Kimberlites, Diatremes, and Diamonds: Their Geology, Petrology, and Geochemistry

Henry O. A. Meyer
F. R. Boyd
editors

Proceedings of the Second
International Kimberlite Conference
Volume 1

American Geophysical Union
Washington, D.C. 20009
1979

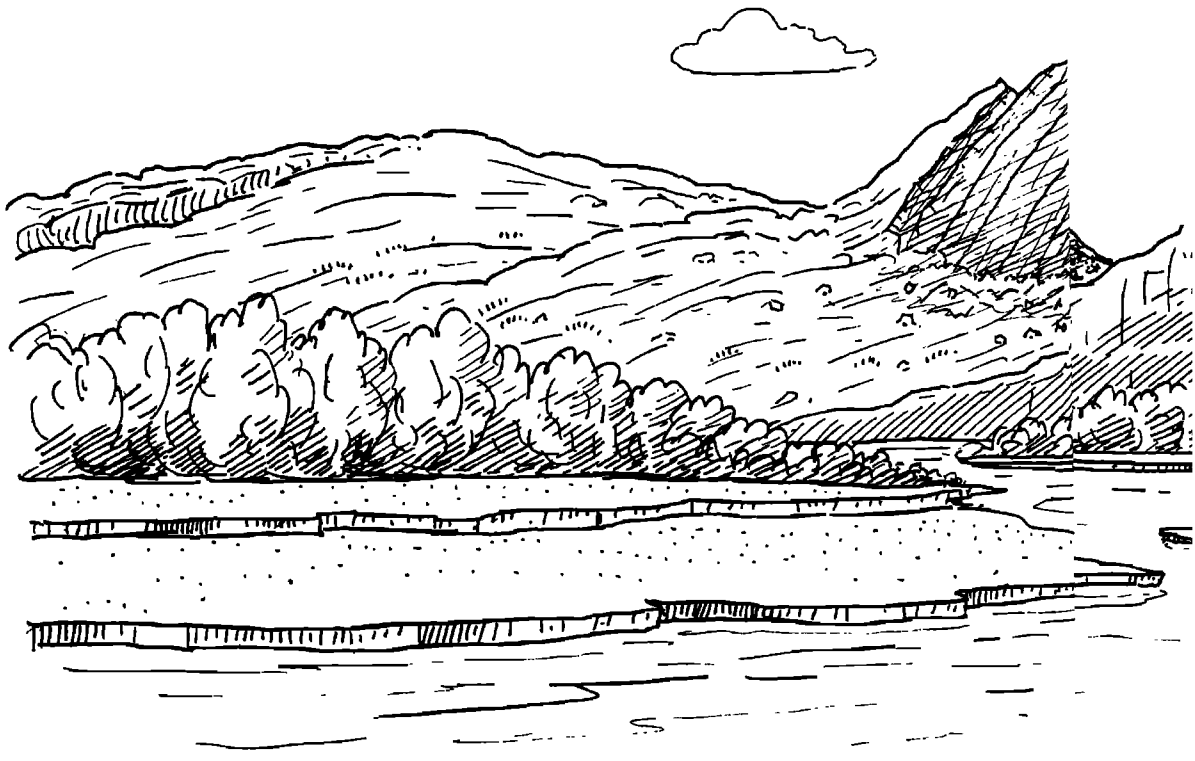

Preface

Since the first edition was published in 1979, the Third International Kimberlite Conference was held in Clermont-Ferrand in 1982. Nevertheless, several of the problems addressed by papers in the first edition of this publication are still valid and remain unanswered today. For example, we still do not understand the spatial and temporal relationship between kimberlite, xenocrysts and xenoliths, nor do we understand why kimberlites occur where they do or why they often intruded ancient cratonic areas periodically throughout geologic time. There is a growing suspicion that continental rifting or perhaps doleritic/basaltic volcanism is a precursor to kimberlitic activity, but the links are tenuous and often conflicting.

The problems of definition and adequate classification of kimberlites, especially for the southern African rocks, are nearing resolution. Hopefully, others will embrace this classification, and misnomers concerning rocks now misleadingly referred to as kimberlite will be removed.

Diamonds received attention during the intervening years between the two Kimberlite Conferences, but still there persists the belief that diamonds and kimberlite are genetically related. And this in spite of the fact that the richest diamond-bearing rock in the world is a tuffaceous lamproite in northwest Australia.

Interestingly, geochemical studies of kimberlite have not been numerous. This may be because of the brecciated nature of kimberlite and the presence of numerous macro- and micro-inclusions of foreign material. The field is ripe for study if one can separate out the essential minerals of kimberlite. This comment is pertinent to isotopic studies as well. Curiously, an area that is lacking is the determination of ages of various xenoliths and xenocrysts. Admittedly, this is difficult, but the results would be of significance with regard to the evolution of the upper mantle, a subject covered in volume 2 of these Proceedings.

Henry O. A. Meyer

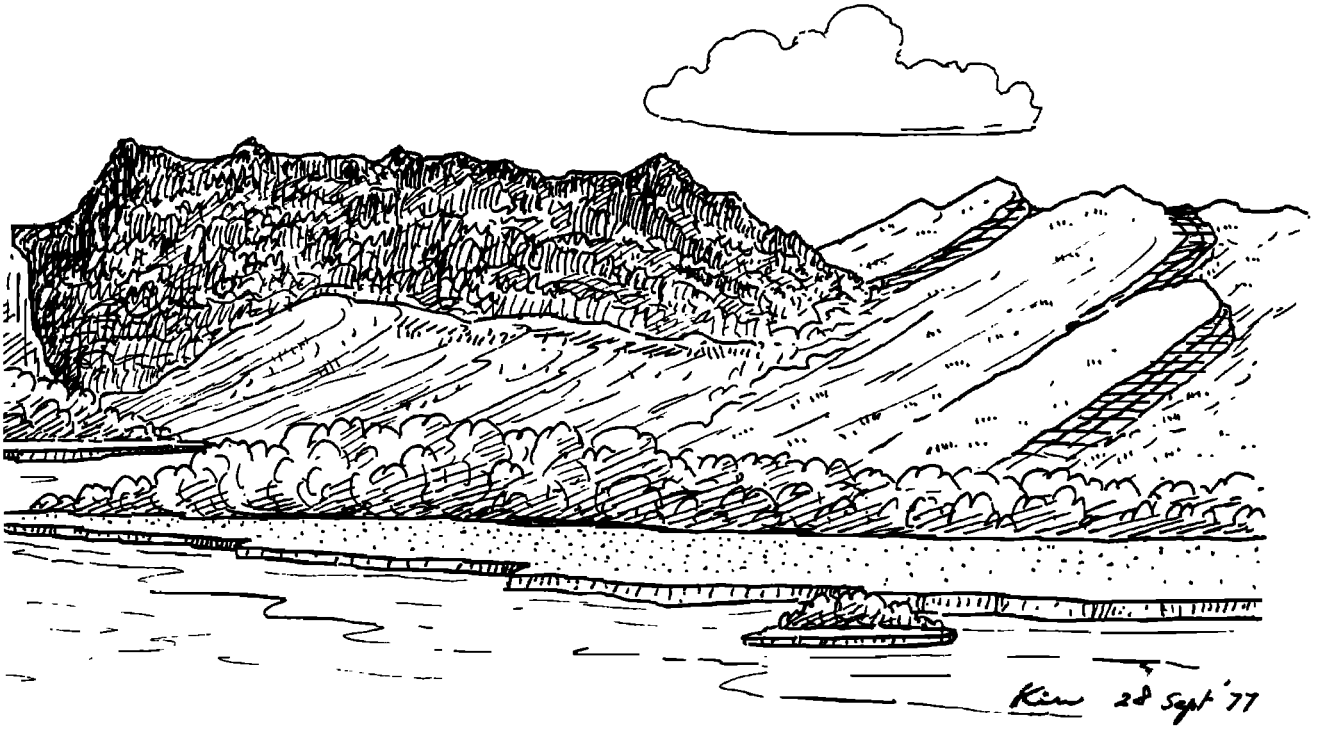

CONTENTS

I. DIAMONDS

II. KIMBERLITES

FIELD RELATIONS

MINERALOGY AND PETROLOGY

I. DIAMONDS

SILICATE AND OXIDE INCLUSIONS IN DIAMONDS FROM THE FINSCH KIMBERLITE PIPE

J.J. Gurney

Geochemistry Department, University of Cape Town, Rondebosch 7700, S. Africa

J.W. Harris

Grant Institute of Geology, University of Edinburgh, Edinburgh EH9 3JW, U.K.

R.S. Rickard

Geochemistry Department, University of Cape Town, Rondebosch 7700, S. Africa

Abstract. A systematic search of 14,500 carats of diamonds (approximately 232,000 stones) from the Finsch kimberlite yielded 1024 diamonds with microscopic inclusions. Sulphides (358), graphite (132) and clouds (23) constitute almost exactly half of these. Of the rest 501 inclusions are minerals of peridotitic composition whilst 10 are eclogitic.

The mineral inclusions appear to be in equilibrium with each other and diamond.

The peridotitic minerals are: olivine (60%), orthopyroxene (20%), garnet (20%) and chromite (1%). The eclogitic minerals are garnet, clinopyroxene and kyanite.

A total of 100 minerals from 80 diamonds have been analysed including 14 garnet/olivine, 2 garnet/orthopyroxene, 1 olivine/chromite, 1 orthopyroxene/silica phase, 1 garnet/clinopyroxene and 1 clinopyroxene/phlogopite pairs.

The peridotitic minerals are distinctively depleted in calcium and have high Mg/Fe and Cr/Al ratios. The eclogitic minerals have opposite characteristics.

The 2 garnet/orthopyroxene pairs could have formed at virtually identical temperatures and pressures. These conditions were within the diamond stability field at a temperature close to 1100°C and a pressure close to 50 kb.

The peridotitic inclusions and the associated diamonds crystallised from a melt formed by a small degree of partial melting of a garnet lherzolite mantle in the presence of water and CO_2. Capture of Ca^{++} by CO_3^{--} is proposed to account for the calcium depleted nature of the mineral inclusions in these diamonds. Based on mineral abundances $\sim$ 98% of the diamonds at Finsch formed during this process.

The remaining $\sim$2% are considered to be derived from a pre-existing diamondiferous eclogite horizon sampled by the kimberlite during its ascent through the mantle.

Introduction

The Finsch Pipe is a major kimberlite mine which has produced diamonds since 1963 at a rate which has been greater than 2 million carats annually in recent years. The mine is about 37 km east of Postmasburg, Cape Province, South Africa.

The diatreme is intrusive into the banded ironstones of the Lower Griquatown (Pretoria) Group, lying outside of the present day extent of the Karoo sedimentary basin. Nevertheless, fragments of Karoo rocks have been seen in the kimberlite and a zircon age of 93 m.y. (Davis, 1977) groups this occurrence with the post-Karoo kimberlite intrusives of virtually contemporaneous age from Botswana, the Kimberley District and Northern Lesotho.

The surface kimberlite at Finsch has been completely altered. Ruotsala (1974) has described this material as friable yellow ground which persists to a depth of approximately 130 feet. The yellow ground grades into blue over approximately the next 100 feet. Some aspects of the general petrography of the Finsch kimberlite have been presented by Clement (1975).

More than 90% of the heavy mineral concentrate produced during the diamond recovery process in the mining operation at Finsch is garnet. Ilmenite and diopside are both very rare. The predominance of garnet is thought to be only in part due to weathering in the surface kimberlite. Olivine and orthopyroxene would be completely removed by this process, but we have seen chrome

diopside and ilmenite persist in yellow ground elsewhere and, in addition, current mining operations are in less altered material with no obvious change in concentrate character. The garnets from the concentrate have been studied by Gurney and Switzer (1973).

Objectives

It was the aim of this study to determine which minerals occur as inclusions in diamonds from the Finsch Mine, and to find the range in chemical composition for individual mineral species. It was also intended to investigate the conditions under which these minerals might crystallise and hence to gain an insight into the natural process of diamond formation. In this respect it was obvious that diamonds containing more than one mineral species as inclusions would be particularly important.

Although inclusions in diamonds have been studied and analysed by various workers in recent years, the comprehensive sampling of a single locality in the manner of this study has not previously been possible. It was hoped that the restriction of the sampling to inclusions from one locality would simplify interpretation of the new data.

The Finsch locality was of particular interest because of the presence of low calcium, high magnesium, high chromium garnets in the concentrate (Gurney and Switzer, 1973). The present study was expected to show that the xenocryst garnets were identical to the diamond inclusions as predicted in the earlier work.

In so far as possible, it was intended to compare the inclusions in the diamonds with the same minerals in mantle xenoliths from the same kimberlite. However, the practical difficulty experienced in sampling the xenoliths at Finsch has restricted this comparison to only a few rocks.

Diamond Selection

The diamonds were selected from that part of the general production defined by the -6 to +5 diamond sieve class. The diamonds are less than 1.83 mm. in largest dimension and average approximately 0.056 carat/stone. This relatively small size was considered acceptable as there is no evidence to relate inclusion size or type to diamond size and it is much easier to extract inclusions from a small diamond than a large crystal.

The diamonds were first inspected by binocular microscope and those containing inclusions were separated and divided into categories of mineral assemblages. The sampling information and a breakdown of the categories are summarised in Table 1. As the ten categories in Table 1 were compiled on observational evidence only, it was not possible to distinguish between certain mineral species whilst they were still inside the diamond.

No attempt was made to allocate olivine, orthopyroxene or other essentially colourless mineral inclusions to separate categories; they were all termed colourless inclusions. Subsequent inclusion analyses showed that more than 70% of these are olivine. The rest are orthopyroxene, except for very rare high Si phases, believed to be coesite.

Olivine is often found in the eye of sulphide inclusions (Harris, 1972) but these are frequently masked from view so the sulphide category will include a certain number of olivines; sulphide more rarely disguises other inclusions such as purple garnet or eclogitic minerals.

TABLE 1. The Relative Abundance of Inclusions in Diamonds of Sieve Class -6 +5[a] from the Finsch pipe

		No
1.	Peridotite Paragenesis	
	Colourless inclusions	381
	Colourless inclusions + purple garnet	50
	Purple garnet	63
	Purple garnet + sulphide	3
	Chromite	4
		501
2.	Eclogite Paragenesis	
	Orange garnet	8
	Orange garnet plus sulphide	2
		10
3.	Other Inclusions: Paragenesis not defined	
	Sulphides[b]	358
	Graphite	132
	Clouds (dense particles)	23
		513
	Totals (1 + 2 + 3)	1024
	Estimated No. of carats inspected	14,500
	Estimated No. of stones inspected	232,000

(a) Sieve class -6 +5. Diameter of circular aperture = 1,829 m.m. Approximate average weight in carats/stone =0.056 ct.

(b) Sulphides occur with both peridotite paragenesis and eclogite paragenesis minerals. The majority of such silicates are olivine (i.e. peridotite paragenesis).

(c) In a subsequent search of additional diamonds eclogitic clinopyroxene, an eclogitic garnet/clinopyroxene pair, a kyanite and a phlogopite were found. These minerals are included in the discussion but not in this abundance table.

It was difficult to distinguish sulphides from graphite and at present we have no information on the sulphide inclusion breakdown nor their compositions. We cannot therefore assess the extent of misidentification in this category of essentially black-looking inclusions.

The purple and the orange garnet categories have been found analytically to correspond to chrome-rich and chrome-poor compositions respectively, whilst all the spinels are high chromium chromites.

Clinopyroxenes are so rare in Finsch diamonds that none were found in the initial sampling. Subsequently four chrome-poor clinopyroxenes were found in an inspection of several different size ranges of Finsch production; one co-exists with chrome-poor garnet. During this later search an extremely magnesian, low calcium garnet with an unexpected green colour (F87: Table 2), a kyanite (Table 3) and additional chromites (Table 2) were found and analysed. Although the bright green colour of chrome diopsides should make them easily visible in a diamond, none were found either in the initial sampling of $\sim$ 232,000 stones or subsequently.

Mineral Inclusion Selection and Diamond Characteristics

In accordance with our principal objective, inclusions were selected for analysis in such a way as to allow investigation of their range in chemistry, both within single diamonds and within the diamond suite as a whole. Care was taken to analyse all identified inclusions of relatively rare mineral type (clinopyroxenes, chromite, kyanite), as well as all inclusions of unusual colour or lustre. Particular attention was given to the selection of diamonds with more than one inclusion.

In addition to the nature of inclusions, attention was given to the characteristics of the host diamonds, in order to investigate relationships between inclusion types and the diamond habit and colour. Six shape categories of diamonds (octahedron, dodecahedron, flattened dodecahedron, macle, irregular and aggregate) and two principal colour types (colourless and brown) were determined. In those inclusion groups (Table 1), where the numbers of diamonds were relatively large (e.g. peridotitic olivines and garnets), inclusion-bearing diamonds were chosen in order to represent each of the shape and colour categories. For rarer inclusion groups, all inclusions were investigated.

In most groups there were insufficient data to make a meaningful assessment of the relationships between diamond shape, diamond colour, and inclusion chemistry. Where a number of inclusions were found - that is for the peridotitic olivines and garnets - the restricted range of the inclusions (discussed below) prevented the detection of any correlation.

The shape classification of inclusion-bearing diamonds did reveal, however, that over 60% of diamonds containing peridotitic inclusions were macles. This percentage is three times that of macles in the same size range from the general diamond production at Finsch (see Harris et al., 1975; Harris and Gurney, 1978).

Analytical Procedure

The inclusions were released from the diamond by mechanical crushing and fracturing. The individual inclusions, usually 0.1 - 0.5 mm. in size were suitably mounted and polished and analysed by an electron microprobe analyser, using standards of similar composition and applying the data correction procedure Abfan II (Boyd, Finger and Chayes, 1969). Detection limits for each element are given in Table 4.

Inclusions Studied

A total of 100 minerals in 80 diamonds have been analysed. These include one garnet/clinopyroxene and one clinopyroxene/phlogopite pair from the eclogitic suite together with 14 garnet/olivine, 2 garnet/orthopyroxene, one olivine/chromite and one orthopyroxene/silica phase of peridotitic origin. The total is made up of 50 garnets, 22 olivines, 6 orthopyroxenes and 8 chromites from the peridotitic suite, 6 garnets, 4 clinopyroxenes, a phlogopite and a kyanite of eclogitic character and 2 silica rich phases believed to be coesite.

The inclusions were wholly enclosed within the diamonds and were not located in cracks, nor along fractures nor annealed fractures. They show little or no signs or alteration. Irrespective of inclusion type many of the inclusions are clearly xenohedral (Prinz et al., 1975), and commonly exhibit equant or elongate cubo-octahedral morphologies, with inclusion faces closely parallel to the (100) and (111) planes in the diamonds. Where more than one inclusion of the same mineral was found in one diamond, the crystal morphologies were often different.

In some instances more than one inclusion of the same mineral was found in one diamond and seventeen such cases were investigated. In agreement with the majority of previous studies of this aspect; for example by Sobolev (1974) or Prinz et al., (1975); no analytically significant differences in composition were recorded for grains of the same mineral in one diamond.

In addition to the above it was also noted that the compositions of different minerals in the same diamond were systematically co-variant. For instance, the most iron-rich olivine co-exists with iron-rich garnet (see Figs. 1 and 3) whilst more magnesian olivine and garnet are found together in 12 diamonds. Orthopyroxene is always more magnesian than olivine as it is in the peridotite xenoliths. In all of these respects our results are entirely consistent with other previously published information on diamond inclusions as reviewed by Meyer and Tsai (1976).

We consider that this evidence is strongly in

TABLE 2. Selected Analyses of Peridotitic Inclusions in Finsch Diamonds

	Garnet-Olivine Pairs						Garnet-Orthopyroxene Pairs								
Sample No.	F9		F13		F14		F16		F41		F45		F71	F73	F87
Mineral	Gt	Ol	Gt	Ol	Gt	Ol	Gt	Ol	Gt	Opx	Gt	Opx	Cte	Cte	Gt
SiO_2	41.4	40.6	41.8	41.4	42.0	41.0	41.0	40.4	42.2	58.2	42.2	58.7	0.11	0.09	41.9
TiO_2	ND	ND	ND	ND	0.08	ND	0.14	ND	ND	ND	ND	ND	0.08	0.07	ND
Al_2O_3	15.1	ND	19.3	ND	14.0	ND	18.3	ND	19.3	0.66	19.4	0.26	7.95	6.71	18.1
Cr_2O_3	11.6	ND	7.06	ND	11.2	ND	7.06	ND	7.34	0.34	7.32	0.15	63.2	63.1	8.32
*FeO	5.87	5.83	5.09	5.49	5.82	5.92	5.83	7.70	5.09	3.38	5.51	3.48	10.8	14.0	3.33
MnO	0.28	0.07	0.21	0.04	0.20	0.08	0.20	0.12	0.18	0.08	0.19	0.09	0.63	0.16	0.15
MgO	24.1	52.1	24.6	51.3	24.4	52.3	20.1	50.6	25.1	37.1	24.6	36.9	16.1	14.7	27.5
CaO	0.65	ND	0.34	ND	1.10	ND	6.12	ND	0.74	0.13	0.75	0.11	0.09	0.10	0.09
Na_2O	ND	ND	ND	ND	ND	ND	ND	ND	ND	ND	ND	0.14	ND	ND	ND
Total	99.0	98.6	98.4	98.2	98.8	99.3	98.7	98.8	99.9	99.9	100.0	99.8	99.0	98.9	99.4
							Ionic Proportions								
Si	3.011	0.992	2.993	1.011	3.059	0.994	2.991	0.993	2.982	1.980	2.985	1.998	0.004	0.003	2.963
Ti					0.004		0.008						0.002	0.002	
Al	1.295		1.629		1.202		1.574		1.608	0.026	1.618	0.010	0.305	0.262	1.509
Cr	0.667		0.400		0.645		0.407		0.410	0.009	0.409	0.004	1.625	1.651	0.465
Fe	0.357	0.119	0.305	0.112	0.355	0.120	0.356	0.158	0.301	0.096	0.326	0.099	0.294	0.388	0.197
Mn	0.017	0.001	0.013	0.001	0.012	0.002	0.012	0.002	0.011	0.002	0.011	0.003	0.017	0.004	0.009
Mg	2.612	1.896	2.626	1.866	2.649	1.890	2.185	1.853	2.643	1.881	2.594	1.872	0.780	0.725	2.899
Ca	0.051		0.026		0.086		0.478		0.056	0.005	0.057	0.004	0.003	0.004	0.007
Na												0.009			
Total	8.008	3.008	7.992	2.989	8.013	2.006	8.011	3.007	8.010	4.003	8.001	3.999	3.030	3.039	8.049
Oxygens	12	4	12	4	12	4	12	4	12	6	12	6	4	4	12

*Total iron as FeO
ND = Not detected. See Table 4 for analytical detection limits.

TABLE 3. Eclogitic Inclusions in Finsch Diamonds

Mineral-Sample No.	Gt-F67	Gt-F68	Gt-F84	Gt-F89[a]	Gt-F90	Gt-F91	Cpx F70[b]	Cpx F85	Cpx F86	Cpx F89[a]	Kyte F88	Phl-70[b]
SiO_2	39.2	39.7	39.9	39.3	39.8	39.9	54.5	55.2	54.6	54.1	36.4	40.7
TiO_2	0.31	0.21	0.15	0.84	0.49	0.40	0.49	0.47	0.35	0.43	0.11	1.71
Al_2O_3	22.0	22.2	22.6	21.2	21.9	22.7	6.73	9.27	7.49	7.73	62.8	13.2
Cr_2O_3	0.05	0.09	0.12	0.06	0.16	0.09	0.11	0.13	0.06	ND	ND	0.93
*FeO	22.6	20.8	18.8	18.4	16.3	16.8	6.84	6.50	6.46	5.73	0.16	5.38
MnO	0.69	1.00	0.97	0.28	0.31	0.43	0.06	ND	ND	ND		0.06
MgO	8.73	11.7	14.3	8.15	10.1	10.2	11.4	10.6	10.9	10.3		25.9
CaO	6.72	3.33	3.11	10.9	10.7	9.79	16.3	12.0	16.3	15.5		0.05
Na_2O	0.20	0.20	0.15	0.23	0.18	0.20	3.62	5.67	3.77	4.33		0.08
K_2O							0.48	0.16	0.03	0.04		10.2
Total	100.5	99.2	100.1	99.4	99.9	100.5	100.5	100.0	100.0	98.2	99.5	98.2
							Ionic Proportions					
Si	2.982	3.005	2.965	3.002	2.988	2.975	1.972	1.979	1.975	1.985		
Ti	0.018	0.012	0.008	0.048	0.028	0.022	0.013	0.013	0.010	0.012		
Al	1.973	1.981	1.980	1.909	1.938	1.995	0.287	0.392	0.319	0.334		
Cr	0.003	0.005	0.007	0.004	0.009	0.005	0.003	0.004	0.002			
Fe	1.438	1.317	1.169	1.175	1.023	1.048	0.207	0.195	0.195	0.176		
Mn	0.044	0.064	0.061	0.018	0.020	0.027	0.002					
Mg	0.990	1.320	1.584	0.928	1.130	1.133	0.615	0.566	0.588	0.563		
Ca	0.548	0.270	0.248	0.892	0.861	0.782	0.632	0.461	0.632	0.609		
Na	0.030	0.029	0.022	0.034	0.026	0.029	0.254	0.394	0.264	0.308		
K							0.022	0.007	0.001	0.002		
Total	8.026	8.004	8.044	8.010	8.024	8.017	4.007	4.011	3.988	3.990		
Oxygens	12	12	12	12	12	12	6	6	6	6		

*Total iron as FeO
ND = Not detected
(a) and (b) are coexisting pairs.

TABLE 4. Analytical Detection Limits for Mineral Analysis by Electron Microscope

Element Oxide	Detection Limit wt.%
SiO_2	0.03
TiO_2	0.03
Al_2O_3	0.02
Cr_2O_3	0.04
FeO	0.04
MnO	0.03
MgO	0.03
CaO	0.02
Na_2O	0.05
K_2O	0.03

favour of equilibrium crystallisation of the diamond host and its inclusion mineral or minerals and conclude that the original mineral compositions have not changed since diamond formation.

At Finsch the silicate inclusions are dominated by olivine (see Table 1). Chrome garnet and orthopyroxene clearly can co-exist with olivine since they have been found in the same diamond. (See Table 1). All three, together with chromite, since they resemble the minerals found in mantle peridotite from kimberlite fall within the grouping termed the ultramafic suite (Meyer and Tsai, 1976), or the peridotite suite (Harris and Gurney, 1978).

Previous studies of diamond inclusions have identified another major suite of minerals which have been termed "eclogitic" on the basis of the major component similarity of these inclusions compared to minerals found in the occasionally diamondiferous kimberlite xenolith, eclogite. This second suite is present at Finsch, but forms only a very minor part (<2%) of the silicate inclusion population at this locality. In this respect Finsch appears to be similar to Mir (Sobolev, 1974).

The Eclogite Inclusions

The eclogite inclusions are so rare that out of the initial sampling of 1024 inclusions from approximately 232,000 diamonds only 10 were visually identified to be of eclogitic origin. Whilst a further search in different size ranges of diamonds confirmed this rarity, a number of additional eclogitic minerals were recovered and have been analysed. Analyses of all the eclogitic minerals will be found in Table 3.

The garnets and clinopyroxenes are both iron-rich, but within the reported range from other localities as shown for garnets (Fig. 2). The garnets fall into the field D in Figs. 4A and 2 and plot the furthest away from the Mg apex of all garnets found at Finsch. Both the garnets and clinopyroxenes show wide variations in chemistry which are difficult to interpret without additional inclusions from which to attempt to develop some compositional trends. They are however chemically related to the eclogite xenoliths in the pipe which are also characterised by iron enrichment and variability in composition providing the four small samples available for our study (see Fig. 4A) are representative of the eclogite suite as a whole. The single kyanite inclusion in a diamond is considered to show an association with kyanite eclogite which, it is inferred, will be found in the Finsch kimberlite as sampling progresses. Kyanite, however, is usually associated with grossular garnet, and it is regarded as certain that the limited number of eclogitic minerals sampled do not completely define the compositional variations of eclogitic minerals at the Finsch locality.

The high sodium contents of eclogite garnet inclusions were first commented upon by Sobolev et al. (1971) and are confirmed at Finsch. They are not restricted to the inclusions since one of the four analysed xenolith garnets has 0.14 wt. % Na_2O.

Although eclogite minerals in diamond are very rare at Finsch, one garnet/clinopyroxene pair was analysed (F89: Table 3). Application of the Fe/Mg.gt/cpx geothermometer (Raheim and Green, 1974) gives temperatures of 1019°C, 1095°C and 1171°C at pressures of 40, 50 and 60 kb. respectively. This range of values intercepts the diamond/graphite reaction curve at 1030°C and 42 kb., and defines a line close to and parallel to the peridotite wet solidus of Kushiro et al. (1968), (see Fig. 6), thereby implying hydrous melting assuming that the inclusions equilibrated with a melt. Wood (1976) has expressed reservations about the accuracy of the gt/cpx geothermometer on both experimental and theoretical grounds and since the calcium content of the garnet, at 10.9 wt. % CaO, is outside the range of the experimental calibration, the calculation could be inaccurate. It does, however, predict conditions of

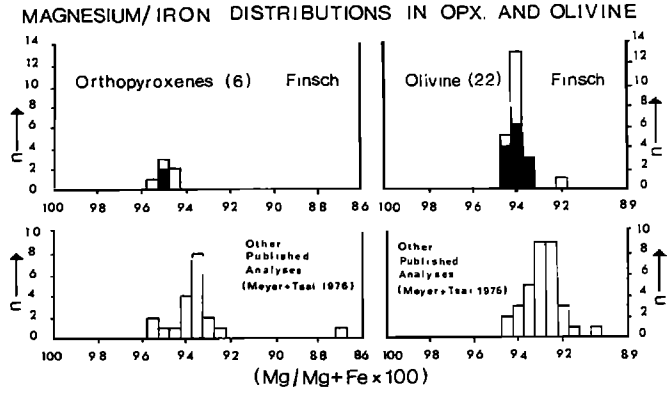

Figure 1. Mg/Mg and Fe ratios for orthopyroxene and olivine inclusions in diamonds.

formation which are similar to those which we have calculated for garnet/orthopyroxene pairs from two Finsch diamonds.

Eclogite xenoliths from kimberlite are occasionally found to contain diamonds (e.g. Rickwood et al., 1969; Reid et al., 1976) and since the eclogite xenoliths at Roberts Victor are demonstrably non-cognate to the kimberlite (Kramers, 1977), we have no evidence which contradicts the views of Sobolev (1974) and others, that the eclogitic inclusions are found in diamonds released from disaggregated eclogite xenoliths sampled by chance by the protokimberlite at depth. Indeed, we suggest that the lead isotope ratios obtained by Kramers (1977) for Finsch sulphide inclusions, on which is based the non-cognate origin of the diamonds in the kimberlite, may relate only to the eclogite derived fraction of the diamond population.

The Peridotite Inclusions

The twenty-two analysed olivines are forsterites; twenty-one have a very restricted range in composition (Fo 93.5 - 94.75) whilst one is Fo 92. TiO_2, Al_2O_3, Cr_2O_3 and CaO are in all cases on or below the analytical detection limit (see Table 4). The high Cr_2O_3 contents (>0.05%) reported by other workers (e.g. Meyer and Boyd, 1972) are not present in this sampling of Finsch olivine inclusions, which have been very carefully checked. Sobolev (1974) gives similar results for inclusions from Mir and has shown that high Cr olivines are in equilibrium with the most chromiferous garnets. Garnet inclusions at Finsch frequently have less than 8% Cr_2O_3. Twelve of the olivines spanning the full compositional range co-exist with garnet.

The six orthopyroxenes are very magnesian enstatites with 100 (Mg/Mg + Fe) in the range 94.5 - 95.5. Two co-exist with garnet. One contains 0.26 wt.% Al_2O_3 and the other 0.66 wt.% Al_2O_3. These values are the limits of Al_2O_3 contents found in all orthopyroxene inclusions. Calcium is very low (0.09 wt.% - 0.27 wt.% Ca). The range in sodium is 0.06 wt.% - 0.14 wt.% Na_2O. Titanium was not detected (D.L.~0.03wt.%).

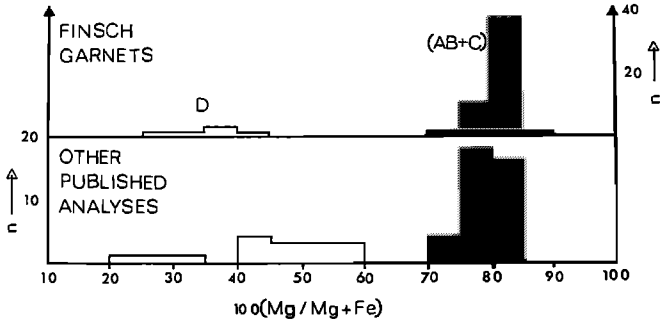

Figure 2. Mg/Mg and Fe ratios for garnet inclusions in diamonds (See text for discussion of groups ABC and D.)

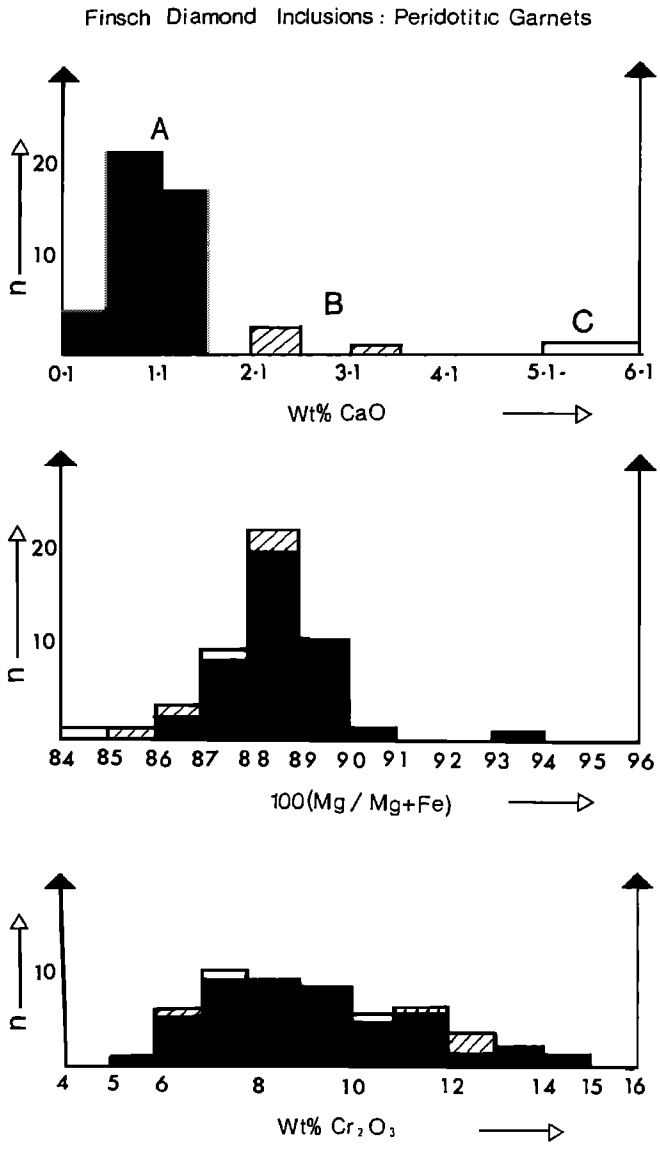

Figure 3. CaO, Mg/Mg and Fe and Cr_2O_3 in peridotitic garnet inclusions in Finsch diamonds.

The Cr_2O_3/Al_2O_3 ratio is fairly constant (0.41 - 0.59).

The Mg/Fe distributions in the orthopyroxenes and olivines are summarised in Fig. 1 where they are compared with other published analyses of inclusions in diamonds and some xenolith data from Finsch. A similar plot for all the Finsch garnets is presented in Fig. 2. The Finsch peridotitic inclusions, olivine, orthopyroxene and garnet, fall within the range of Mg/Mg + Fe reported elsewhere but to the magnesian side of the median in all three cases. Selected analyses of the peridotite minerals are given in Table 2.

The variation in composition of the peridoti-

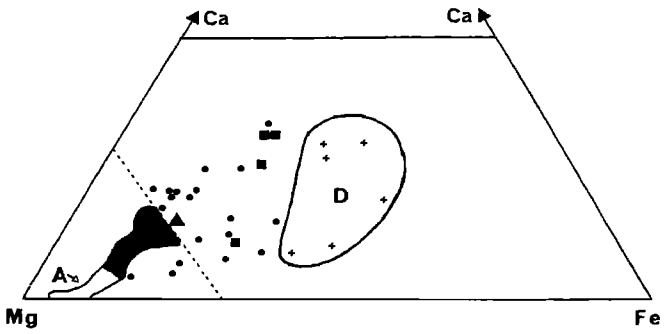

Figure 4A. Ca:Mg:Fe diagram for garnets from Finsch.

Symbols : ■ :Eclogite Xenoliths
▲ :Garnet Websterite Xenolith
● :Concentrate Xenocrysts
+ :Eclogitic inclusions in diamond (Field D).

Field A (unshaded Area): field of group A inclusions in diamonds. Black field: see Fig.4B.

tic garnet inclusions is largely defined by the ranges in Mg/Mg + Fe ratio, Cr_2O_3 and CaO illustrated in Figs. 3, 4 and 5. For convenient reference the peridotitic garnets have been broken up into three groupings A, B and C on the basis of calcium content, whilst the eclogitic garnet inclusions are called Group D (Fig. 2). Forty-four out of fifty peridotitic garnets have very low calcium contents and fall in Group A. Therefore Group A garnets predominate over a minor component of rare garnet compositions (Groups B and C). The analyses need no assigned Fe^{3+} to fill the trivalent lattice site since (Al^{3+} + Cr^{3+}) = 2.00 ± 0;03 for all fifty garnets. Titanium was detected in only five garnets, sodium in none and manganese is always within the range 0.15 - 0.30 wt.% MnO. The extremely low calcium contents of the Group A garnets in Finsch diamonds, compared to those which apparently equilibrated with clinopyroxene, are shown in Fig. 5.

The range in Mg/Mg + Fe determined for the three silicate minerals is small and garnet and olivine have been found as co-existing pairs across this full range (see Figs. 1 and 3). In two cases orthopyroxene has been shown to occur with garnet in the same diamond. Fortuitously these orthopyroxenes have the highest and lowest recorded alumina contents respectively, and therefore the restricted equilibration conditions generated by F41 and F45 in Fig. 6 and discussed in detail later may represent the maximum range of conditions for all the orthopyroxenes.

The chromites found in Finsch diamonds are all characterised by Cr_2O_3 contents greater than 61 wt.%, (Table 2) and are thereby similar to those reported from elsewhere previously (e.g. Meyer and Boyd, 1972; Sobolev, 1974). Since chromite is a refractory mineral occasionally reported in peridotite xenoliths it is considered to be a minor member of the peridotite suite.

Evidence in favour of inclusion equilibration within a single diamond was advanced in an earlier section and from this, the above and Table 1, it is deduced that garnet, orthopyroxene and olivine were in equilibrium during the period of formation of the majority of the diamonds at Finsch.

It is relevant to compare the peridotitic inclusions in the diamond with the compositions of concentrate xenocrysts and the component minerals of peridotite from Finsch.

In addition therefore to the inclusion data, data on garnet xenocrysts described in the paper by Gurney and Switzer (1973) have been included in Figs. 4A and 4B and, in addition, some partial analyses from that source are utilised in Fig. 5. Garnet compositions from xenoliths from the Finsch Mine have been plotted in the same figures. Xenoliths from Finsch have been sought on several occasions but have chiefly been found as remnants of garnet in a mass of serpentine and other low temperature secondary products within the yellow ground. Over a number of visits the

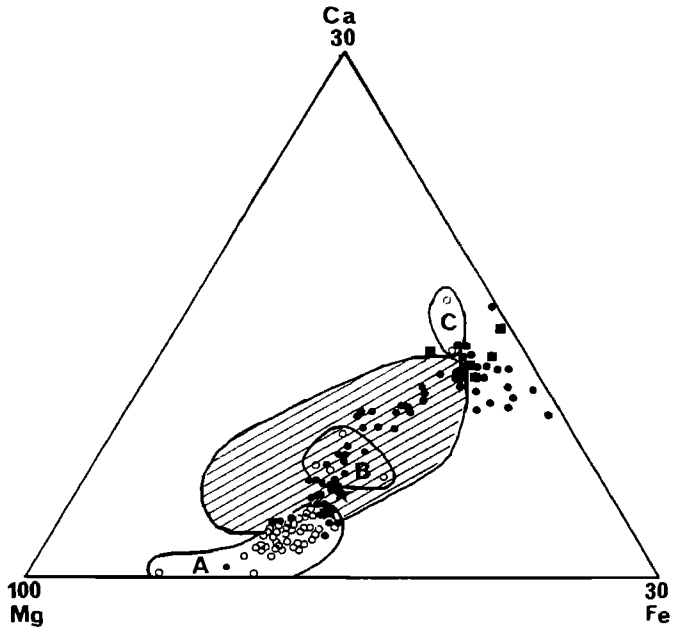

Figure 4B. Magnesian apex of Fig. 4A (see dotted line in 4A). Garnet compositions.

Symbols: ■ :Peridotite Xenoliths
✱ :Garnet Serpentinites
● :Concentrate Xenocrysts
○ :Inclusions in diamond
▨ :Shaded field: field of diamond inclusions defined by published analyses (Lawless 1974).

mine geologist has collected six garnet lherzolites, one garnet websterite, two small fragments which appear to have been garnet harzburgites and three eclogites. All the xenoliths are small (~ 4 cm. in largest dimension) and some phases are completely altered. In three cases, two garnet lherzolites and a garnet websterite, the mineral compositions are set out in Table 5.

The garnet lherzolites are similar to coarse garnet-lherzolites found at Bultfontein (Dawson et al., 1975; Boyd and Nixon, 1977) or Matsoku (Cox et al., 1973) and many other South African

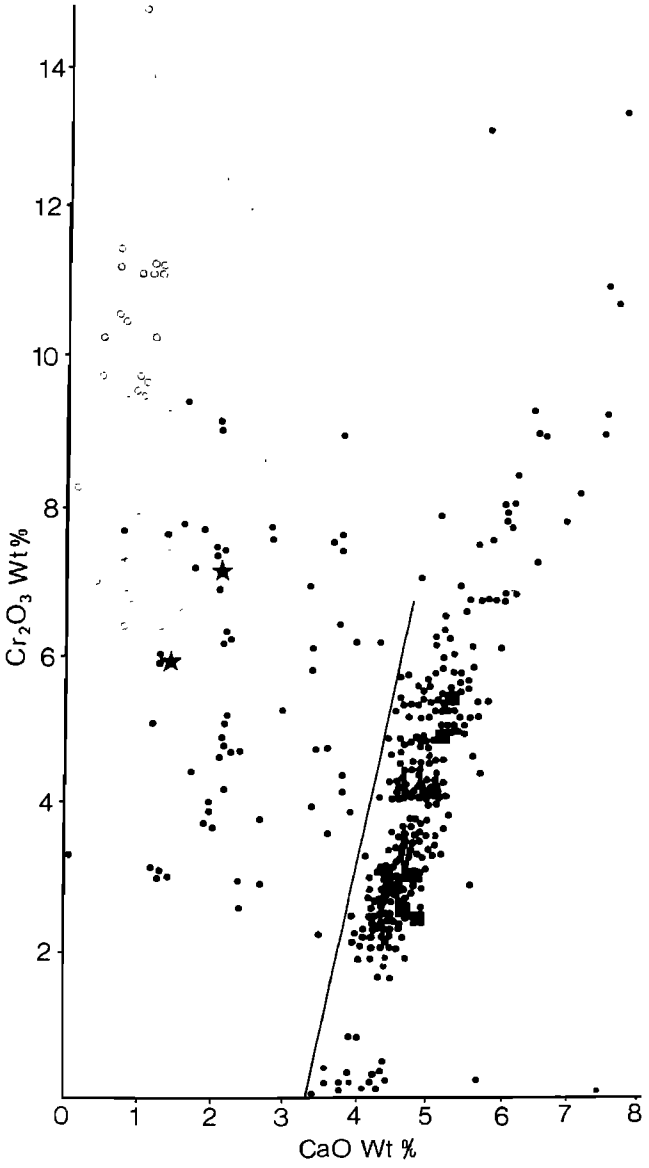

Figure 5. Plot of Cr_2O_3 against CaO for Finsch peridotitic garnets.

Symbols: ▲:Garnet Websterite
Rest :as for Fig. 4B.

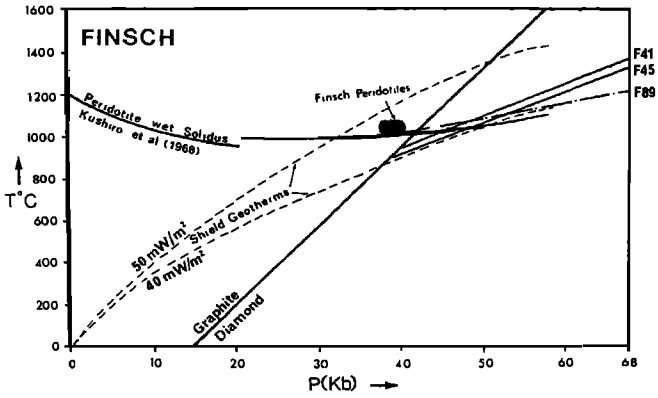

Figure 6. Schematic diagram to illustrate possible conditions of formation of the diamond inclusions at Finsch (See text for data sources and discussion).

localities (e.g. Frank Smith, Monastery, De Beers, Du Toit's Pan, Wesselton, Jagersfontein, Northern Lesotho, etc.). However, whereas such lherzolites typically have Al (En) contents >0.7 wt.% Al_2O_3, the four garnet-lherzolites from Finsch have orthopyroxenes with 0.53 - 0.66 wt.% Al_2O_3. This range overlaps the higher Al_2O_3 contents of the 6 analysed orthopyroxene inclusions from diamond.

In the diamonds, the low calcium garnets (Groups A and B: Figs. 3, 4A and 4B), the orthopyroxenes, and all the olivine inclusions (except one) are more magnesian than the same minerals in the xenoliths. The Group A and B garnets and all 6 orthopyroxenes are depleted in calcium relative to garnet lherzolite minerals (see Fig. 5 for garnet data). The orthopyroxenes also have less Na_2O and the lowest Al_2O_3 contents, although there is overlap as mentioned earlier.

The calcium depleted nature of the peridotitic inclusions is further emphasised by the complete absence of chrome diopside as an inclusion in the diamonds studied. Sobolev (1974) notes that chrome diopside is the most strikingly noticeable inclusion in diamond. We believe that it is most unlikely that such inclusions have been overlooked, and consider that the extreme calcium depletion of most of the garnets in diamonds compared to garnets in lherzolites, as shown in Fig. 5, is only possible in the absence of clinopyroxene.

Since we have deduced, as a result of this study, that garnet, orthopyroxene and olivine are in equilibrium with each other during the major phase of diamond formation at Finsch, it is possible that minerals matching the diamond inclusions might be found in garnet harzburgite fragments. Unfortunately no such rocks have been found, except possibly for two fragments which were extensively serpentinised and in which only the garnets could be analysed. The garnet compositions are plotted on Figs. 4 and 5, and are peripheral to the main group of diamond inclusion data. Garnet harzburgites from elsewhere e.g.

TABLE 5. Mineral Compositions of 2 Finsch Garnet Lherzolites and One Garnet Websterite

Sample No	JJG 147				JJG 479				JJG 545		
Rock type	Garnet Lherzolite				Garnet Lherzolite				Garnet Websterite		
Mineral	Gt	Cpx	Opx	Ol	Gt	Cpx	Opx	Ol	Gt	Cpx	Opx
SiO_2	41.5	54.9	57.6	40.7	42.0	54.4	57.0	40.6	41.2	54.5	56.7
TiO_2	0.05	ND	ND	ND	0.33	0.16	0.11	ND	0.53	0.18	0.10
Al_2O_3	19.6	1.16	0.53	ND	21.4	1.75	0.64	ND	20.0	2.23	0.65
Cr_2O_3	5.37	0.91	0.23	0.05	3.10	0.95	0.11	ND	4.40	1.21	0.24
*FeO	7.27	2.57	5.11	8.65	7.29	2.61	5.31	8.60	9.28	3.77	6.84
MnO	0.35	0.08	0.11	0.10	0.28	0.07	0.09	0.09	0.31	0.10	0.12
MgO	19.5	18.7	34.8	49.4	20.5	18.4	0.67	50.2	19.3	18.0	34.4
CaO	5.67	20.2	0.73	0.08	4.84	20.1	0.11	0.08	4.88	18.4	0.73
Na_2O	ND	1.10	0.13	ND	ND	1.38	ND	ND	0.06	1.89	0.19
Total	99.4	99.7	99.3	99.0	99.8	99.9	99.7	99.7	100.0	100.3	100.0
					Ionic Proportions						
Si	3.007	1.997	1.991	1.002	2.998	1.968	1.966	0.993	2.982	1.966	1.966
Ti	0.003				0.018	0.004	0.003		0.029	0.005	0.003
Al	1.673	0.050	0.022		1.802	0.075	0.026		1.706	0.095	0.027
Cr	0.307	0.026	0.006	0.001	0.175	0.027	0.005		0.252	0.035	0.007
Fe	0.440	0.078	0.148	0.178	0.435	0.079	0.153	0.176	0.561	0.114	0.198
Mn	0.021	0.002	0.003	0.002	0.017	0.002	0.003	0.002	0.019	0.003	0.004
Mg	2.108	1.015	1.793	1.812	2.180	0.994	1.830	1.831	2.081	0.968	1.778
Ca	0.440	0.789	0.027	0.002	0.370	0.779	0.025	0.002	0.378	'.712	0.027
Na		0.077	0.009			0.097	0.007		0.008	0.132	0.013
Oxygens	12	6	6	4	12	6	6	4	12	6	6

* Total iron as FeO
ND = Not detected

Premier Mine (Danchin and Boyd, 1976), Bultfontein (Gurney, unpublished data), Sloan (Eggler and McCallum, 1975) all have >3 wt.% CaO and would plot between Groups B and C in Fig. 4B (cf. also Fig. 3) well away from the Group A garnets.

The xenocryst minerals in the kimberlite are predominantly garnet with the compositions plotted in Figs. 4A, 4B and 5. It can be seen that certain xenocryst garnets fall into the diamond inclusion field defined by published analyses (Lawless, 1974), but that in general they have less Cr_2O_3 and more CaO than the Group A Finsch diamond inclusions, which are extremely low in CaO and lie partly outside the previously reported compositional field for inclusions (see Fig.4).

Xenocrysts which form an intermediate grouping between the lherzolite garnets and Group A (see Fig. 4B) are detailed in Gurney and Switzer (1973), who suggested that (i) they would be identical to peridotitic garnet inclusions in Finsch diamonds, and (ii) that they were derived from disaggregated harzburgite. This study has shown that the xenocryst compositions are represented in diamond only by garnet Groups B and C which are very subordinate in abundance to Group A garnets. The selected xenocrysts define a well developed continuous compositional trend from the garnet lherzolite field to the edge of the Group A inclusion field in Fig. 4B.

These concentrate xenocrysts are very important in the final analysis of the Finsch diamond inclusion garnet population. They are homogeneous and clearly distinguishable in composition from garnet in garnet lherzolite. It is unlikely that they are all derived from disaggregated garnet harzburgite since garnets in harzburgite with less than 3.5 wt.% CaO are rare. Most significant is the fact that as xenocrysts they have not been protected by diamond. Their presence in the concentrates demonstrates that armouring is not a pre-requisite for the preservation of compositional differences in the peridotitic garnets at Finsch and that we are not dealing with two chemically distinct populations of (i) peridotitic garnet inclusions in diamond and (ii) garnets in lherzolites or harzburgites, but with a continuum of compositions, which might be linked in a single evolutionary process. Indeed the majority of the peridotitic minerals have such a specific and unusual chemistry that we consider that they cannot represent randomly sampled mantle material but must reflect a definite mode of formation.

Equilibration Conditions

Diamond Inclusions

In the peridotitic suite of diamond inclusions the only clues with respect to the temperatures and pressures of equilibration we have deduced are derived from the orthopyroxenes, in particular the two orthopyroxenes (F41 and F45) which co-exist with garnet.

The compositions of these co-existing mineral pairs are given in Table 2. It can be seen that F41 opx contains 0.66 wt.% Al_2O_3 and F45 opx 0.26 wt.%.

The Al_2O_3 content of orthopyroxene in the presence of garnet is both temperature and pressure sensitive (e.g. McGregor, 1974). A garnet/orthopyroxene pair cannot, therefore, define a unique value for either variable, but can be used to derive a locus of PT values which define all the possible solutions to the observed mineral chemistry. McGregor's experimental data does not straddle the observed range of Al_{En} in the Finsch diamond inclusions and his experiments were carried out in the simple system MAS. Whilst the silicates which crystallised with the diamond are largely defined by this system, direct application of McGregor's data would predict equilibration pressures for F41 and F45 which would differ by approximately 14 kb. at temperatures above 1000°C, and at 1100°C indicate pressures of 67.8 kb. and 54.5 kb. for F41 and F45 respectively. Yet these two orthopyroxenes are indistinguishable with respect to Mg and Fe and are part of a compositionally tightly restricted and unusual (by comparison with peridotites) group of minerals.

The difference in equilibration conditions is apparently almost completely removed when consideration is taken of the effect of the additional components (especially Fe, Ca, Cr and Na) present in the natural system. Wood and Banno (1973) and Wood (1974) have considered these effects from a thermodynamic standpoint. We have used Wood (1974, Equation 12) and a similar procedure devised by Fraser (Fraser and Lawless, 1978) to define equilibration conditions for F41 and F45 at various temperatures. Results for 1100°C are summarised in Table 6. The Wood (1974, Equation 12) charge balanced calculation after O'Hara and Yarwood (1977) predicts pressures within 2 kb. of each other for F41 and F45 at any fixed temperature. The calculation using the method of Fraser predicts lower pressures and it is this method which was used to generate the straight lines F41 and F45 in Fig. 6 which are truncated by the graphite-diamond reaction curve, and will be discussed later.

We consider that the coincidence of some of the corrected values is a more accurate reflection of the actual conditions of formation of these two mineral assemblages, than the uncorrected data provides.

TABLE 6. Calculations of Possible equilibration conditions

(a) Garnet/opx diamond inclusions F41 and 45

Mineral Pair	Assumed T°C	P(Kb) (i)	(ii)	(iii)	(iv)
F41	1100	54.4	46.4	52.6	50.4
F45	1100	67.8	60.1	54.1	52.4

(b) Xenoliths

Sample No.	Wells T°C	P(Kb) (iii)	(iv)
JJG 147	1050	39.9	37.0
JJG 479	1030	40.8	40.8
JJG 545	1050	39.1	37.3

(i) Al in M1 = Al/2. (McGregor 1974)

(ii) Al in M1 = Al/2. (Wood 1974. Equn.12)

(iii) Charge balanced (Wood: Equn. 12 as in O'Hara and Yarborough 1977)

(iv) Charge balanced (Fraser and Lawless 1978)

Xenoliths

We have similarly calculated the equilibration pressures for xenoliths from Finsch using temperatures derived from the clinopyroxene compositions after Wells (1977). These are also listed in Table 6.

Discussion

The information on equilibration conditions for the diamond inclusions and the xenoliths at Finsch are summarised in Fig. 6. The solidus of peridotite when $P_{H_2O} = P_{total}$ (Kushiro et al., 1968), the graphite-diamond reaction curve, and two possible shield geotherms (Pollack and Chapman, 1977) are also plotted.

Since F41 and F45 are inclusions in diamonds, the straight line denoting possible equilibration Ts and Ps is not extended into the graphite stability field. The xenoliths lie in the graphite field. The eclogitic assemblage F89 is denoted by two points which represent temperatures calculated for pressures of 50 and 60 kb. using the equation derived by Raheim and Green (1974).

These temperature and pressure elements show that the diamond inclusions F41, F45 and F89 could not have formed unless the shield geothermal gradient was considerably less steep than that calculated by Pollack and Chapman (1977) for a surface heat flow of 50 mW/m^2. At a surface flow

of 40 mW/m^2 the inclusions could have formed but only at temperatures and pressures close to the geotherm and close to the "wet" solidus temperature of peridotite. Heat flow measurements for South Africa at the present time range from 33.5 mW/m^2 to 75 mW/m^2 , with the majority of values between 40 and 70 mW/m^2 (Carte and van Rooyen, 1969). In general the higher values occur in the continental margins and the lower values on the Transvaal Craton.

The higher heat flow measurements would appear to indicate a geothermal regime in the mantle in which "wet" peridotite must melt outside the field of diamond stability (Fig. 6). Only at very low geothermal gradients could diamond be stable at temperatures which are above both the geotherm and the "wet" peridotite solidus and yet within the diamond stability field. The"wet" peridotite solidus has been well determined by several experimentalists (e.g. Kushiro et al., 1968); Boettcher et al., 1975; O'Hara et al., 1975) and the diamond graphite reaction curve is well defined experimentally and theoretically (Kennedy and Kennedy, 1976). If the geothermal regime within the earth's crust and upper mantle were equally well quantified, the results would imply an important restriction of the diamondiferous kimberlites to areas of low surface heat flow.

Calculation of geothermal gradients, however, involves assumptions with respect to crustal and mantle compositions and structure and the physical properties of minerals at high temperatures and pressures which are not well known and these and other factors can lead to considerable uncertainty in the calculation of the geothermal gradient. An alternative "adiabatic" geotherm calculated by Harte (1977), cuts steeply across the Pollack and Chapman (1977) geotherms at temperatures above 1000°C and would suggest that in this temperature region the geotherms for areas of different surface heat flow will be convergent. This convergence however is least for low surface heat flows and such low geothermal gradients would still allow small volumes of water/CO_2 saturated melts to form within the diamond stability field.

Since an increase in pressure and an increase in temperature have opposing effects on garnet solid solution in orthopyroxene, the locus of points generated from the geobarometry for the garnet/orthopyroxene pairs F41 and F45 closely parallels likely geotherms, as shown in Fig. 6. These lines, therefore, cannot be used to restrict the conditions of diamond formation to narrow limits. The evidence presented in Fig. 6 permits temperatures of formation of the mineral pairs above 1050°C. However, other evidence appears to favour the lower part of these ranges. We have determined the compositions of chrome diopside inclusions in diamond from Koffiefontein, another Karoo kimberlite pipe and these have Ca/Ca + Mg ratios in the range 0.42 - 0.45 which are indicative of temperatures in the approximate range of 1075°C ± 50°C. Meyer and Tsai (1976) have previously described a calcic peridotitic clinopyroxene in a diamond inclusion pair from Jagersfontein, another cretaceous kimberlite in the Karoo province.

The very low alumina contents in the orthopyroxene inclusions as compared to orthopyroxenes in garnet-peridotite xenoliths of coarse and deformed types does not suggest an association of the diamond inclusions with high temperature peridotites supposedly sampled at 170 - 200 km depths, such as those described by Boyd and Nixon (1975), which have Al_2O_3 >1.2 wt.% in opx. The orthopyroxenes in diamond show more affinity with the cooler and lower pressure coarse grained garnet-peridotites. The small amounts of titanium in the inclusions generally, their higher Mg/Mg + Fe ratios and their low calcium contents support this conclusion. The inclusions do not, therefore, appear to be related to the high temperature mantle samples (deformed peridotite or megacryst) which occur in kimberlite.

On the basis of the foregoing, we therefore favour diamond formation at Finsch to have occurred at temperatures of approximately 1100 ± 50°C. If diamond crystallisation occurred within the specified temperature range then the chemistry of the two garnet/orthopyroxene pairs, F41 and F45, and the peridotite "wet" solidus restrict the possible equilibration pressure to a small range of 50 ± 3 kb; as can be seen by inspection of Fig. 6.

We propose the following hypothesis for the formation of those diamonds which are connected with the peridotite paragenesis. We believe this to be close to 98% of all diamonds at Finsch, having assumed that since olivine is the commonest silicate to be found with sulphide, the sulphide inclusions can be assigned in the same proportions as the silicates.

1. A partial melt of garnet lherzolite or garnet harzburgite mantle in the presence of water, CO_2 and probably other volatiles is initiated in the mantle, within the diamond stability field. The residual mantle is garnet harzburgite. The melting temperature is at or only slightly above the ambient geothermal temperature at the pressure concerned.

2. It is suggested that the presence of abundant CO_2 generates an initial melt of carbonatitic-kimberlitic affinities (Wyllie and Huang, 1976) which preferentially dissolves Ca as compared with other cations and renders the solid silicates in equilibrium with it very poor in CaO (Harte, Gurney and Harris; in preparation).

3. When the silicate phases in equilibrium with the melt have become extremely calcium poor, due to the progressive capture of calcium by $CO_3^=$ in the melt, conditions become particularly favourable for diamond formation. Under the same conditions sulphides (chalcopyrite, pyrrhotite and pentlandite mixtures: Harris, 1972) are formed. These and the sub-calcic silicates are occasionally included in the diamond.

4. Subsequently, this total system comprising silicate melt, cumulate minerals (including diamonds) and the remaining volatile phase is rapidly emplaced into the crust as the kimberlite itself or an essential component of it. The coarse peridotite xenoliths and the eclogite represent shallower mantle overlying the proto-kimberlite which was sampled en route to the surface. The development of an over-pressure by sudden change in CO_2 solubility as described by Wyllie and Huang (1976) is a potential trigger mechanism for this event.

The hypothesis is a process which assumes that diamonds at Finsch formed from a mantle liquid in the presence of CO_2 and water. Diamonds have been shown to contain abundant CO_2, H_2O, N_2, CH_4, Ar and possibly H_2 (Melton et al., 1972) and all these constituents could well be concentrated in the postulated volatile phase. $CO_3^=$ and OH^- ions have been identified in diamonds (Chrenko et al., 1967). A cloud-like region in a diamond from Arkansas appeared to consist of H_2O, CO_2 and H_2 (Giardini and Melton, 1975). Similar cloud-like regions have been observed in Finsch diamonds and are reported in Table 1.

Further evidence for the presence of volatiles and a melt during the growth of Finsch diamonds is provided by Fesq et al. (1975) who detected minute quantities of impurities which they regarded as melt material trapped during diamond growth. They estimated that the diamonds crystallised from an H_2O-rich picritic magma in the presence of Fe-Ni-Cu-Co sulphides; a conclusion entirely compatible with our own observations and proposed mechanism for diamond formation. When these facts are considered together with the extremely narrow range of unusual mineral compositions the crystallisation of diamond from a silicate melt is considered more probably than any other. We certainly consider that the mineral compositions cannot represent randomly sampled mantle compositions but must reflect a definite mode of formation.

In the proposed hypothesis the diamonds with the ultramafic mineral inclusions would be cognate with respect to the kimberlite genesis. The kimberlite at Finsch forms part of the post-Karoo igneous event (Davis, 1977) but work by Kramers (1977, 1978) has shown that the lead isotopic characteristics of at least some sulphide inclusions in diamonds at Finsch are quite incompatible with derivation from the kimberlite; the lead ratios giving an age of some 2.5 b.y. This apparent anomaly can be reconciled if the diamonds containing the sulphide inclusions belong to the eclogitic rather than the peridotitic mineral association. Kramer points out that the great inequality in the lead contents between the various analyses suggests that the lead is contained in only one or two of the diamonds in each sample. It is possible therefore that the age determined relates to an earlier eclogitic paragenesis and not to the origin of the majority of Finsch diamonds.

Acknowledgments. The authors acknowledge gratefully the financial assistance of De Beers Consolidated Mines, the Diamond Research Laboratories and the University of Cape Town.

The project was made possible and constantly encouraged by J.B. Hawthorne. The diamonds were sorted by Ms. H. Hartley and A. van Niekerk in the Kimberley Sorting Offices.

The manuscript was critically reviewed by Ben Harte; a contribution which is underemphasised by this brief acknowledgment.

A computer print-out of all the analytical results for the diamond inclusions, the xenocrysts and the xenoliths may be obtained from the senior author on request.

References

Boetcher, A.L., Mysen, B.O., and Modreski, P.J., Melting in the mantle : phase relationships in natural and synthetic peridotite-H_2O and peridotite-H_2O-CO_2 C-H-O-S with application to kimberlite. Phys. Chem. Earth IX, Ed. L.H. Ahrens et al., Pergamon Press, 855-867, 1975.

Boyd, F.R., Finger, L.W., and Chayes, F., Computer reduction of electron probe data, Carnegie Inst. Year Book, 67, 210-215, 1969.

Boyd, F.R., and Nixon, P.H., Origins of the ultramafic nodules from some kimberlites of Northern Lesotho and the Monastery Mine, South Africa, Phys. Chem. Earth IX, Ed. L.H. Ahrens et al., Pergamon Press, 431-454, 1975.

Boyd, F.R., and Nixon, P.H., Ultramafic nodules from the Kimberley pipes, South Africa, Geo. et Cosmochim Acta, in press, 1978.

Bravo, M.S., and O'Hara, M.J., Partial melting of phlogopite-bearing synthetic spinel- and garnet-lherzolites, Phys. Chem. Earth IX, Ed. L.H. Ahrens et al., Pergamon Press, 845-854, 1975.

Carte, A.E., and van Rooyen, A.I.M., Further measurements of heat flow in South Africa, Geol. Soc. S.A., Spec. Pub. No. 2, 445-448, 1969.

Chrenko, R.M., McDonald, R.S., and Darrow, K.A., Infra-red spectra of diamond coat, Nature, 213, 474-476, 1967.

Clement, C.R., The emplacement of some diatreme-facies kimberlites, Phys. Chem. Earth IX, Ed. L.H. Ahrens et al., Pergamon Press, 51-60, 1975.

Cox, K.G., J.J. Gurney, and B. Harte, Xenoliths from the Masoku pipe, in Lesotho Kimberlite, edited by P.H. Nixon, pp 76-92. Cape and Transvaal printers, Cape Town, South Africa, 1973.

Danchin, R.V., and Boyd, F. R., Ultramafic nodules from the Premier kimberlite pipe, Carnegie Inst. Year Book, 75, 531-538, 1976.

Davis, G.L., The ages and uranium contents of zircons from kimberlites and associated rocks, Extended Abstr., 2nd Internat. Kimberlite Conf., Santa Fe, 1977.

Dawson, J.B., Gurney, J.J., and Lawless, P.J., Palaeogeothermal gradients derived from xenoliths in kimberlite, Nature, 257, 299-300, 1975.

Eggler, D.H., and McCallum, M.E., Diamond-bearing peridotite in a Wyoming kimberlite pipe, Annual Meeting Geol. Soc. Amer. Abstr., 1, 1065, 1975.

Fesq, H.W. et al., A comparative trace element study of diamonds from Premier, Finsch, and Jagersfontein Mines, South Africa, Phys. Chem. Earth IX, Ed. L.H. Ahrens et al., Pergamon Press, 817-836, 1975.

Fraser, D.G., and Lawless, P.J., Pyroxene geotherms : mantle probes or measures of pyroxene diffusion rates, in prep., 1978.

Giardini, A.A., and C.E. Melton, The nature of cloud-like inclusions in two Arkansas diamonds, Amer. Min., 60, 931-933, 1975.

Gurney, J.J., and G. Switzer, The discovery of garnets closely related to diamonds in the Finsch pipe, South Africa, Contrib. Mineral. Petrol., 39, 103-116, 1973.

Harris, J.W., Black material on mineral inclusions and in internal fracture planes in diamond, Contrib. Mineral. Petrol., 35, 22-33, 1972.

Harris, J.W., J.B. Hawthorne, M.M. Oosterveld, and E. Wehmeyer, A classification scheme for diamond, and a comparative study of South African diamond characteristics, in Phys.Chem. Earth IX, edited by L. Ahrens, J.B. Dawson, A.R. Duncan, and A.J. Erlank, pp 765-783. Pergamon Press, Oxford, England, 1975.

Harris, J.W., and J.J. Gurney, Inclusions in diamond in The Properties of Diamond, edited by J.E. Field, pp 555-592. Academic Press, London, England, 1978.

Harte, B., Kimberlite nodules, upper mantle petrology and geotherms, Phil. Trans. R. Soc. Lond. A., 288, 487-500, 1978.

Harte, B., Gurney, J.J., and Harris, J.W., The origin of CaO poor silicate inclusions in diamonds, in prep., 1978.

Kennedy, C.S., and Kennedy, G.C., The equilibrium boundary between graphite and diamond, J. Geophys. Res., 81, 2467-2470, 1976.

Kramers, J.D., Lead and strontium isotopes in inclusions in diamonds and in mantle-derived xenoliths from southern Africa, Extended Abstr., 2nd Internat. Kimberlite Conf., Santa Fe, 1977.

Kramers, J.D., Pb, U, Sr, K and Rb in inclusion-bearing diamonds and mantle-derived xenoliths from southern Africa, Contrib. Mineral. Petrol., in press, 1978.

Kushiro, I, Syono, Y, and Akimoto, S., Melting of a peridotite nodule at high pressures and high water pressures, J. Geophys. Res., 73, 6023-6029, 1968.

Lawless, P.J., Some aspects of the geochemistry of kimberlite xenocrysts, M.Sc. thesis, Univ. of Cape Town, pp. 121, 1974.

MacGregor, I.D., The system $MgO-Al_2O_3-SiO_2$: solubility of Al_2O_3 in enstatite for spinel and garnet peridotite compositions, Amer. Min., 59, 110-119, 1974.

Melton, C.E. et al., The observation of nitrogen, water, carbon dioxide, methane and argon as impurities in natural diamonds, Amer. Min., 57, 1518-1523, 1973.

Meyer, H.O.A., and Boyd, F.R., Composition and origin of crystalline inclusions in natural diamonds, Geo. et Cosmochim. Acta, 36, 1255-1274, 1972.

Meyer, H.O.A., and Tsai, H.M., The nature and significance of mineral inclusions in natural diamond : a review, Mineral. Sci. and Eng. News, 8, 242-261, 1976.

O'Hara, M.J., M.J. Saunders, and E.L.P. Mercy, Garnet-peridotite, primary ultrabasic magma and eclogite; interpretation of upper mantle processes in kimberlite, in Phys. Chem. Earth IX, edited by L. Ahrens, J.B. Dawson, A.R. Duncan, and A.J. Erlank, pp 571-604. Pergamon Press, Oxford, England, 1975.

O'Hara, M.J., and Yarwood, G., High pressure-temperature point on an archaean geotherm, magma genesis by implied anatexis and consequences for garnet-pyroxene thermometry and barometry, Phil. Trans. R. Soc. Lond. A., 288, 441-453, 1978.

Pollack, H.N., and Chapman, D.A., On the regional variation of heat flow, geotherm and lithospheric thickness, Tectonophysics, 38, 279-296, 1977.

Prinz, M. et al., Inclusions in diamonds : garnet lherzolite and eclogite assemblages, Phys. Chem. Earth IX, Ed. L.H. Ahrens et al., Pergamon Press, 797-816, 1975.

Raheim, A., and Green, D.H., Experimental determination of the temperature and pressure dependence of the Fe-Mg partition coefficient for coexisting garnet and clinopyroxene, Contrib. Mineral. Petrol., 48, 179-203, 1974.

Reid, A.M. et al., Garnet and pyroxene compositions in some diamondiferous eclogites, Contrib. Mineral. Petrol., 58, 203-220, 1976.

Rickwood, P.C., Gurney, J.J., and White-Cooper, D.R., The nature and occurrence of eclogite xenoliths in the kimberlites of southern Africa, Geol. Soc. S.A., Spec. Pub. No. 2, 371-393, 1969.

Ruotsala, A.P. Alteration of Finsch kimberlite pipe, South Africa, Economic Geology, 70, 587-590, 1975.

Sobolev, N.V., Deep-seated inclusions in kimberlites and the problem of the composition of the Upper Mantle, Eng. translation : D.A. Brown, Ed. F.R. Boyd, A.G.U. Publication, 1974.

Sobolev, N.V. and Lavrent'ev, Yu. G., Isomorphic sodium admixture in garnets formed at high pressures, Contrib. Mineral. Petrol., 31, 1-12, 1971.

Wells, P.R.A., Pyroxene thermometry in simple and complex systems, Contrib. Mineral. Petrol., 46, 1-15, 1977.

Wood, B.J., The solubility of alumina in orthopyroxene co-existing with garnet, Contrib. Mineral. Petrol., 46, 1-15, 1974.

Wood, B.J., The partitioning of iron and magnesium between garnet and clinopyroxene,

Carnegie Inst. Yearbook, 75, 571-573, 1976.

Wood, B.J., and Banno, S., Garnet-orthopyroxene and orthopyroxene-clinopyroxene relationships in simple and complex systems, Contrib. Mineral. Petrol., 42, 109-124, 1973.

Wyllie, P.J., and Huang, W.L., Carbonation and melting reactions in the system $CaO-MgO-SiO_2-CO_2$ at mantle pressures with geophysical and petrological applications, Contrib. Mineral. Petrol., 54, 79-107, 1976.

MINERAL INCLUSIONS IN DIAMOND: PREMIER, JAGERSFONTEIN AND FINSCH KIMBERLITES, SOUTH AFRICA, AND WILLIAMSON MINE, TANZANIA

Hsiao-ming Tsai and Henry O.A. Meyer

Department of Geosciences, Purdue University, West Lafayette, Indiana 47907

Jules Moreau

Lab de Mineralogie, Univ. Catholique de Louvain, 3 Place L. Pasteur, 1348 Louvain-la-Neuve, Belgium

H. Judith Milledge

Dept. of Chemical Crystallography, Univ. College London, Gower St., London, W.C.I. England

Abstract. Over 50 diamonds containing inclusion have been examined from four African localities; Premier, Jagersfontein and Finsch kimberlites in South Africa, and the Williamson (or Mwadui) Mine, Tanzania. The results of the study confirm the previously reported observation that most mineral inclusions in diamond are generally similar irrespective of world-wide occurrence. For example, the inclusions belong to two distinct suites; one ultramafic (olivine, enstatite, Cr-pyrope, diopside, chromite) and the other eclogitic (pyrope-almandine, omphacite). In detail some chemical differences do exist, but these were insufficient to characterize the inclusions from any one mine. In general, however, compared to other world wide occurrences diamonds from the Premier Mine appear to contain more eclogitic-suite minerals (e.g. clinopyroxene and pyrope-almandine). Furthermore, a unique acmitic diopside was obtained in a diamond from this same mine. Diamonds from Jagersfontein contained two unusual pyropic garnets that appear transitional between the normal eclogitic and Cr-pyrope garnet inclusions. Possibly these two unusual minerals, the acmitic pyroxene and pyropic garnets may indicate a more diverse chemical environment than hitherto considered for diamond genesis.

Introduction

The studies of mineral inclusions in diamonds have provided significant information regarding the physics and chemistry of the upper mantle, as well as the genesis of diamond. However, up to the present time most studies, apart from those from Russia (Sobolev, et al., 1971a), have been based on diamonds from regional areas (e.g. South Africa, Brazil, Ghana), and not from any specific diamond-bearing kimberlite. Accordingly, the present investigation is a reconnaissance study of mineral inclusions in diamonds from four specific localities in Africa. Altogether about 50 diamonds with inclusions were examined from the Pre-Cambrian Premier kimberlite (South Africa), the Phanerozoic Finsch and Jagersfontein kimberlites (South Africa) as well as the Williamson kimberlite (Tanzania) (Fig. 1). This is the first description of diamond inclusions from East Africa (Williamson Mine, Tanzania).

Mineral inclusions in natural diamonds have been reported from a variety of African localities, Venezuela and Thailand (Meyer, 1967; Meyer and Boyd, 1968, 1972), Siberia and the Urals (Sobolev, et al., 1971a, 1971b; Sobolev, 1974), Brazil (Meyer and Svisero, 1975), and some unknown localities (Prinz et al., 1975). In general the chemistry of the inclusions of each mineral type is remarkably similar and comparable to minerals occurring in kimberlite and associated xenoliths, although, some notable differences do exist. A good example is the presence of greater amounts of chromium in mineral inclusions than usually observed in kimberlitic minerals.

Two distinct suites of inclusions have also been reported (Meyer and Boyd, 1972; Meyer and Svisero, 1975; Prinz et al., 1975). One suite contains minerals that resemble the mineral assemblages in ultramafic xenoliths, whereas the other contains minerals comparable to those occurring in eclogite. Individual members of one suite are never found coexisting in the same diamond with those from the other. However, mineral assemblages from both suites have been observed in diamonds from the same kimberlite. The results of this present reconnais-

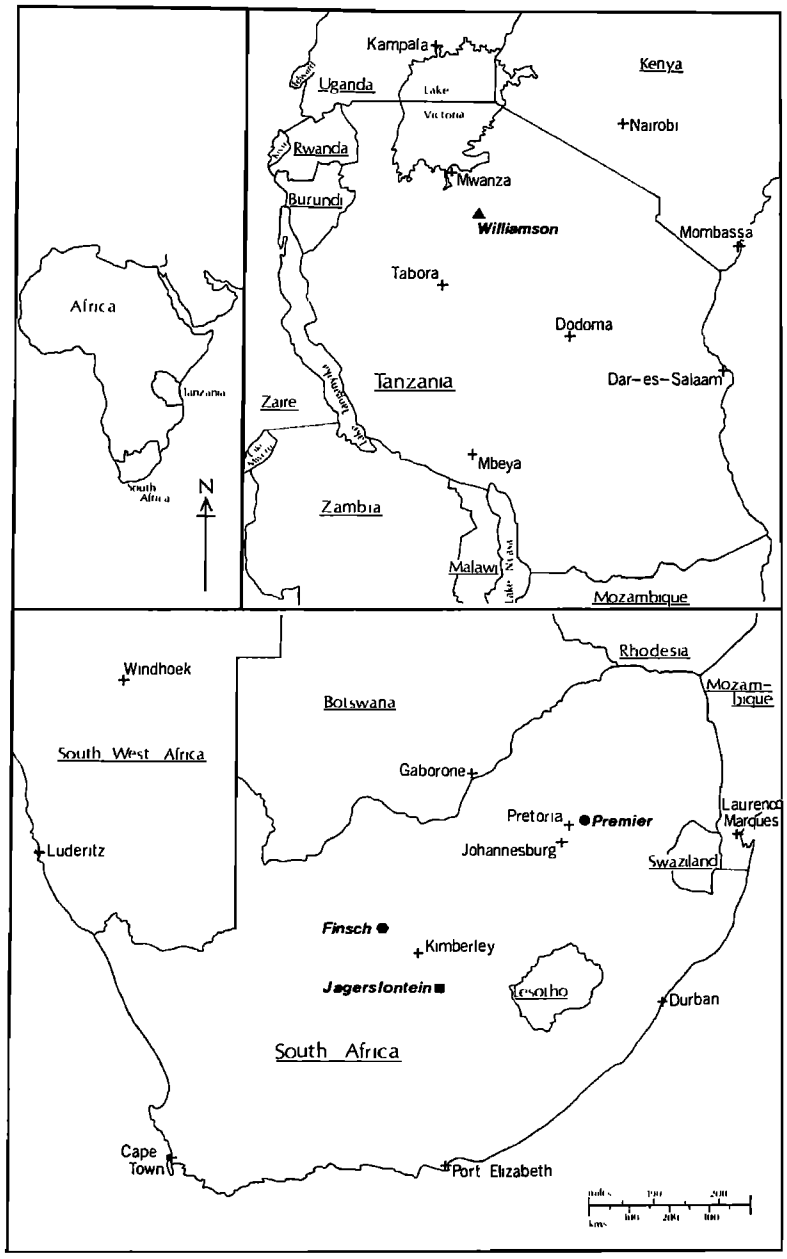

Fig. 1. Locality map of Premier, Jagersfontein and Finsch kimberlites, South Africa, and Williamson (Mwadui) kimberlite, Tanzania.

sance study suggest that in certain instances a particular mineral is relatively abundant in diamonds from a specific locality. For example, diopside, which is relatively rare in most diamonds, appears to be a predominant inclusion in Premier diamonds. The relationship between diamond inclusions and kimberlite, as well as associated xenoliths is not entirely understood at this time, but it is obvious that more detailed studies of mineral inclusions in diamonds and comparable minerals in kimberlite will reveal significant information on the constituents and origin of upper mantle rocks. There is a distinct possibility based on the chemical nature of the inclusions that diamonds have a xenocrystic relationship to the host kimberlite.

Mineralogy

The present study is based on diamonds with silicate or oxide inclusions from four kimberlite pipes, Premier, Jagersfontein, Finsch, and Williamson. The inclusions obtained in this investigation were generally less than 100μm in

TABLE 1. Analyses of Cr-pyrope garnet inclusions in diamond.

	Premier		Finsch		Williamson					Jagersfontein	
Oxide	2	7[a]	1	5[b]	7	12	20	32	33	W2-1	B5-1
SiO_2	42.6	43.1	42.3	42.7	41.7	41.9	41.4	42.2	42.3	40.3	41.3
TiO_2	0.07	0.30	0.04	<0.01	0.04	0.03	0.04	0.03	0.04	0.59	0.71
Al_2O_3	15.2	17.2	16.7	19.8	18.2	16.1	16.9	18.5	19.1	17.5	19.4
Cr_2O_3	9.59	6.53	9.61	6.29	7.19	8.06	7.62	7.64	5.22	1.93	1.27
FeO*	5.34	5.81	5.46	5.80	5.96	5.36	5.62	6.22	5.65	15.5	12.8
MgO	23.0	21.8	25.2	22.5	23.2	22.8	22.4	23.7	21.9	16.8	18.2
CaO	3.85	5.30	0.69	2.63	2.25	4.14	4.16	2.25	5.53	5.42	5.28
NiO	<0.01	0.06	<0.01	<0.01	0.01	<0.01	0.01	<0.01	0.02	<0.01	<0.01
Na_2O	0.09	0.08	0.10	<0.01	<0.01	<0.01	0.04	0.07	0.04	<0.01	0.07
K_2O	0.02	<0.01	0.01	<0.01	<0.01	<0.01	<0.01	0.10	0.01	<0.01	<0.01
Total	99.8	100.2	100.2	99.7	99.5	98.4	98.2	100.6	99.8	98.1	99.0
	Number cations on the basis of 12 oxygens (x1000)										
Si	3069	3077	3010	3029	3011	3050	3020	2990	3020	3048	3042
Ti	2	15	1	0	0	0	0	0	0	33	39
Al	1292	1443	1402	1657	1545	1384	1453	1548	1612	1560	1680
Cr	545	366	539	351	409	463	438	428	293	115	73
Fe*	321	345	323	344	358	325	342	368	338	979	786
Mg	2469	2321	2670	2378	2500	2474	2438	2503	2330	1893	1997
Ca	296	404	53	200	173	322	323	170	422	439	414
Ni	0	2	0	0	0	0	0	0	0	0	0
Na	10	10	12	0	0	0	4	8	4	0	8
K	0	0	0	0	0	0	0	0	0	0	0
Total	8005	7984	8010	7959	7997	8019	8019	8016	8019	8066	8039

* All Fe reported as FeO
a, Coexists with enstatite and diopside
b, Coexists with olivine and enstatite

size, and are garnet, diopside, enstatite, olivine and chromite. The chemistry of these minerals is similar to other published data from worldwide localities. Although the majority of the inclusions are monomineralic, several important coexisting minerals have been observed. For example, olivine + enstatite + garnet (Cr-pyrope), enstatite + diopside + garnet (Cr-pyrope), and garnet (pyrope-almandine) + omphacite are among the assemblages that have been found.

The diamonds used in this study are generally less than 2mm in size, and they are mostly clear, well-formed octahedra or dodecahedra. Inclusions were extracted from the diamonds by either cracking, or burning in air at 830°C for 3~4 hours. Chemical analyses of the inclusions were obtained using an automated M.A.C. 500 microprobe with on-line computer reduction of data via a modified Bence-Albee (1968) and Albee and Ray (1970) matrix refinement which includes background, deadtime, drift, fluorescence and atomic number effects. Standards were predominantly glasses except for K, Cr, Fe and Mn in which carefully analyzed minerals were used. The analyses are believed correct to within ±2% of the concentration for major elements. For minor elements the accuracy is much less but reproducibility is usually to within 0.02 wt%.

Garnet

Two types of garnet inclusions have been reported (Meyer and Boyd, 1972; Prinz et al., 1975). One is a purple-colored Cr-rich, low-Ca pyrope, comparable in many respects to the garnets from ultramafic xenoliths; and the other one is orange-colored pyrope-almandine, which resembles the garnets from eclogitic xenoliths. The low-Ca garnets contain a high proportion of the Cr-pyrope molecule ($Mg_3Cr_2Si_3O_{12}$) and are restricted to diamonds and rare occurrences in kimberlite concentrate (Gurney and Switzer, 1973) (Tables 1 and 2).

The significant chemical difference among the garnet inclusions can be shown in terms of $Cr_2O_3/Cr_2O_3 + Al_2O_3$ vs. MgO/MgO + FeO and

TABLE 2. Analyses of pyrope-almandine garnet inclusions in diamond.

	Premier						Jagersfontein	
Oxide	5	6	8	12[a]	13	14	R4-1	R3-1
SiO_2	40.7	42.3	41.3	40.4	41.7	40.2	42.2	45.2
TiO_2	0.25	0.25	0.31	1.01	0.86	0.73	0.24	0.13
Al_2O_3	22.2	22.2	22.4	21.1	20.6	21.1	19.5	15.4
Cr_2O_3	0.05	0.21	0.11	0.10	0.29	0.05	0.11	0.21
FeO*	13.3	14.3	14.7	17.7	12.3	13.5	13.8	13.5
MgO	11.2	16.8	13.5	13.7	18.6	9.82	16.2	19.7
CaO	11.5	4.14	7.35	5.10	4.66	13.7	7.91	5.74
NiO	0.01	<0.01	<0.01	<0.01	0.05	<0.01	-	-
Na_2O	0.23	0.03	0.35	0.14	0.13	0.09	0.33	0.42
K_2O	<0.01	<0.01	<0.01	<0.01	<0.01	<0.01	<0.01	<0.01
Total	99.4	100.2	100.0	99.3	99.2	99.2	100.6	100.3
	Number cations on the basis of 12 oxygens(x1000)							
Si	3028	3057	3032	3020	3039	3022	3100	3284
Ti	13	13	17	55	47	40	13	6
Al	1941	1893	1935	1859	1768	1872	1676	1313
Cr	2	10	6	4	15	2	6	10
Fe*	825	862	903	1105	751	848	839	816
Mg	1239	1808	1472	1521	2018	1099	1757	2126
Ca	916	320	577	408	364	1104	619	445
Ni	0	0	0	0	2	0	-	-
Na	33	4	49	20	17	11	45	57
K	0	0	0	0	0	0	0	0
Total	7997	7996	7991	7991	8020	7996	8055	8058

*All Fe reported as FeO

a, Coexists with omphacitic pyroxene

$Cr_2O_3/Cr_2O_3 + Al_2O_3$ vs. CaO/CaO + MgO (Fig.2). The relatively high Cr_2O_3 content and the restricted MgO/MgO + FeO of most Cr-pyrope inclusions are well illustrated in this figure and contrast markedly those inclusions which are comparable to eclogitic garnet with virtually no Cr. The Cr-rich garnets display a variation in CaO/CaO + MgO between 1 and 22%. The eclogitic garnet inclusions have a much wider range in CaO/CaO + MgO value (15-60%) in keeping with characteristics of most eclogite garnets.

Clinopyroxene

Clinopyroxene are observed as diamond inclusions in only two of the four kimberlites; Jagersfontein and Premier. Of all the inclusions clinopyroxene appear to show the greatest diversity in chemical composition. In general two major groups, diopsidic and omphacitic, can be recognized, however, there is considerable variation in element content within each group (Fig. 3). A unique acmitic pyroxene was obtained from a Premier diamond.

Diopside. Three diopsides were obtained in the present study (Table 3). One specimen from Premier Mine (PRE-7) coexists with enstatite and Cr-pyrope; whereas one from Jagersfontein (W8-1) coexists with enstatite. This latter diopside contains approximately 2 wt% each of Na_2O, Al_2O_3 and Cr_2O_3, and is thus comparable with Cr-diopside inclusions from Russian diamond (Sobolev et al., 1970, 1971a). The other two diopsides contain much less Na, Al and Cr, and differ from each other in their contents of FeO, MgO and CaO. In all three diopsides, TiO_2 is less than 1 wt%. It is possible that PRE-7 equilibrated at a higher temperature than the other two on the basis of $\frac{Ca}{Ca+Mg}$ (Fig. 4).

Omphacite. In contrast to the rare occurrences of clinopyroxene inclusions in diamond,

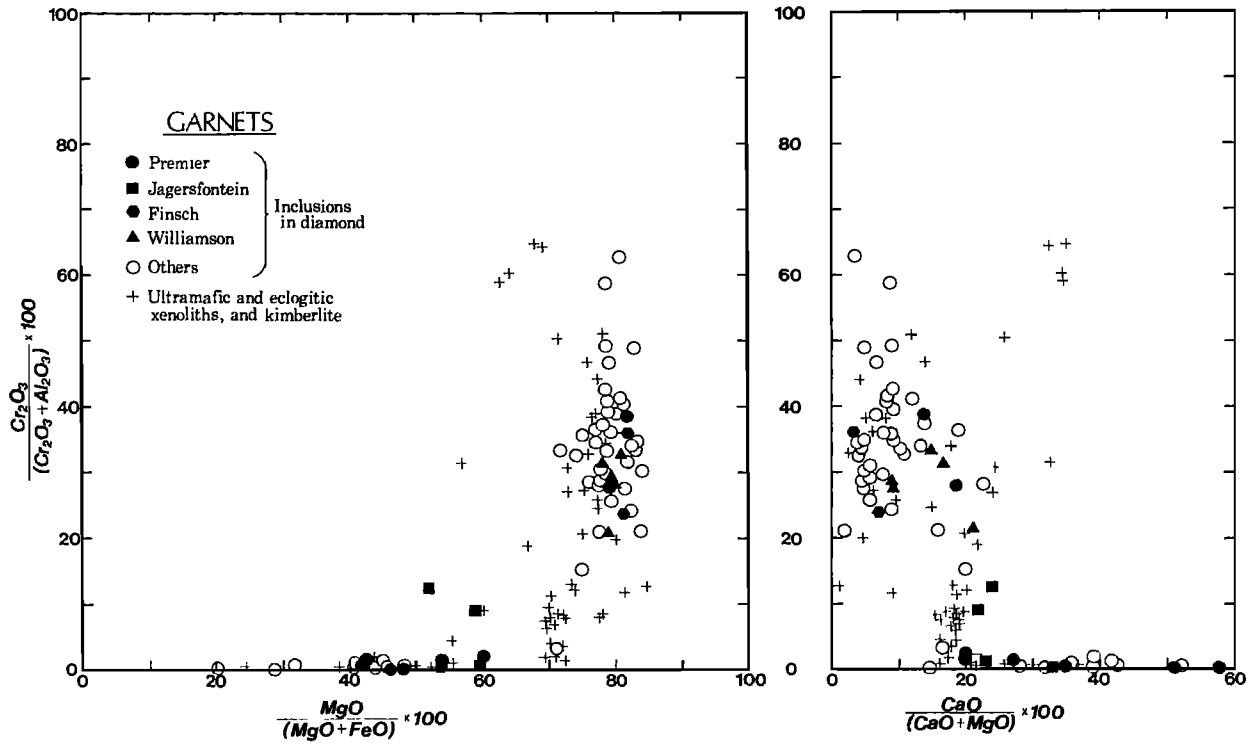

Fig. 2. Chemical variations of garnet inclusions in diamonds from Premier, Jagersfontein, Finsch and Williamson compared with similar inclusions in diamonds from other localities (Meyer and Boyd, 1972; Sobolev et al., 1969, 1973; Prinz et al., 1975; Meyer and Svisero, 1975 and Harris and Gurney, 1976). Garnets from kimberlites and associated xenoliths included for comparison.

five omphacitic pyroxenes were recovered and analysed from Premier diamonds. Only one of these coexists with an eclogitic type garnet (PRE-12), but there are two other pyroxenes of comparable composition (PRE-1 and PRE-17) (Table III). The two remaining omphacites are more Ca-rich and contain less Na and Al (Table 3, Fig. 4). Inclusions with similar composition have been recorded by Prinz et al. (1975) and Sobolev et al. (1971a).

Acmitic pyroxene. An unusual pyroxene inclusion from Premier Mine contains insufficient Al and Cr to balance the high Na content, thus requiring the formation of the acmite molecule ($NaFe^{3+}Si_2O_6$) (∿15%). It is also unusual in that it has one of the highest Ti contents observed in diopside inclusions (Table III). In the pyroxene quadrilaterial (Fig. 4) this inclusion plots close to the region of omphacitic pyroxene, but is distinct from them that it has much lower Al content (Al_2O_3∿ 0.89 wt%). This acmitic inclusion is also generally distinct from pyroxenes that are present in the xenoliths and the only other occurrence of an inclusion requiring the presence of acmite molecule is the pyroxene M of Meyer & Boyd (1972). Obviously it is closest in composition to eclogitc-suite inclusions but assignment to this suite is not entirely satisfactory.

Orthopyroxene

In keeping with previous observations, orthopyroxene inclusions in this study show a rather restricted range of composition, Mg/Mg+Fe ranging from 0.93 to 0.95 (Table 4 and Fig. 4). Four of the orthopyroxene inclusions coexist with other minerals; PRE-7 coexists with diopside and Cr-pyrope; JAG 8-1 occurs with diopside; JAG2-1 is present with olivine; and FIN 5 occurs with both Cr-pyrope and olivine. An interesting observation is that the two enstatites coexisting with diopside show significantly higher contents of Ca (Fig. 4) than the remaining five orthopyroxenes (Table 4), although this is somewhat different from the result reported by Prinz et al. (1975) who noted orthopyroxene with low-Ca coexisting with clinopyroxene. A slightly higher Al content is also noticeable for these two enstatites with diopside. The variation of all other minor elements is fairly small, and in agreement with other published enstatite inclusions (Meyer and Boyd, 1972; Prinz et al., 1975).

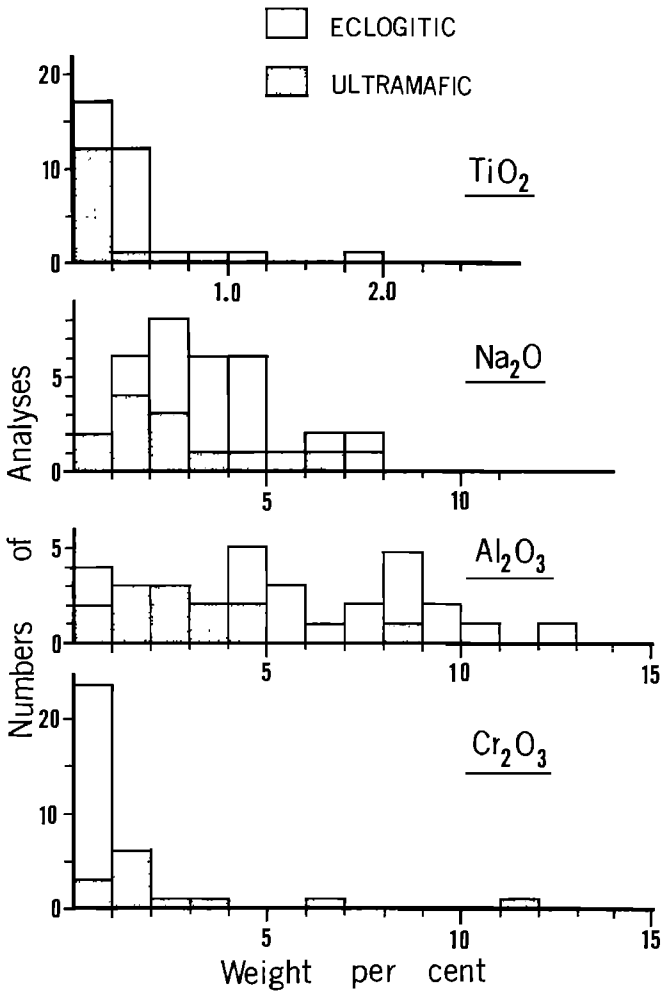

Fig. 3. Variation of TiO_2, Na_2O, Al_2O_3 and Cr_2O_3 in eclogitic (omphacite) and ultramafic (diopside) pyroxene inclusions. Data from Meyer and Boyd, 1972: Prinz et al., 1975; Sobolev et al., 1970, 1971a, 1971b, 1972; Harris and Gurney, 1976.

Olivine

Olivine, normally the most commonly observed inclusion in diamond, is relatively less abundant in this study, because of selectivity exercised in choosing specific diamonds. However, the nine olivine inclusions, obtained and analyzed in this study confirm the previously published results, indicating a uniform composition of olivine inclusions from worldwide localities (Table 5 and Fig. 4) (Meyer and Boyd, 1972; Prinz et al., 1975; Meyer and Svisero, 1975).

Chromite

Two chemically different chromite inclusions were obtained from the Finsch and Jagersfontein Mines, and the analyses are presented in Table 6. The one from Jagersfontein is unusual in that it contains higher FeO and less Cr_2O_3, MgO and Al_2O_3 than the majority of chromite inclusions that have previously been found (Fig. 5). The only similar inclusion to that of Jagersfontein is one from Sierre Leone (Meyer and Boyd, 1972), but this chromite inclusion is also unique in its presence of ZnO. The one from Finsch is comparable to most chromite inclusions (Sobolev et al., 1971a; Meyer and Boyd, 1972) in that they are all extremely rich in chromium, but vary in Mg/Mg+ Fe^{2+} (Fig. 5).

Discussion

The results of the present study confirm the previous observation that diamond inclusions fall into two general categories. One group, particularly emphasized by the Williamson inclusion, is predominantly ultramafic in nature, whereas the other is eclogitic. For example the garnet and pyroxene in Premier diamond are pyrope-almandine and omphacitic diopside which are all characteristic of eclogite. Interestingly, although diamond is often found in eclogite xenoliths from kimberlite (Gurney et al., 1969; Reid et al., 1976) diamond in ultramafic xenoliths is relatively rare (Dawson and Smith, 1975; McCallum and Eggler, 1976). Surprisingly, this is the reverse of the relative abundance observed in diamond inclusions since it appears from the data available that the ultramafic suite of inclusions is more common than the eclogitic one. With regard to this latter suite it is noteworthy that both pyrope-almandine and omphacite are much more common in Premier diamond than from any other locality. Whether this abundance is due to the Pre-Cambrian age of this pipe (Allsopp et al., 1967) is unknown. However, diamonds from other areas where pipes

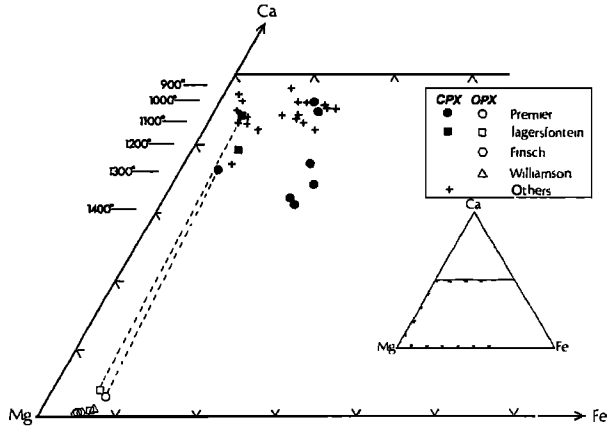

Fig. 4. Mg-Ca-Fe relationships of clinopyroxene and othopyroxene inclusions in diamond. Data from Meyer and Boyd, 1972; Prinz et al., 1975; and Sobolev et al., 1970, 1971a, 1971b, 1972.

TABLE 3 Analyses of clinopyroxene inclusions in diamond.

	Diopside			Omphacite					Acmitic
	Premier Jagersfontein			Premier					Premier
	7[a]	W8-1[b]	W4-1	1	11	12[c]	15	17	19
SiO_2	56.1	55.3	54.0	54.5	54.7	54.3	53.1	55.1	54.8
TiO_2	0.07	0.04	0.03	0.54	0.17	0.94	0.19	0.28	1.23
Al_2O_3	0.92	2.39	0.83	8.08	4.71	7.43	4.77	5.78	0.89
Cr_2O_3	0.72	2.01	0.17	0.05	0.01	0.09	0.01	0.08	0.12
FeO*	2.84	1.95	4.11	7.26	6.99	8.18	6.60	8.73	9.21
MgO	21.1	16.2	19.5	11.9	12.8	12.5	12.9	14.6	16.6
CaO	17.9	19.2	19.1	13.0	19.5	12.1	19.6	11.8	14.0
NiO	0.02	0.05	0.04	0.02	0.03	0.05	<0.01	0.05	0.05
Na_2O	0.67	2.17	0.61	3.80	2.29	4.34	2.27	3.16	2.64
K_2O	0.03	0.24	0.07	0.04	<0.01	0.09	<0.01	0.09	0.05
Total	100.4	99.5	98.5	99.2	101.2	100.0	99.4	99.7	99.6
	Number of cations on the basis of 6 oxygens (x1000)								
Si	1996	2000	1984	1975	1975	1962	1957	1993	2014
Ti	1	0	0	14	4	26	4	8	34
Al	39	102	35	345	200	316	207	246	38
Cr	20	57	4	1	0	2	0	2	3
Fe*	84	58	126	219	211	247	203	263	283
Mg	1120	874	1066	642	690	675	707	772	909
Ca	684	737	752	503	755	470	774	457	549
Ni	0	1	0	0	0	1	0	1	1
Na	46	151	43	267	160	303	162	222	188
K	1	10	2	1	0	3	0	3	2
Total	3991	3992	4012	3965	3994	4003	4012	3960	4021

* All Fe reported as FeO

a, Coexists with Cr-pyrope and enstatite
b, Coexists with enstatite
c, Coexists with pyrope-almandine

are believed to have been erupted during Pre-Cambrian time (e.g. Ghana, Venezuel and Dimantina, Brazil) do not show this character.

It should be noted that in general most unequivocal pre- or syngenetic inclusions in diamond do not chemically resemble the present constituent minerals of kimberlite. As previously mentioned the inclusions mirror the compositions of eclogite and peridotite xenoliths, and associated xenocrysts in kimberlite. The evidence at present, based on undeniably primary inclusions is that diamond does not form in kimberlite as it is presently defined but in some other chemical environments. Thus diamond is a xenocryst in kimberlite and not a phenocryst directly genetically related to kimberlite.

At the present time several minerals have been observed as inclusions in diamond but the temporal relation between inclusion and host is not entirely clear. These minerals include those referred to as epigenetic as well as several problematic ones such as quartz (Harris, 1968; Meyer and Svisero, 1975), sanidine and magnetite (Prinz et al., 1975) and micas (Meyer and Boyd, 1972; Prinz et al., 1975; Giardini et al., 1974). The presence of known low pressure phases inside diamond (e.g. kaolinite, serpentine, goethite) could be interpreted, if caution is not used, as indicating diamond has formed under crustal pressures. The cause of misunderstanding lies in the manner in which the host diamond encloses the included material. In early chemical studies of diamond inclusions (Meyer and Boyd, 1967, 1968, 1972; Harris, 1968) the identification of syngenetic or epigenetic nature was based on whether visible flaws, fractures or cleavage extended from the inclusion to the surface of the host diamond. This criteria, however, may not be entirely equivocal since several inclusions have

TABLE 4. Analyses of orthopyroxene inclusions in diamond.

	Premier	Finsch			Williamson	Jagersfontein	
Oxide	7[a]	5[b]	8	9	2	W8-1[c]	R2-1[d]
SiO_2	57.4	58.2	57.8	57.5	57.2	57.3	57.6
TiO_2	0.02	<0.01	<0.01	<0.01	<0.01	<0.01	<0.01
Al_2O_3	0.77	0.46	0.45	0.41	0.74	0.55	0.56
Cr_2O_3	0.39	0.37	0.29	0.26	0.47	0.25	0.27
FeO*	4.79	3.64	3.33	3.31	4.45	4.17	3.99
MgO	34.7	37.0	37.4	37.4	35.6	34.7	36.0
CaO	1.38	0.24	0.21	0.15	0.46	2.32	0.20
NiO	0.06	0.10	0.14	0.13	0.13	0.11	-
Na_2O	0.17	0.06	<0.01	<0.01	0.11	0.22	0.79
K_2O	<0.01	0.02	0.01	0.02	<0.01	<0.01	0.04
Total	99.7	100.1	99.6	99.2	99.2	99.6	98.8
	Number of cations on the basis of 6 oxygens (x1000)						
Si	1979	1981	1973	1972	1976	1978	1986
Ti	0	0	0	0	0	0	0
Al	32	18	18	16	29	22	22
Cr	10	10	7	7	12	6	7
Fe*	138	103	94	94	127	119	114
Mg	1782	1879	1907	1911	1831	1785	1853
Ca	56	8	7	5	16	85	9
Ni	1	1	3	3	3	2	-
Na	11	3	0	0	7	14	6
K	0	0	0	1	0	0	0
	4009	4003	4009	4009	4001	4011	3997
En	93	95	95	95	94	93	94

* All Fe reported as FeO

a, Coexists with diopside and Cr-pyrope
b, Coexists with olivine and Cr-pyrope
c, Coexists with diopside
d, Coexists with olivine (R2-2)

been observed that satisfy the requirements of being primary (no crack to diamond surface) but upon detailed examination are found to be partly oxidized or hydrated, e.g. olivine inclusions partly altered to serpentine. It is important that these problems be understood when one is discussing the genesis of diamond based on the nature of its inclusions. Physical studies on the nature of fractures and cleavage planes associated with inclusions and diamond may provide significant insight and possible solution to this problem.

Recently, Meyer and Tsai (1976b) and Harris and Gurney (1976) have reviewed the current literature on inclusions in diamond and their relation to diamond genesis and upper mantle mineralogy. Meyer and Tsai (1976a) have attempted to determine final equilibration conditions for assemblages of different inclusions within the same diamond. Typical assemblages are the Premier 7 diopside - enstatite - Cr-pyrope and the Jagersfontein 8 diopside-enstatite. Based on the pyroxene geothermometer of Davis and Boyd (1966) and the Al_2O_3 geobarometer of MacGregor and Basu (1974) the Premier assemblage has apparently equilibrated at 1270°C and 65kb whereas the Jagersfontein specimen reached final equilibration at 1010°C and 53kb. These conditions are in the general range for equilibration of garnet-lherzolite xenoliths from kimberlite (Boyd, 1973; Nixon and Boyd, 1973).

Unfortunately, with regard to the eclogitic assemblage inclusions it is not possible to determine both pressure and temperature. However, using the models of Akella and Boyd (1974) and Raheim and Green (1974) it is possible to estimate the temperature of equilibration.

TABLE 5. Analyses of olivine inclusions in diamond.

	Premier		Finsch	Williamson				Jagersfontein	
Oxide	3	16	5[a]	8	20	30	76	R2-2[b]	W3-1
SiO_2	41.6	41.3	41.2	40.9	40.6	40.9	40.7	41.6	40.7
TiO_2	0.02	0.01	0.01	<0.01	0.01	<0.01	<0.01	0.01	<0.01
Al_2O_3	<0.01	<0.01	0.05	<0.01	<0.01	0.02	<0.01	0.04	0.05
Cr_2O_3	0.03	0.01	<0.01	0.03	0.02	0.02	<0.01	0.02	0.11
FeO*	6.37	7.36	6.17	7.31	7.24	6.86	6.40	6.71	8.87
MgO	52.8	51.5	51.3	52.1	51.6	52.3	52.1	52.3	48.4
CaO	0.04	0.06	0.02	0.02	0.04	0.04	<0.01	<0.01	0.10
NiO	0.48	0.45	0.36	0.33	0.40	0.39	0.49	-	0.25
Na_2O	<0.01	<0.01	<0.01	<0.01	0.04	0.02	0.01	0.05	0.04
K_2O	<0.01	<0.01	<0.01	<0.01	<0.01	<0.01	<0.01	<0.01	<0.01
Total	101.3	100.7	99.1	100.7	100.0	100.6	99.7	100.8	98.5
	Number of cations based on 4 oxygens (x1000)								
Si	992	996	1002	985	986	985	987	997	1008
Ti	0	0	0	0	0	0	0	0	0
Al	0	0	0	0	0	0	0	0	1
Cr	0	0	0	0	0	0	0	0	2
Fe*	126	148	125	147	146	138	129	134	183
Mg	1876	1850	1859	1874	1870	1881	1884	1867	1785
Ca	1	1	0	0	0	0	0	0	2
Ni	9	8	7	5	7	7	9	-	4
Na	0	0	0	0	1	0	0	2	1
K	0	0	0	0	0	0	0	0	0
	3004	3003	2994	3011	3011	3012	3009	3000	2986
Fo	94	93	94	93	93	93	94	93	91

*All Fe reported as FeO

a, Coexists with enstatite and Cr-pyrope
b, Coexists with enstatite (R2-1)

Applying these models to the pyrope-almandine-omphacite assemblage in Premier diamond (PRE-12) a temperature of 1250°C is obtained. Admittedly, these physical conditions may require reassessment when more vigorous models are available but at present serve to indicate the general region in which crystallization may have occurred.

A significant problem with respect to diamond inclusion research is the nature of sampling the source location. This is not done by the inclusion investigator who normally has to rely on already sorted diamonds provided through the courtesy of interested parties. Often this results in insufficient samples for significant interpretation but may provide tantalizing suggestions as in the present study. In this context the apparent common occurrence of clinopyroxene in Premier diamonds makes this locality unique, and furthermore the rare peridotite-type inclusion garnets from Jagersfontein may characterize diamonds from this pipe. Previously, Sobolev et al. (1971a, 1975) have observed that pyroxenes in the Mir kimberlite from Yakutia are particularly rich in Cr and Na in contrast to most other pyroxene inclusions from worldwide localities.

It is important that future studies of mineral inclusions be undertaken on diamonds from known sources, and even from known areas within a specific kimberlite pipe. The results of such investigations together with comparable studies of the mineral chemistry of kimberlite and associated xenoliths (e.g. Danchin and Boyd, 1976) will add considerably to our understanding of the upper mantle. For example, it will aid in understanding how unique the sampling is in each kimberlite and in comparison how the xenoliths and xenocrysts compare with the inclusions in diamond. However, the problem still remains of

TABLE 6. Analyses of chromite inclusions in diamond.

	Finsch*	Jagersfontein
Oxide	7	B12-1
SiO_2	0.16	0.12
TiO_2	0.48	0.18
Al_2O_3	7.16	4.17
Cr_2O_3	63.9	56.2
FeO**	10.7	33.6
MgO	14.7	6.01
CaO	0.05	0.02
NiO	0.11	-
Na_2O	<0.01	<0.01
K_2O	<0.01	<0.01
Total	97.3	100.3

Number of cations based on 4 oxygens (x1000)

Si	5	3
Ti	12	4
Al	280	176
Cr	1678	1591
Fe**	296	1007
Mg	726	321
Ca	1	0
Ni	2	-
Na	0	0
K	0	0
	3000	3102

*Very small inclusion
**All Fe reported as FeO

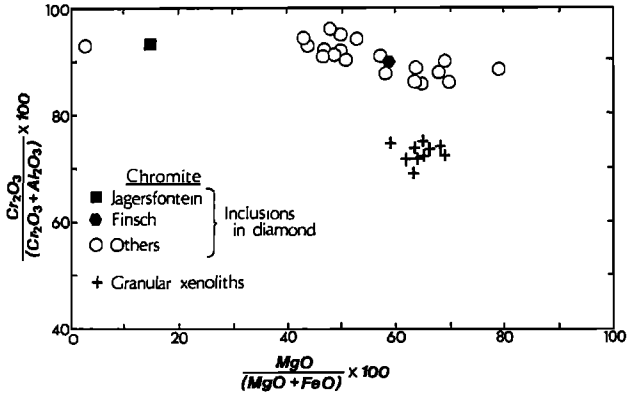

Fig. 5. Composition of chromite inclusions from Finsch and Jagersfontein diamond compared with chromites from other localities and granular xenoliths. Data from Meyer and Boyd, 1972; Meyer and Svisero, 1975; Prinz et al., 1975; Sobolev et al., 1971a and Nixon and Boyd, 1973.

incorporating the mineral chemical and petrologic data into a unified and coherent odyssey.

Acknowledgments. We thank the National Science Foundation Earth Sciences Section for financial aid with respect to this study (Grants GA-43990 and DES72-01659). J.M. gratefully acknowledges the use of facilities at Purdue University while on sabbatical leave from University of Neuve Louvain, and HMT is pleased to acknowledge the financial aid of a David Ross Fellowship from Purdue Research Foundation. To all those who supplied diamond specimens we give thanks, and also to Dr. M. Prinz whose critical comments considerably improved the manuscript.

References

Akella, J. and F.R. Boyd, Petrogenetic grid for garnet peridotites. Carnegie Inst. Wash. Year Book, 73, 269-273, 1974.

Albee, A.L., and L. Ray, Correction factors for electron probe microanalysis of silicates, oxides, carbonates, phosphates and sulphates. Anal. Chem. 42, 1408-1414, 1970.

Allsopp, H.L., A.J. Burger, and C. Van Zyl, A minimum age for the Premier kimberlite pipe yielded by biotite Rb-Sr measurements, with related galena isotopic data. Earth Planet. Sci. Lett., 3, 161-166, 1967.

Bence, A.E., and A.L. Albee, Empirical correction factors for the electron microanalysis of silicates and oxides. Jour. Geol., 76, 382-403, 1968.

Boyd, F.R., The pyroxene geotherm. Geochim. Cosmochim. Acta, 37, 2533-2546, 1973.

Danchin, R.V., and F.R. Boyd, Ultramafic nodules from the Premier kimberlite pipe, South Africa. Carnegie Inst. Wash. Year Book, 75, 531-538, 1976.

Davis, B.T.C., and F.R. Boyd, The join $Mg_2Si_2O_6$-$CaMgSi_2O_6$ at 30 kilobars pressure and its application to pyroxenes from kimberlites. J. Geophys. Res., 14, 3567-3576, 1966.

Dawson, J.B., and J.V. Smith, Occurrence of diamond in a mica-garnet lherzolite in kimberlite. Nature, 254, 580-581, 1975.

Giardini, A.A., V.J. Hurst, C.E. Melton, and J.C. Stormer, Biotite as a primary inclusion in diamond: its nature and significance. Am. Mineral., 59, 783-789, 1974.

Gurney, J.J., J.C. Siebert, and G.G. Whitfield, A diamondiferous eclogite from the Roberts Victor Mine. Trans. Geol. Soc. S. Afr., Spec. Pub. 2, 351-359, 1969.

Gurney, J.J., and G.S. Switzer, The discovery of garnets closely related to diamonds in the Finsch pipe, South Africa. Contr. Mineral. Petrol., 39, 103-116, 1973.

Meyer, H.O.A., Inclusions in diamond. Carnegie Inst. Wash. Year Book, 66, 446-450, 1967.

Harris, J.W., The recognition of diamond inclusions. Pt. 1: Syngenetic mineral inclusions.

Pt. 2: Epigenetic mineral inclusions. Indust. Diamond Rev., 402-410, 458-461, 1968.
Harris, J.W., and J.J. Gurney, Inclusions in diamond. In Properties of Diamond, Ed. J.E. Field. Oxford Univ. Press, Oxford, 1976.
MacGregor, I.D., and A.R. Basu, Thermal structure of the lithosphere: A petrologic model. Science, 185, 1007-1011, 1974.
McCallum, M.E., and D.H. Eggler, Diamonds in an upper mantle peridotite nodule from kimberlite in Southern Wyoming. Science, 192, 253-256, 1976.
Meyer, H.O.A., and F.R. Boyd, Mineral inclusions in diamonds. Carnegie Inst. Wash. Year Book, 67, 130-135, 1968.
Meyer, H.O.A., and F.R. Boyd, Composition and origin of crystalline inclusions in natural diamond. Geochim. Cosmochim. Acta, 36, 1255-1273, 1972.
Meyer, H.O.A., and D.P. Svisero, Mineral inclusions in Brazilian diamonds. Phys. Chem. Earth, 9, 785-795, 1975.
Meyer, H.O.A., and H.M. Tsai, Mineral inclusions in diamond: Temperature and pressure of equilibration. Science, 191,849-851, 1976a.
Meyer, H.O.A., and H.M. Tsai, Mineral inclusions in natural diamond - their nature and significance: A review. Minerals Sci. Engineering, 8, 242-261, 1976b.
Nixon, P.H., and F.R. Boyd, Petrogenesis of the granular and sheared ultrabasic nodule suite in kimberlites. In Lesotho Kimberlites, Ed. P.H. Nixon, Lesotho Nat. Dev. Corp., Maseru, 48-56, 1973.
Prinz, M., D.V. Manson, P.F. Hlava, and K. Keil, Inclusions in diamonds: Garnet lherzolite and eclogite assemblages. Phys. Chem. Earth, 9, 797-815, 1975.
Raheim, A., and D.H. Green, Experimental determination of the temperature and pressure dependence of the Fe-Mg partition coefficient for coexisting garnet and clinopyroxene. Contr. Mineral. Petrol., 48, 179-203, 1974.
Reid, A.M., R.W. Brown, J.B. Dawson, G.G. Whitfield, and J.C. Siebert, Garnet and pyroxene compositions in some diamondiferous eclogites. Contr. Mineral. Petrol., 58, 203-220, 1976.
Sobolev, N.V., The deep seated inclusions in kimberlites and the problem of the upper mantle composition. Nauk Publish. House, Siberian Branch, Novosibirsk, 264 pp., 1974.
Sobolev, N.V., Z.V. Bartoshinsky, E.S. Yefimova, Yu. G. Lavrent'yev, and L.N. Pospelova, Association of olivine, garnet and chrome-diopside in a Yakutsk diamond. Dokl. Akad. Nauk SSSR, 192, 1349-1353, 1970.
Sobolev, N.V., A.I. Botkunov, Yu. G. Laurent'yev, and L.N. Pospelova, Peculiarities of the composition of minerals coexisting with diamond from Mir pipe, Yakutia. Zap. Vses. Mineral. Obshch., 100, 558-564, 1971a.
Sobolev, N.V., M.A. Gnevushev, L.N. Mikhailovskaya, S.I. Futergendler, E.I. Shemanina, Yu. G. Lavrent'yev, and L.N. Pospelova, The compositin tion of garnet and pyroxene inclusions from the diamonds of the Urals. Dokl. Akad. Nauk. SSSR, 198, 190-193, 1971b.
Sobolev, N.V., Yu.G. Lavrent'yev, N.P. Pokhilenko, and V.S. Sobolev, Chrome pyropes from diamonds in Yakutia. Dokl. Akad. Nauk. SSSR, 189, 162-165, 1969.
Sobolev, N.V., Yu. G. Lavrent'yev, N.P. Pokhilenko, and L.V. Usova, Chrome-rich garnets from the kimberlites of Yakutia and their parageneses. Contr. Mineral. Petrol., 40, 39-52, 1973.
Sovolev, V.S., N.V. Sobolev, and Yu.G. Lavrent'yev, Inclusions in diamond extracted from a diamondiferous eclogite. Dokl. Akad. Nauk. SSSR, 207, 164-167, 1972.
Sobolev, V.S., N.V. Sobolev, and Yu.G. Lavrent'yev, Chrome-rich clinopyroxenes from the kimberlites of Yakutia. N. Jb. Miner. 123, 213-218, 1975.

REGIONAL AND LOCAL VARIATIONS IN THE CHARACTERISTICS OF DIAMONDS FROM SOME SOUTHERN AFRICAN KIMBERLITES

J.W. Harris

Grant Institute of Geology, West Mains Road, Edinburgh EH9 3JW, Scotland

J.B. Hawthorne

Geology Department, De Beers Consolidated Mines Ltd., P.O. Box 616, Kimberley South Africa

M.M. Oosterveld

Computer Services Department, De Beers Consolidated Mines Ltd., P.O. Box 616, Kimberley, South Africa

Abstract. Studies, additional to those of Harris et al. (1975) on diamonds from the Finsch and Koffiefontein mines, show that with increasing depth in both diatremes the morphological character of the diamonds remains virtually constant but that colour variations are evident. At Premier mine, diamonds derived from distinct kimberlite units at the same level within the diatreme also show morphological similarity and colour variation.

Described for the first time are physical characteristics of diamonds from the Zwartruggens dyke swarm, the Letseng-le-terai diatremes, and the Ebenhaezer and the Kimberley group of diatremes. Diamonds from Zwartruggens are distinctively characterised by cubic shape, the virtual absence of macles, and orange-colours; those at Letseng-le-terai by a scarcity (<2%) of octahedra and absence of transparent green-coated stones; those at Ebenhaezer by a few relatively large cubo-octahedral diamonds, and those within the Kimberley group of diatremes by the constancy of diamond morphology.

The results of these studies are that diamond crystal form and colour are respectively diagnostic of most of the individual kimberlite sources from which diamonds were examined, but collectively, on a regional basis, these characteristics do not define any geographic pattern in southern Africa.

Variation of diamond morphology and colour is discussed in relation to chemical and physical conditions pertaining to the 'peridotitic' and 'eclogitic' growth environments of diamond, and the subsequent processes which affected these diamond populations in specific kimberlites.

Introduction

The classification scheme for diamond based on physical features as a function of diamond size (Harris et al., 1975) has been used to obtain new data about the characteristics of diamonds from several of the major kimberlite occurrences in southern Africa. Diamonds were obtained for classification not only from the general productions at Koffiefontein, 1975, and Zwartruggens, 1976, but also, between 1973 and 1977, from development levels at Finsch, Koffiefontein, and the Main Pipe at Letseng-le-terai in Lesotho. In addition, diamond parcels especially obtained for valuation have provided information about the variation of diamond characteristics in two specific kimberlite types at Premier, and other special diamond parcels from the Ebenhaezer diatreme adjacent to Koffiefontein and the Satellite Pipe at Letseng-le-terai have enabled some comparisons to be made between the diamonds from different diatremes in the same kimberlite complex. A preliminary investigation of the diamond characteristics from the Kimberley group of mines (Bulfontein, De Beers, Dutoitspan and Wesselton) has also been completed.

Classification Procedure

The classification scheme followed is that discussed in detail by Harris et al. (1975). In the present study the diamonds were sized by sieving prior to examination. To define the major morphological divisions of a diamond sample such physical properties as crystal form, angularity and regularity are determined as a

TABLE 1. Diamond Sieve Information

Sieve Class*	Diameter in mm of aperture (lower screen)	Approximate average weight in carats per stone
-23 +21	7,925	4,853
-21 +19	6,350	2,476
-19 +17	5,740	1,574
-17 +15	5,410	1,256
-15 +13	4,521	0,860
-13 +12	4,089	0,561
-12 +11	3,454	0,371
-11 + 9	2,875	0,211
- 9 + 7	2,464	0,123
- 7 + 6	2,159	0,0896
- 6 + 5	1,829	0,0557
- 5 + 3	1,473	‡0,029
- 3 + 2	1,321	‡0,015
- 2 + 1	1,092	‡0,008

‡ Logarithmic midpoints
* Diamond sieves with circular apertures

function of size. Other diamond subdivisions depend on properties such as transparency or opacity, colour, the numbers of inclusions, and surface features. The full range of sieve classes used, the diameter of aperture and corresponding average weight per diamond are listed in Table I. This enables the reader to locate the sieve classes on the abscissae in the subsequent figures. The smaller sieve classes (< +7) are included in Table I because unlike previous studies (e.g. Harris et al., 1975), all diamonds in some parcels were categorised. For studies on diamond samples from the general productions at Koffiefontein and Zwartruggens either the total, or at least 1000 stones in each of the sieve classes between +7 and +21 were examined.

Diamonds obtained from development projects or special valuation parcels were usually classified over the full range of diamond sizes. This procedure was adopted because, unlike diamonds in the general production, there is only a specific number of stones in these parcels and the parcels contain diamonds in most of the sieve classes. Invariably, this procedure resulted in complete classification of all the diamonds in the parcel.

Diamonds in sieve classes smaller than +6 were usually classified with the aid of a binocular microscope, but for larger stones, the standard 5(x 2.5 mag.) or 10(x 3.5 mag.) headloop used by daimond sorters was employed.

Once classified the data were computed, and the computer programme compares the various divisions of the classification as a function of diamond size. A modification to the original programme now enables the results to be plotted directly in graph form, but the computer programme still records values to the nearest half percent.

For the purposes of these studies diamond twins (macles) are considered as being independent of crystal shape. This procedure was preferred as there was often insufficient numbers of macles in certain sieve classes in the special parcels to justify as worthwhile a more detailed breakdown of this morphological division.

Results

From the computation of the diamond data two important relationships are presented in the results. There are the variations of (i) crystal form, and (ii) colour, as functions of diamond size. These relationships are the principal means by which the diamonds from the various sources can be defined, and also these parameters provide information about the environment, during and subsequent to, diamond growth.

No values are given if the population in a group is less than 100 diamonds for such data were considered to be unrepresentative, and for some samples the numerical symbols designating crystal form and colour differ from those used in 1975. The results are divided into three sections.

A) Studies on diamonds from single kimberlite diatremes.

B) Studies on diamonds from a kimberlite dyke swarm at Zwartruggens.

C) Studies on diamonds from adjacent kimberlite diatremes.

A) Studies on Diamonds from Single Kimberlite Diatremes

1. Koffiefontein. In view of the relatively small number of diamonds characterised during 1973 (Harris et al., 1975), a further sample was examined from the 1975 production at the 100-160 m levels. The effect of adding the new results to those previously obtained, Figures 1a and 1b, did not change the values of the various crystal forms as a function of diamond size by more than a few percent (Figure 1a). Similarly colours did not vary markedly (Figure 1b), excepting for diamonds of greater than one carat where there was about a 5% increase in green and about a 15% increase in yellow stones at the expense of colourless diamonds (cf. Figure 1b with Figure 3 Harris et al., 1975).

Between 1973 and 1977 the 244 m and 488 m development levels were completed at Koffiefontein. The diamonds from each level were initially examined in parcels related to geological divisions within the pipe, but for the purposes of comparing diamond characteristics with depth, the data for diamonds from each level were combined; results are shown in Figures 1c, 1d, 1e and 1f.

Although there is not a full overlap of crystal form as a function of diamond size with depth (cf. Figures 1a, 1c and 1e) there are

clearly only minor variations of morphology between the three levels at this mine. The more marked discrepancy occurring with the larger stones at the 244 m level compared with the surface, is probably the result of insufficient number of diamonds in the relevant sizes at the 244 m level.

With increasing depth there are, however, significant changes in diamond colour (Figures 1b, 1d, 1f). The most marked over the common diamond size range is the increase in the proportion of yellow and brown stones at the expense of colourless. For the three levels colourless diamonds decrease in proportion from about 60% to 40% and yellow and brown stones increase from about 30% to 50%. There is also a slight increase in proportion of green diamonds on the 488 m level relative to other coloured stones, although there are small numbers of diamonds in those sieve sizes. On each of the levels, the relative proportion of yellow to brown stones increases, as the size of diamond increases.

2. Finsch. A comparison of diamond crystal form between the surface and the 348 m development level at the Finsch Mine is shown in Figures 2a and 2c. There are only minor variations of morphology between these two levels, and as the variations occur principally among the larger stones where diamond numbers on the 348 m level are small, these differences may not be significant.

The variation of colour with diamond size between these two levels is shown in Figures 2b and 2d. The predominant feature to note is the marked decrease in transparent green-coated stones from 10-20% at surface to less than 2% at the 348 m level. This change is accompanied by a complementary increase in the brown and colourless stones and a slight decrease in the proportion of grey stones (cf. Figures 2b and 2d). On both levels, however, the proportion of yellow stones increases with increasing diamond size, whereas the proportion of brown stones steadily decreases.

Since about 1975 there has been a marked decrease in the proportion of transparent green-coated diamonds recovered from the surface production at the Finsch Mine, and the virtual disappearance of diamonds with this colour appears to be closely linked to the change in state of the kimberlite from altered and weathered "yellow" ground to the less altered "blue" ground at the deeper levels.

3. Premier. Diamond samples have been recovered from two specific kimberlite types at the 520 m level at this mine. At this level the brown kimberlite occupies about one-fifth of the pipe area at the south-eastern end of the diatreme. The grey kimberlite occupies most of the remainder of the diatreme apart from a small volume of black kimberlite containing carbonate-rich dykes near the north-western end of the pipe.

The morphological differences between diamonds from the two kimberlites are shown in Figures 3a and 3c. Variations in morphology are small. The brown kimberlite has fewer octahedral diamonds and slightly more dodecahedral and flattened dodecahedral diamonds than the grey kimberlite.

Figures 3b and 3d illustrate the marked differences in diamond colour between these two kimberlite types. Relative to the brown kimberlite there is a 10% decrease in colourless diamonds, a 20-25% decrease in yellow diamonds, an 8-10% decrease in transparent green-coated diamonds, and a 30% increase in brown diamonds. The diamonds from both kimberlites also show an increase in the proportion of yellow stones at the expense of brown diamonds with increasing diamond size.

The present results can also be compared to similar data determined for the diamonds recovered from the underground production levels between 200 and 350 m at Premier during 1971-73 (Harris et al., 1975). Over the size range common to both studies the variations of diamond morphologies are small, but the results from the grey kimberlite and the general production are particularly close (compare Figures 3a and 3c with Figure 3e).

No similar clear collation emerges, however, if diamond colours from the general production (Figure 3f) are compared to those from the 520 m level (Figures 3b and 3d). The proportion of colourless diamonds for example, is about 10% higher in the general production than in either the brown or grey kimberlites. On this basis, colour derivation solely from diamonds in the two kimberlite types would only be possible if the diamond colour varied in some way, either within these kimberlites or as a function of depth.

B) Studies on Diamonds from a Kimberlite Dyke Swarm at Zwartruggens

The Zwartruggens dyke swarm is situated 60 km west of Rustenburg, Transvaal, and comprises a number of narrow east-west striking near vertical kimberlite dykes. Although diamonds were classified from two localities, few differences were noted and the results from the individual occurrences were combined and are presented in Figures 4a and 4b.

The diamond morphology from this source is unique in comparison to other southern African diamond deposits studied to date because there are less than 1% macles in the mine (see Figure 4a). Other kimberlites have a macle content of at least 10%. Another prominent feature is the presence of 5-10% cubes; other sources so far studied have less than 1%.

These diamonds also show several distinctive colour characteristics (Figure 4b). There are 2-5% of orange and amber stones compared to less than 1% elsewhere (see for example Figure 3b). There are noticeable numbers of diamonds with multiple colours (ambers and colourless) and over part of the diamond size range there are up

to about ½% of blue stones. The latter proportion is comparable with that at Premier but diamonds of this colour have not been encountered elsewhere. There is also a high proportion, (about 25%) of transparent green-coated diamonds.

C) Studies of Diamonds from Adjacent Kimberlite Diatremes

1. The Main and Satellite Pipes at Letseng-le-terai. The two pipes at Letseng-le-terai in the north-eastern highlands of Lesotho are separated at the surface by 300 m of basalt wall rock. The Main Pipe has a surface area of 15.9 ha. and the Satellite Pipe 4.7 ha. (1 hectare = 10,000 m^2 = 2.47 acres). Prior to the present open cast mining operations the surfaces of both mines were extensively worked by local diamond diggers.

From the Main Pipe diamonds were examined from sampling operations carried out, over the whole pipe, at surface and the 60 m level. Although different kimberlite types were encountered on both levels, no appreciable differences in characteristics were observed, and the results from all the localities studied were combined (Figure 5a). At the Satellite Pipe only surface sampling (0-5 m) was completed and no distinctive kimberlite types were observed. Diamonds were recovered from all areas of this pipe but the number classified was small (Figure 5c).

The distinctive morphological feature of the diamonds from the Main Pipe (Figure 5a) is the low octahedral content, less than 2%, coupled with the unusually low proportion of macles, at about 10%. An equally low octahedral content was determined for the Brown kimberlite at Premier, but the macle content from this kimberlite is twice that at Letseng (cf. Figures 3a and 5a). In the Satellite Pipe (Fig. 5c) there are less octahedra and macles but more dodecahedra than in the Main Pipe.

The colour data for the diamonds from both pipes are shown in Figures 5b and 5d. There are wide differences in the proportion of brown and grey stones in these pipes, and an unusual feature is the absence in both diatremes of transparent green-coated diamonds.

The differences in morphology and colour of diamonds from these two diatremes, however, may not be significant, as relatively few diamonds were classified from the Satellite Pipe, and these had been recovered from the surface which had already been worked by local diamond diggers.

2. Koffiefontein and Ebenhaezer Diatremes. These two pipes are situated in the western Orange Free State, South Africa, and are separated at surface by only 120 m of Karroo wall rock. The Koffiefontein diatreme is 10 ha. in area at surface and the Ebenhaezer 7.5 ha. The Ebenhaezer Pipe was sampled at the surface and the 60 m level. The diamonds were classified and the results from both levels combined (Figures 6a and 6b).

An important morphological feature of the diamonds from Ebenhaezer is the presence of a few cubo-octahedrons among the smaller stones (Figure 6a). These diamond shapes have been noted at the Premier Mine but only in the much smaller diamond sizes, (e.g. 0.02 carats per stone as opposed to 0.08 carats per stone at Ebenhaezer).

A comparison of morphology between Ebenhaezer and the Koffiefontein data presented earlier (Figures 1a, 1c, 1e) reveals that at Ebenhaezer there is a slightly higher proportion of flattened dodecahedra, at the expense of dodecahedra, than in the three levels studied at Koffiefontein, but otherwise, the morphology of diamond from these two mines is similar.

No unusual colours were found at Ebenhaezer (Figure 6b), but a colour comparison with Koffiefontein (Figures 1b, 1d, 1f) shows that the proportion of specific colours varies between the two diatremes. The diamond colour at Ebenhaezer, for example, corresponds more closely to the diamond colours from the 244 m and 488 m levels at Koffiefontein, than to the surface production.

3. The Kimberley Group of Mines. In a preliminary study, a limited number of diamonds from special valuation parcels, from the Bulfontein, De Beers, Dutoitspan and Wesselton Mines have been examined and classified. For individual sources there were insufficient diamonds to allow comparisons to be made on the basis of individual diatremes. It was nevertheless apparent that morphologically the diamonds were similar whereas colour differences were evident.

In view of the colour variation between individual diatremes no combined results of colour versus diamond size for these mines are presented, but Figure 7a gives the combined morphology results which are regarded as being representative of diamond morphology in the Kimberley group of mines.

Discussion

Comparison of Diamond Morphology from Various Groups of Kimberlite

The characteristics of diamond from each of the six kimberlite groups indicate that on a local basis distinctions between individual sources can be made. The completion of the preliminary study of the diamond characteristics of the Kimberley group of diatremes also enables a general comparison of morphology to be made of diamonds from several important kimberlite sources in southern Africa. No similar exercise is attempted for diamond colours because of the local variability of this characteristic. For the morphological comparison, data from adjacent kimberlites were combined in the following ways.

a) Premier group: The results shown in Figure 7b were obtained by combining the diamond morpho-

logies from grey and brown kimberlites with those from general productions.

b) Koffiefontein group: Figure 7c shows the results of combined diamond morphological data from the various levels of the Koffiefontein and Ebenhaezer diatremes.

c) Zwartruggens group: The morphology of diamonds from both localities is shown in Figure 7d.

d) Finsch mine: Morphological data are combined for diamonds from the 100-150 m production level and from the 348 m sampling level, Figure 7e.

e) Letseng-le-terai group: Only the morphology of diamonds from the Main pipe is shown in Figure 7f, as it was considered that there were insufficient data from the Satellite pipe.

The diamond morphology data shown in Figures 7a-7f can be divided into a number of groups. The diamonds from the Kimberley, Koffiefontein and Finsch mines (Figures 7a-7c-7e) have similar morphologies with roughly the same proportion of flattened dodecahedra, macles and polycrystalline aggregates. They also show roughly the same proportion of octahedra which steadily increase with diamond size. In the case of Finsch this change is at the expense of the proportion of dodecahedra, whereas in the Kimberley and Koffiefontein kimberlite groups the proportion of dodecahedrons does not appreciably decrease with increasing diamond size. The three mines show distinct differences, however, in the proportions of irregular diamonds.

The Premier, Zwartruggens and Letseng-le-terai pipes (Figures 7b-7d-7f) form another group. These sources have much lower proportions of octahedral diamonds, and these percentages are essentially constant throughout the size ranges studied. These mines, however, vary individually in respect of the proportions of dodecahedra, macles, cubes and irregular stones.

The diamond morphology data can also be divided on the basis that the Koffiefontein and Finsch data (Figures 7c and 7e) are distinct from the other sources since the macle proportions at these two mines are constant with respect to diamond size.

However, there appears to be no distinguishing regional characteristics from these various large-scale morphological groupings which can be used to separate the kimberlites. In general, only relative differences exist between the same diamond morphologies in five of the kimberlite sources, and these variations probably relate to processes which subsequently modified the original crystals (see below). The presence of cubes at Zwartruggens is only of local significance, for its nearest kimberlite neighbour, Premier Mine, has no cubes in its diamond population.

The emplacement ages of six of the kimberlites range from Pre-Cambrian to Cretaceous. Premier Mine is Pre-Cambrian (Allsopp et al., 1967) and Allsopp and Barratt (1975), using Rb/Sr ratios, have dated Zwartruggens at 147 ± 4 m.y., and obtained a mean age of 86 ± 3 m.y. for the four Kimberley mines, which is in close agreement to the zircon ages of 91 ± 2 m.y. determined by Davis et al. (1976). As the kimberlites at Finsch, Koffiefontein and Letseng are also part of the post-Karoo kimberlite event in southern Africa, it would therefore appear that there is no relationship between the principal morphologies of diamonds and the emplacement ages of the kimberlites in which they are found.

Of the nine occurrences Zwartruggens is the only kimberlite dyke swarm, and this mine contains very distinctive diamond morpholgies. These morphologies, however, can not be related to the mode of kimberlite intrusion, as a preliminary study of the diamonds from the Bellsbank kimberlite dyke swarm in the Cape Province reveals morphologies and colours similar in type and proportion to the major kimberlite sources discussed above. The morphology of diamonds from Zwartruggens, therefore, is a characteristic peculiar to that particular locality.

The Variation of Diamond Morphology as a Function of Diamond Size and Kimberlite Type

Harris et al.(1975) discussed the varying proportions of diamond crystals found in different kimberlites in terms of primary populations of octahedra, macles, cubes, combined forms and aggregates. Subsequent modifications produced dodecahedra and flattened dodecahedra from the original octahedra, rounded many of the other primary diamond shapes, and created most of the irregular crystals.

The initial part of this hypothesis assumed that all the diamonds in a specific kimberlite formed in a single location as part of a single growth process, and such a unique source now seems unlikely. Quantitative chemical analyses of representative samples of the syngenetic mineral inclusions in diamonds from known sources, clearly indicates that there are two major, and chemically distinct, environments for diamond growth in the upper mantle. Studies of the abundances of these syngenetic minerals moreover, indicates that the proportion of diamonds belonging to each of these two environments also varies between kimberlite sources. For example, Harris and Gurney (1978) have shown that at the Finsch Mine, a very high proportion (>98%) of diamonds are derived from a 'peridotitic' environment whilst at the Premier and Koffiefontein mines there is roughly equal proportions of 'peridotitic' and 'eclogitic' diamonds in the diamond populations.

These different environments, however, do not appear to seriously influence the growth mechanism of the diamond. At Finsch, Koffiefontein and Premier, it is clear that the octahedra and its twin the macle are the predominant primary diamond crystal habits, irrespective of the silicate assemblage present during their formation. With the cubes at Zwartruggens, and the few cubo-octahedra classified at Premier and Eben-

haezer, it is likely that their morphologies are related to variations in the physical conditions during diamond formation. Morphological studies on synthetic diamonds by Klyuyev et al. (1973) have shown that cubes and cubo-octahedra require, relative to octahedra, either lower temperatures or higher pressures for their formation.

The consistently low proportion of aggregated octahedra and macles from five of the sources, and the equally low proportion of aggregated octahedra and cubes at Zwartruggens, indicate that changes in diamond nucleation were not accompanied by abrupt changes in the physical conditions, but proceeded more or less steadily once the environmental conditions were appropriate. In fact, the similarity between the morphologies of diamonds from the 'peridotite' and 'eclogite' environments, as well as the similarity of the imposed morphologies of the different syngenetic mineral inclusions present in these two distinct groups of diamonds (Harris and Gurney 1978), suggest that, in general, the pressure/temperature conditions between these two environments were not very different. This conclusion is supported by the available evidence on the geothermometry and geobarometry of the mineral inclusions in diamond (e.g. see Gurney et al., 1978, in press).

The principal morphological variation which is likely to be related to the prevailing chemical, rather than, physical conditions, is the proportion of macles in a specific diamond population, as the macle proportion probably reflects differences in the degree of carbon saturation during the initial stages of diamond growth.

The virtual absence of macles and the presence of cubes, at Zwartruggens, and vice versa for the other mines, does not mean that these two crystal habits are always mutually exclusive. They have been found together as coated stones in the diamond population from Koidu No. 1 Pipe Sierra Leone (Grantham and Allan, 1960), and are a common feature, again as coated stones, in the diamonds from Zaire, although in this case no studies have been completed on specific kimberlite or alluvial diamond sources.

The diamond contributions from the 'peridotitic' and 'eclogitic' sources, and the ratios of the primary crystal habits in each of these sources, are the two unknowns which generally prevent a more detailed interpretation of the systematic morphological trends shown by the primary diamond crystal habits in the various figures. At Finsch, however, the diamonds are derived almost solely from a 'peridotitic' environmnet and have a constant octahedron to macle ratio irrespective of diamond size. Such data (Figure 7e), suggests that in this initial diamond growth environment the level of nucleation of the octahedra was greater than that of the macles, but that the nucleation rates for both morphologies were the same.

Moore and Lang (1974) clearly demonstrated that rounded dodecahedral diamonds are resorbed forms of diamond octahedra, and a resorption process has obviously affected all the diamond populations in the present investigation. Apart from the octahedra, similar rounded surfaces have been found on macles and octahedral aggregates from all the mines studied, and the rare tetrahexahedron (a solution form of the cube) has been observed at Zwartruggens.

At present it is uncertain whether the resorption process occurred whilst the diamonds were present in their original 'peridotitic' or 'eclogitic' environments or whether the kimberlite was principally responsible. Some resorption has been observed on octahedral diamonds recovered from eclogite nodules (Robertson, in press) but the systematic variation in the ratio between octahedra and dodecahedra with diamond size at Kimberley, Finsch and Koffiefontein (see Figures 7a, 7c and 7d) may indicate that it is in the

---

KEY TO FIGURES 1 THROUGH 7:

(Form as a Function of Size) - Numbers on graphs refer to different shapes of diamond as follows:

1- Octahedra
2- Dodecahedra
3- Flattened Dodecahedra
4- Cube-Octahedra
5- Cube-Dodecahedras
6- Cubes
7- Macles
8- Spheres
9- Irregular
10- Cube-Octahedra-Dodecahedra
11- Octahedra-Dodecahedra
12- Tetrahedron
13- Polycrystalline
14- Uncertain

(Colour as a Function of Size) - Numbers on graphs refer to different colours of diamond as follows:

1- Colourless
2- Yellow
3- Brown
4- Green
5- Orange & Amber
6- Pink & Mauve
7- Blue
8- Black
9- Multiple
10- Steel Grey & Grey
11- Smokey
12- Uncertain

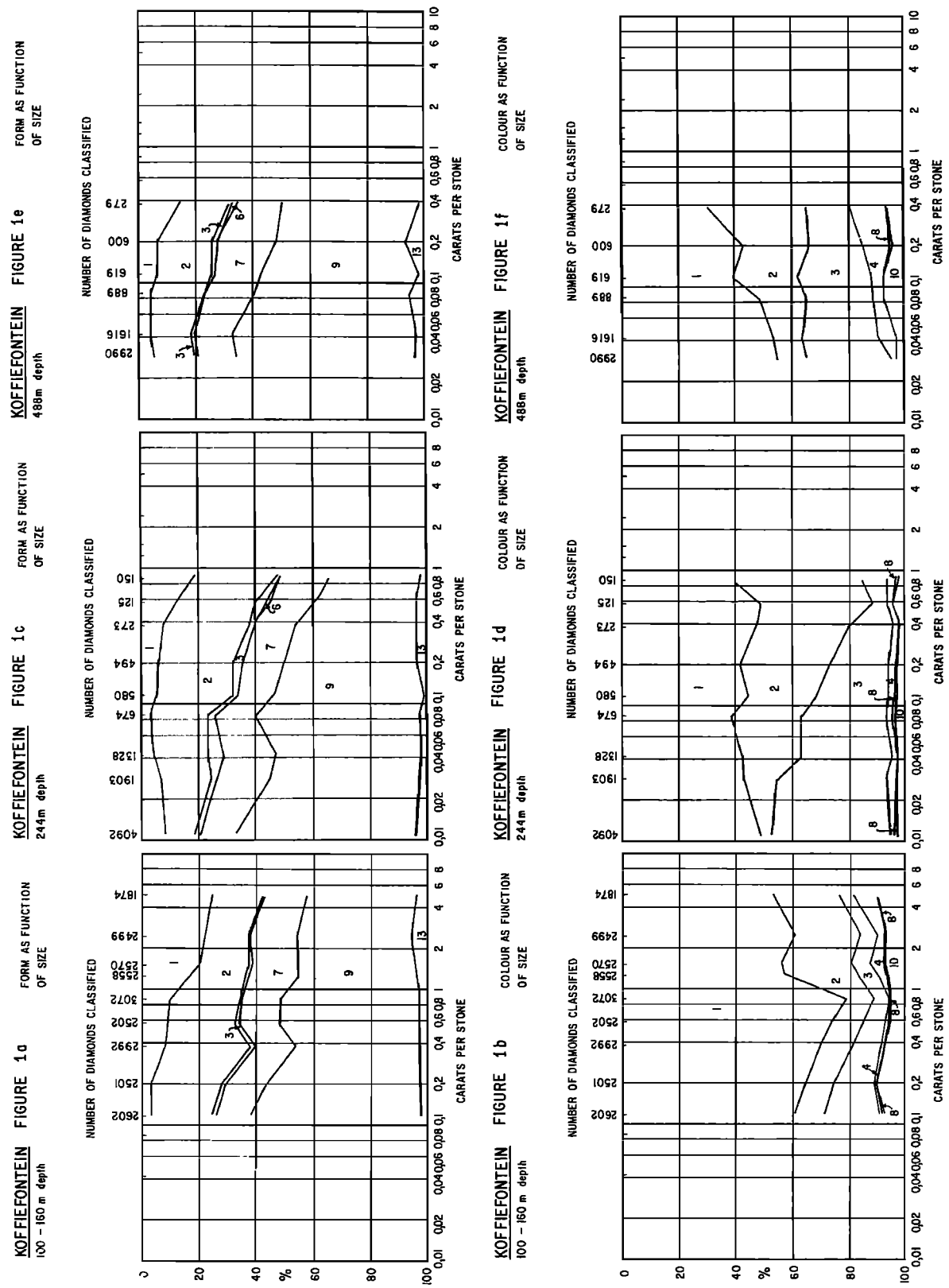

Figure 1

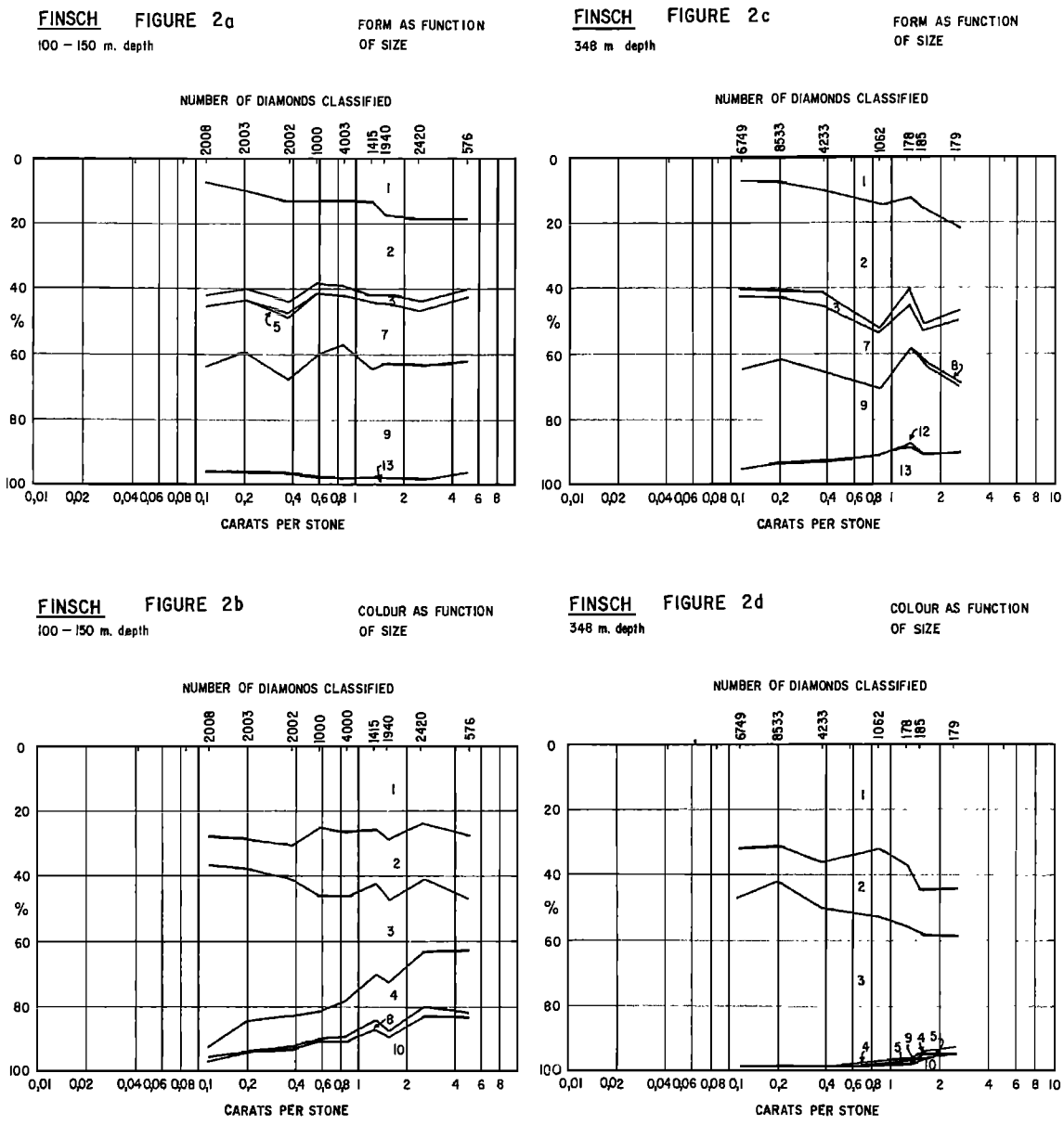

Figure. 2

kimberlite, during some stage of fluid or volatile ascent, that this process occurs.

At Premier, Zwartruggens and Letseng-le-terai (Figures 7b, 7d, 7f) the consistently low octahedron proportion suggests that the solution process was more severe. It would seem that the number of octahedra attacked in a particular diamond size class is a fixed proportion of the total number of octahedra in that size, and the resorption causes an exponential reduction in the numbers of octahedra in each size class until a common minimum is approached.

At all the mines, a large proportion of the diamonds are classified as irregular (see above). Diamonds which are broken invariably fracture along diamond cleavage planes, and fracture surfaces can be defined as "old" or "new" (Williams 1932). In the first case, the surface has been partially resorbed subsequent to fracture, and the edges of the fracture surface are smooth and rounded. With "new" fracture surfaces, no resorption has occurred and surface edges are sharp.

The presence, from all the mines studied, of broken dodecahedra of all sizes with "old" fractures, indicates that the event or events that caused these diamonds to break, largely post-

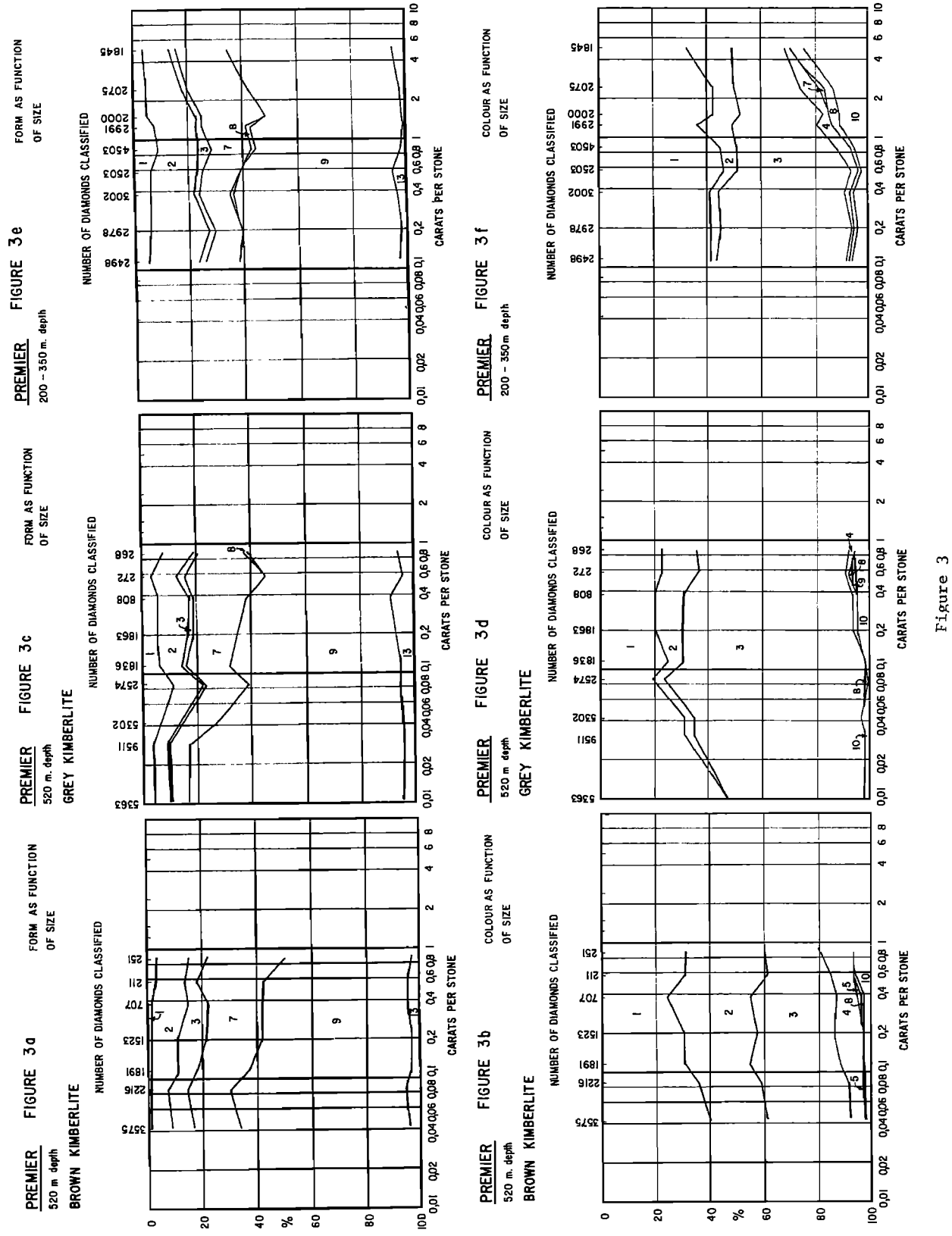

Figure 3

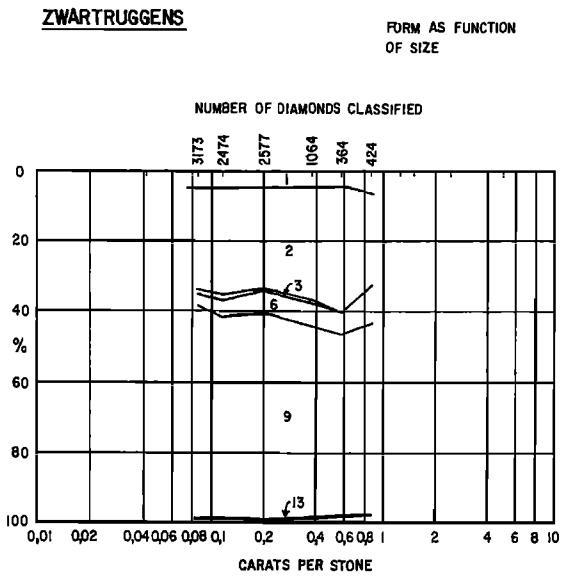

FIGURE 4a

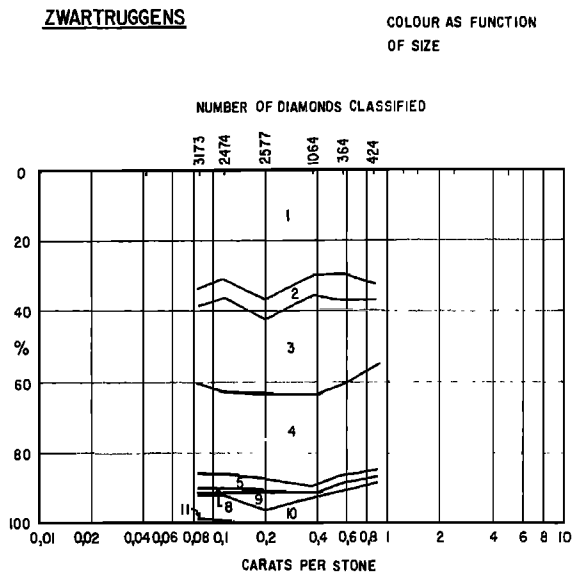

FIGURE 4b

Figure 4

dates diamond resorption. It is likely that during kimberlite ascent, either sudden upward movement of the kimberlite, or internal strain caused by the ever-increasing differential expansion rates between diamond and its inclusions as the pressure drops (see Harris et al., 1970) would provide opportunities for diamond to fracture, but these events would also allow sufficient time for partial resorption of broken surfaces by fluids or volatiles.

'New' fractured diamonds may derive from the explosive nature of kimberlite emplacement, or from mining and milling processes used in diamond recovery. At present, however, no data are available from the various mines about the relative contributions these two factors make to the proportion of irregular diamonds with 'new' fracture.

The diamonds recovered from the brown and grey kimberlites at Premier mine showed only slight morphological differences (cf. Figure 3a and 3c). Only slight differences were also recorded for diamonds obtained from the adjacent Koffiefontein and Ebenhaezer kimberlite diatremes (cf. Figures 1a, 1c, 1e and 6a). In both cases, the morphological differences relate to small variations in the ratios of the proportions of octahedra to dodecahedra or flattened dodecahedra. These results strongly suggest that the diamonds from the two kimberlites at Premier were initially part of the same combined diamond population, and morphological variations reflect the different degrees to which the diamonds in the two kimberlites were subsequently modified during ascent and emplacement. A similar conclusion can be drawn from the comparison of the diamonds from Koffiefontein and Ebenhaezer, although in this case, the kimberlites carrying the diamonds formed two adjacent diatremes rather than two intrusions within the same vent.

The Variation of Colour as a Function of Diamond Size, Kimberlite Type and Depth Within a Diatreme

Diamond colour, like the primary diamond shapes, does not obviously appear to be controlled by the two diamond growth environments. The principal diamond colours in both the 'peridotitic' and 'eclogitic' environments are colourless, yellow and brown.

In the present study diamonds with these three colours predominate in all the kimberlites examined, and except in Zwartruggens, display a common colour trend in the combined diamond populations; yellow diamonds increase in proportion over brown ones as diamond size increases. The proportion of yellow to brown diamonds not only varies between the individual diatremes, but also between individual kimberlites at the same level, as at Premier, and with depth in the same kimberlite, as at Koffiefontein.

The yellow versus brown colour variation was first noted during earlier work on South African diamonds by Harris et al. (1975). To account for these trends they suggested that dispersed nitrogen might migrate at appropriate temperatures and form nitrogen aggregates, or nitrogen platelets within the lattice during diamond growth. A more detailed evaluation of these colour trends however must await the determination of the amount of nitrogen present in the

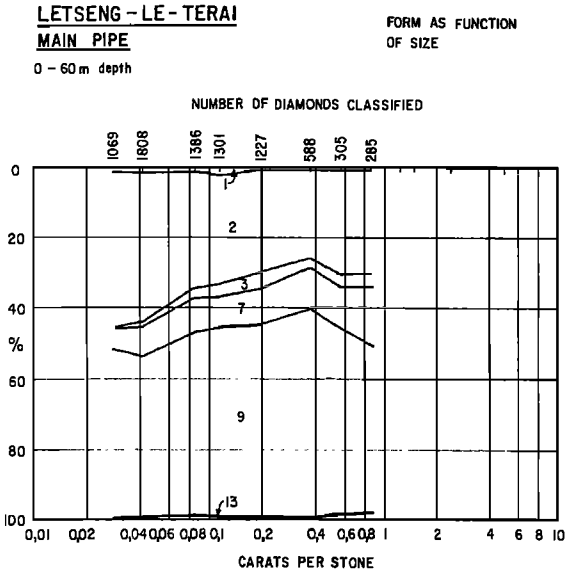

FIGURE 5a

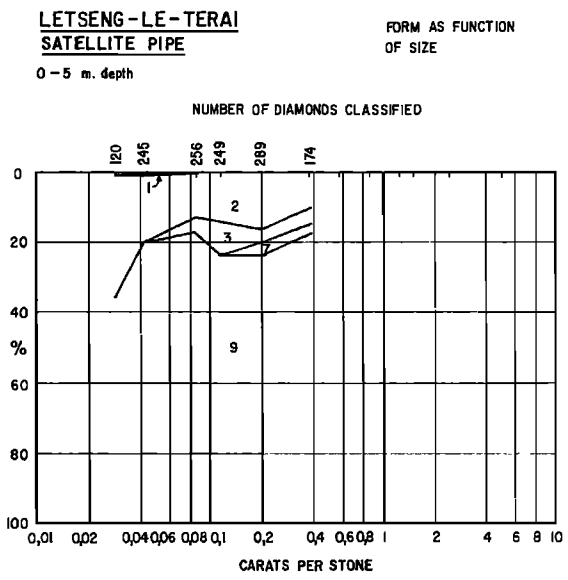

FIGURE 5c

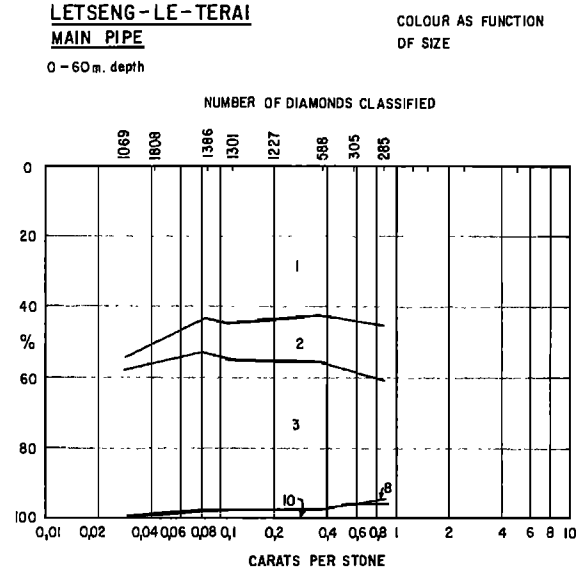

FIGURE 5b

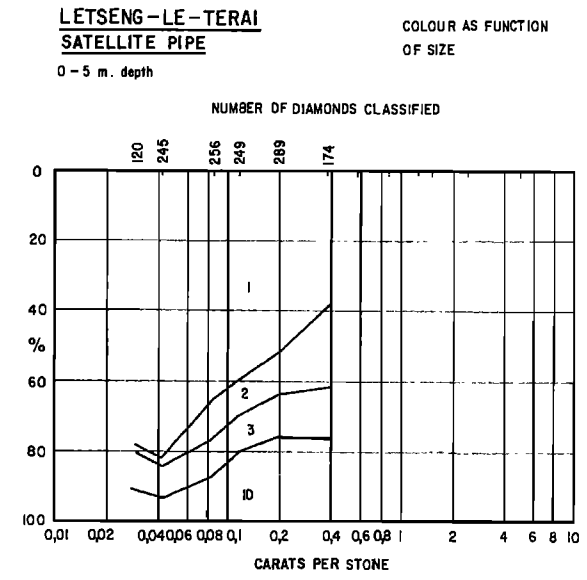

FIGURE 5d

Figure 5

'peridotitic' and 'eclogitic' growth environments of diamond. In this regard, a study is to be completed of the nitrogen content in diamonds recovered from eclogite nodules.

At Zwartruggens, the presence of amber-coloured diamonds indicates that in addition to physical aggregation, nitrogen has also substituted for carbon in the diamond lattice, and produced the so-called type Ib diamond (Bruton, 1970). Whether or not these two processes occurred at the same time is uncertain, but the presence of amber diamonds and the absence of a distinct colour trend may be related.

The variations of diamond colour with depth and diamond size are unlikely to be controlled by temperature differences during the final stages of kimberlite intrusion. Whilst different lattice sites may contain impurities with different mobilities, the emplacement histories of diamonds found in the closely spaced present

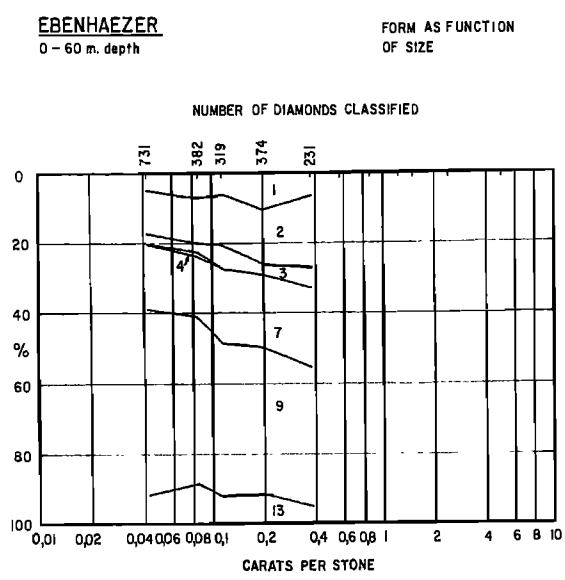

FIGURE 6a

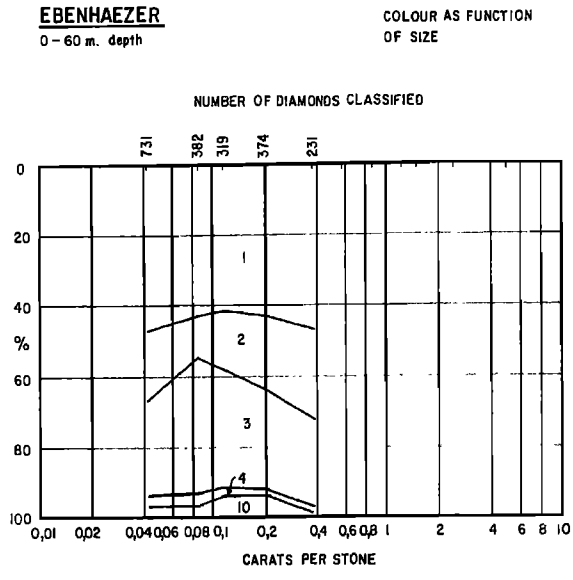

FIGURE 6b

Figure 6

mining levels are not likely to be sufficiently different to have caused the colour variations observed. Evans and Rainey (1975) have shown that it is very difficult to change the original body colour of a diamond, and the conditions required to do so, 2000-2300°C at 48 kb (4.8 GPa), are unlikely to prevail after the kimberlite has reached the surface.

If, however, the assumption is made that the size distribution of a diamond population in a kimberlite varies with the depth from which it is extracted, and Wagnér (1914) presents some evidence for this premise, then the observed colour variation with depth would follow as a corollary, since diamond colour has been shown to be a function of diamond size. In any specific kimberlite this prediction will not be seriously influenced by the diamond morphology as primary crystal habits appear to be largely independent of depth (see above).

One other aspect of diamond colour which will need to be determined if a more detailed interpretation of the present colour trends is to be made, will be the proportion of nitrogen-free diamonds (the so-called Type II's) in a particular diamond population. Type II diamonds are usually coloured brown because of minute amounts of graphitic or amorphous carbon which lie on the diamond (111) lattice planes, the carbon impurity having formed in response to plastic deformation of the diamond, (Urusovskaya and Orlov 1964). Evans (1976) has suggested that plastic deformation occurs preferentially in Type II diamonds firstly because platelets in Type I diamonds will tend to inhibit the movement of dislocations, and secondly because Type II diamonds appear to have a higher initial density of dislocations.

Although no quantitative studies have yet been completed, diamonds exhibiting plastic deformation are particularly common at Premier mine and are also easily found in all the other major kimberlite sources studied. Plastically deformed diamonds can usually be recognised by the presence of single or multiple ⟨110⟩ striation lines running partly or completely around the surface of the diamond. This surface feature is found on diamonds of all sizes, and with the possible exception of the cube and combined habits (see Harris et al., 1975), occurs on all diamond forms. The uncertainty with respect to the cube and the combined forms arises because although striation lines have not been observed on these morphologies, relatively few of them have been encountered in the course of these studies. Excluding brown diamonds, striation lines have also been observed on colourless stones and very occasionally on yellows.

Apart from the influence plastically deformed diamonds may have on the colour trends, they are also important because they indicate that established diamond populations have been subjected to differential stresses which must have been in a wholly crystalline environment, or one in which there was at least grain boundary contacts between the minerals. The plastic deformation of diamond most probably occurred at mantle depths since there is abundant evidence for differential stress in the mantle as demonstrated by the deformation textures found in mantle peridotite in

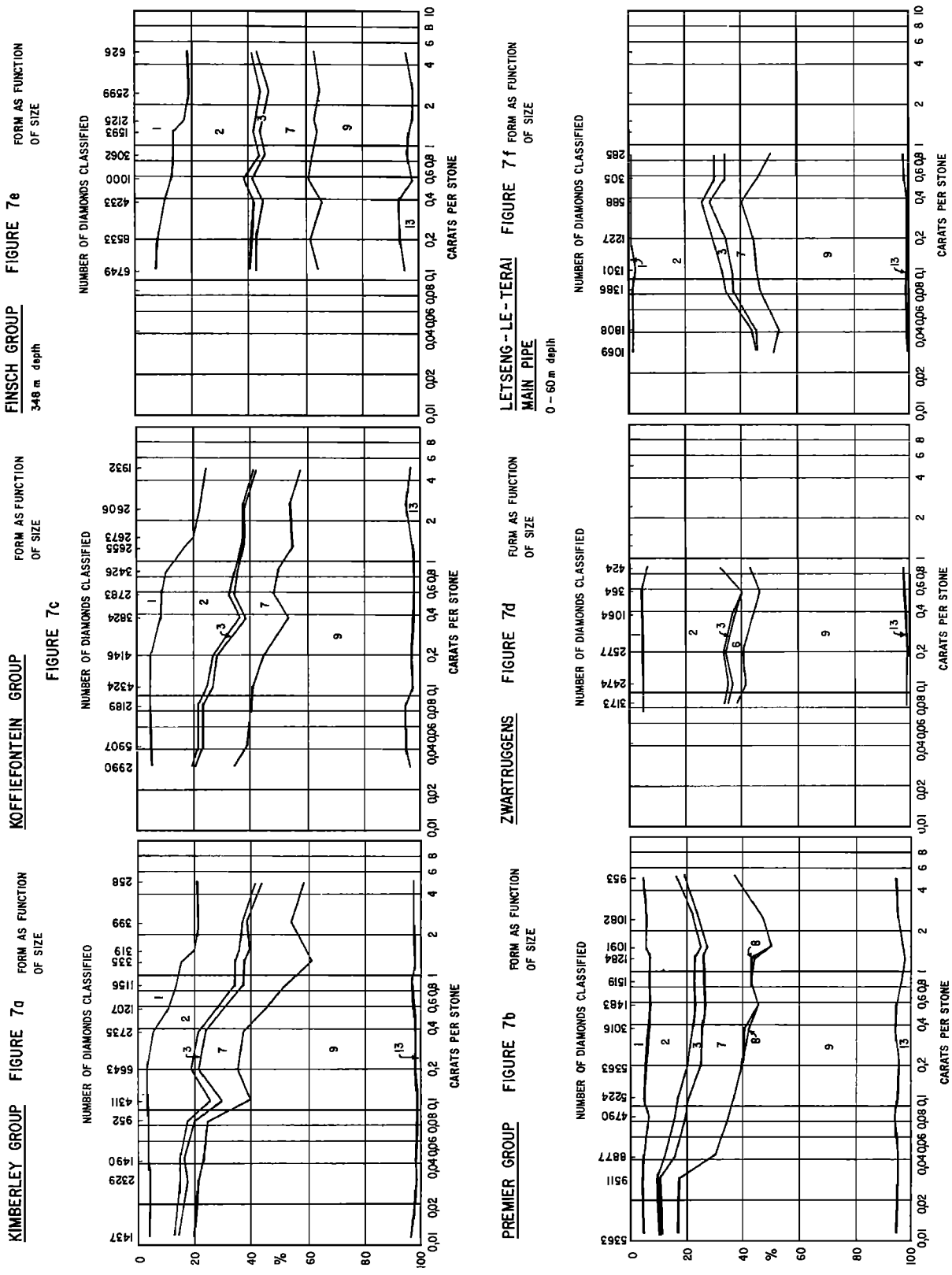

Figure 7

several diamondiferous kimberlites. If this is the case, the deformation may either reflect a widespread process of mantle creep, or a local event associated with diapirism during kimberlite genesis (Harte et al., 1975).

The ductility of diamond at high pressures and temperature has been determined by DeVries (1975) who showed that, in as little as 5 minutes, extensive plastic deformation occurred at temperatures as low as 900-1100°C over the pressure range 60-10 kb (6 to 1 GPa). These deformation temperatures are at least 200°C lower than the available equilibration temperatures for co-existing mineral pairs included in diamond during its growth (Meyer and Tsai 1976; Gurney et al., in press), and the ease of dislocation motion implied by the deformation experiments, may also indicate that the preservation of deformation lamellae on diamond necessitates the deformation to be closely linked to a kimberlite genesis.

The predominance of Type II brown diamonds over Type II colourless ones also raises the question of whether the deformation took place whilst the diamond was in its own stability field, or in the stability field of graphite. The presence of both diamond colours could indicate that plastic deformation occurred across the diamond/graphite boundary. Alternatively, the deformation could have occurred entirely within the graphite stable region, the colourless Type II diamonds having insufficient graphite on their (111) planes to subsequently affect the absorption of light. Internal graphitisation of diamond outside its stability field need not necessarily lead to the total conversion of the crystal, and a mechanism for restricted graphitisation has been suggested by Howes (1962).

Transparent Green-Coated Diamonds. Diamonds with this type of colour coat have been found in all the diamond sources studied with the exception of Letseng-le-terai. Usually their proportion at a particular mine averages less than 10%, but the current diamond productions at Zwartruggens, and until recently at Finsch, averaged between 10-25%.

This type of colour coat is probably the result of natural α-particle bombardment by uranium and thorium atoms in the kimberlite, the damage to the surface of the diamond occurring over long periods of time but after kimberlite emplacement and cooling to below 500°C, (Vance et al., 1973). Thus, if the kimberlites at Letseng-le-terai are grouped with other post-Karoo kimberlite intrusives in the same region, at approximately 90 m.y. old (see Davis et al., 1976), then the absence of transparent green-coated diamonds suggests that in this mine the EU content is much less than the expected 15-30 ppm (see Vance et al., 1973). (EU-the equivalent uranium concentration of a material is that uranium concentration which has the same α-activity as the actual radioelement mixture in the material).

At Finsch, recent mining operations recovered diamonds from below the leached and oxidised near surface kimberlite and the proportion of transparent green-coated diamonds dropped to less than 2%. Vance et al. (1973) suggested that the original high proportion of green-coated diamonds at Finsch was caused either by radioactive enrichment or segregation within the surface levels, and the new evidence supports this conclusion. After emplacement and cooling, groundwater would mobilise and concentrate the uranium and thorium particularly, and an aqueous radioactive source will produce even green surface coats on diamond (Vance and Milledge, 1972). The irregular migration of the groundwater through the kimberlite would also ensure that a relatively high proportion of the diamonds within the groundwater zone were damaged. Below this zone, however, diamonds would only be damaged according to the original distribution of radioactive elements in the unweathered kimberlite (see Vance et al., 1973).

There is no information available on the radioactive content of the kimberlite dykes at Zwartruggens but they have been dated by Allsopp and Barrett (1975) at 147 $\pm$ 4 m.y. The present high proportion of green-coated diamonds, therefore, suggests two possibilities. Firstly that radioactive enrichment in groundwater is responsible, or secondly, that there is in fact an above average EU content in this kimberlite. Gurney and Hobbs (1973) have shown that the Bellsbank fissure mine has an EU value of 25.4 ppm and it may be that relatively high radioactivity is a feature of kimberlite dykes.

Concluding Remarks

The results of this study have shown that there is a general similarity between the morphology and the colour of diamonds from six widely separated kimberlite sources in southern Africa, but that these physical features vary sufficiently between the individual sources to enable diamond populations to be uniquely defined. The data have also allowed some predictions to be made about the initial growth environments of diamonds originating in the upper mantle beneath southern Africa, and the possible ways in which diamond populations subsequently undergo modifications during kimberlite ascent and intrusion.

Apart from providing information about diamond characteristics the classification scheme forms the framework within which several related projects are currently in progress. These studies include the determination of the relative abundances of the syngenetic minerals found in diamonds, the chemical analysis of representative inclusion samples, and the determination of carbon isotope ratios. In each project an observation or analysis is specifically related to the source, size, morphology and colour of the diamond. It is hoped that integrated studies of

this type will lead to a more complete understanding of the environments in which diamond grew and evolved.

Acknowledgements. The authors wish to thank the De Beers Diamond Sorting Office and Computer Services Department, Kimberley for their co-operation during the course of this work, in particular to Miss J. Hartley and Miss A. Van Niekerk and Messrs. C.R. Loveday and M.V. Irwin.

Thanks are also due to the Bobbejaan Mining Co. Ltd. and to the Helam Diamond Mining Company for permission to examine diamonds from Bellsbank, and Zwartruggens.

The authors would also like to thank Dr. J.J. Gurney, Mr. N.F. Best, Mr. P.M. Jackson and Mr. D. Robinson for constructive criticism of the manuscript.

Finally we wish to thank De Beers Consolidated Mines Ltd., and De Beers Industrial Diamond Division Ltd. for permission to publish this manuscript.

References

Allsopp, H.L., and D.R. Barrett, Rb-Sr age determinations on South African Kimberlite Pipes, in Physics and Chemistry of the Earth, edited by L. Ahrens, J.B. Dawson, A.R. Duncan, A.J. Erlank, vol. 9, pp. 605-617. Pergamon Press, Oxford, England, 1975.

Allsopp, H.L., A.J. Burger and C. Van Zyl, A minimum age for the Premier Kimberlite pipe yielded by biotite Rb-Sr measurements, with related galena isotopic data, Earth Planet. Sci. Lett. 3, 161-166, 1967.

Bruton, E., Diamonds, N.A.G. Press Ltd., London, England, 1970.

Davis, G.L., T.E. Krogh, and A.J. Erlank, The ages of zircons from kimberlites from South Africa, Carnegie Inst. Wash. Yearb. 75, 821-824, 1976.

DeVries, R.C., Plastic deformation and "work-hardening" of diamond, Mat. Res. Bull. 10, 1193-1200, 1975.

Evans, T., and P. Rainey, Changes in the defect structure of diamond due to temperature and high pressure treatment, Proc. Roy. Soc. Lond. A 344, 111-130, 1975.

Grantham, D.R., and J.B. Allen, Kimberlites in Sierra Leone, Overseas Geology and Mineral Resources 8, 5-25, 1960.

Gurney, J.J., and J.B.M. Hobbs, Potassium, Thorium and Uranium in some kimberlites from South Africa, Extended Abstracts, First International Kimberlite Conference, Cape Town, South Africa, 143-146, 1973.

Gurney, J.J., J.W. Harris, and R.S. Rickwood, Silicate and oxide inclusions in diamonds from the Finsch kimberlite pipe, Proceedings of the Second International Kimberlite Conference, in press.

Harris, J.W., and J.J. Gurney, Inclusions in diamond, in The Properties of Diamond, edited by J.E. Field, pp. 555-592. Academic Press, London, England, 1978.

Harris, J.W., H.J. Milledge, T.H.K. Barron, and R.W. Munn, Thermal expansion of garnets included in diamond, J. Geophys. Res. 75, 5775-5792, 1970.

Harris, J.W., J.B. Hawthorne, M.M. Oosterveld, and E. Wehmeyer, A classification scheme for diamond, and a comparative study of South African diamond characteristics, in Physics and Chemistry of the Earth, edited by L. Ahrens, J.B. Dawson, A.R. Duncan and A.J. Erlank, vol. 9, pp. 765-783. Pergamon Press, Oxford, England, 1975.

Harte, B., K.G. Cox, and J.J. Gurney, Petrography and geological history of upper mantle xenoliths from the Matsoku kimberlite pipe, in Physics and Chemistry of the Earth, edited by L. Ahrens, J.B. Dawson, A.R. Duncan and A.J. Erlank, vol. 9, pp. 477-506, Pergamon Press, Oxford, England, 1975.

Howes, V.R., The graphitisation of diamond, Proc. Roy. Soc. Lond. A 80, 648-662, 1962.

Klyuyev, Yu.A., Yu.A. Dudenkov, and V.I. Nepsha, Derivation of diamond growth conditions from growth forms and the distribution of optical centres, Geochem. International 10, 781-787, 1973.

Meyer, H.O.A., and H. Tsai, Mineral inclusions in diamond: temperature and pressure of equilibration, Science 191, 849-851, 1976.

Moore, M., and A.R. Lang, On the origin of the rounded rhombic dodecahedral habit of natural diamond, J. of Crystal Growth 26, 133-139, 1974.

Robertson, D.N., Diamond and graphite in eclogite xenoliths in kimberlite, Proceedings of the Second International Kimberlite Conference, in press

Urusovskaya, A.A., and Yu.L. Orlov, Nature of plastic deformation of diamond crystals, Doklady Akad. Nauk. SSSR 154, 112-115, 1964.

Vance, E.R., and H.J. Milledge, Natural and laboratory α-particle irradiation of diamond, Mineral. Mag. 38, 878-881, 1972.

Vance, E.R., J.W. Harris, and H.J. Milledge, Possible origins of α-damage in diamonds from kimberlites and alluvial sources, Mineral. Mag. 39, 349-360, 1973.

Wagner, P.A., The Diamond Fields of Southern Africa, Transvaal Leader, Johannesburg, South Africa, 1914. (Reprinted 1971, Struik (Pty) Ltd., Cape Town, South Africa).

Williams, A.F., The Genesis of Diamond, Benn Ltd., London, England, 1932.

DIAMONDS FROM KIMBERLITES IN THE COLORADO-WYOMING STATE LINE DISTRICT*

M. E. McCallum
Colorado State University, Fort Collins, Colorado 80523
and U.S. Geological Survey, Box 25046, Denver Federal Center, Denver, Colorado 80225

C. D. Mabarak
318 South Loomis, Fort Collins, Colorado 80521

H. G. Coopersmith
Cominco American Inc., St. Charles, Missouri 63301

Abstract. Seventy-eight diamonds recovered from weathered kimberlite from diatremes in the Colorado-Wyoming State Line district are described in terms of size, weight, morphology, color, fluorescence, nd inclusions. The stones are subdivided into two groups: small diamonds, those approximately >1 mg and >1 mm; and microdiamonds, those ≤1 mg and ≤1 mm. Total combined weight of all diamonds in both groups is about 84 mg. (0.42 carat).

Octahedral forms are most abundant in the microdiamond fraction and octahedra/dodecahedra ratios show a general decrease with size (O/D = 6.0 for <0.3-1.0 mm range and 1.2 for 1.0->2.0 mm range). Octahedra and macles appear to be primary growth forms, and dodecahedral forms evolved from octahedra.

Variations in size and form are reflected by weak to moderate trends in color, fluorescence, and inclusion content.

Introduction

Following the discovery in 1975 of diamonds in a serpentinized garnet lherzolite nodule from a kimberlite diatreme (Schaffer 3 in School Section 16) in southern Wyoming (McCallum and Eggler, 1976), a program was initiated at Colorado State University to test the kimberlites in the region for diamonds. Weathered kimberlite from selected pipes in the Colorado-Wyoming State Line and Iron Mountain, Wyoming, districts was evaluated by preliminary reconnaissance, and during the summer of 1975, 21 small diamonds were recovered from two of the Colorado diatremes (8 from the Sloan 1 pipe and 13 from the Sloan 2 pipe) (McCallum and Mabarak, 1976a). Subsequent testing in 1975-1976 led to the recovery of small diamonds from the Schaffer 10, 15, 16, and 19 pipes and the Aultman pipe (McCallum and Mabarak, 1976b). By August 1977, diamonds had also been isolated from weathered kimberlite of the Schaffer 3 and 13 pipes, and from two of the Nix pipes, and the total number of crystals recovered from the district had reached 78. (See McCallum and others, 1977, and Smith and others, in press, for pipe locations.) No diamonds have yet been found in kimberlite from the Iron Mountain district.

Most of the diamonds range from approximately 0.2 mm to 2.0 mm in average diameter and <0.5 mg to 4.0 mg in weight (Table 1). Maximum concentration of diamonds is in the 0.3-0.5 mm and 0.5-1.0 mm size fractions (Fig. 1A). As would be expected, weight of diamonds per size interval along with weight percent per size interval increases appreciably in the larger size units (Figs. 1B and C). The largest crystal recovered to date was taken from the Sloan 2 pipe, weighs 11.8 mg (0.059 carat) and is approximately 1.3 x 1.75 x 2.8 mm in size (Fig. 2) (McCallum and Mabarak, 1976b). The diamonds have been arbitrarily subdivided into two groups: 1) small diamonds and 2) microdiamonds. The small diamond group includes 24 crystals that are greater than 1 mm in size and 1 mg in weight. Microdiamonds are equal to or less than 1 mm in size and 1 mg in weight, and 54 have been recovered from the State Line district (Table 1). The total weight of the 78 diamonds is about 84 mg or approximately 0.42 carat. Small diamonds comprise nearly 64 mg or 0.32 carat of the total, whereas microdiamonds account for the remaining 20 mg or 0.10 carat (Table 1, Fig. 1).

*Publication authorized by the Director, U.S. Geological Survey.

TABLE 1. Weight as a function of size.

	Size mm*	No. of crystals	Average weight		Total weight	
			mg.	Carat	mg.	Carat
Micro-diamonds	<0.3	10	∿0.20	∿0.0010	∿2.0	∿0.0100
	0.3-0.5	22	∿.30	∿.0015	∿6.6	∿.0330
	0.5-1.0	22	∿.54	∿.0027	∿11.85	∿.0593
	Totals (ave.)	54	(∿0.38)	(∿0.0018)	∿20.45	∿0.1023
Small diamonds	1.0-1.5	15	1.60	0.0080	23.95	0.1198
	1.5-2.0	7	3.20	.0160	22.42	.1121
	>2.0	2	8.72	.0436	17.43	.0872
	Totals (ave.)	24	(2.60)	(0.013)	63.80	0.3191
	Overall totals (ave.)	78	(∿2.37)	(∿0.012)	∿84.25	∿0.4214

*Categorized according to largest dimension.

Recovery Procedure

Weathered kimberlite was collected in 50-100 pound (∿23-46 kg) samples from pipe surfaces; several samples were taken from each of the larger pipes (e.g., Sloan 1 and 2, Schaffer 13 and 15). The samples, which generally contain variable amounts of weathered granitic host rock material, were sieved through 3.3 mm and 1.5 mm screens. Material larger than 3.3 mm was scanned visually, but to date no diamonds have been recovered from this sample fraction. The 1.5-3.3 mm and <1.5 mm splits were run separately through a six-foot (∿1.85-meter)-long sluice with one-inch (2.54-cm) riffle spacing to concentrate the heavy mineral fraction. For each 50 pounds (∿23 kg) of sample processed, approximately 7 pounds (3.2 kg) of material was recovered, of which about 50 percent has a specific gravity of greater than 3.0 (McCallum and Mabarak, 1976b, p. 22). The sluice concentrates were dried and immersed in 52-percent hydrofluoric acid for from two to four weeks utilizing the method developed by Neuerberg (1975). In most runs the acid was changed every four to five days. After four weeks of treatment, most silicates are digested and only about 1 percent of the original sample volume remained (McCallum and Mabarak, 1976b). The residual, acid-insoluble fraction was run through a Franz magnetic separator[1] (side slope setting 20 degrees, front slope setting 23 degrees), that effectively removed most of the paramagnetic minerals. The remaining heavy mineral concentrate was then examined under a regular binocular microscope and suspected

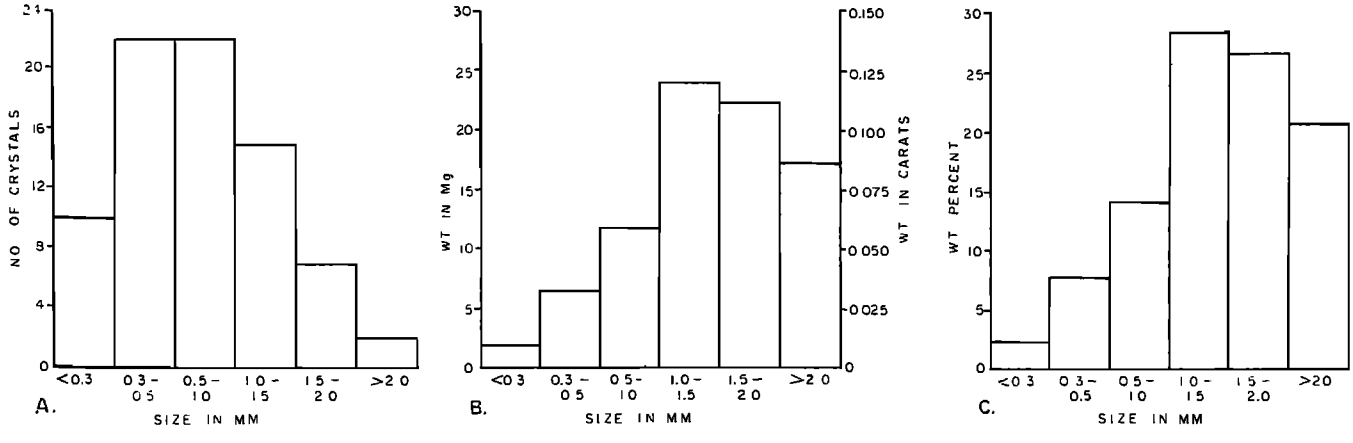

Figure 1. Size distribution of State Line diamonds. A. Number of crystals per size interval. B. Weight per size interval. C. Weight percent of total per size interval.

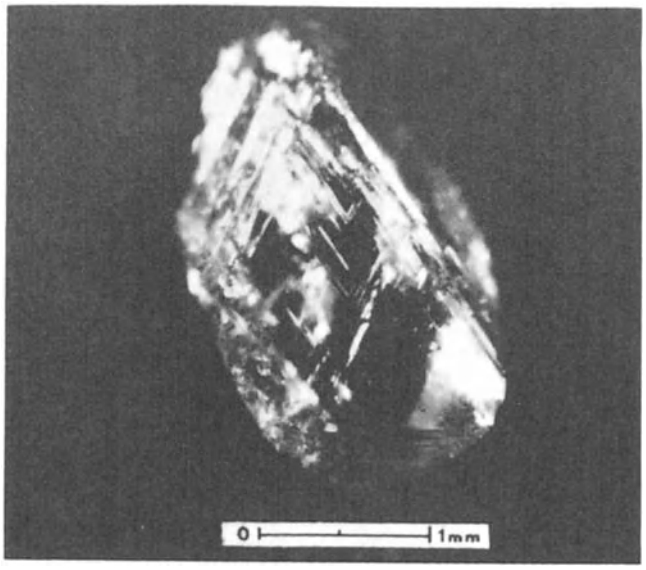

Figure 2. Distorted octahedral diamond from the Sloan 2 pipe. It weighs 11.8 mg (0.059 carat) and is the largest stone included in this report.

diamonds were tested under a polarizing microscope for isotropy and refractive index. Less fragile appearing diamonds were checked for hardness and a few of the first recovered crystals were X-rayed with a Gandolfi camera by W. N. Sharp of the U.S. Geological Survey. A number of crystals have also been examined by scanning electron microscope in order to better evaluate surface features.

Diamond Classification

The diamonds are described according to the six-fold classification of Whitelock (1973). This system is based on predominant crystal forms and subdivides stones into octahedra, rhombic dodecahedra, flattened dodecahedra, macles, aggregates, and irregular shapes. In addition, a seventh category of rounded crystals transitional between octahedra and dodecahedra is included. The assignment of crystals to the appropriate category necessitated the establishment of abritrary cutoffs determined by relative percentages of predominant versus subordinate forms. These assignments are somewhat similar but not identical to those developed by Whitelock (1973). For octahedral-dodecahedral forms, all crystals having more than approximately 75 percent {111} faces are classified as octahedra, whereas those with more than 75 percent {110} faces are designated dodecahedra. All crystals with intermediate combinations of {111} and {110} faces are assigned to the octahedra-dodecahedra transitional group, which is apparently comparable to the large intermediate category defined by Milashev (1965). Broken or partially formless crystals are classified according to the relative percentage of faces present or preserved. If the crystal exhibits more than 50 percent identifiable faces, it is assigned to the appropriate crystal form group; otherwise, it is designated as an irregular (broken or formless). This 50 percent cutoff is the same as that adopted by Harris and others (1975) as opposed to the 60-70 percent cutoff employed by Whitelock (1973).

TABLE 2. Morphological classification of State Line diamonds as a function of size.
[O = octahedra, O-D = transitional octahedra-dodecahedra, D = dodecahedra, F = flattened dodecahedra, M = macles, A = aggregates, I = irregular shapes, O/D = ratio of octahedra to dodecahedra, O/D^+ = ratio of octahedra to dodecahedra including O-D group with dodecahedra.]

	Size mm*	O	O-D	D	F	M	A	I	Total	O/D	O/D^+
Micro-diamonds	<0.3	5	1	0	0	1	2	1	10	---	5.0
	0.3-0.5	3	2	0	1	4	10	2	22	3.0	1.0
	0.5-1.0	4	6	0	1	2	9	0	22	4.0	0.57
	Totals (ave.)	12	9	0	2	7	21	3	54	(6.0)	(1.09)
Small diamonds	1.0-1.5	2	3	1	2	1	4	2	15	0.67	0.33
	1.5-2.0	3	1	1	1	0	1	0	7	1.5	1.0
	>2.0	1	0	0	0	0	1	0	2	---	---
	Totals (ave.)	6	4	2	3	1	6	2	24	(1.2)	(0.67)
	Overall totals (ave.)	18	13	2	5	8	27	5	78	(2.57)	(0.90)

*Categorized according to largest dimension.

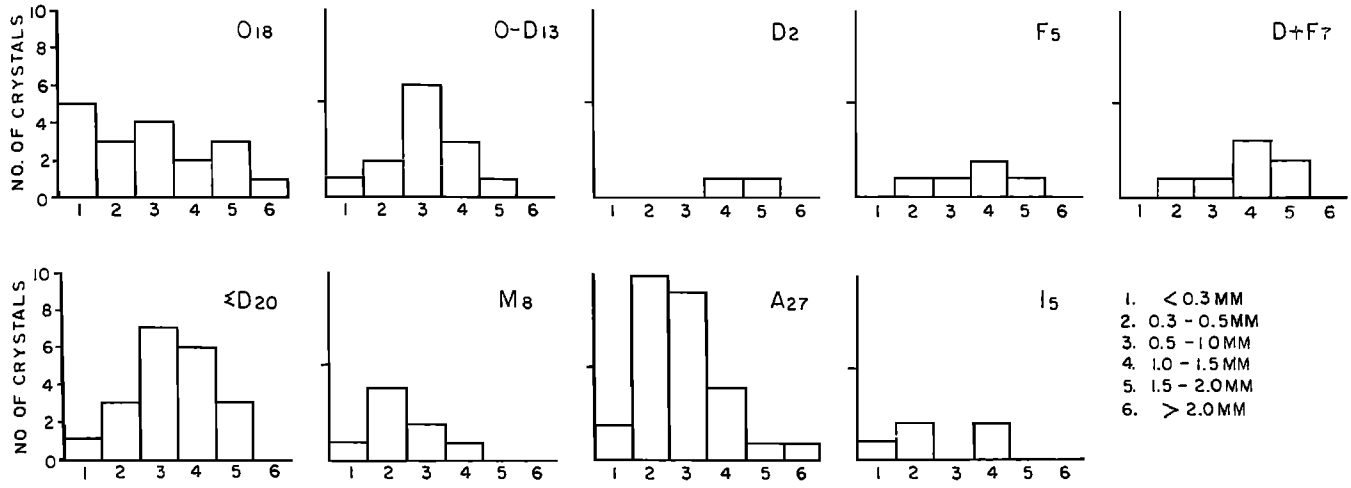

Figure 3. Crystal form as a function of size. Form symbols same as in Table 2 with the addition of D + F = dodecahedra and flats, and ΣD = total dodecahedral forms. Subscripts on form symbols indicate number of crystals of that type.

Aggregate types and octahedra predominate (27 and 18 diamonds, respectively--Table 2, Fig. 3). Most aggregates are comprised of octahedral forms and complex interpenetrations of octahedra. Transitional octahedra-dodecahedra types also are relatively abundant (13 stones) and, as with octahedra and aggregates, the majority are in the microdiamond group. All but one of the eight macles described are microdiamonds, as are three of the five irregulars. Dodecahedral types are the only crystal forms that predominate in the larger size fraction; both of the two regular dodecahedra and three of five flattened dodecahedra belong to the small diamond group (Table 2, Fig. 3).

General Morphological Features

To date, no attempt has been made to classify the diamonds in terms of Types Ia, Ib, or IIa, IIb. However, the presence of well-developed crystal forms in the majority of the diamonds suggests that most if not all of the stones are almost certainly of the general Type I variety.

Octahedral faces are the most common morphological feature of the State Line district diamonds. Most of the diamonds have at least a few octahedral faces; in octahedra, transitional octahedra-dodecahedra, and aggregate types these faces are generally abundant and well-developed. Dodecahedral faces, although subordinate to octahedral forms, are prominent in many of the aggregates as well as the various dodecahedra types. Many of the dodecahedral faces are characterized by the presence of fine ridges or seams along the short diagonals of the unit rhombs producing a partial development of tetrakishexahedral forms similar to those described by Whitelock (1973, p. 129).

Surface Features

Lamellar buildup of thin platelets (growth hillocks) on {111} surfaces is very prominent in many of the State Line diamonds, especially octahedral forms (Figs. 4 and 5). When platelet growth is nearly continuous across individual faces but with slight decreases in size, stepped surfaces develop and the crystals appear to be laminated (e.g., Figs. 4B, C, D, and 5A, C). Where layers are only partially developed on faces, triangular-shaped growth platelets or terraces are formed, similar to those described by Grantham and Allen (1960) and Whitelock (1973) (Figs. 4A, E, and 5B). Trigons (triangular shaped pyramidal or flat-bottomed depressions) are relatively common, particularly on {111} surfaces of octahedra (Fig. 4E), although they have also been observed in dodecahedral forms (Figs. 4B and F). The trigons are oriented in a reverse direction to that of the face on which they occur (Fig. 4E), and they are considered to be solution features (Franks and Lang, 1965). Natural etch pits ranging from regular to highly irregular shapes are present on the surfaces of many of the diamonds (Fig. 4F). The etch pits, commonly in association with abundant near-surface mineral inclusions (Figs. 4B, F), may give a corroded appearance to the crystal.

Octahedra

Octahedra (18 stones) include regular and distorted planar and laminated types (Figs. 2, 4A, C, D, E, and 5), and they grade into dodecahedral forms. Most of the octahedra exhibit pronounced lamellar buildup on {111} surfaces (Figs. 4 and 5), and the largest crystal recovered to date from the district is a 0.059-carat

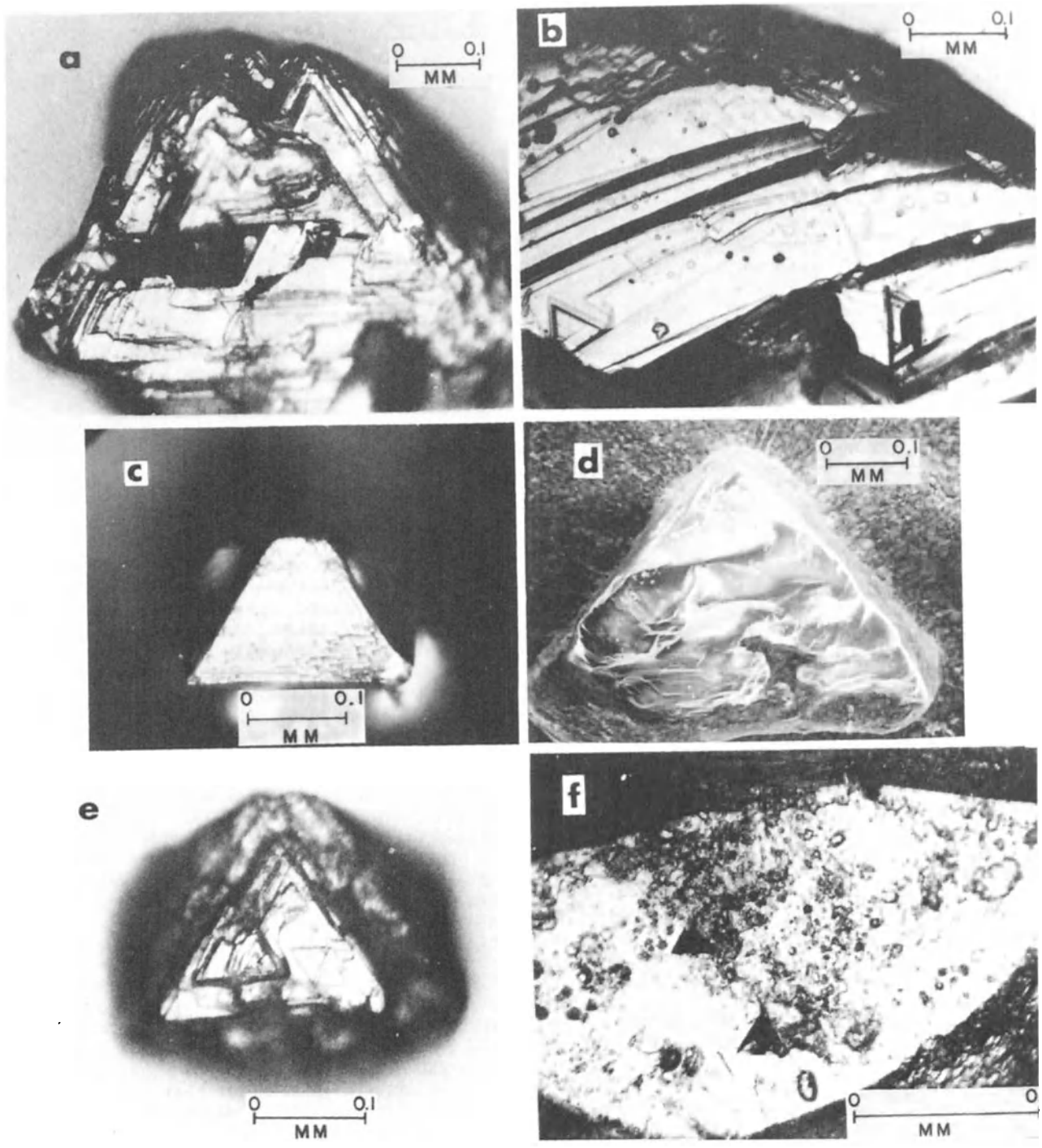

Figure 4. Lamellar buildup and surface features of {111} faces of diamonds from the Sloan 1 and 2 pipes. A. Triangular shaped growth platelets of a complex, distorted laminated octahedron. B. Growth lamellae and trigon (lower left corner) on a relict (111) face of a flattened dodecahedron (flat). C. Fine triangular platelets of a slightly distorted planar octahedron. D. Slightly curviplanar growth lamellae on an irregualr surface of a planar octahedron (SEM photo). E. Pronounced triangular platelets and trigons on built-up face of a laminated octahedron. F. Trigons and natural(?) etch pits on a relict (111) face of the flattened dodecahedron in B. (Note abundant tiny inclusions.)

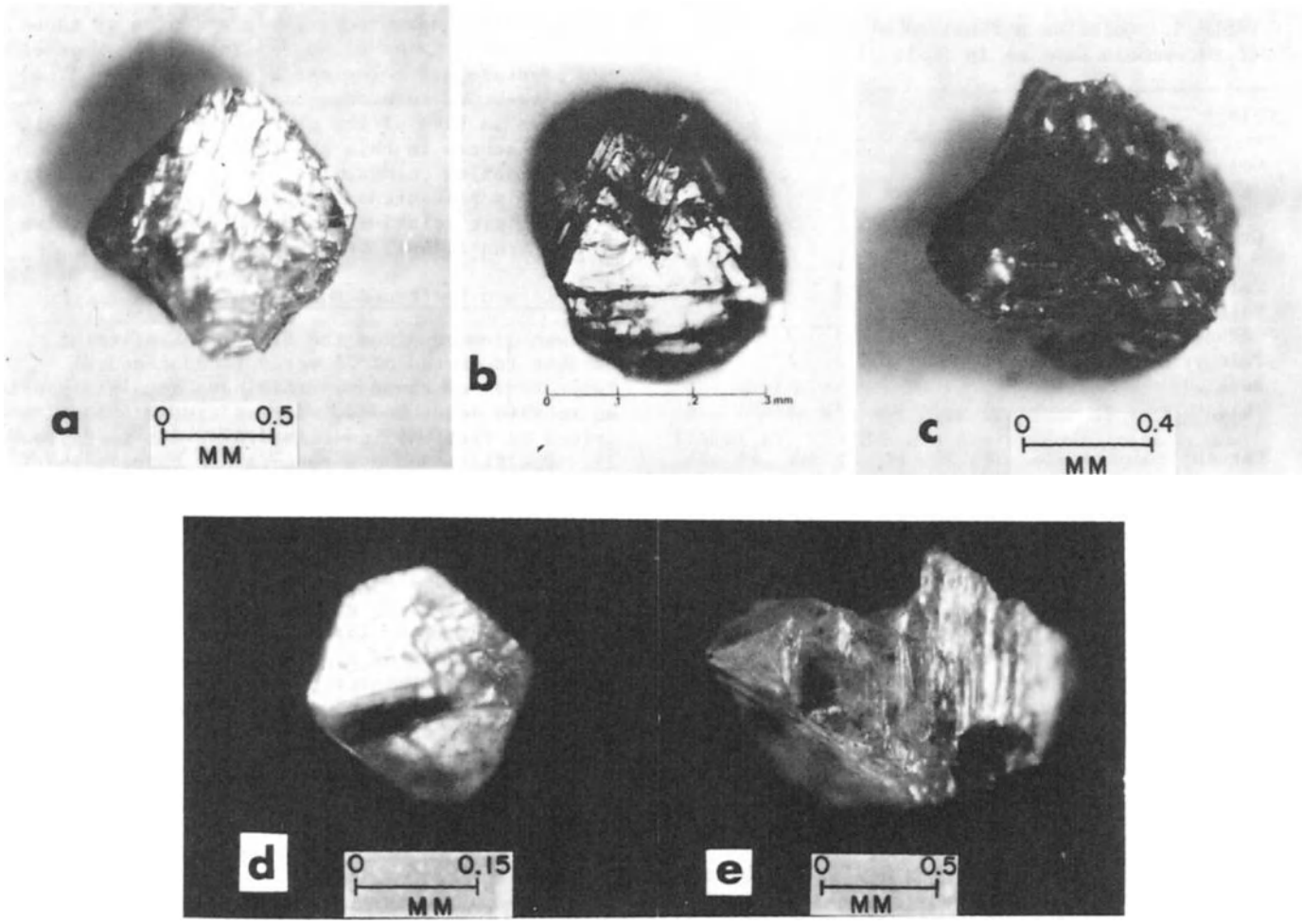

Figure 5. Octahedral forms. A. Regular laminated octahedron with well-developed triangular platelet buildup on {111} faces. B. Complex laminated octahedron with very pronounced triangular growth platelets that have produced incipient rounding of the crystal. C. Back side of laminated octahedron from A exhibiting dark coloration imparted by abundant small graphite (?) platelets along near-surface {111} cleavage planes. D. Slightly distorted regular planar octahedron. E. Broken distorted laminated octahedron showing prominent thin tabular inclusions of graphite (?) along {111} cleavage planes.

distorted octahedron with prominent growth platelets (Fig. 2). Well-laminated octahedra exhibit a rounded appearance that is caused by the progressive decrease in platelet size on {111} surfaces (e.g., Figs. 4E, and 5A, B, C). This platelet size decrease also gives rise to the formation of incipient dodecahedra at edge sites. Triangular growth platelets, trigons, and natural etch pits are well developed on many of the crystals. Although two-thirds of the octahedra (12) are less than 1.0 mm in size (microdiamonds), four of the nine largest crystals (>1.5 mm) of all diamonds recovered to date are octahedra (Table 2). Thirteen crystals of this group are colorless to glassy, but the remaining five range from white to pale orange brown, pale yellow, and dark gray (Table 3).

Coloration of the dark-gray crystal is imparted by the presence of small graphite(?) platelets along {111} cleavage surfaces (e.g., Fig. 4C). Octahedra are for the most part non-fluorescent, although three crystals fluoresce pale yellow and another three are bright yellow (Table 4). Most of the octahedra contain at least some tiny unidentified inclusions of both dark- and light-colored minerals (Table 5). Although these inclusions have not yet been definitely identified, it appears that at least garnet, olivine, and pyroxene are present. Several crystals are characterized by generally small black platey to flake-like mineral grains that parallel octahedral cleavage planes and appear to be concentrated near surface. These inclusions range up to nearly 0.3 mm in largest

TABLE 3. Color as a function of crystal form (form symbols same as in Table 2).

Color	O	O-D	D	F	M	A	I	Total
Colorless to glassy	13	8	1	3	6	15	3	49
White	2	0	0	0	1	2	0	5
Gray to gray white	0	0	0	0	1	5	0	6
Pale brown	0	1	0	1	0	3	2	7
Pale orange to orange brown	1	1	1	1	0	0	0	4
Pale yellow	1	3	0	0	0	1	0	5
Dark gray to black	1	0	0	0	0	1	0	2
Percent colored	28	38	50	40	25	44	40	37

dimension (e.g., Fig. 5E) and are thought to be graphite.

Transitional Octahedra-Dodecahedra

A complete transition between octahedra and dodecahedra is observed in the State Line district diamonds (Figs. 5 and 6). Octahedral forms become progressively more rounded as dodecahedral faces are developed (Fig. 6C). Many of the dodecahedral faces in the transition series show partial formation of tetrakishexahedral forms (Fig. 6D). Crystals of this transition category exhibit octahedral and dodecahedral faces in combinations with a maximum of 75 percent of one form and a minimum of 25 percent of the other. Two crystals of combined octahedral-dodecahedral face development are somewhat anomalous in that they show octahedral forms on one side of the crystal and dodecahedral forms on the other in a fashion similar to those described by Harris and others (1975). These do not exhibit the rounded nature and intimate interrelationship of face growth seen in the other transitional types, and they were both categorized as octahedra on the basis of a predominance of {111} faces.

Thirteen rounded octahedra-dodecahedra transition crystals were recognized, and nine of these are classed as microdiamonds (Table 2). Most of the crystals are colorless although pale-yellow and pale-brown to orange-brown colors were observed in five of the crystals (Table 3). All but two stones in this group fluoresce; eight exhibit yellow colors, whereas two are blue white and one is pale orange (Table 4). Mineral inclusions are relatively abundant in all but five of the transitional octahedra-dodecahedra.

Rhombic and Flattened Dodecahedra

Seven diamonds from the State Line district exhibit in excess of 75 percent dodecahedral faces. Two of these crystals have been classed as rhombic dodecahedra, whereas five are described as flattened dodecahedra or flats (Table 2). The flattened dodecahedra are characterized by one axis that is generally less than one-half the length of the other two. This distinction between dodecahedral types is comparable to that established by Harris and others (1975) who stated that rhombic dodecahedra when viewed at nearly right angles to a {110} face exhibit five "facets" with four in perspective, whereas in flats three of the five "facets" are dominant, producing a triplet of {110} faces centered about a [111] axis.

The two rhombic dodecahedra are both greater than 1 mm in diameter and one weighs approximately 4.5 mg (0.0225 carat). The larger of the two crystals is a very well developed pale-amber to white non-fluorescent dodecahedron (Fig. 6A). It exhibits thin lamellar growth platelets (octahedral lamellae) that converge on one of the triad axes, and small trigons are present on several faces. Numerous tiny mineral inclusions of unknown composition are concentrated in and near a small internal zone of amber coloration. The second rhombic dodecahedron is a broken fragment (Fig. 10, middle crystal, bottom row) (>50 percent of original) that is slightly more complex in nature than the crystal shown in Figure 6A. Relict octahedral faces are preserved (comprising less than 25 percent of the total faces) and poorly developed tetrakishexahedral forms are defined by fine ridges along the short diagonals of many rhombic faces. The crystal is

TABLE 4. Fluorescence as a function of crystal form (form symbols same as in Table 2).

Color	O	O-D	D	F	M	A	I	Total
Yellow to bright yellow	3	2	0	1	0	5	2	13
Pale yellow	3	6	0	2	0	3	1	15
Blue white	0	2	1	0	0	0	0	3
Pale orange	0	1	0	0	0	6	0	7
Non-fluorescent*	12	2	1	2	8	13	2	40
Percent fluorescent	33	85	50	60	0	52	60	49

*Most of the microdiamonds are non-fluorescent or very weakly fluorescent.

TABLE 5. Variation in abundance of inclusions as a function of crystal form.

Inclusions	O	O-D	D	F	M	A	I	Total
None	5	5	1	3	6	7	3	30
Rare < 5	3	2	0	0	0	6	1	12
Moderate 5-20	5	4	1	1	0	10	0	21
Abundant > 20	5	2	0	1	2	4	1	15
Total	18	13	2	5	8	27	5	78
Percent inclusion-bearing	72	62	50	40	28	74	40	38

clear to glassy and inclusion-free, contains numerous complex growth lamellae, and fluoresces blue-white (Tables 3, 4, and 5).

The flattened dodecahedra are characterized by rounded edges and curved to irregular elongated faces that locally are conchoidally fractured and pitted (e.g., Figs. 6E and F; Fig. 10, lower left corner; Fig. 11, upper right corner). Prominent growth lamellae are present on some surfaces (Figs. 4B and 6F), and trigons and natural etch pits are locally abundant (Figs. 4B and F). Three of the flats are greater than 1 mm in size whereas two fall into the microdiamond category (Table 2). The two smaller crystals are both colorless to glassy whereas the larger flats are glassy, pale brown, and pale orange (peach), respectively (Table 3). All flats show considerable brilliance, and three exhibit pale to bright-yellow fluorescence (Table 4). Only two of the flats contain inclusions, and most of these are clear to white. Clear mineral inclusions (possibly olivine) appear to be relatively abundant in at least one crystal (Fig. 4F).

Macles

Eight macles were recognized and all but one are classed as microdiamonds (Table 2). The macle category includes the generally flattened crystals that are twinned according to the spinel twin law (Fig. 7). In addition, thin tabular crystals that appear to be individuals of twins cleaved along the twin plane are also included in this category. Faces adjacent to the twin plane are characterized by re-entrant or proud angles converging on the twin plane seam (Fig. 7F). One strongly laminated macle exhibits a very pronounced herringbone pattern expressed by lamellae that converge and diverge on opposite sides of the twin plane (Figs. 7A and B). Several of the macles show a somewhat distorted triangular shape (e.g., Fig. 7C), although most typically express two regular triangular {111} faces paralleling one another across a spinel twin plane.

The macles are predominantly colorless to glassy. The only other varieties include one white and one gray-white crystal. All State Line macles recovered to date are non-fluorescent (Table 4), and most are free of inclusions (Table 5). Inclusions are present in only two crystals and are extremely small, though abundant.

Aggregates

Aggregate diamonds are those comprised of two or more crystals that have grown together either randomly, as interpenetrant twins, or as combinations thereof (Figs. 8, 9A, and 10, upper left and right corners; Fig. 11, lower left). Although intergrowths of octahedra predominate (Figs. 8B, D, and E), dodecahedral forms are also common (especially so in larger crystals) and generally occur in combination with octahedral forms (Figs. 8A and C). Lamellar platelet buildup is very prominent on many of the {111} faces present in the aggregates, and well-defined triangular platelets, trigons, and etch pits are locally abundant.

Many of the octahedra intergrowths are controlled by interpenetrant twin laws. The most common twin type involves a series of uniformly oriented intergrown octahedra that have mutually parallel "a" axes. The diamond in Figure 8E includes such a twinned intergrowth, although the twin penetrations are not well exposed in the viewing angle. A rarer interpenetrant twin type consists of the simple penetration growth of two planar octahedra that relate to one another by mutually inclined "a" axes (Fig. 9A). The twin law is apparently defined by a [111] axis. The twinned crystal shown in figure 9A is approximately 0.5 x 0.5 x 0.8 mm and is part of the first diamond recovered from a Colorado pipe. The stone was originally about 50 percent larger but was broken during testing (McCallum and Mabarak, 1976b, p. 25-26). The missing portion was a highly lustrous pale-brown irregular-surfaced overgrowth that completely engulfed the clear glassy twin aggregate.

Twenty-seven aggregate stones have been described, and most of these (21) are less than 1 mm in size (Table 2). However, the second largest diamond recovered from the district is a 5.63-mg intergrowth of irregular octahedra (aggregate size 1.25 x 1.5 x 2.25 mm). More than

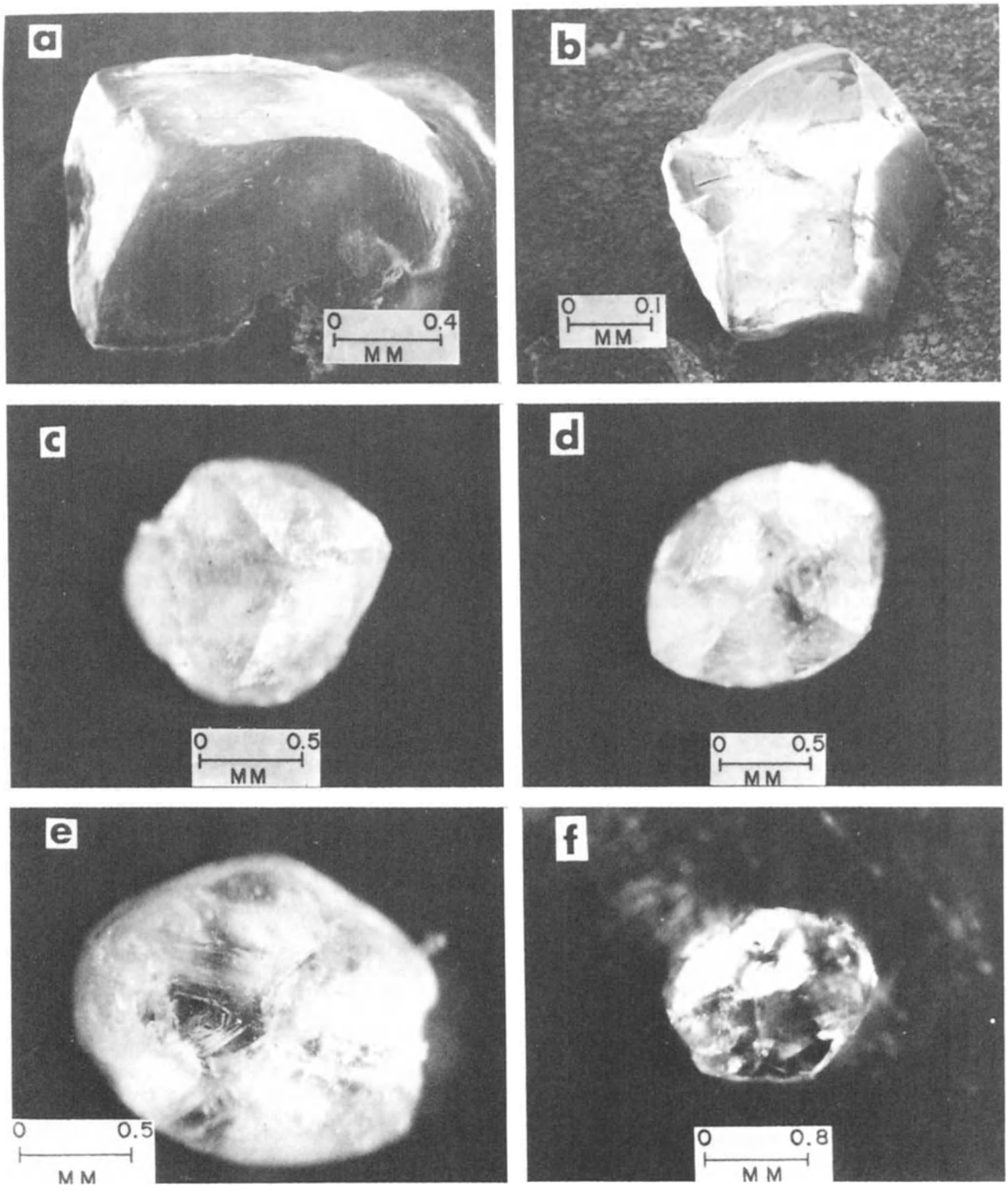

Figure 6. Dodecahedral forms. A. Rhombic dodecahedron showing triad and tetrad axes (SEM photo). B. Slightly distorted dodecahedron transitional from an octahedron (SEM photo). C. Triad view of a rhombic dodecahedron showing weak development of a partial tetrakishexahedral form. D. Rhombic dodecahedron showing moderately well-developed partial tetrakishexahedral form and poorly preserved relict octahedral faces. E. Rounded, flattened dodecahedron showing growth lamellae in a depression. F. Flattened dodecahedron showing pronounced growth lamellae.

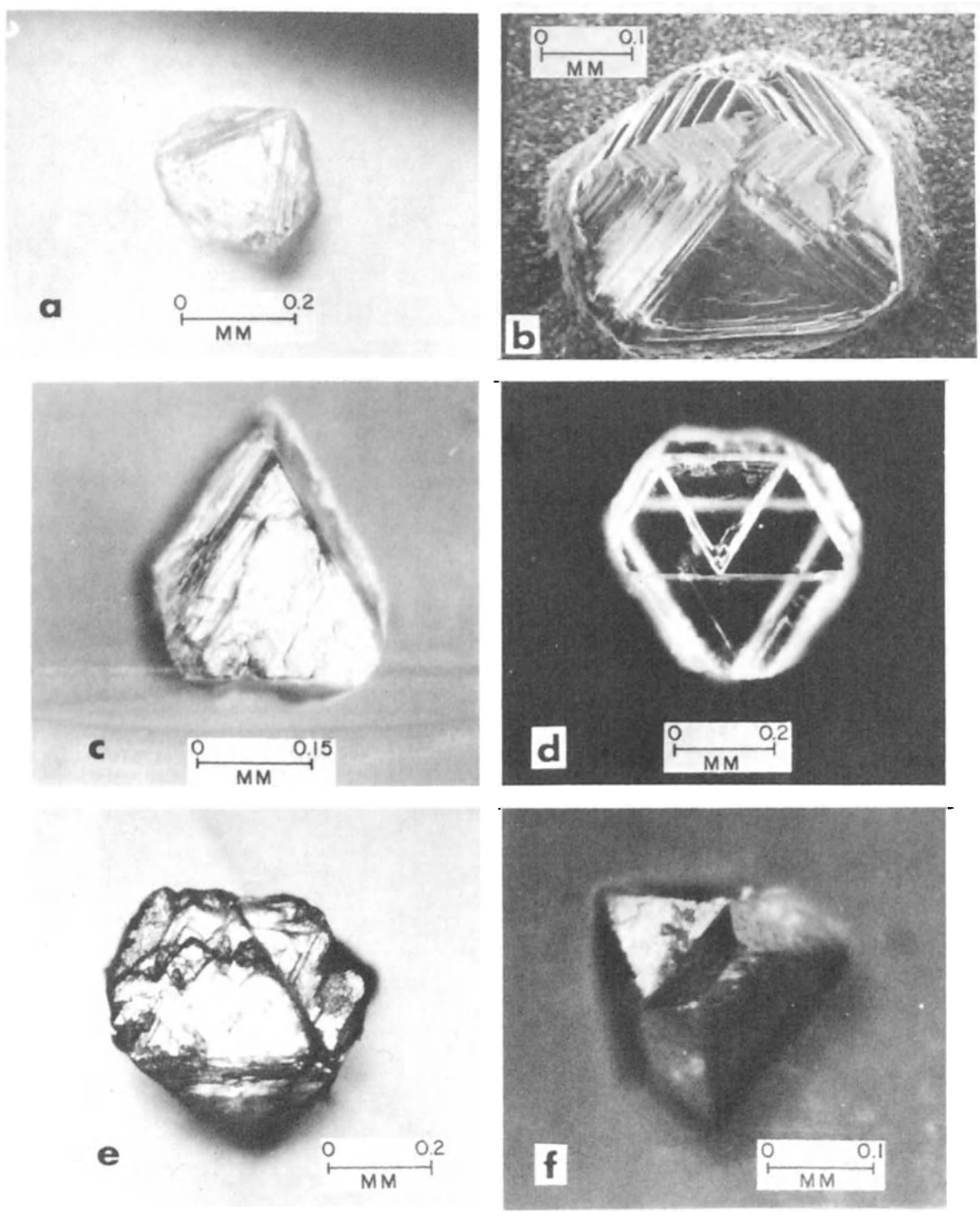

Figure 7. Macle forms. A. Laminated macle resting on (111) face paralleling twin plane. B. Laminated macle in A showing prominent "herringbone" pattern across the twin seam (SEM photo). C. Laminated triangular flat macle chip. D. Transparent glassy flat macle showing well-developed triangular growth platelet on (111) surface. E. Complex macle with irregular development of triangular platelets, resting on (111) face paralleling twin plane. F. Macle with planar octahedral faces exhibits pronounced re-entrant and proud angles along twin plane.

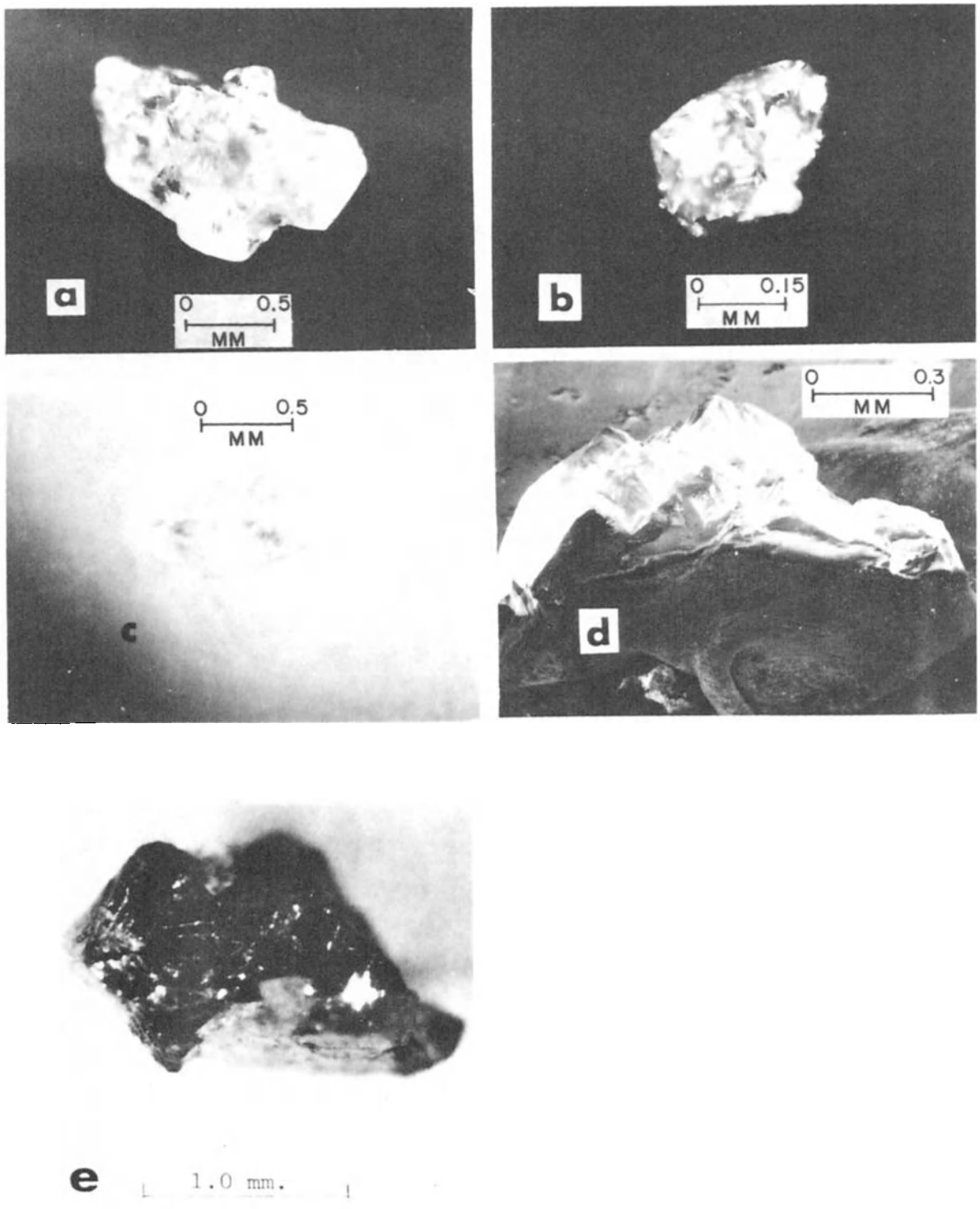

Figure 8. Aggregate forms. A. Elongated flattened dodecahedron penetrated by distorted octahedra. B. Multiple intergrowths of octahedra. C. Octahedra-dodecahedra intergrowths. D. Multiple intergrowths of octahedra (SEM photo). E. "Large" octahedra intergrown with smaller octahedra.

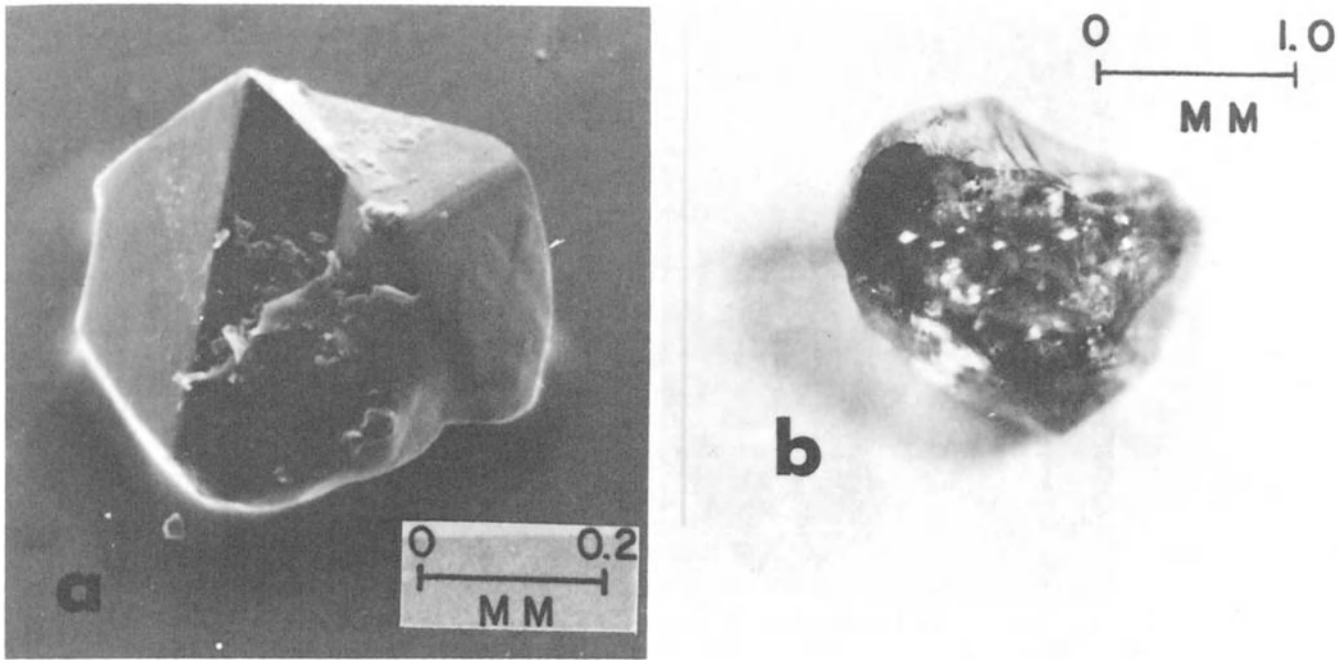

Figure 9. Penetration twin aggregate and irregular formless diamonds. A. Interpenetrant twin of planar octahedra from the Sloan 2 pipe (first diamond recovered from Colorado kimberlite) (SEM photo by R. B. Taylor, U.S. Geological Survey). B. Rounded irregular formless diamond.

half of the aggregate stones (15) are colorless to glassy; five are gray to gray white; and the remainder are white, pale brown, pale yellow, and dark gray (Table 3). Non-fluorescent varieties are most prevalent, but pale-orange to pale- and bright-yellow fluorescent colors are relatively common (Table 4). Aggregate diamonds contain the highest proportion of mineral inclusions of all diamond types (Table 5). The inclusions are typically very small (less than

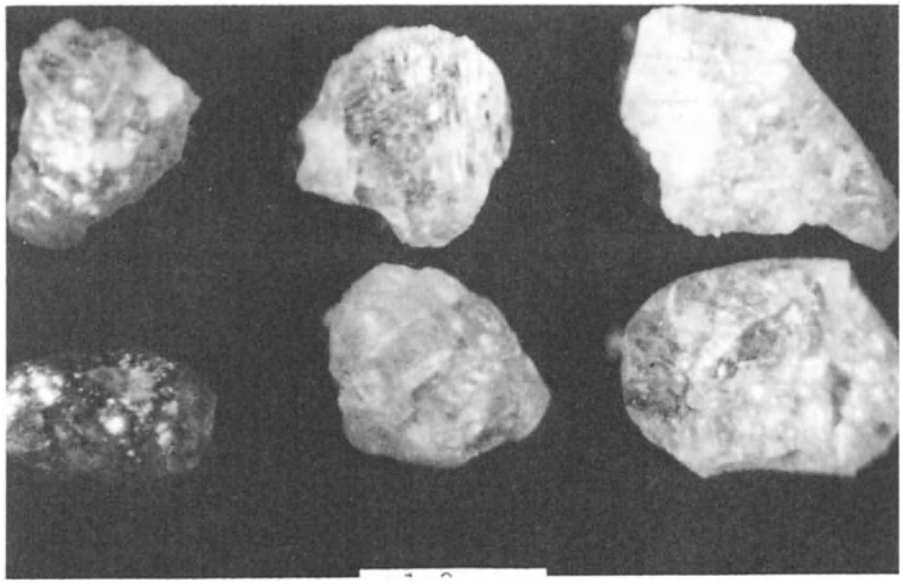

Figure 10. Representative diamonds from the Sloan 1 pipe (composite weight of the six stones is approximately 14.0 mg or 0.07 carat). Morphological types are as follows: Top row, left to right: aggregate; distorted, rounded laminated octahedron; aggregate. Bottom row, left to right: flattened dodecahedron; irregular shape (formless).

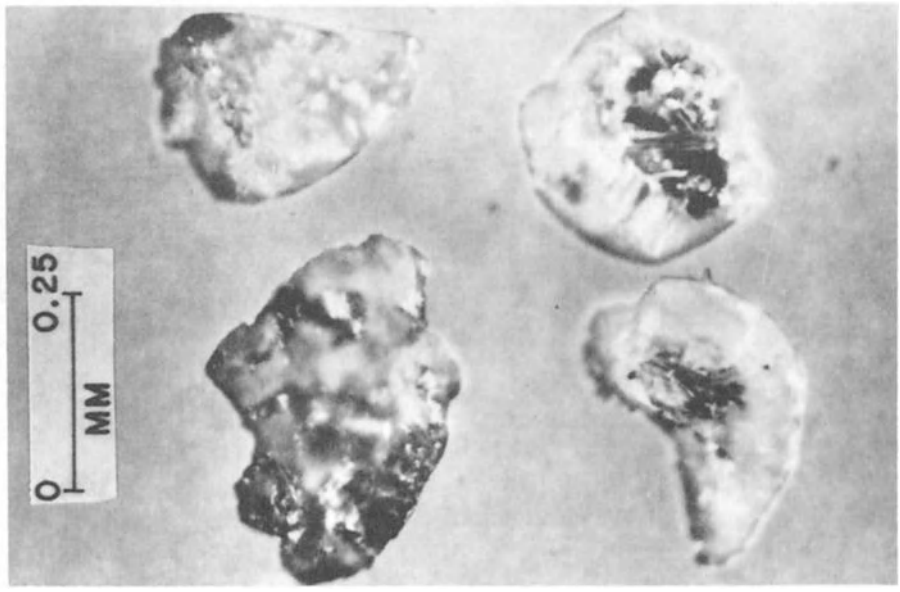

Figure 11. Representative diamonds from Wyoming pipes (composite weight of the four stones is approximately 2.0 mg or 0.01 carat). Morphological types are as follows: upper left, irregular shape (fragment); upper right, flattened dodecahedron; lower left, aggregate; lower right, irregular shape (fragment).

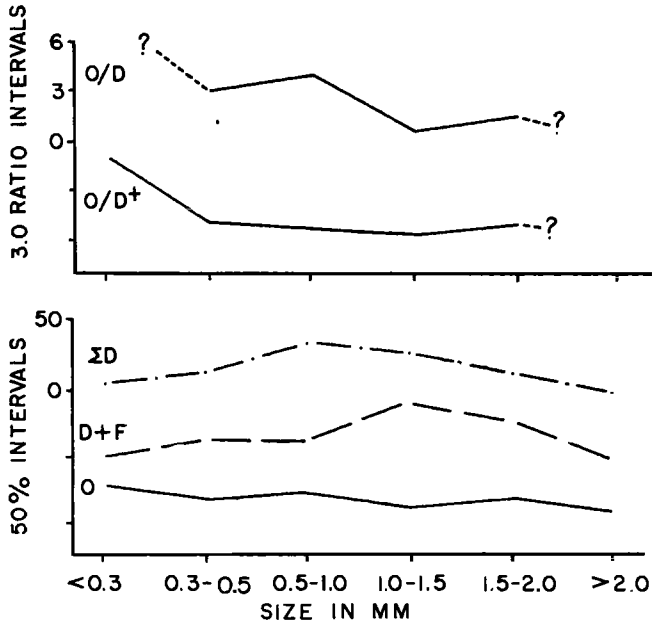

Figure 12. Variation curves showing size distribution of octahedral (O) and dodecahedral (D + F, ΣD)$_+$ forms and octahedra/dodecahedra ratios (O/D, O/D$^+$) (Form symbols same as in Table 2.) Small sample populations limit statistical application, especially in larger size range. Dashed and queried portion of octahedra/dodecahedra ratio curves reflect an absence of dodecahedra for the indicated size fraction.

0.1 mm) and, although their compositions have not yet been determined, many appear to be small flakes of graphite.

Irregular Shapes

Irregular-shape diamonds include both formless stones and fragments of other morphological types in which less than 50 percent of the crystal exhibits well-defined forms. Of the five diamonds assigned to this category, only one is essentially devoid of crystal faces (Fig. 9B). It has irregular rounded surfaces, shows growth lamellae on the margins of a local depression, and has abundant irregular shaped etch pits. This formless stone weighs 3.3 mg, is clear to glassy with zones of pale brown, fluoresces yellow, and is free of inclusions.

The four irregular fragments (e.g., Fig. 9B; Fig. 10, lower right; Fig. 11, upper left) appear to be pieces of octahedra and dodecahedra, but face distribution is not adequate to permit classifying these stones on the basis of predominant form type. Three of the fragments are less than 1 mm wide and are colorless; the single larger fragment is pale brown (Tables 2 and 3). The fragments are either non-fluorescent or fluoresce yellow (Table 4), and only one contains abundant inclusions (Table 5).

General Trends of Diamond Characteristics and Properties

Physical properties of the State Line diamonds show several general trends that may be indica-

TABLE 6. Color as a function of crystal size.

Size mm*	Colorless to Glassy	White	Gray to White	Pale Brown	Pale Orange to Orange Brown	Pale Yellow	Dark Gray to Black	Percent Colored
<0.3	9	1	0	0	0	0	0	10
0.3-0.5	16	1	3	2	0	0	0	27
0.5-1.0	11	2	2	1	2	4	0	50
1.0-1.5	8	1	1	2	1	1	1	47
1.5-2.0	3	0	0	2	1	0	1	57
>2.0	2	0	0	0	0	0	0	0
Total	49	5	6	7	4	5	2	37

*Categorized according to largest dimension.

tive of their growth evolution. It must be emphasized, however, that based upon the very low concentrations of stones, especially in the larger size range, these trends are apparent only; presentation of more quantitative data must await recovery of larger quantities of diamonds.

Crystal Form and Octahedra-Dodecahedra Ratios

The most prominent trend in crystal form is the apparent decrease in octahedra and increase in dodecahedra with increasing crystal size (Figs. 3 and 12). This trend is well reflected by macle distribution that also decreases with increasing crystal size, and plots of octahedra/dodecahedra ratios (Table 2, Fig. 12) strongly express the trend. Octahedra are more abundant in the microdiamond fraction, and octahedra/dodecahedra ratios show a general decrease with size (O/D = 6.0 for mircrodiamond versus 1.2 for small diamond); if the transitional octahedra-dodecahedra are included as dodecahedral forms, the resulting ratios (O/D^+, Table 2) are 1.09 for microdiamonds and 0.67 for small diamonds. This is just the opposite of octahedra-dodecahedra trends established for diamonds from several South African kimberlites (e.g., Whitelock, 1973; Harris and others, 1975), although Whitelock (1973, p. 30) reported that octahedra are more prevalent in the lower size range in non-quarry samples from the Kao,

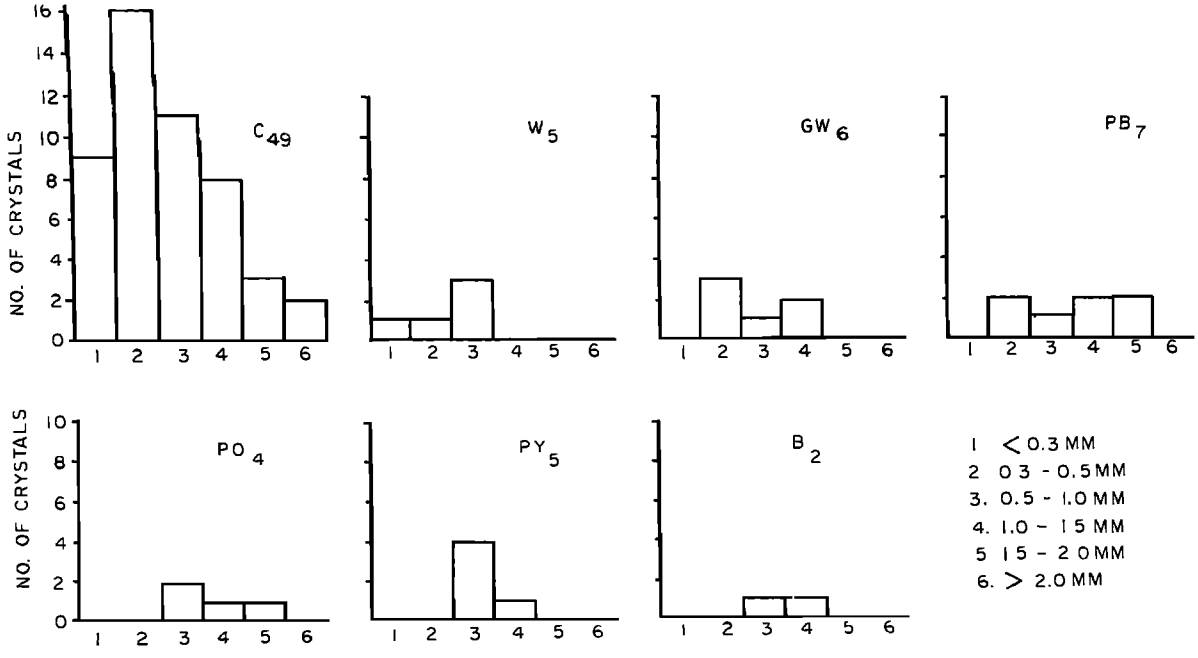

Figure 13. Color as a function of crystal size. C = colorless to glassy, W = white, GW = gray-white, PB = pale brown, PO = pale orange to orange brown, PY = pale yellow, B = dark gray to black. Subscripts on color symbols indicate number of crystals of that color.

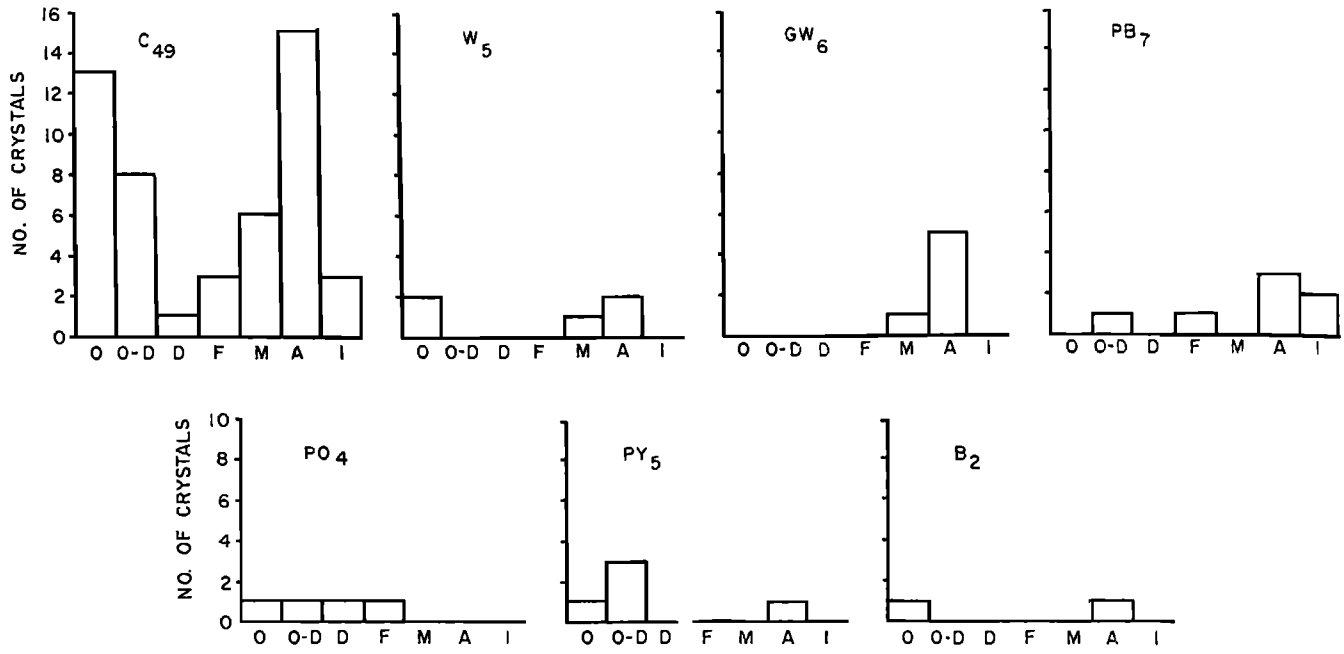

Figure 14. Color as a function of crystal form. Form symbols same as in Table 2, color symbols same as in Figure 13. Subscripts on color symbols indicate number of crystals of that color.

Lesotho, diamond district. However, comparison between distribution trends in Africa and State Line diamonds is probably meaningless, in that the smallest diamond included in the African studies is larger than the largest crystal used in the evaluation of Colorado-Wyoming diamonds.

Color

Thirty-seven percent of the diamonds are colored at least to some extent. In general, the percentage of colored diamonds appears to increase with increasing size in the microdiamond

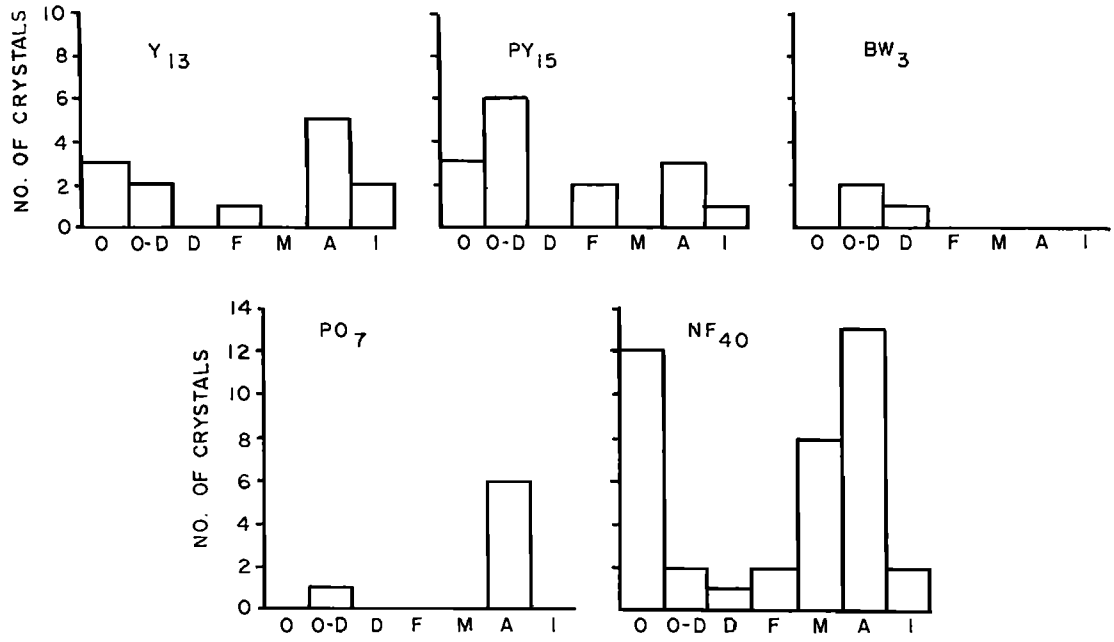

Figure 15. Fluorescence as a function of crystal form. Form symbols same as in Table 2. Y = yellow to bright yellow, PY = pale yellow, BW = blue-white, PO = pale orange, NF = non-fluorescent. Subscripts on color symbols indicate number of crystals of that color.

category and decrease slightly in small diamonds excluding the sample population of two in the >2.0-mm size range (Table 6, Fig. 13). Colored crystals comprise approximately 22 percent of the lowest two size fractions (<0.5 mm), but increase to 48 percent of the four larger size categories (0.5->2.0 mm). No one form exhibits a significant increase in percentage of colored stones over other forms; however, the macles and octahedra show the lowest concentration of colored varieties (Table 3, Fig. 14). Pale yellow coloration is restricted to stones having octahedral face forms (chiefly in the transitional octahedra-dodecahedra group).

Fluorescence

Nearly half the diamonds show some degree of fluorescence in ultraviolet light, shades of yellow being most abundant, especially in crystals with octahedral forms (Table 4, Fig. 15). Striking trends in fluorescence are evident for both transitional octahedra-dodecahedra forms and macles. The macles are uniformly non-fluorescent whereas 85 percent of the transitional octahedra-dodecahedra fluoresce (most pale yellow). In addition to the predominant pale- to bright-yellow colors, blue-white and pale-orange fluorescence colors were also observed. Blue-white coloration is restricted to transitional octahedra-dodecahedra and rhombic dodecahedra crystals, whereas pale-orange shades occur primarily in aggregate forms. Most microdiamonds are either non-fluorescent or only very weakly fluorescent.

Inclusions

Concentrations of mineral inclusions in the various diamond types exhibit no apparent significant trends, although macles contain the fewest inclusion of all stones (Table 5). Aggregates and octahedra contain the greatest number of inclusions. The inclusions range from extremely minute formless(?) blebs (<0.01 mm) of unknown composition to larger subhedral to nearly euhedral crystals as much as 0.3 mm in diameter. The larger inclusions range from colorless to pale green to black, and some have been tentatively identified as garnet, olivine, pyroxenes, and graphite. (Microprobe and X-ray analyses are planned for definitive identification.) Small black platelets of graphite occur along cleavage planes in some crystals. The graphite inclusions all appear to be concentrated near the surface of crystals and are probably the result of graphitization of diamond along planes of weakness (stress planes). Numerous minute, clear, rounded to irregular inclusions are abundant in some samples, and these may be olivine, although diamond has been suggested as a possibility for some (H. O. A. Meyer, 1977, pers. commun.).

Discussion

Although the sample population of diamonds evaluated from the Colorado-Wyoming State Line district is inadequate for reliable statistical treatment, a few semiquantitative trends that may be of some significance have evolved from the study of these stones. The most informative trend reflected by the State Line diamonds is probably that of increasing development of dodecahedral forms at the expense of octahedra. Octahedra/dodecahedra ratios range from O/D = 6.0 (or $O/D^{+} = 1.09$) for microdiamonds to O/D = 1.2 (or $O/D^{+} = 0.67$) for small diamonds (Table 2, Fig. 12). These trends coupled with the relative abundance of transitional forms indicate that most if not all of the State Line diamonds apparently formed originally as octahedra and many were later modified to dodecahedral forms. This agrees in principle with the view expressed as early as 1911 by Fersmann and Goldschmidt (quoted from Harris and others, 1975, p. 777) that dodecahedra are developed by resorption or solution processes operating on primary growth octahedra, a view that has been subsequently supported by the work of many others (e.g., Whitelock, 1973; Harris and others, 1975; Stolin and Gvozhdyara, 1971). Whitelock (1973, p. 138) has suggested that "all diamonds which form initially are primarily octahedra" and cited as supporting evidence the fact that primary growth features were observed only on octahedral faces of the diamonds he evaluated from several South African locations. Similar growth evidence has been observed on the State Line diamonds. Moreover, it is concluded that macles are also primary growth forms.

Color trends also appear to support the contention that octahedra and macles are primary forms. Most of the octahedra and macles, as well as aggregate stones with predominantly octahedral forms, are colorless to glassy (Table 3, Fig. 14). This trend is also reflected in large part by colors of fluorescence in ultraviolet light. Approximately two-thirds of the octahedra and octahedrally dominant aggregates are non-fluorescent, as are all of the macles. It is assumed that the early crystallizing diamonds were relatively free of impurities or contained nitrogen in platelets, a form of impurity that is common to colorless stones (Harris and others, 1975). This could also account for weak or nonexistent fluorescence colors. Initial coloration of many of the diamonds may have been caused by the introduction of small atomic aggregates of nitrogen associated with platelet nitrogen in a fashion similar to that described by Harris and others (1975, p. 780). Intro-

[1]Brand or manufacturers' names mentioned in this report are for descriptive purposes only and do not constitute endorsement by the U.S. Geological Survey.

duction of the aggregate nitrogen may be enhanced by environmental conditions that favor the transition to dodecahedra, and the presence of aggregate nitrogen may be at least in part responsible for the generation of fluorescence colors.

Clearly, considerably greater quantities of diamonds must be recovered before truly meaningful trends can be established for the diamonds in this district. However, the major objective of this paper is to report on the occurrence of diamonds in the Colorado-Wyoming State Line pipes and to indicate the general trends of physical properties observed in the stones recovered to date.

Acknowledgments. We wish to thank R. K. Johnson, V. P. Menzer, and C. T. Nadler, who helped with the tedious work of concentrating heavy mineral splits and recovering diamonds. Appreciation is also extended to Frank Yaussi and Jack Gegner for their cooperation and aid in recovering diamonds from the Sloan pipes. The manuscript has benefited from the thoughtful review of E. E. Foord, D. P. Gold, A. J. Gude, 3rd, and H. O. A. Meyer. The study was supported by the Earth Sciences Section of the National Science Foundation (contracts DES 74-13098 and EAR 74-13098 A01), the Wyoming Geological Survey, the U.S. Geological Survey, and the Colorado State University Development Fund.

References

Fersmann, A. von, and V. Goldschmidt, Der Diamant, Heidelberg University Library Publication, 1911.

Franks, F. C., and A. R. Lang, X-ray topography of diamonds, in Physical Properties of Diamonds, edited by R. Berman, Clarendon Press, Oxford, 1965.

Grantham, D. R., and J. B. Allen, Kimberlites in Sierra Leone, Overseas Geology and Mineral Resources, 8, 5-25, 1960.

Harris, J. W., J. B. Hawthorne, M. M. Oosterveld, and E. Wehmeyer, A classification scheme for diamond and a comparative study of South African diamond characteristics, Phys. Chem. Earth, 9, 765-783, 1975.

McCallum, M. E., and D. H. Eggler, Diamonds in an upper mantle peridotite nodule from kimberlite in southern Wyoming, Science, 4. 192, 253-256, 1976.

McCallum, M. E., D. H. Eggler, H. G. Coopersmith, C. B. Smith, and C. D. Mabarak, Colorado-Wyoming State Line kimberlite guide, Second International Kimberlite Conference, Santa Fe New Mexico, 1977.

McCallum, M. E., and C. D. Mabarak, Diamond in kimberlitic diatremes of northern Colorado, Geology, 4, 467-469, 1976a.

McCallum, M. E., and C. D. Mabarak, Diamond in State Line kimberlite diatremes, Albany County, Wyoming, Larimer County, Colorado, Geol. Surv. Wyo., Rept. Invest. No. 12, 36p, 1976b.

Milashev, V. A., Petrochemistry of the kimberlites of Yakutia and characteristics of their diamond mineralization, Leningrad, "NEDRA" publication (English translation by M. Constable), 1965.

Neuerberg, G. J., A procedure, using hydrofluoric acid, for quantitative mineral separations from silicate rocks, U.S. Geol. Survey Jour. Research, 3, no. 3, 377-378, 1975.

Smith, C. B., M. E. McCallum, H. G. Coopersmith, and D. H. Eggler, Petrochemistry and structure of kimberlites in the Front Range and Laramie Range, Colorado-Wyoming, Proceedings of the Second International Kimberlite Conference, in press.

Stolin, O., and P. Gvozhdyara, Morphological evaluations of synthetic diamonds after grading: in Proceedings International Conference on Application of Synthetic Diamonds in Industry, Kiev, 1971.

Whitelock, T. K., Morphology of the Kao diamonds, in Lesotho Kimberlite, edited by P. H. Nixon, pp 128-140, Lesotho Development Corp., Maseru, Lesotho, 1973.

II. KIMBERLITES: FIELD RELATIONS

GEOLOGY OF THE DOKOLWAYO KIMBERLITE AND ASSOCIATED PALAEO-ALLUVIAL DIAMOND DEPOSITS

J. Barry Hawthorne, Anthony J. Carrington, C. Roger Clement and E. Michael W. Skinner

Geology Department, De Beers Consolidated Mines Limited, Kimberley 8300, R.S.A.

Abstract. In 1973 prospecting in northeastern Swaziland resulted in the discovery of the diamond bearing Hlane deposits consisting of grits and conglomerates of Red Bed (upper Triassic) age in Karroo System rocks of the Lebombo monocline. Sedimentological studies of these deposits indicate that they have a westerly provenance. In 1975 the Dokolwayo diamond bearing kimberlite diatreme was discovered 30 km west of the diamond bearing sediments. This diatreme lies outside the present limits of the Karroo basin and has late Archaean, granite-gneiss wallrocks. The kimberlite contains numerous xenoliths of sedimentary rocks including coals. Palynological studies show that the sediments and kimberlite matrix are of predominantly Permian age. The xenoliths must have originated from overlying Karroo rocks which have slumped into the diatreme at the time of its formation; the overlying sediments having subsequently been removed by erosion. Apart from dykes and minor dyke enlargements no other diamondiferous kimberlites have been found between the Triassic diamond bearing sediments and the Dokolwayo diatreme. It therefore appears that the diamonds in the sediments were derived from the Dokolwayo diatreme which must have been emplaced between the Permian and Triassic Eras.

The Dokolwayo diatreme is elongate and has an irregular outline. It measures 2.8 ha at the surface and increases to 3.4 ha at a depth of 50 m. Petrographic and structural features indicate that the diatreme has a central core of kimberlite that was emplaced by essentially gas-solid fluidised intrusion which caused disaggregation of much of the xenolithic sandstone; large quantities of quartz and feldspar grains released during disaggregation are incorporated in the groundmass of the kimberlite. An earlier, narrow zone of porphyritic kimberlite occurs along the diatreme margins.

A comparison of the chemistry of garnets and spinels from the Dokolwayo kimberlite and the Hlane deposits supports the hypothesis that they have a common source.

The age and location of the Dokolwayo diatreme are discussed in relation to the structural framework of southern Africa and to kimberlite magma genesis.

Introduction

During 1973 exploration in northeastern Swaziland resulted in the discovery at several localities of diamond bearing grits and conglomerates of Red Bed (upper Triassic) age in the Karroo System sedimentary rocks of the Lebombo monocline. The richest and most extensive deposits occur within the confines of the Hlane Game Sanctuary (Fig. 1).

Sedimentological studies and paleocurrant analysis of the diamond-bearing beds suggest that these beds were deposited by an ancient river system flowing in a southeasterly direction. Further exploration carried out during 1975 in an upstream direction relative to the paleoslope resulted in the discovery of the Dokolwayo kimberlite diatreme some 30 km from the Hlane deposits.

Despite intensive exploration no other diamondiferous kimberlites, apart from dykes and minor dyke enlargements have been found in the area between the Dokolwayo diatreme and the diamond bearing sediments in the Hlane area.

The geology of the Hlane deposits is described and the possible relationship of these deposits with the Dokolwayo diatreme is evaluated. In addition results of the structure, petrography, xenoliths and mineral chemistry of the Dokolwayo kimberlite are presented. Investigations were directed towards elucidating the age of formation of the diatreme, the mechanism of its emplacement and the origin of the Hlane diamonds.

The Hlane Diamond Deposits

The Hlane palaeo-alluvial diamond deposits occur within the Red Beds near the top of the Karroo sedimentary sequence which lies in a 10 km wide belt along the Swaziland-Mozambique border (Fig. 1). Locally this sequence attains a thickness of about 1000 m. Table 1 shows the typical succession in the area.

The entire sequence lies within the eastern limb of the Lebombo monocline and dips eastwards at 10^{o}-12^{o}. A series of N-S trending faults downthrown to the west dislocates the sequence. The sediments are intruded by numerous dolerite dykes, dolerite sills and rare volcanic breccia plugs. The upper Karroo sediments are poorly ex-

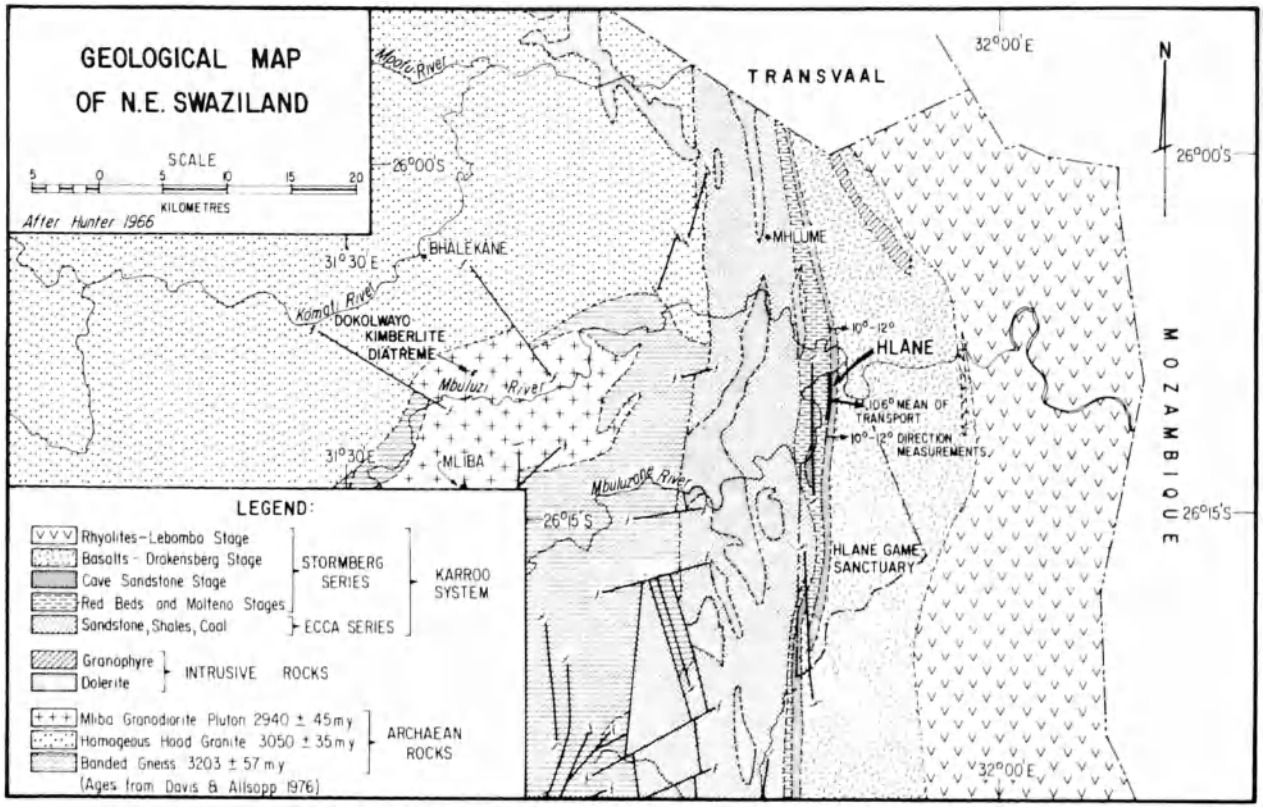

Fig. 1. Geological Map of N.E. Swaziland

posed and most field observations are from the twenty shafts, 1 km of tunnels and seventy-five boreholes sunk in the Hlane area; the ground surface is ± 230 m above sea level.

The suboutcrop of the main diamond bearing horizon has been traced 5 km north-south along the east bank of the Umbuluzane river. Its downdip extension has been established for 1.2 km to the east at a depth of 170 m below surface.

The highest concentrations of diamonds are found in two adjacent units of the basal sediments of the Red Beds. The lower unit is 0.4-2.0 m thick and consists of a sequence of upward-fining cycles of carbonate-cemented sediments that occupy a system of broad irregular undulating channels shallowly incised into a siltstone footwall. Each cycle consists of a basal conglomerate of pebble size and smaller carbonate and siltstone clasts set in a poorly sorted, muddy, grit matrix passing upwards into muddy crossbedded grits and ripple marked sandstones. This unit may consist of up to four cycles but these are rarely complete

TABLE I. Geological Column in N.E. Swaziland.

Stage/Series		Lithology	Thickness	Age
Lebombo and Drakensburg Stages	Stormberg Series	Rhyolites, basalts, agglomerates and stratified tuffs	> 3000 m	Triassic Jurassic
Cave Sandstone Stage		Massive aeolianite	70 m	Upper mid Triassic
Red Beds Stage		Siltstones	50 m	Upper mid Triassic
Molteno Stage		Fluvial sandstones and siltstones	40 m	Upper mid Triassic
Beaufort and Ecca Series		Sandstone, grit, shale and coals	800 m	Permian
Dwyka Series		Tillite	5 m	Upper Carboniferous
		Granite Gneiss		Archaean

*The lowest coals are found in the middle Ecca approximately 250 m above the base of the Karroo succession.

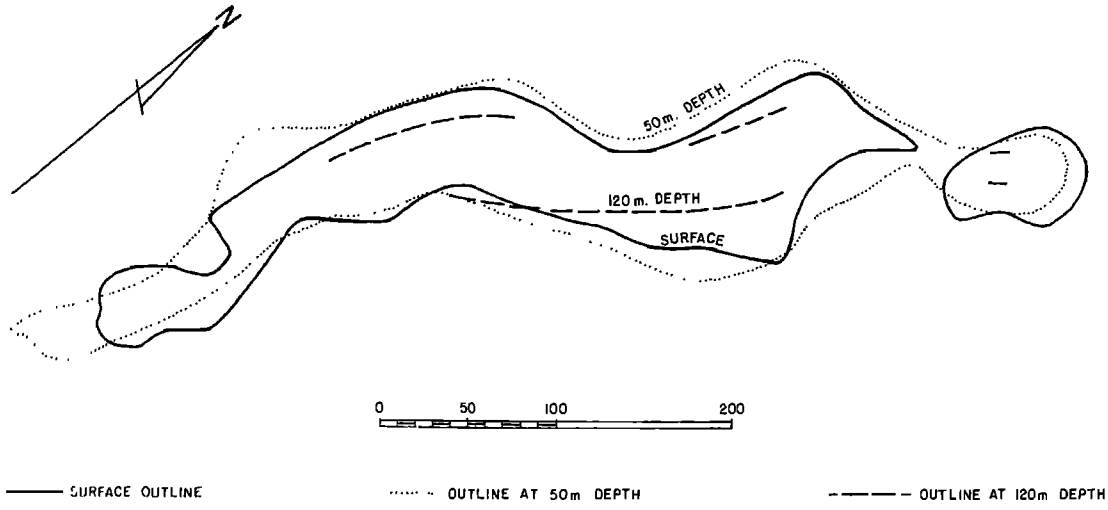

Fig. 2. Dokolwayo Kimberlite Diatreme

having apparently been truncated by pene contemporaneous erosion. The upper unit is 0.5-0.8 m thick and comprises a single sediment cycle lithologically similar to the cycles in the lower unit but perceptibly better sorted and less muddy. Heavy mineral-rich laminae are common and trough and avalanche crossbedding are the primary structures. The upper unit is of greater persistance than the lower unit, extending beyond the channel confines and lapping onto the channel interfluves.

The orientation of the incised channels containing the diamond bearing sediments and the foreset azimuths of the avalanche and trough cross-bedded units indicate that the deposits are derived from the westnorthwest. The vectoral mean of twenty-five directional measurement was 106° from true north with a consistency ratio of 64%.

Both units contain abundant kimberlitic garnet, less common chrome-rich spinel and rare chrome diopside. Non-kimberlitic garnet is present but rare. Diamonds are present in sufficient quantities to warrant detailed investigation of the deposit. The diamonds are moderately sorted, of small size (av. ± 0.008 cts) and include a high percentage of well formed crystals.

The high incidence of kimberlitic garnet in relation to non-kimberlitic garnet and the lack of clasts derived from the Archaean basement rocks suggests that the source of the diamonds and kimberlite-derived minerals was within the Karroo basin during the period of deposition of the Red Beds.

In summary, paleocurrent analysis and sedimentological studies indicate that the diamondiferous sediments were introduced from the westnorthwest by a braided stream system that shallowly incised a broad flood plain of poorly consolidated partly lithified and calcretised overbank sediments which were the source of the carbonate and siltstone clasts in the conglomerates.

No comparable palaeo-alluvial diamond deposits are known in southern Africa. In Siberia, palaeo alluvial diamond deposits of pre-Jurassic age have been found in the close vicinity of the Mir pipe (Rozhkov et al. 1967). These deposits are thought to have formed as a result of infilling of small lakes in depressions in the Ordovician limestones by stream-transported diamond-bearing sands and gravels. In the largest of these deposits, the Pyatachok, lenses of diamond bearing gravel are 1.5-2.4 m thick and the average diamond mass ranges from 0.035 carats to 0.05 carats. The diamond bearing horizons are overlain by clays and brown coals of Rhaetian/Triassic age.

TABLE II. Modal Analyses Representative Samples of Dokolwayo Kimberlite.

Kimberlite type	Central-clastic	Central-clastic	Tuffisitic vein+	Marginal porphyritic
Olivine (altered)	11	22	-	46
Quartz	32	20	54	-
Feldspar	4	6	6	-
Mica	-	7	-	30
Calcite	-	-	2	4
Serpentine	-	-	-	16
Opaque mins. & perovskite	-	1	-	4
Matrix*	34	21	36	-
Xenoliths	19	16	2	-

*Matrix - largely indeterminate, but apparently a mixture of clay minerals, mica, calcite and serpentine.

+Tuffisitic vein cutting central clastic kimberlite.

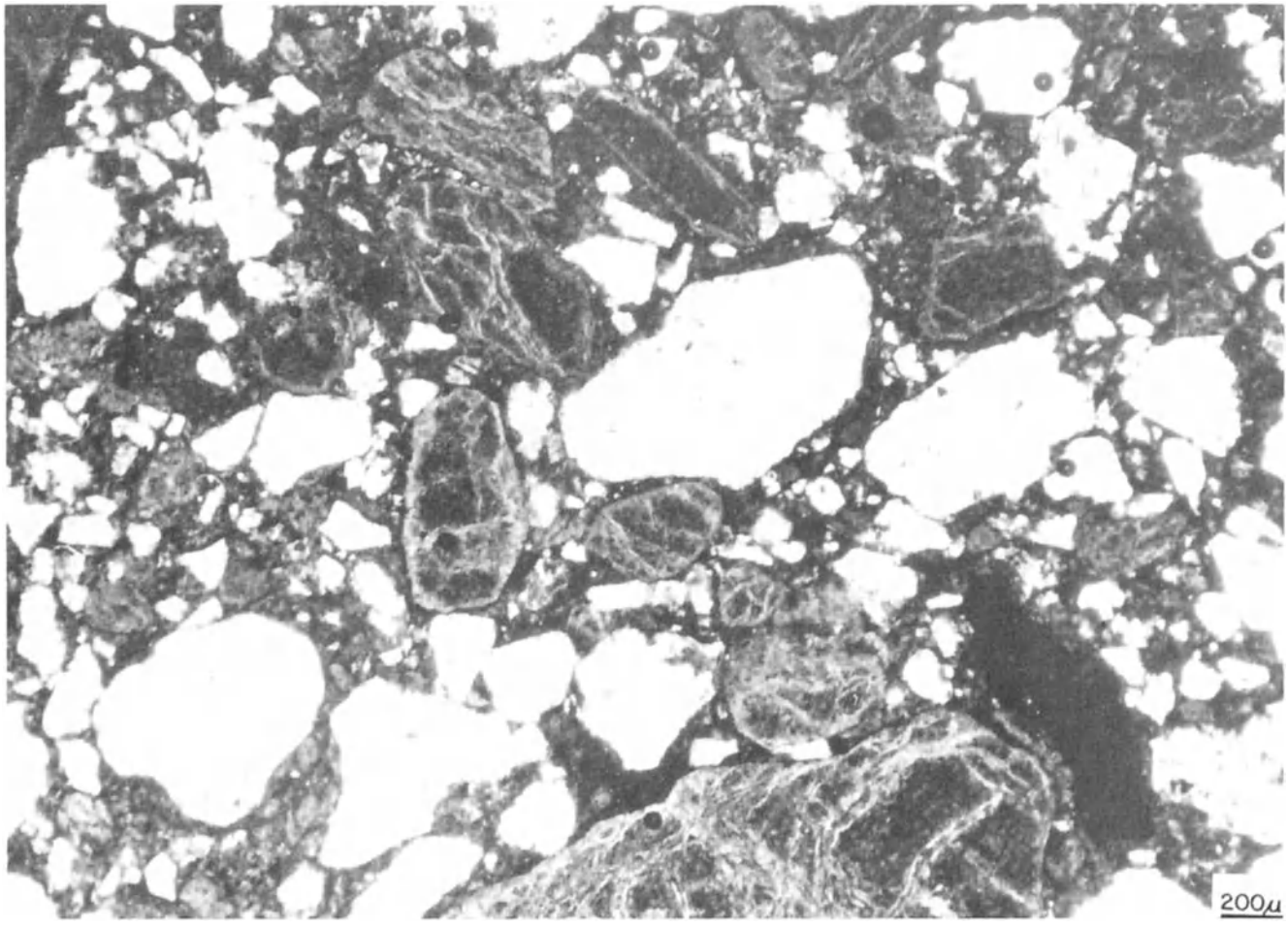

Fig. 3. Photomicrograph of Dokolwayo central clastic kimberlite showing clear light coloured sub-angular quartz and feldspar grains intermingled with anhedral and subhedral altered olivine grains set in a clayey matrix.

The Dokolwayo Kimberlite Diatreme

The Dokolwayo diatreme is located 2 km north of the eastward-flowing Mbuluzi river in northern Swaziland (Fig. 1) at a surface elevation of ±350 metres above sea level. Granite gneisses intruded by the diatreme form part of the Mliba granodiorite pluton (Hunter, 1966) and have been dated at 2940±45 my (Davies and Allsopp, 1976).

The kimberlite in the upper part of the diatreme is highly weathered and is covered by 1-2 m of grey-brown soils composed mainly of the weathering products of the surrounding granite gneisses. Diamond drilling, percussion drilling and pitting have shown that the diatreme is irregularly elongate in outline with steeply dipping walls. The surface area is 2.8 ha increasing to 3.4 ha at a depth of 50 m (Fig. 2). Determination of the pipe outline at a depth of 120 m is in progress.

Petrography

A series of polished slabs and thin sections have been cut from specimens of kimberlite drill cores obtained from depths of 50-120 m below surface. Petrographic examination of these specimens is hindered by severe secondary alteration which persists to the deepest explored levels. Nevertheless, it is apparent that the upper part of the diatreme contains two mineralogically and texturally different types of kimberlite.

The central part of the diatreme contains kimberlite characterized by a clastic texture and abundant xenogenic material. The xenogenic components range from large (>1 m) blocks of country rock to microscopic xenocrysts. The most prominent feature of the central kimberlite is the presence of abundant quartz and feldspar xenocrysts. Modal analyses (Table II) indicate that quartz and feldspar comprise between 25 and 40

vol. % of the rock. These xenocrysts reach 3 mm in size but the majority measure < 0.5 mm. Most of the grains are subangular or subrounded. Sharply angular, broken grains are present locally. (Fig. 3).

The quartz grains are generally clear and unaltered except marginally where replacement by calcite may be evident. Many show strained extinction and recrystallization features. Adjacent grains in microxenolithic quartz aggregates commonly have sutured contacts. The feldspar grains are altered to varying degrees having been partly carbonatized and/or sericitized. Small quartz-feldspar microxenoliths are present but are uncommon.

Also prominent are numerous completely altered olivine grains which reach several millimetres in size. Both relatively large anhedral macrocrysts (>1 mm) and euhedral phenocrysts (<0.5 mm) are represented. Broken grains are common. The altered olivine content varies considerably (even within a single thin section) ranging between 10 and 30 vol. %. The most common alteration or replacement products are a micaceous clay mineral, serpentine and calcite.

Although no rounded garnets were seen in thin section, hand specimens contain rounded garnets with thick kelyphitic rims. Rare angular or subangular garnet grains (0.1-0.5 mm) appear to be broken fragments of original kimberlitic and/or non-kimberlitic macrocrysts and are devoid of kelyphite rims. Small (<0.3 mm long) laths of mica, mostly phlogopite, occur scattered throughout the rock.

Microxenolithic fragments include extremely fine grained, altered, quartz-rich sedimentary material and numerous small coal fragments, commonly traversed by thin calcite veinlets and stringers. Small fragments, compositionally and texturally similar to the host rock, but commonly of finer average grain size and containing relatively abundant phlogopite also occur. These

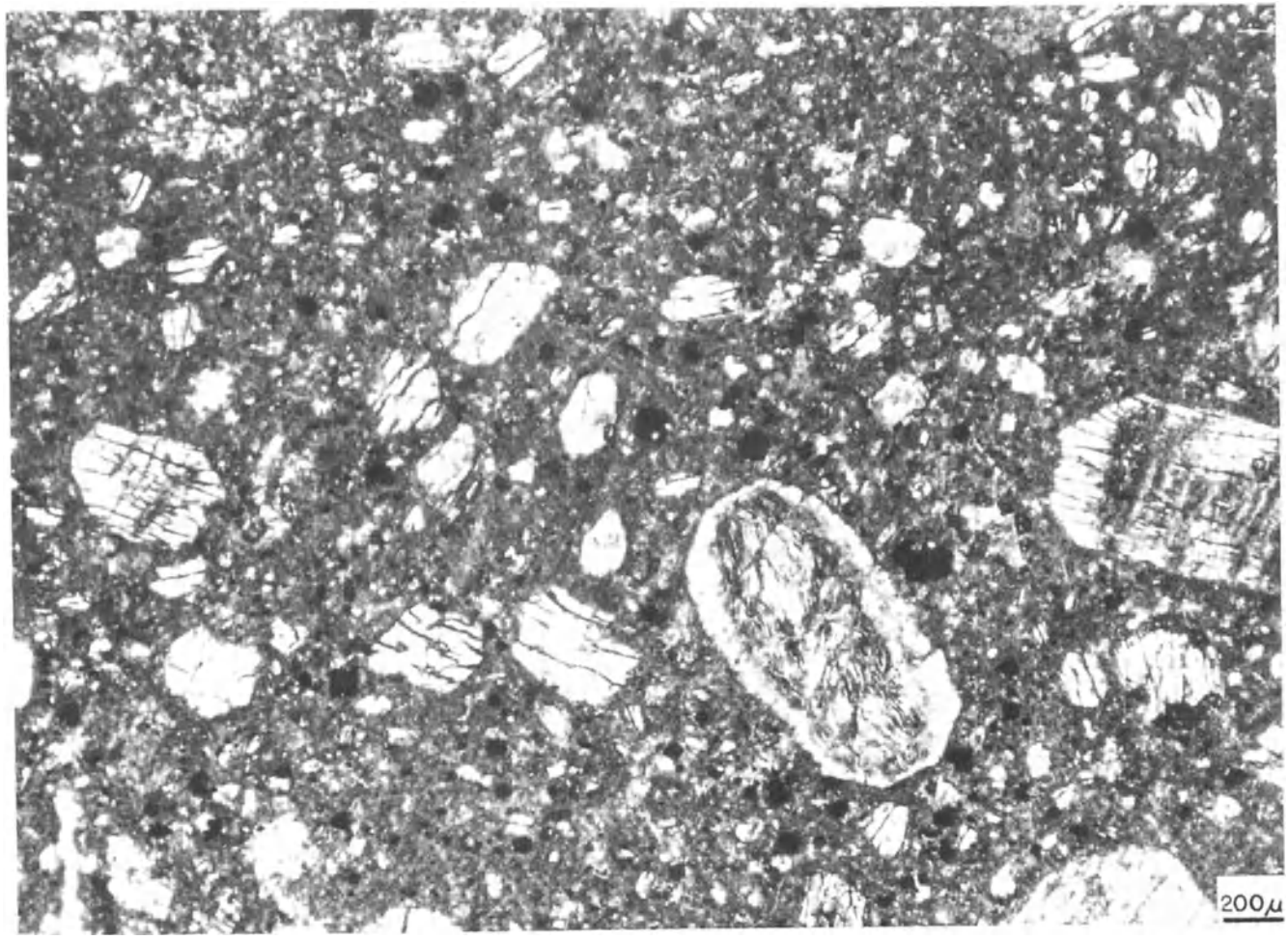

Fig. 4. Photomicrograph of Dokolwayo marginal porphyritic kimberlite showing altered olivine grains set in a matrix of phlogopite, serpentine, carbonate, opaque oxides and clay minerals.

TABLE III. Pre-Cretaceous Kimberlites in Southern Africa.

Locality	Age in my	Method
Swartruggens dykes	150±3	Rb-Sr*
Middelpunt dyke	165±10	Rb-Sr[1]
Dokolwayo diatreme	190±270	Field Relations
	300±20	U-Pb*
Colossus "	490±20	Rb-Sr*
Beit Bridge "	730±60	Pb-Pb*
National "	1180±30	Rb-Sr*
Premier "	1200±1250	Rb-Sr*

*Allsopp & Kramers, 1977
[1]Allsopp & Kramers, (private communication)

must be derived from one or more earlier generations of clastic kimberlite. Fragments of porphyritic kimberlite are also present and are locally abundant. In such areas, an increase in the abundance of kimberlite fragments is accompanied by concomittent decrease in quartz and feldspar grains. The minerals and rock fragments are set in a highly altered, intimately mixed matrix of finely comminuted quartz and feldspar fragments, fairly abundant minute shreds and laths of mica, reddish brown iron oxide weathering products, calcite and considerable yellow-brown clayey material.

In contrast to the central area the marginal parts of the diatreme contain porphyritic kimberlite with numerous altered olivine crystals and scattered small (seldom > 5 cm) wallrock xenoliths set in a greyish-green aphanitic matrix (Fig. 4). Examination in thin section reveals two morphological varieites of altered olivine. Large (1-15 mm), anhedral, commonly rounded, sometimes irregular or broken macrocrysts contrast strongly with smaller (< 0.1-2.0 mm) pseudomorphs of euhedral olivine phenocrysts. Following the interpretation of Boyd and Clement (in press) most of the anhedral macrocrysts commonly present in kimberlites are considered to be xenocrysts derived from upper mantle peridotitic rocks. Olivine in the marginal kimberlite has been completely replaced by talc, serpentine, calcite and clay minerals.

The most abundant groundmass mineral is phlogopite (Table II), and the rock is classed as a phlogopite kimberlite (Skinner and Clement, 1977). Much of this mica occurs as fine-grained (<0.1-0.3 mm), irregular, partly altered plates and laths but euhedral crystals are also present. Locally, the grains occur in irregular aggregates. The bulk of the remaining groundmass consists of serpentine, much of which occurs as an alteration product of phlogopite. Serpentine also occurs in veinlets traversing the rock. Rare elongate to acicular small grains (0.1 mm long), now consisting mainly of serpentine have "ghost" morphology and cross partings suggesting the original presence of apatite.

Calcite occurs locally in the groundmass as small aggregates of anhedral grains (commonly <0.1 mm in diameter) and as scattered larger (up to 0.2 mm) subhedral grains. Scattered opaque minerals occur throughout the groundmass as equant, sometimes euhedral grains, ranging in size from <0.1 mm to about 0.25 mm. The profiles of many of the larger opaque grains are characterized by numerous re-entrants indicative of complex aggregates. Perovskite is a rare component of the kimberlite.

In addition to wallrock xenoliths, a few small fragments of earlier generation porphyritic kimberlite are evident. No kimberlitic garnets have been noted in thin section but they are undoubtedly present in the marginal kimberlite.

Xenoliths

Most of the numerous xenoliths found in the Dokolwayo kimberlite are granite gneiss, granodiorite, sandstone or siltstone. Many small coal fragments are found in close association with the sandstones and appear to be restricted to the clastic kimberlite in the core of the diatreme.

The granitic xenoliths resemble similar rock types found within the Mliba Pluton and it is assumed that they are derived from the diatreme walls. They have no particular significance in relation to the age of emplacement of the diatreme. Xenoliths of sedimentary rock have an important bearing on the age of emplacement of the kimberlite as they must predate the formation of the diatreme and have been derived from overlying strata removed by erosion after the formation of the diatreme. Sandstones are the most common type of sedimentary xenolith and they are usually fine to medium grained, dark grey to white, moderately to poorly sorted, quartz rich and partly silicified. The sand grains are generally angular to subrounded and unsilicified material has a clay carbonate matrix. The content of opaque minerals is low. The less common siltstones are cream to yellow in colour and are fairly friable. Coal xenoliths are brecciated, veined by calcite and somewhat oxidised. Many of the sandstone xenoliths have highly irregular margins and appear to have been "frozen" in the kimberlite matrix whilst in the process of becoming disaggregated.

The abundance of quartz grains in the clastic kimberlite probably reflects extensive disaggregation of sandstone inclusions and erosion of sandstone wallrocks during fluidized intrusion. Quartz grains are highly concentrated in the later tuffisite veins within the clastic kimberlite, and this may be due to mechanical disintegration and winnowing out of less resistant material.

Palynological studies of shale and coal xenoliths and kimberlite matrix were carried out at the Bernard Price Institute for Palaeontological Research, Johannesburg. A diverse fossil miospore assemblage of predominantly lower Permian age was identified (R. Falcon, private communication). It follows that the Dokolwayo clastic kimberlite

must have been emplaced in post lower Permian times.

The nature of the coal xenoliths also provides data regarding the temperature of formation of the clastic kimberlite. Vitrinite reflectance measurements carried out on samples at the laboratories of the Societe Nationale des Petroles d'Aquitaine at Pau, France, gave a value of 1.32 which suggests that the coal xenoliths had not been subjected to temperatures in excess of 250°C. This temperature was established by comparative studies of coals that have been slightly metamorphised by dolerite sills. Commenting on these results, D.M. Rowsell (private communication) states: "In a 'normal' sedimentary basin without any effects of intrusions, a vitrinite reflectance of 1.32 would correspond to a paleotemperature of about 140°C, but in cases such as your kimberlite (or in dolerite contact zones) a higher temperature maintained for a shorter time will have the same effect. I have no disagreement with S.N.P.A.'s conclusion, although if the kimberlite was able to cool much more quickly than a dolerite sill, the temperature might have been slightly higher. In any case it seems safe to say that it could not have been more than about 300°C."

Karroo dolerites and Stormberg lavas have not been found as xenoliths in the Dokolwayo kimberlite These two distinctive, resistant rock types are common xenoliths in many central and southern African kimberlites (Hawthorne, 1975). Their absence lends support to the view that the Dokolwayo diatreme predates the late Triassic period when Stormberg volcanic activity was initiated in southern Africa.

So far, no ultramafic xenoliths have been found in the Dokolwayo kimberlite. However, compositional studies of the kimberlitic garnets suggest that these garnets may have been derived from the disaggregation of eclogite and garnet lherzolite.

Diatreme Formation

In attempting to interpret the mode of formation of the Dokolwayo diatreme two important factors must be considered. Firstly, the diatreme has been subjected to considerable erosion since the time of its formation and, secondly, it is clearly the result of multiple episodes of intrusion which resulted in the emplacement of kimberlites of widely different character.

The presence of abundant xenoliths derived from Karroo strata that are no longer preserved in the area is strong evidence of substantial erosion. A deep level of erosion also is supported by the irregular shape of the body, the approach towards dyke-like form at the present exposure surface, the presence of outward-dipping contact zones, and the presence of "blind" areas where kimberlite failed to penetrate to the present surface (Fig. 2). These features are directly analogous with the deeper parts of the Kimberley pipes (Hawthorne, 1975).

The central kimberlite is best classified as a tuffisite-breccia, interpreted as resulting from turbulent, essentially gas-solid, fluidized intrusion. Evidence supporting this mode of emplacement is summarized below :-

1. The clastic texture of the rock.

TABLE IV. Analyses of Garnets and Spinel from Dokolwayo(D) and Hlane(H).

		Mean Chemical Compositions												
Garnet		Al_2O_3	St.d	FeO	St.d	TiO_2	St.d	CaO	St.d	Cr_2O_3	St.d	MgO	St.d	No. of grains analysed
Colour Range														
Mauve	D	17.6	1.37	6.4	0.88	0.1	0.11	6.2	0.87	7.3	1.50	19.4	1.04	49
	H	20.5	0.83	7.3	0.67	0.4	0.16	4.7	0.21	3.2	0.68	20.5	0.49	50
Cerise	D	20.5	0.83	7.3	0.67	0.4	0.16	4.7	0.21	3.2	0.68	20.5	0.49	48
	H	20.7	0.69	7.2	0.75	0.3	0.13	4.9	0.34	4.0	0.80	20.4	0.58	51
Pink	D	21.0	0.84	7.1	0.40	0.3	0.09	4.6	0.19	2.4	0.70	21.2	0.52	50
	H	21.1	0.67	7.1	0.34	0.3	0.18	4.6	0.28	3.1	0.69	21.1	0.33	28
Red	D	20.9	0.83	8.3	1.05	0.7	0.31	4.5	0.23	2.1	0.67	20.4	0.86	50
	H	21.1	0.74	8.2	1.26	0.7	0.28	4.6	0.20	2.4	0.76	20.8	1.03	50
Dark Orange	D	21.7	0.58	9.8	1.05	0.9	0.18	4.0	0.43	0.4	0.30	20.0	0.75	50
	H	22.1	0.52	10.0	1.87	0.9	0.24	4.2	0.63	0.5	0.43	19.7	1.46	51
Pale Orange	D	22.0	0.44	10.5	1.50	0.8	0.18	3.8	1.05	0.2	0.14	19.5	1.50	52
	H	22.9	0.45	11.4	2.50	0.3	0.23	4.5	1.51	0.1	0.13	18.2	2.50	50
Straw	D	22.9	0.75	11.5	4.89	0.3	0.17	4.5	2.13	0.3	0.33	18.5	4.65	22
	H	23.2	0.36	10.1	2.88	0.1	0.08	4.6	1.38	0.2	0.14	19.4	2.53	38
Spinel	D	5.8	3.75	16.7	3.75	1.4	1.19	0	-	59.9	4.92	13.5	1.57	48
	H	5.3	3.98	17.5	4.45	1.3	1.31	0	-	59.8	6.39	12.8	2.01	20

Analyst : G. Hutchinson
St.d = Standard deviation

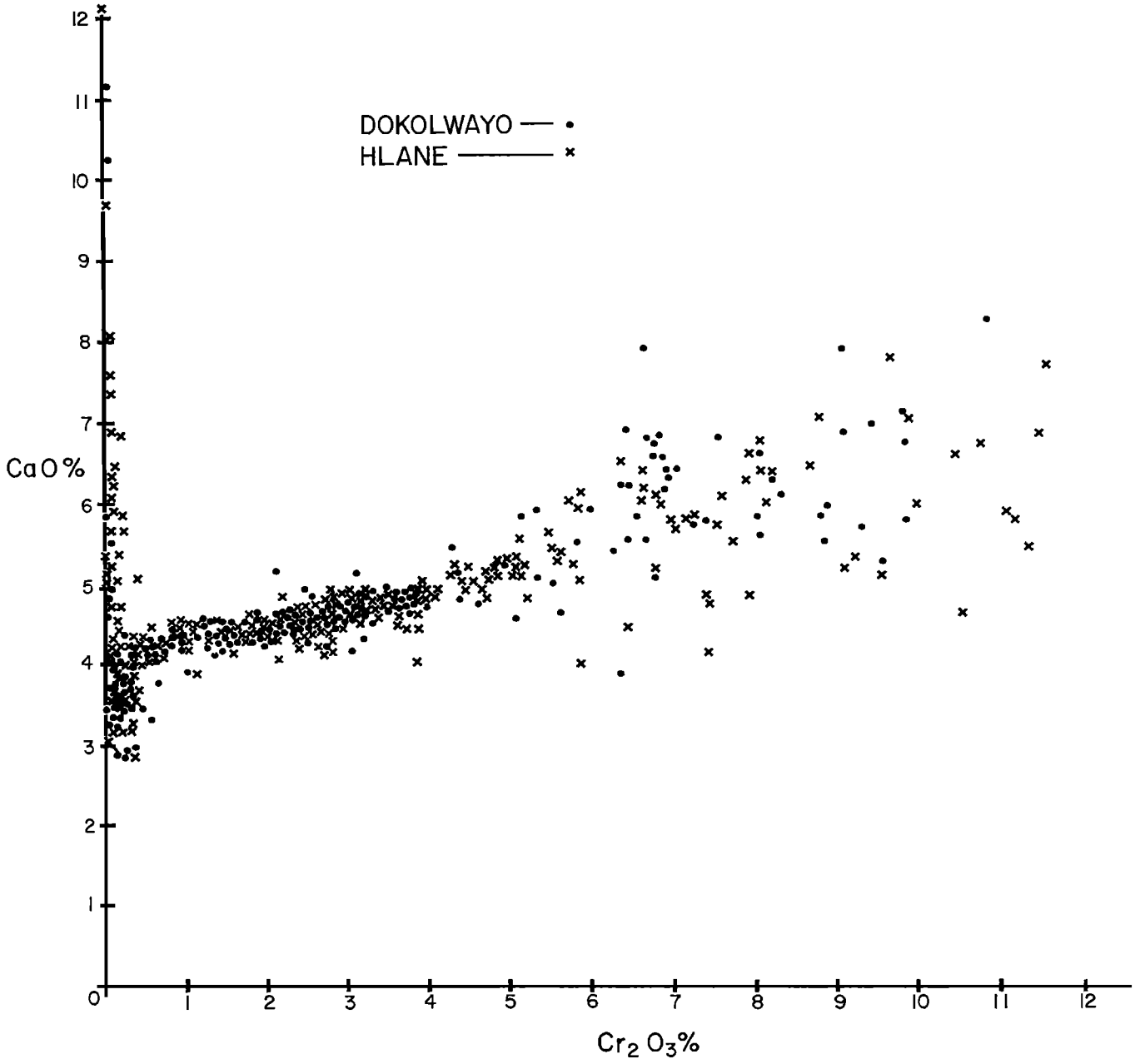

Fig. 5. Composition of garnets from the Dokolwayo kimberlite and the Hlane paleo-alluvial deposit expressed in terms of CaO and Cr_2O_3.

2. The high proportion of incorporated xenogenic material.
3. The high degree of mixing of xenoliths and xenocrysts, of extremely variable size, derived from different stratigraphic horizons.
4. The presence of erratically oriented flow structures including swirl and eddy patterns.
5. Tuffisite veins, commonly containing a high proportion of quartz and feldspar grains (60-70 vol. %), cut the central kimberlite and included xenoliths and locally disrupt and brecciate the latter.
6. The broken nature of many of the mineral grains is ascribed to impact during fluidized intrusion.
7. The low emplacement temperature indicated

by the absence of thermal metamorphic effects on xenolithic components, particularly on heat-sensitive coal inclusions.

8. The presence of spherical kimberlite aggregates in which the average size of the grains decreases outwards, producing a rudely concentric zoning emphasised by concentric alignment of elongate components. These aggregates are considered to be volcanic lapilli that may have formed by accretion in the fluidized system.

Considered collectively these features are strong evidence of at least one major phase of gas-solid fluidized intrusion, probably preceded by explosive breakthrough to the surface of a higher (now eroded) level. The abundance of a tuffisite-breccia further suggests that intrusive activity of this type has played a major role in forming and shaping the diatreme at higher (eroded) levels, a supposition that is in accordance with the views of Dawson (1960, 1962) on the formation of kimberlite pipes.

Features at the present levels of exposure do not suggest, however, that fluidization was responsible for initial formation of the diatreme. Contact relationships exposed in boreholed cores show that the marginal porphyritic kimberlite is older than the tuffisite-breccia (veinlets of the latter cut the former at contacts). The porphyritic kimberlite apparently represents the preserved marginal remnants of an intrusive phase that was largely cored out by the later tuffisite-breccia.

The previously described irregularities in the shape of the pipe suggest that an early stage of diatreme formation involved magmatic stoping, probably accompanied by inward spalling of country rock material. This stage of formation culminated in the emplacement of porphyritic kimberlite, enriched in earlier crystallized material and xenoliths. The intrusion of the porphyritic kimberlite may have been associated with a fluidized phase, developed at a higher level in the diatreme.

The two-phase intrusive history of the Dokolwayo diatreme described above is clearly an oversimplification. The presence of earlier generations of kimberlite as inclusions in both the central and marginal kimberlites indicates a more complex situation involving earlier periods of intrusive activity. Nevertheless, it is considered that the marginal and central kimberlites are evidence of a general time progression from magmatic stoping at an early (embryonic) stage of diatreme formation to later fluidized erosion at higher levels. In a complex diatreme such as the Dokolwayo occurrence this cycle of formation may have been repeated several times.

Age of the Diatreme

No zircon or mica suitable for radiometric dating has been found in the Dokolwayo kimberlite but a tentative age determination by a mineral

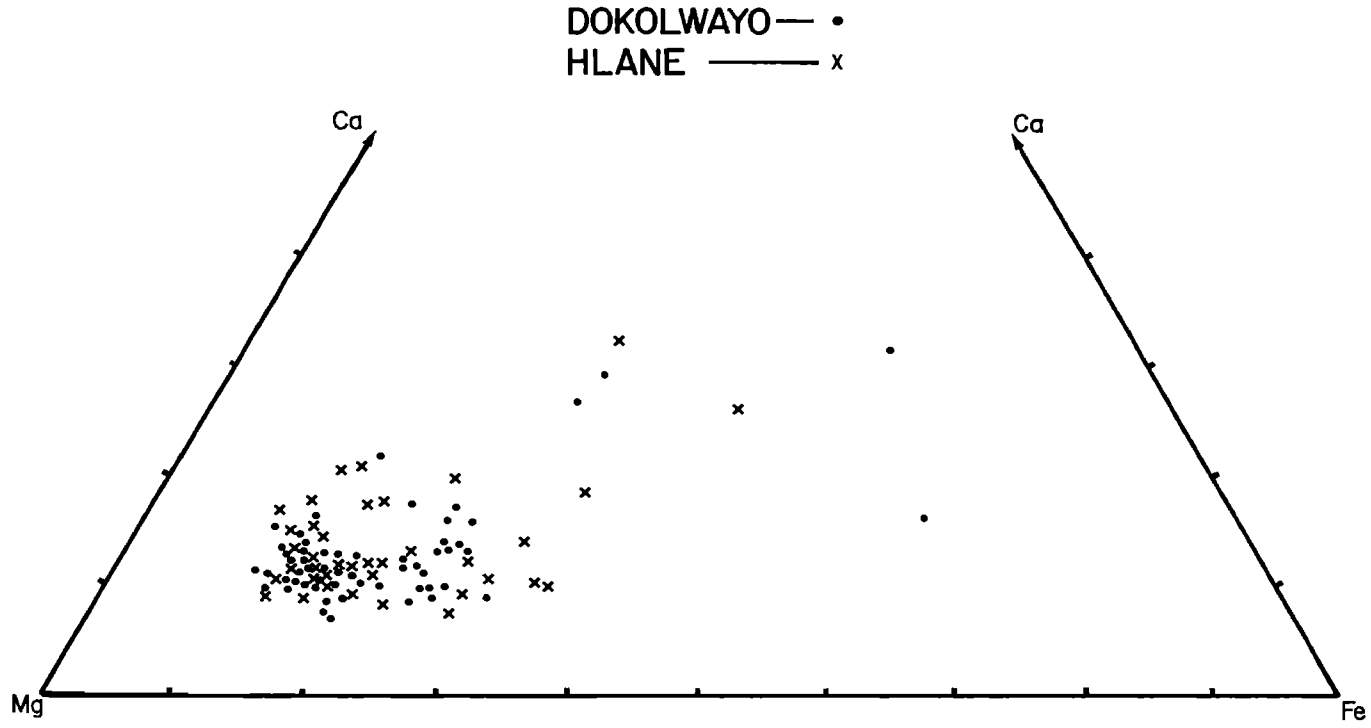

Fig. 6. Composition of garnets from the Dokolwayo kimberlite and the Hlane paleo-alluvial deposit expressed in atomic proportions of Ca, Mg and Fe.

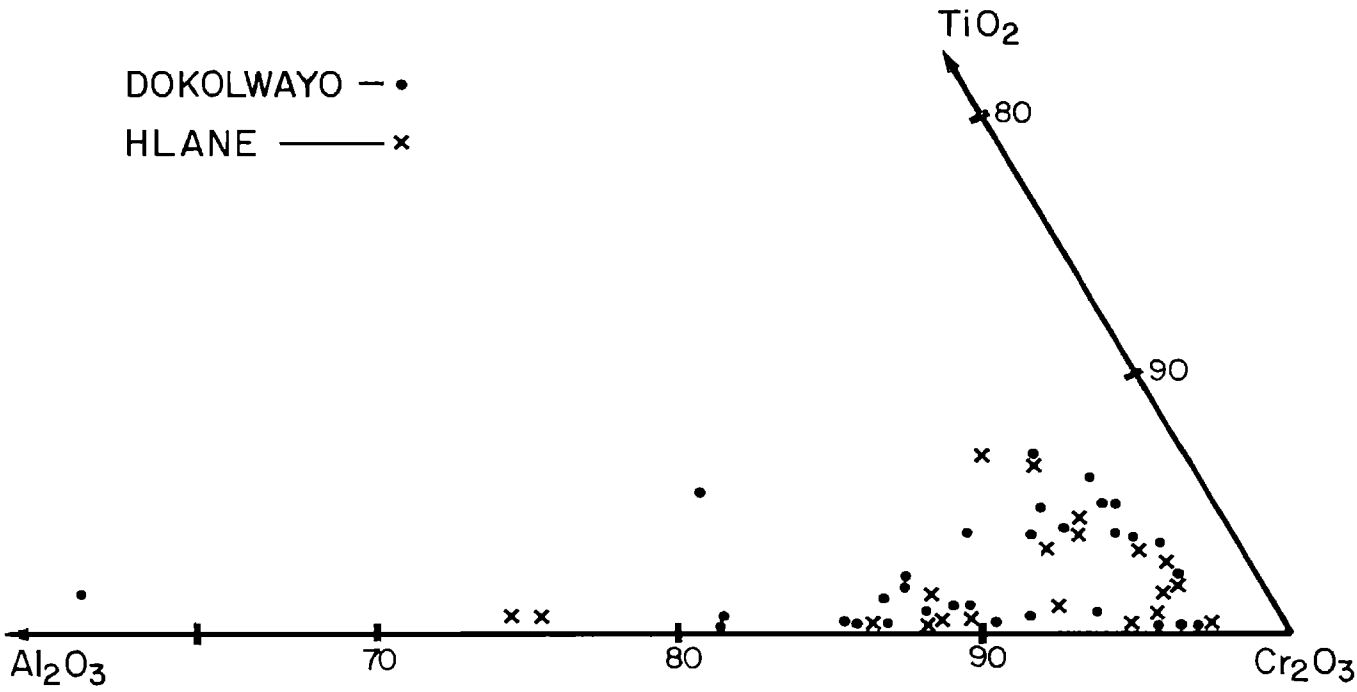

Fig. 7. Composition of spinel from the Dokolwayo kimberlite and the Hlane paleo-alluvial deposit expressed in terms of Cr_2O_3, TiO_2 and Al_2O_3.

isochron U-Pb method indicates an age of 300 ± 20 my (Allsopp & Kramers, 1977). This age has been verified by field relationships.

The maximum age limit of the diatreme is determined by the presence of miospores of predominantly lower Permian age in xenoliths of sandstone and coal in the kimberlite matrix. These xenoliths may be correlated with sandstones and coals found in the middle Ecca (lower Permian) coal measures of the main Karroo basin in Swaziland. It follows that the diatreme formed in post lower Permian times and incorporated fragments of coal and sandstone from Ecca beds present at that time but since removed by erosion. The time interval that elapsed between the deposition of the Ecca coal measures and the intrusion of the diatreme must have been sufficient for the lithification and diagenesis of the Ecca sandstones to have taken place and for the carbonaceous deposits to be converted to coal.

The minimum age limit of the diatreme is fixed by its relationship to the diamondiferous sediments of the Hlane area as there is field and geochemical evidence which suggests that the diamonds and accompanying kimberlite derived minerals in the Hlane Red Beds grits and conglomerates are derived from the Dokolwayo diatreme. No fossils have been identified from these beds but their stratigraphic position and strong resemblance to fossil bearing beds in the main Karroo basin allow reasonable correlation. The Red Beds in the main Karroo basin are of upper to middle Triassic age (du Toit, 1954). Whilst this correlation may be open to question there is no doubt that the Red Beds of the Hlane area pre-date the overlying Stormberg basalts and rhyolites of the Lebombo and associated dolerite dykes. Manton (1968) determined the age of the southern Lebombo acid volcanic rocks as 202 ± 14 my using a Rb decay constant of 1.39. Recalculating this data using a Rb decay constant of 1,42 gave an age of 198 ± 13 my. If the base of the Jurassic is taken to be 195 my it follows that both the Red Beds and the Dokolwayo diatreme must have originated in pre-Jurassic times.

Table III shows the age of emplacement of the oldest of the post-Karroo kimberlites, the Dokolwayo kimberlite, and all the known pre-Karroo kimberlites in southern Africa; none are similar in age to the Dokolwayo diatreme.

Mineral Chemistry

In an attempt to prove that the heavy, resistant kimberlite derived minerals (other than diamond) found in the Hlane deposit could have originated from the Dokolwayo kimberlite, detailed studies of the relative quantity, colour and chemical composition of representative samples of these minerals were carried out. Both deposits contain kimberlitic garnets and chrome spinel but no ilmenite.

Mineral samples were obtained from crushed rock specimens and from surface drainage channels. Mechanical concentrating devices and Bromoform were used to obtain heavy residues in the 4-0.5 mm size range. These residues were examined under a binocular microscope and the kimberlite derived

minerals were separated from the balance of dense mineral grains and rock fragments by visual inspection. Superficial examination of the grains from both sources show a wide colour range of garnets from pale straw to mauve. Unbroken grains commonly have finely cross-hatched surfaces reminiscent of overlapping roof tiles; this feature may be caused by etching. Spinels generally do not exceed 2 mm in diameter and unbroken grains occur as equidimensional octahedra with shiny black surfaces. No ilmenite was found.

Colour comparison was carried out on roughly 1000 garnet grains in the 16-28 (Tyler) mesh size range, selected at random from the larger samples referred to above. These grains were divided into seven colour groups, straw, pale orange, dark orange, red, pink cerise and mauve. The number of grains in each category varied to some extent between the two sources but in both cases more than 60% of the grains fell within the pale orange, dark orange and mauve groups.

Similar studies carried out on other ilmenite free or ilmenite poor kimberlites suggest that the range and proportion of garnet colours may be a diagnostic feature of the particular source. For example, two kimberlite dyke sources in the Eastern Transvaal (the closest known kimberlites to the Dokolwayo occurrence) contain characteristic milky pink to mauve garnets unlike any found at Dokolwayo. Similarly the kimberlite dyke swarm in the Theunissen area in the Orange Free State contains a high proportion of garnets of a flesh pink colour not found elsewhere. A further example is the Jagersfontein kimberlite in the Orange Free State which contains numerous unique pale mauve garnets.

Microprobe analyses of over 700 grains of garnet and spinel from Dokolwayo and Hlane were carried out so that detailed comparison of the mineral chemistry of these grains could be made. From the samples referred to above 20-48 grains of spinel and 22-52 grains of garnet from each colour category were selected at random for analysis. Analyses were carried out at the Anglo American Research Laboratories, Johannesburg, using an A.R.L. SEMQ automated electron microprobe. A summary of the results obtained is presented in Table IV.

Figure 5 shows the composition of the Dokolwayo and Hlane grains in terms of CaO versus Cr_2O_3 and Fig. 6 indicates the compositional range expressed in terms of atomic proportions of Ca, Mg and Fe. All plotted data points were selected to show the extremes of composition. Figure 7 shows the composition of spinel in terms of Al_2O_3, Cr_2O_3 and TiO_2.

Comparison of the results obtained shows that there is a high degree of similarity in chemical composition of the garnet and spinel from the two sources. Whilst this similarity cannot prove that the Hlane garnet and spinel was derived from the Dokolwayo kimberlite it lends strong support to this hypothesis of origin.

Structural Setting

The Dokolwayo diatreme is located near the axis of the Lebombo monocline, a structure regarded by du Toit (1929) as having originated during the eruption of the Stormberg lavas in Jurassic times. The monocline extends almost straight in a north-south direction for 700 km along the western boundary of Mozambique. The axial region of the monocline is characterised by numerous subparallel north-south striking faults and dolerite dyke swarms. Cox (1970) postulates that the Lebombo monocline is controlled by structures that are the southerly continuation of the Mozambique Belt.

Clifford (1966 and 1970) and Dawson (1970) show that in Africa the economically important diamond bearing kimberlites are located within the boundaries of old cratonic areas. The older cratons defined by Clifford (1970) are those areas of continental crust that have not suffered orogenic deformation for at least the past 1500 my.

The Dokolwayo diatreme appears to be marginal to the area defined by Clifford (1970) as the southern African (Transvaal Rhodesia) craton. However, in the vicinity of the diatreme the granite gneisses are 2940 ± 45 my (Davies & Allsopp, 1976) and there is no evidence of younger orogenic deformation. A gentle eastward downwarping is reflected in dips of 10^{o} to 12^{o} in the Karroo rocks. More substantial crustal deformation that reflects the true terminus of the craton may occur further to the east along the axis of a gravity "low" (Reeves, 1976) where acid lavas are extruded and where the Karroo rocks plunge steeply beneath Cretaceous and Tertiary sedimentary formations. It is therefore concluded that the Dokolwayo diatreme lies within the boundaries of the Transvaal Rhodesia craton.

Kimberlite Magma Genesis

Mitchell (1970) states that whilst some geologists consider the constant spatial association and temporal sequence between basaltic magma and kimberlite to be evidence of a genetic relation, others do not subscribe to this point of view. The discovery of the Dokolwayo kimberlite with its unique Permo-Triassic age is a further example of a southern African kimberlite which is not shortly preceded by a major event of basalt extrusion or dolerite emplacement. The vast majority of kimberlites in southern Africa are nevertheless of post Jurassic age and their emplacement shortly followed the Stormberg volcanic event.

With the recognition of the new ages of kimberlite listed in Table IV the time span of kimberlite emplacement in southern Africa resembles more closely that of the Siberian kimberlite province. Milashev (1974), Rozhkov (1967), Kharkiv (1967) and Bogatykh (1976) show that Siberian kimberlites range in age from Paleozoic in the

southerly Malo Botuobiya cluster to Mesozoic in the more northerly clusters; the main body of kimberlites are of Paleozoic age. These authors also show that widespread dolerite intrusion took place both prior to and subsequent to the emplacement of kimberlites.

Although many kimberlite occurrences are linked in time and space with the extrusion of plateau basalts and intrusion of related dolerites, other kimberlites do not share these relationships. It is suggested in these latter cases that there is no genetic link between basalt and the kimberlite magma.

Acknowledgements. The writers are indebted to the Anglo American Corporation of South Africa and to De Beers Consolidated Mines Limited for permission to publish this paper and to the staff of these organisations who assisted in its preparation. Thanks are due also to H. Allsopp and J. Kramers for age determinations carried out on the Dokolwayo kimberlite, to D. Rowsell for arranging for the vitrinite reflectance measurements on the Dokolwayo coal to be carried out at the S.N.P.A. laboratories, to R. Falcon and I. Mclaughlin for palynological studies undertaken on the sedimentary xenoliths from Dokolwayo, to J. Robey, G. Hutchinson, S. Shee and C. Hatton who carried out microprobe analyses on the Dokolwayo and Hlane garnets and spinels and to J. Gurney, R. Danchin and B. Wyatt whose interest, criticism and comments were of great assistance to the writers.

References

Allsopp, H.L., and J.D. Kramers, Rb-Sr and U-Pb age determinations on southern African kimberlite pipes, Ext. Abs. 2nd Int. Kimberlite Conf., Santa Fe, New Mexico, 1977.

Bogatykh, I. Ya., New data on dynamic influence of trapps on kimberlite bodies, Doklady Academy Nauk SSSR, 226, 1, Geologiya, 166-167, 1976. (In Russian).

Boyd, F.R., and C.R. Clement, Compositional zoning of olivines in kimberlite from the De Beers mine, South Africa, in press.

Clifford, T.N., Tectono metallogenic units and metallogenic provinces of Africa, Earth and Planetary Science Letters, 1, 421-434, 1966.

Clifford, T.N., The structural framework of Africa in African Magmatism and Tectonics, edited by T.N. Clifford and I.G. Gass, pp. 321-335, Oliver and Boyd, Edinburgh, 1970.

Cox, K.G., Tectonics and vulcanism of the Karroo period and their bearing on the postulated fragmentation of Gondwanaland in African Magmatism and Tectonics, pp. 211-236, Oliver and Boyd, Edinburgh, 1970.

Davies, R.D. and H.L. Allsopp, Strontium isotopic evidence relating to the evolution of the lower pre-Cambrian granitic crust in Swaziland. Geology, 4, 553-556, 1976.

Dawson, J.B., A comparative study of the geology and petrography of the kimberlites of the Basutoland province, unpublished Ph.D. thesis, University of Leeds, p. 344, Leeds, 1960.

Dawson, J.B., Basutoland kimberlites, Geol. Soc. Am. Bull., 73, 545-560, 1962.

Dawson, J.B., The structural setting of African kimberlite magmatism in African Magmatism and Tectonics, pp. 321-335, Oliver and Boyd, Edinburgh, 1970.

Du Toit, A.L., The volcanic belt of the Lebombo - a region of tension, Trans. Royal Soc. South Africa, XVII, 189-217, 1929.

Du Toit, A.L., The Geology of South Africa, edited by S.H. Haughton, pp. 351-359, Oliver and Boyd, Edinburgh, 1954.

Hawthorne, J.B., Model of a kimberlite pipe, Physics and chemistry of the Earth, 9, 1-15, 1975.

Hunter, D.R., Geological map of Swaziland, 1966.

Kharkiv, A.D., New data on the age of kimberlite pipes of Daaldyno Alakitsky region, Geol. i Geofiz, 4, 124-128, 1967. (In Russian)

Manton, W.I., The origin of associated basic and acid rocks in the Lebombo-Nuanetsi igneous province, Southern Africa, as implied by Strontium isotopes, Journal of Petrology, 9, 23-29, 1968.

Milashev, V.A., Kimberlite Provinces, p.236, Nedra, Leningrad, 1974. (In Russian).

Mitchell, R.H., Kimberlites and related rocks - A critical reappraisal. Journal of Geology, 78, 686-704, 1970.

Reeves, C., The delineation of crustal provinces in southern Africa from a compilation of gravity data, Annual report of the Research Institute of African Geology, The University of Leeds, 36-41, Leeds, 1976.

Rozhkov, I.S., G.P. Mikhalev, B.I. Prokopchuk, and E.A. Shamshina, Diamond Bearing placers of western Yakutia, pp. 127-140, Nauka, Moscow, 1967. (In Russian).

Skinner, E.M.W., and C.R. Clement, Mineralogical classification of Southern African kimberlites, Ext. Abs. 2nd Int. Kimberlite Conf., Sante Fe, New Mexico, 1977.

STRUCTURAL SETTING OF KIMBERLITES IN SOUTH-EASTERN AUSTRALIA

K.J. Stracke

Stockdale Prospecting Limited,
60 Wilson Street, South Yarra, 3141, Victoria, Australia

John Ferguson and L.P. Black

Bureau of Mineral Resources,
Post Office Box 378, Canberra City, 2601, A.C.T., Australia.

Abstract. Recent discoveries have established the existence of fourteen areas where kimberlitic rocks occur in south-eastern Australia, in the States of New South Wales, Victoria, Tasmania and South Australia. One or more intrusions are found in each area, the maximum being twenty-seven. Rb-Sr dating on whole-rock samples and on phlogopite separates have established Permian and Jurassic ages for kimberlitic occurrences in north-western New South Wales and South Australia respectively. Field relations indicate that all the occurrences post-date the Proterozoic and that some are as young as Tertiary.

In an attempt to relate the kimberlitic occurences, and their associated rock types, to a structural framework the following features were investigated: on- and off-shore structures, igneous activity, earthquake activity, general tectonics, gravity and magnetics. It appears that postulated extensions of transform faults, stemming from both the Antarctic and Tasman Sea Ridges, have played the major role in the location of kimberlitic intrusives in south-eastern Australia. Near the eastern seaboard, the NNE projected continental fracture zone, stemming from the Antarctic Ridge, also coincides with a broad belt of Cainozoic igneous activity, an edge of epeirogenic uplift, and the mean line of hot spot migration. All of the kimberlitic occurences near the eastern seaboard of Australia fall within this broad zone of activity. Their location also appears to have been governed by fracture patterns initially developed during pre-breakup times, which later became the sites of continental extensions of transform faulting.

Introduction

Fourteen occurrences of kimberlitic rocks have recently been discovered in south-eastern Australia in the States of South Australia, Victoria, Tasmania and New South Wales (Figure 1 and Table 1). One or more intrusives are found in each area, with a maximum of twenty seven in one cluster. With one exception, the field relations indicate that all occurrences post-date the Proterozoic, and that at least one is as recent as Tertiary. Rb-Sr isotopic analyses have been carried out on whole-rock samples, phlogopite, and other mineral separates from three of the areas. References have been made to "kimberlite" occurrences in four areas in Australia, all located in the south-east (Lovering and White, 1969; Colchester, 1972; Tucker and Collerson, 1972; Ferguson et al., 1977).

This paper attempts to relate the kimberlitic and associated rock types to a structural framework. Relations with the following features have been investigated: on- and off-shore structures, supracrustal igneous activity, granitic activity, earthquake activity, tectonics, gravity and magnetics.

The term "kimberlitic" is used to describe these rocks as there are significant petrographic and chemical differences compared with kimberlites from other areas (see Ferguson and Sheraton this volume).

Rb-Sr Isotopic Analysis

Analytical Techniques

Analytical procedures for Rb and Sr, incorporating a mixed ^{84}Sr-^{85}Rb spike, were based on the techniques outlined in Page et al. (1976) and Williams et al. (1976). A triple-filament ion source was used for both Rb and Sr determinations; the latter were made in a 30 cm radius - 60 degree sector mass-spectrometer from which a $^{87}Sr/^{86}Sr$ mean value of 0.71035 is derived for the NBS 987 standard. Regression of the analytical points is based on the work of McIntyre et al. (1966). A relative deviation of 0.3% has been used for $^{87}Rb/^{86}Sr$ and a standard deviation

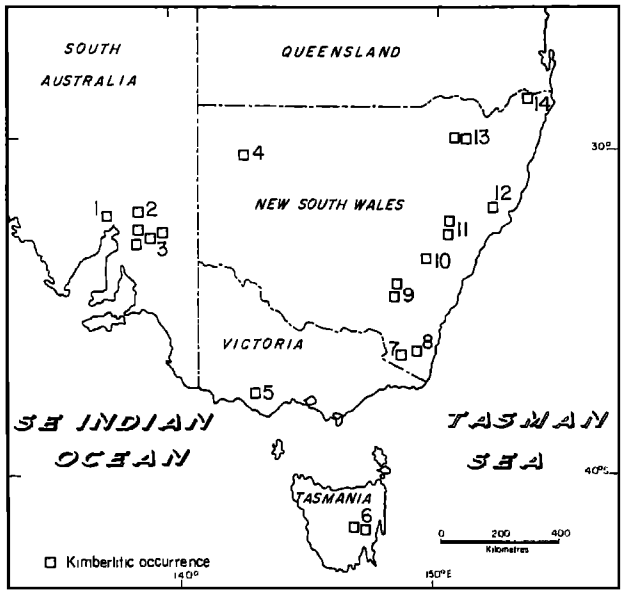

Fig. 1. Localities of kimberlitic occurrences in south-eastern Australia.

Area:	1	Port Augusta	Area:	8	Bombala
	2	Walloway		9	Jugiong
	3	Terowie		10	Abercrombie
	4	White Cliffs		11	Nullo Mountain
	5	Bullenmerri		12	Gloucester
	6	Oatlands		13	Bingara
	7	Delegate		14	Mt. Brown

of 10×10^{-5} has been assigned to $^{87}Sr/^{86}Sr$. The value $1.42 \times 10^{-11} y^{-1}$ (Neumann and Huster, 1972), as provisionally recommended by the August 1976 meeting of the IUGS (International Commission on Stratigraphy, Subcommission on Geochronology), has been used for the decay constant of ^{87}Rb. All uncertainties are expressed at the 95% confidence level. A 6 ng blank correction has been applied to both Rb and Sr analyses where appropriate. Blank-corrected isotopic data appear in Table 1.

Isotopic Data

South Australia. Phlogopite from five separate kimberlite intrusions has been analysed. Total-rock analyses were also made on three of these intrusions (Table 2). The phlogopites are insufficiently enriched in ^{87}Rb relative to ^{86}Sr to allow age estimates independent of initial ratio assumptions. Reasonably reliable ages should, however, be provided by the two phlogopite-total rock pairs, which yield values of 164 m.y. and 172 m.y. for samples 75210090 and 75210434, respectively (Table 2). A K-Ar age determination on the phlogopite separate from sample 75210434 gave an age of 173 ± 4 m.y. These ages are in agreement with that calculated from phlogopite 75210091 - total rock 75210090 at 174 m.y. The two phlogopites which are less enriched in ^{87}Rb are consequently more sensitive to assumed initial ratio; these yield higher and presumably less reliable ages (188 m.y. for 75210085, 199 m.y. for 75210086). All analytical points produce only a poorly-defined isochron with age and initial ratio of 176 ± 29 m.y. and 0.708 ± .004. Carbonatite (75210081) from the Walloway occurrence (intrusive 2) has initial $^{87}Sr/^{86}Sr$ marginally below 0.705.

New South Wales. White Cliffs (Figure 1 area 4). The age of the kimberlites at White Cliffs can be deduced from two independent isotopic arguments. First, a phlogopite (75210021), little enriched in ^{87}Rb relative to ^{86}Sr (Table 2), when combined with its total-rock point, yields a value of 260 m.y. This is supported by data for two eclogite xenoliths from the kimberlite. A clinopyroxene-total rock pair from eclogite 75210033 generates a nodule age of 600 m.y. Garnet, clinopyroxene and total-rock data produce an age of 260 ± 67 m.y. for eclogite 75210025. Both nodule ages presumably represent maximum values for the enclosing kimberlitic rock. The analytical points for 75210025 define a model 1 isochron (i.e., none of the scatter can be attributed to geological causes). This may simply be a consequence of mass-balance considerations, even though an intergranular Rb- and Sr-bearing phase has been established to be present in eclogite nodules (Allsopp et al., 1969; Griffin and Murthy, 1968); it seems likely that Rb and Sr in the garnet would be dominated by kelyphitic material (e.g., Allsopp et al., 1969; Barrett, 1975). The indicated initial $^{87}Sr/^{86}Sr$ ratio for nodule 75210025 is 0.7086 ± .0007 (at 260 m.y.); that for sample 75210033 is 0.7040 (at 600 m.y.). These isotopic data suggest that the former of these chemically similar eclogite nodules may have been isotopically reset during generation or intrusion of the kimberlitic magma.

Jugiong (Figure 1, Area 9). Owing to the absence of phlogopite, isotopic analyses have been restricted to phases less useful for geochronology. Nevertheless, trends which are consistent with the stratigraphical constraints appear to be recognisable on the $^{87}Sr/^{86}Sr$ vs. $^{87}Rb/^{86}Sr$ diagram (Figure 2). Most surface samples of kimberlitic material from intrusion 4 (specimens 75210067 A to D) have indistinguishable $^{87}Sr/^{86}Sr$ ratios (Table 2 and Figure 2). An additional autolith composite (75210104) has a marginally, but possibly significantly higher ratio. A kimberlitic lapillus (75210419) taken from drill core at 97 m has an identical $^{87}Sr/^{86}Sr$ ratio to the 75210067 samples. This may be fortuitous, or alternatively indicate that these two separate diatremes from which they were collected have identical isotopic histories.

A further group of four samples apparently plot on a subhorizontal line with lower indicated initial ratio (about 0.7050 as opposed to 0.7056). Of these, 75210445 and 75210447 represent a kimberlitic lapillus and an autolith, respectively,

TABLE 1A

Area	Co-Ordinates (Centre of Area) (lat/long)	Number and Shapes of Intrusions	Country Rock	"Radiometric Age"
1. PORT AUGUSTA	137°38'E/32°30'S	3 kimberlite sill outcrops, extending along a 25km NW-SE trend; possibly part of same sill. Sills up to 2m thick.	Relatively unfolded sediments overlain by large Proterozoic quartzite formation forming mesa cappings.	
2. WALLOWAY	138°35'E/32°37'S	7 kimberlitic dykes, some with elongated "blows", with northerly trend; largest body 20m long.	Siltstone of the Proterozoic Umberatane Group.	172 m.y.
3. TEROWIE				164-174 m.y.
a) Wonna Group	139°00'E/33°15'S	3 kimberlite pipes ranging from 20x10m to 280x140m; 5 kimberlite dykes up to 1km long and from 0.25 to 2m wide; 1 swarm of small kimberlite dykes. Most dykes have a NW-SE strike but some strike NNE-SSW.	Proterozoic marine sediments.	
b) Pandappa/ Calcutteroo Group	139°12'E/33°07'S	4 kimberlite pipes (20x10m, 20x20m, 110x50m and 160x25m); 4 kimberlite dykes & 1 dykeswarm striking NW-SE and NNE-SSW.		
c) Nackara Group	139°14'E/32°57'S	5 narrow and short kimberlite dykes with NNE-SSW strikes.		
d) Pine Creek Group	139°17'E/33°10'S	1 kimberlite pipe (650x150m) and 3 dykes with northerly trend.		
4. WHITE CLIFFS	142°37'E/30°42'S	1 kimberlite pipe (130x90m); 5 small dykes trending NW-SE.	Precambrian schists.	~ 260 m.y.

taken from drill core at approximately 30 m below surface; 75210041 and 75210055 are total-rock samples from separate intrusions. Two moderately fresh kimberlitic dykes found cutting intrusion 4 (75210448 and 75210102) and a fresh kimberlitic lapillus from intrusion 2 (75210047) have the lowest $^{87}Sr/^{86}Sr$ ratios, being below 0.705, found in the kimberlitic intrusions in the Jugiong area.

An amphibole megacryst (75210067E) of probable

TABLE 1B

Area	Co-Ordinates (Centre of Area) (lat/long)	Number and Shapes of Intrusions	Country Rock	"Radiometric Age"
5. BULLENMERRI	143°07'E/38°15'S	1 kimberlitic body, presumably pipe largely covered by maar.	Tertiary marine sediments generated by late Tertiary volcanics forming craters.	
6. OATLANDS	147°19'E/42°17'S	2 kimberlitic bodies of unknown shape and size.	Sequence of Permo-Triassic sediments intruded by sheets of Jurassic dolerite.	
7. DELEGATE	148°47'E/36°50'S	2 kimberlitic pipes measuring 390x300m and 210x120m.	Intrudes along boundary between Upper Ordovician meta-sediments and Lower Devonian granite.	Middle Jurassic (Lovering and Richards (1964), McDougall and Wellman (1976)).
8. BOMBALA	149°23'E/36°47'S	1 kimberlite pipe 70x40m and 1 small kimberlite dyke striking NE-SW.	Upper Devonian granite.	
9. JUGIONG	148°16'E/34°59'S	8 pipes of which the largest measures 635x425m, 240x170m, 300x120m and 100x100m.	Middle Devonian granites which have intruded Silurian sediments. Two intrusives cut Cainozoic basalt dated at 17.2 m.y.	Cainozoic
10. ABERCROMBIE	149°22'E/33°52'S	1 kimberlitic pipe shape unknown but smallest dimension at least 12m.	Middle Devonian graywacke, underlain by Carboniferous granite.	
11. NULLO MOUNTAIN	150°13'E/32°50'S	2 kimberlitic occurrences of unknown shape.	Sandstones and claystones of the Jurassic Narrabeen Group.	
12. GLOUCESTER	151°42'E/32°04'S	2 elongated kimberlite pipes measuring 140x20m and 100x10m.	Undifferentiated Carboniferous sediments.	
13. BINGARA	150°28'E/30°07'S	3 kimberlitic bodies of unknown shape.	Upper Devonian sandstones.	
14. MT. BROWN	152°46'E/28°38'S	3 tabular kimberlitic occurrences dipping about 30° SSE and extending for at least 1km along strike.	Middle to Upper Jurassic sandstones and mudstones.	

TABLE 2A. Rb-Sr Isotopic Compositions: South Australia

Sample and Location	Rock Type	Rb (μ g/g)	Sr (μ g/g)	$^{87}Sr/^{86}Sr$	$^{87}Rb/^{86}Sr$
Terowie (area 3)					
Intrusion 1					
75210085 phlogopite	kimberlite	400.0	205.5	0.72340	5.629
Intrusion 2					
75210086 phlogopite	"	95.01	25.23	0.73905	10.91
Intrusion 3					
75210090 total rock	"	130.6	461.6	0.71053	0.8170
75210090 phlogopite	"	490.6	62.48	0.76190	22.79
Intrusion 4					
75210091 phlogopite	"	482.8	114.9	0.73863	12.17
Walloway (area 2)					
Intrusion 1					
75210434 total rock	kimberlite dyke	143.3	620.8	0.70735	0.6756
75210434 phlogopite	" "	443.9	100.2	0.73706	12.83
Intrusion 2					
75210081 total rock	carbonatite	5.268	1579	0.70499	0.00963

lower crustal origin, found in intrusion 4, has a lower $^{87}Sr/^{86}Sr$ ratio (0.70406) than the surrounding kimberlitic rock.

Garnet-spinel lherzolite (75210433) and spinel lherzolite (75210117) inclusions from intrusion 3 have statistically indistinguishable $^{87}Rb/^{86}Sr$ and $^{87}Sr/^{86}Sr$ ratios (Table 2). The high Rb and Sr contents and high $^{87}Sr/^{86}Sr$ ratios of the garnets separated from garnet lherzolite nodules (75210059 and 75210062) in intrusion 4 presumably reflect a dominantly kelyphitic component (Table 2). Clinopyroxene from the latter nodule possesses the most primitive $^{87}Sr/^{86}Sr$ ratio (0.7029) found in this study.

In the case of the kimberlitic rocks in the Jugiong area two of the seven diatremes (including intrusion 4) penetrate Cainozoic basalts; nearby lavas give an age of 17.2 m.y. (Wellman and McDougall, 1974b). Given this age constraint the subhorizontal lines shown in Figure 2 for the two major groups of results might be interpreted as isochrons of Quaternary or Tertiary age.

Interpretation

Some of the $^{87}Sr/^{86}Sr$ isotopic differences in the South Australian and Jugiong material possibly relate to the difficulties of obtaining completely unaltered samples but may also, in part, be due to primary factors. The lower $^{87}Sr/^{86}Sr$ ratios found in the Jugiong occurrences correlate with the least altered material. Berg and Allsopp (1972) and Barrett and Berg (1975) have established that low $^{87}Sr/^{86}Sr$ ratios are a feature associated with fresh kimberlites as contrasted with higher values for altered kimberlite; however, micaceous kimberlites also have high values for this ratio. The Jugiong kimberlites have a low mica content, so that percolating groundwater may be responsible for the high $^{87}Sr/^{86}Sr$ values in this variety of altered kimberlite (Barrett and Berg, op. cit). On the other hand the high $^{87}Sr/^{86}Sr$ ratio encountered in the South Australian occurrences may be a reflection of their high mica content and not of secondary alteration. Langworthy and Black (in prep.) argued for a radiogenically-enriched and heterogenous phlogopite-bearing mantle in the source region of a kimberlite-related magma. Such a region would be expected to be enriched not only in K, but also in Rb and its daughter, radiogenic Sr. The possibility of isotopic heterogeneity in the mantle has been noted by many other authors (eg. Harris et al., 1972; Barrett, 1975; Barrett and Berg, 1975), and recently vigorously argued by Brooks et al. (1976).

Structural Settings

Seismic activity is shown in Figure 3, and represents a compilation of recordings since 1900 from data filed in the Bureau of Mineral

TABLE 2B Rb-Sr Isotopic Compositions: New South Wales

Sample and Location	Rock Type	Rb (μg/g)	Sr (μg/g)	$^{87}Sr/^{86}Sr$	$^{87}Rb/^{86}Sr$
White Cliffs (area 4)					
Intrusion 1					
75210021 phlogopite	kimberlite dyke	281.3	141.8	0.72654	5.736
75210021 total rock	" "	64.25	1202	0.70591	0.1543
Intrusion 2					
75210025 total rock	eclogite nodule	7.098	286.8	0.70887	0.07146
75210025 garnet	" "	1.798	4.337	0.71303	1.1975
75210025 clinopyroxene	" "	0.199	118.0	0.70866	0.00487
75210033 total rock	" "	16.15	111.1	0.70761	0.4200
75210033 clinopyroxene	" "	2.124	131.8	0.70441	0.04651
Jugiong (area 9)					
Intrusion 1					
75210041 total rock	kimberlite	26.36	769.7	0.70498	0.09888
Intrusion 2					
75210047 total rock	kimberlite lapillus	64.44	1326	0.70475	0.1403
75210419 total rock	" "	62.48	447.6	0.70559	0.4030
Intrusion 3					
75210055 total rock	kimberlite	47.63	946.0	0.70516	0.1453
75210433 total rock	garnet-spinel lherzolite nodule	7.624	46.29	0.70615	0.4754
75210117 total rock	2-spinel lherzolite nodule	9.594	58.05	0.70623	0.4772
Intrusion 4					
75210059 garnet	garnet lherzolite nodule	0.2527	0.9209	0.71078	0.8082
75210062 garnet	garnet lherzolite nodule	0.6370	1.4017	0.71316	1.313
75210062 clinopyroxene	garnet lherzolite nodule	0.3120	76.81	0.70291	0.01172
75210067A total rock	kimberlite autolith	46.53	785.6	0.70562	0.1710
75210067B total rock	" "	53.05	993.1	0.70558	0.1542
75210067C total rock	kimberlite lapillus	43.07	940.4	0.70567	0.1322
75210067D total rock	" "	35.72	849.0	0.70556	0.1214
75210067E amphibole	megacryst in kimberlite	1.969	118.8	0.70406	0.04783
75210102 total rock	kimberlite dyke	42.58	785.0	0.70484	0.1562
75210104 total rock	2-kimberlite autoliths	64.49	858.0	0.70582	0.2170
75210445 total rock	kimberlite lapillus	52.66	688.9	0.70512	0.2206
75210447 total rock	kimberlite autolith	42.20	777.7	0.70512	0.1566
75210448 total rock	kimberlite dyke	51.87	753.9	0.70448	0.19860

Resources. Tow prominent belts of earthquake activity are apparent (Figure 3), one striking north to north-west through the Flinders Ranges of South Australia and extending to the north-west margin of the continent; the second belt trends north through Tasmania, across Bass Strait into Victoria, and then north-eastwards into New South Wales, and continues offshore in south-eastern Queensland. Cleary and Simpson (1971) have postulated that these two zones of earthquake activity correspond to projected continental extensions of oceanic transform faults originating from the Antarctic Ridge. The separation of Australia from Antarctica began 53 m.y. ago,

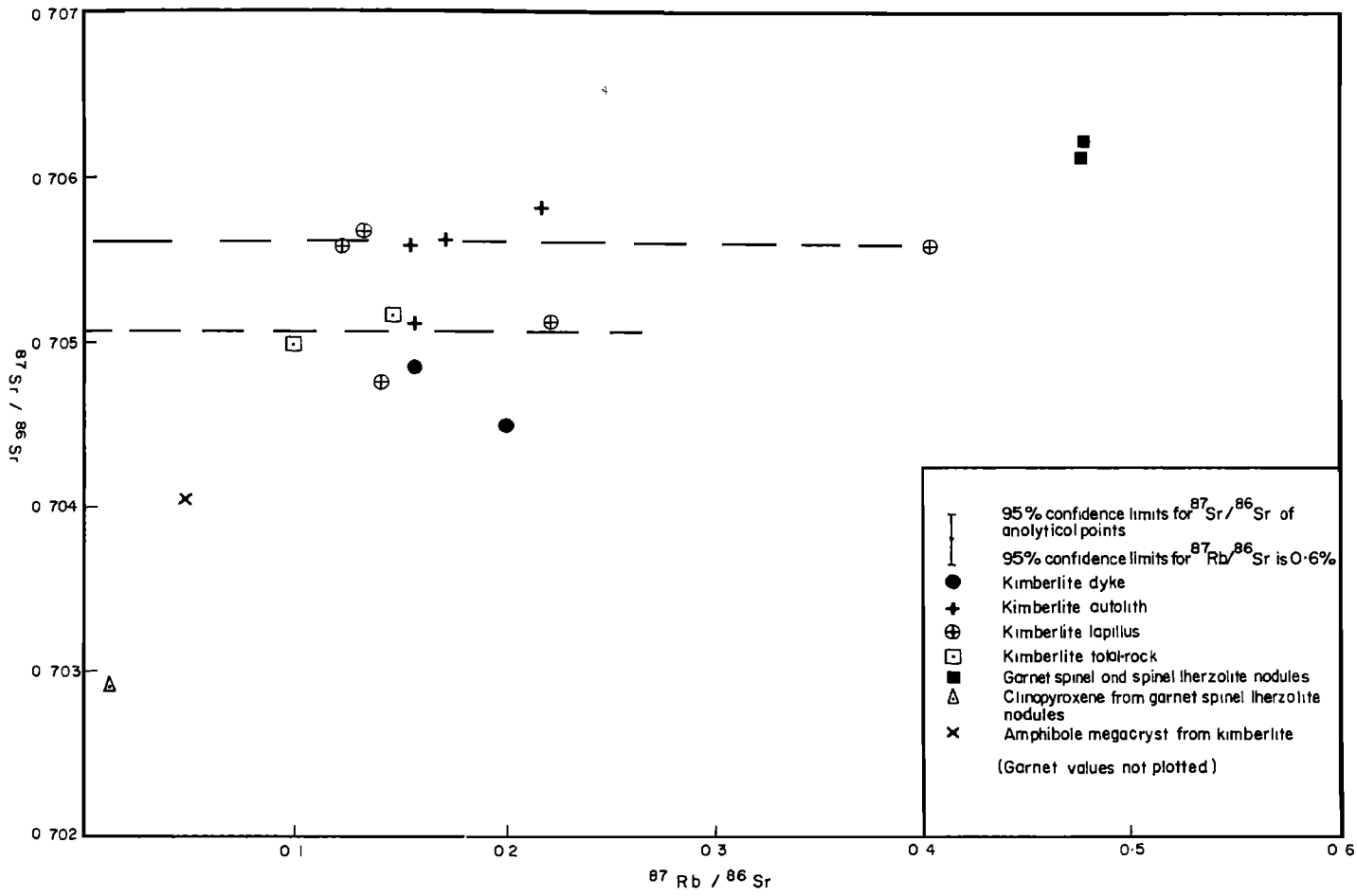

Fig. 2. Plot of $^{87}Sr/^{86}Sr$ versus $^{87}Rb/^{86}Sr$ for sundry rocks and minerals found in the Jugiong kimberlitic rocks (area 9).

and is still continuing (Weissel and Hayes, 1972). The Transform fault postulate is cited by other authors to account for the development of the shear zone feature in the Flinders Range of South Australia (Coward, 1976; Embleton, 1976 and Steward, 1976). Nine of the areas lie on or adjacent to the projected continental extension of these oceanic transform faults. Of the fourteen kimberlitic occurrences, only four lie outside seismically active areas.

Selected structural features and supracrustal igneous activity are shown in Figure 4 and summarised in Table 2. All large scale structural features, both on- and off-shore, are represented in Figure 4; these include lineaments, faults, fold trends, shears and transform faults. The distribution of igneous features shown in this figure represents most of the supracrustal activity in south-eastern Australia. Dense clustering of diatremes can, in part, be schematic or selective, the selection being dependent on whether or not the diatremes contain xenoliths. Further, only those judged to be of upper mantle origin are shown (mostly taken from Wass and Irving, 1976). The reasoning behind this selective process is that as some of the diatremes are similar to kimberlites in their mode of emplacement they may have a spatial and/or genetic affiliation with them.

As indicated by Cleary and Simpson (1971), the edge of epeirogenic uplift on the south-eastern seaboard of Australia (described by David, 1950), coincides roughly with recent earthquake activity, and with a projected oceanic fracture zone stemming from the Antarctic Ridge. All the kimberlitic areas on the south-eastern seaboard of Australia straddle the edge of this epeirogenic uplift which commenced in the Mesozoic and continued intermittently through the Cainozoic (Wellman and McDougall, 1974). Cainozoic basaltic activity is associated with the epeirogenic uplift, occurring in an approximately 300 km-wide zone which incorporates all the kimberlitic areas near the south-eastern seaboard of Australia. This basaltic activity is dominantly alkaline, but in two of the areas the immediate rock types

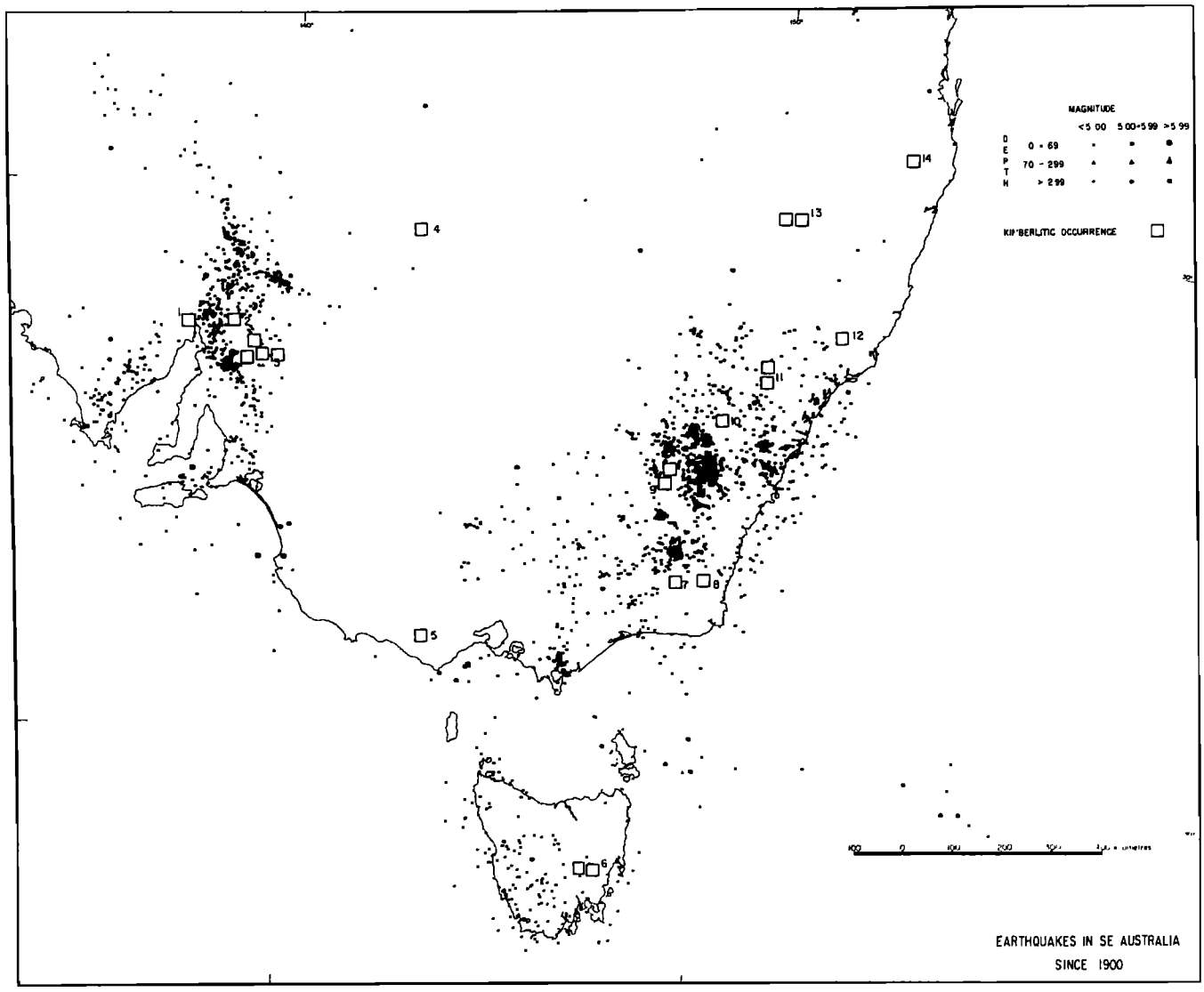

Fig. 3. Earthquake activity in south-eastern Australia. Map compiled from "Earthquake Data File, Bureau of Mineral Resources, Geology and Geophysics, Canberra, A.C.T., Australia". Projected oceanic fracture zones (Cleary and Simpson, 1971).

are sub-alkaline. The Cainozoic mean line of hot spot migration (Wellman and McDougall, 1974a), as defined by central volcano provinces and the present day hot spot sites (Sass, 1964), also passes through the zone of basaltic activity in south-eastern Australia. Areas 9, 10, 11 and 14 lie on or near this mean line of hot spot migration. The Jugiong occurrences (area 9) lie on the mean line of hot spot migration at a site with a deduced age of less than 11 m.y. This age possibly corresponds to the age of the kimberlitic rocks. With one exception, the remaining kimberlitic areas in south-eastern Australia are associated with supracrustal igneous activity (Table 2). The Walloway occurrence (area 2) has a unique spatial association with carbonatite (Tucker and Collerson, 1972).

Hayes and Ringis (1973) have postulated that the Tasman Sea opened up by a process of sea-floor spreading between about 80 and 60 m.y. b.p. As can be seen from Figure 4, the crustal isochrons intersect the continental margin of Australia with a large angular discordance resulting in older oceanic crust being absent north of Tasmania. Basing their views to some extent on these features, Hayes and Ringis (1973) have ascribed this complex relationship to subduction during a limited period of Tasman Sea opening. This interpretation has however, been challenged by Weissel and Hayes (1977) who re-interpret the

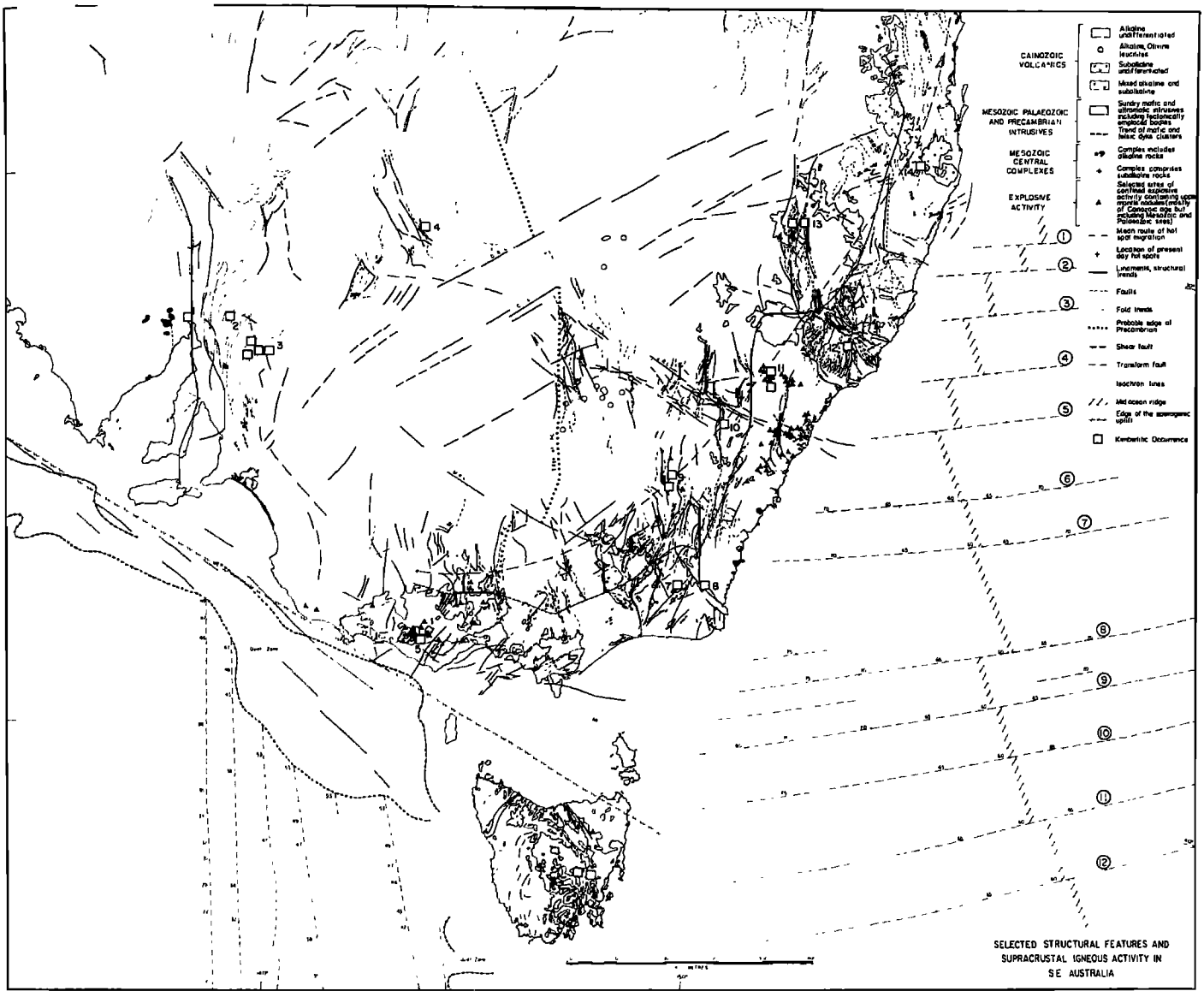

Fig. 4. Selected structural features and supracrustal igneous activity in south-eastern Australia.
Sources:-
Cainozoic Volcanics: Edwards 1950; Spry 1962; Sutherland 1969; Sutherland et al., 1973; Wellman et al., 1970; Wellman 1974; Wellman and McDougall 1974a and b.
Mesozoic and Paleozoic intrusions: "The Geological Map of Australia, 1:2,500,000 scale, Bureau of Mineral Resources, Geology and Geophysics, Canberra, A.C.T., Australia". Harper 1915; Boeson et al., 1961; Evernden and Richards 1962; Brown et al., 1968; Packham 1969; Beams 1975.
Other:-
Diatremes: Adamson 1969; Crawford 1973; Wass and Irving 1976. Hot Spot Activity: Sass 1964; Wellman and McDougall 1974a. Lineaments: Scheibner 1976a; Harrington et al., 1973. Faults, shears and fold trends: "The Geological Map of Australia, 1:2,500,000 scale, Bureau of Mineral Resources, Geology and Geophysics, Canberra, A.C.T., Australia". Giddings and Embleton 1974; Crawford and Campbell 1973; Veevers 1976; Coward 1976. Sea-floor spreading: Weissel and Hayes 1972; Hayes and Ringis 1973; Ringis 1975. Edge of epeirogenic uplift: David 1950; Wellman and McDougall 1974a.

DRL = Darling River Lineament
CIL = Cobar Inglewood Lineament
LRL = Lachlan River Lineament
MRL = Murray River Lineament

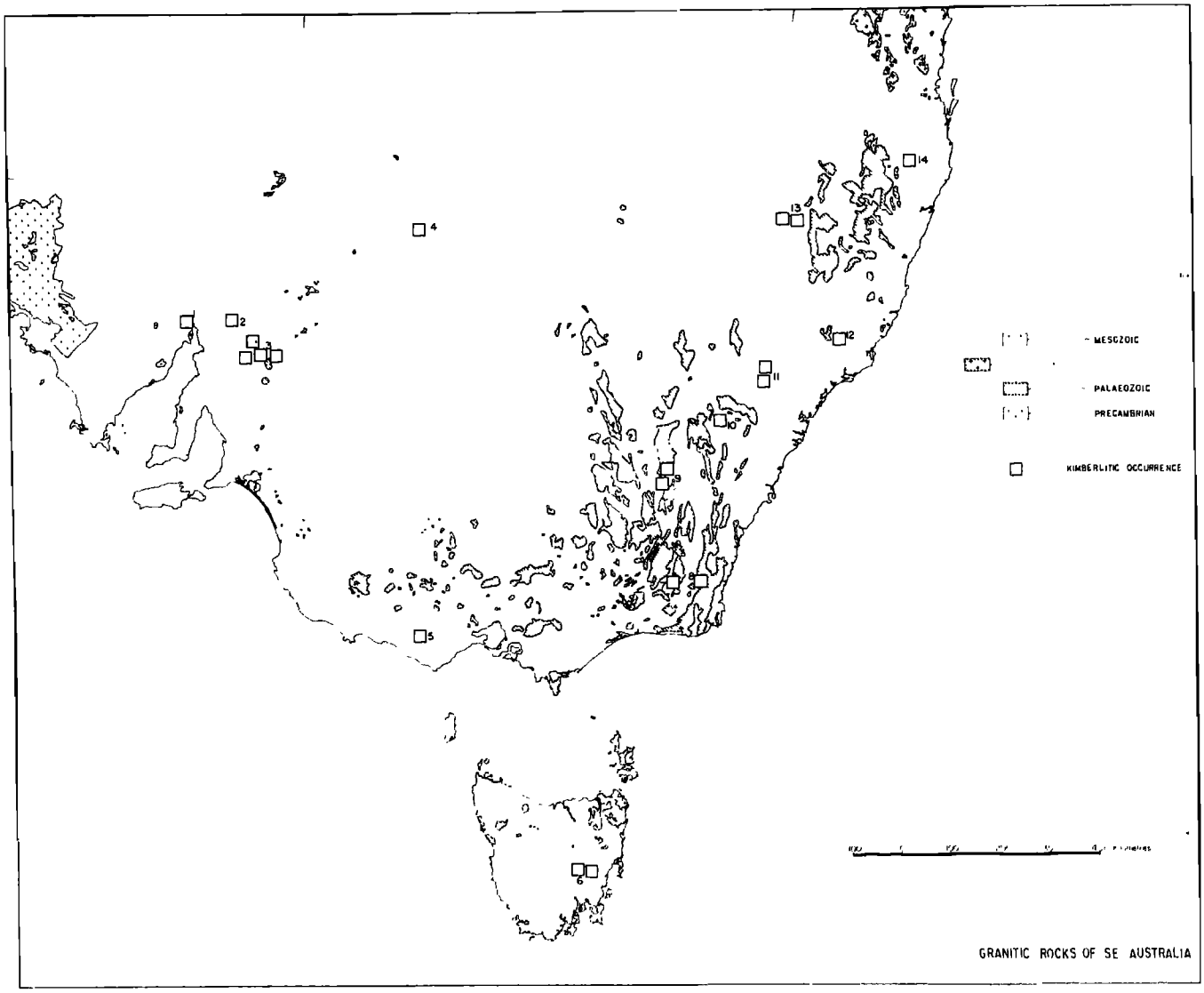

Fig. 5. Granitic rocks of south-eastern Australia. Map compiled from "The Geological Map of Australia, 1:2,500,000 scale, Bureau of Mineral Resources, Geology and Geophysics, Canberra, A.C.T., Australia".

marine magnetic data in terms of a simple two-plate spreading system thereby obviating the need for subduction.

Wilson (1965) developed the hypothesis that lines of weakness in old continental crust determine sites for the development of transform faults; Ringis (1975) has found that this concept has application to the south-eastern Australian margin. An attempt has been made to relate the distribution of kimberlitic rocks from this region to the fracture patterns resulting from the opening up of the Tasman Sea. Following Ringis (1975), the transform faults are numbered for ease of reference (Figure 4).

Lack of information does not yet allow the northernmost kimberlitic occurrence at Mt. Brown (area 14) to be related to possible fracture zones associated with Tasman Sea opening. The postulated continental extensions of fracture zone 2 is a west to north-west boundary line between two structural blocks; additionally, Permian felsic plutons are present on the coast. Fracture zone 3 extension coincides with a boundary between a structural block and sedimentary basin; there is further coincidence here with discordant igneous bodies of Mesozoic age. Permian thrust faulting associated with the Great Serpentine Belt also intersects the coast at this point (Ringis, 1975). As can be seen from Figure 4, the Gloucester and Bingara occurrences (areas 12 and 13) lie near the Great Serpentine Belt. The continental extension of

transform fault 4 coincides with the Hunter-Mooki thrust zone which also forms the northern edge of the Permo-Triassic Sydney Basin (Ringis, op. cit.). One of the Bingara kimberlitic intrusions (area 13) is situated on the north-westerly extension of this thrust zone. The Nullo Mountain occurrence, (area 11) is found to the south of this thrust zone in a dense cluster of Tertiary diatremes.

The Lachlan River Lineament lies on the continental extension of transform fault 5, in the continental shelf region. The extension of this line includes Mt. Woolnough - an inferred mafic igneous body (Ringis, 1975). The dense cluster of Sydney Basin diatremes (Crawford, 1973) lies on the Lachlan River Lineament, as does the Abercrombie kimberlitic occurrence (area 10). Part of the olivine leucitite cluster in central New South Wales also falls on this lineament, which possibly also incorporates the White Cliffs occurrence (area 4) at its extreme western extension.

The on-shore projection of transform fault 6 coincides with the central complex of Milton, a Permian intrusion which contains alkaline rock types (Ringis, op. cit.). Tertiary diatremes, the Jugiong kimberlitic rocks (area 9), and a cluster of olivine leucitites are all located on a WNW projection of this oceanic transform: here, however, it must be stressed that only minor WNW lineaments are present in the continental setting (Figure 4). The Jugiong occurrences are also adjacent to the NNW-trending Coolac Serpentinite Belt (Figure 4) which to the SE is semi-continuous with NW-trending lineaments and faults incorporating the Bombala and Delegate occurrences (areas 8 and 7).

The extended trend of fracture zone 7 into the continental setting includes the three Mesozoic mafic igneous complexes of Mt. Dromedary, Montague Island and Tanja syenite, all of which contain alkaline rock types. Some 70 kilometres inland the Myalla Road syenite complex falls on this trend line, as well as Tertiary diatremes farther to the west. Farther inland the Murray River Lineament forms a possible northwesterly extension of this zonal trend. The Delegate and Bombala occurrences (areas 7 and 8) lie in a fringe area slightly to the south of this postulated lineament.

The extension of fracture zone 8 coincides with the southern edge of the Gippsland Basin (Ringis, op. cit.). A large number of Tertiary and Quaternary diatremes, including the kimberlitic occurrence of Bullenmerri (area 5), are situated on a western projection of this lineament. The Oatlands occurrence in Tasmania (area 6), as well as Tertiary diatremes, could also be construed as lying on the continental projection of transform fault 11.

Should the Tasman Sea transform faults have a continental manifestation, then it must be noted that these postulated extensions change from the slightly curved fracture line patterns of transform fault 5, and those south of it, to strongly curved ones farther north. The strongly curved fracture pattern shown in the northern part of Figure 4 coincides with the area where the oceanic isochrons intersect the continental margin at high angles, and, as noted, may be a possible product of subduction during a limited period of Tasman Sea opening (Hayes and Ringis, 1973). The abundant thrust faulting in the New England Fold Belt began in the Permian as a result of obduction (Scheibner, 1973). Along this strongly-curved grain, first produced in the Permian orogenic episodes, lay the sites of continued reactivation, including the period during the opening of the Tasman Sea. In the area to the south of transform fault 4, the postulated Palaeozoic obduction and subduction zones are sub-parallel to the present-day coastline and thereby approximately at right-angles to the postulated transform fault extensions. This factor could account for the fracture pattern variations.

As pointed out by Ringis (1975) the intrusions on or near the coastline on the projected extensions of the transform faults all predate the $\sim$80 m.y. b.p. opening of the Tasman Sea. This feature is in accordance with the postulate that the sites of transform faults are probably dictated by pre-existing structural weaknesses in the pre-breakup continental crust (Wilson, 1965; Watterson, 1975).

With the exception of four areas, the kimberlitic rocks occur in or near granitic plutons; in three of these four areas the relationships are obscured by young cover (Figure 5). The Walloway occurrence (area 2) intrudes Proterozoic rocks, and is not spatially associated with younger granites. Area 1 kimberlitic rocks are the only ones spatially associated with Precambrian granite plutons; elsewhere the plutons are of Palaeozoic age.

Scheibner divided the Lachlan Fold Belt in New South Wales into anticlinorial and synclinorial zones. "The terms anticlinorial and synclinorial denote to major and composite structural units in fold or orogenic belts of anticlinorial or elevated, and synclinorial or depressed character" (p 10, 1976b). Using published information (see caption Figure 6), this technique was applied to the other States in south-eastern Australia; the composite map is shown in Figure 6. Information is inconclusive in four kimberlitic areas, the remaining occurrences fall equally into anti- and synclinorial zones. By definition, there is, in part, a resulting general coincidence between anticlinoria zones and zones of major granitic development.

In terms of Bouguer anomalies (Figure 7) thirteen of the kimberlitic areas are located in gravity lows; the exception is Bullenmerri (area 5), which occurs in a gravity low but is immediately adjacent to a high-low boundary. On

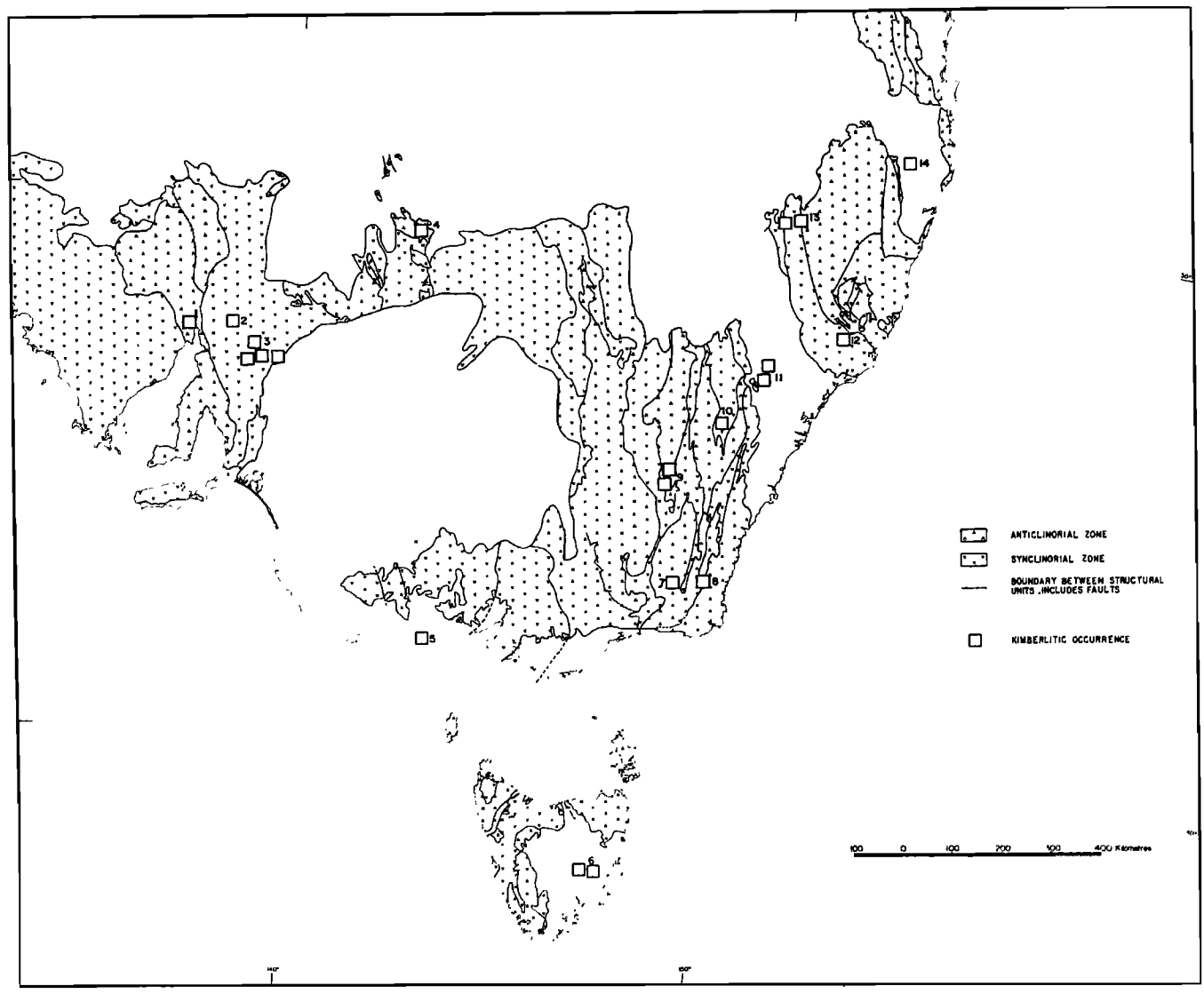

Fig. 6. Anticlinorial and synclinorial zones of south-eastern Australia. Information compiled from:-
General: "Tectonic Map of Australia and New Guinea 1:5,000,000 Geological Society of Australia, 1971", "The Geological Map of Australia, 1:2,500,000 scale, Bureau of Mineral Resources, Geology and Geophysics, Canberra, A.C.T., Australia".
New South Wales: Scheibner 1974, 1976a and b.
Victoria: Spencer-Jones and VandenBerg 1975; VandenBerg 1976; Crook and Powell 1976.
Queensland: Jones 1965.
Tasmania: Banks and Jago 1972; Williams et al., 1975; Williams 1976.
South Australia: Thomson et al., 1975; Katz 1976.

the basis of gravity trends, Wellman (1976) has defined crustal block boundaries which are included in Figure 7. As can be seen, four areas lie on or adjacent to these boundaries, namely the occurrences at Port Augusta, White Cliffs, Jugiong and Bingara (areas 1,4,9 and 13 respectively). There is a broad parallelism between the trends displayed by gravity, tectonic units, and elongation of major granitic belts.

Magnetic coverage is sketchy for south-east Australia; information is limited to ten of the fourteen areas. Of these, most lie in magnetic lows; where the occurrences are on magnetic highs they are immediately adjacent to magnetic

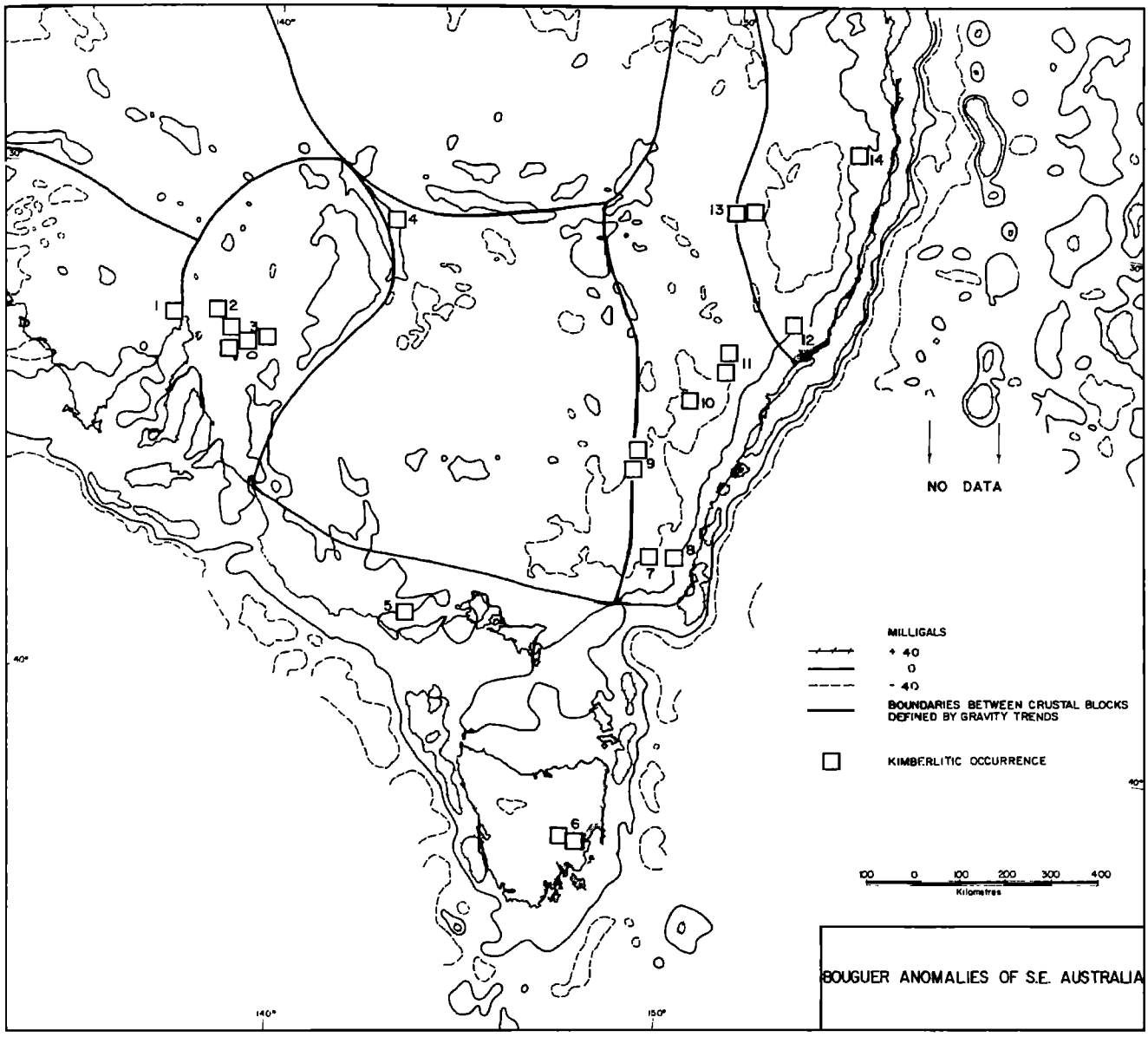

Fig. 7. Bouguer Anomalies of south eastern Australia, contour intervals 40 milligals. Taken from "Compilation and production of the 1976 Gravity Map of Australia (Anfiloff et al., 1976)". Boundaries between crustal blocks defined by gravity trends (Wellman 1976).

low boundaries. Six of the ten areas occur on or adjacent to magnetic high-low boundaries. There is a broad correlation between the magnetic and gravity grain, but no coincidence of highs and lows. There is insufficient magnetic coverage in the main granitic zones, as well as in zones of supracrustal igneous activity, to test a correlation. Although information is sketchy there is a broad superposition of the magnetics and clinoria trends.

The salient features of the fourteen kimberlitic occurrences are tabulated in Table 3.

Conclusion

Postulated continental extensions of transform faults, stemming from both the Antarctic and Tasman Sea Ridges, appear to have played the major role in the location of kimberlitic intrusions in south-eastern Australia. The South Australian kimberlitic occurrences all lie on the continental projection of the oceanic fracture zone arising from present-day spreading associated with the Antarctic Ridge. On the eastern seaboard, this southern spreading ridge is also thought to be

TABLE 3A

Area No. & Locality	1 Port Augusta	2 Walloway	3 Terowie
Map Earthquakes	Lie on W margin of N-S earthquake zone & on W side of projected N-S oceanic fracture zone.	Lie in central part of N-S earthquake zone immediately adjacent to projected N-S oceanic fracture zone.	Lie on E margin of N-S earthquake zone adjacent to projected N-S oceanic fracture zone.
Structural Features	Lies adjacent to N-S lineament which is a fault further to the N. Possible NNW alignment of the three kimberlites.	Lies in Flinders Range "elbow" position. Elongate kimberlitic intrusions parallel to fold grain.	Lies in Flinders Range "elbow" position. Elongate kimberlitic intrusions parallel to fold grain.
Supracrustal Igneous Activity	Immediately to the E of Proterozoic mafic intrusions.	Carbonatites & kimberlitic intrusions intimately associated.	Blank zone.
Granitic Rocks	Near Precambrian granite plutons.	Blank zone.	Near Ordovician granitic plutons.
Anticlinorial and Synclinorial Zones	In central part of anticlinorial zone.	In central part of synclinorial zone.	In central part of synclinorial zone.
Gravity	In gravity low adjacent to crustal block boundary.	In gravity low in marginal part of crustal block.	In gravity low in central part of crustal block.
Magnetics	Two of the intrusions occur in a magnetic high & the third on a high-low boundary.	In a magnetic low.	In the centre of a magnetic low.

TABLE 3B

Area No. & Locality	4 White Cliffs	5 Bullenmerri	6 Oatlands
Map Earthquakes	Blank zone.	Blank zone.	On NE fringe of earthquake region.
Structural Features	Adjacent to fault & NNW lineament. On fringe of W extension of Lachlan River Lineament.	On S flank of edge of epeirogenic uplift & adjacent to NE lineament.	In zone of minor NNW faults.
Supracrustal Igneous Activity	In area of Palaeozoic mafic intrusions.	Lies within cluster of Quaternary diatremes & in a province of alkali basalts.	In area of broad province of Mesozoic mafic intrusion rocks. Tertiary diatremes nearby.
Granitic Rocks	Young cover obscures relationships.	Young cover obscures relationships.	Young cover obscures relationships.
Anticlinorial and Synclinorial Zones	In anti-clinorial zone in complex area.	Situated on projected position of boundary between syn- & anticlinorial zones.	Young cover obscures relationships.
Gravity	In gravity low adjacent to high-low boundary near intersection point of four crustal blocks.	In gravity high immediately adjacent to high-low boundary. Removed from crustal block boundary.	In gravity low near high-low boundary.
Magnetics	In a magnetic low near a high-low boundary.	Right on a high-low boundary.	One kimberlite in high immediately adjacent to high-low magnetic boundary; second occurrence in magnetic low.

TABLE 3C

Area No. & Locality	7 Delegate	8 Bombala	9 Jugiong
Map Earthquake	On E fringe of earthquake activity & adjacent to projected NE oceanic fracture zone.	On E fringe of earthquake activity and adjacent to projected NE oceanic fracture zone.	In area of earthquake activity & adjacent to projected NNE oceanic fracture zone.
Structural Features	Adjacent to NE lineament & on SE flank of edge of epeirogenic uplift.	Adjacent to alkali basalt & in province of central complexes with alkaline varieties.	Lies at the intersection of N striking faults & lineaments. On W flank of edge of epeirogenic uplift.
Supracrustal Igneous Activity	In area of alkali basalts & diatremes.	Adjacent to alkali basalt & in province of central complexes with alkaline varieties.	Adjacent to thrust fault with serpentinite. Tertiary alkali basalts in area. Lies on mean line of hot spot migration.
Granitic Rocks	Intrusion into Silurian granite.	Intrusion into Devonian granite.	Cluster in part intrusion into Silurian granitic pluton.
Anticlinorial and Synclinorial Zones	Central anticlinorial zone.	Centre of area of anticlinoria.	All in anticlinorial zone which is very narrow at this point, hence near synclinorial boundary.
Gravity	In gravity low near crustal block boundary.	In gravity low on flank of high-low boundary.	In gravity low immediately adjacent to crustal block boundary.
Magnetics	No information available.	No information available.	Southern occurrences on high-low boundary; no information for N occurrences.

TABLE 3D

Area No. & Locality	10 Abercrombie	11 Nullo Mtn.	12 Gloucester
Map Earthquakes	In area of earthquake activity & immediately adjacent to projected NNE oceanic fracture zone.	In the area of mild earthquake activity & on E flank of projected NNE oceanic fracture zone.	On N fringe of earthquake activity.
Structural Features	Occurs within the SE trending Lachlan River Lineament & on the W flank of edge of epeirogenic uplift.	On E flank of edge of epeirogenic uplift.	Lies in "elbow" position of the Tamworth Synlinorial Zone & on E flank of edge of epeirogenic uplift.
Supracrustal Igneous Activity	Lies adjacent to mean line of hot spot migration; Sydney Basin diatremes & this area of kimberlites lie on the Lachlan River Lineament.	Lies in area of Tertiary diatreme cluster.	Lies close to S extension of Great Serpentine Belt & general area of Cainozoic alkali basalts.
Granitic Rocks	Adjacent to mid-to-late Palaeozoic granites.	Young cover obscures relationships.	Near Permian granitic plutons.
Anticlinorial and Synclinorial Zones	Central synclinorial zone.	Probably in synclinorial zone occurring in Sydney Basin.	In central part of Tamworth Synclinorial Zone.
Gravity	In gravity low centrally situated in crustal block.	In gravity low near centre of crustal block.	In gravity low near high-low boundary approaching crustal block boundary.
Magnetics	In centre of magnetic low zone.	In magnetic high immediately adjacent to high-low boundary.	No information available.

TABLE 3E

Area No. & Locality	13 Bingara	14 Mt. Brown	General Comment
Map Earthquakes	Two occurrences lie astride projected NNE fracture zone; area devoid of earthquake activity.	Blank zone.	Of the fourteen areas only four lie outside of seismically active zones. Nine of the areas lie on or adjacent to the continental projections of oceanic fracture zones.
Structural Features	Occurs in N extension of Tamworth Synclinorial Zone & on W flank of edge of epeirogenic uplift.	Adjacent to minor NNE trending faults on E flank of edge of epeirogenic uplift.	All areas on the E seaboard straddle the edge of epeirogenic uplift. There is a marked coincidence of the edge of epeirogenic uplift with the projected oceanic fracture zone on the E seaboard. All kimberlites are associated with either faults,lineaments or folds. Three areas are found in "elbow" positions of major flexures.
Supracrustal Igneous Activity	Lies close to Great Serpentine Belt; also in diatreme area. In province of Cainozoic sub-alkaline basalts.	In area of mixed alkaline & sub-alkaline Cainozoic basalt activity & adjacent to mean line of hot spot migration.	All areas on E seaboard are found in areas of basaltic activity which is dominantly alkaline but some areas are associated with sub-alkaline basalts. Only one area (3) is not spatially associated with supracrustal igneous activity. 3 areas (9,12&13) are associated with serpentinites. Areas 9,10, 11&14 lie on or near the mean line of hot spot migration.
Granitic Rocks	Near Permian granitic plutons.	Near Permian granitic plutons.	All areas except for four occur in or near granitic plutons; in three of these four areas the relationships are obscured by younger cover rocks. The Walloway occurrence (area 2) intrudes Proterozoic rocks and is unrelated to younger granites.
Anticlinorial and Synclinorial Zones	Near flanks of Tamworth Synclinorial Zone.	Probable synclinorial zone.	The areas are evenly distributed in syn- and anticlinorial zones; information is uncertain in four areas.
Gravity	In gravity low near crustal block boundary.	In gravity low near gravity high-low boundary removed from crustal block boundary.	Thirteen of the areas are located in gravity lows; the exception is Bullenmerri (area 5) occurring in a gravity high immediately adjacent to a high-low boundary. Four of the areas lie on, or adjacent to, crustal block boundaries as defined by gravity trends.
Magnetics	No information available.	In magnetic low.	Information limited to ten of the fourteen areas. Most of the areas lie in magnetic lows, where in magnetic highs these are immediately adjacent to high-low boundaries. Six of the ten areas occur on or adjacent to magnetic high-low boundaries.

responsible for the projected continental fracture zone, lying within a broad belt of Cainozoic igneous activity in south-eastern Australia between the edge of epeirogenic uplift and the mean line of hot spot migration. All the kimberlitic occurrences near the eastern seaboard of Australia fall within this broad zone of activity. Their location also appears to have been governed by fracture patterns initially developed during pre-breakup times and which later became the sites of continental extensions of transform faulting during the Tasman Sea opening; this spreading commenced 80 m.y. ago and aborted 60 m.y. ago. A number of the kimberlitic occurrences on the eastern seaboard of Australia are located at the intersections of the projected continental transforms stemming from the two spreading centres.

Acknowledgements. We are indebted to Australian Anglo American Limited, De Beers Consolidated Mines Limited, and the Director, Commonwealth of Australia, Bureau of Mineral Resources, Geology and Geophysics, for permission to publish.

We thank Ms. Ann Goleby for help in preparing some of the maps; Mrs. Michele Karakasch for the draughting of maps and figures; J.W. Sheraton and W.B. Dallwitz for critical reading of the manuscript.

References

Adamson, C.L., 1969. Crushed stone and gravel resources of the Sydney Region, New South Wales. Rec. Geol. Surv. N.S.W., 11(2), 93-114.

Allsopp, H.L., Nicolaysen, L.O. and Hahn-Weinheimer, P., 1969. Rb/K ratios and Sr-isotopic compositions of minerals in eclogitic and peridotitic rocks. Earth Planet. Sci.Lett., 5, 231-244.

Anfiloff, W., Barlow, B.C., Murray, A.S., Denham, D. and Sanford, R., 1976. Compilation and production of the 1976 Gravity Map of Australia. BMR J. Aust. Geol. and Geophys., 1, 273-276.

Banks, M.R. and Jago, J.B., 1972. Plate tectonics and the lower Palaeozoic of Tasmania. Nature Phys. Sci., 240, 9-11.

Barrett, D.R., 1975. The genesis of kimberlites and associated rocks: strontium isotopic evidence. Phys. Chem. Earth,9, 637-653.

Barrett, D.R. and Berg, G.W., 1975. Complementary petrographic and strontium-isotope ratio studies of South African kimberlite. Phys. Chem. Earth,9, 619-635.

Beams, S., 1975. Geology and geochemistry of the Wyndham-Whipstick Area, N.S.W. Aust. Nat. Univ., B. Sc. Hons. thesis (unpubl.).

Berg, G.W. and Allsopp, H.L., 1972. Low $^{87}Sr/^{86}Sr$ ratios in fresh South African kimberlites. Earth Planet Sci.Lett., 16, 27-30.

Boeson, R., Irving, E. and Robertson, W.A., 1961. The Palaeomagnetism of some igneous rock bodies in N.S.W. J. Proc. R. Soc. N.S.W., 94, 227-232.

Brooks, C., James, D.E. and Hart, S.R., 1976. Ancient Lithosphere: Its role in young continental volcanics. Science, N.Y., 193, 1086-1094.

Brown, D.A., Campbell, K.S.W. and Crook, K.A.W., 1968. The geological evolution of Australia and New Zealand. Pergamon Press, 409p.

Cleary, J.R. and Simpson, D.W., 1971. Seismotectonics of the Australian Continent. Nature, Lond., 230, (5291), 239-241.

Colchester, D.M., 1972. A preliminary note on kimberlite occurrences in South Australia. J. geol. Soc. Aust., 19(3), 383-386.

Coward, M.P., 1976. Large scale Palaeozoic shear zone in Australia and present extension to the Antarctic Ridge. Nature, Lond., 259, 648-649.

Crawford, E.A., 1973. Igneous rock deposits, central Sydney Basin. Geol. Surv. New South Wales, Report GS 1973/441, 37p.

Crawford, A.R. and Campbell, K.S.W., 1973. Large scale horizontal displacement within Australia-Antarctica in the Ordovician. Nature Phys. Sci., 241, 11-14.

Crook, K.A.W., and Powell, C.McA., 1976. Tasman Geosyncline. Tour Guide 25th Inter. Geol. Cong.

David, T.W.E, 1950. In: W.R. Browne (ed.). The geology of the Commonwealth of Australia, 1. Arnold, London, 747p.

Edwards, A.B., 1950. The petrology of the Cainozoic basaltic rocks of Tasmania. Proc. R. Soc. Vic., 62(1), 97-120.

Embleton, B.J.J., 1976. Large scale Palaeozoic shear zone in Australia. Nature, Lond., 264, 199.

Evernden, J.F. and Richards, J.R., 1962. K/Ar Ages in Eastern Australia. J. geol. Soc. Aust., 9(1), 1-49.

Ferguson, John, Ellis, D.J. and England, R.N., 1977. Unique spinel-garnet lherzolite inclusion in kimberlite from Australia. Geology,5, 278-280.

Ferguson, John and Sheraton, J.W., This volume. Petrogenesis of kimberlitic rocks and associated xenoliths of S.E. Australia.

Giddings, J.W. and Embleton, B.J.J. 1974. Large scale horizontal displacements in Southern Australia - Contrary evidence from Palaeomagnetism. J. geol. Soc. Aust., 21(4), 431-436.

Griffin, W.L. and Murthy, V.R., 1968. Abundances of K, Rb, Sr and Ba in some ultramafic rocks and minerals. Earth Planet. Sci. Lett., 4, 497-501.

Harper, L.F., 1915. Geology and mineral resources of the southern coalfield (1) the south portion. Mem. geol. Surv. N.S.W., 7.

Harrington, H.J., Burns, K.L. and Thompson, B.R., 1973. Gambier-Beaconsfield and Gambier-Sorell fracture zones and the movement of plates in the Australia-New Zealand region. Nature phys. Sci., 245, 109-112.

Harris, P.G., Hutchinson, R. and Paul, D.K., 1972. Plutonic xenoliths and their relation to the upper mantle. Phil. Trans. Soc., London, A271, 313-323.

Hayes, D.E. and Ringis, J., 1973. Sea-floor spreading in the Tasman Sea. Nature, Lond., 243, 454-458.

Jones, O.A., 1965. Geology and mineralization of eastern Queensland. In: McAndrew, J., (ed.) Geology of Australian ore deposits. 8th Commonwealth Mining and Metallurgical Congress, Aust. and New Zealand. Aust. Inst. Min. Metall., 352-360.

Katz, M.B., 1976. Lineament tectonics of the Willyama Block and its relationship to the Adelaide Aulocogene. J. geol. Soc. Aust., 23(3), 275-286.

Langworthy, A.P. and Black, L.P., In Prep. The Mordor Complex: a highly differentiated, potassic intrusion with kimberlitic affinities in Central Australia.

Lovering, J.F. and Richards, J.R., 1964. Potassium-argon age study of possible lower-crust and upper mantle inclusions in deep-seated intrusions. J. geophys. Res., 69, 1895-1901.

Lovering, J.F. and White, A.J.R., 1969. Granulitic and eclogitic inclusions from basic pipes at Delegate, Australia. Contr. Miner. Petrol., 21(1), 9-52.

McDougall, I. and Wellman, P., 1976. Potassium-argon ages for some Australian Mesozoic igneous rocks. J. geol. Soc. Aust., 23(1), 1-10.

McIntyre, G.A., Brooks, C., Compston, W. and Turek, A., 1966. The statistical assessment of Rb-Sr isochrons. J. geophys. Res., 71, 5459-5468.

Neumann, W. and Huster, E., 1972. Neubestimming der Halbwertszeit des ^{87} Rubidiums durch Vergleich von Messungen an der getrenntent Isotopen ^{87}Rb and ^{85}Rb. Z. Naturforschung 27, 862-863.

Packham, G.H. (Editor), 1969. The geology of New South Wales. J. geol. Soc. Aust., 16(1), 654p.

Page, R.W., Blake, D.H. and Mahon, M.W., 1976. Geochronology and related aspects of acid volcanics, associated granites, and other Proterozoic rocks in the granites-Tanami region, north-western Australia. BMR J. Aust. Geol. and Geophys. 1, 1-13.

Ringis, J., 1975. The relationship between structures on the south-east Australian margin and in the Tasman Sea. Bull. Aust. Soc. Explor. Geophys., 6(2-3), 39-41.

Sass, J.H., 1964. Heat flow values from Eastern Australia. J. geophys. Res., 69(18), 3889-3893.

Scheibner, E., 1973. A plate tectonic model of the Palaeozoic Tectonic history of New South Wales. J. geol. Soc. Aust., 20(4), 405-426.

Scheibner, E., 1974. Tectonic map of New South Wales, scale 1:1,000,000. Geol. Surv. N.S.W., Sydney.

Scheibner, E., 1976a. Explanatory Notes on the Tectonic Map of New South Wales. Geol. Surv. N.S.W.

Scheibner, E., 1976b. Tasman Fold Belt System in New South Wales. 25th Inter. geol. Congr. Sydney. Report GS 1976/195, 33p.

Spencer-Jones, D., and Vandenberg, A.H.M., 1975. The Tasman geosyncline in Victoria - Regional Geology. In: Knight, C.L. (ed.). Economic geology of Australia and Papua New Guinea. Aust. Inst. Min. Metall., 1, Metals, Monograph Series 5, 637-645.

Spry, A., 1962. Igneous activity of Tasmania. J. geol. Soc. Aust., 9(2), 256-284.

Stewart, I.C.F., 1976. Fractures and movement in the Adelaide rift zone. Nature, Lond., 264, 198-199.

Sutherland, F.L., 1969. A comparison of the Cainozoic Volcanic Provinces of Victoria and Tasmania. Proc. R. Soc. Vic., 82(2), 179-185.

Sutherland, F.L., Green, D.C. and Wyatt, B.W. 1973. Age of Great Lake Basalts. J. geol. Soc. Aust., 20(1), 85-94.

Thomson, B.P., Forbes, B.G. and Coats, R.P., 1975. Adelaide geosyncline and Stuart Shelf. In: Knight, C.L. (ed.). Economic geology of Australia and Papua New Guinea. Aust. Inst. Min. Metall., 1, Metals, Monograph Series 5, 537-542.

Tucker, D.H. and Collerson, K.D., 1972. Lamprophyric intrusions of probable carbonititic affinity from South Australia. J. geol. Soc. Aust. 19(3), 387-392.

Vandenberg, A.H.M., 1976. The Tasman Fold Belt in Victoria. Geol. Surv. Victoria, Report 1976/3, 44p.

Veevers, J.J., 1976. Early Phanerozoic events on and alongside the Australasian-Antarctic Platform. J. geol. Soc. Aust., 23(2), 183-207.

Wass, S.Y. and Irving, A.J., 1976. XENMEG - A catalogue of occurrences of xenoliths and megacrysts in volcanic rocks of eastern Australia. The Australian Museum, Sydney, 441p.

Watterson, J., 1975. Mechanism for the persistence of tectonic lineaments. Nature, Lond., 253, 520-522.

Weissel, J.K. and Hayes, D.E., 1972. Magnetic Anomalies of the Southeast Indian Ocean. In: Hayes, D.E. (ed.). Antarctic Oceanology II: the Australian-New Zealand Sector, Antarctic Res. Ser., 19, 165-196.

Weissel, J.K. and Hayes, D.E., 1977. Evolution of the Tasman Sea reappraised. Earth Planet. Sci. Lett., 36, 77-84.

Wellman, P., Cundari, A. and McDougall, I., 1970. Potassium-Argon ages for leucite-bearing rocks from New South Wales, Australia. J. Proc. R. Soc., N.S.W., 103, 103-107.

Wellman, P., 1974. Potassium-argon ages on the Cainozoic volcanic rocks of Eastern Victoria, Australia. J. geol. Soc. Aust., 21(14), 359-376.

Wellman, P. and McDougall, I., 1974a. Cainozoic

igneous activity in Eastern Australia. Tectonophysics, 23, 49-65.

Wellman, P. and McDougall, I., 1974b. Potassium-argon ages on the Cainozoic volcanic rocks of New South Wales. J. geol. Soc. Aust., 21(3), 247-272.

Wellman, P., 1976. Gravity trends and the growth of Australia: A tentative correlation. J. geol. Soc. Aust., 23(1), 11-14.

Williams, E., Solomon, M. and Green, C.R., 1975. Geological setting of metalliferous ore deposits in Tasmania. In: Knight, C.L. (ed.). Economic geology of Australia and Papua New Guinea. Aust. Inst. Min. Metall. 1, Metals, Monograph Series 5, 567-581 .

Williams, E., 1976. Tasman Fold Belt System in Tasmania. 25th Inter. geol. Congr., 29p.

Williams, I.S., Compston, W., Chappell, B.W. and Shirahase, T., 1976. Rubidium-strontium age determinations on micas from a geologically controlled, composite batholith. J. geol. Soc. Aust., 22, 497-506.

Wilson, J.T., 1965. A new class of faults and their bearing on continental drift. Nature, Lond., 207, 343-347.

KIMBERLITES IN BRAZIL: AN INITIAL REPORT

Darcy P. Svisero

Instituto de Geosciencias, Universidade de Sao Paulo, Brazil

Henry O. A. Meyer and Hsiao-ming Tsai

Department of Geosciences, Purdue University, West Lafayette, Indiana 47907

Abstract. Although diamonds have been known since the 1700's in Brazil, only in the last decade has unequivocal evidence for kimberlites been obtained. Much of this evidence is in the confidential reports of mining companies; accordingly this brief note is to indicate the occurrence and nature of some of the recently discovered kimberlites in western Minas Gerais. These kimberlites form only part of a larger region of kimberlite activity extending from Minas Gerais, through Gois and Mato Grosso States into Rondonia Territory.

Introduction

A large area of Brazil, approximately 8.5 million km^2, consists of the South American Platform or Shield (Almeida et al., 1976). This platform is similar in many respects to the geological character of the Siberian, African and Australian shields and accordingly the occurrence of kimberlite would not be unusual. Furthermore, the widespread occurrence of diamond in Brazil (e.g. States of Minas Gerais, Mato Grosso, Bahia, and Goias as well as Territories of Rondonia and Roraima) (Fig. 1) also lend crecedence to the possibility of kimberlites. Such ideas have recently proven correct and kimberlites are now documented from several areas in Brazil.

The main purpose of this paper is to place in context the present general situation with regard to research and prospection for kimberlites in Brazil. Such studies are in their infancy and thus only general geological remarks with respect to kimberlite localities are made, although special emphasis is placed on the area in West Minas Gerais State where most of the kimberlites presently known are located.

The Kimberlitic Province of West Minas Gerais

West Minas Gerais State is by far the most important diamondiferous area in Brazil and contains the majority of kimberlites discovered up to the present time. The geographic limits of this Province may be defined roughly by the Paranaiba and Grande Rivers. Most of the well-known centers of diamond production, such as Coromandel, Monte Carmelo, Romaria, Patos, Estrela do Sul, are located within this region.

Detrital diamonds were first discovered in West Minas Gerais about 1750. During the nineteenth century when Brazil was the major world producer of diamond, the washings in West Minas Gerais were responsible for most of the Brazilian production. Furthermore, a characteristic of the area is the periodic finding of large diamonds, such as the Getulio Vargas which weighed 726.6 carats and is still the fifth largest diamond ever found. The occurrence of large stones is still common in the placers of Santo Inacio and Santo Antonio das Aguas Vermelhas River near Coromandel as well as near Estrela do Sul along the Bagagem River. For example, a 83-carat diamond was recently found in placers at the side of Estrela do Sul (Svisero and Haralyi, 1977).

The existence of kimberlites in West Minas Gerais has been a subject of long discussion. Many authors in the past point out the possibility that kimberlite may occur in Brazil, (Derby, 1898; Rimann, 1917; Maack, 1926; Freyberg, 1932), but only recently through systematic surveys were kimberlites actually discovered. Two companies; a French and a Brazilian studied the dispersion of the resistant kimberlite minerals pyrope garnet and Mg-ilmenite and discovered several intrusive bodies with kimberlitic characteristics (Barbosa et al., 1976). More recently another company has reprospected the region and has increased the number of probable kimberlites. In spite of this work the only kimberlite reported in the literature to date is the Vargem diatreme located 20 km southeast of Coromandel (Svisero et al., 1977). Presently several kimberlites including the Limeira, Capo da Erva, Japecanga, Vargem, Santa Clara, Forca, Lagoa Seca, Poco Verde and Santa Rosa have been sampled and are being investigated (Fig. 2).

Fig. 1. Main localities of diamond occurrences in Brazil: 1) Tibagi, 2) Franca, 3) Tiros, 4) Estrela do Sul, 5) Coromandel, 6) Romaria, 7) Abaete, 8) Grão Mogol, 9) Diamantina, 10) Morro do Chapeu, 11) Lençois, 12) Gilbues, 13) Maraba, 14) Tepequen, 15) Uraricoera, 16) Machado, 17) Aripuana, 18) Chapada Guimaraes, 19) Diamantino, 20) Poroxeu, 21) Rondonopolis, 22) Coxim, 23) Barra do Garças, 24) Baliza, 25) Mineiros.

Geology

The geology of West Minas Gerais modified from Barbosa et al., (1970) and Hasui et al. (1976) is summarized in Fig. 3. The most conspicuous feature is a central zone of Precambrian rocks extending NW-SE which constitute the Alto Paranaiba tectonic arc separating the Parana Basin in the southwest from the Alto San-Franciscana Basin on the northeast. The geology of this central zone comprises Upper Pre-cambrian metasediments belonging to the Araxa, Canastra and Bambui Groups. The Araxa Group, the oldest unit in the area, is composed essentially of schists and metabasites of high greenschist and amphibolite facies. It is followed by the Canastra Group (quartzites and phyllites) and Bambui Group (slates and limestones). The former rocks show little or no metamorphism.

Another remarkable feature of the region (Fig. 3) is the occurrence of six large alkaline and carbonatite complexes whose distribution follows the trend of regional structures. However, as will be discussed later the emplacement of these alkaline complexes is linked to major fractures or faults which have probably also controlled the kimberlitic intrusions.

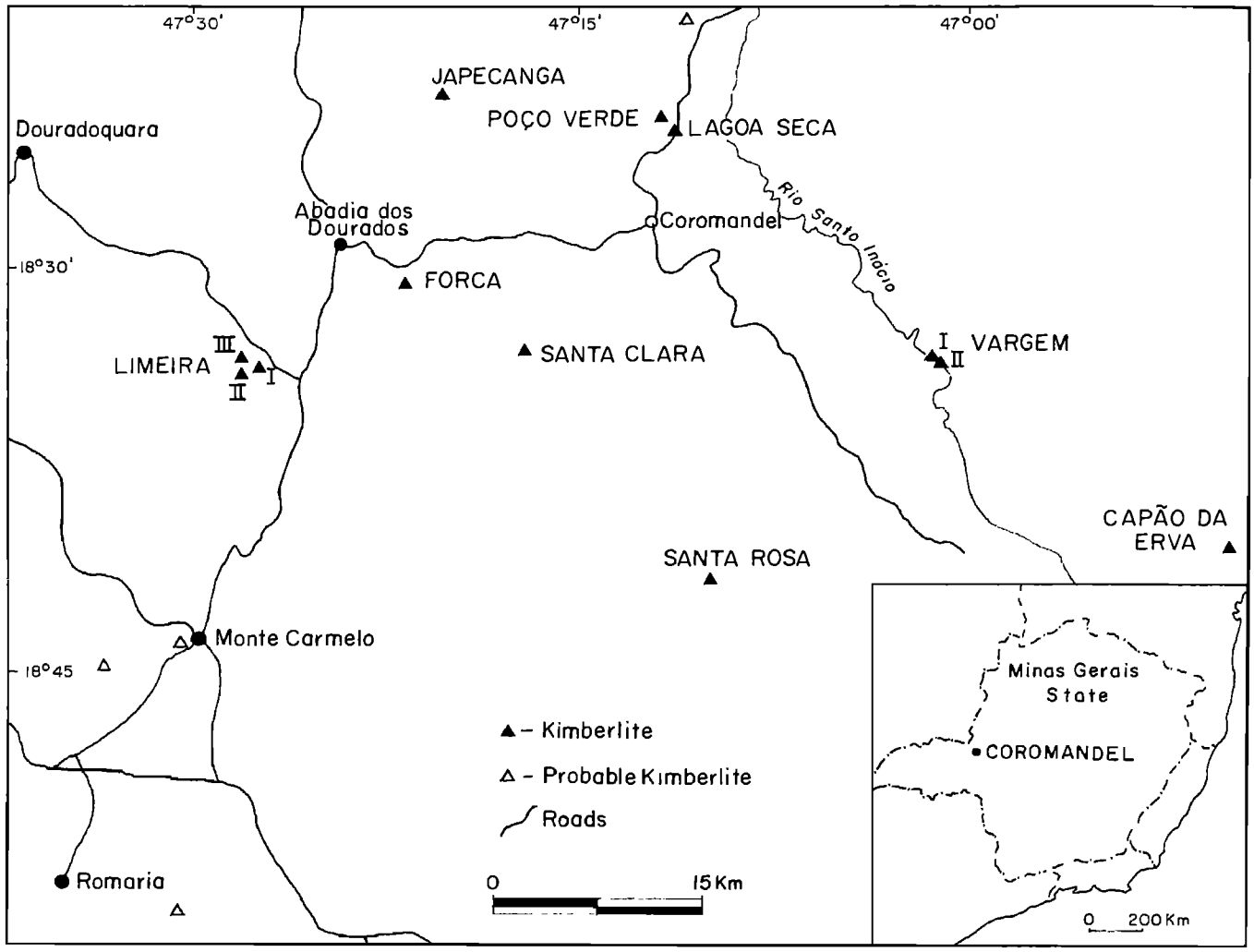

Fig. 2. Geologic location of kimberlites in the Kimberlitic Province of West Minas Gerais.

Geophysics

Several recent geophysical surveys both aeromagnetic (Bosum, 1973; Bosum et al., 1974, Vianna and Schmidt, 1975) and gravimetric (Almeida et al., 1976) have contributed greatly to understanding the structural control of the geology.

In Figure 4 is displayed the aeromagnetic pattern of the area where three different types of anomalies may be distinguished: 1) an irregular type related to the basaltic traps of Parana Basin and Alto San-Franciscana Basin; 2) a large polar type corresponding to the exposed alkaline complexes of Tapira, Araxa, Salitre, Serra Negra, Catalao I and Catalao II; the smaller intrusions of Ibia, Sao Getardo and Perdizes, as well as kimberlites, and other basic and ultrabasic rocks which did not reach the surface; 3) a linear type of anomaly produced by ancient deep faults that have been penetrated by dikes whose ages varies from Cretaceous (diabases, basalts) up to 1000 million years old (metabasites). Almeida (1967) first showed that these deep faults have been periodically reactivated, of which the last period occurred during the Upper Cretaceous and was followed by kimberlite intrusion.

The gravimetric pattern of West Minas Gerais is shown in Fig. 5. The main feature is a central uplift along the NW-SE and NE-SW directions. This uplift corresponds exactly with the tectonic arc of Alto Paranaiba which Hasui et al. (1976) assumes to have been developed during the Upper Cretaceous. This uplift was followed by deep faults on the border and may have localized the kimberlite and carbonatite activity. The kimberlites particularly seem to be concentrated at the juncture of the two deep structures (NW-SE and NE-SW) that intersect near Monte Carmelo and Coromandel (Figs. 3 and 4).

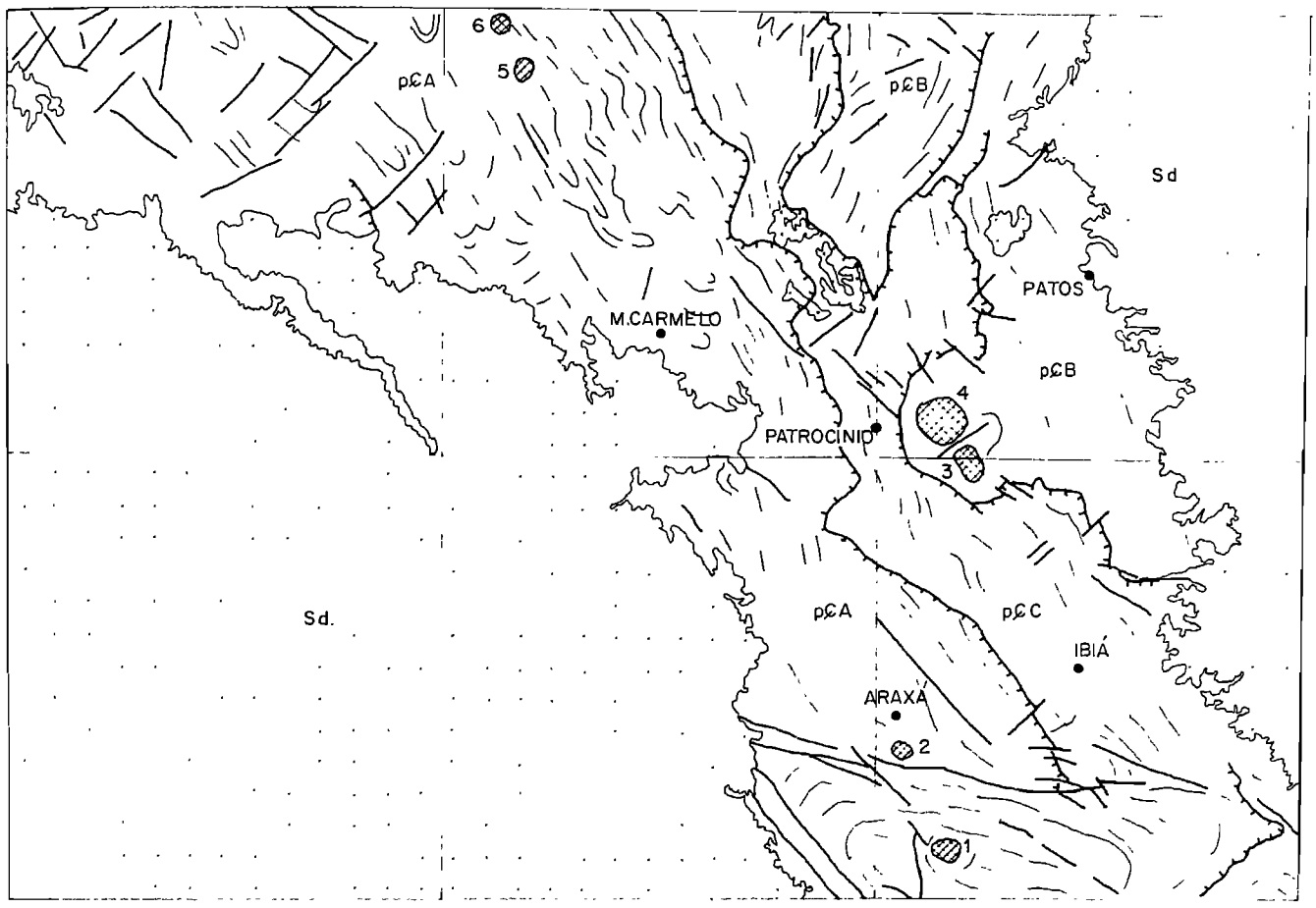

Fig. 3. Geologic sketch of West Minas Gerais State. Symbols: p Є A - Araxa Group, p Є B - Bambui Group, p Є C - Canastra Group, Sd - Mesozoic and Cenozoic sediments. Numbers refer to alcaline diatremes: 1) Tapira, 2) Araxa, 3) Salitre, 4) Serra Negra, 5) Catalão I, 6) Catalão II.

Age of Kimberlites

A number of kimberlite in West Minas Gerais have been dated by zircons (Davis, 1977) and they appear to be Cretaceous in age. This age is supported by field evidences as well as by many other indirect data. The Cretaceous period began in this region with the outpouring of enormous amounts of basaltic lava that intruded the sediments of the Parana Basin about 125 million years ago (Amaral 1972). In the Upper Cretaceous the development of the Alto Paranaiba Area took place, including deep fracturing that enabled the migration of kimberlites, carbonatites and other alkaline rocks into the crust. Other evidence of a Cretaceous age for the kimberlites is provided by the diamond-bearing conglomerate of the Bauru Formation. This conglomerate, the secondary source of diamond in the area, has been mined near the locality of Romaria since 1867. Heavy mineral constituents obtained by washing the conglomerate include (besides diamond) pyrope, and Cr-pyrope garnets as well as Mg-ilmenite together with magnetite perovskite and several other minerals. In general, the conglomerate has a suite of minerals that can be considered to be derived from both kimberlitic and alkaline sources.

Vargem Kimberlite

Presently, the Vargem Kimberlite, located 20 km southeast of Coromandel District, is the only one reported in the geological literature (Svisero et al., 1977). The kimberlite is extremely weathered at the surface but can be sampled in outcrops of yellow ground due to erosion by the Santo Inacio River which flows across a portion of the diatreme (Fig. 2).

Although weathered, the Vargem kimberlite shows a serpentinized and brecciated texture plus a few weathered xenoliths. However, concentrate from the pipe contains deep purple garnets, green diopsides and leucoxenized ilmenite.

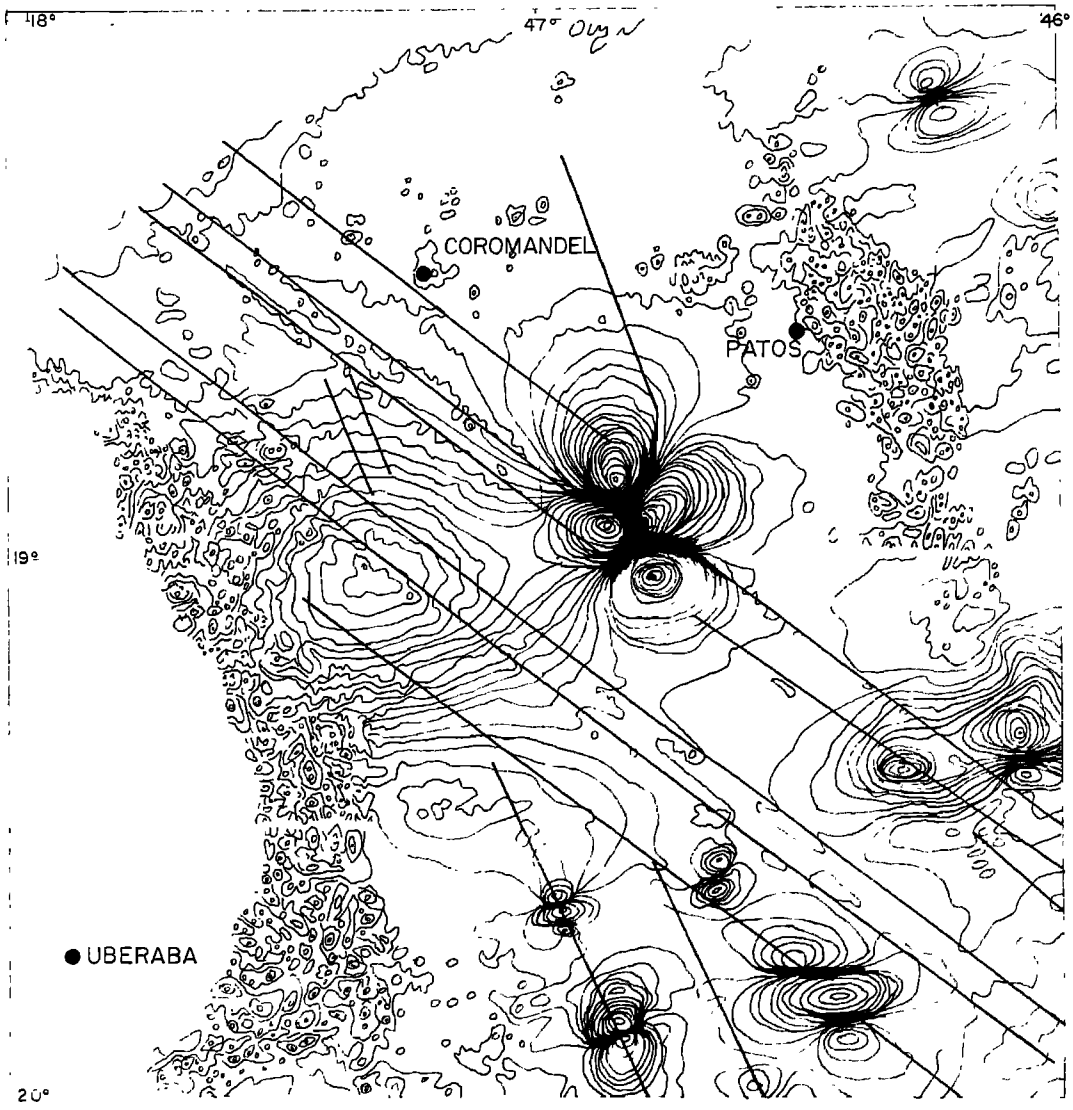

Fig. 4. Aeromagnetometric pattern of West Minas Gerais State.

Electron probe analyses of these minerals are presented in Table 1, and plotted in ternary variation diagrams (Figs. 6, 7, and 8) together with comparable data of African and U.S. kimberlites.

Limeira Kimberlites

Three kimberlites are presently known on the Limeira Farm located a few kilometers from the Monte Carmelo-Douradoquara road. One of these kimberlites, referred as Limeira I, contains a number of xenoliths which unfortunately like the kimberlite are weathered. More resistant kimberlite crops out in a small (dry) river bed that crosses the diatreme. Detailed geological mapping revealed that the Limeira I kimberlite is associated with a small olivine-basaltic plug.

Romaria Kimberlite

As previously mentioned diamond has been exploited at Romaria since the end of nineteenth century. Hussak (1894) based on the results of Romaria concentrates suggested the presence of kimberlites as the source of those diamonds. Recent detailed aerogeophysical survey has led to the finding of three probable kimberlites; two near Monte Carmelo and another near Romaria (Fig. 2). Several lines of evidence, including mineralogical and sedimentological studies, point to kimberlite being the primary source of diamonds in Romaria (Svisero et al., 1978).

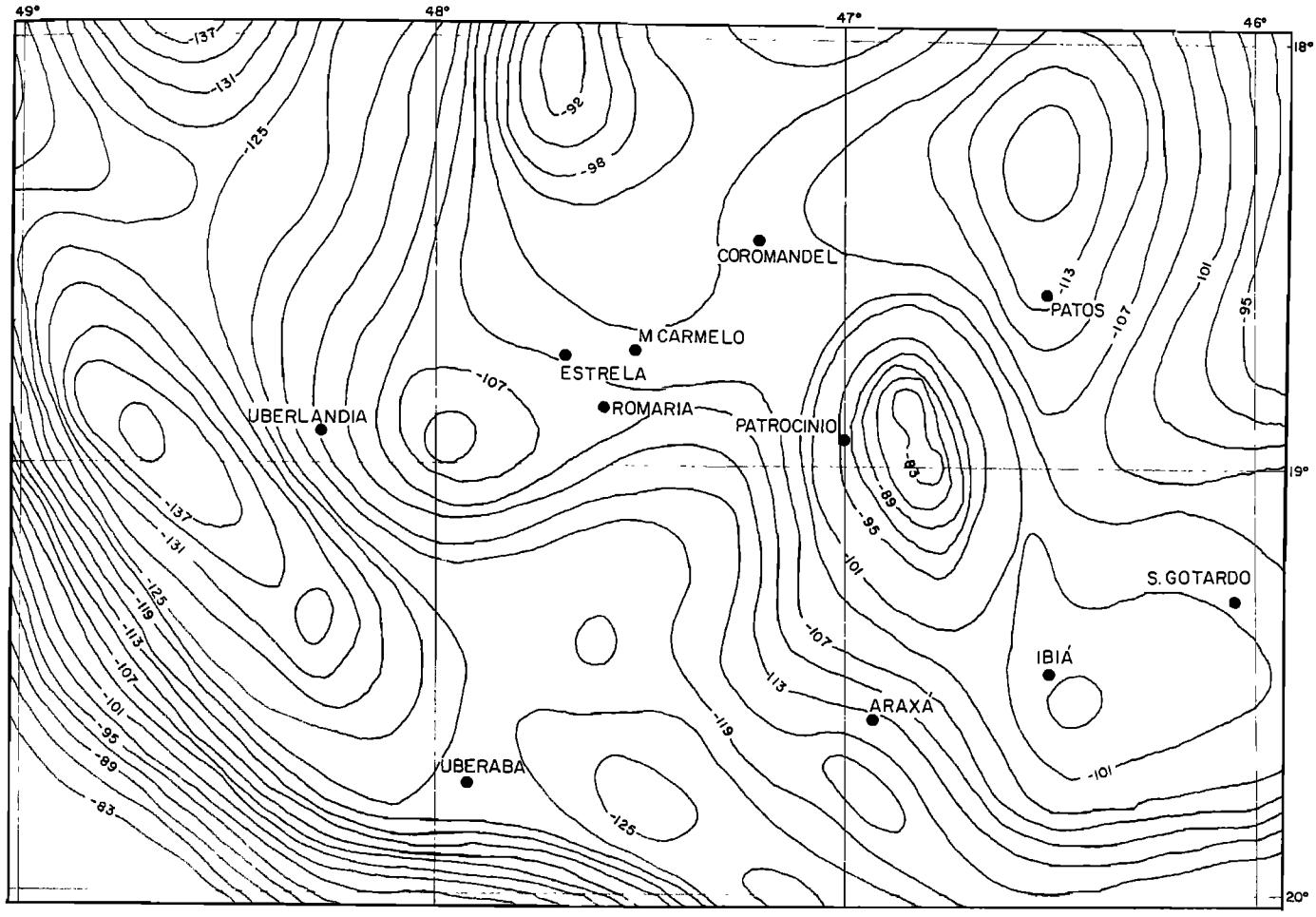

Fig. 5. Gravimetric pattern of West Minas Gerais State.

Other Kimberlite Provinces in Brazil

Kimberlites are not only restricted to West Minas Gerais State and it is possible that South Piaui State probably constitutes another area of kimberlite intrusions. However, only one kimberlite, the Redondao Kimberlite, has been reported in the literature to date (Melo and Porto, 1965; Svisero et al., 1977).

The Redondao was the first kimberlite to be discovered in Brazil, and Melo and Porto (1965) referred to it during a geological reconaissance for oil in South Piaui State. The absence of vegetation plus the presence of an almost circular depression 1 km wide and 70 meters deep, certainly assisted the finding of the Redondao diatreme.

The Redondao kimberlite, as in the case of the Vargem, is weathered at the surface and deep red garnet seems to be the only resistant mineral present in the concentrates. A particular

TABLE 1. Representative Analyses of Minerals from the Vargem Kimberlite.

	Garnet		Clinopyroxene		Ilmenite	
SiO_2	42.8	41.7	54.4	54.3	0.02	0.02
TiO_2	0.30	0.20	0.12	0.06	48.0	50.1
Al_2O_3	21.2	15.5	0.21	2.01	<0.01	0.31
Cr_2O_3	1.35	10.2	0.71	2.35	1.48	2.24
FeO	8.42	8.11	4.39	2.77	42.0	35.4
MnO	-	-	0.11	0.09	0.27	0.25
MgO	21.1	18.3	16.7	15.9	7.36	10.8
CaO	4.66	6.86	22.0	10.0	0.01	0.04
NiO	<0.01	0.02	<0.01	0.01	<0.01	<0.01
Na_2O	0.05	0.07	1.11	2.75	<0.01	0.14
K_2O	<0.01	<0.01	<0.01	0.01	<0.01	<0.01
Total	99.9	100.9	99.7	99.3	99.1	99.3

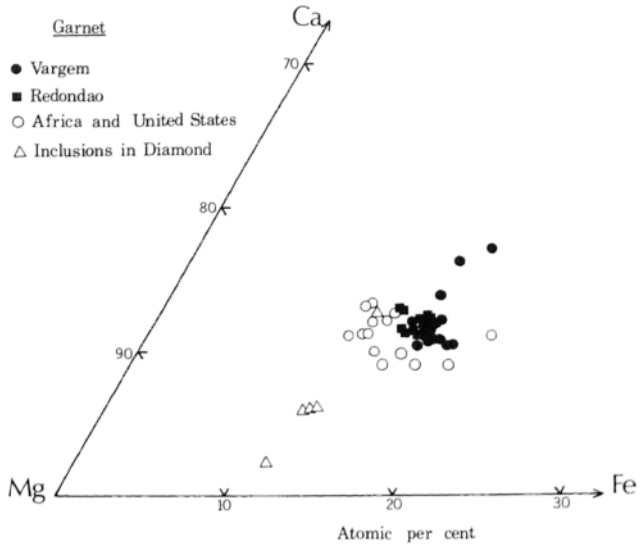

Fig. 6. Garnet from Vargem and Redondão diatremes in terms of Ca-Mg-Fe atomic per cent. Kimberlitic garnets from Southern Africa and North America are shown for comparison (Reid and Hanor, 1970; Cox et al., 1973; Meyer 1975 and Meyer and Svisero, 1975).

feature of the Redondao kimberlite is the presence of numerous xenoliths of crustal and mantle origin. Among the xenoliths have been found a garnet lherzolite about 12 cm in size. Unfortunately, apart from garnet the xenolith was completely serpentinized. Electron probe

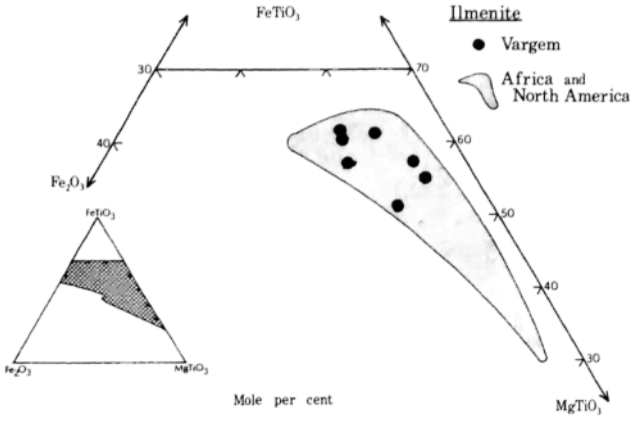

Fig. 7. Compositions of ilmenites from Vargem diatreme expressed in terms of the molecules ilmenite ($FeTiO_3$) Geikielite ($MgTiO_3$) and Hemitite (Fe_2O_3). Recalculation of iron into Fe''' and Fe'' was done following the method of Boyd (1971). Area for kimberlitic ilmenites from Southern Africa and North America is based on data from Mitchell, 1973; McCallister et al., 1975; Boyd and Nixon, 1973).

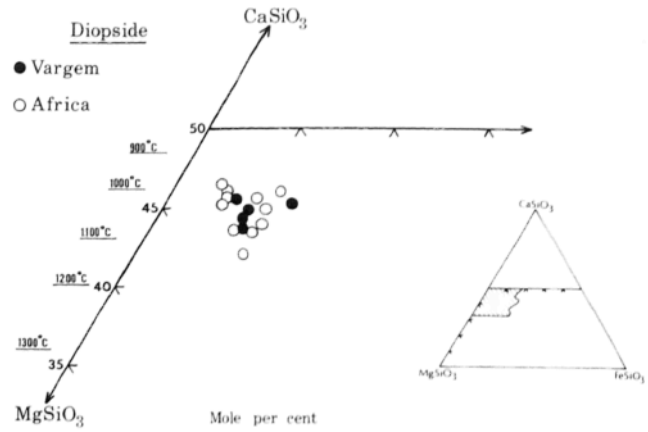

Fig. 8. Compositions of diopside from the Vargem diatreme together with other kimberlitic diopsides from Southern Africa (Cox et al., 1973; Boyd, 1969).

analyzes of garnets from Redondao kimberlite and xenolith are listed in Table 2. Figures 6 and 9 are Ca-Mg-Fe diagrams of the garnets together with comparable ones from other sources.

Besides the Provinces of West Minas Gerais and Southwest Piaui many other places in Brazil are possible potential kimberlite provinces. For example, diamonds are widespread in many remote localities such as north Mato Grosso, central Para, Roraima and Amapa Territories. Geological data on these areas is still restricted to general reconaissance, with some minor recent improvement by ERTS Survey. Kimberlites have been prospected for in some of these localities but the results are still unknown, although a possible diamond-bearing kimberlite in Rondonia Territory has been reported.

TABLE 2. Representative Garnet Analyses from Redondao Kimberlite and Garnet-lherzolite Xenolith.

	Xenolith	Kimberlite		
SiO_2	42.0	42.0	41.8	40.6
TiO_2	0.34	0.22	0.19	0.05
Al_2O_3	21.1	22.6	21.3	20.6
Cr_2O_3	3.39	1.75	2.68	4.20
FeO	5.99	8.37	8.13	7.30
MnO	-	0.36	0.36	0.43
MgO	21.4	20.6	20.7	21.0
CaO	4.91	4.88	4.89	5.14
NiO	<0.01	<0.01	<0.01	0.04
Na_2O	0.09	0.05	<0.01	0.01
K_2O	<0.01	<0.01	<0.01	<0.01
Total	99.2	100.8	100.1	99.4

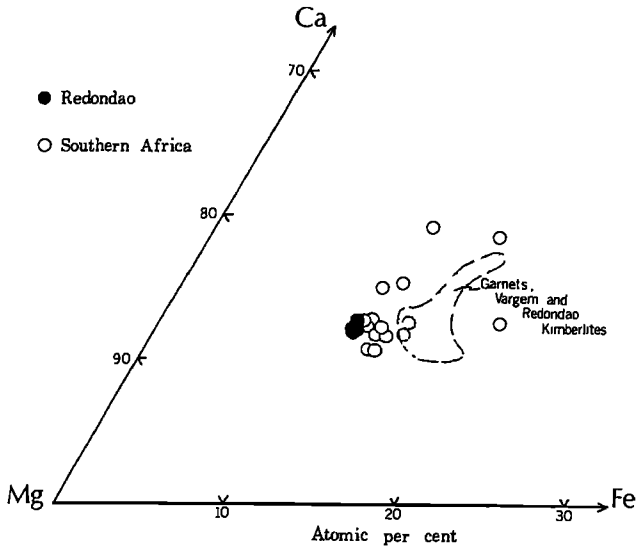

Fig. 9. Compositions of garnets in garnet - "lherzolite" xenolith from Redondao diatreme, Piaui State, in terms of Ca-Mg-Fe atomic per cent. Comparable garnets in ultramafic xenoliths from Southern Africa are shown for comparison (Bloomer and Nixon, 1973; Nixon and Boyd, 1973; Boyd, 1974; Boyd and Nixon, 1975).

Acknowledgements

The authors are indebted to Dr. Octávio Barbosa for helping during field work. The following financial support is gratefully acknowledged: Meyer -- National Science Foundation Earth Science Section Grants GA-36141 and GA-43990; Tsai -- David Ross Fellowship, Purdue Research Foundation; Svisero -- Fundacão de Amparo à Pesquisa do Estado de São Paulo.

References

Almeida, F.F.M., Y. Hasui and B.B.B. Neves, The upper Precambrian of South America, Institute of Geosciences Bulletin, University of Sao Paulo, 7, 45-80, 1976.

Almeida, F.F.M., Y. Hasui, N.L.E. Haralyi and A. Davino, Geophysical evidences of the geodinamical evolution of West Minas Gerais in the Cretaceous, Abst. II Latin American Geological Congress, Acapulco, Mexico, 1976.

Almeida, F.F.M., Origin and Evolution of Brazilian Platform. Departamento Nacional da Produçao Mineral, Bulletin 236, Rio de Janeiro, 36 pp., 1967.

Amaral, G., K/Ar ages of Jacupiranga Alkaline District, São Paulo State, Brazil. Upper Mantle Symposium, Buenos Aires, 2, 333-334, 1972.

Barbosa, O., D.P. Svisero and Y. Hasui, Kimberlites in Alto Paranaiba, Minas Gerais, Abst. 29 Brazilian Geological Congress, 323, Ouro Preto, Belo Horizonte, Minas Gerais, 1976.

Barbosa, O., O.P.G. Braun, R.C. Dyer and C.A.B.R. Cunha, The Geology of Triangulo Mineiro Region. Departamento Nacional da Produnao Mineral, Bulletin 136, 1970.

Bosum, W., S. Paulsen, G. Blumel, W. Eberle, D. Hagen, J. Paulino, G. Lacerda and R.B. Vianna, Methodology of geophysical, geological and geochemical surveys of the Brazilian-German Convention, Departmento Nacional da Produçao Mineral and Companhia de Pesquisas de Recursos Minerais, 14 pp., 9 maps, Belo Horizonte, 1974.

Bosum, W., The aeromagnetic survey of Minas Gerais and Espirito Santo States and its relation with the geological structures, Revista Brazileira de Geociencias, Vol. 3, 149-159, 1973.

Bloomer, A.G. and P.H. Nixon, The geology of Letseng-la-terre kimberlite pipes, in Lesotho Kimberlites, Ed. P.H. Nixon, 30-36, Lesotho Nat. Dev. Corp., Maseru, 1973.

Boyd, F.R. and P.H. Nixon, Origin of the ultramafic nodules from some kimberlites of Northern Lesotho and the Monastery Mine, South Africa, Phys. Chem. Earth, 9, 431-454, 1975.

Boyd, F.R., Ultramafic nodules from the Frank Smith kimberlite pipe, South Africa, Carnegie Inst. Wash. Yearb. 74, 285-294, 1974.

Boyd, F.R. and P.H Nixon, Origin of the ilmenite-silicate nodules in kimberlites from Lesotho and South Africa, in Lesotho Kimberlites, Ed. P.H. Nixon, 254-268, Lesotho Nat. Dev. Corp., Maseru, 1973.

Boyd, F.R., Electron probe study of diopside inclusions from kimberlite, Am. J. Sci., 267-A, 50-69, 1969.

Cox, K.G., J.J. Gurney and B. Harte, Xenoliths from Matsoku Pipe, in Lesotho Kimberlites, Ed. P.H. Nixon, 76-100, Lesotho Nat. Dev. Corp., Maseru, 1973.

Davis, G.L., The ages and uranium contents of zircons from kimberlites and associated rocks, (Abstr.) Second Int. Kimberlite Conf., Santa Fe, 1977.

Derby, O.A., Brazilian evidence on the genesis of the diamond, Journ. Geology, 6, 121-146, 1898.

Freyberg, B. von, Ergebnisse geologish Forschungen in Minas Gerais (Brasilien), Neues Jb. Min. Geol. und Palaont., Sonderband II, XI, 401 pp., Stuttgart, 1932.

Hasui, Y., F.F.M. Almeida, N.L.E. Haralyi, A. Davino and D.P. Svisero, Tectonic context of carbonatites from West Minas Gerais and South Goias States. (In prep.), Int. Symp. Carbonatites, Poços de Caldas, Brazil, 1976.

Hussak, E., On the diamond-bearing deposits of Agua Suja near Bagagem, Minas Gerais, in Report of the Commission for Exploration of Center Brazilian Plateau, H. Lombaerts & Co., Rio de Janeiro, 1894.

Maack, R., Eine forschungsreize uber das hochlan von Minas Gerais zum Paranahyba, Zeitschr. d. Gessellsch. f. Erdk., 310-323, 1926.

McCallister, R.H, H.O.A. Meyer, and D.G. Brookins,

"Pyroxene"-ilmenite xenoliths from the stockdale pipe, Kansas: chemistry, crystallography and origin, Phys. Chem. Earth, 9, 287-293, 1975.

Melo, U. and R. Porto, Geological reconnaissance of the southwest Piaui, Brazil., Petrobras Int. Rept. 244, Belem, 1965.

Meyer, H.O.A., Kimberlite from Norris Lake, Eastern Tennessee: mineralogy and petrology, J. Geol., 83, 518-526, 1975.

Meyer, H.O.A. and D.P. Svisero, Mineral inclusions in Brazilian diamonds, Phys. Chem. Earth, 9, 785-795, 1975.

Mitchell, R.H., Magnesium ilmenite and its role in kimberlite petrogenesis, J. Geol. 81, 301-311, 1973.

Nixon, P.H., The geology of Mothae, Solane, Thaba Putsoa and Boow 13, in Lesotho Kimberlites, Ed. P.H. Nixon, 39-47, Lesotho Nat. Dev. Corp., Maseru, 1973.

Reid, A.M. and J.S. Hanor, Pyrope in kimberlite, Amer. Mineral., 55, 1374-1379, 1970.

Rimann, E., Kimberlite in Brazil, Anais da Escola de Minas do Ouro Preto, 15, 27-32, 1917.

Svisero, D.P., H.O.A. Meyer and H. Tsai, Kimberlite minerals from Vargem (Minas Gerais) and Redondao (Piaui) diatremes, Brazil; and garnet lherzolite-xenolith from Redendao, Revista Brazileira de Geociencias, São Paulo, 7(1): 1-13, 1977.

Svisero, D.P., W. Felitti and J.S. Almeida, The geology of Romaria Diamond Mine, Romaria, Minas Gerais. Proc. of the 7th Symp. on Mining, Porto Alegre (in press), 1978.

Svisero, D.P. and N.L.E. Haralyi, On the Diamond "Princess of Estrela do Sul", Mineraçao and Metalurgia (in press), 1977.

Vianna, R.B. and H. Schmidt, Detailed aerogeophysical survey by helicopter in the Monte Carmelo area, Minas Gerais, Departmento Nacional da Produçao Mineral and Companhia de Pesquisas de Recursos Minerais, 72 pp., 16 maps, Belo Horizonte, 1975.

PRECAMBRIAN ULTRAMAFIC DYKES WITH KIMBERLITE AFFINITIES IN THE KIMBERLEY AREA

C. Roger Clement, E. Michael Skinner, J. Barry Hawthorne, Leendert Kleinjan

Geology Department, De Beers Consolidated Mines, Kimberley 8300, South Africa

Hugh L. Allsopp

Bernard Price Institute of Geophysical Research, University of the Witwatersrand, Johannesburg 2000, South Africa

Abstract. The field relations and major petrographic features of five feldspar free ultramafic dykes are described. These dykes, which contain abundant clinopyroxene and altered olivine, cut the Precambrian wallrocks of the De Beers and Wesselton kimberlite pipes. Rb-Sr dating of one of the dykes indicates an intrusion age of 1910 ± 60 my.

Minerals found within heavy mineral concentrates prepared from samples of these dykes include magnesian ilmenite and pyropic garnet. Compositional data are presented which show that these ilmenites and garnets are chemically identical with those commonly found in kimberlites or in peridotite nodules present as xenoliths in kimberlites. In view of the affinities with kimberlite indicated by the presence of these minerals in the ultramafic dykes, comparisons are drawn between the two rock-types. It is found that, if other mineralogical characteristics, textural features, aspects of the bulk chemistry and some major mineral compositions are taken into account, these dykes cannot be classified as kimberlite.

As a result of this study it is also concluded; that the magma which gave rise to these dykes originated within the upper mantle within the depth range postulated for the genesis of kimberlite magma; that similar ultramafic dykes may be widely distributed under the extensive cover of Karroo shales that blanket the region; and that the dykes were emplaced at higher temperatures than those pertaining during high-level kimberlite intrusion.

Introduction

A suite of unusual ultramafic dykes has been located in underground mine workings near the Wesselton and De Beers kimberlite pipes in the Kimberley area. Five of these dykes contain abundant clinopyroxene and altered olivine and are feldspar-free. Other petrographically similar dykes contain limited amounts of plagioclase. A petrogenetic association between all the dykes is suspected but the plagioclase-bearing occurrences have not been studied in detail and are not discussed in this contribution.

In this paper the field relations, petrography and bulk chemistry of the feldspar-free dykes are reviewed. Mineralogical affinities between these dykes and kimberlite are described and comparisons are drawn between the two rock types. The age of intrusion of the dykes is discussed, and some petrogenetic implications are noted.

Field Relations

The dykes cut the Archaean gneissic basement rocks of the area which have been dated at approximately 2900 my, (Barrett and Berg, 1975) and overlying andesitic lavas, quartz porphyries and quartzites of the Ventersdorp System (2300 my; van Niekerk and Burger, 1964).

The dykes trend in various directions ranging from northwest to due east. Dips vary between 80° and 50° and dyke widths range from a few centimetres to 1.5 m. The widest dyke occurs in the wallrocks of the Wesselton kimberlite pipe, four others are located near the De Beers pipe (Fig. 1).

The Wesselton occurrence was noted by Williams (1932) who classified it as .... "a serpentinised mica augite peridotite or a hardebank (kimberlite) dyke". Underground exposures indicate that this dyke is continuous over a vertical distance of 800 m and it has an established (minimum) strike length, interrupted by the kimberlite pipe, of 700 m. The continuity of the other dykes is less well known and two of the dykes have only been located at single exposures in mine tunnels.

Post-intrusion faulting along at least three of the dykes is evidenced by the development of brecciated zones within or along one contact of the dykes, by the presence of prominent shearing with associated slicken-siding and by off-setting of

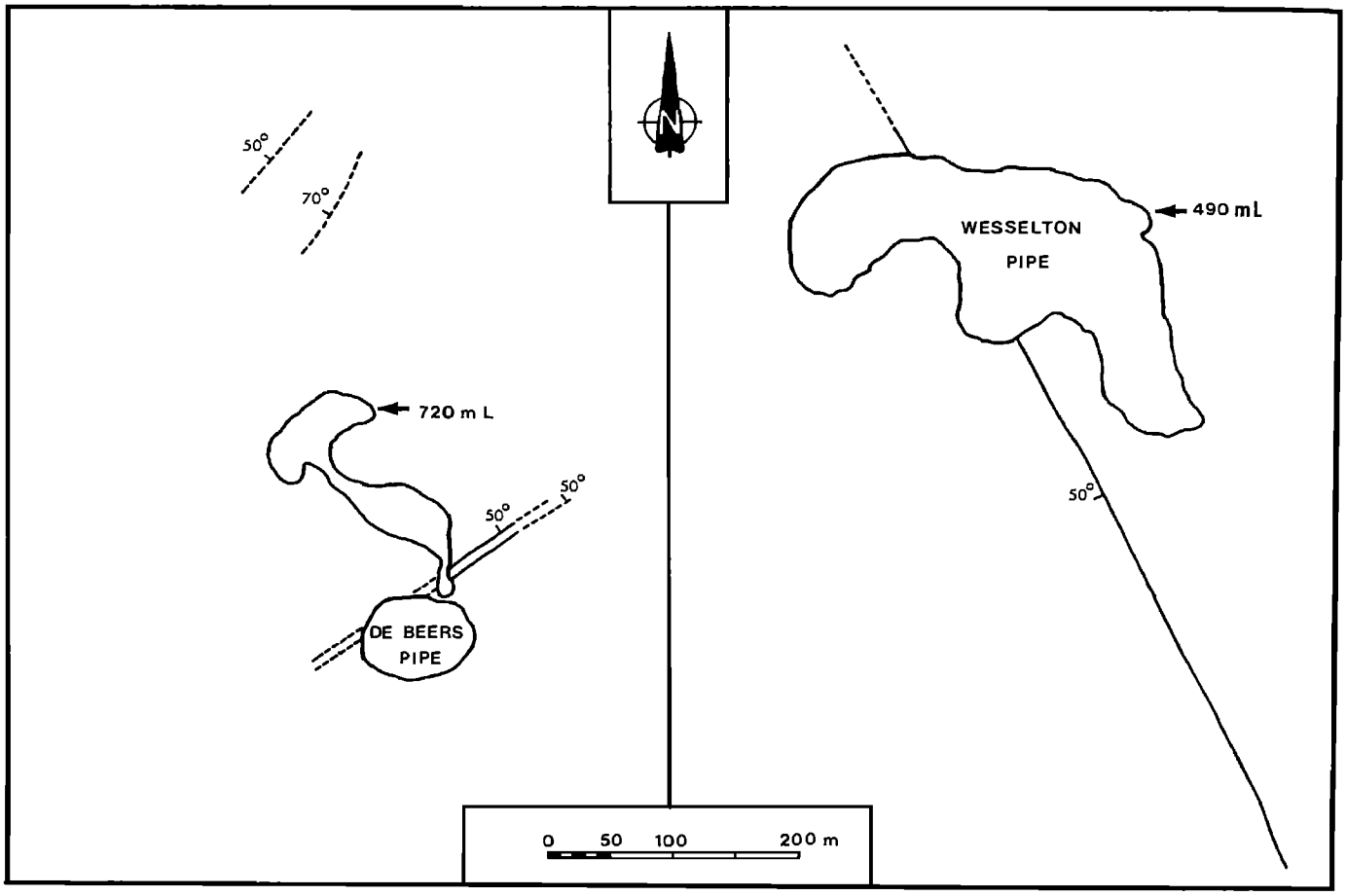

Fig. 1. Locations of the ultramafic dykes near the De Beers and Wesselton kimberlite pipes. The outline of the De Beers pipe at a depth of 720 m is shown. The positions of the two dykes north of the De Beers pipe are projected from higher levels. The shape and size of the Wesselton pipe at a depth of 490 m is indicated.

kimberlite dykes which are younger than the ultramafic dykes but predate the faulting.

Petrography

The dykes are tough, moderately hard, dark grey generally fine-grained rocks. Individual dykes exhibit considerable textural variation and the wider dykes have prominent chilled margins.

The textural variation is particularly well displayed by the dyke at Wesselton mine. The contacts of this dyke are marked by an extremely narrow (1-3 mm) vitrophyric selvedge which consists of altered olivine microphenocrysts commonly less than 0.5 mm in length, set in a dark brown glassy base containing very small (<0.03 mm) opaque granules and scattered microlites of clinopyroxene. Olivine has been pseudomorphously replaced by talc and subordinate serpentine and chlorite. The altered olivine phenocrysts commonly occur in the form of skeletal hopper crystals (Donaldson, 1976) and as complex parallel growth forms similar to those described by Drever and Johnston (1957) from picritic intrusions.

Inwards from the vitrophyric selvedges the groundmass becomes finely crystalline (Fig. 2) and the rock assumes a porphyritic character. The groundmass consists mainly of acicular laths of clinopyroxene up to 0.1 mm in length and similarly fine-grained phlogopite. Other groundmass minerals are serpentine, chlorite (in part an alteration product of clinopyroxene and phlogopite), opaque minerals, rare calcite and clay material. Abundant hopper crystals, ranging between 0.3 and 1.0 mm in size, and parallel growth aggregates of altered olivine are also common in the porphyritic parts of the dyke and occur as prominent phenocrysts (Fig. 2).

The central part of the dyke has a panidiomorphic-granular texture although the euhedral character of the major minerals is partly masked by extensive alteration. This zone contains abundant altered olivine and clinopyroxene crystals which make up 50-60 vol. % of the rock

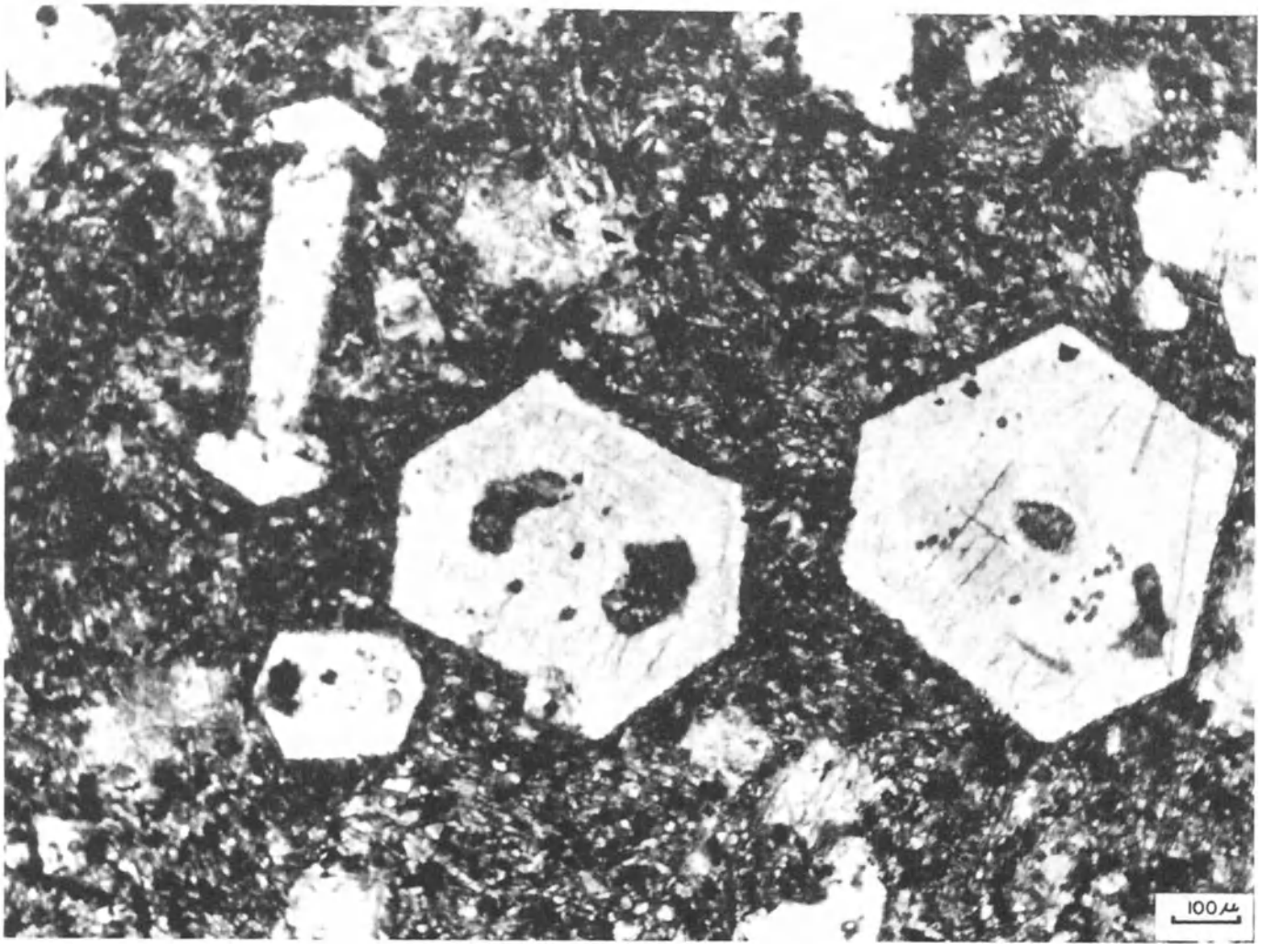

Fig. 2. Hopper crystals of altered olivine in a fine-grained groundmass consisting mainly of acicular clinopyroxene, phlogopite and opaque minerals. Porphyritic zone, Wesselton dyke.

(Table 1). As in the marginal parts of the dyke pseudomorphous replacement of olivine by talc and serpentine is complete. Skeletal grains are much less evident but some hopper crystals which generally approach external morphological completeness are present. Rare pseudomorphs reach 3 mm in length but the majority of the altered olivine grains do not exceed 1 mm. Clinopyroxene occurs as well-formed laths usually between 0.5 and 1.5 mm in length. Extensive steatization and chloritization of the pyroxene has occurred, accompanied by the generation of much fine opaque material.

Phlogopite, chlorite and serpentine are relatively abundant minerals. Phlogopite occurs as laths up to 0.75 mm long and as interstitial material together with serpentine and chlorite between altered olivine and clinopyroxene. This mica is strongly pleochroic ($\beta=\gamma$ brown, α pale yellow-brown) and is often partly altered to chlorite.

Accessory minerals in the central part of the dyke include apatite, opaque oxides, a little calcite and clay (sepiolite or hydromica). Apatite occurs as highly acicular laths up to 0.4 mm in length. Opaque minerals (rarely larger than 0.1 mm and commonly much smaller) occur in various forms including equant subhedral and euhedral crystals and acicular laths. Embayed grains and highly skeletal crystals are noticeable.

The dykes at De Beers mine are texturally and mineralogically similar to the Wesselton occurrence (Fig. 3 and Table 1) but differ in one important respect; mica is rare or absent. Sulphides (mainly pyrite) are common accessory minerals and a little quartz is sometimes present within altered olivine grains.

In addition to opaque oxides heavy mineral concentrates obtained from samples of the Wesselton dyke and three of the De Beers mine dykes contained garnet, rutile, zircon and sulphides. Six

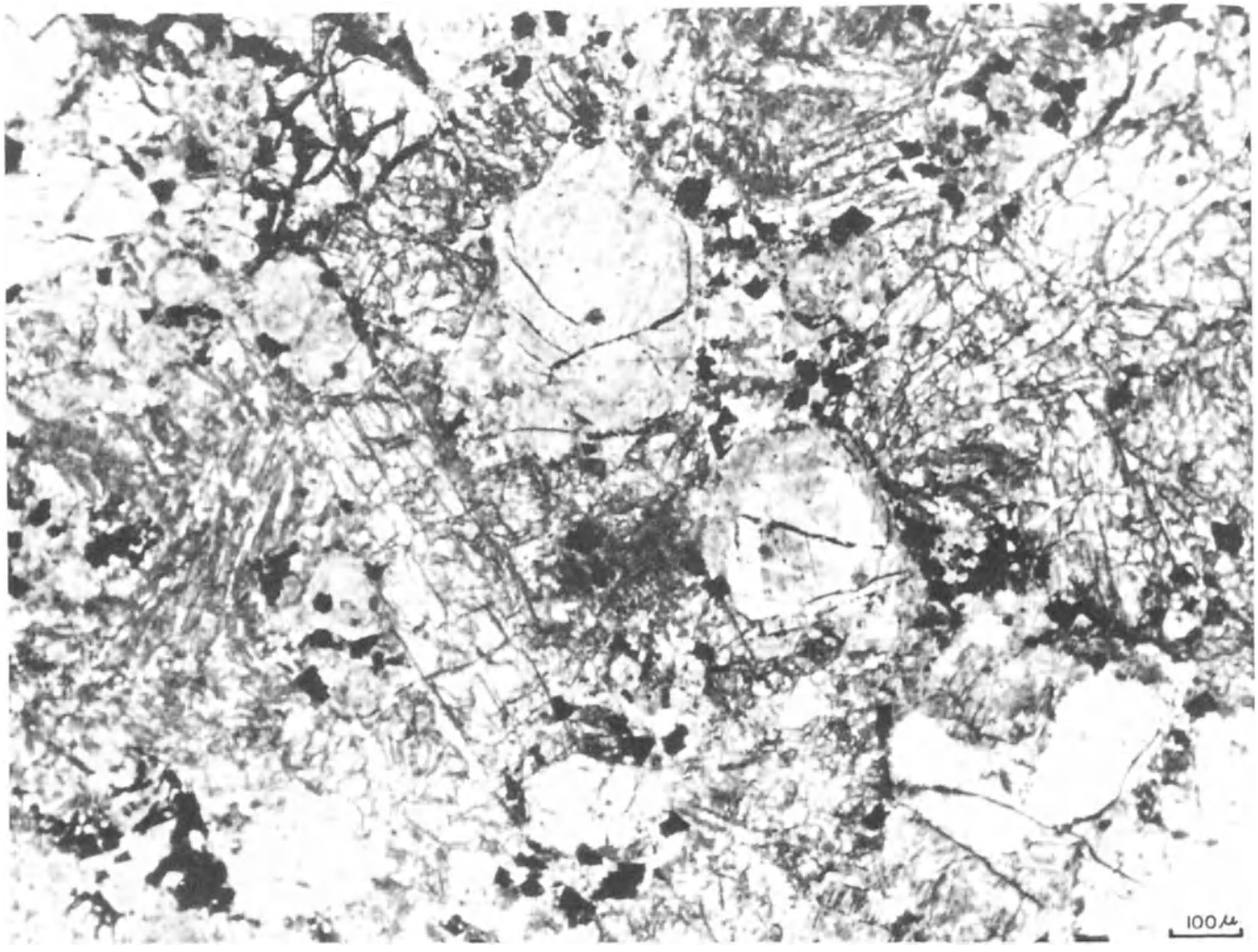

Fig. 3. Altered olivine and fresh clinopyroxene (prominent cleavage) crystals in the central part of an ultramafic dyke near the De Beers kimberlite pipe.

extremely small fragmental diamonds were recovered from a sample of one of the De Beers dykes. Further sampling has confirmed that diamond is a very rare constituent of this dyke. No diamonds were recovered from samples of the other dykes.

Geochemistry

The major element content of samples from four of the dykes has been determined and the analyses are recorded in Table 2 (analyses 1-4). Also shown is the average composition of 14 kimberlite dykes from the Kimberley area (analysis 5) and the composition of a phlogopite-diopside kimberlite (analysis 6) from the Bellsbank dyke system situated 80 km NNW of Kimberley. The Kimberley occurrences include precursor dykes which were intruded before the pipes were formed and late-stage dykes within the major pipes of the area. The two groups of kimberlite dykes do not, with one volatile-rich exception, display wide variations in bulk chemistry. They plot as a well-defined group on the ternary diagram used by Dawson (1967) to illustrate kimberlite compositions (Fig. 4).

It is apparent from Table 2 and Figure 4 that the ultramafic dykes differ geochemically from the Kimberley kimberlite dykes. Although the former are clearly also ultrabasic the SiO_2 content is high relative to the average for the kimberlites. The ultramafic dykes are also characterized by considerably higher iron, alumina and soda and much lower magnesia, lime and volatiles. Similar differences are apparent when the bulk compositions of these dykes are compared with Dawson's average basaltic and micaceous kimberlites (Dawson, 1967). The high CaO and CO_2 figures for the kimberlite dykes are indicative of considerable calcite, a mineral which is a rare constituent of the ultramafic dykes. Depression of the average silica content of the kimberlite dykes

below 30 wt. % is coincident with the generally high content of volatiles and lime.

In several respects the major element chemistry of the ultramafic dykes approximates that of certain diopside-rich kimberlites (Fig. 4). Comparison of the analyses with a phlogopite-diopside kimberlite from the Bellsbank group (analysis 6, Table 2) shows however, that the kimberlite has markedly lower iron and alumina and higher volatiles and K_2O contents; the latter is due to the presence of abundant phlogopite.

Mineral Compositions

Mineral compositions have been determined by electron microprobe analyses at the Anglo American Research Laboratories in Johannesburg using an automated ARL SEMQ instrument.

Severe alteration of the olivine in the dykes is widespread. No unaltered olivine was found in any of the thin sections prepared for microprobe analysis hence no compositional data are available for this mineral.

Clinopyroxene compositions are presented in Table 3. These clinopyroxenes are Fe-rich relative to clinopyroxenes in kimberlite (Fig. 5). Few analyses of primary matrix clinopyroxenes from kimberlite have been published but available data indicate limited compositional variation and restriction to the diopside field as shown in Figure 5. The clinopyroxenes from the ultramafic dykes plot in a clearly separate area in this Ca-Mg-Fe ternary diagram.

Two mica analyses from the Wesselton dyke are also listed in Table 3. Compared with kimberlite phlogopites these micas are Fe-rich. In one case the Mg:Fe ratio is slightly more than 2 and in the other slightly less than 2. Consequently the mica can be regarded as intermediate between phlogopite and biotite. K_2O is low relative to kimberlite phlogopites.

Minerals recovered from heavy mineral concentrates of samples of three De Beers dykes and the Wesselton occurrence are of particular interest. They include garnets and opaque oxides which fall within the compositional ranges of those commonly found in kimberlites or within peridotite xenoliths in kimberlites. Selected analyses are given in Table 4.

The opaque minerals include magnesian ilmenite (commonly containing more than 10% MgO and 1.5% Cr_2O_3), ilmenite and a variety of spinels including high chrome chromites (up to 64% Cr_2O_3). Dawson and Stephens (1975) classified garnets from kimberlite and associated xenoliths according to chemical parameters evaluated on a statistical cluster analyses basis. Many of the garnets in these dykes have compositions which coincide with a cluster group dominated by garnets from four-phase garnet lherzolite nodules in kimberlite (Fig. 6). They are titanium-poor pyrope garnets generally containing moderate Cr_2O_3 (3.5-5%) and low CaO (4.5-6%). Non-kimberlitic Fe and Mn-rich garnets are also present in the ultramafic dykes (Table 4).

TABLE 1. Modal Analyses

Dyke No.	K3 P1	K3 P2	K3 P3	K3 P4	K4 P1
Olivine	28	25	22	30	30
Clinopyroxene	36	37	36	32	23
Serpentine/ Chlorite/Clay	30	32	32	30	23
Phlogopite	-	-	Tr	0	16
Opaque minerals	6	5	8	6	7
Other*	-	-	<1	2	1

*Mainly calcite and apatite

K3 P1 - K3 P4 Modal analyses of dykes at De Beers mine.

K4 P1 Modal analyses of the dyke at Wesselton mine.

TABLE 2. Chemical Analyses

No.	1	2	3	4	5	6
SiO_2	44.8	40.4	41.7	41.7	27.40	46.77
TiO_2	1.87	2.05	1.98	2.90	2.06	1.77
Al_2O_3	6.62	7.20	7.18	5.44	2.20	3.96
Fe_2O_3	15.1*	18.7*	16.7*	17.3*	5.03	7.52*
FeO					3.89	
Cr_2O_3	0.27	0.30	0.28	0.22	0.25	0.37
MnO	0.20	0.28	0.25	0.25	0.18	0.05
MgO	14.3	16.4	17.1	16.9	28.11	17.99
CaO	8.41	1.40	1.68	5.16	12.91	4.97
Na_2O	0.70	0.74	0.96	0.61	0.24	0.43
K_2O	0.66	0.45	0.33	1.86	0.88	2.52
P_2O_5	0.18	0.21	0.19	0.40	1.20	0.96
S	n.d.	n.d.	n.d.	n.d.	0.07	n.d.
LOI_+	n.d.	n.d.	n.d.	n.d.	14.33	10.81
H_2O^+	5.16	7.12	6.85	4.95	n.d.	n.d.
CO_2	1.27	0.51	0.58	1.04	8.36	n.d.
H_2O^-	0.96	3.09	2.76	0.94	0.82	n.d.
NiO	0.12	0.16	0.13	0.12	0.13	n.d.

Analyses 1-3 Ultramafic dykes near the De Beers kimberlite pipe.

Analysis 4 Ultramafic dyke near the Wesselton kimberlite pipe.

Analysis 5 Average of 14 kimberlite dykes in the Kimberley area (unpublished analyses - C.R. Clement and J.J. Gurney)

Analysis 6 Bellsbank kimberlite dyke (unpublished analysis - E.M.W. Skinner).

*Total Fe as Fe_2O_3

n.d. not determined.

Age of the dykes

Field relations indicate that these dykes predate the Cretaceous kimberlite pipes in the Kimberley area which have been dated by Allsopp and

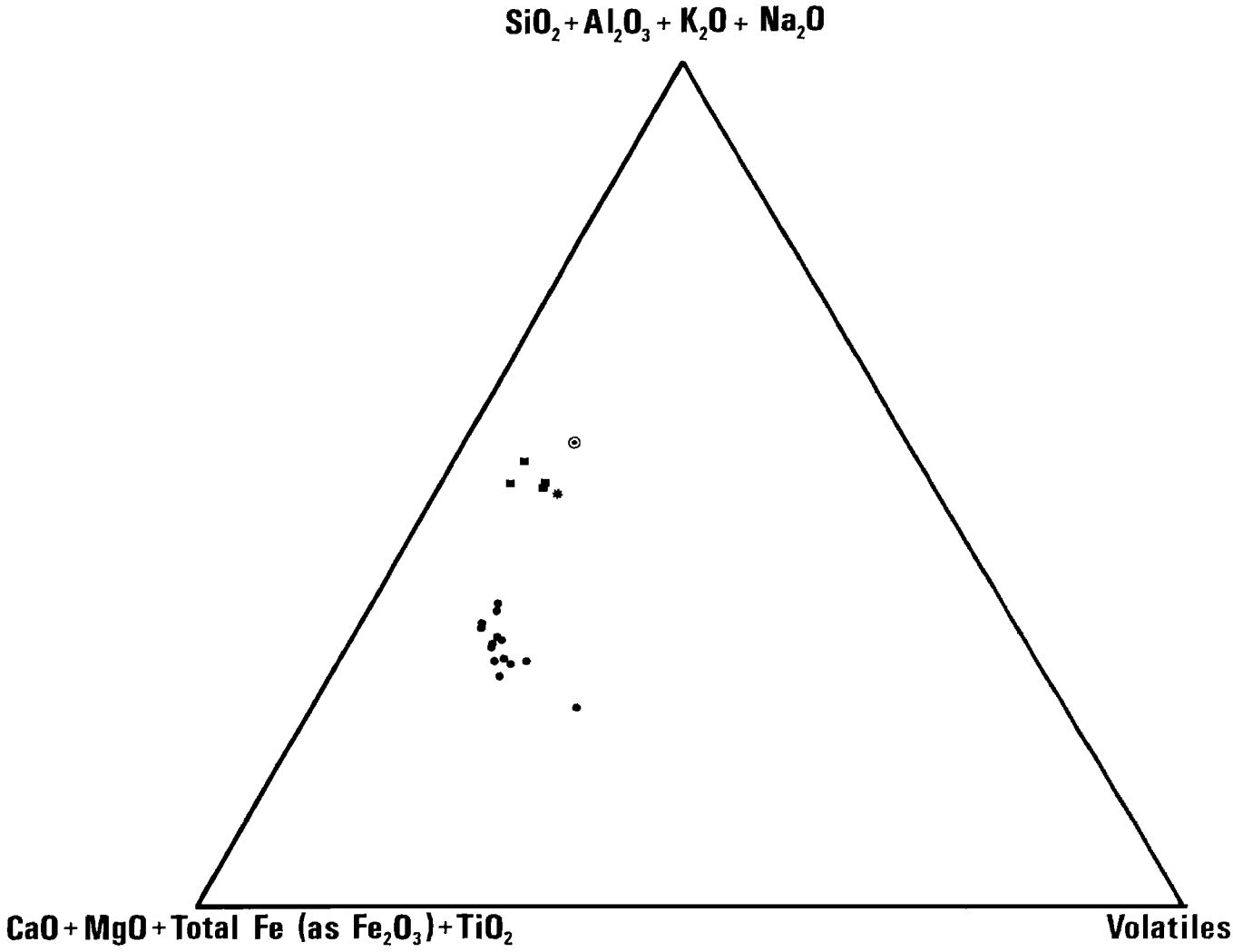

Fig. 4. Ternary diagram illustrating differences in bulk composition between the ultramafic dykes (solid squares) and kimberlite dykes in the Kimberley area (solid circles). Phlogopite and diopside bearing kimberlites from the Bellsbank area (star) and the Swartruggens dyke system (open circle with central dot) plot fairly close to the ultramafic dykes.

Barrett (1975) at 84 ± 3 my (recalculated using $\lambda Rb = 1.42 \times 10^{-11}\ yr^{-1}$). Truncation of the dykes at the contacts of the pipes is evident at both De Beers and Wesselton mines (Fig. 1). Furthermore the dykes do not cut Upper Carboniferous Dwyka shales of the Karroo System which form the upper 130 m of the geological succession in the area. The dykes cut the gneissic basement rocks of the area (dated at ∿2840 my - recalculated using $\lambda Rb = 1.42 \times 10^{-11} \times\ yr^{-1}$; Barrett and Berg, 1975) and the Ventersdorp System rocks (dated at ∿2300 my; van Niekerk and Burger, 1964). A post-Ventersdorp System pre-Karroo age is therefore indicated. To determine the age of the dykes more precisely radiometric dating, by the Rb-Sr method, was carried out on one whole-rock and four fine-grained mica concentrates from two samples of the Wesselton dyke.

Partial chloritization of the mica is common and many grains are coated with an unidentified white amorphous material. However, examination of the microprobe data (Table 3) reveals that the extent of the alteration is not severe: if the volatile content, unaccounted for in the probe analyses, is assumed to be water, the water content at 6-7% more closely resembles that of fresh biotites and phlogopites (4-5%) than that in chlorites (12-13%). Repeated agitation in an ultrasonic water bath followed by careful hand-picking under a microscope yielded samples 10-20 mg in weight that appeared free from alteration. A few per cent of residual pyroxene in the mica concentrates was, however, unavoidable but this is unlikely to have affected the validity of the age-measurements.

Conventional techniques were used for the chem-

TABLE 3. Clinopyroxene and mica analyses

	1	2	3	4	5	6	7	8
Source	K3 P2	K3 P2	K4 P1	K4 P1	K4 P1	K4 P1	K4 P1	K4 P1
SiO_2	50.15	51.92	51.95	52.46	51.91	51.93	39.02	36.94
TiO_2	1.43	1.23	1.25	0.92	1.13	0.95	4.80	4.12
Al_2O_3	3.27	2.79	1.40	0.85	0.88	0.83	11.46	11.56
Cr_2O_3	0.15	0.27	0.24	0.20	-	0.01	-	0.01
FeO*	11.38	9.49	7.78	7.65	8.54	8.67	13.59	16.55
MnO	0.17	0.14	0.11	0.11	0.15	-	0.07	0.08
MgO	15.34	15.92	15.70	16.02	15.34	15.29	17.39	16.89
CaO	18.52	19.44	21.23	21.17	20.95	20.78	0.09	0.05
Na_2O	0.53	0.48	0.57	0.51	0.57	0.68	0.71	0.34
K_2O	-	0.07	0.01	0.01	-	-	7.00	6.44
NiO	0.03	0.04	0.07	0.05	0.01	-	0.06	0.08
Total	100.97	101.79	100.31	99.95	99.48	99.14	94.19	93.06

Analyses 1 and 2 Clinopyroxenes from an ultramafic dyke at De Beers mine.
Analyses 3-6 Clinopyroxenes from an ultramafic dyke at Wesselton mine.
Analyses 7 and 8 Micas from the dyke at Wesselton mine.
*Total Fe as FeO

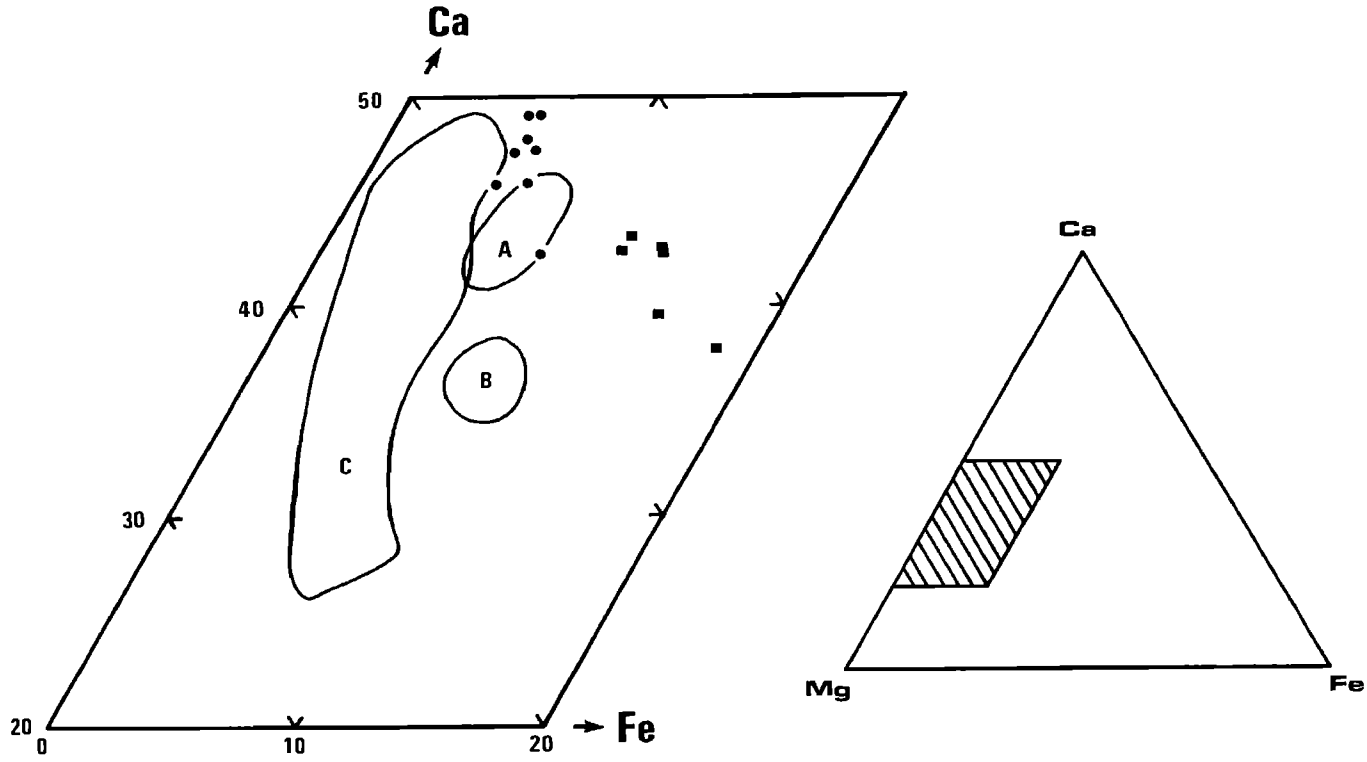

Fig. 5. Compositions of clinopyroxenes from kimberlites and associated xenoliths and from two of the ultramafic dykes expressed in terms of Ca, Mg and Fe. Fields A, B and C show the composition ranges of clinopyroxene from xenoliths in kimberlite (from Dawson, et al., 1977), solid circles represent kimberlite groundmass diopsides (from Dawson et al., 1977 and Emeleus and Andrews, 1975), solid squares represent the compositions of clinopyroxenes from the ultramafic dykes.

TABLE 4. Selected analyses of heavy minerals from concentrates

No.	1	2	3	4	5	6	7	8	9	10	11	12	13
SiO_2	-	-	0.3	-	-	-	-	42.02	41.17	42.21	36.28	36.19	37.22
TiO_2	51.12	54.68	48.8	0.42	3.45	0.25	92.19	-	-	0.06	-	-	-
Al_2O_3	-	0.19	0.1	3.94	2.36	11.62	-	20.79	20.74	20.10	21.31	21.11	21.83
Cr_2O_3	2.42	1.84	0.1	64.02	56.21	55.50	4.28	4.68	4.92	5.34	0.02	0.03	0.01
FeO*	35.11	29.01	43.4	15.67	27.81	18.74	2.65	6.12	6.69	6.45	17.40	24.79	29.95
MnO	0.31	0.17	3.4	0.27	0.30	0.18	-	0.28	0.32	0.34	21.84	14.53	3.57
MgO	10.85	14.28	0.3	12.31	9.31	12.11	-	20.60	21.03	19.93	1.75	0.86	3.62
CaO	-	-	0.1	-	-	-	-	5.15	5.36	5.44	2.10	1.66	4.66
Total	99.81	100.17	96.5	96.63	99.44	98.40	99.12	99.64	100.23	99.87	100.70	99.17	100.86

Analyses 1 and 2 Kimberlite-type magnesian ilmenite
Analysis 3 Ilmenite
Analyses 4-6 Spinels
Analysis 7 Rutile
Analyses 8-10 Kimberlite-type garnet
Analyses 11-13 Non-kimberlitic garnet

* Total Fe as FeO

ical separation of Rb and Sr and for the mass-spectrometric analyses. Data for the E & A standard Sr, analysed by the same method, yielded a $^{87}Sr/^{86}Sr$ ratio of 0.70795 ± 0.00002. Measurements on the NBS standard SRM-607 showed that the Rb and Sr concentration determinations are accurate to within 1%. The experimental data for the whole-rock and mica samples are listed in Table 5.

Fitting a straight line by the method of York (1966) would be the most direct way of handling the above data. As indicated below this is probably not a valid approach in the present instance, but for completeness the computed results (using a value of 1.42×10^{-11} yr^{-1} for the decay constant of ^{87}Rb) are: Age = 1763 ± 40 my; Initial $^{87}Sr/^{86}Sr$ ratio = 0.7068 ± .0009, where the errors listed are 1 sigma values.

In an earlier section the severe alteration of the dyke rocks was described. In particular it was noted that pyroxene, the main Sr-bearing mineral, is extensively altered to steatite and chlorite. It is probable therefore that the Rb-Sr data for the whole-rock sample has been influenced by groundwater exchange; that this is the case is supported by the fact that the initial $^{87}Sr/^{86}Sr$ ratio referred to above is unusually high for a presumed mantle-derived rock of this age. Barrett and Berg (1975) obtained $^{87}Sr/^{86}Sr$ ratios of 0.710 - 0.720 for groundwater from the Kimberley area, and partial exchange with such water is feasible. The isochron approach to the interpretation of the age-determination data is therefore rejected.

Estimated initial $^{87}Sr/^{86}Sr$ ratios for 1900 my-old mantle derived rocks range from approximately 0.701 to 0.704 according to the models of Faure and Powell (1972) and Davies et al. (1970). An intermediate value of 0.7025 has been assumed and the calculated ages based on this assumption are also listed in Table 5. The uncertainty arising from the choice of the initial Sr ratio is approximately ± 25 my, which is less than the uncertainty due to the scatter of the data. The mean mica age (see footnote to Table 5) is 1910 ± 60 my. The possibility that this age represents a resetting event cannot be excluded, but no pervasive 1900 my thermal event, that could give rise to resetting, has been recognised in the Kimberley area.

Comparison with kimberlite

The heavy mineral suite in these rocks clearly suggests a link between the dykes and kimberlite as does their occurrence in an area of intensive, albeit much later, kimberlite intrusion. In other respects, however, the dykes differ considerably from kimberlite.

Modal analyses (Table 1) indicate that clinopyroxene is generally volumetrically more abundant than olivine. Although diopside occurs as an essential mineral in some kimberlites (Skinner and Clement, 1977) it is commonly less abundant than olivine.

There is a complete absence in the dykes of anhedral, commonly rounded, macrocrysts of olivine which together with smaller euhedral phenocrysts, form the typical olivine assemblage in kimberlite. Similarly the silicate and oxide heavy mineral suites, although compositionally akin to those present in kimberlite, are unusual in that none of the minerals occur as macrocrysts. The majority of the grains recovered lie between 100 and 28 mesh (Tyler) screen sizes.

Textural features and the morphological characteristics of some essential minerals differ markedly from those reported from kimberlite. Notable in these respects are the hypidiomorphic-granular to panidiomorphic-granular textures of

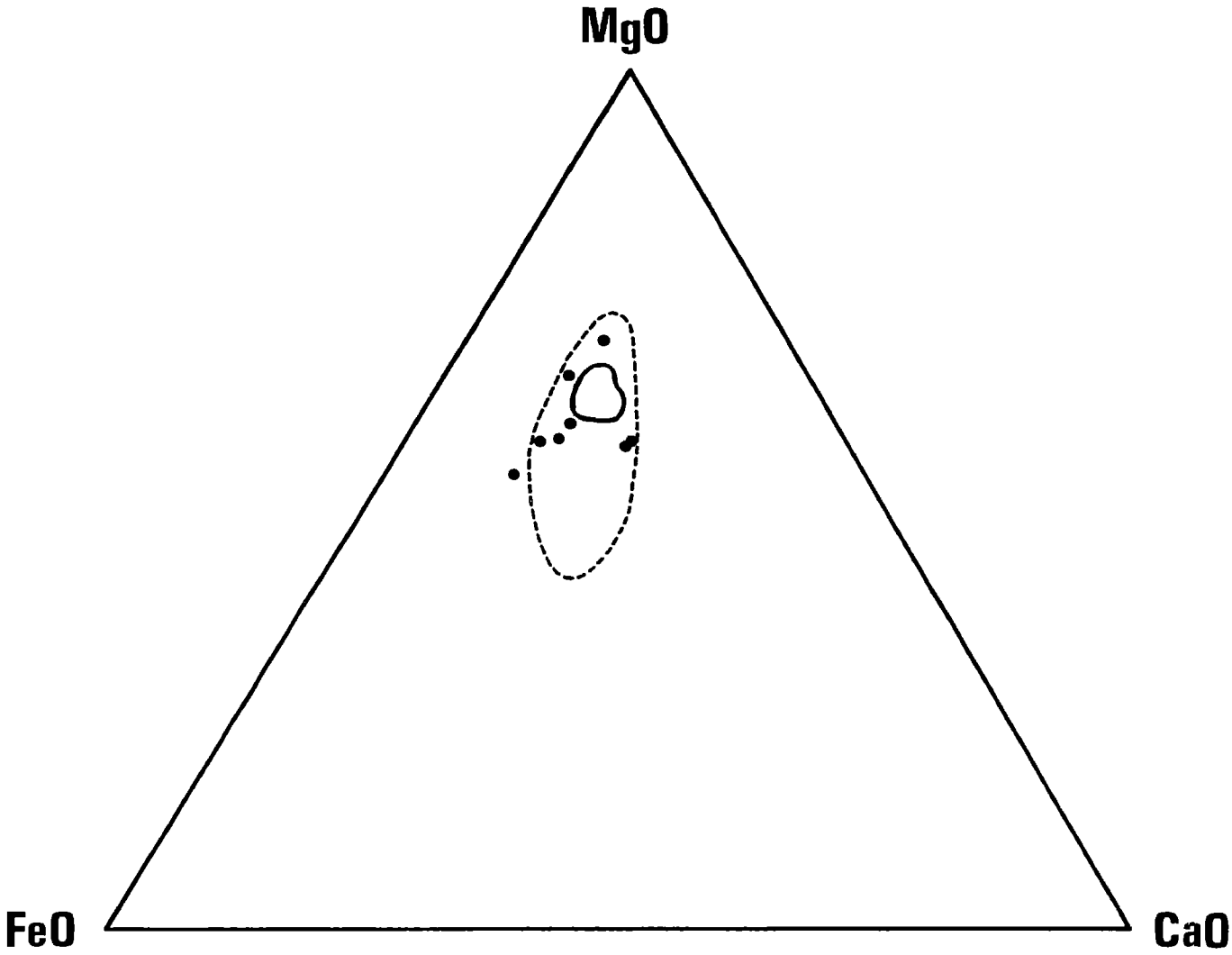

Fig. 6. Compositions of garnets from the ultramafic dykes in terms of MgO, FeO and CaO. 36 Garnets from these dykes plot within the field outlined by a solid line. Additional garnets are plotted as solid circles. The dotted line outlines a compositional field of statistically clustered garnets from kimberlite and associated xenoliths. Most of these garnets are derived from garnet lherzolite nodules (from Dawson and Stephens, 1975).

the major (central) parts of the dykes and the skeletal olivines which have not been found in kimberlite. The abundance of parallel growth forms of olivine is also atypical relative to kimberlitic olivine.

Textural features of the ultramafic rocks indicate that crystallization of the major minerals occurred more or less in situ. It is therefore concluded that the dykes were emplaced as liquids at considerably higher temperatures than have been suggested to pertain during high level kimberlite intrusion. The glassy margins and fine-grained character of the dykes indicate rapid cooling after emplacement. The skeletal nature of many olivine grains suggests rapid olivine growth (Donaldson, 1976).

The differences between these ultramafic dykes and kimberlite noted above, together with previously discussed differences with respect to bulk chemistry and some mineral compositions, are considered sufficient to rule out classification of these rocks as kimberlite.

Conclusions

Three main conclusions can be drawn from this study;

Firstly the intrusion of Cretaceous kimberlites in the Kimberley area was preceded by a much earlier period of ultrabasic magmatism resulting in the intrusion of these dykes which may be widely

TABLE 5. Rb-Sr Radiometric Dating - Experimental Data

Sample	^{87}Rb	^{86}Sr	$^{87}Rb/^{86}Sr)A$	$^{87}Sr/^{86}Sr)N$	Apparent age (my)
Whole-rock	12.49	36.84	0.3351	0.7153	-
Mica - 1	54.06	25.83	2.069	0.7636	2050
2	53.56	24.31	2.178	0.7623	1907
3	60.69	29.64	2.024	0.75699	1871
4	56.44	25.60	2.180	0.76212	1899

Note: The concentrations of ^{87}Rb and ^{86}Sr are expressed in ppm.
$^{87}Rb/^{86}Sr)A$ is the atomic ratio, and $^{87}Sr/^{86}Sr)N$ is normalised to $^{88}Sr/^{86}Sr = 8.375$.
The whole-rock sample and the mica concentrates 1 and 2 are from sample K4 P/1, and the other two micas are from sample K4 P/2.
The Sr measurement for the Mica-1 sample was of poor quality, and the data for this sample was accordingly given less weight in calculating the mean age.

distributed under the extensive cover of Karroo rocks in the region.

Secondly, although these rocks cannot be classed as kimberlites, it is concluded on the basis of some of the heavy minerals present, that the magma which gave rise to the dykes originated within the upper mantle in the depth range postulated for the genesis of kimberlite.

Thirdly a direct genetic association between the dykes and the kimberlites in the area can be considered but seems unlikely in view of the long time interval between the two periods of intrusion.

Acknowledgements. Our thanks are due to members of the staff of the Anglo American Research Laboratories, particularly G. Hutchinson for the mineral analyses given in this paper. The Kimberlite Research Unit at the University of Cape Town is thanked for providing whole rock geochemical data. We are grateful to Mrs. B. Booysen for typing the manuscript. Finally, we are indebted to the Anglo American Corporation of South Africa and De Beers Consolidated Mines for permission to publish this paper.

References

Allsopp, H.L., and D.R. Barrett, Rb-Sr age determinations on South African Kimberlite pipes, Phys. Chem. Earth, 9, 605-617, 1975.

Barrett, D.R., and G.W. Berg, Complementary petrographic and strontium-isotope ratio studies of South African kimberlite, Phys. Chem. Earth, 9, 619-635, 1975.

Davies, R.D., H.L. Allsopp, A.J. Erlank, and W.I. Manton, Sr-isotopic studies on various layered intrusions in southern Africa, Geol. Soc. S. Afr., Spec. Publ. 1, 576-593, 1970.

Dawson, J.B., Geochemistry and origin of kimberlite, in Ultramafic and Related Rocks, edited by P.J. Wyllie, pp. 269-278, John Wiley & Sons, New York, 1967.

Dawson, J.B., J.V. Smith, and R.L. Hervig, Late-stage diopsides in kimberlite groundmass, Extended Abstracts, 2nd International Kimberlite Conf., Santa Fe, New Mexico, 1977.

Dawson, J.B., and W.E. Stephens, Statistical classification of garnets from kimberlite and associated xenoliths, J. Geol., 83, 589-607, 1975.

Donaldson, C.H., An experimental investigation of olivine morphology, Contrib. Mineral. Petrol., 57, 187-213, 1976.

Drever, H.I., and R. Johnston, Crystal growth of forsteritic olivine in magmas and melts, Trans. Roy. Soc. (Edinburgh), 63, 289-315, 1957.

Emeleus, C.H., and J.R. Andrews, Mineralogy and petrology of kimberlite dyke and sheet intrusions and included peridotite xenoliths from South West Greenland, Phys. Chem. Earth, 9, 179-197, 1975.

Faure, G., and J.L. Powell, Sr-isotope Geology, 188 p., Springer-Verlag, 1972.

Skinner, E.M.W., and C.R. Clement, Mineralogical classification of southern African kimberlites, Extended Abstracts, 2nd International Kimberlite Conf., Santa Fe, New Mexico, 1977.

Van Niekerk, C.B., and A.J. Burger, The age of the Ventersdorp System, Ann. Geol. Surv. S. Afr., 3, 75-86, 1964.

Williams, A.F., The genesis of the diamond, 636 p. Ernest Benn, London, 1932.

York, D., Least squares fitting of a straight line, Can. J. Phys., 44, 1079-1086, 1966.

KIMBERLITIC, MELILITITIC, TRACHYTIC AND CARBONATITE ERUPTIVES AT SALTPETRE KOP, SUTHERLAND, SOUTH AFRICA

J.R. McIver

Department of Geology, University of the Witwatersrand, Johannesburg, South Africa, 2001

John Ferguson

Bureau of Mineral Resources, Geology and Geophysics, Canberra, Australia

Abstract. Kimberlitic, melilititic, trachytic, and carbonatite eruptives occur in association at Saltpetre Kop, Sutherland, South Africa. This magmatic assemblage is believed to have originated as a result of crystal fractionation, liquid immiscibility and crystal-liquid reaction phenomena operative in an ascending kimberlitic magma generated by limited mantle melting in the depth range 100 - 200 km. The kimberlitic rocks at Saltpetre Kop are considered to represent part of the original magma which erupted from a relatively low pressure regime (20 - 25 kb). Slow uprise of the remainder was accompanied by olivine fractionation, separation of an immiscible carbonatite phase and the onset of an olivine-liquid reaction resulting in the formation of olivine melilitite; continued fractionation of the magma to beyond the limit of melilite stability gave rise to the feldspathic assemblages of the trachytic eruptives.

Introduction

The close association in space and time of olivine melilitite, carbonatite, kimberlite and other ultramafic alkaline rocks has long been interpreted by many authors as being indicative of a genetic link between them (see Tuttle and Gittins, 1966; Heinrich, 1966; for summaries). Current opinion has it that carbonatitic liquids are associated with kimberlites either as late-stage residual fluids or as immiscible phases developed during kimberlite crystallisation (Franz and Wyllie, 1967; McGetchin and Nikhauj, 1973; Gittins et al., 1975; Griffin and Taylor, 1975; Ferguson et al., 1975). Less agreement appears to exist on a genetic relationship between kimberlite and olivine melilitite. Taljaard (1936) considered that kimberlite represented hydrothermally altered olivine melilitite, and Holmes (1936) considered olivine melilitite to be kimberlite magma devoid of xenolithic minerals, H_2O, CO_2, P_2O_5 and CO_3^{2-}. Frankel (1956) concluded that olivine melilitite represented a portion of the magma from which kimberlite was derived. Bultitude and Green (1968) considered olivine melilitite to be a primary melt of hydrous mantle material or to have been generated by extreme fractionation of picritic melts. Eggler (1974) and Boettcher et al. (1975) have stressed the importance of the presence of CO_2 in mantle melting events for the production of melilite-bearing assemblages. Yoder (1973, 1975) has recorded that under anhydrous conditions the stability of akermanite is limited to pressures less than 14 kb, that in the presence of excess H_2O stability is limited to pressures less than 10.2 kb and that in the presence of excess CO_2 akermanite stability is limited to pressures less than 6 kb. Accordingly, constraints are placed on the regions where melilite-bearing rocks may crystallise; such relatively low pressure regimes are unlikely to be sites of generation of olivine melilitites and associated magmas (Bultitude and Green, 1968).

Following his study of the Gross Brukkaros volcano in South West Africa, Janse (1971) proposed that kimberlite represented relatively unmodified magma which appeared at the surface following rapid ascent from depth. The same magma if arrested en route and modified by carbonate removal was considered to give rise to monticellite-bearing assemblages under low pressure conditions and melilite- and nepheline-bearing assemblages under higher or fluctuating pressure conditions. Danchin et al. (1975) applied the technique of cluster analysis (Rhodes, 1969;

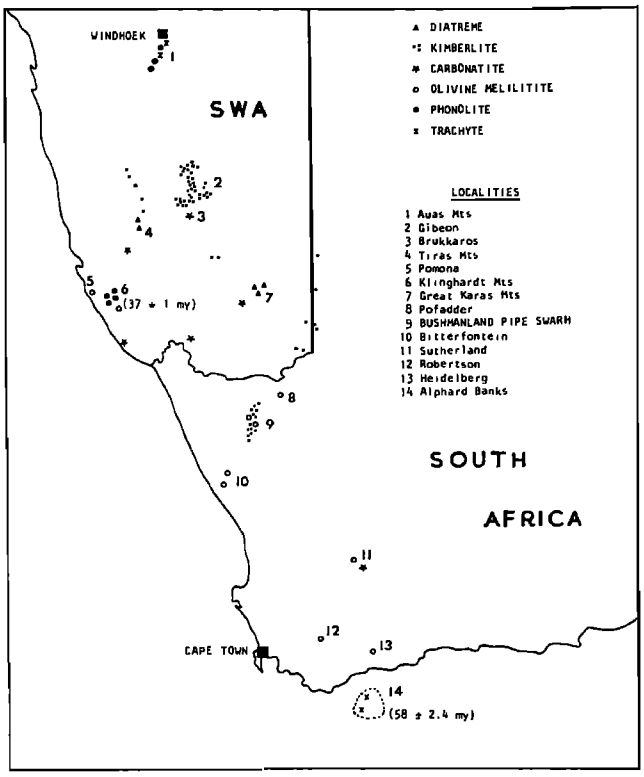

Fig. 1. Map showing locality of Sutherland and the distribution of dominantly alkaline eruptive centres parallel to the coast of South and South West Africa, after Cornelissen and Verwoerd, 1975.

Lenthall, 1972) to 109 chemical analyses of kimberlites and spatially associated ultramafic alkaline rocks reported in the literature and found that at an arbitrarily selected distance coefficient of 3 the analyses defined seven major cluster Groups (see Table III). Groups 1 to 3 contained only non-kimberlitic rocks and are dominated by melilite-bearing and monticellite-bearing ultramafics; Groups 5 to 7 contained only kimberlites while Group 4 is transitional containing both kimberlite and non-kimberlitic material. Considered in terms of the modified CMAS system (O'Hara, 1968), the average analyses of the cluster Groups define an olivine control line extending from the magnesium-rich kimberlites to the non-kimberlitic ultramafics (Ferguson et al., 1975). From this it was concluded that kimberlites and associated rocks could be genetically related by polybaric olivine-dominated fractionation coupled with a reaction relationship involving olivine, ilmenite and carbonated magma to produce melilite, perovskite and under low pressure conditions, monticellite.

To further test these conclusions the igneous assemblages associated with kimberlitic rocks of the Saltpetre Kop diatreme were studied.

The Saltpetre Kop Eruptive Centre

The Saltpetre Kop volcano, situated some twenty kilometres southeast of the village of Sutherland, Cape, South Africa, is one of a large number of predominantly alkaline eruptive centres occurring in a zone parallel to the west coast of South and South West Africa (Fig. 1). Cornelissen and Verwoerd (1975) point out that while ages are imperfectly known it is reasonable to postulate that this vulcanism is related to young continental warping associated with the opening of the south Atlantic. Saltpetre Kop forms a prominent cone-shaped hill rising some 250 m above the surrounding countryside and comprises post-Karroo intrusive and extrusive rocks which include trachyte, carbonatite, olivine melilitite and pyroclastic kimberlitic eruptives. Olivine melilitites are also exposed on the Sutherland town lands and at Tonteldoosfontein 15 km further to the south. The geology of the Saltpetre Kop eruptives has been described by Rogers and du Toit (1903, 1904), Taljaard (1936), Gerrard (1958) and more recently by de Wet (1974) to whom free reference is made in the following section.

The Saltpetre Kop vent forms the centre of a regular circular updomed region within the sedimentary Beaufort Formation of the Karroo Supergroup. The regional 2-3° northerly dip of the shales and sandstones becomes affected some 4 km from the vent and increases progressively until near the main vent the outward dip of the strata reaches 60°. The main vent at Saltpetre Kop is filled with lithic pyroclasts and occupies an area some 1500 x 1000 metres; fragments of Karroo sediments predominate, but fragments of quartzite and dolerite are present as are rare xenocrysts of hornblende, ilmenite and biotite. Silicification of the central vent breccia is common, but in the vicinity of carbonatite outcrops, carbonate becomes important as a cementing material. Rogers and du Toit (1903, 1904) recorded that within 4 square kilometres around Saltpetre Kop some twenty volcanic necks and vents are developed; recent mapping by de Wet (1974) has categorised these eruptives in more detail. According to de Wet the eruptive rocks around Saltpetre Kop comprise trachytic materials which are the most abundant volcanics together with less abundant and less voluminous carbonatite and olivine melilitite. Pyroclastic rocks bearing a strong macroscopic resemblance to some types of kimberlite are present within the ring of disturbed rocks some three kilometres west of Saltpetre Kop in the form of the so-called Silver Dam pyroclastics. According to de Wet (1974) the order of intrusion is given as olivine melilitite, trachytic eruptives and carbonatite; the relative age of the pyroclastics is unknown.

Olivine melilitite is present as dyke-like and

TABLE 1. Analyses of Minerals from Sutherland Eruptives

Number	1*	2*	3*	4*	5*	6*	7*	8*	9*	10+	11*	12+
Sample Number	C8	C8	C8	C8	C8	C31	C31	C30	C30	C29	C30	C30
SiO_2	0.00	0.01	52.02	50.44	49.90	36.71	38.30	40.45	37.99	39.31	39.78	39.59
TiO_2	46.06	44.74	0.11	0.99	0.62	0.03	0.04	0.08	0.00	0.01	0.01	0.02
Al_2O_3	0.27	0.31	2.03	3.40	3.49	0.01	0.00	0.03	0.00	0.05	0.00	0.04
MgO	4.87	5.76	17.09	13.13	13.42	41.16	41.03	47.05	33.25	45.77	43.26	47.20
FeO_t	49.29	48.26	6.53	7.28	9.14	23.21	21.17	10.06	29.02	13.49	16.64	14.20
Cr_2O_3	0.00	0.02	0.49	0.00	0.00	0.00	0.04	0.00	0.02	0.04	0.04	0.03
MnO	0.17	0.34	0.02	0.08	0.02	0.08	0.08	0.13	0.51	0.16	0.08	0.15
NiO	0.00	0.18	0.06	0.00	0.07	n.d.	0.01	0.24	0.03	n.d.	0.20	n.d.
CaO	0.00	0.05	21.54	22.33	20.16	0.12	0.25	0.00	0.07	0.26	0.06	0.28
Na_2O	0.00	0.02	0.37	1.59	2.26	0.00	0.11	0.06	0.15	0.00	0.00	0.01
K_2O	0.03	0.00	0.01	0.02	0.09	0.03	0.00	0.06	0.01	0.00	0.06	0.00
	100.69	99.78	100.27	99.26	99.17	101.35	101.03	99.03	101.03	99.09	100.13	101.52
						Fo_{76}	Fo_{77}	Fo_{88}	Fo_{65}	Fo_{86}	Fo_{82}	Fo_{86}

Analyst : * C. Frick, Geological Survey of South Africa
+ B. Wyatt, Anglo American Corporation of South Africa

1. Ilmenite, Silver Dam Pyroclasts
2. Ilmenite, Silver Dam pyroclastics
3. Clinopyroxene xenocryst, Silver Dam pyroclastics
4. Clinopyroxene xenocryst, Silver Dam pyroclastics
5. Clinopyroxene xenocryst, Silver Dam pyroclastics
6. Groundmass olivine, olivine melilitite, Sutherland town lands
7. Groundmass olivine, olivine melilitite, Sutherland town lands
8. Groundmass olivine, olivine melilitite, Sutherland town lands
9. Groundmass olivine, olivine melilitite, Sutherland town lands
10. Groundmass olivine, olivine melilitite, Sutherland town lands
11. Olivine phenocryst, olivine melilitite, Sutherland town lands
12. Olivine phenocryst, olivine melilitite, Sutherland town lands

TABLE 1.(continued) Analyses of Minerals from Sutherland Eruptives

Number	13*	14*	15*	16*	17+	18+	19+	20+	21+	22+	23+	24+
Sample Number	C31	C31	C31	C32	C29	C29	C29	C29	C29	C27	C27	C27
SiO_2	37.35	37.36	39.37	40.10	37.92	39.95	40.06	39.44	39.90	40.27	39.64	39.86
TiO_2	0.05	0.08	0.06	0.00	0.00	0.00	0.01	0.02	0.00	0.01	0.02	0.01
Al_2O_3	0.02	0.04	0.02	0.00	0.02	0.06	0.07	0.19	0.03	0.05	0.05	0.04
MgO	40.76	41.98	41.55	47.55	37.42	50.40	48.98	47.21	47.73	48.94	47.25	46.13
FeO_t	21.19	21.17	20.68	10.92	24.87	10.49	10.41	10.16	11.70	10.68	11.84	13.15
Cr_2O_3	0.00	0.00	0.04	0.14	0.02	0.09	0.08	0.03	0.09	0.07	0.06	0.04
MnO	0.07	0.00	0.06	0.26	0.45	0.12	0.14	0.19	0.13	0.11	0.12	0.13
NiO	0.23	0.15	0.19	n.d.	n.d.	n.d.	n.d.	n.d.	n.d.	n.d.	n.d.	n.d.
CaO	0.00	0.10	0.07	0.00	0.06	0.26	0.25	0.85	0.15	0.19	0.14	0.08
Na_2O	0.00	0.00	0.00	0.00	0.01	0.00	0.00	0.00	0.00	0.01	0.02	0.00
K_2O	0.00	0.00	0.00	0.04	0.01	0.00	0.01	0.02	0.00	0.00	0.00	0.00
	99.67	100.88	102.04	99.01	100.79	101.35	100.01	98.11	99.73	100.32	99.14	99.44
	Fo_{77}	Fo_{77}	Fo_{78}	Fo_{88}	Fo_{73}	Fo_{89}	Fo_{89}	Fo_{89}	Fo_{88}	Fo_{90}	Fo_{88}	Fo_{87}

Analyst : * C. Frick, Geological Survey of South Africa
+ B. Wyatt, Anglo American Corp. of South Africa

13. Olivine phenocryst, olivine melilitite, Sutherland town lands
14. Olivine phenocryst, olivine melilitite, Sutherland town lands
15. Olivine phenocryst, olivine melilitite, Sutherland town lands
16. Olivine phenocryst, olivine melilitite, Sutherland town lands
17. Olivine phenocryst, olivine melilitite, Sutherland town lands
18. Olivine phenocryst, olivine melilitite, Sutherland town lands
19. Core and rim of olivine phenocryst, olivine melilitite, Sutherland town lands
20. Core and rim of olivine phenocryst, olivine melilitite, Sutherland town lands
21. Olivine phenocrysts, olivine melilitite, Sutherland town lands
22. Olivine phenocryst ex autolith, olivine melilitite, Saltpetre Kop
23. Olivine phenocryst ex autolith, olivine melilitite, Saltpetre Kop
24. Olivine phenocryst ex matrix olivine melilitite, Saltpetre Kop

TABLE 1. (continued) Analyses of Minerals from Sutherland Eruptives

Number Sample Number	25+ C27	26+ C30	27+ C30	28* C32	29* C32	30* C30	31+ C29	32+ C29	33+ C29	34+ C29	35+ C30	36+ C29
SiO_2	39.85	38.10	39.75	46.45	42.18	40.87	37.40	37.70	36.79	37.37	48.80	44.55
TiO_2	0.01	0.01	0.02	0.00	0.04	0.01	0.08	0.08	0.05	0.07	0.00	0.14
Al_2O_3	0.03	0.02	0.06	4.23	4.10	0.02	0.04	0.04	0.51	0.31	33.93	32.49
MgO	46.11	37.15	47.29	11.29	12.02	20.03	20.66	21.56	19.08	22.91	0.01	0.43
FeO_t	13.99	25.40	13.54	3.93	2.29	8.54	8.92	8.21	8.67	6.94	0.00	1.23
Cr_2O_3	0.04	0.01	0.04	0.00	0.00	0.00	0.03	0.03	0.03	0.03	0.04	0.01
MnO	0.16	0.50	0.13	0.11	0.00	0.32	0.35	0.36	0.36	0.32	0.00	0.01
NiO	n.d.	n.d.	n.d.	0.02	0.12	0.00	n.d.	n.d.	0.00	0.00	0.00	n.d.
CaO	0.10	0.07	0.19	28.72	33.63	29.64	33.26	33.32	33.87	33.63	16.49	0.28
Na_2O	0.01	0.00	0.01	4.18	4.02	0.19	0.09	0.14	0.00	0.00	0.52	12.45
K_2O	0.00	0.01	0.00	0.18	0.21	0.00	0.01	0.03	0.06	0.02	0.00	8.48
	100.30	101.27	101.03	99.09	98.61	99.62	100.84	101.47	99.42	101.32	99.79	100.07
	Fo_{85}	Fo_{73}	Fo_{85}									

Analyst : *C. Frick, Geological Survey of South Africa
+B. Wyatt, Anglo American Corporation of South Africa

25. Olivine phenocryst ex matrix olivine melilitite, Saltpetre Kop
26. Olivine phenocryst in xenolithic olivine melilitite, Sutherland town lands
27. Olivine phenocryst in xenolithic olivine melilitite, Sutherland town lands
28. Melilite, olivine melilitite, Sutherland town lands
29. Melilite, olivine melilitite, Sutherland town lands
30. Monticellite associated with anorthite pseudomorphing olivine, olivine melilitite, Sutherland town lands
31. Monticellite in reaction rim around olivine, olivine melilitite, Sutherland town lands
32. Monticellite in reaction rim around olivine, olivine melilitite, Sutherland town lands
33. Monticellite in reaction rim around olivine, olivine melilitite, Sutherland town lands
34. Monticellite in reaction rim around olivine, olivine melilitite, Sutherland town lands
35. Anorthite associated with monticellite (analysis 30)
36. Nepheline, olivine melilitite, Sutherland town lands.

Fig. 2. Olivine replaced by an assemblage of tabular melilite, magnetite and marginal phlogopite, pp. light, X40.

sill-like bodies of small extent intruded into the Beaufort sediments in the vicinity of Saltpetre Kop. Unaltered material is disappointingly scarce and extensive carbonation in the vicinity of carbonatites is not uncommon. One sill 500 metres south of the main vent is notable in that it contains an abundance of 2 cm diameter autolithic nodules (Ferguson et al., 1973) estimated by de Wet (1974) to make up 30% of the exposed portion of the sill. The olivine melilitite exposed on the town lands at Sutherland village may represent sills or dykes of shallow dip (Taljaard, 1936; Gerrard, 1958). The town lands olivine melilitite exposures differ from those of Saltpetre Kop in that they are somewhat coarser grained, relatively unaltered and more noticeably porphyritic in hand specimen; inclusions of older olivine melilitites are not infrequent in some specimens studied.

de Wet (1974) distinguishes between contaminated and almost inclusion-free trachytic eruptives. The latter are present as narrow steeply dipping dykes of K-rich trachyte in sharp contact with the surrounding sedimentary strata; unweathered material is reddish brown, but becomes cream-coloured on exposure. Apart from the main vent, trachyte contaminated by an abundance of wall rock sediments and minor dolerite and quartzite comprises the largest intrusions around Saltpetre Kop. The contaminated trachyte occurs as irregular dykes up to one kilometre in length and with widths measured in tens of metres.

Small plug-like and dyke-like bodies of carbonatite occur around Saltpetre Kop and attention is drawn by de Wet (1974) to the abundance of hornblende, biotite and ilmenite megacrysts within some outcrops. Carbonatitic rocks show finer grained selvages against olivine melilitites when in contact thus establishing their age relationship (de Wet, 1974). The Silver Dam type pyroclastics are present in several vents having diameters of 10-30 metres. The vents are filled with country rock sediments and less-abundant igneous and metamorphic rock fragments set in a grey-blue earthy matrix containing an abundance of amphibole, pyroxene,

Fig. 3. Portion of an olivine crystal replaced by euhedral monticellite (high relief) and anorthite (low relief), pp. light, X225.

ilmenite and brown mica megacrysts measuring several centimetres across. The megascopic resemblance of this material to some kimberlites encouraged the exploration of these vents by shallow excavations in earlier times.

In the vicinity of Saltpetre Kop the generally cream-coloured Karroo sediments show marked red/brown discoloration due to the introduction of iron oxides especially along joint planes. de Wet (1974) records the presence of introduced barite crystals along joints in sandstones over a wide area around Saltpetre Kop.

Petrography and Mineralogy

Silver Dam type pyroclastics

Inclusions and groundmass make up almost equal volumes of many portions of these rocks. The groundmass consists of highly decomposed fine-grained rock composed of carbonate and finely divided perovskite together with cryptocrystalline indeterminate materials. Ghost outlines of pre-existing crystals within the groundmass possibly represent original olivine grains. Rock fragments mainly of sedimentary origin make up the largest proportion of the inclusions present; also present are fragments of granite, gneiss, dolerite and a gabbro characterised by purple clinopyroxene crystals. Mineral fragments include ilmenite in crystals up to 2.5 cm across, brown amphibole crystals up to 3 cm across, purple augite up to 0.5 cm across and prominent biotite flakes. Brown amphibole and augite are surrounded by reaction rims in which fine biotite is prominent. Chemical analyses of two ilmenite grains (Table I, Nos. 1 and 2) from the pyroclastics are included in Table I as are two analyses of clinopyroxene grains and a clinopyroxene occurring in a gabbro xenolith (Table I, Nos. 3, 4 and 5). Comparison of the latter 3 analyses suggests that the pyroxene grains are xenolithic rather than cognate.

Olivine Melilitite

The olivine melilitites of the Sutherland town lands have been studied by Taljaard (1936) and Gerrard (1958) while de Wet (1974) dealt with the olivine melilitites in the vicinity of Saltpetre Kop. In general, outcrops on the town lands are less altered and contain larger phenocrysts of olivine and magnetite. Several olivine melilitites from Saltpetre Kop show extensive replacement by carbonate which in places is accompanied by fluorspar.

The olivine melilitites are invariably porphyritic or microporphyritic rocks containing abundant olivine phenocrysts (up to 10 mm) and less common magnetite set in an aphanitic groundmass; most olivine grains show corrosion effects resulting from reaction. The matrices of the olivine melilitites show wide variation in grain size, composition and degree of alteration. Extremely fine-grained cryptocrystalline types have been interpreted by Gerrard (1958) as resulting from very rapid crystallisation. Matrices of coarser crystallinity are composed of variable proportions of melilite, phlogopite, olivine, augitic pyroxene, magnetite, perovskite, apatite, zeolites and rare monticellite and nepheline. Ilmenite is reported as a rare mineral by Taljaard (1936) and Gerrard (1958) but was not encountered in the specimens studied here. Xenolithic, generally rounded fragments of older olivine melilitite are of common occurrence within the samples studied.

Olivine phenocrysts in the olivine melilitites have been corroded and embayed by reaction with the surrounding liquid, producing rims of phlogopite followed by melilite (Table I, No. 29), magnetite, perovskite and minor monticellite (Table I, Nos. 30-34) and anorthite (Table 1, No. 35) with secondary carbonate and zeolite. Figure 2 illustrates an advanced stage of replacement where the crystalline aggregate is composed of olivine remnants, tabular melilite, phlogopite and magnetite.

Monticellite is not an abundant phase in the olivine melilitite suite. Gerrard (1958) records monticellite as a replacement of olivine and attributes the process to contact metamorphism resulting from a younger intrusion. Both

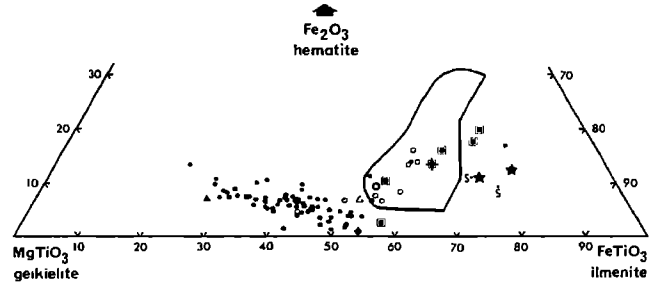

Fig. 4. Variation in mol. per cent $MgTiO_3$, $FeTiO_3$ and Fe_2O_3 for kimberlitic ilmenites: filled circles - autolith groundmass ilmenites, Wesselton; ringed filled circle - average composition (Danchin et al., 1975); open circles - autolith groundmass ilmenites, Lesotho, ringed open circle - average composition (Danchin et al., 1975); double squares - autolith nucleus ilmenites; crossed double square - average composition (Danchin et al., 1975); filled triangle - secondary Liqhobong ilmenite (Haggerty, 1973); open triangle-primary Liqhobong ilmenite (Haggerty, 1973); filled diamond - secondary ilmenite in lherzolite (Boyd and Nixon, 1973); enclosed area - kimberlitic ilmenites after Frick (1973); filled stars - ilmenites from alnoites (Frick, 1973); S, ilmenites, Silver Dam pyroclastics, Saltpetre Kop.

Taljaard (1936) and Gerrard (1958) record the presence on the Sutherland town lands of a fine-grained porphyritic rock consisting of phenocrysts of magnetite and olivine (up to 5 mm) set in a fine granular matrix of monticellite, magnetite and an isotropic to near isotropic unidentified mineral. Microprobe studies showed the latter to be laumonite and also that in the granular groundmass monticellite (Table I, Nos. 31 to 34) is subordinate to fine-grained olivine. Extensive marginal replacement of phenocrystal olivine by fine granular monticellite is in evidence and "ghost textures" seen under low magnification suggest that the present groundmass includes completely replaced olivine phenocrysts.

Another occurrence of monticellite was recorded from a Sutherland town lands olivine melilitite which contains an olivine phenocryst (Fig. 3) which has been completely replaced by a granular aggregate of euhedral monticellite crystals (Table I, No. 30) set in a matrix of anorthite (Table I, No. 35); the latter mineral has not been previously recorded from the Sutherland eruptives. Other olivine phenocrysts in the same thin section show reaction rims in which melitite is prominent.

Trachyte

de Wet (1974) has described the trachytes present in the vicinity of Saltpetre Kop as being porphyritic rocks composed of generally corroded sanidine phenocrysts set in a microcrystalline matrix of lath-shaped feldspar microlites together with finely disseminated iron oxides. Small crystals of nepheline occur in the vicinity of sanidine phenocrysts. Biotite is a scarce phase while apatite, and more rarely, fluorspar are present as accessory minerals. The specimens studied by the writers contain xenolithic fragments of cryptocrystalline, apparently highly altered rock considerably richer in fine-grained iron oxide than the enveloping trachyte. A feature of this highly altered material is the presence of prominent iron oxide rimmed, near euhedral crystals of fluorspar.

Carbonatitic Rocks

de Wet (1974) has recognised sövitic and ankeritic varieties of carbonatite together with a biotite metacarbonatite which is described as a biotite-rich rock extensively replaced by calcite. de Wet (1974) further reports that, in contrast to most other Southern African occurrences of carbonatitic rocks Ba is always in excess of Sr. Gross Brukkaros is an exception showing more similarity to Saltpetre Kop than to other occurrences in this respect. Pyrochlore octahedra 40 to 50 microns in diameter are disseminated in sövite occurring within the central vent.

Geochemistry

(a) Methods

Rock samples intended for chemical analyses were reduced in an agate-lined swing mill and dried at 110°C. Fe, Mn, Ti, Ca, K, P, Si, Al and Mg were determined on a Philips PW1410 semi-automatic X-ray spectrometer using the fusion method of Norrish and Hutton (1969). Pressed powder pellets were used for Na without matrix correction. Water and ignition losses were determined at 110°C and 1000°C respectively. CO_2 and ferrous iron were determined by standard wet chemical procedures. Mineral analyses were carried out using a Jeol JXA50 and an ARL-SEMQ microprobe. Analysed mineral standards were employed in both cases and the raw data were corrected according to the Bence-Albee (1968) procedure.

(b) Minerals

Ilmenite (Table I, Nos. 1 and 2) was recorded as a phenocrystal phase only within the Silver Dam pyroclastic assemblage and the analyses are compared with the fields of kimberlitic ilmenite established by various authors in Figure 4. The Silver Dam ilmenites contain less than 5 per cent MgO and accordingly plot with the less magnesian ilmenites found in kimberlites and in the field of ilmenites occurring in alnöites (see Frick, 1973 and Danchin et al., 1975). According to Haggerty (1973) the compositions of the Silver Dam ilmenites would compare most closely with those of primary high-pressure ilmenites, although their close chemical correspondence to alnöitic ilmenites (Frick, 1973) would suggest a relatively low-pressure regime for their formation.

Twenty-two analyses of olivines from the Saltpetre Kop melilitite suite are presented in Table I. They range from Fo_{65} to Fo_{90} with some specimens showing little variation (Fo_{76-78}, Sample C31, Table I, Nos. 6, 7, 13, 14, 15) while others show a spread of values of Fo_{65}-Fo_{83} within the same thin section (Table I, Nos. 8, 9, 11, 12). Olivines in older xenolithic olivine melilitite fragments returned values of Fo_{73} and Fo_{85} (Table I,Nos.26,27). Compositional determinations on the core and rim of a large olivine grain failed to reveal a zonal structure (Table I, Nos. 19, 20). No distinct ranges in composition characterise groundmass and phenocrystal olivines; nevertheless, the wide range of compositions present in sample C30 (Table I) suggests in this specimen at least, that the olivines do not represent an equilibrium assemblage and include xenocrystic grains. Comparison of matrix and autolith olivines from the autolith-rich olivine melilitite at Saltpetre Kop yielded no significant difference in composition(Table I, Nos. 22, 23, 24, 25).

TABLE II. Chemical Analyses

Number	1	2	3	4	5	6	7	8	9	10	11
Sample Number	C25	C27	C27A	C27M	C28	C29	C30	C31	C32	G1	G2
SiO_2	36.39	32.75	37.24	30.96	35.24	31.72	31.30	35.30	34.01	37.13	37.98
TiO_2	2.36	1.86	1.35	1.79	3.21	2.93	2.97	3.03	3.03	3.61	3.97
Al_2O_3	7.49	6.88	6.63	6.62	7.68	6.98	6.92	7.25	7.23	10.58	9.07
Fe_2O_3	0.61	0.06	1.43	1.52	1.69	2.19	0.90	2.13	1.79	2.00	2.19
FeO	9.41	8.54	6.93	8.30	8.29	10.20	11.47	8.42	9.40	10.43	10.36
MnO	0.19	0.18	0.28	0.31	0.18	0.28	0.25	0.19	0.24	0.26	0.22
MgO	17.92	14.18	13.58	14.38	18.78	19.16	19.74	20.16	19.88	19.12	18.51
CaO	15.89	13.71	11.83	13.12	15.32	18.18	18.59	14.97	16.72	13.02	11.58
Na_2O	2.79	1.54	1.33	1.27	0.55	2.85	2.13	1.17	2.59	1.32	3.13
K_2C	1.35	2.67	3.22	2.75	2.60	1.05	1.01	1.94	1.52	0.51	1.64
P_2O_5	1.07	0.87	0.63	0.94	1.00	1.58	1.67	0.77	1.42	0.00	0.84
H_2O^-	0.28	0.29	0.16	0.81	0.50	0.23	0.32	0.41	0.27	0.37	0.22
LOI	3.92	7.21	4.46	8.79	5.17	1.49	2.01	3.70	1.41	0.83	0.89
CO_2	n.d.	9.04	9.23	7.02	n.d.	n.d.	n.d.	n.d.	n.d.	0.47	0.16
Cl	-	-	-	-	-	-	-	-	-	-	-
	99.67	99.78	98.30	99.58	100.21	98.84	99.28	99.44	99.51	99.65	100.76

Nos. 1 - 9 Analysts : T.S. McCarthy and S.J. Barnes

1. Olivine melilitite, Saltpetre Kop
2. Autolith-bearing olivine melilitite, Saltpetre Kop, whole-rock anslysis
3. Autolith from No. 2, Saltpetre Kop
4. Matrix of No. 2, Saltpetre Kop
5. Olivine melilitite, Sutherland town lands
6. Olivine melilitite, Sutherland town lands
7. Olivine melilitite, Sutherland town lands
8. Olivine melilitite, Sutherland town lands
9. Olivine melilitite, Sutherland town lands
10. Olivine melilitite, Klaasvoodgs (Taljaard, 1936)
11. Olivine melilitite, Klaasvoogds (Taljaard, 1936)

TABLE II.(continued) Chemical Analyses

Number	12	13	14	15	16	17	18	19	20	21	22
Sample Number	G4	G5	G6	G7	G8	G9	G10	C8	C9	C21	C41
SiO_2	36.15	36.95	31.17	30.54	38.30	33.41	34.45	45.02	44.33	50.02	53.73
TiO_2	2.30	4.95	2.96	2.74	2.30	8.19	5.21	2.27	2.50	0.42	0.68
Al_2O_3	15.18	7.85	6.25	10.23	11.56	5.35	8.99	9.81	9.35	15.73	16.32
Fe_2O_3	4.87	4.78	3.22	4.75	5.43	4.78	6.20	10.56(t)	2.71	-	1.13
FeO	9.11	8.70	9.64	8.86	6.53	9.76	8.25	n.d.	7.80	3.77	5.01
MnO	0.33	0.20	-	0.24	0.39	0.18	0.26	0.27	0.31	0.22	0.24
MgO	13.63	15.87	19.90	20.05	9.10	17.43	17.22	10.20	10.40	0.11	0.66
CaO	11.40	13.36	17.76	14.58	17.40	12.59	11.47	11.52	11.39	11.00	5.34
Na_2O	2.42	2.32	2.03	3.30	3.48	1.87	1.85	3.56	3.17	0.58	0.36
K_2O	1.81	2.04	2.51	0.75	1.53	0.99	1.31	0.89	0.91	10.75	11.07
P_2O	0.26	0.83	-	-	0.54	1.84	0.97	0.89	0.75	1.33	0.96
H_2O^-	0.37	0.49	0.40	0.46	0.30	0.79	0.54	1.45	1.62	0.19	0.62
LOI	1.95	1.64	2.05	1.30	2.35	0.26	2.59	4.17	4.58	6.57	3.99
CO_2	-	0.66	-	1.78	0.08	0.42	0.33	n.d.	n.d.	n.d.	n.d.
Cl	-	-	-	-	-	0.24	0.54	-	-	-	-
	100.43	100.25	99.62	100.88	99.29	98.10	100.08	100.61	99.82	100.87	100.11

Nos. 19 - 22 Analysts : T.S. McCarthy and S.J. Barnes

12. Olivine melilitite, Spiegel River (Rogers and du Toit, 1903)
13. Olivine melilitite, Spiegel River (Holmes, 1936)
14. Olivine melilitite, Sutherland (Wagner, 1914)
15. Olivine melilitite, Sutherland (Taljaard, 1936)
16. Olivine melilitite, Dreyerrucken, S.W.A. (Kaiser, 1926)
17. Olivine melilitite, Gamoep 4 (Taljaard, 1936)
18. Olivine melilitite, Gamoep 13 (Taljaard, 1936)
19. Silver Dam pyroclastic, Saltpetre Kop
20. Silver Dam pyroclastic, Saltpetre Kop
21. Trachyte, Saltpetre Kop
22. Trachyte, Saltpetre Kop

TABLE II. (continued) CIPW Norms

Number	1	2	3	4	5	6	7	8	9	10
Sample Number	C25	C27	C27A	C27M	C28	C29	C30	C31	C32	G1
cc	-	-	-	-	-	-	-	-	-	2.75
ap	2.59	2.42	1.73	2.66	-	3.32	3.41	1.87	3.08	-
il	4.67	4.24	3.04	4.15	6.04	5.04	4.97	6.04	5.38	6.89
or	-	-	-	-	-	-	-	-	-	-
ab	-	-	-	-	-	-	-	-	-	-
an	5.37	4.77	3.08	5.17	10.71	2.85	5.59	9.23	3.37	21.54
mt	0.92	0.11	2.46	2.69	2.43	2.87	1.15	3.24	2.43	2.91
di	5.34	4.83	25.66	1.33	-	-	-	2.22	-	8.15
he	1.38	1.54	6.51	0.38	7.27	10.36	11.63	0.35	8.59	1.79
fo	30.87	28.16	19.73	30.18	32.49	30.26	30.37	36.16	32.42	30.88
fa	10.87	11.33	6.32	10.78	6.78	8.81	10.81	7.19	8.10	8.59
ne	13.33	8.68	7.23	7.10	2.50	11.82	8.61	5.63	11.09	6.08
lc	6.53	14.88	17.68	15.56	11.28	-	-	9.44	1.88	2.38
la	18.92	19.25	6.59	20.00	20.01	21.49	20.46	18.62	20.26	8.63
kp	-	-	-	-	-	3.19	2.99	-	-	-

Number	11	12	13	14	15	16	17	18	21	22
Sample Number	G2	G4	G5	G6	G7	G8	G9	G10	C21	C41
cc	-	-	0.28	-	7.32	1.95	-	-	-	-
ap	1.96	0.62	1.96	-	-	4.36	4.43	2.41	3.27	2.33
il	7.59	4.48	9.59	5.17	4.70	15.91	16.14	5.11	0.84	1.35
or	-	-	-	-	-	-	-	-	32.87	68.52
ab	-	-	-	-	-	-	-	-	-	1.66
an	5.88	25.87	5.08	0.48	9.84	3.35	3.40	13.81	9.07	10.66
mt	3.19	7.25	7.07	4.29	6.23	7.09	7.10	9.63	-	1.71
di	11.96	1.28	21.46	-	-	28.62	27.97	14.10	0.63	1.79
he	2.50	0.13	2.00	9.69	4.53	0.45	0.44	1.83	13.27	7.30
fo	28.58	23.99	21.28	31.93	31.63	26.20	22.47	27.63	-	-
fa	7.56	7.42	2.51	7.21	5.77	0.43	0.44	4.52	-	-
ne	14.42	11.38	10.85	8.55	13.67	8.77	8.89	9.09	2.83	0.83
lc	7.65	8.61	9.65	-	-	4.70	4.76	5.62	27.20	-
la	8.72	8.80	8.29	24.93	14.04	2.55	3.86	6.25	-	-
kp	-	-	-	7.76	2.28	-	-	-	-	-

Note : Norms 1 - 9 calculated on CO_2-free basis

Two analyses of melilite are presented in Table I (Nos. 28 and 29). One of these (No. 28) is of the melilite illustrated in Figure 2 while the other (No. 29) is of the melilite from a reaction rim around olivine; the latter is poorer in silica and richer in magnesia. Both melilites have compositions closer to melilite than to either akermanite or gehlenite. Five analyses of monticellite occurring as one of the replacement products of olivine are listed in Table I (Nos. 30-34).

(c) Rocks

Table II lists analyses and norms of nine melilitites from the Sutherland area, a trachyte and trachyte breccia from Saltpetre Kop and two pyroclastics from the Silver Dam occurrence. Also listed in Table II are analyses of other Southern African olivine melilitites.

The olivine melilitite analyses (Table II) were compared statistically with 126 analyses of kimberlites and associated ultrabasic rocks and the seven major cluster Groups established for the latter by cluster analysis by Danchin et al. (1975) and Ferguson et al. (1975). At the same distance coefficient (3.0) employed by Ferguson et al. (1975) the Sutherland/Saltpetre Kop olivine melilitite cluster with the analyses of the melilite- and monticellite-bearing ultramafic rocks which dominate Groups 2 and 3 of Ferguson et al. (1975) while the olivine melilitites

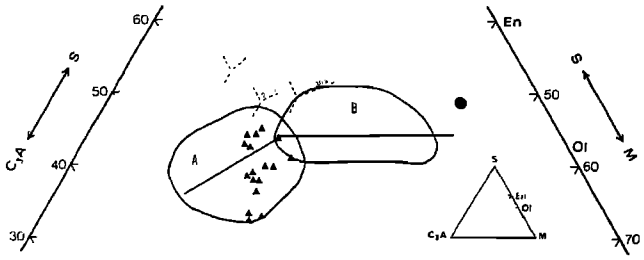

Fig. 5. Projection (Wgt %) of olivine melilite analyses (Table II) from or towards diopside into the plane C_3A-M-S. A, field of non-kimberlitic rocks; B, field of kimberlitic rocks, after Danchin et al., (1975). Triangles - olivine melilitite; circle - GLIK (average garnet lherzolite in kimberlite, Ito and Kennedy, 1967) Phase boundaries volatile-free after O'Hara (1968).

listed by Gerrard (1958) cluster with Group 1 which contains rocks of similar mineralogy to Groups 2 and 3. The olivine melilitites listed in Table II were further compared with the seven cluster Groups established by Ferguson et al. (1975) by consideration of their positions within the CMAS tetrahedron (O'Hara, 1968). As pointed out by Ferguson et al. (1975) the average compositions of the initially established cluster Groups define a trend along an olivine-dominated control line which links the most magnesian kimberlites to the least magnesian of the spatially associated ultrabasic rocks. The control line is subparallel to the CAM plane of the tetrahedron and appears unrelated to pseudo-invariant points applicable to 30 kb or less (O'Hara, 1968). In Figures 5 and 6 the Sutherland and other Cape olivine melilitites plot as additional points within the fields occupied by the non-kimberlitic ultramafics while in Figures 7 and 8 the average of the olivine melilitites listed in Table II provides an additional point on each of the olivine control lines.

Figure 9a shows the kimberlite-melilitite trend projected into the CMS plane of the CMAS tetrahedron where it is compared with the ultrabasic komatiite-tholeiite trend of the Onverwacht eruptives of the Barberton Mountain Land, South Africa (McIver and Lenthall, 1974). While widely divergent, both trends are largely linearly away from the olivine point indicating the importance of olivine fractionation in both series. As shown in Figure 9a the kimberlite-melilitite trend is initially at a high angle to the Di-Fo join suggesting a possible crossing of this join during movement towards the larnite normative compositions characteristic of melilite-bearing or potentially melilite-bearing rocks (Yoder, 1973). The Onverwacht trend, in contrast, is away from the Di-Fo join towards quartz-normative compositions. The two divergent trends shown in Figure 9a represent compositional loci of evolving magmas providing natural parallels to the two trends predicted by Boettcher et al. (1975) and illustrated in Figure 9b. The latter authors concluded that the experimentally determined CO_2-rich trend gives rise to liquids which "may mimic kimberlite-carbonatite magmas and exhibit many chemical similarities to olivine melilitites and olivine nephelinites which are ultimately spatially associated with many kimberlites". Experimental work has therefore offered independent support for the validity of the evolutionary trend from kimberlite to non-kimberlitic melilitic compositions established by consideration of natural specimens (Danchin et al., 1975; Ferguson et al., 1975).

The mantle-melting event giving rise to the Onverwacht trend in Figure 9a very likely took place at depths considerably less than the 200 km or more envisaged for the nascency of kimberlite (see Gurney, 1974). Consideration of the predicted phase relationships of the Onverwacht sequence (McIver, 1975; Howells et al., 1975), however, indicates their relationship to mantle melting at depths possibly in excess of 135 km (45 kb). According to McIver and Lenthall (1974) the composition of the parental magma to the Onverwacht sequence would be close to point 2 on the Onverwacht trend. Such compositions are likely to be related to melting at an invariant point which would project as a pseudo-invariant point within the area Di-En-Ol (Onverwacht trend) of Figure 9a.

Eggler (1974) has shown that under CO_2-saturated conditions the minimum melting point in the assemblage Fo-En-Di moves to the larnite-normative side of the Di-Fo join between 15 and 30 kb. Other recent experimental results show that carbonate would be a stable phase in the presence of CO_2 and H_2O vapour for most projected P-T conditions in the upper mantle (Newton and Sharp, 1975; Kushiro et al., 1975). Furthermore, it has been shown by the former authors that in the upper mantle regimes expected

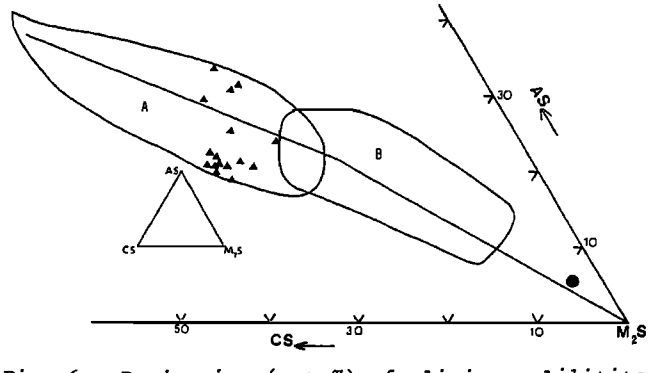

Fig. 6. Projection (wgt %) of olivine melilitite analyses (Table II) from or towards S into the plane M_2S-CS-AS. A, field of non-kimberlitic rocks; B, field of kimberlitic rocks, after Danchin et al., (1975). Ornamentation as in Fig. 5.

for kimberlite generation Fo is incompatible with CO_2 at high activity by the reaction Di + Fo + V → En + Dol. Eggler (1975), however, points out that inclusions of olivine are common in diamonds but that clinopyroxene is rarely present and suggests that in deep mantle regions CO_2 was possibly sufficiently abundant to react out clinopyroxene but insufficient to react out olivine.

In Figure 9a the kimberlite trend line between points 6 and 5 in the C-S-M projection strongly suggests that olivine and orthopyroxene were fractionating phases from a melt initiated in the larnite-normative field during the early stages of kimberlite evolution. This suggestion is supported by the work of Eggler (1974) who has shown that orthopyroxene and olivine are liquidus phases in larnite normative melts resulting from melting in the system Fo-Di-En-CO_2 at high pressure. Brey and Green (1975) have also shown that the effect of the CO_2 in upper mantle regions is to bring orthopyroxene and garnet onto the liquidus of olivine melilitite liquids. While the effect of garnet is less clear in the trends shown in Figures 8 and 9a the initial portion of the trend can apparently be satisfactorily accounted for by olivine and orthopyroxene fractionation.

Brey and Green (1976) have shown that at <17 kb and 950°C a pyrolite composition, less 40% olivine, together with excess CO_2 and H_2O (MH buffered, $XCO_2 = H_2O = 0.5$) has En + Di + Ol + CO_2 as stable phases. Accordingly it is feasible to suggest that the strong olivine control evident in the trend from point 5 in the kimberlite sequence to less magnesian compositions (Fig. 9a) can be accounted for by olivine stability in association with CO_2 at lower pressures coupled with expansion of the olivine primary phase volume with decreasing pressure in the uprising magma column.

In order to assess further the evolutionary model relating more magnesian members of the kimberlite trend to less magnesian compositions

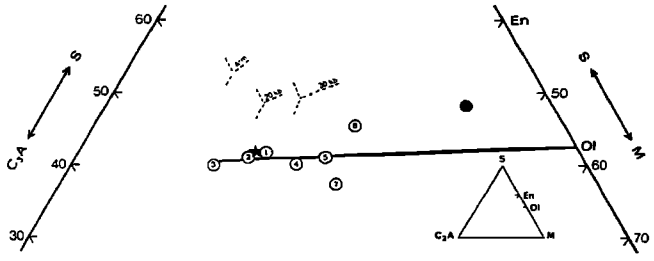

Fig. 7. Projection (wgt %) from or towards diopside into the plane C_3A-M-S of average analyses of the seven cluster Groups (see Fig. 8B, Ferguson et al., 1975) and the average of the olivine melilitite analyses from Southern Africa (Table II). Circled figures, average cluster group analyses (CO_2 free); star, average olivine melilitite; circle, GLIK.

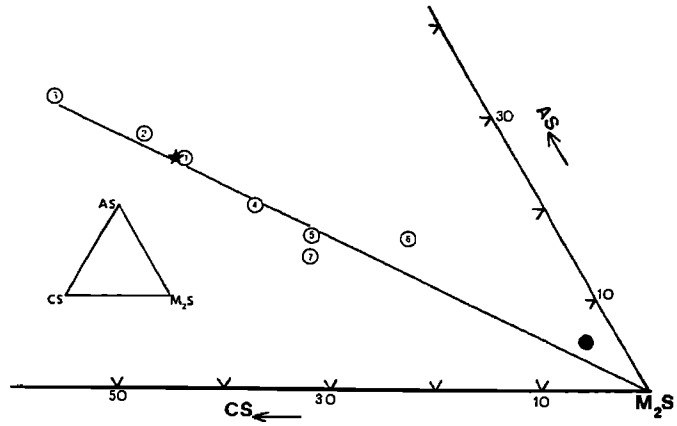

Fig. 8. Projection (wgt %) from or towards S into the plane M_2S-CS-AS of the average analyses of the seven cluster Groups (see Ferguson et al., 1975, Fig. 8A) and the average of the olivine melilitite analyses from Southern Africa (Table II). Ornamentation as in Fig. 7.

initially by olivine-orthopyroxene-dominated fractionation followed by olivine-dominated fractionation, a series of least squares linear mixing calculations were performed. In these calculations use was made of the average compositions of the seven kimberlite cluster Groups (Danchin et al., 1975; Ferguson et al., 1975) in combination with analysed olivines from Saltpetre Kop and an orthopyroxene from an Australian kimberlite. Cluster Groups 4 and 5 (Fig. 9a) could not be related on the basis only of olivine subtraction from the latter. However, subtraction of both olivine (Fo_{90}) and orthopyroxene (En_{90}) from cluster Group 6 yielded calculated compositions for cluster Groups 4, 5 and 7 which show close agreement with the observed compositions of the latter. In Table III observed compositions of cluster Groups 4, 5 and 7 are compared with the compositions calculated for these cluster Groups following extraction of the indicated proportions of olivine and orthopyroxene (Table III, B, C) from cluster Group 6. Subtraction only of olivine (Fo_{78}, Table III) in the proportions indicated in Table III from cluster Group 4 yielded calculated compositions for cluster Groups 1, 2 and 3 which especially in terms of major elements are in turn similar to the observed compositions of the latter. The results of the mixing calculations thus appear to be consistent with the polybaric evolutionary model of kimberlitic and associated rocks suggested by consideration of the CMAS system.

Discussion

The development of magma compositions such as those of the olivine melilitites listed in Table II by polybaric fractionation of kimberlitic magma is indicated by the evidence presented in

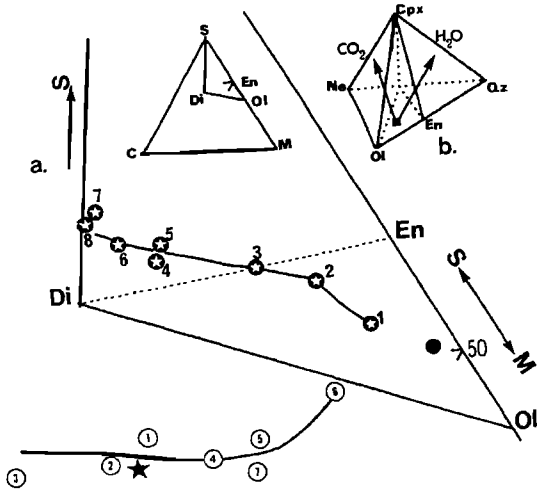

Fig. 9a. Projection (wgt %) from A into the C-S-M plane of the average analyses of the seven cluster Groups (Ferguson et al. 1975), the average of the olivine melilitite analyses from Southern Africa (Table II) and the average analyses of the Onverwacht peridotite-komatite, basaltic komatiite and tholeiitic eruptives from the Barberton Mountain Land. Circled figures - average cluster Group analyses (CO_2 free); solid star - average olivine melilitite; circled stars - Onverwacht eruptives,

1. high magnesia peridotitic komatiites,
2. basal Sandspruit peridotitic komatiites,
3., 4., 5. Geluk, Badplaas and Barberton basaltic komatiites,
6., 7., 8. tholeiitic eruptives (see McIver and Lenthall, 1974).

Circle - GLIK

Fig. 9b. Inferred magmatic trends occasioned by mantle melting in the presence of H_2O and CO_2, after Boettcher et al., 1975).

Figures 5, 6, 7, 8 and 9a. Support is therefore to be found for the generalised models of kimberlite-melilitite evolution proposed by Janse (1971) and Ferguson et al. (1975) as at Gross Brukkaros volcano.

Amphibole megacrysts are a prominent feature of the Silver Dam pyroclastics at Saltpetre Kop and Boyd (1971) has commented on the paucity of amphibole megacrysts in kimberlitic rocks as opposed to the appearance of this mineral in basaltic rocks. On the basis of McGetchen's (1970) analysis of kimberlite eruption Boyd (1971) points out that xenolithic fragments in these rocks are likely to originate at the same mantle depth as the matrix. This being the case the amphibole megacrysts present in the Silver Dam pyroclastics suggest an eruption from depths similar to those applicable to basaltic magmas. According to the amphibole stability fields established by Boettcher et al. (1975) the Silver Dam pyroclastics could have equilibrated at pressures of 20-25 kb and the Silver Dam pyroclastics would thus represent a kimberlitic assemblage that equilibrated at shallower levels than many other kimberlites.

In this respect the iron-rich nature of the ilmenites in the Silver Dam pyroclastics poses some contradictions. On the MgO vs TiO_2 plot for kimberlitic ilmenites (Green and Sobolev, 1975) the Silver Dam ilmenites plot with ilmenites having the lowest MgO and TiO_2 contents and are similar in this respect to the autolith ilmenite nuclei reported by Ferguson et al. (1973). According to Haggerty (1973) progressive crystallisation results in magnesium enrichment in kimberlitic ilmenites and iron-rich ilmenites should therefore be characteristic of less rather than more evolved compositions. Compared with the results of Frick (1973) it is found that the Silver Dam ilmenites resemble those found in alnöitic rocks which are related to more evolved compositions in the kimberlite - non-kimberlite trends of Figures 5, 6, 7, 8 and 9a. Support for the possibility that the Silver Dam ilmenites represent relatively lower temperature equilibration products in the kimberlite evolutionary sequence is indicated by the experimental work of Green and Sobolev (1975). The latter authors have shown that in coexisting synthetic garnet-ilmenite parageneses TiO_2 contents are proportional to temperatures of equilibration and decrease with falling temperature. As garnet was not observed in the Silver Dam specimens studied it follows that interpretation of the low-TiO_2 Silver Dam ilmenites as being indicative of lower temperature equilibration than many other kimberlitic rocks must be treated with some reserve. However, the possibility of coexistence in depth of garnet and ilmenite in the Silver Dam kimberlitic magma cannot be discounted. Frick (1973) has commented on the instability of ilmenite in kimberlite at the time of emplacement and considers that ilmenite in reaction with carbonated magma gives rise to magnetite and perovskite. The change from ilmenite as the major opaque phase in the Silver Dam pyroclastics to magnetite in the olivine melilitites is possibly explained by a liquid ilmenite reaction in relatively shallow environments.

Possibly the most striking petrographic feature of the Sutherland melilitite suite is the reaction relationship between olivine and liquid. Schairer and Yoder (1964), Schrairer (1967), Platt and Edgar (1972) and Gupta et al. (1973) have demonstrated the instability of forsterite relative to melilite in synthetic compositions simulating ultrabasic alkaline liquids in the Ne-Fo-La-SiO_2 system. Within this system the forsterite-liquid reaction permits development of melilite nephelinites (diopside, melilite, nepheline) from olivine- nepheline- melilite-diopside-liquid assemblages. At lower temperat-

TABLE III. Average Analyses of Kimberlite Cluster Groups, Computed Compositions of Kimberlite Cluster Groups Resulting from Least Squares Linear Mixing Calculations and Analyses of Olivine and Orthopyroxene used for Mixing Calculations

	A	B	C	D	E	F	G	H	I	J	K	L	M	N	O	P
SiO_2	39.57	40.27	55.49	35.75	35.67	30.86	30.90	31.97	31.35	39.37	36.29	34.61	35.63	34.68	36.37	34.31
TiO_2	1.80			2.44	2.35	1.65	2.24	3.31	3.64		2.93	6.42	3.24	5.92	3.40	6.23
Al_2O_3	4.36		3.95	4.18	5.22	3.53	4.30	4.66	6.74		8.53	9.04	7.01	8.33	9.42	8.77
Fe_2O_3	6.92			5.46	9.02	7.37	8.62	8.10	13.98		3.82	15.72	3.56	14.48	5.33	15.25
FeO	3.59	10.68t	6.80t	4.55	1.38	2.45	1.86	5.43	-1.48	20.68t	8.73	-3.87	8.47	-2.09	8.00	-3.37
MnO	0.14	0.11	0.00	0.19	0.16	0.14	0.17	0.23	0.23	0.06	0.20	0.40	0.18	0.38	0.25	0.39
MgO	32.03	48.94	32.93	26.83	26.44	28.42	27.42	23.74	23.75	41.55	17.05	17.12	18.59	18.73	17.50	17.39
CaO	6.66	0.19	0.64	10.46	11.37	13.97	14.00	14.58	12.55		15.09	15.46	13.93	14.62	14.29	15.62
Na_2O	0.47			0.46	0.61	0.56	0.59	0.48	0.95	0.07	3.23	0.93	1.21	0.86	1.86	0.90
K_2O	0.89			1.90	1.16	0.28	1.11	1.11	1.80		1.52	2.15	2.76	1.98	1.35	2.09
P_2O_5	0.64			1.67	0.83	0.26	0.80	0.91	1.29		0.23	1.77	0.78	1.63	0.64	1.71
CO_2	2.76			5.77	5.77	10.15	8.00	5.21	5.21		1.27	0.23	0.49	0.50	0.70	0.70
% ol:opx subtracted from A					18:9		5:23		24:26							
% ol subtracted from H												36		32		35

A. Most magnesian kimberlite cluster Group, (Danchin et al., 1975; Ferguson et al., 1975)
B. Olivine (Fo_{90}) from olivine melilitite, Sutherland, No. 22, Table I, this paper
C. Orthopyroxene (En_{90}), kimberlite, Australia, unpublished data, B.M.R., Canberra, Australia
D. Cluster Group 5; observed composition (Danchin et al., 1975; Ferguson et al., 1975)
E. Cluster Group 5; calculated composition after subtraction of 18% ol. (Table III, B) and 9% opx (Table III, C) from cluster Group 6 (Table III, A).
F. Cluster Group 7; calculated composition after subtraction of 5% ol. (Table III, B) and 23% opx (Table III, C) from cluster Group 6)Table III, A).
G. Cluster Group 7; calculated composition after subtraction of 5% ol. (Table III, B) and 23% opx (Table III, C). from cluster Group 6 (Table III, A)
H. Cluster Group 4; observed composition (Danchin et al., 1975; Ferguson et al., 1975)
I. Cluster Group 4; calculated composition after subtraction of 24% ol (Table III, B) and 26% opx (Table III, C) from cluster Group 6 (Table III, A).
J. Olivine (Fo_{78}), olivine melilitite, Sutherland, No. 15, Table I, this paper
K. Cluster Group 3; observed composition (Danchin et al., 1975; Ferguson et al., 1975)
L. Cluster Group 3; calculated composition after subtraction of 36% ol (Table III, J) from cluster Group 4 (Table III, H)
M. Cluster Grour 2; observed composition (Danchin et al., 1975; Ferguson et al., 1975)
N. Cluster Group 2; calculated composition after subtraction of 32% ol (Table III, J) from cluster Group 4 (Table III, H)
O. Cluster Group 1; observed composition (Danchin et al., 1975; Ferguson et al., 1975)
P. Cluster Group 1; calculated composition after subtraction of 35% ol (Table III, J) from cluster Group 4 (Table III, H).

TABLE III. (continued) CIPW Norms (CO_2 free)

	A	D	E	F	G	H	I	K	L	M	N	O	P
ap	1.53	4.13	2.04	0.67	1.99	2.23	3.11	0.55	3.96	1.90	3.72	1.51	3.86
il	3.52	4.94	4.74	3.46	4.58	6.65	7.18	5.70	11.77	6.45	11.07	6.56	11.53
or	5.42	-	-	-	-	-	-	-	-	-	-	-	-
ab	2.83	-	-	-	-	-	-	-	-	-	-	-	-
an	7.37	3.97	8.57	6.95	6.25	7.70	9.15	4.39	13.64	5.81	12.81	13.58	13.36
mt	7.01	8.43	-1.95	3.94	0.06	9.16	-10.18	5.67	-16.69	5.41	-15.66	7.85	-16.35
hm	2.29	-	10.92	5.42	9.23	2.25	21.54	-	26.68	-	25.05	-	26.13
en	-	-	-	-	-	-	-	-	-	-	-	-	-
fs	-	-	-	-	-	-	-	-	-	-	-	-	-
di	17.40	16.64	14.16	-	-	3.77	0.00	7.11	10.25	6.54	11.00	12.00	9.36
he	2.29	0.37	-	-	-	-	-	1.23	-	-	-	1.23	-
fo	51.93	44.46	44.38	54.75	51.50	42.61	43.05	28.17	25.50	31.90	28.59	27.13	26.52
fa	-	0.12	-	-	-	-	-	6.15	-	5.77	-	3.53	-
ne	0.68	2.24	2.97	2.83	2.91	2.33	4.52	15.17	4.11	5.82	3.88	8.66	4.02
lc	-	9.39	5.71	-	-	5.45	3.20	7.22	9.62	13.42	9.04	6.36	9.44
la	-	5.46	8.47	20.95	19.46	17.86	14.47	18.65	11.15	16.05	10.51	11.58	12.13
kp	-	-	-	1.04	4.02	-	3.97	-	-	-	-	-	-

ures melilite in turn is resorbed in liquid-diopside-melilite-nepheline assemblages to produce potential wollastonite in nepheline-feldspar-diopsite assemblages which could mimic phonolite (Platt and Edgar, 1972).

The olivine-liquid reaction preserved in the Sutherland olivine melilitites would appear to provide the natural analogue of the forsterite-liquid reaction in the Ne-Fo-La-SiO_2 system; in the natural system melilite was accompanied by phlogopite, perovskite, monticellite and zeolite. The stability limit of melilite in the presence of excess CO_2 is less than 6 kb ± (Yoder, 1975) and this would imply a maximum depth of 18 km ± for the onset of the olivine reaction interval. In Figures 5 and 6 a change of slope is apparent in the mean trend-lines defined by the fields of kimberlitic and non-kimberlitic rocks. This change takes place at the points of overlap of the two fields and is possibly a consequence of the change of fractionating phases occasioned by the olivine-liquid reaction at 6 kb ± in the natural equivalent of the Ne-Fo-La-SiO_2 system. Trend-lines based on average cluster Group analyses do not show the change in trend (Figs. 7,8). Ferguson et al. (1975), Danchin et al. (1975) and Janse (1971) favoured the development of monticellite as a relatively late-stage mineral during high-level arrest and equilibration of evolving magma of the kimberlite trend. More recent work has revealed the not infrequent presence of monticellite in many South African kimberlites (Clement et al., 1975). Accordingly monticellite does not have the unique position among the more evolved members of the kimberlite series assigned to it by Janse (1971), Ferguson et al. (1975) and Danchin et al. (1975).

Separation of a carbonatite liquid from the carbonated kimberlitic magma either by a process of fractionation (Yoder, 1975; Wyllie and Huang, 1975) or immiscibility (von Eckerman, 1961) is another feature which would be expected to manifest itself at lower pressure regimes than those at which magma generation took place. Whether this separation took place at Saltpetre Kop before or after the onset of the olivine reaction interval is uncertain. Carbonate extraction would, however, result in a residual liquid consisting of olivine crystals together with monticellite and potential or crystalline nepheline, melilite and phlogopite depending on depth. This liquid could be considered as a potential melilite-nepheline-phlogopite peridotite, continued fractionation of which in a crustal regime would result in the formation of nepheline-phlogopite-melilitite, which in turn could give rise to an assemblage containing nepheline and feldspar. This latter assemblage is that of the Saltpetre Kop trachytes which probably represent the natural equivalent of the residual liquids which Platt and Edgar (1972) suggest mimic phonolite in the K-free synthetic system.

Two reactions (Yoder, 1973) which possibly took place at an advanced stage of evolution, but before the disappearance of olivine are:

$$2\,Ak + 3Lc + (x+1)Fo \rightarrow 4Di + 3Ks + xFo \qquad (1)$$

$$Di + 3Ks + (x+4)Fo + 3H_2O + CO_2 \rightarrow \text{Phlogopite} + \text{Calcite} + xFo \qquad (2)$$

The amount of Fo available at the time of the reaction will determine the proportion of oliv-

ine in the final assemblage which apart from olivine agrees closely with the minor intrusives of metacarbonatite (calcite and biotite) described from Saltpetre Kop by de Wet (1974). The incompatibility of melilite and feldspar in the presence of olivine (Yoder, 1973) precludes the possibility that the anorthite-monticellite-melilite-olivine assemblage encountered in these rocks is in equilibrium.

A Model For Saltpetre Kop

Kimberlitic magma with dissolved CO_2 and H_2O was generated by partial melting of hydrous carbonate-bearing garnet lherzolite (Wyllie and Huang, 1975) at depths probably between 100-200 km. Initial slow uprise of this magma was accompanied by olivine and orthopyroxene fractionation. Arrest of some of the magma in a pressure regime where amphibole was a stable phase was followed by rapid transport to surface of this magma to give rise to the Silver Dam pyroclastics. Arrest of the evolving magma at depths of less than 18 km allowed fractionation towards the olivine reaction interval to produce melilite-monticellite-phlogopite-perovskite-zeolite assemblages together with disequilibrium or excess olivine in the olivine melilitites. Possibly concomitantly with the arrest of the magma and the onset of the olivine reaction interval a carbonatite phase began to separate; volatile pressure increased to the point where it exceeded the lithostatic pressure; doming took place culminating in the formation of the central vent at Saltpetre Kop. Radial and tangential fractures developed during updoming were then intermittently exploited by olivine melilititites, trachytic eruptives and carbonatites. The trachytes developed as a result of continued fractionation of magma in a crustal regime to beyond the limit of melilite stability to produce a potassium-rich feldspar-bearing system.

Acknowledgements

The authors wish to extend their appreciation to the following: The Council of the University of the Witwatersrand and the Council for Scientific and Industrial Research for financial support; the geological staff and management of Rand Mines Ltd. for assistance during the field work; Dr. C. Frick and Mr. B. Wyatt of the Geological Survey of South Africa and Anglo-American research laboratories respectively for undertaking analyses of rocks and minerals; Mr. G. Levin for supplying maps of the South Western Cape area and Dr. B.W. Chappell of the Australian National University for making his mixing program available. Drs. R.G. Cawthorn and S.W. Richardson and Messrs. R.N. England and G.P. Brey are sincerely thanked for critically reviewing the manuscript. One of us (J.F.) acknowledges permission for publication from the Director, Bureau of Mineral Resources, Geology and Geophysics, Canberra.

References

Bence, A.E. and A.L. Albee, Empirical correction factors for the electron microanalysis of silicates and oxides. J. Geol., 78, 382-403, 1968.

Boettcher, A.L., Mysen, B.O. and P.J. Modreski. Melting in the mantle: phase relationships in natural and synthetic peridotite-H_2O-CO_2 systems at high pressures. Physics and Chemistry of the Earth, 9, 855-868, 1975.

Boyd, F.R., Pargasite-Spinel peridotite xenolith from the Wesselton Mine. Carnegie Inst. Yearbk. 70, 138-142, 1971

Boyd, F.R. and P.H. Nixon, Origin of the ilmenite-silicate nodules in kimberlites from Lesotho and South Aprica. In: Lesotho Kimberlites (ed. P.H. Nixon), 254-268: Lesotho National Development Corporation, Maseru, 1973.

Brey, G. and D.H. Green, The role of CO_2 in the genesis of olivine melilitite. Contrib. Mineral. Petrol., 49, 93-104, 1975.

Brey, G. and D.H. Green, Solubility of CO_2 in olivine melilitite at high pressures and role of CO_2 in the earths upper mantle. Contrib. Mineral. Petrol., 55, 217-236, 1976.

Bultitude, R.J. and D.H. Green, Experimental study at high pressures on the origin of olivine nephelinite and olivine melilitite magmas. Earth Planet. Sci. Letters, 3, 325-337, 1968.

Clement, C.R., Gurney, J.J. and E.M.W. Skinner, Monticellite- an abundant groundmass mineral in some kimberlites. Ext. Abs. Kimberlite Symposium, Cambridge, U.K., 1975.

Cornelissen, A.K. and W.J. Verwoerd, The Bushmanland kimberlites and related rocks. Physics and Chemistry of the Earth, 9, 71-80, 1975.

Danchin, R.B., Ferguson, J., McIver, J.R. and P.H. Nixon, The composition of late stage kimberlitic liquids. Physics and Chemistry of the Earth, 9, 235-245, 1975.

de Wet, J.J., Carbonatites and related rocks at Saltpetre Kop, Sutherland, Cape Province. Unpubl. M.Sc. thesis, Univ. Stellenbosch, 1974.

Eggler, D.H., Effect of CO_2 on the melting of peridotite. Carnegie Iest. Yearbk., 73, 215-224, 1974.

Eggler, D.H., Peridotite-carbonate relations in the system CaO-MgO-SiO_2-CO_2, Carnegie Inst. Yearbk., 74, 468-474, 1975.

Ferguson, J., Danchin, R.V. and P.H. Nixon, Petrochemistry of kimberlite autoliths. In: Lesotho Kimberlites (ed. P.H. Nixon), 285-293. Lesotho National Development Corporation, Maseru, 1973.

Ferguson, J., Martin, H., Nicolaysen, L.O. and R.V. Danchin, Gross Brukkaros: a Kimberlite-Carbonatite Volcano. Physics and Chemistry of the Earth, 9, 219-234, 1975.

Frankel, J.J., An inclusion-bearing olivine melilitite from Mukorob, South West Africa. Trans. roy. Soc. S. Afr., 35, 115-124, 1956.

Franz, G.W. and P.J. Wyllie, Experimental studies in the system CaO-MgO-SiO_2- CO_2- H_2O. In: Ultramafic and Related Rocks (ed. P.J. Wyllie).

John Wiley and Sons., Inc., New York, 1967.
Frick, C., Kimberlitic ilmenites. Trans. geol. Soc. S. Afr., 76, 85-94, 1973.
Gerrard, I., The olivine melilitites from the Western Cape. Unpubl. M.Sc. thesis, Univ. Cape Town, 1958.
Gittins, J., Hewins, R.H. and A.F. Laurin, Kimberlitic-Carbonatitic Dikes of the Saguenay River Valley, Quebec, Canada. Physics and Chemistry of the Earth, 9, 137-148, 1975.
Green, D.H. and N.V. Sobolev, Coexisting garnets and ilmenites synthesized at high pressures from pyrolite and olivine basanite and their significance for kimberlite assemblages. Contrib. Mineral. Petrol., 50, 217-229, 1975.
Griffin, W.L. and P.N. Taylor, The Fen Damkjernite: Petrology of a Central-Complex kimberlite. Physics and Chemistry of the Earth, 9, 163-178, 1975.
Gupta, A.K., Venkateswaren, G.P., Lidiak, E.G. and A.D. Edgar, The system diopside-nepheline-akermanite-leucite and its bearing on the genesis of alkali-rich mafic and ultramafic volcanic rocks. J. Geol., 81, 209-218, 1973.
Gurney, J.J., The origin of kimberlite: Modern concepts. Trans. geol. Soc. S. Afr., 77, 353-362, 1974.
Haggerty, S.E., Spinels of unique composition associated with ilmenite reactions in the Liqhobong kimberlite pipe, Lesotho. In: Lesotho Kimberlites (ed. P.H. Nixon), 149-158, Lesotho National Development Corporation, Maseru, 1973.
Heinrich, E., The geology of carbonatites. Rand McNally and Co., Chicago, 1966.
Holmes, A., Contributions to the petrology of kimberlites and its inclusions. Trans. geol. Soc. S. Afr., 39, 379-428, 1936.
Howells, S., Begg, C. and M.J. O'Hara, Crystallisation of some natural eclogites and garnetiferous ultrabasic rocks at high pressure and temperature. Physics and Chemistry of the Earth, 9, 895-902, 1975.
Ito, K. and G.C. Kennedy, Melting and phase relations in a natural peridotite to 40 kb. Am. J. Sci., 265, 519-539, 1967
Janse, A.J.A., Monticellite bearing porphyritic peridotite from Gross Brukkaros, South West Africa. Trans. geol. Soc. S. Afr., 74, 45-56, 1971.
Kushiro, I., Satake, H. and S. Akimoto, Carbonate-silicate reactions at high pressures and possible presence of dolomite and magnesite in the upper mantle. Earth Planet. Sci. Letters, 28, 116-120, 1975.
Lenthall, D.H., The application of discriminatory and cluster analysis as an aid to the understanding of the acid phase of the Bushveld complex. Econ. Geol. Research Unit, Univ. of the Witwatersrand Inform. Circ. No. 72, 33pp, 1972.
McGetchin, T.R., Mechanism of emplacement of kimberlite and related breccia at Moses-Rock dike, Utah. Program and Abstracts, Int. Symposium on Mechanical Properties and Processes in the Mantle, Flagstaff, Arizona, 7-8, 1970.
McGetchin, T.R. and Y.S. Nikhauj, Carbonatite-kimberlite relations in the Cave Valley diatreme, San Juan County, Utah. J. Geophys. Res. 78, 1854-1869, 1973.
McIver, J.R. and D.H. Lenthall, Mafic and ultramafic extrusives of the Barberton Mountain Land in terms of the CMAS system. Precamb. Res., 1, 327-343, 1974.
McIver, J.R. Aspects of some high magnesia eruptives in Southern Africa. Contrib. Mineral. Petrol., 51, 99-118, 1975.
Newton, R.C. and W.E. Sahrp, Stability of forsterite and CO_2 and its bearing on the role of CO_2 in the mantle. Earth Planet. Sci. Letters, 26, 239-252, 1975.
Norrish, K. and J.T. Hutton, An accurate X-ray spectrographic method for the analysis of a wide range of geological samples. Geochem. Cosmochim. Acta, 33, 431-453, 1969.
O'Hara, M.J., The bearing of phase equilibria studies in synthetic and natural systems on the origin and evolution of basic and ultrabasic rocks. Earth Sci. Rev., 4, 69-133,1968.
Platt, R.G. and A.D. Edgar, The system nepheline-diopside-sanidine and its significance to the genesis of melilite- and olivine-bearing alkaline rocks. J. Geol., 80, 224-236, 1972.
Rhodes, J.M., The application of cluster and discriminatory analysis to mapping granite intrusions. Lithos, 2, 223-238.1969.
Rogers, A.W. and A.L. du Toit. Annual report of the Geological Commission of the Cape of Good Hope, 1903.
Rogers, A.W. and A.L. du Toit, The Sutherland volcanic pipes and their relationship to other vents in South Africa. Trans. Phil. Soc. S. Afr., 15, 61-74, 1904.
Schairer, J.F. Phase equilibria at one atmosphere related to tholeiitic and alkali basalts. In: (ed. P.H. Abelson): Researches in geochemistry John Wiley and Sons, New York, 1967
Schairer, J.F. and H.S. Yoder, Crystal and liquid trends in simplified alkali basalts. Carnegie Inst. Yearbk., 63, 64-74, 1964.
Taljaard, M.S., South African melilite basalts and their relations. Trans. geol. Soc. S. Afr., 39, 281-316, 1936.
Tuttle, O.F. and J. Gittins., Ed: Carbonatites. John Wiley and Sons, New York, 1966.
von Eckerman, H., The petrogenesis of the Alnö Alkaline Rocks. Bull. geol. Inst. Univ. Upsala, 40, 25-36, 1961.
Wyllie, P.J. and W.L. Huang, Peridotite, kimberlite and carbonatite explained in the system $CaO-MgO-SiO_2-CO_2$. Geology 3, 621-624, 1975.
Yoder, H.S. Melilite stability and paragenesis. Fortschr. Miner., 50, 140-173, 1973.
Yoder, H.S., Relationship of melilite-bearing rocks to kimberlite. A preliminary report on the system akermanite-CO_2. Physics and Chemistry of the Earth, 9, 883-894, 1975.

MINERALOGY AND PETROLOGY

MINERALOGICAL CLASSIFICATION OF SOUTHERN AFRICAN KIMBERLITES

E. Michael W. Skinner and C. Roger Clement

Geology Department, De Beers Consolidated Mines Limited, P.O. Box 616, Kimberley 8300, R.S.A.

Abstract. Previous mineralogical classifications of kimberlites are considered inadequate principally because they fail to take into account the full range of primary minerals that occur in these rocks. A new classification is therefore proposed based on the relative abundances in kimberlites of five primary minerals. These minerals are diopside, monticellite, phlogopite, calcite and serpentine.

Olivine is always an abundant mineral in kimberlites but is of limited use in classification since the abundance of olivine is largely independent of the relative abundances of the other minerals present. Furthermore, adequate distinction cannot be made between olivine derived directly from the kimberlite magma and xenocrystic olivine.

Deuteric alteration of kimberlites is a common feature but alteration due to deuteric processes does not seriously hinder classification. Severe weathering or metasomatism may, however, make reliable mineralogical classification impossible.

Modal analyses of twelve southern African kimberlites are presented to demonstrate the practical application of the proposed classification and to illustrate the wide mineralogical range exhibited by kimberlites.

Introduction

Examination of the fine-grained constituents of kimberlites has been and is to some extent a comparatively neglected aspect of petrographic studies of these rocks. In contrast many detailed investigations have been undertaken with respect to the larger (often xenocrystic or xenolithic) components of kimberlites. Two main reasons for this can be advanced. Firstly many of the coarse components are considered to be representatives of minerals and rocks which occur in the Earth's upper mantle and consequently they are of considerable geological importance. The true relationship of these components to kimberlites is poorly understood. Secondly the fine-grained components have been regarded as rather elusive constituents which are commonly extensively altered. We believe, however, that a better understanding of the fine-grained minerals is essential if the nature of kimberlite and its relationship with other rocks is to be fully understood. We also believe that previous mineralogical classifications of kimberlite are generally inadequate because they fail to take into account the full range of primary minerals that may be present in kimberlites.

A fundamental requirement for the mineralogical classification of any suite of rocks is the delineation of valid petrographic limits. For our proposed classification we consider that such limits are embodied in the definition of kimberlite proposed by Clement et al. (1977). The most relevant part of this definition is as follows: "The matrix contains as prominent primary phenocrystal and/or groundmass constituents, olivine and several of the following minerals: phlogopite, calcite, serpentine, diopside, monticellite, apatite, spinels, perovskite and ilmenite. Other primary minerals may be present in accessory amounts."

Review and Discussion of Some Previous Classifications

Early classifications of kimberlite such as those introduced by Lewis (1897) and by Wagner (1914), tend to combine a number of physical characteristics, including the degree of weathering and textural variation, with variation in mineral content. Two main types of kimberlite were recognised. These are basaltic (mica-poor) and lamprophyric (micaceous) kimberlites.

The terms used by Lewis and Wagner have become widely accepted and still form the basis of most modern classifications. For example, the elaborate classification devised by Milashev (1963; cited by Frantsesson, 1970) is based, from a mineralogical standpoint, on initial subdivision into basaltic and lamprophyric types. Further subdivision is made according to specific groups of minerals which Milashev regarded as principal primary constituents. Basaltic kimberlite was divided into types containing (a) olivine, clinopyroxene and/or melilite(?) and (b) olivine or olivine and monticellite. Lamprophyric kimberlite was divided into types containing (a) olivine, phlogopite, clinopyroxene and/or melilite(?) and

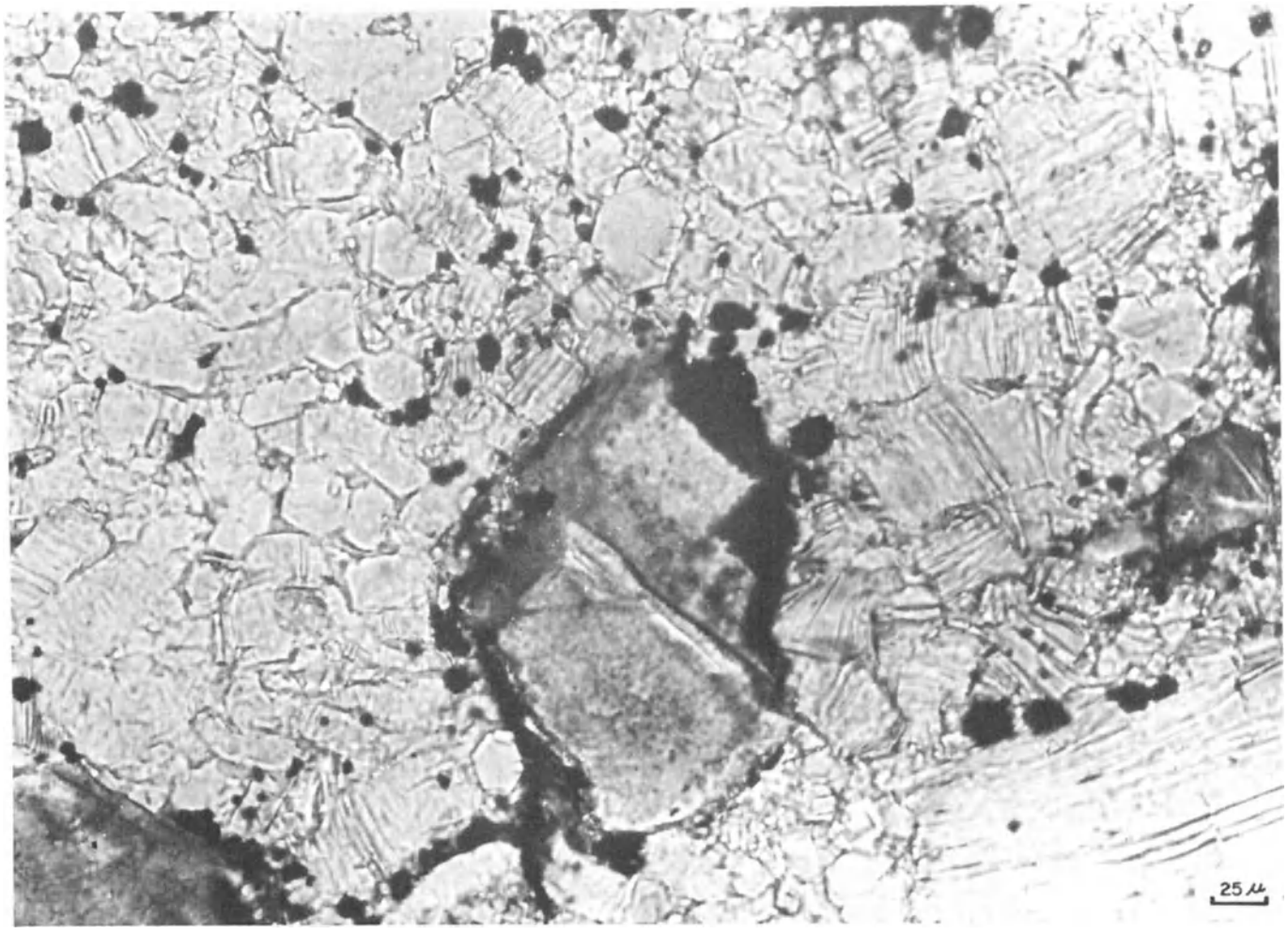

Fig. 1. A phlogopite kimberlite from the Sydney-on-Vaal dyke. Serpentinized olivine phenocrysts are set in a groundmass consisting mainly of small, euhedral, phlogopite crystals.

(b) olivine and phlogopite or olivine, monticellite and phlogopite.

The inclusion of melilite in Milashev's classification as a principal primary mineral is questionable. In the kimberlites which we have examined we have not found melilite or any other feldspathoid minerals, but we admit that our sample is regionally biased. Milashev regarded both calcite and serpentine as secondary minerals. It has, however, since been shown (Watson, 1967; Emeleus and Andrews, 1975; Clement, 1975 and others) that these minerals also occur as primary constituents.

The widespread acceptance of Lewis' and Wagner's terms is surprising. The term 'basaltic' is geologically incorrect in the context of these authors as kimberlites are feldspar-free and do not typically display a basaltic texture. Furthermore both 'basaltic' and 'lamprophyric' are vague terms for which no compositional limits are set. Kimberlite classification based on these terms is therefore subjective and may lead to confusion.

In an alternative classification proposed by Mitchell (1970) kimberlites were subdivided according to the relative abundances of olivine, phlogopite and carbonate. Three main types, kimberlite (equivalent to basaltic kimberlite), micaceous kimberlite and calcareous kimberlite, were recognised. We consider that this classification like others, is inadequate, mainly because it fails to account for the full range in type and abundance of principal primary minerals. An additional criticism is that use of the term 'kimberlite' to describe a specific variety is confusing. 'Kimberlite' is used, and will continue to be used, as a collective term uniting all members of the kimberlite suite incorporating all mineralogical variations and including epiclastic, pyroclastic and igneous types.

The presence or relative abundance of olivine has been utilized as a basis for the subdivisions of kimberlites by Milashev (op. cit.) Mitchell (op. cit.) and others. We have found, however, that the abundance of olivine is largely indepen-

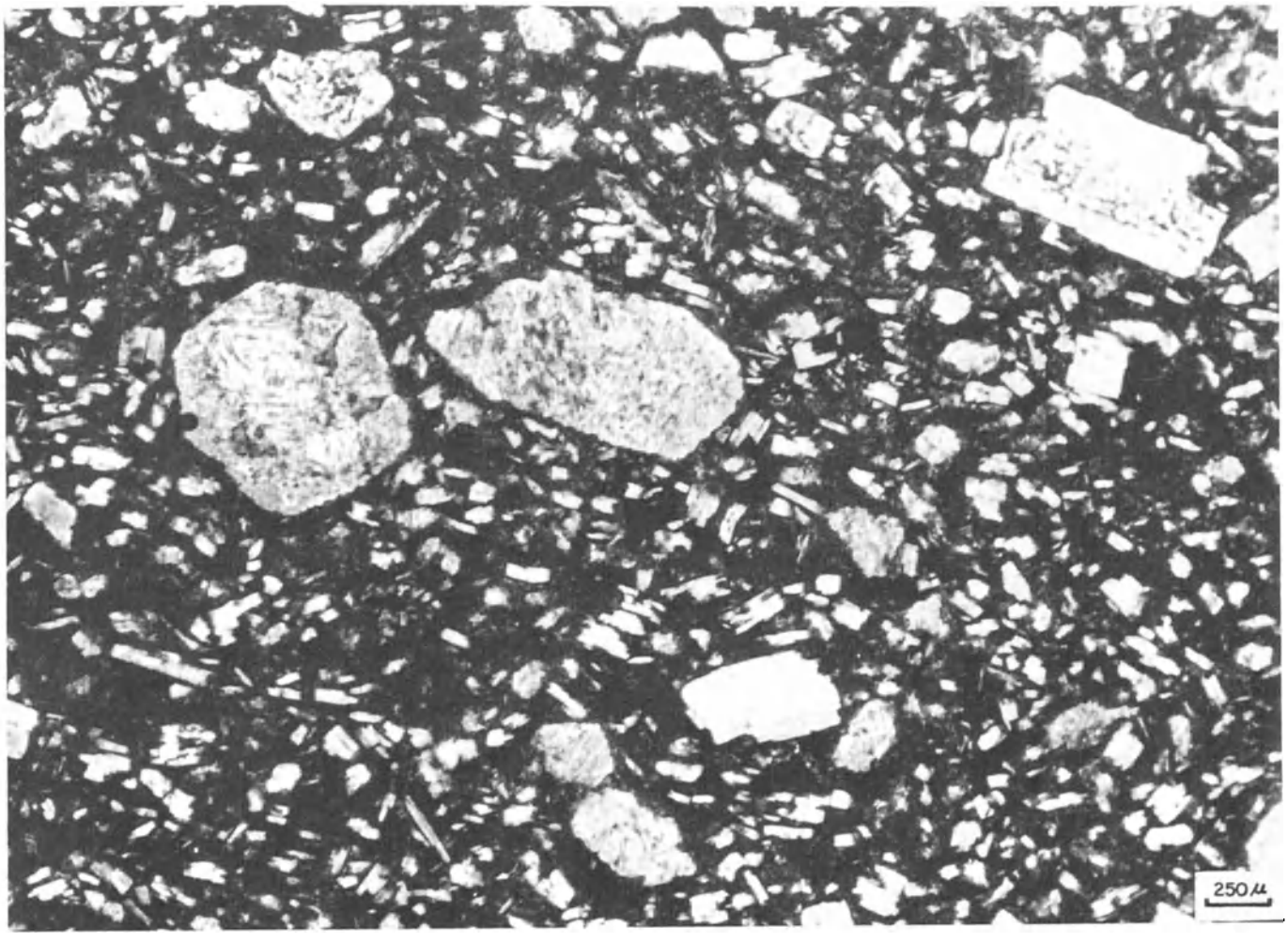

Fig. 2. A phlogopite kimberlite, from the Main dyke of the Swartruggens group. Steatized olivine plus large and small phlogopite phenocrysts are set in an extremely fine-grained phlogopitic groundmass. Note the sub-parallel orientation of elongate crystals.

dent of the variation in abundance and type of other major constituents. Hence olivine is of limited use for classification purposes. Evidence exists to indicate that many anhedral crystals of olivine are xenocrysts (e.g. Boyd and Clement, 1977) while others may represent corroded phenocrysts. Adequate distinction between these olivines is not as yet possible. The proportion of olivine derived directly from the kimberlite magma cannot therefore be accurately assessed. This problem further limits the use of olivine in classification.

The Proposed Mineralogical Classification of Kimberlite

This classification is based on the examination of approximately 2000 thin sections representing more than 200 kimberlites located within South Africa, Lesotho, Botswana and Rhodesia. This study has indicated that, in addition to olivine, any one of five other minerals may be present as a major primary constituent of kimberlite. These minerals are diopside, monticellite, phlogopite, calcite and serpentine. Accordingly we propose the recognition of five basic subdivisions of kimberlite depending upon (and named after) whichever one of these five minerals is volumetrically most abundant. Olivine is omitted in view of the previously discussed limitations.

Further subdivision can be made if one or more of these or any other mineral is present in sufficient abundance for it to qualify as a characterizing accessory or modifier. We have found it useful to accept, as characterizing accessories, those minerals which are present to the extent of, or exceed two-thirds of the volumetric abundance of the dominant mineral. We accept the possibility that, in addition to the five minerals listed above, some other mineral may occur as a

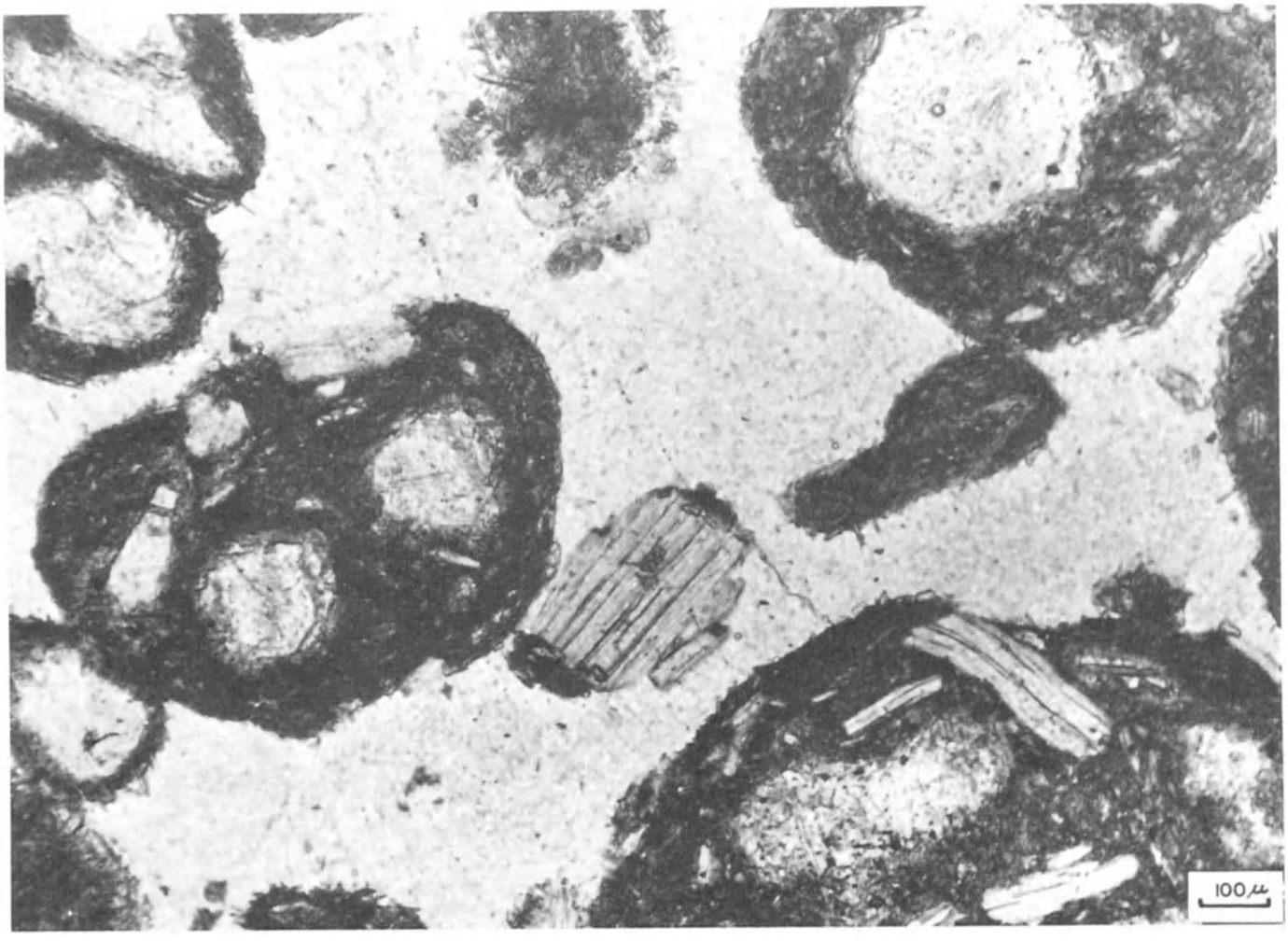

Fig. 3. A serpentine-phlogopite kimberlite, from the Finsch pipe. Globular segregations (autoliths) contain mainly phenocrysts of olivine (serpentinized) and phlogopite plus very fine-grained phlogopite and diopside. The interautolithic material is essentially serpentine.

major constituent of kimberlite. In this event our primary subdivision could be extended.

In the kimberlites which we have examined only one other mineral has been found to occasionally occur in sufficient abundance for it to qualify as a characterizing accessory. This mineral is apatite. It is, however, also true that the total opaque-mineral content accounts for a major proportion of some kimberlites. Opaque minerals often cannot be identified during point-counting in transmitted light. Ideally a combination of reflected and transmitted light studies are required to remedy this inadequacy. As a temporary measure we have qualified all kimberlites containing abundant opaque-minerals as 'opaque-mineral-rich'.

All other primary minerals present in the kimberlites that we have examined invariably occur as minor accessories. They do not therefore affect classification of the rocks.

Kimberlites sometimes contain more than one generation of phlogopite. Some of this phlogopite may have a cryptogenic (unknown) origin. Such phlogopite has, however, not been found in sufficient abundance for it to hinder accurate classification of the rock.

Alteration Effects

Adequate mineralogical classification of any rock is partly dependent on the degree to which the rock has been altered. Extensive alteration introduces a subjective element into classification as interpretive assessment of the nature of the original minerals becomes necessary.

Kimberlites may be altered by deuteric, metasomatic and weathering processes. Deuteric alteration, generally reflected by partial or complete pseudomorphous replacement of original minerals, is evident to some degree in all the

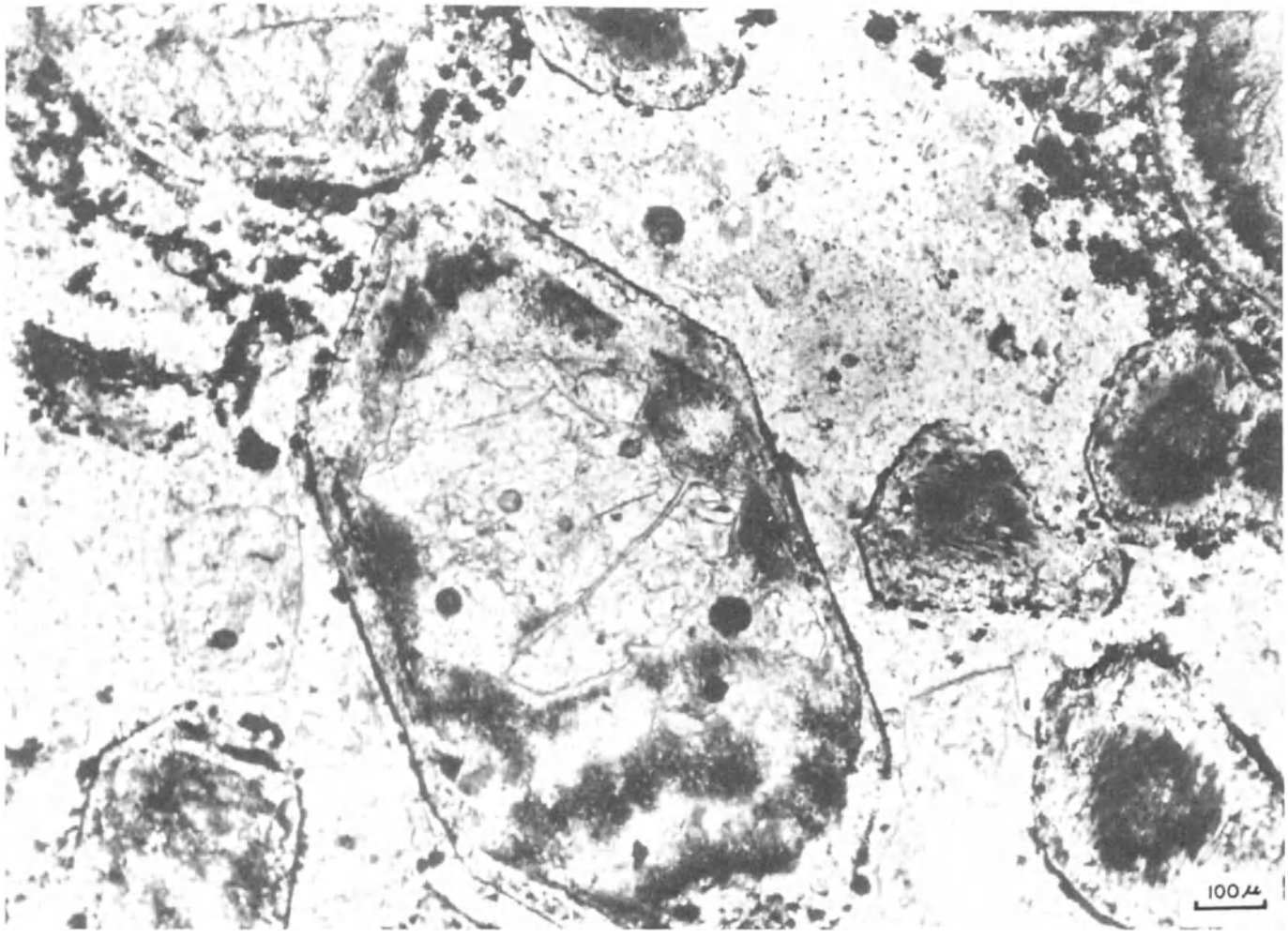

Fig. 4. A calcite-serpentine kimberlite, from a dyke in the country-rock of the Dutoitspan pipe. Altered (mainly serpentinized and chloritized) olivine phenocrysts (rimmed by small opaque-minerals) and rafts of calcite (eg. bottom-right of large olivine) are set in a groundmass of serpentine which is speckled with small flakes of secondary clay minerals.

kimberlites that we have examined. As deuteric processes are the direct consequence of the consolidation of the magma, the resulting alteration products, for purposes of this classification are regarded as primary constituents. Alteration of this type does not therefore pose a serious problem with respect to classification.

Alteration due to metasomatic and/or weathering processes in kimberlites is generally reflected by the development of clay, and/or chlorite and/or abundant carbonate minerals. Replacement resulting from metasomatic and weathering processes seldom takes place in pseudomorphous fashion. Thus, according to the nature of the alteration products and the form of replacement, it is commonly possible to distinguish between deuteric and other alteration effects with sufficient accuracy to ensure adequate classification.

In those cases where many of the original minerals are masked by the products of extensive alteration, and where the nature of the alteration processes cannot be determined, reliable mineralogical classification may be rendered impossible.

In practice, during point-counting to establish modal proportions, the following situations may arise:

1. Unaltered minerals may be encountered.
2. Partly or completely altered minerals may be encountered but the nature of the original minerals can be recognised by mineral relicts and/or preservation of original mineral morphologies and/or relict textural features.
3. Completely altered minerals may be encountered and the nature of the original minerals cannot be determined but the processes responsible for the alteration can be identified as having been deuteric.
4. Completely altered minerals may be encountered and the nature of the original minerals cannot

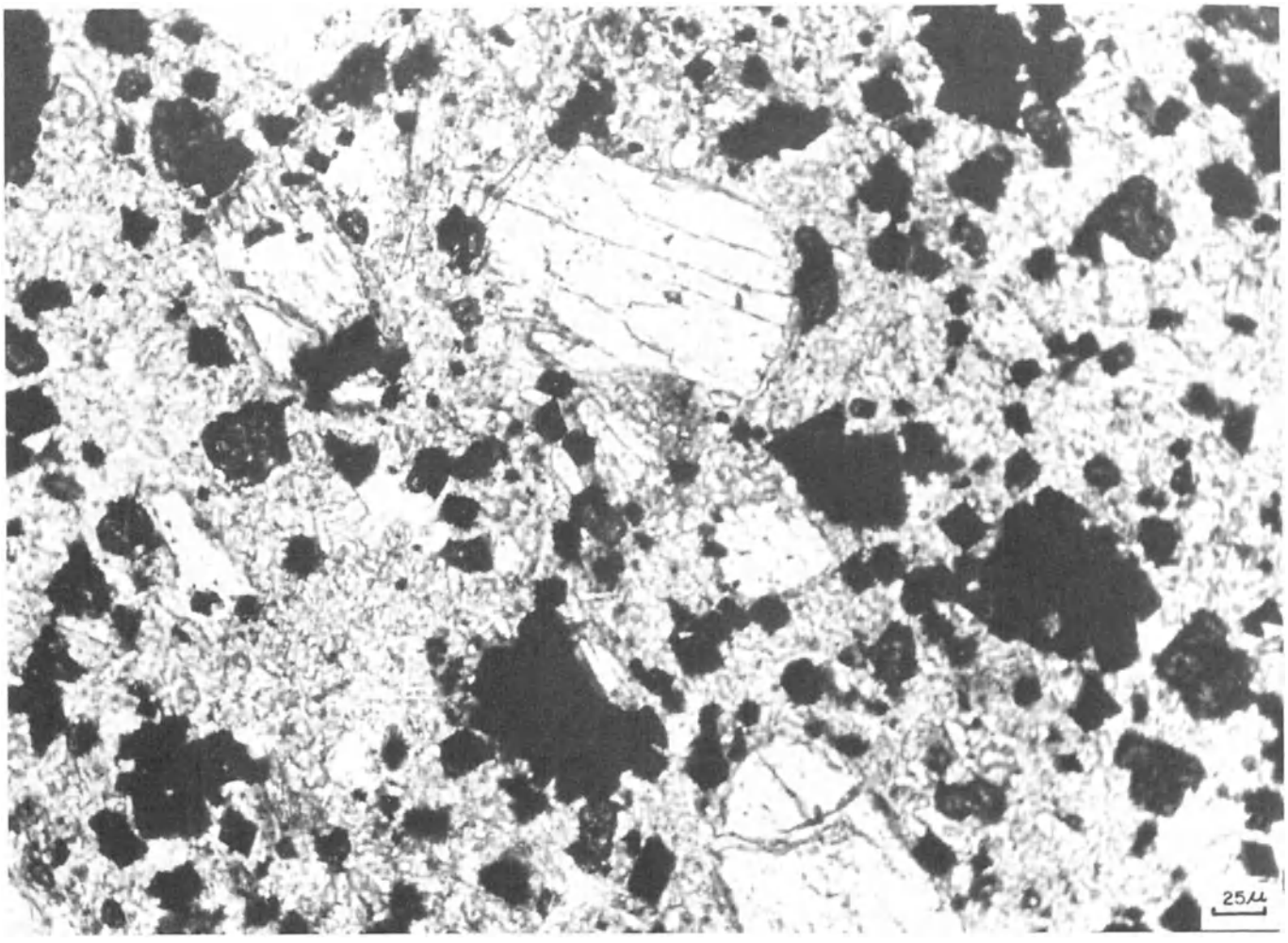

Fig. 5. An 'opaque-mineral-rich' calcite kimberlite, from a dyke within the Wesselton pipe. Microphenocrysts of fresh olivine, opaque minerals, perovskite and apatite are set in a groundmass of calcite.

be determined but the alteration can be identified as having been due to metasomatic and/or weathering processes.

5. Completely altered minerals may be encountered but neither the nature of the original minerals nor the processes responsible for the alteration can be identified.

In determining modal proportions no problems are experienced with respect to points 1, 2 and 3. In the case of points 4 and 5 classification is hindered or may not be possible because original modal proportions cannot be determined. We suggest that highly weathered kimberlites that cannot be classified be named according to the dominant alteration process as indicated by the alteration products present (e.g. carbonatized kimberlite).

Application of the Proposed Classification

We have found that, for most of the kimberlites that we have examined, limited point-counting (eg. 500 points over a single thin section measuring 600 mm^2) is adequate to establish modal proportions with sufficient accuracy for meaningful classification. In other cases, where the petrography of the kimberlites varies significantly over short distances, we have found it necessary to point-count several thin sections from different specimens. For example, additional point-counting was needed to account for petrographic variations created by the effects of flowage differentiation in the case of the Swartruggens kimberlite dyke (analysis 3, Table I and Fig. 2).

Eighteen modal analyses of kimberlite from twelve southern African occurrences are presented in Table I. Included in this table are modal proportions recalculated on an olivine-free basis. These highlight the relative abundances of the other primary minerals. The modal analyses have been selected to demonstrate the practical application of the classification and to illustrate the large variation in content of major primary minerals.

Analyses 4 and 5, from coarse and fine-grained zones within the same kimberlite, are included as

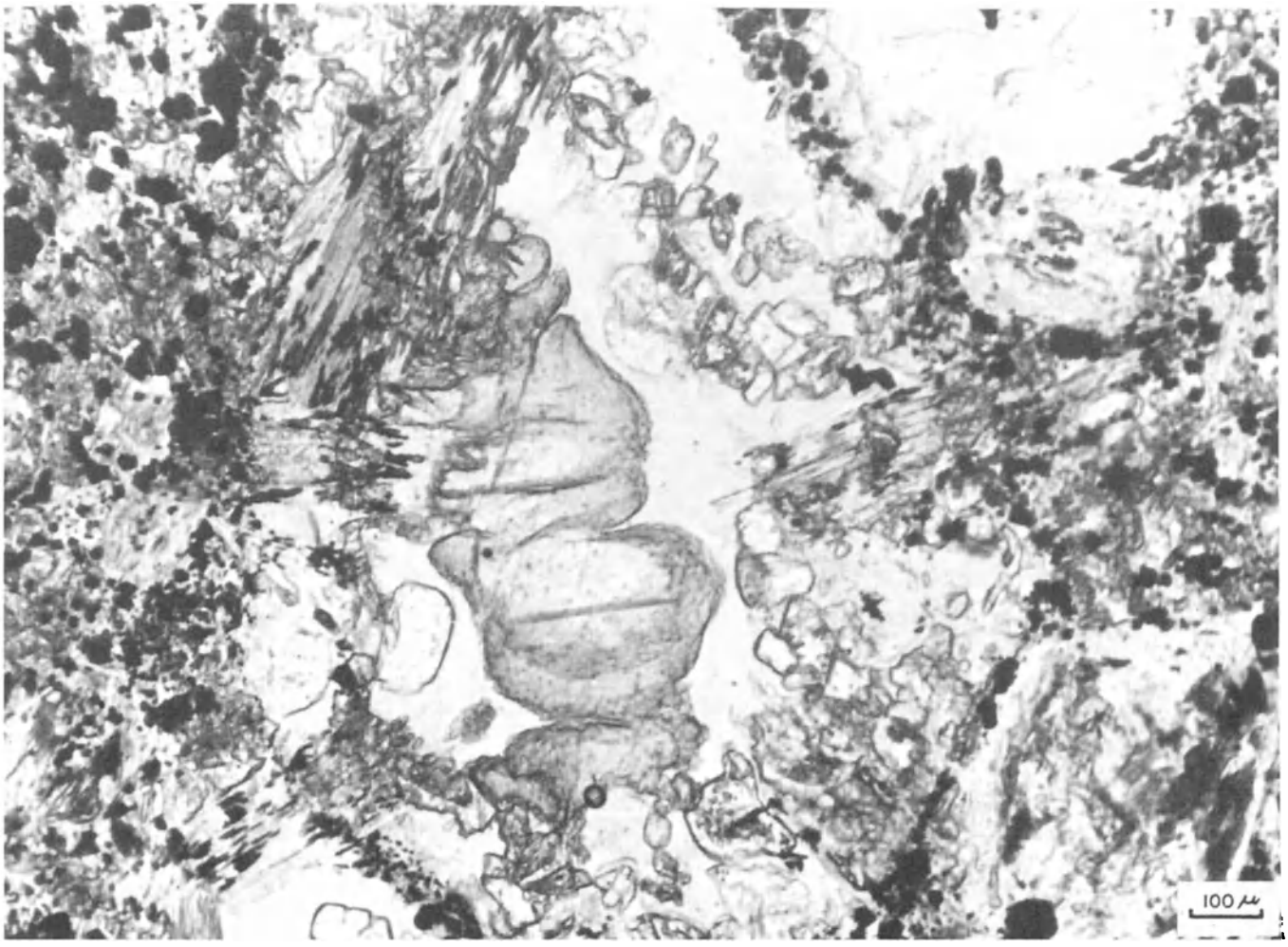

Fig. 6. A serpentine-phlogopite-calcite kimberlite, from the Wesselton pipe. Groundmass serpentine (centre) encloses rafts of calcite (some with corroded margins) and is bordered by phlogopite laths, altered olivine grains and microphenocrysts of opaque minerals and perovskite.

an example illustrating that the abundance of olivine has little effect on the relative proportions of the minerals used for classification. Analysis 9 is included to illustrate the problem resulting from the presence of abundant opaque minerals (Figure 5). Comparison of analyses 2 and 18 (Figures 9 and 10) which represent neighbouring kimberlite intrusions in the same pipe and which differ markedly in mineral content, stresses the need for a detailed mineralogical classification of kimberlite.

Twelve photomicrographs of some of the kimberlites represented in Table I are presented to graphically illustrate variations in petrographic features including variations in mineral content.

Conclusion

The proposed classification is based on quantitative modal analysis. It therefore provides a practical basis for subdividing kimberlite in terms of mineral content. Although this classification is based on the examination of southern African kimberlites, published mineralogical descriptions of kimberlites from elsewhere, indicate that it may have wider application.

The use of this scheme for classifying many different kimberlites of variable mode of occurrence and texture has met with few problems. The most serious of these are those resulting from extensive alteration. In this respect we feel that progress has been made in interpreting the nature of the alteration processes affecting kimberlite. We admit, however, that this interpretation may, in some cases, be subjective.

We hope that this classification will provide a broader base for comparing kimberlites of divergent and like mineralogy and for comparing kimberlites with other rock types.

TABLE 1. Modal analyses of selected southern African kimberlites

Source	1		2		3		4		5		6		7		8		9		10		11		12		13		14		15		16		17		18	
	A	B	A	B	A	B	A	B	A	B	A	B	A	B	A	B	A	B	A	B	A	B	A	B	A	B	A	B	A	B	A	B	A	B	A	B
Phlogopite	44	67	43	73	67	85	61	73	46	69	28	38	<1	1	13	23	9	15	13	24	-	-	<1	1	1	2	22	34	24	37	20	34	16	29	1	2
Calcite	8	12	tr	tr	6	5	13	16	11	16	<1	1	29	50	14	25	19	32	12	22	14	32	25	34	5	10	tr	tr	1	2	4	7	-	-	tr	tr
Serpentine	4	6	7	12	3	4	3	>3	4	6	25	35	11	19	12	22	6	10	14	27	21	47	28	39	14	28	16	25	9	14	5	9	7	14	6	13
Diopside	-	-	-	-	2	3	1	1	1	1	18	25	-	-	-	-	-	-	-	-	-	-	-	-	27	54	26	40	20	31	-	-	-	-	-	-
Monticellite	-	-	-	-	-	-	-	-	-	-	-	-	-	-	6	11	-	-	-	-	-	-	-	-	-	-	-	-	-	-	18	31	22	41	26	58
Apatite	1	1	7	12	-	-	3	>3	3	>4	tr	tr	5	9	1	2	-	-	4	7	3	7	6	8	-	-	tr	tr	-	-	tr	tr	1	2	tr	tr
Opaque Minerals	6	9	1	2	1	1	2	3	2	3	<1	1	11	19	7	13	20	33	8	15	6	14	10	14	1	2	1	1	5	8	5	9	4	8	8	17
Perovskite	3	5	<1	1	-	-	-	-	-	-	-	-	1	2	2	4	6	10	<3	5	tr	tr	3	4	2	4	-	-	5	8	5	9	3	6	4	9
Olivine	34		41		21		17		33		28		42		45		40		47		56		27		50		34		36		42		46		55	

Column A Volume percentages recalculated to exclude all cryptogenic constituents except olivine.
Column B Volume percentages of A recalculated to exclude all olivine.

Analysis 1	Sydney-on-Vaal -dyke	Phlogopite kimberlite
" 2	De Beers - pipe	Phlogopite kimberlite
" 3	Swartruggens -Main dyke	Phlogopite kimberlite
" 4	Star -Byrnes dyke (fine zone)	Phlogopite kimberlite
" 5	Star -Byrnes dyke (coarse zone)	Phlogopite kimberlite
" 6	Finsch -pipe	Serpentine-phlogopite kimberlite
" 7	De Beers -dyke	Calcite kimberlite
" 8	Wesselton -pipe	Serpentine-phlogopite-calcite kimberlite
" 9	Wesselton -dyke	Opaque mineral-rich calcite kimberlite
" 10	Frank Smith -pipe	Calcite-phlogopite-serpentine kimberlite
" 11	Dutoitspan -dyke	Calcite-serpentine kimberlite
" 12	Wesselton -dyke	Calcite-serpentine kimberlite
" 13	Letlhakane DK1 -pipe	Diopside kimberlite
" 14	Bellsbank -Intermediate dyke	Phlogopite-diopside kimberlite
" 15	Letseng Satellite -dyke	Diopside-phlogopite kimberlite
" 16	Matsoku -pipe	Monticellite-phlogopite kimberlite
" 17	Wesselton -pipe	Phlogopite-monticellite kimberlite
" 18	De Beers -pipe	Monticellite kimberlite

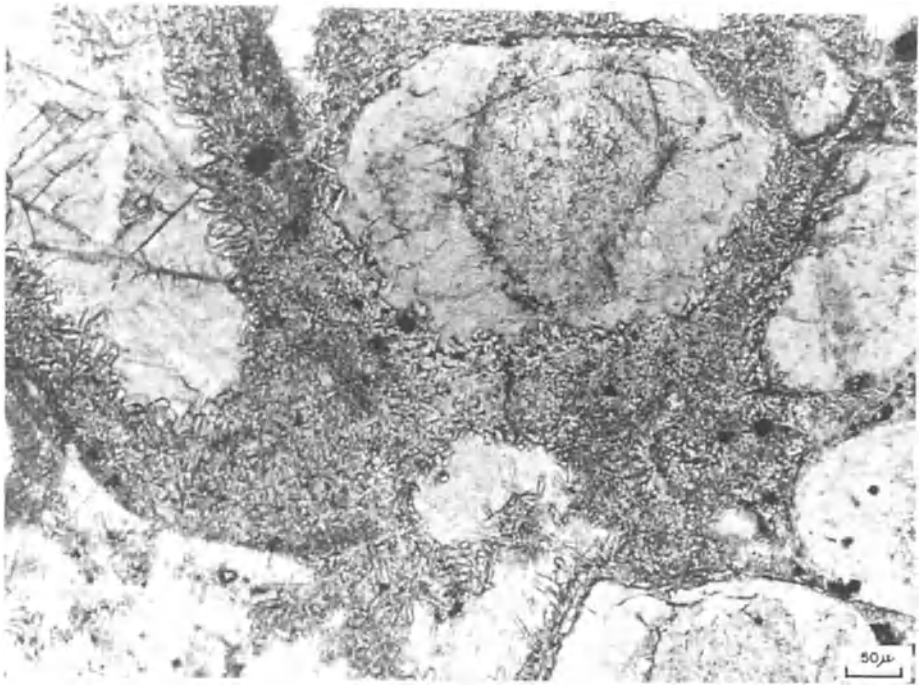

Fig. 7. A diopside kimberlite from the Letlhakane DK1 pipe. Fine crystals of diopside are set in a base of serpentine (bottom). They surround altered olivine phenocrysts (eg. top middle) and also enclose calcite in orbicular, geode-like, structures (top, left).

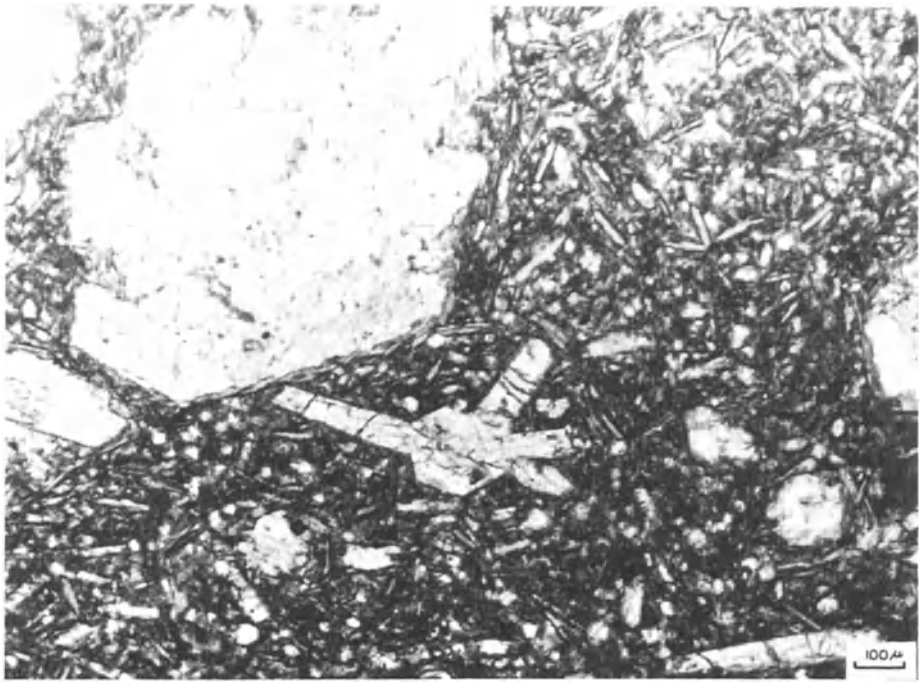

Fig. 8. A phlogopite-diopside kimberlite, from an Intermediate dyke of the Bellsbank group. Phenocrysts of altered olivine (top left) and diopside (small aggregate, centre) are set in a groundmass of finer-grained diopside, phlogopite and serpentine.

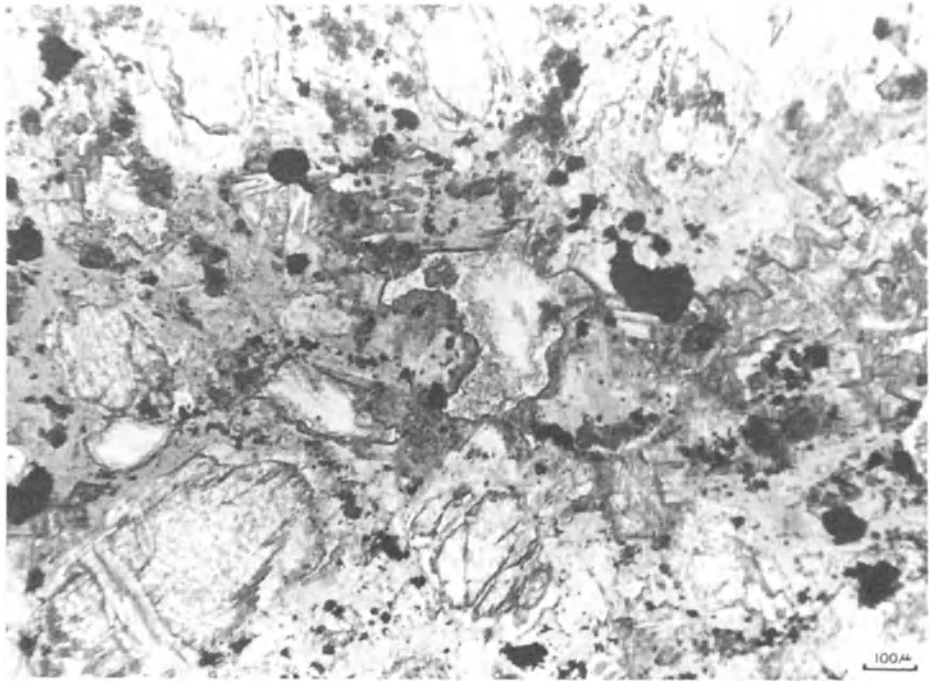

Fig. 9. A phlogopite kimberlite, from the 'Core kimberlite' in the south-eastern part of the De Beers pipe. Partially altered and marginally corroded phenocrysts of olivine are set in a groundmass of phlogopite, lesser serpentine (centre) and apatite (acicular crystals, top-left of centre).

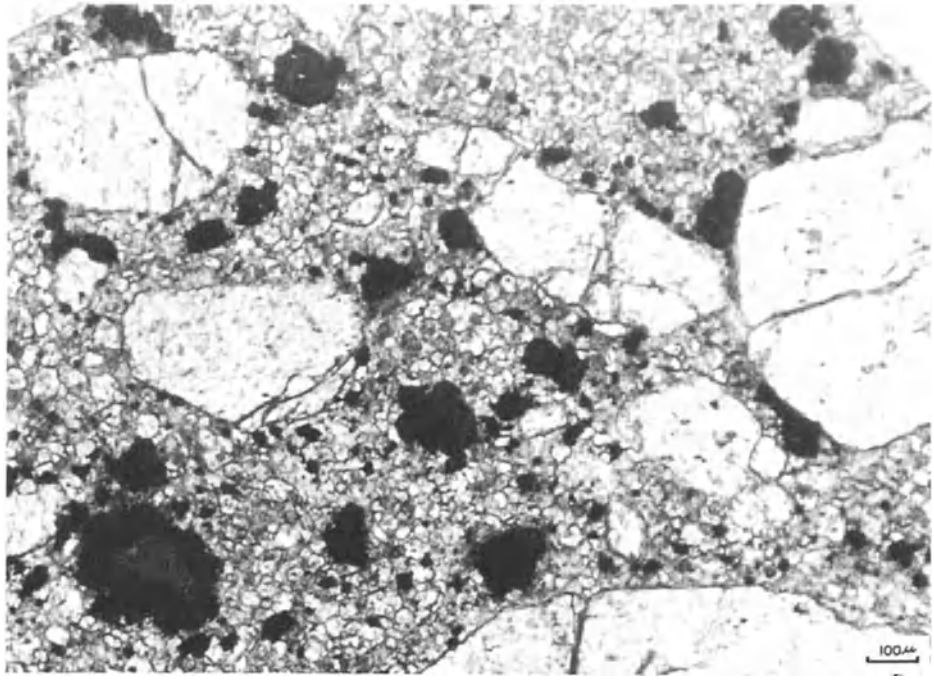

Fig. 10. A monticellite kimberlite from the 'Peripheral kimberlite' in the south-eastern part of the De Beers pipe. Comparatively fresh olivine crystals and microphenocrysts of opaque minerals and perovskite are set in a granular groundmass of monticellite. Individual monticellite grains generally measure less than 40μ.

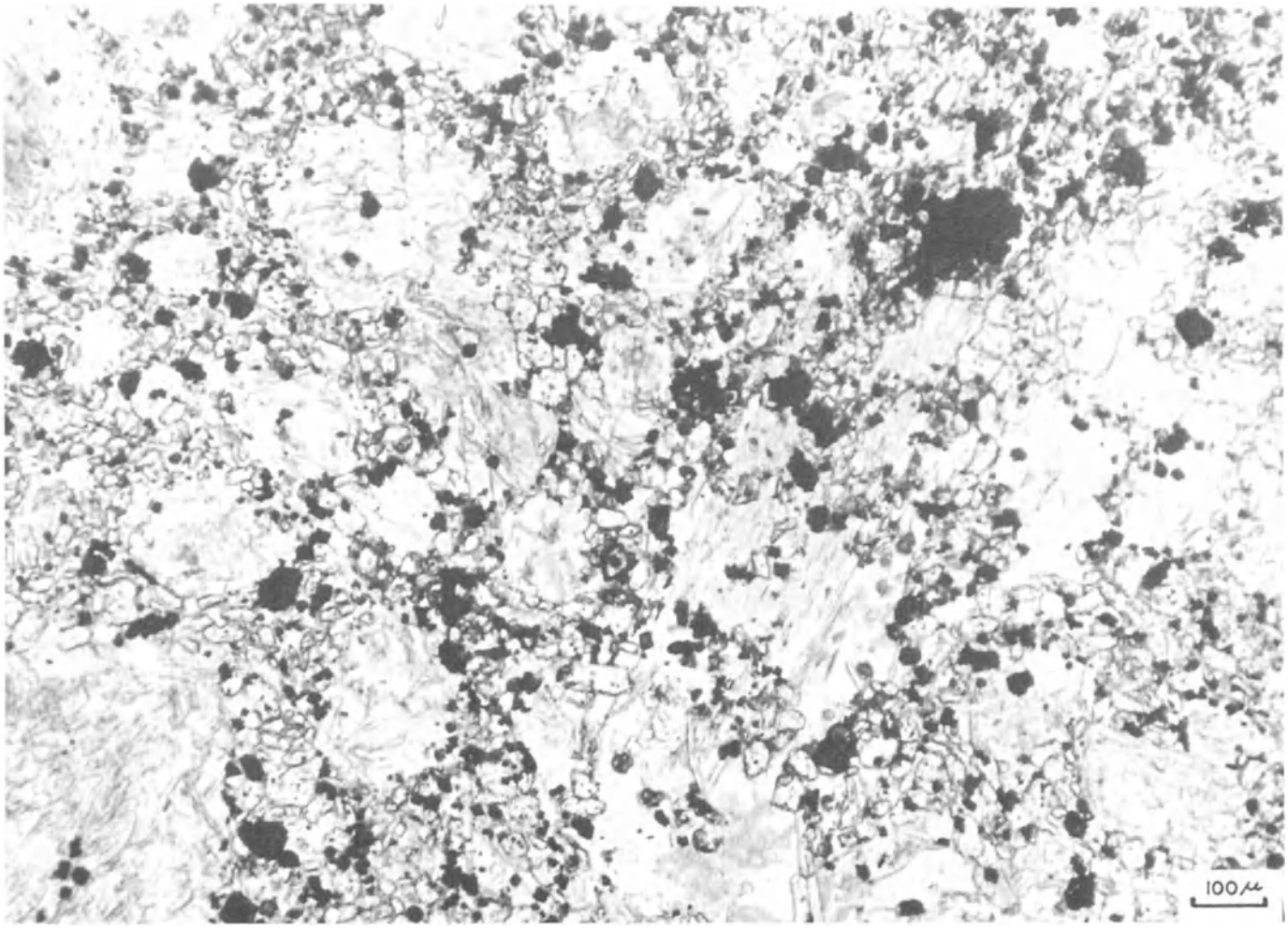

Fig. 11. A phlogopite-monticellite kimberlite, from the Wesselton pipe. Altered (mainly serpentinized and phlogopitized) olivine phenocrysts are surrounded by small crystals of monticellite, opaque-minerals, perovskite and mica all of which are set within either larger sized mica plates (eg. centre) or irregular patches of serpentine.

Acknowledgements. The writers are indebted to the Anglo American Corporation of South Africa and to De Beers Consolidated Mines Limited for permission to publish this paper. The staff of the Geological Department, De Beers Consolidated Mines Limited, especially Mrs. B. Booysen, are thanked for their help in the preparation of the manuscript.

References

Boyd, F.R. and C.R. Clement, Compositional zoning of olivines in kimberlite from the De Beers Mine, Kimberley, South Africa, Carnegie Inst., Washington, Year Book 76, 485-493, 1977.

Clement, C.R., The emplacement of some diatreme facies kimberlites, Phys. Chem. Earth, 9, 51-59, 1975.

Clement, C.R., E.M.W. Skinner, and B.H. Scott, Kimberlite redefined, Extended Abstracts, 2nd International Kimberlite Conf., Santa Fe, New Mexico, 1977.

Emeleus, C.H., and J.R. Andrews, Mineralogy and petrology of kimberlite dyke and sheet intrusions and included peridotite xenoliths from South-west Greenland, Phys. Chem. Earth, 9, 179-197, 1975.

Mitchell, R.H., Kimberlite and related rocks - a critical reappraisal, J. Geol. 78, 686-704, 1970.

Frantsesson, E.V., The petrology of the kimberlites, translated by D.A. Brown, 195 p., Aust. Nat. Univ. Canberra, 1970.

Lewis, H.C., Papers and notes on the genesis and matrix of the diamond, edited by T.G. Bonney, London, 1897.

Wagner, P.A., The diamond fields of southern Africa, 355 p., The Transvaal Leader, Johannesburg, 2nd impression C. Struik.

PETROGENESIS OF KIMBERLITIC ROCKS AND ASSOCIATED XENOLITHS OF SOUTHEASTERN AUSTRALIA

John Ferguson and J. W. Sheraton

Bureau of Mineral Resources, P.O. Box 378, Canberra City, A.C.T. 2601 Australia

Abstract. Fourteen widely-separated occurrences of kimberlitic rocks have recently been discovered in southeastern Australia. Those that have been dated have given ages ranging from Permian to Cainozoic. One occurrence exhibits an intimate spatial association with carbonatite. Lherzolite nodules, with garnet and/or spinel, have been found in two areas; eclogite nodules are more widespread. Most of the clinopyroxenes and garnets in the kimberlites are chemically similar to those from the lherzolite or eclogite nodules. Garnet and clinopyroxene from one eclogite (grinquaite) nodule are of identical composition to those from garnet lherzolite from the same area, suggesting derivation from a common mantle source region. Other eclogites are considerably more iron-rich, and apparently originated at higher levels in the upper mantle or lower crust. Ilmenites from three occurrences plot within the field of those found in olivine melilitite with low Mg and high Fe contents. A fourth occurrence contains ilmenite that is enriched in Mg and Ti, suggesting derivation from garnet peridotite.

Kimberlitic rocks from southeastern Australia which have been analyzed may be divided into two chemically distinct groups which define divergent trends within the CMAS tetrahedron. Those from Walloway, South Australia, fall on the more evolved part of the "normal" kimberlite trend shown by kimberlites and related alkaline ultramafic rocks of southern Africa. Rocks of this type are considered to have been formed by less than one percent of melting of garnet lherzolite at depths in excess of 125 km, followed by olivine and orthopyroxene dominated fractionation; garnet and clinopyroxene do not appear to have been significant fractionating phases. The Cainozoic kimberlitic rocks from Jugiong, New South Wales, are relatively enriched in Al_2O_3 and Na_2O, and depleted in MgO, and have close chemical affinities with olivine nephelinites. Consideration of phase relations in the CMAS tetrahedron indicates equilibration pressures of about 20 kb, and the chemical variations may be explained in terms of only minor olivine and possibly orthopyroxene fractionation. Temperature estimates based on compositions of coexisting minerals in lherzolite and eclogite nodules, and the occurrence of a unique garnet-spinel lherzolite inclusion falling on the quasi-univariant boundary between the garnet and spinel lherzolite fields, show that the nodules equilibrated at about 1240°C and 22 kb. This is in good agreement with the data obtained for the host rocks, and suggests that the olivine nephelinite magmas were derived by partial melting of garnet lherzolite at depths of about 70 km. The abnormally high geothermal gradient implied by these data is higher than the calculated mean oceanic geotherm, and intersects the graphite-diamond stability curve at considerably higher temperatures and pressures than those indicated by the nodules, so that it is most unlikely that diamondiferous kimberlites of Cainozoic age occur in this part of New South Wales.

Introduction

Fourteen widely-separated areas of kimberlitic rocks, which include olivine nephelinite and carbonatite, have recently been discovered in southeastern Australia in the states of South Australia, Tasmania, Victoria, and New South Wales. Localities are shown in Figure 1, and details of the occurrences and structural relations are given by Strake, et al. (this vol.). Reference has previously been made to these occurrences (Lovering and White, 1969; Colchester, 1972; Tucker and Collerson, 1972; Ferguson, et al., 1977).

Analyses were carried out on concentrates comprising one or more of the minerals, clinopyroxene, garnet, and ilmenite, separated from kimberlitic rocks from seven of the areas. Lherzolite nodules were obtained from three kimberlitic intrusions in two areas, and eclogite nodules from four areas. Temperature-pressure estimates were calculated for these inclusions and a palaeogeotherm constructed, and petrogenetic models tested using chemical mineralogical data.

In this paper we have used the term "kimber-

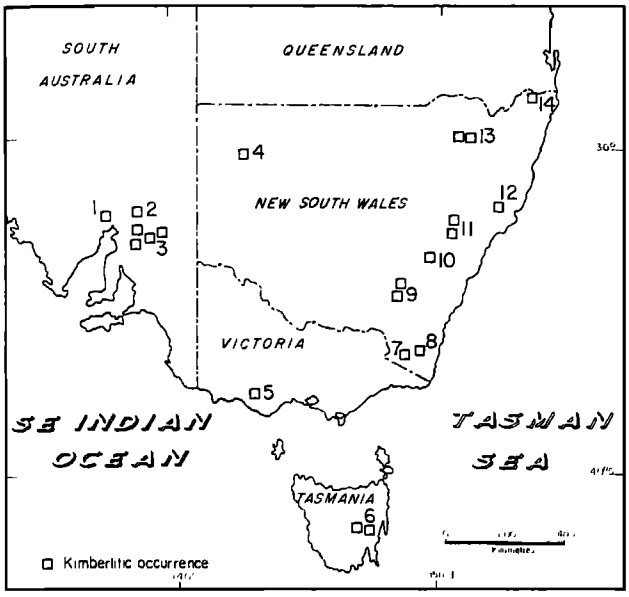

Fig. 1. Localities of kimberlitic occurrences in southeastern Australia. Areas: 1 = Port Augusta, 2 = Walloway, 3 = Terowie, 4 = White Cliffs, 5 = Bullenmerri, 6 = Oatlands, 7 = Delegate, 8 = Bombala, 9 = Jugiong, 10 = Abercrombie, 11 = Nullo Mountain, 12 = Gloucester, 13 = Bingara, 14 = Mount Brown.

litic" to describe these rocks as there are significant petrographic and chemical differences compared with kimberlites from other areas. Mineral compositions are typical of those found in kimberlites from other localities, although bulk compositions of rocks from two areas (White Cliffs and Jugiong) are more comparable with olivine nephelinites and related alkaline ultramafic rocks. Intrusives from Walloway have bulk compositions similar to kimberlites.

Petrography of Kimberlitic Rocks

Owing to the weathered nature of much of the material, petrographic investigations were restricted to moderately fresh samples from four areas (2, 3, 4, and 9, Fig. 1).

Walloway, Terowie and White Cliffs (Areas 2, 3 and 4)

Narrow kimberlitic dykes which occur in these areas are of the micaceous variety. Phenocrysts comprise phlogopite, up to 2 mm long, and euhedral pseudomorphed olivine, up to 1 mm long. The olivine is replaced by carbonate, serpentine and chlorite. The groundmass (<0.1 mm) consists of phlogopite, magnesite, opaque minerals, and in some cases, brown spinel and perovskite.

At Walloway (area 2) carbonated kimberlitic intrusives are associated with carbonatite. Phlogopite phenocrysts are common, and olivine is replaced by serpentine and carbonate. $\delta^{13}C$ values of carbonates from kimberlitic rocks from both the Walloway and Jugiong areas are compatible with the primary carbonates being magmatic (T. H. Donnelly, pers. comm., 1977).

Jugiong (Area 9)

Two types of kimberlitic intrusives are found in this area. The dominant type is a massive, dark, fine-grained, porphyritic rock, but two of the seven intrusions are brecciated (equivalent to the diatreme-facies kimberlite of Dawson, 1971). Both types are extensively altered, but most of the freshest material came from this area.

Massive kimberlitic rocks. These rocks occur as neck fillings (up to 40 m wide), and as narrow dykes up to 30 cm thick. Euhedral olivine, or its pseudomorphs, forms phenocrysts up to 1 mm across; angular xenocrysts, up to 5 mm in diameter, comprise olivine, orthopyroxene, clinopyroxene, garnet and spinel (i.e. lherzolite assemblage). The very fine-grained groundmass contains aegirine, aegirine-augite, augite, richterite, orthoclase, magnesite and minor amounts of albite, analcite, chlorite, perovskite and magnetite. Some of these phases are probably secondary, and serpentine, brown mica and magnesite are abundant replacement minerals. A feature of the rocks is the presence of spherical or irregular ocelli, up to 5 mm across. They are slightly coarser grained than the groundmass, and more felsic, olivine being absent. There is a correlation between the compositions of the olivine phenocrysts, which range from Fo_{91} to Fo_{86} in different intrusions, and mineralogical variations in the groundmass and ocelli. In rocks with more magnesian olivine phenocrysts, the ocelli consist of magnesite, analcite and only minor augite. With decreasing Fo values, clinopyroxene becomes more abundant and more sodic (aegirine), richterite appears, and orthoclase becomes the predominant felsic mineral. In the most evolved rocks a brown mica is present, and richterite forms mantles to xenocrystic pyroxene and olivine.

Xenocrystic olivine is usually Fo_{91}, but a few grains are Fo_{84}, and there is also a group between Fo_{86} and Fo_{88}. Orthopyroxene is consistently En_{91}, and spinel xenocrysts have molecular Al/Cr ratios of about 3. Rare composite fragments are also present - e.g., an orthopyroxene host with olivine inclusions. Many of these xenocrysts have compositions identical to those of minerals in the lherzolite nodules.

Although having many features characteristic of kimberlites, these rocks appear to have petrographic affinities with olivine analcitites and monchiquites. However, the degree of

Table 1. Compositions of co-existing minerals in typical lherzolite and eclogite nodules from Jugiong (area 9; lherzolites from intrusion 3, eclogite from intrusion 4) and White Cliffs (area 4, intrusion 2). Averages of type I and type II eclogite clinopyroxenes and garnet are from Edwards, et al. (in prep.).

	Spinel lherzolite				Garnet-spinel lherzolite				
Sample No.	75210418				75210052/39				
	Ol	Opx	Cpx	Sp	O_1	Opx	Cpx	Gt	Sp
SiO_2	40.32	54.62	52.15	n.d.	40.93	55.41	52.64	42.36	n.d.
TiO_2	n.d.	0.17	0.56	0.45	n.d.	n.d.	n.d.	n.d.	n.d.
Al_2O_3	n.d.	4.14	5.90	48.98	n.d.	4.53	5.55	22.50	47.30
FeO*	9.60	6.11	3.15	12.15	8.81	5.17	2.61	6.30	11.24
MnO	0.19	0.23	0.21	n.d.	n.d.	n.d.	n.d.	0.27	0.33
MgO	49.88	33.38	15.84	20.28	50.25	33.47	16.72	21.09	19.47
CaO	n.d.	0.78	18.91	0.07	n.d.	0.88	19.94	5.39	n.d.
Na_2O	n.d.	n.d.	1.74	n.d.	n.d.	n.d.	1.26	n.d.	n.d.
Cr_2O_3	n.d.	0.59	1.53	18.06	n.d.	0.53	1.28	2.10	21.66
O=	4	6	6	4	4	6	6	12	4
Si	0.985	1.884	1.883	-	0.997	1.904	1.895	2.992	-
Al^{iv}	-	0.116	0.117	1.535	-	0.096	0.105	0.008	1.500
Al^{vi}	-	0.052	0.134	-	-	0.088	0.131	1.866	-
Ti	-	0.004	0.015	0.009	-	-	-	-	-
Cr	-	0.016	0.044	0.380	-	0.014	0.036	0.117	0.460
Fe^{3+}	0.031	0.039	0.031	0.067	0.006	-	0.026	0.024	0.040
Fe^{2+}	0.165	0.137	0.064	0.203	0.173	0.149	0.053	0.348	0.212
Mn	0.004	0.007	0.006	-	-	-	-	0.016	0.007
Mg	1.815	1.716	0.852	0.804	1.824	1.714	0.897	2.220	0.780
Ca	-	0.029	0.732	0.002	-	0.032	0.769	0.408	-
Na	-	-	0.122	-	-	-	0.088	-	-
$Mg/(Mg+Fe^{2+}+Fe^{3+})$	0.903	0.907	0.900	0.748	0.911	0.920	0.919	0.856	0.756

* Total Fe as FeO Ol = Olivine Cpx = Clinopyroxene Sp = Spinel
n.d. Not detected Opx = Orthopyroxene Gt = Garnet

alteration makes more precise classification difficult.

Brecciated kimberlitic rocks. Brecciated (diatreme-facies) kimberlitic rocks are found in two intrusions which have a minimum depth of 200 m. These rocks contain nucleated autoliths (Ferguson, et al., 1973), and angular to rounded fragments similar to the lapilli found in kimberlites from the Kao pipe, Lesotho (Clement, 1973). Lapilli and nucleated autoliths can make up as much as 40 percent, by volume, of the rock, lapilli being the more abundant. The lapilli are characterised by a range of grainsize produced by a mixture of phenocrysts and xenocrysts, whereas the autoliths, typically 1-12 cm across, are more even-grained. The nuclei of the autoliths comprise mantle or crustal rock or mineral fragments, and rarely, kimberlitic lapilli.

Both crustal and mantle xenoliths are common. The former are mostly granite, with minor basalt and granulite fragments and kaersutite crystals. Mantle rock inclusions include griquaites (Nixon, 1973), as well as garnet, spinel, and garnet-spinel lherzolites.

Petrography of Nodules

Nodules in the kimberlitic rocks are of three main types - lherzolites, eclogites and crustal rocks (granite, basalt and mafic granulite).

All the lherzolite nodules studied, apart from a single example from Gloucester (area 12), come from the Jugiong (area 9). Garnet, spinel and garnet-spinel lherzolites are all found in the Jugiong area, and mainly form small nodules 1 or 2 cm across with an average grainsize of about 1 mm. The main constituents are olivine Fo_{90-92} (40-60%), enstatite En_{90-92} (20-40%), and pale green chrome diopside (10-25%), with small amounts of pyrope-rich garnet (0-10%) and greenish brown or reddish brown aluminous, or rarely chrome-rich spinel (0-5%) (Table 1). Many of the xenocrysts in the kimberlitic rocks are of identical composition, and are probably fragments of lherzolite. Scapolite and phlogopite were found in a few nodules. Olivine is commonly slightly serpentinised, pyroxenes have finely granulated margins, and in most rocks garnet shows extensive replacement by orange-

Table 1. Cont.

Garnet lherzolite				Eclogites						
75210424				75210414		Type I		Type II		
Ol	Opx	Cpx	Gt	Cpx	Gt	Cpx	Gt	Cpx	Gt	Sample No.
40.04	54.47	51.56	41.39	52.44	41.83	52.38	39.73	52.60	40.85	SiO_2
n.d.	0.16	0.67	0.22	0.31	0.10	0.62	0.11	0.54	0.07	TiO_2
n.d.	4.43	6.59	22.93	6.41	24.38	9.04	21.62	11.49	22.60	Al_2O_3
10.26	6.55	3.42	7.89	2.88	6.61	7.52	20.31	2.99	13.20	FeO*
0.24	0.22	0.18	0.47	0.15	0.41	0.06	0.49	0.03	0.32	MnO
49.41	32.82	15.66	20.62	16.05	21.45	9.65	8.44	10.75	14.36	MgO
n.d.	0.77	18.86	4.87	19.46	4.55	17.04	9.21	18.02	8.50	CaO
n.d.	n.d.	1.75	n.d.	1.80	0.33	3.62	0.05	3.53	0.05	Na_2O
0.05	0.58	1.33	1.62	0.53	0.35	0.06	0.04	0.05	0.05	Cr_2O_3
4	6	6	12	6	12	6	12	6	12	O=
0.981	1.885	1.861	2.935	1.882	2.928	1.913	3.019	1.882	2.984	Si
-	0.115	0.139	0.065	0.118	0.072	0.087	-	0.118	0.016	Al^{iv}
-	0.066	0.141	1.852	0.153	1.940	0.302	1.937	0.367	1.931	Al^{vi}
-	0.004	0.018	0.012	0.008	0.005	0.017	0.006	0.015	0.004	Ti
0.001	0.016	0.038	0.091	0.015	0.019	0.002	0.002	0.001	0.003	Cr
0.038	0.028	0.046	0.099	0.058	0.146	0.006	0.017	-	0.081	Fe^{3+}
0.172	0.161	0.057	0.369	0.029	0.240	0.223	1.273	0.089	0.725	Fe^{2+}
0.005	0.006	0.006	0.028	0.005	0.024	0.002	0.032	0.001	0.020	Mn
1.803	1.692	0.842	2.179	0.859	2.238	0.525	0.956	0.573	1.564	Mg
-	0.029	0.729	0.370	0.748	0.341	0.667	0.750	0.691	0.665	Ca
-	-	0.122	-	0.125	0.045	0.256	0.007	0.245	0.007	Na
0.896	0.900	0.891	0.822	0.908	0.853	0.696	0.426	0.886	0.660	Mg/(Mg+Fe^{2+}+Fe^{3+})

* Total Fe as FeO
n.d. Not detected
Ol = Olivine
Opx = Orthopyroxene
Cpx = Clinopyroxene
Gt = Garnet
Sp = Spinel

brown kelyphitic material and pale greenish-brown spinel. Clinopyroxene in the Gloucester lherzolite is partly replaced by pale brownish amphibole. In only one garnet-spinel lherzolite (75210052/39) is there an equilibrium assemblage (Ferguson, et al., 1977).

Eclogite nodules are more widespread than lherzolites, and were found in kimberlitic rocks from Port Augusta, White Cliffs, Jugiong and Gloucester (areas 1, 4, 9 and 12, respectively). They have also been described from Delegate (area 7, Lovering and White, 1969). Those from White Cliffs have been described by Edwards, et al. (in prep.). Pale green clinopyroxene (40-70%) and pale pink garnet (30-50%) are the main constituents, although there are appreciable amounts of plagioclase, quartz and scapolite (sulphur-rich mizzonite in an eclogite from Gloucester: 75210096) in some nodules. Orthopyroxene is present in one of the eclogites from Jugiong, kyanite occurs in some of the White Cliffs eclogites, and several nodules from Port Augusta contain up to 10 percent of brownish amphibole. Minor constituents are apatite, rutile, sphene and opaque minerals. Garnet commonly shows extensive alteration to kelyphite, predominantly magnesian gedrite. Other secondary minerals include pale green aluminous spinel, analcite, brownish mica, carbonate and chlorite.

Clinopyroxene and garnet from one of the Jugiong eclogite nodules are almost identical in composition to those from lherzolite nodules from the same pipe, and minerals from a second eclogite are only slightly more Fe-rich (see below). This suggests a source at similar depths in the mantle for both bypes of nodule. There is a slight layering in some nodules which suggests that cumulates of eclogite composition may form part of the garnet lherzolite assemblage. These mantle-derived eclogites (or griquaites: Nixon, 1973) are distinct from more Fe-rich, probably crustal eclogites from the other localities. Fragments of undoubted crustal material (orthopyroxene-clinopyroxene-plagioclase and garnet-orthopyroxene-clinopyroxene-plagioclase granulites, granite and basalt) occur in kimberlites from the Port Augusta and Jugiong areas.

Mineral Chemistry

Heavy mineral concentrates of unaltered minerals from residual weathered kimberlitic rocks were obtained from eight areas. Analyses of these concentrates, which comprised one or

Table 2. Compositions of garnets from mineral concentrates, and lherzolite and eclogite nodules.

	Concentrates														
	Cluster 3			Cluster 5			Cluster 9								
Area No.	3	5	9	3		9	3		4	8	9				12
Intrusion No.	6	1	7	1	5	6	1	5	2	1	2	5	6	7	1
Sample No.*	5	15	2	1	2	1	7	2	2	2	3	3	3	6	8
SiO_2	39.80	41.12	40.70	39.52	38.11	37.23	41.49	41.69	41.74	42.43	42.12	41.86	41.63	41.79	41.49
TiO_2	n.d.	0.12	0.06	n.d.	n.d.	0.11	0.39	0.06	n.d.	0.08	0.10	n.d.	n.d.	0.08	0.05
Al_2O_3	22.45	23.17	23.20	22.81	22.03	22.11	21.68	22.07	22.65	24.09	23.08	23.82	23.10	22.62	23.73
FeO**	20.22	13.54	13.63	23.86	29.55	30.61	9.25	7.56	7.82	6.71	7.24	9.16	8.67	6.97	7.64
MnO	0.36	0.29	0.31	0.14	0.69	0.96	0.26	0.23	0.33	0.15	0.20	0.08	0.18	0.17	0.27
MgO	10.38	16.27	16.20	13.13	8.23	7.22	19.62	20.59	20.67	21.38	21.14	18.70	19.76	20.97	20.29
CaO	6.76	5.37	5.54	0.56	1.22	1.36	5.06	5.02	5.06	5.07	4.76	6.38	5.18	5.27	4.74
Na_2O	n.d.	0.03	0.13	n.d.	0.17	0.41	0.06	0.1	n.d.	n.d.	0.12	n.d.	0.21	0.12	0.69
Cr_2O_3	0.03	0.09	0.21	n.d.	n.d.	n.d.	2.18	2.67	1.72	0.1	1.25	n.d.	1.28	2.00	1.09
							0 = 12								
Si	2.993	2.984	2.953	2.964	2.949	2.895	2.969	2.961	2.959	2.977	2.970	2.980	2.955	2.953	2.921
Al^{iv}	0.007	0.016	0.047	0.036	0.051	0.105	0.031	0.039	0.041	0.023	0.030	0.020	0.045	0.047	0.079
Al^{vi}	1.984	1.966	1.938	1.981	1.959	1.922	1.798	1.809	1.852	1.970	1.889	1.979	1.888	1.838	1.890
Ti	-	0.007	0.003	-	-	0.006	0.021	0.003	-	0.004	0.005	-	-	0.004	0.003
Cr	0.002	0.005	0.012	-	-	-	0.123	0.150	0.096	0.006	0.070	-	0.072	0.112	0.061
Fe^{3+}	0.032	0.036	0.109	0.054	0.125	0.238	0.076	0.088	0.093	0.038	0.078	0.041	0.113	0.105	0.217
Fe^{2+}	1.240	0.785	0.718	1.443	1.787	1.753	0.478	0.361	0.371	0.356	0.349	0.504	0.402	0.307	0.233
Mn	0.023	0.018	0.019	0.009	0.045	0.063	0.016	0.014	0.020	0.009	0.012	0.005	0.011	0.010	0.016
Mg	1.164	1.760	1.752	1.468	0.949	0.836	2.092	2.179	2.184	2.236	2.221	1.984	2.091	2.209	2.129
Ca	0.545	0.418	0.431	0.045	0.101	0.113	0.388	0.382	0.384	0.381	0.360	0.487	0.394	0.399	0.358
Na	-	0.004	0.018	-	0.026	0.062	0.008	0.014	-	-	0.016	-	0.029	0.016	0.094
$Mg/(Mg+Fe^{2+}+Fe^{3+})$	0.478	0.682	0.679	0.495	0.332	0.296	0.791	0.829	0.825	0.850	0.839	0.784	0.802	0.843	0.826

* For the concentrates, the number of analyses included in each average is indicated. For the nodules, individual BMR sample numbers are given (all are prefixed 7521). For the White Cliffs area (4), averages of type I and type II eclogite garnets are given (from Edwards et al., in prep.).

** Total Fe as FeO.

n.d. Not detected.

Table 2. Cont.

Garnet-spinel lherzolites				Garnet lherzolites				Eclogites				
Cluster 9				Cluster 9				Cluster 9		Cluster 3		
9				9				9		12	4	
3				3			4	4		1	2	
0052/39	0115/5	0429	0433	0416	0424	0432	0060	0413	0414	0096	1	11
42.36	42.02	41.82	41.81	41.41	41.39	41.33	41.89	41.01	41.83	39.66	39.73	40.85
n.d.	n.d.	0.18	0.14	0.09	0.22	0.15	n.d.	0.16	0.10	0.11	0.11	0.07
22.50	22.83	24.01	23.62	22.95	22.93	23.13	23.08	23.96	24.38	23.42	21.62	22.60
6.30	7.42	6.29	6.14	7.01	7.89	6.94	7.12	10.98	6.61	17.21	20.31	13.20
0.27	0.28	0.41	0.44	0.49	0.47	0.27	0.17	0.43	0.41	0.51	0.49	0.32
21.09	20.73	20.85	20.62	20.76	20.62	20.62	21.32	18.28	21.45	9.27	8.44	14.36
5.39	5.03	4.45	4.82	5.08	4.87	5.27	5.02	4.39	4.55	8.77	9.21	8.50
n.d.	0.15	0.83	0.82	0.36	n.d.	0.57	n.d.	0.42	0.33	0.58	0.05	0.05
2.10	1.55	1.17	1.60	1.87	1.62	1.71	1.40	0.36	0.35	0.49	0.04	0.05
						0 = 12						
2.992	2.970	2.928	2.936	2.922	2.935	2.911	2.954	2.913	2.928	2.968	3.019	2.984
0.008	0.030	0.072	0.066	0.078	0.065	0.089	0.046	0.087	0.072	0.032	-	0.016
1.866	1.872	1.910	1.888	1.831	1.852	1.832	1.872	1.920	1.940	2.034	1.937	1.931
-	-	0.009	0.007	0.005	0.012	0.008	-	0.009	0.005	0.006	0.006	0.004
0.117	0.087	0.065	0.089	0.104	0.091	0.095	0.078	0.020	0.019	0.029	0.002	0.003
0.024	0.091	0.190	0.187	0.182	0.099	0.043	0.096	0.188	0.146	0.041	0.017	0.081
0.348	0.348	0.178	0.173	0.232	0.369	0.291	0.324	0.465	0.240	1.036	1.273	0.725
0.016	0.017	0.024	0.026	0.029	0.028	0.016	0.010	0.026	0.024	0.032	0.032	0.020
2.220	2.184	2.176	2.156	2.183	2.179	2.165	2.241	1.935	2.238	1.034	0.956	1.564
0.408	0.381	0.334	0.362	0.384	0.370	0.398	0.379	0.380	0.341	0.703	0.750	0.665
-	0.021	0.113	0.112	0.049	-	0.078	-	0.058	0.045	0.084	0.007	0.007
0.856	0.833	0.855	0.857	0.841	0.822	0.866	0.842	0.748	0.853	0.490	0.426	0.660

* For the concentrates, the number of analyses included in each average is indicated. For the nodules, individual BMR sample numbers are given (all are prefixed 7521). For the White Cliffs area (4), averages of type I and type II eclogite garnets are given (from Edwards et al., in prep.).

** Total Fe as FeO.

n.d. Not detected.

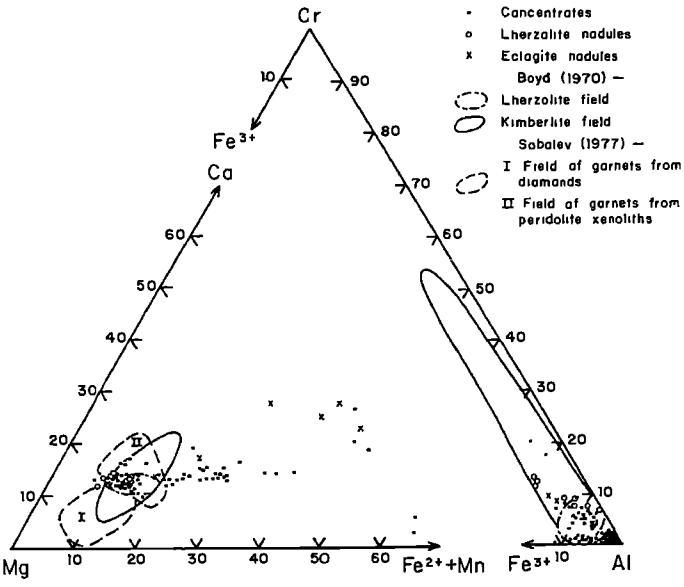

Fig. 2. Compositions of garnets from lherzolite and eclogite nodules and mineral concentrates from kimberlitic intrusives of southeastern Australia plotted on variation diagrams for the 6 and 8-coordinated sites.

more of the minerals garnet, clinopyroxene and ilmenite, and of the various phases in the ultramafic nodules, were carried out on a T.P.D. energy-dispersive electron microprobe using the methods described by Reed and Ware (1975). The results were normalized to 100 weight percent to aid comparisons, and Fe^{3+}/Fe^{2+} ratios were calculated assuming ideal stoichiometric compositions (Tables 1-4).

Garnet

Garnets were analyzed from concentrates obtained from six of the kimberlitic areas (3, 4, 5, 8, 9 and 12), eclogite nodules from three areas (4, 9 and 12), and garnet and garnet-spinel lherzolite inclusions from two occurrences in the Jugiong area (9) (Table 2).

These garnets were classified in terms of the cluster groups established by Dawson and Stephens (1975) for garnets from kimberlites and associated xenoliths. All of the garnets fall into cluster groups 9, 5 and 3. Cluster 9 is the largest group, and includes all those from lherzolite xenoliths, from a spinel pyroxenite inclusion from Delegate (area 7; Lovering and White, 1969) and from two eclogite nodules from Jugiong (area 9). Concentrates from all areas except 5 include cluster 9 garnets. All such garnets from south-eastern Australia, except for some of those from the Terowie kimberlites (area 3), fall in, or very close to, the lherzolite xenolith and kimberlite fields defined by Boyd (1970) and Sobolev (1977) (Figure 2). Most of the cluster 9 garnets found in Australia are Ca-rich and Cr-poor compared with garnet inclusions in diamond (Gurney and Switzer, 1973), although two of those from Terowie have relatively high Cr contents (Figure 2).

Garnets of cluster group 5, which includes examples from both kimberlites and eclogites (Dawson and Stephens, 1975), are confined to concentrates from two areas (3 and 9) and are absent from nodules. These are the most Fe-rich garnets found in kimberlites (Table 2).

Cluster group 3 garnets are characterized by relatively high FeO and CaO, and correspondingly low MgO contents, and are found in concentrates from three areas (3, 5, and 9), and in eclogite nodules from White Cliffs and Gloucester (areas 4 and 12). Those from the Bullenmerri concentrates (area 5) and from one of the intrusives in the Terowie area (area 3) are restricted to this cluster. Garnet in eclogites from Delegate (area 7) is also of this type (Lovering and White, 1969). Most of the garnets from concentrates show a relatively large scatter on the Ca-Mg-(Fe^{2+} + Mn) plot; enrichment in Fe^{2+} + Mn ensures that they plot well outside the fields of kimberlite and lherzolite xenolith garnets (Figure 2). Dawson and Stephens (1975) point out that this is a moderately large cluster containing most of the common eclogite garnets.

In terms of the garnet end-members (Al + Sp)-(Gr + An)-Py, three of the White Cliffs (area 5) garnets belong to group B eclogites (Coleman, et al., 1965), which is the group dominated by eclogites derived from high-grade crustal metamorphic facies, whereas one of the garnets from this area falls into group A, as do the two Jugiong (area 9) eclogite garnets. These group A eclogite garnets also fall into the field of garnets from eclogites and gros-

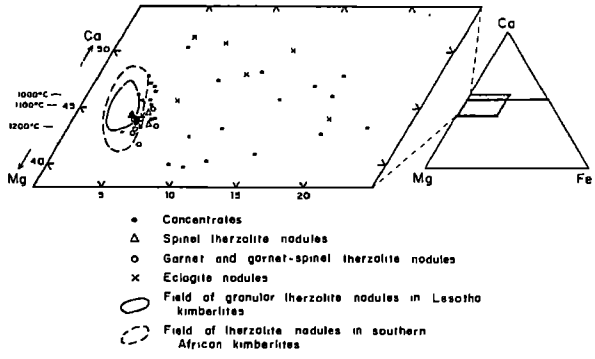

Fig. 3. Compositions of clinopyroxenes from lherzolite and eclogite nodules and mineral concentrates from kimberlitic intrusives of southeastern Australia. Fields of clinopyroxenes from granular lherzolite nodules in Lesotho kimberlites (Nixon and Boyd, 1973) and lherzolite nodules in southern African kimberlites (MacGregor, 1975) are shown. Temperatures are for the enstatite-diopside solvus at 30 kb (Mori and Green, 1975).

Table 3. Compositions of clinopyroxenes from mineral concentrates, and lherzolite and eclogite nodules.

	Concentrates							Spinel lherzolites			
Area No.	3	6					10	9			
Intrusion No.	5,6	1	4	5	6	7	1	3			
Sample No.*	2	3	2	2	2	2	3	0108	0110	0118/5	0418
SiO_2	54.87	52.26	53.08	52.94	53.68	52.38	52.88	52.59	53.68	52.41	52.15
TiO_2	n.d.	0.15	0.43	0.1	n.d.	0.36	0.1	0.23	n.d.	0.23	0.56
Al_2O_3	1.37	5.67	5.14	4.72	3.58	6.17	5.07	5.70	3.58	6.21	5.90
FeO**	2.37	2.85	2.81	3.08	2.31	2.91	2.41	2.63	2.31	3.04	3.15
MnO	n.d.	n.d.	n.d.	n.d.	n.d.	n.d.	n.d.	n.d.	n.d.	n.d.	0.21
MgO	17.23	16.18	16.54	16.89	17.26	15.99	16.05	16.50	17.26	15.76	15.84
CaO	21.96	20.95	19.34	20.29	20.71	18.93	21.57	19.62	20.71	19.45	18.91
Na_2O	0.93	1.04	1.39	0.95	1.02	1.85	1.04	1.48	1.02	1.72	1.74
Cr_2O_3	1.28	0.91	1.27	1.03	1.47	1.43	0.89	1.25	1.47	1.19	1.53
					O = 6						
Si	1.986	1.888	1.913	1.912	1.936	1.884	1.911	1.893	1.936	1.888	1.883
Al^{iv}	0.014	0.112	0.087	0.088	0.064	0.116	0.089	0.107	0.064	0.112	0.117
Al^{vi}	0.044	0.129	0.131	0.113	0.088	0.146	0.127	0.135	0.088	0.152	0.134
Ti	-	0.004	0.012	0.003	-	0.010	0.003	0.006	-	0.006	0.015
Cr	0.037	0.026	0.036	0.029	0.042	0.041	0.025	0.036	0.042	0.034	0.044
Fe^{3+}	-	0.022	-	0.006	0.004	0.039	0.005	0.028	0.004	0.034	0.031
Fe^{2+}	0.072	0.064	0.085	0.087	0.065	0.049	0.068	0.051	0.065	0.057	0.064
Mn	-	-	-	-	-	-	-	-	-	-	0.006
Mg	0.929	0.871	0.888	0.909	0.928	0.857	0.864	0.885	0.928	0.846	0.852
Ca	0.852	0.811	0.747	0.785	0.800	0.730	0.835	0.757	0.800	0.751	0.732
Na	0.065	0.073	0.097	0.067	0.071	0.129	0.073	0.103	0.071	0.120	0.122
Mg/(Mg+ Fe^{2+}+ Fe^{3+})	0.928	0.910	0.913	0.907	0.931	0.907	0.922	0.918	0.931	0.903	0.900
Ca/(Ca+Mg)	0.478	0.482	0.457	0.463	0.463	0.460	0.491	0.461	0.463	0.470	0.462
% Jadeite	2.9	2.5	6.1	3.1	2.5	5.0	4.3	3.9	2.5	5.2	4.7

* For the concentrates, the number of analyses included in each average is indicated. For the nodules, individual BMR sample numbers are given (all are prefixed 7521). For the White Cliffs area (4), averages of type I and type II eclogite clinopyroxenes are given (from Edwards et al., in prep.).

** Total Fe as FeO.

n.d. Not detected.

Table 3. Cont.

Garnet-spinel lherzolites				Garnet lherzolites				Eclogites				
9				9				9		12	4	
3				3			4	4		1	2	
0052/39	115/5	0429	0433	0416	0424	0432	0060	0413	0414	0096	I	II
52.64	52.36	52.56	52.50	51.90	51.56	52.48	52.61	51.91	52.44	51.49	52.38	52.60
n.d.	0.42	0.57	0.47	0.42	0.67	0.14	0.32	0.52	0.31	0.54	0.62	0.54
5.55	6.48	7.21	7.00	5.93	6.59	5.65	6.18	7.14	6.41	7.04	9.04	11.49
2.61	2.96	2.64	3.07	3.05	3.42	2.73	2.90	3.86	2.88	5.88	7.52	2.99
n.d.	n.d.	0.24	0.27	0.23	0.18	n.d.	n.d.	0.19	0.15	n.d.	0.06	0.03
16.72	15.35	15.46	15.66	16.04	15.66	16.36	16.24	14.42	16.05	12.58	9.65	10.75
19.94	19.30	17.55	17.42	19.05	18.86	19.58	18.75	19.25	19.46	20.39	17.04	18.02
1.26	1.85	2.60	2.44	1.82	1.75	1.71	1.74	2.14	1.80	1.65	3.62	3.53
1.28	1.30	1.19	1.15	1.56	1.33	1.36	1.28	0.56	0.53	0.42	0.06	0.05
						0 = 6						
1.895	1.887	1.882	1.883	1.870	1.861	1.886	1.892	1.874	1.882	1.885	1.913	1.882
0.105	0.113	0.118	0.117	0.130	0.139	0.114	0.108	0.126	0.118	0.115	0.087	0.118
0.131	0.162	0.186	0.179	0.122	0.141	0.125	0.154	0.178	0.153	0.189	0.302	0.367
-	0.011	0.015	0.013	0.011	0.018	0.004	0.009	0.014	0.008	0.015	0.017	0.015
0.036	0.037	0.034	0.033	0.044	0.038	0.039	0.036	0.016	0.015	0.012	0.002	0.001
0.026	0.019	0.048	0.051	0.069	0.046	0.061	0.022	0.054	0.058	0.001	0.006	-
0.053	0.070	0.031	0.042	0.023	0.057	0.021	0.065	0.062	0.029	0.179	0.223	0.089
-	-	0.007	0.008	0.007	0.006	-	-	0.006	0.005	-	0.002	0.001
0.897	0.825	0.825	0.837	0.861	0.842	0.876	0.870	0.776	0.859	0.686	0.525	0.573
0.769	0.745	0.673	0.669	0.735	0.729	0.754	0.722	0.745	0.748	0.800	0.667	0.691
0.088	0.129	0.180	0.170	0.127	0.122	0.119	0.121	0.150	0.125	0.117	0.256	0.245
0.919	0.903	0.913	0.900	0.903	0.891	0.914	0.909	0.870	0.908	0.792	0.696	0.866
0.462	0.475	0.449	0.444	0.461	0.464	0.463	0.454	0.490	0.465	0.538	0.560	0.547
2.6	7.3	9.8	8.7	1.4	3.8	2.0	6.3	8.0	5.2	10.4	24.8	24.8

* For the concentrates, the number of analyses included in each average is indicated. For the nodules, individual BMR sample numbers are given (all are prefixed 7521). For the White Cliffs area (4), averages of type I and type II eclogite clinopyroxenes are given (from Edwards et al., in prep.).

** Total Fe as FeO.

n.d. Not detected.

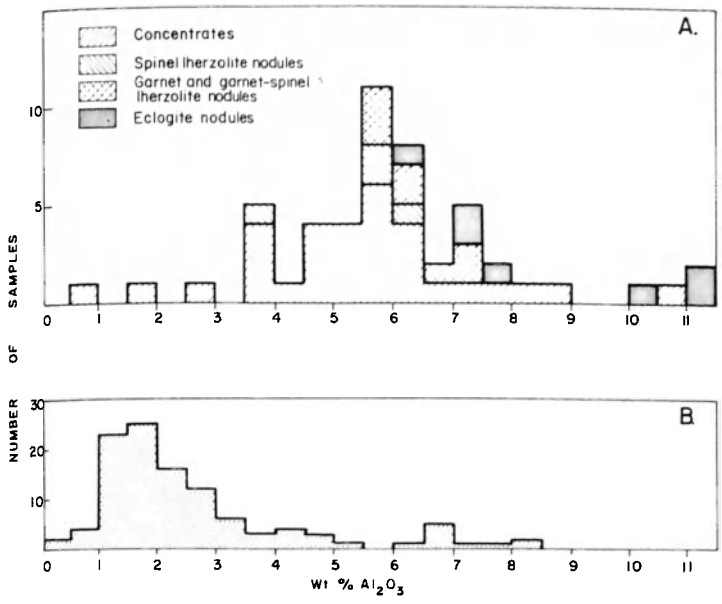

Fig. 4. Histograms showing Al_2O_3 contents of clinopyroxenes from (A) lherzolite and eclogite nodules and mineral concentrates from kimberlitic intrusives of southeastern Australia; and (B) ultramafic associations from kimberlites (Sobolev, 1977).

pydites in kimberlites from Russia and southern Africa (Lovering and White, 1969). One of the Jugiong eclogite garnets (75210414) bears a close resemblance to those from the garnet and garnet-spinel lherzolites found in kimberlitic intrusives from the same area, and the other (75210413) is only slightly richer in FeO.

Clinopyroxene

Clinopyroxene in concentrates from eight areas (3, 4, 5, 6, 8, 9, 10 and 12), and in twelve lherzolite nodules from two of the Jugiong occurrences and three eclogite nodules from Jugiong and Gloucester, were analyzed. Over half the concentrate clinopyroxenes (from Terowie, Oatlands, Jugiong and Abercrombie: areas 3, 6, 9 and 10, respectively) are chrome diopsides with Mg/(Mg + Fe) ratios between 0.89 and 0.93, and Ca/(Ca + Mg) ratios of 0.45 to 0.50 (Table 3, Figure 3). Diopside from garnet, spinel, and garnet spinel lherzolite inclusions, and an eclogite nodule (75210414) from two of the Jugiong occurrences are virtually identical in composition to those in concentrates from the same intrusions, and diopside from a second eclogite nodule (75210413) from this locality is only slightly richer in Fe and poorer in Mg (Table 3). This suggests that many of the clinopyroxenes from concentrates represent xenocrystic diopsides derived by fragmentation of similar nodular material. These diopsides are typical of clinopyroxene found in lherzolite inclusions and as xenocrysts in kimberlites from other localities (e.g., Nixon and Boyd, 1973; MacGregor, 1975; Sobolev, 1977). However, none compares with subcalcic diopsides from sheared lherzolite nodules, which are thought to have originated relatively deep in the mantle, in Lesotho kimberlites (Nixon and Boyd, 1973). TiO_2, Na_2O and Cr_2O_3 contents are generally similar to those of kimberlitic clinopyroxenes, although the diopsides are slightly poorer in SiO_2, and Al_2O_3 contents are higher by a factor of two or three (Figure 4). The high Al_2O_3 contents reflect those of the host rocks, and may indicate relatively high Al_2O_3 in the source regions. Jadeite contents are fairly low (less than about 8%), but Tschermak's component is slightly higher than in most kimberlitic clinopyroxenes.

The remaining group of clinopyroxenes (mainly augites and salites) is relatively rich in Fe, (Figure 3) and includes concentrates from the Terowie, White Cliffs, Bullenmerri, Bombala, Jugiong and Gloucester areas (3, 4, 5, 8, 9 and 12, respectively, not included in Table 3); this group probably originated at shallower depths than did the diopsides, possibly within

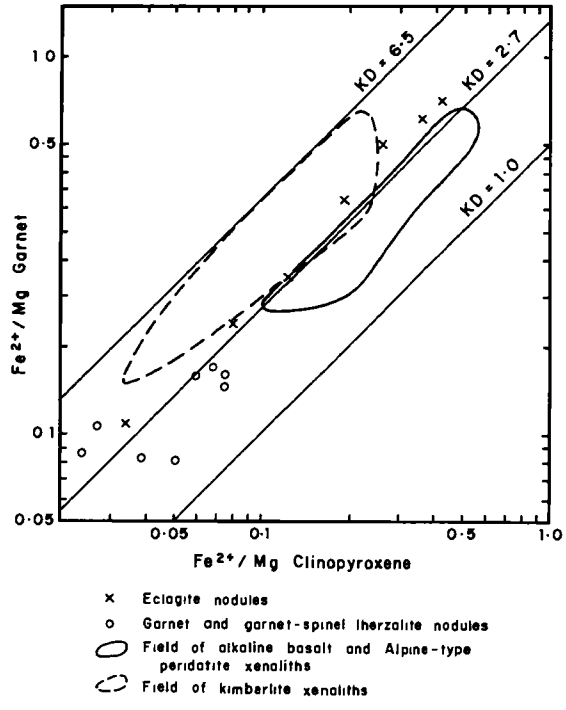

Fig. 5. Distribution of Fe^{2+}/Mg between coexisting garnet and clinopyroxene (after Banno and Matsui, 1965) for lherzolite and eclogite nodules of southeastern Australia. Fields of alkali basalt and Alpine-type peridotite xenoliths (Irving, 1974) and eclogite xenoliths in kimberlites (Lovering and White, 1969; Irving, 1974) are shown.

Table 4. Compositions of ilmenites from mineral concentrates.

Area No.	3		5		8	9							12
Intrusion	1		1		1	2							1
TiO_2	50.88	46.54	46.53	44.26	47.90	50.65	48.73	47.09	46.85	46.69	45.50	45.29	47.83
Al_2O_3	0.23	0.11	0.99	0.58	0.66	0.54	0.37	0.43	0.51	0.38	0.58	0.54	0.74
FeO*	40.49	43.87	47.73	52.66	45.11	40.74	44.36	46.79	47.13	47.84	48.50	49.10	44.53
MnO	0.30	0.34	0.23	0.34	0.44	0.27	0.53	0.22	0.36	0.44	0.25	0.30	0.35
MgO	7.84	7.16	4.38	2.16	5.89	7.64	5.85	5.23	5.05	4.51	4.90	4.77	6.33
CaO	0.08	n.d.	n.d.	n.d.	n.d.	n.d.	n.d.	n.d.	0.11	n.d.	0.09	n.d.	n.d.
Cr_2O_3	0.19	1.98	0.14	n.d.	n.d.	0.16	0.16	0.24	n.d.	0.15	0.17	n.d.	0.21
						0 = 6							
Ti	1.810	1.660	1.689	1.634	1.722	1.802	1.756	1.702	1.694	1.697	1.645	1.639	1.713
Al	0.013	0.006	0.056	0.033	0.037	0.030	0.021	0.024	0.029	0.021	0.033	0.031	0.041
Cr	0.007	0.074	0.005	-	-	0.006	0.006	0.009	-	0.006	0.007	-	0.008
Fe^{3+}	0.361	0.600	0.562	0.700	0.519	0.359	0.461	0.562	0.583	0.579	0.671	0.691	0.524
Fe^{2+}	1.241	1.140	1.364	1.462	1.284	1.253	1.317	1.319	1.312	1.354	1.278	1.285	1.249
Mn	0.012	0.014	0.009	0.014	0.018	0.011	0.022	0.009	0.015	0.018	0.010	0.012	0.014
Mg	0.553	0.506	0.315	0.158	0.420	0.539	0.418	0.375	0.362	0.325	0.351	0.342	0.450
Ca	0.004	-	-	-	-	-	-	-	0.006	-	0.005	-	-

* Total Fe as FeO n.d. Not detected

the crust. They are generally similar in composition to clinopyroxenes from pyroxenite inclusions in basalts (Ellis, 1976) and to some eclogite clinopyroxenes, including those in eclogites associated with amphibolites and granulites (Lovering and White, 1969) and in the group B eclogites of Coleman, et al., 1965. Cr_2O_3 and Mg/(Mg + Fe) are relatively low, whereas TiO_2, Na_2O and jadeite contents tend to be higher than in the main group of diopsides. Al_2O_3 contents are comparable with those of clinopyroxenes from eclogite inclusions in kimberlites (Sobolev, 1977), but appreciably lower than those of eclogites from basic pipes at Delegate (area 7, Lovering and White, 1969). Clinopyroxene (salite) concentrates from the White Cliffs occurrence are similar to those of type I eclogite nodules from the same pipes (Edwards, et al., in prep.), and some of the Terowie concentrates compare with a salite from an eclogite nodule from Gloucester (area 12) (Table 3), strongly suggesting that many of the more Fe-rich xenocrystic clinopyroxenes are fragments of eclogitic material.

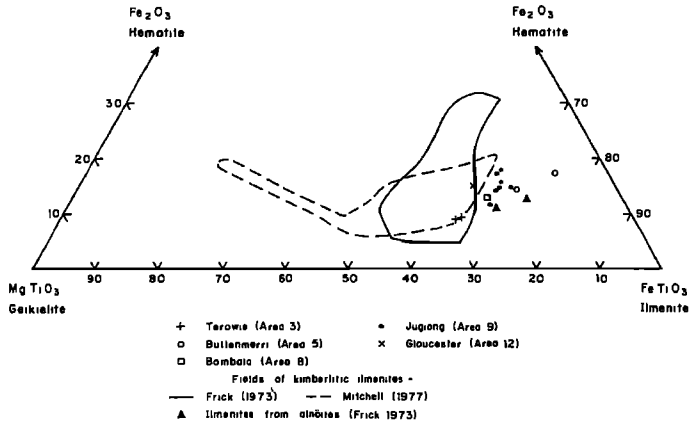

Fig. 6. Compositions of ilmenite from mineral concentrates from kimberlitic intrusives of southeastern Australia. Fields of kimberlitic ilmenites from diverse localities in Russia and Africa (Frick, 1973), and discrete ilmenites from southern African kimberlites (Mitchell, 1977) are shown.

Iron-Magnesium Distribution Coefficients

Figure 5 (after Banno and Matsui, 1965) shows partition of Fe^{2+} and Mg between coexisting garnet and clinopyroxene in the garnet and garnet-spinel lherzolite and eclogite nodules. As the Fe^{2+} contents were calculated assuming ideal stoichiometric compositions, this diagram is subject to errors, although the general distribution of points is reasonably accurate. Values of $K_D/(Fe^{2+}/Mg)_{Gt}/(Fe^{2+}/Mg)_{Cpx}/$ range from 1.6 to 3.9, the lherzolite and two eclogite nodules from Jugiong having lower Fe^{2+}/Mg ratios and slightly lower K_D values than eclogites from White Cliffs and Gloucester. This supports the conclusion that the lherzolites and eclogites from Jugiong have a common mantle source. The K_D values are similar to those of eclogites in kimberlites, garnet pyroxenite xenoliths in alkali basalts, and layers in Alpine-type peridotites (Irving, 1974), as well as eclogite inclusions from the Delegate pipes (Lovering and White, 1969). The lower K_D values of the nodules from Jugiong indicate higher equilibration temperatures than those of the eclogites from White Cliffs and Gloucester (Banno and Matsui, 1965; Råheim and Green, 1974).

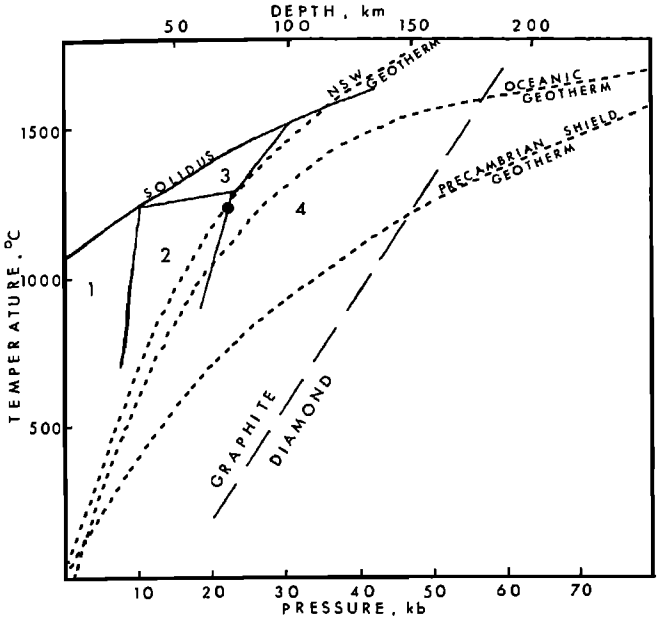

Fig. 7. Pressure-temperature fields of mineral assemblages in pyrolite III composition (Green and Ringwood, 1967) 1 = plagioclase lherzolite, 2 = spinel lherzolite, 3 = aluminous pyroxene lherzolite, 4 = garnet lherzolite. Oceanic and Precambrian shield geotherms are from Ringwood (1966); the New South Wales (NSW) geotherm is taken from one of the theoretical steady-state temperature profiles of the eastern province of Australia (Sass, et al., 1976). Solid circle represents the temperature-pressure plot of a spinel-garnet lherzolite nodule (75210052/39) from Jugiong.

Ilmenites

Ilmenite concentrates were obtained from the kimberlitic occurrences of Terowie, Bullenmerri, Bombala, Jugiong and Gloucester (areas 3, 5, 8, 9 and 12, respectively). The analyses (Table 4) are compared with the fields of kimberlitic ilmenites, as established by Frick (1973) and Mitchell (1977), in terms of the ternary plot of the molecular proportions of ilmenite-geikielite-hematite (Figure 6). The ilmenites from Terowie and Gloucester fall into the kimberlitic fields, whereas the remainder lie on the ilmenite-rich side, and have chemical similarities to ilmenites occurring in alnöites (Figure 6; and Frick, 1973). Most of the southeast Australian ilmenites have low MgO and Cr_2O_3, and moderate TiO_2 contents relative to typical kimberlitic ilmenites (Ferguson, et al., 1973; Haggerty, 1975; Sobolev, 1977).

As pointed out by Mitchell (1977), kimberlitic ilmenites have a wide range of compositions which may be a reflection of minor changes in temperature and liquid composition. Frick (1973) also ascribes the chemical variations to reactions between ilmenite and carbonate fractions in the kimberlite.

P-T Estimates of Lherzolite and Eclogite Nodules

P-T conditions of crystallization of lherzolite assemblages have been estimated from the compositions of coexisting minerals (Davis and Boyd, 1966; MacGregor, 1974; Wood and Banno, 1973). Early estimates of this type were based on the diopside-enstatite solvus (Davis and Boyd, 1966) and the pressure-dependent solubility of Al_2O_3 in enstatite coexisting with garnet or spinel (MacGregor, 1974).

Additional constraints can be obtained from thermodynamic modelling of the pyroxenes (Wood and Banno, 1973). Mori (1977) has summarized the present status of temperature calculations on spinel lherzolites, and has presented additional data on subsolidus equilibria in the system $CaO-MgO-Al_2O_3-SiO_2$ and in a range of minerals from a natural spinel lherzolite. Refinement of the earlier work results particularly from the demonstration of a pressure effect on the pyroxene solvus (Howells and O'Hara, 1975; Mori and Green, 1975, 1976) and recognition that the pyroxene solvus is dependent on the Al_2O_3 content in pyroxene (Boyd, 1970), as well as on other elements in complex natural systems.

Three methods of Mori (1977) that are the basis of our geothermometry depend on the chemical equilibria:

$$\underset{\text{orthopyroxene}}{Mg_2Si_2O_6} = \underset{\text{clinopyroxene}}{Mg_2Si_2O_6} \qquad (T_1)$$

$$\underset{\text{clinopyroxene}}{CaMgSi_2O_6} + \underset{\text{spinel}}{MgAl_2O_4} = \underset{\text{clinopyroxene}}{CaAl_2SiO_6} + \underset{\text{olivine}}{Mg_2SiO_4} \qquad (T_2)$$

$$\underset{\text{orthopyroxene}}{Mg_2Si_2O_6} + \underset{\text{spinel}}{MgAl_2O_4} = \underset{\text{orthopyroxene}}{MgAl_2SiO_6} + \underset{\text{olivine}}{Mg_2SiO_4} \qquad (T_3)$$

Method 3 is critically dependent upon experimental data for alumina solubility in orthopyroxene coexisting with spinel at various pressures, and at present these data are inconsistant (MacGregor, 1974; Wood, 1975; Fujii and Takahushi, 1976; Obata, 1976; Stroh, 1976). Therefore, we have placed more reliance on the first two methods in presenting our data. The presence of garnet coexisting with aluminous spinel in some lherzolites allows independent T estimates using the data pertaining to the partitioning of Mg and Fe between coexisting garnet and clinopyroxene, as experimentally determined by Råheim and Green (1974).

All our P-T determinations were made on nodules from the Jugiong area. One lherzolite (75210052) contains both garnet and spinel, apparently in equilibrium, with no evidence of reaction or zonation, suggesting crystallization on the quasi-univariant boundary separating the spinel and garnet lherzolite fields. Experimental studies using complex

Table 5. Chemical analyses of kimberlitic rocks, carbonatite, and garnet-spinel lherzolite nodule from southeastern Australia.

	A	B	C	D	E	F	G	H
Area No.	2	2	2	2	2	4	9	9
Intrusion No.	1	1	2	3	4	1	1	2
SiO_2	21.99	6.33	32.65	26.92	24.60	23.51	42.86	36.13
TiO_2	1.83	1.63	3.40	4.71	4.48	1.76	1.96	3.18
Al_2O_3	3.40	2.80	7.66	4.47	3.83	5.56	7.42	9.86
Fe_2O_3	10.39*	4.50	6.04	5.69	3.92	8.89*	10.61*	11.38*
FeO		1.34	5.05	3.47	2.81			
MnO	0.22	0.16	0.17	0.18	0.16	0.16	0.15	0.15
MgO	22.23	4.67	20.25	17.96	18.12	11.27	17.06	9.64
CaO	17.03	40.91	6.01	11.32	13.93	20.73	9.40	14.51
Na_2O	0.03	0.13	0.17	0.11	0.07	0.44	2.19	3.11
K_2O	0.10	0.85	2.70	2.92	2.18	1.49	0.97	0.91
P_2O_5	1.72	1.36	2.88	0.93	0.69	0.98	0.76	1.33
H_2O^+		1.56	6.39	3.29	2.81	1.43	2.70	4.15
H_2O^-		0.82	3.96	1.77	1.33	6.52	1.18	0.76
CO_2	11.2	31.79	1.89	14.64	20.17	15.8	2.2	5.05
S		0.05	0.08	1.52	0.67			
Total		98.92	99.30	99.90	99.77			
-O for S		0.02	0.04	0.76	0.33			
Total		98.90	99.26	99.14	99.44	98.54	99.46	100.16
				Trace elements in parts per million				
Sc	23	35	27	30	25	34	22	27
V	198	231	270	340	335	291	136	160
Cr		970	212	940	970			
Co		100	121	76	102			
Ni	523	268	170	447	510	389	895	115
Cu	65	70	62	79	54	79	49	87
Zn	100	66	102	96	75	97	94	100
Ga		3.5	14.5	10.5	10.0			
Rb	5	32.5	140	119	95	63	29	66
Sr	1700	1250	615	570	343	1300	824	1400
Y	25	17	17	18	15	19	19	30
Zr	430	274	170	301	214	197	204	310
Nb	418	323	190	220	215	175	86	174
Ba	3000	3080	2360	1890	1530	1410	949	1910
La	392	225	47	141	117	179	60	100
Ce	472	431	88	297	284	289	105	163
Pb		29	16	15	12			
Th	54	43.0	7.2	26.0	28.5	23	11	18
U		13.5	3.6	4.0	4.0			
Si/Mg	0.77	1.05	1.25	1.16	1.05	1.62	1.95	2.90
K/Rb	166	217	160	204	190	196	278	114
Zr/Nb	1.03	0.85	0.89	1.37	1.00	1.13	2.37	1.78
Nb/Y	17	19	11	12	14	9.2	4.5	5.8
mg^+	0.81	0.60	0.77	0.79	0.84	0.71	0.76	0.62
k^+	0.68	0.81	0.91	0.94	0.95	0.69	0.23	0.16

* Total Fe as Fe_2O_3. + Niggli values (atomic proportions Mg/(Mg+Fe+Mn) and K/(K+Na), respectively).

A. Carbonated micaceous kimberlitic rock (75210081); B. Carbonatite (75210101); C. Micaceous kimberlitic dyke (75210434); D. Carbonated micaceous kimberlitic dyke (75210468); E. Carbonated micaceous kimberlitic dyke (75210469); F. Carbonated olivine nephelinite dyke (75210021); G. Olivine nephelinite (75210041); H. Olivine nephelinite lapilus (75210047).

Analyses by X-ray fluorescence in Bureau of Mineral Resources and Department of Geology, Australian National University laboratories, except Na (determined by atomic absorption) and H_2O^+, H_2O^- and CO_2 (determined gravimetrically).

Table 5. Cont.

I	J	K	L	M	N	P	Q	R	
9	9	9	9	9	9	9	7	-	
2	3	4	4	4	4	3	-	-	
35.83	41.93	40.30	38.27	38.30	37.41	42.99	41.24	40.36	SiO_2
2.93	1.96	2.22	2.25	2.10	2.07	0.17	2.42	4.12	TiO_2
8.14	8.69	6.94	7.23	6.33	6.25	2.64	10.20	10.54	Al_2O_3
7.74	11.21*	10.21*	10.10*	9.76*	4.66	2.10	4.93	4.03	Fe_2O_3
6.11					5.42	6.34	6.69	8.38	FeO
0.16	0.16	0.14	0.13	0.12	0.17	0.15	0.20	0.18	MnO
16.83	15.26	12.38	12.26	12.73	18.51	37.50	15.87	12.66	MgO
5.00	10.29	11.32	11.78	11.70	9.68	3.00	11.92	10.28	CaO
2.14	2.16	1.36	1.39	1.21	2.56	0.37	2.88	3.63	Na_2O
1.32	1.99	1.11	1.13	1.09	0.91	0.22	0.48	1.12	K_2O
1.04	0.92	0.93	0.88	0.82	0.81	0.03	1.04	0.79	P_2O_5
4.62	2.70	2.05	2.40	2.65	2.44	1.25	1.89	2.27	H_2O^+
5.27	0.66	3.75	3.46	3.71	0.66	0.18	0.19	0.66	H_2O^-
2.24	3.65	6.0	7.55	8.65	7.65	2.46	0.04	0.64	CO_2
0.16					0.04				S
99.53					99.24				Total
0.08					0.02				-O for S
99.45	101.58	98.71	98.83	99.17	99.22	99.40	100.02	99.66	Total
					Trace elements in parts per million				
20	23	20	23	17	19	19			Sc
141	95	151	217	143	159	61			V
670					910	2530			Cr
98					82	129			Co
1090	737	692	742	803	820	2080			Ni
44	49	45	50	51	47	18			Cu
112	104	87	99	95	94	67			Zn
16.0					9.5	3.0			Ga
61	46	49	59	48	43.0	6.8			Rb
447	955	835	1095	1050	840	42			Sr
23	24	23	25	28	20	3			Y
248	222	223	244	230	196	13			Zr
164	96	95	105	102	84	2			Nb
645	1210	729	1010	902	845	35			Ba
61	68	68	67	58	59	1			La
127	117	113	113	115	106	4			Ce
15					7	3			Pb
24.0	18	16	22	20	15.0	0.4			Th
2.4					2.2	0.2			U
1.65	2.13	2.52	2.42	2.33	1.57	0.89	2.01	2.47	Si/Mg
180	359	188	159	188	176	269			K/Rb
1.51	2.31	2.35	2.32	2.25	2.33	6.5			Zr/Nb
7.1	4.0	4.1	4.2	3.6	4.2	0.7			Nb/Y
0.68	0.73	0.70	0.70	0.72	0.77	0.89	0.72	0.65	mg^+
0.29	0.38	0.35	0.35	0.37	0.19	0.28	0.10	0.17	k^+

* Total Fe as Fe_2O_3. + Niggli values (atomic proportions Mg/(Mg+Fe+Mn) and K/(K+Na), respectively).

I. Olivine nephelinite lapillus (75210419); J. Olivine nephelinite (75210055); K. Olivine nephelinite autolith (75210067A); L. Olivine nephelinite autolith (75210067B); M. Olivine nephelinite lappilus (75210067C); N. Olivine nephelinite dyke (75210102); P. Garnet-spinel lherzolite nodule (75210433); Q. Olivine nephelinite from Delegate N.S.W. (R58 of Lovering and White, 1969). R. Olivine analcitite from Murrumburrah, N.S.W. (M3 of Irving and Green, 1976). Analyses by X-ray fluorescence in Bureau of Mineral Resources and Department of Geology, Australian National University laboratories, except Na (determined by atomic absorption) and H_2O^+, H_2O^- and CO_2 (determined gravimetrically).

natural rocks or model mantle compositions have established the position of the quasi-univariant boundary (Green and Ringwood, 1967, 1970; O'Hara, et al., 1971). Mori's (1977) T_1 and T_2 temperature parameters have respective values for this nodule of 1243°C and 1237°C (Ferguson, et al., 1977). Other garnet-spinel lherzolite nodules from Jugiong have minor kelyphitic rims, which in most cases contain aluminous spinel, developed around the garnet. Temperature estimates for these nodules (average of T_1 and T_2) range from 1204° to 1221°C. As shown by Ferguson, et al., 1977, application of the 1240°C temperature estimate to the boundary curve separating the spinel and garnet lherzolite fields yields a pressure of 21 kb (O'Hara, et al., 1971) or 22 kb (Green and Ringwood, 1970). In view of the fact that increasing P raises the T_1 and T_2 estimates, and that the experimental work was carried out at 16 kb (Mori, 1977), the 1240°C estimate for this nodule at 22 kb represents a minimum. However, according to Mori (1977) the estimated temperature at 22 kb would be less than 50°C higher than that at 16 kb. The spinel lherzolite nodules found in the Jugiong occurrences indicate temperatures of equilibration very similar to those of the garnet-spinel lherzolites, the range being 1214° to 1258°C (average of T_1 and T_2).

The Jugiong eclogite (griquaite) showing mineralogical similarities to the clinopyroxene and garnet in the lherzolites gives a T estimate

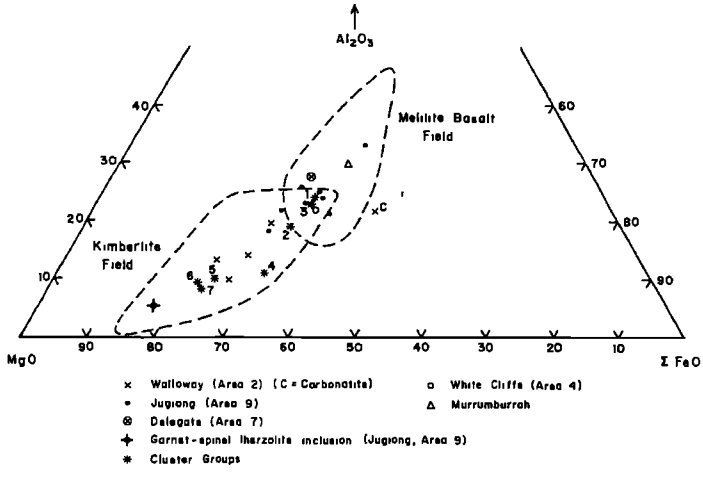

Fig. 8. Al_2O_3-MgO-total FeO diagram for kimberlitic rocks of southeastern Australia, showing kimberlite and melilite basalt fields of Cornelissen and Verwoerd (1975). Compositions of a garnet-spinel lherzolite nodule (75210433) from Jugiong, the kimberlitic cluster groups (1-7) of McIver and Ferguson (this vol.), olivine nephelinite from Delegate, N.S.W. (Lovering and White, 1969), and olivine analcitite from Murrumburrah, N.S.W. (Irving and Green, 1976) are also indicated.

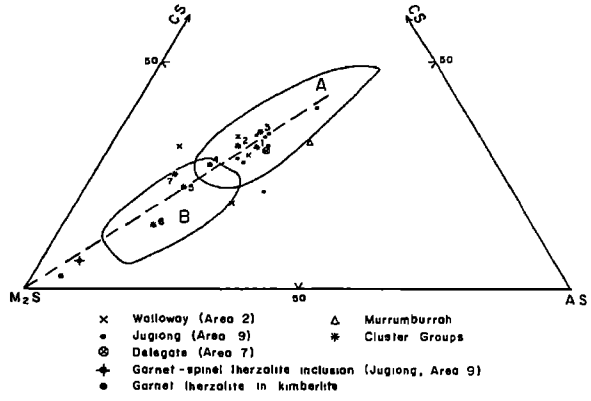

Fig. 9. Projections from, or towards, S onto the M_2S-CS-AS plane in the CMAS tetrahedron for kimberlitic rocks of southeastern Australia. The kimberlitic cluster groups (1-7) and fields of kimberlites (B) and associated kimberlitic rocks (A) of McIver and Ferguson (this vol.), and the average garnet lherzolite in kimberlite (Ito and Kennedy, 1967) are shown.

of 1228°C at 22 kb (Råheim and Green, 1974). In comparison, eclogite nodules from White Cliffs have given values of 850-900°C and 19-25 kb (Edwards, et al., in prep.). Alternative estimates of T_1, T_2 and T_3 may be compared with those based on Mori's methods (1977). For T_1, the Herzberg and Chapman (1976) method gives excellent agreement, whereas the T_2 their values are about 100°C higher than those of Mori (1977); MacGregor's (1974) and Obata's (1976) data give values for T_3 50-100°C lower. In the case of the garnet-spinel lherzolites it was found that the Råheim and Green (1974) method of temperature estimation at 22 kb gave results fairly consistent with those of Mori's T_1 and T_2. The method of Wood and Banno (1973) gave results 40-80°C higher than Mori's (1977). Equilibration temperatures calculated from the Ca/(Ca+Mg) of the diopsides, using the diopside solvus of Davis and Boyd (1966), and Mori and Green (1975), at 30 kb, produce values 100 to 150°C below the average of T_1 and T_2 obtained using the Mori (1977) method. A further independent empirical estimate of P and T can be derived from the intersection of the alumina-in-orthopyroxene contours of the garnet lherzolite field with the spinel lherzolite-garnet lherzolite boundary. Using this method, only the data of Green and Ringwood (1970) give results approximating to those already estimated - 1220°C at 22 kb. We therefore consider that a T-P estimate of 1240°C and 22 kb is well founded using the above methods of P-T estimation.

The close temperature grouping of the lherzolite nodules does not allow as estimate of the variation of T with P. However, the equilibrium garnet-spinel lherzolite assemblage falling, as it does, on the quasi-univariant curve at

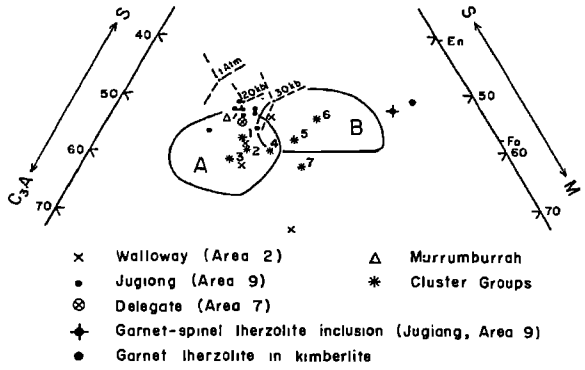

Fig. 10. Projections from, or towards, diopside onto the C_3-A-M-S plane in the CMAS tetrahedron for kimberlitic rocks of southeastern Australia. Positions of the pseudo-invariant points are from O'Hara (1968). En = enstatite, Fo = forsterite; fields as Figure 9.

1240°C and 22 kb, indicates an abnormally high geothermal gradient (Figure 7), actually exceeding the estimated oceanic geotherm (Ringwood, 1966). Irving (1975) considers that xenoliths are genetically related to processes of magma generation, and so by their very nature would exemplify a perturbed regional mantle geotherm. The age of the geothermal gradient indicated by the garnet-spinel lherzolite assemblage is probably that of the intrusion, namely late-Tertiary or Quaternary. In eastern Australia, emplacement of kimberlitic magma was preceded by widespread Cainozoic basaltic activity. Theoretical steady-state temperature profiles of the eastern province of Australia indicate the presence of abnormally high gradients in some areas (Sass, et al., 1976). These results are consistent with that predicted by the equilibrium garnet-spinel lherzolite assemblage found in the Jugiong kimberlitic occurrences (Figure 7).

It would then seem likely that the nodules from Jugiong represent samples from a region marking a perturbed steady-state geotherm generated during Tertiary times, and continuing to the present day. The abnormally high geothermal gradient indicated here intersects the diamond/graphite inversion curve at depths and temperatures greatly in excess of those shown for the inclusions (Figure 7), thereby making the prospect of finding diamondiferous kimberlites of Cainozoic age in this part of New South Wales highly improbable.

Geochemistry

Thirteen kimberlitic rocks from Walloway, White Cliffs, and Jugiong (areas 2, 4 and 9, respectively), as well as a carbonatite from Walloway and a garnet-spinel lherzolite nodule from Jugiong, were analyzed (Table 5). Analyses of an olivine nephelinite from Delegate (area 7) (Lovering and White, 1969) and an olivine analcite from Murrumburrah, N.S.W. (Irving and Green, 1976) are also given (Table 5, Anals. Q and R, respectively).

The samples from Walloway, with the exception of the carbonatite, are chemically similar to evolved kimberlitic rocks and alkaline ultramafic rocks associated with kimberlites (Ferguson, et al., 1973). They plot within the kimberlite field of Cornelissen and Verwoerd, 1975, on an Al_2O_3-MgO-FeO diagram (Figure 8), and have relatively high Niggli mg (0.77-0.84) and k (0.68 - 0.95). Si/Mg ratios are slightly higher than those suggested by Fesq, et al., 1975, as being typical of uncontaminated kimberlites (<0.9), but this is considered to reflect their more evolved nature, involving fractionation of a phase with low Si/Mg (e.g., olivine). Trace-element contents mostly fall within the range of kimberlites and associated rocks - high Cr, Ni, Rb, Sr, Nb, Ba, La, Ce, Pb, and Th. Nb/Y ratios are particularly high, similar to those of kimberlites from South Africa (Kable, et al., 1975), and comparable with those of highly alkaline mafic rocks in general (Pearce and Cann, 1973). The low Zr/Nb and K/Rb ratios are also similar to those of kimberlites from other localities (Dawson, 1971; Kable, et al., 1975).

Rocks, including nucleated autoliths, from the Jugiong area have a range of compositions, but differ from normal kimberlites in the relatively high SiO_2, Al_2O_3, Na_2O, and lower MgO contents. Niggli Mg values are consequently slightly lower (all except one are in the range 0.62 to 0.77), and k values are considerably lower (0.19 - 0.38), than in the kimberlitic rocks from Walloway. Some of these chemical features may be due to the effects of a CO_2-rich vapour phase during partial melting of postulated parent lherzolite, which would favour the production of liquids enriched in Al_2O_3, CaO, and alkalis (Boettcher, et al., 1975). Most samples plot in the region of overlap of the melilite basalt and kimberlite fields (Cornelissen and

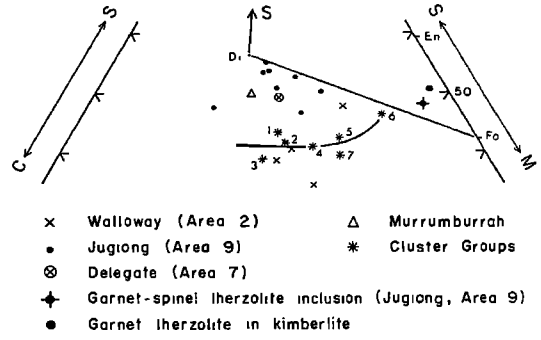

Fig. 11. Projections from A onto the C-S-M face of the CMAS tetrahedron for kimberlitic rocks of southeastern Australia. En = enstatite, Fo = forsterite, Di = diopside; fields as Figure 9.

Verwoerd, 1975) on the Al_2O_3-MgO-FeO diagram, although 75210041 and 75210102 plot further into the kimberlite field, and the most evolved sample (75210047) plots well inside the melilite basalt field (Figure 8). Trace-element contents are similar to those of the alkaline ultramafic rocks, including kimberlites, although Si/Mg and Zr/Nb ratios are higher, and Nb/Y lower, than in the Walloway kimberlites. The single rock from White Cliffs plots with the main group of Jugiong samples on the Al_2O_3-MgO-FeO diagram, although in some respects - high Niggli k and Nb/Y, and low Zr/Nb - it resembles kimberlites from Walloway.

Chemically, the Jugiong rocks quite closely resemble olivine analcitite from Murrumburrah, N.S.W. (Irving and Green, 1976) and the olivine nephelinite from Delegate (Lovering and White, 1969), although most are slightly poorer in Al_2O_3, and contain considerable amounts of CO_2 (Table 5). There is also some similarity with ankaramite from the Lashaine volcano, Tanzania (Rhodes and Dawson, 1975), and with average South African olivine melilite (McIver and Ferguson, this vol.) (Figure 8). The Jugiong rocks are considered to have close chemical affinities with the olivine nephelinite suite, a precise petrographic classification being difficult owing to the degree of alteration, although it is probable that analcite was a primary phase in some of the analyzed samples. They plot in or near the nephelinite field on a normative colour index vs. normative plagioclase diagram (Irvine and Baragar, 1971), whether or not the norm is calculated volatile-free. On a volatile-free basis, all are diopside- and olivine-normative, and all except sample 75210067A are nepheline-normative, although the presence of large amounts of carbonate, some of which may be primary, makes the norms unreliable. Several of the carbonate-rich kimberlites from Walloway, and the White Cliffs sample, are larnite-normative if CO_2 is excluded from the norm calculation, but hypersthene-normative if it is included.

The garnet-spinel lherzolite nodule from Jugiong (Table 5, P) is similar in composition to garnet lherzolite inclusions in kimberlite from other localities, although it has slightly lower MgO, and higher Al_2O_3, CaO, Na_2O, and K_2O than most such nodules (Rhodes and Dawson, 1975; O'Hara, et al., 1975). It is also relatively undepleted in trace elements including Rb, Sr, Y, and Zr (Rhodes and Dawson, 1975).

CMAS Projections

Chemical analyses of the kimberlites and kimberlitic rocks of southeastern Australia have been recalculated in terms of the four CMAS components (O'Hara, 1968). The results are presented graphically in figures 9 to 11 which represent planes within, or forming a side of, the tetrahedron. Studies of the planar projections of these analyzed rocks are compared with the experimentally determined phase boundaries, as well as with seven groups of rocks representing 126 analyses of kimberlites and associated alkaline ultramafic rocks from southern Africa established from statistical cluster analysis (Danchin, et al., 1975; Ferguson, et al., 1975). As pointed out by McIver and Ferguson (this vol.), the trend displayed by these seven cluster groups indicates that olivine and orthopyroxene were the dominant fractionating phases during the early stages of kimberlite evolution, whereas the more evolved rocks are accounted for by olivine-dominated fractionation.

Figure 9 shows the projection of the southeastern Australian analyses from or towards S onto the plane M_2S-CS-AS; it can be seen that the analyses plot on a linear trend extending from the olivine corner, which is coincident with that of the established cluster groups (McIver and Ferguson, this vol.). Most of the samples plot in the field of alkaline ultramafic rocks associated with kimberlites, although one of the Walloway rocks (75210434) plots in the kimberlite field (Danchin, et al., 1975). The linear trend away from the olivine corner defined by the southeastern Australian rocks indicates that olivine, orthopyroxene, or both, were significant fractionating phases, whereas garnet and clinopyroxene were not. In Figure 10, the analyses are projected from or towards diopside onto the C_3A-M-S plane; here two distinct groups are apparent. The Walloway rocks 75210468 and 75210469 group near the evolved end of the established trend defined by the seven cluster groups of kimberlites and associated rocks. As can be seen, this control line appears to be unrelated to the pseudo-invariant points applicable to 30 kb or less (from O'Hara, 1968). The remaining samples, representing the Delegate and Jugiong rocks (areas 7 and 9, respectively), group around the 20 kb pseudo-invariant point - an indication that this was the last pressure of equilibration. This pressure is also consistent with the estimate of $\approx$22 kb calculated from the lherzolite nodules found in the Jugiong intrusives. The presence of amphibole megacrysts in the Jugiong rocks suggests eruption from depths applicable to basaltic magma generation (Boyd, 1971; McGetchen, 1970). If this is the case, the amphiboles probably equilibrated at pressures of 20-25 kb, thus offering further confirmation of the depth of origin of these rocks. Plotting of stereographic pairs of the CMAS tetrahedron indicates that most samples plot near the CMS side, and fall closest to a plan roughly parallel to it. Consequently, following McIver and Ferguson (this vol.), the southeastern Australian rocks are projected from the A apex onto the CMS face of the tetrahedron, which gives minimal distortion. From this plot the two divergent trends seen in Figure 10 are better defined. The Walloway compositions tend to fall near

the established kimberlite and associated alkaline ultramafic rock trend, which initially lies at a high angle to the Di-Fo join. The remaining southeastern Australian rocks define a trend more enriched in the S component, and sub-parallel to the Di-Fo join (Figure 11). The two trends shown in this projection are consistent with the model of derivation by partial melting of an upper mantle source rock of composition similar to the garnet lherzolite inclusions found in kimberlitic rocks, including those from Jugiong. The melting event giving rise to the "normal" kimberlite trend, as shown by the southern African and Walloway rocks, very likely took place at depths exceeding 125 km, whereas the upper mantle event giving rise to the Jugiong-Delegate trend probably took place at depths of about 70 km. Alternatively, the latter trend could have originated by melting at greater depths followed by equilibration at $\approx$70 km before rapid emplacement near the surface. It is worth emphasizing that the calculated geothermal gradient in the Jugiong area is in excess of the mean oceanic geotherm (see above), with predicted temperatures of about 1300° at a depth of 70 km. Bultitude and Green (1968) and Green (1970), have demonstrated that under hydrous conditions a small degree of melting of rocks of upper mantle composition takes place at around 27 kb and 1250°C. Therefore at a postulated temperature of about 1300°C at 70 km depth it seems likely that partial melting of garnet lherzolite could have taken place, and, coupled with relatively minor fractionation involving olivine and possible orthopyroxene, produced the observed trend.

Thus, from a consideration of the planar projections within the CMAS tetrahedron, both trend lines can be attributed to a small degree of melting within the upper mantle, but at different temperatures and pressures, followed by olivine and orthopyroxene fractionation. The composition of the garnet-spinel lherzolite nodule found in the Jugiong intrusive (Table 5, P) compares very well with that of the upper mantle, as suggested by the world-wide occurrence of garnet lherzolite inclusions in kimberlite (Ito and Kennedy, 1967), as well as with the theoretical pyrolite composition (Ringwood, 1966).

Discussion and Conclusions

The investigated kimberlitic rocks of southeastern Australia may be divided into two chemically distinct groups, which define divergent trends within the CMAS tetrahedron. The South Australian kimberlites, notably those from the Walloway area, form part of the typical trend shown by kimberlites and related alkaline ultramafic rocks of southern Africa (Danchin, et al., 1975; McIver and Ferguson, this vol.), and fall towards the more evolved end of this trend. Kimberlitic rocks of this type are considered to have been formed by small degrees of melting of phlogopite-bearing garnet lherzolite at depths in excess of 125 km (equivalent to about 40 kb) (O'Hara, 1970). Olivine and orthopyroxene were the main fractionating phases during the early stages of kimberlite evolution, whereas the more evolved rocks may be explained on the basis of olivine-dominated fractionation; garnet and clinopyroxene do not appear to have been significant fractionating phases.

The kimberlitic rocks of the Jugiong and Delegate areas have close chemical affinities with olivine nephelinites and related rocks, and appear to be unrelated to the "normal" kimberlite trend. Consideration of phase relationships in the CMAS tetrahedron (O'Hara, 1968) indicate equilibration pressures of about 20 kb, and the observed chemical variations in these rocks may be explained on the basis of relatively minor olivine and possibly orthopyroxene fractionation. The presence of amphibole megacrysts is also consistent with equilibration at pressures of 20-25 kb (Boettcher, et al., 1975). T-P conditions of 1240 ± 20°C and 22 ± 1 kb are indicated by compositions of coexisting minerals in lherzolite and eclogite nodules, together with the occurrence of a unique garnet-spinel lherzolite inclusion containing an equilibrium assemblage falling on the quasi-invariant boundary between the spinel and garnet lherzolite fields. This is well-supported by the data obtained for the host rocks. The very high geothermal gradient implied by these estimates suggests that kimberlitic magma could have been generated by small degrees of partial melting of garnet lherzolite at depths of about 70 km and at temperatures of about 1300°C. Bultitude and Green (1968, 1971) have suggested that 3 to 6 percent melting of mantle pyrolite (lherzolite) containing 0.1 to 0.2 percent H_2O at depths of 80-120 km may lead to the production of olivine nephelinite and olivine-melilite nephelinite magmas (see also Irving and Green, 1976).

The justification for regarding olivine nephelinites and related rocks, such as those of the Jugiong area, as belonging to the kimberlitic association rests on their mode of occurrence and, more particularly, on their characteristic suite of mantle inclusions. We consider that both olivine nephelinite and kimberlite (s.s.) magmas may be derived directly by small degrees of melting of four-phase lherzolite, possibly phlogopite-bearing, in the mantle, although rocks of chemistry generally similar to olivine nephelinite (including olivine melilitites and related rocks) may also be derived by fractionation of kimberlite magma (Ferguson, et al., 1975). The observed fractionation trend would be dependent on the depth at which melting began, which would, in turn, depend on the geothermal gradient. Under geothermal gradients appropriate to Precambrian shield areas, the "normal" kimberlite evolutionary trend, as typified by the southern African

and South Australian kimberlites, would apply, whereas with high geothermal gradients, such as apparently existed in New South Wales during the Cainozoic (Ferguson, et al., 1977), initial melts would be of olivine nephelinite type. O'Hara (1968) has shown that initial melts of four-phase lherzolite in the 10-20 kb range are nepheline-normative, whereas above 20 kb they are hypersthene-normative, becoming richer in normative olivine with increasing pressure. The actual degree of melting is undoubtedly also of importance, as rare-earth contents suggest that kimberlite magmas are produced by less than 1 percent melting of garnet lherzolite (Mitchell and Brunfelt, 1975). The situation is further complicated by the amount and composition of a fluid phase. The considerable amounts of carbonate in the Australian kimberlitic rocks indicate that a CO_2-rich vapour phase may have been involved in magma generation. In the presence of such a vapour phase, the liquid would be SiO_2-undersaturated and relatively enriched in Al_2O_3, CaO, and alkalis, and the solidus temperature would be raised (Boettcher, et al., 1975; Eggler, 1975). Nevertheless, we suggest that the two distinct chemical trends shown by the kimberlitic rocks of southeastern Australia can, to a large extent, be explained by the different pressures under which the magmas were formed. In principle, there is no reason why transitional types between these two extremes should not be found, depending on the local geothermal gradient.

The abnormally high geothermal gradient present when the kimberlitic (olivine nephelinite) magmas of the Jugiong area were generated intersects the diamond/graphite inversion curve at much greater pressures and temperatures than those indicated by the nodules, so that it is highly unlikely that diamondiferous kimberlites of Cainozoic age occur in this part of New South Wales.

An eclogite nodule from one of the Jugiong intrusives contains garnet and clinopyroxene of identical compositions to those of garnet lherzolite nodules from the same area, strongly suggesting a common mantle source. Such eclogites, or griquaites according to the usage of Nixon (1973), are considered to be of cumulate origin. Eclogites from other localities (White Cliffs, Delegate, and Gloucester) are considerably more iron-rich, and apparently originated at higher levels in the upper mantle or lower crust.

Kimberlitic activity has occurred over a period of several hundred million years in southeastern Australia. The White Cliffs occurrences are of Permian age, the South Australian kimberlites are Jurassic, and a late Cainozoic age is suggested for the Jugiong intrusives (Stracke, et al., this vol.). Despite their chemical similarity, the Jugiong and Delegate olivine nephelinites are not manifestations of the same phase of magmatic activity, as the latter have given Jurassic agea (Lovering and Richards, 1964). However, the Jugiong occurrences may be related to the extensive late Cainozoic Newer Basalts of Victoria and South Australia, which include olivine analcitites and olivine nephelinites (Irving and Green, 1976), or to the leucite-bearing volcanics of New South Wales (Cundari, 1973).

Acknowledgements. We are indebted to Australian Anglo-American Limited, De Beers Consolidated Mines Limited, and the Director, Bureau of Mineral Resources, Geology and Geophysics, for permission to publish.

We gratefully acknowledge the donation of rock specimens by Mr. Glen H. Griffiths, Utah Development Company, and by Mr. D. M. Colchester. Thanks are due to B. W. Chappell and J. G. Pyke for chemical analyses, N. G. Ware of the Australian National University for microprobe facilities, Ms. Judith Montgomerie and Mrs. Michele Karakasch for drafting, N. J. Davis for drafting and laboratory assistance, K. J. Stracke of Stockdale Prospecting Limited for encouragement and help, and W. B. Dallwitz and R. J. Ryburn for critical comments on the manuscript.

References

Banno, S., and Y. Matsui, Eclogite types and partition of Mg, Fe, and Mn between clinopyroxene and garnet, Proc. Jap. Acad., 41, 716-721, 1965.

Boettcher, A. L., B. O. Mysen, and P. J. Modrski, Melting in the mantle: phase relationships in natural and synthetic peridotite - H_2O and peridotite - H_2O - CO_2 systems at high pressures, Phys. Chem. Earth, 9, 855-867, 1975.

Boyd, F. R., Garnet peridotites and the system $CaSiO_3$-$MgSiO_3$-Al_2O_3, Mineral. Soc. Amer. Spec. Pap., 3, 63-67, 1970.

Boyd, F. R., Pargasite-spinel peridotite xenolith from the Wesselton mine, Carnegie Inst. Wash. Yearb., 70, 138-142, 1971.

Bultitude, R. J., and D. H. Green, Experimental study at high pressures on the origin of olivine nephelinite and olivine melilite nephelinite magmas, Earth Planet. Sci. Lett., 3, 325-337, 1968.

Bultitude, R. J. and D. H. Green, Experimental study of crystal-liquid relationships at high pressure in olivine nephelinite and basanite compositions, J. Petrol., 12, 121-147, 1971.

Clement, C. R., Kimberlites from the Kao pipe, Lesotho, in Lesotho kimberlites, P. H. Nixon (ed.), Lesotho National Development Corporation, Maseru, 110-121, 1973.

Colchester, D. M., A preliminary note on kimberlite occurrences in South Australia, J. Geol. Soc. Aust., 19, 383-386, 1972.

Coleman, R. C., D. E. Lee, L. B. Beatty, and

W. W. Brannock, Eclogites and eclogites: their differences and similarities, Bull. Geol. Soc. Amer., 76, 483-508, 1965.

Cornelissen, A. K., and W. J. Verwoerd, The Bushmanland kimberlites and related rocks, Phys. Chem. Earth, 9, 71-80, 1975.

Cundari, A., Petrology of the leucite-bearing lavas in New South Wales, J. Geol. Soc. Aust., 20, 465-492, 1973.

Danchin, R. V., J. Ferguson, J. R. McIver, and P. H. Nixon, The composition of late stage kimberlite liquid as revealed by nucleated autoliths, Phys. Chem. Earth, 9, 235-245, 1975.

Davis, B. T. C., and F. R. Boyd, The join $Mg_2Si_2O_6$ - $CaMgSi_2O_6$ at 30 kilobars pressure and its application to pyroxene from kimberlites, J. Geophys. Res., 71, 3567-3576, 1966.

Dawson, J. B., Advances in kimberlite geology, Earth Sci. Rev., 7, 187-214, 1971.

Dawson, J. B., and W. E. Stephens, Statistical classification of garnets from kimberlite and associated xenoliths, J. Geol., 83, 589-607, 1975.

Edwards, A.C., J. F. Lovering, and J. Ferguson, High pressure basic inclusions from the Kayrunnera kimberlitic breccia pipe in New South Wales (in prep.).

Eggler, D. H., CO_2 as a volatile component of the mantle: the system Mg_2SiO_4-SiO_2-H_2O-CO_2, Phys. Chem. Earth, 9, 869-881, 1975.

Ellis, D. J., High pressure cognate inclusions in the Newer Volcanics of Victoria, Contrib. Mineral. Petrol., 58, 149-180, 1976.

Ferguson, J., R. V. Danchin, P. H. Nixon, Petrochemistry of kimberlite autholiths, in Lesotho kimberlites, P. H. Nixon (ed.), Lesotho National Development Corporation, Maseru, 285-293, 1973.

Ferguson, J., D. J. Ellis, and R. N. England, Unique spinel-garnet lherzolite inclusion in kimberlite from Australia, Geology, 5, 278-280, 1977.

Ferguson, J., H. Martin, L.O. Nicolayson, and R. V. Danchin, Gross Brukkaros: a kimberlite-carbonatite volcano, Phys. Chem. Earth, 9, 219-234, 1975.

Fesq, H. W., E. J. D. Kable, and J. J. Gurney, Aspects of the geochemistry of kimberlites from the Premier Mine, and other selected South African occurrences with particular reference to rare earth elements, Phys. Chem. Earth, 9, 687-707, 1975.

Frick, C., Kimberlitic ilmenites, Trans. Geol. Soc. S. Afr., 76, 85-94, 1973.

Fujii, T., and E. Takahaski, On the solubility of alumina in orthopyroxene coexisting with olivine and spinel in the system MgO - Al_2O_3 - SiO_2, Mineral J. (Japan), 8, 1976.

Green, D. H., the origin of basaltic and nephelinitic magmas, Trans. Leicester Lit. Phil. Soc., 64, 26-54, 1970.

Green, D. H., and A. E. Ringwood, The stability fields of aluminous pyroxene peridotite and garnet peridotite and their relevance to upper mantle structure, Earth Planet. Sci. Lett., 3, 151-160, 1967.

Green, D. H., and A. E. Ringwood, Mineralogy of peridotitic compositions under upper mantle conditions, Phys. Earth Planet. Interiors, 3, 359-371, 1970.

Gurney, J. J., and G. S. Switzer, The discovery of garnets closely related to diamonds in the Finsch pipe, South Africa, Contr. Mineral. Petrol., 39, 103-116, 1973.

Haggerty, S. E., The chemistry and genesis of opaque minerals in kimberlites, Phys. Chem. Earth, 9, 295-307, 1975.

Herzberg, C. T., and N. A. Chapman, Clinopyroxene geothermometry of spinel-lherzolites, Amer. Mineral., 61, 626-637, 1976.

Howells, S., and M. J. O'Hara Palaeogeotherms and the diopside-enstatite solvus, Nature, 254, 406-408, 1975.

Irvine, T. N., and W. R. A. Baragar, A guide to the chemical classification of the common volcanic rocks, Can. J. Earth Sci., 8, 523-548, 1971.

Irving, A. J., Geochemical and high-pressure experimental studies of garnet pyroxenite and pyroxene granulite xenoliths from Delegate basaltic pipes, Australia, J. Petrol., 15, 1-40, 1974.

Irving, A. J., On deducing palaeogeotherms from xenolith suites in basalts and kimberlites; A Heisenbergain uncertainty? Extended abstracts, Int. Conf. on Geothermometry and Geobarometry, Penn. State Univ., 1975.

Irving, A. J. and D. H. Green, Geochemistry and petrogenesis of the newer basalts of Victoria and South Australia, J. Geol. Soc. Aust., 23, 45-66, 1976.

Ito, K., and G. C. Kennedy, Melting and phase relations in a peridotite to 40 kilobars, Amer. J. Sci., 265, 519-538, 1967.

Kable, E. J. D., H. W. Fesq, and J. J. Gurney, The significance of the inter-element relationships of some minor and trace elements in South African kimberlites, Phys. Chem. Earth, 9, 709-734, 1975.

Lovering, J. F., and J. R. Richards, Potassium-argon age study of possible lower-crust and upper-mantle inclusions in deep-seated intrusions, J. Geophys. Res., 69, 4895-4901, 1964.

Lovering, J. F., and A. J. R. White, Granulitic and eclogitic inclusions from basic pipes at Delegate, Australia, Contr. Mineral. Petrol., 21, 9-52, 1969.

MacGregor, I. D., The system MgO - Al_2O_3 - SiO_2: solubility of Al_2O_3 in enstatite for spinel and garnet peridotite compositions, Amer. Mineral., 59, 110-119, 1974.

MacGregor, I. D., Petrologic and thermal structure of the upper mantle beneath South Africa in the Cretaceous, Phys. Chem. Earth, 9, 455-466, 1975.

McGetchin, T. R., Mechanism of emplacement of kimberlite and related breccia at Moses-Rock

dike, Utah. Program and extracts, Int. Symposium on Mechanical Properties and Processes in the Mantle, Flagstaff, Arizona, 7-8, 1970.

McIver, J. R., and J. Ferguson, Kimberlitic, melilititic, trachytic and carbonatite eruptives at Saltpetre Kop, Sutherland, South Africa (this vol.).

Mitchell, R. H., Geochemistry of magnesian ilmenites from kimberlites in South Africa and Lesotho, Lithos, 10, 29-38, 1977.

Mitchell, R. H., and A. O. Brunfelt, Rare earth element geochemistry of kimberlite, Phys. Chem. Earth, 9, 671-686, 1975.

Mori, T., Geothermometry of spinel lherzolites, Contr. Mineral. Petrol., 59, 261-279, 1977.

Mori, T., and D. H. Green, Pyroxenes in the system $Mg_2Si_2O_6$ - $CaMgSi_2O_6$ at high pressures, Earth Planet. Sci. Lett., 26, 277-286, 1975.

Mori, T., and D. H. Green Subsolidus equilibria between pyroxenes in the CaO - MgO - SiO_2 system at high pressures and temperatures, Amer. Mineral., 61, 616-625, 1976.

Nixon, P. H., Perspective, in Lesotho kimberlites, P. H. Nixon (ed.), Lesotho National Development Corporation, Maseru, 300-318, 1973.

Nixon, P. H., and F. R. Boyd, Petrogenesis of the granular and sheared ultrabasic nodular suite in kimberlites, in Lesotho kimberlites, P. H. Nixon (ed.), Lesotho National Development Corporation, Maseru, 48-56, 1973.

Obata, M., The solubility of Al_2O_3 in orthopyroxenes in spinel and plagioclase peridotites and spinel pyroxenite, Amer. Mineral., 61, 804-816, 1976.

O'Hara, M. J., The bearing of phase equilibria studies in synthetic and natural systems on the origin and evolution of basic and ultrabasic rocks, Earth Sci. Rev., 4, 69-133, 1968.

O'Hara, M. J., Upper mantle composition inferred from laboratory experiments and observation of volcanic products, Phys. Earth Planet. Interiors, 3, 236-245, 1970.

O'Hara, M. J., S. W. Richardson, and G. Wilson, Garnet-peridotite stability and occurrence in crust and mantle, Contr. Mineral. Petrol., 32, 48-68, 1971.

O'Hara, M. J., M. J. Saunders, and E. L. P. Mercy, Garnet-peridotite primary ultrabasic magma and eclogite; interpretation of upper mantle processes in kimberlite, Phys. Chem. Earth, 9, 571-604, 1975.

Pearce, J. A., and J. R. Cann, Tectonic setting of basic volcanic rocks determined using trace element analyses, Earth Planet. Sci. Lett., 19, 290-300, 1973.

Råheim, A. and D. H. Green, Experimental determination of the Fe-Mg partition coefficient for coexisting garnet and clinopyroxene, Contr. Mineral. Petrol., 48, 179-204, 1974.

Reed, S. J. B., and N. G. Ware, Quantitative electron microprobe analysis of silicates using energy-dispersive x-ray spectrometry, J. Petrol., 16, 499-518, 1975.

Rhodes, J. M., and J. B. Dawson, Major and trace element chemistry of peridotite inclusions from the Lashaine Volcano, Tanzania, Phys. Chem. Earth, 9, 545-577, 1975.

Ringwood, A. E., The chemical composition and origin of the Earth, in Advances in earth science, P. M. Hurley (Ed.), M.I.T. Press Cambridge, Mass., 287-356, 1966.

Sass, J. H., J. C. Jaeger, and R. J. Munroe, Heat flow and near-surface radioactivity in the Australian continental crust, U.S. Geol. Survey, Open-file Rept., 76-250, 1976.

Sobolev, N. V., Deep seated inclusions in kimberlites and the problem of the composition of the upper mantle (translated from Russian), American Geophysical Union, Washington, 279p., 1977.

Stracke, K. J., J. Ferguson, and L. P. Black, Structural setting of kimberlites in southeastern Australia (this vol.).

Stroh, J. M., Solubility of alumina in orthopyroxene plus spinel as a geobarometer in complex systems. Applications to spinel-bearing alpine-type peridotes, Contr. Mineral. Petrol., 54, 173-188, 1976.

Tucker, D. H., and K. D. Collerson, Lamprophyric intrusions of probable carbonatitic affinity from South Australia, J. Geol. Soc. Aust., 19, 387-391, 1972.

Wood, B. J., The application of thermodynamics to some subsolidus equilibria involving solid solutions, Fortschr. Mineral., 52, 21-45, 1975.

Wood, B. J. and S. Banno, Garnet-orthopyroxene and orthopyroxene-clinopyroxene relationships in simple and complex systems, Contr. Mineral. Petrol., 42, 109-124, 1973.

MINERALOGY OF THE TUNRAQ KIMBERLITE SOMERSET ISLAND, N.W.T., CANADA

Roger H. Mitchell

Department of Geology, Lakehead University, Thunder Bay, Ont., Canada

Abstract. The Tunraq diatreme is a multiple intrusion of massive kimberlite cut by a composite dike of massive and fissile micaceous kimberlite. Megacrysts common to all facies are niobian rutile, ilmenite and garnet. Ilmenites are magnesian (8.4-17.5%MgO), the most magnesian types occurring as mantles on rutile. Garnets are pyrope, Ti-pyrope, low Cr (<2.5%Cr_2O_3) pyrope and high chrome pyrope. The latter are considered to be derived by framentation of ultramafic xenoliths and the others to be true phenocrysts. Phlogopite (2-6%TiO_2) is present as laths which are rounded, distorted and kink banded, and appear to have formed prior to fluidization. Phenocrystal and groundmass olivines range in composition from Fo_{92} to Fo_{87}, the euhedral groundmass olivines being in general richer in FeO and CaO than the rounded pre-fluidization phenocrysts. Other groundmass minerals include iron rich serpentine, calcite, perovskite and spinel. The spinel assemblage is different to that observed in other Somerset Island kimberlites in being poorer in Al_2O_3. Spinels are all suhedral post-fluidization spinels of wide compositional range. In the massive kimberlite and fissile micaceous kimberlite the spinels range from titaniferous-magnesian-chromite to magnesian ulvospinel-ulvospinel-magnetite and in the massive micaceous kimberlite from titaniferous-magnesian-chromite to Ti-free magnetite. All three facies are considered to have been derived from the same batch of mantle derived magma by differing degrees of fractional crystallization at low pressure. The generation of micaceous kimberlites is considered not to be a function of low pressure differentiation of kimberlite as the trend towards micaceous kimberlite, as exemplified by the presence of Al_2O_3 poor spinels, is induced in the mantle; low pressure differentiation merely emphasizes that trend. Thus the occurrence of kimberlite and micaceous kimberlite within the same kimberlitic magma province probably reflects different degrees of partial melting of the mantle and/or differentiation under high pressure.

Introduction

The Tunraq (Inuit; a protective spirit) kimberlite is the only occurrence of micaceous kimberlite within the Somerset Island kimberlite province (figure 1). The kimberlite is one of a group of kimberlites lying on the eastern bank of the Elwin River, eastern Somerset Island and is an ovoid diatreme c.350 m., in its maximum dimension. The intrusion is cut by an east-west tributary of the Elwin River which exposes a 130 m., true outcrop on its southern bank. The remainder of the diatreme area is composed of a frost heaved regolith of kimberlite and country rock limestone fragments. The bulk of the kimberlite is a black coarse grained massive kimberlite containing widely variable amounts of angular to rounded country rock xenoliths. Garnet and ilmenite are visible in hand specimen. Petrographically the kimberlite consists of garnet, ilmenite, olivine and phlogopite phenocrysts set in a groundmass of spinel, perovskite, serpentine and calcite. The eastern portion of the outcrop in the stream bank is cut by a composite dike (c.20 m.) of micaceous kimberlite. The bulk of this dike is a massive grey-green micaceous kimberlite containing large (1 cm.) phenocrysts of phlogopite and olivine together with rare garnet and ilmenite set in a groundmass of spinel, perovskite, serpentine and calcite. Phlogopite is randomly oriented, and this differs from the black kimberlite petrographically only in the modal amount of phlogopite. Within the massive micaceous kimberlite is a thin (2 m.) dike of fissile fine grained green micaceous kimberlite. The fissility is imparted by a relatively small amount of small crystals of oriented phenocrystal mica. Large phenocrysts of mica are absent and olivine phenocrysts are rare. The groundmass is identical to that of the other facies but is richer in calcite. The western edge of the diatreme can be seen to be in sharp contact with the country rocks. The contact kimberlite is a very fine grained grey rock consisting of olivine phenocrysts pseudomorphed

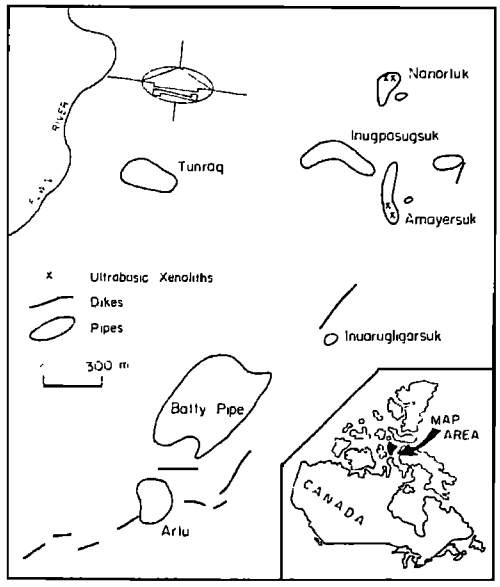

Fig. 1. The Batty Bay group of kimberlites and the location of the Tunraq kimberlite, Somerset Island, N.W.T., Canada.

by calcite set in a groundmass of perovskite, spinel, serpentine and calcite laths. This rock is gradational into massive black kimberlite containing abundant country rock xenoliths with phlogopite and fresh olivine phenocrysts set in a groundmass of perovskite, spinel, serpentine, calcite laths and irregular lobate patches of calcite and serpentine. This is the only occurrence of carbonate segregations at Tunraq similar to the segregations attributed to liquid immiscibility in other Somerset Island kimberlites (Clarke and Mitchell, 1975). Typically at Tunraq the carbonate does not segregate but remains intimately intermixed with the serpentine groundmass.

Minerals in the kimberlite were analysed at Purdue University using an automated MAC 500 microprobe (Finger and Hadidiacos, 1972).

Rutile

Rutile has been found only as discrete grains (0.04 - 0.2 mm.) rimmed by magnesian ilmenite in heavy mineral concentrates. Rutile has been described in kimberlites as rutile-ilmenite intergrowths derived by the breakdown of armalcolite (Haggerty, 1975), as a primary phase (?) being replaced by ilmenite (Mitchell, 1973), as rutile serpentine rims about magnesian ilmenite (Clarke and Mitchell, 1975) and as epitaxial overgrowths of rutile on perovskite (Mitchell and Clarke, 1976). This latter paragenesis of rutile, typical of the Peuyuk kimberlite, is absent in the Tunraq kimberlite.

Rutile compositions are given in Table 1, the principal variation being in the Cr_2O_3 and Nb_2O_5 contents. Rutile of a similar composition, although with slightly higher Fe_2O_3 contents has been described by Dawson and Smith (1977) from lherzolite and mica-amphibole-rutile-ilmenite-diopside (MARID) xenoliths in kimberlite. Such rutiles differ notably from the low Cr_2O_3(0.5%) and low Nb_2O_5(0.5%) rutiles associated with diamonds and eclogites (Smith and Dawson, 1975; White and Taylor, 1973). Dawson and Smith (1977) consider that the MARID xenoliths crystallized from a kimberlite magma at 500-100 km., depth. This together with the occurrence of metasomatically introduced rutile in lherzolite xenoliths in kimberlite (Harte and Gurney, 1975) indicates that niobian rutile is probably a primary early crystallizing phase in kimberlite magmas.

Ilmenite

Tunraq is unusual amongst the Somerset Island kimberlites in that both facies of the intrusion contain abundant discrete grains of magnesian ilmenite. The grains range up to 1 mm., in size, are typically rounded and rimmed by perovskite. Representative analysis are given in Table 2 and the compositional variation illustrated in figure 2. Zoning within individual grains, composed of three to four single crystals ranges from moderate e.g. 13.6 to 15.3% MgO over 1 mm., to insignificant over 0.4 mm. Zonation when present is irregular relative to the margins of the crystals. The ilmenites are similar to ilmenites in other kimberlites in exhibiting a wide range in composition (MgO, 8.4-17.5%), and especially to the high MgO group of ilmenites found in the Frank Smith, Wesselton and Premier kimberlites (Mitchell,1977a; Gurney et al. 1973). The most magnesian ilmenites occur as mantles upon rutile, a feature observed at Wesselton by Mitchell (1973). Compositional trends are interpreted to be from high to low MgO contents with increasing Fe_2O_3 contents. No correlation of Cr_2O_3 with MgO is evident (r=0.3) and no "parabolic relationship" between these two elements of the kind described by Haggerty (1975) is present. MnO exhibits a good positive correlation with MgO(r=0.76), the opposite to that observed by Mitchell (1977a) in several South African examples (r=0.46). Niobium

Table 1. Representative analyses of rutile in the Tunraq kimberlite.

	1	2	3	4	5	6
TiO_2	93.3	92.8	94.9	93.5	98.1	98.3
Al_2O_3	0.1	0.0	0.1	0.0	0.2	0.2
Cr_2O_3	3.9	3.2	3.4	3.9	0.0	0.1
Fe_2O_3*	0.9	1.2	0.2	0.3	0.5	0.7
MnO	0.0	0.0	0.0	0.0	0.0	0.0
MgO	0.2	0.9	0.0	0.1	0.3	0.1
Nb_2O_5	1.8	1.5	1.8	1.3	1.2	0.3
	100.3	99.6	100.5	99.3	99.5	99.7

*Total Fe expressed as Fe_2O_3

contents are 0.0-2.1% Nb_2O_5 and similar to other kimberlite ilmenites in being enriched in niobium relative to ilmenite from other basic and ultrabasic rocks (Mitchell 1977a).

Garnet

Garnet occurs as rounded megacrysts up to 1 mm., in diameter in both facies of the kimberlite. Colors range from orange to deep red to purple with increasing MgO, Cr_2O_3 and CaO and decreasing FeO. Megacryst garnets (76 analyses) fall into 3 groups using the statistical classification of Dawson and Stephens (1975) i.e. groups 1 (34%), group 2 (3%) and group 9 (63%). The major element variation is illustrated in figure 3 which shows that group 9 garnets are divisable into 2 groups, a relatively iron rich low Cr (<2.5% Cr_2O_3) group and a relatively iron poor high Cr(>2.5% Cr_2O_3) group of variable Ca content. The high Cr group 9 garnets are identical to garnets found in garnet lherzolite xenoliths in Somerset Island kimberlites and elsewhere (figure 3). Dawson and Stephen's (1975) group 9 is apparentely bimodal as it stands and probably incorporates garnets of two different origins. Further subdivision on the basis of CaO and Cr_2O_3 should be attempted. The high Cr group 9 garnets found in this and many other kimberlites, are best considered to be derived by fragmentation of ultrabasic xenoliths, even though such xenoliths are apparently lacking at Tunraq.

The groups 1 and 2 garnets vary in their Mg/Mg+Fe ratios from 0.82-0.76, increasing Fe being accompanied by a slight increase in Ca (figure 3). Groups 1 and 2 have high TiO_2 and low Cr_2O_3 relative to group 9 garnets. Dawson and Stevens (1975) and Mitchell (1978) consider that 1 and 2 garnets probably form a continuum of compositions rather than 2 discrete groups. Figure 3 indicates that low Cr, group 9 garnets might also be included in this continuum.

The groups 1 and 2 and low Cr group 9 garnets are compositionally very similar to garnet

Table 2. Representative analyses of ilmenite.

	1	2	3	4	5	6	7	8
TiO_2	48.0	49.0	49.3	52.5	53.2	52.2	54.0	55.9
Cr_2O_3	1.2	0.7	1.7	0.2	0.2	0.4	0.8	1.9
Fe_2O_3*	14.4	15.5	13.6	10.2	9.7	11.1	9.1	6.0
FeO*	27.9	24.4	23.1	23.8	22.0	19.8	19.7	18.5
MgO	8.4	10.9	11.7	12.8	14.3	15.0	16.0	17.6
MnO	0.2	0.3	0.3	0.2	0.2	0.4	0.3	0.4
	100.1	100.8	99.7	99.4	99.5	98.9	99.8	100.4
Mol.% end member molecules								
$MnTiO_3$	0.4	0.6	0.6	0.4	0.5	0.8	0.6	0.8
$MgTiO_3$	30.1	37.9	41.1	44.4	48.9	51.3	54.1	58.6
$FeTiO_3$	56.0	47.6	45.6	46.2	42.2	38.1	37.3	34.6
Cr_2O_3	0.5	0.3	0.8	0.1	0.1	0.2	0.3	0.8
Fe_2O_3	13.0	13.6	12.0	8.9	8.3	9.6	7.8	5.1

*Fe_2O_3 and FeO calculated by Carmichael's (1967) method.

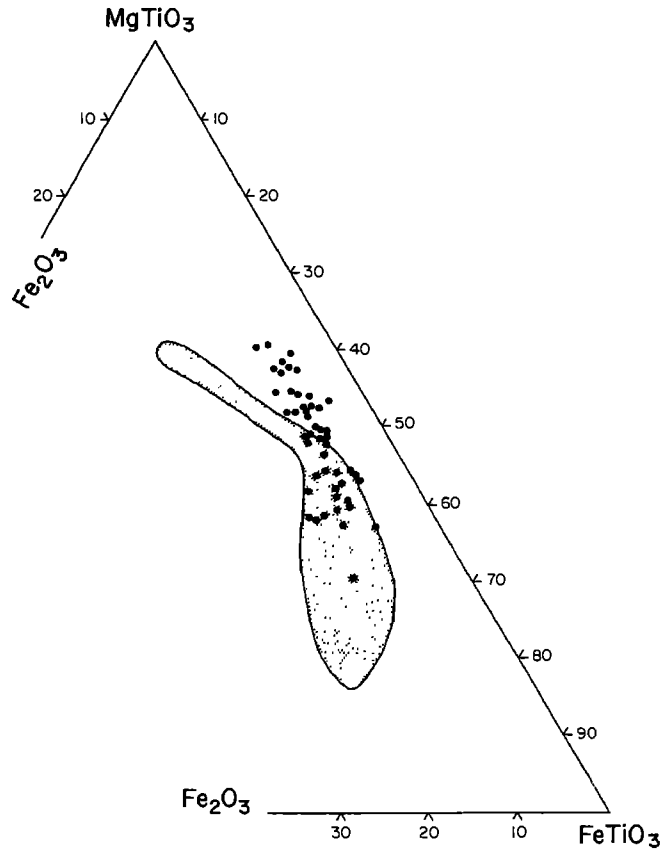

Fig. 2. Composition of Tunraq ilmenites. Compositional field of Southern African ilmenites from Mitchell (1977a).

megacrysts from the Frank Smith and Monastery kimberlites (Boyd and Dawson, 1972), the Artur de Paiva kimberlite (Boyd and Danchin, 1974), the Sloan diatreme (Eggler and McCallum, 1974) and the Elwin Bay monticellite-kimberlite (Mitchell, 1978), which are now being recognized as characteristic megacrysts of kimberlite which are not of xenocrystal origin and which appear to be true phenocrysts.

The Tunraq garnets are in general slightly richer in iron than garnets from Elwin Bay where the Mg/Mg+Fe is 0.83 to 0.79, and are distinctly poorer in TiO_2 e.g. Tunraq group 1 garnets comprise 93% of the total group 1 and 2 population, whilst at Elwin Bay they make up 41% of that population. In addition garnets at Elwin Bay are very much larger (1-2 cm.). The relative enrichment in Ti of the Elwin Bay garnets may be a reflection of the apparent failure of this kimberlite to crystallize abundant ilmenite during the pre-fluidization crystallization history.

The Tunraq and Elwin Bay garnet data indicate that subtle differences are present in the nature of the garnet suites between individual diatremes with the same kimberlite province.

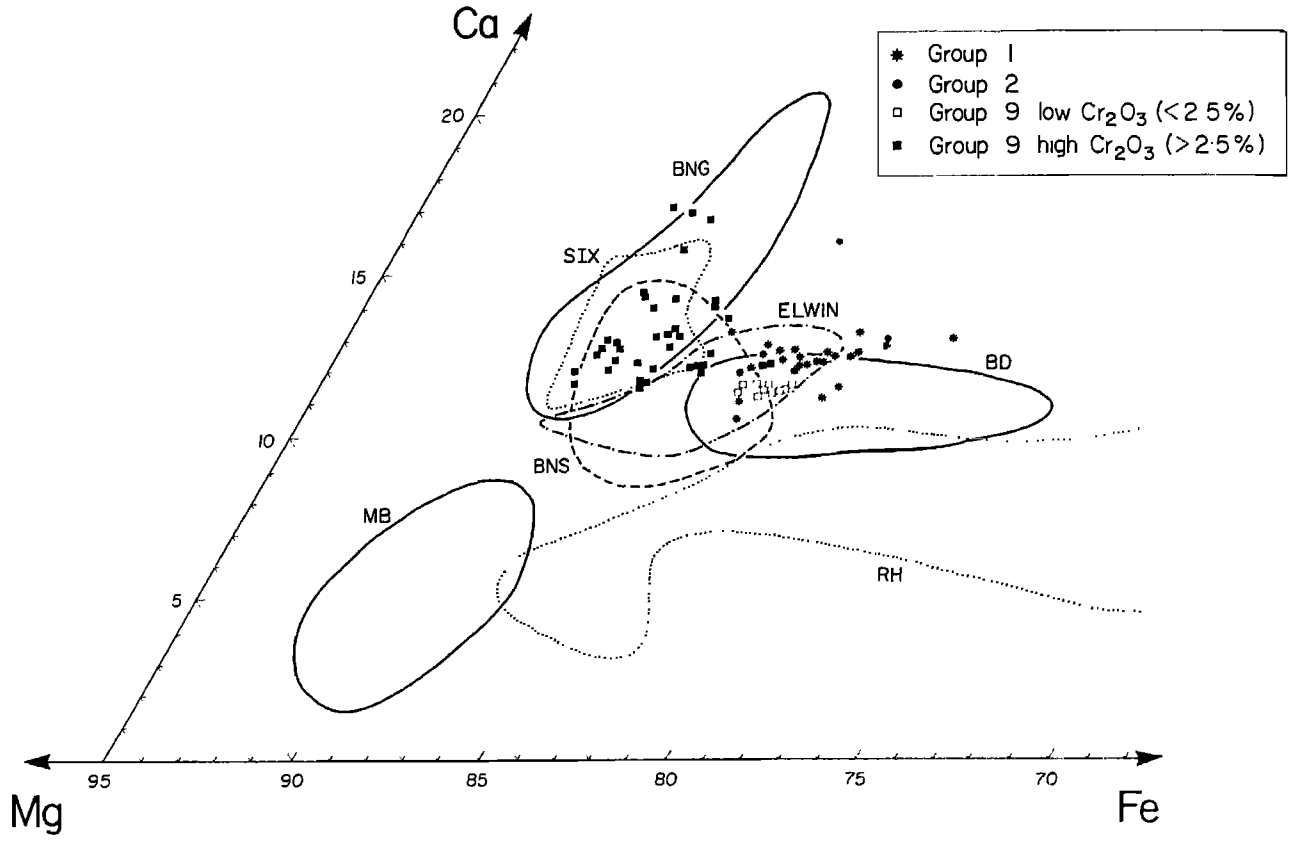

Fig. 3. Composition of garnets in Elwin Bay kimberlite compared with that of other mantle derived garnets. MB, diamonds (Meyer and Boyd, 1972); BNG, BNS, granular and sheared lherzolites, Lesotho (Boyd and Nixon, 1975); SIX, Somerset Island lherzolites (Mitchell, 1977b, unpub. data); BD, Frank Smith and Monastery megacrysts (Boyd and Dawson, 1972); RH, Kimberley megacrysts (Reid and Hanor, 1970); ELWIN, Elwin Bay megacrysts (Mitchell, 1978a).

Phlogopite

Mica, in the Tunraq kimberlite, massive and fissile micaceous kimberlite, is present only as phenocrysts. Groundmass (post-fluidization) mica appears to be absent. All of the phenocrysts are either broken, rounded, twisted or kink banded and exhibit undulatory extinction. Chloritization is rare but replacement by penetration of calcite along cleavage planes is common. All the micas are single crystals and there are no aggregates of mica which might suggest that a cumulate body of mica or glimmerite xenoliths has been fragmented. Deformation of the mica probably occurred during fluidization. A prefluidization origin for the mica implies crystallization at depth, either in the mantle or lower crust. Representative compositions are given in Table 3. No compositional differences exist between micas in the different facies of the kimberlite and very little range (0.87-0.92) is found in Mg/Mg+Fe ratios. TiO_2 and Cr_2O_3 show considerable variation (but no correlation with FeO). Figure 4 illustrates that high TiO_2 (>2.0%) contents are characteristic of the Tunraq micas. Mica compositions lie well outside of the field of mica megacrysts in kimberlite as defined by Dawson and Smith (1975) and this field should therefore

Table 3. Representative analyses of mica megacrysts.

	1	2	3	4	5
SiO_2	41.7	40.4	39.6	39.0	37.8
TiO_2	1.6	3.8	5.4	5.3	5.5
Al_2O_3	12.0	12.7	13.8	13.2	13.0
Cr_2O_3	0.2	0.0	0.4	0.9	1.1
FeO*	5.3	6.2	4.8	4.4	4.7
MnO	0.0	0.0	0.0	0.0	0.0
MgO	24.1	22.5	21.6	21.3	21.0
CaO	0.7	0.0	0.0	0.0	0.0
Na_2O	0.3	0.3	0.3	0.2	0.2
K_2O	9.5	10.1	10.1	9.7	10.0
NiO	0.1	0.1	0.1	0.1	0.1
	94.8	96.1	96.2	94.1	93.4
Mg/Mg+Fe	0.89	0.87	0.89	0.90	0.89

*Total Fe expressed as FeO

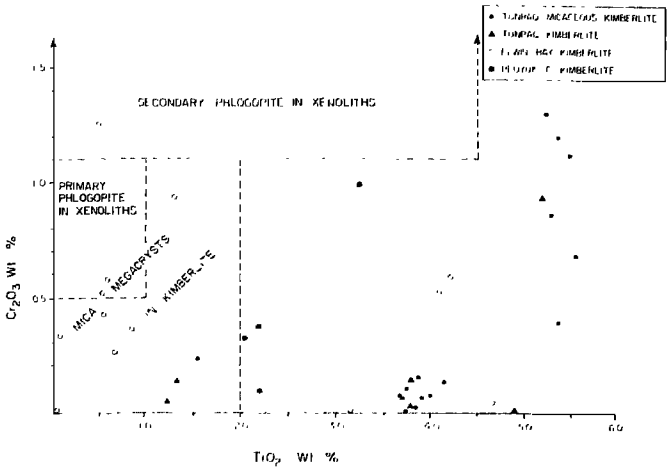

Fig. 4. Plot of Cr_2O_3 vs. TiO_2 for micas from Tunraq and other Somerset Island kimberlites. Compositional fields for other micas from Dawson and Smith (1975) and Carswell (1975).

be extended up to at least 6% TiO_2. None of the micas lie within the fields of primary and secondary phlogopite in xenoliths. Micas of comparable composition to the low Cr_2O_3 (<0.5%) moderate TiO_2(1-4%) phenocrysts are known from MARID xenoliths but the Tunraq micas have generally higher Mg/Mg+Fe ratios and lower NiO contents (figure 5), as well as having no deficiency in Al^{IV}. No compositional data exist comparable with the high TiO_2 high Cr_2O_3 phlogopites. Figure 4 also gives data for Elwin

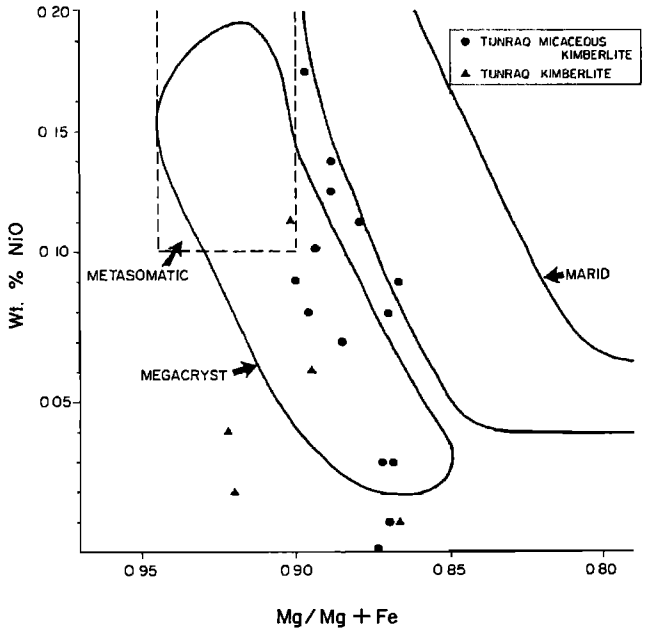

Fig. 5. Plot of NiO vs. Mg/Mg+Fe for Tunraq micas. Compositional fields for other micas from Dawson and Smith (1977).

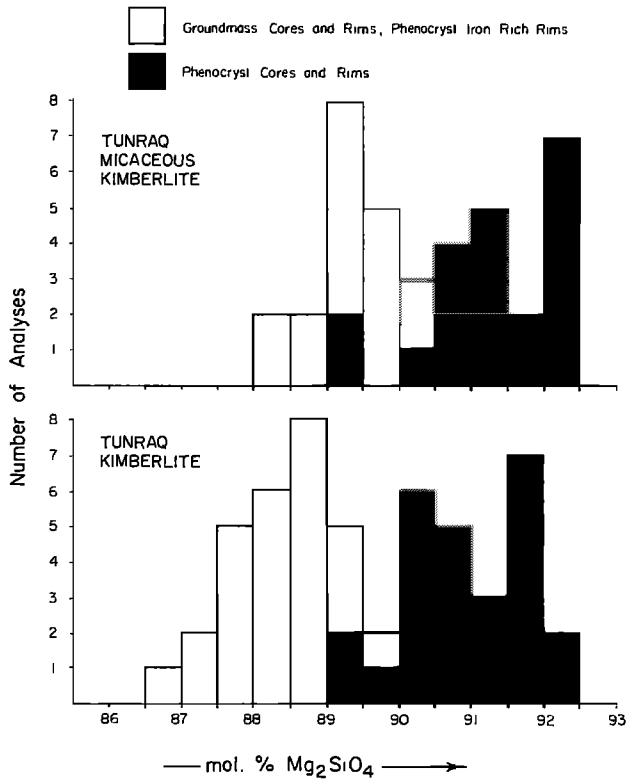

Fig. 6. Compositions of phenocrystal and groundmass olivines in Tunraq kimberlite and micaceous kimberlite.

Bay mica. This kimberlite contains both phenocrystal and groundmass mica. The evolutionary trend of mica compositions being towards lower TiO_2 and Cr_2O_3 contents. Micas are in general less titaniferous than those found at Tunraq. By analogy, the Tunraq micas may evolve from high to low TiO_2 and Cr_2O_3 contents.

Olivine

In both the kimberlite and micaceous kimberlite olivine occurs in two generations, an earlier one of rounded to subhedral phenocrysts and a second generation of euhedral to subhedral groundmass olivines. Because the rounding of phenocrystal olivine by the fluidized intrusive process is not as pronounced as in many kimberlites and because of the pervasive secondary alteration it is difficult to distinguish phenocrystal and groundmass olivines on the basis of habit. An arbitrary size limit of 1 mm. is taken as being the boundary between the two types. All of the olivines are extensively pseudomorphed by a yellow-brown serpentine. This serpentine is an iron rich variety (9.7% FeO) apparently peculiar to kimberlites (Emeleus and Andrews, 1975; Mitchell, 1978) and which can form either as a primary or secondary phase. Iron rich serpentine of this type only appears

Table 4. Representative analyses of spinels.

	1	2	3	4	5	6	7	8	9	10	11	12	13	14	15	16	17
TiO_2	0.4	0.5	2.9	3.2	0.9	1.5	3.0	4.8	7.6	11.5	14.7	16.7	18.2	15.7	7.0	6.2	0.0
Al_2O_3	11.4	13.2	10.7	10.3	2.7	2.3	1.8	2.3	3.9	7.5	8.0	8.7	8.4	6.2	0.2	0.3	0.0
Cr_2O_3	54.2	55.1	50.3	51.6	58.7	61.0	55.4	47.8	43.9	27.1	19.3	2.4	1.5	3.8	11.0	26.5	0.0
FeO*	19.2	15.8	21.4	19.4	25.1	21.9	26.6	33.2	28.3	36.9	41.2	52.2	52.4	51.0	70.4	58.1	92.0
MnO	0.3	0.3	0.3	0.4	0.5	0.4	0.4	0.5	0.5	0.5	0.5	0.5	0.5	0.5	0.3	0.3	0.2
MgO	13.9	14.7	14.3	15.3	11.4	12.1	11.1	9.6	13.8	14.5	15.3	15.7	15.0	16.0	5.2	5.2	0.9
	99.4	99.6	99.9	100.2	99.2	99.3	98.3	98.1	97.8	98.8	96.1	97.2	97.3	94.1	96.1	94.1	93.1
Recalculated analyses+																	
Fe_2O_3	7.3	4.5	7.8	7.1	11.0	8.0	10.4	13.2	12.1	18.1	20.6	32.2	30.5	28.6	46.0	32.5	69.4
FeO	12.6	11.7	14.3	13.0	15.2	14.7	17.2	21.3	17.4	20.6	22.6	23.2	25.9	25.3	29.0	28.9	29.5
	100.1	100.0	100.7	100.8	100.3	100.0	99.3	99.5	99.1	99.7	100.8	99.3	99.9	100.2	98.7	99.8	100.1
$MgAl_2O_4$	20.5	23.8	18.6	17.8	4.5	4.3	3.2	4.1	6.6	11.5	11.6	12.0	11.5	8.5	0.3	0.4	-
Mg_2TiO_4	1.3	1.7	9.8	10.7	3.0	5.3	10.4	16.4	24.3	33.7	33.5	31.9	30.0	34.9	15.0	15.8	-
Mn_2TiO_4	-	-	-	-	-	-	-	-	-	0.2	0.8	0.7	0.7	0.8	0.5	0.6	-
Fe_2TiO_4	-	-	-	-	-	-	-	-	-	-	6.6	11.7	16.6	15.3	5.1	3.0	-
$MnCr_2O_4$	0.8	0.9	0.8	0.9	1.4	1.2	1.0	1.2	1.1	0.7	-	-	-	-	-	-	-
$MgCr_2O_4$	40.9	41.0	31.2	34.7	44.2	45.6	34.4	17.0	19.9	-	-	-	-	-	-	-	-
$FeCr_2O_4$	23.8	24.8	26.5	24.2	27.0	29.4	32.6	38.8	28.5	27.2	18.8	2.2	1.4	3.5	11.3	29.1	-
Fe_3O_4	12.7	7.8	13.0	11.7	19.4	14.2	18.2	22.4	19.6	26.7	28.7	42.2	39.8	37.1	67.7	51.1	-

*Total Fe expressed as FeO. + Fe_2O_3 and FeO calculated by Carmichael's (1967) method; 1-2, aluminous-magnesian-chromite; 3-4, titaniferous-magnesian aluminous chromite (TIMAC); 5-11, titaniferous-magnesian-chromite (TMC); 12-14, magnesian ulvospinel-ulvospinel-magnetite (MUM); 15-16, titaniferous chromite (TC); 17, magnetite.

to form under conditions of low oxygen fugacity and when iron in serpentinized olivines is not expelled as magnetite during the alteration process. Calcite pseudomorphs occur, but are not characteristic of the Tunraq kimberlites. Olivines rarely show stress induced undulatory extinction. The variation in composition of olivine in the different facies is shown in figure 6. Early phenocrysts are essentially homogeneous (Fo_{92}-Fo_{90}) with thin iron enriched margins (Fo_{90}-Fo_{88}). Groundmass olivines are weakly zoned from cores of Fo_{92}-Fo_{90} to margins of Fo_{87}. Reverse zoning occurs rarely from Fo_{86}-Fo_{88}. Figure 6 illustrates that there is no significant difference in composition between kimberlite and micaceous kimberlite olivines. Phenocrystal olivines can be distinguished from groundmass olivine by the latter invariably containing greater than 0.1% CaO. The low CaO content of the olivines, even when crystallizing from a fluid which eventually crystallizes calcite, is in agreement with Warner and Luth's (1973) data for the Mg_2SiO_4-$CaMgSiO_4$ solvus which indicates that olivines contain less than 1 mol.% $CaMgSiO_4$ in solid solution at low temperatures. NiO is strongly depleted in the margins of some of the olivines but remains constant from core to rim in others. The NiO depleted rims are similar to those found by Mitchell and Fritz (1973) in the Peuyuk kimberlite, in which the Ni depletion is contemporaneous with the crystallization of nickeliferous pyrite. Ni-bearing sulphides have not yet been noted at Tunraq.

No xenocrystal olivines derived by the fragmentation of ultramafic xenoliths are evident at Tunraq, except perhaps the rare strained olivines. The presence of xenocrystal garnet and pyroxene indicates that such olivines might be present, but no chemical and few textural criteria are available to distinguish them from phenocrystal olivines.

The range in olivine composition seen at Tunraq is similar to that of olivine in other Somerset Island kimberlites and demonstrates that olivine compositions do not reflect the different degrees or directions of evolution of kimberlite magma within individual diatremes. Olivines in kimberlites seem on a world wide basis to commence crystallization at about Fo_{92}, in both phenocrysts and groundmass and evolve to iron rich compositions of about Fo_{87} (Mitchell, 1973, Emeleus and Andrews, 1975, Boyd and Clement, 1978).

Spinel

Representative analyses of spinels are given in Table 4. Spinel compositions are plotted in figure 7 as end member spinel molecules in a reduced iron spinel prism as outlined by Mitchell and Clarke (1976). This type of projection in which total iron is calculated as FeO is useful for kimberlite spinels, which have probably formed under relatively reducing conditions, in that it includes all the major elements determined. The prism does not however indicate possible variations in Fe_3O_4 and $MgFe^{3+}O_4$. Magnetite variations are shown in figure 8.

In each phase of the diatreme, spinels occur

initially as large (up to 0.5 mm.) euhedral to subhedral crystals. The latest spinels are all small (0.05 mm.) euhedral crystals. No atoll spinels (Mitchell and Clarke, 1976) are present. All the spinels appear to be post-fluidization spinels as no large rounded transparent red aluminous-magnesian-chromite (AMC), typical of the Peuyuk and Elwin Bay kimberlites is found. TiO_2 poor spinels at Tunraq which plot near the base of the spinel prism are Al_2O_3 deficient and opaque and lie at the Cr_2O_3 rich end of the Peuyuk AMC compositional trend. Each facies of the diatreme has a distinct spinel assemblage.

Spinel crystallization in the kimberlite commenced with the relatively uncommon Al_2O_3 poor aluminous-magnesian-chromites (Table 4, anals. 1-2) and evolved via rare titaniferous-magnesian-aluminous-chromite (TIMAC, Table 4, anals. 3-4) to large crystals of titaniferous-magnesian-chromite (TMC, Table 4, anals. 5-11). Within the TMC spinels Al increases as Ti increases. Increasing Fe^{3+} and Ti at approximately constant Fe/Fe+Mg ratios leads to the development of members of the magnesian ulvospinel-ulvospinel-magnetite series (MUM, figures 7 and 8; Table 4, anals. 12-14) of hexahedral habit. Ti-free magnetite does not terminate the spinel compositional trend.

The massive micaceous kimberlite initially crystallized TMC identical to that of the early spinels in the kimberlite but the trend towards Ti enrichment at constant Fe/Fe+Mg ratio does not exceed 3% TiO_2, therefore members of the MUM series are not developed. Spinels richest in TiO_2 (6-7%) are unusual in being Al and Mg poor titaniferous chromites (TC, Table 4, anals. 15-16) and are shown in figure 7 as the 5 analyses with Fe/Fe+Mg ratios greater than 0.8. The most abundant spinel is a Ti-free magnetite (Table 4, anal. 17) of octahedral habit. The TC spinels and the lack of MUM spinels indicate that in this facies spinels were rapidly depleted in Al and Mg and although insufficient data are as yet available to accurately delineate this trend it is possible that the trend is initially along the axis of the spinel prism with increasing Fe/Fe+Mg ratios, culminating in the formation if Ti-free magnetite.

The fissile micaceous kimberlite initially crystallized TMC with TiO_2 greater than 7%, which evolved into members of the MUM series. The trend is identical to that of the kimberlite spinels excepting that the early spinels of low TiO_2 content are absent. No Ti-free magnetite is formed.

Spinel compositional trends are in general similar to those determined for other kimberlites (Haggerty, 1975, Mitchell and Clarke, 1976) in showing Ti and Fe^{3+} enrichment as crystallization proceeds. Figures 8 and 9 illustrate that the Tunraq spinels are deficient in Al_2O_3 relative to the Peuyuk spinels, and that they have a similar evolutionary trend towards MUM spinels at approximately constant Fe/Fe+Mg. The lack of

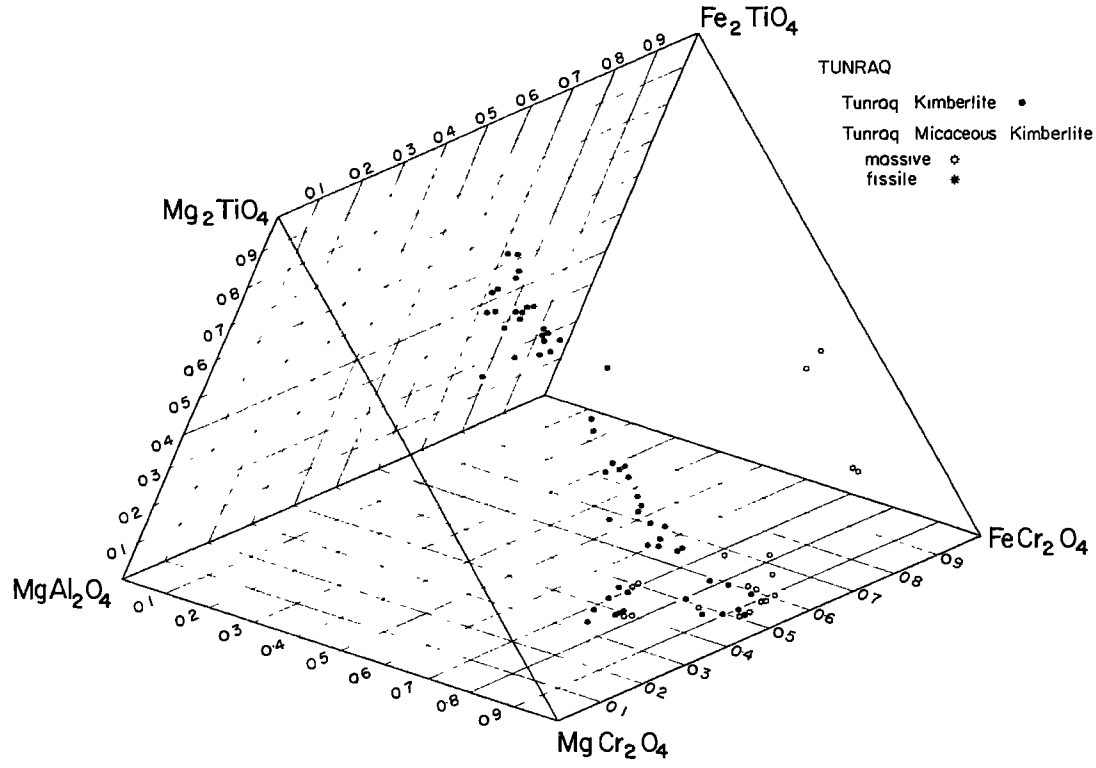

Fig. 7. Composition of spinels plotted in a reduced iron spinel prism.

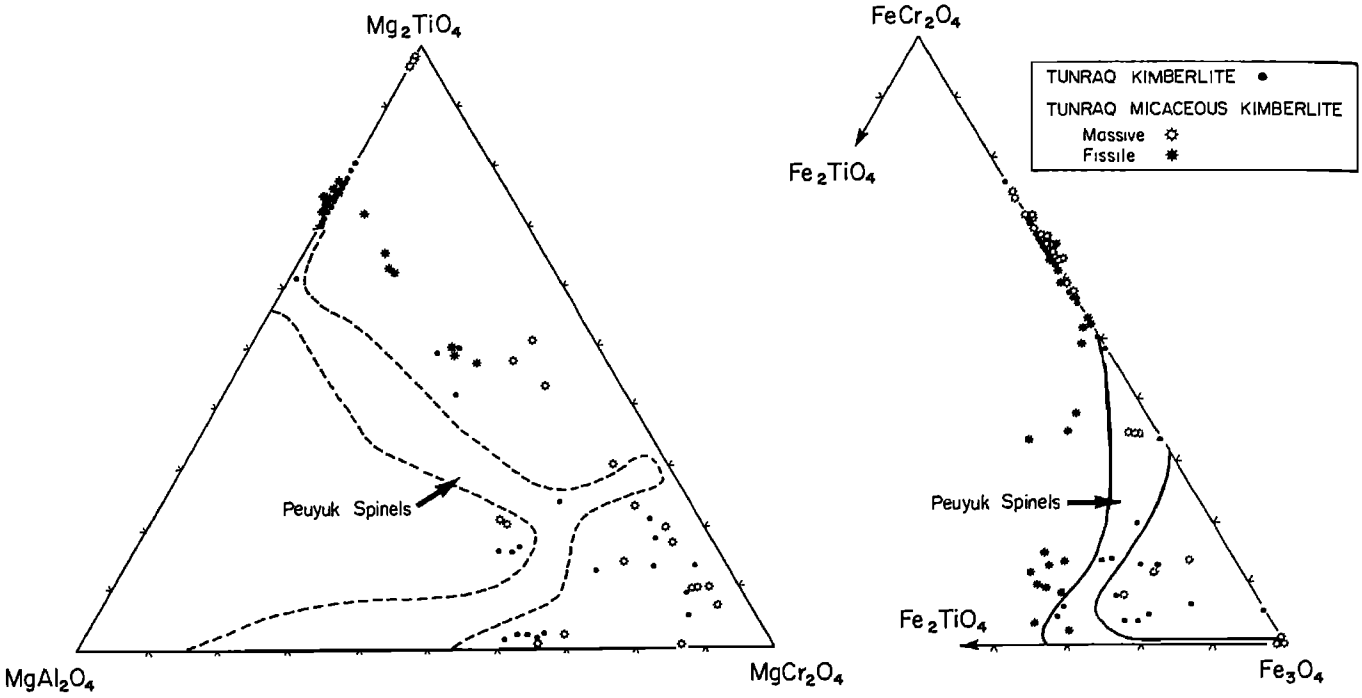

Fig. 8. Ternary molecular percentages of $MgAl_2O_4$-$MgCr_2O_4$-Mg_2TiO_4 and $FeCrO_4$-Fe_3O_4-Fe_2TiO_4 of spinels. Molecular components calculated as in Mitchell and Clarke (1976).

Al_2O_3 rich AMC spinels at Tunraq is well illustrated in figure 8. Compositional data for spinels in other micaceous kimberlites is unavailable except for a study of the Kirkland Lake (Ontario) micaceous kimberlite (Mitchell, 1978b), the compositional trend of which is shown in figure 9. Those spinels are even more depleted in Al and have higher Fe/Fe+Mg ratios than the Tunraq spinels. The evolutionary trend is however very similar. The Kirkland Lake spinels do not show the magnesian depletion trend of the Tunraq massive micaceous kimberlite. Comparable spinels to those of this latter trend are seen in the titaniferous chromites exsolved from ilmenite in the Premier kimberlite (Danchin and D'Orey, 1972), the Ti-poor chromites in diamond (Meyer and Boyd, 1972) and the overall trend of lunar spinels (Haggerty, 1972).

Perovskite

Perovskite occurs in abundance as a groundmass phase as discrete euhedral to rounded brown crystals and as reaction rims upon magnesian ilmenite megacrysts. The reation rims demonstrate that magnesian ilmenite was not in equilibrium with the magma which eventually formed the groundmass. The perovskites lack the epitaxial rutiles characteristic of the Peuyuk kimberlite (Mitchell and Clarke, 1976), and common in the Elwin Bay kimberlite (Mitchell, 1978a).

Representative partial analyses are given in Table 5. Low totals are due to the presence of rare earths not determined. No differences in the composition of perovskite in the different facies exists. The perovskites are similar in composition to perovskite in other kimberlites, in having low and constant FeO contents and significant Nb_2O_5 contents. Where perovskite and ilmenite coexist it is found that the perovskite always had the greater Nb_2O_5 content, confirming that perovskite is the major carrier of Nb in kimberlites (Mitchell, 1972).

Clinopyroxene

Clinopyroxene is found as single crystals only in heavy mineral concentrates, it does not at any time crystallize as a post-fluidization liquidus phase. The clinopyroxene is a green chrome diopside (1.6-2.3% Cr_2O_3) with Mg/Mg+Fe ratios of 0.92-0.94 and Ca/Ca+Mg ratios of 0.446-0.484. The diopsides are identical to pyroxenes found in lherzolite xenoliths in other Somerset Island kimberlites and give solvus equilibration temperatures of 905-1060°C (Davis and Boyd, 1966), similar to those of coarse granular garnet lherzolite (Mitchell, 1977b). The clinopyroxenes are undoubtedly derived by fragmentation of such nodules. No orthopyroxene has yet been found, possibly because of the ease with which this mineral is serpentinized.

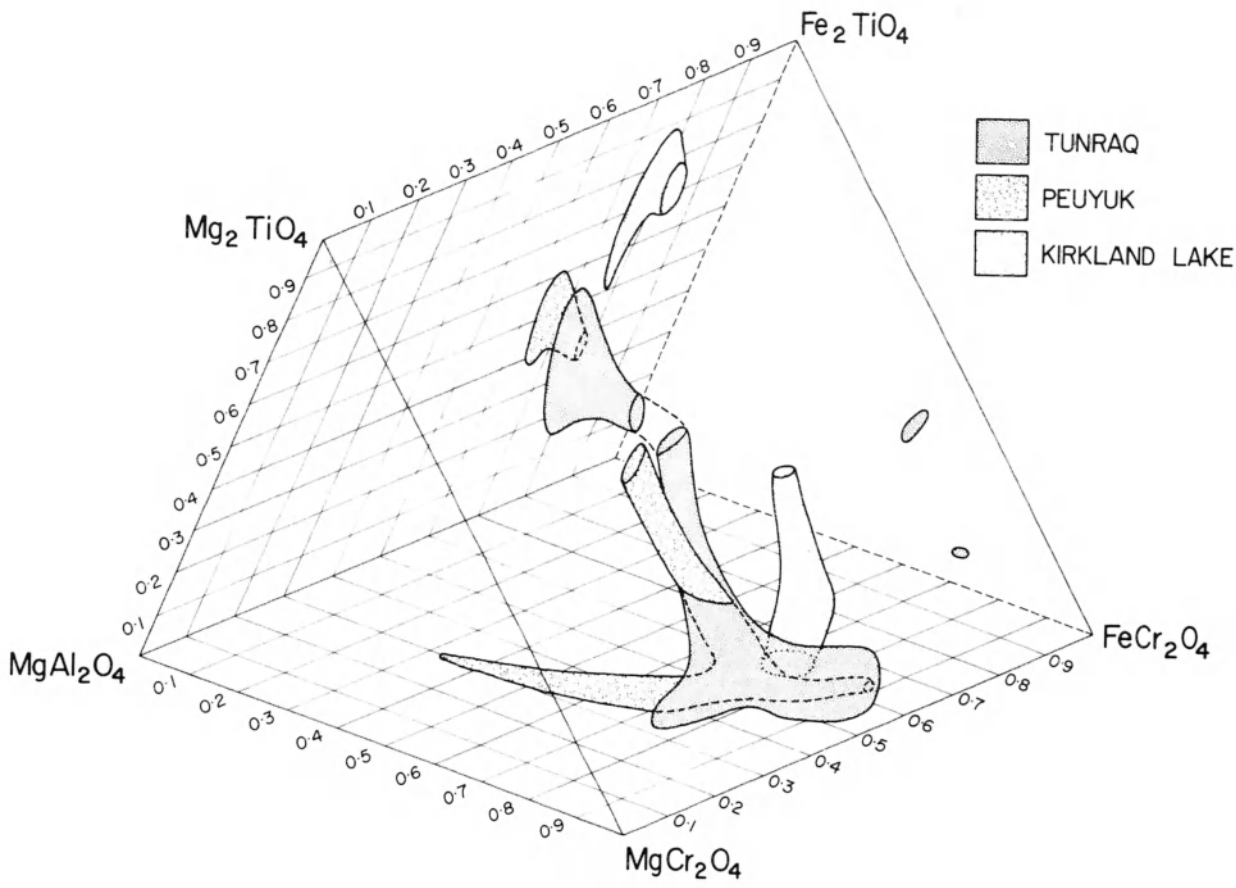

Fig. 9. Compositional fields of spinels from the Tunraq, Peuyuk (Mitchell and Clarke, 1976) and Kirkland Lake kimberlites (Mitchell, 1978).

Discussion

The mineralogy and petrography of the Tunraq kimberlite indicates that the phases which are common to all three facies and which crystallized in the mantle are niobian rutile (minor), magnesian ilmenite, pyrope, (groups 1, 2, low Cr 9) and probably olivine. With decreasing pressure as the magma ascends towards the crust pyrope and ilmenite cease to crystallize and phlogopite replaces garnet as the aluminous liquidus phase in the lower crust and uppermost parts of the mantle. This crystallization sequence is very different to that deduced for the Elwin Bay and Peuyuk kimberlites in which aluminous-magnesian-chromite is abundant, ilmenite is absent or insignificant and in which only minor amounts of phlogopite formed. The Tunraq kimberlites demonstrate that the evolutionary trend towards micaceous kimberlite is established in the mantle and that this trend is merely emphasized in the lower crust and post-fluidization crystallization history. The "least evolved" magma at crustal levels at Tunraq is represented by the massive black kimberlite. (Although this kimberlite lacks abundant modal mica it might be thought of as being a micaceous kimberlite because of the inherent alumina deficiency in the post-fluidization spinel compositions). This kimberlite crystallized only a small amount of mica prior to emplacement and spinels evolved towards MUM spinels at approximately constant Fe/Fe+Mg ratios. The fissile micaceous kimberlite can be thought of as being a late fraction of this magma because of the similar spinel composition trend. In contrast abundant crystallization of phlogopite prior to emplacement resulted in the very different spinel evolutionary trend of the massive micaceous kimberlite. This may have been the result of pooling of the magma or a slower ascent rate of that magma batch. At Tunraq the post-fluidization crystallization did not result in the seperation of immiscible carbonate rich fluids except on a minor scale at the margins of the intrusion.

Detailed mineralogical studies of three different kimberlite diatremes within the Somerset Island kimberlite province e.g. the Peuyuk kimberlite and calcareous kimberlite (Mitchell and Clarke, 1976), the Elwin Bay monticellite

Table 5. Representative composition of perovskite.

	1	2	3	4	5	6	7
CaO	38.8	38.5	38.1	37.8	37.5	38.8	36.0-40.2
TiO_2	56.2	55.3	55.7	54.8	54.8	56.9	52.4-55.9
Al_2O_3	0.2	0.2	0.2	0.3	0.2	0.2	0.2- 0.4
Cr_2O_3	0.1	0.1	0.1	0.1	0.1	0.2	- -
FeO*	1.1	1.2	0.9	1.1	1.2	0.9	1.0- 2.1
MnO	0.0	0.1	0.1	0.0	0.0	0.0	- -
MgO	0.5	0.4	0.5	0.5	0.4	0.4	0.1- 0.2
Nb_2O_5	0.6	0.8	0.4	0.6	0.5	0.5	0.6- 1.5
	97.6	96.4	96.0	95.3	94.9	97.8	

*Total Fe expressed as FeO.
1-2, kimberlite; 3-4, massive micaceous kimberlike; 5-6, fissile micaceous kimberlite; 7, Range in composition of kimberlite perovskite (Mitchell 1972).

kimberlite (Mitchell 1978) and the Tunraq micaceous kimberlite, have shown that each diatreme exhibits both subtle and gross differences in their post and pre-fluidization crystallization histories, and that the observed differentiation trends are imposed upon the individual magma batches in the mantle. All three diatremes are a part of same cycle of kimberlite magmatism and the differences probably reflect different degrees of partial melting and/or amounts of high pressure differentiation. In particular the replacement of aluminous-magnesian-chromite by phlogopite and the development of the Tunraq micaceous kimberlite might be due to smaller amounts of partial melting (or compositional differences) of the source material than required to generate the Peuyuk kimberlite e.g. enrichment of the melt is K_2O and H_2O.

It will be of interest to determine whether or not each of Somerset Island diatremes has distinct mineralogical characteristics. If so, such studies should provide much evidence concerning the petrogenesis of kimberlite.

Acknowledgements. This work is supported by the National Research Council of Canada. Henry Meyer is thanked for access to the Purdue University microprobe. The field work was undertaken as a part of the Geological Survey of Canada's Project Boothia, and J.W. Kerr is thanked for much help and logistical assistance. The assistance and hospitality provided by personnel of Diapros Canada Ltd., is highly appreciated and R.J. Davies and J.B. Howkins in particular are thanked for their interest in this project. Marsha Mitchell is thanked for field assistance.

References

Boyd, F.R., and C.R. Clement, Compositional zoning of olivines in kimberlite from the De Beers Mine, Kimberley, South Africa. Carnegie Institution of Washington Geophysical Laboratory Yearbook 76, 485-493, 1977.

Boyd, F.R., and R.V. Danchin, Discrete nodules from the Artur de Paiva kimberlite, Angola. Carnegie Institution of Washington Yearbook, 73, 278-282, 1974,

Boyd, F.R., and J.B. Dawson, Kimberlite garnets and pyroxene-ilmenite intergrowths. Cargegie Institution of Washington Year Book, 71, 373-378, 1972.

Boyd, F.R. and P.H. Nixon, Origins of ultramafic nodules from some kimberlites of Northern Lesotho and the Monastery mine. Physics and Chemistry of the Earth, 9, 431-454, 1975.

Carmichael, I.S.E., The iron-titanium oxides of salic volcanic rocks and their associated ferromagnesian silicates. Contribution to Mineralogy and Petrology, 14, 36-74, 1967.

Carswell, D.A., Primary and secondary phlogopites and clinopyroxenes in garnet lherzolite xenoliths. Physics and Chemistry of the Earth, 9, 417-429, 1975.

Clarke, D.B. and R.H. Mitchell, Mineralogy and petrology of the Somerset Island kimberlite, N.W.T., Canada. Physics and Chemistry of the Earth, 9, 123-235, 1975.

Danchin, R.V. and F. D'Orey, Chromian spinel exsolution in ilmenite from the Premier Mine, Transvaal, South Africa. Contributions to Mineralogy and Petrology, 35, 43-49, 1972.

Davis, B.T.C. and F.R. Boyd, The join $Mg_2Si_2O_6$-$CaMgSi_2O_6$ at 30 kb. pressure and its application to pyroxenes from kimberlite. Journal of Geophysical Research, 71, 3567-3576, 1966.

Dawson, J.B. and J.V. Smith, Chemistry and origin of phlogopite megacrysts in kimberlite. Nature 253, 336-338, 1975.

Dawson, J.B. and J.V. Smith, The MARID (mica-amphibole-rutile-ilmenite-diopside) suite of xenoliths in kimberlite. Geochemica et Cosmochimica Acta., 41, 309-323, 1977.

Dawson, J.B. and W.E. Stephens, Statistical classification of garnets from kimberlite and associated xenoliths. Journal of Geology, 83, 589-607, 1975.

Eggler, D.H. and M.E. McCallum, Xenoliths in diatremes of the Western United States. Carnegie Institution of Washington Year Book, 73, 254-300, 1974.

Emeleus, C.H. and J.R. Andrews, Mineralogy and petrology of kimberlite dike and sheet intrusions and included peridotite xenoliths from South West Greenland. Physics and Chemistry of the Earth, 9, 179-197, 1975.

Finger, L.E. and C.Q. Hadidiacos, Electron microprobe automation. Carnegie Institution of Washington Year Book, 71, 598-600, 1972.

Gurney, J.J., H.W. Fesq and E.J.D. Kable, Clinopyroxene-ilmenite intergrowths from Lesotho kimberlites: a re-appraisal. In. P.H. Nixon (Editor), Lesotho Kimberlites, Lesotho National Development Corporation, 238-253, 1973.

Haggerty, S.E., Luna 16. An opaque mineral study and a systematic examination of compositional

variations of spinels from Mare Fecunditatis. Earth and Planetary Science Letters, 13, 328-352, 1972.

Haggerty, S.E., The chemistry and genesis of opaque minerals in kimberlite. Physics and Chemistry of the Earth 9, 295-307, 1975.

Harte, B. and J.J. Gurney, Ore mineral and phlogopite mineralization within ultramafic nodules from the Matsoku kimberlite pipe, Lesotho. Carnegie Institution of Washington Year Book, 74, 528-536, 1975.

Meyer, H.O.A. and F.R. Boyd, Composition and origin of crystalline inclusions in natural diamonds. Geochemica et Cosmochimica Acta. 36, 1255-1273, 1972.

Mitchell, R.H., Composition of perovskite in kimberlite. American Mineralogist 57, 1748-1753, 1972.

Mitchell, R.H. Magnesian ilmenite and its role in kimberlite petrogenesis. Journal of Geology 81, 301-311, 1973a.

Mitchell, R.H., Composition of olivine, silica activity and oxygen fugacity in kimberlites. Lithos 6, 65-81, 1973b.

Mitchell, R.H., Geochemistry of magnesian ilmenites from kimberlites in South Africa and Lesotho. Lithos 10, 29-37, 1977a.

Mitchell, R.H., Ultramafic xenoliths from the Elwin Bay kimberlite, the first Canadian Paleogeotherm. Canadian Journal of Earth Science, 14, 1202-1210, 1977b.

Mitchell, R.H., Mineralogy of the Elwin Bay kimberlite, Somerset Island, N.W.T., Canada. American Mineralogist, 63, 47-57, 1978a.

Mitchell, R.H., Composition of spinels from the Upper Canada Mine micaceous kimberlite, Kirkland Lake, Ontario. Canadian Mineralogist, in press, 1978b.

Mitchell, R.H. and D.B. Clarke, Oxide and sulphide mineralogy of the Peuyuk kimberlite, Somerset Island, N.W.T., Canada. Contributions to Mineralogy and Petrology 56, 157-172, 1976.

Mitchell, R.H. and P. Fritz, Kimberlite from Somerset Island, District of Franklin, N.W.T., Canadian Journal of Earth Science, 10, 757-764, 1973.

Reid, A.M. and J.S. Honor, Pyrope in kimberlites. American Mineralogist 55, 1374-1379, 1970.

Smith, J.V. and J.B. Dawson, Chemistry of Ti-poor spinels, ilmenites and rutiles from peridotite and eclogite xenoliths. Physics and Chemistry of the Earth 9, 309-322, 1975.

Warner, R.D. and W.C. Luth, Two phase data for the join monticellite ($CaMgSiO_4$) - forsterite (Mg_2SiO_4): Experimental results and numerical analysis. American Mineralogist 58, 998-1008, 1973.

White, A.J.R. and J.R. Taylor, Some trace elements in rutile from eclogites and their implications. First International Conference on Kimberlites. Extended Abstracts, 309-311, 1973.

MINERALOGICAL STUDIES ON THE DIAMONDIFEROUS KIMBERLITE OF THE WAJRAKHARUR AREA, SOUTHERN INDIA

Jagannadham Akella

University of California, Lawrence Livermore Laboratory, Livermore, California 94550

P. Satyanarayana Rao

Geological Survey of India, Southern Circle, Madras-6, India

Robert H. McCallister

Department of Geosciences, Purdue University, West Lafayette, Indiana 47907

F. R. Boyd

Geophysical Laboratory, 2801 Upton St., N.W., Washington, D.C. 20008

Henry O. A. Meyer

Department of Geosciences, Purdue University, West Lafayette, Indiana 47907

Abstract. Diamond-bearing kimberlites occur in Andhra Pradesh at Wajrakharur and Lattavaram. In general, the kimberlites at the surface are elliptical with their longer axes trending approximately N70°E. The pipes have intruded PC Dharwarschists, granites, and gneisses but have very limited surface exposure.

The kimberlite near Lattavaram is hard and compact, but slight differences in mineralogy are obvious between the two pipes at this locality. One kimberlite pipe consists predominantly of phenocrysts of olivine (Fo_{92}) partly serpentinized in a medium- to fine-grained groundmass of magnetite-rich spinel, chromite, phlogopite, and monticellite. Pectolite is also present. However, a remarkable feature of this kimberlite is the ubiquitous occurrence of needle-like crystals of nickel sulfide in the serpentine.

The second kimberlite at Lattavaram also is predominantly of serpentinized olivine, picroilmenite, and minor garnet in a matrix of calcite, phlogopite, and opaque phases including Cr-rich ilmenite. Minor phases such as sphene and perovskite are also present. Olivine ranges between Fo_{88} to Fo_{92}; and garnet is about 75% pyrope, 11% grossular with between 2.5 to 3 wt % Cr_2O_3. Up to the present time, a few mantle xenoliths have been recovered from drill cores, but crustal xenoliths (e.g., amphibolites) are not uncommon.

Introduction

Although diamond has been known in India from historical times, the presence of kimberlite has been the subject of much speculation and controversy. However, in the late nineteenth century, igneous rocks, supposedly the host rocks for diamonds at Pannah and Wajrakharur, were described but were discounted as being kimberlite (Foote, 1889; Lake, 1890). The source rock for the diamonds was subsequently investigated by others (Pitchamuthu and Rao, 1932; Mathur and Singa, 1963; Mehr, 1953) but generally considered that kimberlite was not present. In 1963, Rao and Phadtre, after a preliminary study of the geology and petrography for four igneous bodies near Wajrakharur, Andhra Pradesh, concluded they were kimberlitic. The present study concentrates on the mineralogy and mineral chemistry of phases from two of the diatremes near Lattevarems, which is six miles SSW of Wajrakharur. Unfortunately, paucity of ultramafic xenoliths from these diatremes makes it impossible to draw any major conclusion regarding the upper mantle petrology beneath the South-Indian shield.

Geology

Four pipe-like bodies are located in the region of Wajrakharur. Two are near this village and the other two are near Lattavaram six miles SSW of Wajrakharur. These bodies are somewhat oval in shape, trending roughly N70°E and have intruded pre-cambrian Dharwar Schists, granite, and gneiss.

The Archaean early Proterozoic rocks of the Indian shield are divided into six provinces on the basis of structural trends and litho-stratigraphic developments (Naqvi et al., 1974). The rocks in the present area of study are classed into the Dharwar province of Mysore and Andhra Pradesh. Sarkar (1968) assigned 2.5-3.0 b.y. for the Dharwars, and the post-Dharwarian granites and gneiss are assigned 1.2 b.y. Murty of the Geological Survey of India (private communication) from field observations believes that the kimberlites and associated rocks could be around 1025 m.y.

The material in the pipes is highly weathered near the surface and consists of serpentine, calcite, clay minerals, and fragments of crustal and local host country rock. At Lattavaram the

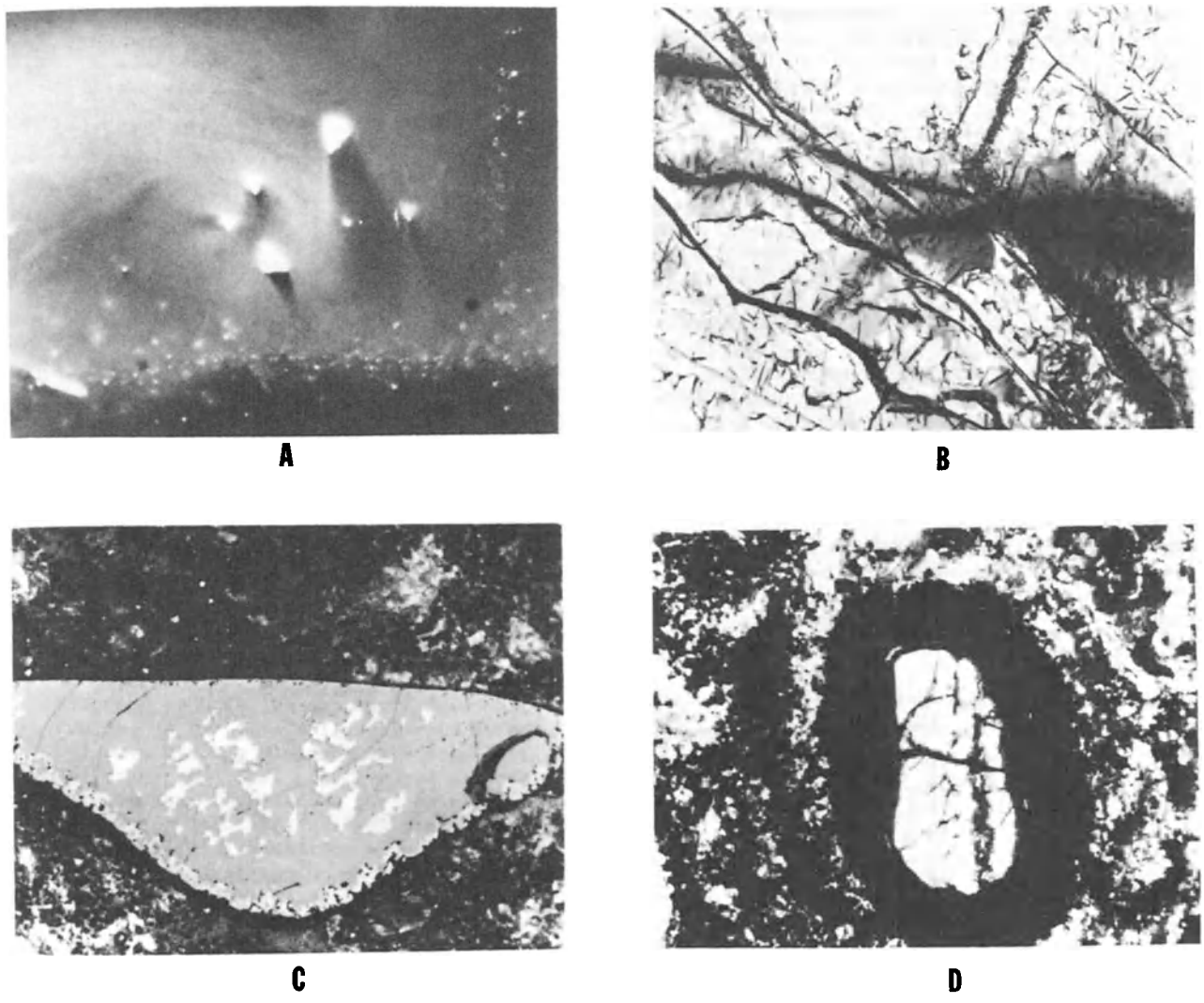

Fig. 1. (a) Nickel-sulfide phase. The grains are ∿2μm in size. (b) Needle-like nickel-sulfide phase in serpentine. The cross section of needles is triangular (A). Note some unaltered olivine also in the serpentine. (c) Ilmenite in L-2 kimberlite rock. Note rutile inside and along the grain boundary. (d) Thick kelyphitic rim around the garnet. An intermediate zone of alteration is present between the unaltered garnet and the kelyphitic rim.

kimberlite is somewhat more durable and compact than at Wajrakharur, and it is thus possible to distinguish slight mineralogical and petrographic differences between the two pipes. Rao and Phadtre (1963) report the occurrence of eclogite and peridotite xenoliths from this locality, recovered from the drill cores. For the most part, xenoliths consist of amphibotite or other crustal fragments only.

Petrography and Mineral Chemistry

Petrographically the two kimberlites near Lattavaram are distinct. One kimberlite (L_1) is dark blue in color, hard and compact, and it is fine- to medium-grained and porphyritic. This kimberlite consists of relatively small (average about 1 mm) phenocrysts of olivine in a very dark, fine-grained matrix of serpentine, calcite, phlogopite and magnetite-rich spinel. Minor monticellite and pectolite were also noted. Sometimes monticellite is seen as a thin rim around the Mg-olivine.

Olivine is colorless in polarized light with high birefringence and 2V nearly 90°. Serpentinized olivine phenocrysts are interesting in that the veins of serpentine contain numerous minute needles approximately 2 μm in length and with triangular cross sections. We analyzed this phase using electron microprobe; and after making appropriate corrections for the serpentine

surrounding the needle, a maximum content of 72 wt % Ni was obtained for this mineral. This strongly suggests it is hazelwoodite (Ni_3S_2). The occurrence of this phase is believed to be due to late stage sulfurization of the olivine, accompanying serpentinization, with the Ni being derived from the original olivine, which contains 0.2 to 0.3 wt % NiO (Figs. 1a and 1b).

Chemical analyses of various phases in L-1 are presented in Table 1. Olivine from the L-1 pipe rock is generally close to Fo_{92} in composition. Unaltered olivine contains 0.2-0.3 wt % NiO and is very low in chromium. Monticellite in this rock has ∿8 wt % FeO in it. The Ca:Mg:Fe ratio of monticellite is 47:44:9.

Spinels in this rock appear to be of two types; a minor number are rich in chromium (7-11 wt % Cr_2O_3, Table 1) whereas the second group have generally about 2-4 wt % Cr_2O_3. These two types could not be distinguished from the other optically under microscope. The Mg/(Mg + Fe) ratio for these spinels ranges from 0.12 to 0.15, and the Cr/(Cr + Al) ratio ranges between 0.65 to 0.86. Akella et al. (1976) have shown experimentally that the Cr/(Cr + Al) ratio of the spinel is sensitive to the Mg/(Mg + Fe) ratio of the spinel. Even though both types of spinels in these kimberlites have similar Mg/(Mg + Fe) ratio, their chrome contents are different by a factor of three. It is conceivable that the Cr_2O_3-rich spinels have minute inclusions of chromite, which we were not able to identify.

TABLE 1. Representative analyses of minerals from Lattavaram-1 kimberlite.

	Olivine	Spinel (1)	Spinel (2)	Monticellite	Pectolite	Serpentine
SiO_2	41.50	---	---	37.25	52.40	42.57
TiO_2	0.02	9.80	7.32	0.27	0.04	0.02
Al_2O_3	---	0.95	1.17	0.06	0.50	0.97
Cr_2O_3	0.09	2.63	10.69	---	0.04	0.13
FeO	7.84†	27.73	24.18	8.05†	0.52†	1.07†
Fe_2O_3		51.52	47.76			
MgO	50.86	6.69	7.16	21.63	0.23	39.46
CaO	0.10	---	---	32.46	33.73	0.77
MnO	0.12	0.54	0.58	0.29	0.13	0.23
Na_2O	---	---	---	0.06	9.34	0.09
K_2O	---	---	---	0.05	0.04	0.05
NiO	0.34	---	---	0.02	0.01	---
Co	---	0.12	0.14	---	---	---
Cu	---	0.07	0.03	---	---	---
Total	100.87	100.05	99.03	100.14	96.99 (+OH)	85.36 (+OH)
	Number of cations for O = n × 1000					
Si	1000			999		
Ti	---			5		
Al	---			1		
Cr	1			---		
Fe	157			187		
Mg	1827			864		
Ca	2			933		
Mn	2			6		
Na	---			3		
K	---			1		
Ni	6			---		
$\frac{Mg}{(Mg+Fe)}$	0.921			0.822		

†Total Fe as ferrous iron.

Fig. 2. A typical field outcrop of the L-2 kimberlite.

The second kimberlite (Fig. 2) at Lattavaram (L-2) is much more coarsely grained than L-1. The rock is porphyritic, the phenocrysts being mostly olivine, and occasionally garnet. Olivine phenocrysts are for the most part serpentinized. Other major phases are ilmenite and garnet. Minor phases such as sphene and perovskite have also been observed. These two phases are seen as discrete grains in thin section. The groundmass consists predominantly of serpentine, calcite, minor phlogopite, and opaque phases, including spinel and ilmenite. One noteworthy feature in this rock is the absence of the nickel-sulphide phase in the serpentine.

Chemical analyses of various phases from L-2 kimberlite are presented in Table 2. Composition of L-2 olivines is similar to those from L-1 kimberlites, except for the lower Mg/(Mg + Fe) ratio for the former. Ilmenite (Fig. 1c) ranges from 30-50 μm in size and is evenly distributed in the thin section. Chemically there are two species of ilmenites, one of which is six times richer in chromium (ilmenite 1, Table 2) compared to the other. The chrome-rich ilmenite has ∿50% geikilite component in it, whereas the chrome-poor variety has ∿32%. Geikilite component of these ilmenites is compatible with that reported for kimberlite ilmenites in the literature. It is presumed that the earlier formed ilmenites are more iron-rich and also relatively poorer in chromium, and as the crystallization progressed, the later formed ilmenites have become magnesian with higher concentrations of chrome. It is not presently understood whether the as-

TABLE 2. Representative analyses of minerals in Lattavaram-2 kimberlite.

	Olivine	Garnet	Ilmenite(1)	Ilmenite(2)	Phlogopite	Serpentine	Sphene
SiO_2	41.28	42.77	0.24	0.16	39.92	42.42	29.71
TiO_2	0.05	0.11	53.37	53.18	0.58	0.05	37.08
Al_2O_3	0.02	21.53	0.30	0.38	13.64	0.74	1.34
Cr_2O_3	0.06	2.82	4.03	0.79	0.03	0.02	---
FeO†	11.23	7.58	23.73	35.48	2.80	4.32	1.66
MgO	48.23	21.28	16.43	10.08	25.67	37.76	0.13
CaO	0.21	4.48	0.34	0.02	0.01	0.12	27.53
MnO	0.15	0.36	0.54	0.25	0.02	0.20	0.05
Na_2O	0.03	---	0.01	0.06	---	---	---
K_2O	---	---	---	---	10.10	---	0.01
NiO	0.23	---	0.05	---	0.01	0.19	0.01
Tot.	101.49	100.93	99.04	100.39	92.78 (+OH)	85.82 (+OH)	97.52 (+OH) (+F)
	Number of cations for O = n × 1000						
Si	1002	3012	11	8			
Ti	---	3	1835	1891			
Al	---	1785	16	21			
Cr	1	153	145	29			
Fe	228	444	907	1403			
Mg	1746	2235	1120	710			
Ca	5	336	17	1			
Mn	2	21	21	10			
Na	1	---	---	3			
K	0	---	---	---			
Ni	4	---	---	---			
$\frac{Mg}{(Mg+Fe)}$	0.884	0.835	0.553	0.336			

†Total Fe as ferrous iron.

sumed progressive crystallization took place during the process of kimberlite formation or during its ascent before emplacement.

Garnets in L-2 kimberlite are light pink in color and have very thick kelyphitic rims around them (Fig. 1d). Chemical analyses for the garnets are presented in Table 2. These garnets contain 2.5-3 wt % Cr_2O_3 and are very poor in TiO_2 (0.11 wt %). Reid and Hanor (1970) have shown for the garnets from the Kimberley area that the Cr_2O_3 content of the kimberlite garnets is low, <0.6 wt %, except in the more magnesian variety, Mg/(Mg + Fe) > 0.81, where Cr_2O_3 varies from 1.6 to 2.7 wt %. The garnets they examined were also low in MnO ≤0.4 wt %. Garnets from L-2 pipe have an Mg/(Mg + Fe) ratio 0.84, and the amounts of Cr_2O_3 and MnO in them is in agreement with Reid and Hanor's observation. The Ca:Mg:Fe ratio of these garnets is 11:74:15. Boyd and Nixon (1973) and Akella (1974) have shown that natural kimberlitic garnets and garnets synthesized at ∿45-kilobars pressure, contain 10-14 mole % of the grossular molecule. The grossular content of L-2 garnets is in the range of their observation. Analysis for the L-2 kimberlite garnets, plotted in the Ca:Mg:Fe ternary diagram, is well within the composition field for garnets from pipes in the Kimberley area (Reid and Hanor, 1970).

Xenoliths

Numerous fragments of amphibolite and/or other crustal materials are common in the kimberlite pipes. However, in the kimberlite pipe rocks near Lattavaram, we found two eclogite xenoliths that are approximately 6 cm in cross section and a fragment of a diopside phologopite chip. An ilmenite megacryst was also recovered from the highly weathered pipe rock near Wajrakharur.

The dominant phases in the eclogite FRB 549 are Fe-rich garnet and diopside (Table 3) with a grain size of 1-3 mm. Irregular patches of white alteration material (clay?) can be seen between the grains. The diopside is inhomogeneous in Ti, Al, Fe, Mg, and Na. The second eclogite chip FRB 551 contains garnet that is considerably more magnesian than the garnet from FRB 549 (Table 3).

Ilmenite megacryst FRB 548 from the Wajrakharur kimberlite pipe contains inclusions of diopside and rather Fe-rich garnet (Table 4). The Mg(Mg+Fe) ratio for the garnet is 0.374, and it contains ∿19% grosular. The giekilite content of

TABLE 3. Chemical analyses for diopside and garnet from eclogites, FRB-549 and FRB-551.

	FRB-549		FRB-551	
Oxide	Diopside	Garnet	Diopside	Garnet
SiO_2	52.16	39.51	55.61	42.54
Al_2O_3	4.23	21.57	2.77	22.11
TiO_2	0.70	0.07	0.30	0.21
Cr_2O_3	0.07	0.11	1.02	2.05
FeO	6.49	23.04	1.18	6.54
MgO	12.91	8.43	16.49	21.11
CaO	22.02	6.45	21.68	4.64
MnO	0.06	0.60	0.06	0.35
Na_2O	1.37	0.00	1.62	0.02
K_2O	0.00	0.00	0.00	0.00
NiO	0.00	0.00	0.00	0.00
Total	100.01	99.78	100.73	99.57
	Number of cations for O = n × 1000			
Si	1925	3027	1984	3018
Al	184	1947	116	1849
Ti	19	4	8	11
Cr	2	7	29	115
Fe	200	1476	35	388
Mg	710	963	877	2233
Ca	871	529	829	353
Mn	2	39	2	21
Na	98	---	112	3
K	---	---	---	---
Ni	---	---	---	---
	4012	7992	3992	7990
Mg/(Mg+Fe)	0.780	0.395	0.961	0.852

the ilmenite is ∿39% and is within the range found for other kimberlitic ilmenites.

Discussion

The geologic occurrence, plus the petrographic character of these rocks, and the similarity of mineral compositions with other well-studied South African kimberlites are sufficient evidence to support Rao and Phadtre (1963) in their conclusion that these are true kimberlites.

It is possible to estimate the temperature of equilibration for the xenoliths found in these kimberlites using the Mg-Fe partitioning data between the coexisting garnet and clinopyroxene (Akella and Boyd, 1974; Raheim and Green, 1974). Eclogite sample FRB 551 gives an equilibration temperature of 945°C using Akella and Boyd's data, and FRB 549 eclogite gives 880°C. However, the estimated temperature for FRB 549 eclogite is not too meaningful in view of the compositional inhomogeneities in the diopside. Temperatures estimated using Raheim and Green's equation at 30 kbar are approximately 20°C lower than those obtained with Akella and Boyd's data.

TABLE 4. Chemical analyses of minerals from ilmenite megacryst, FRB-548.

Oxide	Diopside	Garnet	Ilmenite
SiO_2	50.86	39.14	0.00
Al_2O_3	5.10	21.26	0.55
TiO_2	0.53	0.10	52.96
Cr_2O_3	0.07	0.13	0.77
FeO	7.21	23.45	27.36
Fe_2O_3	0.00	0.00	7.36
MgO	12.36	7.87	11.17
CaO	21.23	6.86	0.02
MnO	0.05	0.61	0.32
Na_2O	1.47	0.00	0.00
K_2O	0.00	0.00	0.00
NiO	0.00	0.00	0.00
Total	98.88	99.42	100.51
Number of cations for 0 = n × 1000			
Si	1904	3023	---
Al	225	1935	15
Ti	15	6	921
Cr	2	8	14
Fe^{2+}	226	1514	529
Fe^{3+}	---	---	128
Mg	690	906	385
Ca	851	568	---
Mn	2	40	6
Na	107	---	---
K	---	---	---
Ni	---	---	---
	4021	8000	2000
Mg/(Mg+Fe)	0.753	0.374	

Mg-Fe partitioning between the coexisting diopside and garnet inclusions in the ilmenite megacryst FRB 548 shows its temperature of equilibration to be 900°C using Akella and Boyd's data. The equilibration temperature for a variety of diopside-ilmenite nodules from South Africa ranged between 980°-1250°C, according to Boyd and Nixon (1973). Thus, it is interesting to note that this ilmenite megacryst has a substantially lower equilibration temperature than most African intergrowths.

Boyd and Nixon (1975) postulated that the discrete nodules and lamellar ilmenites are xenocrysts derived by crystallization of melts in the low velocity zone of the mantle. Their hypothesis is based on the premise that the discrete nodule assemblage in kimberlite was formed in equilibrium with silicates similar to those found in intergrowths and that they are a part of the assemblage ilmenite-chinopyroxene-orthopyroxene-garnet. On the other hand, if the ilmenite megacryst from Lattavaram is a high-pressure phenocryst in a proto-kimberlitic magma, as suggested by Mitchell (1977), then the magma must be rather surprisingly cool.

Acknowledgments. One of the authors (JA) wishes to thank the Carnegie Institution of Washington, D.C., for making money available to go to India and collect the samples while the author was associated with the Geophysical Laboratory. Thanks are also due to Dr. N.G.K. Murty, Deputy Director, and Sri S. Rajaraman, Senior Geologist, both from Geological Survey of India, Hyderabad, for their advice and help during the field work. Jagan Akella is personally thankful to Dr. F. R. Boyd and Dr. H. S. Yoder, Jr., for their encouragement during the progress of the work.

Work performed under the auspices of the U.S. Department of Energy by the Lawrence Livermore Laboratory under contract number W-7405-ENG-48. Meyer gratefully acknowledges support from National Science Foundation Earth Science Section Grants EAR 76-22698 and GA-43990.

References

Akella, J., and F. R. Boyd, Petrogenetic grid for garnet peridotites, Carnegie Inst. Wash. Yearbook 73, 269-273, 1974.

Akella, J., Solubility of Al_2O_3 in orthopyroxene coexisting with garnet and clinopyroxene for compositions on the diopside-pyrope join in the system $CaSiO_3$-$MgSiO_3$-Al_2O_3, Carnegie Inst. Wash. Yearbook 73, 273-278, 1974.

Akella, J., R. J. Williams, and O. Mullins, Solubility of Cr, Ti and Al in co-existing olivine, spinel, and liquid at 1 atm, Proc. Lunar Sci. Conf. 7th, 1, 1179-1194, 1976.

Boyd, F. R., and P. H. Nixon, Structure of upper mantle beneath Lesotho, Carnegie Inst. Wash. Yearbook 72, 431-445, 1973.

Boyd, F. R., and P. H. Nixon, Origins of the

ultramafic nodules from some kimberlites of northern Lesotho and the Monastery mine, S. Africa, Phys. Chem. of the Earth, 9, 431-454, 1975.
Boyd, F. R., and P. H. Nixon, Origin of the ilmenite-silicate nodules in kimberlites from Lesotho and S. Africa, in Lesotho Kimberlites, edited by P. H. Nixon, pp. 254-268, Lesotho National Development Corp., Maseru, Lesotho, 1973.
Foote, R. B., Rec. Geol. Surv. Ind., 22, 1889.
Lake, P., Rec. Geol. Surv. Ind., 23, 1890.
Mathur, S. M., and H. N. Singa, Bull. Geol. Surv. Ind., 21, 1963.
Mehr, S., Quart. J. Min. Met. Soc. Ind., 24, 125-132, 1953.
Mitchell, R. H., Geochemistry of magnesian ilmenites from kimberlites in S. Africa and Lesotho, Lithos, 10, 29-37, 1977.
Naqvi, S. M., V. Divakara Rao, and H. Narain, The protocontinental growth of the Indian shield and the antiquity of its rift valleys, Precambrian Res., 1, 345-398, 1974.
Pichamuthu, C. S., and R. Rao, Proc. Ind. Sci. Cong., 19th Session, 1932.
Raheim, A., and D. H. Green, Experimental determination of the temperature and pressure dependence of the Fe-Mg partition coefficient for coexisting garnet and clinopyroxene, Contrib. Min. Pet., 48, 179-203, 1974.
Rao, P. S., and R. N. Phadtre, Geol. Soc. Ind., 7, 118-123, 1963.
Reid, A. M., and J. S. Hanor, Pyrope in kimberlite, Am. Min., 55, 1374-1379, 1970.
Sarkar, S. N., Precambrian stratigraphy and geochemistry of peninsular India, Dhanbad Publishers, Dhanbad, India, 1968.

PETROCHEMISTRY AND STRUCTURE OF KIMBERLITES IN THE FRONT RANGE AND LARAMIE RANGE, COLORADO-WYOMING

C. B. Smith*
Colorado State University, Fort Collins, Colorado 80523

M. E. McCallum
Colorado State University, Fort Collins, Colorado 80523,
and U.S. Geological Survey, Denver, Colorado 80225

H. G. Coopersmith
Cominco American, Inc., St. Charles, Missouri 63301

David H. Eggler
The Pennsylvania State University, University Park,
Pennsylvania 16802

Abstract. Four transitional varieties of kimberlite from northern Colorado and southern Wyoming can be distinguished on the bases of textures and modal compositions: 1) massive to porphyritic, 2) carbonate-rich massive to porphyritic, 3) intrusive breccia, and 4) carbonate-rich intrusive breccia. Massive to porphyritic kimberlite occurs in dikes, sills, and small plugs, whereas intrusive breccia is restricted to diatremes. Carbonate-rich kimberlite contains increased amounts of carbonate (greater than 45 percent), some of which is interpreted to be primary and some of which probably formed by autometasomatic replacement. Kimberlite in the Iron Mountain, Wyoming, district consists of abundant massive to porphyritic kimberlite in an extensive dike or fissure system along which occur sporadic pipe structures, whereas kimberlite in the Colorado-Wyoming State Line district to the south consists primarily of intrusive breccia in pipe structures. The Iron Mountain fissure system is interpreted to represent a diatreme root zone that is exposed at a lower erosional level than the pipes in the State Line district.

Introduction

Ninety-one kimberlite bodies have been discovered in the Front Range of northern Colorado and southern Wyoming since 1960 (McCallum et al., 1975). Thirty-two of the known kimberlites occur as pipes and smaller pluglike bodies in the State Line district, which encompasses an area of about 300 km^2 astride the Colorado-Wyoming State boundary (Fig. 1). Fifty-seven pipes and dikes occur in the Iron Mountain district, an area of about 50 km^2 on the east flank of the Laramie Range, approximately 70 km north of the State boundary (Fig. 1). One small kimberlite pipe (Green Mountain diatreme--30 m in diameter) is situated immediately west of Boulder, Colorado, 120 km south of the State line (Kridelbaugh et al., 1972; Kridelbaugh and Meyer, 1973; Meyer and Kridelbaugh, 1977; Boctor and Meyer, 1977). A single kimberlite dike was recently discovered near Estes Park, Colorado, about 60 km south of the State boundary (J. C. Cole, oral communication, 1976).

Published accounts of these kimberlite occurrences have been restricted primarily to evaluation of xenoliths and megacrysts of upper mantle and lower crustal derivation (e.g., Eggler and McCallum, 1974, 1976; Eggler et al., 1977; McCallum et al., 1975; McCallum, Eggler and Smith, 1977) and to diamonds in kimberlite of the State Line district (McCallum and Eggler, 1976; McCallum and Mabarak, 1976a, b; McCallum, Mabarak and Coopersmith, 1977). Additional discussions have pertained to emplacement mechanisms as related to intrusive form and alteration processes (Woolsey et al., 1975; McCallum, 1976) and lower Paleozoic sedimentary xenoliths (e.g., Chronic et al., 1969; McCallum et al., 1975). Owing to poor exposure of pipes

*Present address: Bernard Price Institute of Geophysical Research, University of Witwatersrand, Johannesburg 2001, South Africa

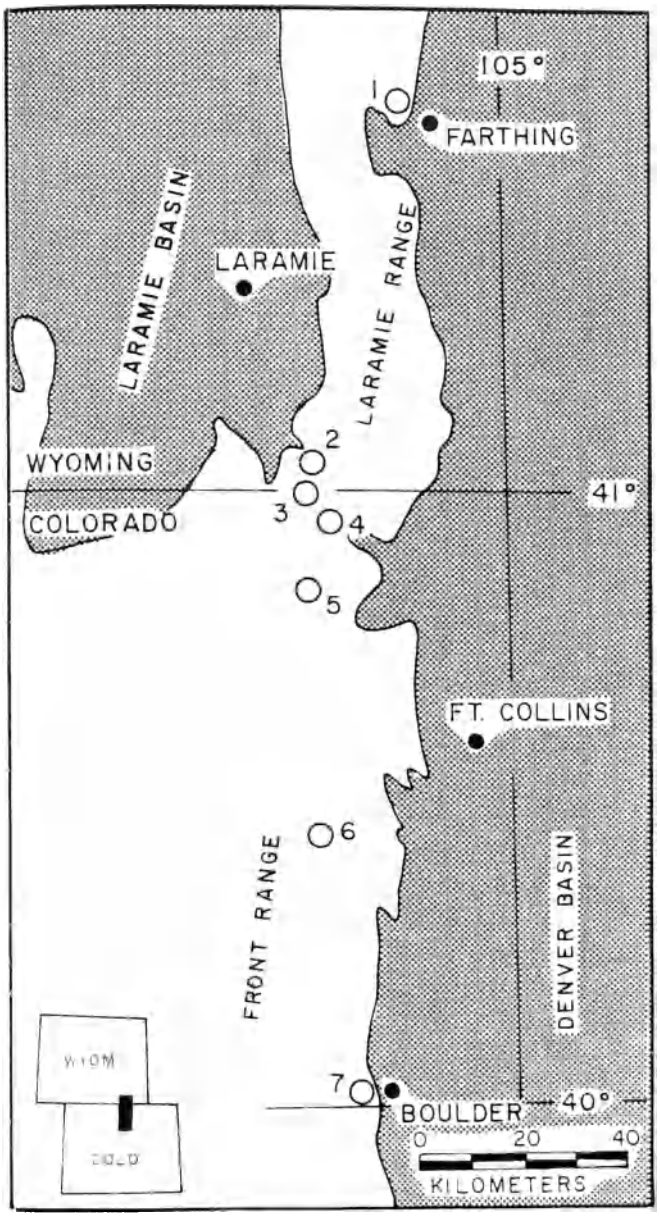

Figure 1.--Location map. 1--Iron Mountain district; 2--Ferris and Aultman pipes; 3--Schaffer pipes; 4--Nix and Moen pipes; 5--Sloan pipes; 6--Estes Park dike; 7--Boulder pipe (Green Mountain); 2, 3, 4 and 5 are collectively designated the State Line district.

and dikes, relatively little emphasis has been placed on the petrography and petrology of the kimberlite itself, although kimberlite in the Sloan 1 diatreme, the largest and best exposed of any in the area, has been described in detail by McCallum and Eggler (1971), and Iron Mountain district kimberlite has been discussed by Smith (1977) and Smith et al. (1977).

Geologic Setting

Kimberlites intrude Precambrian granitic and metamorphic rocks of the Front Range along a 200-km north-south trend and are presumed to represent a single episode of emplacement, possibly related to the structural evolution of the eastern front of the southern Rocky Mountains (McCallum et al., 1975). A probable Devonian age for kimberlite emplacement is suggested by fission-track dating of zircons (Naeser and McCallum, 1977), and this age agrees favorably with the post-Silurian and pre-Mississippian age previously established by geologic evidence (Chronic et al., 1969; McCallum et al., 1975; Smith, 1977).

Structural control of kimberlite emplacement in the State Line district consists primarily of southwest- to northeast-trending joints of variable dip in granitic rocks. Diatremes of the Nix and Sloan groups (Fig. 1) are spatially associated with major faults, although only the Sloan 1 and 2 pipes are unquestionably fault-controlled. The Sloan 1, the largest known diatreme, occurs at the intersection of two faults that have controlled the size and shape of the pipe (McCallum and Eggler, 1971).

The most prominent near-surface control of kimberlite emplacement in the Iron Mountain district is pervasive jointing in the Precambrian Sherman Granite. Fault control is not evident from the surface geology; however, the strong southwest-northeast linear trend of the dike system may reflect deep-seated structural control along a major fracture related to, or part of, the Precambrian Nash Fork-Mullen Creek shear zone as projected through this part of the Laramie Range by Hills and Armstrong (1974). Possible structural controls of comparable magnitude are not apparent for kimberlites in the State Line, Estes Park, or Green Mountain localities.

Field Relations and Intrusive Form of Kimberlite

Kimberlite from both the State Line and Iron Mountain districts is truncated by late Tertiary to Pleistocene erosion surfaces, and most exposures consequently have negligible relief and little or no outcrop. Kimberlite is generally deeply weathered and often covered by a thin veneer of colluvial granitic material (grus) and/or alluvium. Some pipes are prominently expressed in positive relief due, in part, to silicification of kimberlite and adjacent wall rocks.

Kimberlite occurs in a variety of intrusive forms including dikes, sills, plugs, blind ("roofed") diatremes, and diatremes. Plugs and diatremes predominate in the State Line district, in contrast to the Iron Mountain district where kimberlite is characterized by a higher density of exposures in a dike or fissure

system along which occur sporadic small diatremes and blind diatremes. Dikes or dike-like features, in the State Line district are uncommon relative to pipe structures. They are generally traceable for less than a few meters and are closely associated with pipes. In contrast, Iron Mountain dikes can be traced for as much as 1.5 km, are irregularly shaped and have nonparallel walls, vary from less than 1 to nearly 50 m in width, and have numerous sinuous apophyses of variable sizes subsidiary to the main dikes. The dikes commonly open into small diatremes. One sill has been recognized at Iron Mountain.

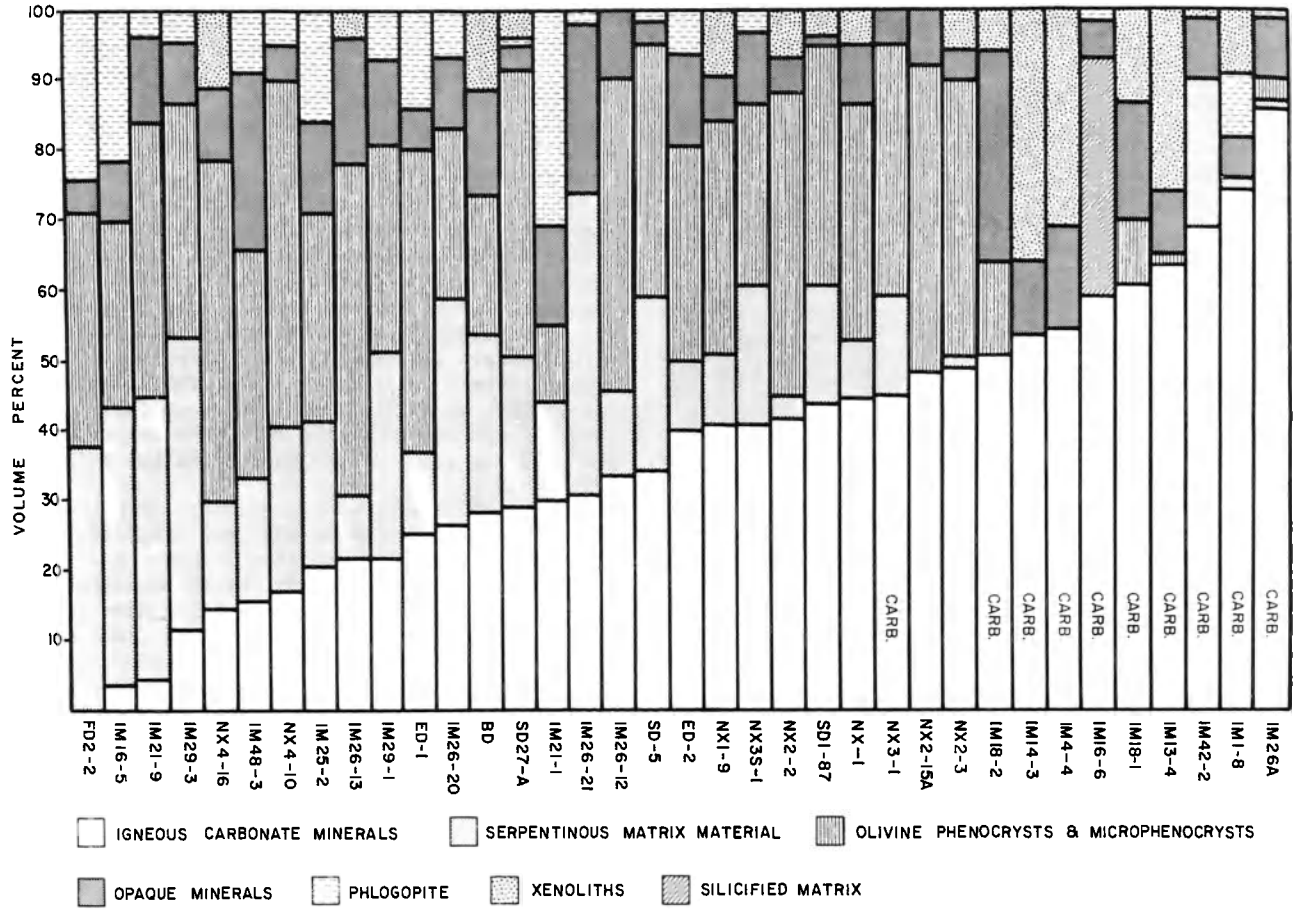

Figure 2.--Modal analyses of kimberlite. Trace amounts of primary and secondary minerals (e.g. apatite, chlorite) are not included. Carbonate minerals include primary and secondary calcite and dolomite. Olivine phenocrysts and microphenocrysts include unaltered and serpentinized olivine. Opaque minerals are predominantly magnetite, perovskite, and/or hematite. CARB.=carbonatized samples in which groundmass and phenocryst-xenocryst minerals are replaced by carbonate. Decreased amounts of minerals other than carbonate in carbonatized samples are due to replacement by carbonate. Modal analyses do not reflect xenolith components in all samples, because the megascopic nature of most xenoliths precludes accurate volume determinations from thin sections. Most samples are massive to porphyritic kimberlite. Samples classified as breccia are BD, SD27-A, SD-5, SD1-87, IM14-3, IM4-4, IM13-4, and IM42-2. Samples transitional between breccia and massive to porphyritic kimberlite are FD2-2, NX1-9, NX3S-1, NX-1, NX3-1 and IM1-8. Prefixes indicate origin of samples, as follows. State Line district: FD--Ferris 2 pipe; NX--Nix 1, 2, 3, or 4 pipes; SD--Sloan 1 pipe; IM--Iron Mountain district; BD--Boulder pipe (Green Mountain); ED--Estes Park dike.

The kimberlite at Estes Park is a narrow linear dike averaging 0.5 to 1 m in width that can be traced for about 0.5 km on the basis of vegetative and soil contrasts with the country rock.

Petrography of Kimberlite

General Compositions

Four varieties of kimberlite are recognizable: massive to porphyritic, carbonate-rich massive to porphyritic, breccia, and carbonate-rich breccia. Massive to porphyritic kimberlite (equivalent to the massive variety of Dawson (1967) or the picrite porphyrites of Frantsesson (1970)) typically contains only minor amounts of xenolithic constituents and is most commonly restricted to dikes and small plugs, although it may be found locally in larger pipe structures. Brecciated kimberlite is distinguished by higher xenolith contents and is, with rare exceptions, restricted to diatremes or blind diatremes. Because of the poor exposures and highly weathered nature of surface kimberlite, the existence of composite intrusions is uncertain. Crosscutting relationships between massive and brecciated varieties have not been observed, even on the relatively well exposed Sloan 1 pipe.

The compositional variability of Colorado-Wyoming kimberlite can be attributed to a wide range of carbonate content (Fig. 2). Carbonate (calcite and subordinate dolomite) occurs as primary groundmass minerals, secondary replacement products, and minor amounts of post-solidification veinlets. Carbonatized kimberlite is most abundant at Iron Mountain; known carbonatized kimberlite in the State Line district occurs only in the SH13 and NX3 pipes.

Olivine phenocrysts and microphenocrysts constitute 10 to 50 percent of most kimberlite and are generally serpentinized. The apparent decrease of olivine (and other minerals) in carbonatized kimberlite (Fig. 2) is a result of inclusion of carbonatized minerals in the carbonate fraction, because carbonatized silicates are difficult to distinguish from groundmass carbonate in thin section. Most kimberlite contained 30 to 40 volume percent olivine prior to alteration.

Opaque minerals range from 5 to 36 percent in kimberlite and consist dominantly of magnetite and perovskite in carbonate-poor rocks, and of secondary (?) hematite, leucoxene, and unidentified fine-grained phases in carbonate-rich kimberlite. Only trace amounts of groundmass ilmenite (less than 1 mm) have been recognized in Colorado-Wyoming kimberlite.

Phlogopite occurs in significant amounts only in carbonate-poor dike-facies kimberlite at Iron Mountain, Estes Park, and one State Line district locality (dike related to Schaffer 13 pipe).

Diamond has been recovered from deeply weathered kimberlite from several pipes in the State Line district, but has not yet been found in kimberlite from Iron Mountain, Estes Park, or Boulder. Table 1 summarizes the textural, structural, and compositional relationships and intrusive forms of the various types of Colorado-Wyoming kimberlite.

Massive to Porphyritic Kimberlite

Massive to porphyritic kimberlite is best exposed in the Iron Mountain district, where it occurs in dikes and in small plugs that are expressed as enlarged portions of dikes. In the State Line district, this variety of kimberlite is much less common. There it forms what appear to be small plugs (e.g., Nix 2 and 4 occurrences), minor dikes or dikelike exposures, and localized bodies in pipes (e.g., in the Sloan 1 pipe). The Estes Park dike is also composed of massive to porphyritic kimberlite.

In hand specimen this variety of kimberlite is generally green to dark green and massive to porphyritic, depending on size and abundance of olivine phenocrysts (Fig. 3). This variety of kimberlite is not brecciated and, at Iron Mountain, is relatively free of mantle- or crustal-derived xenoliths. Inclusions are relatively more abundant at the State Line and Estes Park localities. Irregular flow structures defined by alinement, stratification, and size sorting of olivine and altered olivine phenocrysts are locally present. These structures are most likely the result of flow differentiation during emplacement (Simkin, 1967; Bhattacharji, 1967). However, in no instance are outcrops sufficiently extensive to allow detailed study of flow structures relative to dike geometry.

In thin section this type of kimberlite is characterized by as much as 50 percent rounded to subrounded olivine and subordinate (less than 1 percent) enstatite phenocrysts (1 mm to 3 cm in length) and olivine microphenocrysts (0.1 to 1 mm in length) set in a fine-grained chaotic matrix of serpentine, calcite, dolomite, phlogopite, magnetite, perovskite, apatite, rutile, hematite, pyrite, chalcopyrite, and, locally, chlorite and talc. Secondary minerals are ubiquitous, but because of their typically fine grain size, most have not been studied in detail. Serpentine, dolomite, hematite, magnetite, and minor iddingsite replace olivine phenocrysts. Secondary matrix minerals include hematite, magnetite, chlorite, talc, phlogopite, leucoxene, pyrite, and chalcopyrite.

Olivine. The large volume of olivine and virtual absence of other xenocrysts or xenoliths in the massive to porphyritic Colorado-Wyoming kimberlite is considered strong support for a phenocrystic origin for virtually all of this olivine. Mitchell (1973) has pointed out that groundmass microphenocrysts in kimberlites are commonly slightly less magnesian than

phenocrysts. A limited number of microprobe analyses of olivine in a dike from Iron Mountain are consistent with those observations. The largest analyzed phenocryst is Fo 91.9; three other phenocrysts average Fo 90.6, whereas the one analyzed microphenocryst is Fo 87.4. No zoning was detected in the olivine crystals, but because phenocryst margins are serpentinized, accurate analyses of the margins are impossible to obtain. No monticellite has been recognized.

Perovskite. Brown anhedral perovskite as much as 0.2 mm in diameter is distributed throughout the matrix in amounts of as much as 5 volume percent. Perovskite analyzed by microprobe (from Iron Mountain) proved to be homogeneous and similar in composition to kimberlitic perovskite from Wesselton and Bulfontein, South Africa, and Ison Creek, Kentucky (Mitchell, 1972) and from Greenland (Emeleus and Andrews, 1975).

Magnetite. Anhedral to euhedral magnetite ranges from less than 0.01 to 0.05 mm in diameter and is present as three discrete types that represent at least two generations of crystal growth. Magnetite of probable primary origin occurs in two forms: (1) anhedral, wormy blebs with prominently embayed grain margins; and (2) larger euhedral crystals (as much as 0.05 mm in diameter). These two varieties display epitaxial and composite grain relationships with perovskite; either mineral may occur as thin rinds on the other or as composite or discrete grains. Type (3) magnetite occurs within or at the margins of serpentinized olivine phenocrysts and is of obvious secondary origin. Much of this type of magnetite is likely dispersed throughout the matrix.

Phlogopite. At least two generations of phlogopite are present in massive to porphyritic kimberlite. The first occurs as 1 mm to 1 cm pleochroic anhedral grains that are commonly chloritized along cleavage planes, and the crystals are typically mechanically deformed. The Estes Park dike is distinct in containing the highest amounts of phlogopite (as much as 5 volume percent) and rare polycrystalline aggregates.

The second type of phlogopite occurs as fine-grained (0.1-0.5 mm in length) ragged laths and plates within the matrix, is non-pleochroic to faintly green or reddish brown, and poikilitically encloses opaque minerals of the groundmass, the most common of which are perovskite and magnetite.

Phlogopite does not exhibit flowage around phenocrysts, and in some samples it occurs as crisscrossing laths that form a reticulate network throughout the groundmass. Such a texture could not develop in a moving liquid or crystal-liquid mush. Phlogopite of the groundmass is probably of secondary post-emplacement origin (Brookins, 1969; Dawson, 1962).

Apatite. Primary apatite occurs in trace amounts (as much as 1 percent) as radial aggregates of acicular crystals and, more commonly, as prismatic crystals from 0.1 to 0.5 mm in length.

Serpentine. Serpentine occurs as secondary fibrous pseudomorphs after olivine and enstatite and as an important phase in the groundmass. In most samples, serpentinous material in the matrix is a turbid, hydrated mixture of optically unidentifiable microcrystalline serpentine, clay minerals, altered perovskite, minor sphene (?), and Mg-Fe-Ti oxides or hydroxides. In a few carbonate-rich samples, matrix serpentine (serpophite) occurs as homogeneous, nearly isotropic patches that display emulsion-like texture with carbonate.

Groundmass serpentine may be secondary after microcrystalline olivine and/or pyroxene, or is possibly a primary phase that crystallized from a Mg- and H_2O-rich silicate fluid at temperatures below 500°C (Robinson, 1975; Emeleus and Andrews, 1975).

Carbonate. Massive to porphyritic kimberlite contains as much as 45 modal percent matrix carbonate. Staining tests (Dickson, 1965) indicate that the carbonate is dominantly calcite and ferrous calcite with minor amounts of dolomite. Groundmass carbonate most commonly occurs as interstitial anhedral blebs (0.2-0.5 mm in diameter) or reticulate patches distributed throughout the rock. The igneous nature of groundmass carbonate in the Sloan 1 diatreme of the State Line district has been demonstrated by carbon and oxygen isotope determinations (McCallum and Eggler, 1971; Deines and Gold, 1973). The emulsion-like texture in some samples suggests that, at least locally, silicate and carbonate liquids were immiscible (e.g., Clement, 1975; Griffin and Taylor, 1975) during the final stages of emplacement and that solidification of the two was nearly simultaneous. Late-stage veining and/or replacement textures are rare.

Carbonate-rich Massive to Porphyritic Kimberlite

Carbonate-rich massive to porphyritic kimberlite is dark gray to black, gray, or greenish-gray in color and occurs in dike segments proximal to pipe structures and within pipes. The rock is texturally similar to the massive variety described above, but is compositionally dissimilar in that it contains greater amounts of carbonate, much of which occurs as replacement products of phenocryst-xenocryst minerals and serpentinous groundmass material. In the most intensely altered samples, carbonatized phenocryst-xenocryst "ghosts" occur in a matrix of essentially massive carbonate where carbonatization is most intense. Consequently, porphyritic textures are less conspicuous in hand specimen and thin section.

TABLE 1. Principal Kimberlite Textural Types in the State Line District.

Characteristics	Type 1 Massive to porphyritic kimberlite	Type 2 Massive to porphyritic carbonatized kimberlite	Type 3 Kimberlite breccia	Type 4 Carbonatized kimberlite breccia
Composition				
a) phenocryst -xenocryst	Fresh to serpentinized, rounded olivines abundant; lesser orthopyroxene, clinopyroxene, ilmenite, garnet, chromite, phlogopite, and rutile. 0.1-20 mm.	Carbonatized to variable degrees with minor silification and rare serpentinization. Otherwise similar to massive porphyritic kimberlite.	Same as Type 1 but generally more altered; all olivine and orthopyroxene serpentinized.	Carbonatized and silicified with minor fresh garnet and diopside. Olivine and orthopyroxene replaced by carbonate and preserved as pseudomorphs.
b) groundmass	Serpentine and primary carbonate. Commonly patchy with a mixture of serpentine and calcite. Very fine-grained (0.1 mm) euhedral magnetite and perovskite and minor phlogopite. Carbonate-rich blebs and laths.	Carbonatized to variable degrees,with serpentine either absent or chaotically and intimately mixed through matrix. Carbonate is a fine-grained, chaotic mixture of primary and secondary calcite and dolomite Minor carbonate veining. Perovskite and magnetite commonly altered. Most abundant at Iron Mountain.	Serpentinized with minor carbonate. Generally more "flooded" with serpentine. Mineralogy same as Type 1.	Very fine grained calcite, patchy silicification. Opaque minerals altered to leucoxene (?) and fine-grained Fe oxides. Original minerals virtually completely altered. Many fresh, angular pieces of country rock in various degrees of comminution. Additional calcite, dolomite, and ankerite. Some serpentine intimately mixed with groundmass carbonate.
Texture	Fine-grained massive to porphyritic. Commonly a bimodal size range of olivine.	Massive to porphyritic but not as distinct because of carbonatization of phenocrysts.	Brecciated, some autoliths and abundant rounded to angular inclusions of country rock. Texture similar to Type 1, where xenoliths are less abundant.	Brecciated, similar to Type 3, but commonly with more abundant angular country rock fragments and higher amounts of pulverized fragmental material in groundmass.

TABLE 1. (continued)

Structures	Local flow structures defined by alignment, layering, and size sorting of phenocrysts-xenocrysts, carbonate laths, and groundmass opaque minerals.	Similar to Type 1 though flow structures are not as abundant.	Flow structures rare.	Flow structures rare.
Xenoliths	Rare to moderately abundant locally, rounded, generally <8 cm, some quite fresh. Includes mantle-derived megacrysts and peridotite. Crustal rocks notably scarce.	Rare to moderately abundant locally. Similar to Type 1 kimberlite, with the addition of minor angular to elongate granitic wall-rock fragments.	Common--rounded to angular, generally less than 12 cm but may be as large as 30 cm--fresh to completely serpentinized, carbonatized, fenitized, or silicified. Includes mantle-derived peridotite, eclogite, and megacrysts; lower and upper crustal rocks.	Relatively common, rounded, 1-10 cm; usually completely carbonatized and/or silicified. Abundant angular wall-rock granitic fragments at Iron Mountain.
Emplacement type	Dikes, sills, and plugs and enlargements of same. May include previously consolidated kimberlite.	In dikes, sills, and plugs closely associated with diatremes or blind diatremes.	Diatremes and "blind" diatremes.	Diatremes and "blind" diatremes
Exposure geometry	Narrow, irregular, elongate to ovoid.	Similar to Type 1 kimberlite.	Irregular, commonly elongate to pipelike, of variable size.	Similar to Type 3.
Wall-rock alteration	Very minor to completely lacking.	Not well exposed, but apparently some carbonatization and silicification, with rare mechanical brecciation.	Generally minor, locally mechanical brecciation of wall rock and/or serpentinization or saussuritization.	Generally minor with local mechanical brecciation, carbonatization, and silicification. Generally more intense than in other types.
Level in system (See Fig. 6)	Root zones with later intrusion into pipes.	Root zones closely associated with pipes, and as late intrusions into pipes.	Upper root zones and pipes.	Upper root zones and pipes.

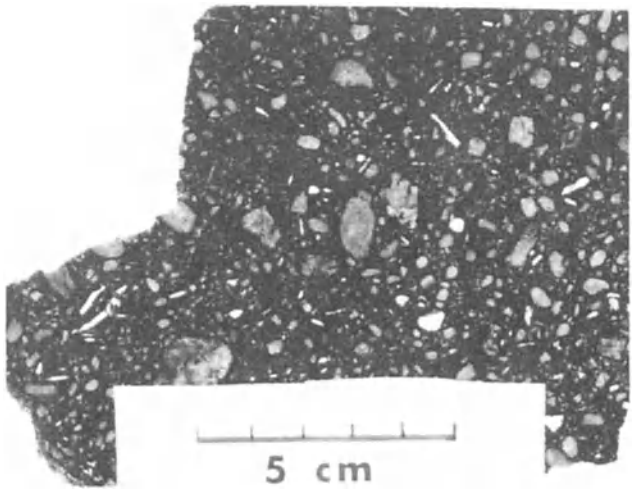

Figure 3.--Porphyritic kimberlite from Nix 4 locality, State Line district. Predominantly subrounded to elongate olivine and minor enstatite set in dense black matrix composed of serpentine and carbonate. White angular laths are composed of secondary carbonate and are of uncertain origin.

The variable intensity of carbonatization and superimposed weathering have resulted in greater textural and mineralogical variation than in carbonate-poor massive to porphyritic kimberlite. Magnetite is generally altered to hematite, and altered olivine phenocrysts are commonly rimmed by or contain hematite. Perovskite is altered to finely crystalline or amorphous mixtures of rutile, leucoxene, and

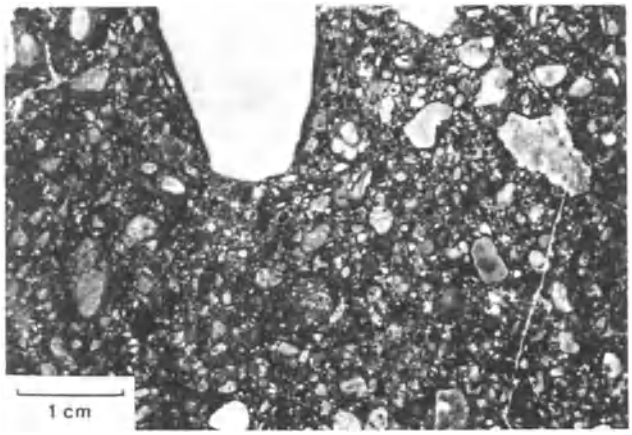

Figure 4.--Kimberlite breccia from Sloan 1 diatreme, State Line district. Primarily light-colored Paleozoic limestone fragments, altered olivine, "pellets" of earlier generation kimberlite (low center of photo), and opaque minerals set in a fine grained chaotic mixture of fragmental material, serpentine, and carbonate. Horizontal field of view is 6 cm.

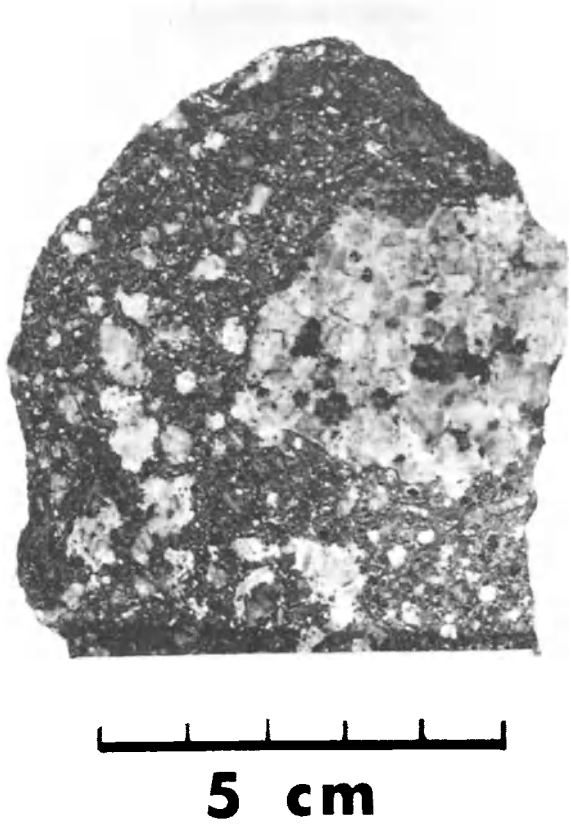

Figure 5.--Carbonatized kimberlite breccia from the Iron Mountain district (IM14 pipe). Light-colored granitic fragments in matrix of carbonate, and carbonatized and pulverized granitic and kimberlitic components.

sphene (?); and phlogopite is generally absent. The rock is locally silicified to a variable extent (e.g., IM16-6, fig. 2).

Kimberlite Breccia and Carbonate-rich Kimberlite Breccia

Kimberlite breccias are restricted to the pipe structures and are distinct from dike-facies kimberlite in that they contain greater numbers of xenoliths of more variable size. Brecciated kimberlite is generally structureless relative to massive to porphyritic kimberlite, in that flow banding or compositional layering is very rare.

Angular to rounded xenoliths include lower Paleozoic sedimentary rocks; upper and lower crustal Precambrian crystalline rocks (granite, gneiss, schist, basalt, pyroxenite, and granulite); and upper mantle nodules of spinel and garnet peridotite, garnet clinopyroxenite and websterite, dunite, eclogite, monomineralic megacrysts, and carbonatite. Deep-seated xenoliths of all types are mostly poorly

preserved, commonly being carbonatized, silicified, serpentized, or hematized. Upper crustal xenoliths (predominantly granitic or sedimentary) are generally less altered than deep-seated xenoliths.

Three types of brecciated kimberlite have been recognized on the bases of composition, texture, and intrusive form. The first is compositionally and texturally similar to, and gradational into, massive to porphyritic carbonate-poor kimberlite, but is defined as breccia because of slightly higher xenolith content (about 5 to 10 percent) and pipelike geometry.

The second breccia type is a green to dark green variety (Fig. 4) that is well exposed at the Sloan 1 pipe in Colorado (McCallum and Eggler, 1971). Subrounded to subangular sedimentary carbonate fragments (1 to 5 cm in diameter) and olivine phenocrysts and microphenocrysts are set in a fine-grained matrix of serpentine, carbonate, perovskite, magnetite, hematite, and a wide variety of secondary minerals. Sloan 1 kimberlite is unique relative to other Colorado-Wyoming brecciated phases in that it contains as much as 10 percent of indistinct 0.1 to 1 cm diameter, angular and rounded fragments of earlier generation kimberlite similar to kimberlite "pellets," described by Clement (1973) from the

TABLE 2. Chemical Analyses of Colorado-Wyoming Kimberlite.

Oxide	NX3s-1	IM1-8	ED1-1	SD1-86	SDI-88	IM16-5	NX4-10	NX4-16
SiO_2	24.8	25.7	29.6	30.4	32.5	33.6	34.2	34.2
TiO_2	1.4	2.6	5.2	0.90	0.60	3.0	0.75	0.95
Al_2O_3	3.1	2.1	2.7	1.9	1.9	2.8	2.4	2.7
Cr_2O_3	0.10	0.10	0.19	0.14	0.10	0.14	0.13	0.16
Fe_2O_3	7.0	8.7	5.6	4.0	3.5	7.7	3.7	6.4
FeO	1.3	0.87	5.0	2.0	1.9	3.8	2.1	1.5
MnO	0.15	0.16	0.25	0.13	0.09	0.18	0.13	0.14
NiO	0.07	0.07	0.08	0.11	0.10	0.10	0.14	0.12
MgO	22.2	12.6	23.1	25.9	27.4	28.4	31.2	30.7
CaO	16.2	19.9	10.2	14.8	12.5	5.1	7.9	6.8
Na_2O	0.07	0.05	0.03	0.04	0.03	0.05	0.07	0.09
K_2O	0.16	1.0	0.94	0.29	0.20	1.4	1.1	0.42
P_2O_5	1.4	0.35	0.09	0.35	0.15	0.35	0.15	0.3
BaO	0.06	0.07	0.07	0.03	0.01	0.08	0.07	0.08
CO_2	10.5	21.0	5.8	8.9	7.0	1.7	3.5	2.2
L.O.I.	10.0	4.4	9.9	10.2	11.6	11.2	9.8	14.0
Total	98.5	99.7	98.8	100.0	99.6	99.6	98.3	100.7

ED=Estes Park dike
State Line district: NX=Nix pipes, SD=Sloan pipes
IM=Iron Mountain district
L.O.I.=Loss on ignition at 1000°C
Analyses by Skyline Labs, Inc., Wheatridge, Colorado

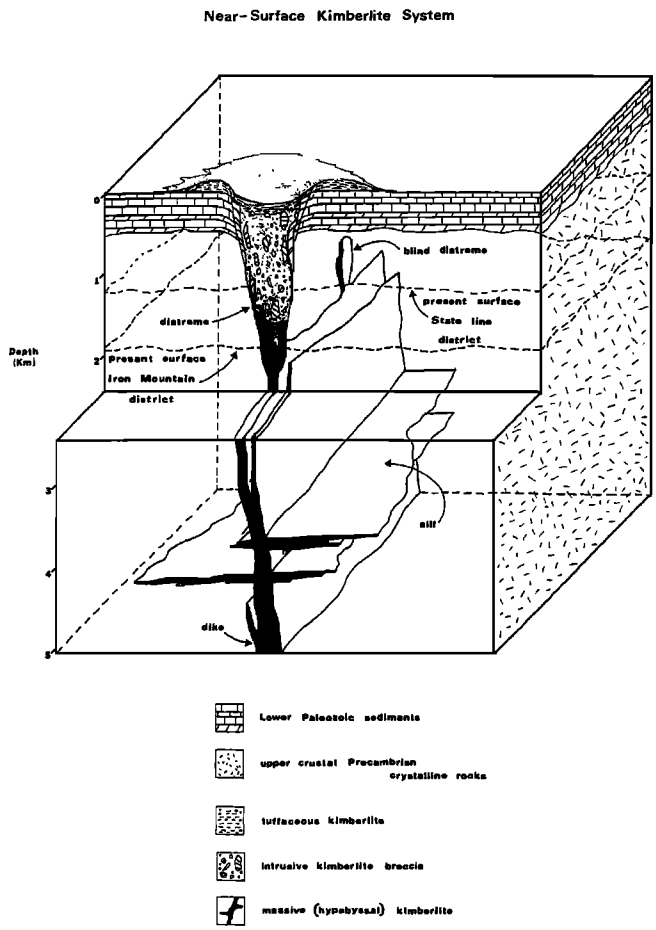

Figure 6.--Kimberlite emplacement model (from McCallum and Mabarak, 1976b).

Kao pipe and which he termed lapilli. Nucleated autoliths (Danchin et al., 1975; Ferguson et al., 1973) are present in minor quantities and are unique to the Sloan 1 breccia.

Carbonate-rich breccias occur predominantly in the Iron Mountain district diatremes (IM14-3, IM13-4, IM42-2, in Fig. 2). They are composed of as much as 70 percent angular host-rock granitic fragments, in various degrees of comminution, set in a chaotic matrix of finely crystalline carbonate, hematite, and carbonatized, rounded olivine (?) microphenocrysts (Fig. 5). Locally, intrusive kimberlite breccia consists of intensely pulverized granitic fragments resembling fault gouge, with no trace of the kimberlitic fluid phase preserved in the groundmass.

The most intense wall-rock alteration of Colorado-Wyoming kimberlite occurs in these breccia pipes. Minute carbonate veinlets permeate wall rock to as much as 30 m from the contact in one exposure, resulting in incipient carbonatization of granitic rocks.

Major Oxide Chemistry

Major oxide analyses of Colorado-Wyoming kimberlites span a broad compositional range (Table 2). The most distinct chemical variability is due to antithetic serpentine and carbonate contents. Carbonate-poor, massive to porphyritic and brecciated kimberlites have the highest MgO contents (23.1 to 31.2 percent) and generally lower CaO and CO_2 contents. Of the three carbonate-rich samples analyzed, the one from Iron Mountain (IM1-8) is carbonatized, displays extensive replacement of phenocryst and groundmass phases, and contains the highest carbonate content. The other two carbonate-rich samples (NX3S-1 and SD1-86, from the State Line district) are not carbonatized according to petrographic criteria, but rather consist of serpentinized olivine microphenocrysts set in a carbonate matrix with minor serpophite (?) in which replacement effects are not apparent. Carbonatized kimberlite from Iron Mountain has high SiO_2, MgO, and low CaO relative to carbonatitic dikes of the Saguenay River Valley, Quebec, Canada (Gittens et al., 1975) and is more similar to the composite analysis of the Benfontein sill, South Africa (Hawthorne, 1968).

Emplacement

The presence of nonbrecciated massive to porphyritic and brecciated kimberlite in both the State Line and Iron Mountain districts is consistent with models suggesting that volatile-rich kimberlite magma is intruded into dike and sill systems, from which diatreme formation is initiated at depths of 2 to 3 km (e.g., Dawson, 1967, 1971, 1972; McCallum and Mabarak, 1976b, Fig. 8). The Iron Mountain district, characterized by larger amounts of massive to porphyritic kimberlite in an extensive dike system in contrast to the predominance of intrusive breccia in State Line district pipes and plugs, is thought to reflect a deeper erosional level than the State Line district. The Iron Mountain kimberlite district probably represents a diatreme root zone composed of massive to porphyritic hypabyssal dike facies and brecciated diatreme-facies kimberlite. At Iron Mountain, fluidized cells were apparently only rarely developed or fluidization was aborted after brief intrusive activity, and most of the breccia pipes appear to represent incipient diatremes "frozen" in the initial stages of development.

Carbonatization accompanied diatreme formation in some State Line district pipes and in all exposed Iron Mountain district pipes and proximal dikes. There is some question as to whether carbonatization of dike-facies kimberlite is magmatic (pre-solidification and pre-diatreme formation) or autometasomatic (post-solidification and synchronous with or post diatreme formation). In contrast to the

South African Premier kimberlite, where "vapor-rich liquids" were responsible for localized metasomatic alteration of wall-rock kimberlite (Robinson, 1975), carbonatization of Iron Mountain dike segments has occurred on a more extensive scale and was not accompanied by intense carbonate veining or brecciation. The most viable mechanism for carbonatization of the Colorado-Wyoming kimberlites is autometasomatic alteration by an exsolved vapor phase during final crystallization of dike-facies kimberlitic, concurrent with initiation of diatreme formation.

Conclusions

The most significant results of our investigations of kimberlite from the Colorado-Wyoming State Line and Iron Mountain, Wyoming, districts are as follows:

1. Four transitional varieties of kimberlite have been defined: massive to porphyritic, carbonate-rich massive to porphyritic, intrusive breccia, and carbonate-rich intrusive breccia.
2. Massive to porphyritic kimberlite occurs in dikes, sills, and plugs and generally reflects deeply eroded levels of the intrusive system.
3. Brecciated kimberlite is restricted to diatremes and blind diatremes, reflecting higher levels within the intrusive system.
4. Carbonate-rich kimberlite appears to be closely related to pipe structures and proximal dikes. Intense carbonatization is considered an autometasomatic process associated with initiation of diatreme formation.
5. Matrix carbonate and serpentine in some kimberlite dike samples show emulsion-like textures that suggest crystallization from immiscible liquids. The presence of liquids, together with the presence of two generations of olivine (some euhedral), indicates that the kimberlite is magmatic.

Acknowledgments

Studies of the kimberlite would have been impossible without the generous cooperation of the ranchers in the area. Special appreciation is extended to P. Brownell, whose hospitality and interest greatly facilitated the work. The aid given by F. Yaussi, C. D. Mabarak, and R. B. Thompson has been invaluable. We thank G. L. Snyder and M. A. Kuntz of the U.S. Geological Survey for critical reviews which resulted in substantial improvement of the manuscript.

The research was supported by the Earth Sciences Section of the National Science Foundation (contracts DES 74-13098 and EAR 74-13098 A01) and by the U.S. Geological Survey.

References

Bhattacharji, S., Scale model experiments on flowage differentiation in sills, in Ultramafic and Related Rocks, edited by P. J. Wyllie, pp. 69-70, John Wiley & Sons, Inc., New York, 1967.

Boctor, N. Z., and H. O. A. Meyer, Oxide and sulfide minerals in kimberlite from Green Mountain, Colorado, Extended Abstracts, Second International Kimberlite Conference, Santa Fe, New Mexico, 1977.

Brookins, D. G., A list of minerals found in Riley County kimberlites, Trans. Kansas Acad. Sci. 72, 365-373, 1969.

Chronic, J., M. E. McCallum, C. S. Ferris, Jr., and D. G. Eggler, Lower Paleozoic rocks in diatremes, southern Wyoming and northern Colorado, Geol. Soc. Amer. Bull. 80, 149-156, 1969.

Clement, C. R., Kimberlites from the Kao pipe, Lesotho, Lesotho Kimberlites, edited by P. H. Nixon, pp. 110-121, Lesotho National Development Corporation, Maseru, Lesotho, 1973.

Clement, C. R., The emplacement of some diatreme-facies kimberlites, Phys. Chem. Earth, 9, 51-60, 1975.

Danchin, R. V., J. Ferguson, J. R. MacIver, and P. H. Nixon, The composition of late stage kimberlite liquids as revealed by nucleated autoliths, Phys. Chem. Earth, 9, 235-246, 1975.

Dawson, J. B., Basutoland kimberlites, Geol. Soc. Amer. Bull., 73, 545-560, 1962.

Dawson, J. B., A review of the geology of kimberlites, Ultramafic and Related Rocks, edited by P. J. Wyllie, pp. 241-257, John Wiley & Sons, Inc., New York, 1967.

Dawson, J. B., Advances in kimberlite geology, Earth Sci. Rev., 7, 187-214, 1971.

Dawson, J. B., Kimberlites and their relation to the mantle, Phil. Trans. Roy. Soc. London, A., 297-311, 1972.

Deines, P. and D. P. Gold, The isotopic composition of carbonatite and kimberlite carbonate and their bearing on the isotopic composition of deep-seated carbon, Geochim. et Cosmochim, Acta, 37, 1709-1733, 1973.

Dickson, J. A. A., A modified staining technique for carbonates in thin section, Nature, 205, 587, 1965.

Eggler, D. H., and M. E. McCallum, Preliminary upper mantle-lower crust model of the Colorado-Wyoming Front Range, Carnegie Inst. Wash. Year Book, 73, 295-300, 1974.

Eggler, D. H., and M. E. McCallum, A geotherm from megacrysts in the Sloan kimberlite pipes, Colorado, Carnegie Inst. Wash. Year Book, 75, 538-541, 1976.

Eggler, D. H., M. E. McCallum, and C. B. Smith,

Discrete nodule assemblages in kimberlites from northern Colorado and southern Wyoming: evidence for a diapiric origin of kimberlite, Extended Abstracts, Second International Kimberlite Conference, Santa Fe, New Mexico, 1977.

Emeleus, C. H., and J. R. Andrews, Mineralogy and petrology of kimberlite dikes and sheet intrusions and included peridotite xenoliths from southwest Greenland, Phys. Chem. Earth, 9, 179-198, 1975.

Ferguson, J., R. V. Danchin, and P. H. Nixon, Petrochemistry of kimberlite autoliths, Lesotho Kimberlites, edited by P. H. Nixon, pp. 285-293, Lesotho National Development Corporation, Maseru, Lesotho, 1973.

Frantsesson, E. V., The petrology of the kimberlites, translated by D. A. Brown, Publication no. 150, Canberra, Department of Geology, Australian National University, A. C. T., 194 pp., 1970.

Gittens, J., R. H. Hewins, and A. F. Laurin, Kimberlitic-carbonatitic dikes of the Saguenay River Valley, Quebec, Canada, Phys. Chem. Earth, 9, 126-148, 1975.

Griffin, W. L., and P. N. Taylor, The Fen damkjernite: petrology of a "central-complex kimberlite," Phys. Chem. Earth, 9, 163-178, 1975.

Hawthorne, J. B., Kimberlite sills, Geol. Soc. South Africa Trans. 71, 291-311, 1968.

Hills, F. A., and R. L. Armstrong, Geochronology of Precambrian rocks in the Laramie Range and implications for the tectonic framework of Precambrian southern Wyoming, Precambrian Research, 1, 213-225, 1974.

Kridelbaugh, S. J., R. Hobblitt, K. Kellogg, and E. Larson, Petrologic and paleomagnetic implications of the Green Mountain diatreme (abs.), Geol. Soc. Amer. Abstr. Prog., 4 (no. 6), 386, 1972.

Kridelbaugh, S. J., and H. O. A. Meyer, Kimberlite from Green Mountain, Colorado: Mineralogy and Petrology (abs.), EOS, 84, 1224, 1973.

McCallum, M. E., An emplacement model to explain contrasting mineral assemblages in adjacent kimberlite pipes, Journal of Geol., 84, 673-684, 1976.

McCallum, M. E., and D. H. Eggler, Mineralogy of the Sloan diatreme, a kimberlite pipe in northern Larimer County, Colorado, Am. Mineralogist, 55, 1735-1749, 1971.

McCallum, M. E., and D. H. Eggler, Diamonds in an upper mantle peridotite nodule from kimberlite in southern Wyoming, Science, 192 (no. 4236), 253-256, 1976.

McCallum, M. E., D. H. Eggler, and L. K. Burns, Kimberlite diatremes in northern Colorado and southern Wyoming, Phys. Chem. Earth, 9, 149-161, 1975.

McCallum, M. E., D. H. Eggler, and C. B. Smith, Discrete nodule assemblages in kimberlite from northern Colorado and southern Wyoming, Extended Abstracts, Second International Kimberlite Conference, Santa Fe, New Mexico, 1977.

McCallum, M. E., and C. D. Mabarak, Diamond in kimberlite diatremes of northern Colorado, Geology, 4, 467-469, 1976a.

McCallum, M. E., and C. D. Mabarak, Diamond in State Line kimberlite diatremes, Albany County, Wyoming, Larimer County, Colorado, Wyo. Geol. Survey Report of Invest., no. 12, 36 p., 1976b.

McCallum, M. E, C. D. Mabarak, and H. G. Coopersmith, Diamonds from kimberlite in the Colorado-Wyoming State Line district, Extended Abstracts, Second International Kimberlite Conference, Santa Fe, New Mexico, 1977.

Meyer, H. O. A., and S. J. Kridelbaugh, Green Mountain kimberlite, Colorado: Mineralogy and petrology, Extended Abstracts, Second International Kimberlite Conference, Santa Fe, New Mexico, 1977.

Mitchell, R. H., Composition of perovskite in kimberlite, Amer. Mineralogist, 57, 1748-1753, 1972.

_____, Composition of olivine, silica activity, and oxygen fugacity in kimberlite, Lithos., 6, 65-81, 1973.

Naeser, C. W., and M. E. McCallum, Fission-track dating of kimberlitic zircons, Extended Abstracts, Second International Kimberlite Conference, Santa Fe, New Mexico, 1977.

Robinson, D. N., Magnetite-serpentine-calcite dikes at Premier Mine and aspects of their relationship to kimberlite and to carbonatite of alkalic carbonatite complexes, Phys. Chem. Earth, 9, 61-70,1975.

Simkin, T., Flow differentiation in the picritic sills of North Skye, Ultramafic and Related Rocks, edited by P. J. Wyllie, pp. 64-68, John Wiley & Sons, Inc., New York, 1967.

Smith, C. B., Kimberlite and mantle derived xenoliths at Iron Mountain, Wyoming, unpubl. M. S. thesis, Colorado State University, 218 p., 1977.

Smith, C. B., M. E. McCallum, and D. H. Eggler, Kimberlite with carbonatitic affinities at Iron Mountain, Wyoming (abs.), Geol. Soc. Amer. Abstr. Prog., 9 (no. 6), 763, 1977.

Woolsey, T. S., M. E. McCallum, and S. A. Schumm, Modeling of diatreme emplacement by fluidization, Phys. Chem. Earth, 9, 29-42, 1975.

PETROGENESIS OF KIMBERLITES AND ASSOCIATED POTASSIC LAMPROPHYRES FROM CENTRAL WEST GREENLAND

B.H. Scott*

Grant Institute of Geology, University of Edinburgh, West Mains Road,
Edinburgh EH9 3JW, Scotland

Abstract. A suite of kimberlite and potassic lamprophyre (or lamproite) dykes occur in the area of Holsteinsborg, Central West Greenland. These dykes are extremely fresh and apparently uncontaminated and, therefore, particularly suitable for a whole-rock geochemical study.

The dykes were formed by multiple injections of magma. Most of the kimberlites are diopside-phlogopite-kimberlites, and their chemistry is typical of micaceous kimberlites. Dunites form a large proportion of the ultrabasic inclusions found in the kimberlite dykes. The potassic lamprophyres are rather unusual in that (i) some have ubiquitous titaniferous phlogopite, pseudoleucite, potassic richterite and olivine as major constituents and (ii) they have very high K_2O contents (up to 10 wt%) together with high volatile contents while still containing substantial amounts of (MgO+FeO). These dykes, therefore, show many similarities to other ultrapotassic magnesian rocks such as lamproites. The potassic lamprophyres can be distinguished chemically from the kimberlites by higher SiO_2, K_2O, Al_2O_3, Na_2O, P_2O_5, Rb, Sr, Y, Zr, Ba, Ce and La but lower MgO, FeO, Fe_2O_3, CaO, MnO, H_2O^+, Cr, Ni and Cu.

Recalculating whole-rock analyses on a volatile-free basis, the interpretation of the geochemistry of the Holsteinsborg dykes using mainly extract calculations and variation diagrams is consistent with the following petrogenetic model: (i) the modification of a parental kimberlitic magma by olivine (with minor chromite) fractionation to a liquid that was then intruded to form the kimberlite dykes (ii) the evolution of the initial lamprophyric magma from a parental kimberlitic magma by the fractionation of olivine plus spinel (titano-magnetite) (iii) further evolution of the lamprophyric magma by olivine plus clinopyroxene plus phlogopite (± pseudoleucite) fractionation prior to intrusion.

*Present address: Anglo American Research Laboratories, P.O. Box 106, Crown Mines, 2025, Transvaal, South Africa.

Introduction

In the region south of Holsteinsborg, Central West Greenland, numerous post-tectonic dykes intrude the Precambrian basement gneisses. These dykes are mostly kimberlites and potassic lamprophyres. The localities, field relations, petrography and mineral chemistry of these dykes are to be published elsewhere and have been discussed in detail in Scott (1977). These dykes are extremely fresh and apparently free of contamination by crustal material and so are very suitable for a whole-rock geochemical study. Few such studies have been completed for other kimberlites because they are often substantially altered. The close relationship in space, and possibly in time, of these kimberlites with the potassic lamprophyres (which could also be termed lamproites) provides an exceptional opportunity to study the well-documented, but little understood, association of kimberlites with other alkaline mafic rocks.

Salient Features of the Dykes

The majority of dykes discussed in this paper occur in the coastal area between Holsteinsborg and Itivdleq, 50 km to the south. The kimberlite dykes are confined to the northern-most 10 km while the lamprophyres are found in the central and southern parts of this coastal area.

All these dykes are narrow intrusions which have fairly consistent strike directions and can sometimes be followed for 2-3 km. Features such as internal contacts suggest that they were formed by multiple injections of magma.

The kimberlites have macrocrysts (terminology after Clement et al.1977) of olivine, phlogopite, picroilmenite and rare pyrope garnet in a matrix of olivine, phlogopite, clinopyroxene, carbonate, serpentine, apatite, perovskite and spinel. Most of the rocks are diopside-phlogopite-kimberlites using the classification of Skinner and Clement (1977). Parts of the dykes contain high concentrations of rounded inclusions dominated by dunites, an unusual inclusion suite in comparison with inclusion suites from other

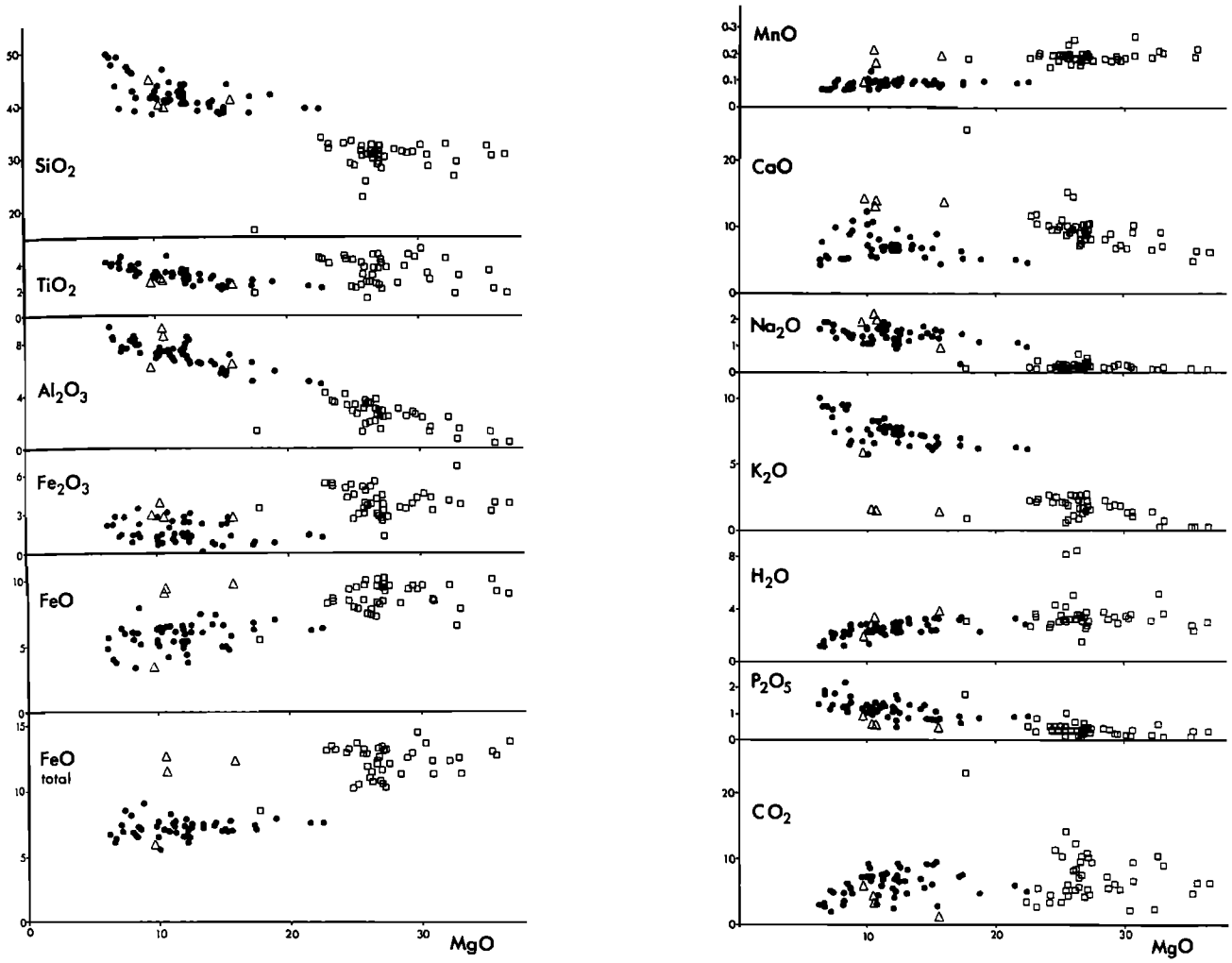

Fig. 1. Major oxide (wt%) variation diagrams of the Holsteinsborg dykes, plotted with MgO as the abscissa. Squares = kimberlites; circles = potassic lamprophyres; triangles = anomalous lamprophyres.

kimberlites. Lherzolites, wehrlites, harzburgites, garnet-granulites and eclogites are also found.

The potassic lamprophyres have macrocrysts of phlogopite, pseudoleucite, olivine and diopside set in a finer-grained groundmass which may include phlogopite, potassic richterite, diopside, alkali feldspar, priderite, carbonate and serpentine. Numerous assemblages of these minerals are found among the lamprophyres and as a result it is difficult to find a term which encompasses all the varieties, particularly since the nomenclature of potassium-rich mafic rocks is very confused. This problem is discussed in more detail by Scott (1977, in preparation) but it should be noted firstly, that rocks with felsic phenocrysts should not strictly be called lamprophyres, and secondly, that although "lamproite" may be an equally good term for some of the Holsteinsborg dykes, it does not emphasise the volatile- and olivine-rich nature of many of the dykes.

Abundant deep red-brown titaniferous phlogopite, often with rims of tetraferriphlogopite (term after Rimskaya-Korsakova and Sokolova 1966), and groundmass diopside, carbonate, apatite and serpentine are features common to nearly all the dykes. The primary carbonate and serpentine often form relatively large patches or segregations. The olivine compositions, particularly in the kimberlites, have a wide range of Mg/(Mg + Fe) ratios ($Mg_{78-92.5}$).

The mineralogy and chemistry of a few dykes from the Holsteinsborg area did not obviously fit into the pattern of lamprophyre intrusion and hence are referred to as the "anomalous lamprophyres". A few samples from these dykes were included in the geochemical study but will not be discussed in any detail.

Whole-Rock Geochemistry

The Holsteinsborg dykes are mostly ultrabasic and when compared to other ultrabasic rocks are relatively rich in K_2O, TiO_2, CaO, Rb, Sr, Y, Zr and Ba. The whole-rock data are summarised in the form of histograms in Scott (1977, in preparation) and on oxide versus oxide variation diagrams in this paper (Figures 1 and 2). Some representative whole-rock analyses are given in Tables 1 and 2 and the analytical techniques are given in Appendix 1. These data show that the Holsteinsborg dykes include rocks with a wide range of compositions, particularly in MgO and K_2O. The dykes, however, do form two compositionally distinct groups which are consistent with the division into kimberlitic and lamprophyric types using field, petrographical and mineralogical evidence.

The lamprophyres are distinguished from the kimberlites by higher SiO_2, K_2O, Al_2O_3, P_2O_5, Rb, Sr, Y, Zr, Ba, Ce and La but lower MgO, FeO, Fe_2O_3, CaO, MnO, H_2O^+, Cr, Ni and Cu. All the dykes are rich in CO_2.

Major Element Chemistry

The Holsteinsborg kimberlites have all the chemical characteristics of micaceous kimberlites (Dawson 1967) except for lower H_2O^+ contents. High CO_2 values typical of kimberlites are found, but in samples where SiO_2 values are less than 30 wt% the CO_2 contents are greater than 10 wt% and these are referred to as

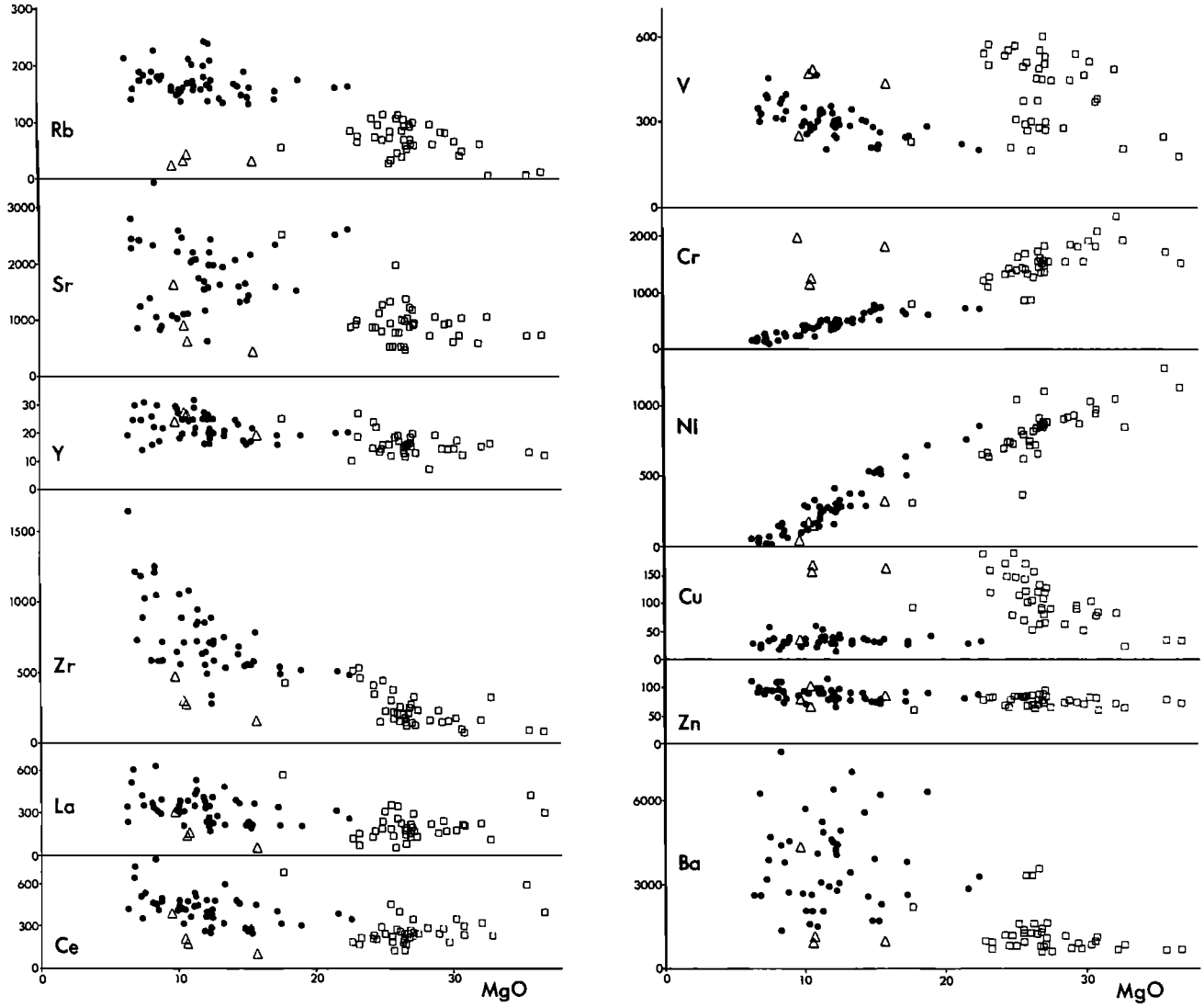

Fig. 2. Trace element variation diagrams for the Holsteinsborg dykes (ppm) with MgO (wt%) as the abscissa. (Symbols as for Fig. 1).

TABLE 1. Representative Whole-Rock Chemical Analyses of the Holsteinsborg Kimberlite Dykes (nd = not detected).

SAMPLE	5508	5607	5699	5820	5903	5907	5932	5966	5973	5997	5999A
Major Oxides (wt%)											
SiO_2	31.18	32.42	31.33	26.53	30.45	16.40	30.30	29.98	32.98	30.78	33.06
TiO_2	2.57	3.88	3.80	1.84	2.12	1.94	3.36	3.82	4.07	4.67	4.36
Al_2O_3	3.38	3.77	2.47	0.61	0.44	1.28	1.72	2.37	3.50	2.64	3.34
Fe_2O_3	3.71	4.18	3.50	6.68	3.95	3.49	4.26	2.77	5.42	3.82	4.53
FeO	7.69	9.49	9.33	6.50	9.23	5.45	8.44	9.57	8.42	9.50	9.50
MnO	0.18	0.19	0.18	0.22	0.23	0.19	0.27	0.18	0.20	0.18	0.20
MgO	26.00	26.63	28.91	32.78	35.75	17.24	30.84	27.49	23.24	29.33	25.01
CaO	9.78	8.04	9.44	9.58	6.50	24.81	9.49	8.34	12.02	7.09	10.16
Na_2O	0.28	0.26	0.12	0.06	0.05	0.14	0.11	0.25	0.17	0.35	0.31
K_2O	2.84	2.10	1.88	0.09	0.29	0.99	1.40	1.58	2.27	2.00	2.12
H_2O^+	3.59	3.16	3.34	5.64	2.91	3.16	3.82	3.29	3.86	3.51	3.12
P_2O_5	0.44	0.25	0.49	0.66	0.40	1.80	0.32	0.41	0.91	0.34	0.50
CO_2	8.29	5.88	5.31	10.58	6.71	23.39	6.67	9.61	2.72	6.10	3.78
Total	99.93	100.25	100.10	101.77	99.03	100.78	101.00	99.66	99.78	100.31	99.99
Minor Elements (ppm)											
V	271	496	456	224	269	247	372	450	518	550	574
Cr	1357	1467	1822	1912	1756	816	1840	1565	1172	1798	1380
Ni	770	663	918	840	1275	329	994	880	652	922	739
Cu	102	161	102	23	34	91	78	79	157	87	145
Zn	69	73	71	65	80	60	82	73	82	78	86
Rb	107	95	62	nd*	9	53	43	58	75	82	68
Sr	793	499	1078	1090	749	2524	744	961	908	918	806
Y	18	15	19	16	13	25	17	13	18	14	14
Zr	209	179	234	327	90	412	101	229	535	154	440
Ba	1298	1309	754	789	688	2210	932	649	766	906	848
La	276	177	164	114	443	582	238	153	82	251	201
Ce	291	193	247	231	604	687	313	249	173	288	217

carbonate-rich kimberlites. The average Mg/Fe(t) and K/Na ratios of 1.75 and 8.1 respectively are typical of micaceous kimberlites. The Fe^{3+}/Fe^{2+} ratios for all the Holsteinsborg dykes lie within the range 0.3 - 0.4 and vary sympathetically with the H_2O^+ content. Values of less than 1 for this ratio are usual for other ultrabasic rocks such as peridotites and dunites, but Dawson (1967) suggests a much higher value of 7.5 for kimberlites. It has already been noted that the Holsteinsborg dykes contain considerably less H_2O^+ than other kimberlites and show significantly less alteration than, say, many South African kimberlites. It appears, therefore, that the Fe^{3+}/Fe^{2+} ratio varies with the H_2O^+ content and generally reflects the degree to which these rock types have been altered, particularly through serpentinisation.

The lamprophyre dykes are characterised by high K_2O contents (up to 10 wt%) and therefore, are referred to as potassic lamprophyres. These extreme K_2O contents, which are very unusual in such magnesian rock types, together with certain mineralogical features of the Holsteinsborg lamprophyres indicate a similarity with the rare ultrapotassic volcanics, such as lamproites, from the Leucite Hills, Wyoming (Carmichael 1967b) and West Kimberley, Western Australia (Wade and Prider 1940). The high K_2O content, along with high Al_2O_3, reflects not only abundant phlogopite in these rocks but also the pseudoleucite macrocrysts, groundmass feldspar and potassic richterite.

These major element data have been summarised using simple oxide versus oxide variation diagrams in Figure 1. With decreasing MgO the kimberlites show poorly defined increases of K_2O, Al_2O_3 and CaO, while the potassic lamprophyres show increases of TiO_2, Al_2O_3 and K_2O. It can also be seen from many of these variation diagrams that the potassic lamprophyres tend to plot on a continuation of the kimberlite trends, possibly implying a genetic relationship between the two groups.

The undersaturated nature of the kimberlite dykes is reflected in the high normative percentage of ol, the occurrence of ne and lc and occasionally cs (Ca_2SiO_4). In contrast, the potassic lamprophyres are silica saturated and mostly hy normative and a few samples are even qtz normative. The high normative or in part reflects the abundant phlogopite. The occurrence of ks and ns (K_2SiO_3 and Na_2SiO_3 respectively),

which are rarely found in norms, reflect the peralkaline nature of these rocks.

The combination of both the hy normative and peralkaline nature of these rocks is unusual but has been noted in similar rock types including wyomingites and orendites from the Leucite Hills (Carmichael 1967b), and wolgidites, cedricites, fitzroyites and mamilites from West Kimberley (Wade and Prider 1940).

Trace Element Geochemistry

The trace element concentrations of some of the Holsteinsborg dykes are given in Tables 1 and 2 while all the data are summarised in variation diagrams in Figure 2.

The main characteristic of the trace element contents of the Holsteinsborg dykes is their often extremely high concentrations. The trace elements fall into the same two contrasting groups recognised in kimberlites by Dawson (1962, 1967). One suite of elements, including Cr and Ni, occur in amounts characteristic of ultrabasic rocks and the second suite, including Rb, Sr, Y, Zr, Ba, Cu, V and La, occur in greater amounts than is usual for ultrabasic rocks. It is also well known that potassic lamprophyres (or lamproites) show similar trace-element patterns to kimberlites, and that many of these unusual characteristics are further intensified in carbonatites. This also holds for the Holsteinsborg dykes.

Petrogenesis

For a discussion about the petrogenesis of these rock types to be meaningful the analyses should be considered on a volatile-free basis. Although the CO_2 and H_2O^+ are considered to be primary constituents of the magma some attempt must be made to account for the random loss or relative movement of either volatiles or an immiscible volatile-rich fluid during emplacement. In the Holsteinsborg dykes this late-stage H_2O- and CO_2-rich fluid is now represented by groundmass serpentine and calcite which often form relatively large patches or segregations. In some dykes the segregations are concentrated

TABLE 2. Representative Whole-Rock Chemical Analyses of the Holsteinsborg Potassic Lamprophyre Dykes (nd = not detected).

	Potassic Lamprophyres												Anom. Lampro-phyre
Sample	5611	5622A	5623	5629	5630	5634	5637	5652	5653	5664	5942	5945	5672
Major Oxides (wt%)													
SiO_2	38.28	39.21	41.58	40.22	41.37	41.92	41.91	49.60	40.13	41.39	49.06	41.63	40.45
TiO_2	2.24	2.24	3.46	3.11	4.00	3.15	2.65	4.15	2.88	2.84	4.05	3.11	2.38
Al_2O_3	5.60	5.01	7.11	6.47	7.44	7.01	5.94	8.64	6.59	6.54	9.26	7.70	6.43
Fe_2O_3	2.33	1.49	1.28	0.12	1.31	2.46	0.97	2.21	1.36	0.98	1.41	1.24	2.72
FeO	4.83	6.14	6.19	7.41	7.86	5.27	6.93	4.75	5.97	6.09	5.65	6.14	9.76
MnO	0.09	0.10	0.09	0.09	0.10	0.10	0.10	0.07	0.10	0.09	0.08	0.10	0.19
MgO	15.30	21.61	12.02	13.44	8.75	11.17	18.95	6.32	12.53	17.38	7.32	9.88	15.84
CaO	8.99	5.02	7.40	7.37	9.69	6.65	5.22	4.32	7.37	5.37	4.98	10.14	13.66
Na_2O	1.60	1.13	1.59	1.55	1.14	1.95	1.16	1.60	1.54	1.49	1.56	1.34	0.84
K_2O	6.27	6.25	7.54	7.36	6.81	7.54	6.10	10.03	7.25	7.09	9.19	6.89	1.14
H_2O^+	3.30	3.36	2.25	2.96	2.84	2.43	2.36	1.12	2.27	3.17	1.86	2.71	3.65
P_2O_5	0.76	0.94	1.60	1.39	1.65	1.31	0.88	1.26	1.05	0.65	1.30	1.26	0.33
CO_2	9.00	5.94	5.33	6.29	4.45	6.68	4.73	2.93	8.81	7.24	1.98	7.10	0.77
Total	98.59	98.44	97.44	97.78	97.41	97.64	97.90	97.00	97.85	100.32	97.70	99.24	98.16
Minor Elements (ppm)													
V	219	236	364	352	407	318	288	359	300	253	400	298	437
Cr	755	744	509	536	285	393	657	164	486	627	208	257	1797
Ni	557	782	250	294	94	291	728	54	342	505	89	98	306
Cu	30	28	41	28	39	53	42	26	46	35	35	39	159
Zn	75	81	82	91	73	99	89	111	79	76	96	86	82
Rb	144	162	180	133	180	159	125	216	170	138	176	160	30
Sr	1385	2549	1582	1940	857	2174	1578	2365	1994	1619	2419	1114	409
Y	17	19	27	21	30	25	19	19	20	16	25	20	18
Zr	557	505	730	759	714	844	516	1648	586	495	894	648	142
Ba	1730	2838	6405	7002	2764	3149	6379	2590	3017	2622	3883	2738	990
La	221	322	395	486	390	351	206	344	235	215	421	308	42
Ce	284	384	487	598	477	441	298	423	364	312	523	413	103

in certain areas, often towards the margin of the dyke. It appears, therefore, that the amount of carbonate and associated minerals included in a rock after solidification is not governed by the evolution of the magma but by the conditions controlling the movement or escape of the more mobile volatile-rich fluid. The whole-rock analyses for the Holsteinsborg dykes, therefore, were replotted having removed the H_2O^+ and CO_2 as $Ca(Mg)CO_3$ and recalculating to 100%. Most of the carbonate in the kimberlite dykes is calcite, sometimes with minor magnesian contents, so the CO_2-free analyses were calculated by the removal of $CaCO_3$. This might not be quite so accurate for the lamprophyre dykes because higher MgO contents (up to 22 wt%) were more frequently found. For some analyses the removal of $CaCO_3$ (equivalent to the CO_2) gave a small negative CaO content and this was compensated for by removing an equivalent amount of MgO. For some oxides the adjusted analyses, recalculated to 100%, show less scatter when plotted on similar variation diagrams to those in Figures 1 and 2.

This treatment of the whole-rock data on a $Ca(Mg)CO_3$- and H_2O^+-free basis is even further justified if the carbonate-rich segregations are indicative of liquid immiscibility at the time of intrusion. It has often been suggested that the volatile-rich and silicate fractions of kimberlites (Clement 1975) and other alkaline ultrabasic rocks (Ferguson and Currie 1971) are immiscible.

(a) Extract Calculations

It has already been noted that the continuous trends obtained on some of the variation diagrams may indicate a simple genetic relationship between the kimberlites and potassic lamprophyres. Extract calculations, using a modification of the least-square-fit computer program of Wright and Doherty (1970), were performed in an attempt to obtain a solution which might substantiate this possible relationship. Table 3 lists representative analyses of minerals found in the Holsteinsborg dykes which may be important in the evolution of the magmas. The average kimberlite and potassic lamprophyre compositions given in Table 4 (calculated free of $Ca(Mg)CO_3$ and H_2O^+ were used to represent the parent and evolved magmas. Using spinel (192 from Table 3) and pure forsterite and fayalite as possible precipitating phases the following solution was obtained:

$$\underset{\text{magma}}{\text{kimberlite}} = 28.96\% \underset{\text{magma}}{\text{lamprophyre}} + 55.66\% \text{ olivine } (Mg_{91.5}) + 15.38\% \underset{192}{\text{spinel}}$$

This solution gives the sum of the residuals as 0.24 and, as values of less than one are generally considered to be meaningful, it strongly suggests a simple genetic relationship between the kimberlites and lamprophyres. This calculation shows that the fractionation of a kimberlite magma with the formation of a precipitate of 22% spinel and 78% olivine would result in a liquid with the composition of the average lamprophyre. A more detailed petrogenetic model based on the above solution is developed by presenting the whole-rock geochemistry in other ways.

(b) Variation Diagrams

The major element analyses of the Holsteinsborg dykes are plotted on MgO versus oxide variation diagrams in Figure 1. Although the use of variation diagrams is debatable they are useful for illustrating the compositional relations within groups of rocks. It has already been shown, however, that it is more appropriate to use volatile-free analyses. Figure 3 shows the main compositional fields for the kimberlites and potassic lamprophyres using the $Ca(Mg)CO_3$- and H_2O^+-free analyses on similar variation diagrams to Figure 1. With decreasing MgO (i) the kimberlites show an increase of Al_2O_3, K_2O and TiO_2 and a poorly defined decrease of FeO (total) and MnO, (ii) the lamprophyre dykes show an increase of SiO_2, TiO_2, Al_2O_3, K_2O, P_2O_5 and possibly Na_2O and poorly defined decreases of FeO (total) and MnO. There is little change in the plot of P_2O_5 versus MgO from Figure 1 to Figure 3 and so P_2O_5 should perhaps have been considered as a volatile, particularly as the apatite in these rocks is generally associated with the calcite, and their co-crystallisation in carbonatitic-like fluids has been suggested by Biggar (1969).

Possible fractionating phases have also been plotted on Figure 3 (largely from Table 3). The variation in chemistry within each group of dykes can be explained mainly by olivine fractionation or enrichment. The kimberlite trend leads away from an olivine with the composition, Mg_{85}, found for the euhedral crystals in the kimberlite dykes. The lamprophyres, however, trend away from an olivine with a composition of $Mg_{91.5}$, which is the mean composition of the olivines found in the lamprophyre dykes. It can be seen from Figure 3 that in detail the lamprophyre trend might be more accurately explained by extracting relatively minor amounts of clinopyroxene and phlogopite in addition to the olivine. The control point for the lamprophyre trend, therefore, would lie within the triangle joining olivine, clinopyroxene and phlogopite, but close to the olivine apex. The position of this point is difficult to define because of the uncertainty in the composition of the fractionating phlogopite (the analysed macrocrysts show considerable variation in chemical composition).

Since most of the rocks considered in this study are porphyritic, it is difficult to

TABLE 3. Selected Mineral Analyses from the Holsteinsborg Dykes

	Kimberlites						Dunite Inclusions			Potassic Lamprophyres					
Mineral	OL	OL	SP	ILM	PLG	PLG	OL	OL	CHR	OL	CPX	PLG	PLG	FELD	PSD
Sample Number	5975	5512	5518G	5518G	5518G	5966(2)	5984b	5518G	5951	5612	5693	5646	5693	5632	5693
Analysis Number	375	173	192	214	200	129	469	187	119	424	143	165	137	519	138
SiO_2	39.92	40.98	0.30	0.04	40.76	37.49	40.48	41.78	0.09	41.20	53.35	39.58	39.81	63.30	64.37
TiO_2	0.05	nd	20.87	52.12	0.44	4.44	0.04	0.01	0.05	nd	1.11	7.32	6.65	0.30	0.01
Al_2O_3	0.03	nd	1.86	0.99	11.52	15.36	0.05	0.03	3.18	-	0.51	11.65	9.70	15.94	18.25
Cr_2O_3	0.09	0.11	0.93	1.87	nd	0.21	nd	nd	61.71	0.05	0.67	0.62	nd	nd	nd
FeO	14.28	8.03	61.13+	33.00x	10.21	7.26	13.07	8.06	24.09o	8.10	2.95	5.64	7.61	2.85	0.13
MnO	0.14	0.18	0.77	0.28	0.09	0.05	0.22	0.18	0.91	0.12	0.04	0.02	nd	nd	nd
NiO	0.29	0.40	0.10	0.12	0.03	-	0.36	0.34	-	0.37	nd	0.14	0.12	nd	nd
MgO	45.79	50.93	10.19	11.06	21.99	19.64	46.25	50.56	10.16	49.63	16.97	20.80	20.49	0.03	nd
CaO	0.12	0.08	0.72	0.03	0.01	nd	0.11	nd	nd	0.06	23.29	0.07	0.03	0.03	0.02
Na_2O	nd*	0.05	0.03	nd	0.04	0.32	-	0.02	nd	-	0.47	0.11	0.09	0.40	0.03
K_2O	0.03	nd	nd	nd	10.17	9.59	-	nd	nd	-	0.02	9.96	9.61	15.73	16.58
Total	100.74	100.76	96.90	99.51	95.26	94.36	100.58	100.98	100.19	99.53	99.38	95.91	94.11	98.58	99.39
Formula															
Si	0.993	0.991	0.010	0.002	5.958	5.467	1.002	1.006	0.003	1.007	1.960	5.659	5.838	12.049	11.993
Ti	0.001	-	0.543	1.817	0.048	0.487	0.001	-	0.001	-	0.031	0.787	0.733	0.043	0.001
Al	0.001	-	0.076	0.005	1.985	2.640	0.001	0.001	0.127	-	0.022	1.963	1.677	3.576	4.007
Cr^{3+}	0.002	0.002	0.025	0.069	-	0.024	-	-	1.645	0.001	0.019	0.070	-	-	-
Fe^{2+}	-	-	0.791	0.237	-	-	-	-	0.215	-	-	-	-	-	-
Fe	0.297	0.162	0.977	1.043	1.248	0.885	0.271	0.162	0.469	0.165	0.091	0.674	0.933	0.454	0.020
Mn	0.003	0.004	0.023	0.011	0.011	0.006	0.005	0.004	0.026	0.002	0.001	0.002	-	-	-
Ni	0.006	0.008	-	0.004	0.004	-	0.007	0.007	-	0.007	-	0.016	0.014	-	-
Mg	1.698	1.837	0.525	0.764	4.791	4.269	1.707	1.814	0.515	1.808	0.929	4.432	4.479	0.009	-
Ca	0.003	0.002	0.027	0.001	0.002	-	0.003	-	-	0.002	0.917	0.011	0.005	0.006	0.004
Na	-	0.002	0.002	-	0.011	0.090	-	0.001	-	-	0.033	0.030	0.026	0.148	0.011
K	0.001	-	-	-	1.896	1.784	-	-	-	-	0.001	1.816	1.768	3.820	3.941
O	4.000	4.000	4.000	6.000	22.000	22.000	4.000	4.000	4.000	4.000	6.000	22.000	22.000	32.000	32.000
Atomic Ratio															
$\frac{Mg}{Mg+Fe}$	0.85	0.92	-	-	0.79	0.83	0.86	0.92	-	0.92	-	0.87	0.83	-	-

Explanation

* nd = not detected; + recalculated analysis (after Carmichael 1967a) FeO = 33.8, Fe_2O_3 = 30.4; x FeO = 26.9, Fe_2O_3 = 6.8; o FeO = 16.5, Fe_2O_3 = 8.4; OL 375 - 0.5 mm euhedral olivine; OL 173 - 3 mm anhedral olivine; SP 192 - <0.1 mm subhedral oxide; ILM 214 -0.7 mm ragged anhedral oxide; PLG 200 - centre of a 1 mm euhedral tabular phlogopite macrocryst; PLG 129 - small groundmass phlogopite; OL 469 - an olivine from small granuloblastic dunite; OL 187 - large olivine from a coarse dunite; CHR 119 - opaque oxide in a coarse dunite; OL 424 - 3 mm anhedral olivine; CPX 143 - 1.2 mm subhedral clinopyroxene macrocryst; PLG 165 - 1 mm slender phlogopite lath; PLG 137 - 0.75 mm basal section phlogopite; FELD 519 - groundmass feldspar lath; PSD 138 - large pseudoleucite macrocryst.

TABLE 4. The Average Major Oxide Compositions of the Holsteinsborg Kimberlite and Potassic Lamprophyre Dykes. (calculated using the 41 kimberlite and 52 lamprophyre analyses).

	Average Kimberlite	Average Potassic Lamprophyre
SiO_2	30.18	41.76
TiO_2	3.39	3.12
Al_2O_3	2.48	7.17
Cr_2O_3	0.22	0.08
Fe_2O_3	3.92	1.85
FeO	8.68	5.85
MnO	0.19	0.10
MgO	27.53	11.84
CaO	9.65	7.85
Na_2O	0.25	1.42
K_2O	1.82	7.05
H_2O^+	3.70	2.49
P_2O_5	0.51	1.14
CO_2	7.39	5.72

distinguish that part of the trend due to liquid evolution from the part which may be the result of phenocryst and/or xenocryst accumulation in the liquid. In these rocks it is virtually impossible to differentiate between xenocrysts and phenocrysts. The few composite olivine macrocrysts might be considered to be xenocrysts, but they would have little effect on the whole-rock chemistry of the dykes as they represent a very small proportion of the total olivine present. In any event, the dunite inclusions in the Holsteinsborg kimberlites are thought to represent cumulates from the olivine fractionation of the dykes rather than exotic xenolithic material. The wide range and close match of the compositions of olivine occurring as macrocrysts and in the dunite inclusions is the main evidence supporting this conclusion.

The wide range of Mg/(Mg + Fe) ratios found among the olivines, particularly in the kimberlites ($Mg_{78-92.5}$) does imply that olivine fractionation has taken place. Both the kimberlite and lamprophyre dykes, therefore, may have resulted from pulsatory eruption from magma systems fractionating primarily olivine.

It has already been suggested from the extract calculations that the lamprophyres may be genetically related to the kimberlites and both groups of samples also plot on a fairly continuous trend in many of the variation diagrams in Figure 3. Any discussion of possible relationships between the two groups requires an estimate of the composition of the initial liquids from which the two groups of dykes evolved, probably by the fractionation processes just discussed. The average compositions of each group of dykes (given in Table 4) were taken to represent these initial liquid compositions. For the lamprophyre dykes the average composition is similar to the most magnesian, aphyric rock analysed (sample 5653, see Table 2). It should be noted that some modification to the proposed initial liquid compositions within the range of observed compositions does not alter the principal conclusions of the following discussion.

The extract calculations and wide range of olivine compositions have already been used to suggest that olivine fractionation was an important control on the composition of magmas forming the Holsteinsborg dykes. It is clear from Figure 3, however, that the variation in chemistry of the group as a whole cannot be explained solely by olivine fractionation. In the plot of MgO vs. TiO_2 (Figure 3), for example, the evolution from a kimberlitic parental magma to a lamprophyric magma with a similar TiO_2 content cannot be explained by the fractionation of a TiO_2-free phase, such as olivine. To explain the deviations from an olivine control line requires the crystallisation of a Fe-Ti phase together with olivine. Titanomagnetite is an abundant Ti-rich mineral in the kimberlite dykes. The titanomagnetite analysis 192 (see Table 3) and an olivine of composition $Mg_{91.6}$ (analysis 424, see Table 3) were fractionating phases suggested by the extract calculations. Using these mineral compositions possible olivine plus spinel fractionation trends are illustrated in Figure 3. It can be seen from Figure 3 that the evolution of the initial lamprophyre liquid from the parental kimberlitic magma (represented by the average compositions) is consistent with the fractionation of approximately 78% olivine of composition Mg_{92} and 22% spinel with a composition similar to analysis 192.

The fractionation of titanomagnetite is not often considered to be important in the generation of magmas. The K_2O-Al_2O_3-TiO_2 (wt%) ternary variation diagram given in Figure 4, however, confirms that a TiO_2-bearing phase appears to have an important control in the evolution of the magmas forming the Holsteinsborg dykes. No trends should be evident in this plot if the variation in composition was purely a result of olivine fractionation and this is found to be the case only for the lamprophyre dykes. The trend within the kimberlites (see Figure 4) away from spinel (or more generally TiO_2) is strongly indicative of spinel being a significant fractionating phase in the kimberlites. The lamprophyres plot on the TiO_2-poor extension of the kimberlite trend and so, with respect to the three components being considered here, the lamprophyres could be formed by removal of spinel from a kimberlitic magma.

In summary, it is proposed that: (i) a kimberlitic parental magma evolved by olivine and minor spinel fractionation to a liquid that was then intruded to form the kimberlite dykes,

(ii) a lamprophyric magma evolved from a parental kimberlitic magma by the fractionation of 78% olivine plus 22% spinel, (iii) the lamprophyric magma evolved further by olivine plus clinopyroxene plus phlogopite (± pseudoleucite) fractionation before intrusion.

(c) 'FMA' diagram

Figure 5, which gives the 'FMA' plot for the Holsteinsborg dykes, shows that the two main groups of dykes lie on different trends reflecting the separate evolution of the lamprophyres and kimberlites. The scatter among the MgO-poor lamprophyres may be accounted for by some pseudoleucite (or leucite) fractionation. The fractionation within the kimberlites appears to be controlled by olivine with a mean composition of Mg_{85} but could also be explained (in this plot) by fractionating a more Mg-rich olivine together with 10% spinel. A similar combination of phases, but with about 22% spinel, fractionating from a kimberlitic magma could produce a liquid of lamprophyric composi-

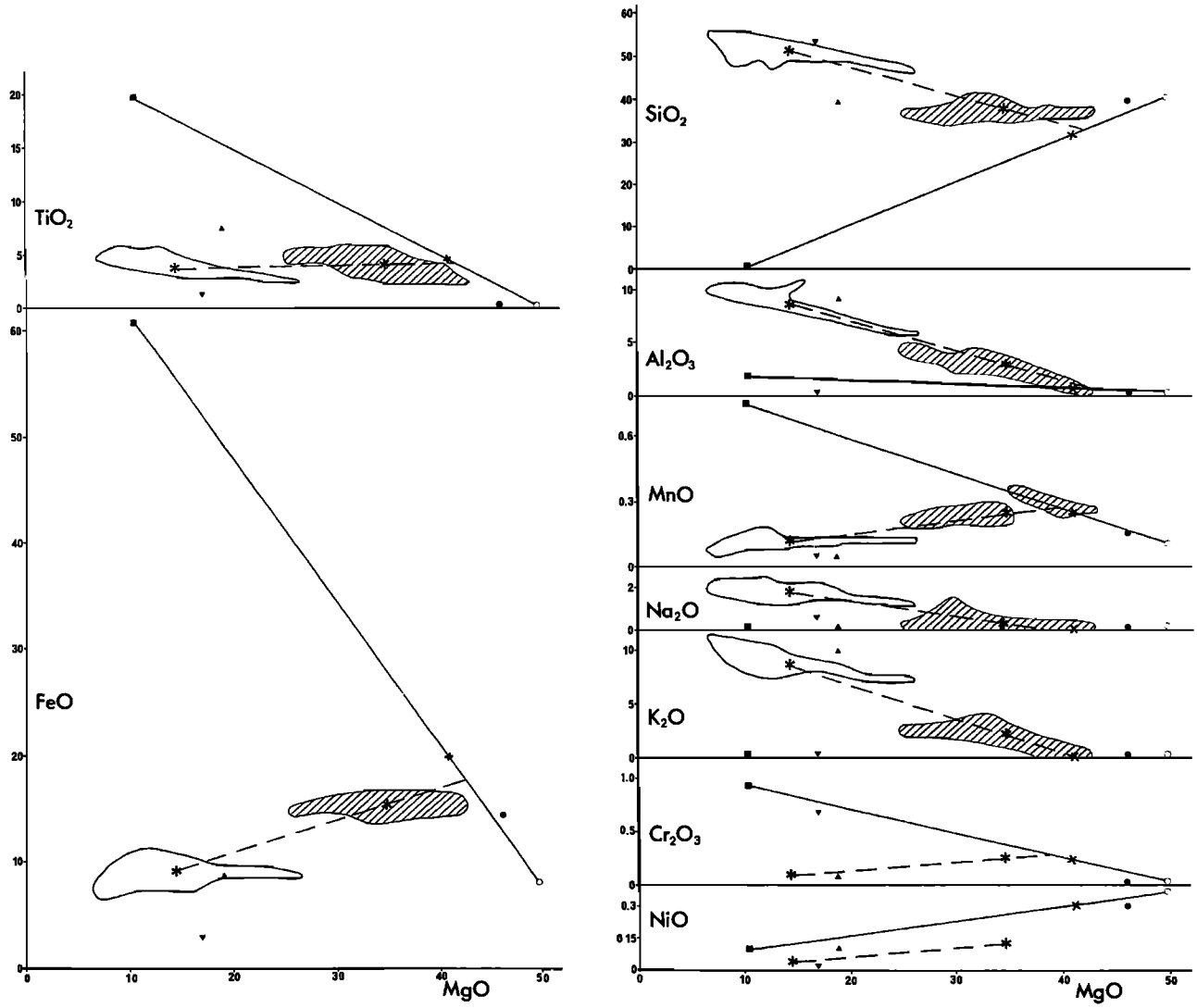

Fig. 3. Compositional fields of the kimberlites and lamprophyres on variation diagrams using $Ca(Mg)CO_3$- and H_2O^+- free analyses; some possible fractionating phases have also been plotted: shaded areas = kimberlite dyke compositions; white areas = potassic lamprophyre dyke compositions; asterisks = average chemical compositions of the kimberlite and potassic lamprophyre dykes (recalculated from Table 4); open circle = olivine, $Mg_{91.5}$ (analysis 424, Table 3) from a lamprophyre dyke; closed circle = euhedral olivine, Mg_{85} from a kimberlite dyke; square = spinel (titanomagnetite analysis 192, Table 3); triangle = first generation phlogopite (analysis 37 from Scott 1977); inverted triangle = clinopyroxene (analysis 143, Table 3).

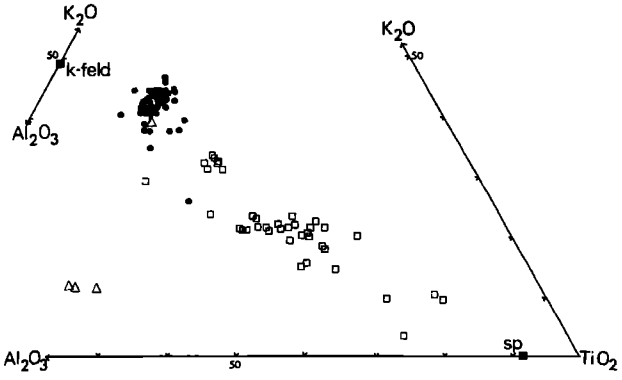

Fig. 4. K_2O-Al_2O_3-TiO_2 ternary (wt%) variation diagram for the Holsteinsborg dykes: K-feld = potassium feldspar; ol = olivine, $Mg_{91.5}$; sp = spinel (analysis 192); squares = kimberlites; circles = potassic lamprophyres; triangles = anomalous lamprophyres.

tion and this is consistent with the proposed model.

(d) Molar ratio comparisons

It is sometimes difficult to discriminate between rival hypotheses for magmatic evolution using variation diagrams and ternary weight per cent plots. To overcome this problem and to determine possible extraction compositions Pearce (1968, 1970) suggested the use of molar ratios comparisons, where molar ratios of the oxides are calculated using one specific oxide as the constant divisor and these values are used to plot variation diagrams.

Examination of the variation diagrams (Figure 3) suggests that K_2O and Al_2O_3, which lie on good and fairly continuous trends and might almost be considered as incompatible elements, would be most suitable for use as the constant divisor for Pearce's method. K_2O is independent of the suggested fractionating phases and so can be used to normalise the other components. Plotting MgO/K_2O vs. SiO_2/K_2O (moles), as shown in Figure 6, a good linear trend is obtained for the kimberlites but is less well defined for the lamprophyres. The slope of the trend obtained should give the MgO/SiO_2 ratio of any extract. The slope of the best fit line for the kimberlites only is approximately 1.83 which indicates that the fractionating phases are most likely to be olivine, $Mg_{91.5}$ plus 10% spinel.

The calculated slope of the line which would join the plots of the suggested initial kimberlite and lamprophyre magmas (from Table 4) on such a diagram is 1.98. This value is close to that predicted for the fractionation of 22% spinel together with 78% olivine, $Mg_{91.5}$ and so is consistent with the proposed model.

On this diagram the anomalous lamprophyre dykes define a line with a less steep gradient relative to the other dykes and is consistent with clinopyroxene fractionation.

(e) C-M-A-S

O'Hara (1968) devised a scheme for representing analytical data for basic and ultrabasic rocks in terms of a pseudo-quaternary system C-M-A-S, the natural analogue of the synthetic quaternary system CaO-MgO-Al_2O_3-SiO_2. The method of projection and location of phase boundaries are given by O'Hara (1968) and Jamieson (1969, 1970). Depending on the position of the points within the tetrahedron some of the projection planes are prone to distortion. A stereoscopic examination of the position of the points within the tetrahedron (as given in Scott 1977) shows that the points representing the Holsteinsborg dyke compositions lie close to a plane parallel to CAM (at S = 40%) and on a line trending away from olivine.

In considering kimberlites and related rock types in terms of the C-M-A-S system a number of uncertainties arise. First, CO_2 is an oxide not accounted for in this scheme and kimberlitic rocks contain high and variable amounts of CO_2, carbonate being an important constituent of these rocks. Kimberlites have been interpreted using the C-M-A-S system by Ferguson et al. (1975) where the analyses were used both complete and CO_2-free, removing the CO_2 as dolomite. In this paper the analyses were used CO_2-free but removing the CO_2 as essentially calcite ($Ca(Mg)CO_3$). Another problem with kimberlitic rocks in the C-M-A-S tetrahedron is their relationship to experimentally determined

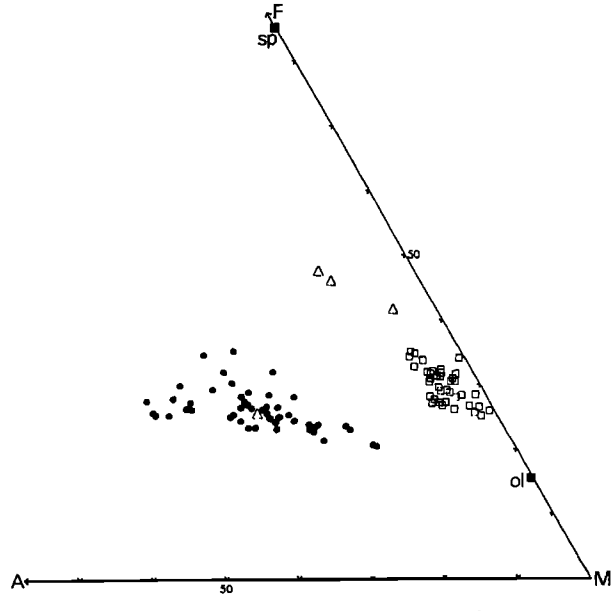

Fig. 5. 'FMA' diagram for the Holsteinsborg dykes: F = FeO + Fe_2O_3; M = MgO; A = Na_2O + K_2O. (Symbols as for Fig. 4).

phase boundaries. Jamieson (1969) has suggested that differences in content of some 'minor' elements (Ti, K, P) may cause shifts in the position of phase boundaries in the C-M-A-S system and the Holsteinsborg dykes do show extreme and variable concentrations of these elements.

Bearing in mind these possible modifying factors the C-M-A-S system can be used to interpret the petrogenesis of the Holsteinsborg dykes.

The projection plane of silica into $CS\text{-}M_2S\text{-}AS$ is close to the plane cutting the tetrahedron in which the Holsteinsborg dykes plot while also passing through the olivine point. Plotting the Holsteinsborg dykes using complete analyses in this projection (not shown) there is a fair amount of scatter but the points lie fairly close to an olivine control line. Plotting the recalculated $Ca(Mg)CO_3$- and H_2O^+-free analyses (as shown in Figure 7) the amount of scatter is reduced significantly and the trends are displaced slightly. The lamprophyre dykes still lie on an olivine trend again indicating that olivine fractionation is the main control of compositions within the lamprophyres. The less magnesian lamprophyres are trending towards the potassium feldspar (or leucite) point. The kimberlite trend, however, shifted away from a true olivine control line towards spinel supporting the earlier suggestion that some spinel may be fractioning together with olivine in the kimberlite magma. This trend is similar to that found for the ultramafic extrusives of the Onveracht Group, South Africa (McIver and Lenthall 1974) which were considered to be the parental to the less magnesian extrusives in that area and were also suggested to have been derived by partial melting at depth.

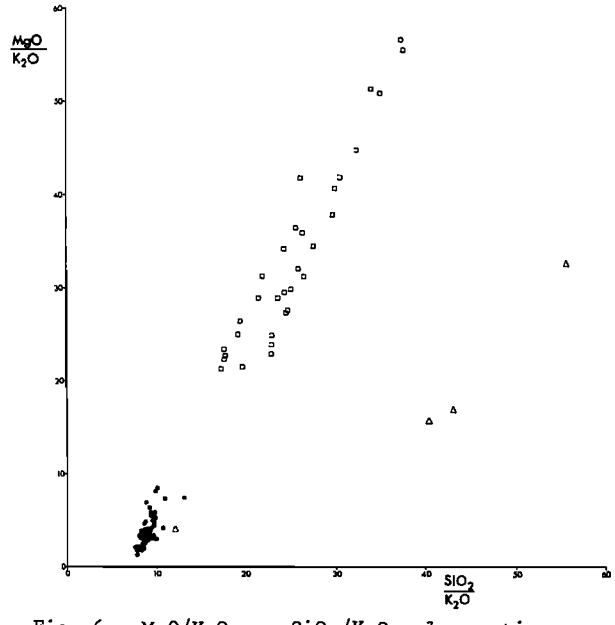

Fig. 6. MgO/K_2O vs. SiO_2/K_2O molar ratio variation diagram for the Holsteinsborg dykes. (Symbols as for Fig. 1).

This plot is also consistent with the derivation of a lamprophyre magma from a parental kimberlite magma by olivine plus spinel fractionation. The clinopyroxene enrichment of the anomalous dykes is again illustrated.

(f) Trace element geochemistry

Although the concentration of trace elements is sensitive to fractionation processes, in this instance they are not so useful in the discussion of the proposed petrogenetic model for the Holsteinsborg dykes because it is difficult to estimate the trace element composition of any possible fractionating phases. It is evident, however, that none of the trace element data contradict the proposed model.

The trace element variation diagrams (Figure 2) generally show a high degree of scatter, but Cr and Ni are the exceptions. Although the NiO vs. MgO variation diagram (Figure 2) reveals a good linear trend, it appears from Figure 3 that the suggested high pressure fractionating phases, Ni-bearing olivine and spinel 192, cannot explain the observed trend. The distribution coefficient for Ni between olivine and silicate liquids, however, is sensitive not only to pressure but also to the composition of the liquid (O'Hara et al. 1975, Hart et al. 1976, Mysen 1976, Irvine and Kushiro, 1976). Hart et al. (1976) suggest that D_{Ni} varies inversely with MgO. The olivine involved in the proposed first stage and relatively high pressure fractionation may, therefore, have had a very low nickel content. If this was the case, the slope of the olivine-spinel tie line given in Figure 3 would be reversed and could be consistent with the proposed fractionation model. The Ni content of olivine, as well as the Fe^{2+}/Mg ratio, may also be affected by the oxygen fugacity of the magma as suggested by Moore and Erlank (1977).

The good trend obtained for Cr vs. MgO (Figure 2) is consistent with approximately 22% spinel plus olivine fractionation (see Figure 3). The expected smear of points towards olivine reflecting the proposed second stage fractionation, however, is not present. This plot, therefore, may suggest that the minor phases fractionating together with olivine and controlling the composition within each group of dykes may contain significant Cr_2O_3. For the kimberlites this phase may be spinel or even chromite while Cr-bearing clinopyroxene is more likely in the case of the lamprophyres.

The remaining trace elements, especially Ba, Ce, La, V and Sr, have a fairly random distribution relative to MgO (Figure 2). The

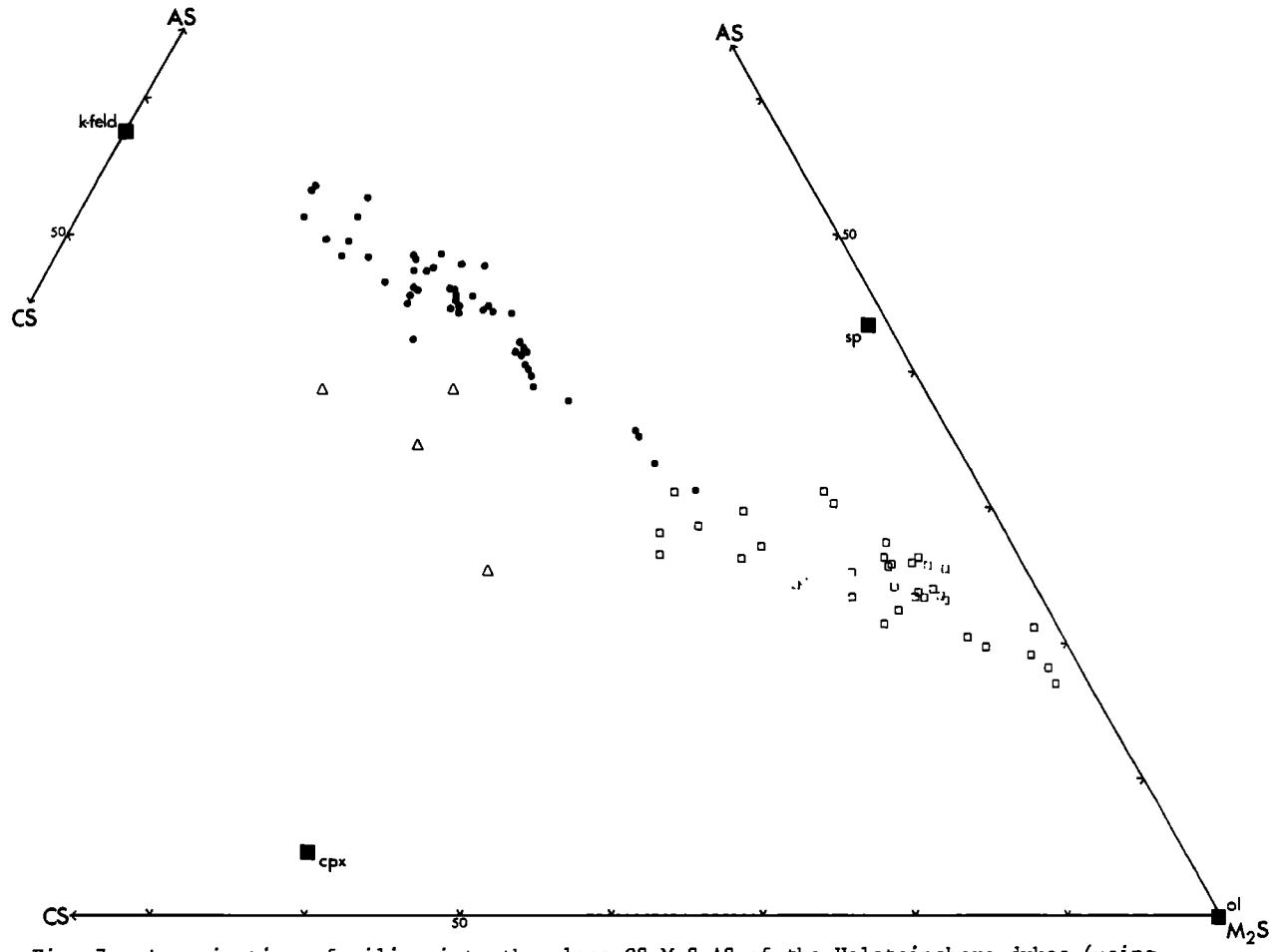

Fig. 7. A projection into the plane CS-M_2S-AS of the Holsteinsborg dykes (using $Ca(Mg)CO_3$- and H_2O^+- free analyses): squares = kimberlites; circles = potassic lamprophyres; triangles = anomalous lamprophyres; ol = olivine; sp = spinel (analysis 192); cpx = clinopyroxene; K-feld = potassium feldspar.

apparently random concentrations of many of the trace elements may be a more sensitive indicator than the major oxides of any inhomogeneity in the rocks which is particularly characteristic of kimberlites. There is also the possibility of a random loss of some of the elements along with the volatile-fraction of the intruding magma. The carbonate-rich kimberlites do show a relative enrichment of Ba, Sr, Ce, La and P (see analysis 5907, Table 1).

These variation diagrams, however, do not appear to be inconsistent with the proposed fractionation hypothesis. Examining the Cu vs. MgO diagram, for example, shows the kimberlites and lamprophyres to have different trends but both away from olivine and may reflect the separate second stages of fractionation. As Cu is likely to substitute in spinel the fractionation of a Cu-bearing spinel and olivine could account for the evolution of a lamprophyric magma containing less Cu than its parental kimberlitic magma.

There seems to be no simple correlation of trace elements with concentrations of major elements for which they commonly substitute (except for K and Rb in the kimberlites).

In addition to the other trace elements, F, Cl, S and B were also determined for a few selected samples. The kimberlites were found to contain up to 0.21 wt% F, 0.14 wt% Cl, 0.20 wt% S while the lamprophyres contained more F (up to 0.44 wt%) and 0.20-0.30 wt% S but no detectable Cl. Boron was not detected in any samples.

Discussion

Many of the high concentrations of certain elements are intensified not only in the carbonate-rich Holsteinsborg dykes but also in carbonatites in general. These enrichments appear to be related to the carbonate fraction in these rock types. It is suggested that the Holsteinsborg kimberlite magma originated in the mantle. If the mantle is considered to be

garnet lherzolite, the assemblage is virtually barren with respect to many of the elements concentrated in kimberlites and potassic lamprophyres. Even with small degrees of partial melting followed by extreme crystal fractionation, it is difficult to explain many of the concentrations reported. Several other phases, however, have been proposed as being part of the stable mantle assemblage and include phlogopite (Dawson 1971, Boettcher et al. 1975, Carswell 1975, Beswick 1976), rutile and apatite (Kable et al. 1975), amphibole (Oxburgh 1964, Millhollen et al. 1974) and carbonate (Eggler 1976, Wyllie 1977). Small degrees of partial melting of a mantle containing such phases might produce ultrabasic magmas with significant concentrations of many elements which have been difficult to explain using other petrogenetic models. Phlogopite in the mantle would provide a source not only of K but probably also of Ti, Al, Rb, Ba and F. Bravo and O'Hara (1975) have shown experimentally that at 1080°C and 30 kb a liquid with 3.6 wt% K_2O is in equilibrium with a phlogopite-garnet-lherzolite; this liquid, however, does not resemble a kimberlite. They also suggest that at pressures greater than 30 kb the initial melt of a phlogopite-garnet-lherzolite may be rich in K_2O and resemble a kimberlite. Boettcher et al. (1975) formed liquids with 0.6 wt% K_2O by the partial melting of phlogopite-spiked (1 wt% K_2O) peridotites. The assumption that the magma parental to all the Holsteinsborg dykes contained 1.82 wt% K_2O (see Table 4), therefore, seems realistic and the derivation of more potassic dykes by crystal fractionation becomes feasible.

There is now convincing evidence that both CO_2 and H_2O do exist in the upper mantle and Eggler (1976) and Wyllie (1977) suggest that at upper mantle pressures carbonate (calcic dolomite) is stable. Recent experimental data (e.g. Wyllie and Huang 1975a and 1975b, Mysen and Boettcher 1975a and 1975b, Eggler 1976) led Wyllie (1977) to suggest that incipient melting of carbonated peridotite produces a carbonatitic liquid and that the interstitial fluid at the top of the low velocity zone may therefore be carbonatitic and probably enriched in alkalis and a host of trace elements. At deeper levels this liquid becomes more siliceous, but still undersaturated, to give kimberlitic compositions. Wyllie also considers that the distribution of carbonate, phlogopite and amphibole in peridotite strongly influences the composition of mantle-derived magmas. Amphibole is not thought to be stable at the pressures and temperatures required for the formation of kimberlitic magmas. It seems that the presence of carbonate and phlogopite in the mantle are important, or even essential, in explaining many of the unusual characteristics of potassic magnesian rocks, kimberlites and carbonatites.

Interpretation of the whole-rock geochemistry of the Holsteinsborg kimberlites together with the wide range of Mg/(Mg + Fe) ratios found in the olivines indicates that the variation in composition of the kimberlites away from the estimated parental magma is largely the result of olivine fractionation. In the detailed interpretation of the data, however, it was suggested that a relatively minor amount of another phase may also be involved in the fractionation and is likely to be spinel. If this spinel was a titanomagnetite it would fall in well with the derivation of a lamprophyre magma by the extract of the same fractionating phases, but with a higher proportion of titanomagnetite, from a kimberlite magma. If the spinel was a chromite it would fit with the suggestion that the unusually abundant dunite inclusions represent cumulates from this fractionation. These dunites contain minor amounts of chromite but no titanomagnetite and are interpreted as cumulates rather than depleted mantle because of the Fe-rich nature of the olivines which also show a wide range of Mg/(Mg + Fe) ratios ($Mg_{82-92.5}$) as well as from the textures in the coarse dunites (Scott 1977, in preparation). The occurrence of cumulate dunite inclusions in the kimberlites supports the suggestion of olivine fractionation being the main control in the evolution of the kimberlite magma.

Although conditions were obviously not suitable for deep-seated rocks to be transported to the surface by the lamprophyre magma, one might expect some indication of olivine plus titanomagnetite cumulates among inclusions in kimberlite. Since such inclusions are not found perhaps the conditions suitable for the proposed fractionation preclude the eruption to near surface of kimberlite magmas carrying inclusions. The appropriate conditions may simply occur at depths which are shallower than those from which the kimberlites begin their relatively rapid ascent to the surface and then representative cumulates would not be expected at the surface. Dawson and Hawthorne (1973) report olivine + spinel + perovskite cumulate layers in the Benfontein kimberlites which presumably resulted from relatively shallow level crystallisation. Clarke and Mitchell (1975) suggest that the epitaxial zones of titanomagnetite with a composition similar to many of Holsteinsborg spinels found round chromite grains are a post-fluidisation crystallisation phase. This chromite to titanomagnetite crystallisation trend is consistent with those suggested by Haggerty (1976). It follows, therefore, that the spinel crystallising together with olivine at depth would be chromite, as found in the dunites from the Holsteinsborg kimberlites, but at shallower depths the spinel would be a titanomagnetite as proposed for the evolution of the initial lamprophyric magma. Some of the chromites from the dunite inclusions have unusually high Cr_2O_3 contents (up to 62.18 wt%)

that are characteristic of diamond inclusions and therefore may indicate that the dunites have crystallised at depths within the diamond stability field.

An alternative suggestion is that the Fe-Ti-rich phase crystallising together with olivine to form the lamprophyric magma was ilmenite which is sometimes considered to be a stable mantle phase (Boyd and Nixon 1973, Goff 1973). Using ilmenite rather than titanomagnetite, however, does not give consistent results from an interpretation of the whole-rock geochemistry similar to that presented in this paper.

Conclusions

Although it is possible to distinguish between the Holsteinsborg kimberlites and potassic lamprophyres, their close association and numerous similarities suggest that they are genetically related. One hypothesis for this relationship has been discussed here and involves an essentially simple fractionation process. The relationship of the potassic lamprophyres to the kimberlites proposed here for the Holsteinsborg dykes is similar to that suggested by Ferguson et al. (1975) and Danchin et al. (1975) for similar rock types. It should be noted, however, that although in the model proposed here it is implied that the Holsteinsborg potassic lamprophyre and kimberlite dykes were both derived from the same body of magma, this need not necessarily be the case. The model may apply to processes whereby potassic lamprophyres, in general, are derivatives of kimberlitic magmas which have been substantially modified during their relatively slow ascent to the surface. The spatial association of kimberlites and potassic lamprophyres of either similar or different ages, therefore, is consistent with this model. The episodic generation and intrusion of kimberlitic magmas separated by long time intervals is well known in certain parts of Southern Africa, for example in the Kimberley area.

The main conclusions from this study are summarised below in terms of a petrogenetic model for the Holsteinsborg dykes:

(1) A magma with a kimberlitic composition was generated, probably by the partial melting of a phlogopite-, carbonate-bearing mantle.

(2) Fractionation of substantial olivine, with minor chromite, then occurred. The dunite inclusions found in the kimberlite dykes represent cumulates from this period of crystallisation.

(3) During this fractionation, the kimberlite magma was continually tapped and then intruded along fractures to form narrow composite dykes in the near surface parts of the crust.

(4) The kimberlitic magma carried crystals of olivine, chromite, picroilmenite, phlogopite and garnet and continued to crystallise olivine, phlogopite and oxides at lower pressures. Diopside, apatite, calcite and serpentine crystallised from residual fluids close to the time of intrusion.

(5) A separate portion of an initial kimberlitic magma was either erupted slowly to near surface regions or its ascent was arrested one or more times. During an early part of the magma's ascent extensive fractionation of olivine and an Fe-Ti-spinel occurred resulting in the relative enrichment of many elements in the liquid. The composition of this liquid was then lamprophyric in character.

(6) At a higher level, probably less than 40km, the protolamprophyric magma was modified by the crystallisation of olivine, diopside, phlogopite and leucite. The interstitial liquid crystallised to form a fine-grained groundmass which included phlogopite, potassic richterite, diopside, potassium feldspar, carbonate, apatite and serpentine.

(7) The anomalous lamprophyre dykes probably represent a part of the initial lamprophyric magma which has accumulated abundant clinopyroxene.

Appendix I

Analytical Techniques

All obvious xenolithic and weathered material was removed from thin slices of the rock specimens. Large samples of each specimen (up to 1.5 kg) were used in the preparation of the rock powders. Eighty seven samples were analysed using largely X-ray fluorescence techniques. The major element concentrations were determined by a method similar to Rose et al. 1963, using fused rock powders while pressed powders were used for the trace elements. All determinations were made using a 24 channel automatic, Phillips PW1212 X-ray fluorescence spectrometer. FeO, Na_2O, H_2O^+ and CO_2 were determined using standard wet-chemical techniques.

Generally the kimberlite analyses gave totals close to 100 % but the major oxide totals for the lamprophyre samples tended to be low. This discrepancy is partly accounted for by the "minor" element concentrations, in particular Ba and Sr. F, Cl, S and B were found not to be particularly significant components of the lamprophyres.

Six full wet-chemical analyses (analysts M.J. Saunders, University of Edinburgh and A.C.S. Smith of the University College, London) of samples from the Holsteinsborg dykes were also carried out and used as standards in the other determinations.

Details of all the analytical techniques, samples analysed, sample localities and results are available in Scott (1977) or from the author. Representative analyses are given both in Tables 1 and 2 and in Scott (in preparation).

Acknowledgements. I am indebted to Dr. J. Watterson, Mr. J. Grocott and Dr. J. Diggens for their help, particularly during fieldwork in Greenland and also to the Greenland Geological Survey (G.G.U.) for putting their facilities in Holsteinsborg at our disposal. I would also like to thank Dr. J.W. Harris, Prof. M.J. O'Hara Dr. B.G.J. Upton, Mr. B.A. Wyatt, Dr. R.V. Danchin, Prof. J.B. Dawson, Dr. D.B. Clarke and Prof. P.G. Harris for stimulating discussions and critical reading of drafts of this manuscript; Mr. M.J. Saunders, Dr. P.G. Hill, Dr. A.C.S. Smith, Mr. G. Angell and Mr. J. Bowles for their interest and invaluable assistance with analytical work; the staff at the Grant Institute for their help and advice, and Dr. D.H. Eggler for his constructive suggestions and comments when reviewing this paper.

Financial support from the Natural Environmental Research Council, Science Research Council, De Beers Consolidated Mines Ltd., Central Research Fund of the University of London, British Universities Students Travel Association and the Anglo American Corporation of South Africa is gratefully acknowledged.

References

Beswick, A.E., K and Rb relations in basalts and other mantle derived materials, Is phlogopite the key? Geochem. cosmochim. Acta, 40, 1167-1184, 1976.

Biggar, G.M., Phase relationships in the join $Ca(OH)_2$-$CaCO_3$-$Ca_3(PO_4)_2H_2O$ at 1000 bars, Mineralog. Mag., 37, 75-82, 1969.

Boettcher, A.L., B.O. Mysen, and P.J. Modreski, Melting in mantle: phase relationships in natural and synthetic peridotite-H_2O and peridotite-H_2O-CO_2 systems at high pressures, Physics. Chem. Earth, 9, 855-867, 1975.

Boyd, F.R., and P.H. Nixon, Origin of the ilmenite-silicate nodules in kimberlites from Lesotho and South Africa, In: Lesotho Kimberlites, Editor P.H. Nixon, Lesotho National Development Corporation, Maseru, pp. 254-268, 1973.

Bravo, M.S., and M.J. O'Hara, Partial melting of phlogopite-bearing synthetic spinel- and garnet-lherzolites, Physics Chem. Earth, 9, 845-854, 1975.

Carmichael, I.S.E., The iron-titanium oxides of salic volcanic rocks and their associated ferromagnesian silicates, Contrib. Mineral. Petrol., 14, 36-64, 1967a.

Carmichael, I.S.E., The mineralogy and petrology of the Leucite Hills, Wyoming, Contrib. Mineral. Petrol., 15, 24-66. 1967b.

Carswell, D.A., Primary and secondary phlogopites and clinopyroxene in garnet lherzolite xenoliths, Physics Chem. Earth, 9, 417-429, 1975.

Clarke, D.B., and R.H. Mitchell, Mineralogy and petrology of the kimberlite from Somerset Island, N.W.T., Canada, Physics Chem. Earth, 9, 123-135, 1975.

Clement, C.R., The emplacement of some diatreme-facies kimberlites, Physics Chem. Earth, 9, 51-59, 1975.

Clement, C.R., E.M.W. Skinner, and B.H. Scott, Kimberlite redefined, Extended Abstracts, Second International Kimberlite Conference, Santa Fe, New Mexico, 1977.

Danchin, R.V., J. Ferguson, J.R. McIver, and P.H. Nixon, The composition of late stage kimberlite liquids as revealed by nucleated autoliths, Physics Chem. Earth, 9, 235-245, 1975.

Dawson, J.B., Basutoland kimberlites, Bull. geol. Soc. Am., 73, 545-559, 1962.

Dawson, J.B., Geochemistry and origin of kimberlite, In: Ultramafic and Related Rocks, Editor, P.J. Wyllie, Wiley, New York, pp. 269-278, 1967.

Dawson, J.B., The genesis of kimberlite, In: Diamond Research for 1971, Industrial Diamond Information Bureau, London, pp. 2-7, 1971.

Dawson, J.B., and J.B. Hawthorne, Magmatic sedimentation and carbonatitic differentiation in kimberlite sills at Benfontein, South Africa, Jl. geol. Soc. Lond., 129, 61-85, 1973.

Eggler, D.H., Does CO_2 cause partial melting in the low-velocity layer of the mantle? Geology, 4, 69-72, 1976.

Ferguson, J., and K.L. Currie, Evidence of liquid immiscibility in alkaline ultrabasic dykes at Callender Bay, Ontario, J. Petrology, 12, 561-585, 1971.

Ferguson, J., H. Martin, L.O. Nicolaysen, and R.V. Danchin, Gross Brukkaros : a kimberlite-carbonatite volcano, Physics Chem. Earth, 9, 219-245, 1975.

Goff, S.P., The mineralogy and geochemistry of a kimberlite dyke from Søndre-Isortoq Fjord, South West Greenland, M.Phil. Thesis, University of Leicester (unpubl.), 1973.

Haggerty, S.E., Opaque mineral oxides in terrestial igneous rocks, in: Oxide Minerals, Min. Soc. Amer. Short Course Notes, 3, (Ed. D. Rumble III), Hg 101-Hg 300, 1976.

Hart S.R., K.E. Davis, I. Kushiro, and E. Watson, Partitioning of nickel between olivine and silicate liquids, Abstracts of 1976 Annual Meetings, Geol. Soc. Am., 8, no. 6, 906-907, 1976.

Irvine, T.N., and I. Kushiro, Partitioning of Ni and Mg between olivine and silicate liquids, Carnegie Inst. Wash. Yearb., 75, 668-675, 1976.

Jamieson, B.G., Natural rock projection into a pseudo-quarternary system, Progress in Experimental Petrology, First Progress Report, N.E.R.C., p. 152-155, 1969.

Jamieson, B.G., Phase relations in some tholeiitic lavas illustrated by the system R_2O_3-XO-YO-ZO_2, Mineralog. Mag., 37, 537-554, 1970.

Kable, E.J.D., H.W. Fesq, and J.J. Gurney, The significance of inter-element relationships of some minor and trace elements in South African kimberlites, Physics Chem. Earth, 9, 709-734, 1975.

McIver, J.R., and D.H. Lenthall, Mafic and ultramafic extrusives of the Barberton Mountain Land in terms of the CMAS system, PreCamb. Res., 1, 327-343, 1974.

Millhollen, G.L., A.J. Irving, and P.J. Wyllie, Melting interval of peridotite with 5.7 per cent water to 30 kilobars, J. Geol., 82, 575-587, 1974.

Moore, A.E., and A.J. Erlank, Olivine compositional complexity in olivine melilitites from Namaqualand, South Africa, and its bearing on kimberlite genesis, Extended Abstracts, Second International Kimberlite Conference, Santa Fe, New Mexico, 1977.

Mysen, B.O., Nickel partitioning between upper mantle crystals and partial melts as a function of pressure, temperature and nickel concentration, Carnegie Inst. Wash. Yearb., 75, 662-668, 1976.

Mysen, B.O., and A.L. Boettcher, Melting of a hydrous mantle: I. Phase relations of a natural peridotite at high pressures and temperatures with controlled activities of water, carbon dioxide and hydrogen, J. Petrology, 16, 520-548, 1975a.

Mysen, B.O., and A.L. Boettcher, Melting of a hydrous mantle: II. Geochemistry of crystals and liquids formed by anatexis of mantle peridotite at high pressures and high temperatures as a function of controlled activities of water, hydrogen and carbon dioxide, J. Petrology, 16, 549-593, 1975b.

O'Hara, M.J., The bearing of phase equilibria studies in synthetic and natural systems on the origin and evolution of basic and ultrabasic rocks, Earth Sci. Rev., 4, 69-133 1968.

O'Hara, M.J., M.J. Saunders, and E.L.P. Mercy, Garnet-peridotite, primary ultrabasic magma and eclogite; interpretation of upper mantle processes in kimberlite, Physics Chem. Earth, 9, 571-604, 1975.

Oxburgh, E.R., Petrological evidence for the presence of amphibole in the upper mantle and its petrogenetic and geophysical implications, Geol. Mag., 101, 1-19, 1964.

Pearce, T.H., A contribution to the theory of variation diagrams, Contrib. Mineral. Petrol., 19, 142-157, 1968.

Pearce, T.H., Chemical variations in the Palisade Sill, J. Petrology, 11, 15-32, 1970.

Rimskaya-Korsakova, O.M., and E.P. Sokolova, Iron-magnesium micas with reverse absorption, Mineralog. Abstr., 17, 504, 1966.

Rose, H.J., I. Adler, and F.J. Flanagan, X-ray fluorescence of the light elements in rocks and minerals, Appl. Spectrosc., 17, 81-85, 1963.

Scott, B.H., Petrogenesis of kimberlites and associated potassic lamprophyres from Central West Greenland, Ph.D. Thesis, University of Edinburgh (unpubl.), 1977.

Scott, B.H., Kimberlites and potassic lamprophyre dykes from the region of Holsteinsborg, Central West Greenland, (in preparation).

Skinner, E.M.W., and C.R. Clement, A mineralogical classification of Southern African kimberlites, Extended Abstracts, Second International Kimberlite Conference, Santa Fe, New Mexico, 1977.

Thornton, C.P., and O.F. Tuttle, Chemistry of igneous rocks : part I, differentiation index, Am. J. Sci., 258, 664-684, 1960.

Wade, A., and R.T. Prider, The leucite-bearing rocks of the West Kimberley Area, Western Australia, Jl. geol. Soc., 96, 39-98, 1940.

Wright, T.L., and P.C. Doherty, A linear programming and least squares computer method for solving petrologic mixing problems, Bull. geol. Soc. Am., 81, 1995-2008, 1970.

Wyllie, P.J., (Editor) Ultramafic and Related Rocks, Wiley, New York, 1967.

Wyllie, P.J., and W.L. Huang, Influence of mantle CO_2 in the generation of carbonatites and kimberlites, Nature, Lond., 257, 297-299, 1975a.

Wyllie, P.J., and W.L. Huang, Peridotite, kimberlite and carbonatite explained in the system $CaO-MgO-SiO_2-CO_2$, Geology, 3, 621-624, 1975b.

Wyllie, P.J., Mantle fluid compositions buffered by carbonates in peridotite-CO_2-H_2O, J. Geol., 85, 187-207, 1977.

THE OXIDE AND SILICATE MINERAL CHEMISTRY OF A KIMBERLITE FROM THE PREMIER MINE: IMPLICATIONS FOR THE EVOLUTION OF KIMBERLITIC MAGMAS

Don Elthon and W. Ian Ridley

Lamont-Doherty Geological Observatory of Columbia University and the
Department of Geological Sciences, Columbia University,
Palisades, New York 10964

Abstract. A detailed microprobe study of the oxide and silicate minerals in a very fresh kimberlite from the Premier Mine provides a variety of information on the crystallization of kimberlitic magmas. Olivines are characterized by two populations; one corresponds to the xenocrystal and/or high pressure regime (Fo_{91}-Fo_{94}), the other to the groundmass crystallization (Fo_{88}-Fo_{89}). On the basis of Cr_2O_3, FeO* and Al_2O_3, it is possible to distinguish phlogopites which crystallize directly from the kimberlitic magma versus those which are xenocrystal. The chemistry of some phlogopite megacrysts is consistent with their direct crystallization from the kimberlitic melt, for other phlogopite megacrysts a xenocrystal origin is more probable. The mineral chemistry of the garnets, opx and cpx indicates that these are xenocrystal.

Picroilmenite grains are ubiquitously mantled by perovskite and Ti, Mg, Cr, Al magnetites. This peritectic-like reaction involving picroilmenite, perovskite, $magnetite_{ss}$, and the magma is a convenient point to divide the crystallization of the kimberlitic magma into the high pressure and groundmass regimes. There are extensive intergranular variations in the chemical composition of many of the groundmass phases. This is probably due to local disequilibrium at a very small scale reflecting the heterogeneities in A_{CO_2}, A_{H_2O}, and f_{O_2} during ascent and crystallization.

Introduction

Kimberlites represent a valuable source of information concerning processes occurring in the upper mantle. The study of ultramafic nodules incorporated in kimberlitic magmas during their ascent to the surface has yielded a vast amount of knowledge on the physiochemical state of the upper mantle. The presence of diamonds in kimberlites, together with studies of pressure-sensitive minerals in garnet peridotite nodules indicate that kimberlitic magmas originate at pressures equivalent to 150-200 kilometers deep in the earth's mantle (Boyd, 1977). However, the origin and evolution of kimberlitic melts remain poorly understood.

The chemical and physical changes that occur during the ascent and crystallization of kimberlitic magmas are inherently reflected in the mineral chemistry of phases that crystallize during cooling, lithostatic pressure release, and de-volatilization of the magma. Previous studies have shown that several silicate and oxide phases may crystallize and that individual phases can be compositionally complicated (Mitchell and Clarke, 1976; Haggerty, 1975; Gittins et al., 1975). In order to further understand the conditions of crystallization in kimberlite magmas we have performed detailed microprobe analyses of oxide and silicate minerals occurring as phenocrysts, xenocrysts, and groundmass phases in a very fresh kimberlite from the Premier Mine, South Africa.

Petrography and Mineral Chemistry

The samples studied are all "micaceous" kimberlites characterized by abundant phlogopite grains. The groundmass consists of perovskite, $magnetite_{ss}$, olivine, phlogopite, carbonates, "serpentine", chlorite, sulfides ± apatite. Olivine is the dominant mineral displaying three modes of occurrence. Individual, euhedral to subhedral crystals of olivine are disseminated throughout the thin sections, aggregates of polycrystalline olivine are occasionally found, and olivine also occurs in partially fragmented peridotitic nodules. The olivine crystal boundaries have usually been slightly serpentinized.

Phlogopite occurs in partially dismembered xenoliths but the majority of phlogopite grains are dispersed throughout the groundmass. Megacrysts of phlogopite are rarely found; often these show kink banding and other indications of deformation, and commonly they contain inclusions of rutile.

Picroilmenites (Mg-rich ilmenites) are

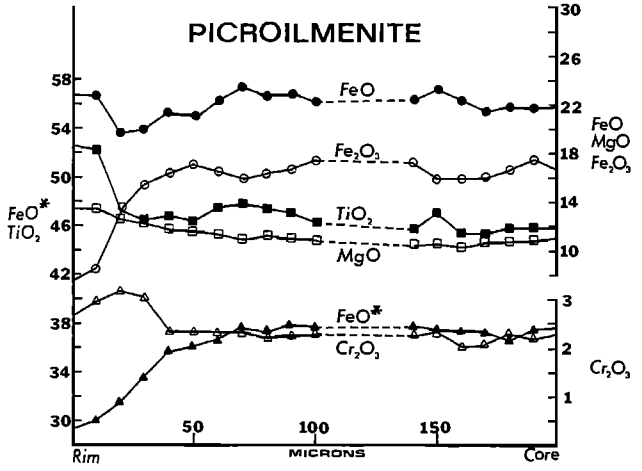

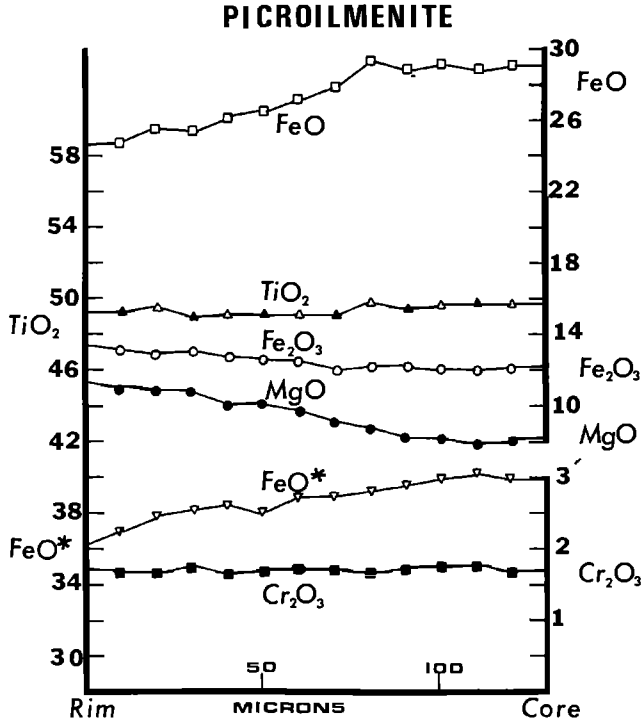

Figure 1A and 1B. Figures 1A and 1B show the major element variations in rim to core traverses across picroilmenite grains. In Figure 1A, FeO remains relatively constant while Fe_2O_3 increases from rim to core. The rim is enriched in TiO_2, MgO, Cr_2O_3 and CaO (not shown) relative to the core. In Figure 1B, Fe_2O_3 remains relatively constant while FeO increases from rim to core. Again, MnO and CaO (not shown) are enriched in the rim relative to the core. In the majority of picroilmenites that are zoned, Fe_2O_3 decreases from core to rim. Note that only one-half of the essentially symmetrical traverses are shown.

common but always display reaction mantles of perovskite and magnetite.

Garnet, ortho- and clinopyroxenes are preserved in partially dismembered xenoliths and occasionally are dispersed in the groundmass. Garnet is usually fractured, often displaying kelyphytic rims. Ortho- and clinopyroxenes also show evidence indicating disequilibrium with the kimberlite magma.

Oxide Mineral Chemistry

Picroilmenites

Picroilmenite is the most distinctive kimberlite oxide mineral, occurring as small disseminated grains, as large nodules, and as eutectic-like intergrowths with diopside or enstatite (Mitchell, 1973). In this study, we have found only small, disseminated grains, 0.1-2 mm across. Generally, 3-4 irregularly shaped, ovoid picroilmenite grains are found per thin section.

These picroilmenites can be divided into two general categories: 1) inversely zoned crystals (MgO, TiO_2, MnO, CaO enriched rims) which are generally small, and 2) unzoned, large crystals which often have granoblastic, recrystallised textures similar to those reported by Mitchell (1973). The inversely zoned picroilmenites have highly contrasting patterns of major element distribution in systematic microprobe traverses across the grains.

Figures 1A and 1B demonstrate the two "end member" types of zoning associated with these picroilmenites. In both figures, only one-half of the nearly symmetrical traverse is shown. In Figure 1A, FeO remains relatively constant across the grain TiO_2, MnO, and CaO (not shown), in addition to MgO, are enriched in the rim relative to the core. Cr_2O_3 and Al_2O_3 remain relatively constant from rim to core. The traverse shown in Figure 1A is represented by Line A in Figure 2.

Figure 1B shows the other "end member" zonation pattern in picroilmenites where FeO increases from rim to core while Fe_2O_3, TiO_2, and Cr_2O_3 remain relatively constant. Al_2O_3 and MnO are irregular but relatively constant. The traverse shown in Figure 1B is represented by Line B in Figure 2. Most picroilmenites display a zonation pattern which is a composite of these two end members, i.e. both FeO and Fe_2O_3 increase from rim to core. For the individual samples studied, the internal variations in picroilmenite zonation patterns within a single thin section are essentially the extent of variation within the entire suite of samples. Thus these variations in FeO, Fe_2O_3, and FeO/Fe_2O_3 amongst individual grains in the same thin section are interpreted to be the result of local disequilibrium and local variations in f_{O_2}.

The picroilmenite composition can be expressed in terms of three major components: ilmenite, geikielite, and hematite. From the examination

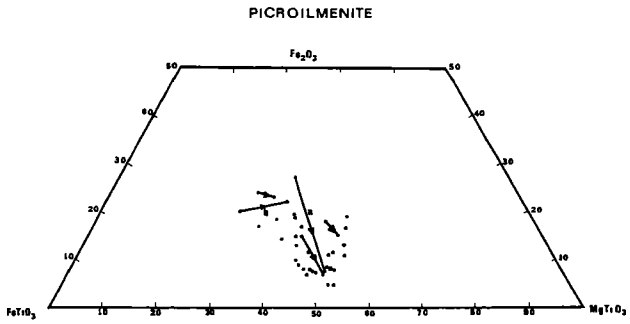

Figure 2. Ilmenite vs. geikielite vs. hematite - The compositions of picroilmenites in this study are plotted in the Ilm-Gk-Hema ternary diagram. Lines a and b correspond to the zoning observed in Figures 1A and 1B, respectively. Arrows point toward the rim composition. The overall trend due to magmatic processes is towards higher $MgTiO_3$ and lower Fe_2O_3 with $FeTiO_3$ remaining constant. The shaded area is the range of picroilmenite analyses reported by Boyd and Nixon (1973), Mitchell (1973), and Haggerty (1975).

of Figure 2, the microprobe analyses reported here are within the limits reported by Boyd and Nixon (1973), Mitchell (1973) and Haggerty (1975). The trend most commonly observed in the zonation patterns of these picroilmenite grains is the tendency towards enrichment in $MgTiO_3$ and depletion in Fe_2O_3 in the picroilmenite grains during the evolution of the kimberlite magma.

The substitution of $MgTiO_3$ for the Fe_2O_3 component is the main substitution effect related to magmatic variations (Figure 2). These trends are similar to those observed by Haggerty et al. (1977) for chemical variations due to magmatic processes in kimberlitic magmas. Submicron exsolution lamellae of hematite (?) are occasionally observed in picroilmenite hosts. While these may be common in the small, zoned picroilmenite grains, lamellae are very rare in the polycrystalline, granoblastic textured picroilmenites, possibly as a result of post-exsolution annealing and recrystallization.

One characteristic of all picroilmenites in the samples studied, in addition to the zoning previously mentioned, is the ubiquitous presence of reaction mantles of perovskite and Ti, Mg, Cr, Al - magnetites. Textural evidence indicates that this association is produced by a peritectic -like reaction between picroilmenite and the kimberlitic liquid to produce the assemblage of perovskite and magnetite$_{ss}$. In Figure 3, the perovskite and Ti, Mg, Cr, Al - magnetites can be seen replacing picroilmenite. In many cases, remnants of picroilmenite can be found encapsulated within these late forming perovskite and Ti, Mg, Cr, Al - magnetite reaction mantles (Figure 4).

Similar mineralogically complex mantles on picroilmenite were reported by Haggerty (1973). However, the small picroilmenites encapsulated within perovskite and Ti, Mg, Cr, Al magnetites have been interpreted to be secondary in origin. There is much evidence supporting the hypothesis

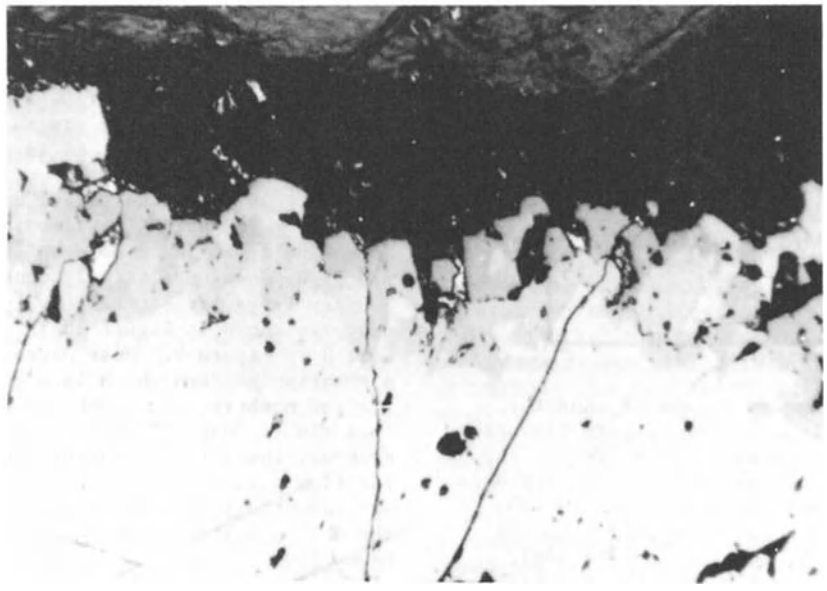

Figure 3. Photo shows reaction mantle of perovskite plus magnetite$_{ss}$ replacing picroilmenite. Oil immersion, reflected light photomicrograph. The field of view is 0.5 mm across.

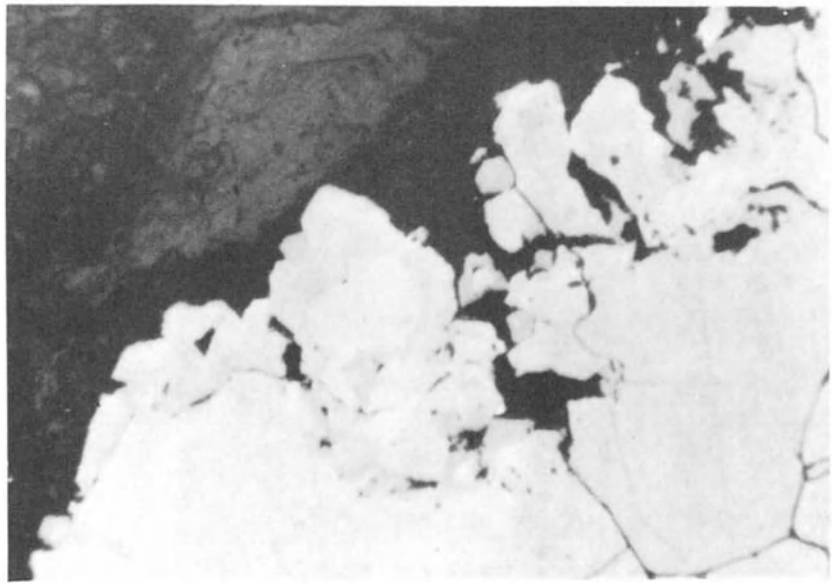

Figure 4. Where the reaction of picroilmenite with the kimberlitic magma to produce perovskite and magnetite$_{ss}$ is heterogeneous and incomplete, the preservation of small picroilmenite relicts in the reaction mantle is observed. Oil immersion, reflected light photomicrograph. The photo is 0.5 mm across.

that these small picroilmenites are not secondary but rather the remnants of the original picroilmenite rim, most of which has been replaced by reaction with the groundmass kimberlitic magma. Firstly, both the large picroilmenite and the small grains on the rim are pleochroic and simultaneously reach maximum extinction. Secondly, where the large picroilmenite grains are zoned, for example with MgO-rich rims, these small picroilmenites on the rim are extremely MgO-rich. Thirdly, the textural evidence (Figure 3) shows the reaction relationship of the picroilmenite with the kimberlitic magma resulting in the replacement of picroilmenites by reaction mantles of perovskite plus magnetite$_{ss}$. Also, in many instances the replacement of picroilmenite with perovskite and magnetite$_{ss}$ has been incomplete with several of those "rim picroilmenites" remaining connected to the large picroilmenite (Figure 4).

Perovskite

Perovskite is found in reaction mantles on picroilmenite, in reaction mantles on rutile, scattered throughout the groundmass, and very rarely in reaction mantles (associated with Ti, Mg, Cr, Al magnetites) on some chromium spinels. The perovskites from all four types of occurrences are chemically indistinguishable. In all of these perovskites, Fe_2O_3, Al_2O_3, and Cr_2O_3 are the major dilutants although their sum rarely is more than 2% (Table 1). However, the perovskite in picroilmenite mantles are slighty zoned with Cr-rich and Al-poor regions adjacent to the picroilmenite and the Cr-poor and Al-rich rim adjacent to the groundmass. It is also assumed the perovskite is the major mineralogical "sink" for Nb, Zr and REE.

Rutile

Rutile is found in many mineralogical associations in the kimberlites we have studied, and in other kimberlites (e.g. Haggerty, 1975; Clarke and Mitchell, 1975). Rutile is commonly observed in parallel, lensoidal intergrowths within picroilmenite grains (Figure 5) and occasionally within perovskite mantling the picroilmenite where the rutile previously enclosed within picroilmenite, has not been completely replaced by the reaction of picroilmenite with the melt to produce perovskite plus magnetite$_{ss}$.

Although we have not observed armalcolite in the samples studied here, its occurrence has been reported in De Toitspan kimberlites (Haggerty, 1975) as well as in lamproites from Smoky Butte, Montana, U.S.A. (Velde, 1975). It is possible that some of these rutile-picroilmenite intergrowths could have resulted from the breakdown of armalcolite.

Rarely, rutile is found as distinct crystals, not associated with picroilmenite. A minor portion of these rutile grains are disseminated

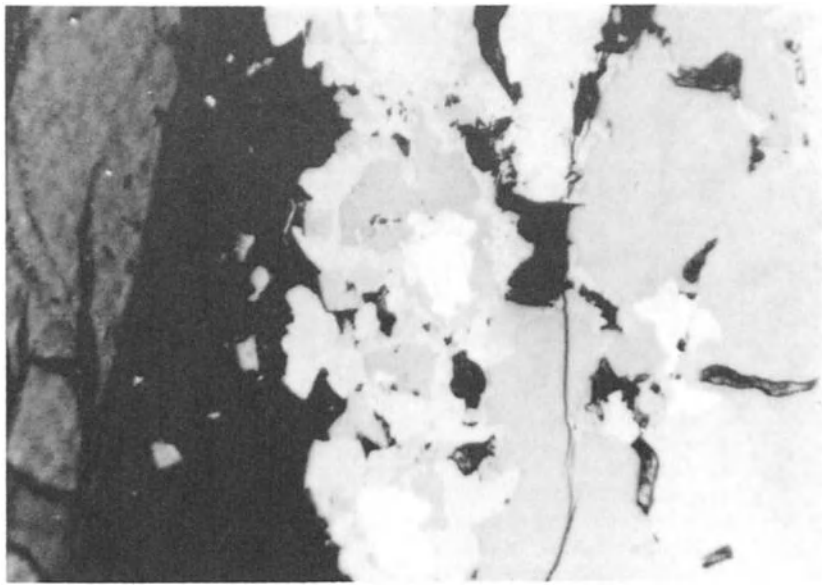

Figure 5. These rutile (white)-picroilmenite (grey) intergrowths are common in some picroilmenite crystals. Possibly they represent the breakdown products of armalcolite. Oil immersion, reflected light photomicrograph. The field of view is 0.5 mm across.

throughout the groundmass and mantled by perovskite with very minor Ti, Mg Cr, Al magnetites. More commonly, these rutile grains are found encapsulated within phlogopite megacrysts. These rutile grains have been poikilitically enclosed by later crystallizing phlogopites and have not developed perovskite and Ti, Mg, Cr, Al magnetite reaction mantles formed during the groundmass crystallization. Instead, these rutile grains have developed a semi-continuous, single phase reaction corona between the rutile and surrounding phlogopite. It has not been possible to quantitatively determine the composition of this phase, but qualitative measurements indicate that it is a potassium bearing rutile-like mineral with ∿8-9% K_2O, 85% TiO_2.

TABLE 1. Representative Compositions of Perovskite and Rutile.

SiO_2	.00	.02	.02	.05	.00	.00
TiO_2	56.18	57.76	57.00	56.42	97.89	98.36
Al_2O_3	.44	.47	.47	.42	.36	.37
Cr_2O_3	.49	.01	.20	.05	.59	1.21
Fe_2O_3	1.48	1.07	.98	.81	.00	.00
MnO	.08	.04	.07	.05	.00	.00
MgO	.00	.00	.00	.00	.00	.00
CaO	40.17	39.96	38.03	40.38	.16	.17
ZnO	.00	.00	.02	.00	.00	.00
Total	98.84	99.13	96.79	98.13	99.00	100.11

Note: All iron calculated as Fe_2O_3

The major dilutants in the rutiles are Cr_2O_3 (∿ 1%), Fe_2O_3 (∿ 1%), MgO (∿ 1%) and Al_2O_3 (∿ 0.5%) (Table 1). Zr and Nb, although not analyzed, may also be significant (Clarke and Mitchell, 1975; Dawson and Smith, 1977). Thus, rutile is an important accessory mineral whose chemistry is very similar to those from "MARID" nodules (Dawson and Smith, 1977). The chemistry of rutiles from lherzolite nodules have somewhat higher Cr_2O_3 (1.6-7.2%) while rutiles from eclogites are characterized by low Cr_2O_3 (∿ 0.0n%). Hence, the chemistry of rutiles from these kimberlite samples would seem to preclude their direct derivation from a peridotitic or eclogitic source. We feel that their chemistry is the result of magmatic processes and their presence is not related to incidental incorporation of these as xenocrysts.

Spinels

Four types of spinels are found in the kimberlite samples studied. Chromium spinels are very rare (<<1%) and are usually found as subhedral inclusions within pyroxenes, although some are found within the groundmass. From the examination of Table 2 there are 3 types of chromium spinels found in the kimberlites studied. Type "A" spinels are very rare and occur as spinel-apatite vermicular intergrowths. The type "A"

TABLE 2. Representative Spinel Analyses.

	Chromium Spinels							Groundmass Spinels		
	'A'		'B'			'C'				
				*		*	*			
TiO_2	.25	.67	10.81	9.49	8.40	5.22	5.41	20.03	19.14	16.01
Cr_2O_3	62.22	58.73	39.32	34.57	37.24	29.11	28.62	2.17	5.34	.92
MnO	.36	.21	.52	.48	.58	.46	.43	.74	.71	.88
FeO*	16.09	16.67	32.29	34.16	34.46	55.32	55.65	55.54	54.83	55.59
NiO	.12	-	.08	-	.09	.08	.05	-	-	-
SiO_2	.20	.06	.07	.04	.21	.14	.09	.11	.00	.31
CaO	.03	.02	.00	.07	.00	.00	.00	.32	1.18	.55
MgO	14.13	13.14	12.89	13.51	12.77	4.72	4.79	12.81	12.52	14.94
Al_2O_3	6.20	10.88	3.80	6.04	4.47	.72	.68	4.61	4.65	7.66
Total	99.60	100.38	99.78	98.36	98.22	95.77	95.72	96.33	98.37	96.86
$MgAl_2O_4$	8.68	15.22	5.26	8.39	6.26	1.00	1.00	6.40	6.54	10.67
Mg_2TiO_4	.48	1.28	21.67	19.10	16.85	8.82	8.99	21.99	21.19	23.27
Mn_2TiO_4	-	-	-	-	-	.66	.67	1.10	1.10	1.33
Fe_2TiO_4	-	-	-	-	-	1.57	2.01	24.37	23.03	10.29
$MnCr_2O_4$	1.11	.67	1.56	1.55	1.78	-	-	-	-	-
$MgCr_2O_4$	54.61	34.04	2.50	7.31	12.11	-	-	-	-	-
$FeCr_2O_4$	26.86	40.29	53.50	40.74	38.95	42.98	42.08	3.13	7.83	1.34
Fe_3O_4	8.10	3.94	16.21	22.69	23.62	46.07	45.38	41.67	40.29	52.09
Total	99.84	100.44	100.70	99.78	99.57	101.10	100.13	98.66	99.98	99.48

Type 'A' chromian spinels occur as vermicular intergrowths with apatite.
Type 'B' chromian spinels are generally found included within pyroxenes. The type 'B' spinel with the asterisk occurs as a disseminated grain in the groundmass (rimmed by magnetite$_{ss}$) but is very similar to those 'B' spinels enclosed by pyroxenes.
Type 'C' chromian spinels are disseminated throughout the groundmass and are rimmed by magnetite$_{ss}$.
The groundmass spinels compositions are representative of the variable nature of these complex magnetite$_{ss}$.

spinels are rich in chromium but contain relatively minor TiO_2 and FeO. When calculated into the component species, these are very rich in the $MgCr_2O_4$ and $MgAl_2O_4$ end members but contain much less of the Mg_2TiO_4 and Fe_3O_4 end members in comparison to the other types of chromium spinels.

In contrast, type "B" spinels are included within xenocrystic pyroxene crystals and are much richer in TiO_2 and FeO* but contain somewhat lower Al_2O_3 and Cr_2O_3. As a result, when these spinels are recalculated into ideal end members, Mg_2TiO_4 and Fe_3O_4 molecules represent a larger percentage while the $MgAl_2O_4$ and $MgCr_2O_4$ components decrease.

Finally, the type "C" spinels contain much less Cr_2O_3, MgO and Al_2O_3 than either types "A" or "B" while FeO* increases to over 55%. When recalculated, these spinels consist dominantly of Fe_3O_4 and $FeCr_2O_4$ components with an intermediate proportion of Mg_2TiO_4 (see Table 2).

In Table 2, those analyses of chromium spinels (type "B" and "C") which are not included within pyroxenes are marked with an asterisk while those included within pyroxenes are unmarked. The type "B" spinels are, with only one exception, preserved within megacrysts of ortho- or clinopyroxene, neither of which is observed as a groundmass mineral. Thus, the chemical similarity of these spinels to spinels from peridotite xenoliths as well as their mode of occurrence suggests that these Cr-spinels are xenocrystic. It is probable that the chemical variations present within these spinel groups is probably due to variations in the depth in the mantle from which these spinels are derived.

The type "C" spinels are not included within pyroxenes but are found dispersed within the

rock, and are mantled by magnetite$_{ss}$. Their chemistry is unusual and may indicate a partial equilibration of the spinel (possibly xenocrystic) with the kimberlitic magma. These type "C" spinels have a high magnetite component similar to the groundmass spinels but remain compositionally distinct from the groundmass magnetite.

A fourth type of spinel, Ti, Mg, Cr Al - magnetite is abundant with perovskite on the reaction mantles of picroilmenite and rutile, in the groundmass, and on mantles surrounding chromium spinels if they are exposed to the crystallizing groundmass. Their chemistry is highly variable (see Table 2), with the chemical variations of these spinels on the rims of a single picroilmenite grain being as great as the variations within the entire suite of samples. Also, the chemistry of spinels in the groundmass is just as variable, even within grains a millimeter apart. The size of these magnetite$_{ss}$ grains is usually too small to determine if they are zoned, but the few larger grains analysed are unzoned. Local disequilibrium, on the submillimeter scale seems to have resulted in these intergrain variations in chemistry.

Silicate Mineral Chemistry

Olivine

Olivine represents the most abundant silicate mineral in these kimberlites, occurring as phenocrysts, xenocrysts and groundmass crystals. Examination of the two histograms in Figure 6 shows that there are two principal chemical groups. The groundmass olivines are small, unzoned or very slightly zoned and have a composition of Fo_{88-89}. The more magnesian olivines [Fo_{91-94}] are larger and usually zoned to Fo_{88-89} rims. These are interpreted to be both phenocrysts and xenocrysts with forsterite-rich cores which have been rimmed by more fayalitic olivine during the crystallization of the kimberlite groundmass. The more magnesian rims on olivines (Figure 6) are found on large olivine crystals whose rims (assumed to be $\sim Fo_{88-89}$) have been replaced during low temperature alteration.

Phlogopite

The ubiquitous presence of phlogopite, commonly in two generations, is a striking feature of kimberlites and other lamprophyres even on the hand-specimen scale. However, phlogopites found in kimberlites have many potential sources. The most obvious and probably most important process producing these abundant phlogopites is direct crystallization from the vapor- and potassium-rich kimberlitic magma. Other potential sources of phlogopite include the upper mantle, peridotite nodules carried by the kimberlitic magma and secondary reaction processes occurring in kimberlites.

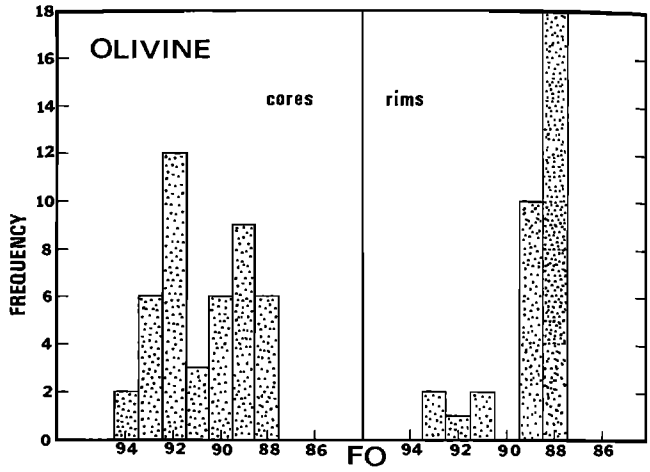

Figure 6. Histogram showing the compositions of disseminated olivine crystals in the kimberlitic matrix. The cores of olivine crystals fall into two groups: those analyses approximating Fo_{90-88} which are generally small, unzoned crystals and those analyses approximating Fo_{94-91} which are generally larger and zoned. From the compositions of the rims, it is shown that the groundmass crystallization of olivine has produced compositionally uniform rims of Fo_{88-89}. Those olivine crystals with Fo_{93-91} rims have undergone moderate serpentinization replacing the (assumed) more iron-rich rims.

The examination of Figure 7 shows three compositional groups. The FeO*-poor and Cr_2O_3-rich population labelled "nodules" consists of phlogopites which can be demonstrated texturally to be xenocrystic and includes analyses from the literature of phlogopites from ultramafic nodules (Carswell, 1975). These analyses are consistent with the field of phlogopites from peridotites delineated by Dawson and Smith (1977).

The Cr_2O_3-poor population of phlogopite analyses (Figure 7) consists of analyses of both groundmass phlogopite and phlogopite phenocrysts which cannot be demonstrated texturally to be xenocrystic. Note the complete overlap of analysis from MARID xenoliths and kimberlite phlogopite phenocrysts. The chemical similarity of phlogopite crystals from MARID nodules to the groundmass phlogopites in the kimberlites in this study suggest that the MARID nodules may represent the result of crystal accumulation from a kimberlitic magma at 50-100 km (Dawson and Smith, 1977).

In Figure 8, again it is apparent that there are three distinct sources of phlogopite crystals in kimberlites. The low Cr_2O_3 and low Al_2O_3 analyses are phenocryst and groundmass phlogopites. The population of analyses labelled "nodules" are xenocrystic phlogopites from this study as well as primary phlogopites from peridotite nodules (Carswell, 1975). The third group represents secondary phlogopites in peridotite

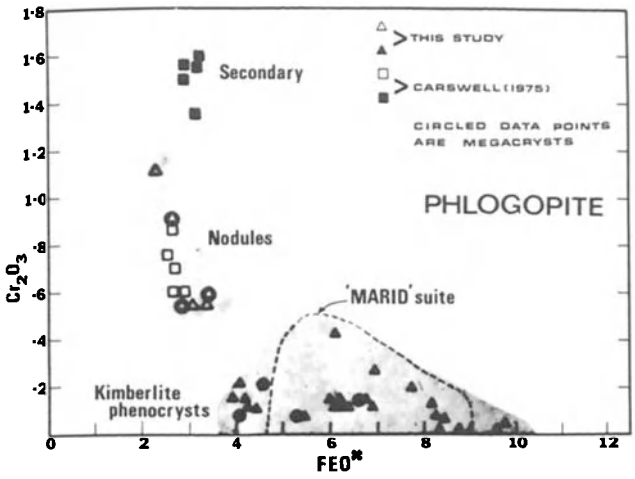

Figure 7. FeO* vs. Cr_2O_3 in phlogopite crystals. Note the three distinct groupings of phlogopite analyses. The "kimberlite phenocrysts" group includes small, disseminated phlogopite crystals as well as phlogopite megacrysts. Due to their chemical similarity, these phlogopite megacrysts appear to be crystallized from the kimberlitic melt rather than being xenocrystic in origin. Also note the similarity of kimberlitic phlogopite phenocrysts to the phlogopites from the "MARID" suite of nodules (Dawson and Smith, 1977). Both of these are chemically distinct from primary phlogopites in nodules or from phlogopites produced by secondary processes in the mantle (see text).

nodules (Carswell, 1975). As can be seen from Figure 7 and Figure 8, these secondary phlogopites are distinctly different from the groundmass phlogopite, indicating quite different conditions of crystallization, perhaps involving metasomatic processes within the mantle.

Many of the phlogopite crystals analysed contain up to 1-2 wt.% TiO_2 (Figure 9), reflecting the titanium-rich nature of kimberlitic magma. Those phlogopites with low TiO_2 contents occasionally contain rutile grains, although the TiO_2 contents of phlogopites with rutile inclusions is highly variable.

There is significant grain-to-grain variation in the chemistry, (FeO, Cr_2O_3, Al_2O_3) within the kimberlitic phenocryst and groundmass phlogopites (Table 3) although individual grains are homogeneous and unaffected by low temperature alteration. The variations in chemistry between grains can thus be related to changing conditions in the kimberlitic magma during the crystallization of phlogopite and the failure of early crystallizing phlogopite grains to re-equilibrate with the magma. Similar observations have been observed by Gittins et al. (1975) from kimberlitic-carbonatitic dikes from the Saquenay River Valley, Canada.

Garnets

Garnet is a rare mineral in the kimberlites studied. Garnet is generally found as highly fractured grains associated with pyroxenes ± olivine, and ± phlogopite in megacrysts. The chemistry of these garnets (Table 4) is typical of garnets from garnet lherzolite nodules (Danchin and Boyd, 1976) and they are interpreted to be xenocrystal, derived from partially dismembered ultramafic nodules.

Pyroxenes

Both ortho- and clinopyroxenes are found in these kimberlites as well as most kimberlites. In the samples studied here they occur in partially dismembered xenoliths or as large megacrysts. Neither is observed as a groundmass mineral and both are believed to be xenocrystal.

Discussion

Petrologically, kimberlites are extremely complicated. From their derivation in the upper mantle at ≥ 200 km to their emplacement in the crust they typically will entrain peridotitic, eclogitic, crustal, and other assorted nodules of various and disputed origin. The result of this fragmentation and engulfment process during their ascent and cooling is to produce a rock that consists not only of minerals directly crystallized from the melt but an assortment of xenocrysts and partially dismembered nodules. Therefore, it is necessary to establish criteria to evaluate whether a given mineral is the result of direct crystallization from the kimberlitic melt or from

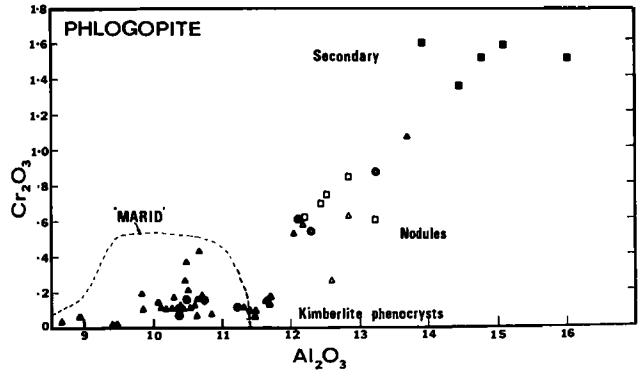

Figure 8. Al_2O_3 vs. Cr_2O_3 in phlogopite. As in Figure 7, notice the three distinct chemical groupings. Again, the kimberlite phenocrysts are similar to "MARID" phlogopites. The chemical dissimilarity between secondary phlogopite crystals in nodules to kimberlite phenocrysts suggest that the secondary phlogopites are not produced by interaction with the kimberlitic melt during eruption.

fragmentation of the various types of nodules included within the kimberlite itself.

The exact origin of discrete picroilmenite grains has been the subject of much dispute over the years. They have been interpreted to be formed by crystallization under high-pressure in the kimberlitic melt (Mitchell, 1973) or to be xenocrystic in origin (Boyd and Nixon, 1975). There is a body of circumstantial evidence bearing on their origin. Within peridotite and eclogite nodules collected from kimberlite pipes picroilmenite is not a common mineral (Smith and Dawson, 1975; and Mitchell, 1973), but picroilmenite is abundant within the kimberlite matrix. Additionally, throughout the crystallization intervals of kimberlitic magmas there is a continuous presence of at least one titanium-rich phase i.e., rutile and picroilmenite (plus armalcolite?) crystallize whilst at depth, perovskite plus Ti, Mg, Cr, Al-magnetites crystallize as groundmass phases. The kimberlitic magma clearly has a high a_{TiO_2}, a prerequisite only if the picroilmenites are truly phenocrystic phases. Therefore, the universal presence of picroilmenite in kimberlites, the scarcity of picroilmenite in peridotite and eclogite nodules as well as the titaniferous nature of kimberlitic melts suggests that the origin of picroilmenite is by direct crystallization from the kimberlite melt.

As described earlier, the variations in chemistry in picroilmenites is quite significant. Unzoned, granoblastic picroilmenites and inversely zoned picroilmenites have been previously described by Mitchell (1973) and Haggerty (1973), respectively. The granoblastic picroilmenites are generally much larger than the inversely zoned picroilmenites and may have undergone an annealling event as proposed by Mitchell (1973),

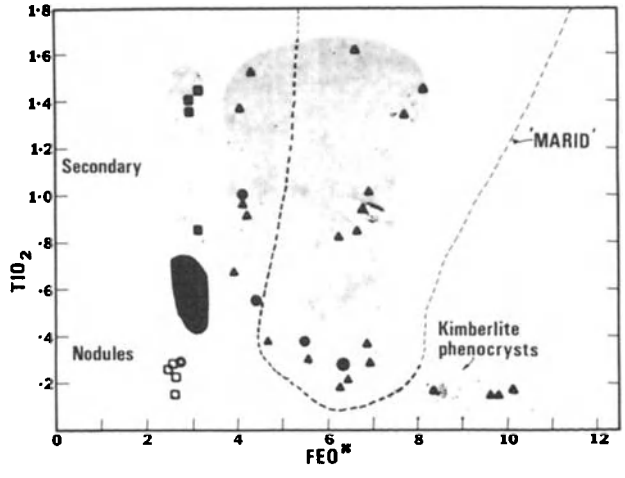

Figure 9. TiO_2 vs. FeO* in phlogopite. The TiO_2 contents of phlogopites are highly variable in the mantle and kimberlitic environments and is not much use in distinguishing possible petrogenesis of kimberlitic phlogopites.

TABLE 3. Phlogopite Analyses.

	1	2	3	4	5	6
SiO_2	42.70	42.73	41.98	43.02	42.45	42.57
TiO_2	.53	.29	.15	.51	.71	.93
Al_2O_3	12.05	10.25	8.46	12.17	11.39	10.60
Cr_2O_3	.53	.11	.00	.62	.16	.16
FeO*	3.20	6.42	9.64	2.82	3.95	6.87
MnO	.02	.03	.04	.00	.03	.09
MgO	25.61	25.24	24.43	25.74	25.51	23.71
CaO	.03	.14	.05	.05	.02	.05
NiO	n.d.	.14	.06	.19	n.d.	.11
Na_2O	.30	.07	.04	.43	.23	.19
K_2O	10.43	9.97	9.98	9.58	10.64	9.61
P_2O_5	.00	.07	.01	.00	.00	.02
Total	95.39	95.46	94.85	95.20	95.09	94.89

1. Phlogopite from partially dismembered ol-opx-cpx-gnt-phl nodule
2. Groundmass phlogopite
3. Groundmass phlogopite
4. Phlogopite metacryst with numerous deformation lamellae and rounded grain boundaries (pre-fluidization)
5. Phlogopite from partially dismembered ol-opx-cpx-gnt-phl nodule
6. Phlogopite megacryst (post-fluidization)

sufficient to homogenize individual grains.

Within the groundmass of the kimberlites studied here, the following minerals crystallized: calcite, perovskite, Ti, Mg, Cr, Al magnetites, phlogopite, olivine, apatite and assorted sulfides. As mentioned earlier, the groundmass olivines are $Fo_{(88-89)}$. Those olivines with more magnesium rich cores are usually zoned to rims of $Fo_{(88-89)}$ (see Figure 6). The ubiquitous presence of perovskite and Ti, Mg, Cr, Al magnetites on the rims of picroilmenite and rutile indicates that perovskite and Ti, Mg, Cr, Al magnetites rather than picroilmenite or rutile are stable during the groundmass crystallization.

In view of the very fresh nature of these kimberlites, the abundance of calcite in the groundmass and as subhedral to anhedral crystals cannot be attributed to secondary alteration processes common in kimberlites. Rather, the carbonate phase has crystallized directly from a CO_2-saturated kimberlite melt, along with both silicate and oxide phases.

The evolution and crystallization of kimberlite magma

Judging from studies of pressure-sensitive mineral pairs in garnet peridotite xenoliths, kimberlites must originate at depths in excess of 150 km (Boyd, 1976). In a CO_2-bearing mantle at

TABLE 4. Garnet and Pyroxene Analyses.

	Garnets				cpx		opx	
	1	2	3	4	5	6	7	8
SiO_2	42.16	41.58	41.14	41.30	55.27	53.78	57.97	57.47
TiO_2	.08	.00	.04	.10	.14	.83	.07	.00
Al_2O_3	20.27	21.27	21.16	18.67	1.40	.81	.25	.96
Cr_2O_3	4.48	3.33	3.53	6.11	2.32	.23	.02	.29
FeO*	6.74	6.17	6.93	6.58	2.50	4.00	7.23	4.16
MnO	.39	.33	.04	.38	.11	.20	.20	.09
MgO	20.88	22.71	21.18	20.63	16.42	18.80	34.82	36.89
CaO	5.06	2.92	4.40	5.27	20.68	19.30	.31	.35
NiO	.00	.00	.00	.00	n.d.	n.d.	n.d.	n.d.
Na_2O	.02	.00	.04	.04	2.02	.64	.00	.04
K_2O	.00	.00	.00	.00	.00	.09	.00	.00
P_2O_5	.09	.02	.04	.07	.05	.12	.00	.00
Total	100.17	98.33	99.19	99.16	100.91	98.79	100.86	100.27

1 and 2. Garnets in partially dismembered nodules
3 and 4. Garnet megacrysts
5. cpx megacryst
6 and 7. Coexisting cpx and opx in partially dismembered nodule
8. opx megacryst

this depth the stable assemblage would be a carbonated garnet peridotite, which might also contain primary phlogopite (Wyllie and Huang, 1976a,b; Wyllie, 1977). A small degree (<1%) of melting would produce a silicate melt, saturated with CO_2 and H_2O, the precursor to a kimberlite melt. This protokimberlite would thus have olivine, orthopyroxene, clinopyroxene, garnet, phlogopite and carbonate as liquidus or near-liquidus phases.

Within the region of magma genesis the a_{SiO_2} in the melt would be buffered by the equilibrium of olivine + orthopyroxene + melt (note, however that γ_{SiO_2} must be sensitive to the amount of CO_2, H_2O in the melt). As the carbonated melt ascends towards the surface, its a_{SiO_2} may no longer be buffered by olivine and orthopyroxene if it fails to maintain equilibrium with mantle minerals (Nichols et al., 1971), and the silica activity continues to fall with decreasing pressure and as CO_2 degasses from the melt. The near-surface value of a_{SiO_2} must be relatively low, in order to stabilize perovskite as a ubiquitous matrix mineral (Carmichael et al., 1970; Mitchell, 1975). It seems probable that the various Ti-bearing oxide and silicate phases observed to crystallize in kimberlites, do so in response to variations in f_{O_2} and a_{SiO_2} during magma ascent. A specific example would be the peritectic-like reaction between picroilmenite and kimberlite melt to produce perovskite + magnetite$_{ss}$.

Kimberlites, unlike most other silicate magmas, due to their origin at high pressures can initially dissolve large quantities of both CO_2 and H_2O if the degree of partial melting is very small. Since both CO_2 and H_2O solubility decrease dramatically with decreasing pressure, loss of these constituents during ascent must drastically change both the structure of the kimberlite liquid and the activities of the remaining oxide species, expecially if the latter are unbuffered by mantle minerals. Hence, the final kimberlite magma may be chemically quite heterogeneous with regard to dissolved volatiles, chemical species and overall melt structure. All of these features probably combine to limit diffusion through the melt upon crystallization, resulting in local chemical disequilibrium effects developing in terms of f_{O_2}, f_{CO_2}, a_{MgO}, a_{FeO}, etc. The lack of achievement of chemical equilibrium on this restricted scale is now reflected in significant intergrain chemical variation.

Post-Amble

Unlike almost all other silicate melts, the crystallization history of kimberlites is closely tied to the dissolution of CO_2 and H_2O during ascent. The fact that the matrix of kimberlites generally contains a carbonate phase strongly supports the view that the melt has been continuously saturated with CO_2 during its evolution; in this case large volumes of CO_2 must degas from the melt during ascent (Wyllie, 1977). Not

surprisingly, the phases crystallizing at depth from such a melt are not those crystallizing from the near-surface, CO_2-depleted melt. In this discussion, we have conveniently separated the crystallization of kimberlite into two intervals separated by the reaction of picroilmenite with the magma to form perovskite + magnetite. The earliest period involved crystallization of picroilmenite, rutile, olivine, phlogopite, and possibly orthopyroxene, clinopyroxene, garnet, spinel and armalcolite. The later period (essentially the near-surface environment) involved perovskite, magnetite, olivine, phlogopite, carbonate, apatite and sulfides. Since the matrix mineralogy of kimberlites is so variable (Clements et al., 1977), the above scenario should not necessarily be applicable to kimberlites in general. Probably variations in f_{O_2}, f_{H_2O} and f_{CO_2} in different kimberlites have a strong influence on the silicate and oxide mineral chemistry and paragenesis.

Lamont-Doherty Geological Observatory Contribution No. 2706.

Acknowledgements. We would like to thank Charles Stern for a critical review of the manuscript and J. Hamlyn for her typing expertise. The microprobe facilities are supported by National Science Foundation grant EAR-76-82456 and NASA grant NGR-33-008-199.

References

Boyd, F.R., and P.H. Nixon, Origin of the ilmenite-silicate nodules in kimberlites from Lesotho in South Africa, In: Lesotho kimberlites (ed. P.H. Nixon), 254-268, 1973.

Boyd, F.R., and P.H. Nixon, Origins of the ultramafic nodules from some kimberlites of Northern Lesotho and the Monastery Mine, South Africa, In: Phys. Chem. Earth, 9, 431-454, 1975.

Carmichael, I.S.E., J. Nicholls, and A.L. Smith, Silica activity in igneous rocks, Am. Mineral., 55, 246-263, 1970.

Carswell, D.A., Primary and secondary phlogopites and clinopyroxenes in garnet lherzolite xenoliths, In: Phys. Chem. Earth, 9, 417-430, 1975.

Carter, D.L., and A. Okaya, Electron paramagnetic resonance of Fe^{3+} in TiO_2, Phys. Review, 118, 1485-1490, 1960.

Clarke, D.B. and R.H. Mitchell, Mineralogy and petrology of the kimberlite from Somerset Island, N.W.T., Canada, In: Phys. Chem. Earth, 9, 123-135, 1975.

Clement, C.R., E.M.W. Skinner, and B.H. Scott, Kimberlite redefined, Sec. International Kimb. Conf. Extended Abst., 1977.

Danchin, R.V., and F.R. Boyd, Ultramafic nodules from the Premier kimberlite pipe, South Africa, Ann. Report of the Director, Geophysical Laboratory, 531-538, 1976.

Dawson, J.B., and J.V. Smith, The MARID suite of xenoliths in kimberlite, Geochem. Cosmochim. Acta, 41, 309-323, 1977.

Gittins, J., R.H. Hewins, and A.F. Laurin, Kimberlitic-carbonatitic dikes of the Saquenay River Valley, Quebec, Canada, In: Phys. Chem. Earth, 9, 137-148, 1975.

Haggerty, S.E., Spinels of unique composition associated with ilmenite reactions in the Lighbong kimberlite pipe, Lesotho, In: Lesotho Kimberlites (ed. P.H. Nixon), 149-158, 1973.

Haggerty, S.E., The chemistry and genesis of opaque minerals in kimberlites, In: Phys. Chem. Earth, 9, 295-307, 1975.

Mitchell, R.H., Magnesian ilmenite and its role in kimberlite petrogenesis, J. Geol., 81, 301-311, 1973.

Mitchell, R.H., and D.B. Clarke, Oxide and sulphide mineralogy of the Peuyuk Kimberlite, Somerset Island, N.W.T., Canada, Contrib. Mineral. Petrol., 56, 157-172, 1976.

Nicholls, J., I.S.E. Carmichael, and J.C. Stormer, Silica activity and P_{total} in igneous rocks, Contrib. Mineral. Petrol., 33, 1-20, 1971.

Smith, J.V., and J.B. Dawson, Chemistry of Ti-poor spinels, ilmenites, and rutiles from peridotite and eclogite xenoliths, In: Phys. Chem. Earth, 9, 309-322, 1975.

Velde, D., Armalcolite-Ti-phlogopite-diopside-analcite-bearing lamproites from Smoky Butte, Garfield County, Montana, Am. Mineral., 60, 566-573, 1975.

Wyllie, P.J., Mantle fluid compositions buffered by carbonates in peridotite-CO_2-H_2O, J. Geol., 85, 187-207, 1977.

Wyllie, P.J., and W.L. Huang, Carbonation and melting reactions in the system CaO-MgO-SiO_2-CO_2 at mantle pressures with geophysical and petrological applications, Contrib. Mineral. Petrol., 54, 79-107, 1976a.

Wyllie, P.J., and W.L. Huang, High CO_2 solubilities in mantle magmas, Geology, 4, 21-24, 1976b.

OXIDE AND SULFIDE MINERALS IN KIMBERLITE FROM GREEN MOUNTAIN, COLORADO

Nabil Z. Boctor* and Henry O. A. Meyer

Department of Geosciences, Purdue University, West Lafayette, Indiana 47907

Abstract. The opaque minerals in kimberlite from Green Mountain, Colorado are represented by an assemblage of spinel solid solutions, ilmenite, rutile, perovskite, and minor sulfide minerals.

The spinels in the groundmass and in reaction mantles on ilmenite nodules are generally enriched in Ti and Mg and depleted in Cr. Spinels in ilmenite reaction mantles have the highest TiO_2 (up to 33 wt. %), high MgO (19.5 wt. %), and high FeO (33 wt. %), whereas spinels in reaction mantles on rutile-ilmenite intergrowths are the richest in Cr_2O_3 (up to 12 wt. %). Groundmass spinels are more enriched in Fe_2O_3 and Al_2O_3 relative to the spinels in the reaction mantles.

The complex reaction mantles on ilmenite nodules and on rutile-ilmenite intergrowths display different mineralogy and chemistry in different specimens. These differences are controlled by the changes in the activities of Mg, Ti, and Al in the liquid with progressive crystallization and by local buffering of the fO_2 during the reaction between the xenocrysts and liquid. The mineral assemblages in the complex reaction mantles reflect variations in fO_2 which were probably induced by changes in the CO/CO_2 and H_2/H_2O ratios during the crystallization and equilibration of the different mineral phases in the mantles. The variations in fO_2 apparently continued during the crystallization of the groundmass.

Perovskite is remarkably enriched in Nb and REE. This enrichment is attributed to the presence of a CO_2 rich fluid that provided the complexing ions ($CO_3^{=}$, HCO_3^{-}) necessary for the enrichment of these elements.

Sulfide minerals are represented by heazlewoodite and bornite that are commonly associated with serpentine. Their mineralogy and texture are not suggestive of an origin by sulfide liquid immiscibility. More likely, they are the products of sulfurization reactions during serpentinization.

Introduction

In recent years, the opaque oxides in kimberlites have been the subject of various investigations (Boyd and Nixon, 1973; Danchin and D'Orey, 1972; Danchin et al., 1976; Dawson and Hawthorne, 1973; Haggerty, 1973, 1975; Mitchell, 1973; Mitchell and Clark, 1976). These investigations have demonstrated the importance of oxide minerals in kimberlites as indicators of the physical-chemical environment during crystallization, fluidization, emplacement, and final cooling of kimberlitic magma. The approach adopted in the present investigation was to study the oxide mineral assemblages in the complex reaction mantles on ilmenite nodules and in the groundmass of a suite of specimens selected from a single kimberlite pipe at the Green Mountain, near Boulder, Colorado. The mineralogy of the sulfide minerals in this kimberlite was also studied.

*Now at the Geophysical Laboratory, Carnegie Institution of Washington, Washington, D. C. 20008.

Geological Setting

The kimberlite at the Green Mountain is represented by a single diatreme, roughly circular in surface exposure, which has intruded Precambrian granite. The original geometry of the intrusion has been modified subsequently by the Laramide orogeny, and attempts to date the intrusion using paleomagnetic data proved ambiguous (Kridelbaugh et al., 1972). Meyer (1976) and Meyer and Kridelbaugh (1977) suggested that the Green Mountain kimberlite is most likely comparable in age with those of the Colorado-Wyoming state line region, which are supposedly Devonian. The major minerals in Green Mountain kimberlite are diopside ($Ca_{0.76}Mg_{0.98}Fe_{0.10}Si_{1.98}O_6$) ilmenite (up to 12 wt. % MgO), Cr-rich and Cr-poor almandine, olivine (Fo_{93}), orthopyroxene (En_{91}), biotite, phlogopite (up to 6 wt. % TiO_2), serpentine, and calcite (Kridelbaugh and Meyer, 1973; Meyer and Kridelbaugh, 1977). Several types of xenolith, including fragments of Boulder granite and garnet granulite, occur in the kimberlite.

Analytical Methods

The specimens were studied by reflected light microscopy and occasionally in transmitted light. The minerals were chemically analyzed using an automated M.A.C. 500 electron microprobe. Data reduction was performed by the α program which employs the correction schemes of Bence and Albee

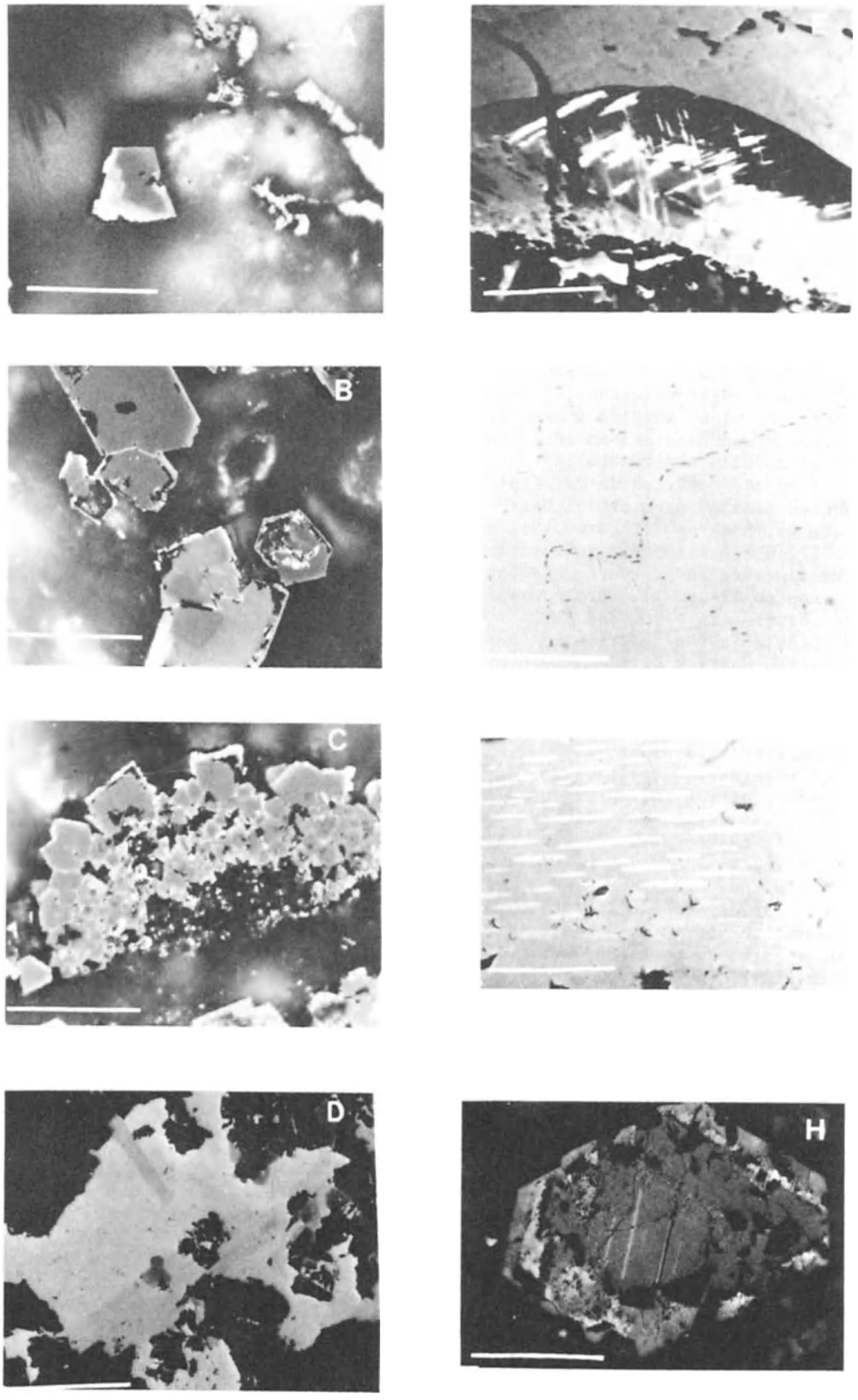

(1968) and Albee and Ray (1970). Magic IV computer program (Colby, 1971) was used for data reduction of perovskite analyses. Ferric iron was calculated using the method of Finger (1972).

Oxide Minerals

Oxide minerals in Green Mountain kimberlite are represented by: 1 - a complex assemblage of spinel solid solutions in the groundmass and in reaction mantles on ilmenite nodules and on rutile-ilmenite intergrowths, 2 - ilmenite nodules, groundmass ilmenite, and secondary ilmenite in the reaction mantles, 3 - rutile-ilmenite intergrowths, and 4 - perovskite.

Groundmass Spinels

Spinels occur in the groundmass of Green Mountain kimberlite as zoned or unzoned subhedral to euhedral crystals (15-50 μm). Zoned crystals have dark, grayish brown cores and light brown rims of a higher reflectance than the core (Fig. 1a, b). Occasionally an outermost zone of titaniferous magnetite mantles the rim, with or without a thin intervening film of silicates. In certain instances, the cores are corroded and show partial resorption. Microprobe analyses (Table 1, Analysis 1) show a decrease in MgO and TiO_2 and an increase in Fe_2O_3 from core to rim. In some cases, zoned spinels form aggregates of interlocking idiomorphic crystals (Fig. 1c). Unzoned spinels are homogeneous in composition and their chemistry is, in general, similar to that of the rims of zoned spinels (Table 1, Analyses 2 and 3). In a single specimen, however, the groundmass spinel was a titanomagnetite containing small amounts of MgO, Al_2O_3, and Cr_2O_3 (Table 1, Analysis 4). Magnetite-ilmenite intergrowths occasionally occur in the groundmass and are characterized by a network of ilmenite parallel to the octahedral planes of magnetite. In a few instances, the magnetite encloses a few zoned idiomorphic crystals of spinel that served as nucleation sites for large tabular lamellae of ilmenite (Fig. 1d).

The groundmass spinels in the Green Mountain diatreme are characterized by their low Cr content. Thus they differ from the Cr rich spinels commonly observed in kimberlites (Haggerty, 1975; Mitchell and Clark, 1976) and from spinel inclusions in diamond (Meyer and Boyd, 1972).

Ilmenite

Ilmenite nodules (0.4 to 2.0 cm) are common in all specimens investigated. Some are recrystallized into a mosaic of interlocking crystal aggregates, whereas others show evidence of shearing and development of deformation twinning particularly near their peripheries (Fig. 1e). The ilmenite commonly displays fine exsolutions of spinel (Fig. 1f). Unfortunately, the composition of these exsolutions cannot be determined as their size is smaller than the quantitative resolution of the microprobe. Microprobe traverses across the lamellae show substantial increase in the count rates for Mg, Cr, and Al. Some ilmenite nodules show abundant lamellae of titanomagnetite parallel to their (0001) planes (Fig. 1g). Euhedral ilmenite crystals (Fig. 1h) that show lamellar intergrowths of titanomagnetite are also present in the groundmass and may occur in the same specimen with magnetite-ilmenite intergrowths. A secondary magnesian ilmenite (Table 1, Analysis 11) occurs in reaction mantles on ilmenite nodules and in the groundmass. In carbonate rich specimens, Mg poor and Mn rich ilmenite (Table 1, Analysis 12) occurs in the groundmass and in reaction mantles on rutile-ilmenite intergrowths.

Reaction Mantles on Ilmenite Nodules

Complex reaction mantles on ilmenite nodules in Green Mountain kimberlite are common. Nodules

Fig. 1a. Spinel showing growth zoning with a Ti, Mg rich core and an outermost zone of titaniferous magnetite, reflected light, bar = 0.05 mm.
Fig. 1b. Similar to Fig. 1a, the intermediate spinel zone is well developed in some of the crystals, a thin film of intervening silicate is present rimmed by magnetite. Note the presence of titaniferous magnetite rims on idiomorphic silicate, reflected light, bar = 0.05 mm.
Fig. 1c. Aggregates of interlocking spinel crystals in groundmass, reflected light, bar = 0.02 mm.
Fig. 1d. Magnetite with coarse lamellae of ilmenite, which nucleated on zoned spinel crystals, reflected light, bar = 0.02 mm.
Fig. 1e. Sheared ilmenite showing 2 sets of deformed twin lamellae, reflected light, partially crossed nicols, bar = 0.1 mm.
Fig. 1f. Ilmenite nodule with spinel lamellae, reflected light, bar = 0.05 mm.
Fig. 1g. Ilmenite nodule showing titanomagnetite lamellae parallel to (0001) of the host, reflected light, bar = 0.02 mm.
Fig. 1h. Ilmenite crystal in groundmass showing titanomagnetite lamellae and perovskite rim, reflected light, bar = 0.02 mm.

TABLE 1. Representative Electron Microprobe Analyses of Spinels and Ilmenite

	Zoned Spinel		Unzoned Spinels			Reaction Mantle Spinels					Ilmenite		
	1		2	3	4	5	6	7	8	9	10	11	12
Oxide wt. %	Core	Rim											
TiO_2	22.82	19.77	19.77	18.27	5.55	33.25	25.76	9.85	0.99	23.66	54.39	56.40	52.33
FeO	15.79	19.97	21.15	22.51	33.46	31.75	32.88	12.65	30.85	27.09	25.78	10.39	42.28
Fe_2O_3	24.68	30.69	28.91	29.85	53.87	11.93	21.73	52.73	66.85	12.33	5.57	6.60	--
MnO	0.82	0.55	1.01	0.73	1.66	0.97	2.99	0.91	0.28	2.19	0.25	0.64	4.96
MgO	24.45	19.97	18.90	17.72	0.69	19.43	13.00	17.80	1.65	19.57	12.86	22.63	0.66
CaO	0.08	0.02	0.03	0.08	0.88	0.01	0.02	0.05	0.02	0.12	0.04	0.04	0.07
Al_2O_3	9.28	9.54	9.17	10.10	2.89	1.84	1.27	5.45	0.05	3.63	0.51	0.33	0.01
Cr_2O_3	1.11	0.82	1.48	0.78	0.35	0.85	1.56	0.48	0.03	11.79	0.65	2.16	0.04
	99.06	100.60	100.42	100.02	99.33	100.03	99.28	100.72	100.72	100.38	100.05	99.19	100.35

in different samples display mantles of different mineral assemblages:

1 - The outermost rims of the ilmenite nodule is remarkably enriched in Mg relative to the cores (22.6 versus 12.9 wt. % MgO). The magnesian ilmenite is mantled by a discontinuous zone of rutile-ilmenite intergrowths. A spinel rich in TiO_2, MgO, and FeO mantles the rutile-ilmenite intergrowth (Table 1, Analysis 5). This type of reaction mantle is not as well defined as those described by Haggerty (1973), and frequently the spinel mantles the rutile-ilmenite intergrowth on both sides with islands of secondary magnesian ilmenite in the inner rims (Fig. 2a). The lamellar ilmenite intergrowths in rutile occasionally show cores of Mg and Cr rich spinel (Fig. 2b) which seems to share the same crystallographic plane as the ilmenite and may also occur in the rims of secondary magnesian ilmenite surrounding the rutile-ilmenite intergrowth (Fig. 2c). The bulk compositions of the rutile-ilmenite intergrowth are commonly similar to that of armalcolite. The groundmass spinels coexisting with ilmenite nodules that display this type of reaction mantle are of the zoned type and are more enriched in Fe_2O_3 and Al_2O_3 and more depleted in TiO_2 relative to the spinels in the reaction mantles.

2 - The ilmenite nodule is mantled by an inner zone of Ti rich spinel (Table 1, Analysis 6) along its peripheries or along calcite veinlets that transect the nodule. The spinel zone is followed by a discontinuous zone of magnesian ilmenite which is mantled by a magnesian titanomagnetite that is more enriched in MgO, Al_2O_3, and Fe_2O_3 and more depleted in TiO_2 (Table 1, Analysis 7) relative to the spinel of the inner zone. The outermost spinel shows oscillatory zoning and may occur in contact with the spinel of the inner zone with no intervening ilmenite (Fig. 2e). Ti poor magnetite (Table 1, Analysis 8) either fills the median part of the calcite veinlets or occurs in direct contact with Ti rich spinel of the inner zone or with ilmenite (Fig. 2f). The groundmass spinels coexisting with ilmenite nodules displaying this type of reaction mantle are magnetite-ilmenite intergrowths and Ti poor magnetite. Rutile-ilmenite intergrowths in the same specimens are mantled by Cr and Ti rich spinels.

3 - The ilmenite nodule is mantled by a rim of perovskite and rarely an intervening zone of Ti rich spinel. Commonly the outer rim is an intimate mixture of ilmenite and perovskite, but occasionally the perovskite occurs as subhedral to euhedral crystals (Fig. 3a). The groundmass spinels coexisting with perovskite mantled ilmenite nodules are of the unzoned Ti rich type.

Ilmenite nodules that do not display reaction mantles are rare in Green Mountain kimberlite, and the spinel coexisting with such nodules is titanomagnetite (5.6 wt. % Ti) depleted in Mg and Al.

Rutile-ilmenite Intergrowths

Rutile-ilmenite intergrowths occur in the groundmass in addition to their occurrence in the reaction mantles. They are commonly associated with Ti rich phlogopite. Commonly they are mantled by secondary magnesian ilmenite which occasionally shows fine spinel exsolutions (Fig. 3b). In some cases, the ilmenite is mantled by a Ti and Cr rich spinel which is the richest in Cr in the Green Mountain kimberlite (Cr_2O_3 8.5 - 11.8 wt.%). Rarely the rutile-ilmenite intergrowths are mantled by Mn rich ilmenite that is depleted in Cr and Mg (Table 1, Analysis 12) which is in turn mantled by Ti and Cr rich spinel (Table 1, Analysis 9; Fig. 3c), the ilmenite being more enriched in Mn relative to the spinel. Occasionally the rutile-ilmenite intergrowths are directly mantled by spinel which occurs as idiomorphic crystals without an intervening zone of ilmenite (Fig. 3d).

Perovskite

In addition to its occurrence in the reaction mantles, perovskite occurs in the groundmass. Perovskite in the groundmass occurs as subhedral crystals or crystal aggregates that are commonly mantled by rutile or anatase which appears to be of secondary origin (Fig. 3e). Both the mantle and groundmass perovskites are characterized by their high Nb_2O_5 and REE oxides (Table 2). The Nb content in perovskite is variable within the same specimen. Occasionally, perovskite crystals show zoning with a decrease of Nb from core to rim.

Sulfide Minerals

The sulfide minerals in Green Mountain kimberlite are rare, being represented by heazlewoodite and Ni bearing bornite with minor amounts of covellite. None of the primary sulfides, pyrrhotite, pentlandite, and chalcopyrite, that commonly occur as accesory minerals in other kimberlites were observed in the samples studied from Green Mountain kimberlite. Heazlewoodite occurs as veinlets and irregular masses in serpentine and rarely as oriented platelets in this mineral. Bornite occurs either as a discrete mineral, partially replaced by covellite, or as thin, discontinuous rims on heazlewoodite (Fig. 3f).

Discussion

The Green Mountain kimberlite is characterized by the presence of Ti and Mg rich spinels that are different in composition from the chromites, chromite-picrochromites, and titanian chromites that are common in kimberlites. The composition of the spinel minerals in the groundmass and in ilmenite reaction mantles were plotted (Fig. 4) in the reduced spinel prism (Haggerty, 1971) by the method of Irvine (1965). All iron was calculated as Fe^{2+}. The data were also projected on the base of the spinel prism, its front rectangular face, and its front triangular face (Fig. 5). The same symbol was used for coexisting spinels in the groundmass and in the reaction mantles of each specimen for easy comparison.

The first striking feature about the spinels in Green Mountain kimberlite is that they are confined mainly to the front rectangular face bound by the components Mg_2TiO_4-Fe_2TiO_4-$MgAl_2O_4$-$FeAl_2O_4$. However, since Fe^{3+} is not taken into account in the reduced spinel prism, two additional components, Fe_3O_4 and $MgFe_2O_4$ which are necessary for representation of the spinel solid solution compositions are not represented. A single exception is the groundmass spinels in one specimen, the compositions of which plot in the front triangular face bound by the components Fe_2TiO_4-$FeCr_2O_4$-$FeAl_2O_4$. The known kimberlitic spinels that are confined to the quartenary system, Mg_2TiO_4-$MgAl_2O_4$-$FeAl_2O_4$-Fe_2TiO_4, are those from Benfontein kimberlitic sills (Dawson and Hawthorne, 1973); the spinels in the complex ilmenite reaction mantles at Liqhobong (Haggerty, 1973); phase c spinels in Peuyuk kimberlite (Mitchell and Clark, 1976); and spinels in the groundmass of nucleated autoliths from South and Southwest African kimberlites (Danchin et al., 1975). Early formed spinels in kimberlite which are confined to the quartenary system $FeCr_2O_4$-$MgCr_2O_4$-$FeAl_2O_4$-$MgAl_2O_4$ (Haggerty, 1975) were not encountered in the specimens studied from the Green Mountain kimberlite.

The spinels in the Green Mountain kimberlite are apparently the products of late stage crystallization from a Ti rich liquid. The occurrence of Ti rich spinels in the ilmenite reaction mantles; the idiomorphic nature of most of the groundmass spinels; and the presence of thin mantles of Ti rich spinels on silicate minerals seem to support this conclusion. The spinels display oscillatory zoning and resorption textures; they are not in equilibrium with other phases in the reaction mantles on ilmenite nodules; and they plot within the experimentally determined solvi of Muan et al. (1972), although they do not display exsolution textures. These features suggest that they did not crystallize under equilibrium conditions.

The origin of the rutile-ilmenite intergrowths in kimberlite is not well understood. The similarity of the bulk composition of some of these intergrowths to that of armalcolite, and the occurrence of armalcolite as a kimberlitic mineral suggest that some of the rutile-ilmenite intergrowths are the products of a breakdown of armalcolite (Haggerty, 1975). Experimental investigations (Lindsley et al., 1975; Friel et al., 1977) indicate that armalcolite with Fe/(Fe + Mg) ratio of 0.5 is stable at 1200°C and 10 Kb. It breaks down with increasing pressure to rutile, a more magnesian armalcolite, and ilmenite solid solution. At 14 Kb this assem-

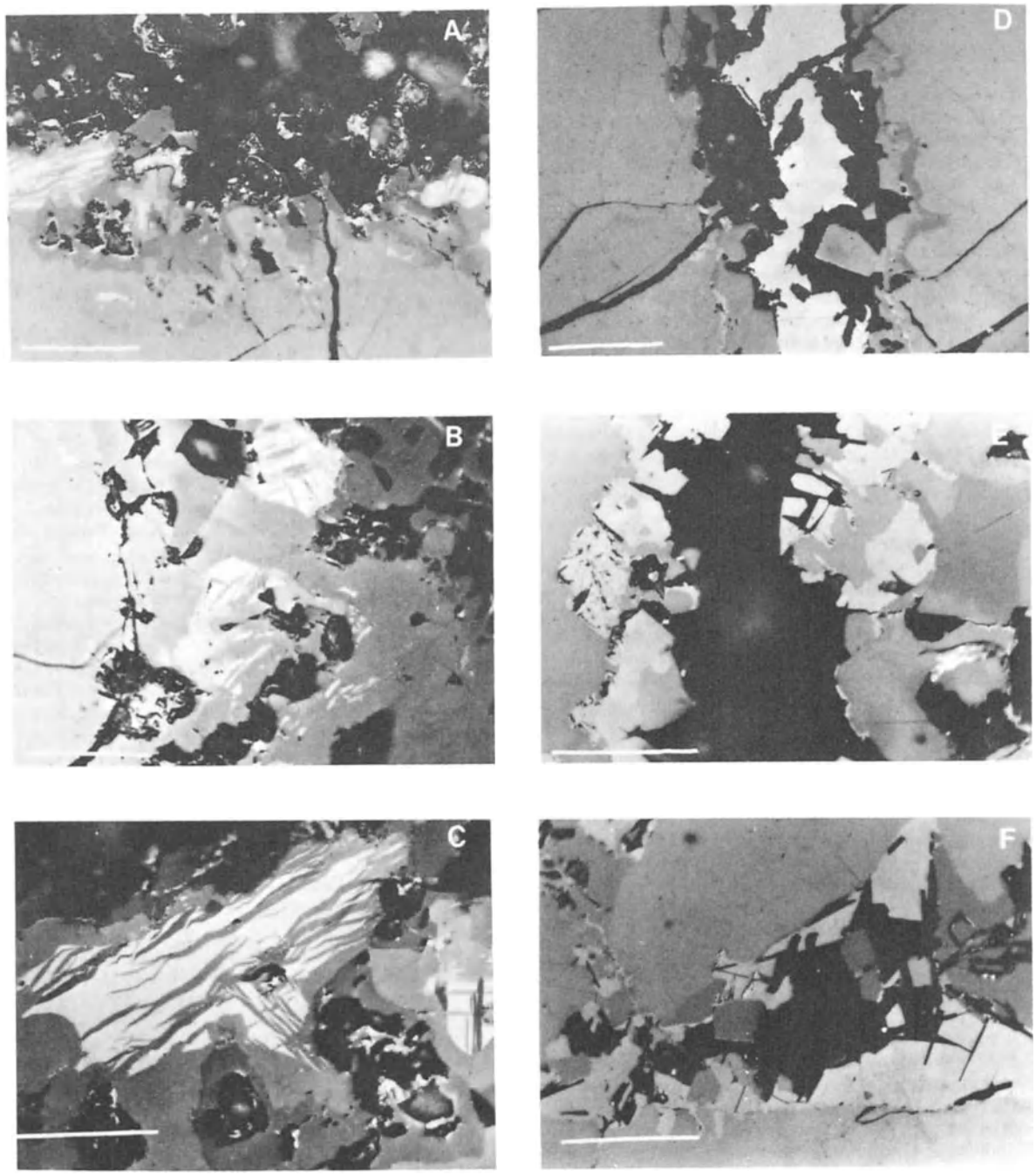

Fig. 2a. Reaction mantle showing rutile-ilmenite intergrowth rimmed on both sides by Ti, Mg rich spinel with islands of ilmenite in the inner rim, reflected light, bar = 0.1 mm.
Fig. 2b. Rutile-ilmenite intergrowth in reaction mantle, the ilmenite lamellae show cores of spinel, reflected light, bar = 0.02 mm.
Fig. 2c. Spinel lamellae sharing the same plane with ilmenite in rutile-ilmenite intergrowth, adjacent ilmenite rim shows fine lamellae of spinel, reflected light, bar = 0.02 mm.
Fig. 2d. A veinlet of calcite transecting an ilmenite nodule, magnetite fills the median part of the vein; a zone of Ti rich spinel mantles the ilmenite, followed by a discontinuous zone of ilmenite and an outer zone of spinel showing oscillatory zoning, reflected light, bar = 0.1 mm.
Fig. 2e. Spinel showing oscillatory zoning in direct contact with Ti rich spinel in inner zone. Ti poor magnetite mantles the ilmenite in the upper part of the photograph, reflected light, bar = 0.05 mm.
Fig. 2f. Magnetite in direct contact with ilmenite on one side with Ti rich spinel on the other side, reflected light, bar = 0.05 mm.

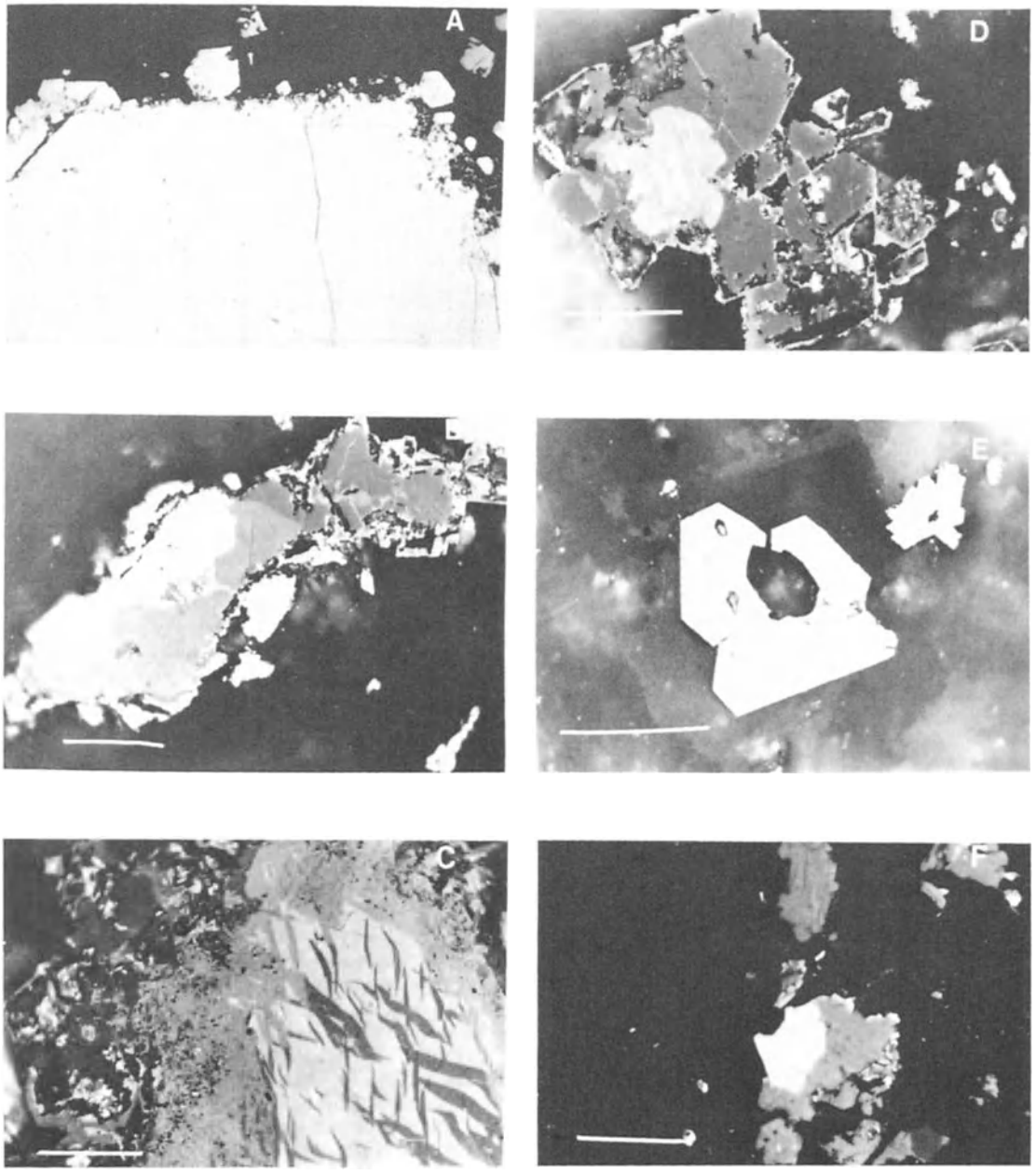

Fig. 3a. Ilmenite with perovskite rim; note crystals of perovskite in the outermost part of the rim, reflected light, bar = 0.05 mm.
Fig. 3b. Rutile-ilmenite intergrowth mantled by ilmenite which is rimmed by Ti, Cr bearing spinel, the outer most light colored rim is magnetite, reflected light, bar = 0.02 mm.
Fig. 3c. Rutile-ilmenite intergrowth mantled by Mn rich ilmenite with an outer zone of Cr and Ti bearing spinel, reflected light, bar = 0.02 mm.
Fig. 3d. Rutile-ilmenite intergrowth with idiomorphic crystals of spinel on its rim with no intervening ilmenite, reflected light, bar = 0.02 mm.
Fig. 3e. Perovskite crystals replaced at their rims by anatase, reflected light, bar = 0.05 mm.
Fig. 3f. Heazlewoodite (white) rimmed by bornite (gray), reflected light, bar = 0.05 mm.

TABLE 2. Representative Electron Microprobe Analyses of Perovskite*

Oxide wt. %	1	2	3	4
SiO_2	0.03	0.16	0.01	0.04
TiO_2	43.00	45.70	46.60	48.70
ZrO_2	0.01	0.01	0.01	0.01
FeO	2.58	2.78	2.04	1.92
MgO	0.34	0.37	0.19	0.13
CaO	30.00	31.20	31.70	33.10
Y_2O_3	0.08	0.04	0.01	0.04
La_2O_3	1.98	1.86	1.58	0.73
Ce_2O_3	5.88	5.73	4.93	3.56
Pr_2O_3	0.81	0.72	0.52	0.24
Nd_2O_3	1.64	1.90	1.11	1.37
Ta_2O_5	0.01	0.01	0.06	0.18
Nb_2O_5	11.50	7.11	8.60	6.81
Na_2O	1.88	1.43	1.54	1.72
	99.7	99.0	98.9	98.5

*Analyses 1 and 2, Groundmass perovskite; Analyses 3 and 4, Reaction mantle perovskite

TABLE 3. Representative Electron Microprobe Analyses of Sulfides

Element wt. %	Heazlewoodite			Bornite
S	26.70	26.90	27.00	25.60
Fe	1.04	1.10	1.22	11.30
Ni	72.60	71.90	72.20	1.28
Cu	0.01	0.01	0.01	61.10
	100.3	99.9	100.4	99.3

blage is replaced by a two phase assemblage of rutile and magnesian ilmenite solid solution (dT/dP 30°/Kb). This suggests that the rutile-ilmenite intergrowths in the Green Mountain kimberlite, if they were the result of armalcolite breakdown, must have formed at a minimum pressure of 14 Kb. The prsence of Al^{3+}, Cr^{3+}, and Ti^{3+} in armalcolite, however, stabilizes it to temperatures lower than that at which ideal armalcolite is stable, and also raises its breakdown temperatures by approximately 35°C/Kb (Kesson and Lindsley, 1975). The presence of Cr bearing spinels as lamellae in the magnesian ilmenite component of some rutile-ilmenite intergrowths in the Green Mountain kimberlite suggests that if these intergrowths are products of breakdown of armalcolite, the latter was Cr and Al bearing and therefore its breakdown temperature may have been higher than that of ideal armalcolite.

The mineral assemblage in the reaction mantles on ilmenite nodules differs in mineralogy and chemistry from one specimen to another. These differences are controlled by the changes in the activities of Mg, Ti, and Al in the liquid with progressive crystallization and by local buffering of the fO_2 during the reaction between the nodules and liquid. The mineral assemblages in the reaction mantles reflect variations in fO_2 which are demonstrated by the presence in some reaction mantles of Ti rich spinel with low Fe_2O_3/FeO ratio and of titanomagnetite or Ti poor magnetite, occasionally with an intervening zone of magnesian ilmenite. Variations in fO_2 apparently continued during the crystallization of the groundmass as demonstrated by the presence in some specimens of magnetite-ilmenite intergrowths formed by subsolidus oxidation together with ilmenite that displays oriented titanomagnetite lamellae produced by subsolidus reduction. The variations in fO_2 are probably a reflection of the changes in CO/CO_2 and H_2/H_2O ratios in the residual fluids during the crystallization and equilibration of the mineral assemblages in the reaction mantles and the groundmass (see also Haggerty, 1973).

Perovskite in Green Mountain kimberlite is remarkably enriched in Nb and rare earth elements. The niobium content is much higher than that previously reported for kimberlitic perovskite (Mitchell, 1972). The enrichment of Nb in perovskite from the Green Mountain kimberlite is reminiscent of carbonatitic perovskite. Perovskite from Green Mountain also seems to contain higher concentrations of rare earth elements in comparison to other kimberlitic perovskite; for example, the sum of total REE oxides and ThO_2 in perovskites from Koidu and DeBeer pipes are 3.11 and 2.4 wt. %, respectively (Grantham and Allen, 1960). The REE contents of perovskite in Green Mountain are comparable to those reported by Smith (1970) for nephelinites and mellilite nephelinites and by Carmichael (1967) in Madupite lavas from Leucite Hills, Wyoming.

It is interesting to note that perovskite enriched in REE in Green Mountain kimberlite coexist with what appears to be a primary carbonate. REE are known to form stable complexes with volatiles and supercritical fluids (Loubet et al., 1972). Kimberlitic magma is known to be enriched in volatiles, and Eggler (1975) has demonstrated experimentally that the vapor phase coexisting with such magma is CO_2 rich. Fesq et al. (1975) suggested that REE enrichment and fractionation in kimberlitic magma are dominantly controlled by selective formation and removal of mobile REE carbonate complexes into CO_2 rich fluids which separate from the kimberlitic magma during em-

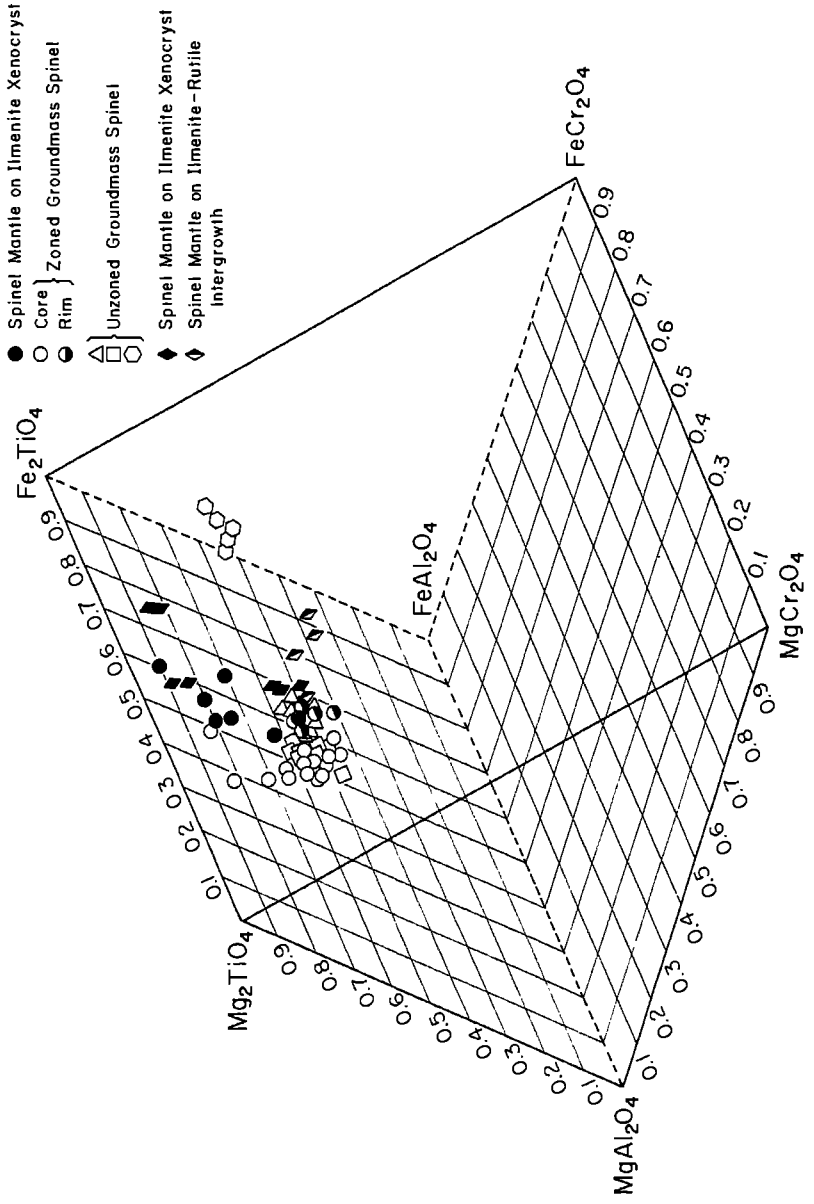

Fig. 4. Spinel compositions in groundmass and on reaction mantles on ilmenite nodules and rutile-ilmenite intergrowths plotted in the reduced spinel prism.

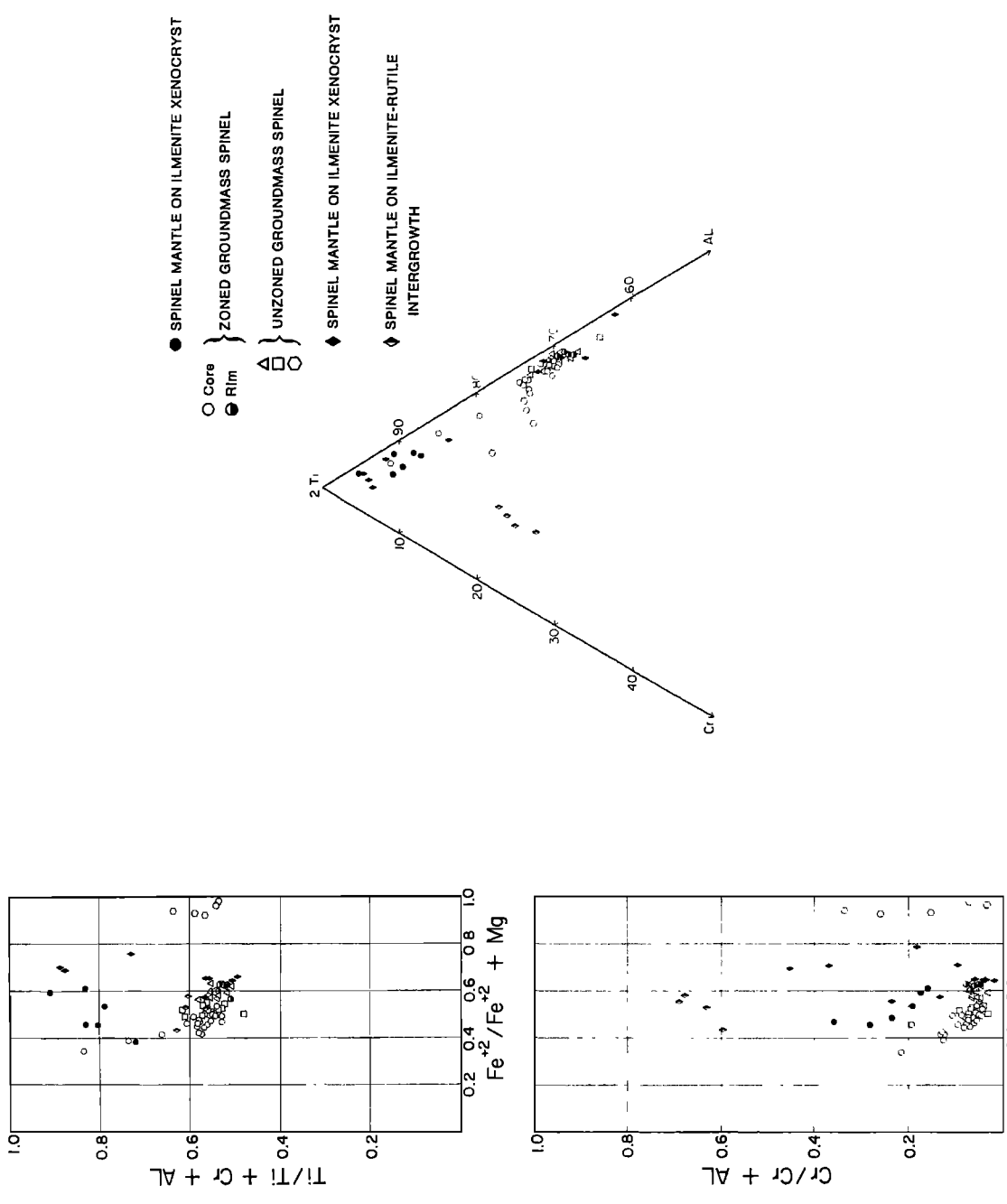

Fig. 5. Projections of the spinel compositions on the base, front rectangular face, and front triangular face of the spinel prism.

placement. The enrichment of REE in perovskite from Green Mountain is attributed to the presence of CO_2 rich fluid which provided the complexing ions (e.g., HCO_3^- and $CO_3^=$) necessary for concentration and transport of the REE. It is interesting to note that Nb, which was also enriched in the residual kimberlitic liquid from which perovskite crystallized, forms stable complexes in the presence of ions such as OH, $CO_3^=$, and F^-, which are considered by Kable et al. (1975) to be responsible for enrichment of this element in Bellsbank kimberlite. This suggests that the separation of CO_2 rich fluid from the kimberlitic magma may have been responsible for enrichment of both Nb and REE in perovskite from the Green Mountain.

The sulfide minerals in the specimens studied from Green Mountain kimberlite are mainly heazlewoodite and bornite. These minerals are characterized by their low sulfur to metal ratios and are commonly formed during serpentinization (Ramdohr, 1967). Heazlewoodite and bornite in the Green Mountain kimberlite are commonly associated with serpentine; they do not display the primary textures suggestive of sulfide liquid immiscibility and are interpreted as products of sulfurization reactions during serpentinization. Therefore, there seem to be two distinct sulfide mineral assemblages in kimberlite: a primary assemblage of pyrrhotite, pentlandite, and chalcopyrite and a secondary assemblage of Cu, Fe, and Ni sulfides that are occasionally associated with native Cu and Fe-Ni. The primary sulfide assemblage originates from an immiscible sulfide liquid that separates in the early stages of crystallization of the kimberlitic magma, whereas the secondary sulfide assemblage forms in an environment of low fS_2 during serpentinization when the primary sulfide minerals undergo partial or complete breakdown.

Acknowledgments. The authors wish to thank Dr. S. E. Haggerty, B. Wayatt, and J. D. Pasteris for reviewing the manuscript. N. Z. Boctor is grateful to Drs. F. R. Boyd, H. O. A. Meyer, and H. S. Yoder for providing funds to attend the Second International Kimberlite Conference.

References

Albee, A. L., and L. Ray, Correction factors for electron probe microanalysis of silicates, oxides, carbonates, phosphates, and sulfates, Anal. Chem., 42, 1408-1414, 1970.

Bence, A. E., and A. L. Albee, Empirical correction factors for the electron microanalysis of silicates and oxides, J. Geol., 76, 382-403, 1968.

Boyd, F. R., and P. H. Nixon, Origin of the ilmenite-silicate nodules in kimberlite from Lesotho and South Africa, in Lesotho Kimberlite, edited by P. H. Nixon, pp. 254-268, Lesotho National Development Corporation, Maseru, Lesotho, 1973.

Carmichael, I. S. E., The mineralogy and petrology of the volcanic rocks from Leucite Hills, Wyoming, Contrib. Mineral. Petrol., 15, 24-66, 1967.

Colby, J. W., Magic IV - A computer program for quantitative electron microprobe analysis, Bell Telephone Laboratories, Inc., Allentown, Pennsylvania, 1971.

Danchin, R. V., and F. D'Orey, Chromium spinel exsolution in ilmenite from the Premier Mine Transv., South Africa, Contrib. Mineral. Petrol., 35, 43-49, 1972.

Danchin, R. V., J. Ferguson, J. R. McIver, and P. H. Nixon, The composition of late stage kimberlite liquids as revealed by nucleated autoliths, Phys. Chem. Earth, 9, 235-245, 1975.

Dawson, J. B., and J. B. Hawthorne, Magmatic sedimentation and carbonatitic differentiation in kimberlite sills at Benfontein, South Africa, J. Geol. Soc. Lond., 129, 61-85, 1973.

Eggler, D. H., CO_2 as a volatile component of the mantle: The system Mg_2SiO_4-H_2O-CO_2, Phys. Chem. Earth, 9, 869-881, 1975.

Fesq, H. W., E. J. D. Kable, and J. J. Gurney, Aspects of the geochemistry of kimberlites from the Premier Mine and other selected South African occurrences with particular reference to the rare earth elements, Phys. Chem. Earth, 9, 687-705, 1975.

Finger, L. W., The uncertainty in the calculated ferric iron content of a microprobe analysis, Carnegie Inst. Yearbook, 71, 600-603, 1972.

Friel, J. J., I. Harker, and G. C. Ulmer, Armalcolite stability as a function of pressure and oxygen fugacity, Geochim. et Cosmochim. Acta, 41, 403-410, 1977.

Grantham, D. R., and J. B. Allen, Kimberlites in Sierra Leone, Overseas Geol. Miner. Resour., 8, 5-25, 1960.

Haggerty, S. E., Compositional variation in lunar spinels, Nature, Phys. Sci., 233, 156-160, 1971.

Haggerty, S. E., Spinels of unique composition associated with ilmenite reaction mantles in the Liqhobong kimberlite pipe, Lesotho, in Lesotho Kimberlites, edited by P. H. Nixon, pp. 149-158, Lesotho National Development Corporation, Maseru, Lesotho, 1973.

Haggerty, S. E., The chemistry and genesis of opaque minerals in kimberlites, Phys. Chem. Earth, 9, 295-307, 1975.

Irvine, T. N., Chromian spinel as a petrogenic indicator. Part 1. Theory, Can. J. Earth Sci., 2, 648-672, 1965.

Kable, E. J. D., H. W. Fesq, and J. J. Gurney, The significance of the inter-element relationships of some minor and trace elements in South African kimberlites, Phys. Chem. Earth, 9, 709-734, 1975.

Kesson, S. E., and D. H. Lindsley, The effect of Al^{3+}, Cr^{3+}, and Ti^{3+} on the stability of armalcolite, Proc. Lunar Sci. Conf., 6, 911-920, 1975.

Kridelbaugh, S. J., R. Hobbit, K. Kellogg, and E. Larson, Petrologic and paleomagnetic implications of the Green Mountain diatreme, Geol. Soc. Am., Program with Abstr., 4, 386, 1972.

Kridelbaugh, S. J. and H. O. A. Meyer, Kimberlite from Green Mountain, Colorado, Eos, 84, 1224, 1973.

Lindsley, D. H., S. E. Kesson, M. J. Hartzman, and M. K. Cushman, The stability of armalcolite: Experimental studies in the system MgO-Fe-Ti-O, Proc. Lunar Sci. Conf., 5, 521-534, 1974.

Loubet, M., M. Bernat, M. Javoy, and C. J. Allegre, Rare earth contents in carbonatites, Earth Planet. Sci. Lett., 14, 226-232, 1972.

Meyer, H. O. A., The kimberlites of the continental United States: A review, J. Geol., 84, 377-404, 1976.

Meyer, H. O. A., and F. R. Boyd, Composition and origin of crystalline inclusions in natural diamonds, Geochim. et Cosmochim Acta, 36, 1255-1273, 1972.

Meyer, H. O. A., and S. J. Kridelbaugh, Green Mountain kimberlite, Colorado: Mineralogy and petrology, Extended Abstr., Second International Kimberlite Conference, 1977.

Mitchell, R. H., Composition of perovskite in kimberlite, Am. Mineral., 57, 1748-1753, 1972.

Mitchell, R. H., Magnesian ilmenite and its role in kimberlite petrogenesis, J. Geol., 81, 301-311, 1973.

Mitchell, R. H., and D. B. Clarke, Oxide and sulfide mineralogy of the Peuyuk kimberlite, Somerset Island, N. W. T., Canada, Contrib. Mineral. Petrol., 56, 157-172, 1976.

Muan, A., J. Hauck, and T. Lofall, Equilibrium studies with a bearing on lunar rocks, Proc. Lunar Sci. Conf., 3, 185-196, 1972.

Ramdohr, P., A wide spread mineral association, connected with serpentinization, N. Jahrb. Min., 107, 241-265, 1967.

Smith, A. L., Sphene, perovskite and coexisting Fe-Ti oxide minerals, Am. Mineral., 55, 264-269, 1970.

ZIRCON-OXIDE REACTIONS IN DIAMOND-BEARING KIMBERLITES

Ellen Raber and Stephen E. Haggerty

Department of Geology, University of Massachusetts, Amherst, Massachusetts 01003

Abstract. In a petrographic and electron microprobe study of zircons ($ZrSiO_4$) intergrown with ilmenite ($FeTiO_3$) and/or rutile (TiO_2) from kimberlites in southern Africa we have established: (1) The compositions of ilmenites associated with zircons have a narrow range in MgO (8-10 wt%) and in Cr_2O_3 (0.02-0.85 wt%) contents which may be indicative of a characteristic P-T regime. (2) Subsolidus reactions, along the zircon-ilmenite interfaces, yield an exotic mineral assemblage consisting of zirconolite ($CaZrTi_2O_7$), Ti-rich baddeleyite ($[TiZr]O_2$), and diopside ($CaMgSi_2O_6$) in association with calcite ($CaCO_3$). (3) Ilmenite/rutile-zircon assemblages consist of zirconolite + baddeleyite + diopside at ilmenite-zircon interfaces, and baddeleyite + sphene ($CaTiSiO_5$) at rutile-zircon interfaces; both assemblages are in association with calcite. (4) Rutile-zircon assemblages consist only of Zr-armalcolite ($[FeMg]Ti_2O_5$) and ilmenite when not in association with calcite. We propose that assemblages along calcite-associated interfaces are the result of reactions due to the availability of a *carbonatitic* fluid which induced an intercrystalline reaction between zircon and either ilmenite or rutile. This is the first reported occurrence of terrestrial zirconium-bearing armalcolite. Based on phase equilibria studies the conditions inferred for the coexisting mineral assemblages are T = 1450-1550°C, P = 8-12 Kb, and $fO_2 < 10^{-12}$ atms. The Ti/Zr ratios of zirconolites are evaluated as a possible geothermometer, but it is recognized that the application to kimberlites is limited because of the indeterminate effects of pressure.

Introduction

Zircons ($ZrSiO_4$) and ilmenites ($FeTiO_3$) in kimberlites have widely contrasting distributions: the former are as rare or rarer than diamonds, whereas the latter are characteristic constituents that are commonly in high modal abundances. Our working hypothesis is that zircons and diamonds may be genetically related and consequently those ilmenites which are commonly associated with zircons provide the best estimate of ilmenite compositions which are likely to form during diamond nucleation and growth.

Ilmenites are widely used as placer prospecting guides to kimberlites, because they have distinctively high MgO contents, low to intermediate Fe_2O_3 contents, and the presence of Cr_2O_3. However, to our knowledge no chemical criteria are available on distinguishing barren kimberlites from diamondiferous kimberlites based on associated mineralogy. Studies by Kresten et al. (1975) suggest that some properties of kimberlitic zircons may reflect the diamond grade of the host rock, but that has yet to be established with any degree of confidence.

A detailed reflection microscopy and electron-microprobe study was undertaken on the associations of zircons intergrown with either ilmenite and/or rutile from the Kimberley pipes, the Monastery mine, and the Mothae pipe, in southern Africa. The objectives of this study are as follows: (1) to determine the compositions of ilmenites associated with zircons; (2) to determine the differences between rutile-zircon (RUZ), zircon-ilmenite (ZIL), and zircon + rutile + ilmenite (Z-RIL) assemblages; (3) to characterize the reactions at the rutile-zircon and ilmenite-zircon interfaces in each of the three types of assemblages; and (4) to relate these interface reactions to pressure, temperature and kimberlite petrogenesis.

Results and Mineral Chemistry

Petrographic and electron microprobe analyses were undertaken on: (1) intergrown zircon-ilmenite (ZIL) assemblages from the Monastery and Mothae localities; (2) rutile-zircon (RUZ) assemblages from the Mothae pipe; and (3) rutile and ilmenite-zircon (Z-RIL) assemblages from Kimberley. Photomicrographs of these specimens are illustrated in Fig. 1.

Analytical data on rutiles and zircons in this study show that these approach stoichiometric TiO_2 and $ZrSiO_4$, respectively, with minor concentrations of other elements (Table 1). These data compare favorably with analyses by other investigators (e.g., Haggerty, 1975; Nixon et al., 1963; and Kresten et al., 1975).

Analyses of ilmenites associated with zircons (Table 1) are also in agreement with the ranges of kimberlitic ilmenite compositions that have been

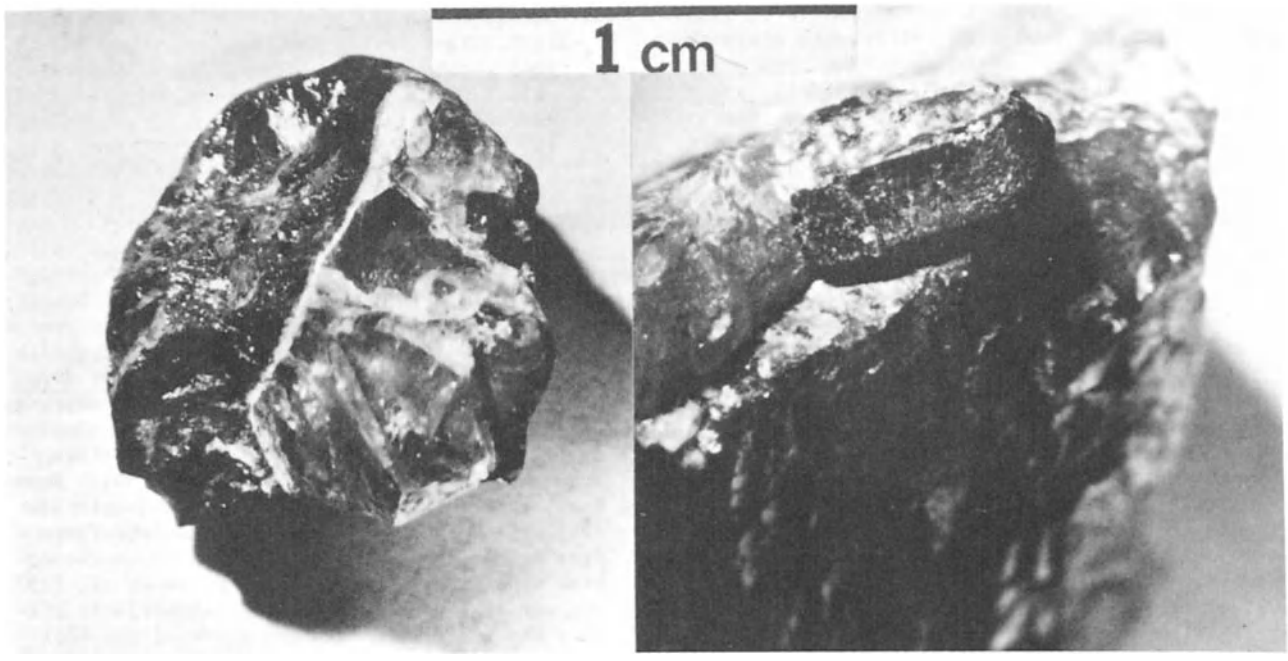

Fig. 1. Photomicrographs of an intergrown ilmenite (dark) - zircon (light glassy) assemblage with reaction interface from the Monastery Mine (left), and an intergrown rutile (dark) - zircon (light glassy) assemblage from the Mothae pipe, Lesotho (right).

determined by Haggerty (1975), Mitchell (1973), and Boyd and Nixon (1973) being distinctive in their high MgO contents, low to intermediate Fe_2O_3 contents and variable Cr_2O_3 concentrations.

In a previous study of over 200 kimberlitic ilmenites (Haggerty, 1975), a relatively smooth parabolic relationship was shown to exist between MgO and Cr_2O_3 contents reaching a minima at values of MgO between 6 and 10 wt%. This minima is characterized by a relatively small number of data points, which we now propose reflects those ilmenites which formed in association with zircons. This relationship is shown in Fig. 2 and it has been suggested (Haggerty, 1975) that it may be indicative of a pressure dependence. That high Cr_2O_3 contents are possible within the ilmenite structure is suggested by the presence of chromite lamellae in kimberlitic picroilmenites (e.g., Danchin and D'Orey, 1972; Haggerty, 1975) and by high pressure phase equilibria studies (Wyatt, 1978). These data contrast, furthermore, with equilibria at one atmosphere in which the solid-solubility of Cr_2O_3 in $FeTiO_3$ is shown to be <1 wt%. Trivalent substitutions of the form Cr^{3+}

TABLE 1. ELECTRON MICROPROBE ANALYSES OF KIMBERLITIC ZIRCONS AND ASSOCIATED ILMENITES.
(Average analyses of at least 10 points.)

OXIDES	ZIL Zircon (Monastery)	ZIL Zircon (Mothae)	Z-RIL Zircon (Kimberley)	ZIL Ilmenite (Monastery)	ZIL Ilmenite (Mothae)	Z-RIL Ilmenite (Kimberley)
MgO	0.00	0.00	0.02	9.88	8.06	7.32
Al_2O_3	0.00	0.02	0.12	0.17	0.16	0.02
ZrO_2	72.40	71.14	67.96	0.26	0.22	0.24
SiO_2	27.10	27.73	30.47	0.00	0.00	0.02
CaO	0.00	0.01	0.00	0.03	0.00	0.01
TiO_2	0.00	0.01	0.07	46.64	44.87	51.99
Cr_2O_3	0.03	0.02	0.06	0.85	0.71	0.04
MnO	0.02	0.03	0.08	0.29	0.30	0.20
FeO	0.01	0.12	0.00	24.06	25.79	33.62
Fe_2O_3	-	-	-	17.16	19.53	5.82
TOTAL	99.56	99.08	98.78	99.34	99.64	99.26

ZIL are zircon-ilmenite associations; Z-RIL are zircon-rutile and ilmenite associations.

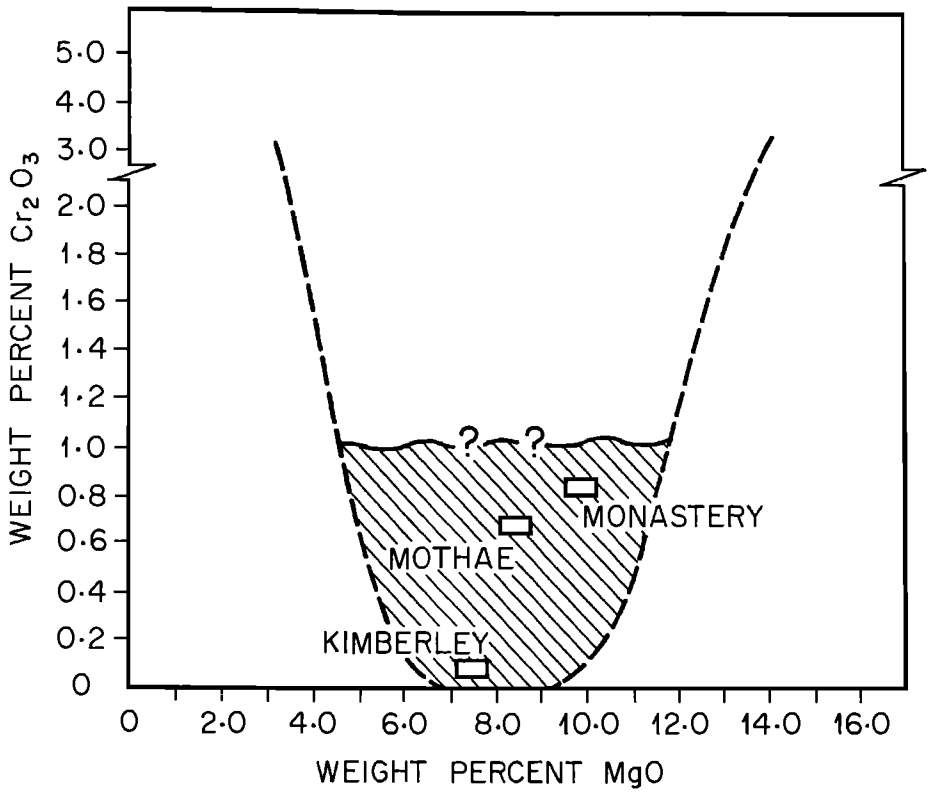

Fig. 2. Cr_2O_3 *versus* MgO for kimberlitic ilmenites from Lesotho and West Africa (Haggerty, 1975). The approximated parabolic curve is drawn through data maxima. The open rectangular symbols are for those ilmenites which formed in association with zircons in diamondiferous kimberlites. The shaded region represents an ilmenite compositional regime which is suitable for zircon formation and is possibly also within the diamond stability field.

$\rightarrow Fe^{3+}$ or $2Cr^{3+} \rightarrow Fe^{2+} + Ti^{4+}$ are invoked but whether simple ionic or diadochic exchange is preferred at high pressures has not been determined. The compositions of ilmenites associated with zircons from diamond-bearing kimberlites (Monastery, Mothae and Kimberley) have a narrow range in MgO (8-10 wt%) and in Cr_2O_3 (0.02-0.85 wt%) contents. These ilmenite compositions may, therefore, be indicative of a characteristic P-T regime which is not only suitable for zircon formation, but possibly also for diamond.

Analyses were concentrated on the interface areas in which an earlier reflection microscopy study had disclosed the presence of other microcrystalline phases. Zircon-ilmenite interfaces in ZIL samples contain an exotic mineral assemblage consisting of zirconolite ($CaZrTi_2O_7$), Ti-rich baddeleyite ($[TiZr]O_2$), and diopside ($CaMgSi_2O_6$); this assemblage is contrasted with RUZ intergrowths which have Ti-rich baddeleyite and sphene ($CaTiSiO_5$) at rutile-zircon interfaces. RIL assemblages that are not associated with calcite consist of zirconium-bearing armalcolite ($[FeMg]Ti_2O_5$) and ilmenite ($FeTiO_3$) but we note that this may not be a general characteristic because it was observed in only one sample from the Mothae pipe, Lesotho. Analyses of these assemblages are summarized in a simplified tetrahedron showing the relative positions of each of the identified phases in Fig. 3.

Baddeleyite, zirconolite and armalcolite are extremely rare in terrestrial, lunar and meteoritic associations and, in fact, their common association has been identified in only one lunar highland anorthosite (Haggerty, 1973). Because of the rarity of these minerals, little geochemical work has been undertaken on their genetic associations. In particular, there has been no attempt to establish the equilibrium reaction for the formation of zirconolite in nature. It is therefore, our intent to discuss, in detail, the results of our analyses for the associated interface assemblages in an attempt to better understand the physical parameters necessary for their formation.

Baddeleyite (ZrO_2)

Baddeleyite was identified along interfaces in all of the kimberlitic assemblages associated with calcite (ZIL and Z-RIL) as illustrated in Fig. 4. Mineral grains are mostly anhedral, al-

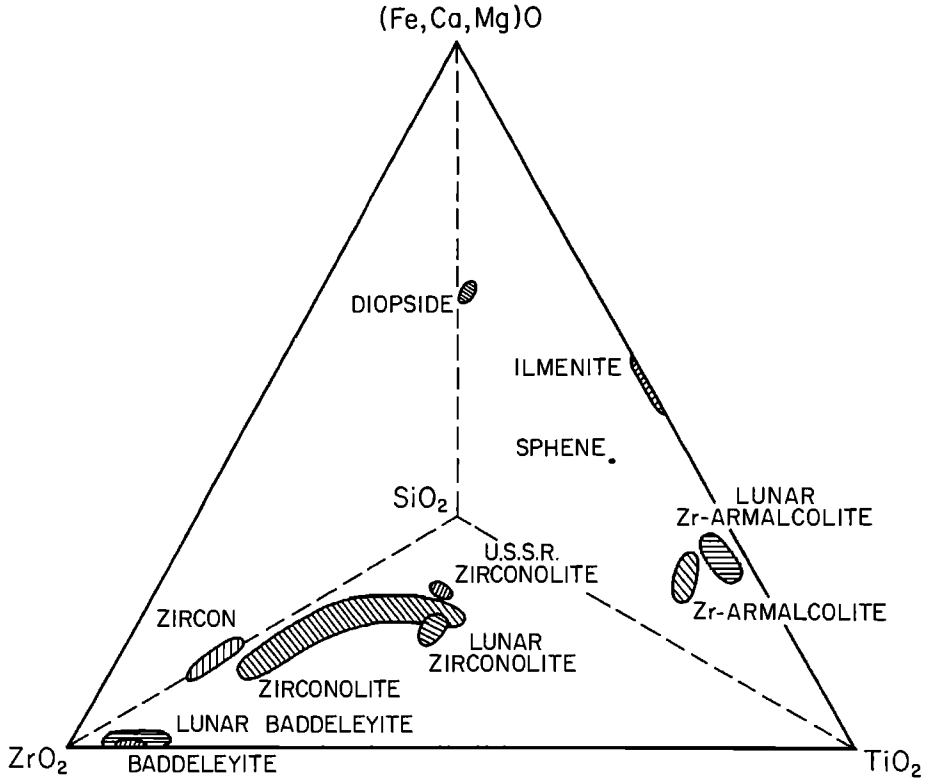

Fig. 3. A compositional tetrahedron showing the relative positions of mean analyses for kimberlitic interface assemblages. Comparative analyses are given for zirconolite, baddeleyite and Zr-armalcolite from other terrestrial and lunar examples. Sphene is plotted as stoichiometric $CaTiSiO_5$. All analyses are in oxide wt%.

though baddeleyite in the Monastery sample tended to show distinct euhedral crystals. A comparison of kimberlitic interface baddeleyites with lunar baddeleyites, also in association with zirconolite (Table 2), show that there are both minor differences and similarities in oxide concentrations. The outstanding feature is that both types are titaniferous (3.68-7.93 wt% TiO_2), a property which is not displayed by primary baddeleyite in some terrestrial gabbros (Keil and Fricker, 1974); however, this may simply be a reflection of bulk chemistry which averages ~0.5 wt% TiO_2 in the gabbros reported.

Zirconolite ($CaZrTi_2O_7$)

Zirconolite is identified at the three kimberlite localities in which zircons and ilmenites are associated with calcite (Fig. 4). These are the first reported occurrences of zirconolite in kimberlites. Although lunar occurrences have been reported, only four other terrestrial localities are presently known: zirconolite from a decomposed magnetite pyroxenite in Sao Paulo, Brazil (Hassak, 1894); varieties of zirconolite from Ceylon (Blake and Smith, 1913); and zirconolite from the amphibolized pyroxenites of the Afrikanda (Kola Peninsula) and Arbarastkh (Aldan) massifs in the U.S.S.R. (Wark et al., 1973).

Electron microprobe analyses (Table 3) show that the ZrO_2 contents of the three kimberlitic zirconolites vary between 41.9 and 71.3 wt%; those from the Arbarastkh and the Afrikanda massif vary between 33.0 and 33.5 wt%; and the lunar examples have ZrO_2 contents between 30.06 and 41.25 wt%. For TiO_2, the variations from these localities are 16.70-40.48 wt%, 30.43-31.57 wt%, and 25.48-35.79 wt%, respectively. It should be noted that the kimberlitic examples have ZrO_2 contents substantially higher than those from other sources, whereas the TiO_2 content is both higher and lower. Although we have yet to undertake a detailed REE study of the kimberlitic zirconolites, preliminary data suggest that the REE abundances are lower than the U.S.S.R. and the lunar examples which range from 3.48 wt% to 17.52 wt%. The divalent cations are relatively constant for all zirconolites, and these are in the range 14-18 wt%.

Structural formulae and the Ti/Zr ratios are of particular interest because phase-equilibria studies (Wark et al., 1973) indicate the possibility that this ratio may be temperature sensitive. Experimental data yield Ti/Zr at 1500°C = 1.30, Ti/Zr at 1450°C = 1.53, and Ti/Zr at 1300°C = 2.51.

The relationship of Ti/Zr to temperature is linear as illustrated in Fig. 5. From this we estimate T = 1450-1525°C for lunar zirconolites, and T = 1475°C for the U.S.S.R. zirconolites. The formation temperatures for the Monastery, Kimberley and Mothae kimberlite localities are 1430°C, 1470°C and 1640°C, respectively.

Armalcolite ($[FeMg]Ti_2O_5$)

The Mothae kimberlite locality is the second terrestrial occurrence of armalcolite (Fig. 4). The first occurrence (Haggerty, 1975) from DuToitspan, is in association with rutile and MgO-rich ilmenite. Zirconium-bearing armalcolite has only been recognized in lunar samples from the Apollo 15 and 16 sites (Haggerty, 1973), and, hence, the Mothae RUZ sample is the first reported terrestrial occurrence.

Electron microprobe analyses (Table 2) show that the Mothae zirconium armalcolites are distinctive in that they contain Ba (2.2-2.4 wt% BaO), Sr (1.4-1.8 wt% SrO), Zn (~0.4 wt% ZnO) and K (~0.5 wt% K_2O). Our identification of this mineral as a member of the armalcolite solid solution series is based on optical properties (color, reflectivity, anisotropy) and stoichiometry, with cation totals that range between 2.958-2.972 (theoretical = 3.0 cations) on the basis of 5 oxygen atoms. X-ray data on the mineral, however, have not been obtained and there is the likelyhood that this mineral is structurally related to the crichtonite, senaite, davidite, landauite, loveringite series ($AM_{21}O_{38}$) in which A is the dominant large cation and is respectively, Sr, Pb, REE, Na and Ca, and M are the smaller cations, Ti, Zr, Cr, Al, Fe, Mg and Mn (Gatehouse et al., 1978). It should be noted that members of this series have previously been identified in kimberlites in which either Ba (Haggerty, 1975) or K (Smyth et al., 1978) is the dominant large cation. In most other respects the Mothae zirconium mineral is compositionally similar to zirconium armalcolites in the lunar samples (Table 2); in particular, Zr and Ti contents are constant, with $ZrO_2 \simeq 6$ wt% and $TiO_2 \simeq 66$ wt%. There are, however, differences in CaO, Al_2O_3 and Cr_2O_3 contents, and the most notable is that of chromium which varies between 4.3-11.5 wt% Cr_2O_3 in lunar zirconium armalcolites, in contrast to the uniformly low concentrations (<0.5 wt% Cr_2O_3) that are present in the Mothae mineral. X-ray structural data are required to clarify this mineral's affinity to either armalcolite or crichtonite.

It is perhaps significant to note, furthermore, that all three of the ilmenite/rutile zircon assemblages from Kimberley and the Mothae sample

TABLE 2. COMPARATIVE TABLE OF ELECTRON MICROPROBE ANALYSES OF (KIMBERLITIC, GABBROIC AND LUNAR) BADDELEYITES, AND (KIMBERLITIC AND LUNAR) Zr-ARMALCOLITES. (Average analyses of at least 10 discrete grains)

	BADDELEYITE					Zr-ARMALCOLITE	
OXIDES	ZIL Monastery	ZIL Mothae	(1) Lunar Sample 61156,5	(1) Lunar Sample 15102,12	(2) Gabbroic Sample	(1) Lunar Sample 61156,5	RUZ Mothae
MgO	0.19	0.09	0.10	0.09	-	2.31	4.16
Al_2O_3	0.51	0.11	0.15	0.12	-	1.49	0.19
ZrO_2	93.22	90.63	87.25	93.49	97.80	6.01	6.71
SiO_2	0.00	0.00	0.21	0.29	0.08	0.23	0.00
CaO	0.09	0.65	0.53	0.12	-	3.40	1.61
TiO_2	3.68	6.10	7.93	2.94	0.56	66.52	66.08
Cr_2O_3	0.18	0.11	0.27	0.14	-	10.31	0.13
MnO	0.18	0.05	0.16	0.17	-	0.13	0.20
FeO	0.68	0.63	0.80	1.22	1.30	9.33	15.23
Y_2O_3	-	-	1.27	1.47	-	<0.05	0.01
Nb_2O_5	-	-	1.03	0.65	-	0.37	0.00
HfO_2	-	-	-	-	0.93	-	-
SrO	-	-	-	-	-	-	1.63
K_2O	-	-	-	-	-	-	0.52
BaO	-	-	-	-	-	-	2.37
NiO	-	-	-	-	-	-	0.07
ZnO	-	-	-	-	-	-	0.41
PbO	-	-	-	-	-	-	0.01
TOTAL	98.73	98.38	99.70	100.68	100.67	100.10	99.33

(1) Lunar Sample analyses from Haggerty (1973)
(2) Gabbroic analysis from Keil and Fricker (1974), Rock A 394 (Locality: Canadian Arctic Archipelago)
ZIL are zircon-ilmenite associations. RUZ is a rutile-zircon association.

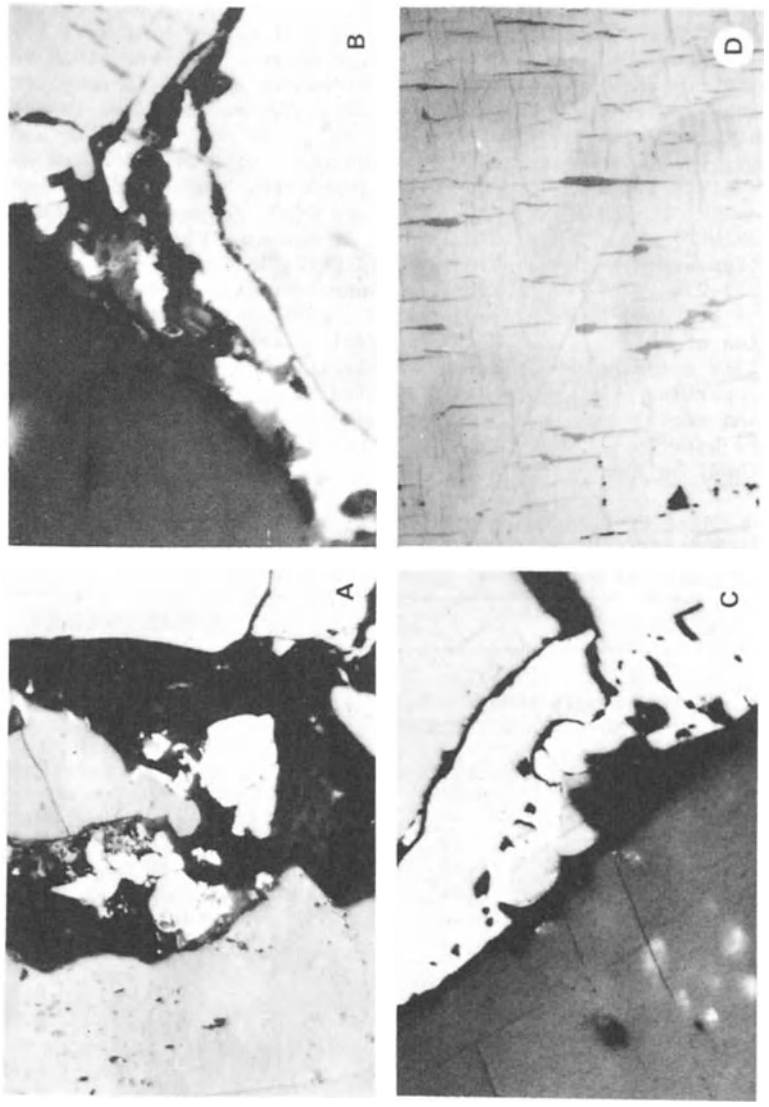

Fig. 4. Interface Assemblages: (A) Zircon (gray left) + ilmenite (right) with an associated reaction. This zone contains microcrystalline calcite and a multi-component assemblage (center area) of diopside (dark gray) + symplectic grains of zirconolite and baddeleyite (light gray). Monastery Mine. (B) Zircon (gray left) + rutile (right) in reaction contact along an interface zone which is produced by the introduction of microcrystalline calcite to yield baddeleyite (light anhedral crystals) + sphene (gray anhedral crystals and stringers). The dark gray lamellae within rutile are oriented ilmenite. Kimberley Pool. (C) Where no calcite is present, zircon (gray left) and rutile (right) are found in association with primary Zr-armalcolite (light gray); the armalcolite appears as oblate crystals in the rutile along the reaction interface. Mothae. (D) An example of sigmoidal ilmenite lenses in a rutile host which is due possibly to the breakdown of primary armalcolite. Kimberley Pool. Field of view = 0.340 mm. Oil immersion and reflected light.

contain oriented sigmoidal lenses of ilmenite (7-9 wt% MgO) in the rutile host. Although no armalcolite is present in those from Kimberley, the suggestion has been made that the assemblage, ilmenite + rutile may result from the decomposition of pre-existing primary armalcolite (Haggerty, 1975). We propose, therefore, that the Mothae sample may originally have had two generations of armalcolite, a Zr-free variety and the Zr-variety, and that it was only the former that decomposed to rutile + ilmenite. Whether all of the rutile + ilmenite assemblages examined in this study are the result of primary armalcolite breakdown cannot be unequivocally demonstrated.

Reaction Chemistry

In addition to the minerals already discussed, diopside, sphene and calcite are also present in the interface reaction zones. To explain these associated mineral assemblages the following mechanisms are proposed: The exotic mineral assemblages occur only in those samples that include calcite along the mineral interfaces and because CaO is a major component of the interface assemblages, we suggest that the intercrystalline reaction was triggered by a *carbonatitic* fluid. CaO is the only component necessary for the formation of these minerals because Zr, Si, Fe, Mg and Ti are already present in zircon and ilmenite. Neither the precise timing of this reaction nor the stage of kimberlite formation can yet be established; however, we consider that it is a secondary reaction which may have developed during fluidization or emplacement. The reaction believed to have occurred between the ilmenite-zircon interfaces, to account for zirconolite, baddeleyite and diopside in the calcite-bearing kimberlites from all three localities is as follows:

$$2(FeMg)TiO_3 + 4ZrSiO_4 + 3CaCO_3 \rightarrow$$

Ilmenite + Zircon + Calcite $\rightarrow$

$$3ZrO_2 + CaZrTi_2O_7 \qquad (1)$$

Baddeleyite + Zirconolite

$$+ 2Ca(FeMg)Si_2O_6 + 3CO_2\uparrow$$

+ Diopside + Carbon Dioxide

Our reflected light microscopy study shows clear evidence of successive stages of alteration (Fig. 4) in the form of symplectitic textures of diopside-baddeleyite-zirconolite, zircon-baddeleyite, and baddeleyite-zirconolite, so that the reaction along the interface may not be a single stage event as is suggested by equation (1).

In the Z-RIL samples from the Kimberley locality, the interface assemblages between rutile and zircon grains consist of baddeleyite and sphene. Reaction (2) between rutile and zircon could ac-

TABLE 3. ELECTRON MICROPROBE ANALYSES OF ZIRCONOLITES.

Locality	KIMBERLITIC			U. S. S. R.		LUNAR				
	1	2	3	4	5	6	7	8	9	10
Sample	Monastery	Mothae	Kimberley	Arba-rastkh	Afrikanda	15102,12	14257,3	10046,20	10047,20	14305,77
MgO	1.20	0.31	0.49	0.14	0.10	0.89	0.69	0.65	0.01	1.15
Al_2O_3	0.13	0.04	0.23	0.10	0.09	0.80	1.36	1.07	0.48	0.67
ZrO_2	51.12	71.27	41.91	33.54	32.96	41.25	40.40	37.21	33.60	30.06
SiO_2	0.00	0.00	0.00	0.00	0.00	0.28	0.42	0.00	-	0.26
CaO	10.11	9.09	11.10	12.61	11.44	7.32	8.80	7.31	2.63	6.15
TiO_2	29.16	16.70	40.48	31.57	30.43	35.79	34.40	32.61	25.48	29.62
Cr_2O_3	1.10	0.06	0.09	0.00	0.00	0.68	0.54	0.56	0.07	0.50
MnO	.11	0.15	0.11	0.00	0.00	0.15	0.00	0.11	-	-
FeO	6.94	2.38	5.15	2.30	2.84	5.63	6.10	5.95	9.06	4.23
Fe_2O_3	0.00	0.00	0.00	2.78	3.15	-	0.00	-	-	-
Y_2O_3	-	-	-	0.28	0.31	4.21	3.60	3.06	7.80	7.70
Nb_2O_5	-	-	-	4.85	4.71	0.72	1.00	1.85	2.75	4.34
Trace El.	-	-	-	8.73	10.78	-	3.48	8.74	17.52	14.58
TOTAL	99.87	100.00	99.56	97.42	96.81	97.72	100.79	99.12	99.40	99.26

Analyses: 1-3: South African kimberlites (average analyses of at least 10 discrete grains)
4: Arbarastkh massif, Aldan, U.S.S.R. (Wark et al., 1973)
5: Afrikanda massif, Kola Peninsular, U.S.S.R. (Wark et al., 1973)
6: (Haggerty, 1973)
7: (Bushe et al., 1972)
8-10: (Wark et al., 1973)

TABLE 4. STRUCTURAL FORMULAE OF ZIRCONOLITE CALCULATED ON THE BASIS OF 7 OXYGENS.

Locality	KIMBERLITIC			U. S. S. R.		LUNAR				
	1	2	3	4	5	6	7	8	9	10
Sample	Monastery	Mothae	Kimberley	Arbarastkh	Afrikanda	15102,12	14257,3	10046,20	10047,20	14305,77
Mg	0.1101	0.0302	0.0430	0.001	0.013	0.070	0.062	0.600	0.000	0.113
Al	0.0096	0.0031	0.0162	0.008	0.007	0.051	0.096	0.780	0.040	0.52
Zr	1.5330	2.2718	1.1992	1.047	1.043	1.065	1.185	1.119	1.140	0.969
Si	-	-	-	-	-	0.016	0.025	0.108	-	0.017
Ca	0.6660	0.6366	0.6976	0.866	0.795	0.413	0.567	0.483	0.196	0.435
Ti	2.6980	0.8207	1.7860	1.520	1.486	1.425	1.560	1.512	1.333	1.473
Cr	0.0532	0.0031	0.0042	-	-	0.025	0.026	0.27	0.004	0.026
Mn	0.0059	0.0082	0.0056	-	-	0.006	-	0.006	-	-
Fe^{2+}	0.3570	0.1210	0.2527	0.123	0.154	0.248	0.307	0.307	0.527	0.234
Fe^{3+}	-	-	-	0.134	0.154	-	-	-	-	-
Y	-	-	-	0.009	0.011	0.121	0.115	0.100	0.289	0.271
Nb	-	-	-	0.139	0.138	0.019	0.027	0.052	0.086	0.130
Trace El.	-	-	-	0.173	0.230	-	0.457	0.247	0.401	0.287
Ti/Zr	1.760	0.361	1.489	1.45	1.42	1.34	1.32	1.35	1.17	1.52

Analyses: 1-3: South African kimberlites (average analyses of at least 10 discrete grains)
4: Arbarastkh massif, Aldan, U.S.S.R. (Wark et al., 1973)
5: Afrikanda massif, Kola Peninsular, U.S.S.R. (Wark et al., 1973)
6: (Haggerty, 1973)
7: (Bushe et al., 1972)
8-10: (Wark et al., 1973)

count for this mineral assemblage as follows:

$$TiO_2 + ZrSiO_4 + CaCO_3 \rightarrow$$

Rutile + Zircon + Calcite →

$$CaTiSiO_5 + ZrO_2 + CO_2\uparrow \quad (2)$$

Sphene + Baddeleyite + Carbon Dioxide

Therefore, with the introduction of $CaCO_3$ (as a fluid phase) along mineral grain boundary interfaces, reaction (1) would take place when only ilmenite and zircon are present (Monastery and Mothae samples), and reaction (2) would occur if only rutile and zircon were present. Where both rutile and ilmenite are present (possibly due to armalcolite decomposition), we suggest that reactions (1) and (2) occur simultaneously along their respective oxide interfaces. There is good textural evidence for the existence of reaction (1), but it is perhaps significant that we have not yet observed the association of sphene and zirconolite or either of these minerals in association with perovskite. Their associations are most directly related to a_{SiO_2} although P-T and fO_2 may also be effective parameters in governing the respective partitioning coefficients of Ca, Zr, Ti and Si among minerals in the assemblage. No thermodynamic data are available on zirconolite and the rarity of the mineral in nature makes any further assessment on the likelihood of these reactions extremely difficult.

Discussion

The association of baddeleyite with zircon in these samples allows for an evaluation of the P-T conditions necessary for the two phases to coexist. From the experimental data and proposed phase diagram for the system ZrO_2-SiO_2 at 1 atm (Butterman and Foster, 1967), we can establish that zircon is stable in association with monoclinic baddeleyite at T < 1170°C and in association with tetragonal baddeleyite at T < 1676°C. At temperatures greater than 1676°C zircon decomposes to baddeleyite + cristobalite ($ZrSiO_4 \rightarrow ZrO_2 + SiO_2$). This reaction has been reported in high temperature impactite glasses where baddeleyite and cristobalite coexist as metastable phases (El Goresy, 1965; Kleinman, 1969).

Experimental data are not available on the effect of pressure on the reaction zircon → baddeleyite + cristobalite, but impactite studies show that the P-T curve of the reaction does have a positive slope (estimated at 5°C/kb) and that cristobalite is stable at T ≅ 1600°C and P ≅ 7 kb. Available thermodynamic data show that zircon and baddeleyite can coexist at high pressures (Nicholls et al., 1971) and in fact may coexist in the diamond stability field at T = 1327°C and P = 55.7 kb. Further calculations are necessary to determine a more extended range of values for this three phase coexisting assemblage.

Evidence for the development of a possible baddeleyite-zirconolite solid solution series is apparent from the experiments by Coughanour et

al. (1955) on the system $CaO-TiO_2-ZrO_2$ (Fig. 6) at 1 atm and T = 1450-1550°C. Our analyses clearly show that any reaction taking place to form these zirconium minerals in kimberlites must have occurred below the solvus, because both discrete grains of zirconolite and baddeleyite, as well as symplectitic grains, were found to exist.

Although our estimated formation temperatures, based on the Ti/Zr zirconolite geothermometer, are exceptionally high, 1430°C, 1470°C and 1640°C for the Monastery, Kimberley and Mothae localities, respectively, an evaluation can be made for the reality of these temperatures from experimental data in the system $CaO-ZrO_2-TiO_2$ at 1 atm and T = 1450-1550°C (Coughanour et al., 1955). Fig. 6 shows the phase relationships of the system and the positions of the zirconolites which are associated with baddeleyite. Note that all of the samples, except Mothae, have estimated temperatures compatible with that of the experimental system and that all except the Mothae sample plot within the correct phase regicn where both baddeleyite and zirconolite coexist. The Mothae sample plots in the one phase titanian-baddeleyite$_{ss}$ field which supports the contention that the Ti/Zr ratio is indicative of a higher temperature of formation than that of the experimental phase diagram. Because the Mothae sample did not contain cristobalite, we assume that the temperature could not have been in excess of 1676°C (Butterman and Foster, 1967) because at this temperature zircon decomposes to baddeleyite + cristobalite. The possibility does exist, however, that the Ti/Zr zirconolite ratio may also be pressure sensitive.

Experimental studies (Lindsley et al., 1974; Friel et al., 1977) indicate that armalcolite is stable as a single phase at 1300°C and 10 kb. With increasing pressure, decomposition occurs and armalcolite breaks down to a more magnesium armalcolite plus Geik-Ilm$_{ss}$ plus rutile (dT/dP = 20° C/kb). At 14 kb and 1200°C this three phase assemblage is replaced by rutile plus Geik-Ilm$_{ss}$ in 1:1 proportions (dT/dP = 30° C/kb). These studies show that zirconium has the effect of decreasing armalcolite stability and decomposition occurs at 1-2 kb less than that of Zr-free armalcolite; with the addition of Mg, however, the stability of the end member $MgTi_2O_5$ is increased to at least 20 kb. Therefore, the interface Zr-armalcolite must clearly have formed at pressures <12 kb and if we attribute the sigmoidal lenses of ilmenite plus rutile to the decomposition of Zr-armalcolite, then the pressures estimated must also have been

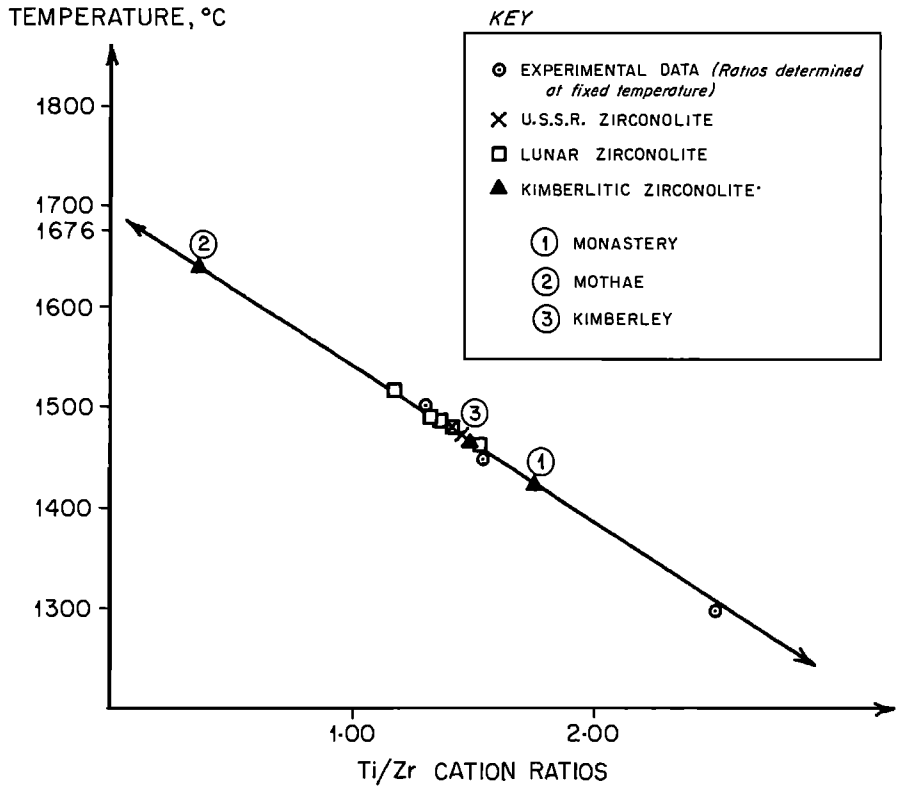

Fig. 5. Ti/Zr ratio *versus* temperature (T^0C) for experimentally synthesized zirconolites (Wark et al., 1973). Ratios for lunar, U.S.S.R. and kimberlitic zirconolites (from Table 3) are plotted on this linearly estimated trend.

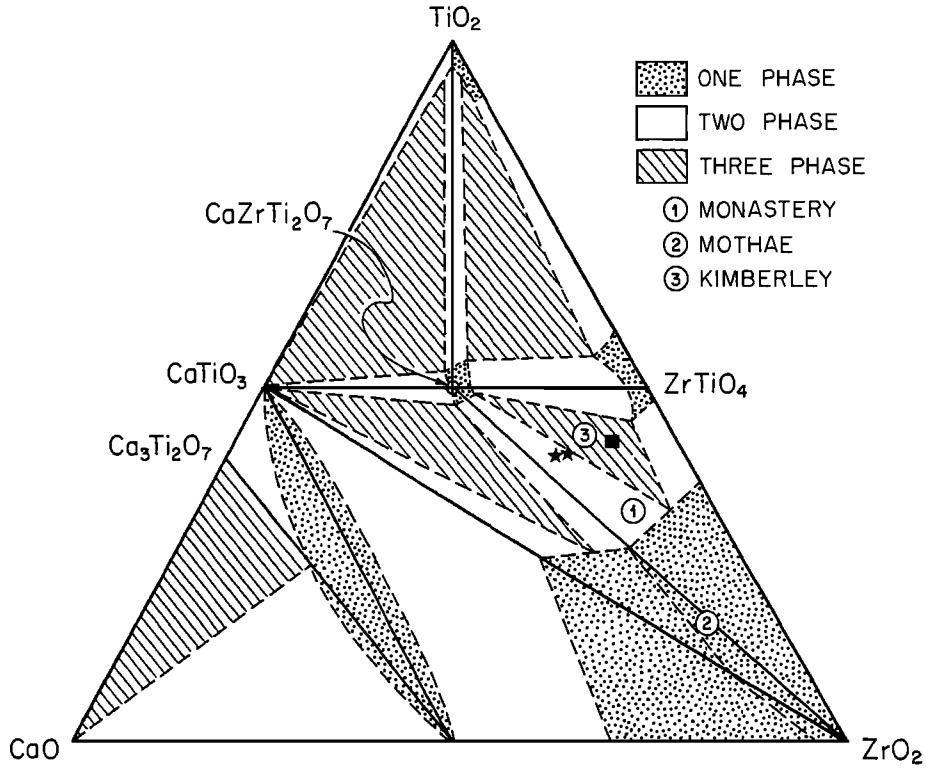

Fig. 6. Estimated trends of solid-solution development in the system $CaO-ZrO_2-TiO_2$ at T = 1450 - 1550°C and at 1 atm., (Coughanour et al., 1955). Baddeleyite with associated zirconolite analyses (from Table 3) from the kimberlitic samples (open circles, numbered 1-3), the U.S.S.R. samples (stars), and the lunar sample 66156,6 (full square) are plotted. The dashed line near the ZrO_2 apex separates the cubic ZrO_2 field on the left from the tetragonal field to the right.

>8 kb, and the range, therefore, is 8-12 kb.

Furthermore, experiments on the stability of armalcolite as a function of oxygen fugacity (Friel et al., 1977), show that only those samples prepared between $10^{-9.5}$ and $10^{-10.5}$ atm contain single-phase armalcolite, while those at $10^{-12.2}$ and $10^{-12.8}$ atm consisted of primary armalcolite and ilmenite. Because primary ilmenite is present, in addition to Zr-armalcolite, fO_2 must have been $<10^{-12.2}$ as well as at a pressure >8 kb and <12 kb, to account for all the coexisting phases. Although Zr-armalcolite has not as yet been identified in the other samples, we attribute this to a marginal sample population.

Summary and Conclusions

Zirconolite ($CaZrTi_2O_7$), armalcolite ([FeMg]-Ti_2O_5) and baddeleyite (ZrO_2) have been found to exist in kimberlitic intergrown RUZ, ZIL, and Z-RIL assemblages. This is the first reported occurrence of zirconolite in kimberlitic rocks and the Mothae locality is the second to contain armalcolite. Zirconolite and baddeleyite exist as a result of a secondary reaction, and because CaO is a major component of the interface assemblages, we suggest that the presence of a *carbonatitic* fluid phase is an essential constituent to promote intercrystalline reaction between zircon and ilmenite and/or rutile interfaces. Armalcolite was found in only one sample which was not associated with calcite along grain boundary interfaces and, therefore, is assumed to be a primary phase. It is also believed that those samples which contain both rutile and ilmenite are the result of primary Zr-armalcolite decomposition.

Physical constraints for this *carbonatitic* reaction can be made from an evaluation of the P-T conditions which are necessary for these minerals to coexist. This can be deduced from available experimental and thermodynamic data in which we note: (1) zircon is stable at T < 1676°C in association with tetragonal ZrO_2 (Baddeleyite) and at T < 1170°C in association with monoclinic ZrO_2; (2) impactite and phase-equilibria studies show that at temperatures >1676°C and P ≈ 7 kb, zircon reacts to form baddeleyite + cristobalite; (3) if the Ti/Zr ratios of zirconolites associated with baddeleyites are considered to be temperature dependent, those which are compatible with the experimental system $CaO-ZrO_2-TiO_2$ at 1 atm and T = 1450-1550°C plot in a correct phase region where

zirconolite + baddeleyite coexist. The Mothae assemblage, is a higher temperature (T = 1640°C), assemblage and plots incorrectly in the one phase titanian-baddeleyite$_{ss}$ field; (4) zircon and baddeleyite can coexist in the diamond stability field at T = 1327°C and P = 55.7 kb; and (5) Zr-Armalcolite + Rutile + Ilm$_{ss}$ (due to primary Zr-armalcolite decomposition) in association with primary ilmenite is stable at P < 12 kb and fO_2 < $10^{-12.2}$ atms.

Therefore, the formation of these minerals at rutile-zircon and ilmenite-zircon interfaces must have taken place at P < 12 kb with fO_2 < $10^{-12.2}$ atms (based on Zr-armalcolite decomposition and primary ilmenite association), and T = 1450-1550°C (based on the zirconolite geothermometer) in which tetragonal ZrO_2 should be present. We assume that T must be <1676°C because no cristobalite was observed in any of the samples. If monoclinic baddeleyite were present, inferring that T < 1170°C, it could imply that the Ti/Zr ratio in zirconolite must also be pressure sensitive.

In summary, we propose that the zircon-ilmenite and/or rutile assemblages may be useful tools in establishing initial P-T parameters and that perhaps zirconolite may be a definitive clue in determining the temporal relationships and the stages of carbonatitic immiscibility. A broader conclusion from this study is that the compositions of ilmenites associated with zircons are in a critical range of Mg and Cr which may well be constrained by a P-T relationship which is compatible with that of diamond stability.

Acknowledgments. We are especially grateful to Tony Erlank, Joe Boyd and Barry Hawthorne for providing us with zircon-ilmenite/rutile assemblages from various kimberlites. In addition, we would like to thank both Nabil Boctor and Richard Williams for their critical and most helpful comments in the review of this manuscript. This research was supported by the National Science Foundation (principal investigator S.E.H.) through grant number EAR 76-23787. Credit for skillful drafting is due to Marie Litterer.

References

Blake, G. S. and G. F. H. Smith, On varieties of zirkelite from Ceylon, Min. Mag., 16, 309-316, 1913.

Boyd, F. F. and P. H. Nixon, Origin of the ilmenite-silicate nodules in kimberlites from Lesotho and South Africa, In: Lesotho Kimberlites (editor P. H. Nixon), 254-268, 1973.

Bulakh, A. G., G. A. Hinskii, and A. A. Kukharenke, Zirkelite from deposits of the Kola Peninsula. Zapinski Vesesoyuz, Mineral. Obshchestua, 89, 261-273 (in Russian), 1960.

Busche, F. D., M. Prinz, K. Keil and G. Kurat, Lunar zirkelite: A uranium-bearing phase, Earth and Planet Sci. Lett., 14, 313-321, 1972.

Butterman, W. C. and W. R. Foster, Zircon stability and the ZrO_2 - SiO_2 phase diagram, 52, Am. Min., 52, 880-885, 1967.

Coughanour, L. W., R. S. Roth, S. Marzullo, and F. E. Sennett, Solid-state reactions and dielectric properties in the systems magnesia-zirconia-titania and lime-zirconia-titania, Jour. Research Nat. Bur. Stds., 54, 191-199, 1955.

Danchin, R. V. and F. D'Orey, Chromium spinel exsolution in ilmenite from the Premier Mine, Transvaal, South Africa, Contr. Min. Pet., 35, 43-49, 1972.

El Goresy, A., Baddeleyite and its significance in impact glasses, Jour. Geophys. Res., 70, 3453-3456, 1965.

Friel, J. J., I. Harker, and G. C. Ulmer, Armalcolite stability as a function of pressure and oxygen fugacity, Geochim. Cosmochim. Acta, 41, 403-411, 1977.

Gatehouse, B. M., I. E. Grey, I. H. Campbell, and P. Kelley, The crystal structure of loveringite--a new member of the crichtonite group, Amer. Min., 63, 28-36, 1978.

Haggerty, S. E., Armacolite and genetically associated opaque minerals in the lunar samples, Geochim. Cosmochim. Acta Suppl., 4, 777-797, 1973.

Hussak, E., Über den baddeleyit (syn. Brazilit) von der eisenmine Josupiranganis, Sao Paulo. Ischerm. Mineral. Petrogr. Mitt., 14, 395-414, 1894.

Keil, K. and P. E. Fricker, Baddeleyite (ZrO_2) in gabbroic rocks from Axel Heilberg Island, Canadian Arctic Archipelago. Am. Min., 59, 249-253, 1974.

Kleinmann, B., The breakdown of zircon observed in the Libyan desert glass as evidence of its impact origin, Earth and Planet Sci. Lett., 5, 497-501, 1969.

Kresten, P., P. Fels, and G. Berggen, Kimberlitic zircons--a possible aid in prospecting for kimberlite, Mineral. Deposita, 10, 47-56, 1975.

Lindsley, D.H., S. E. Kesson, M. J. Hartzman, and M. K. Cushman, The stability of armalcolite: experimental studies in the system: MgO-Fe-Ti-O. Proc. Fifth Lunar Sci. Conf., Geochim. Cosmochim. Acta, Suppl., 5, 521-534, 1974.

McTaggart, G. D. and A. I. Andrews, Immiscibility area in the system TiO_2-ZrO_2-SiO_2, Journal of the Amer. Ceram. Soc., 40, 167-170, 1957.

Mitchell, R. H., Magnesium ilmenite and its role in kimberlite petrogenesis, J. Geol., 81, 301-311, 1973.

Muan, A., J. Hauck, and T. Lofall, Equilibrium studies with a bearing on lunar rocks, Proc. Third Lunar Sci. Conf. Suppl. 3, Geochim. Cosmochim. Acta, 1, 185-96, 1972.

Nicholls, J., I. S. E. Carmichael, and J. C. Stormer, Jr., Silica activity and P total in igneous rocks, Contr. Min. and Pet., 33, 1-20, 1971.

Nixon, P. H., O. Von Knorring and J. M. Rooke, Kimberlites and associated inclusions of

Basutoland: A mineralogical and geochemical study, Amer. Min., 48, 1090-132, 1963.
Smyth, J. R., A. J. Erlank, and R. S. Rickard, A new Ba-Sr-Cr-Fe titanate mineral from a kimberlite nodule, (abstract), E. O. S. Amer. Geophys. Union, 59, 394, 1978.
Wark, D.A., A. F. Reid, J. F. Lovering, and A. El Goresy, Zirconolite (versus zirkelite) in lunar rocks, Abs. Proc. IV Lunar Sci. Conf., Houston, 764-766, 1973.
Wyatt, B. A., Phase relationships in the system picroilmenite-clinopyroxene - Cr_2O_3 (this volume), 1978.

K, Rb AND Ba IN MICAS FROM KIMBERLITE AND PERIDOTITIC XENOLITHS, AND IMPLICATIONS FOR ORIGIN OF BASALTIC ROCKS.

J. V. Smith and R. L. Hervig

Department of the Geophysical Sciences,
The University of Chicago, Chicago, Illinois 60637

D. Ackermand

Mineralogisch-Petrographisches Institut der Universität
Kiel, W. Germany

J. B. Dawson

Department of Geology, University of St. Andrews, Scotland

Abstract. Electron microprobe analyses of high sensitivity (~40ppmw, 2σ) of micas gave ranges and means: primary texture in peridotite xenolith Rb_2O 160-520(312) BaO 320-7000(1,725); secondary texture in peridotite xenolith <50-600(340), 330-7200(2,170); MARID xenoliths 470-700(580), 340-800(420); megacryst in kimberlite 290-1060 (760), 130-970(380); rare type I groundmass xenocryst in kimberlite 240-630(470), 1,030-4,300 (2,670); abundant type II groundmass 90-820(420), 470-5,800(2,620); clinopyroxene-rich suite 340-900 (650), 90-480(280).

The negative correlation between K/Rb and K/Ba might result from mica having higher K/Rb and lower K/Ba than coexisting liquid, as implied by comparing means for the MARID and megacryst suites with those for type II groundmass micas. The negative correlation for both primary and secondary peridotite micas may result from partial melting in the mantle, or perhaps from mica-clinopyroxene exchange reaction.

A model composition for the bulk Earth (based on same K/Rb as C1 meteorite, and one-sixth K/Ba) falls in the range for peridotite micas. Most volcanic rocks fall on a single positive trend between K/Rb and K/Ba, which apparently poses a problem for differentiation models based just on mica-liquid partitioning. Most continental rocks have K/Rb (~300) and K/Ba (30) which lie inside the range for peridotite micas and close to the model values for the bulk Earth. Tholeiite and alkali basalt from oceanic islands have higher K/Rb(430) and most mid-ocean ridge basalts have much higher K/Rb(~1,100). Whereas most continental rocks could obtain their K,Rb and Ba simply from total extraction of phlogopite during partial melting of peridotite, rocks with high K/Rb could not. Data for amphibole and clinopyroxene do not allow simple models for total extraction of K,Rb and Ba. Complex models involving partial extraction, combinations of minerals, and crystal-liquid differentiation during magma ascent may be needed. Island-arc volcanic rocks give three major groups, of which the calc-alkaline association falls in the range of peridotitic micas whereas the tholeiitic association has higher K/Rb (~900).

To explain rocks with low K/Rb and K/Ba, it may be necessary to consider relationships with carbonatitic rocks and inclusions in diamond which have low ratios, especially the latter. Type I groundmass micas in kimberlite have K/Rb and K/Ba near to those for micas from the Oka carbonatite.

Introduction

Major and minor elements in individual minerals of xenoliths from the upper mantle may provide controls for models on (a) bulk composition of the upper mantle, and (b) crystal-liquid fractionation therein, especially w.r.t. partial-melting models for the origin of basalt. Bulk chemical analyses of mineral separates have great value, as exemplified by the trace element study of diamonds (Fesq et al., 1975a) and of clinopyroxenes (Shimizu, 1975). Ideally, however, techniques should allow spot analyses directly relatable to texture studied optically in a thin section. Particularly valuable for major and minor elements is the electron microprobe, and just coming over the horizon for trace elements and isotope ratios is the ion microprobe. Although analyses reliable to 25% are now being attained for certain trace elements in the range 0.01-10ppm (e.g. Steele et al., 1978), the technical problems of the ion microprobe are so great that it is desirable to lower the detection level of the elec-

tron microprobe as far as possible. Careful attention to the background, and use of high beam current and long counting time, allows detection of 20ppm (2σ) for many elements between Na and U.

Major carriers of alkalis in the upper mantle are amphibole (not stable below ~100km), phlogopite mica (stable down to ~150km, and perhaps deeper for low geothermal gradient) and diopside (stable to perhaps ~300km depth). Garnet (stable to perhaps ~500km depth) and perhaps olivine (Hervig et al., 1977) may become major carriers below 150km depth. Sanidine is potentially stable to high pressure in Si-rich, Mg-poor material (Smyth and Hatton, 1977). K bearing sulfides (Clarke et al., 1977) may be significant. Sensitive electron-microprobe analyses for Na and K are reported by Bishop et al. (1978) for garnet, pyroxenes and olivines in peridotite and eclogite xenoliths from kimberlites, following earlier studies by A. J. Erlank and N. V. Sobolev. We now report sensitive analyses for Na,K,Rb and Ba in micas from kimberlites and enclosed xenoliths. The K/Rb and K/Ba ratios are used to test whether phlogopite could be a major contributor of K,Rb and Ba to the source regions of kimberlite and basalts, and indeed whether it would be the sole contributor of K and Rb (Beswick, 1976).

Phlogopite-rich mica occurs in kimberlite as (a) "primary" and "secondary" crystals in peridotite xenoliths (Carswell, 1975) and eclogite xenliths (Carswell, 1975) and eclogite xenoliths, (b) mica-rich nodules of the mica-amphibole-rutile-ilmenite-diopside (MARID)-suite, interpreted as igneous cumulates (Dawson and Smith, 1977), (c) isolated megacrysts, most of which may be high-pressure phenocrysts, and (d) groundmass crystals. Dawson and Smith (1975) and Smith and Dawson (1975) attempted to classify the micas from their major and minor elements, and further work has confirmed the gross features but indicated further complexities which require detailed description in a series of papers. Smith et al. (1977b, 1978) found that the groundmass micas of micaceous kimberlites occur as very rare Type I crystals [xenocrysts from an intrusive precursor (carbonatitic?) to kimberlite] and abundant Type II crystals (crystallized after emplacement). Detailed textural and chemical data have been published for the MARID suite, and are in process of publication for the other types. We are currently investigating a suite of nodules rich in clinopyroxene whose provenance is not yet clear. The specimens range from (a) single crystals of clinopyroxene containing oriented mica crystals, to (b) polycrystalline specimens obviously produced by deformation and subsequent partial recrystallization, and to (c) polycrystalline specimens of uncertain origin. The micas are chemically similar to megacryst micas. Here we report only the analyses for Na,K,Rb and Ba (Table 1). An extended abstract (Smith et al., 1977a) was based on a smaller data set, and unfortunately contained incorrect analyses of amphibole and serpentine (see later).

Analytical Procedure

Analyses of K and Na made by routine procedures (Smith et al., 1978) are accurate to ~0.2 wt.% (1σ) for K and ~0.02 wt.% (1σ) for Na.

Special study revealed a linear background around the Ba L_α peak. Analyses were made at 15kV, 1.5μA beam current, 15-20μm spot diameter, 200sec on peak and 100sec at backgrounds ±0.05Å, LiF monochromator. The standard was Corning W glass assumed to have 0.56 wt.% Ba. An INAA analysis at Oregon State gave 0.57 wt.% Ba (A. A. Chodos, pers. comm.).

The Rb L_α peak lies on the tail of the Si K_α peak and detailed profiles were measured for several micas (Smith et al., 1977, Fig. 1). Although the background is non-linear, accurate analyses were obtained with backgrounds at ±0.015Å from the peak. The monochromator was ADP, and other analytical conditions were the same as for Ba. Corning W glass was the standard. A careful atomic-absorption analysis by Jun Ito gave Rb_2O 0.49 wt.%. This analysis was calibrated against several standards, agrees well with 0.50 found by wet chemical analysis (A. A. Chodos, pers. comm.), but disagrees with 0.82 from INAA analysis (quoted by A. A. Chodos).

Albee-Ray factors calculated from the major element compositions of the micas and standards were sufficiently close to unity to be ignored. Hence the Rb_2O and BaO analyses were proportioned directly to 0.49 and 0.62 wt.%, respectively.

Analyses were made initially at two spots, one near the center of the crystal, and one near the edge, but avoiding any altered rim revealed by optical study. Additional analyses were made if the first two analyses disagreed within statistical error (~2σ). Several grains were checked in most thin sections. Uniform analyses were obtained for nearly all specimens when grains were preselected for uniformity of color, and lack of alteration. Low K_2O analyses were typical of altered grains. Rubidium was unstable using the high beam current of the present analytical conditions, and the peak reading was taken on a different spot to the one for background readings to make the loss trivial. Mean analyses in Table 1 have a detection level near 40ppm (2σ), and are rounded-off to the nearest 10ppm. The accuracy depends on both the reliability of the standard and the statistical error, but should be near 10% (2σ) at 500ppm and near 5% at 2000ppm.

Discussion

Data on Micas

Table 1 and Figure 1 contain the range and mean of BaO, Rb_2O, K/Rb and K/Ba (wt.% or ratio), and Figures 2-5 show the correlations K/Rb vs. K/Ba, Rb_2O vs. FeO, BaO vs. FeO and Rb_2O vs. Na_2O.

There are wide overlapping ranges for all types of micas, and the following discussion mainly concentrates on the broad trends.

TABLE 1. Analyses of Na_2O, K_2O, Rb_2O, BaO in mica.

Label	Na_2O %	K_2O %	Rb_2O ppm	BaO ppm	K/Rb wt.	K/Ba wt.	Locality
(a) "primary" peridotite							
JVS 73-59	0.25	10.4	280	6,970	337	14	Bul
BD 1368	0.97	9.35	230	4,000	377	22	Mona
CHE-MON 4	0.76	9.69	160	3,530	550	25	"
BD 1143	0.82	9.90	330	2,020	273	46	Bul
CHE-BT7	0.21	9.50	260	1,720	332	51	"
JVS 73-63	0.35	10.5	240	1,380	397	70	"
JVS 73-64	0.15	10.5	160	960	596	101	"
BD 1197	0.26	10.6	320	880	301	112	DeB
BD 1359	0.13	10.3	365	700	254	136	Mat
BD 2125	0.06	10.3	440	620	212	154	Mot
JVS 73-72	0.15	10.7	320	350	304	283	Bul
JVS 73-75A	0.22	10.9	360	360	275	281	"
BD 1141A	0.16	10.7	390	340	249	292	"
HOAM 73-1800X	0.22	11.0	520	320	192	319	?
mean	0.34	10.3	312	1,725	332	136	
(b) "secondary" peridotite							
JVS 73-113-2j	0.20	10.1	200	7,170	458	13	Bel
JVS 73-113-1n	0.21	10.2	110	6,990	842	14	"
BD 1698	0.21	10.5	530	3,540	530	27	RV
BD 1692	0.43	10.0	340	3,300	267	28	"
BD 1079	0.68	9.6	<50	2,970	-	30	Wes
BD 1155	0.81	8.5	140	2,380	551	33	Bul
BD 1154	0.60	9.9	360	1,890	250	49	"
BD 1688	0.60	9.9	230	1,740	391	53	Dut
BD 1126	0.50	9.9	420	1,450	196	57	Jag
BD 1544(a)	0.28	10.0	460	910	197	102	Las
BD 1544(b)	0.47	9.86	320	970	280	94	"
BD 1780/1	0.16	11.0	370	820	269	124	New
unknown	0.07	10.4	330	780	286	124	?
JVS 73-165	0.48	10.4	430	750	220	128	Let
BD 1368	0.34	10.2	500	490	184	192	Mona
BD 2036/5	0.63	9.91	410	460	219	200	Kam
BD 1780/2	0.18	10.5	600	330	159	295	New
mean	0.40	10.0	340	2,170	331	92	
(c) MARID (mica-amphibole-rutile-ilmenite-diopside)							
BD 1671(a)	0.19	10.7	550	800	177	124	Bul
BD 1671(b)	0.19	10.7	600	470	162	211	"
BD 1159	0.08	10.2	540	380	171	248	"
BD 1082	0.13	9.89	620	350	145	262	Wes
BD 1778	0.18	10.6	700	350	137	280	New
BD 1158	0.17	10.5	470	340	203	286	Bul
BD 1165	0.05	10.7	600	340	162	286	RV
BD 1160	0.16	10.6	540	340	178	288	Bul
mean	0.14	10.5	580	420	167	248	
(d) mica megacryst							
BD 1124	0.19	10.6	670	970	144	102	Jag
BD 1079	0.16	10.4	950	930	99	103	Wes
BD 1088	0.28	10.2	290	800	319	118	NeE
BD 1712	0.13	10.4	810	810	116	139	RV
BD 1775	0.05	10.6	1,060	580	91	170	Kli
BD 1823	0.06	10.6	870	490	111	201	Exc
BD 1268	0.10	9.16	750	280	111	303	Hel
BD 1083/1	0.17	9.93	970	280	93	330	Wes
BD 1380	0.26	10.4	890	280	106	344	Mona
BD 1091	0.11	10.6	770	270	125	364	Sta
BD 1118	0.18	10.1	760	200	121	469	Jag
BD 1381	0.22	9.90	940	180	96	511	Mona
BD 1116	0.20	10.3	740	160	126	594	Jag
BD 1788	0.21	10.5	640	160	149	608	Wel
BD 1395	0.11	10.0	715	140	127	661	Mona
BD 1070	0.18	10.4	900	140	105	688	Dut
BD 1717	0.11	10.1	330	130	278	722	RV
BD 768	0.21	10.2	670	130	138	726	Hol
mean	0.16	10.2	760	380	136	397	
(e) (rare Fe-rich) type I groundmass							
BD 1611(a)	0.3	9.5	630	4,320	137	20	Uca
BD 1268(a)	0.32	9.2	240	3,080	348	28	Hel
BD 1611(b)	-	9.9	400	2,800	225	33	Uca
BD 1268(b)	0.45	9.8	470	2,100	189	43	Hel
BD 1100	0.2	9.8	600	1,030	148	88	Mont
mean	0.32	9.6	470	2,670	209	42	
(f)							
BD 1089(a)	0.08	10.0	320	5,780	284	16	NeE
BD 1611	-	9.7	600	4,950	147	18	Uca
BD 1097(a)	0.06	8.9	580	4,120	139	20	Sta
BD 1089(b)	0.08	10.1	150	3,900	611	24	NeE
BD 1268(a)	0.29	9.5	400	2,400	216	37	Hel
BD 1100	-	9.9	350	2,120	257	43	Mont
BD 1088(a)	0.13	10.2	270	1,180	343	80	ZeZ
BD 1097(b)	0.16	10.3	90	650	1,039	147	Sta
BD 1088(b)	0.21	10.4	620	600	152	161	ZeZ
BD 1268(b)	0.22	10.1	820	470	112	199	Hel
mean	0.12	9.9	420	2,620	330	74	
(g) clinopyroxene megacryst and clinopyroxenite							
JVS 73-113-1i	0.03	10.8	900	480	109	209	Bel
BD 1977/1	0.06	10.6	580	460	169	218	"
JVS 73-113-1k	0.03	11.0	770	400	130	255	"
JVS 73-113-1ℓ	0.06	10.8	550	380	178	263	Bel
BD 1977/2	0.21	10.6	610	290	156	335	"
BD 2746	0.16	10.8	340	290	287	344	Kim
JVS 73-113-2e	0.04	10.5	610	260	116	374	Bel
JVS 73-113-2a	0.04	10.7	540	220	180	451	"
JVS 73-113-2c	0.04	10.9	610	200	162	505	"
BD 2997	0.22	10.5	730	170	130	572	Bul
BD 2999	0.12	10.8	820	120	120	836	"
BD 2998	0.21	10.4	730	90	129	1,072	"
mean	0.10	10.7	650	280	156	453	

Bel Bellsbank, Bul Bultfontein, DeB DeBeers, Dut Dutoitspan, Exc Excelsior, Hel Helam, Hol Hololo, Jag Jagersfontein, Kam Kamfersdam, Kim Kimberley, Kli Klipfontein, Las Lashaine, Let Letseng, Mat Matsoku, Mona Monastery, Mont Monteleo, Mot Mothae, NeE New Elands, New Newlands, RV Roberts Victor, Sta Star, Uca U. Canada, Wel Weltvreden, Wes Wesselton, ZeZ Zout en Zuur

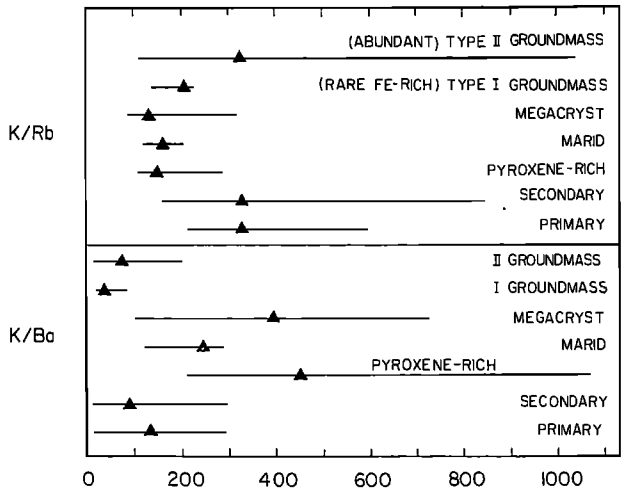

Fig. 1. Range and mean of K/Rb and K/Ba (Table 1) for seven types of micas in the kimberlite environment.

In general, K/Ba decreases as K/Rb increases, and a single broad band encompasses most of the data (Fig. 2). Several other weak correlations can be found, but none are really good. Thus for the primary-peridotite group, Rb tends to correlate positively with total Fe (Fig. 3) and negatively with Ba. These correlations have weakened as data were obtained for additional specimens, and will be checked as further specimens become available for analysis.

Type II groundmass and MARID micas have insufficient Al and Si to fill the tetrahedral sites. A substantial fraction of the iron must be ferric (Smith et al., 1978), probably resulting from oxidation during movement and emplacement of the kimberlite. There is a fairly good correlation between total Fe and Rb (positive) and Ba (negative) in Figs. 3 and 5 for the primary peridotite and "pyroxene" groups, whereas the megacryst and

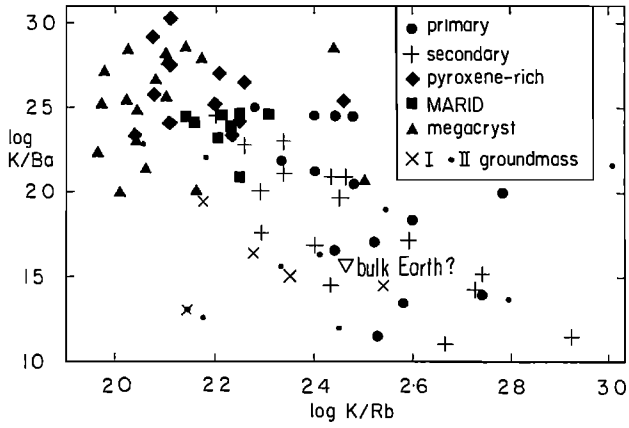

Fig. 2. Log K/Ba vs. log K/Rb for micas. Data in Table 1.

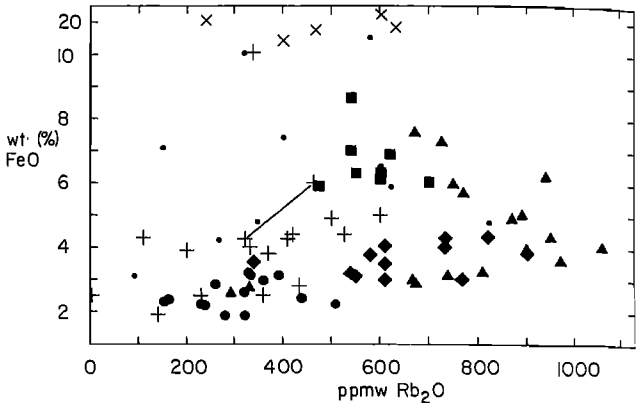

Fig. 3. Wt.% of total Fe expressed as FeO vs. part-per-million-weight Rb_2O for micas. Data in Table 1. List of symbols in Fig. 2.

secondary peridotite groups overlap but tend towards higher Fe. MARID micas are strongly displaced to higher Fe, perhaps because of substantial ferric iron. Micas from the kimberlite groundmass are widely scattered but tend to lie at high Fe. There may be a reasonable correlation between just ferrous iron and Rb (positive) and Ba (negative), but this cannot be tested until some technique is devised for obtaining the Fe^{2+}/Fe^{3+} ratio for small grains.

Returning to the negative correlation of K/Ba with K/Rb (Fig. 2), there is no definitive explanation. Two obvious possibilities are (a) mica-liquid fractionation, and (b) mica-clinopyroxene fractionation, both of which can be examined with reference to the expected values of K/Ba and K/Rb for the bulk Earth. Of course, these values cannot be obtained directly from experimental measurements, but a combination of well-known cosmochemical and geochemical arguments (most recently summarized by Smith, 1977) suggests that the bulk Earth should have the same K/Rb ratio as Cl meteorite viz. (544±75)/(1.88±0.36) = 289±~100) and a K/Ba ratio about 6 (±1?) times

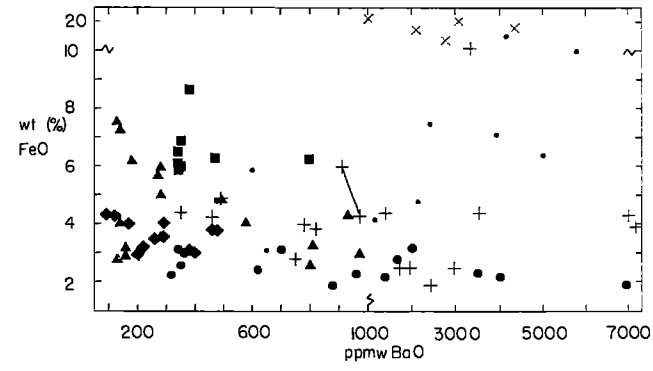

Fig. 4. Wt.% of total Fe expressed as FeO vs. ppmw BaO for micas. Data in Table 1. List of symbols in Fig. 2. Note changes of scale.

smaller than the Cl value of 216. This model composition for the bulk Earth falls into the region occupied by peridotitic micas (Figs. 2 and 6), and allows the possibility that some fractionation process resulted in formation of upper-mantle micas whose overall composition incorporates K,Rb and Ba with the ratios for the bulk Earth.

Beswick (1976) emphasized that micas should have K/Rb about three times lower than coexisting liquid, and used this to explain differences of K/Rb among several types of basalt (see later). The interpretation of megacryst and MARID micas as phenocrysts and cumulates from kimberlite crystallizing during ascent to the surface is consistent with Beswick's suggestion since these two groups have K/Rb about 3 times lower on average than for type II groundmass micas (Fig. 2). The negative correlation between K/Ba and K/Rb for all the micas then indicates that mantle micas have higher K/Ba than coexisting liquid.

Since there are no direct experimental data on the partitioning of K,Rb and Ba between mica and magma at upper-mantle conditions, we assume a working model that (i) phlogopite has taken up most of the K,Rb and Ba of the upper mantle, (ii) that the average composition of the phlogopite is K/Rb ~290 and K/Ba ~36, and (iii) that crystal-liquid fractionation has produced local inhomogeneities in peridotites resulting in a negative correlation between Rb and Ba of the phlogopites.

The other suggestion of mica-clinopyroxene fractionation can be examined from Fig. 6. Unfortunately the Rb content of mantle-derived clinopyroxenes is too low for electron microprobe analysis, and it is difficult to obtain clean samples for bulk analysis. However, the mass-spectrometer analyses by Shimizu (1975) were based on carefully purified samples, and the data fall in a systematic trend based on micas from granular (G) and sheared (S) lherzolite nodules from kimberlite, and in discrete mica nodules (D). Also plotted are data by Philpotts et al. (1972) for two omphacites (O)

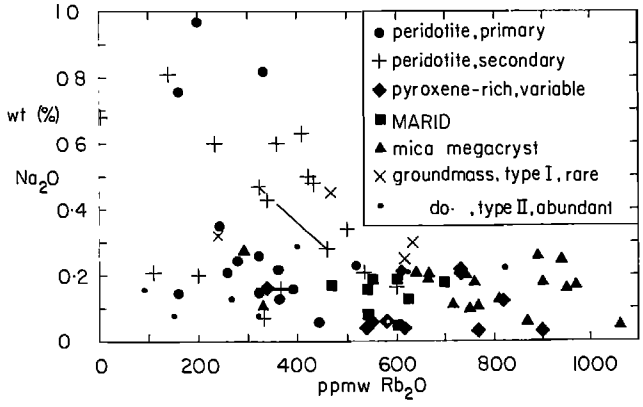

Fig. 5. Wt.% Na_2O vs. ppmw Rb_2O for micas. Data in Table 1.

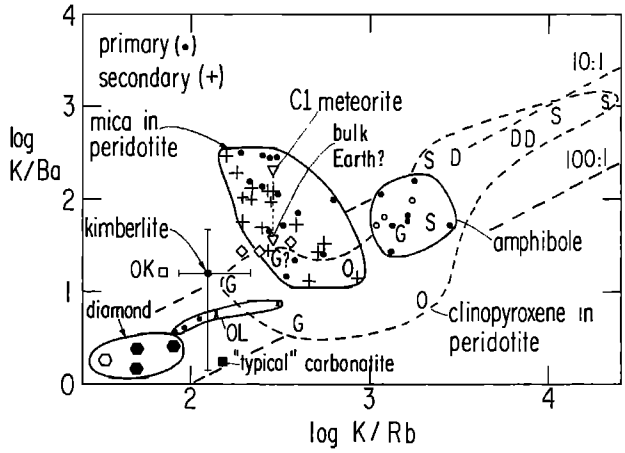

Fig. 6. Log K/Ba vs. log K/Rb for mica, pyroxene and amphibole, and for kimberlite and diamond. See text for sources of data and explanation of most symbols. The data for clinopyroxene are shown by placing a symbol (G granular, S sheared, D discrete, O omphacite) at the data point. The diamond-shaped symbols and open square are for micas and host carbonatite from Oka (OK). Three phonolite and nephelinite rocks (dots) and two sodium carbonate lavas (crosses) are enclosed in the ring for Oldoinyo Lengai (OL). The data for amphibole are distinguished by dot (Basu and Murthy, 1977) and open circle (Philpotts and Schnetzler, 1970).

from Roberts Victor eclogites, which fall in the same overall trend. The data allow that the K/Rb/Ba bulk content of the upper mantle might be altered by mica-clinopyroxene fractionation, followed by some process for mechanical separation of the two minerals. Clinopyroxene, rich in K,Rb and Ba, might have exsolved these elements as mica, as in some eclogites (Reid et al., 1976). Simple mica-liquid fractionation, is preferred to mica-pyroxene fractionation because of greater ease of solid-liquid than solid-solid fractionation.

Because the textural type of mica in a peridotite does not affect the composition range (Fig. 6), the chemical arguments presented here do not depend on the processes responsible for the observed textures in peridotites. However, major chemical fractionations (scale of 1km?) may be followed by minor fractionations (scale down to 1mm?).

We shall assume from now on that mica-liquid fractionation was the dominant process in causing variation in mica compositions, and that mica-clinopyroxene fractionation might be an additional subsidiary process.

Comparison with bulk analyses.

Mass-spectrometer analyses of >98% pure separates of mainly fresh mica (Allsopp and Barrett,

1975) yielded 369-489ppm Rb for all but one of Wesselton "nodule" micas, which overlaps with but tends to be lower than our range of 430-640 for MARID micas (Table 1). Aoki (1974), however, recorded Rb_2O analyses of MARID micas which are twice higher (0.11-0.18 wt.%) than ours (0.05-0.07). Allsopp and Barrett recorded 624-880ppm Rb for Monastery megacrysts, which range lies inside our wider range of 290-1060ppm (mean 760ppm) for megacryst micas from twelve kimberlite localities, but tends to be lower than our values of 715, 890 and 940ppm for three megacrysts from Monastery.

Bulk analyses of micas from peridotite nodules probably represent mixtures of texturally "primary" and "secondary" micas. Furthermore there may be a substantial amount of serpentinization which is not always identifiable by optical methods. The range of 231-555ppm Rb obtained by Allsopp and Barrett for De Beers, Bultfontein and DuToitspan peridotite micas overlaps our range of 146-475ppm Rb for "primary" and <50-550ppm for "secondary" peridotite micas. Our mean values for "primary" and "secondary" micas are identical within experimental uncertainty (332 and 331).

Rhodes and Dawson (1975) reported a range of 75-234 (mean 175) for Rb in sixteen peridotites from Lashaine, and summarized earlier data for peridotite inclusions in kimberlite which have K/Rb typically at 254 in three studies and averaging at 186 for another study of 61 inclusions. These values tend to be lower than our range of 159-842 (mean 332) for peridotite micas, and there is no satisfactory explanation for the difference of the mean values. The assumed Rb value of our standard may be wrong, and the INAA value might be correct: however, this is believed to be very unlikely because of the good agreement between standard chemical and atomic absorption analyses. A second possibility is that the K/Rb ratio of bulk peridotite nodules is not determined solely by the mica, and that other components are important. Thus bulk kimberlites have K/Rb 88-207 (see later), and metasomatism of the peridotite may have reduced K/Rb. Originally we suspected that serpentine might have a much lower K/Rb ratio than mica, and indeed early analyses listed by Smith et al. (1977) apparently confirmed this. Unfortunately a numerical error in the background used in a computer program had given falsely high results, and new analyses yielded no detectable Rb at the 40ppm detection level. Rhodes and Dawson (1975, Table 6) reported the following typical or average values of K/Rb for other types of peridotite: inclusions in basalt 278; spinel-peridotite inclusions from the Central Massif, France 367; ones from the Mid-Atlantic Ridge 410; and alpine-type ultramafic rocks 269. These values actually surround our mean value of 332 for peridotite micas, and we shall assume that our value applies to all types of peridotites within an uncertainty of ~25%.

Our data for Type II groundmass micas are only exploratory, and quite insufficient to determine the composition range within a single kimberlite and between different kimberlites. Smith et al. (1977b) found wide variations of major and minor elements between different Type-II crystals of the same kimberlite, and this also occurs for trace elements. The exploratory data give K/Rb 112-1039 (mean 330), which range is mostly higher than K/Rb values for bulk kimberlites: Fesq et al. (1975b), 88-217; Barrett and Berg (1975), 93-207; Harris and Middlemost (1969), mean 196. We cannot explain why our values for Type II mica tend to be higher than for bulk kimberlite, but it is only necessary for serpentine, which has roughly equal abundance as mica, to contain ~20ppm Rb for K/Rb to be lowered from ~330 for a mica to ~100-~200 for bulk kimberlite.

Smith et al. (1977b) tentatively suggested that rare xenocrysts of Type I groundmass micas came from a carbonatitic precursor. Unfortunately there are no detailed electron microprobe analyses of micas from carbonatites, and existing bulk analyses of micas appear to be biased by contamination. Rimsaite (1969) reported the following values for bulk micas from the Oka carbonatite: green K/Rb 359 K/Ba 33; brown 243,27; orange 194,26 (Fig. 6; open diamonds). Our values for 5 Type I crystals (K/Rb 137-348, mean 209; K/Ba 20-88, mean 42) overlap the values for these bulk carbonatitic micas.

There are fewer data for Ba than for Rb in peridotite and peridotitic micas. Ridley and Dawson (1975) reported K/Ba 18 and K/Rb 121 for phlogopite from a Lashaine peridotite. Although taken separately the K/Ba and K/Rb values fit within our ranges for peridotitic mica, taken together they lie outside the main trend in Fig. 2. Perhaps the occurrence of Ba (and K) in clinopyroxene (Shimizu, 1975) is causing complications. Fesq et al. (1975b) reported K/Ba 273 and K/Rb 193 in phlogopite from a Bultfontein garnet peridotite, which values plot in the main trend in Fig. 2. They also reported K/Ba 1.4-46 for 13 S. African kimberlites, which values are mostly below our range of 16-199 for Type II groundmass micas. However baryte is a common minor constituent of kimberlite, and Ba probably occurs as a substituent of carbonate, thereby providing an explanation of the bias in the ranges.

Origin of kimberlite and differentiation therein.

If the data in Fig. 6 are correct, kimberlite cannot have acquired its K,Rb and Ba merely by total incorporation of these elements from mica during partial melting of a peridotite similar to any of the mica-bearing peridotites listed in Table 1. However this does not rule out a hypothetical mica-bearing peridotite not yet sampled in suites of nodules.

Perhaps the origin of kimberlite should be set in a wider context. Also plotted on Fig. 6 are

(a) neutron-activation data for three sets of inclusion-bearing diamonds (filled hexagons) and optically-clear diamonds (open hexagon) obtained by Fesq et al. (1975a), (b) a single datum (filled square) for typical bulk carbonatite (Gold, 1966), and a single datum (open square) for both carbonatite from Oka (Rimsaite, 1969), and (c) three data for phonolite and phonolitic nephelinite rocks (dots) and two data for sodium carbonate lavas (crosses) from Oldoinyo Lengai volcano (Dawson, 1966). These data were selected after an extensive search for materials with low K/Ba and K/Rb. All other volcanic rocks have higher K/Ba and K/Rb (Fig. 7). Fesq et al. proposed that the analyses of 26 elements in diamond can be explained by variable amounts of H_2O-CO_2-rich fluid and Fe-Ni-Cu-Co sulfides as well as a more abundant silicate phase. Perhaps the unusual Oldoinyo Lengai rocks are related to the trapped inclusions in diamond. It is impossible to give an answer to the source of these materials, but it seems necessary to take into account the possible existence in the upper mantle of fluids with K/Ba and K/Rb values much lower than the values found in peridotitic micas. Probably the fluids are dominated by carbonate (and sulfide?), and have very different properties from silicate-rich fluids. Perhaps kimberlite may derive its K,Rb and Ba from a mixture of peridotitic mica and carbonatitic source material. Clinopyroxene may also be a significant contributor.

The differentiation of kimberlite has already been mentioned in the earlier discussion of the difference of composition between micas of the MARID, megacryst and type II groundmass suites. Type I groundmass micas tend to lie to the lower left of the trend in Fig. 2, and overlap with micas from the Oka carbonatite (Rimsaite, 1969; open diamonds, Fig. 6). Type II groundmass micas occupy a similar composition range to peridotitic micas (Fig. 2). Preliminary electron microprobe analyses of amphiboles in MARID specimens gave the following data: specimen 1082, K_2O 5.28 wt.%, BaO 20? ppm; 1159, 5.28, 30?; 1160, 5.12, 0?; 1671, 4.92, 60; 1778, 5.88, 40. Since the accuracy of the BaO analyses is about 40ppm (2σ), no confidence can be placed in resulting K/Ba ratios except that they are in the region of 1,000 or more. Preliminary analyses revealed no Rb_2O at the 40ppm level, indicating K/Rb ratios greater than 1,000. Crystallization of amphibole should cause a decrease of K/Rb and K/Ba of the kimberlite magma. Electron microprobe analyses of serpentine and carbonate are too insensitive to yield reliable data. Analyses of mineral separates by techniques sensitive to the ppm level will be needed to clarify the distribution of K,Rb and Ba in kimberlites. Furthermore, it will be necessary to consider the possible extent of change of composition of kimberlite during ascent and after emplacement in any attempt to determine the differentiation sequence in a kimberlite. Certainly the occurrence of MARID nodules, mica megacrysts, and Type I groundmass micas demonstrate that substantial differentiation may have occurred during ascent.

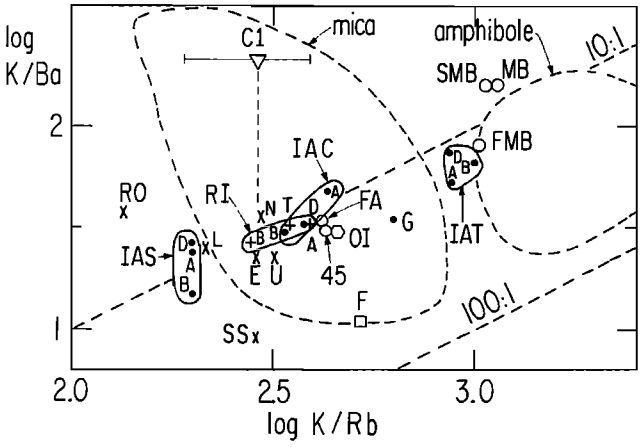

Fig. 7. Log K/Ba vs. log K/Rb for rocks. See Table 2 for data and key to symbols. The ranges for mica and amphibole are taken from Fig. 6. The model composition for bulk Earth is at the end of the arrow projecting downwards from the composition for Cl meteorite.

Origin of basalts and other volcanic rocks.

Readers are referred to Carmichael et al. (1974) for a review of the origin of basalts and other volcanic rocks. There is an enormous literature on the use of K, Rb and other trace elements to place limits on the processes involved in the source regions and during ascent and crystallization in magma chambers. The present discussion is strictly confined to the possible roles of mica, clinopyroxene and amphibole in the source regions of volcanic rocks. Particular emphasis is placed on whether phlogopite-melt equilibria can explain the variation of K/Rb, as advocated by Beswick (1976) and disputed by Menzies (1978). Here, the variation of K/Ba will also be considered as an extra constraint.

Table 2 contains a selection of rocks for which both K/Rb and K/Ba were measured. The symbols in Fig. 7 give a quick visual distinction between continental environment (cross), mid-ocean ridge (open circle), and island-arc (dot). Except for unusual rocks (Roman Region high-alkali rocks; Shonkin Sag shonkinite) and two rock types shown merely to illustrate possible compositions in the lower crust (granulites and charnockitic parent magma), K/Ba and K/Rb are positively correlated.

Continental rock types, as typified by Ross Island, Eifel, Uganda and Dunedin specimens, lie close to the model composition for the bulk Earth. Only slight K/Rb/Ba differentiation has occurred between the basanitoid, trachybasalt and anorthoclase phonolite sub-groups of the Ross Island volcanic rocks, and to a first approxima-

TABLE 2. K/Rb and K/Ba for selected rocks.

Symbol	Location; rock type	n	K/Rb	K/Ba	Ref.
SS	Shonkin Sag, shonkinite	2	284,293	9.1,9.3	1
RO	Roman region; high-K lavas	13	109-180(136)	12-49(38)	2
E	Eifel, W. Germany; high-K lavas	17	289	23	3
U	Uganda; high-K lavas	23	323	23	3
L	Lesotho; tholeiitic basalts	22	108-685(213)	12-46(25)	4
IAT	island arc tholeiites; general	(B)	1,000	67	5
	description; B basalt, A	(A)	890	53	5
	andesite, D dacite	(D)	870	75	5
IAC	island arc calc-alkaline association;	(B)	340	30	5
	general description; B basalt,	(A)	430	48	5
	A andesite, D dacite	(D)	380	33	5
IAS	island arc shoshonitic association;	(B)	200	15	5
	general description; B basalt, A	(A)	200	24	5
	andesite, D dacite	(D)	200	27	5
MB	typical mid-ocean-ridge basalt	-	1,130	160	6
SMB	slow-spreading mid-ocean-ridge	7	1,080	162	7
FMB	fast-spreading mid-ocean-ridge	8	1,040	80	7
45	45°N mid-ocean-ridge basalt	-	430	31	6
FA	37°N mid-ocean-ridge basalt	10	324-566(416)	29-42(34)	8
OI	oceanic islands; tholeiite, alkali basalt	225	450	31	6
RI	Ross Island; basanitoid (B),	(B)12	208-493(283)	18-32(27)	9
	trachybasalt (T); anorthoclase	(T)6	278-408(352)	25-43(32)	9
	phonolites (A)	(A)4	365-431(390)	30-36(33)	9
N	Dunedin, NZ; alkaline lavas	12	158-394(297)	24-51(35)	10
G	Brazil; granulites	62	626	20	11
F	France; charnockitic parent magma	-	519	11	12
-	Archean tholeiite	-	350	30	13

n number of samples or bracketed symbol of rock type. The range and mean, or just the mean, is given for K/Rb and K/Ba.

References: 1. Nash and Wilkinson, 1970; 2. Cox et al., 1976; 3. Lloyd and Bailey, 1975; 4. Cox and Hornung, 1966; 5. Jakeš and White, 1972; 6. Erlank and Kable, 1976; 7. Hart, 1971; 8. White and Bryan, 1977; 9. Goldich et al., 1975; 10. Price and Taylor, 1973; 11. Sighinolfi, 1971; 12. Leyreloup et al., 1977; 13. Sun and Nesbitt, 1977.

tion the whole set of data can be taken to indicate approximately the K/Rb of the parent magmas before differentiation. More specifically, the Ross Island basanitoid data have been measured carefully, and the basanitoid group of rocks is likely to have undergone the least post-ascent differentiation. The mean K/Rb and K/Ba ratios for this group (283 and 27) are quite close to the values of 290 and 36 listed earlier for a model bulk Earth. Furthermore, the entire set of data for these continental volcanic rocks lies within the field for peridotite micas, thereby allowing the hypothesis that these volcanic rocks obtain their K,Rb and Ba contents by total extraction of mica during partial melting of upper-mantle peridotite. The only exception is the set of data for Lesotho tholeiitic basalts whose mean K/Rb and K/Ba values are much lower; however, there are wide ranges for individual hand specimens and the analyses are rather old, and the K data are rather imprecise.

Island-arc rocks have been classified into tholeiite (IAT), calc-alkaline (IAC) and shoshonitic associations (IAS) with sub-groups of basaltic, andesitic and dacitic types, but increasing complexities are appearing. There are only insignificant variations of K/Rb and K/Ba between the three rock types of each association, thereby showing that post-ascent differentiation has little effect on these ratios, as is well known. The major distinctions between the three associations require explanation in terms of some process or processes involved with generation of the magmas. In island-arc rocks, Rb apparently increases faster than K does with respect to the depth of the earthquake foci under the extruded rock (reviewed by Beswick, 1976). This trend was explained by Beswick in terms of different degrees of phlogopite-liquid fractionation in the partial melting process, but this process may be untenable when K/Ba is also considered. If the negative trend of K/Ba vs. K/Rb in peridotite micas is the result of crystal-liquid fractionation, as suggested earlier, the trend for island-arc rocks should be negative instead of positive.

For oceanic islands, both tholeiitic and alkali

basalts have similar K/Rb ~450 and K/Ba ~31. Mid-ocean ridge rocks fall into two groups, (a) the well-known group of basaltic rocks (MB), whose ratios apparently are fairly similar for slow-moving (SMB) and fast-moving (FMB) ridges, and (b) ones from the 37°(FA for FAMOUS) and 45°N latitudes of the Mid-Atlantic Ridge. The former have high K/Rb ~1000 and the latter fall close to the oceanic island group. Alteration of submarine basalts may change Ba by 50% (Philpotts et al., 1969), but the above data should be for unaltered samples.

Fig. 6 allows tests of simple models involving minerals other than mica. Analyses for amphibole crystals (kaersutites; Basu and Murthy, 1977; amphiboles from two camptonites and one andesite, Philpotts and Schnetzler, 1970) define a fairly small region which has too high K/Rb to fit with the mid-ocean ridge basalts. The ill-defined trend for clinopyroxenes does not fit either. Total extraction of just one mineral does not seem a promising model for the origin of K,Rb and Ba in mid-ocean ridge basalts with high K/Rb. Apparently it is necessary to turn to complex models involving more than one mineral, or models involving partial extraction, or both, when considering the origin of these rocks.

The island-arc shoshonitic association falls just to the left of the range for peridotitic micas, and overlaps the trend for the Oka carbonatitic micas. Much further thinking is needed about the origin of rocks in the shoshonitic association, and indeed of all the high-K lavas. Quantitatively they are very insignificant, as are carbonatites, and special processes involving extraction of a minute fraction of material from the upper mantle may be involved, together with strong fractionation during ascent and emplacement.

Conclusion

Whatever the ultimate conclusions about the origin of K,Rb and Ba in volcanic rocks, it is perhaps worth emphasizing that most rocks have K/Rb and K/Ba which fall in the central bloc in Fig. 7, fairly close to the datum for the bulk Earth model, and inside the field for peridotitic mica. The answer to Beswick's question "Is phlogopite the key?" could be "Yes" for most magmas, but the details of the processes may be rather different from those envisaged by him.

The incomplete nature of the present data, and the tentativeness of the suggestions, are fully recognized by us, but we feel that discussion is needed to provoke further experimentation. Particularly needed are data on the trace-element contents of carbonate, serpentine and other minerals in peridotites, kimberlites, and carbonatites. Unfortunately the electron microprobe is of little use below 100ppm for most elements in most minerals, and it will be necessary to develop new techniques for spot analyses at the 1-10ppm level. Furthermore, controlled experiments of element partitioning at upper-mantle conditions will be needed before observed distributions can be interpreted with confidence.

Acknowledgements. We thank C. H. Emeleus and H. O. A. Meyer for donating specimens listed in Table 1(a). J. V. Smith gratefully acknowledges grants NSF-EAR-76-03604 and NASA 14-001-171 Res, as well as general support from the Materials Research Laboratory funded by NSF. Technical support from I. M. Steele, T. Solberg, I. Baltuska and O. Draughn is gratefully acknowledged.

References

Allsopp, H. L., and D. R. Barrett, Rb-Sr age determinations on South African kimberlite pipes, Phys. Chem. Earth, 9, 605-617, 1975.

Aoki, K., Phlogopites and potassic richterites from mica nodules in South African kimberlites, Contr. Mineral. Petr., 48, 1-8, 1974.

Barrett, D. R., and G. W. Berg, Complementary petrographic and strontium-isotope ratio studies of South African kimberlite, Phys. Chem. Earth, 9, 619-635, 1975.

Basu, A. R., and V. R. Murthy, Kaersutites, sub-oceanic low-velocity zone, and the origin of mid-ocean ridge basalts, Geology, 5, 365-368, 1977.

Beswick, A. E., K and Rb relations in basalts and other mantle derived materials. Is phlogopite the key?, Geochim. Cosmochim. Acta, 40, 1167-1183, 1976.

Bishop, F. C., J. V. Smith, and J. B. Dawson, Na,K,P and Ti in garnet, pyroxene and olivine from peridotite and eclogite xenoliths from African kimberlites, Lithos in press, 1978.

Carmichael, I. S. E., F. J. Turner, and J. Verhoogen, Igneous Petrology, McGraw-Hill, New York, 1974.

Carswell, D. A., Primary and secondary phlogopites and clinopyroxenes in garnet lherzolite xenoliths, Phys. Chem. Earth, 9, 417-429,

Clarke, D. B., G. G. Pe, R. M. MacKay, K. R. Gill, M. J. O'Hara, and J. A. Gard, A new potassium-iron-nickel sulphide from a nodule in kimberlite, Earth Planet Sci. Lett., 35, 398-410, 1977.

Cox, K. G., and G. Hornung, The petrology of the Karroo basalts of Basutoland, Amer. Miner., 51, 1414-1432, 1966.

Cox, K. G., C. J. Hawkesworth, R. K. O'Nions, and J. D. Appleton, Isotopic evidence for the derivation of some Roman Region volcanics from anomalously enriched mantle, Contr. Mineral Petr., 56, 173-180, 1976.

Dawson, J. B., Oldoinyo Lengai - an active volcano with sodium carbonatite lava flows, In "Carbonatites", edited by O. F. Tuttle and J. G. Hines, Interscience, New York, 1966.

Dawson, J. B., and J. V. Smith, Chemistry and origin of phlogopite megacrysts in kimberlite, Nature, 253, 336-338, 1975.

Dawson, J. B., and J. V. Smith, The MARID (mica-amphibole-rutile-ilmenite-diopside) suite of

xenoliths in kimberlite, Geochim. Cosmochim. Acta, 41, 309-323, 1977.
Erlank, A. J., and E. J. D. Kable, The significance of incompatible elements in Mid-Atlantic Ridge basalts from 45°N with particular reference to Zr/Nb, Contr. Mineral. Petrol., 54, 281-291, 1976.
Fesq, H. W., D. M. Bibby, C. S. Erasmus, E. J. D. Kable, and J. P. F. Sellschop, A comparative trace element study of diamonds from Premier, Finsch and Jagersfontein mines, South Africa, Phys. Chem. Earth, 9, 817-836, 1975a.
Fesq, H. W., E. J. D. Kable, and J. J. Gurney, Aspects of the geochemistry of kimberlites from the Premier mine, and other selected South African occurrences with particular reference to the rare earth elements, Phys. Chem. Earth 9, 687-707, 1975b.
Gold, D. P., The average and typical chemical composition of carbonatites, Int. Mineral. Assoc. Volume, Mineralogical Society of India, 83-91, 1966.
Goldich, S. S., S. B. Treves, N. H. Suhr, and J. S. Stuckless, Geochemistry of the Cenozoic volcanic rocks of Ross Island and vicinity, Antarctica, J. Geol., 83, 415-435, 1975.
Harris, P. G., and E. A. Middlemost, The evolution of kimberlites, Lithos, 3, 77-88, 1969.
Hart, S. R., K, Rb, Cs, Sr and Ba contents and Sr isotope ratios of ocean floor basalts, Phil. Trans. R. Soc. London, A 268, 573-587, 1971.
Hervig, R. L., J. V. Smith, and J. B. Dawson, Minor element content of olivine and orthopyroxene in upper-mantle xenoliths, Extended Abstracts, Second International Kimberlite Conference, Santa Fe, New Mexico, 1977.
Jakeš, P., and A. J. R. White, Major and trace element abundances in volcanic rocks or orogenic areas, Geol. Soc. Amer. Bull., 83, 29-40, 1972.
Leyreloup, A., C. Dupuy, and R. Andriambololona, Catazonal xenoliths in French neogene volcanic rocks: constitution of the lower crust, Contr. Mineral. Petrol., 62, 283-300, 1977.
Lloyd, F. E., and D. K. Bailey, Light element metasomatism of the continental mantle: the evidence and the consequences, Phys. Chem. Earth, 9, 389-416, 1975.
Menzies, M., Comment on "Is phlogopite the key?" by A. E. Beswick. Geochim. Cosmochim. Acta, 42, 146-149, 1970. Author's reply, 149-150.
Nash, W. P., and J. F. G. Wilkinson, Shonkin Sag laccolith, Montana: pt. I, mafic minerals and estimates of temperature, pressure, oxygen fugacity and silica activity, Contr. Mineral. Petrol., 25, 241-269, 1970.
Philpotts, J. A., and C. C. Schnetzler, Phenocryst-matrix partition coefficients for K, Rb, Sr and Ba, with applications to anorthosite and basalt genesis, Geochim. Cosmochim. Acta, 34, 307-322, 1970.
Philpotts, J. A., C. C. Schnetzler, and S. R. Hart, Submarine basalts: some K, Rb, Sr, Ba, rare earth, H_2O and CO_2 data bearing on their alteration, modification by plagioclase and possible source materials, Earth Planet. Sci. Lett., 7, 293-299, 1969.
Philpotts, J. A., C. C. Schnetzler, and H. H. Thomas, Petrogenetic implications of some new geochemical data on eclogitic and ultrabasic inclusions, Geochim. Cosmochim. Acta, 36, 1131-1166, 1972.
Price, R. C., and S. R. Taylor, The geochemistry of the Dunedin volcano, East Otago, New Zealand: rare earth elements, Contr. Mineral. Petrol., 40, 195-205, 1973.
Reid, A. M., R. W. Brown, J. B. Dawson, G. G. Whitfield, and J. C. Siebert, Garnet and pyroxene compositions in some diamondiferous eclogites, Contr. Mineral. Petrol., 58, 203-220, 1976.
Rhodes, J. M., and J. B. Dawson, Major and trace element chemistry of peridotite inclusions from the Lashaine volcano, Tanzania, Phys. Chem. Earth, 9, 545-557, 1975.
Ridley, W. I., and J. B. Dawson, Lithophile trace element data bearing on the origin of peridotite xenoliths, ankaramite and carbonatite from Lashaine volcano, N. Tanzania, Phys. Chem. Earth, 9, 559-569, 1975.
Rimsaite, J., Evolution of zoned micas and associated silicates in the Oka carbonatite, Contr. Mineral. Petrol., 23, 340-360, 1969.
Shimizu, N., Geochemistry of ultramafic inclusions from Salt Lake crater, Hawaii, and from Southern African kimberlites, Phys. Chem. Earth, 9, 655-669, 1975.
Sighinolfi, G. P., Investigations into deep crustal levels: fractionating effects and geochemical trends related to high grade metamorphism, Geochim. Cosmochim. Acta, 35, 1005-1021, 1971.
Smith, J. V., Possible controls on the bulk composition of the earth: implications for the origin of the earth and moon, Proc. 8th Lunar Sci. Conf., 333-369, 1977.
Smith, J. V., and J. B. Dawson, Chemistry of Mg-rich micas from kimberlites and xenoliths, with implications for volatiles in upper mantle, Geol. Soc. Amer., Abstr. with Programs, 7, 1275-1276, 1975.
Smith, J. V., R. Brennesholtz, and J. B. Dawson, Chemistry of micas from kimberlites and xenoliths, Geochim. Cosmochim. Acta, in press, 1978.
Smith, J. V., R. L. Hervig, D. Ackermand, and J. B. Dawson, K, Rb and Ba in micas from kimberlite and peridotitic xenoliths, Extended Abstracts, Second International Kimberlite Conference, Santa Fe, New Mexico, 1977a.
Smith, J. V., R. Brennesholtz, and J. B. Dawson, Late-stage micas in kimberlite groundmass, Extended Abstracts, Second International Kimberlite Conference, Santa Fe, New Mexico, 1977b.
Smyth, J. R., and C. J. Hatton, A coesite-sanidine grospydite from the Roberts Victor kimberlite, Earth Planet. Sci. Lett., 34, 273-283, 1977.
Steele, I. M., I. D. Hutcheon, and J. V. Smith,

Ion microprobe analysis of plagioclase feldspar ($Ca_{1-x}Na_xAl_{2-x}Si_{2+x}O_8$) for major, minor and trace elements, Proc. 8th Int. Conf. X-ray Optics and Microanalysis, in press, 1978.

Sun, S., and R. W. Nesbitt, Chemical heterogeneity of the Archaean mantle, composition of the Earth and mantle evolution, Earth Planet. Sci. Lett., 35, 429-448, 1977.

White, W. M., and W. B. Bryan, Sr-isotope, K, Rb, Cs, Sr, Ba, and rare-earth geochemistry of basalts from the FAMOUS area, Geol. Soc. Amer. Bull., 88, 571-576, 1977.

GEOCHEMISTRY

VARIATIONS IN STABLE ISOTOPE COMPOSITIONS FOR CARBON AND OXYGEN IN SOME SOUTH AFRICAN AND LESOTHAN KIMBERLITES

B.J. Kobelski[1], D.P. Gold, and P. Deines

Department of Geosciences, The Pennsylvania State University,

University Park, Pa. 16802

Abstract. The mean isotopic composition of carbonates in 142 kimberlite samples from 12 kimberlite localities in southern Africa were determined as $\delta^{13}C = -5.92‰$ vs PDB ($\sigma \pm 2.42$), and $\delta^{18}O = 12.91‰$ vs SMOW ($\delta \pm 3.23$). The only carbonate minerals detected by XRD analysis are calcite and dolomite. The mean isotopic compositions of carbonates in different habits (matrix, and inclusions or segregations) are presented below by location:

Location	Matrix		Inclusions		Total (Mean)	
	$\delta^{13}C$	$\delta^{18}O$	$\delta^{13}C$	$\delta^{18}O$	$\delta^{13}C$	$\delta^{18}O$
Benfontein	-5.21	11.62	-4.91	9.42	-5.07	10.56
DeBeers	-5.99	12.82	-7.11	16.22	-6.65	14.82
Wesselton	-4.88	10.62	-5.44	13.98	-5.12	11.97
Monastery	-4.50	16.26	-4.03	12.96	-4.23	14.37
National	-4.41	13.70	-2.90	15.70	-3.44	14.98
Premier	-7.18	11.38	-9.10	13.87	-7.77	12.14
Ngopetsou	-4.60	11.40	-4.59	12.09	-4.59	11.68
Star	-7.61	11.04	-6.33	10.66	-7.18	10.91
Pipe 200	-6.84	14.71	-6.22	13.14	-6.61	14.12
Kao	-8.89	17.10			-8.89	17.10
Marakabei	-4.74	12.23			-4.74	12.23
Roberts Victor	-6.81	12.23	-11.20	17.74	-7.91	13.61

Angular carbonate xenoliths have similar $\delta^{13}C$ values as the matrix carbonate. Xenocrystic carbonates tend to be enriched in ^{13}C (heavier) with respect to the matrix. Unzoned and rounded carbonate nodules yield similar isotopic values to the matrix carbonates, and they are interpreted as cognate xenoliths. Ocelli in the Benfontein sill have a similar $\delta^{13}C$ value to the matrix carbonates, but are heavier by about 1‰ than early "quench" carbonate "needles". Pisolitic kimberlite lapilli and the carbonate matrix, that occur in pipe-like habit in the Star Mine, have similar $\delta^{13}C$ values, suggesting they originated from the same source. Both the $\delta^{13}C$ and $\delta^{18}O$ values of "replacement" carbonates are highly variable and distinctive from those of the matrix carbonates.

Although the mean carbon isotopic composition is comparable to the values established for diamonds and carbonatites, the mean oxygen isotopic composition of these kimberlites is enriched in ^{18}O by several permil with respect to primary igneous carbonatites. The $\delta^{13}C$ and $\delta^{18}O$ values range from 0.24‰ to -11.76% , and 6‰ to 24‰ respectively. Massive, fragmental, and carbonatitic kimberlite (usually as late dikes) were distinguished on textural, petrographic and isotopic criteria. Their mean carbon and oxygen isotopic compositions are respectively: massive (type 1), 5.41‰ and 11.26‰; fragmental (or type 3), -5.67‰ and 13.90‰; and the carbonatitic kimberlite (or type 2), -7.24% and 12.56‰ . The trend to heavier oxygen values in the fragmental type is thought to be due to interaction with meteoric water during emplacement. A significant difference in the mean ^{13}C of kimberlites from different localities is indicated. For those kimberlite locations where the differences between their mean $\delta^{13}C$ and $\delta^{18}O$ values are too great to be explained by a "combined isotopic effect process", then an inhomogeneous source reservoir of carbon isotopes is inferred.

Introduction

Kimberlites are as interesting geologically as they are rare, because they are the only known primary source of terrestrial diamond, and they may contain samples of the upper mantle and lower crust incorporated during their ascent. Although the importance of carbon in the evolution of kimberlitic rocks had long been realized, it was only in the 1950's that systematic studies

[1] present address Exxon Co. USA, P.O. Box 496, Harvey, LA 70059.

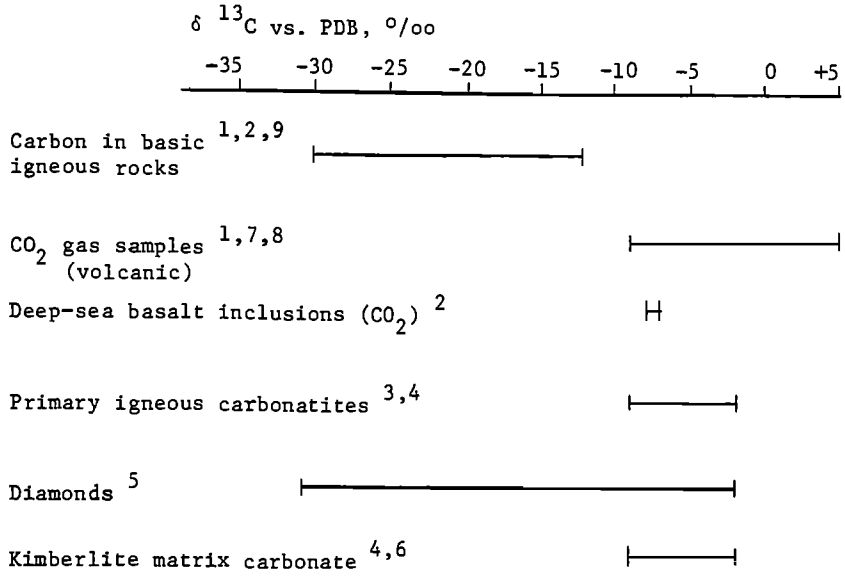

Fig. 1. Comparison of the range of carbon isotopic compositions from various materials believed to represent deep-seated carbon. The data are from: 1, Craig (1953); 2, Pineau et al. (1976); 3, Taylor et al. (1967); 4, Deines and Gold (1973); 5, compiled by Deines and Gold (1973) and Sheppard and Dawson (1975) from various sources; 6, Sheppard and Dawson (1975) (The data for the kimberlite matrix carbonate do not contain analyses from this investigation); 7, Cheminee et al. (1969); 8, Gunter and Musgrave (1971); 9, Hoefs (1973).

were initiated (von Eckermann et al., 1952; Craig, 1953; Wickman, 1956) to characterize the isotopic ratios in ultramafic rocks. Since then studies on the stable isotopes of some rock suites and their constituent minerals have provided information on the degree of equilibrium (isotopic), crystallization temperature, and by use of appropriate fractionation models estimates can be made on the isotopic composition of the source material and the genetic sequence in a petrographic suite. The carbonatites and kimberlites are important links in understanding the carbon and oxygen geochemical cycles because the carbon-bearing phases (diamond, graphite, elemental carbon, fluid inclusions, and carbonate minerals) are the only deep-seated materials currently accessible for study.

Under equilibrium conditions, the graphite-diamond inversion requires between 46 and 47 kb at 1000°C; conditions met in the upper mantle (Kennedy and Kennedy, 1976). Assuming that diamonds have crystallized within their phase stability range, then they must represent a form of mantle carbon. Diamonds from several localities have been analysed for their carbon isotopic composition, and a mean value of $\delta^{13}C$ = -5.8‰ ±1.8 (60 analyses, excluding carbonado analyses) has been determined (Deines and Gold, 1973). For comparison the ranges of the carbon isotopic composition of several materials that are believed to represent deep-seated carbon are plotted in Figure 1.

Kimberlites have not been studied in as much detail as the carbonatites with regard to their carbon isotopic composition. The previous works contain $\delta^{13}C$ and $\delta^{18}O$ values of Premier Mine carbonatite dikes (Baertschi, 1957; Deines and Gold, 1973; Suwa et al., 1975), Siberian kimberlite pipes (Vinogradov et al., 1965), Colorado diatremes (Deines and Gold, 1973), and an unnamed South African kimberlite (Craig, 1953), and a number of kimberlite occurrences in South Africa and Lesotho (Deines and Gold, 1973; Sheppard and Dawson, 1975). The range of the carbon isotopic composition of these kimberlitic carbonates are included in Figure 1.

Deines and Gold (1973) have calculated the mean carbon isotopic composition of the kimberlites studied as $\delta^{13}C$ = 4.7‰ ±1.2, and the mean oxygen isotopic composition of these samples were found to be enriched in ^{18}O by several permil compared to carbonatites. Sheppard and Dawson (1975) report a range of $\delta^{13}C$ from -3‰ to -7.5‰ and $\delta^{18}O$ from 7‰ to 21‰ for carbonates from 17 samples of matrix, xenolith, and kimberlite carbonatized dike, and they note the compositional overlap with diamonds and carbonatites.

At present, relatively few isotopic analyses

of kimberlite carbonates have been documented in the literature. All published analyses, except for a $\delta^{13}C = -23‰$ value reported by Craig (1953), have been plotted in Figure 2. A limited range from -2% to -10% in carbon isotopic composition is apparent for these samples. The availability of samples from South African and Lesothan kimberlites increased many fold as a result of the field trips associated with the 1973 International Kimberlite Conference in Cape Town, South Africa. A study of 12 of these localities was undertaken to (1) determine the isotopic variability of carbon and oxygen in carbonates from southern African kimberlites, (2) determine the mean carbon and oxygen isotopic composition of each of these kimberlite occurrences, (3) test correlations of isotopic variability between matrix and inclusion types, geological type of kimberlite based on field and petrographic criteria, and geographic setting, and (4) give geological meaning to anomalous values such as found by Deines (1968) and Craig (1953).

Experimental Technique

The kimberlite samples were collected (D.P.G.) during September and October, 1973 as part of a general study on diatremes. The kimberlite bodies selected for this study are indicated in Figure 3. In general, the freshest kimberlite specimens were sampled from underground mines, quarry walls, and drill cores.

The carbonate mineralogy of the kimberlite specimens was determined by X-ray diffraction patterns from a Norelco X-ray diffractometer with Ni-filtered $Cu_{K\alpha}$ radiation ($\lambda = 1.5418$ Å) set at 40 kv and 16 mA. A Neir-type mass spectrometer at the Pennsylvania State University was used for the carbon and oxygen isotope analyses (Deines 1967, 1970b). An IBM System/360 computer at the Pennsylvania State University Computer Center facilitated the reduction of the analytical data. Generally, the isotopic composition measurements for the solid carbonate samples were found to have a precision of approximately ±0.15‰. Thin sections of selected samples were studied for petrographic information concerning the distribution of carbonate in the matrix, the nature of carbonate inclusions/xenocrysts, and their classification into textural-mineralogical groups. The carbon isotope ratio ($^{13}C/^{12}C$) is reported in permil (‰) delta (δ) notation versus the PDB standard; the oxygen ratio ($^{18}O/^{16}O$) is reported in permil delta notation versus the SMOW standard.

Results

Petrographic Analysis

The dominant phase of kimberlite carbonate was determined by X-ray diffraction methods to be

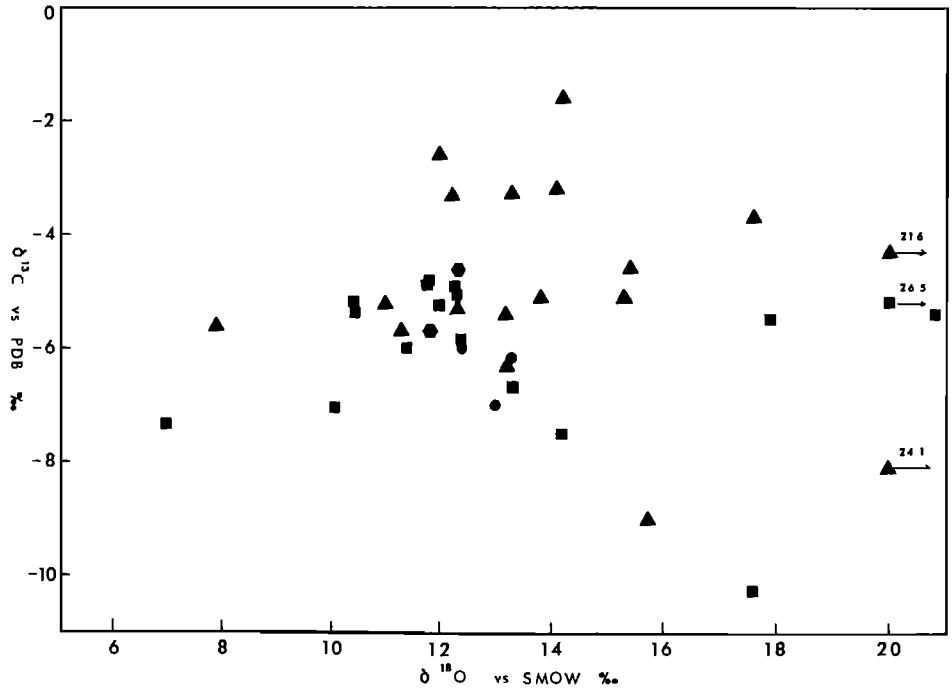

Fig. 2. The isotopic composition of kimberlite carbonates from South African localities. Symbols represent: ● = Baertschi, 1957, ▲ = Deines and Gold, 1973, ■ = Sheppard and Dawson, 1975, ● = Suwa et al., 1975.

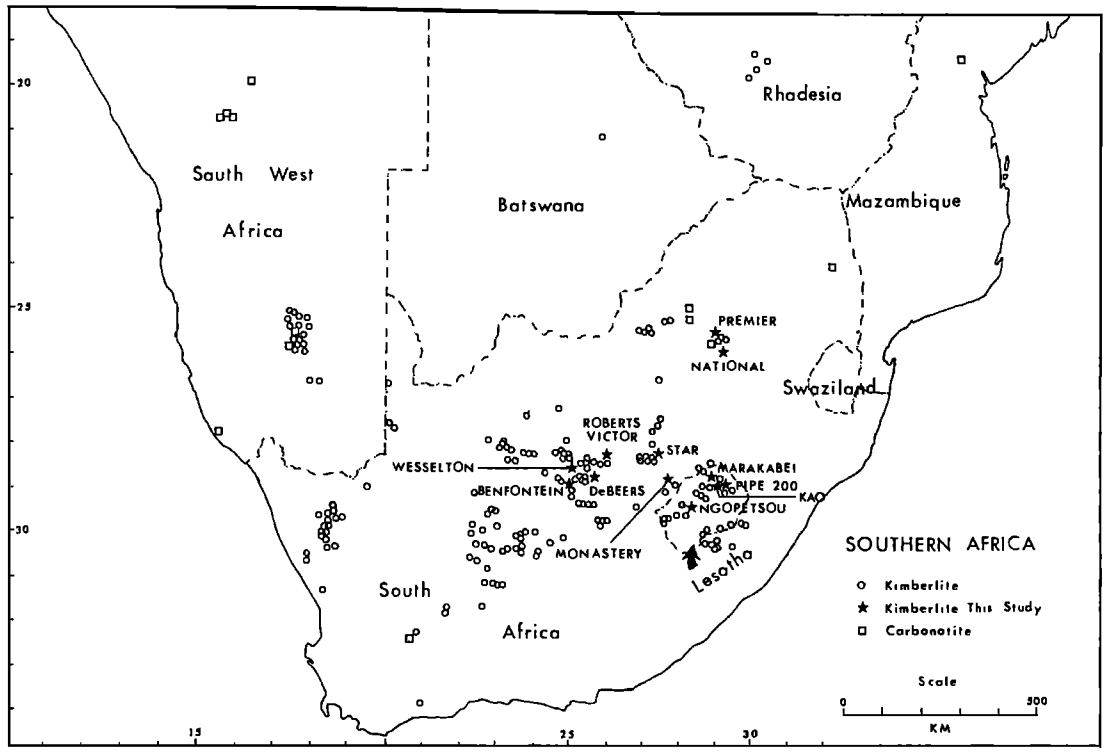

Fig. 3. The distribution of kimberlites and carbonatites in Southern Africa.

calcite. Dolomite was detected as a minor carbonate phase in the Benfontein sill and the DeBeers pipe. In addition to the X-ray mineral identification, other parameters such as hand specimen and thin section petrography, and field relationships were used to classify the samples of this study into three groups; massive, carbonatite-like, and fragmental.

The first group (42 samples), or type 1, is termed massive kimberlite. This type is inferred to be emplaced non-violently or by a slow eruptive process (Hawthorne, 1968), to account for the lack of a fragmental or brecciated phase (Frantsesson, 1970; Dawson, 1971). Rounded phenocrysts of olivine and serpentinized olivine, pyrope garnet, ilmenite, magnetite, and pyroxenes are set in a characteristic dense, dark matrix, which may appear aphanitic even under high magnifications. The matrix is composed of minute grains of olivine, serpentine, ilmenite, small fibrous aggregates of phlogopite, and carbonate. The carbonate may occur in one or more of the following habits: (1) distinct carbonate inclusions and ocelli, (2) acicular and/or dendritic crystals, (3) fine-grained anhedral carbonate disseminated in the matrix, and (4) carbonate pseudomorphs, generally after olivine. Massive kimberlite may include both basaltic and micaceous varieties of other workers (e.g., Dawson, 1967a and b).

The second group (23 samples), or type 2, consists of specimens of carbonatitic kimberlite dikes that are believed to have been emplaced either late in the intrusive process or in a separate event (Robinson, 1975) tapping the residual liquid of a kimberlite magma. Generally pale grey in color and medium to fine-grained in texture, these rocks are composed mainly (up to 60%) of anhedral calcite crystals, with minor amounts of interstitial fibrous serpentine. Magnetite and ilmenite are disseminated in the calcite, and rare flakes of phlogopite occur as an accessory mineral. This type 2 group also includes the metasomatized and carbonatized kimberlite adjacent to the dike, such as the 'Piebald kimberlite' type at Premier Mine (Clements et al., 1973).

The third group, or type 3, constitutes the bulk of the samples (77) of this study. They are termed fragmental kimberlite because of their heterogeneous nature and breccia-like appearance in hand specimen. In some pipes (e.g., Premier Mine) fragmental kimberlite is present with other kimberlite types, in others (e.g., Benfontein sills) it is absent (Hawthorne, 1968). Phenocrysts of rounded olivine, serpentinized olivine pyroxene, pyrope garnet, together with fragments of country rocks occur in a dense matrix of serpentine, phlogopite, and carbonate. Lapilli of earlier generation kimberlite are an important but rare autolithic

component. The carbonate may occur as angular fragments (inclusions), rounded nodules (cognate? xenoliths), small crystalline aggregates, and as finely dispersed grains in the matrix.

Isotopic Analysis

The results are plotted by geographic locality in $\delta^{13}C/\delta^{18}O$ coordinate space (see Fig. 4). The carbon values are more variable than has been reported previously (cf., Fig. 2). The average carbon and oxygen isotopic compositions of the kimberlite bodies are summarized in Table 1 under titles of matrix, inclusions, and the total (weighted mean). Figure 5 is a $\delta^{13}C$ versus $\delta^{18}O$ plot of the mean carbon and oxygen isotopic composition for each kimberlite location. The error bars in this figure are standard deviations from the mean values. Each location is numbered, except for the solid square and circle which represent respectively the mean isotopic composition of the carbonatite-kimberlite dikes (type 2) and the fragmental kimberlite (type 3) from the Premier Mine pipe.

The mean carbon and oxygen isotopic compositions for the different types of kimberlite are presented in Table 2. The mean isotopic composition for 142 samples of kimberlitic carbonates from South Africa/Lesotho is $\delta^{13}C$ = -5.92‰, s = ±2.42, and $\delta^{18}O$ = 12.91‰, s = ±3.23. This mean carbon isotopic composition is compatible with a mantle origin of kimberlite and is similar to the mean $\delta^{13}C$ of carbonatites (-5.1‰, s = ±1.4) and diamonds (-5.8‰, s = ±1.8) (Deines and Gold, 1973). The mean $\delta^{18}O$ of the kimberlite carbonates of this study are enriched in ^{18}O compared to primary igneous carbonatites (Deines and Gold, 1973).

Statistical Analysis of the Data

Introduction

A compilation of the carbon and oxygen isotopic data of kimberlite carbonates from southern Africa reveals a considerable range for these values ($\delta^{13}C$ from +0.24‰ to -11.76‰ and $\delta^{18}O$ from 6.62‰ to 23.93‰). For most kimberlite bodies the range of $\delta^{13}C$ and $\delta^{18}O$ values tend to overlap. Some localities have a limited isotopic range, but this may be due to a limited sample size. Figure 6 depicts the overlap of the carbon isotopic composition for kimberlites of this investigation by location and type, matrix or inclusion carbonate, and includes for comparison the $\delta^{13}C$ range for carbonatites and diamonds.

Although the analytical reproducibility of isotope analysis is extremely good (approximately ±0.15‰) single determinations and even sub-

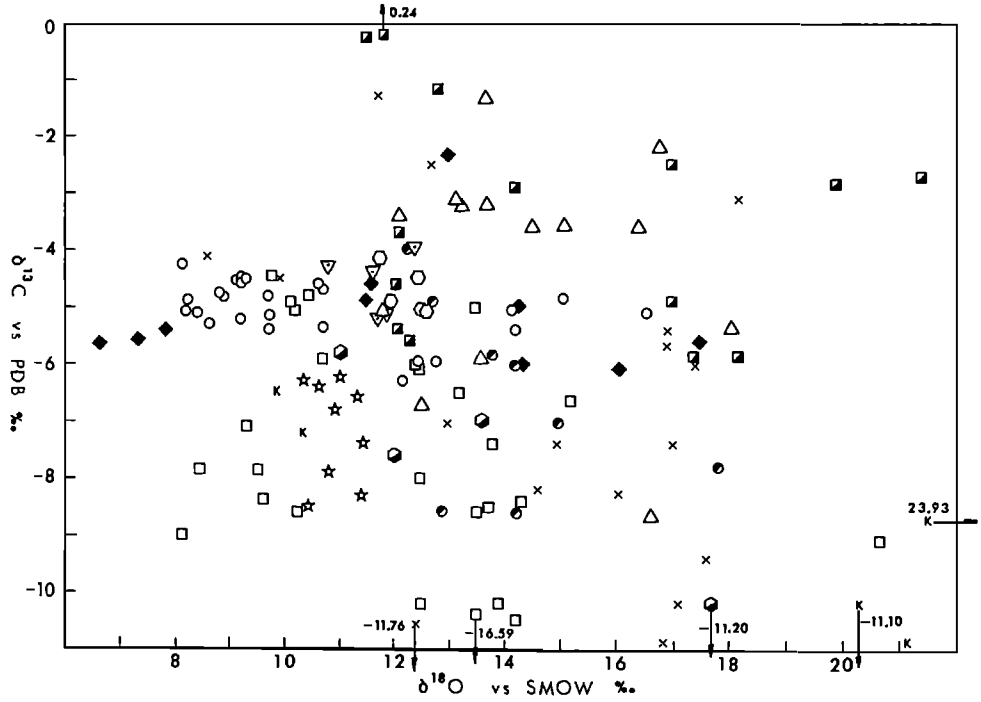

Fig. 4. Isotopic composition of South African and Lesothan kimberlite carbonates of this investigation. Symbols are for localities and represent : ○ = Benfontein Sill, × = DeBeers Mine, ◆ = Wesselton, △ = Monastery Mine, ◪ = National, □ = Premier, ▽ = Ngopetsou, ☆ = Star Mine, ◐ = Pipe 200, K = Kao, ● = Marakabei, ◑ = Roberts Victor.

TABLE 1. Mean Carbon and Oxygen Isotopic Composition of Kimberlites.

	Location	Matrix	Inclusion	Total
$\delta^{13}C$ vs PDB	Benfontein Sill	-5.21 ±0.54 (13)	-4.91 ±0.38 (12)	-5.07 ±0.48 (25)
(°/oo)	DeBeers Pipe	-5.99 ±2.29 (7)	-7.11 ±3.45 (10)	-6.65 ±3.00 (17)
	Wesselton Pipe	-4.88 ±1.32 (6)	-5.44 ±0.65 (4)	-5.12 ±1.10 (10)
	Monastery Pipe	-4.50 ±2.30 (6)	-4.03 ±1.73 (8)	-4.23 ±1.92 (14)
	National Pipe	-4.41 ±1.17 (5)	-2.90 ±2.29 (9)	-3.44 ±2.05 (14)
	Premier Pipe	-7.18 ±1.86 (18)	-9.10 ±3.37 (8)	-7.77 ±2.52 (26)
	Ngopetsou Blow	-4.60 ±0.41 (3)	-4.59 ±0.86 (2)	-4.59 ±0.52 (5)
	Star Mine	-7.61 ±0.80 (6)	-6.33 ±0.04 (3)	-7.18 ±0.90 (9)
	Pipe 200	-6.84 ±1.51 (5)	-6.22 ±2.29 (3)	-6.61 ±1.71 (8)
	Kao Pipes	-8.89 ±2.09 (5)	-	-8.89 ±2.09 (5)
	Marakabei Dike	-4.74 ±0.41 (5)	-	-4.74 ±0.41 (5)
	Roberts Victor	-6.81 ±0.89 (3)	-11.20 (1)	-7.91 ±2.31 (4)
$\delta^{18}O$ vs SMOW	Benfontein Sill	11.62 ±2.86	9.42 ±0.92	10.56 ±2.39
(°/oo)	DeBeers Pipe	12.82 ±2.72	16.22 ±2.23	14.82 ±2.93
	Wesselton Pipe	10.62 ±4.21	13.98 ±1.85	11.97 ±3.74
	Monastery Pipe	16.26 ±1.29	12.96 ±0.72	14.37 ±1.94
	National Pipe	13.70 ±3.47	15,70 ±3.31	14.98 ±3.38
	Premier Pipe	11.38 ±2.11	13.87 ±3.14	12.14 ±2.68
	Ngopetsou Blow	11.40 ±0.51	12.09 ±0.46	11.68 ±0.57
	Star Mine	11.04 ±0.38	10.66 ±0.32	10.91 ±0.39
	Pipe 200	14.71 ±1.95	13.14 ±1.02	14.12 ±1.77
	Kao Pipes	17.10 ±6.56	-	17.10 ±6.56
	Marakabei Dike	12.23 ±0.39	-	12.23 ±0.39
	Roberts Victor	12.23 ±1.31	17.74	13.61 ±2.95

samples cannot be used as reliable criteria for distinguishing kimberlitic types. Many analyses are necessary, and it is essential to treat the results statistically. Several statistical procedures were utilized to determine (1) the frequency distribution and normality of the isotopic data, (2) the significance of $\delta^{13}C$ and $\delta^{18}O$ values respectively for geologic categories and geographic location (emplacement level), (3) the within sample variation.

Analysis of the Carbon Isotope Data

^{13}C Distribution. Frequency distribution plots (histograms), means ($\bar{x}$), standard deviations (s), skewness ($\sqrt{b1}$, and kurtosis (b2), and tests for the normality of the data distribution were calculated using a NORMSTAT computer program available as a library program from the Pennsylvania State University Computer Center. These statistics, summarized in Table 3 and the frequency distributions (Figs. 7 & 9) of the various kimberlite groups are not significantly different from normal i.e., $\sqrt{b1}$ = 0, and b2 = 3, when tested against their appropriate standard error (Pearson and Hartley, 1954). The histogram of all $\delta^{13}C$ data (Fig. 7) shows an approximately normal distribution, with the class intervals of highest frequency limited to a small $\delta^{13}C$ range.

The dolomite samples trend towards heavier carbon isotopic values. The histograms for matrix and inclusion categories (Fig. 8) test normal even though they appear bimodal. However, it is expected that these distributions will appear normal if a larger class interval in the NORMSTAT program were used. The $\delta^{13}C$ values for kimberlite carbonates by petrographic/geologic criteria are given as the histogram plots of Figure 9.

Analysis of Variance by Geologic Type. It is apparent from Figure 5 that the mean carbon isotopic composition of kimberlite carbonates varies with location. For a comparison between geographic locations to have validity, only the carbon isotopic compositions for similar kimberlite geologic types should be considered. The distinction of the kimberlite samples of this study into three general petrographic/geologic types suggests one test for discrimination. A comparison of kimberlite samples by location cannot be undertaken unless significant differences do not exist between these types. Generally, the mean $\delta^{13}C$ values of massive kimberlite (-5.41 ‰) and fragmental kimberlite (-5.67 ‰) appear to be different from the mean $\delta^{13}C$ value of the carbonatite-kimberlite (-7.42‰) at locations where both are sampled.

An analysis of variance procedure becomes appropriate when comparing the means of more than two sets of data. Analysis of Variance (ANOVES) comprises the division of the total variation

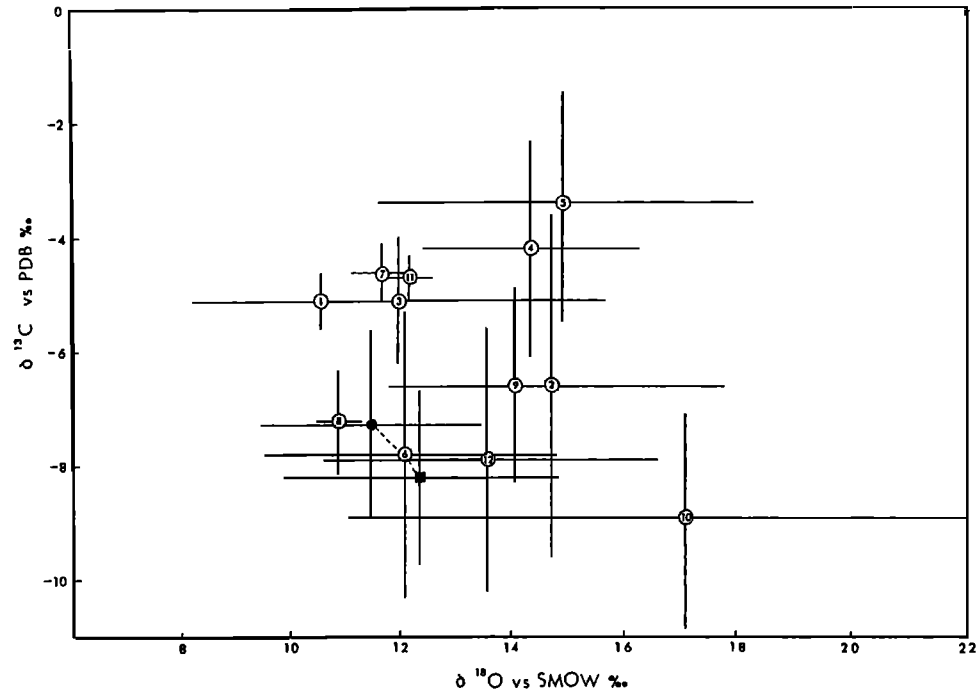

Fig. 5. The mean isotopic composition for kimberlite carbonates by location. Numbers within circles represent: 1 = Benfontein Sill, 2 = DeBeers Mine, 3 = Wesselton, 4 = Monastery Mine, 5 = National, 6 = Premier Mine, 7 = Ngopetsou, 8 = Star Mine, 9 = Pipe 200, 10 = Kao, 11 = Marakabei, 12 = Roberts Victor.

into parts which can be assigned to the sources making up the variation (Griffiths, 1967). The test of significance is an F test; and if the means for the sets of data vary more than the observations within a set, their calculated variance ratio (F) will exceed the tabulated value of F and the null hypothesis is rejected at an appropriate level of significance (op. cit.). The analyses for the $\delta^{13}C$ data were calculated by an ANOVES/ANOVUM computer program provided by the Pennsylvania State University Computer Center. Where observations for a particular sample group or cell are equal, or if there is one factor of variation, the ANOVES program is used; while unequal cell frequencies are treated by the ANOVUM program. ANOVUM handles unequal cells by the unweighted means technique. Every cell total calculated is replaced by the mean for that cell and the number of observations is set to one. The Analysis of Variance is then performed on this adjusted data (Kahn, 1954).

A comparison was made for the three geologic kimberlite types, the nature of carbonate within hand samples (matrix, inclusion), and the interaction of the geologic type and nature of carbonate. The results of an example of ANOVUM analysis is summarized in Table 4. These results indicate that a significant difference exists among the means of the three types of kimberlites when they are compared. The calculated F ratio of 8.20 is significant at the 1% probability

TABLE 2. Mean Isotopic Composition of Kimberlites by Geologic Type (this study).

Item		Matrix	Inclusion	Total
$\delta^{13}C$ (°/oo)	Type 1	-5.67 ± 1.46(29)	-4.84 ± 0.44(13)	-5.41 ± 1.29(42)
	Type 2	-7.09 ± 2.19(15)	-7.58 ± 1.17(7)	-7.24 ± 3.64(22)
	Type 3	-6.01 ± 2.08(38)	-5.38 ± 3.00(39)	-5.67 ± 2.59(77)
$\delta^{18}O$ (°/oo)	Type 1	11.98 ± 2.11	9.64 ± 1.18	11.26 ± 2.16
	Type 2	11.73 ± 2.30	14.33 ± 3.59	12.56 ± 2.96
	Type 3	13.40 ± 4.40	14.39 ± 2.68	13.90 ± 3.43

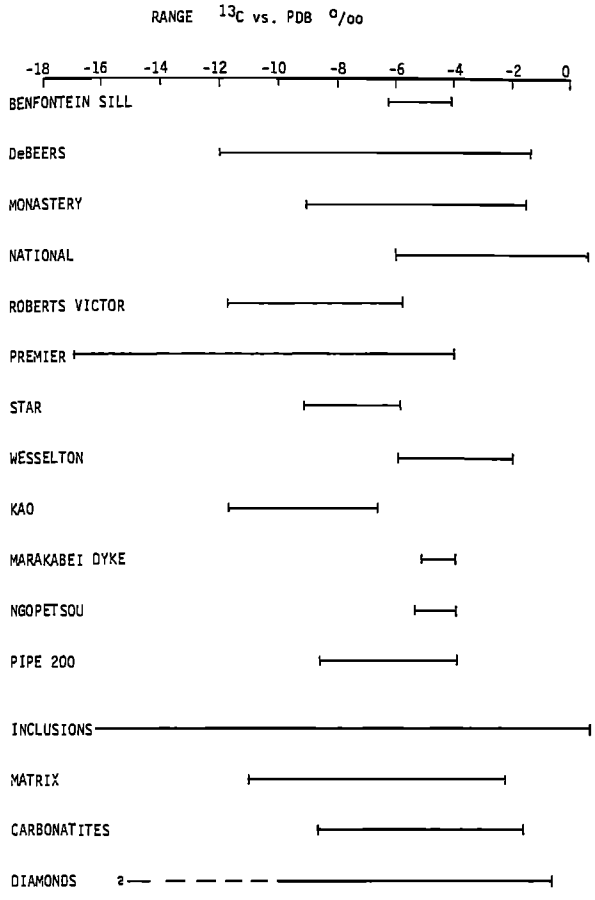

Fig. 6. The overlap of the carbon isotopic composition for kimberlite carbonates from the kimberlite localities of this study. Data for carbonatites and diamonds were compiled by Deines and Gold (1973) from various works.

level (F_{01} = 4.75). In order to determine which kimberlite type mean contributed the greatest part of this significance, subsequent computer analyses were performed. The comparisons of each kimberlite geologic type by an ANOVES F ratio test are given in Table 5. The large F ratios involving the comparisons of type 2 kimberlite (carbonatite-kimberlite) indicate it is of a distinctly different carbon isotopic composition than either type 1 or 3 kimberlites. Type 1 and type 3 kimberlites, however, are alike with respect to $\delta^{13}C$. The analysis of Table 4 also compared the mean $\delta^{13}C$ values of the nature of carbonate, and it appears that matrix and inclusion carbonates within a given kimberlite geologic type are not significantly different with respect to their carbon isotopic composition (F = 0.562).

Analysis of Variance by Kimberlite Location

The $\delta^{13}C$ data was compared, using the ANOVUM procedure, to see if the average carbon isotopic composition of the different petrographic/geologic types varied with geographic location or elevation. Because the type 2 kimberlite represents a very restricted group of carbonatite-like dikes that yield a distinctly different $\delta^{13}C$ values from the types 1 (massive) and 3 (fragmental) kimberlites, they were excluded from the analysis. Thus only types 1 and 3 kimberlite specimens were used from the nine best sampled kimberlite bodies.

Statistics from a NORMSTAT program suggest that these samples are normally distributed. The Analysis of Variance by the ANOVUM program indicates that there are significant differences between kimberlite locations with respect to their mean isotopic composition. The calculated F ratio of 6.10 is significant at the 1% probability level (F_{01} = 2.72).

Summary

1) A range exists in the $\delta^{13}C$ of kimberlite carbonates from Southern Africa with the mean value being $\delta^{13}C$ = -5.84‰ , s = ±2.25 (141 samples).

2) Normal frequency distributions occur for the groups determined by kimberlite geology and petrography, and by the nature of carbonate material (matrix and inclusions).

3) The dolomite samples appear enriched in ^{13}C compared to calcite samples at the Benfontein Sill. This will be discussed in a later section.

4) The values of $\delta^{13}C$ from type 2 carbonatite-kimberlites (-7.24‰) at several locations appear isotopically distinct when compared to the mean $\delta^{13}C$ of type 1 (-5.41 ‰) and type 3 (-5.67‰) kimberlites.

5) Type 1 (massive) and type 3 (fragmental)

TABLE 3. Summary Statistics for the Carbon Isotopic Data.

Item (n)	$\bar{x}$	s	$\sqrt{b1}$	b2	χ^2 (d.f.)	$P(\chi^2)$
All samples (141)	-5.84	± 2.25	-0.262	3.29	36.88 (16)*	.0022
Matrix (82)	-6.08	± 1.95	-0.435	2.81	28.96 (14)	.0110
Inclusion (59)	-5.50	± 2.59	-0.329	3.28	22.48 (12)	.0324
Type 1 (42)	-5.41	± 1.29	-0.938*	4.15*	29.61 (12)*	.0032
Type 2 (22)	-7.24	± 1.91	-0.684	3.20	9.09 (8)	.3349
Type 3 (77)	-5.67	± 1.59	-0.301	3.01	16.92 (14)	.2603

* Significant when tested against the appropriate standard error at the 1% probability level.

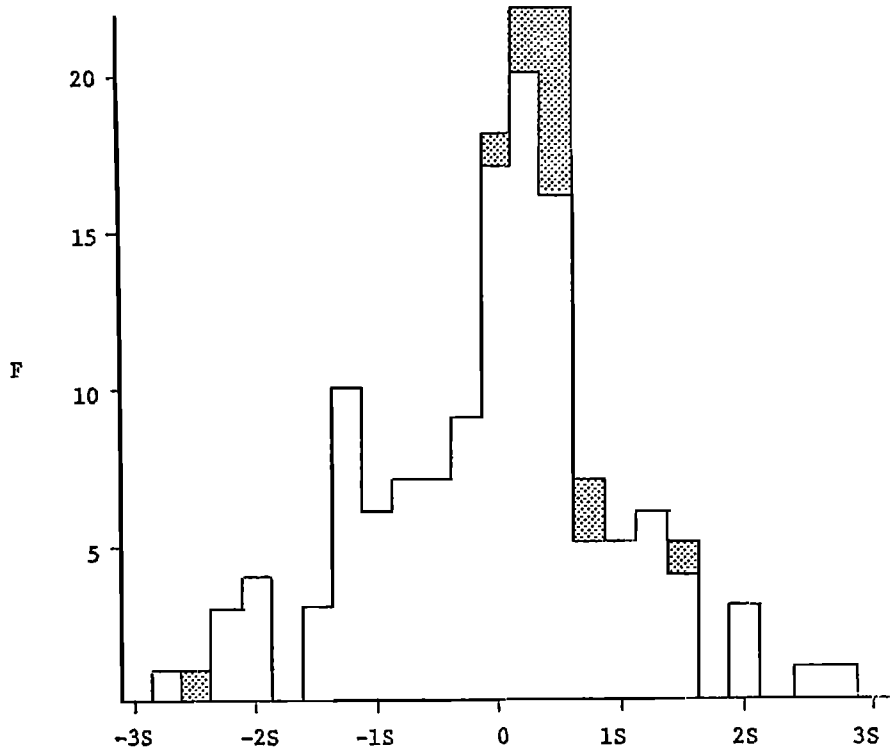

Fig. 7. Histogram of the carbon isotopic compositions of kimberlite carbonates from this study. The dotted area indicates dolomite samples, the remaining area-calcite samples.

kimberlites are alike with respect to their carbon isotopic compositions. But no significant difference between the mean $\delta^{13}C$ of matrix and inclusion carbonate appears to exist.

6) By deleting the type 2 kimberlite from the total distribution, a normal distribution for type 1 plus 3 kimberlite $\delta^{13}C$ data from nine well sampled kimberlites is found. There is a significant difference statistically of the mean $\delta^{13}C$ values from these kimberlites when compared by geographic location. For example, the mean carbon isotopic composition of the National Pipe ($\delta^{13}C$ = -3.44% , s = ±2.05 is distinct from the Kao kimberlite ($\delta^{13}C$ = -8.89%, s = ±2.09).

Analysis of Oxygen Isotopic Data

The values of the $\delta^{18}O$ data from the kimberlite carbonates studied range from 6%. to 24%., a variation much greater than encountered with the $\delta^{13}C$ data. Frequency distributions constructed from various $\delta^{18}O$ parameters are shown in Figures 10 to 12. For several groupings of $\delta^{18}O$ data, the statistical tests for normality (particularly $\sqrt{b1}$ and b2) using the NORMSTAT program, exceeded the calculated values of their appropriate standard (Arkin and Colton, 1966). Therefore caution must be exercised in the analysis and interpretation of the $\delta^{18}O$ data.

From the summary statistics given in Table 6, it is noted that although the mean $\delta^{18}O$ values are distinctive, their standard deviations are large and there is considerable overlap.

An Analysis of Variance using the ANOVUM program was initially run to test for possible correlations in oxygen isotopic composition with geologic kimberlite type. This program is similar to that used for analysis of the $\delta^{13}C$ data, but the results summarized in Table 7 yielded a much larger error term. The F ratio test showed the significance of the geologic type of kimberlite, and more importantly the significance of an interaction between geologic type and the nature of carbonate. Because this interaction is significant, no determinations can be conclusive. Some source of variation is contributing more to the total variation than the error source of variation. By then assuming that this interaction term is the error for testing the main effects of variation, a calculated F ratio of 1.592 was found to be not significant, that is, the geologic type means are not varying more than the interaction; which is disquieting as the interaction is large.

The significance of geographic location was tested by ANOVUM for possible effects on the $\delta^{18}O$ variation. The type 2 kimberlites were deleted from the distribution and data from the

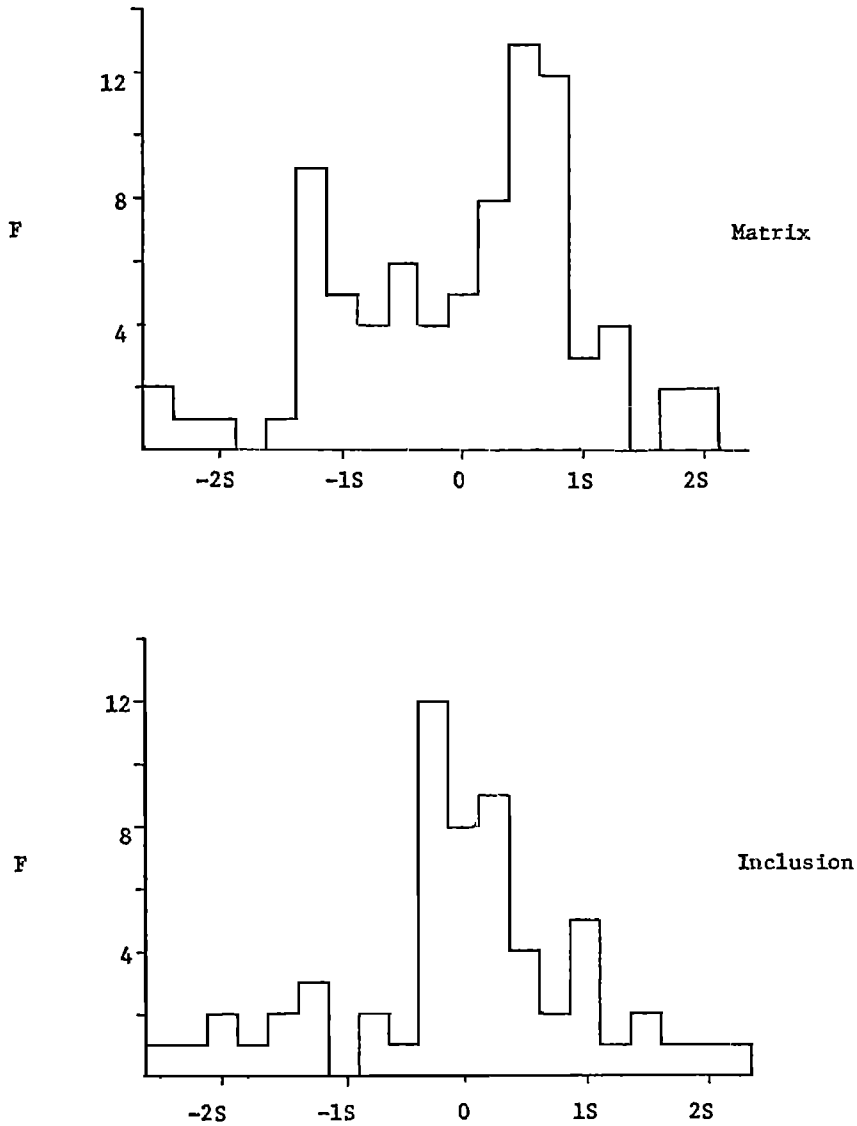

Fig. 8. Histograms of the carbon isotopic composition of matrix and inclusion corbonate from kimberlites in this study.

nine best sampled localities were utilized. The summary table (Table 8) reveals that geographic location is a significant factor when comparing mean $\delta^{18}O$ values of the nine kimberlites. The emplacement level of kimberlite pipes and sills may be reflected by this location factor.

Summary

1) The total $\delta^{18}O$ variation for kimberlite carbonates is large; mean $\delta^{18}O$ = 12.90‰, s = ±3.23 (141 samples).

2) Analysis of variance procedures for $\delta^{18}O$ data indicate that; a) conclusive results cannot be obtained when considering the data by geologic type of kimberlite, and b) the geographic location of the kimberlite, possibly reflecting level of emplacement, is a significant factor when comparing mean $\delta^{18}O$ values.

3) The results obtained by these methods should be interpreted with caution as error terms are large, and the histogram plots and some tests for normality do not support a normal population distribution.

Calcite-Dolomite Relationships

Previously, it had been noted that the frequency distribution of all carbon isotopic compositions (Fig. 7) indicated that the dolomite samples trend towards heavier $\delta^{13}C$ values compared to the calcites. This ^{13}C enrichment in dolomites is a characteristic of many carbonatites (Deines,

1970a), and it appears to be true for kimberlites as well. Table 9 summarizing the $\delta^{13}C$ and $\delta^{18}O$ of coexisting calcites and dolomites at the Benfontein Sill.

In order to determine if these isotopic differences were statistically significant, a small sample t-test was run (Griffiths, 1967). A t-value of 4.28 on 23 degrees of freedom was calculated for the $\delta^{13}C$ data. As $t_{01} = 2.81$ (Arkin and Colton, 1966), this test indicates that there is less than one chance in 100 that such a value is due to chance. Apparently the observed enrichment of $\delta^{13}C$ in the dolomitic kimberlite carbonate samples is statistically valid for the Benfontein Sill. Some process has caused the concentration of $\delta^{13}C$ in the dolomite samples relative to the calcites. The carbonates at the Benfontein Sill are regarded as primary minerals (Hawthorne, 1968). It is envisioned that such a preferential enrichment of $\delta^{13}C$ in the dolomites occurred before or during the crystallization of the coexisting calcites.

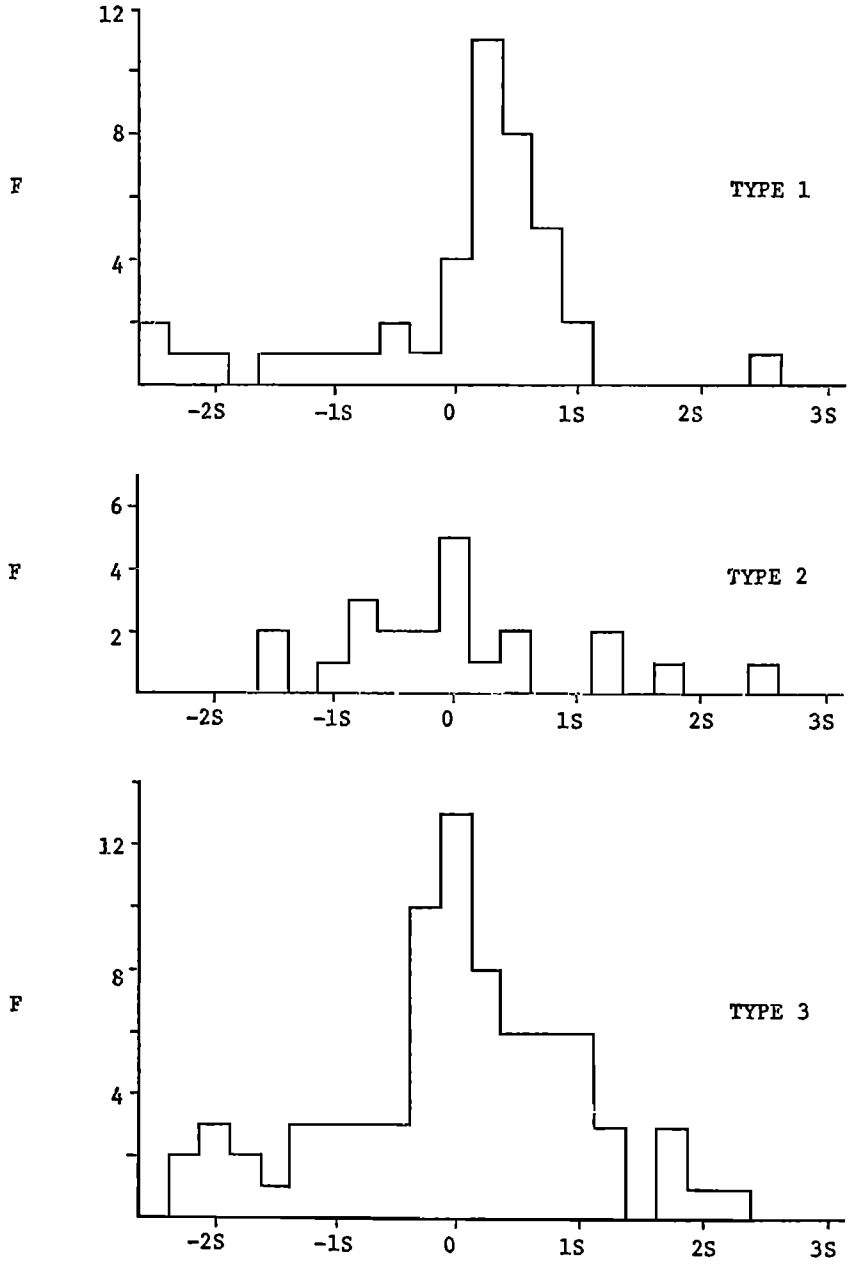

Fig. 9. Histograms of the carbon isotopic composition of the three types of kimberlite classified in this study.

TABLE 4. Analysis of Variance Summary Table for $\delta^{13}C$ Data by Geologic/Petrographic Type Kimberlite.

Source of Variation	Degrees of Freedom	Sum of Squares	Mean Square	F Ratio	F_{01}
Three Geologic Types of Kimberlite	2	77.773	38.886	8.20 **	4.75
Nature of the Carbonate (Matrix or Inclusion)	1	2.667	2.667	0.56 NS	6.81
Geology by Nature Interaction	2	8.229	4.115	0.87 NS	4.75
Error	135	640.292	4.743		
Total Sum of Squares	5518				
Correction Term	3578				
Corrected Total Sum of Squares	5296				

** Significance at 1% probability level
NS No significance at 1% probability level

A calculated t-value of 0.44 on 23 degrees of freedom for the $\delta^{18}O$ data ($t_{50} = 0.685$) from the carbonates at the Benfontein Sill indicates that the observed difference of the oxygen isotopic composition between calcites and dolomites is not significant. The only other kimberlite with calcite-dolomite pairs occurred at the DeBeers Mine, but the analyses (2) were too few for serious consideration. The dolomite of sample DB 1-a was enriched in ^{13}C by 1.55% compared to coexisting calcite, but dolomite in sample DB 2a was depleted in ^{13}C by 1.50% compared to its calcite pair. None of the other kimberlite samples studied contained carbonate pairs.

Petrographic Considerations and Isotopic Compositions

There is no guarantee that the correct factors have been chosen for the statistical tests. This short-coming is not due to inefficiency of the statistical approach as much as to the inexperience of geologists/petrologists in understanding non-equilibrium systems such as kimberlites. Even in a single hand specimen large isotopic variations can exist between different parts of the matrix and the inclusions (Deines, 1968), and equilibrium assemblages may be present only in small domains within the kimberlite body. To some extent the difficulty of addressing the problem of the kimberlite matrix is reflected by the disproportionate amount of study on the xenoliths, xenocrysts, and discrete nodules.

Table 5. ANOVES Comparison of $\delta^{13}C$ Values.

Comparison of Types	n	d.f.	F 01	F Ratio Calculated
1 vs. 2	64	62	7.080	23.09 **
2 vs. 3	89	87	6.900	8.13 **
1 vs. 3	119	117	6.840	0.62 NS

** Significant 1% probability level, NS = not significant

A number of hand specimens (27) were selected for detailed petrographic study and sampling in domains as small as 2-3 mm across. Although ANOVES/ANOVUM procedures considered only two morphological natures of carbonate (matrix and inclusions), additional petrographic distinctions can be made (e.g., replacement carbonate, ocelli, cognate xenoliths, veins, dikes, inclusions, etc.). Some of the carbon and oxygen isotopic variations can be rationalized to processes within these smaller petrographic domains.

1) First, it should be realized that although the analysis of variance indicates no significant difference among mean $\delta^{13}C$ and $\delta^{18}O$ values for matrix and inclusion samples, the isotopic variation within a hand specimen may be large, e.g. the matrix in DeBeers sample DB-2-a has a $\delta^{13}C = -4.48\%$, $\delta^{18}O = 9.92\%$ and an inclusion a $\delta^{13}C = -10.21\%$, $\delta^{18}O = 17.71\%$. Obviously these two subsamples of DB-2-a have distinct isotopic compositions, and each may represent a different isotopic reservoir. Alteration zoning in the inclusion, and its angular form suggest it is crustal carbonate (sedimentary ?) incorporated during kimberlite emplacement.

2) Carbonate nodules, such as those from the Monastery Mine (Mon 16-b, Mon 17, Mon 18), DeBeers (7-b), Ngopetsou (Ngo 2, Ngo 6), and Premier Mine (Pr 3a) tend to be rounded and unzoned. These carbonates are interpreted as cognate xenoliths. Other well-formed carbonate crystals in the kimberlite matrix (Mon 16-a, Mon 19, Mon 20; DB 5a-b), most of which are coarse-grained, have been interpreted as primary constituents of the kimberlite (Whitelock, 1973; Clement 1973, 1975). The $\delta^{13}C$ values of these inclusions are in close accord with the $\delta^{13}C$ of the surrounding matrix carbonate, with differences between the subsamples usually less than 1% . The $\delta^{18}O$ values of these inclusions are slightly more variable.

3) Some carbonates appear milky or translucent even in thin section and may be interpreted as

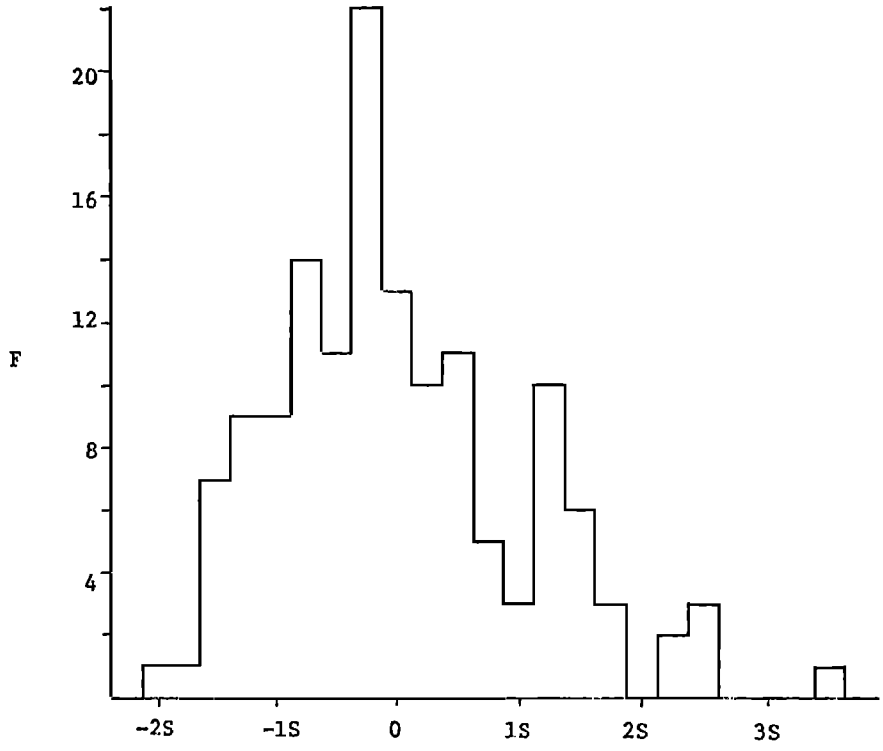

Fig. 10. Histogram of the oxygen isotopic composition of kimberlite carbonates from this study.

xenocrysts because; a) they seldom exhibit crystal form, b) they may appear fragmental or subangular indicating some disruptive mode of transport, and c) they usually feature reaction rims indicating partial metasomatism by the surrounding kimberlite matrix. The xenocryst carbonates from the National Pipe (Nat 1-a, Nat 1-b, Nat 1-c) are heavier in $\delta^{13}C$ not only to surrounding matrix carbonate in hand sample, but also to other kimberlitic material studied in this investigation. Nat 1-c (3) with a $\delta^{13}C$ = +0.24% is isotopically heavy compared to its matrix, $\delta^{13}C$ = -4.59% . The $\delta^{18}O$ values of these inclusions is highly variable. Possible interaction with substances of distinctly different isotopic compositions is suspected. This type of isotopic variation suggests that late fluids responsible for the serpentinization of the matrix were isotopically light compared to the material that was responsible for the xenocrysts.

4) The carbonate ocelli, diapiric ocelli, and the carbonate layer near the top of the lower Benfontein Sill have been interpreted as the products of an immiscible carbonate liquid in the silicate + CO_2 kimberlite melt (Hawthorne, 1968; Clement et al., 1973). The $\delta^{13}C$ analyses of subsamples in Ben 6-b and Ben 6-c show a less than 0.5 % difference between this ocelli material and the kimberlite matrix. Isotopic equilibrium is suggested by this finding. The maximum $\delta^{18}O$ variations within and between hand samples are respectively less than 2 or 3% .

5) The carbonate replacement of a number of primary kimberlite minerals (olivine, enstatite) may occur; a) during the crystallization of initial kimberlite, b) immediately after kimberlite emplacement by hydrothermal fluids, or c) at a later time by ground water precipitation of carbonate (Clement, 1973, 1975; Sheppard and Dawson, 1975). Examples of carbonate replacement of olivine are found in DB 2-a, Pipe 200 12, Pr 3-b, Wes 5a, and Wes 10. The original form of the olivine is preserved and an alteration halo of serpentine, chlorite, and carbonate surrounds the coarse carbonate pseudomorphs. A carbonate replacement rim of an olivine in Pr 3-b (2) has a $\delta^{13}C$ of -16.59%., a value close to that of a fresh water limestone (Keith and Weber, 1964). Both the carbon and oxygen isotopic compositions of these replacement carbonates are highly variable and distinctive from the matrix carbonate.

6) Carbonates occurring as 'needles' in the Benfontein Sill samples have a mean $\delta^{13}C$ = -6% , about 1% lighter than the carbonate ocelli. However, this carbon isotopic composition supports the primary cyrstallizing mineral theory of Mal'kov (1975) for these quench crystals. But the mean $\delta^{18}O$ values for these carbonates is about 4%. heavier than the other primary forms of carbonate at Benfontein.

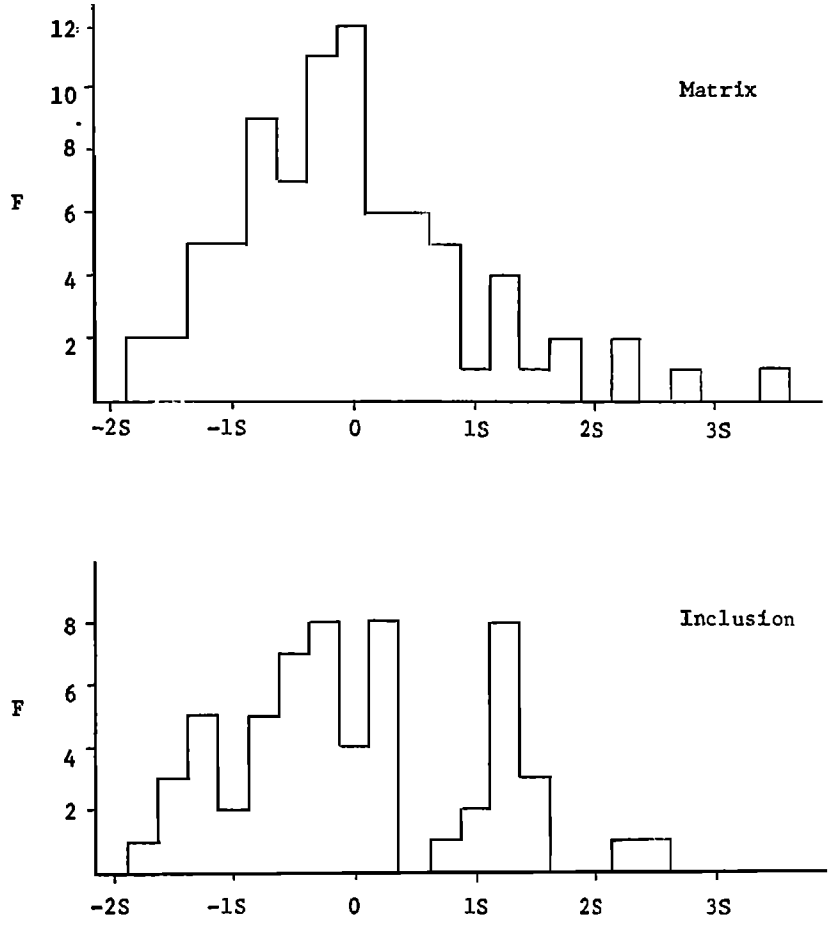

Fig. 11. Histograms of the oxygen isotopic composition of matrix and inclusion carbonates from kimberlites in this study.

7) Pisolitic kimberlite samples from the Scar Mine are of interest because they indicate two generations of crystallization products. Rounded pisolites of previously consolidated kimberlite have been formed by a subsequent fluidization phase of a calcite-rich fluid. Surprisingly, the $\delta^{13}C$ and $\delta^{18}O$ values of the subsamples show the least variation of any hand sample studied in detail, and suggests that isotopic equilibrium was reached between the initial main phase kimberlite and the fluidization phase.

8) Generally, there is an indication that kimberlites termed 'micaceous' are lighter in their carbon isotopic composition than the 'basaltic' kimberlites. The average $\delta^{13}C$ of 13 Star Mine and Roberts Victor micaceous kimberlites is -7.40‰.

Discussion of the Results

Sampling Considerations

An Analysis of Variance procedure assumes that (a) each parent population is normal, (b) each parent population has a similar variance, and (c) each combination of treatments is a random sample from a homogeneous population (Davis, 1973). Although the first two conditions are satisfied, a problem exists with the third because of the difficulty of establishing what a random sample is in practice (Griffiths, 1967).

Variation of the Carbon and Oxygen Isotopic Composition

Introduction. The wide range of values for δ^{13} (+0.24‰ to -11.76‰) in kimberlite carbonates may be attributed to:

1) contamination from country rock, incorporated into the kimberlite during its ascent;

2) fractionation process(s) that may preferentially concentrate or remove ^{13}C;

3) inhomogeneous isotopic composition of the source material of the kimberlite magma.

Most values for the oxygen isotopic composition of kimberlite carbonates are enriched in $\delta^{18}O$ with respect to primary igneous carbonatites (Deines and Gold, 1973). Some of the following

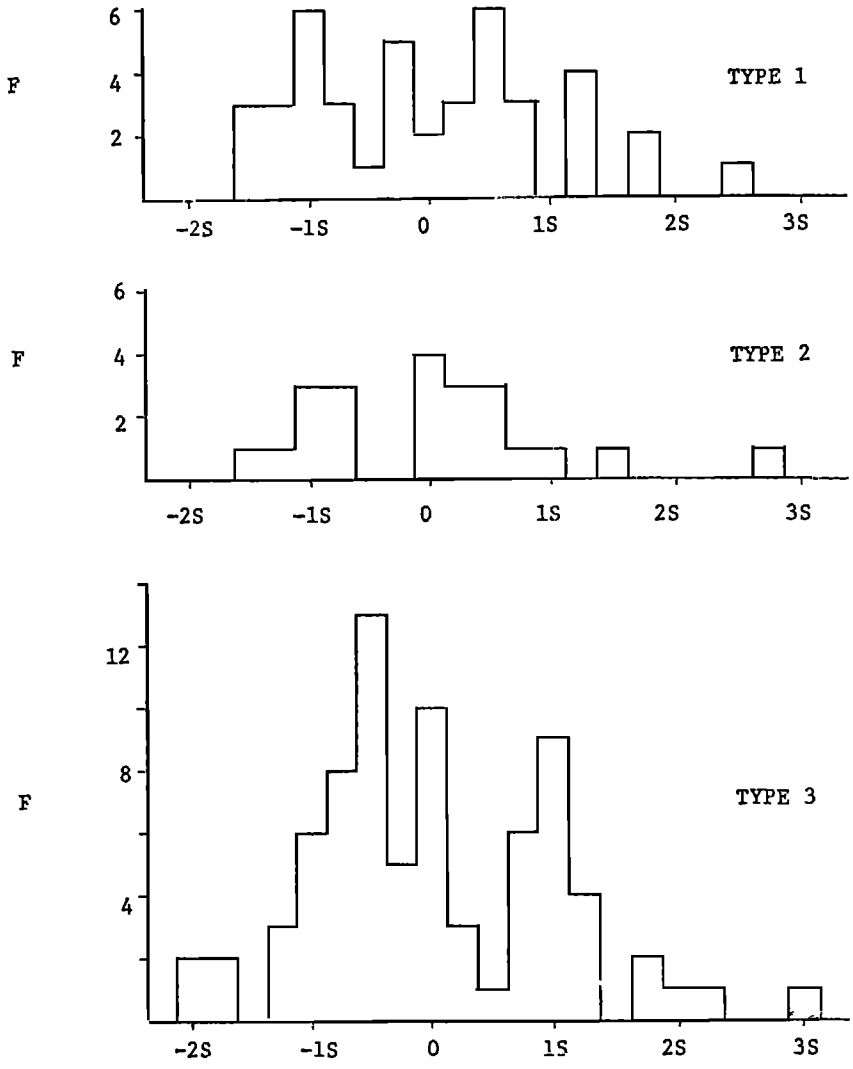

Fig. 12. Histograms of the oxygen isotopic composition of the 3 groups of kimberlite in this study.

factors may contribute to the range of between 10 -18% for $\delta^{18}O$ measured in this study:

1) loss of isotopically light water during the emplacement of the kimberlite (Deines and Gold, 1973);

2) influx of meteoric water (op. cit.);

3) meteoric-hydrothermal fluid interaction with the kimberlite during or after emplacement (Sheppard and Dawson, 1975). This fluid interaction may take greatest effect during the serpentinization process. A temperature from 50°C to 200°C, calculated from calcite-serpentine and calcite-phlogopite temperature dependent fractionation factors appear to be the best range for fluid interaction effects;

4) emplacement level of the kimberlite (Deines and Gold, 1973).

The similarity of the mean oxygen isotope ratios of ultramafic rocks (Taylor, 1968) suggest that the source areas in the mantle are homogeneous with regard to their oxygen isotope compositions.

Causes for the $\delta^{13}C$ & $\delta^{18}O$ Variations in Kimberlites. The type 2 kimberlites (carbonatite dikes) are isotopically lighter in $\delta^{13}C$ by approximately 2‰ compared to types 1 and 3 kimberlites. A possible cause is from assimilation or admixing of isotopically lighter country rock carbonates. The abundance or inclusions in some kimberlites indicates a mechanism, but the essenially cold emplacement and low reactivity of kimberlite magmas (Dawson, 1967a) are likely to produce heterogeneous mixtures with a greater range in isotope ratios than is indicated by our samples. In addition, it is doubtful that suff-

TABLE 6. Summary Statistics for the Oxygen Isotopic Data.

Item (n)	$\bar{x}$	s	$\sqrt{b1}$	b2	χ^2 (d.f.)	$P(\chi^2)$
All samples (141)	12.90 ±	3.23	0.706*	3.39	30.557 (16)	0.0153
Matrix (82)	12.59 ±	3.23	0.923*	4.24*	13.470 (14)	0.4900
Inclusion (59)	13.34 ±	3.20	0.436*	2.46*	27.786 (12)	0.0060
Type 1 (42)	11.26 ±	2.16	0.399	2.40*	20.980 (12)	0.0507
Type 2 (22)	12.56 ±	2.96	0.770	3.73	10.560 (8)	0.2280
Type 3 (77)	13.90 ±	3.43	0.435	2.99	25.600 (14)	0.0290

* Significant when tested against appropriate standard error at the 1% probability level.

icient isotopically light country rock could be incorporated into the carbonatite-kimberlite dikes to account for the observed $\delta^{13}C$ difference. The characteristic isotopic composition of the late carbonatite dikes in kimberlites of different terranes and age, suggests that the process(es) is more fundamental than chance contamination.

An alternate hypothesis involves some type(s) of isotopic fractionation process(es). The kimberlite magma has been regarded as a two phase system, where liquid immiscibility exists between a silicate + CO_2 component and a carbonatite ($CaCO_3$) transporting fluid (Clement, 1975). If theoretical computations of Bottinga (1969) are considered, the carbon in the CO_2 of the silicate phase of the kimberlite magma will be isotopically heavier by up to 3‰ than the later eruptive phase, the $CaCO_3$-rich carbonatite fluid. This would account for the observed differences in our data and some of the other $\delta^{13}C$ variations within these kimberlites.

It may be argued that the samples of type 2 carbonatite-kimberlite were collected from too few localities to warrant meaningful comparison with the other kimberlite types, and that any difference may be geographic. For Premier Mine samples a t-test comparison between fragmental kimberlite (-6.19‰ (7)) and carbonatitic kimberlite (-8.32‰ (17)) was found to be significant at the 1% probability level for a calculated t value of 2.84 on 22 degrees of freedom.

If a fractionation process is solely responsible for the carbon isotopic composition variation of kimberlite carbonates, one would expect that the initial kimberlite phase would be heaviest and the final phase lightest with respect to $\delta^{13}C$ in any kimberlite type. At Kao, the initial 'Quarry' kimberlite has a heavier $\delta^{13}C$ (-6.53‰) than the successive 'Fragmental' (-7.20‰) and 'Transitional' (-8.69‰) kimberlite phases. Of course, each value in this case represents only one sample and a more detailed study is needed to substantiate this finding. Also, at Pipe 200 the mean $\delta^{13}C$ of the initial kimberlite phase, -5.31‰ (3), is isotopically heavier than the subsequent eruptive phases of kimberlite (-7.60‰ (5)).

However, with available data no clear trends in the variation of $\delta^{18}O$ values by geologic type of kimberlite can be shown by a similar fractionation process. The $\delta^{18}O$ variation within the types and from location to location is too large for the number of samples analyzed for critical appraisal. Very large oxygen isotopic variation is found at the hand sampled level as well. One should also give consideration to the $\delta^{18}O$ variation as being caused by the crystallization of various minerals from the initial melt (kimberlitic?). The changes in carbon isotopic composition of the melt are determined by cryst-

TABLE 7. Analysis of Variance Summary Table for $\delta^{18}O$ Data by Geologic/Petrographic Type Kimberlite

Source of Variation	Degrees of Freedom	Sum of Squares	Mean Square	F Ratio	F_{01}
Three Geolgoic Types of Kimberlite	2	162.569	81.284	9.389 **	4.75
Nature of the Carbonate (Matrix or Inclusion	1	4.175	4.175	0.482 NS	6.81
Geology by Nature Interaction	2	102.132	51.066	5.900	4.75
Error	135	1168.798	8.658		
Total Sum of Squares	24942				
Correction Term	15278				
Corrected Total Sum of Squares	23993				

** Significance at 1% probability level
NS Not Significant

TABLE 8. Analysis of Variance Summary Table for $\delta^{18}O$ Type 1 Plus Type 3 Kimberlite by Geographic Location.

	Degrees of Freedom	Sum of Squares	Mean Square	F Ratio	F_{01}
Nine Kimberlite Locations	8	185.010	23.126	4.320 **	2.69
Nature of Carbonate (Matrix or Inclusion)	1	3.864	3.864	0.721 NS	6.90
Location by Nature Interaction	8	95.901	11.988	2.240 NS	2.69
Error	87	466.475	5.362		
Total Sum of Squares	18448				
Correction Term	11918				
Corrected Total Sum of Squares	15447				

** Significance at the 1% probability level
NS Not significant

allization of only one or two solid carbonate phases, while the changes in the oxygen isotopic composition of the melt are not only due to the crystallization of the carbonate phases, but silicates and oxides as well (Deines, 1970a).

The interaction of the kimberlite with meteoric, ground, and hydrothermal waters, and the loss of isotopically heavy $CO_2 + H_2O$ during the degassing process after emplacement can be a substantial cause of isotopic variation (Sheppard and Dawson, 1975). The petrographic study of the carbonate mineralogy of the hand samples indicates that late-stage carbonate replacement is evident. The composition of this carbonate appears isotopically distinct when compared to samples believed to represent primary carbonate material. This is particularly true for the oxygen isotopic compositions which are substantially heavier than the mean $\delta^{18}O$ of 12.91‰. If the oxygen isotopic compositions of these samples appear modified by late stage processes then there is reason to expect that the carbon isotopic compositions are modified as well.

Although the degassing theory of carbon and oxygen isotopic variation is impossible to prove, it is feasible to postulate the opposite. If the isotopically heavy $CO_2 + H_2O$ were retained, the observed $\delta^{13}C$ and $\delta^{18}O$ variation would be small. The Benfontein Sill kimberlite apparently never actually reached the surface (Clement et al., 1973); therefore one can assume that the $CO_2 + H_2O$ phase was retained and accounts for the remarkable uniformity in $\delta^{13}C$ and $\delta^{18}O$ values (cf. Fig. 5). In general small kimberlite bodies, e.g.,

Table 9. Mean Isotopic Values of Carbonates from Benfontein Sill

Item	$\bar{x}$ Calcite (n)	$\bar{x}$ Dolomite (n)	δDol-δCt
$\delta^{13}O‰$	-5.35±0.42(14)	-4.70±0.27(11)	+0.65
$\delta^{18}O‰$	10.76±2.53(14)	10.31±2.29(11)	-0.45

Marakabei and Ngopetsou in Lesotho exhibit only a limited isotopic variation, but such a process does not explain why kimberlites at deep levels, such as a Premier and DeBeers, have considerable isotopic variation.

Even though only type 1 plus type 3 kimberlites (similar mean $\delta^{13}C$ by geologic type) are considered, one must also realize that all the other factors mentioned are possible causes of the $\delta^{13}C$ variation. The variation of mean $\delta^{13}C$ values of types 1 and 3 kimberlites with location also reflects depth of emplacement. The kimberlites of Lesotho are at fairly high levels of emplacement, whereas Kimberley and Premier area kimberlites have undergone considerable erosion and only the throats of the pipes are available for study (Hawthorne, 1975). The carbon isotopic composition of kimberlite carbonates in Lesotho appear isotopically lighter than kimberlite carbonates of the Kimberley Area (cf. Fig. 5). But $\delta^{13}C$ values from the Premier Mine are similar to the Lesotho kimberlites. A temporal factor causing isotopic variation may be indicated here as not all of the kimberlites considered are of similar age.

Although a 'combined isotopic effect process'may account for observed carbon and perhaps oxygen isotopic variation in some kimberlite bodies it is difficult to envisage how such a process could account for the distinctly different isotopic compositions for several of the kimberlites investigated (cf. Fig. 5). The stratification of carbon in the mantle has been suggested because not all kimberlites are generated from the same depths (Nixon et al., 1973). From a study of ultrabasic nodules, Nixon et al. (1973) infer an elevation of the continental plate shear zone beneath southeast Lesotho that caused a lowering in the depth of the graphite-diamond inversion field to the source regions of some kimberlite magmas and therefore preclude the development of diamonds. However, if the regional depths of kimberlite generation of 150 km for South-West Africa, 200 km for Kimberley, and 190 km for Lesotho, (McGregor, 1975) are correct and the mantle is stratified isotopically, then one would expect regional similarities in the carbon

isotopic composition. The mean $\delta^{13}C$ for Kimberley, Lesotho, and Premier areas are calculated respectively as -5.97% , -5.50% and -6.25% , which do not test significantly different in a t-test comparison. These data do not disprove any vertical $\delta^{13}C$ gradients in the mantle, but suggest that there may be relatively large horizontal inhomogeneities.

Summary, Conclusions, and Recommendations

Specimens of kimberlite matrix, some containing fragments and nodules were collected from some diamond-bearing pipes and other kimberlite bodies visited on the field trips associated with the 1st International Kimberlite Conference in 1973. These rocks were grouped into three types in a compound classification scheme based on, (a) descriptions in the literature, (b) textural, mineralogical and petrographic descriptions on the hand specimens and thin sections, and (c) field relationships within each kimberlite body. They are:

Type 1 or massive kimberlite is characterized by a paucity of fragments and a dense, dark matrix composed of olivine, serpentine, ilmenite, small fibrous aggregates of phlogopite, and carbonates. The carbonates in the 42 samples analysed occur in one or more of the following habits: (a) segregations or ocelli; (b) serrated blades of carbonate crystals that look like a quench product; (c) disseminated anhedral grains; (d) replacement products in sub- or anhedral olivine grains.

Type 2 group, represented by 23 samples, occurs generally in tabular bodies composed predominantly (>60%) of anhedral carbonate, with minor magnetite or ilmentite and serpentine, and accessory phlogopite in a medium to fine-grained hypautomorphic granular textured rock. These "dikes" differ in color (grey) and texture (granular and locally poikilitic) from the adjacent kimberlite, and they are considered to be "late stage" carbonatite-kimberlites. Carbonate metasomatism of the host rock has produced the "piebald kimberlite" at Premier Mine.

Type 3 group (77 samples) is termed fragmental kimberlite due to their brecciated appearance. Phenocrysts of "rounded" olivine, serpentinized olivine, pyroxene, pyrope garnet, and angular fragments of country rocks may occur in a dense matrix of serpentine, phlogopite, and carbonates. Lapilli of earlier generated kimberlite are an important but rare autolithic component. The carbonate minerals occur in the following habits: (a) large "rounded" nodules of coarsely crystalline limestone; (b) angular limestone fragments (sedimentary); (c) small aggregates of carbonates in the matrix; (d) finely dispersed grains in the matrix.

Angular carbonate xenoliths have similar $\delta^{13}C$ values as matrix carbonate. Xenocrystic carbonates tend to be enriched in $\delta^{13}C$ with respect to the matrix. Unzoned and "rounded" carbonate nodules yield similar isotopic values to matrix carbonates, and are interpreted as cognate xenoliths. Ocelli in the Benfontein sills have a similar $\delta^{13}C$ value to the matrix carbonates, but are heavier by about 1% than early "quench" carconate needles. Pisolitic kimberlite lapilli and the carbonate matrix, that occur in pipe-like habit in the Star Mine, have similar $\delta^{13}C$ values, suggesting they originated from the same source. Both the $\delta^{13}C$ and $\delta^{18}O$ values of "replacement" carbonates are highly variable and distinctive from those of the matrix.

There are limitations in the sampling program that could be improved by: (a) more isotopic analyses to establish a more precise range for the isotopic variation of kimberlite carbonates; (b) sampling other kimberlite localities and provinces, including barren pipes; (c) a detailed study of carbon and oxygen variation in a deep diamond mine where grid sampling can be attempted; (d) the isotopic characterization of the different forms of carbon (elemental, diamond, graphite, carbonates) in a single pipe; (e) a rigorous statistical analysis of the isotopic data and an integration with other geochemical data.

Application of the Central-Limit Theorem to the $\delta^{13}C$ and $\delta^{18}O$ means for both matrix and inclusions of the types 1, 2, and 3 kimberlites shows that the samples analysed are good estimates of the population for $\delta^{13}C$ data from the types 1, 2, and 3 matrices. The $\delta^{13}C$ means of types 1 and 3 are similar, and therefore are valid for comparison by geographic locality and emplacement level; type 2 is a distinctive population. The populations for $\delta^{18}O$ data in type 1 inclusions and type 2 matrix are not homogeneous. The $\delta^{18}O$ data for the types 1 and 3 means may not be representative of the entire population.

Statistical treatments of the data were utilized to construct frequency distributions and to test the various categories for normality. Each of the several groups of kimberlites were analysed with regard to their mean carbon isotopic composition by an Analysis of Variance procedure (ANOVES/ANOVUM). The mean $\delta^{13}C$ of type 2 (carbonatite-kimberlite) was found to test significantly different from the others, and the types 1 and 3 kimberlites were found to be similar isotopically. The mean $\delta^{13}C$ of the three general groups are:

Type 1 = -5.41% , ±1.29;
Type 2 = -7.24% , ±3.64;
Type 3 = -5.67% , ±2.59.

Another test (ANOVUM) showed that the mean $\delta^{13}C$

of isotopically similar kimberlite types (e.g., 1 & 3) may be significantly different with locality. A similar analysis of the $\delta^{18}O$ data yielded inconclusive results. However, a comparison of the mean $\delta^{18}O$ values of kimberlites by their geographic location reveals a possible significant difference.

A fractionation model evolving towards lighter carbon isotopes is used to explain (a) the relatively lower values for the carbonatite-kimberlite dikes (-8.32) intruding the fragmental kimberlite (-6.19) at Premier Mine; (b) at Kao $\delta^{13}C$ values are lower in the successive "fragmental" (-7.20‰) and "transitional" (-8.69‰) kimberlite phases than in the initial "Quarry" kimberlite phase (-6.53‰); (c) in Pipe 200 the mean $\delta^{13}C$ of the initial phase (-5.31‰) is heavier than the subsequent eruptive phases; (d) dolomite samples from the Benfontein sills were found to be significantly heavier in ^{13}C (+0.65‰) than coexisting calcites. However, the enrichment of $\delta^{13}C$ in dolomites also is characteristic of carbonatites.

A comparison between sub-samples with different habits of carbonate indicates there is a high "in sample" variability, and that steep isotopic gradients can occur between different phases. This comparison, the statistical tests of the $\delta^{13}C$ and the $\delta^{18}O$ data, and a search of the recent literature suggests that the observed isotopic variation may be due to a number of factors, the most likely being:

1) Carbon isotopic fractionation process between an initial "heavy" silicate + CO_2 kimberlite phase, and a later "light" carbonatite phase;

2) Meteoric-hydrothermal fluid interaction with the kimberlite after emplacement, evidenced by isotopically distinctive replacement carbonates within the kimberlite. The variable nature and trend to $\delta^{18}O$ enrichment in kimberlites (12.91‰) with respect to plutonic carbonatites (6 to 8‰) and other ultramafic rocks (5.5 to 7‰) probably is due to interaction with metamorphic or meteoric water during or after emplacement;

3) a degassing process of the isotopically heavy CO_2 - H_2O phase during emplacement;

4) isotopic inhomogeneities due to geography and elevation, which may be a function of, (a) a "combined isotopic effect" of all the above factors, (b) isotopic inhomogeneity of the kimberlite magmas, and (c) isotopic inhomogeneity of carbon in the mantle.

Acknowledgments. The samples were collected through the courtesy of the DeBeers Organization, the Lesotho National Development Corporations, and the management and head office (Goldfields of South Africa Ltd.,) of the Star Diamond Mine. In particular we wish to thank Barry Hawthorne (DeBeers), and Mr. S. Van Schalkwyk (Star Mine) and Dr. J. Jeppe for their help in collecting and shipping samples, and to Dr. J. C. Griffiths (Penn State Univ.) for assisting with the statistical work. The Mineral Constitution Laboratory and Experimental Station of the College of Earth and Mineral Sciences provided funds for the analytical work and computer time. The National Science Foundation provided some travel funds for D.P. Gold to attend the First International Kimberlite Conference, and the South African Council for Scientific and Industrial Research defrayed part of the field trips expenses.

References

Arkin, H., and R. Colton, Tables for Statisticians, Barnes and Noble, Inc., New York, 2nd Ed., 168 p, 1966.

Baertschi, P. Messung und deuting relativer Haufigkeitsvariationen von O-18 in karbonatgesteinen und mineralien, Schweiz. Mineral. Petrog. Mitt., 37, 73-158, 1957.

Bottinga, Y., Carbon isotope fractionation between graphite, diamond, and carbon dioxide, Earth Planet. Sci. Lett., 5, 301-307, 1969.

Cheminee, J., R. Letolle and P.H. Olive, Premieres donnes isotopiques sur des fumerolles de volcans Italiens, Bull. Volcanol., 32, #3, 469-475, 1969.

Clement, C.R., Kimberlites from the Kao pipe, Lesotho, in Lesotho Kimberlites, P.H. Nixon, ed., Lesotho National Development Corp., 110-121, 1973.

Clement, C.R., The emplacement of some diatreme-facies kimberlites, in Physics and Chemistry of the Earth, 9, Progress Series, Pergamon Press, Oxford, 51-60, 1975.

Clement, C.R., J.B. Dawson, G.J. Geringer, J.J. Gurney, J.B. Hawthorne, L. Krol, L. Kleinjan, and A.A. Van Zyl, Guide for the First Field Excursion of the International Conference on Kimberlites, 41 p, 1973.

Craig, H., The geochemistry of the stable carbon isotopes, Geochem. et Cosmochim. Acta, 12, 133-149, 1973.

Davis, J.C., Statistics and Data Analysis in Geology, John Wiley and Sons, New York, 500 p, 1973.

Dawson, J.B., A review of the geology of kimberlites, in Ultramafic and Related Rocks, P.J. Wyllie, ed., John Wiley and Sons, New York, 241-251, 1967a.

Dawson, J.B., Geochemistry and origin of kimberlite, in Ultramafic and Related Rocks, P.J. Wyllie, ed., John Wiley and Sons, New York, 269-278, 1967b.

Dawson, J.B., Advances in kimberlite geology, Earth Sci. Reviews, 7, 187-214, 1971.

Deines, P., Stable carbon and oxygen isotopes of carbonatite carbonates and their interpretation, Unpublished PhD. Thesis, The Pennsylvania State University, 230 p., 1967.

Deines, P., The carbon and oxygen isotopic composition of carbonates from a mica peridotite dike near Dixonville, Pennsylvania, Geochem. et Cosmochim. Acta, 32, 613-625, 1968.

Deines, P., The carbon and oxygen isotopic composition of carbonates from the Oka Carbonatite Complex, Quebec, Canada, Geochem. et Cosmochim. Acta, 34, 1199-1225, 1970a.

Deines, P., Mass spectrometer correction factors for the determination of small isotopic composition variations of carbon and oxygen, Int. Jour. Mass Spectro. Ion Phys., 4, 283-295, 1970b.

Deines, P., and D.P. Gold, The isotopic composition of carbonatite and kimberlite carbonates and their bearing on the isotopic composition of deep-seated carbon, Geochem. et Cosmochim. Acta, 37, 1709-1733, 1973.

Eckermann, H. von, H. von Ubisch and F.E. Wickman, A preliminary investigation into the isotopic composition of carbon from some alkaline intrusions, Geochem. et Cosmochim. Acta, 2, 207-210, 1952.

Frantsesson, E.V., The Petrology of the Kimberlites, D.A. Brown, ed., Australian National Univ., Canberra, Dept. Geol. Spec. Pub. #150, 194 p, 1970 (translation date).

Griffiths, J.C., Scientific Method in Analysis of Sediments, McGraw-Hill, New York, 508 p, 1967.

Griffiths, J.C. and C.W. Ondrick, Sampling a geological population, Computer Contribution 3C, State Geol. Surv., Univ. of Kansas, Lawrence, Kansas, 53 p. 1968.

Gunter, B.D. and B.C. Musgrave, New evidence on the origin of methane in hydrothermal gasses, Geochem. et Cosmochim. Acta, 35, 113-118, 1971.

Hawthorne, J.B., Kimberlite sills, Trans. Geol. Soc. S. Afr., 71, 291-311, 1968.

Hawthorne, J.B., Model of a kimberlite pipe, in Physics and Chemistry of the Earth, 9, Progress Series, Pergamon Press, Oxford, p. 1-16, 1975.

Hoefs, J., Stable Isotope Geochemistry, Springer-Verlag, Berlin-Heidelberg-New York, 140 p, 1973.

Kahn, J., The measurement of packing in sandstones, Unpublished M.S. Thesis, The Pennsylvania State University, 135 p, 1954.

Keith, M.L., and J.N. Weber, Carbon and oxygen isotopic composition of selected limestones and fossils, Geochem. et Cosmochim. Acta, 28, 1787-1816, 1964.

Kennedy, C.S. and G.C. Kennedy, The equilibrium boundary between graphite and diamond, Jour. Geophys. Res., 81, 2467-2470, 1976.

MacGregor, I.D., Petrologic and thermal structure of the upper mantle beneath South Africa in the Cretaceous, in Physics and Chemistry of the Earth, 9, Progress Series, Pergamon Press, Progress Series, Pergamon Press, Oxford, 455-466, 1975.

Kobelski, B.J., South African and Lesothan Kimberlites with Emphasis on the Variation of the Stable Carbon and Oxygen Isotopic Composition of Kimberlite Carbonatites, Unpublished M.S. Thesis, The Pennsylvania State University, 164 p, 1977.

Mal'kov, B.A., Carbonatite-kimberlite, a new type of diamond bearing rock, Doklady Akad. Nauk SSSR, 221, 193-195, 1975.

Nixon, P.H., F.R. Boyd, and A. Boullier, The evidence of kimberlite and its inclusions on the constitution of the outer part of the earth, in Lesotho Kimberlites, P.H. Nixon ed., Lesotho National Development Corporations, p. 312-318, 1973.

Pearson, E.S., and H.O. Hartley, Biometrika Tables for Statisticians, Cambridge University Press, p. 183-184, 1954.

Pineau, F., M. Javoy, and Y. Bottinga, $^{13}C/^{12}C$ ratios of rocks and inclusions in 'popping' rocks of the Mid-Atlantic Ridge and their bearing on the problem of the isotopic composition of deep-seated carbon, Earth Planet, Sci. Lett., 29, 413-421, 1976.

Robinson, D.N., Magnetite-serpentine-calcite dykes at Premier Mine and aspects of their relationship to kimberlite and carbonatite of alkalic carbonatite complexes, in Physics and Chemistry of the Earth, 9, Progress Series, Pergamon Press, Oxford, 61-70, 1975.

Sheppard, S.M.F., and J.B. Dawson, Hydrogen, carbon, and oxygen isotopic studies of megacrysts and matrix minerals from Lesothan and South African kimberlites, in Physics and Chemistry of the Earth, 9, Progress Series, Pergamon Press, Oxford, 747-764, 1975.

Suwa, K., S. Oana, H. Wada, and S. Osaki, Isotope geochemistry and petrology of African carbonatites, in Physics and Chemistry of the Earth, 9, Progress Series, Pergamon Press, Oxford, 735-746, 1975.

Taylor, H.P.., Jr., The oxygen isotope geochemistry of igneous rocks, Contr. Mineral. Petrol., 19, 1-71, 1968.

Taylor, H.P., Jr., J. Frechen, and E.T. Degens, Oxygen and carbon isotope studies of carbonatites from the Laacher See District, West Germany and the Alno District, Sweden, Geochem. et Cosmochim. Acta, 31, 407-430, 1967.

Vinogradov, A.P., O.I. Kropotova, and V.I. Ustinov, Possible sources of carbon in diamonds as indicated by the $^{12}C/^{13}C$ ratios, Geochem. Int., 2, 495-503, 1965.

Whitelock, T.K., The Monastery Mine Kimberlite, in Lesotho Kimberlites, P.H. Nixon ed., Lesotho National Development Corporations, 214-218, 1973.

Wickman, F.E., The cycle of carbon and the stable carbon isotopes, Geochem. et Cosmochim. Acta, 9, 136-153, 1956.

ABUNDANCES OF PALLADIUM, IRIDIUM AND GOLD IN KIMBERLITES AND ASSOCIATED NODULES

D.K. Paul
Geological Survey of India, Calcutta, India

J.H. Crocket
McMaster University, Hamilton, Canada

P.H. Nixon
University of Papua New Guinea, Port Moresby, Papua New Guinea

Abstract. A suite of eleven kimberlites and eleven ultrabasic nodules, mainly garnet lherzolites, were analysed for Pd, Ir and Au by neutron activation. Most of the samples were from Lesotho and South Africa except for four kimberlites from India. The following average noble metal contents were obtained:

	Pd	Ir	Au	(ppb)
Kimberlites	8.1	3.0	12	
Nodules	3.8	18	6.2	

Pd and Au are enriched in kimberlites relative to nodules by a factor of approximately two in contrast to Ir which is depleted in kimberlite by a factor of six. The most consistent metal ratio, Pd/Ir, is significantly different in both kimberlites and nodule from the chondritic Pd/Ir ratio of 1.1. The average Pd/Ir of the nodules, 0.56, is unusual as sulfur-poor silicate rocks with Pd/Ir < 1 are rare. The average Ir content of the nodules, 18ppb, is very high in comparison with other sulfur-poor ultrabasic rocks.

No correlation of kimberlite-noble metal content with chemical parometers sensitive to kimberlite fractionation was found. Presumably partial melting of a peridotite source modelled by the nodules governs the noble metal content of the kimberlites. The opposite partition trends of Ir relative to Pd and Au tentatively suggest Ir is hosted by a different and more refractory phase than Pd or Au.

There is no simple correlation of noble metal content of the nodules with mantle depth. There is some evidence however that the deepest and relatively undepleted nodules have the most chondritic Pd/Ir ratios.

Introduction

Garnet peridotite nodules found in kimberlites are accepted as direct samples of the mantle. Extensive geochemical studies have been undertaken on these nodules to understand the nature and composition of the upper mantle. From these studies the upper mantle has been found to be geochemically heterogeneous, the scale of the heterogeneity ranging from mineral to regional. The study of kimberlite geochemistry has also received attention in recent years, and the geochemical characteristics of different types of kimberlite have been established. Noble metal abundances in kimberlites and associated nodules are, however, poorly known. Some data have been obtained from the Russian occurrences by spectrochemical and neutron activation methods (Yashko-Zakarova and Ilupin, 1973). Direct comparison of noble metal data obtained by different analytical procedures is difficult as much of the variation may result from the analytical procedures.

Based on the variable distribution of Au in igneous rocks (Tilling et al., 1973) and Au and Ir in basalts (Gottfried and Greenland, 1972), it has been concluded that the source region in the mantle may be heterogeneous in respect to these metals. The main aim of the present work is to provide noble metal abundance data on ultramafic nodules and to relate these to their source region in the upper mantle. Secondly, it is argued that the distribution of the noble metals in kimberlites and, particularly, their partition between kimberlites and nodules, provide some insight into the behavior of these metals during melting in a mantle environment.

Samples Analysed

This work reports abundances of Pd, Ir and Au in twenty-two kimberlites and associated nodules from India and Southern Africa. The Indian kimberlite samples are from two separate petrographic provinces of central and south India. Nodules have not yet been reported from the Indian kimberlites. The samples from southern Africa were selected from widely separated regions representing variable composition and environmental set-

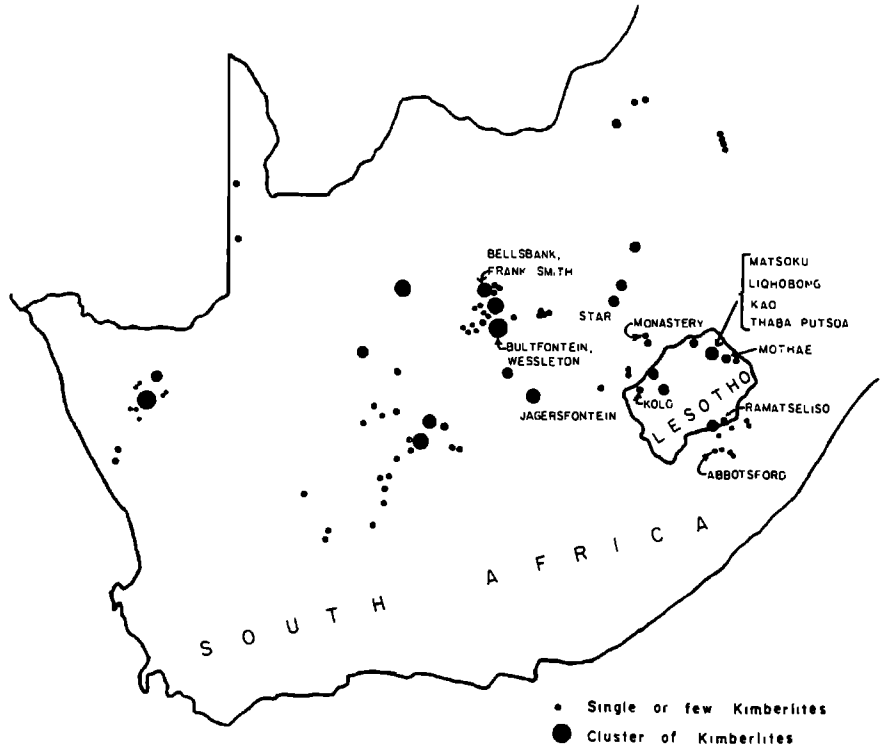

Fig. 1 Location map for Southern African kimberlite and nodule occurrences sampled in this study.

ting (location map, Fig. 1). Detailed petrology and chemistry of the kimberlites and nodules analysed here have been published elsewhere (Nixon and Boyd, 1975; Paul et al., 1975). A short description of the samples is given in the Appendix.

Analytical Method

A radiochemical neutron activation method described by Crocket et al. (1968) was used. Approximately 150 mg of rock powder together with appropriate chemical standards were irradiated in the McMaster University Nuclear Reactor. The samples were subsequently dissolved together with noble metal carriers by an alkali peroxide fusion, and individual noble metals separated and purified by ion exchange and solvent extraction. Metal concentrations were determined by counting the following induced radiations:

Metal			
	198	109	192
Radiation	2.69 Au	13.5 hour Pd	74 day Ir
Counted	412 KeVγ	960 KeVβ	316 KeVγ

Results

The contents of Pd, Ir and Au in individual samples are given in Table 1. The range and average noble metal contents in kimberlites and nodules together with abundances in Type I carbonaceous chondrites, and in some ultrabasic and basic rocks are given in Table 2. Rozhkov et al., (1973) reported gold contents ranging from 1.2 to 18 ppb (mean 3.9 ppb) in Siberian kimberlites. The Au content of associated nodules was similar with a mean of 4.8 ppb. These results compare most closely with our Au values on southern African kimberlites and nodules which average 7.0 and 6.2 ppb respectively (sample PHN 2829 is not included in the nodule average). The Indian kimberlites which average 22 ppb Au are significantly higher. Kaminskiy et al. (1974) determined the platinum metal contents in some Siberian kimberlites and nodules by a spectrophotometric method, and found average Pt, Pd and Ir contents of 187, 53 and 7.6 ppb respectively. Corresponding averages for ultramafic inclusions were 35, 80 and 70 ppb. These values are considerably higher than the averages obtained in this study. Other relevant results are those of Ehmann et al. (1970) who obtained values of 0.8 - 2.6 ppb Au and 1.8 ppb Ir for two samples of ≯ garnet peridotite and one kimberlite.

Discussion

Geochemical characteristics of noble metals

Fig. 2 is a plot of the Pd, Ir and Au proportions in kimberlites and nodules. For the majority of samples kimberlites and nodules lie in distinctly separate fields in Pd-Ir-Au coordinates. The following generalizations are noted.

1) The gold-rich character of the Indian kimberlites is evident.

2) The Pd/Ir ratios of the kimberlites average 2.7 ± 1.4 and are more consistent than those of the nodules which average 0.56 ± 0.85. Both averages are significantly different from the chondritic Pd/Ir average of 1.1. The kimberlite average is similar to that of an alpine peridotite although lower than that of komatiitic peridotites (Table 2). The average Pd/Ir ratio of the nodules is unusual as, to our knowledge, sulfur-poor silicate rocks with Pd/Ir<1 are rare.

3) Ratios of Pd or Ir with respect to gold are highly variable due to the great range in gold contents of both nodules and kimberlites.

The average concentrations of noble metals in kimberlites and nodules (Table 2) are also of some interest. Thus the average Ir content of the nodules is approximately six times that of the kimberlites whereas the reverse is true for Pd and Au in that these metals are lower by a factor of two in the nodules (omitting PHN 2829). A similar pattern emerges in the Siberian kimberlites, especially for Ir, although the Ir contents are apparently higher (Kaminskiy et al., 1974). Further, the Ir contents of the nodules are very high by comparison with sulfur-poor basic or ultrabasic rocks. Exceptions to this generalization include chromitite cumulates in layered basic-ultrabasic plutons such as the Stillwater Complex (Page et al., Table 1, 1975). However, in our nodule suite Ir does not correlate with Cr nor is spinel more than a minor phase, and it is unlikely that spinel is a major host for Ir in the nodules.

The Ir contents of the kimberlites are significantly more uniform than either Pd or Au. A petrographic study of the kimberlites indicates that there is a variable degree of serpentinization. One explanation of the higher Pd and Au variability in the kimberlites is that these elements were remobilized during serpentinization. This conclusion was reached by Crocket and Chyi (1972) for peridotites and dunites of the Mount Albert Pluton. A less extensive redistribution of Ir perhaps reflects the stability of the Ir-bearing phase with respect to serpentinization.

Contamination of nodules by kimberlite

It has been shown that nodules may be contaminated by introduction of K, Rb, Cs, U and Th from the host kimberlite (Gurney et al., 1966). The distribution pattern of the noble metals, however, indicates that contamination of the nodules by

TABLE 1. Pd, Ir and Au contents in kimberlites and associated nodules.

Sample No.	Locality	Pd	Ir	Au	Pd/Ir
		in ppb			
Kimberlite					
UG 84	Majhgawan, Central India	4.1	5.9	24	0.7
MG 6	Majhgawan, Central India	4.3	1.5	2.3	2.9
LM 4/9	Lattavaram, South India	2.3	1.5	43	1.5
WK 2/9	Wajraharur, South India	1.3	0.49	17	2.7
PHN 1598	Thaba Putsoa, Lesotho	7.7	3.5	11	2.2
PHN 1334	Kolo, Lesotho	5.0	2.0	5.2	2.5
PHN 1725	Ramatseliso, Lesotho	15	5.0	6.4	3.0
PHN 1867	Monastery, South Africa	3.5	2.2	0.34	1.6
PHN 3249	Frank Smith, South Africa	19	5.9	0.14	3.3
PHN 2811	Jagersfontein, South Africa	8.9	2.6	10	3.4
PHN 2732	Wessleton, South Africa	18	2.8	16	6.4
Nodules					
PHN 2848	Thaba Putsoa, Lesotho	0.27	33	16	0.008
PHN 1569	Thaba Putsoa, Lesotho	1.0	32	4.1	0.03
PHN 2823	Liqhobong, Lesotho	1.0	6.3	12	0.16
PHN 2860	Matsoku, Lesotho	1.3	5.5	4.1	0.24
PHN 2829	Kao No. 2, Lesotho	11	4.9	103	2.3
PHN 2771	Monastery, South Africa	3.4	21	0.28	0.16
PHN 2782	Frank Smith, South Africa	1.2	13.5	8.9	0.09
PHN 2814	Jagersfontein, South Africa	4.6	53	5.3	0.09
PHN 2759	Bultfontein, South Africa	0.7	12	9.6	0.06
PHN 2764	Bultfontein, South Africa	7.1	7.8	2.0	0.9
PHN 3040	Abbotsford, South Africa	9.3	4.5	0.16	2.1

TABLE 2. Comparison of Pd, Ir and Au contents in kimberlites and nodules with mafic and ultramafic rocks and meteorites.

	Sample	Pd, ppb range	Pd, ppb $\bar{x}$[1]	Pd, ppb n[1]	Ir, ppb range	Ir, ppb $\bar{x}$	Ir, ppb n	Au, ppb range	Au, ppb x	Au, ppb n	Pd/Ir	Ref[1]
Ultramafics	All kimberlites	1.3-19	8.1	11	0.49-5.9	3.0	11	0.14-43	12	11	2.7	o
	Indian kimberlites	1.3-4.3	3.0	4	1.49-5.9	2.3	4	2.3-43	22	4	2.0	o
	S. African kimberlites	3.5-19	11	7	2.0-5.9	3.4	7	0.14-16	7.0	7	3.2	o
	Ultramafic nodules	0.27-11	3.8	11	4.5-53	18	11	0.16-103	6.2	10	0.56	o
	Komatiitic peridotite, S. Africa & Munro Twp., Ont.[2]	5.2-11.3	8.3	11	0.42-2.7	1.1	11	0.4-1.7	1.1	8	7.5	a;l;l
	Alpine peridotite-dunite, Mt. Albert, Quebec	2.8-11	7.9	5	1.6-3.3	2.4	5	0.64-1.6	1.1	5	3.3	e
Basalts	Sea-floor basalt, MAR[3], Leg 37	<0.1-3.5	<0.7	13	<0.01-0.11	<0.025	11	0.8-11	2.8	13	-	f
	Intra-plate and mid-ocean ridge islands[4]		2.0	10	1.13-0.58	0.33	20	0.2-6.6	2.1	41	6.1	i,k,m,n; d;b,h,j
	Continental plateau-building basalt (mainly tholeiite)[5]	0.33-26	5.5	31	0.009-0.49	0.10	36	0.50-11	3.3	31	55	a,k;k;k
	Skaergaard, marginal facies		-			0.26			4.6		-	-;b;m
	Great Lake dolerite, Tasmania		-			0.067			3.6		-	j
	Type I, Carbonaceous chondrites		570			510			140		1.1	g

Footnotes

1. $\bar{x}$, arithmetic average; n, number of samples; ref, references as listed below.
2. The gold data are for the S. African occurrences. Pd and Ir data are for Munro Twp.
3. MAR, mid-Atlantic ridge.
4. Mainly Hawaii, but including Tahiti, Samoa, Reunion, Galapagos, St. Helena, Azores, Ascension.
5. Sierra Geral, Brazil; Columbia River, USA; Stromberg Basalts, S. Africa.
6. Sample no. PHN 2829 omitted from the average.

References

If more than one data source is involved, references are listed with respect to Pd, Ir and Au in that order and are separated by semi-colons.

a. Anhaeusser et al., 1975 b. Baedecker et al., 1971 c. Crocket, unpublished d. Crocket and Skippen, 1966 e. Crocket and Chyi, 1972 f. Crocket and Teruta, 1977 g. Crocket et al., 1968 h. Crocket et al., 1973 i. Ehmann et al., 1970 j. Gottfried and Greenland, 1972 k. Gottfried et al., 1972 l. MacRae and Crocket, unpublished m. Vincent and Crocket, 1960 n. Wasson and Baedecker, 1970.

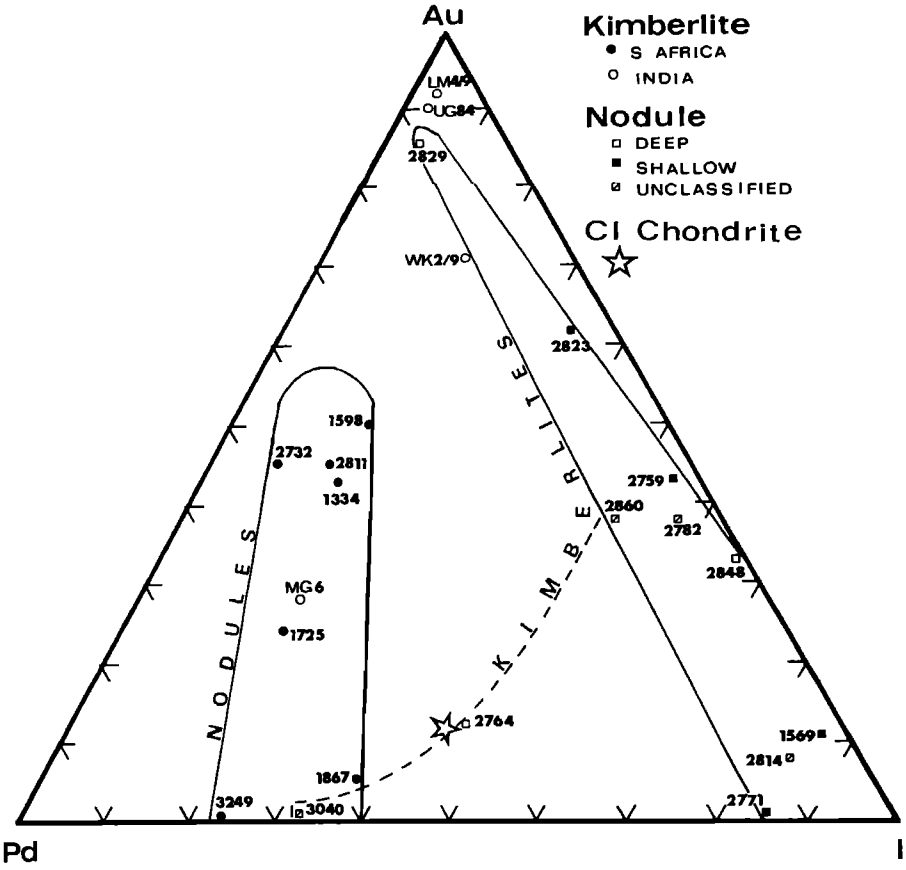

Fig. 2 Proportions of Pd, Ir and Au in kimberlites and ultramafic nodules. Kimberlite (circles) and nodule (squares) fields drawn from visual inspection of data. Diagram illustrates a) relatively consistent Pd/Ir ratios of both kimberlites and nodules, particularly the former, b) large variation in Au relative to either Pd or Ir, c) gold-rich character of the Indian kimberlites relative to those from Southern African, d) Ir-rich and Pd-poor character of the nodules relative to kimberlites, e) general lack of correlation of noble metal content with inferred nodule depth.

host kimberlite would not affect the abundances of Ir and Au in the nodules.

Fractionation during kimberlite emplacement

The fractionation of noble metals during magmatic differentiation has been investigated by various workers. Vincent and Crocket (1960) and Gottfried and Greenland (1972) observed that Au abundances are not significantly affected by low pressure crystal fractionation processes. On the other hand, Ir seems to be depleted as a result of effective removal at a very early stage of differentiation of basaltic magma (Gottfried and Greenland, op. cit.).

In the kimberlites 1/3 SiO_2+3$K_2$0-MgO-FeO-CaO has been found a good indicator of the degree of evolution, and significant correlations between this index and total rare earth concentration has been observed (Paul et al., 1975). The distribution of the noble metals in the kimberlites (Table 1) does not show any correlation with this index nor with Fe, P, Ni and Ti despite the tendency of kimberlite to fractionate to a Ti-rich liquid (Haggerty, 1975). This suggests that the noble metals have not been affected by fractionation during emplacement.

Partition of noble metals during partial melting

Recent studies indicate that kimberlites are products of small amounts of partial melting in the mantle (Paul et al., 1975). Theoretical partial melting models using various trace elements have been applied to petrogenetic problems in recent years (Gast, 1968; Shaw, 1970). The concentrations of trace elements in a liquid derived by partial melting depend on crystal-liquid partition coefficients, the degree of partial melting and the composition of the source. Abundances of noble metals in mantle minerals are not well known. Rozhkov et al. (1973) found that the Au content of the major mantle minerals was equal to that of the whole rock. The partition coefficients of Ir in some relevant minerals can be cal-

culated from published data (Gijbels et al., 1976; Crocket et al., 1976; Gottfried and Greenland, 1972). Assuming an equilibrium partial melting case (without fractional melting) the abundance levels of Ir in a hypothetical melt from a mantle composition, $Ol_{70}Opx_{20}Cpx_5Gnt_5$, can be calculated. The mineralogical constraints outlined earlier (Paul et al., 1975) and the following partition coefficients have been used in the calculations: $K^{Ir}_{Cpx-liq} = 1.5$, $K^{Ir}_{Gnt-liq} = 112$ and $K^{Ir}_{Opx-liq} = 1.5$. Assuming a mantle Ir abundance of 15 ppb (as found in some unaltered garnet peridotite nodules), the Ir content of a hypothetical melt would range from 2.6 ppb (1% melt) to 6.3 ppb (10% melt). This range is similar to those found in the kimberlites (Table 1).

The possibility that minor phases are carriers of noble metals cannot be excluded as Fe-Ni-Cu sulfides and metallic phases including Fe, Ni-Fe and Cu are widespread in kimberlitic ultramafic nodules (Bishop et al., 1975; Haggerty, 1975). These phases, normally efficient concentrators of noble metals, should be significant contributors to partial melts produced at low percentages of melting. A preferential partition of Pd and Au into kimberlite relative to the nodules would result if a significant fraction of these metals were hosted in such early melting phases. It must be noted, however, that the partition trend of Ir is opposite to that of Pd and Au. This suggests that a significant portion of the Ir is hosted by a phase of relatively refractory nature, and indicates that all noble metals are apparently not hosted by the same mineral phases in mantle source rock.

Noble metal variability in the mantle

Textural and mineralogical data on the nodules indicate that they are samples of the mantle from depths of up to 200 km. A complex series of events during the evolution of the Kaapvaal craton has produced varying degrees of depletion (of basaltic constituents ?) in the mantle (Nixon and Boyd, 1975). Thus in Lesotho and westward to Jagersfontein the deepest nodules are relatively undepleted whereas in Bultfontein in the older part of the craton the deepest nodules are highly depleted. Hence the compositional variation of the nodules is not strictly depth dependent. Indeed, differing igneous events in various parts of the craton may have caused depletion effects overriding those due simply to depth of origin.

Iridium, a refractory element, is apparently concentrated in the residua when liquid is extracted from mantle peridotite. In contrast, Pd partitions into the liquid resulting in depletion in the source region. Thus the iridium content of the nodules would increase while palladium would decrease in the source region with higher degrees of partial melting, provided their distribution in the source was uniform. However, if the nodules were samples of a heterogeneous mantle, a simple relationship would not exist. The Ir and Pd contents in the garnet peridotite nodules (Table 1) do not, in general, correlate with the abundances of easily extractable elements (unpublished data, P.H. Nixon). This suggests that the Ir and Pd contents in the mantle source region were variable, although extraction of melt may have accentuated the variation. A similar conclusion was reached by Gottfried and Greenland (1972) who interpreted the regional variations in Au and Ir between low-K_2O tholeiites from the ocean ridges and from North Carolina as reflecting heterogeneity in the upper mantle.

There is, however, some evidence that noble metal ratios may be a guide to the degree of depletion of fusible constituents from mantle peridotite. In general Pd/Ir ratios of the nodules are much less than the chondritic value of 1.1. However, the Pd/Ir ratio of three garnet lherzolite nodules, PHN 2829, PHN 2764 and PHN 3040 are within a factor of two of the chondritic ratio. PHN 2829 is the deepest (200 km) and least depleted nodule, PHN 3040 (high Al and Ca) is relatively undepleted and PHN 2764 is from a depth of approximately 170 km but is depleted. Thus in two of three cases undepleted nodules are characterized by Pd/Ir ratios much closer to chondritic values than the Pd/Ir values of the nodules in general. This suggest that nodules with Pd/Ir ratios near the chondritic value (1 to 2) may be relatively undepleted of basaltic constituents.

Appendix

Petrographic description

Kimberlites

UG 84	-	Pale greenish black kimberlite from a 100 m deep shaft, agglomeratic in nature. Composed of completely serpentinised olivine with minor phlogopite, magnetite, chromite, calcite.
MG 6	-	As above and from the same pipe but collected from an open cast mine.
LM 4/9	-	Bluish grey kimberlite with abundant inclusions of crustal rock. Altered olivine set in a matrix of phlogopite, calcite, perovskite, magnetite, chromite, occasional pyroxene.
WK 2/9	-	Tough dark grey, aphanitic kimberlite with fresh olivine phenocrysts up to 5mm across.
PHN 1598	-	Dark blue - green rock consisting of small (< 1mm) magnetite - carbonate matrix.
PHN 1334	-	Fine porphyritic hardebank consisting of partially altered olivine phenocrysts (15% of rock) in a carbonate and serpentine matrix.
PHN 1725	-	Hardebank with xenocrysts of altered olivine and minor garnet, pyroxene and ilmentite occurring in an aphanitic matrix consisting of calcite, magnetite, perovskite, talc (?) and apatite.

PHN 1867 - Pale bluish grey, composed of serpentinised olivine and later calcite. Occasional fresh olivine and ilmenite.

PHN 3249 - Bluish grey hardebank with autoliths.

PHN 2811 - Fine grained with 10 - 15% olivine, orthopyroxene phenocrysts and rare garnet.

PHN 2732 - Kimberlite with olivine phenocrysts and occasional ilmenite and phlogopite.

Ultrabasic nodules

PHN 2848 - Coarse grained rock with olivine, sparse purple garnet and traces of spinel.

PHN 1569 - Coarse grained garnet lherzolite, olivine slightly serpentinised, abundant enstatite, sporadic garnet, chromium diopside and chromite.

PHN 2823 - Green garnet lherzolite with coarse grained to tabular texture. Coarse, macroscopic, rectangular orthopyroxene and rounded garnet. Accessory chromium diopside and phlogopite.

PHN 2829 - Highly 'sheared' nodule with garnet (up to 4 mm across) and clinopyroxene together making up more than 20% of the rock in a fine matrix of olivine and clinopyroxene.

PHN 2771 - Phlogopite rich wehrlite with abundant clinopyroxene and olivine porphyroclasts. No garnet but ilmenite and secondary rutile.

PHN 2782 - Rock with rounded purple garnets and clinopyroxene porphyroclasts in a dark olivine mosaic.

PHN 2814 - Slightly serpentinised coarse grained rock with minor clinopyroxene and garnet.

PHN 2759 - Slightly deformed garnet lherzolite. Olivine and enstatite show peripheral recrystallisation, and garnet (4 mm across) mantled by secondary phlogopite and spinal. Coarse phlogopite has granulated margins.

PHN 2764 - Porphyroclastic garnet lherzolite with recrystallised olivine forming overgrowths, enstatite is deformed.

PHN 3040 - Fresh dark grey garnet lherzolite with coarse grained texture. Approximate mode is Ol_{60},Opx_{25},Cpx_{5},Gt_{10}. Serpentine and magnetite veinlets. Garnet is subangular, olivine is coarse (1 cm).

Acknowledgements. This work was supported by a grant from the National Research Council of Canada. DKP thanks the Director General, Geological Survey of India for permission to publish this paper.

References

Anhaeusser, C.R., Fritze, K., Fyfe, W.S. and Gill, R.C.O., Gold in "primitive" Archean volcanics. Chem. Geol. 16, 129-135, 1975.

Baedecker, P.A., Schaudy, R., Elzie, J.L., Kimberlin, J. and Wasson, J., Trace element studies of rocks and soils from Oceanus Procellarum and Mare Tranquillitatis. Proc. Second Lunar Sci. Conf., Geochim. Cosmochim. Acta Suppl. 2, 2, 1037-1061, 1971.

Bishop, F.C., Smith, J.V. and Dawson, J.B., Pentlandite-magnetite intergrowths in DeBeers spinel lherzolites: review of sulphides in nodules. Phys. Chem. of the Earth, 9, 323-337, 1975.

Crocket, J.H. and Skippen, G.B., Radioactivation determination of palladium in basaltic and ultrabasic rocks. Geochim. Cosmochim. Acta 30, 129-141, 1966.

Crocket, J.H. and Chyi, L., Abundances of Pd, Ir, Os and Au in an alpine utramafic pluton. Proc. 24th Internatl. Geol. Congress, 10, 202-209, 1972.

Crocket, J.H. and Teruta, Y., Palladium, iridium and gold in mafic and ultramafic rocks drilled from the mid-Atlantic ridge, Leg 37, Deep Sea Drilling Project. Can.J. Earth Sci. 14, 777-784, 1977.

Crocket, J.H., Keays, R.R. and Hsieh, S., Precious metal abundances in some carbonaceous and enstatite chondrites. Geochim. Cosmochim. Acta, 31, 1615-1623, 1967.

Crocket, J.H., Keays, R.R. and Hsieh. S., Determination of some precious metals by neutron activation analysis. J. Radioanalyt. Chem., 1, 487-507, 1968.

Crocket, J.H., Macdougall, J.D. and Harriss, R.C., Gold, palladium and iridium in marine sediments. Geochim. Cosmochim. Acta 37, 2547-2556, 1973.

Crocket, J.H., Teruta, Y. and Garth, J., The relative importance of sulfides, spinels, and platinoid minerals as carriers of Pt, Pd, Ir, and Au in the Merensky Reef at Western Platinum Limited, near Marikana, South Africa. Econ. Geol., 71, 1308-1323, 1976.

Ehmann, W.D., Baedecker, P.A. and McKown, D.M., Gold and iridium in meteorites and some selected rocks. Geochim. Cosmochim. Acta 34, 493-507, 1970.

Gast, P.W., Trace element fractionation and the origin of tholeiitic and alkaline magma types. Geochim. Cosmochim. Acta 32, 1057-1086,1968.

Gijbels, R., Henderson, P. and Zels, J., Geochemistry of some trace elements in mineral separates from Rhum Inner Hebrides, with special emphasis on iridium. Econ. Geol., 71, 1364-1370, 1976.

Gottfried, D. and Greenland, L.P., Variation of iridium and gold in oceanic and continental basalts. Proc. 24th Internatl. Geol. Congress, 10, 135-144, 1972.

Gottfried, D., Rowe, J.J. and Tilling, R.I., Distribution of gold in igneous rocks. U.S. Geol. Survey Prof. Paper 727, 42, 1972.

Gurney, J.J., Berg, G.W. and Ahrens, L.H., Observations on caesium enrichment and the potassium/rubidium/caesium relationship in eclogites from the Roberts Victor Mine, South Africa. Nature 210, 1025-1027, 1966.

Haggerty, S.E., The chemistry and genesis of opaque minerals in kimberlites. Phys. Chem. of the Earth, 9, 295-308, 1975.

Kaminskiy, F.V., Frantsesson, Ye.V. and Khostova, V.P., First information on platinum metals in kimberlitic rocks. Doklady Acad. Sci. U.S.S.R. Earth Sci. Sect. 219, 190-193, 1974.

Nixon, P.H. and Boyd, F.R., Mantle evolution based on studies of kimberlitic nodules from South Africa. 19th Annual Report, Dept. of Earth Sciences, Leeds Univ., 26-31, 1975.

Paul, D.K., Potts, P.J., Gibson, I.L. and Harris, P.G., Rare earth abundances in Indian kimberlites. Earth Planet. Sci. Letters 25, 151-158, 1975.

Rozhkov, I.S., Kaminskiy, F.V. and Frantsesson, Ye.V., Gold in kimberlites and ultrabasic inclusions. Geochem. International 10, 1385-1389, 1973.

Shaw, D.M., Trace element fractionation during anatexis. Geochim. Cosmochim. Acta 34, 237-243, 1970.

Tilling, R.I., Gottfried, D. and Rowe, J.J., Gold abundance in igneous rocks: bearing on mineralization. Econ. Geol. 68, 168-186, 1973.

Vincent, E.A. and Crocket, J.H., Studies on the geochemistry of gold. I. The distribution of gold in rocks and minerals of the Skaergaard intrusion, East Greenland. Geochim. Cosmochim. Acta 18, 130-142, 1960.

Wasson, J.T. and Baedecker, P.A., Ga, Ge, In, Ir and Au in lunar, terrestrial and meteoritic basalts. Proc. Apollo 11 Lunar Sci. Conf., Geochim. Cosmochim Acta 34, Suppl. 1, 2, 1741-1750, 1970.

Yushko-Zakarova, O.Ye. and Ilupin, I.P., Distribution of platinum and palladium in mantle inclusions in kimberlite and some aspects of their magmatic fractionation. Doklady Acad. Sci. U.S.S.R. Earth Sci. Sect. 212, 227-229, 1973.

SIGNIFICANCE OF URANIUM ABUNDANCE IN UNITED STATES KIMBERLITES

Douglas G. Brookins, Richard S. Della Valle and Stephen L. Bolivar

Department of Geology, University of New Mexico, Albuquerque, New Mexico 87131

Abstract. The uranium content of some 150 kimberlite samples from United States occurrences has been determined by delayed neutron activation analysis (DNAA). The DNAA method is much more accurate and precise than gamma ray scintillation techniques; the latter method commonly yields equivalent Uranium (eU) values which are 10 to 300 percent too high. Our U data (by DNAA) combined with Th and K data (by DNAA and wet methods) for fewer samples yield results in agreement with those of investigators who have reported on non-United States kimberlites. In general, the U abundances in kimberlites are significantly higher than for other ultramafic rocks, potassium is usually higher, and thorium data are extremely variable. U/Th ratios far in excess of 4 are common.

Kresten (1974) reported on U abundances in some 80 basaltic kimberlites ($\bar{X}$ = 2.35) and 30 micaceous kimberlites ($\bar{X}$ = 4.91 ppm) from non-United States occurrences. The U content in the former exhibited a positive correlation with perovskite. Our study of United States kimberlites indicates that perovskite can only be a plausible host for U in kimberlites containing little or no carbonatitic calcite. When carbonatitic material is present a positive correlation between U and several trace elements typical of carbonatities is evident although correlation between U and $^{87}Sr/^{86}Sr$ ratios is clear in only about 50 percent of the samples. By using combined $^{87}Sr/^{86}Sr$ and U data, however, it is possible to estimate sedimentary carbonate contamination of kimberlites and associated, mantle-derived inclusions.

Data for the Elliott County, KY ($\bar{X}$ = 2.34 ppm), Prairie Creek, AK ($\bar{X}$ = 21.0 ppm for basaltic kimb.; 3.90 ppm for mic. kimb.), Norris Lake TN ($\bar{X}$ = 2.6 ppm), Riley County, KS ($\bar{X}$ = 4.80 ppm: mic. kimb.), Larimer County, WY CO (4.9 ppm: mic. kimb.), Elk Creek, NB (11.5 ppm: carb. -kimb.) for uncontaminated samples indicate heterogeneous and high-U source regions in the mantle and extreme U/Th segregation prior to final emplacement.

Introduction

The uranium content of some 150 kimberlite and other ultramafic rock samples from United States occurrences has been determined by delayed neutron activation analysis (DNAA). The kimberlites in particular are enriched in uranium relative to ultramafic rock with no apparent kimberlitic affinities. Further, there is usually a positive correlation between uranium content and the presence of carbonatitic material within kimberlites. Our data support Kresten's (1974) proposed positive correlation between perovskite content and uranium abundance only for those kimberlites with little or no carbonatitic calcite. When such carbonatitic material is present, then any contribution from perovskite is masked. High uranium abundances due to contamination from included or host rock material from surrounding host rocks to the kimberlite are apparently of local importance only for the following reasons: (1) High uranium content commonly correlates with carbonatitic 87-Sr/86-Sr ratios (0.703 to 0.705). (2) The mean uranium content for many kimberlites is commonly significantly higher than the uranium content of the host rocks. (3) Where sedimentary (or other) contamination is obvious, uranium contents are lower than for uncontaminated parts of the kimberlites and more or less correlate with sedimentary carbonate 87-Sr/86-Sr ratios (0.708 $\pm$ 0.002).

Kresten (1974) has reported on the uranium abundances in some 80 basaltic kimberlites ($\bar{X}$: 2.35 ppm) and 30 micaceous kimberlites ($\bar{X}$: 4.91 ppm) from locations outside the United States. For the basaltic kimberlites, he reported a positive correlation between uranium abundance and perovskite content and proposed that uranium substituted for calcium in the perovskite. No such correlation was apparent for the micaceous kimberlites. Brookins et al. (1976) reported on some United States kimberlites and showed that uranium commonly correlated with carbonatitic calcite for both basaltic and micaceous kimberlites. The amount of carbonatitic calcite was identified by petrography, distinctive trace element suites, or 87-Sr/86-Sr ratios in the range 0.703 - 0.705. Correlation of high total Sr content and low 87-Sr/86-Sr ratios was noted in only about 50 percent of the samples studied, however.

Both Kresten (1974) and Brookins et al. (1976) used DNAA for uranium determinations because this method is superior to uranium determinations by

TABLE 1. Total Uranium and $^{87}Sr/^{86}Sr$ Data.

Sample	U (ppm)	$^{87}Sr/^{86}Sr$	Sr (ppm)*
A. Elk Creek, Nebraska Location			
ST 936.5	7.30	0.7045	2940
ST 944	11.42	0.7048	1140
ST 946	9.12	0.7055	870
ST 938.5	5.45	0.7051	2440
ST 905	12.12	0.7039	1490
ST 943A	17.44	0.7040	1670
ST 952	11.85	0.7032	3500
ST 929.5A	11.64	0.7030	535
ST 921.5	8.19	0.7035	1020
ST 929	12.58	0.7040	1290
ST 936	12.40	0.7055	1440
ST 916	13.94	0.7067	252
ST 913	12.49	0.7085	40
ST 943B	15.18	0.7056	685
ST 929.5B	12.59	0.7043	286
ST 950	10.91	0.7043	565
(*Brookins et al., 1975)			
B. Elliott County, Kentucky* kimberlites			
EL 100	2.73	0.7053	679
EL 107	1.63	0.7078	307
EL 107-leach	----	0.7035	---
EL 110	1.84	0.7056	---
EL 121	2.15	0.7025	358
EL 225-1	2.61	0.7063	708
EL 225-2	2.77	0.7053	---
EL 301	2.35	0.7040	796
EL 304-WR	2.03	0.7059	603
EL 304-xen.	2.40	0.7075	---
(*See Bolivar, 1977; and Bolivar et al., this volume, for more details)			
C. Wyoming-Colorado Diatremes*			
1. kimberlites			
SD 53a	2.62	0.7061	1740
SD 53b	2.85	0.7058	----
SD 54	5.67	0.7076	867
SD 55a	4.69	0.7185	1860
SD 55b	5.02	------	----
SD 56a	6.04	0.7156	----
SD 56b	6.15	------	----
SD 57a	8.02	0.7059	----
SD 57b	8.22	0.7055	----
2. inclusions (with kimberlite)			
3-23 c1	1.82	0.7062	480
3-23 c2	1.95	0.7048	----
3-24 d	2.65	0.7053	620
3-25 d1	3.60	------	1530
3-25 d2	5.06	------	1760
(*See McCallum, this volume, for more details).			

TABLE 1. (Continued).

D. Riley County, Kansas kimberlites

B1046a	5.32	0.7040	2200
B1046b	4.89	0.7039	1980
B1060	4.08	------	----
R1048	3.32	0.7033	2400
R1044	3.75	0.7036	1950
R1043	7.45	------	----

E. Prairie Creek, Arkansas location*

Sample	U (ppm)	Brief Description
Ark-A	1.37	kimberlite breccia (YG), weathered
Ark-B	1.13	kimberlite breccia (YG), weathered
AA	2.70	tuff
BB	1.82	kimberlite breccia (YG)
CC	1.35	kimberlite breccia (blue)
DD	1.76	kimberlite breccia (YG)
FF	1.58	kimberlite breccia (D+H)
HH	0.82	micaceous sandstone (reworked tuff)
II	2.38	kimberlite breccia (blue) weathered
JJ	1.43	kimberlite breccia (blue) weathered
KK	1.43	kimberlite breccia (YG)
LL	2.62	kimberlite breccia (D+H)
MM	1.71	kimberlite breccia (YG)
OO	1.78	kimberlite breccia (blue)
PP	1.61	kimberlite breccia (YG)
QQ	2.09	kimberlite breccia (YG, weathered)
RR	1.62	kimberlite breccia (blue)
SS	1.81	kimberlite breccia (D+H)
TT	1.49	kimberlite breccia (YG)
UU	1.80	kimberlite breccia (D+H)
VV	1.93	fine-grained green micaceous breccia, weathered
XX	2.21	fine-grained green micaceous breccia
ZZ	1.99	massive-yellow soil
B-5	3.21	fine-grained green micaceous breccia
3-1a	1.47	kimberlite breccia (YG), surface soil sample
3-1c	2.45	kimberlite breccia, very green, sample taken 4' deep
3-3b	1.76	kimberlite breccia (YG), different aliquot of 3-1
3-9b	1.80	kimberlite breccia (YG), weathered
3-10b	1.25	kimberlite breccia (YG), weathered soil sample
3-12	1.36	kimberlite breccia (YG)
3-13	1.19	kimberlite breccia (grn. YG), weathered
3-16	1.73	kimberlite breccia (YG), weathered
3-21	1.65	kimberlite breccia (green YG), weathered
3-23b	2.14	micaceous peridotite, relatively fresh aliquot of sample 3-23
3-29	3.44	tuff-float
3-34b	1.48	kimberlite breccia (YG)
3-36	2.57	micaceous peridotite, exterior sand fractures filled with $CaCO_3$
2-CH	3.41	fine-grained green micaceous breccia
2-CHb	3.41	soil sample from Canary Hill
4-2	1.51	kimberlite breccia (YG)
4-4	2.42	massive yellow soil, probable alteration of peridotite

TABLE 1. (Continued).

4-7	2.54	massive yellow soil, probable alteration of peridotite
4-8	3.74	massive yellow soil, alteration of peridotite taken near creek
4-10	1.96	massive yellow soil, alteration of peridotite
4-12b	2.32	micaceous peridotite, fresh but exterior and fractures filled with $CaCO_3$, different aliquot of 4-12a
4-15	2.58	same as above
4-17	3.30	massive yellow soil, alteration of peridotite
4-19b	2.21	"fresh" green xenolith out of tuff (mudstone?)
4-20	4.66	tuff
4-20ssa	1.78	sandstone xenolith from tuff
4-20ssb	1.02	as above
4-21	4.46	tuff, weathered
4-22	1.71	kimberlite breccia (blue)
4-23	4.92	tuff, weathered
4-24	3.16	massive yellow soil - could be breccia or peridotite alteration
4-25	1.40	as above
4-26	1.45	kimberlite breccia (YG)
4-27	1.27	fine-grained green micaceous breccia
4-28	2.60	massive yellow soil - probable alteration of breccia
4-29	3.13	as above, alteration of peridotite
4-30	1.89	kimberlite breccia (blue-YG)
4-31	3.43	kimberlite breccia (green-YG)
4-32	1.23	kimberlite breccia (YG)
4-34	6.25	kimberlite breccia (blue)
4-36	2.81	kimberlite breccia (blue)
4-B-1	2.78	black soil - surface sample
4-B-2	2.49	as above
4-B-3	3.56	as above
4-MH	2.35	micaceous peridotite, relatively fresh

(*See Bolivar, 1977; and Bolivar and Brookins, this volume, for more details)

other methods. For limited thorium and potassium data wide variation for U/Th are noted and K contents do not correlate well with either U or Th although all three elements are higher than in ultramafic rocks not associated with kimberlites.

Analytical Methods

The analytical methods for the Sr data reported in Table One are given by Brookins (1967). For uranium analyses, we have chosen the delayed neutron activation analysis (DNAA) method as described by Gale (1967) and Cumming (1974) and modified for the present study as described by Balestrini et al. (1977). The Omega West Reactor at the Los Alamos Scientific Laboratory was made available for this study.

The DNAA method is superior to most other methods for uranium analyses as pointed out by Stuckless et al. (1977). X-ray fluorescence methods are not sensitive enough for uranium contents in the low ppm range and gamma scintillation counting is subject to very large uncertainties even in the presence of small amounts of K and Th (Stuckless et al., 1977). The DNAA method as used for this study is both accurate and precise. Our precision in the 2 to 20 ppm range is $\pm$ 3 percent (2σ), $\pm$ 5 percent in the 2 to 0.5 ppm range, and $\pm$ 15 percent in the 0.1 to 0.5 ppm range. For samples containing less than 0.1 ppm preliminary results indicates our precision to be $\pm$ 20-25 percent in the 30 to 100 ppb range. Since most of our errors result from counting statistics, increased sample size normally improves the precision. Thus while one gram samples are adequate for most analyses, two- to three-gram samples are used for samples containing less than one ppm.

Background Information on the Sites Chosen for Study

As part of an on-going study of kimberlites and other ultramafic rocks and their cognate xeno-

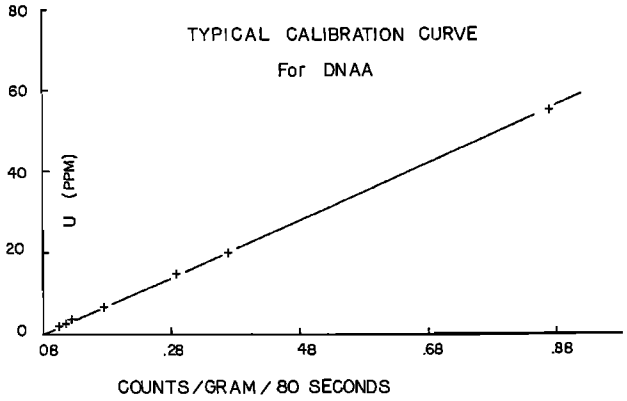

Fig. 1. Calibration Curve for Uranium Analysis by Delayed Neutron Activation Analysis (DNAA). Standards used include U.S.G.S. samples plus standards prepared at the Los Alamos Scientific Laboratory where uranium content was determined by isotope dilution.

liths of the mid-Continental and United States we have been systematically analyzing samples for their Rb, Sr systematics in conjunction with detailed mapping and geophysical studies plus petrography for several years. The present study integrates some previously reported Sr data with U data. Th, REE and related data are in progress.

The Prairie Creek, Arkansas and Elliott County, Kentucky locations have been described thoroughly by Bolivar (1977) and elsewhere in this volume (Bolivar and Brookins) and the Larimer County, Wyoming and Colorado diatremes are also described in this volume (McCallum and Eggler).

The Riley County, Kansas kimberlites are located along the southwesternmost extention of the mid-continent gravity high extending from the Lake Superior region. The kimberlites exhibit magnetic characteristics indicating structural control by the northeast trending, basement tectonic elements (Brookins and Meyer, 1974); they are in close proximity to both the Nemaha and Abilene anticlines of the north-central Kansas. They are not located on the east-west trending "38th Parallel" lineament described by Snyder and Gerdemann (1965) (Re: popular misconceptions on this point). The Riley County kimberlites contain a typical suite of forsteritic olivine, chrome diopsides, pyropic garnet (and knorringite?), Mg-ilmenite, perovskite, phlogopite plus abundant carbonatite. Xenoliths from these kimberlites have been studied by Brookins (1970; 1971), Meyer and Brookins (1971; 1965), Brookins and Wood (1970).

The Elk Creek, Nebraska carbonatite also lies close to the axial trace of the mid-continent gravity high (Brookins et al., 1975; Treves et al., 1972a,b). It is not exposed at the surface but inspection of drill cores and isotopic and other geochemical studies (Brookins et al., 1975; Treves, 1972) have shown it to be a carbonatite with minor kimberlitic material mixed with it.

The diatremes near Avon, Missouri have been the subject of controversy for some time; recently Mansker et al. (1976) have summarized earlier work on the eighty or so diatremes, dikes and breccias known from southeastern Missouri. They report that, while many of the ultramafics are more typical of mica peridotites than other ultramafic rocks, some do possess kimberlitic affinities. The Avon diatreme, in particular, has been shown to contain two generations of forsteritic olivine, phlogopite, minor ilmenite, clinopyroxene, Cr-spinel, Ti-magnetite, and a suite of xenoliths including carbonatites, pyroxenites, serpentinized dunite (?) and others. Garnet has not been observed, however. The serpentine-olivine relations indicate that serpentinization occurred at depth, as serpentine and magnetite veinlets within serpentine after olivine are offset by kink bands assumed to accompany shock processes before and/or during emplacement. Some of the carbonate-rich xenoliths are interpreted as carbonatitic based on low $^{87}Sr/^{86}Sr$ ratios from 0.7033 to 0.7049. These carbonatitic nodules were highly reactive with the ultramafic silicate host and yielded xonotlitic + salitic pyroxene + phlogopite in places. Fluid inclusion temperatures for the carbonatitic nodules vary from 291°C to 306°C (Mansker et al., 1976) which agrees with the local thermal meta-

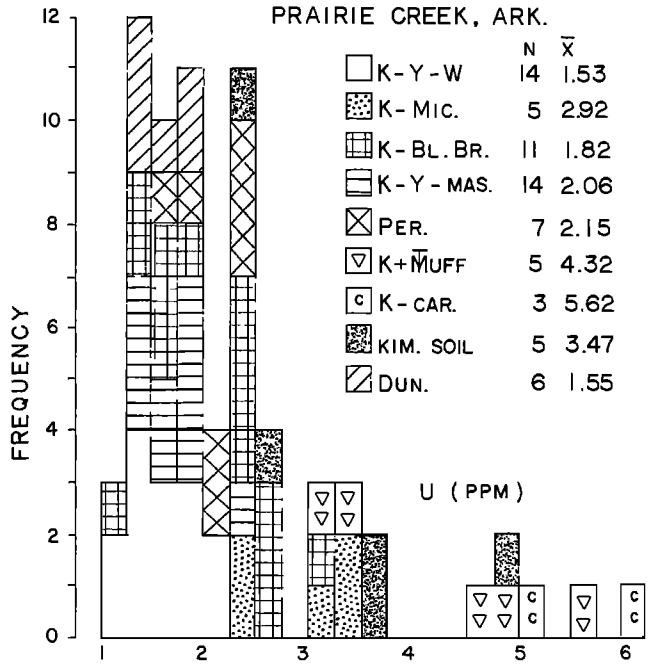

Fig. 2. Prairie Creek, Arkansas Location; frequency versus uranium content for various rock types. Symbols: K = kimberlite, Y = yellow, W = white, Mic. = micaceous, Bl. = blue, Br. = breccia, mas. = massive, Per. = peridotite, Kim. soil = soil developed in situ over kimberlite, car. = carbonatite, dun. = dunite.

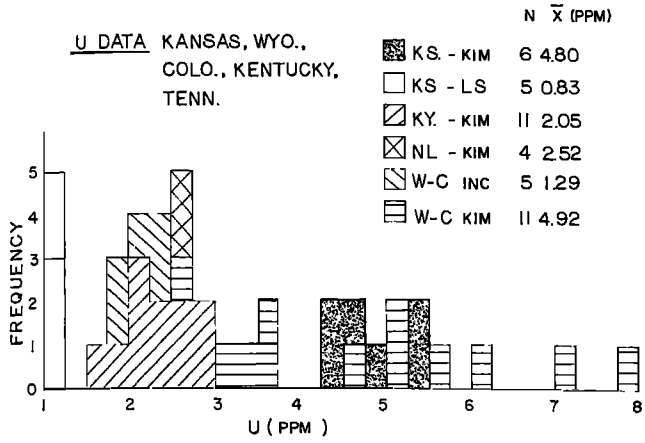

Fig. 3. Frequency plot of uranium content in rocks from several locations. Symbols: KS. = Kansas, kim. = kimberlite, Ls - limestone, KY - Kentucky, NL = Norris Lake (Tennessee), W-C = Wyoming-Colorado, inc. = inclusion.

morphism of the intruded country rock.

Preliminary results show that calcite-rich samples yield U = 2.5- 5.5 ppm while serpentine yields 0.5- 1.3 ppm (unpub. data).

Discussion

Kresten (1974) and Brookins et al. (1976) have pointed out that many ultramafic nodules from kimberlites and related rocks are uranium poor; uranium contents in the 10 to 100 ppm range are not unusual. Many of these ultramafic nodules have been proposed to be genetically linked to the host kimberlite, and it should therefore be possible to predict not only uranium but many other trace element contents in kimberlite formed as a partial melt product of garnet peridotites, eclogites, etc. However, considering the extremely high partition coefficients between some of the typical uranium-rich accessory minerals in kimberlites such as zircon (e.g., U_{zircon}/U_{liquid} = 100; Kresten, 1974) plus the preferential enrichment of uranium in the liquid relative to clinopyroxene (e.g., U_{cpx}/U_{liquid} = 0.012; Kleeman and Lovering, 1973), the high uranium content of xenoliths of kimberlite is attributed to enrichment due to the presence of a 'special' vapor or fluid phase not necessarily linked directly to the kimberlite.

Even many continental basalts, for example, contain less than 1 ppm uranium (a range from 400 ppb to 1.3 ppm for sixty Quaternary basalts has been obtained by the author; report in progress).

For basaltic kimberlites, Kresten (1974) makes a strong case for U:Ca diadochy in perovskite to account for the uranium content noted. His arguments are based on the facts that there simply is not enough high-U zircon present and high-U apatites are not only scarce but clearly due to late stage processes such that the source of uranium must be due to other minerals. Since olivines and pyroxenes (and their serpentinized products) are notoriously U-poor, then the uranium must be, in the absence of any carbonate phases, due to some ubiquitous accessory mineral such as perovskite. By careful size analysis and correlation of high uranium content with the perovskite-rich fraction, Kresten (1974) is able to demonstrate that, for Lesotho kimberlites, perovskite must be the source of most of the kimberlitic uranium. At the same time, however, perovskite as the essential carrier for uranium in micaceous kimberlites (many of which are carbonatitic) is not demonstrated and the source of the higher uranium contents is unknown.

A convenient explanation for the enrichment of any (or many) trace elements in kimberlites is that of contamination, although the suspected contaminant is usually left out of the ensuing discussions unless easily recognizable. For our studies we have commonly chosen to attempt to monitor contamination from suspected sedimentary crustal material by inspection of both total Sr and $^{87}Sr/^{86}Sr$ ratios. Earlier work (Brookins, 1970; Brookins et al., 1976) has shown, however, that while many carbonatites possess high total Sr and low (i.e., 0.703 - 0.705) $^{87}Sr/^{86}Sr$ ratios and Phanerozoic sedimentary carbonate-rich rocks possess lower (150 to 660 ppm) total Sr and higher (0.7065 - 0.7100) $^{87}Sr/^{86}Sr$, the carbonate fractions of many kimberlites do not always reflect such a clear distinction of source of their carbonates on a basis of material balance between carbonatite and sedimentary carbonates. Indeed, very high $^{87}Sr/^{86}Sr$ (i.e., to 0.72) ratios, even in the presence of total Sr in excess of 1000 ppm, are occasionally noted. It must be emphasized, however, that such exceptions are relatively rare. When carbonatitic material is obviously evident based on petrography, chemical studies, etc., then there is usually a clear distinction between carbonatitic material (high Sr, low $^{87}Sr/^{86}Sr$) and sedimentary carbonate material (lower Sr, higher $^{87}Sr/^{86}Sr$) with intermediate Sr and $^{87}Sr/^{86}Sr$ values usually explainable in terms of simple mixing of carbonatitic and sedimentary carbonate material such as noted in groundmass carbonates of

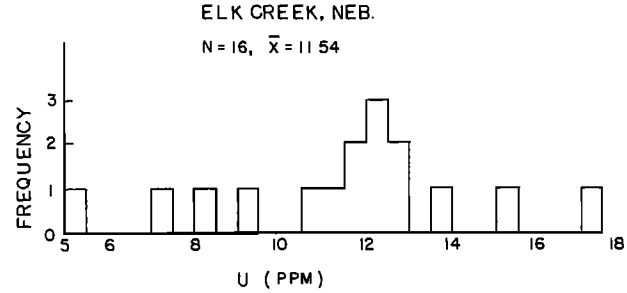

Fig. 4. Frequency plot of uranium content for samples from the Elk Creek, Nebraska location.

TABLE 2. Uranium Content of Kimberlites

Locality	U (ppm) Range	Mean	Number of Samples	References
Elliott Co., Kentucky	1.5 - 3.1	2.33	11	This study
Prairie Creek, Arkansas:				
a) mic. peridotite	1.6 - 2.8	2.35	14	This study
b) kimb. breccia	0.9 - 2.3	1.97	75	This study
c) tuff and kimb. soil	2.2 - 5.9	3.58	17	This study
d) carb. kimb.	5.0 - 6.2	5.62	6	This study
Norris Lake Tennessee	2.0 - 2.9	2.52	4	This study
Riley Co., Kansas	4.2 - 5.7	4.80	6	Brookins et al. (1976)
Larimer Co., Wyoming Colorado				
a) inclusions	1.8 - 2.6	1.35	5	ibid.
b) kimberlite	2.6 - 8.0	5.25	11	ibid.
Elk Creek, Nebraska	5.1 - 17.9	11.54	16	ibid.
Non-U.S.				
a) bas. kimb.	0.5 - 4.5	2.35	82	Kresten (1974)
b) mic. kimb.	2.5 - 12.5	4.91	89	ibid.

the Riley County, Kansas kimberlites (Brookins, 1967).

Attempts at monitoring contamination by carbon and oxygen stable isotopic variations have been only partly successful. Deines and Gold (1973) have shown that while the carbon in carbonatites in association with kimberlites is commonly due to deep sources, the oxygen isotopic variations are so extreme as to preclude use of this parameter alone for attempting quantitative material balance between carbonatitic and sedimentary carbonate materials.

In our (Bolivar and Brookins, this volume) study of the Prairie Creek, Arkansas ultramafic rocks, another complexity results from the fact that when only small amounts of carbonatitic calcite are present, $^{87}Sr/^{86}Sr$ ratios are difficult to use in conjunction with other trace element studies. During leaching of serpentinized samples (Bolivar, 1977) with dilute HCl, for examples, it was found that leaching with 0.1 N HCl for fifteen minutes released Sr with $^{87}Sr/^{86}Sr$ in the range 0.704-0.706 whereas continued leaching with 2 N HCl for an additional 30 minutes released Sr with $^{87}Sr/^{86}Sr$ ranging from 0.705 to 0.711 (mean for thirty samples: 0.7073). This was interpreted to indicate that the 2 N HCl released non-carbonate Sr of higher $^{87}Sr/^{86}Sr$ from relatively loose-bonded sites in silicates. Significantly, the 0.1 N HCl did not leach Rb whereas the 2 N HCl did. A further implication from this study was that the first leached, carbonatitic material was probably mixed in some mechanical fashion, without homogenization with the silicate material. This is important when discussing the trace element contents of kimberlites.

Our data for basaltic kimberlites do not contradict Kresten's (1974) findings. Although we cannot unequivocally equate uranium content with perovskite, high perovskite is noted in thin section for samples with high uranium contents in some cases (Bolivar, 1977). Often, however, the altered nature of the samples makes such a correlation difficult to impossible. It must be emphasized, however, that the nature of the alterations suggests pre-emplacement processes such that contamination form surrounding surface rocks is not suspect. Where data are available (Bolivar, 1977; Brookins, unpub. data), the country rocks commonly contain lower uranium contents than the kimberlites. Further, for fractures in Riley County, Kansas kimberlites filled with sedimentary-derived calcite, the uranium content varies from 0.8 to 1.5 ppm.

A close correlation between phlogopite-bearing kimberlites and suspected carbonatitic material is common. In such occurrences, there also exists close correlation between uranium and carbonate

content. That this is the case is clearly shown in the data presented in Table One. For those occurrences where abundant carbonatitic material has been documented such as at Elk Creek, Nebraska, Riley County, Kansas, some of the Larimer County, Wyoming-Colorado sites, etc., high uranium contents are noted. Even when the suspected carbonatitic material content is lower (i.e., Elliott County, Kentucky, Prairie Creek, Arkansas, Norris Lake, Tennessee, Avon, Missouri) the uranium content varies as the ratio of carbonatite/kimberlite such that high uranium content correlates with low kimberlite and low uranium with high kimberlite contents. Thus the data of Table One suggest that the carbonatitic material controls the uranium budget of the kimberlite-carbonatite mix.

An interesting point to be made is that while high U, K and Th are characteristics of many kimberlites (i.e., relative to other ultramafic rocks), U/Th ratios are commonly very different from the predicted 1/4 ratio commonly assumed. We (See Bolivar, 1977) do not observe systematic K/U nor Th/U variation for the Elliott County, Kentucky or for the Prairie Creek, Arkansas kimberlites but do see a correlation between high total uranium and high carbonatite/kimberlite ratio, then we propose that the uranium budget in at least the micaceous kimberlites is controlled by the presence of carbonatites. Further, if there is a closely controlled process or processes accounting for variation in trace element contents between carbonatite-poor to -absent kimberlites through rocks such as alnoites, then one could logically argue for systematic variation of an element such as uranium from about 50 ppb (e.g., some eclogites, garnet peridotites) to higher values as carbonatite content increases. Yet this systematic variation is not noted and further, eclogite, garnet peridotite and other cognate xenoliths show consistently low uranium contents in the presence of variable uranium contents in the host kimberlites where the variation can be, in many cases, accounted for by the amount of carbonatite present.

Thus our data do not necessarily support nor refute Kresten's (1974) comments concerning micaceous kimberlites; in fact our data are more in line with Middlemost's (1974) comments that the ties between carbonatite and kimberlite may, in many cases, be accidental in that two (or more?) separate magmatic sources are involved and that these sources were not equilibrated with each other.

There is further ramification of this model. Unless it can be unequivocally demonstrated that the Th-U-K budget in kimberlites (with or without carbonatitic material) can be defined in terms of specific minerals or intergranular sites, then total heat budget calculations may be in error. If, as postulated here, uranium is controlled by carbonatite content and thus the Th/U and K/U ratios are suspect, for purposes of heat budget it would be preferable to use measured K and Th contents and assume Th/U = 4 as otherwise erroneous calculations may result.

References

Balestrini, S.J., J.P. Balagna, and H.E. Menlove, Two specialized delayed neutron detector designs for assays of fissionable elements in water and sediment samples, Nuc. Instr. Mehds., 136, 521-524, 1976.

Bolivar, S.L., Geochemistry of the Prairie Creek, Arkansas and Elliott County, Kentucky Intrusions, Ph.D. thesis, University of New Mexico, 286 p., 1977.

Brookins, D.G., The strontium geochemistry of carbonates in kimberlites and limestones from Riley County, Kansas, Earth Plan. Sci. Lttrs., 2, 235-240, 1967.

Brookins, D.G., The kimberlites of Riley County, Kansas, Bull. Ks. Geol. Surv., 200, 32 p., 1970.

Brookins, D.G., and M.J. Woods, High pressure mineral reactions in a pyroxenite granulate from the stockdale kimberlite, Bull. Ks. Geol. Surv., 199, 1-6, 1970.

Brookins, D.G., and H.O.A. Meyer, Crustal and upper mantle stratigraphy beneath eastern Kansas, Geophys. Rev. Lttrs., 1, 269-272, 1974.

Brookins, D.G., R.S. Della Valle, and S.L. Bolivar, Uranium geochemistry of some United States kimberlites, EOS (Trans. Amer. Geophys. Un.), 57, 761, 1976.

Cumming, G.L., Determination of uranium and thorium in meteorites by the delayed neutron activation analysis method, Chem. Geol., 13, 257-268, 1974.

Deines, P., and D.P. Gold, The isotopic composition of carbonatite and kimberlite carbonates and their bearing on the isotopic composition of deep-seated carbon, Geochim. Cosmochim. Acta, 37, 1709-1734, 1973.

Gale, N.G., Development of delayed neutron technique as rapid and precise method for determination of uranium and thorium at trace levels in rocks and minerals, with applications to geochronology, Int. Atom. Energy Agency, Radioactive dating and methods of low level counting, 431-452, 1966.

Kleeman, J.D., and J.F. Lovering, Uranium partitioning in kimberlites and their deep-seated inclusions, Ext. Abs., Int. Conf. Kimbs., Cape Town, 189-190, 1973.

Kresten, P., Uranium in kimberlites and associated rocks, with special reference to Lesotho occurrences, Lithos, 7, 171-180, 1974.

Mansker, W.L., D.G. Brookins, G.P. Landis, and J.W. Husler, Post-Devonian diatremes in southeastern Missouri: investigation of the Avon kimberlite and some emplacement parameters, EOS (Trans. Amer. Geophys. Un.), 57, 761, 1976.

Meyer, H.O.A., and D.G. Brookins, Eclogite xenoliths from the Stockdale kimberlite, Kansas, Contr. Min. Petrol., 34, 60-72, 1971.

Meyer, H.O.A., and D.G. Brookins, Sapphirine, sillimanite and garnet in granulite xenoliths from the Stockdale kimberlite pipe, Kansas, Amer. Mineral., 61, 1194-1202, 1976.

Middlemost, E.A.K., Petrogenetic model for the

origin of carbonatites, Lithos, 7, 275-278, 1974.

Stuckless, J.S., H.T. Millard, C.M. Bunker, I.T. Nkomo, J.N. Rosholt, C.A. Bush, C. Huffman, and R.L. Keil, A comparison of some analytical techniques for determining uranium, thorium and potassium in granitic rocks, U.S. Geol. Surv. Jour. Res., 5, 83-92, 1977.

Treves, S.B., R. Smith, M.P. Carlson, and G. Coleman, Elk Creek carbonatite, Johnson and Pawnee Counties, Nebraska, Geol. Soc. Amer., 4, 297, 1972.

Treves, S.B., R. Smith, and J. Rinehart, Petrography and mineralogy of the Elk Creek carbonatite, Nebraska, Geol. Soc. Amer. Prog. w. Abs., 4, 352-353, 1972a.

GEOPHYSICAL AND Rb-Sr STUDY OF THE PRAIRIE CREEK, AK KIMBERLITE

Stephen L. Bolivar

Los Alamos Scientific Laboratories, Los Alamos, New Mexico 87545

Douglas G. Brookins

Department of Geology, University of New Mexico, Albuquerque, New Mexico 87131

Abstract. Whole-rock and mineral-separate chemical analyses, uranium whole-rock analyses, and Rb-Sr systematics have been determined for the Prairie Creek, Arkansas intrusion. In addition, petrologic data and detailed field investigations, completed as part of a joint University of NM:Purdue University study of mid-continental USA kimberlites, allow the following interpretation. The Prairie Creek intrusion is characterized by three rock types: micaceous peridotite, clearly distinguishable by magnetic data, and kimberlite breccia and associated tuff, not distinguishable by magnetic data. Detailed mapping and geophysical data suggest the sequence of intrusion to be: kimberlite breccia, characterized by a 'typical' diatreme shape; micaceous peridotite, a shallow vertical intrusion of variable thickness; and scattered patches of tuff containing fragments of reworked breccia and peridotite.

Sixty-five Prairie Creek analyses range from 0.7058 to 0.7132 with an arithmetic mean of 0.7094. Variability of $^{87}Sr/^{86}Sr$ total Sr and Rb is attributed to both sample inhomogenity and heterogeneous source regions. The rocks are undateable by the Rb-Sr whole rock method and leaching treatment with 0.1N HCl does not resolve this problem. Preliminary data for Prairie Creek montmorillonite samples suggest that the age of intrusion for this complex may be successfully determined by analyses of clay minerals.

Introduction

In the continental United States, kimberlites occur in at least 12 states (Meyer, 1976). Unfortunately, the available literature is insignificant for most midcontinental occurrences. For example, there are very few geochemical, geophysical or isotopic data for the best known kimberlite in the United States, the diamond-bearing kimberlite at Prairie Creek, Arkansas. Our study provides details of the geology, geophysics, geochemistry and Rb and Sr systematics of the Prairie Creek intrusion.

Location

The Prairie Creek intrusion, near Murfreesboro, Arkansas is the only commercial diamond-bearing kimberlite in North America. After diamonds were discovered in 1906, several mining ventures were undertaken but all ended in failure. Today the area is a state park and tourists are allowed to look for diamonds for a modest fee and several hundred are reported found each year (J. Cannon, personal communication, 1976).

The study area lies on the northern edge of the Gulf Coastal Plain, just south of the Ouachita Mountain region. The rocks in this area are sedimentary and dip gently to the south, with very little surface structure observed. A stratigraphic column is given in Table 1. The intrusion has been dated from field relationships as mid Cretaceous (Miser and Ross, 1923; Bolivar, 1977).

Petrology and Mineralogy

The igneous intrusion, covering 0.3 km^2, at Prairie Creek, Arkansas is characterized by three rock types; a kimberlite breccia, a micaceous peridotite, and an associated tuff (Fig. 1). The kimberlite breccia covers the eastern part of the study area, comprising about 40% of the total intrusion. The shape of this unit is oval-like over 480 m long in a northeast-southeast direction and about 240 m wide. The breccia is an extremely variable porphyritic rock that weathers through blue-green-yellow decomposition products to a black gumbo soil. Veins of quartz (some amethyst), fluorite, and barite cut this unit. The breccia is extremely weathered and serpentinized to at least 70 m and its true mineralogy is unknown (Thoenen et al., 1949). The breccia was divided into 6 subunits: 1) a yellow-green unit which represents the majority of the breccia exposed, 2) a blue-green unit that occurs in scattered

TABLE 1. Comparison of Igneous Rock Types for the Prairie Creek Intrusion

Stratigraphic Column		Igneous Intrusions
Quaternary	Alluvium	
	Terrace Deposits	Tuff and reworked tuff
unconformity		
Upper Cretaceous	Tokio Fm.	
IGNEOUS INTRUSIONS		Micaceous Peridotite
		a) massive yellow clay
Lower Cretaceous	Trinity Fm.	Kimberlite breccia
unconformity		a) fine-grained green micaceous b) massive yellow clay c) yellow-green
Carboniferous	Jackfork sandstone	d) blue-green e) D & H

patches, 3) a green unit, very difficult to distinguish from yellow and blue varieties, 4) a relatively indurated breccia, designated D&H, 5) a massive yellow clay soil, which is an obvious decomposition product of breccia and 6) a fine-grained, green, micaceous breccia, which appears to be a transitional unit between breccias and tuff. The blue-green may represent "fresher" material that ultimately weathers to a yellow breccia although blue-green units (as do other subunits) grade laterally into each other. This suggests, in addition to chemical variations, the possibility of multiple intrusions (pulses) over a short period of time. In thin section the breccia is characterized by serpentinized olivine phenocrysts in a groundmass of serpentinized olivine and phlogopite with minor amounts of spinel, perovskite, secondary biotite, chlorite, and secondary calcite. The lack of magnesian ilmenite, enstatite, and chrome diopside and the rarity of garnet suggest that this rock is not a true kimberlite in the "strictest sense" (Mitchell, 1970); however, the observed mineralogy is not believed to be representative of the original composition because of the extreme alteration of the breccia.

The micaceous peridotite crops out in the northwestern half of the study area, comprising Middle and East Hills. This unit occurs in an oval-like pattern, about 600 m long in a northeast-southwest direction, about 240 m wide, comprising about half of the total intrusive exposed. Small intrusions of peridotite were also noted intruding the breccia in the southwest part. The peridotite is a hard, black to dull brown, porphyritic rock containing olivine phenocrysts that occur as altered black grains. This rock ultimately weathers through a massive yellow-clay to a black gumbo soil (very similar to the breccia yellow-clay). Secondary coatings of carbonate, kerolite, barite and serpentine veins are found. In thin section the peridotite has a porphyritic texture with phenocrysts of subhedral, partially serpentinized olivine (Fo 92) in a groundmass of phlogopite, serpentine and diopside with minor amounts of perovskite, pyrite, amphibole and magnetite. Phlogopite, which alters to chlorite, may reach a maximum dimension of 1 mm and polikilitically encloses opaques, olivine and small, acicular needles of diopside. Spinels are rimmed by magnetite.

The tuff, an extremely variable unit blue-gray in color, occurs in scattered patches throughout the study area but the major exposure is confined to West Hill. The tuff probably formed by fragmentation of peridotite or breccia or both after the initial intrusion, with tuffaceous material from the intrusion washing back into the crater, forming sedimentary features such as flow textures and graded bedding. In thin section the tuff contains quartz, potassic feldspar and biotite in a groundmass of chlorite, serpentine and clay material. Reworked tuff contains up to 50% quartz.

All three rock types contain xenoliths of sandstone and shale but the tuff contains the majority of inclusions, including rare xenoliths of kimberlite breccia and peridotite.

Chemistry

The whole rock and uranium chemistry have been discussed by Bolivar (1977) and Brookins et al.

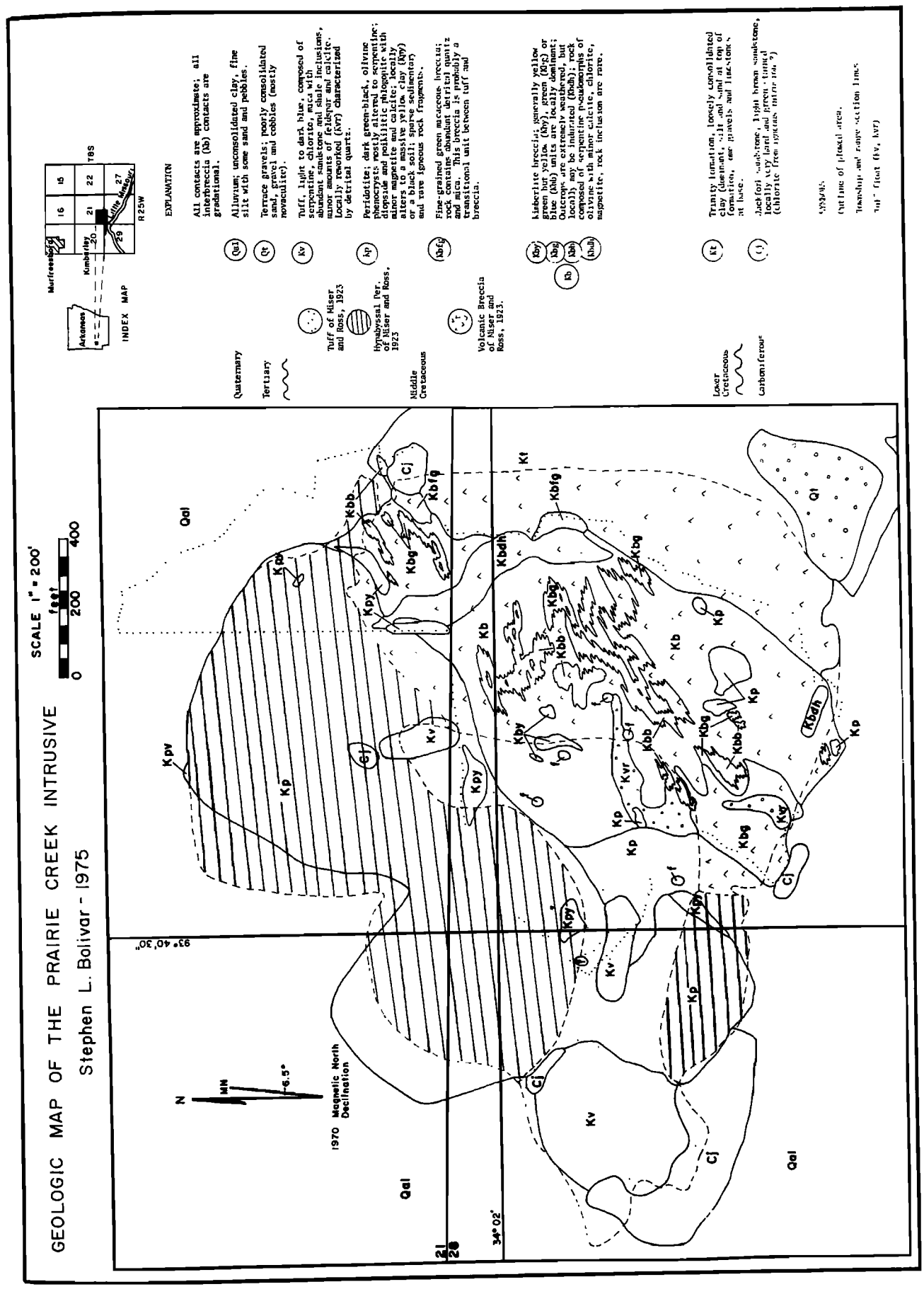

Fig. 1. Geological map of the Prairie Creek Intrusive, Murfreesboro, Ark.

TABLE 2. Chemical analyses and CIPW norms for selected Prairie Creek rocks

A. Tuffs	1	2	3	4
SiO_2	60.24	62.73	54.52	44.77
Al_2O_3	5.40	6.01	4.85	4.34
Fe_2O_3	3.24	2.44	3.70	4.29
FeO	1.64	1.82	1.88	1.59
MgO	7.10	6.35	8.95	15.40
CaO	5.48	3.54	6.33	6.59
Na_2O	1.52	1.52	1.96	0.74
K_2O	5.82	7.50	5.84	5.50
H_2O^+	0.39	1.47	0.28	1.96
H_2O^-	0.56	0.88	1.06	1.39
TiO_2	1.81	1.30	2.32	2.16
P_2O_5	2.15	2.30	3.50	1.21
MnO	0.13	0.11	0.13	0.16
CO_2	4.46	2.22	5.00	9.90
SrO	0.07	0.05	0.13	0.10
S	0.16			
Total	100.17	100.24	100.45	100.10
Q	21.90	24.84	15.04	0
Or	31.54	34.73	28.34	26.71
Ab	0	0	0	0
An	0	0	0	0
Lc	0	0	0	0
Ne	0	0	0	0
Kp	0	0	0	0
Si	11.33	2.26	7.36	21.94
Hy	15.38	18.58	22.77	25.44
Ol	0	0	0	8.65
Ac	9.70	7.20	11.04	5.99
Mt	0	0	0	0
Il	2.65	1.92	3.34	3.06
Hm	0	0	0	1.87
Ap	4.83	5.09	7.83	2.85
$CaTiSiO_4$	0.09	0	0.19	0.50
Pr	.15	0	0	0
Ru	0	0	0	0
Ks	1.58	3.65	2.58	2.98
Ns	0.76	1.63	1.51	0
Cs	0	0	0	0
Mg/Mg+Fe	.74	.74	.75	.83
Total Fe as FeO	4.56	4.02	5.21	5.45

1. P.C. 3-33 Tuff
2. P.C. 2-W4 (BBB) Tuff
3. P.C. 4-19 Tuff
4. P.C. 4-#5 Tuff

(1977) and will only be briefly discussed. Whole rock analyses and CIPW norms are listed in Table 2.

Kimberlite breccia, micaceous peridotite and tuff are distinguished from each other by their SiO_2 contents (%): 44, 40, and 55, respectively. All rock types show considerable variations in the major oxides, but the peridotite contains greater FeO, CaO, TiO_2 and MgO than the breccia and the tuff contains greater CaO, K_2O, Na_2O and Al_2O_3 than the breccia.

The kimberlite breccia is hypersthene normative, the micaceous peridotite is olivine normative and the tuff is quartz normative. The breccia is classified as lamprophyric (Brookins, 1970).

The relationship between the micaceous peridotite and kimberlite breccia is not fully understood, although their similar whole rock chemistry

B. Breccias	1	2	3	4	5	6
SiO_2	44.32	44.30	46.50	43.45	43.59	44.04
Al_2O_3	3.80	3.65	4.20	3.67	4.10	4.52
Fe_2O_3	5.95	5.26	5.82	7.18	7.43	6.10
FeO	1.15	1.04	1.18	0.81	0.57	0.82
MgO	20.00	22.40	19.20	21.70	20.85	16.90
CaO	4.15	3.60	3.70	2.95	2.76	5.24
Na_2O	0.50	0.16	0.23	0.13	0.20	0.14
K_2O	3.07	1.66	2.75	1.48	1.77	1.02
H_2O^+	0.30	3.36	0.58	2.76	0.74	1.70
H_2O^-	3.62	6.25	5.44	6.49	5.02	4.70
TiO_2	2.22	2.20	2.12	2.38	2.44	1.70
P_2O_5	1.85	1.45	0.95	1.15	1.06	2.94
MnO	0.11	0.05	0.12	0.11	0.08	0.20
CO_2	8.85	4.22	7.27	5.15	9.01	10.02
SrO	0.07	0.09	0.06	0.09	0.09	.08
Total	99.96	99.69	100.12	99.50	99.21	100.12
Q	0	0.87	2.99	2.12	2.10	12.21
Or	20.24	11.02	18.29	10.0	12.01	7.15
Ab	2.91	1.61	2.33	1.33	2.06	1.49
An	0	4.88	2.60	5.79	5.81	8.31
Lc	0	0	0	0	0	0
Ne	0	0	0	0	0	0
Kp	0	0	0	0	0	0
Di	5.22	0.77	6.90	0	0	0
Hy	52.33	69.11	56.23	68.51	66.10	55.35
Ol	5.01	0	0	0	0	0
Ac	1.68	0	0	0	0	0
Mt	0	0	0	0	0	0
Il	2.18	1.90	2.27	1.63	1.16	1.88
Hm	4.21	4.12	4.57	5.72	5.95	5.04
Ap	4.32	3.41	2.24	2.75	2.55	7.29
$CaTiSiO_4$	1.91	2.32	1.58	1.58	1.34	0
Pr	0	0	0	0	0	0
Ru	0	0	0	0.55	0.93	0.47
Ks	0	0	0	0	0	0
Ns	0	0	0	0	0	0
Cs	0	0	0	0	0	0
Mg/Mg+Fe	.85	.87	.84	.84	.84	.83
Total Fe as FeO	6.50	5.77	6.42	7.27	7.26	6.31

1. P.C. 3-9 Blue Kimberlite breccia
2. P.C. 3-18 Blue Kimberlite breccia
3. P.C. 3-8 Yellow green Kimberlite breccia
4. P.C. Ark C Yellow green Kimberlite breccia
5. P.C. 3-7 Yellow green Kimberlite breccia
6. P.C. 3-1 Yellow green Kimberlite breccia

implies a genetic relationship. Harker variation diagrams (Bolivar, 1977) suggest that the kimberlite may be a differentiated product of the peridotite, although field relationships suggest that the kimberlite intrusion occurred before the peridotite intrusion which is in conflict with interpretations of previous workers. The sequence of intrusion is believed to be (supported by geophysical data) kimberlite breccia, micaceous peridotite and then tuff.

Geophysical Study

Because of limited field exposure and the extremely weathered nature of the kimberlite, magnetic and gravity surveys were undertaken. A total of 120 permanent stations were surveyed for location and elevation at 30 to 150 m spacings. Temporary stations were then set up at 15 to 30 m intervals. Magnetic measurements were taken at all stations, gravity was taken at permanent

C. Miscellaneous Rocks

	1	2	3	4	5	6	7	8
SiO_2	38.34	40.33	39.26	38.78	42.90	41.48	38.04	37.09
Al_2O_3	5.10	4.00	3.97	3.38	3.75	3.72	3.84	3.69
Fe_2O_3	7.37	5.31	6.48	7.03	3.48	7.47	5.01	4.61
FeO	5.40	2.65	1.81	1.34	4.25	0.88	4.52	8.36
MgO	18.70	26.00	24.55	28.00	27.50	22.25	27.80	26.50
CaO	3.19	4.61	5.32	5.04	4.20	3.63	4.68	5.10
Na_2O	0.24	0.48	0.36	0.22	0.28	0.84	0.23	0.19
K_2O	1.42	2.80	2.41	2.13	4.00	1.80	3.40	2.30
H_2O^+	2.25	0.40	1.02	0.43	0.54	0.12	0.33	3.18
H_2O^-	4.95	0.48	2.59	1.59	0.48	3.01	1.45	1.52
TiO_2	3.80	2.47	2.68	2.61	2.48	2.92	2.10	2.50
P_2O_5	0.85	0.40	.21	0.38	1.01	1.22	0.40	0.28
MnO	0.15	0.12	.12	0.13	.12	0.10	0.14	0.16
CO_2	8.16	9.32	8.86	9.38	5.00	9.94	7.43	4.33
SrO	.14	0.09	.12	0.12	.11	0.13	0.11	0.11
S	.09	0.09			.09			
Total	100.15	99.55	99.75	100.56	100.19	99.51	99.48	99.92
Q	0	0	0	0	0	0	0	0
Or	9.87	17.55	15.57	13.33	20.56	11.89	4.32	6.77
Ab	2.54	4.57	3.53	2.09	0	8.43	0	0
An	10.17	0.52	2.30	2.06	0	1.19	0	2.55
Lc	0	0	0	0	0	0	13.32	6.04
Ne	0	0	0	0	0	0	0.55	1.08
Kp	0	0	0	0	0	0	0	0
Di	1.89	16.98	18.71	14.84	11.68	2.64	17.45	17.99
Hy	57.50	2.96	5.72	4.86	9.96	42.79	0	0
Ol	1.72	48.51	44.27	52.21	46.26	18.41	54.35	56.20
Ac	0	0	0	0	2.02	0	1.00	0
Mt	5.56	1.11	0	0	2.90	0	5.09	5.08
Il	6.23	3.65	3.27	2.42	3.47	1.70	3.05	3.67
Hm	2.34	3.19	4.94	5.19	0	5.82	0	0
Ap	2.09	0.89	0.48	0.84	2.12	2.85	0.87	0.62
$CaTiSiO_4$	0	0	1.22	2.16	0	4.27	0	0
Pr	.09	0.08	0	0	.08	0	0	0
Ru	0	0	0	0	0	0	0	0
Ks	0	0	0	0	0	0	0	0
Ns	0	0	0	0	0	0	0	0
Cs	0	0	0	0	0	0	0	0
Mg/Mg+Fe	.74	.86	.85	.87	.87	.84	.85	.79
Total Fe as FeO	12.03	7.43	7.64	7.67	7.38	7.60	9.03	12.51

1. P.C. R Massive yellow clay soil
2. P.C. 3-25 Micaceous Peridotite
3. P.C. B-11 Micaceous Peridotite
4. P.C. 4-16 Micaceous Peridotite
5. P.C. 3-23 Micaceous Peridotite
6. P.C. 3-20 D+H kimberlite breccia
7. P.C. 4-12 Micaceous Peridotite
8. P.C. 4-18 Micaceous Peridotite

stations only. All magnetic observations were made in a total field intensity Geometric Portable Proton Precision Magnetometer (± 1 gamma). Diurnal corrections were made hourly.

Gravity measurements were made with a Worden Gravity Meter Model 125-Pioneer (± 0.01 mgal). Instrumental, tidal, free air and Bouguer corrections were made, terrain corrections were not.

A regional Bouguer gravity map and regional total field intensity magnetic map (covering about 10 km^2 each) did not indicate any regional anomalies associated with the Prairie Creek intrusion (Bolivar, 1977). The total gravity anomaly over the Prairie Creek intrusion was only 0.5 mgal,

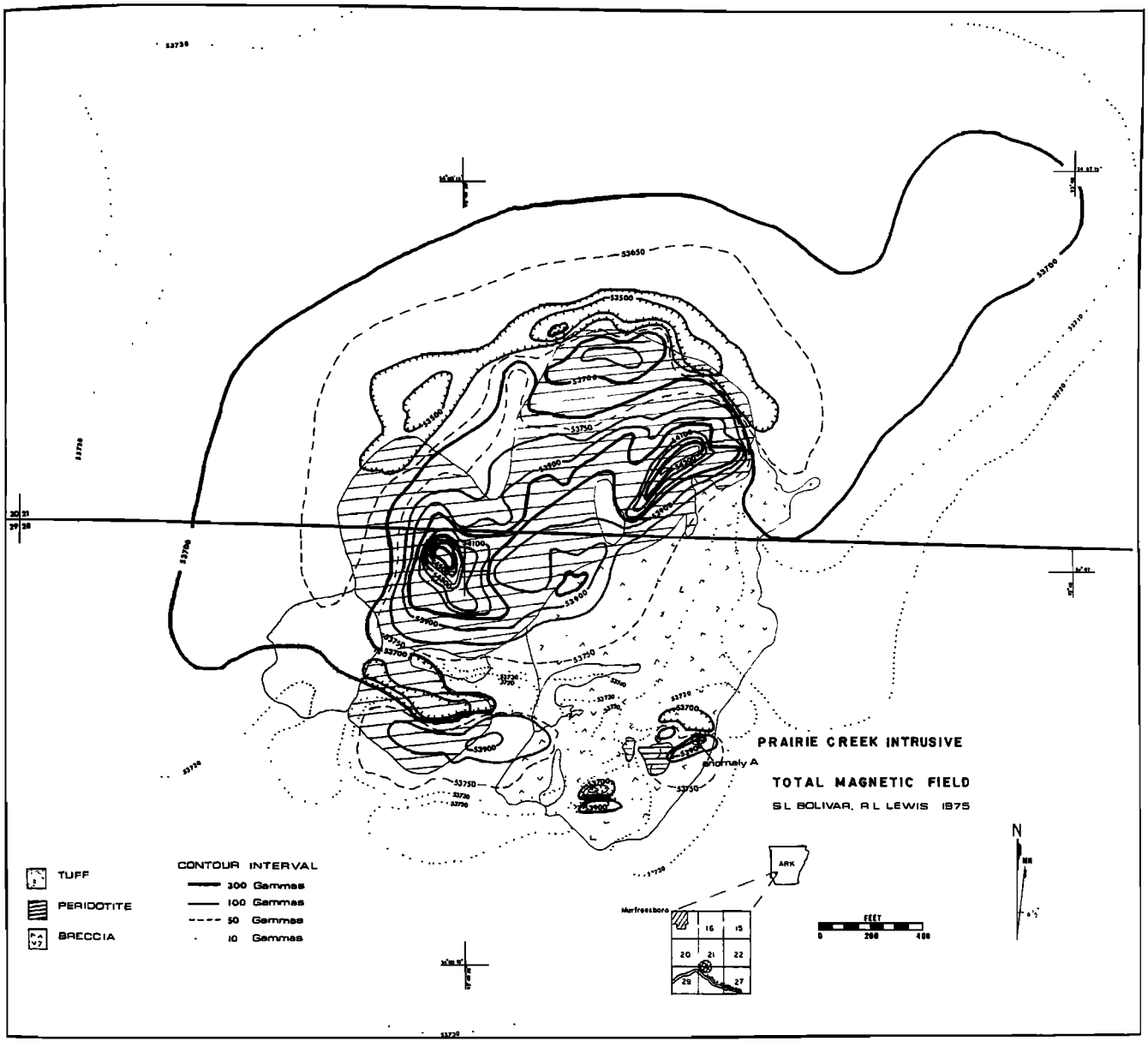

Fig. 2. Total magnetic field map of the Prairie Creek Intrusive.

suggesting the intrusion is very shallow. The gravity data will not be further discussed in this paper.

The detailed total magnetic intensity map (Fig. 2) is dominated by several highs in the northwestern half that reach a maximum of 900 + gammas. Magnetic profiles were examined and showed that magnetic highs occur only over the micaceous peridotite.

Discussion

A detailed geologic map combining geophysical data and field relationships is given in Fig. 1.

Magnetic anomalies are generally caused by differences in magnetic susceptibility which, in general, reflect the magnetite content of the rock. Igneous rocks are commonly more magnetic than sedimentary rocks. Magnetic intensity is an inverse square function; therefore the distance of any magnetic body from a magnetometer affects the size of the anomaly. Consequently, the intrusion of basic igneous rock into sedimentary rock would be expected to produce an anomaly.

Qualitative interpretation of magnetic and gravity data suggest the micaceous peridotite is a shallow, almost vertical, intrusion of slightly variable thickness, dipping slightly to the south.

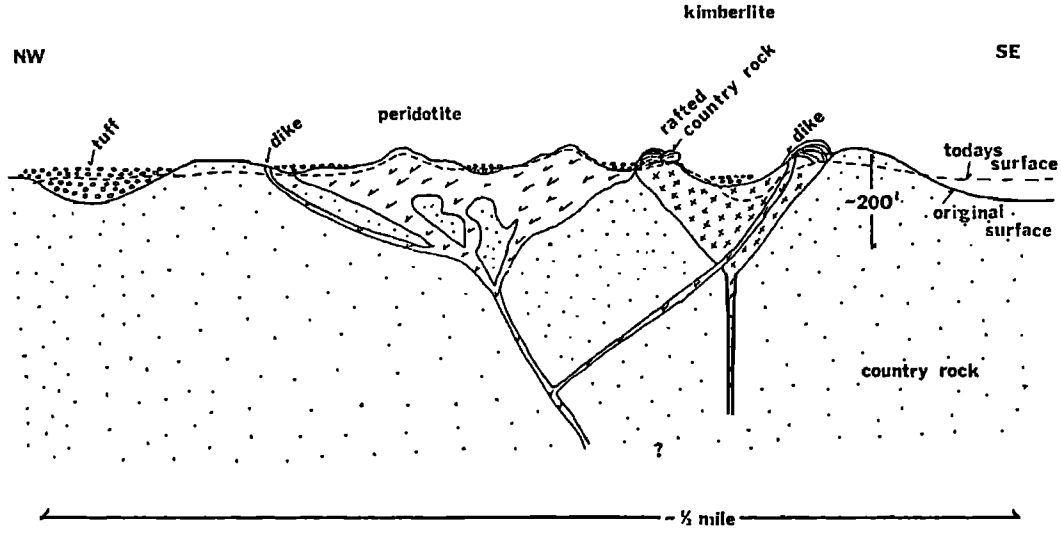

Fig. 3. Hypothetical schematic cross section of the Prairie Creek intrusion (scale exaggerated).

Small intrusions of peridotite in the southeast (Fig. 2) are believed to represent small apophyses of the large peridotite intrusion. Magnetic and gravity readings for one anomaly were taken at 3 m intervals for 30 m traverses for north-south, east-west, northeast-southwest, northwest-southeast legs, respectively. The gravity data reveal no anomaly but the magnetic data confirm the above interpretation.

Boundaries of the peridotite define (Fig. 1) an elongated oval shape, about 600 m long (northeast-southwest) and 240 m wide. By comparison, the kimberlite breccia is not clearly distinguishable by magnetic data but field relationships suggest a similar oval shape, southeast of the peridotite, about 480 m long (northeast-southwest) and 240 m wide. The tuff is indistinguishable from the breccia and country rock and has been mapped by field occurrence only. The relative magnetite content of the breccia, tuff and country rock (alluvium and Cretaceous conglomerates, sandstones and clays) apparently is very similar explaining why these rocks were indistinguishable using magnetic data. Using the above data and field relationships, a hypothetical schematic cross section of the Prairie Creek has been constructed (Fig. 3).

Rb-Sr Isotopy

Analytical Methods

Before analyses were conducted on selected whole rock samples, thin sections were examined for "freshness" on the basis of the criteria of Barrett and Berg (1975), independent of isotopic results.

All mass-spectrometric measurements were made using a 12 inch 90 degree sector, solid source, single filament Nuclide mass spectrometer equipped with a dual electrometer and a strip chart recorder. The $^{87}Sr/^{86}Sr$ ratios were determined on all samples; total Rb and Sr were determined by isotope dilution using ^{84}Sr and ^{87}Rb enriched spikes. Detailed analytical procedures and theories are given in Bolivar (1977). The precision in $^{87}Sr/^{86}Sr$ is generally $\pm$ 0.01% ($1\hat{\sigma}$) or better. The accuracy of the data was established by Eimer and Amend standards ($^{87}Sr/^{86}Sr$ = 0.7080 $\pm$ .0003, $1\hat{\sigma}$) and U.S.G.S. standard determinations ($\pm$ 1%).

Results

Prairie Creek whole rock $^{87}Sr/^{86}Sr$ ratios for all rock units average 0.7094 as shown in Figure 4. Kimberlite breccia (not including micaceous varieties) yield an average of 0.7092, with total Sr 1515-1253 ppm and total Rb 95-196 ppm and micaceous peridotite averages slightly lower (0.7089) with total Sr = 1015-1241 ppm and total Rb = 155-204 ppm. The D&H kimberlite breccia averages 0.7076 for the five freshest samples. Rb/Sr values for kimberlite breccia vary from 0.11 to 0.29, micaceous peridotite vary from 0.13 to 0.19 and tuff from 0.09 to 0.21. Ratios for fine-grained micaceous breccia vary from 0.31 to 0.36.

Plots of Sr versus Rb, $^{87}Sr/^{86}Sr$ versus Sr, $^{87}Sr/^{86}Sr$ versus Rb, Rb versus K_2O, and $^{87}Sr/^{86}Sr$ versus SiO_2 were made and there does not appear to be any relationship between total Sr and total Rb. The plot of $^{87}Sr/^{86}Sr$ versus Sr showed a faint suggestion of an inverse hyperbolic relationship between the two parameters, the highest ratios corresponding to the lowest Sr content for the kimberlite breccia and tuff, but not for the peridotite. If $^{87}Sr/^{86}Sr$ versus 1/Sr is plotted, there is a vague positive slope correlation. For $^{87}Sr/^{86}Sr$ versus SiO_2 only the plot of the tuff samples (a total of 4) suggest a positive corre-

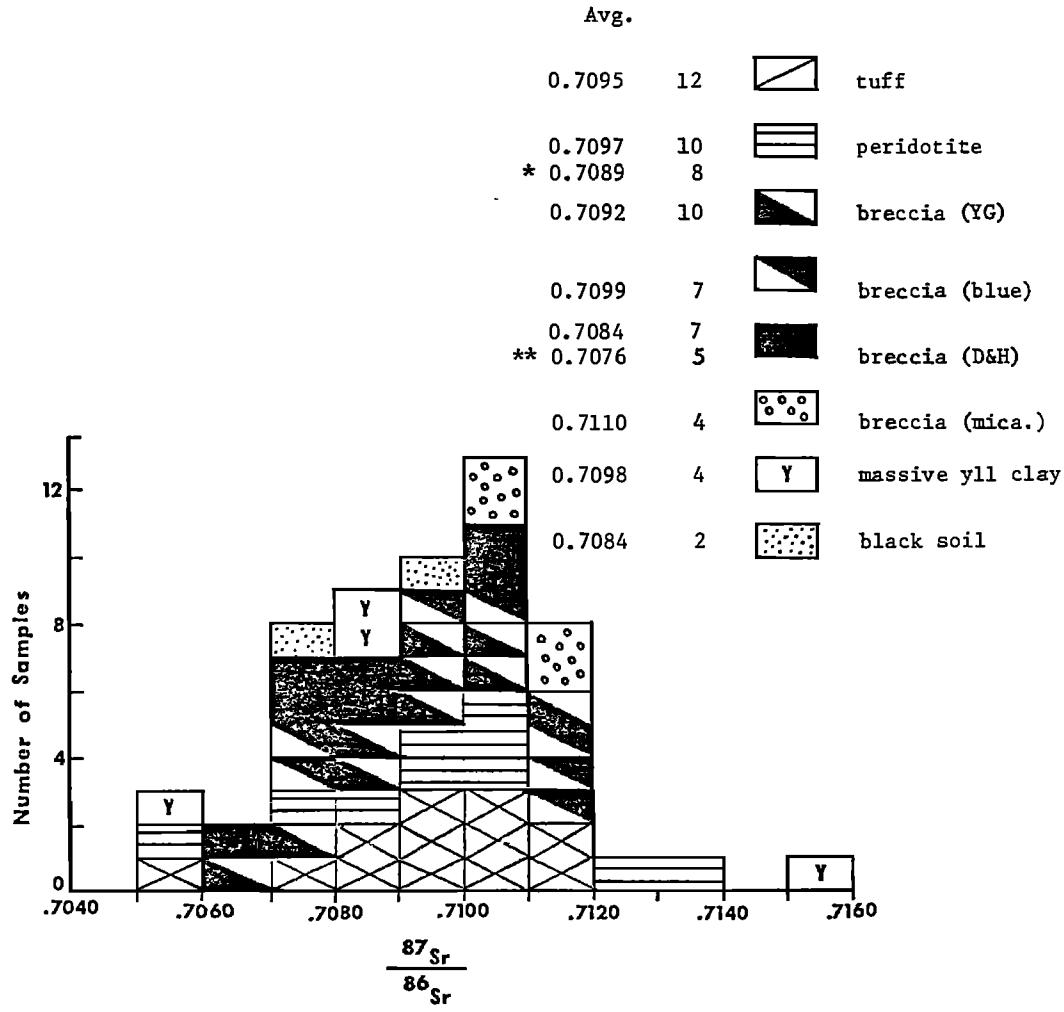

Fig. 4. Histogram-frequency plot of $^{87}Sr/^{86}Sr$, from Prairie Creek rocks. The peridotite total for eight samples (*) does not include two extremely weathered samples with 0.7120 and 0.7132 ratios. The D+H breccia total for five samples (**) does not include two extremely weathered samples with 0.7102 and 0.7104 ratios. The average for 52 samples (not including * and **) is 0.7094.

lation. Kudo et al. (1971) and Faure and Powell (1972) state that these relationships (i.e., a positive correlation for $^{87}Sr/^{86}Sr$ versus SiO_2 and an inverse hyperbolic correlation for $^{87}Sr/^{86}Sr$ versus Sr) suggest, but do not prove, contamination. Samples highest in $^{87}Sr/^{86}Sr$ and low in total Sr support this hypothesis. There does not appear to be any definite relationship between $^{87}Sr/^{86}Sr$ and Rb for any of the samples analyzed. If there has been no loss or gain of Rb one would expect a linear relationship for Rb versus K_2O, but such a relationship is absent for the samples analyzed.

Leach Studies

An extensive leach program using dilute HCl was undertaken to try to reduce the isotopic scatter. Unfortunately, 14 samples analyzed showed variable results for leachates and residues (Table 3). This variability probably results from sample inhomogeneity and possible ground water exchange.

Discussion

Two problems inherent in working with kimberlites are the extremely weathered nature and the heterogeneity of the samples; this is especially applicable to the Prairie Creek samples as all isochron whole-rock plots showed extreme scatter.

Several samples were analyzed in replicate. Laboratory analyses run in duplicate or repeated on the same aliquot produced results within reported error limits; but different aliquots of the

TABLE 3. Rb-Sr Data for Leach Studies*

Sample	Whole Rock - $^{87}Sr/^{86}Sr$		$^{87}Sr/^{86}Sr$ of Residue Relative to Whole Rock	Residue $^{87}Sr/^{86}Sr$
Ark C	(YG kimberlite breccia)	.7094	-	.7094
3-7	(YG kimberlite breccia)	.7093	Δ	.7108
3-8	(YG kimberlite breccia)	.7089	Δ	.7104
3-9	(blue kimberlite breccia)	.7115	∇	.7078
4-1	(D+H kimberlite breccia)	.7081	Δ	.7163
3-11	(D+H kimberlite breccia)	.7074	∇	.7070
3-24	(blue kimberlite breccia)	.7077	Δ	.7093
3-27	(micaceous kimberlite breccia)	.7114	∇	.7095
3-33	(tuff)	.7097	Δ	.7117
3-23	(peridotite)	.7066	Δ	.7069
3-25	(peridotite)	.7099	∇	.7084
4-16	(peridotite)	.7132	∇	.7083
B-11	(peridotite)	.7094	n.d.	n.d.
4-18	(peridotite)	.7020	∇	.7096

Sample	% Residue lower than Whole Rock	Rb Residue (ppm)	Rb Whole Rock (ppm)	Filtrate $^{87}Sr/^{86}Sr$ (leach .1N HCl-15 min.)	$^{87}Sr/^{86}Sr$ of Filtrate Relative to Whole Rock
Ark C	98	93	95	.7055	∇
3-7	100+	115	112	.7060	∇
3-8	96	141	147	.7079	∇
3-9	100+	148	147	.7092	∇
4-1	n.d.	n.d.	n.d.	.7069	∇
3-11	99	161	163	.7073	∇
3-24	99	81	82	.7093	Δ
3-27	100+	135	132	.7066	∇
3-33	100+	112	87	.7103	Δ
3-23	100+	182	155	.7079	Δ
3-25	91	174	191	.7089	∇
4-16	98	174	178	.7093	∇
B-11	n.d.	n.d.	193	.7067	∇
4-18	96	196	204	.7103	∇

Sample	Sr Whole Rock (ppm)	Sr Residue (ppm)	% Residue lower than whole rock	Rb/Sr Whole Rock	Rb/Sr Residue
Ark C	860	413	48	.11	.23
3-7	892	447	50	.13	.26
3-8	515	222	43	.29	.64
3-9	548	241	44	.29	.61
4-1	583	322	55	-	-
3-11	957	487	51	.17	.33
3-24	753	275	37	.11	.29
3-27	432	145	36	.31	.93
3-33	699	242	35	.13	.46
3-23	1151	580	50	.14	.31
3-25	1079	673	62	.18	.26
4-16	1131	765	68	.16	.23
B-11	1201	n.d.	n.d.	-	-
4-18	1241	811	62	.16	.24

*$^{87}Sr/^{86}Sr$ ratios precise to ± .0003 (1σ)

n.d. = not determined

same sample resulted in variable results (i.e., sample inhomogeneity). Minute calcite stringers suggest ground water interaction for many of the samples. There is a faint correlation between $^{87}Sr/^{86}Sr$ and $(K_2O/K_2O + Na_2O)$ for kimberlite breccia and tuff, but not for peridotite. This correlation would be expected because source regions rich in potassium will also be rich in Rb and, in time, rich in ^{87}Sr (Peterman and Hedge, 1971). If not due to contamination, this correlation suggests, due to the low Rb/Sr ratios, that the upper mantle is heterogeneous (Faure and Powell, 1972).

Clay Analyses

Questionable field relationships (Miser and Ross, 1923) bracket an age between Lower Cretaceous and Carboniferous (i.e., probable age of 130 m.y.). Five clay samples yield an isochron age of 108 m.y., but three samples give an age of 235 m.y. (Bolivar, 1977). Two samples can be excluded because they contain abnormal amounts of carbonate which was not removed by leach treatment. The other three samples contain abundant montmorillonite with minor chlorite and kaolinite. These age data are not reliable until more data are available although these preliminary results are encouraging for future studies.

Summary

Based on reproducibility of U.S.G.S. and E & A standards, the variations in $^{87}Sr/^{86}Sr$, total Sr and total Rb are not due to analytical procedures. Variability is predominantly attributed to interaction with ground water (causing isotopic disequilibrium), sample inhomogeneity, and heterogeneous source regions. Extreme care in selecting 'fresh' samples and tedious handpicking to remove xenoliths and megacrysts may (or may not) help to eliminate this scatter. The data were not amenable to isochron treatment.

Acknowledgements. Part of this study was financed by a National Science Foundation grant awarded as a joint investigation between D. G. Brookins, University of New Mexico, and H. O. A. Meyer, Purdue University, for "Study of the Mineralogic, Isotopic, and Geochemical Studies on Ultramafic Rocks and Associated Xenolith from the midcontinental U.S." Special thanks to Richard Lewis and especially Jim Cannon, Superintendent at the Center of Diamonds State Park, for his hospitality and help with the field work.

References

Barrett, D. R., and G. R. Berg, Complementary petrographic and strontium isotope ratio studies of South African kimberlite, Phys. Chem. Earth, 9, 619-635, 1975.

Bolivar, S. L., Geochemistry of the Prairie Creek, Arkansas and Elliott County, Kentucky intrusions, Ph.D. dissertation, Department of Geology, University of New Mexico, 1977.

Brookins, D. G., The Kimberlites of Riley County, Kansas, Kansas Geol. Survey Bull., 200, 1-32, 1970.

Brookins, D. G., R. S. Della Valle, and S. L. Bolivar, Significance of uranium abundance in United States kimberlites, in Extended Abstracts, Second International Kimberlite Conference, 1977.

Faure, G., and J. Powell, Strontium Isotope Geology, Springer-Verlag, New York, 188 p., 1972.

Kudo, A., K. Aoki, and D. G. Brookins, The origin of Pliocene-Holocene basalts of New Mexico in the light of strontium-isotopic and major-element abundances, Earth Planet. Sci. Letter., 13, 200-204, 1971.

Meyer, H. O. A., Kimberlites of the continental United States: A review, Jour. Geol., 84, 377-403, 1976.

Miser, H. D., and C. S. Ross, Diamond-bearing peridotite in Pike County, Arkansas, U. S. Geol. Survey Bull., 735, 279-322, 1923.

Mitchell, R. H., Kimberlite and related rocks -- a critical reappraisal, Jour. Geol., 78, 686-704, 1970.

Peterman, Z. E., and C. E. Hedge, Related strontium isotopic and chemical variations in oceanic basalts, Geol. Soc. Am. Bull., 82, 493-500, 1971.

Thoenen, J. R., R. S. Hill, E. G. Howe, and S. M. Runke, Investigation of the Prairie Creek diamond area, Pike County, Arkansas, U. S. Bureau of Mines Report of Investigations, 4549, 24 p., 1949.

THE CHEMICAL COMPOSITION OF KIMBERLITES COMPARED WITH THE AVERAGE COMPOSITION OF THREE BASALTIC MAGMA TYPES

K. H. Wedepohl and Y. Muramatsu

Geochemical Institute, University of Goettingen, Fed. Rep. Germany

Abstract. New data on Li, F, S, V, Cr, Mn, Co, Mi, Cu, Zn, Rb, Sr, Y, Zr, Nb, Cd, Ba, Hg, Tl, Pb, Bi and the major elements in 11 South African kimberlites do not scatter much about their arithmetic means (exceptions: alkali elements and S). Olivine, serpentine, pyroxene, phlogopite, perovskite, spinel, magnetite and Fe-Ni-Cu-S ores from selected kimberlites have been analyzed by microprobe. Native copper occurs in one sample. Data on about 70 elements in kimberlites, nephelinites, alkali olivine basalts and tholeiitic basalts have been compiled from the literature. These rocks formed from magmas which are thought to be partial melting products of the upper mantle. Therefore, they have been compared chemically with ultramafics. There exist surprising similarities and specific differences between the 4 magma series in the degree of element accumulations or depletions. Cr, Ni, Mg, Co are incorporated in the residual ultramafic material and are increasingly depleted from kimberlites to tholeiites. Mn, Fe, Sc must have bulk distribution coefficients close to one between ultramafics and basaltic melts. Al, Ga and the heavy REE have a tendency towards the residual minerals garnet and orthopyroxene and are low in kimberlites exclusively. Sodium might be specifically transported from kimberlitic magmas to country rocks by CO_2 vapor (fenitization). The so-called incompatible elements Th, U, light REE, Nb, Ta, etc. are almost consistently increasing from tholeiites to kimberlites followed by the heavy alkalies, alkaline earths, Pb, Tl and Li. Regularities in element distribution can be easily explained if magmas represent increasing fractions of partially melted mantle rocks from kimberlites to tholeiitic basalts. Alkali basalts and nephelinites being intermediate between tholeiitic basalts and kimberlites. A constant increase of the heavy sulfur isotope and of the Fe^{3+}/Fe^{2+} ratio from tholeiitic basalts ($\delta^{34}S$-0.3 ‰; Fe_2O_3/FeO = 0.32) to kimberlites ($\delta^{34}S$+4.6 ‰; Fe_2O_3/FeO = 1.3) must be due to losses of light sulfur and of hydrogen from magmas approaching the earth's surface.

Kimberlites

The minor elements Li, F, S (plus S isotopes), V, Cr, Mn, Co, Ni, Cu, Zn, Rb, Sr, Y, Zr, Nb, Cd, Ba, Hg, Tl, Pb, Bi and major elements were determined in 11 South African kimberlites from the Kimberley area (column A of Table 1). Most elemental concentrations scatter little about the arithmetic mean ($\bar{x}$). Exceptions are the alkali elements and sulfur. The majority of values range from $\bar{x}/2$ to $2\bar{x}$. The detailed information on procedures and separate samples has been published by Muramatsu (1977). Additional data (column B of Table 1) on 60 elements in bulk kimberlites have been compiled from the literature (for references see Muramatsu, 1977). The averages for 44 elements are computed of more than 40 values each and those for 20 elements are based on more than 500 separate values. Averages for geographic subgroups scatter about the total average in ranges of different size. For example, the subgroup means for Li, S, Sc, V, Cr, Co, Ni, Cu, Gd and Lu occur in the range from $\bar{x}/2$ to $2\bar{x}$. For the subgroup averages of Be, Zn, Y, Zr, Nb, Sm, Tb, Yb, Hf, Pb and Th the range is $\bar{x}/3$ to $3\bar{x}$ and for B, F, Rb, La, Ce and Nd it is $\bar{x}/4$ to $4\bar{x}$. These ranges generally increase with the absolute abundance in kimberlites. A large scattering of subgroup means has been observed for Sn, Cs, Ba and Eu. Good correlations between Cr-Ni-Co and K-Rb have been observed in the South African kimberlites but correlations between Pb-Tl-K which might have been expected for crystal chemical reasons, do not exist.

The composition of olivine, serpentine, pyroxene, garnet, spinel, magnetite, ilmenite, perovskite, rutile, and Fe-Ni-Cu-S ores from selected South African kimberlites has been investigated by microprobe (see averages in Table 3). The olivine is very close in composition (except Ca, Sr) to olivine from "average" ultramafic rocks as listed in Table 2. The Al content of kimberlitic pyroxenes is less than a fifth of that from ultramafic pyroxenes (Table 2), but sodium and potassium are higher in kimber-

TABLE 1, Page 1

Element in ppm	A[a] Kimberlites (11) This publication	B Kimberlites (N)	C Nephelinites (N)	D Alkali olivine basalts	E Tholeiitic basalts	F Ultramafic rocks	Ratio B/F	Ratio C/F	Ratio D/F	Ratio E/F
Li	~15(A*)	25(75)	16(22)	12	7	2	12.5	8.0	6	3.5
Be		~1(45)			0.7	~ 0.4	~2.5			1.8
B		36(64)			5.8	7	5.1			0.83
C	14800(E)	16200(<670)	205(12)			100	162	2.1		
N						14				
O						429000				
F	1870(E)	1900(93)				97	19.6			
Na	3580(A)	2030(>670)	25300(148)	23000	17580	2230	0.91	11.3	10.3	7.9
Mg	153000(X)	160000(>670)	71200(148)	45230	36910	247500	0.64	0.28	0.18	0.15
Al	17840(X)	18900(>670)	61600(148)	79390	80400	14300	1.3	4.3	5.55	5.62
Si	159000(X)	147000(>670)	188400(148)	226200	239200	203300	0.72	0.93	1.11	1.18
P	4890(X)	3880(>670)	3800(148)	2090	960	220	17.6	17.3	9.5	4.36
S	2180(E)	2000(527)	620(4)			~4000	0.5	0.16		
Cl		300(82)	518(6)			110	2.7	4.7		
K	13300(XA)	10400(>670)	12200(148)	13280	6970	390	26.7	31.3	34.1	17.9
Ca	67500(X)	70400(>670)	90000(148)	65040	72260	27200	2.6	3.3	2.4	2.66
Sc		15(166)	21(8)	20	30	15	1.0	1.4	1.3	2.0
Ti	9110(X)	11800(>670)	16800(148)	14390	9710	780	15.1	21.5	18.4	12.4
V	98(A*)	120(534)	221(63)	213	251	50	2.4	4.4	4.3	5.0
Cr	1380(A*)	1100(594)	344(88)	202	168	3090	0.36	0.11	0.07	0.054
Mn	1240(X)	1160(>670)	1500(148)	1472	1356	1040	1.1	1.5	1.4	1.3
Fe	61400(X)	71600(>670)	91080(148)	90780	85540	64830	1.1	1.4	1.4	1.32
Co	87(A*)	77(591)	52(51)	43	48	110	0.7	0.47	0.39	0.44
Ni	1160(A*)	1050(676)	291(79)	145	134	1450	0.72	0.20	0.10	0.10
Cu	85(A)	80(555)	63(45)	85	90	47	1.7	1.3	1.8	1.91
Zn	85(A)	80(33)	102(40)	108	100	56	1.4	1.8	1.9	1.79
Ga		~10(34)	15(13)	15	17	2.5	~4	6.0	6.0	6.8
Ge		~ 0.5(48)	1.6(3)		1.4	1	~0.5	1.6		1.4
As					1.5	1				1.5
Se		~ 0.15(40)				0.02	7.5			
Br						0.24				
Rb	58(A)	65(148)	39(76)	32	22	1.2	54.1	32.5	26.7	18.3
Sr	632(A*)	740(666)	1350(81)	530	328	22	33.6	61.4	24	14.9
Y	13(X)	22(90)	36(30)	33	28	2.88	7.6	12.4	11.5	9.7
Zr	240(X)	250(517)	205(87)	189	137	16	15.6	12.8	11.8	8.6
Nb	110(X)	110(609)	103(61)	69	13	1.3	84.6	79.2	53.1	10.0
Mo		~0.5(31)			1	0.2	~2.5			5.0
Ru		0.007(10)								
Rh		0.007(10)								

TABLE 1, Page 2

	A	B	C	D	E	F				
Element in ppm	[a] Kimberlites (11) This publication	Kimberlites (N)	Nephelinites (N)	Alkali olivine basalts	Tholeiitic basalts	Ultramafic rocks	Ratio B/F	Ratio C/F	Ratio D/F	Ratio E/F
Pd		0.053(10)				0.01	5.3			
Ag					0.11	0.05				2.2
Cd	0.073(A**)	0.07(11)	0.052(4)	0.082	0.17	0.06	1.2	0.87	1.4	2.8
In			0.034(4)		0.07	0.02		1.7		3.5
Sn		15(18)			1.5	0.52	28.8			2.88
Sb					0.3	0.1				3.0
Te						~ 0.001				
I						0.13				
Cs		2.3(58)			1.1	0.006	383			183
Ba	808(A*)	1000(111)	1046(61)	528	246	20	50	52.3	26.4	12.3
La		150(94)	89(31)	54	15	0.92	163	96.7	58.7	16.3
Ce		200(89)	171(31)	105	32.9	1.93	104	88.6	54.4	17.0
Pr		22(4)	18(22)	28	4.7	0.32	68.8	56.3	87.5	14.7
Nd		85(65)	66(31)	49	18.9	1.44	59	45.8	34.0	13.1
Sm		13(75)	14.5(18)	9.1	4.9	0.40	32.5	36.3	22.8	12.3
Eu		3.0(75)	4.0(18)	3.5	1.5	0.16	18.8	25	21.9	9.4
Gd		8.0(16)	12.1(16)	8.1	5.5	0.74	10.8	16.4	10.9	7.4
Tb		1.0(73)	1.7(9)	1.8	1.2	0.12	8.3	14.2	15.0	10.0
Dy			7.3(18)	4.7	4.9	0.57		12.8	8.2	8.6
Ho		0.55(3)	1.7(9)	1.9	1.3	0.16	3.4	10.6	11.9	8.13
Er		1.45(3)	3.3(14)	2.4	2.8	0.40	3.6	8.3	6.0	7.0
Tm		0.23(3)	0.88(7)	0.7	0.46	0.067	3.4	13.1	10.4	6.9
Yb		1.2(75)	2.3(18)	1.9	2.6	0.38	3.2	6.1	5.0	6.8
Lu		0.16(72)	0.39(17)	0.5	0.46	0.065	2.5	6.0	7.7	7.1
Hf		7(82)	5(2)		2.5	0.6	11.7	8.3		4.2
Ta		9(111)	19(9)		0.5	≤0.1	≥90	≥190		≥5
W			11(5)		0.7	(0.3)?		(36.7)?		(2.3)?
Re						(0.2)				
Os		0.005(10)								
Ir		0.007(10)								
Pt		0.19(10)			0.02	0.06	3.2			0.33
Au		0.004(14)		0.0016	0.004	0.007	0.57		0.23	0.57
Hg	0.008(A**)	0.01(12)	0.02(4)	0.017	0.01	0.03	0.33	0.67	0.57	0.33
Tl	0.22(A**)	0.22(11)	0.009(4)	0.05	0.1	0.010	22	0.9	5	10.0
Pb	8.5(A*)	10(35)	7.8(22)	4.3	3.7	0.20	50	39	21.5	18.5
Bi	0.024(A**)	0.03(11)	0.014(4)	0.03	0.03	0.006	5.0	2.3	5.0	5.0
Th		16(176)	11(24)	3	1.8	0.07	229	157	43	25.7
U		3.1(176)	3.2(11)	0.7	0.5	0.025	124	128	28	20.0

a Analytical methods: A Atomic absorption (flame); A* Atomic absorption (flameless); A** Atomic absorption (with preconcentration); X X-ray fluorescence; E Electrochemical methods

(N) Number of samples

TABLE 2. "Average" elemental abundances (in ppm) in minerals of ultramafic rocks of potential mantle origin (sources of data in footnote).

	Olivine	Clino-pyroxene	Ortho-pyroxene	Cr spinel	Garnet (pyrope-rich)	Phlogo-pite	Parga-sitic amphibole
Na	150	8160	556	n.d.	300	5490	25200
Mg	300000	102500	205700	97200	126700	138700	115800
Al	≤530	21170	16410	164800	112700	66690	70000
Si	188670	245200	258500	3740	195400	193000	204300
K	7	380	25	n.d.	<30	77710	5800
Ca	500	145100	6075	n.d.	32160	145	80000
Ti	210	1750	420	14690	1510	1920[b]	4320
V	5	200	60	530	~150	n.d.	200
Cr	176	7530[a]	2320	177900	31760	48200	11840
Mn	1000	775	853	1000	2640	190	850
Fe	70700	27620	48950	173000	55190	20440	27800
Co	183	40	50	~150	100	n.d.	70
Ni	2800	330	700	~1000	160	1900	70
Cu	50	45	30	n.d.	5	n.d.	7
Zn	65	80	60	(1000)	n.d.	(440)	(350)
Rb	0.03	1	0.3	n.d.	3	255	10
Sr	0.5	~100	7	n.d.	10	18	~400
Ba	0.5	84	14	n.d.	17	1400	260
La	0.06	2.5	0.006	0.62	0.018	225	39
Ce	0.18	6.3	0.019	1.1	1.7	~400	32
Pr	0.015	1.3	0.004	0.14	0.29	68	3.9
Nd	0.08	7.0	0.047	0.54	2.9	222	11
Sm	0.013	1.8	0.05	0.093	1.6	48	2.5
Eu	0.0025	0.75	0.03	0.017	0.73	0.36	0.66
Gd	0.02	3.0	0.15	0.10	2.5	n.d.	2.4
Tb	0.003	0.45	0.04	0.014	0.7	7.3	0.58
Er	0.02	1.5	0.36	0.08	1.5	n.d.	1.2
Yb	0.03	1.0	0.5	0.07	1.5	22	0.9
Lu	0.007	0.19	0.085	0.013	0.48	2.7	0.1
U	0.007	0.12	0.06	n.d.	n.d.	0.24	n.d.

n.d.: no data.
a: in garnet peridotite often higher (Carswell, 1973, etc.).
b: in mica garnet peridotite from Lashaine (Tanzania): 54800 ppm Ti (Dawson, et al., 1970).

Most values from compilation in Wedepohl (1975) except: Ni in phlogopite (Aoki, 1975), Rb in olivine, pyroxenes and garnet, Sr and Ba in olivine (Griffin and Murthy, 1969), several RE in garnet (Shimizu, 1975), RE in phlogopite (Herrmann, 1970), U in olivine, pyroxenes, phlogopite (Dostal and Caperdri, 1975), Cr in garnet (Boyd, et al., 1976).

litic clinopyroxene. Ca and Cr are lower in kimberlitic orthopyroxene. Except for the low Ti and Ca content of kimberlitic garnet from Newland (South Africa) its composition is comparable to garnets from ultarmafics. The kimberlitic phlogopites are appreciably higher in Fe and Ti than those from the reference peridotites. Cr and Na are lower in kimberlitic phlogopite. Perovskite containing 0.5 to 1.9% La_2O_3 and 1.5 to 5.1% Ce_2O_3 occurs as a major host of the REE in kimberlite. The spinels can be very heterogeneous with respect to their Ti content. They contain twice the Cr and a quarter of the Al content of the reference in Table 2. The ore of kimberlite from the De Beers mine (Excursion Stop 4) contains pentlandite, heazlewoodite and native copper. In kimberlite from Loxtondal there is more than 2% pyrite and in Koffyfontein less than 0.1%. Rutile from the De Beers mine contains as much as 2.8% Cr_2O_3.

Magmas of kimberlites, nephelinites and basalts (tholeiites and alkali olivine basalts) are thought to be partial melting products of mantle rocks. Therefore, they are compared chemically with ultramafics from the upper

TABLE 3. Elemental abundances (in ppm) in minerals of kimberlites from the Kimberley area (S. Africa) (Muramatsu, 1977).

	Olivine (N:2)[a]	Clinopyroxene (N:1)[a]	Orthopyroxene (N:1)[a]	Garnet (N:1)[a]	Phlogopite (N:2-5)[a]	Spinel (N:5)[a]
Li	<1	<2	≤3	<1	6	n.d.
F	n.d.	n.d.	n.d.	n.d.	4,800	n.d.
Na	88	12,700	1,200	340	1,980	n.d.
Mg	299,000	100,000	216,000	138,000	154,000	75,600
Al	160	4,900	1,060	92,200	61,900	38,100
Si	191,000	258,000	273,000	198,000	190,000	n.d.
S	90	n.d.	n.d.	n.d.	250	n.d.
K	53[b]	1,300	1,490[b]	1,100[b]	81,300	n.d.
Ca	140	141,000	1,800	22,500	(1,300)	n.d.
Ti	150	1,100	600	360	7,850	15,500
V	5	305	20	200	65	n.d.
Cr	230	8,350	1,200	40,000	2,100	382,000
Mn	1,000	540	930	2,400	n.d.	6,300
Fe	77,000	24,900	48,400	53,100	42,700	170,000
Co	130	24	58	44	73	n.d.
Ni	3,080	440	800	135	1,450	n.d.
Cu	20	23	20	20	51	n.d.
Zn	66	49	61	80	150	n.d.
Rb	<10	<10	<10	<10	550	n.d.
Sr	10	460	32	40	71	n.d.
Cd	0.059	0.010	0.028	0.10	0.022	n.d.
Ba	18	135	58[b]	90[b]	1,140	n.d.
Tl	0.016	0.016	0.015	0.095[b]	0.78	n.d.
Pb	<0.5	1.4	0.8	1.0	2.9	n.d.
Bi	0.007	<0.007	<0.005	<0.007	<0.010	n.d.

a Number of specimens investigated.
b Potential contamination from phlogopite.
n.d. no data

mantle. Accumulations or depletions of several incompatible and refractory elements in kimberlites and basalts relative to ultramafic rocks indicate certain processes of melting and the contribution of specific mantle minerals to kimberlitic and basaltic magmas.

Basaltic Rocks

Analytical data have been compiled for nephelinites, alkali olivine basalts and tholeiitic basalts as for kimberlites. They are listed in columns C, D, E of Table 1. With the exception

TABLE 4. Distribution coefficients (D) for several phases in equilibrium with liquid: basalt or peridotite magma (according to Shaw, 1972) (except U and Zn).

	$D^{cpx-liq}$ (x 100)	$D^{opx-liq}$ (x 100)	D^{ol-liq} (x 100)	$D^{gar-liq}$ (x 100)	$D^{amp-liq}$ (x 100)	$D^{phl-liq}$ (x 100)	D^{sp-liq} (x 100)
K	6	1	0.8	2.5	261	150	
Ni	222	296	1350	85	404	(1000)[b]	1000
Zn	50[a]	(86)[b]	86[a]				
Rb	5	1	0.8	3	115	150	
Sr	20	1	2	1.5	25	8	
Ba	8	1	1	4	800	280	
La	2	0.1	0.8	2	75	10	10
Ce	1.7	0.2	0.9	35	10	10	10
Yb	60	14	2	4000	45	10	5
U	4.1[c]	0.6[c]	0.25[c]				

a Bougault and Hekinian (1974).
b estimated.
c Dostal and Capedri (1975).

TABLE 5. Relative contributions of mantle minerals at the beginning of melting, if the mantle contains 56% olivine, 32.5% orthopyroxene, 5% clinopyroxene, 6% garnet and 0.3% phlogopite. Tentatively computed from elemental abundances of Table 2 and distribution coefficients of Table 4 (Shaw, 1972, etc.).

Element	Olivine %	Orthopyroxene %	Clinopyroxene %	Garnet %	Phlogopite %
K	27	44	17	4	8.4
Ni	55	36	3.5	5.3	≤0.3
Zn	≤ 58	≤31	≤ 11	?	?
Rb	11	51	5.2	31	2.6
Sr	4.6	74	8.1	13	0.2
Ba	5	81	9.3	4.5	0.3
La	22	10	33	0.3	35
Ce	25	6.9	41	0.7	27
Yb	31	42	3	0.1	24
U	≤ 32	≤66	≤ 2.8	?	?

of Sr, Cd and Hg in alkali olivine basalts data and references are the same as reported by Wedepohl (1975). The Sr value is from Faure (1978) and Cd, Hg from Heinrichs (1975). The data on major elements in nephelinites are from publications by Gehnes and Wimmenauer (1975), Hawkins and Natland (1975), Kesson (1973), Lohmann (1964), Nockolds (1954), Varne (1968), Wedepohl (1968), Wilkinson (1975), and Wood (1968). The minor element averages for nephelinites are

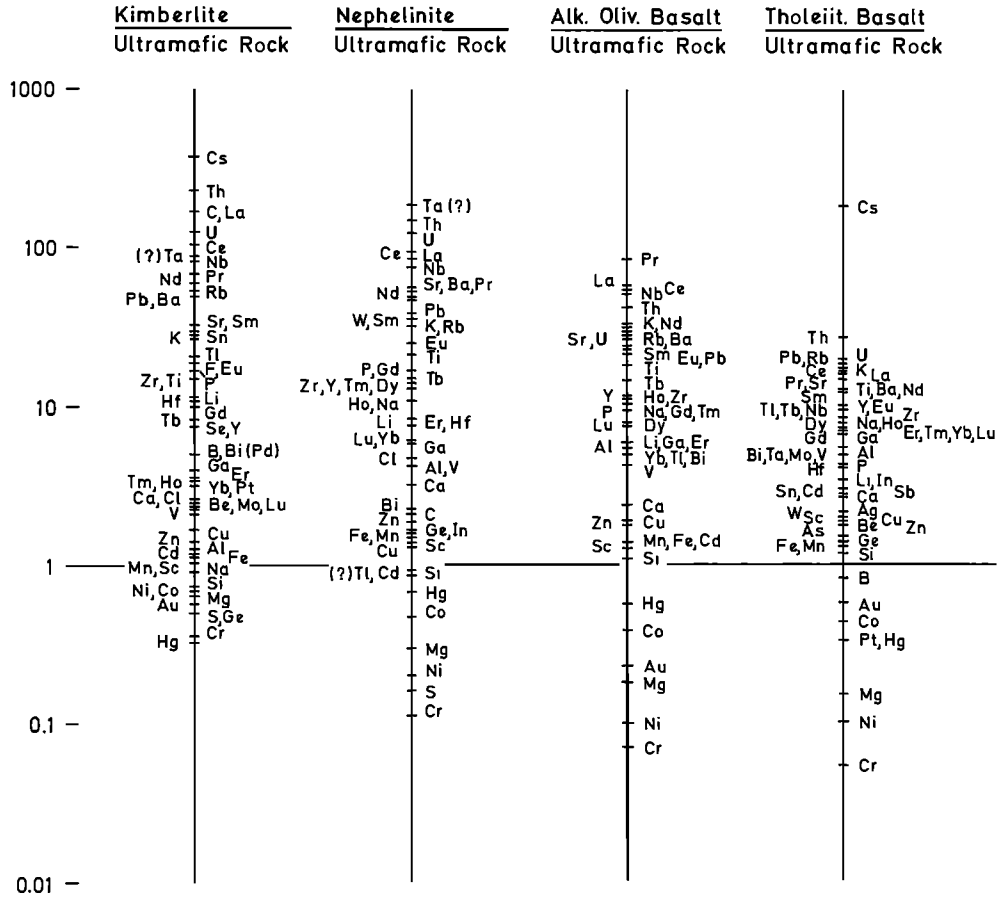

Fig. 1. Abundance of about 60 elements in kimberlites, nephelinites, alkali olivine basalts and tholeiitic basalts relative to their abundance in ultramafic rocks.

computed from results published by Agiorgitis (1967), Borodin and Gladkikh (1967), Brooks (1970), Gehnes and Wimmenauer (1975), Gladkikh and Viktorova (1967), Gottfried, et al. (1972), Gottfried (1977, personal comm.), Hawkins and Natland (1975), Heinrichs (1975), Herrmann (1968), Kay and Gast (1973), Kesson (1973), Lipman, et al. (1973), Lohmann (1964), MacDonald (1968), Mengel (1977), Pourmoafi (1977), Prinz (1967), Schilling and Winchester (1969), Schulz-Dobrick (1971), Wedepohl (1961) and various authors of the Handbook of Geochemistry Vol. II. The number of individual values used for element averages in nephelinites is indicated in column C of Table 1. For alkali olivine basalts (column D) and especially for tholeiitic basalts (column E) even larger sets of data were available.

It might be attractive to discriminate even between subgroups of the three basaltic magma types listed in Table 1 as Velde and Yoder (1976) have recently compiled analyses of melilite-bearing nephelinites. Sufficient data are available for oceanic tholeiitic basalts which are even more depleted in several incompatible elements than tholeiites.

Ultramafic Rocks

Magmas of kimberlites, nephelinites and basalts are thought to be melting products of mantle rocks. Therefore their chemical composition has been compared with that of ultramafic rocks from the upper mantle. For this comparison data on spinel lherzolites and garnet peridotites from the compilation published by Wedepohl (1975) are used. Revised figures on S, Zr, and Ta have been taken from the following references: S: Shima and Naldrett, 1975; Zr: Erlank, et al., 1978; Ta: Wedepohl, 1978.

The average mineral composition of upper mantle rocks has been estimated from lherzolites, harzburgites, etc. of worldwide sampling to be 67% olivine, 24% orthopyroxene, 8% clinopyroxene and 1.5% spinel in case of spinel lherzolites,

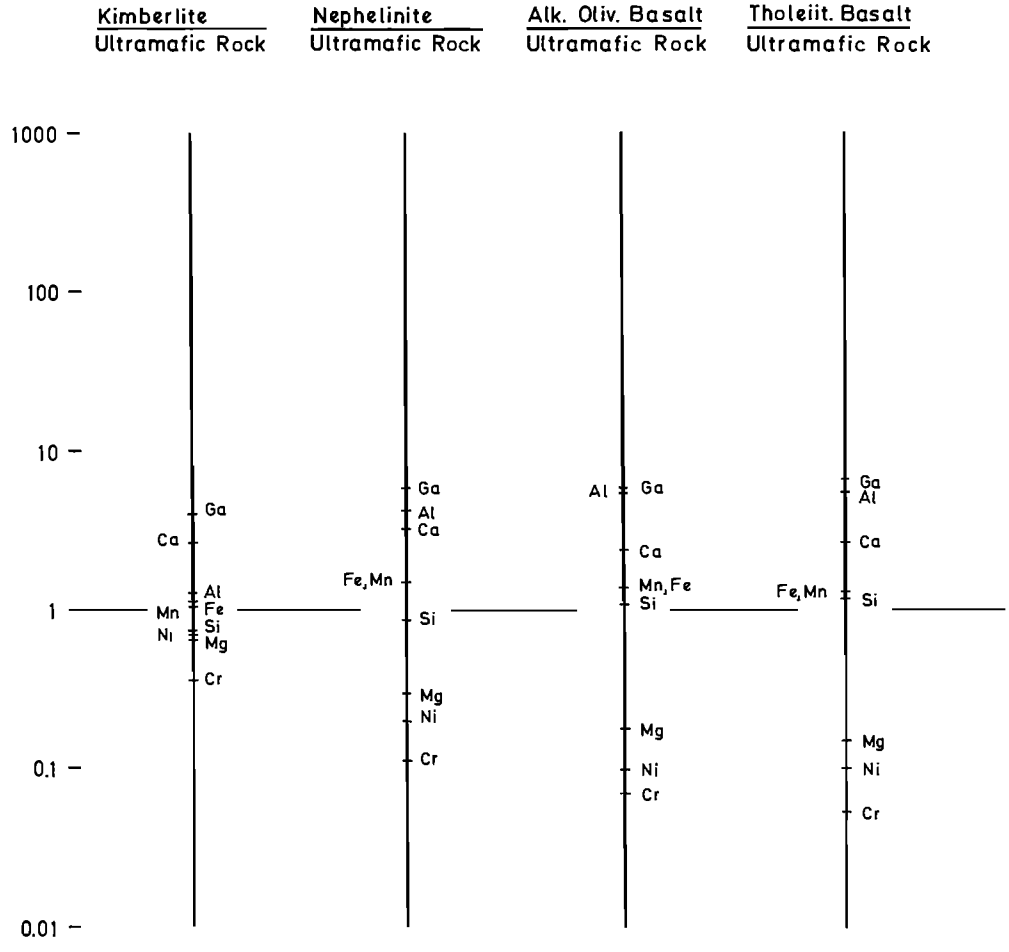

Fig. 1a. Abundance of related elements in kimberlites, nephelinites, alkali olivine basalts and tholeiitic basalts relative to their abundance in ultramafic rocks. Several major elements, Ga and the "residual" elements Mg, Ni, Cr.

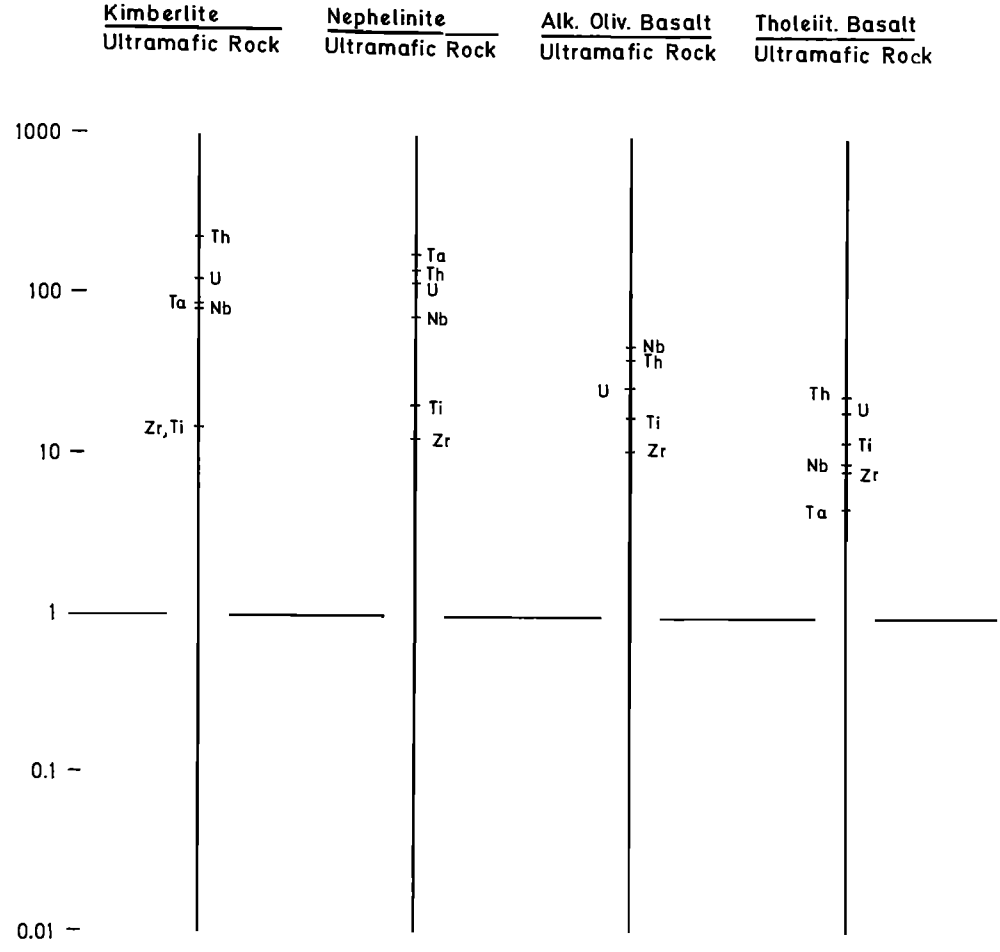

Fig. 1b. Abundance of related elements in kimberlites, nephelinites, alkali olivine basalts and tholeiitic basalts relative to their abundance in ultramafic rocks. Incompatible elements.

and 56% olivine, 32.5% orthopyroxene, 5% clinopyroxene, 6% garnet and 0.3% phlogopite in case of garnet peridotites. Nodules and masses of similar composition are apparently abundant in alkali basalts, kimberlites or occur as peridotite intrusions. It is likely that several of the ultramafic rocks used for analytical investigations and data compilations are residual material from partial melting.

No minerals of ultramafic rocks nor their combinations have the chemical composition of any abundant magma. Therefore element fractionation during partial melting of several mantle minerals must be assumed to be an important process of magma generation.

Origin of Basalt and Kimberlite Magmas

If one knows elemental distribution coefficients (D) between mantle minerals and melts (Table 4), the composition and abundance of mantle minerals (Table 2) and the degree of partial melting, the composition of magmas can be calculated. Such computations have been published by several authors. But the success is usually limited by the quality and availability of distribution coefficients. For our purposes we have used distribution coefficients as compiled by Shaw (1972) and supplemented by values on U from Dostal and Capedri (1975) and on Zn by Bougault and Hekinian (1974). In using these distribution coefficients for genetic considerations one must be aware of their dependence on temperature, pressure and sample composition.

In order to obtain tentative information on relative contributions of mantle minerals at incipient melting we have computed values for 10 elements from data of Tables 2 and 4 and the average garnet peridotite composition mentioned earlier. The formula used for the calculation of the contribution of each mineral fraction at incipient melting is:

$$c_L = (xc_S)D^{-1} \qquad (1)$$

where c_L and c_S are elemental concentrations in melt and mantle minerals respectively and x is the mineral fraction in average mantle rocks.

For 10 elements and incipient melting we have calculated the percentage contribution from individual minerals of a 5-phase garnet peridotite. These data are presented in Table 5. Because of the change of the mineral composition during partial melting or complete reaction of individual minerals our values of individual contributions were restricted to incipient melting.

All elements with low distribution coefficients (D) in major mantle minerals are good candidates to be accumulated in magmas. They can even effectively be contributed to magmas by incipient partial melting of orthopyroxene which crystal chemically is an unfavored host for the large ions of K, Rb, Ba, Sr and U. Relatively high concentrations as those of RE elements in phlogopite combined with a low distribution coefficient make this accessory mineral a good contributor to magmas. If an element has a high distribution coefficient like Ni in olivine, it must be combined with a high Ni concentration and a large abundance of that mineral to influence the magma composition.

For comparison of typical element accumulations and depletions in basalts and kimberlites ratios of element concentrations in the four magmatic rock types relative to those in ultramafic rocks are plotted in Figure 1 (plus 1a, 1b, 1c, 1d).

There are at least six different patterns of element distribution. The following groups can be observed:

1. Elements almost as abundant in basalts and kimberlites as in ultramafic rocks: Fe, Mn, Si (Fig. 1a).
2. Elements almost equally accumulated in all basalts and kimberlites: Ca, Zn, Cu (Figs. 1 and 1a).
3. Elements increasingly accumulated from tholeiitic basalts to kimberlites: U, Th, Nb, Ta (Zr, Hf), P, Cs, Li, Rb, Pb, Ba, light REE (Figs. 1b, 1c, 1d, 1).
4. Elements accumulated almost equally in basalts, but only to a minor degree in kimberlites: Na, Al, heavy REE (Ga, Sc, V) (Figs. 1d, 1a, 1c, 1).
5. Elements with a maximum accumulation

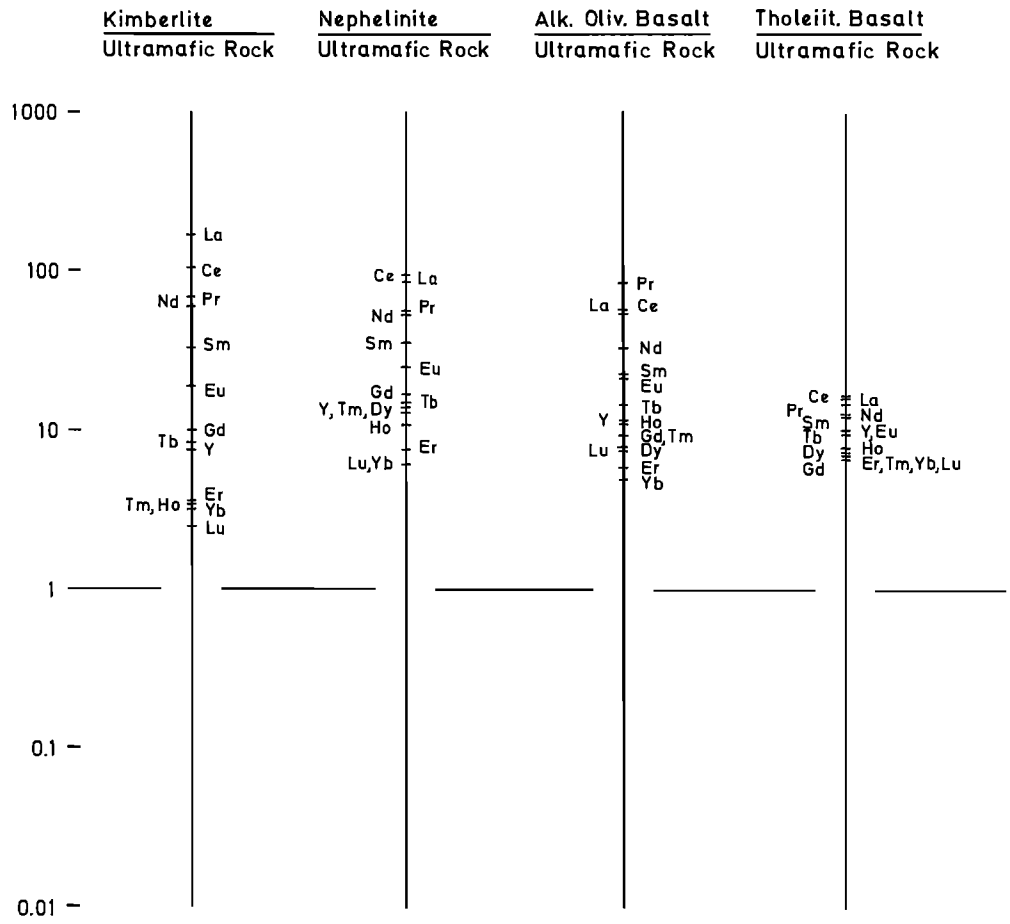

Fig. 1c. Abundance of related elements in kimberlites, nephelinites, alkali olivine basalts and tholeiitic basalts relative to their abundance in ultramafic rocks. RE elements.

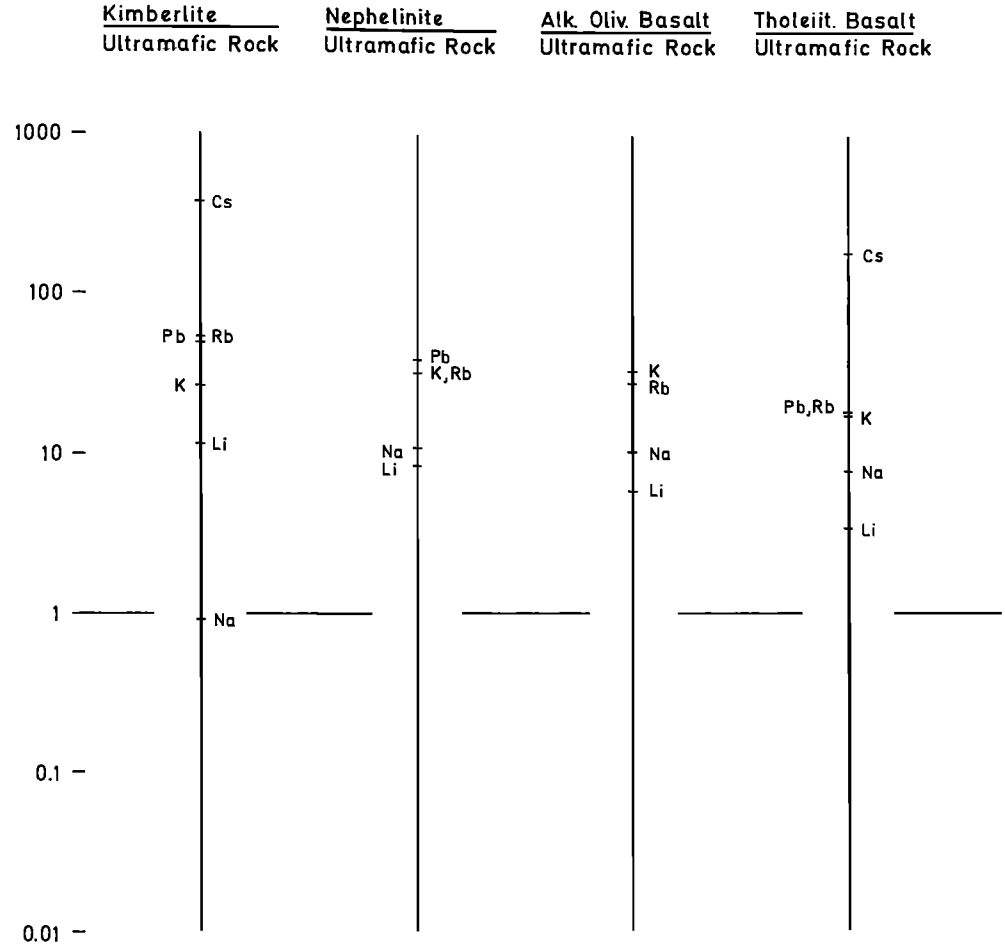

Fig. 1d. Abundance of related elements in kimberlites, nephelinites, alkali olivine basalts and tholeiitic basalts relative to their abundance in ultramafic rocks. Alkali elements and Pb.

exclusively in alkali olivine basalts and nephelinites: Eu to Ho, Sr (K) (Ti) (Figs. 1c, 1).

6. Elements being increasingly depleted from kimberlites to tholeiitic basalts: Ni, Cr, Co, Mg (Figs. 1a, 1).

The characteristic properties in the composition of kimberlites and basalts can be explained by differences in the degree of partial melting, in mantle composition, in total pressure, partial CO_2 and H_2O pressure, and temperature of the mantle environment. Pattern 1 and 2 are probably controlled by distribution coefficients close to one and slightly less than one respectively for the major mantle minerals. A decreasing fraction of partial melting of the major minerals in a homogeneous mantle probably forms pattern 3. A reaction olivine + clinopyroxene + H_2O + CO_2 ⇄ garnet + orthopyroxene + melt + vapor could be assumed to have caused pattern 4 except for Na. Melting experiments of olivine melilitites under high CO_2 + H_2O pressure (30 kb) have demonstrated the persistence of garnet and orthopyroxene as near liquidus phases at increasing vapor proportions (Brey and Green, 1977). Sodium could have been lost from kimberlitic magmas to country rocks by means of CO_2 transport (fenitization). Pattern 5 could be explained by partial melting or complete reaction of phlogopite. A reaction of olivine into melt according to the equation listed for pattern 4 can cause the relative increase of Mg, Ni and Co from tholeiitic basalt to kimberlite (pattern 6).

Some authors expect that unidentified accessory mantle minerals are hosts of several of the minor elements which increase in magmas at decreasing fractions of partial melting. Fesq, et al. (1975), assume that carbonate phosphate minerals may have contributed Th, U, Sr, P and CO_2 from upper mantle assemblages to melts. Newton and Sharp (1975), Kushiro, et al. (1975), Wyllie and Huang (1976) as well as Brey and Green (1976) have presented experimental evidence for the existence of dolomite and magnesite at high CO_2 pressures (above 20 kb).

TABLE 6.

	Tholeiitic basalts	Alkali olivine basalts	Olivine nephelinites	Kimberlites (this publication)
ppm S	subaerial: 65[a] submarine: 780[a]			2200
$\delta^{34}S\,^{o}/_{oo}$	-0.3[a]	+1.3[a]	+3.0[a]	+4.6
Fe_2O_3/FeO	0.32	0.36	0.68	1.3

a Schneider (1970, 1978)

An increase in the average ratio of ferric to ferrous iron from 0.3 to 0.7 and to 1.3 can be observed from tholeiitic basalts to nephelinites and to kimberlites (Table 6). The change in oxygen fugacity from very low values could be explained as a near-surface phenomenon in magmas which have slightly higher water contents from small degrees of partial melting. Water dissociation at temperatures of magmas controls a higher oxygen fugacity if the system becomes open with respect to hydrogen as a magma approaches the earth's surface. Another indication for a partially open system process is the gradient in sulfur isotopic composition as listed in Table 6. If the mantle is almost homogeneous in sulfur $\delta^{34}S$ the increase in heavy sulfur from tholeiitic basalt to kimberlite may be explained by an increasing loss of isotopically light SO_2 and H_2S.

It can be concluded from our observations that many chemical data on kimberlites, basaltic rock series and ultramafic materials can be explained by genetic models in which mantle magmas derived from partial melting. The degree of partial melting of the upper mantle which probably is not very heterogeneous in composition, has mainly controlled the chemical characteristics of the magmas.

References

Agiorgitis, G., Zur Geochemie einiger seltener Elemente in basaltischen Gesteinen, Tschermaks Mineral. Petr. Mitt., 12, 204, 1967.

Aoki, K. I., Origin of phlogopite and potassic richterite bearing peridotite xenoliths from South Africa, Contrib. Mineral. Petrol., 53, 145, 1975.

Borodin, L. S. and V. S. Gladkikh, Geochemistry of zirconium in differentiated alkali basalt series, Geochem. Intern., 4, 925, 1967.

Bougault, H. and R. Hekinian, Rift valley in the Atlantic Ocean near 36° 50' N: Petrology and geochemistry of basaltic rocks, Earth Planet. Sci. L., 24, 249, 1974.

Boyd, F. R., T. Fujii and R. V. Danchin, A noninflected geotherm for the Udachnaya kimberlite pipe, USSR, Carnegie Inst. Annual Rep. Geophys. Lab. Yearbook, 75, 523, 1976.

Brey, G. P. and D. H. Green, Solubility of CO_2 in olivine melilitite at high pressures and role of CO_2 in the earth's upper mantle, Contrib. Mineral. Petrol., 55, 217, 1976.

Brey, G. and D. H. Green, Systematic study of liquidus phase relations in olivine melilitite + H_2O + CO_2 at high pressures and petrogenesis of an olivine melilite magma, Contrib. Mineral. Petrol., 61, 141, 1977.

Brooks, C. K., The concentrations of zirconium and hafnium in some igneous and metamorphic rocks and minerals, Geochim. Cosmochim. Acta, 34, 411, 1970.

Carswell, D. A., Primary and secondary phlogopites and clinopyroxenes in garnet lherzolite xenoliths, Internat. Conf. Kimberlites, Extended Abstr., Rondebosch, 59, 1973.

Dawson, J. B., D. G. Powell and A. M. Reid, Ultrabasic xenoliths and lava from the Lashaine volcano, Northern Tanzania, J. Petrol., 11, 519, 1970.

Dostal, J. and S. Capedri, Partition coefficients of uranium for some rock-forming minerals, Chem. Geology, 15, 285, 1975.

Erlank, A. J., H. S. Smith, J. W. Marchant, M. P. Cardosa and L. H. Aherns, Section 40-E. Abundance in common igneous rock types; crustal abundance, Handbook of Geochemistry, Vol. II, Springer, Berlin, Heidelberg, New York, 1978.

Faure, G., Section 38-E. Abundance in common igneous rock types, Handbook of Geochemistry, Vol. II, Springer, Berlin, Heidelberg, New York, 1978.

Fesq, H. W., E. J. D. Kable and J. J. Gurney, Aspects of geochemistry of kimberlites from the Premier Mine, and other selected South

African occurrences with particular reference to the rare earth elements, Physics Chemistry of the Earth, 9, 687, 1975.
Gehnes, P. and W. Wimmenauer, Geochemical studies on igneous rocks of the Rhine graben region (Germany), N. Jahrb. Miner. Mh., 2, 49, 1975.
Gladkikh, V. S. and M. Y. Victorova, Distribution of niobium and tantalum in the volcanic rocks of the Kuznetskiy Alatan and Maymecha-Kotuy province, Geochem. Intern., 4, 321, 1967.
Gottfried, D., J. J. Rowe and R. I. Tilling, Distribution of gold in igneous rocks, U.S. Geol. Surv. Prof. Pap., 727, 1972.
Gottfried, D., U and Th in 3 nephelinites from Oahu, Hawaii, Personal communication, 1977.
Griffin, W. L. and V. R. Murthy, Distribution of K, Rb, Sr and Ba in some minerals relevant to basalt genesis, Geochim. Cosmochim. Acta, 33, 1389, 1969.
Hawkins, J. W. and J. H. Natland, Nephelinites and basanites of the Samoan linear volcanic chain: their possible tectonic significance, Earth Planet, Sci. L., 24, 427, 1975.
Heinrichs, H., Die Untersuchung von Gesteinen und Gewässern auf Cd, Sb, Hg, Tl, Pb und Bi mit der flammenlosen Atom-Absorptions-Spektralphotometrie, Dissertation, Göttingen, 1975.
Herrmann, A. G., Die Verteilung der Lanthaniden in basaltischen Gesteinen, Contrib. Mineral. Petrol., 17, 275, 1968.
Herrmann, A. G., Section 57-D. Minerals of yttrium and the lanthanides; abundance in rock-forming minerals, Handbook of Geochemistry, Vol. II, Springer, Berlin, Heidelberg, 1970.
Kay, R. W. and P. W. Gast, The rare earth content and origin of alkali-rich basalts, J. Geol., 81, 653, 1973.
Kesson, S. E., The primary geochemistry of the Monaro alkaline volcanics, southeastern Australia - evidence for upper mantle heterogeneity, Contrib. Mineral. Petrol., 42, 93, 1973.
Kushiro, I., H. Satake and S. Akimoto, Carbonate-silicate reactions at high pressures and possible presence of dolomite and magnesite in the upper mantle, Earth Planet. Sci. L., 28, 116, 1975.
Lipman, P. W., C. M. Bunker and C. A. Bush, Potassium, thorium and uranium contents of Upper Cenozoic basalts of the southern Rocky Mountain region and their relation to the Rio Grande depression, J. Res. U. S. Geol. Surv., 1, 387, 1973.
Lohmann, L., Ein Beitrag zur Petrographie Melilith-führender Olivin-nephelinite aus dem Gebiet Fritzlar-Naumburg (Nordhessen), Beitr. Miner. Petrogr., 9, 533, 1964.
MacDonald G. A., Composition and origin of Hawaiian lavas, Geol. Soc. Am. Mem., 116, 477, 1968.
Mengel, K., Alkali- und Erdalkali-Elemente in ausgewählten Basalten der nördlichen hessischen Senke, Dipl.-Arbeit, Göttingen, 1977.
Muramatsu, Y., Geochemische Untersuchungen an Kimberliten, einem Granat-peridotit und einem Eklogit-Einschluß aus Kimberley, Südafrika, PhD-thesis, Göttingen, 1977.
Newton, R. C., and W. E. Sharp, Stability of forsterite + CO_2 and its bearing on the role of CO_2 in the mantle, Earth Planet. Sci. L., 26, 239, 1975.
Nockolds, S. R., Average chemical composition of some igneous rocks, Bull. Geol. Soc. Am., 65, 1007, 1954.
Pourmoafi, M., Übergangselemente (3-d Periode) in ausgewählten Basalten der nördlichen hessischen Senke, Dipl.-Arbeit, Göttingen, 1977.
Prinz, M. Geochemistry of basaltic rocks: trace elements, in, Hess, H. H., and A Poldervaart (eds.), Basalts: The Poldervaart Treatise on Rocks of Basaltic Composition, Vol. 1, Interscience, New York, 1967.
Schilling, J. G. and J. W. Winchester, Rare earth contribution to the origin of Hawaiian lavas, Contrib. Mineral. Petrol., 23, 27, 1969.
Schneider, A., The sulfur isotope composition of basaltic rocks, Contrib. Mineral. Petrol., 25, 95, 1970.
Schneider, A., Section 16-E. Abundance in common igneous rocks, Handbook of Geochemistry, Vol. II, Springer, Berlin, Heidelberg, New York, 1978.
Schulz-Dobrick, B., Die Verteilung des Vanadium in basaltischen Gesteinen aus Nordhessen und Südniedersachsen, Dipl.-Arbeit, Göttingen, 1971.
Shaw, D. M., Development of the early continental crust, Part 1, Use of trace element distribution coeffieient models for the Protoarchean crust, Canad. J. Earth Sci., 9, 1577, 1972.
Shima, H. and A. J. Naldrett, Solubility of sulfur in an ultramafic melt and the relevance of the system Fe-S-O, Econ. Geol., 70, 960, 1975.
Shimizu, N., Rare earth elements in garnets and clinopyroxenes from garnet lherzolite nodules in kimberlites, Earth Planet. Sci. L., 25, 26, 1975.
Varne, R., The petrology of Moroto Mountain, eastern Uganda and the origin of nephelinites, J. Petrol., 9, 169, 1968.
Velde, D., and H. S. Yoder, Jr., The chemical composition of melilite-bearing eruptive rocks, Annual Rep. Carnegie Inst., Geophys. Lab. Yearbook, 75, 574, 1976.
Wedepohl, K. H., Geochemische und petrographische Untersuchungen an einigen jungen Eruptivgesteinen Nordwestdeutschlands, Fortschr. Miner., 39, 142, 1961.
Wedepohl, K. H., Die tertiären basaltischen Gesteine im nördlichen Hessen und südlichen Niedersachsen, Der Aufschluß, Sonderheft, 17, 112, 1968.
Wedepohl, K. H., The contribution of chemical data to assumptions about the origin of magmas from the mantle, Fortschr. Miner., 52, 141, 1975.
Wedepohl, K. H., Section 73-E. Abundance in common igneous rock types, crustal abundance,

Handbook of Geochemistry, Vol. II, Springer, Berlin, Heidelberg, New York, 1978.

Wilkinson, J. F. G., Ultramafic inclusions and high pressure megacrysts from a nephelinite sill, Nandewar Mountains, Northeastern New South Wales, and their bearing on the origin of certain ultramafic inclusions in alkaline volcanic rocks, Contrib. Mineral. Petrol., 51, 235, 1975.

Wood, C. P., A geochemical study of E. African alkaline lavas and its relevance to the petrogenesis of nephelinites, PhD-thesis, Leeds, 1968.

Wyllie, P. J. and W. L. Huang, Carbonation and melting reactions in the system CaO-MgO-SiO_2-CO_2 at mantle pressures with geophysical and petrological applications, Contrib. Mineral. Petrol., 54, 79, 1976.

EXPERIMENTAL STUDIES

A MODEL OF PHASE RELATIONS IN THE SYSTEM $MgO-SiO_2-H_2O-CO_2$ AND PREDICTION OF THE COMPOSITIONS OF LIQUIDS COEXISTING WITH FORSTERITE AND ENSTATITE

David E. Ellis and Peter J. Wyllie

Department of Geophysical Sciences, University of Chicago, Chicago, Illinois 60637

Abstract. A comprehensive model has been developed for the system $MgO-SiO_2-H_2O-CO_2$ on the basis of experimental studies, Schreinemaker's rules, and thermodynamic data. The assemblage forsterite plus enstatite is predicted to melt in the presence of vapor of any H_2O/CO_2 ratio at low pressures, in the presence of vapor whose H_2O/CO_2 ratio is buffered by the presence of magnesite at intermediate pressures, and at a vapor-absent eutectic with brucite and magnesite at high pressures. The composition of the liquid at the solidus for a bulk composition of forsterite plus enstatite plus a small amount of volatiles with a 3/1 H_2O/CO_2 ratio changes from enstatite-quartz normative at 20 kbar, to periclase-forsterite normative at 50 kbar, to forsterite-enstatite normative at 90 kbar and greater pressures. Forsterite cannot coexist with H_2O-CO_2 vapor at pressures greater than 90 kbar. Thus all melting in the earth's mantle at higher pressures must be vapor-absent.

Introduction

In the Proceedings of the First International Kimberlite Conference Eggler (1975) reported on experimental studies in the system $MgO-SiO_2-H_2O-CO_2$ at 20 kbar and Mysen and Boettcher (1975) discussed experimental results on the effects of H_2O and CO_2 on the melting of peridotite at 20 kbar. We have combined their contributions with other phase equilibrium studies to construct a model of phase equilibria in the system $MgO-SiO_2-H_2O-CO_2$ at pressures up to 100 kbar, where the relationships described at 20 kbar are replaced by more complex phase equilibria involving stable hydrates and carbonates. The model outlined here is described in detail in the papers of Ellis and Wyllie (1978a,b,c). The salient features of phase relations in the ternary systems $MgO-H_2O-CO_2$, $MgO-SiO_2-CO_2$, and $MgO-SiO_2-H_2O$ will be discussed, followed by a summary of the quaternary phase relations and the processes of melting and crystallization.

The System $MgO-H_2O-CO_2$

The phase relations of brucite in the system $MgO-H_2O$ are analogous to those determined by Huang and Wyllie (1976) for magnesite in the system $MgO-CO_2$ (see Figure 1). The position of the reaction

$$\text{Brucite} \rightarrow \text{Periclase} + H_2O \qquad (1)$$

has been predicted on the basis of the experimental studies of Walter et al. (1962), Barnes and Ernst (1963), and Irving et al. (1977), thermochemical data, and water fugacities predicted by the modified Redlich-Kwong equation of state (Holloway, 1977). We estimate that reaction 1 maintains a positive P-T slope until brucite melts at the invariant point (MC), at which brucite, periclase, liquid, and vapor coexist. The invariant point (MC) is located near 58 kbar and 1310°C. At pressures greater than or equal to that of point I, where the reaction

$$\text{Magnesite} + \text{Brucite} \rightarrow \text{Periclase} + \text{Vapor} \qquad (2)$$

meets the solidus, brucite and magnesite melt together at a eutectic. The melting model derived by Bradley (1962) for the system $Ca(OH)_2-CaCO_3$ has been used to predict that the composition of the eutectic liquid is 73 mole percent $Mg(OH)_2$ plus 27 mole percent $MgCO_3$. At temperatures below the solidus the composition of vapor coexisting with magnesite-bearing assemblages is buffered.

The System $MgO-SiO_2-H_2O$

The topology for the system $MgO-SiO_2-H_2O$ shown in Figure 2 was derived on the basis of numerous studies of subsolidus reactions, (especially those of Bowen and Tuttle (1949), Chernosky (1976), Evans et al. (1976), Greenwood (1963, 1971), Johannes (1968), Kitahara et al. (1966), and Scarfe and Wyllie (1967)), and from studies

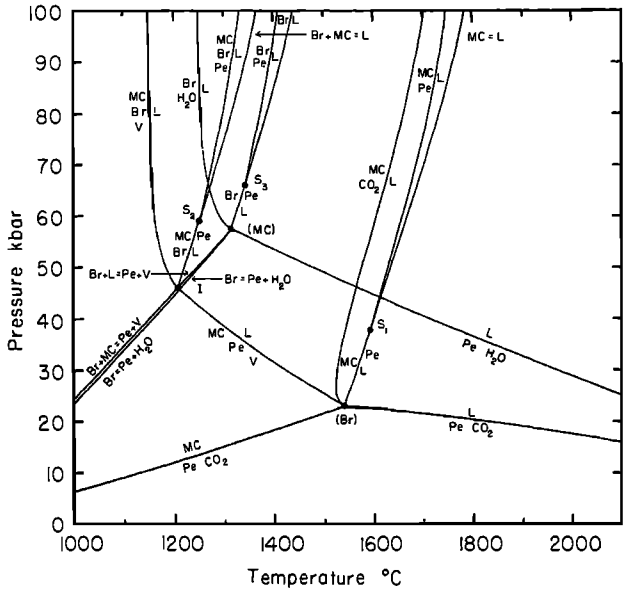

Figure 1. P-T net for the system $MgO-H_2O-CO_2$. Abbreviations used in Figures are Pe = MgO, Br = $Mg(OH)_2$, MC = $MgCO_3$, Q = SiO_2, En = $MgSiO_3$, Fo = Mg_2SiO_4, L = liquid, V = mixed H_2O-CO_2 vapor, H_2O = pure H_2O vapor, CO_2 = pure CO_2 vapor.

of melting relations in this system and related systems (by Eggler (1975), Hodges (1973), Kushiro et al. (1968), Mysen and Boettcher (1975a,b), and Nakumura and Kushiro (1974)). The subsolidus reactions 1 and

$$\text{Brucite} + \text{Enstatite} \rightarrow \text{Forsterite} + H_2O \quad (3)$$

intersect the solidus respectively at the invariant point (En,Q) at about 45 kbar and 1250°C, and the invariant point (Pe,Q) at about 1200°C and 90 kbar. The work of Yamamoto and Akimoto (1977) indicates that the hydrous magnesium silicates, particularly hydroxyl-clinohumite, are not stable at the temperature of the solidus in this system, and thus need not be considered. We assume that the hydrous melting reactions maintain a slight negative slope throughout the range of pressure considered. Near the solidus forsterite plus enstatite coexist with water vapor at low pressures and with brucite at high pressures. At high temperatures water is dissolved in the silicate liquid coexisting with forsterite plus enstatite. If sufficient H_2O is available at pressures greater than 90 kbar, all forsterite will react to form enstatite plus brucite. The assemblage forsterite plus enstatite can not coexist with H_2O at pressures greater than that of the invariant point (Pe,Q).

The System $MgO-SiO_2-CO_2$

The phase equilibria of this system were modeled by Wyllie and Huang (1976). The subsolidus and melting reactions involving magnesite in the system $MgO-SiO_2-CO_2$ take place at higher temperatures and lower pressures than the analogous reactions involving brucite in the system $MgO-SiO_2-H_2O$. The solidus has a positive P-T slope above 25 kbar. Near the solidus of this system, forsterite plus enstatite coexist with CO_2 vapor at low pressure, with magnesite at high pressure, and with silicate liquids containing dissolved CO_2 at temperatures above the solidus. In analogy to the system $MgO-SiO_2-H_2O$, CO_2 may exist as a vapor at high pressures only if all forsterite has been reacted to enstatite plus magnesite.

The System $MgO-SiO_2-H_2O-CO_2$

A model for the system $MgO-SiO_2-H_2O-CO_2$ has been derived from the ternary systems described above. Those reactions which involve the assemblage forsterite plus enstatite are shown in Figure 4. The assemblage forsterite plus enstatite may coexist with a vapor phase only in the low P-T region enclosed by heavy lines. The composition of the vapor phase in the univariant reaction

$$\text{Magnesite}+\text{Forsterite}+\text{Vapor} \rightarrow \text{Enstatite}+\text{Liquid} \quad (4)$$

is buffered by the intersection of the divariant subsolidus reaction surface

$$\text{Magnesite} + \text{Enstatite} \rightarrow \text{Forsterite} + \text{Vapor} \quad (5)$$

with the solidus surface. P-T-X_{CO_2} calculations for reaction 5 show that the vapor present at the solidus must be rich in H_2O at all pressures significantly greater than that of the invariant point labeled A in Figure 4. At pressures

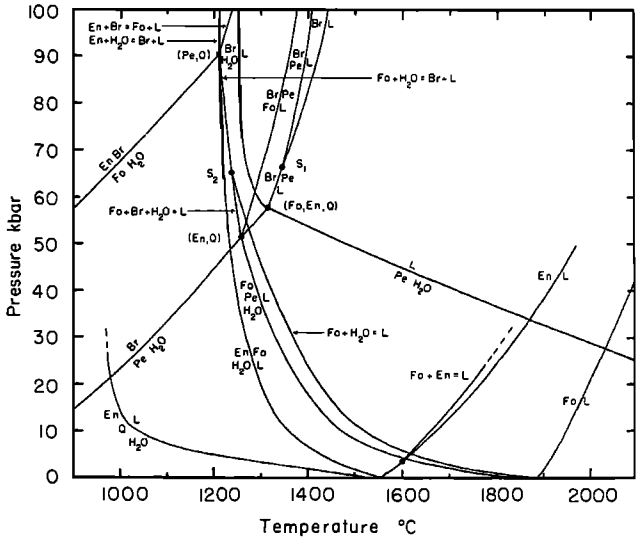

Figure 2. P-T net for the system $MgO-SiO_2-H_2O$.

greater than 90 kbar forsterite is not stable in the presence of vapor of any composition. Forsterite will react with vapor to form enstatite plus magnesite plus brucite until either the vapor or the forsterite is consumed.

The temperature maximum on the solidus surface, shown in Figure 4 as a dashed line, is the locus of isobaric thermal maxima on the reaction

Forsterite + Enstatite + Vapor → Liquid. (6)

It does not exist at pressures below 35 kbar. The temperature maximum originates in the system $MgO-SiO_2-CO_2$ when the rapidly increasing solubility of CO_2 in the silicate liquid which coexists with forsterite and enstatite, associated with the intersection of the subsolidus reaction 5 with the solidus, causes a rapid decrease in the temperature of reaction 6. The thermal maximum on the solidus surface which corresponds to the forsterite-vapor join then begins to migrate away from the CO_2 edge of the $MgO-SiO_2-H_2O-CO_2$ system with increasing pressure. Associated with the thermal maximum on the forsterite-vapor solidus there is a thermal ridge on the vapor-saturated liquidus surface. The forsterite-enstatite boundary on the vapor-saturated liquidus surface traverses this ridge passing through a thermal maximum that chemographic relations show must be located between the forsterite-vapor and the enstatite-vapor joins. As the liquidus ridge retreats from the side forsterite-CO_2 with increasing pressure the

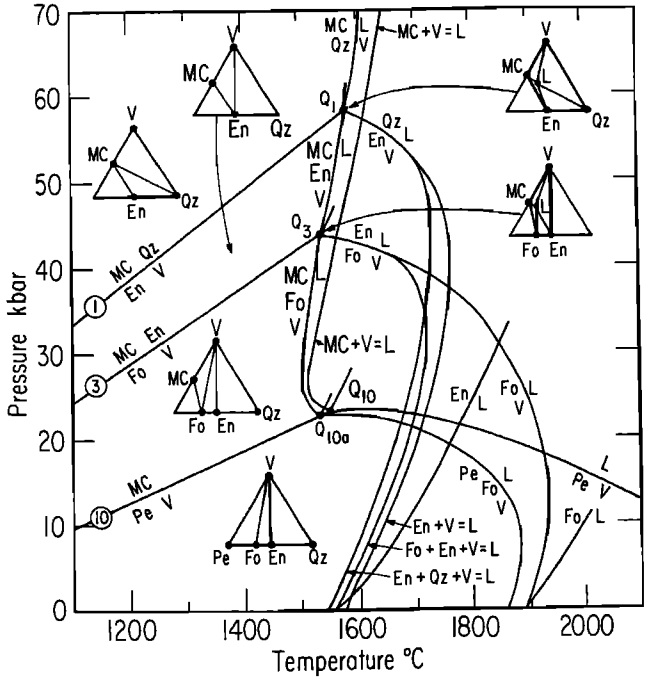

Figure 3. P-T net showing vapor-present univariant reactions in the system $MgO-SiO_2-CO_2$ (Wyllie and Huang, 1976).

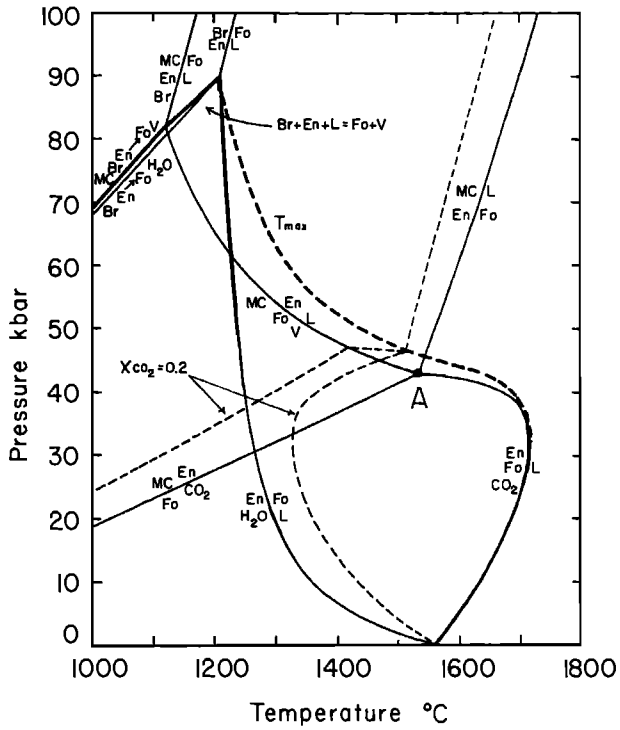

Figure 4. Partial P-T net for the system $MgO-SiO_2-H_2O-CO_2$. Only reactions involving the assemblage forsterite plus enstatite are shown. Vapor may coexist with forsterite plus enstatite only in the P-T region enclosed by the heavy lines. The heavy dashed line shows the position of the thermal maximum on reaction 6.

thermal maximum on the forsterite-enstatite field boundary and the coexisting vapor phase becomes richer in H_2O.

In the presence of mixed H_2O-CO_2 vapor all vapor-present reactions shown in Figure 4 become divariant rather than univariant. Thus the pair of reactions

Enstatite + H_2O → Forsterite + Liquid

and

Forsterite + Enstatite + CO_2 → Liquid

shown in Figure 4 simply represent the two extreme ends of one divariant surface in this system. In order to illustrate how quickly the vapor present along each divariant surface becomes water-rich, the contour for $X_{CO_2} = 0.2$ on three intersecting divariant surfaces has been plotted in Figure 4.

The transition with increasing pressure from vapor-present to vapor-absent melting in this system is illustrated by a series of isobaric sections through Figure 4. These are given in simplified form in Figure 5. The lines shown are the isobaric traces of the divariant

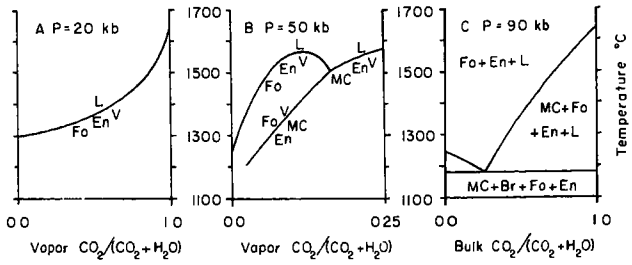

Figure 5. Isobaric sections through the system $MgO-SiO_2-H_2O-CO_2$ at 20, 50, and 90 kbar. The range of vapor compositions which may coexist with forsterite plus enstatite becomes smaller as pressure increases, until at 90 kbar forsterite plus enstatite can no longer coexist with vapor.

surfaces discussed above. Figure 5A shows that at 20 kbar forsterite plus enstatite may coexist with vapor of any X_{CO_2}. At 20 kbar CO_2 is relatively insoluble in the silicate liquid, and does not lower the melting point of the assemblage forsterite plus enstatite nearly as much as H_2O. Eggler (1975) concluded, in agreement with Mysen and Boettcher (1975a,b), that at 20 kbar the vapor-saturated liquid changes from quartz-normative to forsterite-normative as the X_{CO_2} of vapor becomes greater than 0.45.

The thermal maximum shown on reaction 6 at 50 kbar in Figure 5B is the same as that denoted by the heavy dashed line in Figure 4. The composition of the vapor at the thermal maximum changes rapidly from CO_2-rich at 40 kbar to H_2O-rich at 50 kbar. Figure 5B shows that forsterite plus enstatite cannot coexist with vapor richer in CO_2 than that at the isobaric invariant point schematically illustrated, where the subsolidus carbonation reaction intersects the solidus. At temperatures below the solidus the composition of the vapor coexisting with forsterite plus enstatite is buffered by the subsolidus reaction. At the solidus the compositions of both liquid and vapor are fixed. Above the solidus the composition of vapor coexisting with forsterite plus enstatite is buffered by reaction 6, until the temperature of the thermal maximum on that reaction is exceeded. At higher temperatures all vapor is dissolved in the liquid.

Figure 5C illustrates that at 90 kbar and temperatures below the solidus all volatiles are tied up in brucite and magnesite, in the presence of forsterite plus enstatite. A vapor phase is not stable in the presence of the assemblage forsterite plus enstatite. The first melting takes place at a quaternary eutectic involving forsterite, enstatite, brucite, and magnesite.

The P-T net constructed for the system $MgO-SiO_2-H_2O-CO_2$ provides the information necessary to construct isobaric liquidus diagrams, and from them to estimate geometrically the compositions of liquids formed at the solidus. The position of the surface of liquid compositions which coexist with forsterite and enstatite is shown at 20, 40, 70, and 90 kbar in Figure 6. The great change in the position of this surface is due to the increased solubility of CO_2 in the liquid associated with the intersection of reaction 5 with the solidus at about 42 kbar.

The estimated compositions of liquids formed at the solidus at pressures of 20, 50, and 90 kbar are listed in Table 1. These were estimated for a bulk composition consisting of forsterite plus enstatite plus a small amount of volatiles with a 3/1 H_2O/CO_2 ratio. At 20 kbar the first liquid is estimated to be quartz-normative, in agreement with the conclusions of Eggler (1975) and of Mysen and Boettcher (1975a, b). However, at a pressure of 50 kbar the fact that magnesite coexists with forsterite plus enstatite at the solidus causes the first liquid to be highly undersaturated with respect to silica, in fact periclase-forsterite normative. The involvement of magnesite in the melting reaction prevents the SiO_2-enrichment caused at low pressures by vapor with high H_2O/CO_2. At 90 kbar the first liquid coexisting with forsterite plus enstatite is estimated to be enstatite-forsterite normative. The existence of the quaternary eutectic relationship between forsterite, enstatite, brucite, and magnesite at pressures greater than 90 kbar requires that the compositions of the first liquids will be essentially constant at higher pressures, becoming slightly richer in MgO with increasing pressure.

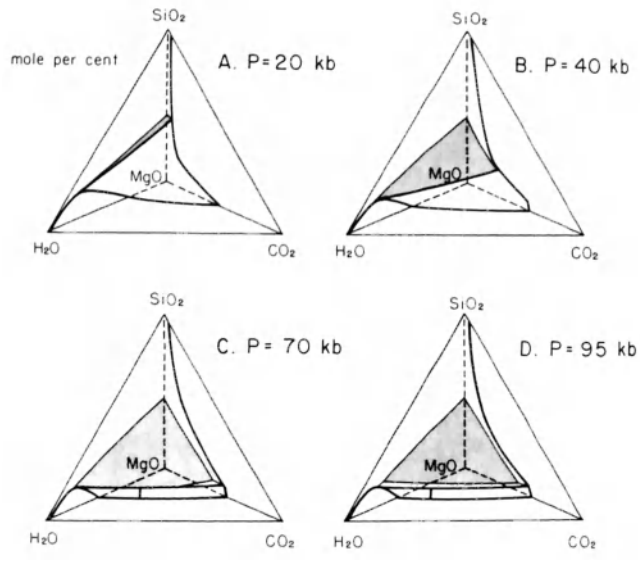

Figure 6. Partial isobaric liquidus diagrams for the system $MgO-SiO_2-H_2O-CO_2$. Heavy lines show liquidus field boundaries on the vapor-saturated liquidus surface. The surface of liquid compositions coexisting with forsterite plus enstatite is stippled. This is vapor absent, but reaches the vapor-saturated liquidus surface in Figures 6A, 6B, and 6C. As pressure increases the volatile-rich parts of the surface become increasingly silica-undersaturated.

TABLE 1. Geometrically estimated compositions of first liquids coexisting with forsterite plus enstatite in a bulk composition with an H_2O/CO_2 ratio of 3/1.

Pressure	Mole Percent				Weight Percent			
	MgO	SiO_2	H_2O	CO_2	MgO	SiO_2	H_2O	CO_2
20 kbar	12	17	70	1	18	37	45	0.x
50 kbar	34	10	31	25	38	17	15	30
90 kbar	32	18	39	11	36	31	19	14

Summary

The model developed for the system $MgO-SiO_2-H_2O-CO_2$ requires that in successively higher pressure ranges, three different types of melting processes characterize the melting of forsterite plus enstatite in the presence of H_2O-CO_2 vapor.

(1) At low pressures the melting reaction is either

Enstatite + Vapor → Forsterite + Liquid

at low X_{CO_2}, or

Forsterite + Enstatite + Vapor → Liquid

at high X_{CO_2}. The composition of the liquids produced varies from quartz-normative in the presence of H_2O to forsterite-normative in the presence of CO_2. This agrees with the conclusions of Eggler (1975) and Mysen and Boettcher (1975a,b). At 20 kbar H_2O is partitioned toward silicate liquids, and CO_2 is partitioned toward the coexisting vapor.

(2) At pressures between 42 and 80 kbar the important melting reaction is 4. The composition of the vapor phase taking part in this reaction is buffered by the subsolidus reaction 5. At temperatures above the solidus for the assemblage forsterite plus enstatite, a thermal maximum exists on the reaction

Forsterite + Enstatite + Vapor → Liquid.

The X_{CO_2} of the vapor at this thermal maximum becomes rapidly smaller as pressure increases.

(3) At pressures above 90 kilobars forsterite plus enstatite melt at a quaternary eutectic with brucite and magnesite, with no vapor present. H_2O/CO_2 of the liquid is fixed at about 3/1 by the eutectic between $Mg(OH)_2$ and $MgCO_3$.

The composition of the first liquid formed in bulk compositions of forsterite plus enstatite and a small amount of volatiles with a 3/1 H_2O/CO_2 ratio changes from quartz-normative to periclase-forsterite normative to enstatite-forsterite normative as pressure increases.

These three kinds of melting reaction must also occur in peridotite, where H_2O and CO_2 are present as vapor, or are stored in amphibole, phlogopite, and carbonate. The distribution of H_2O and CO_2 among liquid crystals and vapor in the simple system $MgO-SiO_2-H_2O-SiO_2$ provides a guide for interpretation of the phase relationships in the complex peridotite-H_2O-CO_2 system (Wyllie, this volume).

Acknowledgments. This research was supported by the Earth Sciences Section, National Science Foundation, NSF Grant EAR 76-20410.

References

Barnes, H. L., and W. G. Ernst, Ideality and ionization in hydrothermal fluids: the system $MgO-H_2O-NaOH$, Am. Jour. Sci., 261, 129-150, 1963.

Bowen, N. L., and O. F. Tuttle, The system $MgO-SiO_2-H_2O$, Geol. Soc. America Bull., 60, 439-460, 1949.

Bradley, R. S., Thermodynamic calculations on phase equilibria involving fused salts. Part I. General theory and application to equilibria involving calcium carbonate at high pressure, Am. Jour. Sci., 260, 374-382, 1962.

Chernosky, J. V., Jr., The stability of anthophyllite—a reevaluation based on new experimental data, Am. Mineral., 61, 1145-1155, 1976.

Eggler, D. H., CO_2 as a volatile component of the mantle: The system $Mg_2SiO_4-SiO_2-H_2O-CO_2$, Phys. Chem. Earth, 9, 869-881, 1975.

Ellis, D. E., and P. J. Wyllie, Carbonation, hydration, and melting relations in the system $MgO-H_2O-CO_2$ at pressures up to 100 kilobars, Am. Mineral., in press, 1978a.

Ellis, D. E., and P. J. Wyllie, Hydration and melting reactions in the system $MgO-SiO_2-H_2O$ at pressures up to 100 kilobars, Am. Mineral., in press, 1978b.

Ellis, D. E., and P. J. Wyllie, Phase relations in the system $MgO-SiO_2-H_2O-CO_2$ and petrological implications, in preparation, 1978c.

Evans, B. W., W. Johannes, H. Oterdoom, and V. Trommsdorff, Stability of chrysotile and antigorite in the serpentinite multisystem, Schweiz. mineral. petrog. Mitt., 56, 79-93, 1976.

Greenwood, H. J., The synthesis and stability of anthophyllite, Jour. Petrol., 4, 317-351, 1963.

Greenwood, H. J., Anthophyllite, corrections and comments on its stability, Am. Jour. Sci., 270, 151-154, 1971.

Hodges, F. N., Solubility of H_2O in forsterite melt at 20 kbar, Carnegie Inst. Wash. Year Book, 72, 495-497, 1973.

Holloway, J. R., Fugacity and activity coefficients of molecular species in fluids at high pressures and temperatures, Carnegie Inst. Wash. Yearbook, 75, 771-775, 1976.

Holloway, J. R., Fugacity and activity of molecular species in supercritical fluids: in Thermodynamics in Geology, D. G. Fraser ed., D. Reidel, Holland, 1977.

Huang, W.-L., and P. J. Wyllie, Melting relationships in the systems $CaO-CO_2$ and $MgO-CO_2$ to 33 kilobars, Geochim et Cosmochim Acta, 40, 129-132, 1976.

Irving, A. J., W.-L. Huang, and P. J. Wyllie, Phase relations of portlandite, $Ca(OH)_2$ and brucite, $Mg(OH)_2$ to 33 kilobars, Am. Jour. Sci., 277, 313-321, 1977.

Johannes, W., Experimental investigation of the reaction forsterite+H_2O = serpentine+brucite, Contr. Mineral. Petrol., 19, 309-315, 1968.

Kitahara, S., S. Takenouchi, and G. C. Kennedy, Phase relations in the system $MgO-SiO_2-H_2O$ at high temperatures and pressures, Am. Jour. Sci., 264, 223-233, 1966.

Kushiro, I., H. S. Yoder, Jr., and M. Nishikawa, Effect of water on the melting of enstatite, Geol. Soc. America Bull., 79, 1685-1692, 1968.

Mysen, B. O., and A. L. Boettcher, Melting of a hydrous mantle: I. Phase relations of natural peridotite at high pressures and temperatures with controlled activities of water, carbon dioxide, and hydrogen, Jour. Petrol., 16, 520-548, 1975a.

Mysen, B. O., and A. L. Boettcher, Melting of a hydrous mantle: II. Geochemistry of crystals and liquids formed by anatexis of mantle peridotite at high pressures and high temperatures as a function of controlled activities of water, hydrogen, and carbon dioxide, Jour. Petrol., 16, 549-593, 1975b.

Nakamura, Y., and I. Kushiro, Composition of the gas phase in $Mg_2SiO_4-SiO_2-H_2O$ at 15 kbar, Carnegie Inst. Wash. Year Book, 74, 255-258, 1974.

Scarfe, C. M., and P. J. Wyllie, Serpentine dehydration curves and their bearing on serpentine deformation in orogenesis, Nature, 215, 945-946, 1967.

Walter, L. S., P. J. Wyllie, and O. F. Tuttle, The system $MgO-CO_2-H_2O$ at high pressures and high temperatures, Jour. Petrol., 3, 49-64, 1962.

Wyllie, P. J., and W.-L. Huang, High CO_2 solubilities in mantle magmas, Geology, 4, 21-24, 1976.

Yamamoto, K., and S.-I. Akimoto, The system $MgO-SiO_2-H_2O$ at high pressures and temperatures—stability field for hydroxyl-chondrodite, hydroxyl-clinohumite, and 10Å-phase, Am. Jour. Sci., 277, 288-312, 1977.

KIMBERLITE MAGMAS FROM THE SYSTEM PERIDOTITE-CO_2-H_2O

Peter J. Wyllie

Department of Geophysical Sciences, University of Chicago, Chicago, Illinois 60637

Abstract. Phlogopite-dolomite-peridotite is the most promising source rock for kimberlites and related magmas. At pressures above about 30 kb, very little CO_2 (low CO_2/H_2O in vapor) is required to produce dolomite in mantle peridotite. If oxygen fugacity is too low, however, CO_2 and carbonate are reduced to carbon, and dolomite is unable to exert its distinctive influence on magma compositions. The oxygen fugacity at various depths in the mantle is a critical factor. Rare diamonds and even rarer carbonates occur in peridotite nodules from kimberlite, and CO_2 is brought to the surface in mantle-derived minerals and lavas. Phase relationships in peridotite-CO_2-H_2O provide a first step for evaluation of the behavior of components C-H-O at depth. Experimental and theoretical data from various sources have been combined for analysis of the near-solidus phase relationships in peridotite-CO_2-H_2O. The divariant solidus surface is traversed by a series of univariant lines where the vapor phase is buffered by amphibole, dolomite (magnesite at higher pressures), phlogopite, or combinations of these. The lines limit the range of vapor-phase compositions that can coexist with peridotite at various pressures. The buffering capacity of dolomite is far greater than that of the hydrous minerals. The buffered curves for partly carbonated peridotite, with and without phlogopite, extend to lower temperatures and higher pressures from an invariant point near 26 kb and 1200°C. Near this line there is a temperature-maximum (a ridge) on the solidus surface, separating the low-pressure surface, where CO_2/H_2O in vapor is higher than in liquid, from the high-pressure surface, where CO_2/H_2O in vapor is lower than in liquid. Enrichment of the high-pressure liquids in CO_2 is associated with the generation of dolomite and low-SiO_2 liquids. Because of this maximum on the solidus, near-solidus magmas rising along an adiabat would evolve volatile components in the depth interval 100-80 km, which could contribute to the explosive eruption of kimberlites. The subcontinental upper mantle is probably heterogeneous with respect to incompatible elements, because local melting due to sparsely distributed CO_2 and H_2O (dolomite and phlogopite) is followed by magmatic flushes, as the melt migrates upwards.

Introduction

Petrological and experimental data appear to be consistent with the conclusion that kimberlite magmas are generated by a small degree of partial melting of mantle peridotite containing H_2O and CO_2, or perhaps other species in the subsystem H-C-O, at depths greater than about 100 kilometers. The evidence that minerals and magmas derived from the upper mantle contain H_2O and CO_2 has been reviewed by Wyllie (1977a) and Eggler (1978). The presence of CO_2 in minerals (Green and Radcliffe, 1975) and basalts (Moore et al., 1977) is established, but carbonates in mantle-derived peridotites are rare (McGetchin and Besancon, 1973). The presence of diamonds and graphite in peridotite and eclogite nodules from kimberlites shows that the oxygen fugacity at depth is not high enough to oxidize all carbon, but there is probably a depth interval within which carbon and carbonate coexist (M. Sato, personal communication, 1977; see also Rosenhauer et al., 1977; Woermann et al., 1977). Evaluation of the system peridotite-CO_2-H_2O is a first step for evaluation of the behavior of components C-H-O in the mantle at depth. At some level, these components assume a form in which H_2O+CO_2 are dominant.

The only comprehensive experimental investigation of the effect of CO_2-H_2O on the melting of natural peridotites (with controlled oxygen fugacities) is that of Mysen and Boettcher (1975). Eggler (1975) studied the effect of CO_2+H_2O on the melting of forsterite+enstatite at 20 kb. These results were presented at the First Kimberlite Conference. Since then, Wyllie and Huang (1975) and Eggler (1976) independently discovered a carbonation reaction which produces striking changes in near-solidus phase relationships between about 20 and 30 kb, and accounts for Eggler's (1974) observation that CO_2 at high pressures generates SiO_2-depleted liquids from forsterite+enstatite+diopside. A preliminary integration of subsolidus carbonation reactions with melting reactions for the system

$CaO-MgO-SiO_2-CO_2-H_2O$ by Wyllie and Huang (1976) illustrated the complexities that would be encountered in experimental studies between about 25 and 40 kb, and Eggler's (1978) experiments included some of these complexities. Brey and Green (1975, 1976) studied the effect of CO_2 and H_2O on the liquidus mineralogy of a selected olivine-melilitite composition, and concluded that this represents a near-solidus liquid for peridotite with H_2O+CO_2 at pressure near 30 kb.

The many uncertainties in experimental results and interpretations up to 35 kb have been discussed extensively (Mysen and Boettcher, 1975; Nehru and Wyllie, 1975; Wyllie and Huang, 1976; Green, 1976; Wyllie, 1977a; Eggler, 1978). A complementary approach is to calculate the positions of specific reactions involving carbonates and hydrous minerals in model systems (Eggler et al., 1976; Ellis and Wyllie, 1978, 1979a, 1979b).

Wyllie (1977a, 1978) and Eggler (1977, 1978) presented analyses of the phase relationships in peridotite-CO_2-H_2O, using available experimental and theoretical data from many sources. They reached broadly similar conclusions, but there are some significant differences of interpretation. They agree that the divariant solidus surface (Mysen and Boettcher, 1975; Eggler, 1975) is traversed by a series of univariant reactions involving amphibole, phlogopite, dolomite, or combinations of these. For CO_2 and H_2O contents below certain limits, the vapor phase composition is buffered to these lines, and isobaric liquid compositions are correspondingly fixed. Some of the differences of interpretation are outlined below with respect to specific figures involving dolomite and phlogopite, the minerals probably required for the generation of kimberlite magmas.

Mantle Peridotite

It is well established that the mantle is heterogeneous, with mineralogy varying from undepleted to depleted in fusible constituents, and contaminated to various extents by metasomatic products including phlogopite (Wyllie, 1971, chapter 6; Ringwood, 1975, chapters 3 and 5; Yoder, 1976; O'Hara, 1975; Harte et al., 1975; Lloyd and Bailey, 1975; Boettcher et al., 1977). This makes generalization difficult. The following analysis of phase relationships for peridotite-CO_2-H_2O involves an average mantle peridotite, with olivine, two pyroxenes, plus spinel or garnet (Wyllie, 1977a; Eggler, 1978). There are large uncertainties in the precise positions of some phase boundaries that have been studied experimentally (e.g. peridotite-H_2O solidus and amphibole stability, see Wyllie, 1977a), and similar uncertainties pertain to the positions of deduced boundaries.

The amounts of H_2O and CO_2 in the upper mantle are normally very low (probably less than 0.1%) and subject to regional variability, and local concentration. For the average model, 0.4% H_2O would produce the maximum possible amount of amphibole, and 0.02% H_2O would produce the maximum possible amount of phlogopite. Metasomatic processes introducing K_2O and H_2O increase the amount of H_2O fixed in phlogopite, which illustrates the arbitrariness of 0.02% H_2O as the level of buffering capacity of phlogopite. It requires approximately 5% CO_2 to convert normal mantle peridotite through dolomite-peridotite and to remove clinopyroxene by carbonation, and it requires about 23% CO_2 to convert peridotite to quartz/coesite-garnet-marble. The capacity of dolomite for buffering a vapor-phase in the mantle is clearly much larger than that of amphibole or phlogopite.

Despite the problem of dealing with an average system, with many uncertainties, the geometrical constraints are such that the general pattern, and the relative positions of the reactions, provide a framework permitting petrological and geophysical conclusions that are not likely to be significantly changed by subsequent precise determinations. We do need much more information on pressures and temperatures, liquid and mineral compositions, and liquid paths within the fusion/crystallization interval.

Peridotite-CO_2

Fig. 1 is a schematic diagram with the effects of CO_2 superimposed on a generalized phase diagram for peridotite. There are no experimental data for peridotite-CO_2. The three decarbonation reactions (Wyllie and Huang, 1976) presented in terms of increasing pressure (carbonation) are:

$$\text{orthopyroxene} + \text{dolomite}_{ss} = \text{olivine} + \text{clinopyroxene} + CO_2 \quad \ldots\ldots(6)$$

$$\text{orthopyroxene} + \text{magnesite}_{ss} = \text{olivine} + \text{dolomite}_{ss} + CO_2 \quad \ldots\ldots\ldots(4)$$

$$\text{quartz/coesite} + \text{magnesite}_{ss} = \text{orthopyroxene} + \text{dolomite}_{ss} + CO_2 \quad \ldots\ldots(2)$$

They terminate at the solidus with excess CO_2 (estimated) at invariant points. With less than 5% CO_2, as in Fig. 1B, there is insufficient to convert all clinopyroxene to dolomite, and reaction (6) is not completed.

The dolomite changes to magnesite through an exchange reaction:

$$\text{dolomite}_{ss} + \text{orthopyroxene} = \text{magnesite}_{ss} + \text{clinopyroxene}$$

(Kushiro et al., 1975) which terminates at invariant point I_0. This reaction does not

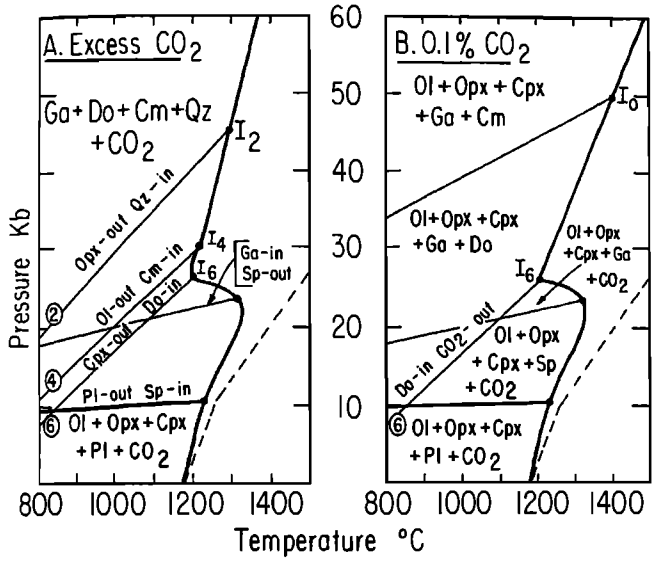

Fig. 1. Peridotite-CO_2, largely schematic (Wyllie, 1978). Dashed line, peridotite solidus (an arbitrary choice; see Wyllie, 1973, for three curves). Solidus slopes above I_6 are estimated.
1A. Excess CO_2, based on combination of Wyllie (1977a, Figs. 1 and 7a), and Wyllie (1971, Figure 6-10).
1B. 0.1% CO_2, based on combination of Fig. 1A and Wyllie (1977a, Fig. 2). Abbreviations: Ol = olivine, Opx = orthopyroxene, Cpx = clinopyroxene, Pl = plagioclase, Sp = spinel, Ga = garnet, Do = dolomite solid solution, Cm = magnesite solid solution, Qz = quartz or coesite.

occur in the presence of CO_2, but it does occur in the presence of CO_2-H_2O on the divariant surface for reaction (6). Thermodynamic calculations by Eggler et al., (1976) are consistent with the figure, but G. Brey (personal communication, 1977) has unpublished experimental data indicating a steeper slope, passing near 900°C at 25 kb. If this is confirmed, the reaction would traverse the divariant surface for reaction (6) with CO_2-H_2O (Fig. 2A).

For mantle peridotite with less than 5% CO_2, Fig. 1B shows that peridotite melts together with calcic dolomite at pressures above I_6. The change from low-pressure melting of peridotite-CO_2 to high pressure melting of dolomite-peridotite involves a remarkable increase in CO_2 solubility within a few kilobars pressure, as the solidus temperature drops to I_6. Wyllie and Huang (1975, 1976) showed that the composition of the near-solidus liquid I_6-I_0 is dominated by the phase relationships in $CaCO_3$-$MgCO_3$ (Irving and Wyllie, 1975). They concluded that the equivalent liquid in the model system CaO-MgO-SiO_2-CO_2 is essentially carbonatitic, with Ca/Mg > 1, 10-15% dissolved silicates, and CO_2 content approaching 40%. Eggler (1976, 1978) concluded that the liquid was somewhat more siliceous, with up to 27% CO_2.

Peridotite-CO_2-H_2O

Consider the effect of adding H_2O to the reactions in Fig. 1A. Each univariant curve extends to a divariant surface, which can be represented in P-T projection by contours for constant vapor-phase composition, as shown in Figs. 2, 3, and 4. The three surfaces in Fig. 2 (exploded diagram for clarity) meet along the heavy line extending from I_6, which is the buffered curve for the beginning of melting of partly carbonated peridotite (dolomite-peridotite) in the presence of H_2O-CO_2. The three surfaces are combined in Fig. 3.

The carbonation surface (Fig. 2A) divides the solidus surface into two parts: Fig. 2B shows the solidus for peridotite-vapor without dolomite, and Fig. 2C shows the solidus for carbonated peridotite (one or more of olivine and pyroxenes reacted away) with vapor. The carbonated surface is traversed by two other lines from I_4 and I_2 (Figs. 2C and 4) marking the intersections of the other carbonation reactions, (4) and (2) from Fig. 1A.

The solidus surface for peridotite-vapor extends uniformly between the low-pressure solidus curves for peridotite-H_2O and excess CO_2 (Fig. 1), with contours spaced according to the data of Mysen and Boettcher (1975), but with different limits adopted for H_2O and CO_2 (see Wyllie, 1978, for details). The surface passes over a temperature-maximum (mn in Fig. 3) of

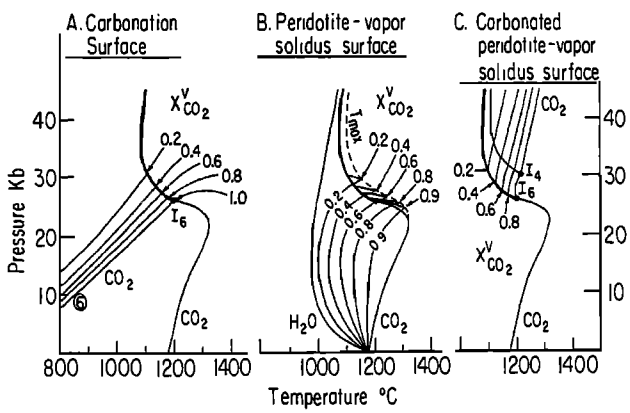

Fig. 2. Vapor-phase contours (mole fraction) on three divariant surfaces for peridotite-H_2O-CO_2, largely schematic, omitting amphibole and phlogopite (Wyllie, 1978). The data of Rosenhauer and Eggler (1975) on diopside-CO_2-H_2O suggest that there could be a shallow temperature minimum on the surface in Fig. 2B, for H_2O-rich vapors. This would add complexity to the diagrams and little of petrogenetic significance, so the prospect is not considered further.

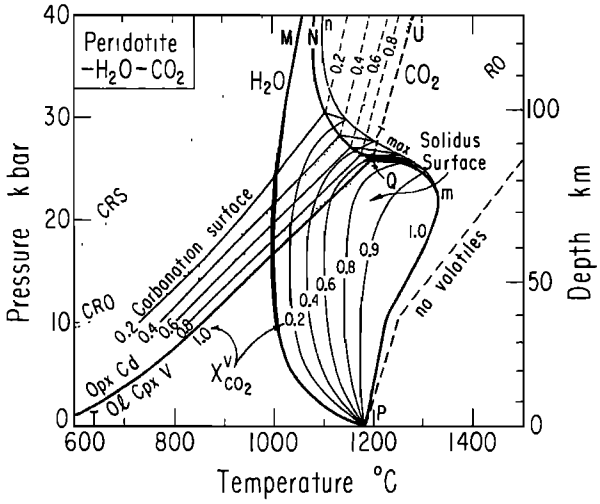

Fig. 3. Peridotite-CO_2-H_2O with excess vapor, combining the three surfaces of the exploded diagram, Fig. 2. Q is equivalent to I_6. The area QNU is dashed, because phase relationships on this surface require more CO_2 than expected in normal mantle. Dotted lines are geotherms: Abbreviations: see Fig. 1; S = shield; O = ocean; CR = Clark and Ringwood (1964); R = Ringwood (1966).

unknown size, and then down to the buffer line from I_6 (QN in Fig. 3). The temperature-maximum (a ridge on the solidus surface) is a significant addition to earlier versions (Wyllie, 1977a; Eggler, 1977, 1978). The limiting contour for CO_2 has a shape consistent with this family of contours. The contour lines on the peridotite-vapor surface (Fig. 2B), do not pass directly from low pressures to corresponding points on the dolomite-buffer line as proposed originally by Wyllie (1977a) and Eggler (1977).

The complete solidus surface is shown in Fig. 4. Fig. 4B is a PX projection of the surface giving a clearer view of vapor-phase compositions. The short-dashed lines for the solidus isotherms, estimated from Fig. 4A, illustrate the geometry of the temperature-maximum on the solidus surface (long-dashed line). For each carbonation reaction, the buffered vapor-phase compositions change from CO_2 to H_2O-rich within a few kilobars above each invariant point, I_6, I_4, and I_2.

Eggler (1977) plotted two versions of the dolomite buffer-line from I_6, each with a pronounced pressure-minimum, using different values for the peridotite-H_2O-CO_2 solidus, and Wyllie (1977a, Fig. 8) indicated a shallow pressure-minimum on this line. Wyllie (1978) discussed the location of this curve as the intersections of the two carbonated surfaces (convex upwards in TX section, Figs. 2A and 2C), concluding that there is no pressure-minimum on the line (Fig. 3).

The temperature-maximum corresponds to the conditions where CO_2/H_2O in vapor equals that in liquid. At lower pressures, Mysen and Boettcher (1975) and Eggler (1975) demonstrated that CO_2/H_2O in vapor was richer than in liquid (because of the low solubility of CO_2 in liquid). Fig. 4B shows that vapors along the dolomite-buffer line from I_6 become so H_2O-rich, that CO_2/H_2O in liquid produced by melting dolomite-peridotite is surely higher than in vapor. Wyllie (1978) concluded that the only way to relate the low-pressure and high-pressure distributions of H_2O and CO_2 between liquid and vapor with internally consistent phase relationships, was by the existence of a temperature-maximum, as shown in Figs. 2, 3, and 4. The hyperdimensional geometrical details cannot be completely defined in such a complex system, but Ellis and Wyllie (1978) traced an equivalent feature across the solidus and liquidus surface of MgO-SiO_2-CO_2-H_2O for the assemblage forsterite+enstatite+vapor.

The shapes of the contours in Fig. 3 are more readily visualized in Fig. 5. Fig. 5A shows the phase fields intersected with vapor of fixed composition, $CO_2/(CO_2+H_2O) = 0.6$. This corresponds to an open system, where CO_2 is added as required to maintain constant vapor-phase composition; 5% CO_2 is required to complete reaction (6), and 23% to pass from peridotite+V through reaction (2). Each line is a contour from a surface, three of which are drawn in Fig. 3, and each point at the intersection of three contours lies on one of the vapor-buffer lines, QN in Fig. 3, and the lines from I_6, I_4, and I_2 in Fig. 4.

In a closed system with fixed bulk composition and the same ratio CO_2/H_2O, the field of peridotite + vapor is bounded by the same reaction contours, as shown in Fig. 5B. Reaction (6) uses up CO_2, so with increasing pressure and continued carbonation, the vapor composition tracks across the divariant surface

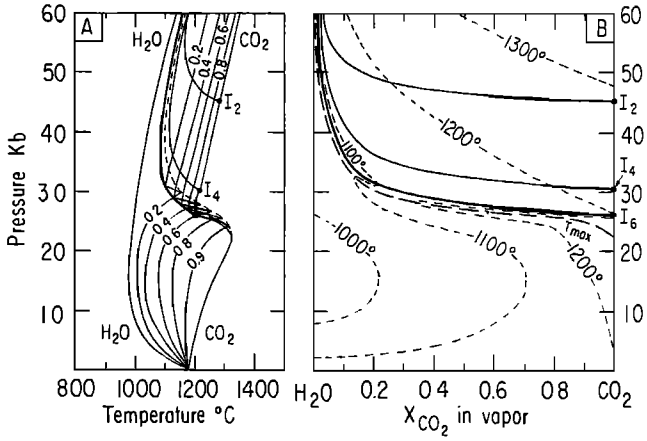

Fig. 4. Solidus surface, partly schematic, for peridotite-CO_2-H_2O. Short dashes: isotherms. Long dashes: temperature-maximum on solidus surface of Fig. 2B, mn in Fig. 3.

(Fig. 2A) becoming enriched in H_2O. With less than 5% CO_2 present, the dolomite-peridotite is unable to leave the divariant surface (6), and reactions (4) and (2) are not encountered at all. Melting begins not along a contour line, as in Fig. 5A, but along a portion of the dolomite-buffer line (QN in Fig. 3).

The isobaric projections in Fig. 6 illustrate the intersections of carbonation reactions with the solidus, the appearance of the temperature-maximum on the solidus, and its migration from CO_2 to H_2O-rich within a few kilobars. Fig. 6A shows the solidus temperature for peridotite-vapor as a function of vapor-phase composition at 20 kb (Mysen and Boettcher, 1975; Eggler, 1975). The solidus at 25 kb is shown by the dashed line in Fig. 6A. The abrupt decrease in temperature of the peridotite-CO_2 solidus between 20 and 25 kb (Fig. 1A) has the effect of producing a temperature-maximum on the H_2O-CO_2 solidus. In Fig. 6B, the solidus just reaches the carbonation reaction at I_6 (Fig. 2, and Q in Fig. 3). The point d in Figs. 6C and D corresponds to a point on the dolomite-buffer line for reaction (6), QN in Fig. 3. Figs. 4B and 6 show that for a very small increase in pressure, the vapor d is strongly enriched in H_2O. The field for peridotite-vapor, and associated divariant solidus surface, is thus restricted.

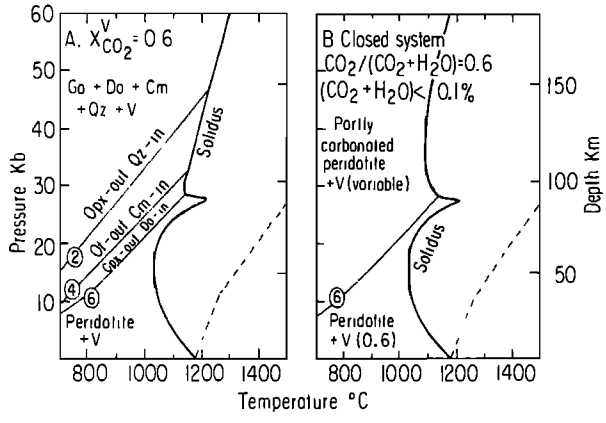

Fig. 5. Peridotite-H_2O-CO_2. Sections based on Figs. 1A, 2A, and 4A. Dashed line is the volatile-free peridotite solidus (Wyllie, 1978). 5A. Phase fields intersected with sufficient CO_2 available to complete the three successive carbonation reactions, [6], [4], and [2]. Each line is a contour for the fixed vapor-phase compositions from a divariant surface. 5B. Phase fields intersected in a closed system. Carbonation begins along the contour from the divariant surface, and continues with increasing pressure as the vapor phase tracks across the surface, becoming enriched in H_2O/CO_2. Abbreviations: see Fig. 1.

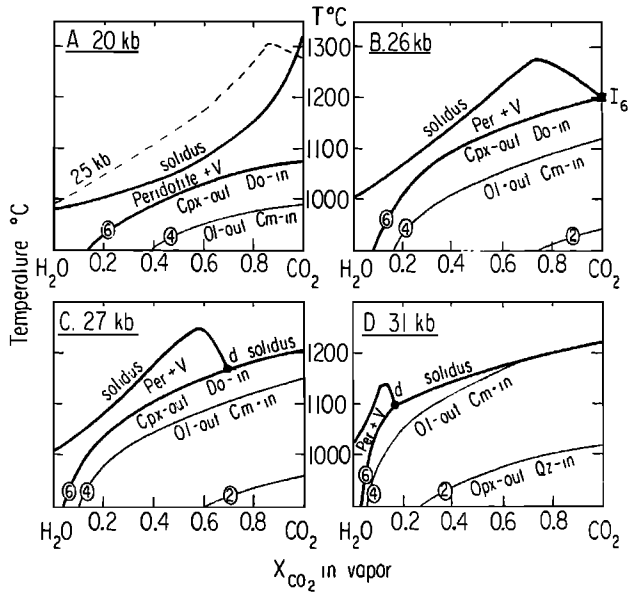

Fig. 6. Schematic isobaric projections for peridotite-H_2O-CO_2 with excess vapor, showing vapor phase compositions (mole fraction). This shows the temperature-maximum on the solidus, and intersections between the solidus and carbonation reactions. Vapor composition d is buffered by the formation of dolomite. See Fig. 10C for 60 kb section.

For peridotite with a small proportion of volatile components, the subsolidus vapor composition is buffered by the line for reaction (6); this curve cannot be crossed unless there is more than 5% CO_2 available to react away all clinopyroxene. With increase in temperature, the vapor-phase is enriched in CO_2. At d, the dolomite-peridotite begins to melt in the presence of vapor d, producing liquid with higher CO_2/H_2O. At pressures greater than 30 kb (Fig. 6D), there is only a limited section of the divariant solidus surface, on the H_2O side of the temperature-maximum, where CO_2/H_2O in vapor is richer than in liquid (corresponding to the low-pressure relations of Fig. 6A). Fig. 10C shows the extreme H_2O-enrichment of vapor at 60 kb.

Phlogopite in Peridotite-CO_2-H_2O

Figs. 7, 8, 9, and 10 illustrate how the subsolidus surface for the dehydration of phlogopite in the presence of H_2O-CO_2 vapor intersects the peridotite-CO_2-H_2O solidus surface (Figs. 7B and 10A), producing a univariant curve for the buffered melting of phlogopite-peridotite. At pressure I_7, this meets the dolomite-buffer line from I_6, and at higher pressures there are two reactions for phlogopite-dolomite-peridotite melting, one with

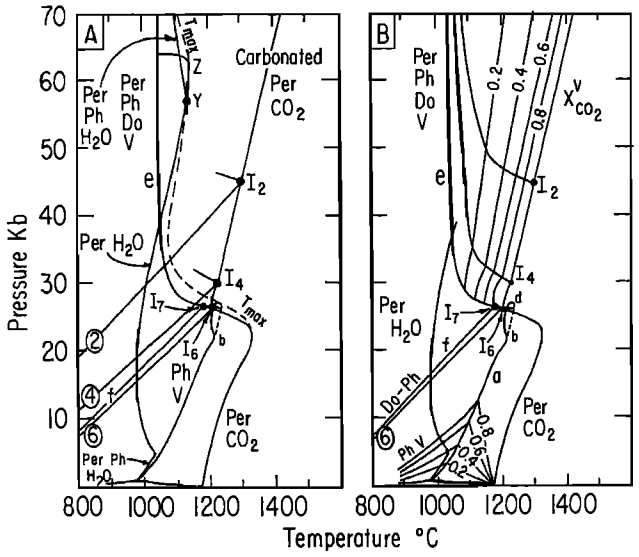

Fig. 7. Peridotite-H_2O-CO_2, largely schematic, for composition with sufficient K_2O to generate phlogopite, omitting amphibole (see Wyllie, 1978 for amphibole).
7A. Many curves are coincident with those of Figs. 1A and 2B.
7B. Vapor-phase contours on three of the surfaces: divariant dissociation of phlogopite, peridotite-vapor solidus, and the solidus for carbonated-peridotite (with phlogopite breakdown products omitted). Abbreviations: see Fig. 1; Ph = phlogopite.

buffered vapor (I_7e) and the other vapor-absent (Fig. 11).

Isochemical phase diagrams for phlogopite-peridotite should include reactions involving kalsilite, leucite and sanidine, the breakdown products of phlogopite. These minerals are not known in mantle peridotites, however, and the reactions have been neglected. The figures include only limits for the occurrence of phlogopite, with the assumption that beyond the stability limit of phlogopite, the small amount of potassium is camouflaged in other minerals, or removed in solution. Wendlandt (1977) illustrated related reactions for the potassic minerals in a simpler magnesite-phlogopite-CO_2-H_2O system, which provides a good model for peridotite reactions.

Phlogopite-peridotite vapor-buffer

Fig. 7A shows univariant lines from peridotite-CO_2 (Fig. 1A), the solidus for peridotite-H_2O (Fig. 2A), and several curves involving phlogopite. The buffered solidus for phlogopite-peridotite (Ph V in Fig. 7A) was located as shown in Fig. 7B; the line abdI_7 marks the intersection between the estimated contours for phlogopite dehydration (Ph V in Fig. 7B) and those for the divariant solidus of peridotite-CO_2-H_2O (Fig. 2B).

Details of the complex intersection line abdcI_7 and vapor-phase compositions are shown in Figs. 8 and 9. The dashed line from b is a temperature-maximum for the melting of phlogopite in peridotite-vapor with high CO_2/H_2O, at temperatures lower than the solidus for peridotite-vapor if phlogopite were absent (the dashed line to higher pressures from Z in Fig. 7A is the equivalent line for vapor with high H_2O/CO_2). The loop between bdcI_7 in PT projection (Figs. 7 and 8) is associated with the intersections of the temperature-maximum on the peridotite solidus, and the temperature-maximum for the melting of phlogopite in the presence of CO_2-H_2O. Fig. 9 shows the variation in buffered vapor composition. With increasing pressure, the vapor coexisting with phlogopite-peridotite (with less than 0.02% H_2O present) becomes enriched in CO_2 along ab, enriched in H_2O along bd as it traverses the ridge on the solidus surface for peridotite-CO_2-H_2O, and then after crossing the temperature-maximum, back along dcI_7 with increasing CO_2/H_2O.

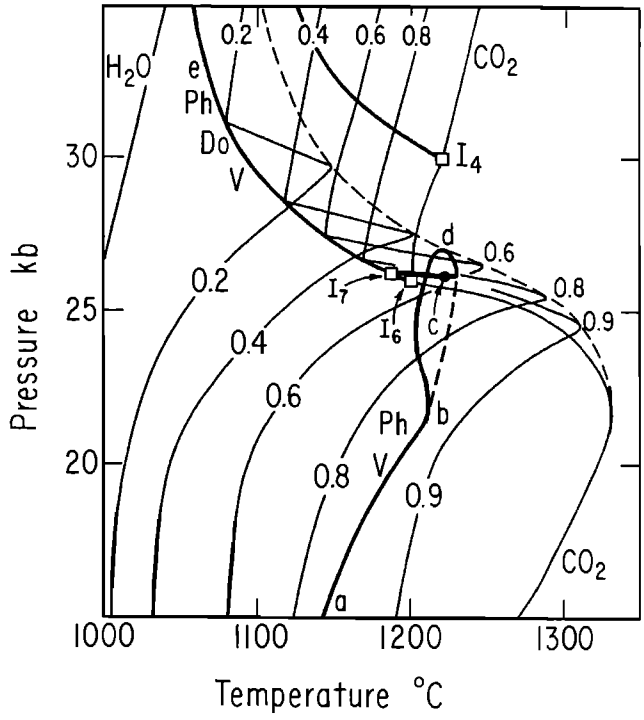

Fig. 8. Details of part of Fig. 7. The univariant intersection line between the peridotite-vapor solidus surface (Figs. 2A and 3) and the schematic dehydration surface for phlogopite-CO_2-H_2O (Fig. 7B). The dashed line from b is a temperature-maximum for the melting of phlogopite in peridotite with high CO_2/H_2O. See Fig. 9 for vapor-phase compositions.

Phlogopite-dolomite-peridotite melting

I_7f in Fig. 7 is the estimated line of intersection between the divariant surfaces for carbonation reaction (6) in Figs. 2A and 3, and for phlogopite dehydration in Fig. 7B. The isobaric projection in Fig. 10A shows a point on the line. At lower temperatures, the two surfaces are replaced by an exchange reaction between dolomite and phlogopite in the presence of peridotite and vapor, with the approximate shape indicated by the isobaric intersection Ph-Do in Fig. 10A. This is based on the reaction determined at 1 kb by Bailey (1966):

orthoclase + dolomite + H_2O =

phlogopite + calcite + CO_2

Additional reactions generated at the isobaric invariant point corresponding to I_7f have been neglected.

The line I_6I_7 in Figs. 7, 8, 9, and 11 is part of the dolomite-peridotite-vapor-buffer line (QN in Fig. 3). The subsolidus dolomite-phlogopite-vapor divariant surface (Fig. 10A) extending from I_7f (Fig. 7) intersects the peridotite-CO_2-H_2O solidus surface along the phlogopite-dolomite-peridotite vapor-buffer line I_7e (Figs. 7, 8, 9, and 11). I_7e is a eutectic reaction, with vapor compositions shown in Fig. 9, and by point e in Figs. 10B and D. The contours for the carbonated solidus surface, $I_6eI_4I_2$ in Figs. 7A and 8 are similar to those for QNU in Fig. 3, but they must fan out to lower temperatures to reach the solidus I_7e, as shown by comparison of Figs. 10C and D. (This is accomplished by the potassic breakdown products of phlogopite, which have been omitted from the phase diagrams).

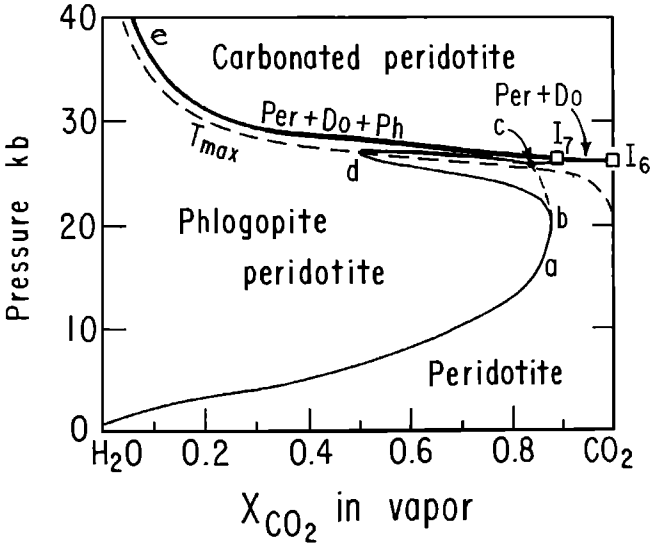

Fig. 9. PX projection of the solidus surface for phlogopite-peridotite-CO_2-H_2O, showing vapor compositions as a function of pressure for univariant curves involving phlogopite, as plotted in Figs. 7 and 8, and 11.

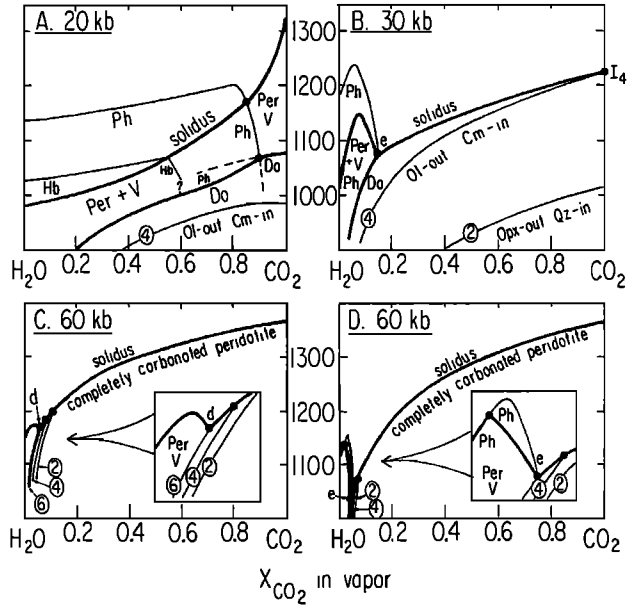

Fig. 10. Schematic isobaric sections through peridotite-H_2O-CO_2 with excess vapor, showing vapor phase compositions (mole fraction), melting of amphibole (Hb), melting of phlogopite (Ph), and eutectic relations between phlogopite- and dolomite-peridotite (liquid coexisting with vapor e). Note the replacement of buffered reaction [6] of Figs. 6 and 10C with a phlogopite-dolomite exchange reaction in Figures 10A, B, and D. Note that vapor e for eutectic melting of phlogopite and dolomite becomes lower than peridotite-H_2O solidus in Figure 10D, as shown in Figure 7. Abbreviations: see Fig. 1.

The isobaric projections in Fig. 10 show the relative vapor-phase compositions for the univariant reactions plotted in Fig. 7. At pressures above 30 kb, the vapor-phase coexisting with phlogopite-dolomite-peridotite has very high H_2O/CO_2, e. The liquid produced at the solidus has lower H_2O/CO_2 than e; the liquid is enriched in CO_2 because dolomite participates in the melting reaction.

The divariant dissociation surface for amphibole intersects the solidus surface at pressure below 25 kb, as indicated in Fig. 10A. Amphibole is not a significant mineral in kimberlite magma generation or crystallization, however, so it has been omitted from this review (see Wyllie, 1978, for details).

Fig. 11 compares many of the solidus reactions for peridotite-CO_2-H_2O. In particular, the solidus for vapor-absent phlogopite-peridotite (Ph), estimated by Wyllie (1977a, Figs. 6 and

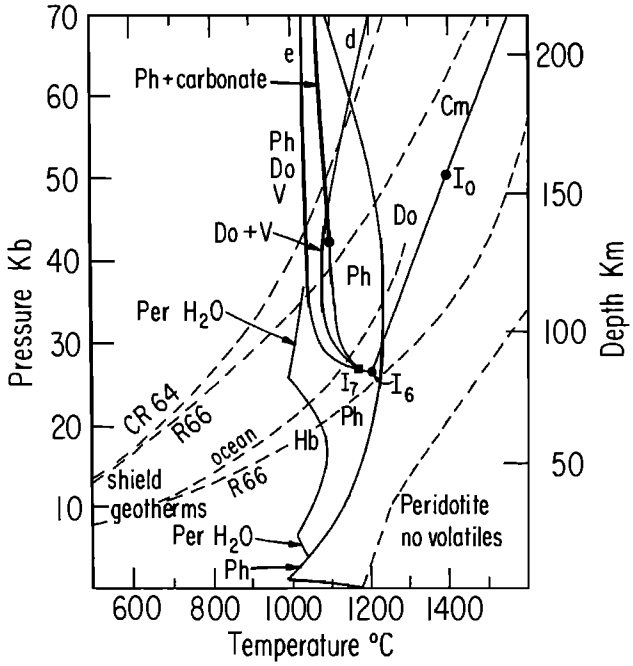

Fig. 11. Selected melting reactions for peridotite-H_2O-CO_2, partly schematic, but with restrictions and internal consistency to constrain their positions. Vapor-absent curves are shown for peridotite with amphibole, phlogopite, carbonate, and carbonate-phlogopite. Buffered vapor-present curves are shown for peridotite with dolomite, and dolomite-phlogopite. Abbreviations: see Figs. 1 and 3.

12A) from experimental data of Modreski and Boettcher (1973), Holloway and Eggler (1976), Markov et al. (1966), and Kushiro et al. (1967), constrains the position of the phlogopite-buffer (abdcI_7 in Figs. 7 and 8) and the two phlogopite-dolomite-peridotite solidus curves extending from I_7. For phlogopite-dolomite-peridotite containing less than 0.02% H_2O and 5% CO_2, melting occurs by the vapor-absent reaction (Ph + carbonate) at a slightly higher temperature than the vapor-buffered reaction I_7e.

The curves in Figs. 7, 8, and 11 that Wyllie (1977a, 1978) referred to as univariant solidus curves with buffered vapor were described as ZIVCs by Eggler (1977, 1978). He defined a "principle of the zone of invariant vapor composition" as: "the region in P-T-X space in which a volatile-bearing mineral coexists with a multicomponent vapor and with its breakdown products in a reaction relation that buffers the vapor composition." There are so many of these for peridotite-CO_2-H_2O, that "ZIVC" occupies almost the same P-T-X space as the solidus surface. The definition is potentially confusing. The ZIVC refers to a region for a univariant curve, yet "invariant" is in the title. The vapor phase is invariant only at constant pressure, but the defined "zone" extends through a wide range of pressures. The vapor-phase composition may vary through almost the complete range of H_2O-CO_2 within a single ZIVC, as shown in Fig. 9. I see no need for a special acronym to distinguish these lines from the standard, univariant buffered curves used by metamorphic petrologists (e.g. Greenwood, 1975).

Mantle Melting

Fig. 11 compares the solidus for peridotite without volatile components with several of the vapor-absent or vapor-buffered univariant solidus reactions that traverse the divariant solidus surface for peridotite-CO_2-H_2O. Even traces of CO_2, H_2O, or CO_2+H_2O lower melting temperatures through hundreds of degrees compared with the solidus for volatile-free peridotite. For the low values of H_2O+CO_2 expected in mantle peridotite, melting is likely to begin not on the divariant surface, but along one of the univariant lines. The four geotherms were calculated by Clark and Ringwood (1964) and modified by Ringwood (1966) before convection was incorporated into the formula, but recent reviews affirm that temperatures between oceans and continents differ to depths of 200 km (Solomon, 1976), and the geotherms are suitable for discussion of processes in this depth range.

According to Fig. 11, amphibole is not involved with melting in stable continental regions. If there is any H_2O or CO_2 present, incipient melting must begin somewhere within the depth range 110-180 km by the fusion of: (1) vapor-absent phlogopite-peridotite or phlogopite-dolomite-peridotite, (2) vapor-buffered assemblages of dolomite-peridotite or phlogopite-dolomite-peridotite, or (3) divariant peridotite-vapor (H_2O rich). The solidus temperature for dolomite(magnesite)-peridotite without H_2O is not reached by 200 km.

The fact that the seismic low-velocity zone beneath continental shields is weakly developed or absent (Solomon, 1976) indicates that mantle peridotite in these regions contains little or no phlogopite, carbonate, and CO_2-H_2O vapor. The fact that kimberlites and other volatile-rich alkalic lavas have been erupted in this environment indicates that H_2O and CO_2 have become concentrated in the mantle, at least locally in time and place. It appears that H_2O and CO_2 are distributed sparsely and irregularly in subcontinental mantle, with periodic magmatic flushes transporting these components into the lithosphere, or through it if tectonic conditions are suitable. This process would produce inhomogeneities in trace element contents of mantle peridotite, both in magmatic source regions and in overlying lithosphere. The ultimate source for replenishment of CO_2, H_2O, and K_2O remains unresolved. These components may come from deeper, or by recycling via subduction. Fig. 11 shows that carbonate is stable in subcontinental mantle to depths greater than 200 km,

in the absence of H_2O. Yamamoto and Akimoto (1977) showed that H_2O could be stored in dense hydrous magnesian silicates at depths greater than 300 km.

Magma Composition

Eggler (1974) demonstrated that CO_2 produced liquids strongly depleted in SiO_2 at pressures just below I_6 (compare Figs. 11 and 1). Wyllie and Huang (1975, 1976) outlined evidence for extreme SiO_2-deficiency, with carbonatitic melts produced near the solidus for dolomite-peridotite (I_6I_0 in Fig. 1B). Eggler (1976, 1978) agreed that such liquids were rich in CO_2. Wyllie (1977a, 1977b) argued that with magma generation along the dolomite-peridotite buffer line $I_6\underline{d}$ in Fig. 11, the first liquid developed could still be carbonatitic, despite the addition of H_2O-rich vapor and solution of H_2O in the melt.

Modreski and Boettcher (1973) measured the composition of glasses quenched from several phlogopite-bearing assemblages modelling the mantle, and concluded that vapor-absent melting of phlogopite-peridotite produces liquids ranging from quartz-normative at 10 and 15 kb to strongly SiO_2-undersaturated, and leucite-normative, at 35 kb. With H_2O present, the liquids were granitic (quartz-normative), owing to the incongruent melting of enstatite with H_2O.

Holloway and Eggler (1976) studied a garnet-lherzolite assemblage with dolomite and phlogopite added (the curve Ph + carbonate in Fig. 11 was passed through their measured solidus temperature of $1125 \pm 25^{\circ}C$ at 30 kb). The liquid was relatively enriched in CO_2, with $H_2O/(H_2O+CO_2) = 0.2$, and they estimated that it was melilitic in composition. Brey and Green (1975) concluded that a specific olivine melilitite composition was in equilibrium with mantle peridotite with H_2O+CO_2 at 30 kb.

For melting along the phlogopite- and dolomite-bearing solidus curves in Fig. 11, the magma composition is controlled more by the buffering minerals than by the CO_2/H_2O ratio. The liquids are enriched in CO_2 (Wyllie, 1977b, 1978) which ensures low SiO_2 (Eggler, 1974). Without phlogopite, Ca/Mg > 1, which fits melilitite compositions rather than kimberlite compositions. With phlogopite present in addition, Mg/Ca in the first liquid would probably be increased, and high K_2O is indicated by the leucite-normative liquid reported by Modreski and Boettcher (1973). Although Modreski and Boettcher measured quartz-normative liquids from phlogopite-peridotite-H_2O, I believe that buffered H_2O-rich vapors coexisting with phlogopite-dolomite-peridotite would not be granitic, because the influence of dolomite would ensure a low SiO_2-content. Wendlandt (1977) described a reaction near 30 kb involving the melting of forsterite+enstatite together with magnesite and phlogopite and vapor with X_{CO_2} near 0.6, with first liquids haplocarbonatitic, and he suggested that "at higher pressures, the liquid is probably kimberlitic".

For each starting assemblage considered, there is a wide temperature interval above the solidus through which liquids present in very small quantities can follow diverse paths through a complex system, with decreasing CO_2, H_2O, and alkalies, increasing SiO_2, and varying Ca/Mg. The liquids range from carbonatitic, through various high alkali, low-SiO_2 compositions including melilitites and kimberlites. From what little is known or deduced at present, I conclude that phlogopite and CO_2 are required in mantle peridotite to produce kimberlite magmas. The CO_2 should be present as dolomite or magnesite to be effective in producing low-SiO_2 liquids; I would be happier about this conclusion if there were more examples of primary carbonates in mantle-derived peridotites (McGetchin and Besancon, 1973).

Magma Generation and Eruption

Fig. 11 shows that if CO_2 and H_2O exist in subcontinental mantle, incipient melting must occur. For an equilibrium situation, the highest level liquid could be carbonatitic or somewhere in the range to kimberlitic or melilitic. With increasing depth, the interstitial liquid would change to more siliceous compositions progressively, as described in the preceding section. However, the liquids would probably rise, producing local concentrations, or intrusions into the lithosphere. Eruptive processes sampling mantle and melts at different levels could produce hybrid magmas, as proposed by Boyd and Nixon (1973), who suggested that kimberlite magmas may be mixtures of silicate liquids from within the asthenosphere with carbonatitic liquids from near the top of the asthenosphere. It is also consistent with the proposal of Franz and Wyllie (1967) that carbonatite magmas could be the fluids involved in the fluidized emplacement of some kimberlites, although in other kimberlites, carbonatite melts may represent an end-product of differentiation (Dawson and Hawthorne, 1973).

Holloway and Eggler (1976) suggested that CO_2-H_2O in mantle peridotite would normally be stored in vapor-absent phlogopite-dolomite-peridotite, and they showed that partial melting could have the effect of leaving a residue of either phlogopite-peridotite, or dolomite-peridotite. Melts of different compositions could be derived from these assemblages. The process is thus an effective means of producing different magmas of specific compositions.

Fig. 11 shows that any process adding small amounts of CO_2 to phlogopite-peridotite, or H_2O to dolomite-peridotite, would have the effect of lowering melting temperatures to the buffered curves $I_7\underline{e}$ or $I_6\underline{d}$, respectively, that is, through more than $200^{\circ}C$ in the depth interval 100-150 km. The metasomatism of mantle peridotite by solutions, reported by Harte et al. (1975),

Lloyd and Bailey (1975), and Boettcher et al. (1977), must have occurred at depths shallower than about 125 km, according to Fig. 11; the metasomatizing solutions would cause melting at greater depths.

Wyllie and Huang (1976) concluded from the shape of the solidus for peridotite-CO_2 (Fig. 1) that kimberlite or carbonatite magmas rising adiabatically must evolve CO_2 at depths of 100-80 km. The temperature-maximum on the peridotite-vapor surface (Figs. 3 and 5) similarly provides a barrier tending to prevent eruption of volatile-rich, deep-seated magmas. A near-solidus magma rising along an adiabat from depth near 125 km would encounter the maximum at a depth near 90 km. (The size of the maximum is not known). If equilibrium were maintained, the magma would be forced to solidify, evolving H_2O+CO_2 at this level (Fig. 5). However, the evolution of gases from the magma could enhance the prospect of crack propogation and explosive eruption, if tectonic conditions were suitable (O. L. Anderson, personal communication, 1977). If explosive events do occur, then equilibrium conditions would not be maintained.

This situation is modified for a melt with dissolved phlogopite components, because the maximum on the solidus for peridotite-CO_2-H_2O, illustrated in Figs. 3 and 5, is at least partially filled by liquid produced from melting of phlogopite, as shown for the area $\underline{bdc}I_7$ in Figs. 8 and 9. Therefore, if equilibrium were maintained, liquids of suitable composition with relatively high CO_2/H_2O would perhaps experience some rather drastic changes in composition when they crossed the solidus maximum shown in Fig. 5, with partial crystallization, and enrichment in the phlogopite components, along with partial evolution of CO_2+H_2O. This region, $\underline{bdc}I_7$, could be a site associated with the formation of some low-SiO_2, potassic magmas of distinctive composition. It could be a region where alkalic magmas from deeper levels become diversified in composition through non-equilibrium crystallization, effervescence, and explosive eruption.

Acknowledgments. This research was supported by the Earth Sciences Section, National Science Foundation Grant EAR 76-20410.

References

Bailey, D. K., Potash feldspar and phlogopite as indices of temperature and partial pressure of CO_2 in carbonatite and kimberlite, Mineral. Soc. India, Internat. Mineral. Assoc. Vol., 5-8, 1966.

Boettcher, A. L., J. R. O'Niel, K. E. Windom, D. C. Stewart, and H. G. Wilshire, Metasomatism and the genesis of kimberlites and alkali basalts, Extended Abstracts, Second International Kimberlite Conference, Santa Fe, New Mexico, 1977,

Boyd, F. R., and P. H. Nixon, Origin of the ilmenite-silicate nodules in kimberlites from Lesotho and South Africa, in Nixon, P. H., ed., Lesotho Kimberlites: Maseru, Lesotho National Development Corporation, p. 254-268, 1973.

Brey, G., and D. H. Green, The role of CO_2 in the genesis of olivine melilitite, Contrib. Mineral. Petrol., 49, 93-103, 1975.

Brey, G., and D. H. Green, Solubility of CO_2 in olivine melilitite at high pressure and role of CO_2 in the earth's upper mantle, Contrib. Mineral. Petrol., 55, 217-230, 1976.

Clark, S. P., and A. E. Ringwood, Density distribution and constitution of the mantle, Review Geophys., 2, 35-88, 1964.

Dawson, J. B., and J. B. Hawthorne, Magmatic sedimentation and carbonatitic differentiation in kimberlite sills at Benfontein, South Africa, Quart. Jour. Geol. Soc. London, 129, 61-85, 1973.

Eggler, D. H., Effect of CO_2 on the melting of peridotite, Carnegie Inst. Washington Yearbook, 73, 215-224, 1974.

Eggler, D. H., CO_2 as a volatile component of the mantle: the system Mg_2SiO_4-SiO_2-H_2O-CO_2, Phys. Chem. of the Earth, 9, 869-881, 1975.

Eggler, D. H., Does CO_2 cause partial melting in the low-velocity layer of the mantle? Geology, 4, 69-72, 1976.

Eggler, D. H., The principle of the zone of invariant vapor composition: an example in the system CaO-MgO-SiO_2-CO_2-H_2O and implications for the mantle solidus, Carnegie Inst. Washington Yearbook, 76, 428-435, 1977.

Eggler, D. H., The effect of CO_2 upon partial melting of peridotite in the system Na_2O-CaO-Al_2O_3-MgO-SiO_2-CO_2 to 35 kb, with an analysis of melting in a peridotite-H_2O-CO_2 system, Amer. Jour. Sci., 278, 305-343, 1978.

Eggler, D. H., I. Kushiro, and J. R. Holloway, Stability of carbonate minerals in a hydrous mantle, Carnegie Inst. Washington Yearbook, 75, 631-636, 1976.

Ellis, D. E., and P. J. Wyllie, A model of phase relations in the system MgO-SiO_2-H_2O-CO_2 and prediction of the compositions of liquids coexisting with forsterite and enstatite, Proceedings of the Second International Kimberlite Conference, in press, 1978.

Ellis, D. E., and P. J. Wyllie, Carbonation, hydration, and melting relations in the system MgO-H_2O-CO_2 at pressures up to 100 kilobars, Amer. Miner., in press, 1979a.

Ellis, D. E., and P. J. Wyllie, Hydration and melting reactions in the system MgO-SiO_2-H_2O at pressures up to 100 kilobars, Amer. Mineral., in press, 1979b.

Franz, G. W., and P. J. Wyllie, Experimental studies in the system CaO-MgO-SiO_2-CO_2-H_2O, in Wyllie, P. J., ed., Ultramafic and Related Rocks, Wiley and Sons, Inc., New York, p. 323-326, 1967.

Green, D. H., Experimental testing of "equilibrium" partial melting of peridotite under water-saturated, high-pressure conditions,

Can. Miner., 14, 255-268, 1976.
Green, H. W., and S. V. Radcliffe, Fluid precipitates in rocks from the earth's mantle, Geol. Soc. America Bull., 86, p. 846-852, 1975.
Greenwood, H. J., Buffering of pore fluids by metamorphic reactions, Amer. Jour. Sci., 275, 573-593, 1975.
Harte, B., K. G. Cox, and J. J. Gurney, Petrography and geological history of upper mantle xenoliths from the Matsoku kimberlite pipe, Phys. Chem. of the Earth, 9, 477-506, 1975.
Holloway, J. R., and D. H. Eggler, Fluid-absent melting of peridotite containing phlogopite and dolomite, Carnegie Inst. Washington Yearbook, 75, 636-639, 1976.
Irving, A. J., and P. J. Wyllie, Subsolidus and melting relationships for calcite, magnesite, and the join $CaCO_3$-$MgCO_3$ to 36 kilobars, Geochim. Cosmochim. Acta, 39, 35-53, 1975.
Kushiro, I., H. Satake, and S. Akimoto, Carbonate-silicate reactions at high pressures and possible presence of dolomite and magnesite in the upper mantle, Earth and Planet. Sci. Lett., 28, 116-120, 1975.
Kushiro, I., Y. Syono, and S. Akimoto, Stability of phlogopite at high pressures and possible presence of phlogopite in the earth's upper mantle, Earth and Planet. Sci. Lett., 3, 197-203, 1967.
Lloyd, F. E., and D. K. Bailey, Light element metasomatism of the continental mantle: the evidence and the consequences, in Physics and Chemistry of the Earth, 9, Pergamon Press, pp. 389-416, 1975.
Markov, V. K., V. P. Petrov, I. S. Delitsin, and Y. N. Ryabini, Phlogopite transformations at high pressures and temperatures, Izvest. Akad. NaukSSSR, Geol. Ser., No. 6, 10-20, 1966.
McGetchin, T. R., and J. R. Besancon, Carbonate inclusions in mantle-derived pyrope, Earth and Planet. Sci. Lett., 18, 408-410, 1973.
Modreski, P. J., and A. L. Boettcher, Phase relationships of phlogopite in the system K_2O-MgO-CaO-Al_2O_3-SiO_2-H_2O to 35 kilobars: a better model for micas in the interior of the earth, Amer. Jour. Sci., 273, 385-414, 1973.
Moore, J. B., J. N. Batchelder, and C. G. Cunningham, Carbon dioxide in vesicles of mid-ocean ridge basalt, Geol. Soc. Amer. Abstracts with Programs, 9, 1100-1101, 1977.
Mysen, B. O., and A. L. Boettcher, Melting of a hydrous mantle, Jour. Petrol., 16, 520-548, 549-593, 1975.
Nehru, C. E., and P. J. Wyllie, Compositions of glasses from St. Paul's peridotite partially melted at 20 kilobars, Jour. Geol., 83, 455-471, 1975.
O'Hara, M. J., M. J. Saunders, and E. L. P. Mercy, Garnet-peridotite, primary ultrabasic magma and eclogite; interpretation of upper mantle processes in kimberlite, Phys. Chem. of the Earth, 9, 571-604, 1975.
Ringwood, A. E., Mineralogy of the mantle, in Advances in Earth Sciences, P. M. Hurley, editor, p. 357-399, M.I.T. Press Cambridge, Massachusetts, 502 p, 1966.
Ringwood, A. E., Composition and Petrology of the Earth's Mantle, McGraw-Hill, New York, 1975.
Rosenhauer, M., and D. H. Eggler, Solution of H_2O and CO_2 in diopside melt, Carnegie Inst. Washington Yearbook, 74, 474-479, 1975.
Rosenhauer, M., E. Woermann, B. Knecht, and G. C. Ulmer, The stability of graphite and diamond as a function of the oxygen fugacity in the mantle, Extended Abstracts, Second International Kimberlite Conference, Santa Fe, New Mexico, 1977.
Solomon, S. C., Geophysical constraints on radial and lateral temperature variations in the upper mantle, Amer. Miner., 61, 788-803, 1976.
Wendlandt, R., The system K_2O-MgO-Al_2O_3-SiO_2-H_2O-CO_2: stability of phlogopite as a function of vapor composition at high pressures and temperatures, Carnegie Inst. Washington Yearbook, 76, 441-448, 1977.
Woermann, E., B. Knecht, M. Rosenhauer, and G. C. Ulmer, The stability of graphite in the system C-O, Extended Abstracts, Second International Kimberlite Conference, Santa Fe, New Mexico, 1977.
Wyllie, P. J., The Dynamic Earth: a Textbook in Geosciences, John Wiley and Sons., Inc., New York, 416 p., 1971.
Wyllie, P. J., Experimental petrology and global tectonics: a preview, Tectonophysics, 17, 189-209, 1973.
Wyllie, P. J., Mantle fluid compositions buffered by carbonates in peridotite-CO_2-H_2O, Jour. Geol., 85, 187-207, 1977a.
Wyllie, P. J., Peridotite-CO_2-H_2O, and carbonatitic liquids in the upper asthenosphere, Nature, 266, 45-47, 1977b.
Wyllie, P. J., Mantle fluid compositions buffered in peridotite-CO_2-H_2O by carbonates, amphibole, and phlogopite, Jour. Geol., 86, in press, 1978.
Wyllie, P. J., and W. L. Huang, Peridotite, kimberlite, and carbonatite explained in the system CaO-MgO-SiO_2-CO_2, Geology, 3, 621-624, 1975.
Wyllie, P. J., and W. L. Huang, Carbonation and melting reactions in the system CaO-MgO-SiO_2-CO_2 at mantle pressures with geophysical and petrological applications, Contrib. Mineral. Petrol., 54, 79-107, 1976.
Yamamoto, K., and S. Akimoto, The system MgO-SiO_2-H_2O at high pressures and temperatures—stability field for hydroxyl-chondrodite, hydroxyl-clinohumite and 10 Å-phase, Amer. Jour. Sci., 277, 288-312, 1977.
Yoder, H. S., Generation of basaltic magma, Nat. Acad. Sciences, Washington, DC, 1976.

EXPERIMENTAL STUDIES ON THE RELATIONSHIP BETWEEN KIMBERLITE MAGMAS AND PARTIAL MELTING OF PERIDOTITE

David H. Eggler

Geophysical Laboratory, Carnegie Institution of Washington,
Washington, D. C. 20008 and
Department of Geosciences, The Pennsylvania State University,
University Park, PA 16802

Richard F. Wendlandt

Geophysical Laboratory, Carnegie Institution of Washington,
Washington D. C. 20008

Abstract. The melting relations of an average Lesotho kimberlite composition have been investigated at 30 and 55 kbar pressure. The content of CO_2 in all experiments was 5.2 wt %, but amounts of H_2O were varied from 0 to about 10 wt %. It can be shown from a theoretical analysis that for nearly all these volatile contents, the solidus temperature of kimberlite composition is not a function of the volatile composition, because at subsolidus conditions, compositions of vapor are buffered by reaction with a carbonate mineral (dolomite at 30 kbar, magnesite at 55 kbar). The subsolidus phase assemblage -- olivine + clinopyroxene + orthopyroxene + garnet + carbonate + phlogopite + vapor -- melts at 1075° ± 25°C at 30 kbar and 1225° ± 25°C at 55 kbar.

At both 30 and 55 kbar, olivine is the liquidus phase at the conditions studied, followed closely in temperature by the crystallization of clinopyroxene and orthopyroxene. At 30 kbar, garnet is consumed immediately above the solidus, but at 55 kbar it persists well into the melting range. Extrapolation of the phase boundaries, in P-T projection, indicates that garnet, olivine, and two pyroxenes crystallize near the liquidus at 60 kbar, a phase field configuration consistent with the hypothesis that kimberlite composition is a primary magma, i.e., is a product at the beginning of melting of a parental peridotite.

A comparison of the experimentally-determined P-T projection of phase equilibria with the Lesotho pyroxene geotherm reveals that beneath Lesotho a liquid of kimberlitic composition coexisted with garnet-olivine-clinopyroxene-orthopyroxene (and perhaps with magnesite or phlogopite as well) at a pressure of 50-60 kbar. Because those phases constitute the Lesotho megacryst assemblage, which equilibrated at about 50-60 kbar, megacrysts are interpreted to be cognate to kimberlite magma.

Inasmuch as partial melting of peridotite containing CO_2 and H_2O will produce liquids of kimberlitic composition at pressures of 50-60 kbar, such liquids may be common in the upper mantle. The rarity of kimberlites as rocks may be attributed to the rarity of tectonic settings conducive to the ascent of appropriate magmas.

Introduction

In many theories of kimberlite petrogenesis, emphasis is placed upon the role of a magmatic, or liquid, phase. The liquid is generally thought to be derived either by partial melting of peridotite (Dawson, 1971; Mitchell and Crocket, 1971; Mysen and Boettcher, 1975) or by fractional crystallization (O'Hara and Yoder, 1967; MacGregor, 1970). Recent experimentation suggests that CO_2 is necessary for the production of kimberlitic-like liquids by partial melting (e.g., Wyllie and Huang, 1975b; Eggler, 1975). The melting of mantle peridotite in the presence of CO_2 (and H_2O) is, however, univariant, by virtue of buffering reactions (Eggler, 1977, 1978a; Wyllie 1977a,b; Eggler and Holloway, 1977). It is then a logical step to suggest that kimberlite can be the liquid composition produced near the univariant solidus at appropriate temperatures and pressures. If that suggestion is true, then experiments on an appropriate natural kimberlite composition should be consistent with the following restrictions: (1) The kimberlite should have a near-liquidus phase assemblage reflecting equilibration with a peridotite phase assemblage at some pressure; (2) The pressure of equilibration of the near-liquidus phases should be con-

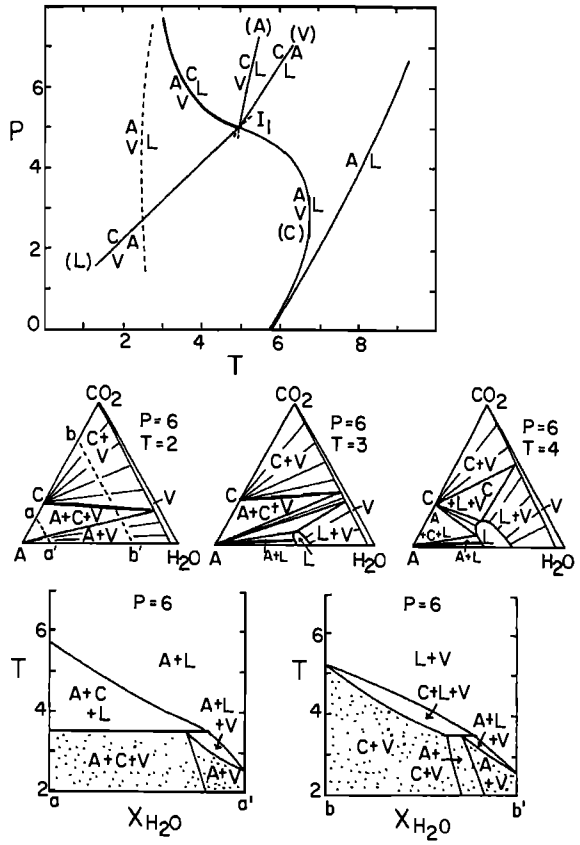

Fig. 1. Phase relations in the model system A-H_2O-CO_2 containing a carbonate mineral, C, including a P-T projection; isobaric, isothermal sections; and isobaric T-composition sections. In the P-T projection, light solid lines refer to reactions in A-CO_2, modeled after behavior in CaO-MgO-SiO_2-CO_2 (Eggler, 1976); the dashed line is the H_2O-saturated solidus in A-H_2O; and the heavy line is the univariant reaction in A-H_2O-CO_2. In sections a-a' and b-b', stippled areas are subsolidus regions. The abscissas denote $X^{sys}_{H_2O}$, not $X^{v}_{H_2O}$ (vapor composition).

sistent with geobarometric estimates of the depth of origin of kimberlite; (3) The liquidus temperature should not be less than the maximum geotherm temperature of the source region. Studies have now been conducted on a natural kimberlite, in addition to the theoretical studies and studies in synthetic systems that are essential to the design and interpretation of the experiments on a natural sample.

Theory of the Zone of Invariant Vapor Composition

The theory of a univariant solidus has been developed by Eggler (1977, 1978a), Eggler and Holloway (1977), and Wyllie (1977a,b). It can be illustrated with a model system A-H_2O-CO_2 (Fig. 1), containing a carbonate mineral, C, and two phases of variable composition, liquid, L, and vapor, V. The P-T relations for A-CO_2 are based on relations in the system CaO-MgO-SiO_2-CO_2 (Eggler, 1976); the univariant reaction (A+V = C+L) can be deduced by inspection. Isothermal, isobaric sections can be constructed using the known distribution of volatiles between liquid and vapor (Eggler and Rosenhauer, 1978), and in turn, pseudobinary T-$X^{sys}_{H_2O}$ joins can be drawn, where $X^{sys}_{H_2O}$ is $H_2O/(H_2O + CO_2)$ in the volatile portion of the bulk composition.

The subsolidus assemblage A+C+V (Fig. 1, section at P=6, T=2) is the key to understanding the melting relations of compositions containing small amounts of volatiles. Such an assemblage exists within a zone of invariant vapor composition (ZIVC), defined as the region in P-T-X space in which a volatile-bearing mineral coexists with multicomponent vapor and with its breakdown products in a reaction relation that buffers the vapor composition. For compositions within the 3-phase triangle A+C+V, insufficient CO_2 is available to carbonate the assemblage completely by the reaction A+CO_2 = C. Moreover, because A and C coexist with a H_2O-CO_2 vapor, and because the vapor composition is buffered by variation in the relative amounts of C and A, that subsolidus assemblage is invariant (at a given P and T).

In order that phase relations at and above the solidus may be understood, two pseudobinary joins have been drawn, one (a-a'), for compositions containing small amounts of volatiles (typical of the mantle) and one (b-b', Fig. 1) for compositions containing relatively large amounts of volatiles (typical of laboratory experiments). On the join a-a', compositions in the ZIVC (the assemblage A+C+V) melt at T=3.5 to A+C+L; the liquid composition is the same for all ZIVC compositions. On the join b-b', on the other hand, the majority of bulk compositions are outside the ZIVC, and the assemblages C+V and A+V melt, at temperatures that are dependent upon the volatile composition, to assemblages that are vapor-present. The compositions of liquids produced at the solidus in section b-b' also vary as a function of the volatile composition.

The P-T coordinates of a ZIVC solidus can be calculated if the $X^{v}_{CO_2}$ [$CO_2/(CO_2+H_2O)$ in the vapor] contours on a decarbonation reaction surface and on a solidus surface are known. This point can be appreciated from Figure 1, section a-a', in which it is seen that the solidus of the assemblage A+C+V occurs at a temperature (and at a $X^{v}_{H_2O}$) corresponding to the intersection of traces of the decarbonation surface (between A+C+V and A+V) and the solidus surface (between A+V and A+L+V).

Decarbonation Reactions and ZIVC-Type Solidi

There are two decarbonation reactions of importance to peridotite assemblages in the mantle:

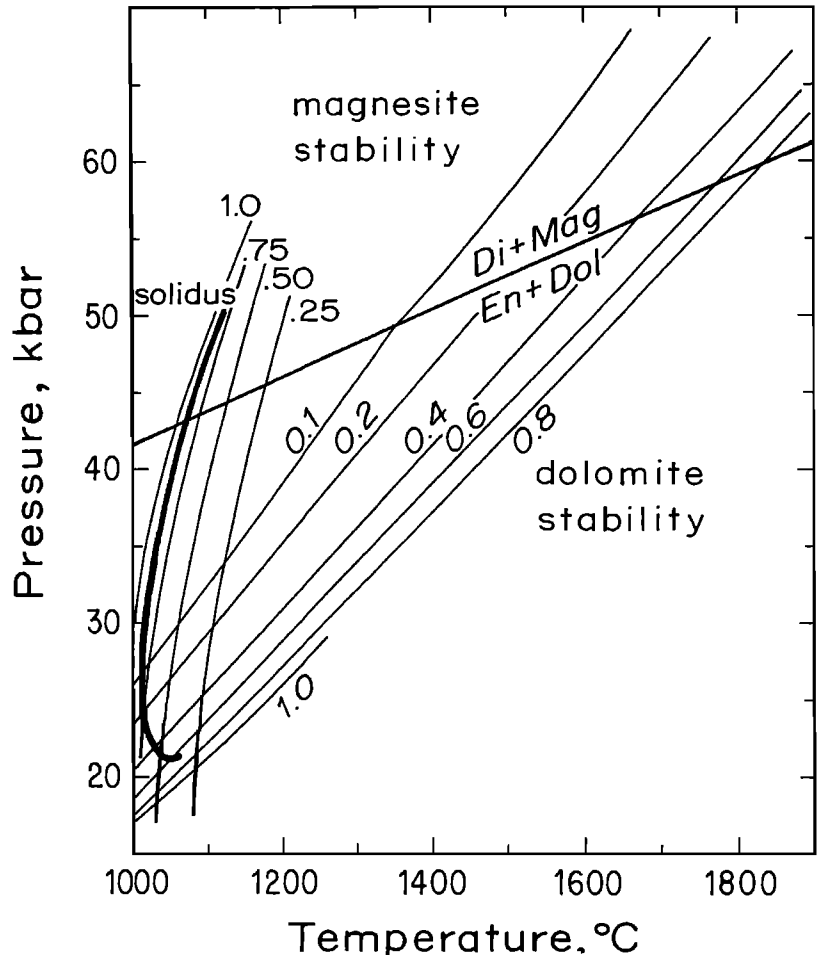

Fig. 2. Divariant surfaces, contoured for $CO_2/(CO_2 + H_2O)$, mol, ($X^v_{CO_2}$) of decarbonation reactions and of a peridotite solidus. The reaction En + Dol = Di + Mag, after Kushiro et al. (1975), separates stability fields for magnesite peridotite from dolomite peridotite. The upper set of contours, for the maximum stability of magnesite in the system $MgO-SiO_2-CO_2-H_2O$ (reaction 1, text), are calculated by the method of Eggler et al. (1976). The bottom set of contours, for the maximum stability of dolomite in the system $CaO-MgO-SiO_2-CO_2-H_2O$ (reaction 2, text), are after Eggler et al. (1976) and Eggler (1977). The H_2O-saturated peridotite solidus is after Kushiro et al. (1968); $X^v_{CO_2}$ contours are estimated. The heavy line is the calculated univariant (ZIVC) solidus buffered by dolomite reaction.

enstatite + magnesite = forsterite + CO_2 (1)

enstatite + dolomite = diopside + forsterite + CO_2 (2)

The compositions of natural phases participating in the first reaction are contained, to a close approximation, in the system $MgO-SiO_2-CO_2-H_2O$. The reaction has been studied, in the absence of H_2O, by Newton and Sharp (1975) and, as a function of CO_2-H_2O vapor composition, by Eggler et al. (1976). Compositions of natural phases participating in the second reaction are contained, to a close approximation, in the system $CaO-MgO-SiO_2-CO_2-H_2O$. The reaction has been studied in that system in the absence of H_2O by Wyllie and Huang (1975a, 1976) and by Eggler (1975, 1976). The divariant surface of the reaction in the presence of H_2O has been calculated by Eggler et al. (1976) and confirmed experimentally by Eggler (1977).

Divariant surfaces on the two reactions, contoured for $X^v_{CO_2}$, mol, are shown in Figure 2, separated by a third vapor-absent reaction determined by Kushiro et al. (1975):

enstatite + dolomite = diopside + magnesite. (3)

At pressures below reaction (3), dolomite is the stable carbonate in equilibrium with peridotite, whereas at pressures above the reaction, magnesite is stable.

It has been shown earlier that ZIVC-type solidi

TABLE 1. Compositions of an Average Lesotho Kimberlite and of the Synthetic Kimberlite Studied

	Lesotho	Lesotho normalized	COOKI-7
SiO_2	33.21	37.88	37.68
TiO_2	1.97	2.25	2.16
Al_2O_3	4.45	5.08	5.11
Cr_2O_3	0.17	0.19	0.23
Fe_2O_3	6.78	0.00	0.00
FeO	3.43	10.87	0.00
CoO	---	---	11.27
MgO	22.78	25.98	25.85
CaO	9.36	10.68	10.62
Na_2O	0.19	0.21	0.22
K_2O	0.79	0.90	0.91
P_2O_5	0.65	0.74	0.74
CO_2	4.58	5.22	5.22
H_2O	10.70	---	---
	99.06	100.00	100.01

can be generated by intersections of such divariant surfaces with solidus surfaces. ZIVC solidi have been discovered in the system CaO-MgO-SiO_2-H_2O-CO_2 by Eggler (1977, 1978a) and in the system K_2O-MgO-Al_2O_3-SiO_2-H_2O-CO_2 by Wendlandt (1977). The solidus surface of peridotite or kimberlite is of more interest. As an example, a peridotite solidus determined by Kushiro et al. (1968) is shown in Figure 2, with estimated $X^v_{CO_2}$ contours. Intersection of the solidus surface with the decarbonation surface defines a ZIVC solidus buffered by dolomite reaction. The composition of vapor buffered by the reaction becomes progressively more H_2O-rich with increasing pressure. (Strictly speaking, the ZIVC solidus of a natural peridotite will not be truly univariant because of limited solid solutions in the crystalline phases. One of the subsolidus minerals will be consumed by melting over a small temperature interval (Mysen and Kushiro, 1977), accordingly, rather than at the solidus. This behavior, which can be called "univariant-like" melting, does not affect the present argument, because the melting interval at a low $X^v_{H_2O}$ should be no different from the melting interval at a high $X^v_{H_2O}$, provided both X_{H_2O}'s are within ZIVC.)

The Composition Studied

A primary concern in carrying out the program of experimentation was selection of the starting composition. Because the number of runs at very high pressure had to be limited, due to excessive breakage of carbide components, only one refractory composition was selected (kimberlite can be usefully considered as an oxide composition plus CO_2 and H_2O). Because some of the most useful geothermometry-geobarometry of nodules has come from Lesotho kimberlites (Boyd, 1973), the average Lesotho kimberlite (Gurney and Ebrahim, 1973) was selected as the starting composition. The composition was modified only by substitution of CoO for FeO (total Fe as FeO). With this procedure, the intrinsically low f_{H_2} of the solid-media assembly (Eggler et al., 1974) can be used to advantage to decrease the loss of a transition element to Pt capsules, while retaining a divalent transition element in the liquid (Coons et al., 1976). The substitution does result in slightly higher solidus and liquidus temperatures (Coons et al., 1976).

The CO_2 content of the Lesotho kimberlite (Table 1) was considered to be entirely of mantle origin. The H_2O content of the Lesotho kimberlite was considered to be largely meteoric (Sheppard and Dawson, 1975). Accordingly, an anhydrous starting material was prepared, to which H_2O was added for individual experiments.

The starting material was prepared as a finely-ground mechanical mixture of titania, cristobalite, $CaMgSi_2O_6$ glass, magnesia, crystalline leucite, calcite, alumina, crystalline $CoSiO_3$, $Ca_3(PO_4)_2$, Cr_2O_3, and Na_2CO_3.

Experimental Procedure

The mixture, with H_2O, was loaded into 1.8 mm-diameter Pt or Pt5Au capsules, about 5 mm long, that were welded shut. The capsules were run, in a vertical position, in talc-pyrex (30 kbar) and talc-boron nitride (55 kbar) assemblies in solid-media, high-pressure apparatus. At 30 kbar, the piston-out procedure was used, with an initial 2 kbar over-pressurization. At 55 kbar, the assembly was heated to about 600°C before the piston (supported by floating steel rings) was advanced to the desired pressure. At both 30 and 55 kbar, nominal pressures are reported. Temperatures, uncorrected for the effect of pressure on emf, were measured with Pt-Pt10Rh thermocouples.

Phase boundaries determined in this study from synthesis runs were not reversed, in large part because of experimental exigencies. Run durations (Table 2) were sufficiently long, however, for equilibrium to have been achieved, based on experience with other carbonate-rich compositions (Eggler, 1978b).

Experimental Results

Phase assemblages were identified in grain mounts with the petrographic microscope. Liquids of CO_2-rich bulk composition at 30 kbar and at high temperatures quenched to glasses that were easily identified by their blue color (Coons et al., 1976), but for lower temperatures and for H_2O-rich compositions at 30 kbar, and for all experiments at 55 kbar, liquids quenched to fine-grained mixtures of crystals, crystallites, and rare glass, which were interpreted to have been

TABLE 2. Results of Quenching Experiments

Composition, wt %			P,	T,	Time,	Stable Phase
COOKI-7	H_2O	CO_2	kbar	°C	hours	Assemblage
94.6	0.0	5.4	30	1300	2.0	ol,opx,cpx,L
94.6	0.0	5.4	30	1400	0.78	ol,opx,cpx,L
94.6	0.0	5.4	30	1500	0.55	ol,cpx,L
94.6	0.0	5.4	30	1600	0.17	ol,L
90.0	4.9	5.1	30	1050	21.25	ol,opx,cpx,gt,ph,dol,V
87.0	8.1	4.9	30	1050	22	ol,opx,cpx,gt,ph,dol,V
89.9	5.0	5.1	30	1100	4	ol,opx,cpx,ph,dol,L
87.4	7.6	5.0	30	1100	3.25	ol,opx,cpx,ph,L
92.4	2.4	5.2	30	1150	3	ol,opx,cpx,L
89.9	5.0	5.1	30	1150	4	ol,opx,cpx,ph,L
90.0	4.9	5.1	30	1200	3.5	ol,opx,cpx,L
84.8	10.4	4.8	30	1200	3	ol,opx,cpx,L
91.1	3.7	5.2	30	1300	2.6	ol,opx,cpx,L
92.2	2.6	5.2	30	1350	3	ol,opx,cpx,L
89.9	5.0	5.1	30	1400	1	ol,L
90.6	4.3	5.1	30	1460	0.5	L
89.0	5.9	5.1	30	1500	1	L
92.7	2.0	5.3	30	1600	0.17	L
85.4	9.7	4.9	55	1200	2	ol,opx,cpx,gt,ph,cm,V
85.4	9.7	4.9	55	1250	2	ol,opx,cpx,gt,ph,L
84.1	11.1	4.8	55	1300	1.5	ol,opx,cpx,gt,L
89.9	5.0	5.1	55	1400	0.5	ol,opx,cpx,gt,L
89.3	5.6	5.1	55	1500	0.5	ol,opx,cpx,L
89.9	5.0	5.1	55	1600	0.17	L

a liquid phase. A vapor phase was not detected at supersolidus conditions. Stable crystalline silicates characteristically appear as euhedra that were unambiguously distinguished from quench crystals; the criteria of Yoder and Kushiro (1969) for distinguishing stable from quench phlogopite were particularly helpful. Stable dolomite or magnesite was distinguished as relatively clear, inclusion-free grains.

At 30 kbar (Fig. 3), compositions containing less than 0.35 weight percent H_2O ($X^{sys}_{CO_2} > 0.94$, wt) have insufficient H_2O to completely hydrate potential phlogopite in the kimberlite composition (Table 1). Phlogopite (Ph) therefore coexists, in the subsolidus region, with its breakdown products, Ks+Sa+Fo, with lherzolite phases [LHZ = diopsidic clinopyroxene (Cpx) + orthopyroxene (Opx) + forsteritic olivine (Fo) + garnet (Gar)], and with dolomite (Dol). (Other minor phases may be present, accounting for the TiO_2 and P_2O_5 contents of the kimberlite.) For bulk compositions containing more H_2O, there is sufficient H_2O to hydrate the potential phlogopite, and in the subsolidus region vapor coexists with LHZ + Dol + Ph (a ZIVC assemblage). Because phlogopite does not coexist with its breakdown products, it cannot buffer the vapor composition. To carbonate the kimberlite composition completely, however, 16.7% CO_2 is required. Because all the compositions studied contain only 5.22 wt% CO_2 (Fig. 3), dolomite coexisted with its breakdown products in all runs and buffered the vapor composition, except for very low and very high $CO_2/(CO_2+H_2O)$. Vapor compositions and the decarbonation boundary can be calculated from reaction (2) in the system $CaO-MgO-SiO_2-CO_2$ (see above).

Inasmuch as the assemblage LHZ + Ph + Dol + V is a ZIVC, melting is, isobarically, invariant-like (see above). The solidus was found to be 1075° ± 25°C at 30 kbar. Garnet is consumed by melting at temperatures immediately above the solidus, but dolomite persists over a small temperature interval, and phlogopite persists over a larger interval. Other details are apparent from the diagram.

Subsolidus assemblages at 55 kbar (Fig. 4) are similar to those at 30 kbar (Fig. 3), except that magnesite (Cm) replaces dolomite as the stable carbonate phase (Kushiro *et al.*, 1975), and the decarbonation boundary (between LHZ + Cm + Ph + V and LHZ + Ph + V) is shifted toward H_2O-rich compositions, due to the higher H_2O content of the buffered vapor (see above). Because H_2O-poor compositions were not studied, the relations between supersolidus magnesite and phlogopite were drawn to be consistent with the data of Wendlandt (1977) on the join $MgCO_3-KMg_3AlSi_3O_{10}(OH)_2-MgSiO_3$ from 32.5–50 kbar. The ZIVC assemblage (LHZ + magnesite + Ph + V) was found to melt at 1225° ± 25°C.

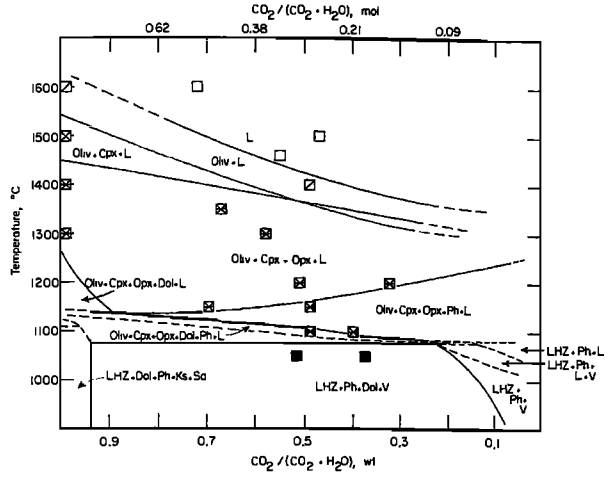

Fig. 3. Phase relations on the join (kimberlite + 5.2 % CO_2)-H_2O at 30 kbar (the composition shown in Table 1, with various amounts of H_2O added). LHZ = Fo + Opx + Cpx + Gar, Ph = phlogopite, Dol = dolomite, Ks = kalsilite, Sa = sanidine, L = liquid, V = vapor. Some phase fields occurring above the vapor-absent solidus are omitted for clarity. The abscissa is $X^{sys}_{CO_2}$, not vapor composition. The decarbonation boundary between the LHZ + Ph + Dol + V and LHZ + Ph + V fields was calculated from Figure 2.

The important discovery in the supersolidus region at 55 kbar was the greatly increased melting range of garnet. For $X^{sys}_{CO_2} \approx 0.5$(wt), garnet persists for almost 300°C above the solidus and to within 100°C of the liquidus. Liquid thus coexists with LHZ over a wide melting range.

The results at 30 and 55 kbar have been combined in Figure 5, a P-T section for one volatile content. The phase fields have been interpolated between 30 and 55 kbar and slightly extrapolated beyond that pressure range.

Discussion

Solidus of Kimberlite and Peridotite

The subsolidus phase assemblages of kimberlite at 30 kbar and at 55 kbar, in the presence of CO_2 and H_2O (Figs. 3 and 4), are the same as those of peridotite composition containing small amounts of CO_2 and H_2O (Eggler, 1977, 1978a). The disparity between these peridotite assemblages and the typical low-pressure groundmass assemblage of kimberlite, olivine + calcite + phlogopite, can be reconciled by a sequence of subsolidus carbonate-silicate reactions (Eggler et al., 1976) that transform the low-pressure assemblage to a high-pressure peridotite assemblage. Kimberlite compositions can be considered, for pressures above about 20 kbar, as exceptionally fertile peridotite compositions, enriched in components partitioned into a liquid phase. The solidi of the two compositions should be approximately the same, accordingly, save for differences arising from variation in the composition of phases.

The vapor-present (ZIVC) kimberlite solidus determined at 30 kbar, 1075° ± 25°C, is close to the solidus predicted for peridotite (Fig. 2), 1025°C. The difference may be ascribed to Co substitution -- a composition with a certain Mg/(Mg + Co) melts at a temperature about 50°C higher than a composition with the same value of Mg/(Mg + Fe) (Coons et al., 1976).

There are few data with which to compare the vapor-present (ZIVC) solidus at 55 kbar, 1225°C ± 25°C (Fig. 3). Clearly, the composition of the buffered vapor at 55 kbar is very H_2O-rich (Fig. 2), and, therefore, the determined solidus can be only slightly higher in temperature than the H_2O-saturated solidus. If a temperature increment is allowed for Co substitution (50°C, as at 30 kbar), a H_2O-saturated solidus of 1160°C would be predicted, a value remarkably close to the solidus in Figure 2, from Kushiro et al. (1968).

Kimberlite as a Primary Magma

At 30 kbar, lherzolite phases (Fo + Opx + Cpx + Gar) are not in equilibirum with liquid except at the solidus of the kimberlite composition (Fig. 3) For that reason, it is unlikely that kimberlite is a primary magma at that pressure, even if compositional variations other than those studied here were taken into consideration. At 55 kbar,

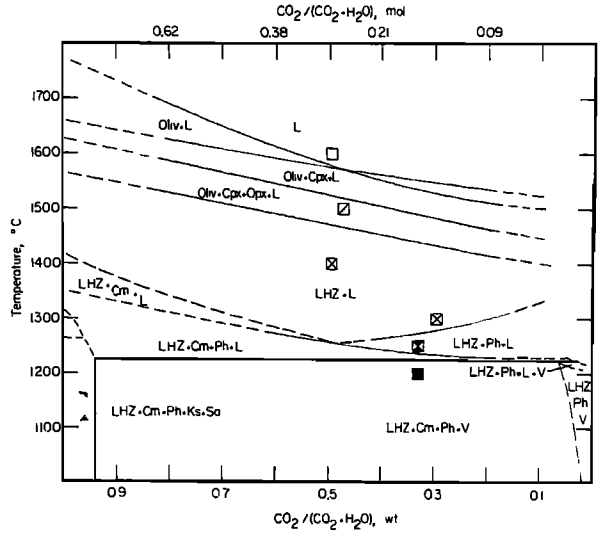

Fig. 4. Phase relations on the join (kimberlite + 5.2% CO_2)-H_2O at 55 kbar (the composition shown in Table 1, with various amounts of H_2O added). Abbreviations same as Figure 3, except that Cm = magnesite. The decarbonation boundary between LHZ + Cm + Ph + V and LHZ + Ph + V was calculated from Figure 2. Some phase fields above the vapor-absent solidus have been omitted for clarity.

however, lherzolite phases coexist with liquid over a temperature range of 200°-300°C, depending on $X^{sys}_{CO_2}$. It is, in fact, remarkable that lherzolite phases were found to coexist near the liquidus at 55-60 kbar (Fig. 5) for $X^{sys}_{CO_2} \approx 0.5$ (wt), because the starting material was only an average kimberlite composition.

The temperature at which a liquid resembling kimberlite could be produced at 55 kbar ranges from 1250°C, near the solidus of this composition, to at least 1500°C, near the liquidus of this composition. The compositions of liquids at the lower temperature are probably slightly more carbonatitic than the bulk composition (Table 1), because the liquid represents the bulk composition minus lherzolite phases.

Immiscible Liquids

The occurrence of carbonatite with kimberlite is common and is often explained by a relationship of liquid immiscibility. No evidence of immiscibility was found in this study, although its occurrence may have been precluded by the selection of relatively low volatile contents or may have been obscured during the quench.

It can be argued from phase equilibria in simple systems (Wyllie and Huang, 1976; Eggler, 1975) that at high pressures kimberlite magmas ranging from carbonate-rich to silicate-rich can be produced solely by partial melting, without recourse to immiscibility. Although there can be no doubt that at low pressures immiscible carbonate magmas exist, both in nature (Dawson and Hawthorne, 1973) and in the laboratory (Koster van Groos and Wyllie, 1973), the role of immiscibility at high pressures is still an open question.

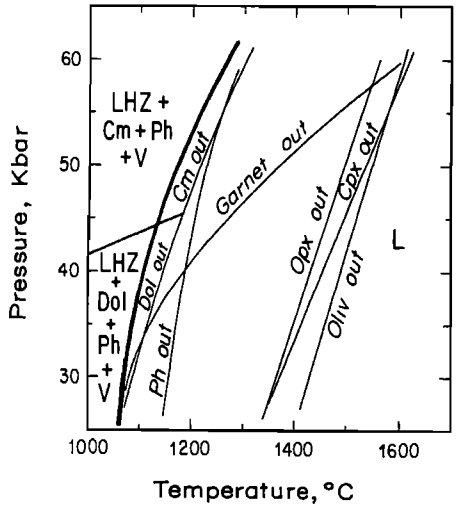

Fig. 5. Phase relations of a kimberlite composition containing 5.0% CO_2 and 5.0% H_2O (wt), interpolated and extrapolated from phase equilibria data at 30 and 55 kbar (Figs. 3 and 4). The heavy line is the univariant (ZIVC) solidus. Abbreviations same as Figure 3.

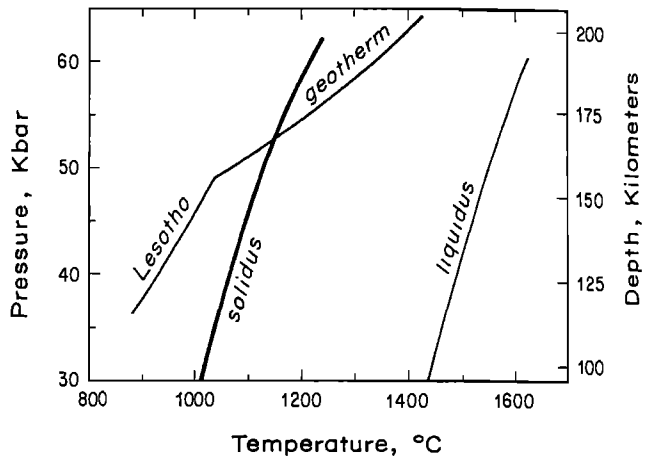

Fig. 6. The solidus and liquidus of a Lesotho kimberlite composition containing 5.0% CO_2 and 5.0% H_2O (wt) (from Fig. 5), with the Lesotho pyroxene paleogeotherm (Boyd, 1973). The solidus has been lowered 50°C from the position in Figure 5 to correct for the substitution of CoO for FeO.

Application to Genesis of Kimberlite

Because the composition investigated is an average Lesotho kimberlite, it is instructive to compare the solidus and liquidus with the pyroxene geotherm of Boyd (1973) calculated from nodules in Lesotho pipes (Fig. 6). The inflected limb of that geotherm intersects the kimberlite solidus at about 53 kbar (if the solidus is lowered 50°C to correct for Co substitution, as discussed above) and continues into the melting range. Because the kimberlite solidus is approximately the same as the peridotite-H_2O-CO_2 solidus, geotherm temperatures are sufficient to partially melt peridotite. Temperatures along the inflected geotherm lie in the supersolidus field of Fo + Opx + Cpx + Gar (± magnesite ± phlogopite) on the kimberlite phase diagram to at least 60 kbar (Fig. 5). Because liquid compositions in that field are also kimberlitic (see above), the composition of the partial melt of peridotite probably was kimberlite. It should be noted that kimberlite has also been proposed to be a partial melt on the basis of rare-earth element (REE) patterns (e.g., Mitchell and Brunfelt, 1975). Heavy REE depletion in kimberlites, indicating equilibrium with a residuum containing garnet, is consistent with derivation from garnet peridotite.

Boyd (1973) found that calculated temperatures of equilibration of discrete nodules (megacrysts) comprising an assemblage of olivine-subcalcic diopside-orthopyroxene-garnet-ilmenite lie along the inflected geotherm. Although megacrysts are usually interpreted to have grown in the presence

of a liquid, there is no agreement on the composition of the liquid. The experimental results obtained here are consistent with proposals that the liquid is kimberlitic (Dawson and Stephens, 1975; Mitchell and Clarke, 1976; Eggler and McCallum, 1976). (Ilmenite was not observed in run products, probably because of the effect of substitution of Co for Fe.) The experimental results suggest, moreover, that a kimberlitic liquid at pressure of less than 60 kbar could also precipitate phlogopite and magnesite. Phlogopite has been identified as a megacryst in kimberlite (Dawson and Smith, 1975), but magnesite megacrysts have not been recognized.

In recent explanations of the inflected limb of the Lesotho geotherm, diapiric flow has been emphasized, whether in the form of an upwelling diapir (Green and Gueguen, 1974), a mantle plume (Parmentier and Turcotte, 1974), or a diapir associated with convective overturn (Boyd, 1976). If a diapir should contain CO_2 and H_2O, and if its temperature distribution at depths of 160-200 km should resemble the Lesotho geotherm (1150°-1400°C), the diapir would partially melt (Fig. 6), and the composition of the melt would be kimberlite. Because there is no reason to assume that diapirs are confined (or have been confined) to areas of known kimberlites, there is also no reason to assume that liquids produced by melting of diapirs (kimberlites, at 160-200 km) are not relatively common in the mantle. The rarity of kimberlite occurrences may then be ascribed to the rarity of tectonic settings conducive to the ascent of kimberlite magmas, not to the rarity of the magmas themselves. There is no reason, in fact, why kimberlitic magmas should not be present beneath ocean basins as well as continents, assuming that the suboceanic mantle contains CO_2 and H_2O (in this regard see Delaney et al., 1977). The apparent absence of kimberlites in oceanic settings may be due to tectonic factors or may be due to the fact that oceanic diapirs can rise high into the asthenosphere. At these relatively shallow depths, the partial melt of the diapir will be not kimberlitic but nephelinitic or basanitic (Eggler, 1978b). Beneath continents, on the other hand, diapiric uprise may be halted near the bottom of the lithosphere, at depths from which ascending liquids will be kimberlitic.

Acknowledgments. This research was supported by the Earth Sciences Section, National Science Foundation, Grants DES 73-00266A01 and EAR 77-15704. We are deeply indebted to Peter M. Bell for use of a high-pressure plate of his design and for his advice in circumventing the many problems encountered during the experimentation at 55 kbar. The manuscript was reviewed by D. C. Presnall, B. O. Mysen, W. Harrison, and H. S. Yoder, Jr.

References

Boyd, F. R., A pyroxene geotherm, Geochim. Cosmochim. Acta, 37, 2533-2546, 1973.

Boyd, F. R., Inflected and noninflected geotherms, Carnegie Inst. Washington Year Book 75, 521-523, 1976.

Coons, W. E., J. R. Holloway, and A. Navrotsky, Co^{2+} as an analogue for Fe^{2+} in high-temperature experiments in basaltic systems, Earth Planet. Sci. Lett., 30, 303-308, 1976.

Dawson, J. B., Advances in kimberlite geology, Earth Sci. Rev., 7, 187-214, 1971.

Dawson, J. B., and J. B. Hawthorne, Magmatic sedimentation and carbonatitic differentiation in Kimberlite sills at Benfontein, South Africa, J. Geol. Sci. Lond., 129, 61-85, 1973.

Dawson, J. B., and J. V. Smith, Chemistry and origin of phlogopite megacrysts in kimberlite, Nature, 253, 336-338, 1975.

Dawson, J. B., and W. E. Stephens, Statistical classification of garnets from kimberlite and associated xenoliths, J. Geology, 83, 589-607, 1975.

Delaney, J. R., D. Muenow, J. Ganguly, and D. Royce, Anhydrous glass-vapor inclusions from phenocrysts in oceanic tholeiitic pillow basalts (abs.), EOS (American Geophysical Union Transactions), 58, 530, 1977.

Eggler, D. H., Peridotite-carbonate relations in the system $CaO-MgO-SiO_2-CO_2$, Carnegie Inst. Washington Year Book 74, 468-474, 1975.

----------Does CO_2 cause partial melting in the low-velocity layer of the mantle?, Geology, 4, 69-72, 1976.

----------The Principle of the Zone of Invariant Vapor Composition: an example in the system $CaO-MgO-SiO_2-CO_2-H_2O$ and implications for the mantle solidus, Carnegie Inst. Washington Year Book 76, 428-435, 1977.

----------The stability of dolomite in a hydrous mantle, with implications for the mantle solidus and the low-velocity zone, Geology, 6, 397-400, 1978a.

----------The effect of CO_2 upon partial melting of peridotite in the system $Na_2O-CaO-Al_2O_3-MgO-SiO_2-CO_2$ to 35 kb, with an analysis of melting in a peridotite-H_2O-CO_2 system, Amer. Jour. Sci., 278, 305-343, 1978b.

Eggler, D. H., and J. R. Holloway, Partial melting of peridotite in the presence of H_2O and CO_2: principles and review: Oregon Dept. Geology Mineral Industires Bull. 96, 15-36, 1977.

Eggler, D. H., I. Kushiro, and J. R. Holloway, Stability of carbonate minerals in a hydrous mantle, Carnegie Inst. Washington Year Book 75, 631-636, 1976.

Eggler, D. H., and M. E. McCallum, A geotherm from megacrysts in the Sloan kimberlite pipes, Colorado, Carnegie Inst. Washington, Year Book 75, 631-636, 1976.

Eggler, D. H., and M. Rosenhauer, Carbon dioxide in silicate melts: II. Solubilities of CO_2 and

H_2O in $CaMgSi_2O_6$ (diopside) liquids and vapors at pressures to 40 kb, Amer. Jour. Sci., 278, 64-94, 1978.

Koster van Groos, A. F., and P. J. Wyllie, Liquid immiscibility in the join $NaAlSi_3O_8$-Na_2CO_3-H_2O, Amer. Jour. Sci., 273, 465-487, 1973.

Kushiro, I., H. Satake, and S. Akimoto, Carbonate-silicate reactions at high pressures and possible presence of dolomite and magnesite in the upper mantle, Earth Planet. Sci. Lett., 28, 116-120, 1975.

Kushiro, I., Y. Syono, and S. Akimoto, Melting of a peridotite nodule at high pressures and high water pressures, J. Geophys. Res., 73, 6023-6029, 1968.

MacGregor, I. D., A hypothesis for the origin of kimberlite, Min. Soc. Amer. Spec. Paper 3, 51-62, 1970.

Mitchell, R. H., and A. O. Brunfelt, Rare earth element geochemistry of kimberlite, Phys. Chem. Earth, 9, 671-686, 1975.

Mitchell, R. H., and D. B. Clarke, Oxide and sulphide mineralogy of the Peuyuk kimberlite, Somerset Island, N. W. T. Canada, Contrib. Mineral. Petrol., 56, 157-172, 1976.

Mitchell, R. H., and J. H. Crocket, The isotopic composition of strontium in some South African kimberlites, Contrib. Mineral. Petrol., 30, 277-290, 1971.

Mysen, B. O., and A. L. Boettcher, Melting of a hydrous mantle: I. Phase relations of natural peridotite at high pressures and temperatures with controlled activities of water, carbon dioxide, and hydrogen, J. Petrology, 16, 520-548, 1975.

Mysen, B. O., and I. Kushiro, Compositional variations of coexisting phases with degree of melting of peridotite in the upper mantle, Amer. Mineral., 62, 843-865, 1977.

Newton, R. C. and W. E. Sharp, Stability of forsterite + CO_2 and its bearing on the role of CO_2 in the mantle, Earth Planet. Sci. Lett., 26, 239-244, 1975.

O'Hara, M. J., and H. S. Yoder, Jr., Formation and fractionation of basic magma at high pressure, Scottish J. Geol., 3, 67-117, 1967.

Parmentier, E. M., and D. L. Turcotte, An explanation of the pyroxene geotherm based on plume convection in the upper mantle, Earth Planet Sci. Lett., 24, 209-212, 1974.

Sheppard, S. M. F., and J. B. Dawson, Hydrogen, carbon and oxygen isotope studies of megacryst and matrix minerals from Lesothoan and South African kimberlites, Phys. Chem. Earth, 9, 747-764, 1975.

Wendlandt, R. F., The system K_2O-MgO-Al_2O_3-SiO_2-H_2O-CO_2: Phase relations of the joins Ph-H_2O-CO_2 and Ph-En-Mag at high temperatures and high pressures and applications to the genesis of alkaline magmas, Extended Abstracts, Second International Kimberlite Conference, Santa Fe, New Mexico, 1977.

Wyllie, P. J., Peridotite-CO_2-H_2O and carbonatitic liquids in the upper asthenosphere, Nature, 266, 45-57, 1977a.

----------Mantle fluid compositions buffered by carbonates in peridotite-CO_2-H_2O, J. Geology, 85, 187-207, 1977b.

Wyllie, P. J., and W. L. Huang, Influence of mantle CO_2 in the generation of carbonatites and kimberlites, Nature, 257,297-299, 1975a.

----------Peridotite, kimberlite, and carbonatite explained in the system CaO-MgO-SiO_2-CO_2, Geology, 3, 621-624, 1975b.

----------Carbonation and melting reactions in the system CaO-MgO-SiO_2-CO_2 at mantle pressures with geophysical and petrological applications, Contrib. Mineral. Petrol., 54, 79-107, 1976.

Yoder, H. S., Jr., and I. Kushiro, Melting of a hydrous phase: phlogopite, Amer. Jour. Sci. 267A, 558-582, 1969.

EXPERIMENTAL STUDY ON TWO PICRITES WITH REFERENCE TO THE GENESIS OF KIMBERLITE

Alok K. Gupta

Department of Geology and Geophysics, University of Roorkee, Roorkee 247672, U.P. India

Kenzo Yagi

Department of Geology and Mineralogy, Hokkaido University, Sapporo, 060 Japan

Abstract. The presence of eclogitic xenoliths often found in kimberlites suggested the possibility of formation of kimberlitic magma by separation of eclogitic fraction from a picritic magma. In order to elucidate this problem both nepheline-normative and hypersthene-normative picrites from Japan have been studied at temperatures and pressures up to 1300°C and 30 kbar in presence of excess water. It is concluded from the present investigation that partial melting of a nepheline - normative picrite at high pressures may produce a kimberlitic magma by subtracting the eclogitic fraction, but a hypersthene-normative picrite is not suitable for the formation of kimberlitic magma. The stability relation of amphibole in the experimental product indicates that kimberlite formation takes place at depth not less than 70 km, or probably 100 km under the condition of low geothermal gradient.

Introduction

The occurrence of eclogitic xenoliths within kimberlites suggested the close genetic relationship between these two rocks. O'Hara (1965) and O'Hara and Yoder (1967) considered that separation of eclogite from a picritic magma at depth of 25 kbar or more might produce a volatile-rich liquid similar to kimberlite. According to Green and Ringwood (1967), however, a nephelinitic but not a kimberlitic magma is formed by the fractionation of a primary picritic melt. In order to elucidate the genetic relationship between a picrite and a kimberlite, melting experiments on a nepheline-normative picrite and a hypersthene-normative picrite from Japan have been made at various temperatures and pressures in presence of excess water.

Petrology of the Samples

A nepheline-normative picritic dolerite from Nosappu Cape of the Nemuro Peninsula, Hokkaido (No.3005, Yagi, 1969) is holocrystalline, coarse-grained, and consists of plagioclase (An_{57-64}), orthoclase cryptoperthite, augite ($Ca_{41}Mg_{47}Fe_{12}$), olivine (Fo_{70}), biotite, Ti-magnetite, and small amount of ilmenite and apatite, and secondary analcite. No distinction between phenocrysts and groundmass is noticed.

A hypersthene-normative picritic basalt from Wakuike, Nagano Prefecture (No.36851, Takeshita, 1974-75) is porphyritic with many megacrysts of plagioclase (An_{92-87}), olivine (Fo_{68-71}), augite ($Ca_{43}Mg_{42}Fe_{15}$- $Ca_{44}Mg_{39}Fe_{17}$) and magnetite phenocrysts in a groundmass of plagioclase, augite ($Ca_{41}Mg_{39}Fe_{20}$), pigeonitic augite ($Ca_{34}Mg_{42}Fe_{24}$), magnetite and slightly devitrified mesostasis.

Presence of abundant megacrysts of anorthite (An_{94}) and olivine (Fo_{81-82}) is remarkable and can be distinguished from other phenocrysts by the absence of zonal structure. Chemical compositions of these two picrites and their normative compsoitions are given in Table 1. It is noted that Nosappu picrite has fairly high content of nepheline, whereas Wakuike picrite has very high content of hypersthene.

Experimental Method

The experiments were carried out by a piston-cylinder high pressure apparatus at temperatures and pressures up to 1300°C and 30 kbar. Powdered sample was put in an Au or Pt capsule with water at the ratio of 4:1, and the sealed capsule was placed in a cell, 1.25 cm in diameter and 5 cm in length. The weight of smaple and water was always measured after each run to ensure that there was no loss of water during the experiment. A hysterisis loop related to the ram thrust during compression and decompression cycles was determined at various temperatures.

The double value of friction was measured by the same method as described by Hariya et al. (1969). The reported pressures are correct to $\pm$ 1 kbar. Temperature was measured by $Pt_{90}Rh_{10}$-Pt and chromel-alumel thermocouples. Effect of pressure on the e.m.f. of the thermocouples was not taken

Table 1. Chemical and Normative Compositions of Picrites.

	1	2		1a	2a
SiO_2	46.07	47.47	Or	11.68	3.56
TiO_2	1.98	0.71	Ab	12.58	12.73
Al_2O_3	11.06	17.09	An	12.51	38.03
Fe_2O_3	5.00	1.32	Ne	5.11	-
FeO	5.44	7.31	Di Wo	18.33	2.62
MnO	0.20	0.24	Di En	14.50	1.71
MgO	9.97	11.31	Di Fs	1.72	0.73
CaO	11.73	9.15	Hy En	-	17.20
Na_2O	2.59	1.51	Hy Fs	-	7.39
K_2O	2.01	0.60	Ol Fo	7.28	6.68
H_2O+	2.22	2.56	Ol Fa	1.02	2.71
H_2O-	1.78	0.64	Mt	7.19	1.86
P_2O_5	0.23	0.18	Il	3.80	1.37
			Ap	0.67	0.40
Total	100.28	100.09			

1 and 1a: Picritic dolerite No.3005 from Nosappu Cape. Analyst: N.Onuki (Yagi, 1969).
2 and 2a: Picritic basalt No.65851 from Wakuike. Analyst: H.Matsumoto (Takeshita,1974-75).

into consideration. Temperatures are accurate to ± 10°C for runs near liquidus or subliquidus, and to ± 15°C for runs near solidus.

Identification of the phases was made by a petrographic microscope, an X-ray diffractometer, and an E.P.M.A. It was frequently observed that mica and amphibole form quench crystals. Therefore special care has been taken to distinguish such quenched phases from equilibrated phases in the liquids.

Experimental Results

Results of the experiments are summarized in Figs. 1 and 2, and some critical runs are given in Table 2. The subsolidus assemblage of the Nosappu picrite consists of clinopyroxene, plagioclase, amphibole, mica, magnetite and vapor at pressures less than 22 kbar, with a solidus at around 700°C (Fig.1). With increasing temperature amphibole disappears first, followed successively by plagioclase, mica, magnetite and clinopyroxene. The liquidus lies around 1200°C with clinopyroxene as the primary phase. At pressures higher than 22 kbar and temperatures less than 1000°C, garnet is always present and there is a fairly wide field of clinopyroxene + garnet + mica + magnetite + liquid + vapor. The mica is phlogopitic in composition. It is noted that mica has much larger stability field compared to amphibole. This fact has already been noted by Yoder and Kushiro (1969) and Modreski and Boettcher (1970), suggesting that the phlogopitic mica may indeed be the source of potassium in the upper mantle. The stability of the amphibole is similar to that of kaersutite studied by the present authors (Yagi et al. 1975).

The subsolidus assemblage of the Wakuike picrite is much simpler, consisting of plagioclase + amphibole + vapor with a solidus around 700°C (Fig.2). With increasing temperature, at about 800°C both clinopyroxene and magnetite begin to crystallize, forming an assemblage of amphibole + plagioclase + clinopyroxene + magnetite + liquid + vapor. With further rise in temperature first amphibole and then plagioclase and magnetite disappear successively. The liquidus with clinopyroxene as the primary phase occurs at about 1250°C, slightly higher than that of the Nosappu picrite, because of higher MgO content. In this picrite garnet appears above 17 - 18 kbar, about 5 kbar lower than the lower stability limit of this mineral in case of the Nosappu picrite. This may be due to the higher concentration of Al_2O_3 and CaO in the rock from Wakuike. Mica is not present at all because of its low content of K_2O.

When the results of these two experiments are compared, it is noted that amphibole and garnet have wider fields of stability in the Wakuike picrite than those in the Nosappu picrite.

Table 2. Critical Runs of the Experiments.

Temp. °C	Pres. Kbar	Time Hr	Phases
A. Picritic Dolerite from Nosappu			
700	10	24	Pl=Cpx > Amph>Mica>Mt:L+V
700	25	24	Cpx > Ga> Mica> Mt: V
750	15	16	Cpx=Pl> Amph>Mica>Mt:L+V
800	20	24	Cpx>>Mica: L + V
800	25	24	Cpx > Ga> Mica> Mt: L + V
950	22	3	Cpx> Ga> Mica> Mt: L + V
1000	25	3	Cpx>>Mica > Mt: L + V
1100	25	3	Cpx>>Mt: L + V
1150	15	1	Cpx>>Mica: L + V
1175	18	1	Cpx: L + V
1200	10	1	L + V
1200	25	1	L + V
B. Picritic Basalt from Wakuike			
675	18	24	Amph>>Pl: V
700	10	20	Amph>>Pl: L + V
700	25	48	Amph> Ga: L + V
750	15	24	Amph> Pl: L + V
800	25	18	Cpx> Ga> Amph> Mt: L + V
900	30	1	Cpx > Ga>>Mt: L + V
950	18	1	Cpx > Amph> Pl> Mt: L + V
950	20	18	Cpx > Ga> Amph> Mt: L + V
1000	10	40	Cpx > Amph > Pl> Mt: L + V
1000	25	20	Cpx> Ga> Mt: L + V
1200	25	1	Cpx> Mt: L + V
1250	15	1	L + V
1300	10	1	L + V

Abbreviations Amph: amphibole, Cpx: clinopyroxene
Ga: garnet, L: liquid, Mt: magnetite,
Pl: plagioclase, V: vapor

Table 3. Analyses of Crystalline Phases and Glasses.

A. Picritic Dolerite from Nosappu

	1	2	3
SiO_2	37.57	49.43	39.23
TiO_2	-	-	3.60
Al_2O_3	19.79	3.52	13.73
FeO	21.44	8.26	12.51
MnO	0.41	0.15	0.18
MgO	8.95	14.09	13.41
CaO	11.85	22.00	8.87
Na_2O	0.08	2.82	2.80
K_2O	-	0.06	1.74
Cr_2O_3	0.21	0.06	-
Total	100.30	100.39	96.07

B. Picritic Basalt from Wakuike

	4	5	6	7
SiO_2	39.57	49.31	46.76	46.67
TiO_2	-	0.49	0.27	0.35
Al_2O_3	20.41	1.94	9.06	12.26
FeO	21.71	13.58	15.55	13.76
MnO	0.29	0.44	0.50	0.43
MgO	10.42	14.68	14.53	15.40
CaO	9.41	16.81	8.32	6.14
Na_2O	0.08	0.35	2.05	0.58
K_2O	-	0.44	0.32	0.10
Cr_2O_3	0.15	0.02	-	-
Total	102.04	98.06	97.36	95.69

A. Picritic dolerite from Nosappu.
1. Garnet crystallized at 800°C and 25 kbar.
2. Clinopyroxene crystallized at 800°C and 25 kbar.
3. Glass formed at 800°C and 25 kbar.

B. Picritic basalt from Wakuike.
4. Garnet crystallized at 1000°C and 25 kbar.
5. Clinopyroxene crystallized at 1000°C and 25 kbar.
6. Amphibole crystallized at 800°C and 20 kbar.
7. Glass formed at 1000°C and 25 kbar.

In analyses Nos.3, 6, and 7, the deficiency from 100% total should correspond to the volatile composnents.

Crystalline Phases

Crystalline phases encountered in the present experiments are described below. E.P.M.A. analyses of garnet, clinopyroxene and amphibole in equilibria with liquids are given in Table 3.

Clinopyroxene forms stout prismatic crystals, 10-20 um across. The extinction angle c^Z ≈ 35-48°. This together with its high birefringence is diagnostic. Sometimes weak pleochroism:

X'...green, Z'...slightly brown

is observed. Twinning on (100) is rarely present. Compositions of clinopyroxenes crystallized at 800°C and 25 kbar from Nosappu picrite and at 1000°C and 25 kbar from Wakuike picrite (Table 3) give the following chemical formulas:

Nosappu: $(Na_{.20}Ca_{.80}Mg_{.77}Fe_{.21})_{1.98}(Si_{1.81}Al_{.15}Fe_{.04}^{3+})_{2.00}O_{6.00}$

Wakuike: $(Na_{.02}Ca_{.69}Mg_{.86}Fe_{.45}^{3+}Ti_{.01}Al_{.03})_{2.06}(Si_{1.94}Al_{.06})_{2.00}O_{6.00}$

When the two compositions are compared, clinopyroxene from Nosappu picrite is omphacitic with fairly high acmite content, whereas that from Wakuike picrite is relatively rich in FeO, and poor in CaO, Na_2O and Al_2O_3, and is more subcalcic augite rather than omphacitic pyroxene.

Amphiboles usually occur as slender prisms, but sometimes as needle-shaped crystals. Those from Nosappu picrite are usually smaller in grain size (10-20 μm), but the amphiboles crystallized from Wakuike picrite are larger (10-50 μm). Extinction angle c^Z = 10-15° for Nosappu sample, and 15-20° for Wakuike sample. Weak pleochroism is as follows: X'... pale green (slightly yellowish)

Z'... grass green.

Composition of an amphibole produced at 800°C and 20 kbar from Wakuike picrite (Table 3), gives the following formula:

$$(Na_{.61}K_{.06}Ca_{1.36})_{2.03}(Mg_{3.32}Mn_{.04}Fe_{1.98})_{5.34}(Si_{7.18}Ti_{.03}Al_{.82})_{8.03}(O,OH)_{24.00}.$$

Quench crystals of amphibole occur in bundle aggregates of slender prisms, by which they can be

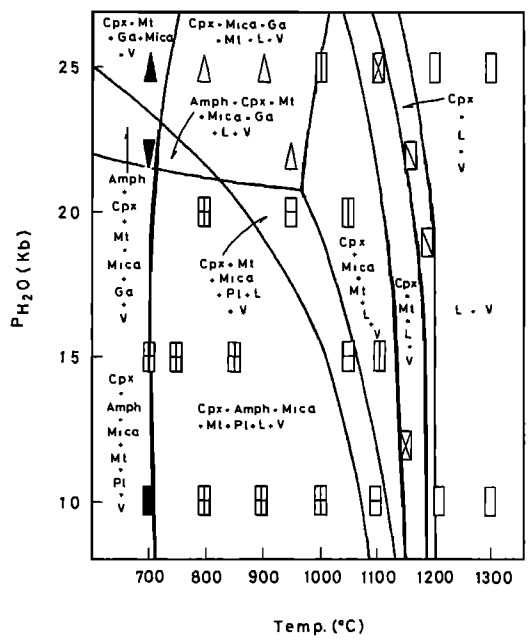

Fig.1. P_{H_2O}- T diagram of the picritic dolerite from Nosappu Cape.

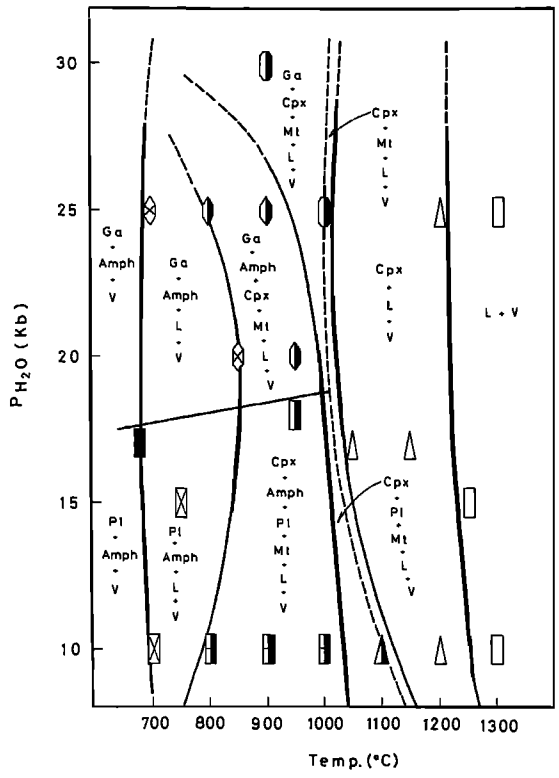

Fig.2. P_{H_2O} - T diagram of the picritic basalt from Wakuike.

distinguished from the equilibrated larger crystals.

Garnet is distinguished by its high relief and isotropism. They often exhibit perfect euhedral crystals (15-40 μm), but also form tiny rounded grains, less than 5 μm. Chemical compositions (Table 3) give the follwoing molecular ratios:

	Nosappu	Wakuike
Almandine	30.4	35.0
Pyrope	35.8	39.5
Grossularite	26.8	16.4
Andradite	7.0	9.1

When compared with garnets from nodules enclosed in kimberlites (Nixon and Boyd, 1973), these garnets are richer in almandine molecule, and poorer in pyrope molecule. It is also noteworthy that the garnets have nearly the same composition in spite of the wide difference in the chemistry of the two picrites. This is quite contrary to the case of clinopyroxenes.

Plagioclase forms thin plates or prismatic crystals (5-10 μm) or needle-shaped crystals. Plagioclase crystallized from Wakuike picrite is very rich in An content judging from its X-ray diffraction patterns.

Mica occurs as thin euhedral to subhedral plates, about 10-20 μm across. It is pale brownish in color, with weak pleochroism. Birefringence is usually high, but sometimes almost isotropic crystals are observed. At higher temperatures sheaf-like aggregates of fibrous mica were sometimes observed, which appear to be quench crystals.

Magnetite occurs as euhedral to subhedral opaque crystals. The size of the crystals increases with duration of runs, and attains even to 100 μm in longer runs, while they are less than 30 μm in shorter runs.

Discussions

In the case of Nosappu picrite, the composition of a glass in equilibrium with the clinopyroxene, garnet, mica and magnetite at 800°C and 25 kbar (Table 3) indicates a drastic decrease in SiO_2 and CaO, and increase in MgO, FeO and TiO_2 contents, compared to the original picrite. However, the CaO and Al_2O_3 contents are still high, and Na_2O and K_2O are still much higher than the average kimberlite from South Africa (Gurney and Ebrahim, 1973). The Na_2O/K_2O ratio is also above 1. The presence of quench crystals of phlogopite may indicate that if the quench phase did not appear, the K_2O and MgO might be still higher.

Thus the composition described here is somewhat similar to some nephelinites, which may support the proposal of Green and Ringwood (1967), that partial melting of picrites may produce nephelinitic magma. However, the most encouraging feature of the present experiment is that SiO_2 has decreased drastically. It is expected, therefore, that further crystallization of Ca- and Na-rich omphacitic clinopyroxene and Ca-rich garnet under isobaric conditions would impoverish the liquids in CaO, Na_2O and Al_2O_3, accompanied by relative enrichment in MgO, thus approaching to a melt of kimberlitic composition.

The composition of the glass in equilibrium with garnet, clinopyroxene, and magnetite at 1000°C and 25 kbar (Table 3) has a SiO_2 content as high as the original picrite, and the composition as the whole is comparable to some piciritic basalts rather than kimberlites. Here the clinopyroxene is subcalcic, but not omphacitic and mica is completely absent, whereas amphibole has much wider stability field.

From the results of the present investigation it is concluded that incipient partial melting of nepheline-normative picrite may produce a kimberlitic magma by subtraction of large amount of eclogitic fraction. However, a hypersthene-normative picrite is not suitable for the production of a melt of kimberlitic composition.

The upper stability limit of amphibole in the case of Nosappu picrite, indicates that the generation of kimberlitic magma occurs at a depth not less than 70 km or 23 kbar, and probably greater than 100 km under the condition of low geothermal gradient, since amphibole is usually absent in kimberlite.

Acknowledgements. The sample of Wakuike picrite was placed at our disposal by the courtesy of Dr.

Hisashi Takeshita of the Moji-Higashi High School. Mr.Shoichi Terada helped us in the preparation of the present paper. Part of the cost of the present experiments was defrayed by the Geodynamics Project grant from the Ministry of Education, Science and Culture, which is gratefully acknowledged.

References

Green,D.H., and A.E.Ringwood, An experimental investigation of the gabbro to eclogite transformation and its petrological applications, Geochim. Cosmochim. Acta,31, 767-833, 1967.

Gurney, J.J., and S.Ebrahim, Chemical composition of Lesotho kimberlites, in Lesotho Kimberlites, edited by P.H.Nixon, pp.280-284, Lesotho National Development Corporation, 1973.

Hariya, Y., W.A.Dollase, and G.C.Kennedy, An experimental investigation of the relationship of mullite to sillimanite, Amer. Mineral.,54 1419-1441, 1969.

Modreski, P.J., and A.L.Boettcher, Phase relationships of phlogopite in the system K_2O-MgO-CaO-Al_2O_3-SiO_2-H_2O to 35 kbar: A better model for micas in the interior of the earth, Amer. J. Sci., 273, 385-414, 1973.

Nixon, P.H., and F.R.Boyd, Petrogenesis of the granular and sheared ultrabasic nodule suite in kimberlites,in Lesotho Kimberlites, edited by P.H.Nixon, pp.48-56, Lesotho National Development Corporation, 1973.

O'Hara, M.J., Primary magmas and the origin of basalts,Scot.J. Geol.,1, 19-40, 1965.

O'Hara, M.J., and H.S.Yoder, Jr., Formation and fractionation of basic magmas at high pressures, Scot. J. Geol.,3, 67-117, 1967.

Takeshita, H., Petrological studies on the volcanic rocks of the northern Fossa Magna region, Central Japan, Pacific Geology, 7, 65-92, 1974 and 10, 1-32, 1975.

Yagi, K., Petrology of the alkalic dolerites of the Nemuro Peninsula, Japan, in Igneous and metamorphic geology, edited by L. Larsen, Geol. Soc. Amer. Memoir 115, pp.103-147, 1969.

Yagi, K., Y.Hariya, K.Onuma, and N.Fukushima, Stability relation of kaersutite, J. Fac. Sci. Hokkaido Univ. Ser.4, 16, 331-342, 1975.

Yoder, H.S.,Jr., and I.Kushiro, Melting of a hydrous phase: phlogopite. Amer. J. Sci. 267A, 558-582.

III. DIATREMES AND CARBONATITES

THE ROLE OF FRACTURE DYNAMICS IN KIMBERLITE PIPE FORMATION

Orson L. Anderson

Institute of Geophysics and Planetary Physics, University of California, Los Angeles, California 90024

Abstract. A fracture dynamic model in which an igneous intrusion of magma within a crack occurs is used to describe the physical processes of kimberlite pipe eruption. A symbiotic relationship exists between the crack and the fluid. The crack tip cannot accelerate faster than the fluid within it can flow in the channel provided by the crack, and the speed of the fluid is limited by its own viscosity. A volatile phase at the tip of the crack at lithostatic pressures will allow the crack to accelerate to high speeds, since the viscosity of a volatile is small.

It is proposed that kimberlite pipes occur in those rare regions of the earth where the composition of rocks at depth are rich in CO_2 compounds. A crack passing through such a region collects abundant CO_2 gas which accumulates in the tip of the crack. This provides the necessary low viscosity for the crack to accelerate. The crack becomes unstable, and the speed approaches the shear velocity of sound as the crack breaks through the earth's surface.

The main problem in this model is that an abundant supply of CO_2 must be available in order for the crack to go all the way to the surface, because the hydrostatic overburden must be balanced by the pressure of the fluid in the crack. The work of Wyllie indicates that CO_2 may be available for rapid crack propagation above 75 km.

Introduction

This paper is concerned primarily with the physical problem of the transport of kimberlite magma from the source area to the surface of the earth. The subject has received little attention in comparison to papers on the geological description of kimberlite pipes, petrologic examination of xenoliths, and the theory of petrogenesis.

We view this subject thus: Under what conditions can a crack be initiated below the earth's crust and grow all the way through the crust, breaking the surface in such a way that xenoliths from the low-velocity zone and the lithosphere can be transported rapidly to the surface?

We view this subject from the standpoint of fracture mechanics. We wish to propose a plausible physical mechanism to explain two general features of a kimberlite pipe: (1) material has been emplaced at the surface from depths as great as 200 km [Wagner, 1914; Dawson, 1962; Boyd and Nixon, 1973]; (2) rocks from this depth, along with others from shallower depths, have ascended very rapidly, by means of a fast-moving high-velocity fluid comprising particulate materials mixed with carbonate-rich fluids or gases [Shoemaker, 1955; McGetchin, 1968; Shoemaker and Moore, 1956; Dawson, 1971, 1972].

The time constraints on the transport of xenoliths to the surface are severe, because ascending diamonds must pass through the graphite stability field and a plausible physical mechanism must account for the presence of diamonds at the earth's surface, where they are metastable.

The diamond-graphite equilibrium diagram [Bundy et al., 1961; Kennedy and Kennedy, 1976] shows that in the diamond phase the temperature must be less than about 1000°C at 150 km and less than about 600°C at 100 km. Any reasonable P-T path transporting the diamond-bearing rock to the surface probably traverses the graphite-stable region. The only way that the diamond phase can be retained in the graphite-stable region is by quenching; that is, the diamond must rapidly lose temperature until a temperature is reached where the rate of reaction from graphite to diamond is very slow. A determination of the quench time is difficult because of unknown reaction times of graphitization. If the diamond is quenched in an inert atmosphere, graphitization would be very slow even at 1000°C. According to Evans [1976], the diamond phase may last 7500 years. However in an environment of the earth's atmosphere, the temperature would have to be maintained below about 400°C [Evans, 1976]. In a very reactive environment, such as the vapors of CO_2 and H_2O in a kimberlite, the rate of graphitization could be rapid at temperatures like 800°C. Diamonds in the interior of xenoliths like eclogite would be protected from a chemically reactive environment, but loose diamonds in the kimberlite itself would have to be quenched rapidly below 400°C in order to be maintained. Since most recovered diamonds are in the kimberlite, it will be assumed that the quench time to 400°C must be a few hours, say five hours.

If rocks containing diamonds travel about 200 km in about 5 hours, then they must be raised at a speed of about 7 meters per second.

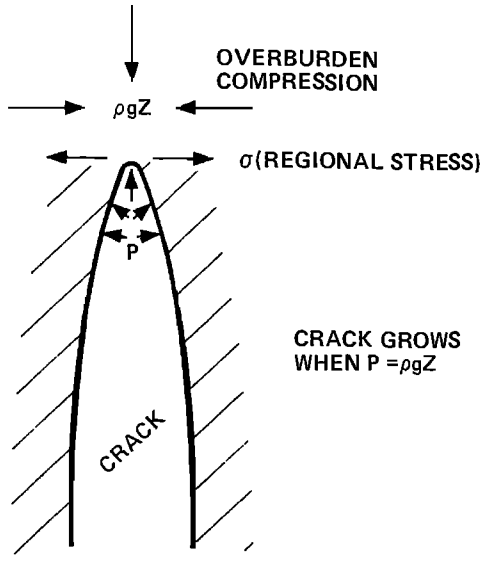

Fig. 1. A schematic curve showing the balance of forces in a growing crack.

This is a very fast rate for fragments of one kind of material to be transported through a solid. A crack must precede the diamond-bearing rock, and it must propagate all the way through the lithosphere to the surface at a speed at least as great as the figures just above, if the diamond is to arrive at the surface simultaneously with the breaching of the surface.

There are limits to the speed at which a crack can travel. A number of theoretical elasticity models have been solved in order to find the terminal velocity of a crack [Roberts and Wells, 1954; Berry, 1960; Erdogen, 1968]. The exact limit depends slightly upon the boundary conditions of the elasticity model assumed, but these investigations all give results suggesting that the terminal velocity is near the shear velocity of sound. For the earth's lithosphere, the shear wave velocity varies, but perhaps 4 km/sec is a reasonable average.

Therefore we will consider two models. In a one-step model of eruption, the crack must propagate to the surface at a velocity of about 7 m/sec, which is an average figure for throughout the lithosphere. In a two-step model of eruption, the crack itself could propagate at a lower speed, but the diamond-bearing rocks brought up in the second step after the crack is formed would have to travel upwards at about 10 m/sec.

Fundamentals of Crack Growth

The formation of a crack in the earth below the lithosphere has been considered by Weertman [1971]. The main obstacle to the formation of a crack lies in the fact that a tensile stress in the lithospheric plate is small compared to the hydrostatic pressure resulting from the overlying burden. Roberts [1970] and Weertman [1971] showed that if the crack is filled with a fluid in equilibrium with the solid then the hydrostatic pressure in the (solid) matrix around the crack is balanced out, and the dynamics of the crack are controlled by the stress field in the lithospheric plate. This is demonstrated in Figure 1. A crack is nucleated under the following conditions: (1) an accumulation of a fluid at the base of the lithospheric plate; (2) the density of the fluid is less than that of a plate; and (3) a tensile stress exists parallel to the surface.

In order for the crack front to move upwards, a fluid must be in the utmost tip of the crack. If the crack moves faster than the fluid, then there is nothing to balance out the hydrostatic component of the lithospheric stress tension in the vicinity of the crack; hence the chief stress components in the vicinity of the crack are compressive and the crack will not grow. The crack will extend upwards, providing the fluid follows in the tip of the extension. A symbiotic relationship therefore exists between the crack and the fluid in the crack, and they both must extend together. The crack cannot grow faster than the fluid can flow in the channel provided by the crack, and this fluid flow is limited by the viscosity of the fluid and the supply of the fluid [Anderson and Grew, 1977].

Since the supply of fluid to the tip of the crack is important, the role of volatiles is crucial. A volatile phase at the tip of the crack because of its low viscosity may allow the crack to accelerate to high speeds, perhaps even to the terminal crack velocity. On the other hand, a liquid magma, due to its high viscosity, would limit the speed of the crack to the order of 1 m/sec or less, depending on the properties of the magma and the crack width [Anderson and Grew, 1977; Maaloe, 1972].

In order to explain the emplacement of large amounts of mantle material including diamonds, at the surface of a kimberlite pipe, it is necessary to postulate an abundant supply of a low-viscosity fluid such as volatiles for the crack propagation mechanism.

As far as the mechanics of crack propagation are concerned, this supply of low-viscosity fluid could either be a reservoir at the base of the crack, or accretions from surrounding rock into the passing crack.

If the crack velocity is slow, as Weertman [1971] has shown, the trailing edges of the crack can join together to form a drop shape. Then the upward motion of the crack and the fluid within the crack geometrically resembles a diapir. In this case, the volume of fluid within the crack is limited by the amount in the reservoir of fluid at the site of the crack initiation. The crack motion exhausts the supply of fluid, closes upon itself, and rises as a diapir. On the other hand, if the crack velocity is very fast the crack will extend all the way back to the site of crack initiation, and the volume of volatiles required to

meet the pressure criterion for crack growth could be large.

According to stress corrosion propagation theory, the initial stages of unstable crack growth is slow. It is in its later stages of growth that it is fast. It is quite possible, even probable, that in early stages the crack and the material in the crack move upwards at geologically slow rates (meters/year). The lapsed time for the slow rates of crack growth could be very long, quite long enough for recrystallization and other equilibrium phenomena to take place within the xenoliths.

In order to preserve the diamond-phase at the surface, the material has to move upwards very rapidly once the graphite→diamond equilibrium curve is crossed. It must be recognized, however, that the fluid in the crack and the crack itself can move very slowly as long as the crack is in the diamond equilibrium field.

In the slow regions of crack growth the rate of crack propagation is controlled by chemical reactions arising from the interaction of the fluid within the crack tip and the solid comprising the crack tip. This region of slow crack propagation is identified as stress corrosion crack propagation. Controlled laboratory experiments have shown that this region extends between 10^{-4} and 10^{-13} km/sec [Anderson and Grew, 1977].

In this region the velocity of crack propagation is governed by a reaction rate equation in which there is a definite activation energy, which is quite high, a temperature according to the typical chemical rate equation, and a stress intensity factor (see Figure 2). The stress intensity factor is a parameter in fracture mechanics which accounts for the nominal stress outside the crack interaction field, and also for the stress multiplaction resulting from the high curvature of the crack. The stress intensity factor is given by

$$K = \text{const} \cdot \sigma \cdot \sqrt{C} \qquad (1)$$

where C is the crack length and σ is the tensile stress component perpendicular to the plane of the crack. The constant in (1) is defined by the precise geometry of the crack and the loading mechanism, and is tabled for various loading systems.

As shown in Figure 2, in the chemical region of crack growth a higher temperature makes the crack go much faster than does a lower temperature. This is a very strong effect and, for oxide compounds, has been found to hold even in the plastic region just below the melting point. In corundum, for example, Evans [1972] showed that in dropping the temperature from 1200°C to 1000°C but keeping K constant, the crack velocity dropped five orders of magnitude.

Applying this to xenolith transport, we could postulate that the upward transport of a slow crack from, say 175 km to 125 km, along the geotherm would result in a substantial decrease in velocity due to the decrease in temperature. Material that is transported within the crack at low depths could be moving fast enough that no changes are made in response to the lower temperature outside the crack. But as the temperature is reduced by the upward motion, the crack could slow down to very low velocity (perhaps as slow as 1 meter/year), in which case there is quite sufficient time for equilibrium to be re-established at this more shallow depth.

Xenoliths that took this path would be interpreted as having gone through a two-stage transport process.

A very slow crack could then be speeded up either by reducing the activation energy (by some chemical reaction at the crack tip by corrosive fluids) or by reducing the viscosity of the fluid.

This hypothesis, briefly discussed above, is a simple illustration of the myriads of paths and histories of rates of motion that could be conceived for the region labeled "chemifracture" in Figure 2.

When the crack is moving slow, the viscous magma within it geometrically resembles a diapir. I propose that the motion of a xenolith from the edge to the center can create strain due to a velocity gradient. From this speculation, one can explain the sharp deformational gradients within the xenolith, as noted by Boullier and Nicolas [1975]. The motion of the crack and the magma would be geometrically equivalent to the diapiric upwelling model envisioned by Green and Guegen [1974].

As the crack goes faster it eventually comes to the speed labeled "viscosity limited growth" in Figure 2. This plateau arises because there is a limit to the speed of a fluid in a narrow channel [Wiederhorn, 1967; Evans, 1972]. The upper limit of the speed of a fluid is controlled by the viscosity of the fluid and the separation between the planes of the channel (the crack width). Now this region is characterized by the fact that the crack velocity is independent of stress. However the plateau is a limit which rises as the viscosity drops [Speidel, 1971], and rises as the crack widens, according to classical calculations on viscous drag. In many ceramics broken in air, this plateau is of the order of 1 cm/sec (Figure 3), two orders below our desired velocity for the rise of diamonds. In materials where the crack is wider, the plateau will be at a higher limit. We expect the crack to be wide (about 1 meter) because the size of xenoliths places a lower limit on this dimension. Ultramafic xenoliths originating at depths greater than 150 km have diameters at least up to 50 cm, and crustal nodules are sometimes quite massive [Boyd, 1978].

This means that the one-step model is possible (the crack goes up followed immediately by the diamond-bearing rocks) because the crack is wide. It must be emphasized that it is very important that the fluid have access to the uppermost tip of the crack, so a rate determining parameter is the curvature of the crack tip. In ceramic fracturing, the tip is sharp, but it may be possible that

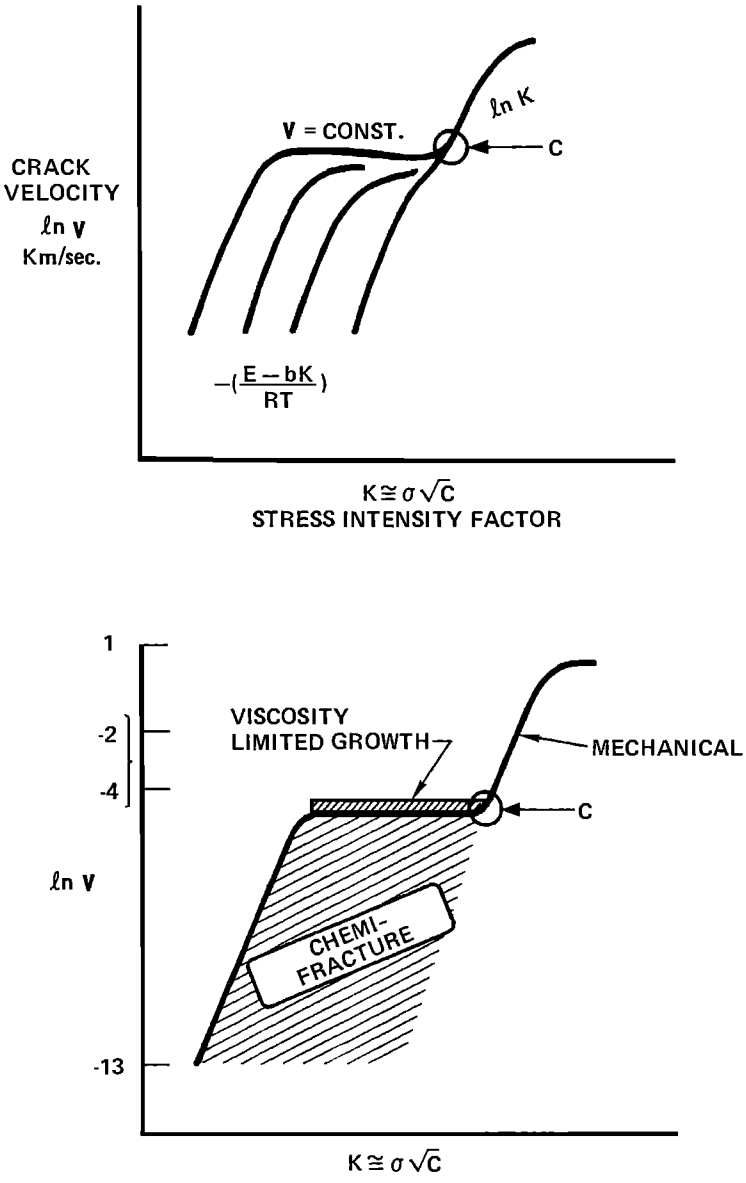

Fig. 2. (Above) A schematic plot of the crack velocity vs stress intensity factor, indicating the three regions of crack growth. (Below) The same plot as above, but showing the names of the three regions of crack growth and indicating the magnitude of their range.

in the mantle the tip curvature is sufficiently large to justify the assumption of wide cracks.

As the crack length C extends, the stress intensity factor K increases as $\sqrt{C}$. When K becomes large enough, the mechanical fracture curve is intersected (point C in Figure 2). At one atmosphere the crack enters the domain of the classical crack and obeys the laws of Griffith [1920] and Mott [1948] for fracture propagation. In this case, the crack rapidly accelerates to the terminal velocity as long as the stress is maintained [see review in Anderson and Grew, 1977].

However, deep in the crust and mantle, the crack cannot enter into the mechanical fracture domain, because the crack tip would outstrip the flow of fluid into the crack, and the hydrostatic overburden pressure would no longer be balanced out. Compression would replace tension at the tip of the crack, and the crack would close ahead of the fluid column. The crack velocity is consequently limited at the critical speed (point C in Figure 2).

In this region the crack can be slowed or stopped by a change in the properties of the solid or

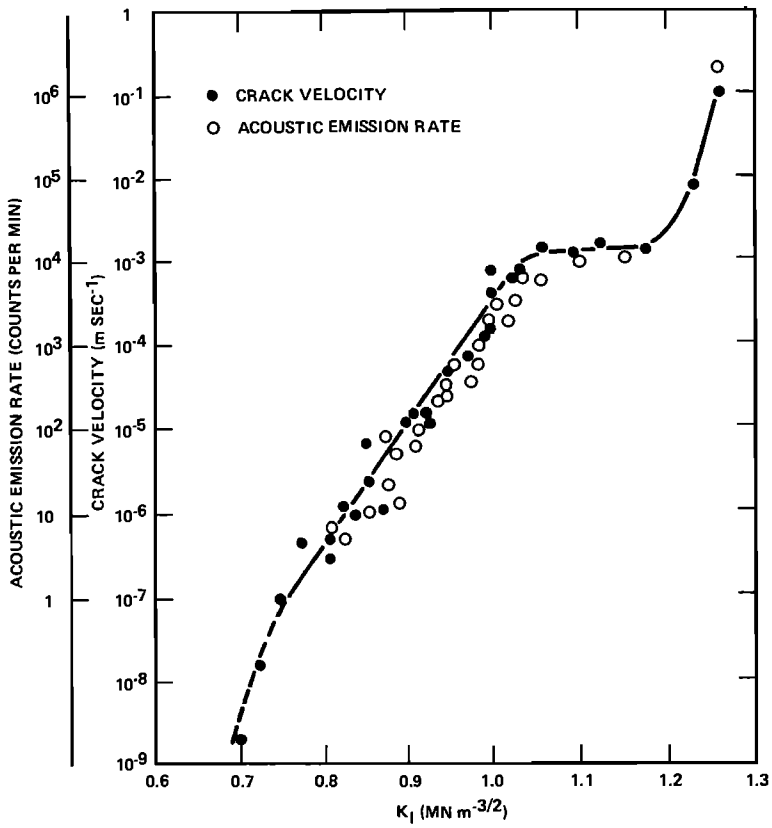

Fig. 3. The variation of crack velocity with stress intensity for corrundum (after A. G. Evans, 1974). Compare with figure 2.

a change in the fluid. If the tensile stress component perpendicular to the crack in the solid vanishes, changes sign to compression, or significantly decreases, the crack can be slowed or stopped. This means however, that there must exist a horizontal deviatoric tension component all the way through the lithosphere above the diamond stability field. (A crack will not propagate all the way through a lithospheric slab in bending, where the top half is in tension and the bottom in compression, or vice-versa.) Also, the crack must obtain a very large supply of a low-viscosity fluid (such as a vapor or gas) in order that the large hydrostatic pressure within the crack tip can be maintained as the crack travels upwards at great speeds.

Near the surface, when the hydrostatic pressure is reduced to the order of the regional stress, the requirements for a high pressure volatile phase in the tip of the crack is diminished. This allows the crack to accelerate well into the mechanical fracture region beyond point C in Figure 2. It is possible that in the last few hundred meters below the surface, the last stages of acceleration bring the crack velocity close to the terminal velocity as it breaches the surface. The reason for this acceleration is that the stress intensity factor is much larger than that corresponding to point C in Figure 1.

The principles of fracture mechanics then put two severe geological restrictions upon diamond-bearing kimberlite formations: (1) the deviatoric stress of the whole lithospheric cross-section at the kimberlite site must be in a state of tension at the time of the extrusion, and (2) somewhere in the lithosphere a large supply of low-viscosity volatiles must be available to accumulate in the tip of the crack.

Data for the crack velocity of corrundum are shown in Figures 3 and 4.

Breaching The Surface

A crack propagating to the surface in advance of the kimberlite material need not have the shape of the kimberlite chimney seen by geologists. It probably will not have this shape, but more that of the typical crack. In the plane parallel to the earth's surface, one dimension will greatly exceed another. The cross-section of the crack need only be approximately linear. It probably will be jerky, irregular, and forked.

Once the surface is breached, the crack model is no longer appropriate. A more likely model is

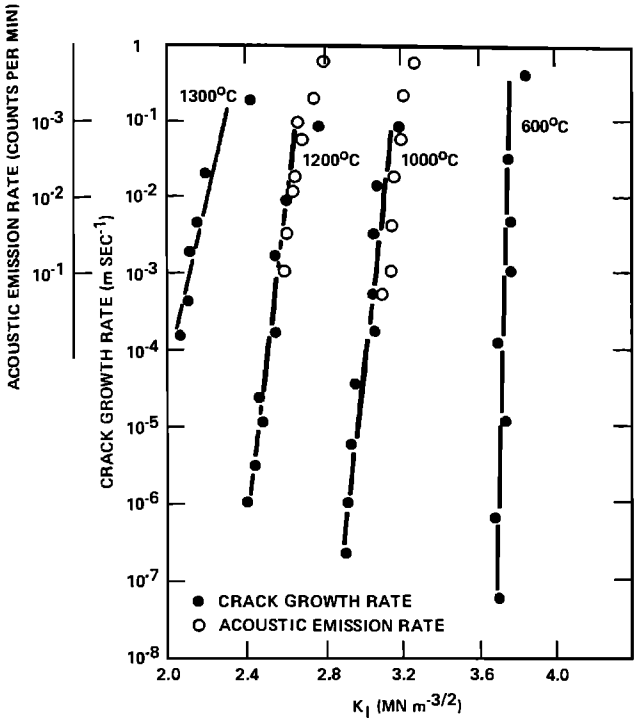

Fig. 4. The variation of crack velocity with the stress intensity factor and temperature for corrundum in the chemi-fracture region (after A. G. Evans, 1974).

that of a long rough pipe, finite in length, in which an incompressible fluid is exhausted through the surface. Such a model has been proposed by McGetchin and Ullrich [1973]. In their solution of this model, they found the exit velocity to be larger than mach one, with a gradual diminishing of velocity as the depth is lowered.

The model developed by Woolsey et al. [1975] using a stream of compressed air to breach layers of sediments, illustrates the probable course of events just before and after the breaching of a crack. According to these models, a fluidization cell develops just below the surface at the time of breaching. Since the velocity of the volatiles exceeds that of the free-fall velocity of the particles, the particles become entrained in a fluidized mixture rising in the center of the column and falling down the edges. This fluidization creates the circular or ellipsoidal pipe shape, roughly the shape of a funnel, being wider at the surface than further down [Hawthorne, 1975, Figure 2].

The cause of this change from a linear crack, during the actual breaching, to a funnel-shaped hole is the same that produces craters from a linear curtain of fire in volcanic eruptions. A minimum in the total energy of the eruption is found when magma erupts from a circular hole [Jackson and Shaw, 1975].

Remnants of the crack trace are observable, if the fluidized material is ejected through the crack away from the main vent. We then see kimberlite dykes radiating away from vents after the eruption has ceased. Varieties of shapes in kimberlites are possible because of the transition from the linear crack to the roughly circular chimney in kimberlite pipes. Examples of these shapes are given by Williams [1932] and Janse [1975, page 85].

Source of the Volatiles

From the point of view of fracture mechanics, a large source of volatiles must be available in order for the crack to propagate upwards rapidly. Without this source, cracks will close under the stress conditions in the crust and mantle. Statements such as "the material will propagate upwards along fault planes" ignore fundamentals of fracture mechanics. Accordingly, the physicist looks to the petrologist to identify these volatiles from the evidence of the xenoliths.

In recent years, there have been more and more reports about the possibility that CO_2, or CO_2-H_2O vapor mixtures, are an important ingredient in mantle structure. The crucial problem is whether or not there can be a large amount of material in the vapor state at mantle conditions. Many authors, in this volume, and in the past literature, have shown how volatiles should be present in the mantle.

All these reports reassure the physicist interested in crack propagation that vapors which are probably rich in CO_2 are available in the mantle for crack propagation if conditions are right. Whether these vapors get into the crack from one deep source, or whether they diffuse into the crack at numerous places along the path of the crack is an important consideration for crack propagation. Wyllie's [1977] report on volatiles in the mantle is worth singling out, because he placed definite limits on the boundary of available volatiles. He examined the phase diagram of peridotite H_2O-CO_2 as a function of pressure and temperature, and showed that magmas containing carbonate compounds "which rise through 85-70 km from greater depths must evolve CO_2 and H_2O." Thus according to Wyllie's model, the presence of a low viscosity volatile is ensured for the fast propagation of the crack upward from about 75 km providing the source of CO_2 is in the magma.

Wyllie's mechanism could possibly work deeper than 75 km, if one considers reactions at a crack boundary. A crack suddenly opening up at a particular depth would create a momentary drop of pressure at the crack wall as the tip moves upward. On the inside of the crack wall, the conditions at 75 km for vapor generation would be realized thus releasing vapor from the magma at the crack wall.

Quenching the Xenoliths

Figure 5 shows the graphite-diamond equilibrium line in relation to the shield geotherm and the

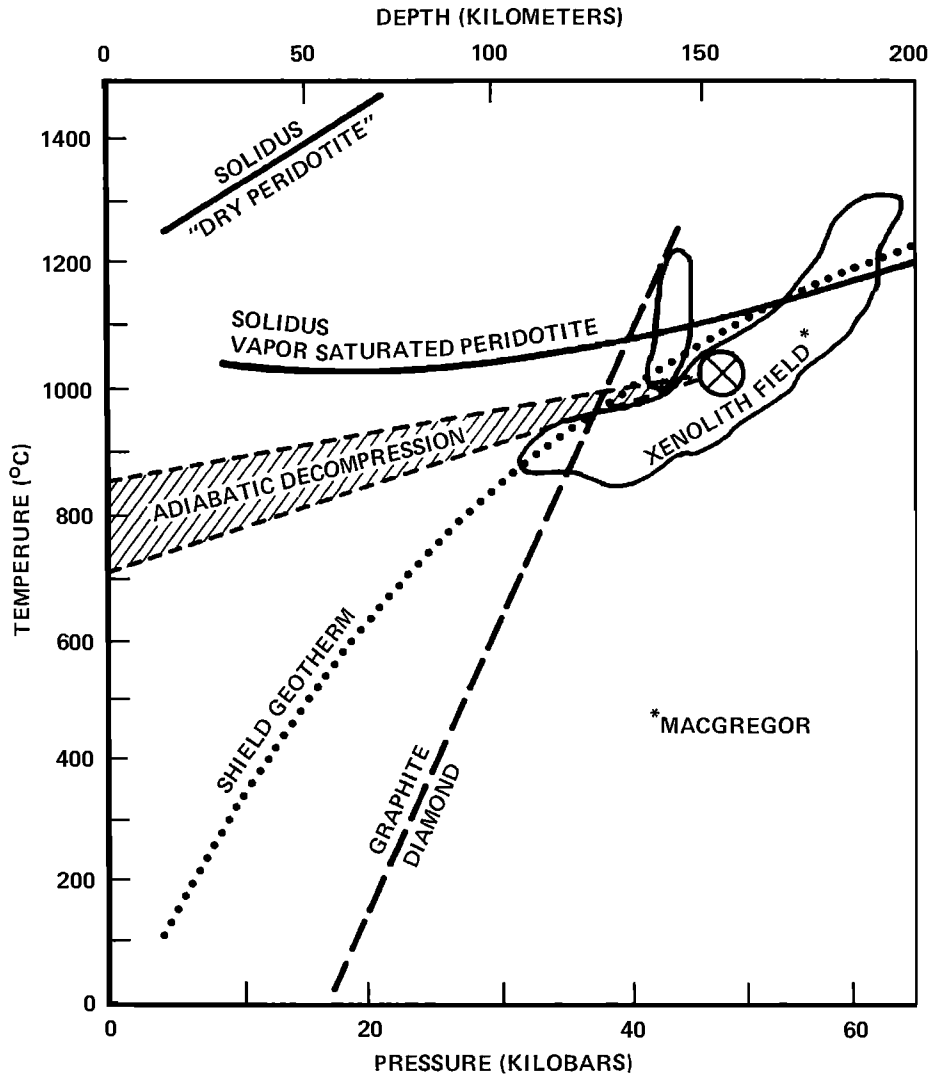

Fig. 5. The solid adiabatic decompression zone plotted in relation to geotherms of the mantle, and various phase equilibrium curves.

solidus line for vapor-saturated peridotite after MacGregor [1975, Figure 4]. Also plotted are the P-T equilibrium values of xenoliths according to MacGregor. We wish to discuss the problem of quenching of the xenoliths so that diamonds are preserved at the surface.

If a crack filled with magma and xenoliths were to propagate slowly to the surface, then thermal equilibrium would be approximated between the surrounding rock and the fluid within the crack. The fluid would then tend to keep the temperature corresponding to the surrounding rock as determined by the geotherm (Figure 5).

At the other extreme the material propagating up in a very fast crack would arrive at the surface with the source temperature, less solid-state adiabatic cooling. We can calculate the temperature drop that a xenolith would experience if the crack moves very fast--so fast that no heat is transferred between the surrounding rock and the magma. This is called adiabatic decompression.

Computing the change of temperature with depth at constant pressure, it is found that the outside limit of dT/dP to be 0.3-0.7°/kbar, the T-P path of adiabatic decompression is plotted as a dashed zone in Figure 3. If a xenolith is suddenly erupted to the surface from the vicinity of the graphite-diamond equilibrium field it will have reduced its temperature at the surface by 150-300°C from its original temperature by solid state adiabatic decompression. It will arrive at the surface at about 800°C, some 700-800°C hotter than the geotherm. If it is adiabatically decompressed from 75 km (Wyllie's depth at which CO_2-H_2O volatile production is possible) it will arrive at about 600°C.

This means that below 75 km the rate determining condition of crack growth is the viscosity of liquid magma, thus ensuring crack growth in the chemi-fracture domain. However, the diamond may be protected from reactive vapors since none exist in the liquid. Assume the diamond travels upward from the diamond-graphite equilibrium curve to the point of vapor release (75 km) in a time less than 7500 years (the time Evans [1976] calculated for graphitization at 1000°C in an inert atmosphere). The magma would be in thermal equilibrium, or about 700°C at 75 km. Vapor is then released according to Wyllie's mechanism, the viscosity of the fluid (now a vapor) in the crack tip drops to about 10-100 poises, and the crack accelerates up to the viscosity limited rate established by the crack width (say 1-10 m/sec). The magma and the crack arrive at the surface in 2 to 20 hours, and by adiabatic decompression of the diamond the temperature is reduced by about 50°. The diamond is in danger of reverting to graphite by being sustained at around 700°C for 2 to 20 hours in a reactive atmosphere.

However, another quenching mechanism is likely to quench the diamonds even further during ascent. From crack fracture experiments it is concluded that the radius of curvature of the crack tip does not change during the fracture [Anderson and Grew, 1977]. Gases in the tip of the crack stay in the tip of the crack under conditions of approximately constant volume. The vapors in the crack suffer a decompression of 75,000 bars to one bar at approximately constant volume as the crack ascends. By the perfect gas law we would calculate a tremendous reduction of temperature in the crack tip; obviously an oversimplification. Nevertheless, we can expect a large quenching effect of the diamond due to decompression of the vapors during the ascent.

Decompression of the volatiles will satisfy the quenching requirements in order to stabilize diamonds. During the several hours of ascent, loose diamonds that later are found in kimberlite, are quenched by being immersed in the decompressing vapors. Diamonds in the interior of xenoliths may not be quenched so readily due to thermal inertia, but on the other hand they may be protected from the chemically reactive environment. The loose diamonds arrive in a metastable state below 400°C at the surface, and the xenolith diamonds, though hotter, can cool at a slower rate without transformation.

Thus we see that a one-step model, in which the magma arrives with the crack, satisfies the criteria for diamond emplacement at the surface. This does not preclude the two-step model postulated by McGetchin and Ullrich [1973], in which diamonds are raised after the surface is breached and fluidization takes place.

If the mechanism of CO_2 vapor production proposed by Wyllie fails, then the two-step model is probably mandatory. In this case, the crack sustained by high viscosity magma in its tip slowly makes its way to the surface. Once the surface is breached, then the model of McGetchin and Ullrich [1973] or its equivalent is invoked to lift and quench the diamonds.

Mercier [1977] in this volume supports the case for a rapid ascent of the xenoliths by examination of the subgrain sizes of olivine in peridotite xenoliths.

Summary

The principles of fracture mechanics appear to provide a theoretical framework for the emplacement of kimberlite pipes and the explanations for the physical appearance of kimberlite xenoliths.

For xenoliths which show evidence of very slow motion, at great depth, one can postulate that the motion of the crack in the diamond-stable field was slow and obeyed the laws of stress corrosion crack propagation where crack velocity depends upon temperature and environment. One can thus explain the sheared nodules with the fine textures which originate at great depths. In this case there is similarity between the crack model and the diapir model.

In the graphite-stable field the crack must move very fast, if diamonds are to be preserved at the surface. In this case one can postulate the classical mechanical crack whose velocity is substantially independent of temperature and environment.

According to fracture mechanics, an abundant supply of low-viscosity fluids (gases) is required to keep the fracture propagating at a rapid rate and is also required to quench the xenoliths containing diamonds at the surface. The volume of this gas is very large and must be derived from upper mantle and lower crustal rocks.

According to the fracture mechanics model, the crack propagating up through the graphite-stable region truly looks like a crack, and not a pipe. Once the crack has breached the surface, fluidization takes place and the roughly circular vent typical of diatremes is formed. Local structural features such as foliation and basement faults have little control over the form and shape of the diatreme, due to the great kinetic energy of the crack and material in the crack at the time of breaching. Fluidization creates a rapidly circulating cell which entraps a large quantity of basement and mantle fragments deep in the pipe and causes a ball-milling action on those xenoliths which escape. Fluidization makes the cracks roughly circular to great depths, but the pipe path becomes irregular at lower depths following the old crack path.

Acknowledgments. The author is grateful to the National Science Foundation (grant number EAR 75-04869) for financial support of this work. This is publication number 1754 of the Institute of Geophysics and Planetary Physics, University of California at Los Angeles.

References

Anderson, E. M., The Dynamics of Faulting, 2nd edition, Edinburgh, Oliver and Boyd, 1951.

Anderson, O. L. and P. C. Grew, Stress corrosion theory of crack propagation with applications to geophysics, Reviews of Geophysics and Space Physics, 15, 77-104, 1977.

Andrews, J. R. and C. H. Emeleus, Structural aspects of kimberlite dyke and sheet intrusion in south-west England, Physics and Chemistry of the Earth, 9, edited by L. H. Ahrens et al., Pergamon Press, 43-50, 1975.

Berry, J. P., Some kinetic considerations of the Griffith criterion for fracture, 1, Equations of motion at constant force, J. Mechanics and Physics of Solids, 8, 194-206, 1960.

Boullier, A. M. and A. Nicolas, Classification of textures and fabrics of peridotite xenoliths from South African kimberlites, Physics and Chemistry of the Earth, 9, 467-475, edited by L. H. Ahrens et al., Pergamon Press, 1975.

Boyd, F. R. and P. H. Nixon, Structure of the upper mantle beneath Lesotho, Carnegie Institution Yearbook, 72, 431-445, 1973.

Boyd, F. R., private communication, 1978.

Bundy, F. P., H. P. Bovenkirk, H. M. Strong, and R. H. Wentorf, Diamond-bearing graphite equilibrium line from growth and crystallization of diamonds, J. Chemistry and Physics, 35, 383-391, 1961.

Clement, C. R., The emplacement of some diatreme-facies kimberlite, Physics and Chemistry of the Earth, 9, 51-59, edited by L. H. Ahrens et al., Pergamon Press, 1975.

Dawson, J. B., Basutoland kimberlites, Geological Society of America Bulletin, 73, 545-560, 1962.

Dawson, J. B., Advances in kimberlite geology, Earth Science Reviews, 7, 187-214, 1971.

Dawson, J. B., Kimberlites and their relation to the mantle, Philosophical Transactions of the Royal Society of London, A 271, 297-311, 1972.

Erdogan, F., Crack propagation theories, Fracture - An Advanced Treatise, edited by Liebowitz, 497-590, Academic Press, New York, 1968.

Evans, A. G., A method for evaluating the time-dependent failure characteristics of brittle materials and its application to polycrystalline alumina, Journal of Materials Science, 7, 1137-1146, 1972.

Evans, T., Diamonds, Contemporary Physics, 17, 45-70, 1976.

Green, H. W., II and Y. Gueguen, Origin of kimberlite pipes by diapiric upwelling in the upper mantle, Nature, 249, 617-620, 1974.

Griffith, A. A., The phenomenon of rupture and flow in solids, Philosophical Transactions of the Royal Society of London, A 221, 163-198, 1920.

Hawthorne, J. B., Model of a kimberlite pipe, Physics and Chemistry of the Earth, 9, 1-15, edited by L. H. Ahrens et al., Pergamon Press, 1975.

Jackson, E. D. and H. R. Shaw, Stress fields in central portions of the Pacific plate, delineated in time by linear volcanic chains, J. Geophys. Res., 80, 1861-1874, 1975.

Janse, A. J. A., Kimberlite and related rocks from the Nama province of south-west Africa, Physics and Chemistry of the Earth, 9, 81-94, edited by L. H. Ahrens et al., Pergamon Press, 1975.

Maaloe, S., Temperature and pressure relations of ascending primary magmas, J. Geophys. Res., 78, 6877-6886, 1973.

MacGregor, I. D., Petrologic and thermal structure of the upper mantle beneath South Africa in the Cretaceous, Physics and Chemistry of the Earth, 9, 455-475, edited by L. H. Ahrens et al., Pergamon Press, 1975.

McGetchin, T. R., The Moses Rock dike: Geology, petrology, and mode of emplacement of a kimberlite-bearing breccia dike, San Juan County, Utah, unpublished Ph.D. thesis, California Institute of Technology, Pasadena, California, 1968.

McGetchin, T. R., L. T. Silver and A. A. Chodase, Titanoclinohumite: A possible mineralogical site for water in the upper mantle, J. Geophys. Res., 75, 255-259, 1970.

McGetchin, T. R. and G. W. Ullrich, Xenoliths in Maars and diatremes with inferences for the moon, Mars and Venus, J. Geophys. Res., 78, 1833-1853, 1973.

Mercier, J.-C. C., Peridotite xenoliths and the dynamics of kimberlite intrusion, Proceedings of the Second International Kimberlite Conference, in press.

Mott, N. F., Fracture of metals: Some theoretical considerations, Engineering, 165, 16-18, 1948.

Roberts, D. K. and Wells, H. C., The velocity of brittle fracture, Engineering, 178, 820-821, 1954.

Roberts, J. L., The intrusion of magma into brittle rocks, Mechanism of Igneous Intrusion, 237-288, edited by G. Newall and N. Rost, Liverpool Press, 1970.

Shoemaker, E. M., Occurrence of uranium in diatremes on the Navajo and Hopi Reservations, Arizona, New Mexico, and Utah, U.S. Geological Survey Professional Paper 300, 179-185, 1955.

Shoemaker, E. M., and Moore, H. J., Diatremes on the Navajo and Hopi Reservations, U.S. Geological Survey Trace Elements Investigative Report 640, 197-203, 1956.

Speidel, M. D., Current understanding of stress corrosion crack growth in aluminum alloys, in The Theory of Stress Corrosion Cracking in Alloys, 345-353, edited by J. C. Scully, the North Atlantic Treaty Organization, Brussels, 1971.

Wagner, P. A., The Diamond Fields of South Africa, Transvaal Leader, 1914.

Weertman, J., Velocity at which liquid-filled cracks move in the earth's crust or in glaciers, J. Geophys. Res., 76, 8544-8553, 1971.

Wiederhorn, S. M., Influence of water vapor on crack propogation in soda-lime glass, J. Am. Ceram. Soc., 50, 407-414, 1967.

Williams, A. F., The Genesis of the Diamond, 2 volumes, Ernest Benn, Ltd., London, p.636, 1932.

Woolsey, T. S., M. E. McCallum, and S. A. Schumm, Modeling of diatreme emplacement by fluidization, Physics and Chemistry of the Earth, 9, 29-42, edited by L. H. Ahrens et al., Pergamon Press, 1975.

Wyllie, P., Kimberlite magmas from the system peridotite-H_2O-CO_2, Extended Abstracts, Second International Kimberlite Conference, Santa Fe, New Mexico, 1977.

PHREATOMAGMATIC ORIGIN OF THE OLIVINE MELILITITE DIATREMES OF THE SWABIAN ALB, GERMANY

Volker Lorenz

Institut für Geowissenschaften der J.Gutenberg-Universität, 6500 Mainz, FR Germany

Abstract. The olivine melilitite diatemes of the Swabian Alb, frequently compared with kimberlite diatremes, are discussed in terms of hydrogeological setting, internal structure and juvenile fraction.

The hydrogeological conditions of the Swabian Alb at the time of diatreme emplacement were characterized by copious amounts of groundwater within the sedimentary cover of the basement. Subsequently to the eruptions groundwater accumulated within the maars of the larger diatremes forming fresh-water lakes as also happened nearby in the Steinheim and Ries impact craters. The diatremes reveal subsidence structures composed of large wall-rock blocks, subaerially deposited pyroclastic beds, and well-bedded reworked pyroclastic debris which accumulated on the floor of the fresh-water crater lakes. The latter fact implies availability of groundwater at the time the diatremes formed.

The juvenile fraction is developed in the shape of spherical to ovoid nucleated autoliths of ash to lapilli size that are macroscopically nearly devoid of vesicles. The autoliths are interpreted as the product of water vapor explosions which took place when rising olivine melilitite magma contacted groundwater and was fragmented into magma droplets. The droplets were rapidly chilled and thus preserved their shape. Because of the hydrogeological data, the diatreme structure, and the chilled nature of the autoliths a phreatomagmatic origin of the Swabian diatremes is suggested.

Introduction

The olivine melilitite diatremes of the Swabian Alb (see Mäussnest 1974a, b for complete list of references) have been known since 1790. Because of the careful analyses of their interior structures by Cloos (1941) they are often referred to in diatreme studies. During the last 20 years new facts and models concerning diatremes and their respective surface structures, i.e. maars and tuff-rings, have been presented which have improved our knowledge about the basic processes within diatremes. One of the most important advances concerns the origin of the gas phase responsible for diatreme formation. When Cloos wrote his account it was a firm belief not requiring proof that the gases were derived from exsolution from the magma involved in diatreme formation. It is now assumed that many diatremes and maars, however, formed because rising magma contacted ground or surface water (e.g. Lorenz 1973, 1975). No paper on diatremes and maars has been published in recent years presenting data which are clearly in favour of a juvenile origin of the gas phase and thus a non-phreatomagmatic origin of the respective volcanic structure.

In 1975 I suggested that groundwater probably played an important role in the formation of the Swabian diatremes. It is the purpose of this paper to give a new interpretation of some field data and to present a revised model on the origin of the Swabian diatremes.

Geological and Hydrogeological Setting

350 diatremes (Mäussnest 1974 a, b) are distributed over an area of 1600 km^2 with the center near Urach. According to faunal evidence from fresh water lake deposits within some of the larger structures the diatremes are Upper Miocene (Tortonian/Sarmatian) in age (Seemann 1926). Some K/Ar ages, 16-11 m.y., obtained from olivine melilitite intrusive in some diatremes are in accord with the faunal data, some, however, give older ages, 20-30 m.y., because of potential excess argon (Lippolt et al. 1973).

At the present surface level the diatremes cut Jurassic lime-, marl-, silt-, clay-, and sandstones. Inclusions in the pyroclastic rocks suggest a downward extension as far as the boundary between the crystalline basement and its Permian/Mesozoic sedimentary cover. The Permian rocks that contain conglomerates with well-rounded pebbles derived from the basement (Bräuhäuser 1918, Carlé 1958) fill a late Hercynian intermontane trough. They are overlain by sand-, silt-, lime-, and marlstones of Triassic age followed by the Jurassic sediments (Wagner 1960). The thickness of the sedimentary cover was about 2 km when

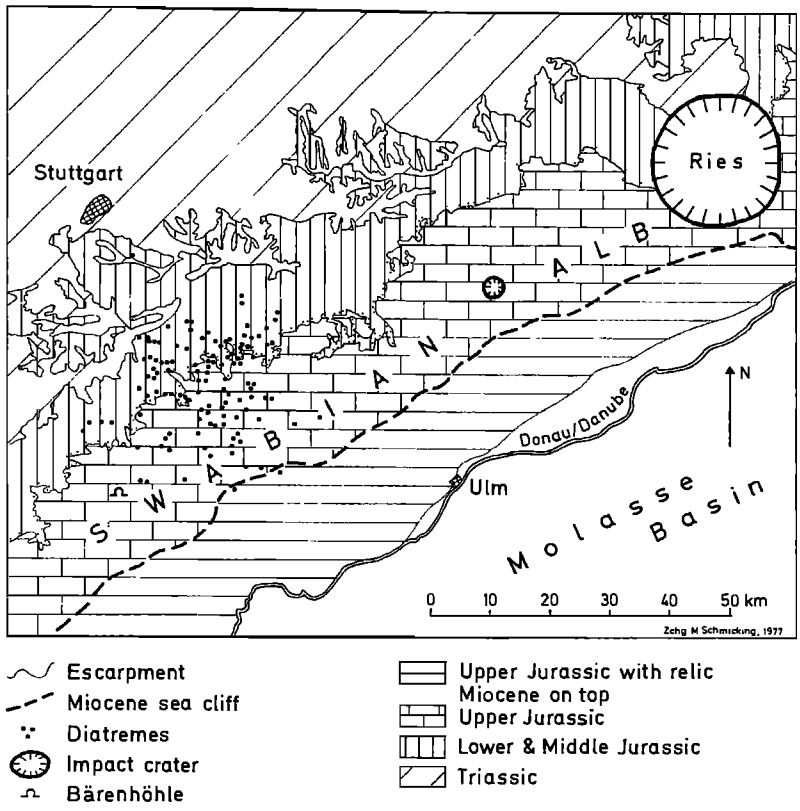

Fig. 1. Geological map of the Swabian Alb, the Swabian diatremes (not all shown), and the Steinheim and Ries impact craters.

the diatremes formed whereas now it is about 1.8 km at the escarpment (Carlé 1958).

During the Lower Tertiary the northern part of the present Swabian Alb was affected by karst activity (Dehm 1961) and it has continued up to the present time. During the Lower Miocene (Burdigalian/Helvetian) the southern half of the Swabian Alb was covered by the shallow sea of the Upper Marine Molasse. Along its northern shore the sea formed a steep cliff up to 70 m high (Eisenhut 1942). The region north of the cliff probably reached elevations of about 100 m above sea level and was dissected to some extent, the cliff presumably being cut by about 50 m deep valleys (Dongus 1972, 1973, 1977). During the Upper Miocene (Tortonian/Sarmatian) limnic and fluviatile sediments of the Upper Freshwater Molasse were deposited south of the cliff on top of the Upper Marine Molasse in part from the region to the north by river and stream transport. At the same time the diatremes were emplaced with the center of activity only 15 km northwest of the cliff. Two diatremes formed south of the cliff (Fig. 1). Fresh water lakes formed within the maars of the larger diatremes (Seemann 1926, Gwinner 1962), including the Jusi diatreme (Fig. 2), immediately after their emplacement.

The Steinheim and Ries impact craters located northeast of the diatreme area on the Swabian Alb formed slightly later (Lippolt et al. 1973). Deep fresh water lakes also formed within their craters.

When the sea covered the southern Swabian Alb it can be assumed that the regional groundwater table was slightly above sea level as the limestones of the 400 m thick Upper Jurassic sediments are well jointed and thus highly permeable. As karst processes had been active already in Lower Tertiary time a potential for accumulation and availability of copious amounts of groundwater is indicated. In deeper levels of the sedimentary cover additional aquifers can be assumed. In contrast the basement is rather dense and therefore assumed to be relatively dry.

In Upper Miocene time deposition of the Upper Freshwater Molasse on top of the Upper Marine Molasse indicates the existance of groundwater at even shallower depth under the northern Swabian Alb. It is therefore no wonder that fresh water lakes formed within the maars of the larger diatremes and the impact craters. The surface of these lakes formed part of the karst water table within the surrounding Upper Jurassic limestones (Dongus 1972, 1974).

In Pliocene time the Danube deposited gravels on the southern Swabian Alb (Dongus 1970) again

indicating a groundwater table within the neighboring limestones at shallow depth. In uppermost Pliocene to early Pleistocene time the early 'Bärenhöhle', a karst cave, formed southwest of the diatremes (Dongus 1973, Wagner 1976), pointing to a karst water table at the present level of 800 m above sea level, i.e. at shallow depth below the Pliocene landsurface.

On the Swabian Alb there are many dry valleys heading south towards the Danube. These valleys are believed to be largely of Pliocene age (Dongus 1973). As indicated above, however, valleys entering the sea of the Upper Marine Molasse must have already existed in Lower Miocene time and contributed debris to the Upper Freshwater Molasse in Upper Miocene time. As erosion leading to formation of valleys frequently follows structural weaknesses such as faults and joints, it can be assumed that a number of Lower Miocene valleys developed into the Upper Miocene and Pliocene valleys on the most prominent structural weaknesses.

It is therefore quite conceivable that copious amounts of groundwater existed in the sedimentary cover of the basement and that a karst water table was established within the Upper Jurassic limestones reaching the valley floors at depths of probably less than 100 m below the general landsurface at the time of diatreme emplacement.

The assumed availability of copious amounts of groundwater at the time the diatremes were emplaced also implies a high probability that groundwater poured into the newly formed fissures along which magma responsible for the diatreme formation rose. From the geological and hydrogeological setting (see also Villinger 1977) it seems to have been inevitable for the rising magma to contact groundwater during its rise towards the surface.

Strong uplift in Plio-/Pleistocene time produced the present elevations of the Swabian Alb (700-800 m in the diatreme area). Subsequent erosion north of the Alb formed the frontal escarpment. As a consequence valleys heading towards the Neckar to the Northwest were deeply incised into the Alb. With time this incision caused a southward retreat of the escarpment and the watershed between the tributaries of the Danube and the Neckar and a considerable lowering of the karst water table.

The Swabian Diatremes

As a result of the lowering of the surface of the Swabian Alb since Upper Miocene time no original structures such as complete maars, tuff-rings, cinder cones, or lava flows are preserved. On the Alb up to 200 m of Upper Jurassic sediments have been eroded exposing structural levels within the diatremes from near the original land surface. Fresh-water lake deposits from the floors of the original craters of some twenty diatremes on the Alb and along its escarpment, however, point to maars as the original surface expression of the diatremes. North of the escarpment erosion has removed up to 800 m of Jurassic

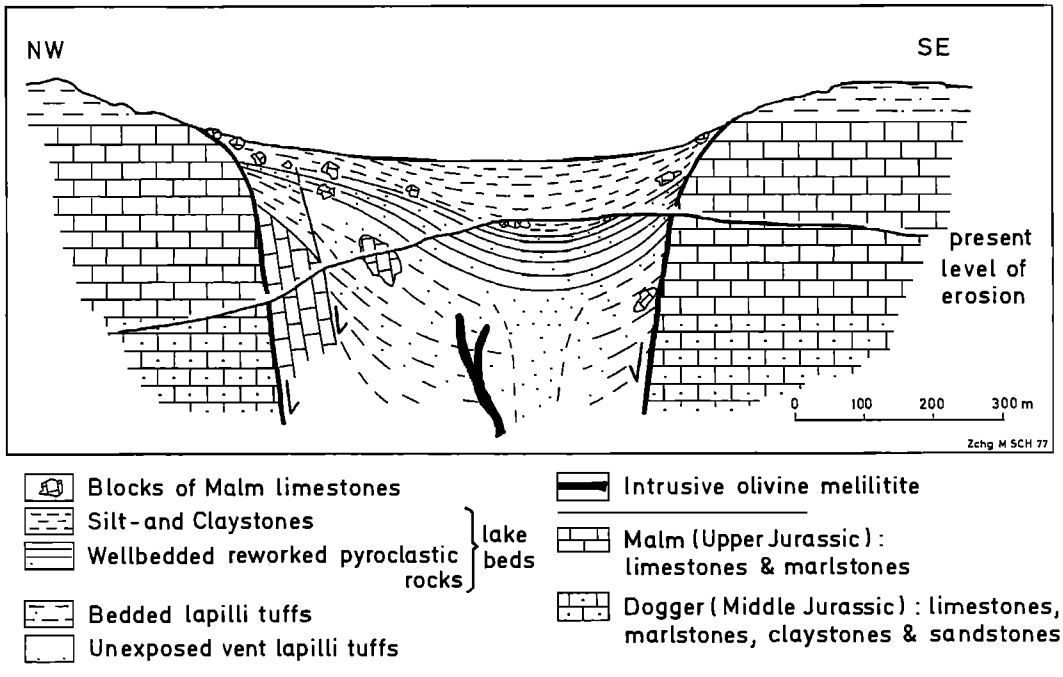

Fig. 2. Schematic cross-section of the main part of the Jusi diatreme, Swabian Alb, northwestern extension omitted.

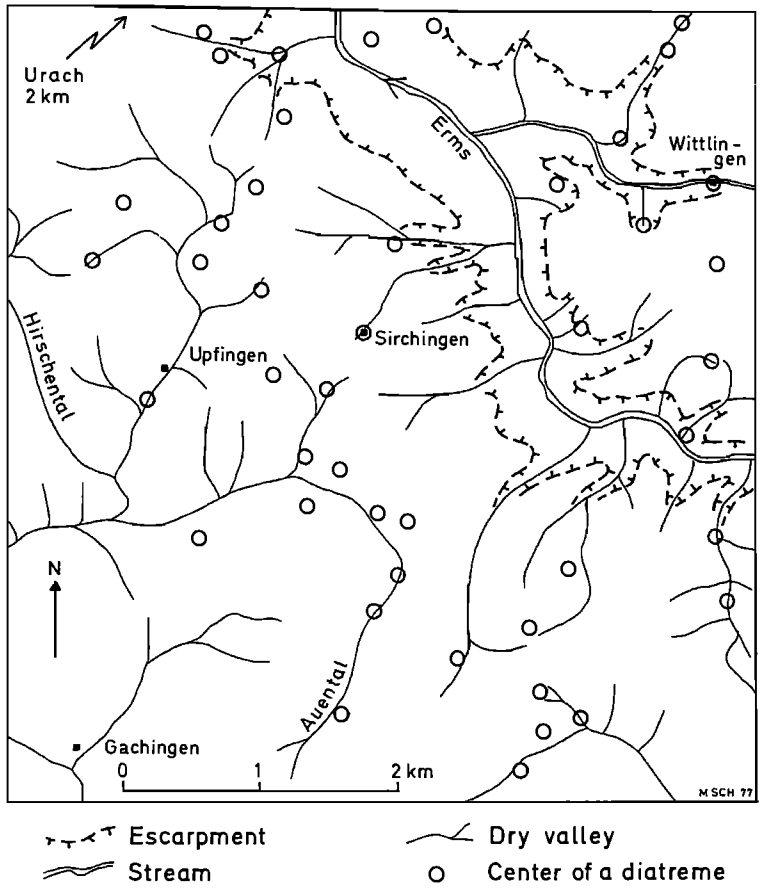

Fig. 3. Map showing part of the diatreme area with relationship between diatremes and valleys on the Swabian Alb south of Urach.

sediments exposing the northern diatremes at rather deep levels. This allows an analyses of the upper 1000 m of the diatreme structure by integration of data from diatremes cut at different erosional levels.

Cloos (1941) has described some diatremes, escecially the Jusi, in such great detail that only some principles will be repeated and new data and interpretations added.

The diatremes range from several tens of meters to about 1.2 km in diameter. They contain pyroclastic rocks, mostly lapilli tuffs, and large blocks of country rocks. In about 20 diatremes olivine melilitite magma intruded at a late stage forming short dikes or small irregular bodies. In addition a number of tuff dikes and one olivine melilitite dike are known from outside the diatremes.

Bedding in Diatreme Rocks

In many diatremes the pyroclastic rocks display bedding that dips at high angles, up to 80°, towards the center as is typical of subsidence structures in diatremes (Lorenz 1973, 1975).Cloos (1941) described several types of bedding, the two most important ones being bedding with well-developed bedding planes and bedding without well-developed bedding planes. The first type is only found in the uppermost parts of some diatremes and was considered by Cloos to be the result of sedimentation under the influence of water, i.e. the rocks represent reworked pyroclastic debris. The bedding of the second type that is developed further down in the diatremes was believed by Cloos to indicate 'less influence of water action' on the deposition of the respective pyroclastic rocks. It is not very clear what Cloos meant by this as he also mentioned fall-back into the open pipe to explain this type of bedding.

As can be observed best at the Jusi, there are additional distinct differences between the two types of bedded rocks. The first type, near the top of the Jusi, is characterized by a higher degree of sorting and of similarity between individual beds. The second type contains levels with more pronounced grainsize differences (both juvenile and wall-rock fragments) or with pronounced concentrations of wall-rock fragments

from specific stratigraphic levels (Upper and Lower Jurassic, Triassic, and Permian). This second type, when compared with bedded rocks from other diatremes and maars, appears to represent the originally bedded primary pyroclastic rocks ejected from the diatremes and deposited at the original surface.

The outcrops in the primary pyroclastic rocks are of limited quality and extent. They rarely show cross-bedding and channels that are typical evidence of pyroclastic surge activity. On the other hand the lack of impact craters under blocks embedded in these lapilli tuffs implies a non-ballistic transport along the ground which implies emplacement by pyroclastic surges.

The steep dip of the primary pyroclastic beds, up to 80°, towards the center of the diatremes and their occurrence down to 440 m below the original surface indicates subsidence of the subaerially deposited beds during and after the volcanic activity (Cloos 1941, Lorenz 1973, 1975). At the Jusi at least 150 m of primary pyroclastic beds subsided differentially for about 150 to 300 m. In all cases the well-bedded rocks overlie the less well-bedded ones. At the Jusi the well-bedded rocks are approximately 40 m thick. They show local interbedding with the overlying silt- and claystones deposited within a former maar freshwater lake. At the Randecker Maar similar well-bedded pyroclastic rocks contain fresh-water fossils (Seemann 1926) and are overlain by fossiliferous papershales and limestones. There is thus clear evidence that the well-bedded rocks represent reworked pyroclastic debris and are of epiclastic origin deposited under the influence of water on the floors of the respective maar fresh-water lakes.

The centroclinal dips of 20 to 40° of the sediments and the well-bedded reworked pyroclastic debris as well as synsedimentary slump structures in the sediments of the Randecker Maar suggest that subsidence of the diatreme fill continued for a prolonged period of time after the eruptions had ended. This post-eruptive subsidence is assumed to have resulted from compaction of the previously unconsolidated fill (Lorenz 1973, 1975).

Blocks of Country-Rocks

Large accidental clasts derived from the wall-rocks are very conspicious in the Swabian diatremes. Because they comprise samples from the Permian/Mesozoic rock sequence, the diatremes can only extend downwards to about the boundary between the basement and its sedimentary cover. This implies rise of the magma through the basement along dikes with the disintegration of the magma into ash particles and lapilli taking place at the base of the sedimentary cover.

Along the margin of some diatremes there are very large blocks of Upper Jurassic lime- and marlstones derived from stratigraphic levels higher than that of the immediate wall (e.g. Jusi, Aichelberg). The largest block of this type occurs at the Jusi and measures about 300 m in diameter.

Cloos considered the process of fluidization as being capable of loosening blocks of this enormous size and of nearly suspending them in the rising gas-particle system. This mechanism has already been contested (Lorenz 1971a, 1975). If such large blocks would subside slowly in a fluidized system then slightly smaller blocks from a deeper level should be able to rise or to be suspended (Lorenz 1971b), but no blocks of the required size and stratigraphic level have been found. The largest blocks from deeper stratigraphic levels reach about one meter and are very rare. This implies that fluidization cannot account for the emplacement of the very large blocks. Lorenz (1971a, 1973, 1975) suggested that differential caldera-like subsidence of wall-rocks and overlying subaerially deposited bedded lapilli-tuffs as a result of enlargement of the initial feeder channel may be the cause for the emplacement of such large blocks of wall-rocks below the stratigraphic level from which they are derived.

Upper Jurassic limestone blocks are also found in the bedded pyroclastic rocks and the overlying sediments. In the siltstones on top of the Jusi the blocks measure several meters in diameter (Fig. 2). Such large blocks exist also in great numbers in the sediments of the Randecker Maar and are assumed to have been emplaced by caving of wall-rocks of the maar (Cloos 1941). They imply unstable crater walls of the respective maars. Because these blocks are much more abundant in the sediments of the Jusi and Randecker Maar than in the underlying primary and reworked pyroclastic beds, the limestones of the crater wall must have been freed from their pyroclastic cover by erosion during deposition of the reworked debris. Continued subsidence of the diatreme content owing to compaction may have contributed to some extent in exposing the upper wall-rocks. The following stages in the development of the diatremes can thus be envisaged:

1. Eruptive stage - Deposition of pyroclastic rocks at the surface, formation of maars due to subsidence of surficial deposits and underlying wall-rocks of the feeder channel during the eruptive processes. Some caving of maar wall-rocks.
2. Post-eruptive stage - Erosion of the bedded pyroclastic debris from the crater rim and walls, deposition of the eroded material on the floors of the fresh-water lakes formed within the larger maars. The maar walls become free from their pyroclastic cover allowing some caving of the Upper Jurassic wall-rocks. Subsidence of the diatreme interior continues due to compaction.
3. Lacustrine stage - Deposition of clay, silt, and limestone within the fresh-water lakes occupying the deeper maars. Caving and slumping of Upper Jurassic limestones from the maar walls (extensive at the Jusi and 'Randecker Maar').

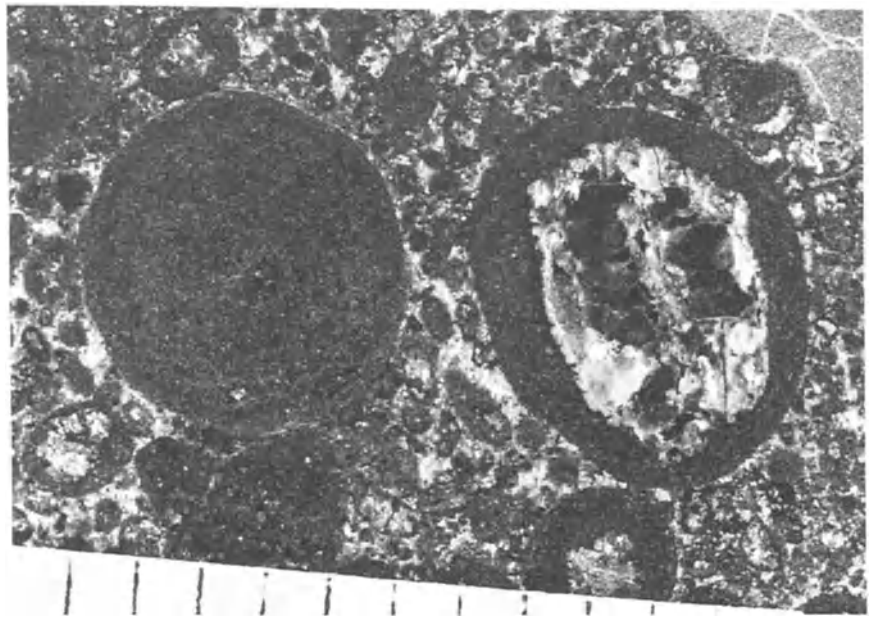

Fig. 4. Olivine melilitite autoliths from Calverbühl diatreme near Urach; left autolith shows concentric layering, right one contains a core of olivine, scale in mm.

Subsidence of the diatreme interior ceases.

In terms of internal structure of the diatremes and bedding of inclosed rocks there are no fundamental differences with those maar-diatreme volcanoes for which a phreatomagmatic origin has been assumed (Lorenz 1973, 1975).

Subsidence of the reworked pyroclastic debris and overlying sediments deposited in fresh-water lakes within the maars and the existance of large slumped blocks within these deposits point out that the lakes formed within a very short period of time after the eruptions had ended. The rapid accumulation of water in the maars also suggests the availability of copious amounts of groundwater within the karstic Upper Jurassic limestones during the time the diatremes erupted.

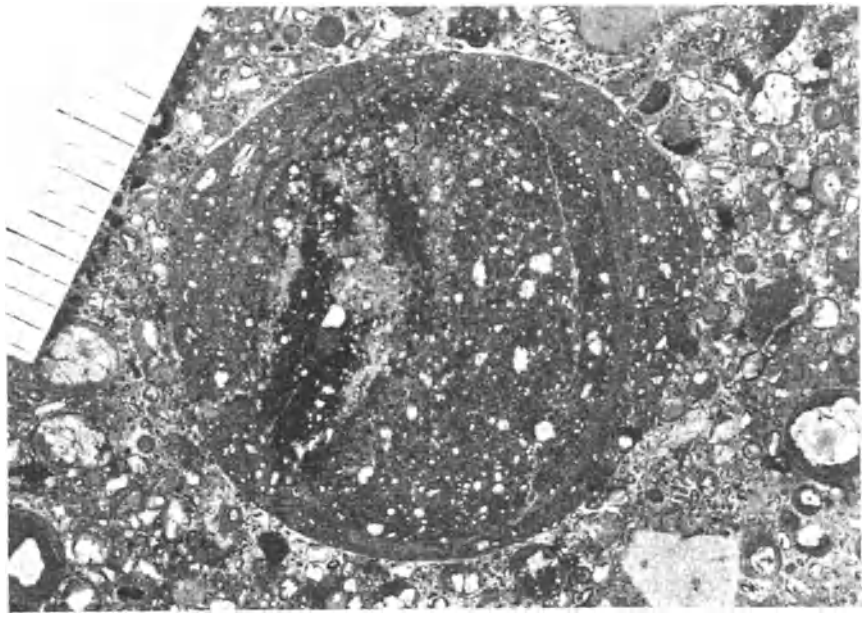

Fig. 5. Olivine melilitite autolith from Calverbühl diatreme near Urach showing concentric layering, scale in mm.

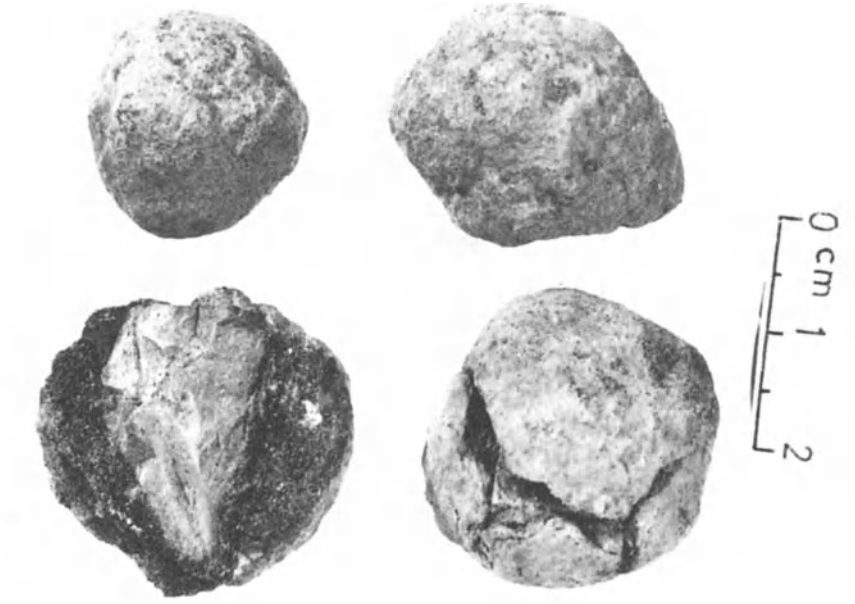

Fig. 6. Autoliths from phreatomagmatic Pulvermaar, West Eifel; a xenolith forms the core of one autolith.

A high proportion of diatremes on the Swabian Alb is located at or very close to the bottom of dry valleys (Fig. 3). The relationship between maars and valleys has been discussed already for the Eifel/Germany and Massif Central/France (Lorenz 1973). On the Alb a number of dry valleys which now preserve the Plio-/Pleistocene stage of erosional development probably existed in a less deeply dissected stage already during Upper Miocene time. These valleys may have formed along zones of structural weakness as discussed above. Some of these structurally weak zones were used by the magma on its way towards the surface. When these zones of weakness opened into fissures to allow rise of the magma they could collect groundwater from the neighboring sediments rather easily.

The Juvenile Fraction of the Pyroclastic Rocks

The juvenile ash grains and lapilli form a large proportion of the pyroclastic rocks. They are typically developed in spheres or ellipsoids with a smooth surface. These round or avoid particles consist of olivine melilitite (Brey 1978, Sick 1970) and many contain a nucleus of either an olivine phenocryst, a piece of slightly more crystallized olivine melilitite or a xenolith (Fig. 4-5). They were believed to represent solidified lava droplets (Cloos 1941, v. Engelhardt & Weiskirchner 1961, Weiskirchner 1967) and qualify for the term autolith (Danchin et al. 1975, Ferguson et al. 1973). The diameter of the nucleated autoliths varies between 0.2 mm and several centimeters. The small ones may only have a thin film of melilitite around a phenocryst. The larger ones may show 1) concentric layering with elongate mineral grains mostly oriented tangentially to the surface, 2) variable states of crystallization of the melt prior to nucleation of the individual autoliths and autolith layers, and 3) a small or large core or no distinct core at all. The xenoliths as cores consist of chips of basement rocks (from Permian clastic rocks?) or Mesozoic marl- or limestones. Obviously the autoliths with a xenolith core imply nucleation of the respective autoliths within or above the diatreme root.

Another important feature of the autoliths is their poor vesicularity. Those vesicles which exist are very small. Therefore, the autoliths did not vesiculate to any appreciable extent once they formed. The few bombs and juvenile blocks are also very poor in vesicle content.

The concentric layering (Fig. 4-5) can be assumed to have formed by successive liquid accretion around a core. The concentrically layered lapilli, therefore, represent the liquid equivalent of accretionary lapilli composed of ash grains (Moore & Peck 1962, Lorenz 1978). The concentric layering and tangential orientation of some microphenocrysts also indicate that surface tension acted on discrete amounts of magma forcing them into droplets. Contact of several droplets prior to solidification apparently caused accretion and thus concentric layering. The fine grain size of the autoliths, the scarcity of indented autoliths due to mutual impact, or rarity of two autoliths welded together suggest extremely rapid solidification of the droplets. Prior to solidification of the droplets the magma must have disintegrated into discrete droplets which were sprayed into a cool void otherwise the effects of surface tension and rapid chilling would not have been preserved in the melt particles.

It has been assumed (Cloos 1941, v. Engelhardt & Weiskirchner 1961, Lorenz et al. 1970) that these droplets imply explosive fragmentation of the magma by rapid exsolution of large amounts of gases. This view is contested now because of several reasons: a) The scarcity of vesicles in the autoliths, bombs, and juvenile blocks implies that the gas phase of the magma had either already exsolved to a high degree while the magma was still fluid or the gasphase had not yet exsolved very much. In both cases no endogenous gases could have disrupted the fluid magma explosively. b) Autoliths have been found at the phreatomagmatic Pulvermaar/West Eifel/Germany (Fig. 6) (Lorenz 1975) and are known in large concentrations from phreatomagmatic phases of cinderconces in the Eifel (Schmincke 1977, Lorenz, unpubl. data). Schmincke demonstrated that the autoliths in the Eifel and elsewhere are products of eruptions transitional between purely magmatic and phreatomagmatic and pointed out that kimberlite autoliths probably formed in a similar fashion. There also seems to exist a close relationship with cauliflower bombs (Lorenz 1973, 1974, 1978) which are also typical of many phreatomagmatic eruptions and form when relatively little external water participates in the eruptions. c) Spherical particals also formed in some water vapor explosion experiments (Fröhlich, pers. communication 1977) when liquid copper was superimposed on water. Breakdown of the vapor film which immediately forms upon contact leads to intimate contact between the cold water and hot liquid metal. The water then flashes into steam and the liquid metal is disrupted explosively and expelled in droplets. The rather high pressures produced in such 'fuel-coolant interactions' are a function of the contact surface between the hot liquid and enclosed water (see also Colgate & Sigurgeirsson 1973, Peckover et al. 1973, Fröhlich 1977).

The large quantities of autoliths in the Swabian diatremes and the favorable hydrogeological setting of the volcanic field suggest that the Swabian autoliths were not the product of transitional but rather of 'normal' phreatomagmatic eruptions. To date nucleated autoliths have only been described from alkali-basaltic and kimberlite magmas (references see above), i.e. from magmas low in silica content. The Swabian olivine melilitites are the most silica-undersaturated rocks of Central Europe (Wimmenauer 1972) and contain only 36% SiO_2 (Brey 1978, Sick 1970). Tholeiitic magmas apparently do not produce autoliths but rather generate angular ash grains and lapilli when involved in phreatomagmatic eruptions. The lower SiO_2 content and thus lower viscosity of the autolith producing magmas in contrast may enable the surface tension to dominate when the magma disintegrates upon contact with water. If the magma has not vesiculated up to the moment of contact, after the explosion rapid chilling should inhibit vesiculation. Nevertheless some juvenile gas may have been released from that part of the melt which disintegrated into dust and may then have participated in the eruption.

The Olivine Melilitite Dikes

Late intrusive olivine melilitite dikes, small irregular intrusives within the diatremes, and one dike outside give additional information. The Jusi, Sternberg, and Eisenrüttel diatremes expose structural levels only a few tens of meters below the original floor of the respective craters. It is quite possible that the Magma reached the surface within the last two diatremes mentioned and formed cindercones on the floors of the maars as is also feasible for the intrusives of other diatremes now exposed only at deeper levels.

In contrast to the central part the chilled margins of most of the intrusives do not contain many vesicles which implies that the previously dissolved gas phase had neither exsolved very much at shallow depth nor very rapidly. This applies also to the Grabenstetten dike which is unrelated to any diatreme near-by and exposed very close to the original surface. Under the assumed hydrogeological conditions it seems reasonable that only in very rare circumstances could the magma rise towards the surface without coming into contact with water to from normal dikes within the country-rocks.
the formation of the diatremes.The internal structure of the diatremes is similar to that of other diatremes for which a phreatomagmatic origin has already been suggested (e.g. Lorenz 1973, 1975). Formation of the fresh-water lakes within the deeper craters immediately after the diatreme emplacement indicates the availability of copious amounts of groundwater in the karstic Upper Jurassic limestones at the time of the eruptive activity.

The juvenile fraction is typically in the form of autoliths that are poor in vesicle content. In contrast to earlier assumptions these autoliths are now believed to have formed when olivine melilitite magma contacted groundwater within the sedimentary cover of the basement. As a result of this analysis the author favors a phreatomagmatic origin of the Swabian diatremes.

Many of the characteristics of the Swabian diatremes are found also in kimberlite diatremes which would support the assumption of a phreatomagmatic origin of the kimberlite diatremes (Lorenz 1973, 1975). The diatremes of the Hegau area southwest of the Swabian field were also emplaced under favorable hydrogeological conditions and some are also characterized by autoliths (Weiskirchner 1967). It is suggested that these diatremes also formed by phreatomagmatic eruptions.

Acknowledgements. The author enjoyed with pleasure a very informative discussion with G. Fröhlich on the subject of water-vapor explosions. G. Abele, D.S. Barker, G. Brey, H.-U.

Schmincke, M.F. Sheridan, and D. Smith kindly reviewed the manuscript.

References

Bräuhäuser, M., Die Herkunft der kristallinen Grundgebirgsgerölle in den Basalttuffen der Schwäbischen Alb, J.Verh.vaterl.Naturkde. Württemberg, 74, 212-274, 1918.

Brey, G., Origine of olivine melilitites - chemical and experimental constraints, J.Volcanology and Geoth.Res., 3, 61-88, 1978.

Carlé, W., Kohlensäure, Erdwärme und Herdlage im Uracher Vulkangebiet und seiner weiteren Umgebung, Z.deutsch.geol.Ges., 110, 71-101, 1958.

Cloos, H., Bau und Tätigkeit von Tuffschloten; Untersuchungen an dem Schwäbischen Vulkan, Geol.Rundschau, 32, 709-800, 1941.

Colgate, S.A. and Sigurgeirsson, T., Dynamic mixing of water and lava, Nature, 244, 552-555, 1973.

Danchin, R.V., Ferguson, J., McIver, J.R., and Nixon, P.H., The composition of late stage kimberlite liquids as revealed by nucleated autoliths, Physics and Chemistry of the Earth, 9, 235-245, 1975.

Dehm, R., Über neue tertiäre Spaltenfüllungen des süddeutschen Jura- und Muschelkalkgebietes, Mitt.Bayer.Staatslg.Pal.hist.Geol., 1, 27-56, 1961.

Dongus, H., Über die Schotter des jungtertiären Albdonausystems und einige geomorphologische Konsequenzen aus ihrer Lage, ihrer Korngröße und ihrer Zusammensetzung, Ber.z.deutsch. Landeskde., 44, 245-266, 1970.

Dongus, H., Einige Bemerkungen zur Frage der obermiozän-unterpliozänen Reliefplombierung im Vorland der Schwäbischen Alb und des Rieses, Ber.z.deutsch.Landeskde., 46, 1-28, 1972.

Dongus, H., Schichtflächenalb, Kuppenalb, Flächenalb (Schwäbische Alb), Z.Geomorph.N.F., 16, 374-392, 1972.

Dongus, H., Die Oberflächenformen der westlichen Mittleren Alb, Abh.Karst- und Höhlenkde., A8, 1-54, 1973.

Dongus, H., Die Oberflächenformen der Schwäbischen Ostalb, Abh.Karst- und Höhlenkde., A11, 1-114, 1974.

Dongus, H., Die Oberflächenformen der Schwäbischen Alb und ihres Vorlandes, Marburger Geographische Schriften, H.72, 1-486, 1977.

Eisenhut, E., Geologische Untersuchungen im Bereich des burdigalen Kliffs zwischen Harthausen und Ingstetten (Schwäbische Alb), N.Jb.Min.Geol.Paläont.Beil.-Bd. (Abh.), Abt.B, 8, 397-458, 1942.

v. Engelhardt, W. and Weiskirchner, W., Einführung zu den Exkursionen der Deutschen Mineralogischen Gesellschaft zu den Vulkanschloten der Schwäbischen Alb und in den Hegau während der 39. Jahrestagung in Tübingen vom 11.-17. Sept. 1961, 1961.

Ferguson, J., Danchin, R.V., and Nixon, P.H., Petrochemistry of kimberlite autoliths. 285-293, in Nixon, P.H. (Ed.): Lesotho kimberlites. 350 p., Lesotho National Development Corporation, (Cape & Transvaal Printers Ltd.), Cape Town, 1973.

Fröhlich, G., Triggerung von Wasserdampfexplosionen, Vortragsreferate, K 9, Frühjahrstagung Essen 1977, Deutsch.Phys.Ges., 1977.

Fröhlich, G., Maximaldruckabschätzungen bei Wasserdampfexplosionen, Vortragsreferate, K 10, Frühjahrstagung Essen, Deutsch.Phys. Ges., 1977.

Gwinner, M.P., Obermiocäner Vulkanismus, In: Samml.Geol.Führer, 40, 159-171, (Bornträger) Berlin, 1962.

Lippolt, H.J., Todt, W. and Baranyi, I., K-Ar ages of basaltic rocks from the Urach volcanic district, SW-Germany, Fortschr.Miner., 50, Beiheft 3, 101-102, 1973.

Lorenz, V., Collapse structures in the Permian of the Saar-Nahe-area, southwest Germany, Geol. Rundschau, 60, 924-948, 1971a.

Lorenz, V., An investigation of volcanic depressions. Part IV. Origin of Hole-in-the-Ground, a maar in Central Oregon. (Geological, geophysical, and energy investigations), NASA progr.rep. (NGR-38-003-012), 113 p., 1971b. Houston, Tex., (Clearinghouse for Federal Scientific and Technical Information, Springfield, Va.: NASA CR-115237.

Lorenz, V., On the formation of maars, Bull. volcanologique, 37, 183-204, 1973.

Lorenz, V., Studies of the Surtsey tephra deposits, Surtsey Res.Progr.Rep., 7, 72-79, 1974.

Lorenz, V., Formation of phreatomagmatic maar-diatreme volcanoes and its relevance to kimberlite diatremes, Physics and Chemistry of the Earth, 9, 17-27, 1975.

Lorenz, V., Accretionary lapilli, In: Green, J. (Ed.), Volcanoes and Volcanology. Ser.of Earth Sciences, 16, in prep., 1978.

Lorenz, V., McBirney, A.R., and Williams, H., An investigation of volcanic depressions. Part III. Maars, tuff-rings, tuff-cones, and diatremes. NASA progr.rep. (NGR-38-003-012), 198 p., Houston, Tex., (Clearinghouse for Federal Scientific and Technical information, Springfield, Va.: NASA CR-115236), 1970.

Lorenz, V., Cauliflower bombs. In: Green, J.,(Ed): Volcanoes and volcanology. Ser.of Earth Sciences, 16, in prep., 1978.

Mäussnest, O., Die Eruptionspunkte des Schwäbischen Vulkans. Teil 1, Z.deutsch.geol.Ges., 125, 23-54, 1974a.

Mäussnest, O., Die Eruptionspunkte des Schwäbischen Vulkans. Teil 2, Z.deutsch.geol.Ges., 125, 277-352, 1974b.

Moore, J.G. and Peck, D.L., Accretionary lapilli in volcanic rocks of the western continental United States, J.Geol., 70, 182-193, 1962.

Peckover, R.S., Buchanan, D.J. and Ashby, D.E.T.F., Fuel-coolant-interaction in submarine volcanism, Nature, 245, 307-308, 1973.

Schmincke, H.-U., Phreatomagmatische Phasen in

quartären Vulkanen der Osteifel, Geol. Jahrbuch, A39, 3-45, 1977.

Seemann, R., Geologische Untersuchungen in einigen Maaren der Albhochfläche, Jh.vaterl. Naturkde.Württemberg, 82, 81-110, 1926.

Sick, U., Über Melilith-Nephelinite der Schwäbischen Alb. 94 p., Dr.rer.nat.thesis, Univ. Tübingen, 1970.

Villinger, E., Über Potentialverteilung und Strömungssysteme im Karstwasser der Schwäbischen Alb (Obere Jura, SW-Deutschland), Geol. Jahrbuch, C18, 1977.

Wagner, G., Einführung in die Erd- und Landschaftsgeschichte. 3. Aufl., 694 p., (Hohenloh'sche Buchhandlung F. Rau) Öhringen, 1960.

Wagner, G., Der Werdegang der Bärenhöhle. 36-42, in:Wagner, G. (Ed.) Die Bärenhöhle bei Erpfingen. 7. Aufl., Sonnenbühl.

Weiskirchner, W., Über die Deckentuffe des Hegaus, Geologie,16, Beiheft 58, 1-90, 1967.

Wimmenauer, W., Gesteinsassoziationen des jungen Magmatismus in Mitteleuropa, Tschermaks Min. Petr.Mitt., 18, 56-63, 1972.

FIELD GEOLOGY, CHEMISTRY, AND PETROLOGY OF BUELL PARK MINETTE DIATREME, APACHE COUNTY, ARIZONA

Michael F. Roden[1] and Douglas Smith

Department of Geological Sciences, University of Texas, Austin, Texas 78712

Abstract. Field relations and rock and mineral chemistry were investigated to understand the volcanology of the minette diatreme, the relationship between minette and kimberlitic tuff, and the genesis of minette varieties at Buell Park, Arizona. Previously, kimberlitic tuff and minette were known to occur together only at Outlet Neck and Buell Park within the Navajo volcanic field, but two new occurrences have been found: The Beast, a minette neck 5 km east of Buell Park, contains a block of kimberlitic tuff, and a small unnamed kimberlitic tuff pipe 8 km east of Buell Park is intruded by a minette dike. Furthermore, at Buell Park where a minette diatreme is nested within a kimberlitic tuff diatreme, evidence indicates an overlap in time of minette and kimberlitic tuff eruptions: the upper 75 m of the layered kimberlitic tuff section contains subrounded, altered minette clasts, and two small ultramafic breccia pipes containing clasts of minette occur along the margins of two late minette intrusions. The bulk of the kimberlitic tuff, however, was erupted before the minette. The minette diatreme, composed of tuff-breccias intruded and capped by massive minette, is now exposed about 200 m below the original maar crater floor.

A mafic olivine- and analcime-bearing minette ring dike forms an arc of 115° around Buell Mountain, which includes the minette diatreme and associated quartz-bearing, felsic minettes. The association suggests that these two rock types were related by fractional crystallization. However, fractional crystallization models require separation of an amount of phlogopite that is inconsistent with its modal proportion and expected settling velocity. The models also require magnetite to separate, but magnetite is restricted to the groundmass of the minettes. More likely, the minette varieties were produced by partial melting of phlogopite-bearing garnet peridotite or crystal fractionation in the mantle.

Diopside phenocrysts in minette throughout the Navajo field contain sparse, distinctive green cores relatively rich in FeO, Al_2O_3, and Na_2O. These cores are most likely xenocrysts mantled by diopside.

Introduction

The Navajo volcanic field [Gregory, 1917; Williams, 1936; Schmitt et al., 1974], a group of minette intrusions and diatremes, and rarer kimberlitic tuff pipes and dikes, lies in an arc along the Arizona-New Mexico and Arizona-Utah borders (Figure 1). The kimberlitic tuff pipes occur in two groups, a northern cluster along the eastern side of the Monument Uplift and a southern group within the Zildlitloi volcanic field (Figure 1), a subdivision of the Navajo volcanic field [Williams, 1936] which consists of an east trending group of minette and kimberlitic tuff diatremes which crosses from Arizona to New Mexico near the town of Navajo, New Mexico. Only in the Zildlitloi field do minette and kimberlitic tuff occur together and at Buell Park (Figure 2) a minette diatreme is preserved within a larger kimberlitic tuff diatreme, 4.5 km in diameter. Within Buell Park, massive, felsic minette caps a sequence of layered kimberlitic tuff on the northern part of Buell Mountain and a minette diatreme forms the southern third (also known as Starrett Mesa) of the mountain. One kilometer to the south, a mafic minette ring dike crops out in an arc of 115° around Buell Mountain (Figure 2). Besides Buell Park, minette and kimberlitic tuff were known to be associated only at Outlet Neck, a minette neck 3 km east of Buell Park. There, a block, 20 m across, of kimberlitic tuff is included in the minette [Allen and Balk, 1954].

Published K-Ar and fission track ages on minette and kimberlitic tuff indicate that these two rock types are of the same age, about 30 million years old [Armstrong, 1969; Naeser, 1971]. New K-Ar dates obtained on phlogopite separates from minettes of the Zildlitloi field

[1]present address: Department of Earth and Planetary Sciences, Massachusetts Institute of Technology, Cambridge, Ma. 02139.

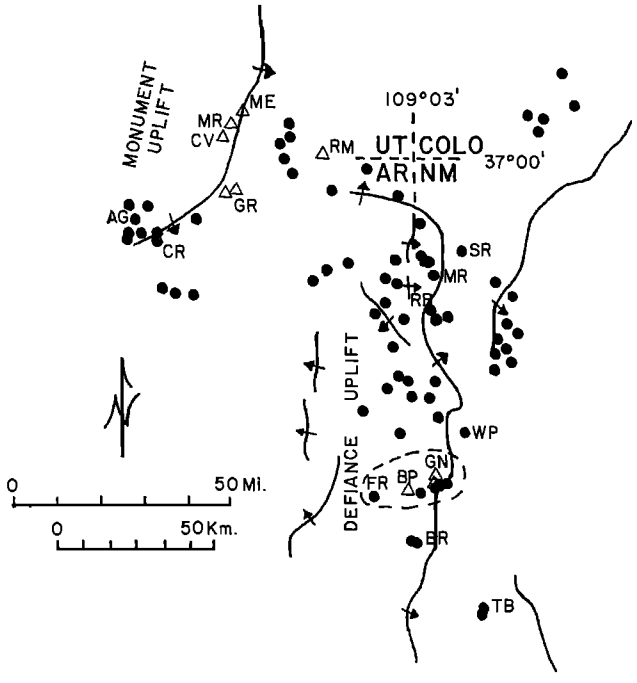

Fig. 1. Sketch map of the Navajo volcanic field. Filled circles are minette diatremes and triangles are kimberlitic tuff pipes. Area outlined by dashed line is the Zildlitloi volcanic field. Major monoclines are indicated by solid lines. Letters identify the following diatremes: ME, Mule Ear; MR, Moses Rock; CV, Cane Valley; GR, Garnet Ridge; RM, Red Mesa; GN, Green Knobs; BP, Buell Park; AG, Agathla; CR, Church Rock; SR, Shiprock; MR, Mitten Rock; RB, Roof Butte; WP, Washington Pass; FR, Fluted Rock; TB, Twin Buttes.

suggest that at least some of the southern diatremes are 5 million years younger than previously thought, and are about 25 million years old [McDowell et al., 1978, in preparation].

"Minette" is used here for the potassium-rich intrusive and extrusive rocks of the Navajo field. These rocks are linked by their potassic nature (3-7.5 weight percent K_2O, $K_2O/Na_2O>1$) and mineralogy. The minettes are pale grey to black, and lamprophyric in texture. Phenocrysts of diopside (to 5 mm long) and phlogopite (to 3 mm in diameter), with or without olivine (to 2 mm long) are embedded in a matrix, commonly trachytic, of sanidine + diopside + oxides + apatite $\pm$ phlogopite $\pm$ quartz $\pm$ amphibole $\pm$ glass. Diopside crystals are euhedral, and large crystals commonly have spongy cores. The mica is a pale brown phlogopite, usually with dark rims, less commonly with dark cores. Olivine is present in the more mafic minettes as phenocrysts and microphenocrysts, often accompanied by a feldspathoid in the groundmass. The feldspathoid, previously identified as leucite [Gregory, 1917] is actually analcime, at least at Buell Park (see section on mineralogy) where it occurs as brown equant grains and interstice fillings in the groundmass of the ring dike. Sanidine occurs sparsely as phenocrysts in the more felsic minettes, but it is generally restricted to the groundmass where it forms a major part of the matrix. Apatite, a ubiquitous accessory, occurs as stubby prisms with cloudy centers due to rod-shaped inclusions aligned parallel to the c-axis. Magnetite is invariably present; ilmenite is rare, but common in the ring dike minette at Buell Park. Both oxides are restricted to the groundmass. Quartz occurs sporadically as interstitial patches and stringers in the felsic minettes of Buell Mountain. Amphibole is very rare, and is known only as an accessory phase from scattered localities in the Navajo field [Williams, 1936; Roden, 1977].

The minettes of the Zildlitloi field display a compositional trend along the strike of the field: the minettes are increasingly mafic to the east. Mineralogically, this trend is best expressed by olivine which is generally absent from minettes west of Zildlitloi Mountain but present in all minettes to the east of Zildlitloi. There is also an increase in analcime(?) to the east. Buell Park occupies an anomalous position in this trend, in that the ring dike contains abundant olivine and analcime, and is similar in composition to the easternmost minettes.

The kimberlitic tuffs are olive green to red-brown microbreccias which at Buell Park underlie the park land and crop out on the lower slopes of Buell Mountain. The tuffs contain, in addition to abundant xenoliths, anhedral xenocrysts of olivine (Fo_{92}, Allen and Balk, 1954), enstatite, Cr-rich diopside, chlorite, and rarer garnet, titanoclinohumite, oxides, and apatite in a fine-grained fibrous matrix of serpentines, clays, chlorite, and talc [Schmitt et al., 1974]. These tuffs differ from typical kimberlites in lacking essential phlogopite, and other minerals rich in incompatible elements [Smith and Levy, 1976], however, "kimberlitic" is used here to describe these rocks in accordance with past usage [for example, Allen and Balk, 1954; Schmitt et al., 1974]. At Buell Park and Green Knobs some of the kimberlitic tuffs are layered, the layering being defined by: (1) lenses 5-10 cm thick of xenolith-rich tuff, (2) alternating light and dark bands of tuff, and (3) weathering. Further descriptions of the field geology and petrography of the kimberlitic tuffs and minettes of the Zildlitloi field have been published by Gregory [1917], Allen and Balk [1954], Schmitt et al. [1974], and Smith and Levy [1976].

The present work is a continuation of that of Schmitt et al. [1974] and involves field, chem-

Fig. 2. Aerial photograph of Buell Park, NASA photograph S-68-13651. Courtesy of NASA and Gordon Swann. North is to the top; the east-west field of view is 6.5 km. Buell Mountain is the wooded mass in the northern part of Buell Park; the ring dike forms a wooded ridge to the south.

ical, and electron microprobe studies of the Buell Park minettes to determine if the minette varieties could be related by crystal fractionation, to outline the volcanic history of the minette diatreme, and to further examine the minette-kimberlitic tuff relationship.

Field Geology and Petrography

Kimberlitic Tuff-Minette Relations

Zildlitloi Field. The association of minette and kimberlitic tuff in the Zildlitloi field has been further documented at two new localities. At The Beast, a minette neck about 5 km east of Buell Park, a wedge of kimberlitic tuff, 10m long, is contained within the minette tuff-breccia. The situation is analogous to that at Outlet Neck [Allen and Balk, 1954]. Eight kilometers east of Buell Park, the small kimberlitic tuff pipe (diameter: 75 m) described by Allen and Balk [1954] is bisected by a 3 m thick minette dike, typical of the olivine-bearing minettes east of Zildlitloi Mountain. The minette is quite vesicular and contains numerous fibrous inclusions of kimberlitic tuff which is xenolith-poor, but in general similar to other kimberlitic tuffs in the field. Pyroxene-feldspar rocks similar to those in minette at nearby Zildlitloi Mountain [Allen and Balk, 1954], are the most common inclusion.

These new localities confirm the intimate relationship between kimberlitic tuff and minette in the Zildlitloi volcanic field; Green Knobs is the only kimberlitic diatreme which lacks associated minette. In contrast, kimberlitic tuff and minette occur separately to the north, in diatremes along the east side of the Monument Uplift [see McGetchin and Silver, 1972].

Buell Park. Schmitt et al. [1974] established the sequence of kimberlitic tuff followed by minette at Buell Park based on cross cutting relationships between the two. However, they noted no overlap of minette and kimberlitic tuff eruptions.

Subrounded, altered minette clasts, generally less than 3 cm in diameter, but up to 10 cm across were found in the upper 75 m of layered kimberlitic tuff (Tkgl, Figure 3) on the northwestern slopes of Buell Mountain. They also occur in layered kimberlitic tuff on the eastern side of Buell Mountain. These clasts are typical minette with diopside and phlogopite phenocrysts in a devitrified matrix (for mode, see Table 1). Judging from the high water content of one clast (see section on rock chemistry) and from their friable nature, much of the groundmass has been altered to clay minerals. In contrast to the well-rounded mantle and lower crustal xenoliths [Schmitt et al., 1974], these minette xenoliths are subrounded to subangular and probably reflect mixing at relatively shallow depths [see discussion in Schmitt et al., 1974].

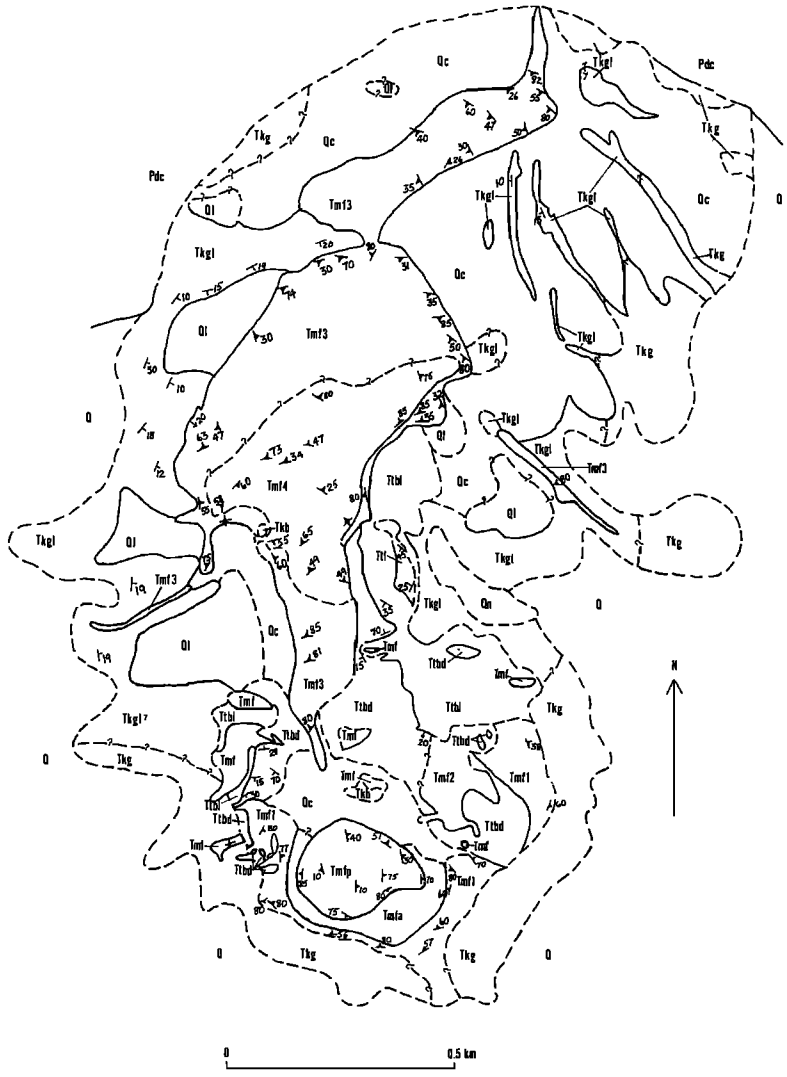

Fig. 3. Geologic map of Buell Mountain. Units are as follows: Q, Quarternary deposits, undifferentiated; Qc, soil and talus; Ql, landslide masses; Qn, stream deposits currently being dissected; Tkb, ultramafic breccia; Tmfp, quartz-bearing felsic minette plug; Tmfa, altered felsic minette; Tmf, felsic minette, undifferentiated; Tmf4, quartz-bearing felsic minette plug(?); Tmf3, platy-cleaved, diopside-rich minette; Tmf2, oxidized felsic minette; Tmf1, phlogopite-rich schistose minette; Ttl, layered minette lapilli tuff; Ttbl, light-colored minette tuff-breccia; Ttbd, dark-colored minette tuff-breccia; Tkgl, layered kimberlitic lapilli tuff; Tkg, massive kimberlitic lapilli tuff; Pdc, De Chelly Sandstone.

There are no major differences between minette-bearing and minette-free kimberlitic tuff. The layering in both is the same, and it appears to be conformable. However, all olivine xenocrysts are completely replaced by serpentines plus oxides in the minette-bearing kimberlitic tuff and the matrix is noticeably dark red, probably due to the presence of disseminated iron oxides. Excluding the minette component, the kimberlitic tuff is identical in texture to the earlier kimberlitic tuffs, albeit more oxidized and hydrated.

Two small, pipe-like outcrops of an ultramafic breccia (Tkb, Figure 3) occur along the margins of two minette plugs. These breccias contain clasts of fine-grained, dark grey minette, quartzite similar to that in the layered kimberlitic tuff, and xenocrysts of kinked olivine (Fo_{89-91}), chrome-rich diopside ($TiO_2 < 0.03$ weight percent, Cr_2O_3 = 0.5 weight percent), and chrome-rich spinel (39.5 weight

percent Cr_2O_3, 25.1 weight percent Al_2O_3) plus xenocrysts derived from the minette. The groundmass consists of poikilitic feldspar(?) enclosing clinopyroxene needles. Many of the clinopyroxene needles are anchored to a clear reaction rim developed around olivine xenocrysts and project radially out into the feldspar. Because of the minette clasts and the location of the pipes along the margins of minette plugs, these breccia pipes probably postdate most if not all minette activity.

Buell Park Minettes

The Buell Park minette diatreme occupies the southern third of Buell Mountain (Figure 3); the northern two thirds consist of layered kimberlitic lapilli tuff (Tkgl, Figure 3) capped and intruded by felsic minette (Tmf3, Tmf4, Figure 3). The diatreme consists of tuff-breccias (Ttbl, Ttbd, Figure 3) and a small block of layered lapilli tuff (Ttl, Figure 3) cut by numerous dikes of, and capped in part by, felsic minette. A cupola of quartz-bearing minette (Tmfp, Figure 3) forms the southwestern corner of the diatreme.

Three types of tuff-breccia [Roden, 1977; Schmitt et al., 1974] are exposed: (1) a light-colored tuff-breccia (Ttbl, Figure 3) which is unsorted and unbedded and contains subangular, nonvesicular, glassy minette clasts (for mode, see Table 1) up to a meter across, (2) an overlying dark colored tuff-breccia (Ttbd, Figure 3) which is crudely bedded, more coherent and contains both subangular minette clasts and flattened bombs (for mode, see Table 1), and (3) a small block of layered lapilli tuff (Ttl, Figure 3) containing tuff-breccias, and graded beds of sub-angular lapilli. The matrix of the light-colored tuff-breccia is a fine-grained, slightly fibrous mix of kimberlitic tuff and minette. In contrast, the matrix of the overlying dark-colored tuff-breccia is devitrified glass, barely distinguishable in thin section from included minette clasts. The minette clasts in both tuff-breccias contain numerous xenoliths and xenocrysts (3-5% volume, Table 1) of many types. Fresh minette glass is preserved in some clasts from the light-colored tuff-breccia.

Massive felsic minettes can be separated into several units based on foliation (Figure 3). The foliation is caused by alignment of phlogopite phenocrysts: abundant phlogopite results in a schistose foliation in contrast to platy foliation developed in relatively phlogopite-poor minette. Massive minette crops out mostly on the northern two-thirds of Buell Mountain, but a minette plug (Tmfp, Figure 3) also forms the southwestern end of Buell Mountain. This plug has a well defined chill zone exposed on the western and southern sides and is surrounded in part by friable, altered minette (Tmfa, Figure 3). The altered minette was originally interpreted to be cataclastic, but diagnostic textures are absent and there is minor sericitization of groundmass feldspars. This minette plug postdates all explosive minette activity in the

TABLE 1. Phenocryst Modes and Groundmass Phases Present, Buell Park Minettes

	1	2	3	4	5	6	7	8
No. of thin sections	3	1	3	3	1	3	3	2
Phenocrysts:								
Diopside	13.0	6.5	9.5	12.4	5.4	12.1	7.0	9.8
Phlogopite	2.3	4.0	6.6	6.7	5.6	3.9	5.6	2.7
Olivine	6.6	-	-	-	-	-	-	-
Sanidine	-	2.5	-	-	Tr	Tr	2.7	2.8
Apatite	-	Tr	Tr	Tr	Tr	Tr	Tr	Tr
Xenoliths	Tr	2.3	3.4	4.1	5.5	2.2	3.4	4.1
Groundmass Phases								
Diopside	+	+	+	+	+	+	+	+
Sanidine	+	+	±	+	+	+	+	+
Phlogopite	+	+	±	+	+	±	+	+
Oxides	+	+	+	+	+	±	+	+
Quartz	-	-	-	-	-	±	±	±
Analcime	+	-	-	-	-	-	-	-
Glass	-	-	±	-	-	-	-	-

1 = ring dike; 2 = minette clast from layered kimberlitic lapilli tuff; 3 = minette clasts from light-colored minette tuff-breccia; 4 = minette clasts from dark-colored minette tuff-breccia; 5 = phlogopite-rich felsic minette (Tmfl, Figure 3); 6 = platy-cleaved, diopside-rich minette (Tmf3, Figure 3); 7 = felsic minette plug (Tmf4, Figure 3); 8 = quartz-bearing felsic minette plug (Tmfp, Figure 3).

diatreme [Schmitt et al., 1974] and was probably contemporaneous with some of the felsic minettes on northern Buell Mountain.

The massive minettes contain variable amounts of phlogopite and diopside phenocrysts (Table 1) in a trachytic matrix consisting of sanidine, diopside, apatite, and magnetite-ulvospinel, with or without phlogopite, quartz, and amphibole. The presence of interstitial patches of quartz in the felsic plug, and sporadically in other units, is significant when contrasted to the mineralogy of the ring dike, described below. Xenoliths and xenocrysts of many types, including pyroxenes, spinel, quartz, feldspars, and crustal rocks, and numerous ultramafic inclusions are locally abundant (Table 1).

In contrast to the quartz-bearing minettes of Buell Mountain, the ring dike minette is a mafic olivine- and analcime-bearing rock. In addition to the presence of olivine and analcime, the minette is distinguished from the felsic Buell Mountain minettes by the lack of a trachytic groundmass, by abundant groundmass ilmenite, by the absence of quartz, and by the rarity of xenoliths and xenocrysts. Phlogopite phenocrysts are sparse (Table 1) and two generations of phlogopite are present: phenocrysts almost completely converted to oxides, and unreacted groundmass phlogopite. Fresh olivine appears to be restricted to the western end of the dike where it is associated with increased groundmass analcime.

Ultramafic Inclusions From Minette

The dense inclusions were previously identified as kimberlite [Schmitt et al., 1974] but in zones of altered minette at Buell Park, the xenoliths weather out as fresh lherzolites and websterites. Two groups of inclusions dominate the ultramafic suite: spinel lherzolite-harzburgites, and websterites. Rarer types include: clinopyroxenites, mica clinopyroxenites, and eclogites. Ultramafic inclusions are also abundant at other minette diatremes in the Zildlitloi field.

The most common group of xenoliths are spinel lherzolites and harzburgites. These occur as rounded inclusions up to 7 cm in diameter, generally altered almost completely to layer silicates. Fresh xenoliths, however, are easily collected in a ravine just south of the felsic plug (Tmfp, Figure 3) where they weather out of altered minette (Tmfa, Figure 3). Texturally, these inclusions are protogranular or transitional between the protogranular and porphyroclastic classes of Mercier and Nicolas [1975]. One porphyroclastic lherzolite was found, but field observations suggest that this texture is rare. In general, the inclusions contain kinked porphyroclasts of olivine and enstatite, and more rarely clinopyroxene, to 5 mm in diameter in a finer-grained matrix of the same plus spinel. The olivines are invariably altered along cracks to serpentines, exsolution lamellae are common in the pyroxenes, and brown spinel occurs both in patches and as vermicular intergrowths with enstatite and diopside [see Smith, 1977]. Some spinel lherzolites and harzburgites collected from a small area of altered minette in the north-central part of Buell Mountain have been almost totally replaced by quartz which coarsens inward from the grain boundaries.

The second abundant group of xenoliths, websterites (to 5 cm in diameter), are more variable both in texture and mineralogy than the spinel lherzolites. The texture is generally allotrophic-granular [Pike and Schwarzman, 1977] although one sample is porphyroclastic. Grain size is generally 1-2 mm across. The porphyroclastic websterite contains large grains of clinopyroxene (1.5 cm in diameter) with lamellae of Ca-poor pyroxene in a finer grained (0.5-1 mm in diameter) matrix of anhedral, equant orthopyroxene and clinopyroxene. Both orthopyroxenes and clinopyroxenes have exsolution lamellae. In no case are the minerals as deformed as their counterparts in the spinel lherzolite suite, and judging from their pleochroism the orthopyroxenes are more iron-rich. The variability in mineralogy lies mainly in the presence or absence of spinel, which may be brown or green; one sample has interstitial plagioclase.

Rare mica clinopyroxenites with accessory apatite are of particular interest because of the possible genetic relationship with the minettes. The mica may be either primary or secondary in texture; the diopsides have spongy rims where they have reacted with the magma. Mineral compositions from a mica clinopyroxenite from The Beast are consistent with a cumulate origin for these xenoliths (M. Roden, unpublished data).

One eclogite with altered, oxidized garnet and spongy pyroxene was found. This is the only reported eclogite from the southern minettes in the Navajo field, although O'Hara and Mercy [1966] described an eclogite from Green Knobs.

Volcanology of Buell Park Minette Diatreme

The land surface at the time of minette eruptions is exposed now at an elevation of 8200 feet on Zildlitloi Mountain [Williams, 1936] while the uppermost minette tuff-breccias on Buell Mountain crop out at 7800 feet. Considering that maar craters, the likely surface expression of diatremes, have floors which typically lie 100 to 650 feet below the surrounding land surface [Lorenz, 1973] and that at Buell Park a minette maar formed within a kimberlitic tuff maar, it is evident that the tuff-breccias formed as part of the maar rim, or immediately below the crater floor. However, the chaotic, unsorted nature of these deposits, especially when compared to the layered lapilli tuffs at Washington Pass [Ehrenberg, 1977a] make their origin as rim deposits

TABLE 2. Representative Microprobe Analyses of Pyroxenes

	BP-35 PC	BP-35 PR	BP-35 G	BPR-5 PC	BPR-5 PR	BPR-5 GR	BP-51 PC	BP-51 PR	BP-29 X	BP-29 X	BP-51 GC	N320 GC
SiO_2	54.6	53.7	54.1	54.6	52.7	51.8	54.5	53.8	55.3	56.8	50.8	50.6
TiO_2	0.21	0.29	0.28	0.35	0.90	1.72	0.25	0.31	<0.03	<0.03	0.29	0.42
Al_2O_3	0.80	0.84	1.00	0.94	0.85	1.08	0.64	0.64	0.76	1.86	3.23	4.41
Cr_2O_3	0.06	<0.04	0.18	0.42	0.30	<0.04	0.30	0.06	0.49	0.36	<0.04	0.08
FeO*	4.22	5.36	5.08	3.77	5.32	7.15	3.37	4.37	1.20	5.09	11.0	9.20
MgO	16.8	16.1	16.3	18.5	16.2	14.4	18.2	17.1	17.8	35.5	11.9	12.6
CaO	22.6	23.0	23.0	21.1	23.0	21.9	22.5	23.1	24.4	0.25	21.9	22.1
Na_2O	0.54	0.46	0.41	0.47	0.30	2.72	0.37	0.37	0.55	<0.03	0.78	0.88
K_2O	0.02	0.02	0.03	<0.02	<0.02	0.02	0.02	0.03	<0.02	<0.02	0.03	0.02
Total	99.9	99.8	100.4	100.2	99.6	100.8	100.2	99.8	100.5	99.9	100.0	100.3

*Total Fe as FeO

PC = phenocryst core, PR = phenocryst rim, X = xenocryst, G = groundmass grain, GC = green core, GR = green rim

Key to sample localities: BPR-6 = olivine-bearing minette, western end of the ring dike, Buell Park; BPR-5 = olivine-bearing minette, central portion of the ring dike, Buell Park; BP-69 = minette clast, layered kimberlitic tuff, Buell Mountain; BP-37 = minette clast, dark-colored minette tuff-breccia, Buell Mountain; BP-51 = minette clast, light-colored minette tuff-breccia, Buell Mountain; BP-41 = felsic minette, northern end of Buell Mountain; BP-35 = quartz-bearing felsic minette plug, southern end of Buell Mountain; BP-29 = ultramafic breccia, Buell Mountain; N320 = Todilto Park minette dike.

unlikely. More likely, the light-colored tuff-breccia is a vent filling and owes its chaotic nature to churning within the vent; the deposit is akin to the tuff-breccias at Shiprock [Williams, 1936]. The dark-colored tuff-breccia with its flattened bombs and crude bedding is interpreted as material that was plastered against the vent walls while still hot enough to be plastic. The block of layered lapilli tuff (Ttl, Figure 3) may be a slump block from the maar rim.

Schmitt et al. [1974] suggested that the massive minettes on the northern part of Buell Mountain were flow remnants but the steep foliation dips (Figure 3) and inward dipping contacts with the underlying kimberlitic tuff (Figure 3) make

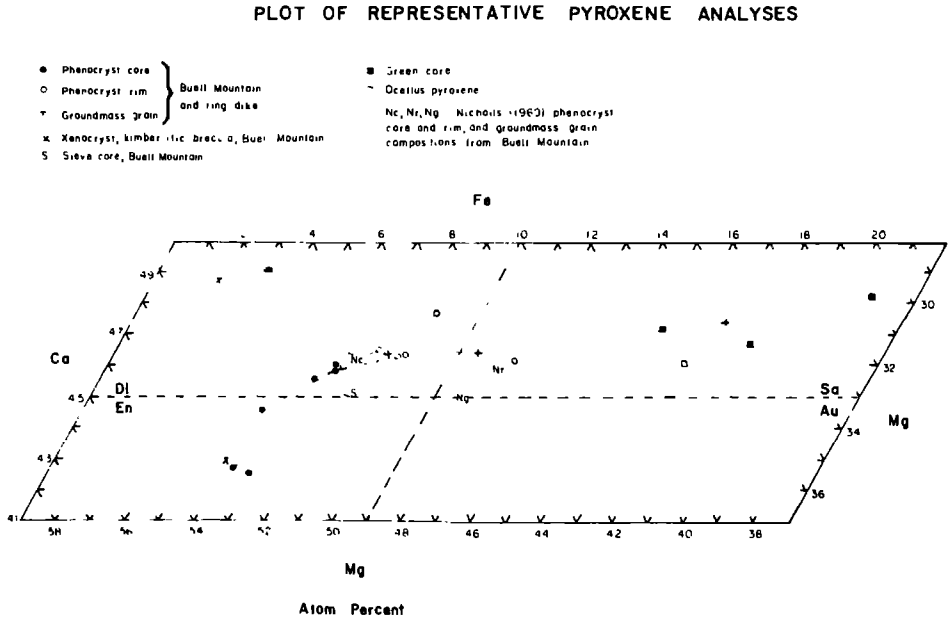

Fig. 4. Portion of Fe-Ca-Mg pyroxene quadrilateral with representative clinopyroxene analyses. Tie lines connect coexisting pyroxenes.

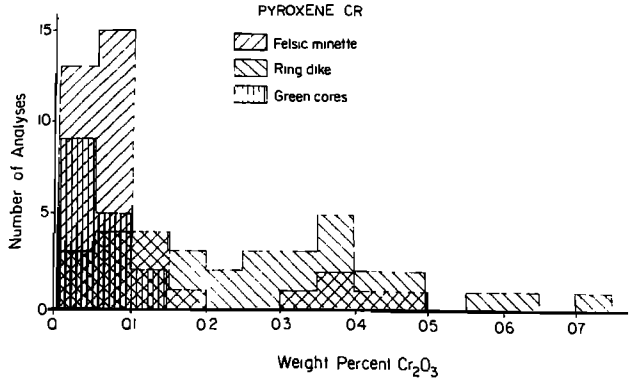

Fig. 5. Histogram of microprobe analyses for Cr_2O_3 in Buell Park pyroxenes and green, salite cores from the Zildlitloi field.

this unlikely. The minette cap was probably a bulbous extrusion, perhaps contemporaneous with the felsic plug (Tmfp, Figure 3) to the south.

The origin of the gas phase during eruption remains a problem. The minette clasts in the tuff-breccias are subangular and vesiculation is rare. This suggests that the volatiles were not juvenile. However, based on abundant pumice at Washington Pass, Ehrenberg [1977a] argued that juvenile volatiles are responsible for the explosive nature of the Navajo volcanic rocks. To the writers' knowledge only at Washington Pass, and Zildlitloi Mountain is vesicular minette common: typical tuff-breccias in the Navajo field contain subangular, nonvesicular clasts of minette. Hence, explosive interaction of minette liquid with groundwater probably supplied the driving force for the eruptions.

Analytical Procedures

All analyses were performed in the Department of Geological Sciences, The University of Texas at Austin. Electron microprobe analyses were made with an Applied Research Laboratories EMX probe system using the correction procedures of Bence and Albee [1968] and Albee and Ray [1970]. Whole rock analyses were performed by modified rapid-method wet chemical techniques by G. K. Hoops. Prior to whole rock analyses, samples of the felsic minettes were handpicked to remove as many xenoliths as possible, however, some contamination was unavoidable.

Mineralogy

Pyroxene

Representative analyses of pyroxenes from Buell Park are compiled in Table 2. The compositions range from endiopside to salite [Poldervaart and Hess, 1951], but cluster in the diopside field (Figure 4). Except for green-cored pyroxenes, described below, most Al is in tetrahedral sites which contain up to 4.5 mole percent Al. Zoning is restricted (Figure 4), and in some cases, erratic. FeO and MgO are the most systematically zoned elements and vary antipathetically: FeO increases toward the rim within any single crystal, but that rim may be as MgO-rich as the core of a neighboring grain. Cr_2O_3 shows the greatest variation, and is typically concentrated in phenocryst cores, but within any given sample some pyroxene rims are richer in Cr_2O_3 than some cores. Na_2O is concentrated in green rims on phenocrysts and in groundmass pyroxenes along with FeO (Table 2). Al_2O_3, SiO_2, and TiO_2 are unzoned except in the ring dike, where phenocryst rims are SiO_2-poor and TiO_2-rich.

Pyroxenes from all the Buell Park minettes overlap in composition, but pyroxenes from the felsic plug (Tmfp, Figure 3) and from the minette cap (Tmf3, Tmf4, Figure 3) on the northern part of Buell Mountain tend to be more FeO-rich and MgO-poor than those from the stratigraphically younger tuff-breccia clasts (Table 2). Although core compositions overlap, ring dike pyroxenes are richer in TiO_2 and Cr_2O_3 than those of felsic minettes. SiO_2 decreases accompanied by an increase in Al_2O_3 towards the rim in the ring dike pyroxenes; it is unzoned in the Buell Mountain pyroxenes.

Large clinopyroxene crystals (greater than 0.5 mm diameter) with green cores and normal, clear diopside rims occur sparsely throughout the Zildlitloi field. The cores may be faintly pleochroic, pale green [α] to pale yellow green [γ], and some have exsolution lamellae of calcum-poor pyroxene or a red-brown mineral, probably hematite or spinel. These green cores are salites [Poldervaart and Hess, 1951] and are

TABLE 3. Representative Microprobe Analyses of Micas

	BP-35 PC	BP-35 PR	BPR-5 PC	BPR-5 G	BP-51 PC	BP-51 PR
SiO_2	40.4	38.4	33.9	36.4	39.2	39.7
TiO_2	4.35	6.13	11.3	9.03	2.72	2.69
Al_2O_3	12.3	12.8	15.4	12.2	12.8	12.7
Cr_2O_3	<0.03	0.08	0.12	0.03	0.12	0.10
FeO*	7.11	8.91	8.09	12.9	7.38	8.89
MgO	21.2	19.2	15.9	14.7	22.1	20.9
CaO	<0.02	<0.02	0.04	<0.02	<0.02	0.03
Na_2O	0.56	0.48	0.59	0.74	0.38	0.37
K_2O	9.52	9.29	8.18	8.70	10.1	9.84
Total	95.5	95.3	93.5	94.7	94.9	95.2
Atom Mg/Fe	5.3	3.8	3.5	2.0	5.3	4.2

*Total Fe as FeO

PC = phenocryst core, PR = phenocryst rim, G = groundmass grain

See Table 2 for sample key

rich in Na_2O, FeO, and Al_2O_3, and poor in Cr_2O_3 and SiO_2 relative to phenocryst clinopyroxene (Table 2, Figure 5). The boundary between core and rim is sharp and occurs over a distance of tens of microns. The green cores from the Zildlitloi field are similar in composition to green cores from The Thumb [Ehrenberg in McGetchin et al., 1977].

Pyroxene xenocrysts from the ultramafic breccia (Tkb, Figure 3) were also analyzed and can be classified into two types: (1) clinopyroxenes typical of minette and (2) clinopyroxenes and orthopyroxenes (BP-29, Table 2) more closely akin to those reported by Smith and Levy [1976] from lherzolite xenoliths and as discrete grains in kimberlitic tuff at Green Knobs. The diopside xenocrysts are lower in Al_2O_3 and Cr_2O_3 than pyroxenes from Green Knobs but have the low TiO_2 and FeO typical of most of the lherzolite pyroxenes [Smith and Levy, 1976]. The enstatite ($Wo_{0.5}En_{92}Fs_7$, Table 2) is indistinguishable from lherzolite orthopyroxenes at Green Knobs, except for slightly lower FeO.

Phlogopite

Most micas (Table 3) are phlogopite with the atom ratio Mg/Fe greater than two [Deer et al., 1963]. Zoning is restricted; only TiO_2, FeO, and MgO are zoned significantly. TiO_2 and FeO generally increase towards the rim while MgO decreases, although some grains are reversely zoned in FeO and MgO. Within grains FeO and MgO vary up to 4 weight percent, but generally less than 2 weight percent. Variations in FeO, MgO, TiO_2, K_2O, and Na_2O define mica compositions characteristic of certain units. Phlogopites from the ring dike (BPR-5, Table 3) are richest in Na_2O while phlogopite from tuff-breccia clasts (BP-51, Table 3) are poorest in Na_2O. High FeO contents characterize micas from the minette cap (Tmf3, Tmf4, Figure 3) on the northern end of Buell Mountain and especially micas from the ring dike.

TABLE 4. Representative Partial Microprobe Analyses of Olivines

	BPR-6 PC	BPR-6 PR	BP-29 X	N320 PC	N320 PR
SiO_2	-	-	40.7	-	-
FeO*	13.4	17.9	9.87	9.10	12.2
MgO	46.8	43.1	50.2	50.4	47.8
CaO	0.16	0.28	<0.02	<0.02	0.23
Total[1]	100.9	100.9	100.6	100.9	101.0
mole %					
Fo	86	81	90	91	87

*Total Fe as FeO

[1]Totals calculated assuming stoichiometry, except for BP-29

PC = phenocryst core; PR = phenocryst rim; X = xenocryst

See Table 2 for key to sample numbers

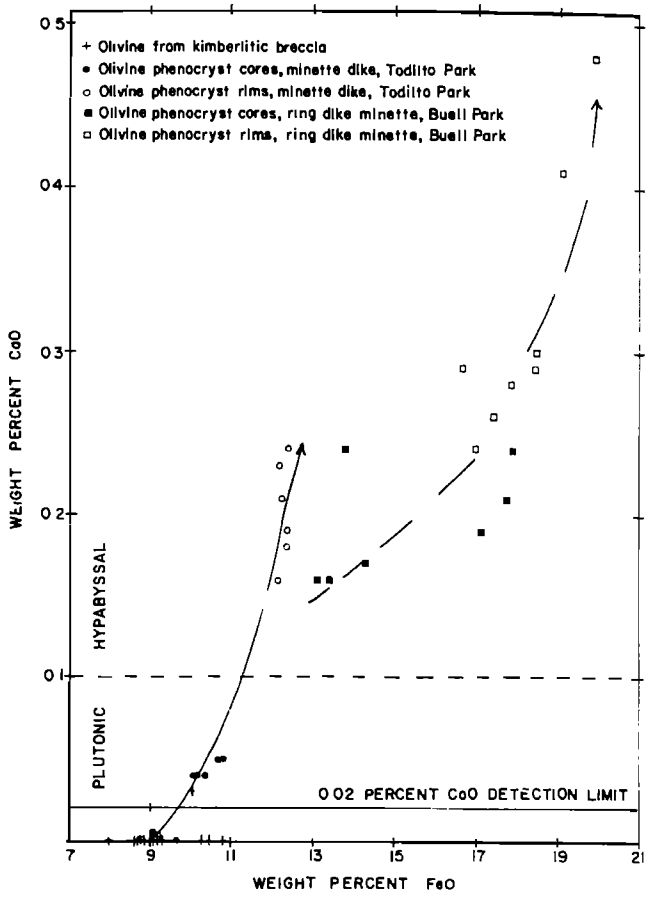

Fig. 6. Plot of CaO versus FeO for olivines from Buell Park ring dike and ultramafic breccia, and Todilto Park minette dike.

TiO_2 contents vary from 2 to 11 weight percent. The massive, felsic minettes (BP-35, Table 3) contain micas which are richer in TiO_2 than those from the stratigraphically younger minette bombs (BP-51, Table 3). In addition, groundmass and phenocryst phlogopite (BPR-5, Table 3) from the ring dike are extremely titaniferous, containing 7.5 to 11.3 weight percent TiO_2. Equally titaniferous phlogopites have been reported from potassium-rich volcanic rocks in West Kimberley, Australia [Carmichael, 1967], New South Wales, Australia [Cundari, 1973], Spain [Borley, 1967], and from Shiprock and Fluted Rock within the Navajo field [Nicholls, 1969].

Olivine

Olivines from the ring dike (Fo_{78-86}), the ultramafic breccia on Buell Mountain (Fo_{89-91}), and a minette dike (Fo_{87-91}) from the eastern end of the Zildlitloi volcanic field in Todilto

TABLE 5. Representative Microprobe Analyses of Oxides

	Ilmenite		Spinel		
	BPR-6 G	BPR-5 G	BP-35 G	BPR-5 G	BP-29 X
SiO_2	-	-	-	-	<0.06
TiO_2	49.8	49.6	28.2	17.0	0.10
Al_2O_3	-	-	0.19	-	25.1
Cr_2O_3	-	-	0.12	-	39.5
FeO*	47.5	48.1	66.5	73.4	21.6
Fe_2O_3[1]	(7.2)	(5.4)	(13.1)	(33.8)	(5.5)
FeO[1]	(41.0)	(43.3)	(54.7)	(43.0)	(16.6)
MnO	-	-	0.23	-	-
MgO	2.16	0.75	1.21	0.80	12.6
Total[2]	100.2	99.1	97.8	94.6	99.5
mole % hematite or ulvospinel	7.4	5.3	80	47	-

*Total Fe as FeO
[1]Fe_2O_3 and FeO calculated on the ilmenite or ulvospinel basis [Anderson, 1968]
[2]Totals calculated after Fe_2O_3 and FeO calculated
G = groundmass grain; X = xenocryst
See Table 2 for key to sample numbers

Park were analyzed (Table 4, Figure 6). The olivines from the three samples are readily distinguished on the basis of CaO and FeO contents (Figure 6). Ring dike olivine phenocrysts are richer in FeO and have relatively high CaO contents, 0.16 to 0.48 weight percent, compared to olivine phenocrysts from the Todilto Park dike. The higher content of MgO in the olivines from Todilto Park is consistent with the increasingly mafic character of minette as one moves from west to east within the Zildlitloi field.

Olivines from the late ultramafic breccia pipes on Buell Mountain do not overlap in composition with the ring dike olivines; there is some overlap with olivine core compositions from Todilto Park. Smith and Levy [1976] reported discrete olivine grain compositions, Fo_{93} to Fo_{88}, from Green Knobs; these olivines also have very low CaO contents, less than 0.05 weight percent [D. Smith, unpublished data]. The association in the ultramafic breccia of olivine with enstatite and Cr_2O_3-rich, TiO_2-poor diopside, and the overlap in composition of the olivine with those from the Green Knobs kimberlitic tuff, suggests that the mineralogy of the breccia from Buell Mountain is of kimberlitic or lherzolitic affinities, not minette affinities.

CaO content in olivine has been shown by Simkin and Smith [1970] to be strongly influenced by pressure and to be independent of FeO content. Olivines with CaO contents less than 0.10 weight percent typically crystallized in a plutonic environment. Stormer [1973] pointed out, on the basis of thermodynamic arguments, that CaO contents of olivines should be influenced by silica activity and temperature also. Noting that olivines from alkaline, undersaturated magmas typically yield steep curves with positive slopes when CaO is plotted against FeO Stormer [1973] concluded that the pressure effect played the dominant role in controlling CaO in olivine for these magmas, and that these magmas have risen rapidly to the surface. The steep curves on the CaO-FeO plot (Figure 6) for the minette olivines suggest that the minettes also rose rapidly to the surface. Furthermore, the CaO content of the olivines suggests that the ring dike olivines and the Todilto Park olivine rims crystallized in a hypabyssal environment while the Todilto Park olivine cores and the ultramafic breccia olivines crystallized in a plutonic environment.

Iron Titanium Oxides

Oxides from the ring dike, the felsic plug, and the ultramafic breccia were analyzed (Table 5); a broad electron beam (approximately 30 microns in diameter) was used where oxidation was obvious. Ferrous and ferric iron were calculated from structural formulas by the method of Anderson [1968]. The low totals for spinel probably reflect subsolidus oxidation. A temperature of 815°C and an oxygen fugacity of $10^{-14.6}$ were calculated from the compositions of coexisting spinel and ilmenite in the ring dike following the method of Buddington and Lindsley [1964]. This value is near the FMQ buffer curve, but the temperature is about 150°C lower than the solidus for the Leucite Hills rocks of similar composition [Carmichael, 1967] and probably reflects subsolidus equilibration.

The Cr_2O_3-rich spinel from the ultramafic breccia (BP-29, Table 5) is obviously not of minette affinities, but is similar to spinels in lherzolite inclusions from Green Knobs reported by Smith and Levy [1976].

TABLE 6. Representative Microprobe Analyses of Analcime and Feldspars

	Analcime	Feldspar		
	BPR-5 G	BPR-5 G	BP-41 G	BP-35 G
SiO_2	53.8	64.7	64.8	64.9
TiO_2	0.06	0.13	-	-
Al_2O_3	23.3	18.3	18.9	18.4
Fe_2O_3*	0.88	0.75	0.67	0.51
Na_2O	10.8	1.87	4.36	4.18
K_2O	0.45	13.9	9.60	10.6
Total	89.3	99.7	98.3	98.6
Na/Na + K		0.17	0.41	0.38

*Total Fe as Fe_2O_3
G = groundmass grain
See Table 2 for key to sample numbers

Feldspar

Representative analyses of feldspars in Table 6 confirm the optical identification of sanidine [Williams, 1936]. FeO has been recast as Fe_2O_3 because iron is probably present as Fe^{3+} [Smith, 1974]. These feldspars are quite iron-rich with variable contents of Na_2O and Fe_2O_3 (Table 6). Low totals probably reflect unanalyzed BaO, SrO, and CaO because Nicholls [1969] reported that these oxides commonly totaled 0.7 to 1.3 weight percent in Navajo feldspars, the bulk being BaO.

Analcime

Microprobe analyses of the mineral previously identified as leucite [Gregory, 1917; Williams, 1936] in the ring dike at Buell Park showed that it is actually analcime. A representative analysis has high water (assmued) and low Na_2O contents. Cation totals are deficient in total Na + K, suggesting that Na_2O volatilized during microprobe analyses. If Na is assumed to equal Al minus K (ignoring the contribution of Ca), as in the ideal formula, the weight percent Na_2O would increase by about 3 weight percent, and water content decrease to about 8 weight percent, values more typical of igneous analcimes [Wilkinson, 1968]

Although much of the analcime is interstitial, some euhedral grains are enclosed in fresh sanidine. Thus, the analcime apparently crystallized earlier than the feldspar and at relatively high temperatures. Experimental work has shown that analcime will not coexist with a silicate melt at water pressures below 4 kbar in the system $NaAlSiO_4$-$NaAlSi_3O_8$-H_2O [Peters et al., 1966]. The addition of K_2O to the system lowered the pressure where analcime and liquid coexisted to 2.3 kbar and 650°C [Peters et al., 1966]. However, the ring dike, which is presently exposed at 7300 feet, probably crystallized less than 400 m below the land surface (see section on volcanology). Thus, P_{H_2O} could not have been high enough to stabilize analcime. Possibly, the analcimes are microphenocrysts which crystallized at higher pressures.

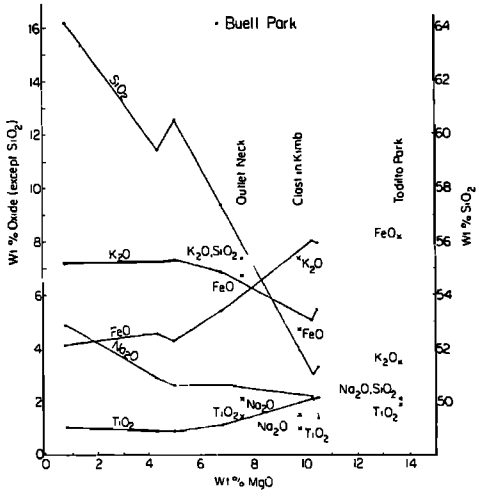

Fig. 7. MgO variation diagram for Buell Park minette analyses, including groundmass glass, plus Outlet Neck [Allen and Balk, 1954] and Dike B, Todilto Park [Williams, 1936]. Note that the clast from the layered kimberlitic tuff does not lie along the trend defined by the other Buell Park minettes.

Rock Chemistry

Six new whole rock analyses and an average of four microprobe analyses of a groundmass glass from a tuff-breccia clast illustrate the peculiar chemistry of minette (Figure 7, Table 7): high MgO and low SiO_2 contents are coupled with high alkali contents and $K_2O/Na_2O>1$. As expected, the more mafic ring dike samples are the most primitive, the tuff-breccia clast occupies an intermediate position, and the felsic plug and massive minette from northern Buell Mountain are relatively differentiated (Figure 7). The groundmass glass is most differentiated of all, and it is syenitic with over 80 percent normative ab + or. This syenitic composition is consistent with the occurrence of sheets of syenite in minette at Agathla, Black Rock, and a small neck 2 km southwest of Twin Buttes [Roden, 1977] which presumably represent residual liquid [see Lindsley et al., 1971]. The felsic minettes are saturated or slightly oversaturated; in contrast, the ring dike minette is saturated or slightly undersaturated. The sample from the western end of the ring dike (BPR-6, Table 7) is undersaturated and has a lower K_2O/Na_2O ratio than the sample (BPR-5, Table 7) from the central part of the dike. This chemical change coincides with an increase of analcime in BPR-6. A minette clast from the kimberlitic tuff (BP-69, Table 7) does not lie along the trends defined by the other Buell Park samples (Figure 7); it appears to have gained MgO, possibly through reaction with the kimberlitic tuff. Also note the high H_2O content of this clast, clearly indicative of alteration. Other analyses from Buell Park have been published by Nicholls [1969], Schmitt et al. [1974], and Allen and Balk [1954].

The range in the minette chemistry at Buell Park encompasses the range in minette compositions within the Navajo field. Most Navajo minettes fall in the range 47-55 weight percent SiO_2 [Williams, 1936], and thus are more mafic than the Buell Mountain minettes but similar to the ring dike minette. Only in the Red Rock Valley, at Sonsela Buttes, and at Washington Pass are felsic minettes similar to those of Buell Mountain associated with more mafic minettes [Ehrenberg, 1977a].

Similar potassium-rich volcanic rocks are

TABLE 7. Chemical Analyses of Buell Park Minettes

	BPR-6	BPR-5	BP-69	BP-37	BP-41	BP-35	BP-51*
SiO_2	49.13	48.94	55.46	56.23	58.88	59.50	61.8
TiO_2	2.02	2.03	0.91	1.08	0.87	0.89	0.99
Al_2O_3	10.51	10.11	10.65	12.14	13.38	12.93	15.3
Fe_2O_3	3.82	4.47	3.68	4.38	3.77	3.02	-
FeO	4.30	3.60	1.08	1.36	1.17	1.46	4.01[1]
MnO	0.12	0.12	0.05	0.08	0.06	0.06	0.07
MgO	9.87	10.03	9.17	6.63	4.31	4.90	0.76
CaO	9.06	8.98	4.34	6.37	6.12	5.30	1.59
Na_2O	2.06	1.28	1.42	2.60	2.87	2.53	4.72
K_2O	4.86	5.22	6.98	6.76	7.20	7.21	6.96
H_2O+	2.38	2.92	2.09	0.84	0.36	0.54	-
H_2O-	0.38	0.80	2.71	0.36	0.08	0.60	-
P_2O_5	0.97	1.08	0.63	0.77	0.74	0.64	-
CO_2	0.00	0.01	0.00	0.02	0.06	0.10	-
Total	99.48	99.59	99.17	99.62	99.87	99.68	96.2
CIPW Norms[2]							
qz	-	-	2.42	-	1.76	4.56	4.16
or	29.72	32.20	43.78	40.65	42.84	43.25	42.72
ab	12.56	11.34	12.78	22.42	24.45	21.75	41.54
an	5.25	6.71	2.18	1.52	2.40	2.68	-
ne	2.96	-	-	-	-	-	-
ac	-	-	-	-	-	-	0.01
di-wo	14.49	13.52	6.81	10.61	9.55	7.99	3.42
di-en	11.67	10.97	5.76	8.51	7.62	6.74	1.70
di-fs	1.12	0.94	0.17	0.87	0.83	0.22	1.64
hy-en	-	2.35	18.47	3.68	3.19	5.66	0.26
hy-fs	-	0.20	0.54	0.38	0.35	0.18	0.26
ol-fo	9.64	8.94	-	3.24	-	-	-
ol-fa	1.02	0.84	-	0.37	-	-	-
mt	5.28	5.35	3.71	3.81	3.47	3.52	3.33
il	3.97	4.03	1.84	2.09	1.67	1.71	1.96
hm	-	-	-	-	-	-	0.23
ap	2.37	2.68	1.59	1.85	1.78	1.54	-
cc	-	0.02	-	0.05	0.14	0.23	-

*Microprobe analyses of groundmass glass (average of four points)
[1]Total Fe as FeO
[2]Calculated after Fe_2O_3 was adjusted to be equal to or less than TiO_2 + 1.5 weight percent [Irvine and Baragar, 1971]; oxides were then normalized to 100%, water-free

See Table 2 for key to samples
Analyst for all samples, except BP-51, was G. K. Hoops

rare, dispersed, and restricted to the continents. They include the volcanic rocks of the Leucite Hills, Wyoming [Carmichael, 1967], the Bearpaw and Highwood Mountains of Montana [Weed and Pirsson, 1895, 1896], leucite-bearing rocks from West Kimberley [Carmichael, 1967] and New South Wales [Cundari, 1973], Australia, and jumillites from Spain [Borley, 1967]. These are all basic rocks with $K_2O > Na_2O$ and peculiar trace element chemistry: Cr, Ni, Ba, Rb, Sr, Nb, Zr, P, and F are all abundant [Carmichael et al., 1974]. The volcanic rocks from the Leucite Hills and West Kimberley are the most extreme members of this suite, having K_2O/Na_2O generally greater than 8 [Carmichael, 1967].

Discussion

Relationship of the Minette Varieties

The association in time and space of mafic and felsic minettes at Buell Park, and their identical initial $^{87}Sr/^{86}Sr$ ratios, 0.708 [Powell and Bell, 1969], suggest that the felsic and mafic minettes are genetically related, and are consistent with the felsic minettes being derived from the mafic minettes by fractionation of the observed phenocrysts: diopside, phlogopite, and olivine. Alternatively, the ring dike minette could be parent plus cumulate. Crystal fractionation was modeled by a MgO-variation diagram [Figure 8] and by a least squares mixing program

TABLE 8. An Example of a Mixing Model: Model A

	Parent	Daughters					Best fit to	
	BPR-5	Diop.	Phlog.	Oliv.	Apat.	BP-37	BPR-5	Residuals
SiO_2	51.29	54.50	36.60	39.40	0.00	57.40	51.68	-0.39
TiO_2	2.13	0.25	11.60	0.00	0.00	1.10	2.48	-0.35
Al_2O_3	10.60	0.64	16.40	0.00	0.00	12.39	10.56	0.04
FeO*	7.99	3.37	8.69	13.42	0.00	5.41	5.73	2.26
MnO	0.13	0.14	0.02	0.18	0.00	0.08	0.08	0.05
MgO	10.51	18.20	17.10	46.80	0.00	6.77	11.09	-0.58
CaO	9.41	22.50	0.04	0.16	56.00	6.50	8.98	0.43
Na_2O	1.34	0.37	0.63	0.00	0.00	2.65	1.86	-0.52
K_2O	5.47	0.02	8.79	0.00	0.00	6.90	5.78	-0.31
P_2O_5	1.13	0.00	0.00	0.00	44.00	0.79	1.73	-0.80
Solution		14.29	14.36	3.32	2.73	64.66		

Sum of Absolute Residuals = 5.54
Sum of Squares of Residuals = 6.86

*Total Fe as FeO

All analyses calculated to 100 percent, water-free

similar to that of Wright and Doherty [1970]. A ring dike minette (BPR-5, Table 7) was chosen as the parent or parent plus cumulate and a minette clast from the tuff-breccias (BP-37, Table 7) was chosen as the daughter to test whether the most mafic of the felsic minettes (Figure 7) could be derived by crystal fractionation from the ring dike minette. Representative mineral compositions, chosen on the basis of histogram plots of microprobe analyses, were normalized to 100 weight percent, water-free, for most models; duplicate models, including water, were run for the best models.

The results can be understood by looking at Figure 8. The crystal cumulate must have a composition within the area outlined by the phase compositions, but all compositions within these areas are too FeO-poor, and most are too SiO_2-rich to cause differentiation of BPR-5 towards BP-37. Relating the more felsic minettes, such as the minette plug (BP-35, Table 7) to the minette clast (BP-37) in a similar model encounters the same difficulties. The residuals from the mixing model (Table 8), and the variation plot (Figure 8) suggest that an Fe-Ti oxide would improve the model. Models C and D (Figure 9, Table 9), which include magnetite as a fractionation phase give better fits to the whole rock chemistry. Fractional crystallization can no longer be ruled out on the basis of the mixing model. The best model (Figure 9) requires fractionation by weight of 18 percent diopside, 12 percent phlogopite, 1.6 percent olivine, 2.2 percent apatite, and 3.1 percent spinel from BPR-5 to obtain BP-37. Sample BP-35 can similarly derived from BP-37 by fractionation of diopside and phlogopite with minor spinel and apatite (Figure 9). Models C and D (Figure 9, Table 9) are similar to fractionation models suggested by Ehrenberg (1977a) to explain mafic and felsic minettes at Washington Pass and Sonsela Buttes.

The best mixing model requires fractionation of magnetite which is unlikely in light of petrography, magma viscosity and density, and phase size and density. In all the Buell Park minettes, primary oxides are restricted to the groundmass. In the chill zone of the ring dike groundmass oxides are approximately 0.025 mm in diameter; oxides in clasts from the tuff-breccia are on the order of 0.05 mm in diameter. Rare large oxide grains have vermicular or embayed edges with reaction rims of phlogopite; some have high Cr_2O_3 contents (53 weight percent, M. Roden, unpublished data). These grains are most likely xenocrysts. Petrographically, the oxides do not appear to have been liquidus phases in either the ring dike minette or in the felsic minette clasts from the tuff-breccia. As Eggler and Burnham [1973] pointed out, it is impossible to derive a daughter magma by subtraction of an oxide from a parent magma if the oxide is not stable near the liquidus of the daughter.

Hypothetical settling velocities of minerals in a liquid of minette composition were investigated [Roden, 1977] to shed further light on the mixing model. Stokes Law behavior was assumed [Shaw et al., 1968; Shaw, 1965; Sparks et al., 1977] and an empirical relation [see discussion in Shaw, 1965] which relates the velocity determined from Stokes Law to the velocity of a particle in a suspension was also used. Olivine and spinel were treated as spheres, diopside as a cylinder, and phlogopite as a disc [McNown and Malaika, 1950]. Viscosity and density were calculated by the methods of Shaw [1972] for viscosity, and Bottinga and Weill [1970] for density with assumed water contents of 3 weight percent for BP-37 and 2

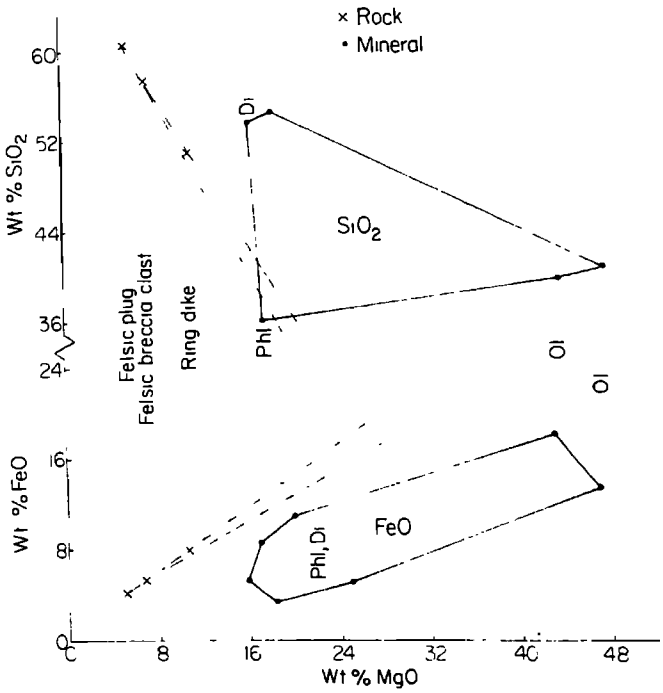

Fig. 8. MgO variation diagram with total Fe as FeO and SiO_2 contents of samples BP-35, BP-37, BPR-5, and phenocrysts of diopside, phlogopite, and olivine. All analyses water-free, recalculated to 100 percent. Net composition of cumulate must lie within outlined areas. Both trends, SiO_2 and FeO, would be more easily explained if an Fe-Ti oxide was also fractionated.

weight percent for BPR-5. The calculated settling velocities show that diopside and olivine settle at approximately the same speed, 1 x 10^{-2} cm sec^{-1}, phlogopite settles about an order of magnitude slower, and magnetite settles 2 orders of magnitude slower than phlogopite. These rates are for 1 bar and 1250°C. With increasing depth the net effect of increasing temperature and pressure is to increase the settling velocities [Kushiro et al., 1976]. The relatively slow settling velocity of spinel is not consistent with the rapid settling velocity needed to fractionate a late crystallizing phase. Furthermore, although the mixing model requires subequal amounts of diopside and phlogopite and essentially no olivine to settle, the greater settling velocities of olivine relative to phlogopite combined with the greater modal proportion of olivine (Table 1) in the ring dike makes the model improbable. A parent with three times as much olivine as phlogopite as in the case of the ring dike, would not likely fractionate subequal amounts of phlogopite and diopside and essentially no olivine. Thus, the settling velocities and the modal proportions are not consistent with the weight percent of the various phases required by the mixing model C.

Intuitively, the abundance of dense inclusions in the felsic minettes appears also to be inconsistent with crystal fractionation. However, Sparks et al. [1977] argued that magmas below the liquidus may behave as Bingham liquids and possess a yield strength. The net result is that xenoliths more than ten times the diameter of the size of the phenocrysts that are causing the Bingham behavior will not settle out, however, the phenocrysts may still settle [see discussion in Sparks et al., 1977, and Shaw et al., 1968]. Clinopyroxene and orthopyroxene xenocrysts of the same size as diopside phenocrysts are common in the felsic minettes and their presence is inconsistent with the crystal settling of diopside and phlogopite, at least in the upper crust.

A final argument against crystal fractionation is based on Sr analyses of the Buell Park minettes [Powell and Bell, 1969]. A felsic minette from Buell Mountain contains 973 ppm Sr, and a ring dike minette contains 1579 ppm Sr. This decrease in Sr from mafic to felsic minettes requires a Sr-rich phase to fractionate from the ring dike minette. The only fractionating phase in the mixing model with a partition coefficient (K_D = concentration of Sr in solid/concentration of Sr in liquid) for Sr greater than 1 is apatite, but its partition coefficient is probably too small, less than 5 (from data in Dasch, 1969) to make the bulk solid/liquid partition coefficient for Sr greater than 1, based on model C. Hence, Sr should increase with fractionation, not decrease as is observed. The mixing models do not satisfactorily explain the Sr data.

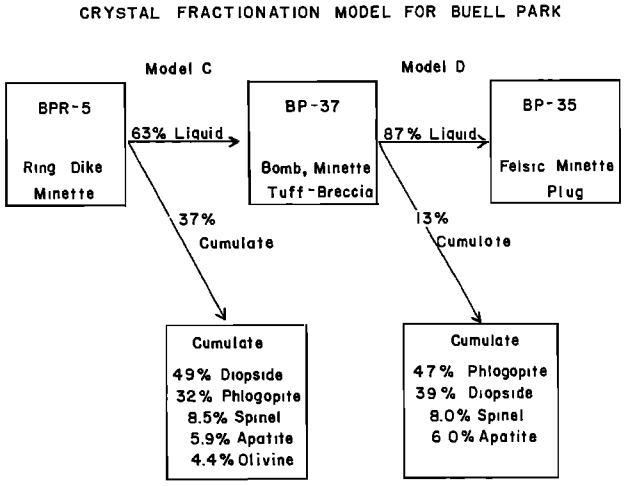

Fig. 9. Fractional crystallization model for the Buell Park minettes based on major element concentrations in whole rocks and phenocrysts.

In summary, crystal fractionation of the observed phenocrysts does not satisfactorily explain the relationship between mafic and felsic minettes. However, the relatively minor chemical variation between felsic minettes on Buell Mountain probably reflects fractionation of diopside and phlogopite with minor amounts of apatite and magnetite. Possibly, a combination of crystal fractionation and assimilation of silicic material in a mafic parent explains the felsic minettes but this possibility remains unexplored. An alternative model involving fractionation in the mantle will be developed in the next section.

Petrogenesis

Hypotheses for the origin of mafic, potassium-rich magmas include fractionation of olivine or eclogite from peridotitic magmas, assimilation of various materials by a wide variety of parent magmas, partial melting of potassium-rich source rocks, and zone refining [see summary in Bell and Powell, 1969]. Most of these hypotheses attribute the peculiar chemistry of these rocks to processes divorced from the source material. However, the Navajo minettes probably represent primary melts from the mantle because of the following characteristics: (1) abundant spinel lherzolite and websterite inclusions, (2) garnet peridotite inclusions which equilibrated at 45 to 52 kbars [Ehrenberg, 1977b], (3) Mg-rich olivine phenocrysts (Fo_{89-91}) in some minette dikes, and (4) the high Ni, 270-360 ppm, and Cr, 300-450 ppm, contents of many minettes [Nicholls, 1969]. If the minettes are primary melts from the mantle, then the source was rich in K_2O and P_2O_5 which were probably contained in accessory phases such as phlogopite, which is stable to 175 km in regions of low geothermal gradient [Modreski and Boettcher, 1972], and apatite, which has been found in some lherzolite inclusions in basalts [for example, Frey and Green, 1974].

TABLE 9. Mixing Models

	BPR-5*	BP-37*	Model B best fit to BP-37	Model C best fit to BPR-5	Model D best fit to BP-37
SiO_2	51.29	57.40	58.09	51.17	57.72
TiO_2	2.13	1.10	1.05	2.69	1.22
Al_2O_3	10.60	12.39	12.42	9.98	12.25
FeO[1]	7.99	5.41	4.59	7.82	5.41
MnO	0.13	0.08	0.06	0.10	0.07
MgO	10.51	6.77	7.04	10.38	6.78
CaO	9.41	6.50	6.42	9.10	6.41
Na_2O	1.34	2.65	2.26	1.84	2.26
K_2O	5.47	6.90	7.13	5.42	6.99
P_2O_5	1.13	0.79	0.99	1.45	0.94
Sum of Absolute Resid.			2.80	2.83	1.33
Sum of Squares of Residuals			1.49	1.22	0.33
Amount of Cumulate, (Wt. %)			14.6	36.3	14.4
Composition of Cumulate	Diop.		5.4	17.8	5.6
	Phlo.		8.2	11.7	6.8
	Oliv.		-	1.6	-
	Magn.		-	3.1	1.2
	Apat.		1.0	2.2	0.9

*Recalculated to 100 percent, H_2O-free
[1]Total Fe as FeO

Model B = BP-37 differentiates to BP-35 without magnetite fractionation
Model C = BPR-5 differentiates to BP-37 with magnetite fractionation
Model D = BP-37 differentiates to BP-35 with magnetite fractionation

For sample key, see Table 2

The Navajo minettes have high initial Sr ratios, 0.7056 to 0.7081, and high Rb, 75-234 ppm, and Sr, 1000-1800 ppm, concentrations [Powell and Bell, 1970]. Sr concentration and $^{87}Sr/^{86}Sr$ ratio are not inversely correlated, and this fact, combined with the high Sr concentrations, makes contamination an unlikely explanation for the high initial $^{87}Sr/^{86}Sr$ ratios. Hence, the isotopic characteristics of the minettes may reflect source characteristics. If this assumption is correct, and if the relatively low Rb/Sr ratio of the mafic minettes, 0.05 [Powell and Bell, 1970], is representative of the source, then the initial $^{87}Sr/^{86}Sr$ ratios of the minettes can be explained if the source of the minettes was enriched in Rb relative to continental mantle [Faure and Powell, 1972] about 1.5 billion years ago ($\lambda[^{87}Rb] = 1.42 \times 10^{-11} yr^{-1}$).

Rare earth elements [Kay and Gast, 1973; Ehrenberg, 1977a, Roden, unpublished data] in the Navajo minettes are highly fractionated relative to chondrites with extreme light rare earth enrichment (La = 320-870 x chondrite, Yb = 2-10 x chondrite). These data suggest that (1) both mafic and felsic minettes formed by a small degree of partial melting of a garnet peridotite in which garnet formed a significant amount of the residuum [Kay and Gast, 1973], or (2) the mafic minettes formed by partial melting of a garnet perdotite as above, while the felsic minettes formed by crystal fractionation from a mafic parent. In the latter case, fractionation of a REE-rich phase such as apatite, must have "buffered" the REE concentrations [Roden and Smith, in preparation].

The writers suggest that the mafic minettes of Buell Park were generated within the garnet peridotite stability field in the upper mantle by partial melting of a phlogopite- and apatite-bearing garnet peridotite. This idea is generally consistent with experimental work by Modreski [1972] who showed that K_2O-rich liquids result when a phlogopite-rich source is melted, and Edgar et al. [1976] who

found that a biotite mafurite equilibrated with olivine, diopside, and phlogopite at pressures to 30 kbars.

The relationship of the felsic minettes to the mafic minettes at Buell Park remains puzzling. Two of the simpler explanations are (1) the felsic minettes, because of their minimal normative olivine contents, were derived by a smaller degree of partial melting than the mafic minettes, or (2) the felsic minettes were derived by crystal fractionation from the mafic minettes, but subtraction of the present phenocryst population does not explain the fractionation as discussed above. This latter fact suggests that a significant period of time or movement occurred between differentiation and extrusion. The abundance of spinel lherzolite inclusions in the felsic minettes contrasted with their absence in the mafic ring dike minettes at Buell Park supports this contention. This difference must be due to the physical properties of the liquids (for example, viscosity), and this difference probably existed prior to the incorporation of the inclusions into the minettes. It is likely that the difference in physical properties between the felsic and mafic minette liquids was a function of their different compositions, and therefore the compositional difference was established in the upper mantle, and not the crust.

The relationship between minette and kimberlitic tuff remains obscure as no intermediate rock type is exposed. The fact that these two rock types occupy the same conduit at Buell Park and neighboring diatremes, and are of the same age, strongly argues that these two rock types are genetically related. The kimberlitic tuff may have been a fluid phase rich in H_2O and CO_2 which separated from the minette magma, perhaps in the upper mantle [see also Smith and Levy, 1976; McGetchin and Silver, 1972].

Origin of Green Pyroxene Cores. The widespread occurrence of the green cores suggests two possibilities for their origin: (1) they are high-pressure phenocrysts, which were later mantled by diopside, or (2) they are xenocrysts from a widespread rock type in the lower crust or upper mantle. Edgar et al. [1976] studied the experimental petrology of a mafic, potassic magma at high pressures. They found that in the range 10 to 30 kbars the clinopyroxene in equilibrium with the melt was lower in Al_2O_3 (0.8 to 1.9 weight percent), Na_2O (0.17 to 0.40 weight percent), and FeO (3.2 to 7.3 weight percent) than the green cores. The diopside compositions observed in the experiments, however, match closely the diopside phenocrysts in the minettes. Furthermore, the green cores have consistently low Cr_2O_3 contents, although their minette host is Cr-rich [Nicholls, 1969], and coexisting diopside phenocrysts have Cr-rich cores (Figure 5, Table 2). Because of the relatively high partition coefficient of clinopyroxene for Cr [for example, Irving, in press], the low Cr_2O_3 contents of the green cores suggests that they are xenocrysts and not phenocrysts. Finally, the presence of exsolutuon lamellae in the cores suggest that the green cores have reequilibrated at a lower temperature than that that they initially crystallized at, a history not compatible with being phenocrysts.

The green cores are probably xenocrysts from a widespread rock type in the upper mantle or lower crust. A logical source is the Colorado Plateau eclogites; however, their pyroxenes are typically more jadeitic (D. Smith, unpublished data). The green cores are, however, similar to salites in garnet granulite xenoliths at The Thumb and S.N. Ehrenberg [McGetchin et al., 1977] has suggested that the granulites are the source for some green cores.

Conclusions

Kimberlitic tuff and minette are associated in four diatremes in the Zildlitloi volcanic field. The minette and kimberlitic tuff were essentially contemporaneous, although the bulk of kimberlitic eruptions was earlier than minette eruptions. At Buell Park there was a time overlap between minette and kimberlitic tuff: minette clasts occur in layered kimberlitic tuff, and two post-minette ultramafic breccia pipes are similar in mineralogy to xenocryst-bearing kimberlitic tuff. The field geology of the Buell Park minette diatreme can be successfully related to a diatreme model in which the tuff-breccias formed as vent filling and splatter plastered on to the sides of the vent throat. The present outcrops are probably on the order of 200 m below the original crater floor.

The mineralogy of the Buell Park minettes is typical of potassium-rich, mafic volcanic rocks: phlogopite, diopside, and sanidine predominate. Most notable is the high TiO_2 content of phlogopite from the ring dike. Crystal fractionation models using phenocryst compositions do not explain the compositional range of the minettes. Inclusion of magnetite as a fractionating phase improves the model, however, the mixing model is generally inconsistent with phase proportions, and probable settling velocities. The mafic and felsic minettes may be related by varying degrees of partial melting of the same source or by crystal fractionation of phases not now observed as phenocrysts plus diopside and phlogopite in the upper mantle.

Green, aluminous salite cores in diopside phenocrysts are widely but sparsely distributed in the Navajo field. These cores are interpreted as xenocrysts because of their exsolution lamellae, and low Cr_2O_3 contents, and because of results from high pressure experiments.

Acknowledgements. This study was supported by grant EAR76-12368 from the Earth Sciences Division, National Science Foundation. Partial

support for field work came from a Sigma Xi Grant-in Aid of Research, and a Penrose Grant from the Geological Society of America to Roden. The Navajo Tribe graciously granted permission for field studies on their land. This work has benefitted at various times from discussion with D.S. Barker, F.A. Frey, J.R. Garrison, F.W. McDowell, and M. Osborne. The project was part of the requirements for a M.A. degree, The University of Texas at Austin.

References

Albee, A. L., and L. Ray, Correction factors for electron probe microanalysis of silicates, oxides, carbonates, phosphates, and sulfates, Anal. Chem., 42, 1408-1414, 1970.

Allen, J. E., and R. Balk, Mineral resources of Fort Defiance and Tohatchi Quadrangles, Arizona and New Mexico, New Mexico Bur. Mines Miner. Resources Bull., 36, 140pp., 1954.

Anderson, A. T., The oxygen fugacity of alkaline basalt and related magmas, Tristan da Cunha, Amer. J. Sci., 266, 704-727, 1968.

Armstrong, R. L., K-Ar dating of laccolithic centers of the Colorado Plateau and vicinity, Geol. Soc. Amer. Bull., 80, 2081-2086, 1969.

Bell, K., and J. L. Powell, Strontium isotopic studies of alkalic rocks: the potassium-rich lavas of the Birunga and Toro-Ankole Regions, East and Central Equatorial Africa, J. Petrology, 10, 536-577, 1969.

Bence, A. E., and A. L. Albee, Empirical correction factors for the electron micro-analysis of silicates and oxides, J. Geol., 76, 382-403, 1968.

Borley, G. D., Potash-rich potassic rocks from southern Spain, Mineral. Mag., 36, 364-379, 1967.

Bottinga, Y., and D. F. Weill, Densities of liquid silicate systems calculated from partial molar volumes of oxide components, Amer. J. Sci., 269, 169-182, 1970.

Buddington, A. F., and D. H. Lindsley, Iron-titanium oxide minerals and synthetic equilivalents, J. Petrology, 5, 310-357, 1964.

Carmichael, I. S. E., The mineralogy and petrology of the volcanic rocks from the Leucite Hills, Wyoming, Contrib. Mineral. Petrol., 15, 24-66, 1967.

Carmichael, I. S. E., F. J. Turner, and J. Verhoogen, Igneous Petrology, McGraw-Hill New York, 1974.

Cundari, A., Petrology of the leucite-bearing lavas in New South Wales, J. Geol. Soc. Australia, 20, 465-492, 1973.

Dasch, E. J., Strontium isotope disequilibrium in a porphyritic alkali basalt and its bearing on magmatic processes, J. Geophys. Res., 74, 560-565, 1969.

Deer, W. A., R. A. Howie, and J. Zussman, Rock-Forming Minerals, vol. 3, Sheet Silicates, 270 pp., Longmans, Green and Co. Ltd., London, 1962.

Edgar, A. D., D. H. Green, and W. O. Hibberson, Experimental petrology of a highly potassic magma, J. Petrology, 17, 339-356, 1976.

Eggler, D. H., and C. W. Burnham, Crystal-liaation and fractionation trends in the system andesite-H_2O-CO_2-O_2 at pressures to 10 kbars, Geol. Soc. Amer. Bull., 84, 2517-2532, 1973.

Ehrenberg, S. N., The Washington Pass volcanic center: evolution and eruption of minette magmas of the Navajo volcanic field, Extended Abstracts, Second International Kimberlite Conference, Santa Fe, New Mexico, 1977a.

Ehrenberg, S. N., Garnet peridotite xenoliths in minette from the Navajo volcanic field, Extended Abstracts, Second International Kimberlite Conference, Santa Fe, New Mexico, 1977b.

Faure, G. and J. L. Powell, Strontium Isotope Geology, 188pp., Springer Verlag, Berlin, 1972.

Gregory, H. E., Geology of the Navajo country. A reconnaissance of parts of Arizona, New Mexico, and Utah, U. S. Geol. Survey Prof. Paper, 93, 161 pp., 1917.

Irvine, T. N., and W. R. A. Baragar, A guide to the classification of the common volcanic rocks, Canadian J. Earth Sci., 8, 523-548, 1971.

Irving, A. J., A review of experimental studies of crystal/liquid trace element partitioning Geochim. Cosmochim. Acta, in press.

Kay, R. W., and P. W. Gast, The rare earth content and origin of alkali-rich basalts, J. Geol., 81, 653-682, 1973.

Kushiro, I., H. S. Yoder, and B. O. Mysen, Viscosities of basalt and andesite melts at high pressure, J. Geophys. Res., 81, 6351-6356, 1976.

Lindsley, D. H., D. Smith, and S. E. Haggerty, Petrography and mineral chemistry of a differentiated flow of Picture Gorge basalt near Spray Oregon: geologic setting and mechanism of differentiation, Carnegie Inst. Wash. Yearb., 69, 264-269, 1971.

Lorenz, V., On the formation of maars, Bull. Volcanol., 37, 183-204.

McDowell, F. W., M. F. Roden, R. J. Arculus, and D. Smith, Potassic volcanism and associated inclusions on the Colorado Plateau (abstract), Geol. Soc. Amer. Abstracts with Prog., 10, 116, 1978.

McGetchin, T. R., and L. T. Silver, A crustal-upper mantle model for the Colorado Plateau based on observations of crystalline rock fragments in the Moses Rock dike, J. Geophy. Res., 77, 7022-7037, 1972.

McGetchin, T. R., D. Smith, S. N. Ehrenberg, M. Roden, and H. G. Wilshire, Navajo kimberlites and minettes, Field Guide, Second International Kimberlite Conference, Santa Fe, New Mexico, 1977.

McNown, J. S., and J. Malaika, Effects of particle shape on settling velocities at low Reynolds numbers, Trans., AGU, 31, 74-82, 1950.

Mercier, J. C., and A. Nicolas, Textures and

fabrics of upper mantle peridotites as illustrated by basalt xenoliths, J. Petrology, 16, 454-487, 1975.

Modreski, P. J., The melting of phlogopite in the presence of enstatite, aluminous enstatite, diopside, spinel, corundum, and pyrope, Carnegie Inst. Wash. Yearb., 71, 392-396, 1972.

Modreski, P. J. and A. L. Boettcher, Phase relationships of phlogopite in the system K_2O-MgO-CaO-Al_2O_3-SiO_2-H_2O to 35 kilobars: a better model for micas in the interior of the earth, Amer. J. Sci., 273, 385-414, 1973.

Naeser, C. W., Geochronology of the Navajo-Hopi diatremes, J. Geophys. Res., 76, 4978-4985, 1971.

Nicholls, J., Studies of the volcanic petrology of the Navajo-Hopi area, Arizona, Ph.D. dissertation, Univ. of California at Berkeley, Berkeley, 1969.

O'Hara, M. J. and E. L. P. Mercy, Eclogite, peridotite and pyrope from the Navajo country, Arizona and New Mexico, Amer. Mineral., 51, 336-352, 1966.

Peters, T., W. C. Luth, and O. F. Tuttle, The melting of analcite solid solutions in the system $NaAlSiO_4$-$NaAlSi_3O_8$-H_2O, Amer. Mineral., 51, 736-753, 1966.

Pike, J. E., and E. C. Schwarzman, Classification of textures in ultramafic xenoliths, J. Geol., 85, 49-61, 1977.

Poldevaart, A. and H. Hess, Pyroxenes in the crystallization of basaltic magma, J. Geol., 59, 472-489, 1951.

Powell, J. L. and K. Bell, Strontium isotopic studies of alkalic rocks: localities from Australia, Spain, and the western United States, Contrib. Mineral. Petrol., 27, 1-10, 1970.

Roden, M. F., Field geology and petrology of the minette diatreme at Buell Park, Apache County, Arizona, M.A. thesis, Univ. of Texas at Austin, Austin, 1977.

Schmitt, H. H., G. A. Swann, and D. Smith, The Buell Park kimberlite pipe, northeastern Arizona, in: Geology of Northern Arizona, Geol. Soc. Amer., Flagstaff Meeting, 672-698, 1974.

Shaw, H. R., Comments on viscosity, crystal setting, and convection in granitic magmas, Amer. J. Sci., 263, 120-152, 1965.

Shaw, H. R., Viscosities of magmatic liquids: an empirical method of prediction, Amer. J. Sci., 272, 870-893, 1972.

Shaw, H. R., D. L. Peck, T. L. Wright, and R. Okamura, The viscosity of basaltic magma: an analysis of field measurements in Makaopuhi Lava Lake, Hawaii, Amer. J. Sci., 266, 225-264, 1968.

Simkin, T., and J. V. Smith, Minor element distribution in olivine, J. Geol., 78, 304-325, 1970.

Smith, D., The origin and interpretation of spinel-pyroxene clusters in peridotite, J. Geol., 85, 476-482, 1977.

Smith, D., and S. Levy, Petrology of the Green Knobs diatreme and implications for the upper mantle below the Colorado Plateau, Earth and Planet. Sci. Letters, 29, 107-125, 1976.

Smith, J. V., Feldspar Minerals, Vol. 2, Chemical and Textural Properties, Springer Verlag, New York, 1974.

Sparks, R. S. J., H. Pinkerton, and R. MacDonald, The transport of xenoliths in magmas, Earth and Planet. Sci. Letters, 35, 234-238, 1977.

Stormer, J. C., Calcium zoning in olivine and its relationship to silica activity and pressure, Geochim. Cosmochim. Acta, 37, 1815-1821, 1973.

Weed, W. H., and L. V. Pirsson, Highwood Mountains of Montana, Geol. Soc. Amer. Bull., 6, 389-422, 1895.

Weed, W. H. and L. V. Pirsson, The Bearpaw Mountains, Montana, Amer. J. Sci., IVth Ser. 1, 283-301, 351-362, 1896.

Wilkinson, J. F. G., Analcimes from some potassic igneous rocks and aspects of analcime-rich igneous assemblages, Contrib. Mineral. Petrol., 18, 252-269, 1968.

Williams, H., Pliocene volcanoes of the Navajo-Hopi country, Geol. Soc. Amer. Bull., 47, 111-172, 1936.

Wright, T. L. and P. C. Doherty, A linear programming and least squares computer method for solving petrologic mixing problems, Geol. Soc. Amer. Bull., 81, 1995-2008, 1970.

THE OKA CARBONATITE COMPLEX: MAGNETITE COMPOSITIONS AND THE RELATED ROLE OF TITANIUM IN PYROCHLORE

Brendan M. McMahon and Stephen E. Haggerty

Department of Geology, University of Massachusetts, Amherst, Massachusetts 01003

Abstract. Electron microprobe analyses of magnetites from the Oka carbonatite complex and associated alkaline rocks show that intermediate members of the melteigite-urtite series, ijolites, contain high concentrations of MnO (~12.0 wt% maximum, with an average of 8.01 wt%), but with TiO_2 (4.5 wt%), Al_2O_3 (2.2 wt%) and MgO (2.8 wt%) contents that are comparable to the compositions of magnetites in diopside-bearing carbonatites. Magnetites of the jacupirangite-okaite series also contain significant contents of MnO; these reach a maximum on the okaite-nepheline okaite end of the series (5.5 wt%) and decrease progressively to jacupirangite (3.5 wt%). Alnoitic magnetites are proportionately lower in MnO (0.5-2.0 wt%), but higher in TiO_2 (3.5 wt%) and MgO contents (7.5 wt%) than those of the associated carbonatites, or those of the alkaline suite. Kimberlites from the Isle Bizard diatreme have low modal concentrations of magnetite; these are low in MnO (<0.25 wt%), have high oxidation indices, $Fe^{3+}/(Fe^{2+} + Fe^{3+}) = 0.636$, and intermediate MgO (3.5-4.5 wt%), and Al_2O_3 (5.5 wt%) contents. The highest MnO contents in magnetite from the complex are in richterite sövites, and these average ~12.0 wt%. Reactions between these magnetites and the calcite matrix results in Mn-siderite, and it is within these areas that pyrophanite-rich ($MnTiO_3$) ilmenites are observed containing between 25-75 mole % $MnTiO_3$.

The results of a coupled pyrochlore study may be summarized as follows: (1) at least six distinct pyrochlore varieties are identified ranging from those that are Zr-rich to others that have high contents of REE; (2) pyrochlore is complexly zoned on the micron to millimeter scale and the most complex zones are at the margins of crystals; (3) the margins of crystals are zoned with respect to TiO_2 and REE, suggesting that the final liquid was enriched in these constituents; (4) Nb is fractionated at an early stage in carbonatite crystallization, followed by TiO_2 and REE, specifically Ce and Nd; (5) in the absence of high U contents, CaO is virtually constant at ~18 wt% and we conclude that the activity of Ca was buffered by CaO saturation.

Carbonatitic magnetites from the Oka complex are characterized by high MnO contents and low TiO_2 concentrations, and we propose that the deficiency in TiO_2 is related to co-precipitating pyrochlore and to the high affinity of Ca for Ti. The observation that the terminal stages of kimberlite formation results in small scale carbonatitic fractionation, with oxides having high MnO contents, is supported by the data on oxides from the Oka complex.

Introduction

Although much debate continues to be centered on the role of immiscible carbonatite fluids, on the relationship of carbonatites and kimberlites (e.g. Mitchell, 1978a) and on the nature of heavy element fractionation in the upper mantle, there is now a growing body of data which tends to indicate that carbonatite liquids are an integral, but enigmatic, phase of the terminal stages of kimberlite formation (e.g. Haggerty, 1975; McMahon and Haggerty, 1976).

Our previous studies have concentrated on the opaque mineral chemistry in kimberlites and these have provided some insight to the progressive changes in composition and in f_{O_2} as a function of kimberlitic evolution (Haggerty, 1973). The early formation of the opaque mineral oxides in kimberlites, their continued growth during a substantial period of crystallization, and their sensitivity to redox changes, makes this mineral group an ideal indicator of the compositional variations that are attendant during kimberlite and carbonatite formation. In a continued effort to understand the potential relationship between kimberlites and carbonatites and kimberlite formation, we have directed our attention in this initial study to a systematic examination of the mineral chemistries of magnetite, ilmenite and pyrochlore in a wide spectrum of host rocks from the Oka carbonatite complex. We conclude that the opaque mineral oxides in the Oka complex are comparable to those produced during the final stages of crystallization typical of many kimberlites, and

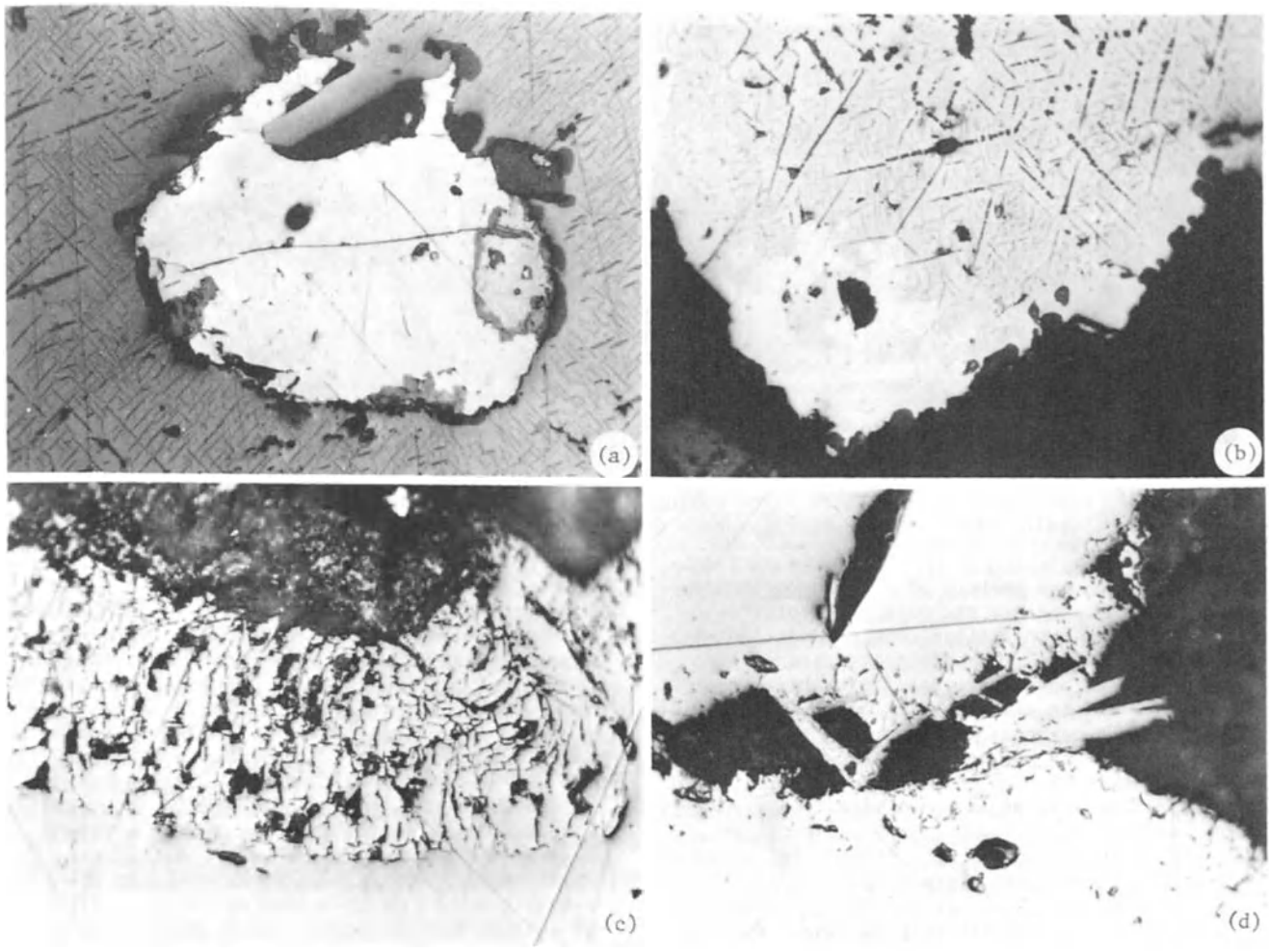

Fig. 1. Photomicrographs of sövite magnetites in which coarse lamellae of pleonaste-hercynite have developed along {lll} spinel planes. The large white inclusion in (a) is a complex intergrowth of pyrrhotite + pentlandite. Alteration of this assemblage along the margins of the inclusion consist of marcasite + magnetite. The light gray area in (b) is maghemite. *Finger-textured*, Mn-depleted magnetite, which is intergrown with Mn-siderite is illustrated in (c). An incipient form of the *finger-texture* is shown in (d) in association with fresh and partially altered pyrophanite laths. Scale: Width of photomicrograph = 0.15 mm. Oil-immersion and reflected light.

that these are characterized by high manganese contents. One of several major differences between kimberlites and carbonatites is the virtual absence of large radius, high valency cations (e.g. Th, U, Ce, Zr, Hf, Nb, Ta) in the former and their widespread association in the latter, specifically in the minerals pyrochlore and latrappite (Nb-perovskite). The magmaphile (i.e. high partitioning coefficients between liquid and crystal) nature of these elements may account for their preferred concentration in carbonatites if it is assumed that carbonatitic liquids persist beyond those of kimberlite formation. Although this study does not shed any new light on the petrological affinities of these elements it has established that the systematics of mineral zonation trends are complex, that Ti partitioning is preferentially into pyrochlore in the presence of coexisting opaque mineral oxides, and that a consistent heavy element paragenesis in pyrochlore is the exception rather than the rule.

The Oka carbonatite complex is located in the Monteregian Hills, 20 miles NW of Montreal, Quebec, Canada. The estimated radiometric age of this atectonic intrusive complex is approximately 117 m.y. (Gold, 1966; Shafiqullah et al., 1969) placing it in the lower Cretaceous. Erosion has exposed the alkaline igneous sequence to the ring dyke and cone sheet level and an entire cross-section of calc-alkaline igneous rocks appears to be present with cross-cutting relationships indicating the relative order of emplacement (Gold, 1966, 1969). Among the alkaline silicate rocks

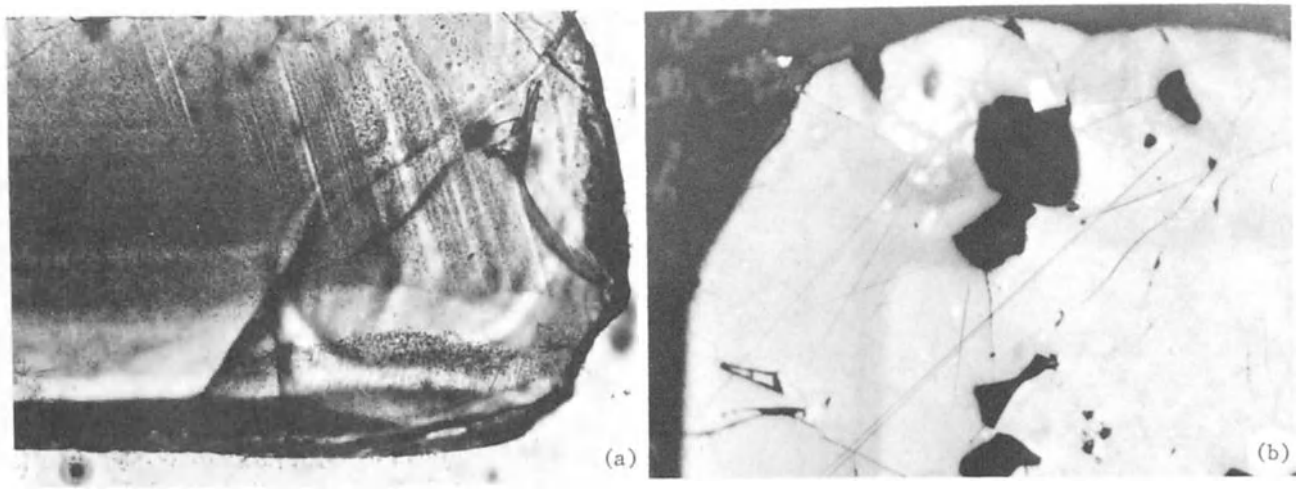

Fig. 2. Repetitive and concentric fine zoning (a), and coarse banded zoning (b) in sövite pyrochlores. Scale: Width of photomicrographs = 0.15 mm. Oil-immersion and reflected light.

in the complex are members of the jacupirangite-okaite series, and members of the melteigite-urtite series (nephelinites), in association with melilitite, kimberlite and alnoite diatremes. The carbonate rocks (sövites) are highly variable in texture and in silicate mineralogy. The matrix of these carbonatites is dominantly calcite, but enrichment trends in manganese and in iron are present in calcite which has undergone partial reaction with adjacent Mn-rich opaque mineral oxides.

Mineral Microscopy

Magnetite is a ubiquitous phase among the variety of rock types in the Oka carbonatite complex. This mineral is commonly present in euhedral to anhedral phenocrysts but it is also a major constituent of the groundmass assemblage. Primary silicate inclusions within magnetite are relatively rare, whereas large ovoid blebs of pentlandite, pyrrhotite and chalcopyrite complexes are widespread (Fig. 1a). The titanium contents of carbonatitic magnetites are typically low (~5 wt.%), and the oxidation exsolution of ilmenite from these spinels is, hence, relatively sparse. On the other hand, although Mg, Cr, and Al are also present in relatively low abundances, the incidence of hercynite-pleonaste exsolution along {111} spinel planes tends to be common (Fig. 1a-b). A characteristic feature of many magnetites is the presence of a peripheral and concentric reaction zone with the carbonate matrix. This zone varies from being a gradational contact in some crystals to others that exhibit a marked discontinuity with the unaltered portions of the crystal; the zone may vary from <10 μm to 50 μm in width and we describe this zone as *finger textured* as illustrated in Fig. 1c-d.

The low bulk titanium contents of carbonatites (0.05-0.30 wt.%) and the variable concentrations of TiO_2 in the associated alkaline suite (0.66 wt.% in urtite-ijolite to 3.7 wt.% in jacupirangite) of the Oka complex (Gold, 1966) is reflected in the mineralogy of these rocks, and is particularly apparent in the low modal concentrations of ilmenite. Primary ilmenite is restricted to the late stage intercrystalline matrix of these carbonatites (Fig. 1d), but is also present as rare oxidation lamellae in magnetite.

Pyrochlore is a prominently developed mineral in most sövites and is also present as a rare associated phase in members of the melteigite-urtite series. It is present in euhedral phenocrysts, contains an abundance of oxide, silicate, and sulfide inclusions, and exhibits pronounced oscillatory zoning on the sub-micron to millimeter scale (Fig. 2).

Magnetite Mineral Chemistry

Magnetite compositions were determined by electron microbeam analyses in the 10 dominant and distinct rock types that constitute the Oka carbonatite complex (Gold, 1966). Mineral averages are listed in Table 1 and these data are summarized on oxide variation diagrams as a function of rock type in Figs. 3-4.

The distinctive characteristics in major element chemistry in the alkaline suite are: (1) alnoitic magnetites have the highest average MgO (7.85 wt.%) and TiO_2 (8.44 wt.%) contents; (2) okaite and ijolite magnetites have higher average MnO contents (6.48-8.01 wt.%) than alnoite or jacupirangite magnetites (1.49-2.71 wt.%); (3) Cr_2O_3 concentrations in this suite are uniformly low (average = 0.3 wt.%); (4) Al_2O_3 contents are relatively constant and vary between 2.19-4.01 wt%; and (5) although the absolute values of Fe_2O_3 vary from 53.66 to 61.85 wt.% in these magnetites, the oxidation ratio of $FeO/(FeO + Fe_2O_3)$ is within narrow limits, between 0.270 for

TABLE 1. MAGNETITE COMPOSITIONAL AVERAGES FOR OKA CARBONATITES AND ASSOCIATED ALKALINE IGNEOUS ROCKS.

	A	B	C	D	E	F	G	H	I	J	K
MgO	3.93	7.85	2.44	2.96	3.14	2.78	1.50	1.59	4.09	4.13	1.30
Al_2O_3	0.68	3.07	2.99	4.01	4.89	2.19	0.59	1.27	1.66	0.13	0.00
ZrO_2	0.11	0.02	0.09	0.03	0.04	0.00	0.00	0.01	0.04	0.00	0.06
CaO	0.00	0.01	0.10	0.04	0.03	0.00	0.00	0.00	0.03	0.00	0.00
TiO_2	5.83	8.44	2.28	2.94	1.91	4.50	3.80	3.15	3.49	6.30	3.77
Cr_2O_3	0.01	0.01	0.05	0.00	0.01	0.00	0.00	0.05	0.01	0.04	0.00
MnO	0.25	1.49	2.71	6.48	6.10	8.01	7.29	8.11	11.26	11.69	4.46
FeO	30.51	25.99	27.17	23.31	22.93	26.01	25.12	23.77	17.06	18.75	27.88
Fe_2O_3*	59.24	53.66	61.45	60.13	61.85	58.31	60.88	62.73	62.86	58.91	61.95
Total	100.56	100.54	99.44	99.90	100.90	101.83	99.18	100.68	100.50	99.95	99.45

A = Kimberlite
B = Alnoite
C = Jacupirangite
D = Okaite
E = Nepheline okaite
F = Ijolite
G = Diopside sövite
H = Niocalite sövite
I = Monticellite sövite
J = Richterite sövite
K = Richterite sövite with pyrochlore
* = Calculated assuming spinel stoichiometry

nepheline okaites and 0.326 for alnoites.

Among the carbonatites, which include diopside sövite, niocalite sövite, monticellite sövite, and richterite sövites (with and without pyrochlore, respectively), we note that these magnetites have high, but variable, concentrations of MnO (richterite sovite = 11.69 wt.%; pyrochlore-bearing richterite sövite = 4.46 wt.%), that TiO_2 is in the range 3.15-6.30 wt.%, and that Al_2O_3 and Cr_2O_3 are rarely in excess of a total of 1.5 wt.%. Magnetites in richterite-(pyrochlore absent) and monticellite-bearing sövites have relatively high MgO contents (~4 wt.%) in contrast to the pyrochlore, diopside and niocalite sövites which are in the range of 1.3-1.6 wt.%. The ratios of $FeO/(FeO + Fe_2O_3)$ in the sövites are, on average, lower than that of magnetites in the alkaline suite with the former varying between 0.241-0.310, and the latter between 0.270-0.326.

The kimberlitic magnetites from the Oka complex have no internally distinct characteristics in terms of major element chemistry. However, these do differ from the magnetites in the alkaline suite and the magnetites in the sövite series in that MnO contents are extremely low (0.25 wt.%) and the oxidation ratio of $FeO/(FeO + Fe_2O_3)$ is relatively high (0.340).

Magnetites containing the highest average MnO contents are those in richterite and monticellite sövites with 11.69 and 11.26 wt.% MnO respectively (Table 1). The richterite sövites also contain the *finger-textured* reaction mantles (Fig. 1c) and a detailed examination of the zonal and reaction trends in major element chemistry are illustrated in Figs. 3 and 4. The cores of magnetites in the monticellite sövites show a slight depletion in MnO, FeO and Fe_2O_3 contents (Fig. 3a), and correspondingly higher concentrations of MgO and Al_2O_3, with constant TiO_2 values. In contrast, there is a marked manganese enrichment from the cores of magnetites in richterite sövites towards the inner margin of the reaction zones; at the reaction zone, and within the *finger textured* magnetite, the MnO content decreases progressively and reaches a minimum of 0.5 wt.% MnO (Fig. 3b). This variation in MnO is mirror-imaged by variations in FeO contents and is compensated by progressive changes in MgO and TiO_2 contents; the trivalent cations Fe^{3+}, Cr and Al appear to behave independently of this reaction chemistry. The relationship of MnO *versus* MgO for the core-mantle variation and the associated reaction assemblage (Fig. 3b) is illustrated in Fig. 4. The protruding magnetite *fingers* that extend into the groundmass (Fig. 1c) alternate with manganiferous siderite which changes progressively away from the reaction rim into calcite. Changes in MgO contents are continuous (Fig. 3b and 4) but there is a 4-7 wt.% MnO depletion in the *fingered* magnetite, and a substantial increase in FeO (Fig. 3b); the absolute margins of magnetite crystals contain <0.05 wt.% MgO and ~2 wt.% MnO. It is

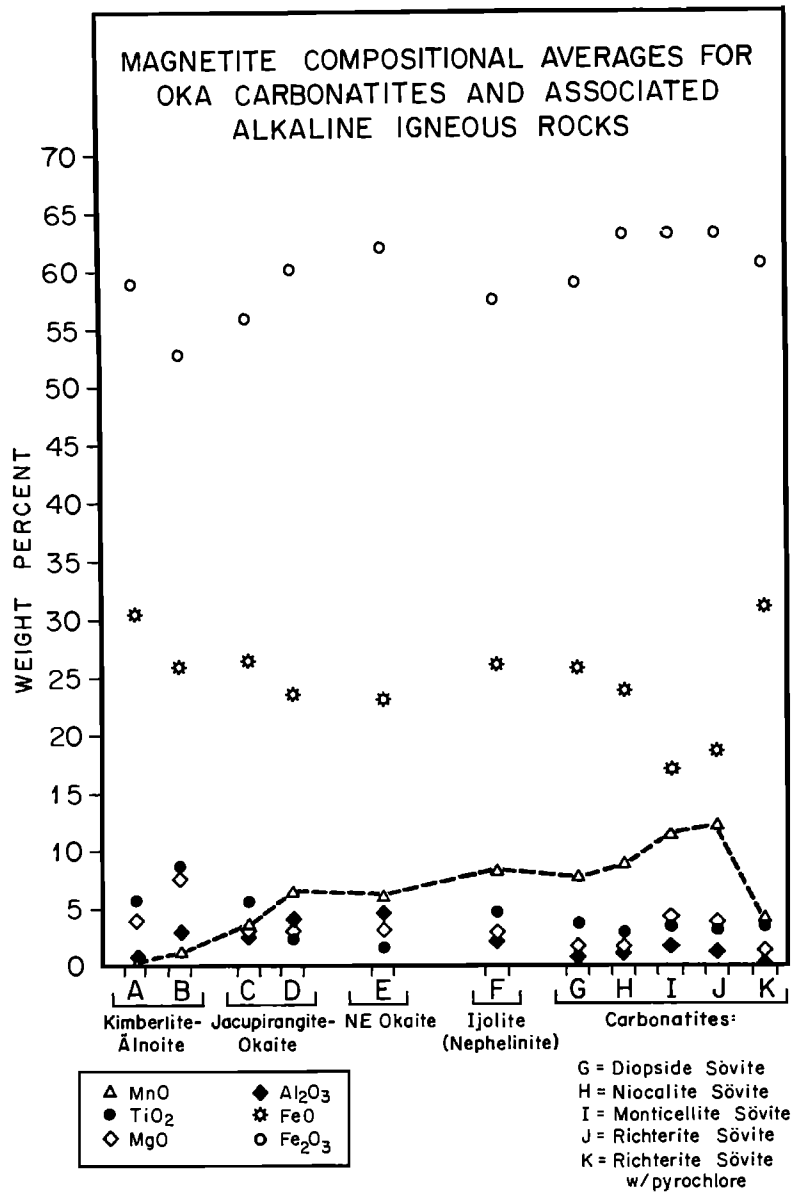

Fig. 3. Oxide variations as a function of rock type for magnetite compositions. The dashed line emphasizes the variation in MnO contents.

within this reaction assemblage that the rare occurrences of discrete crystals of ilmenite-pyrophanite ($FeTiO_3$ - $MnTiO_3$) solid solution members are observed (Fig. 1d). These crystals range from 25-75 mole % pyrophanite and appear unaltered when partially wedged between magnetite phenocrysts, but exhibit extensive alteration to magnetite, Nb-rich rutile, and Mn-siderite in all other regions of the calcite matrix.

In summary, the associated alkaline ultrabasic rocks in their relative order of emplacement are the jacupirangite-okaite series (titanaugite pyroxenites-melilitites), the melteigite-urtite series of the nephelinites (diopside pyroxene-nepheline rocks), and the alnoite-kimberlite diatremes. The magnetites of the jacupirangite-okaite series contain significant MnO contents (5.5 wt.%) on the okaite to nepheline-okaite end of the series and these decrease progressively to the jacupirangite value of 3.5 wt.% (Fig. 4). TiO_2 ranges from 1.5 to 5.5 wt.% with a minimum in nepheline-okaite and a maximum in jacupirangite. Nepheline-okaite magnetites have the lowest Ti/Ti + Cr + Al (cations/24 cations) encountered in this study (0.281). Ti/Ti + Cr + Al increases to 0.325 (Fig. 4) at the titanaug-

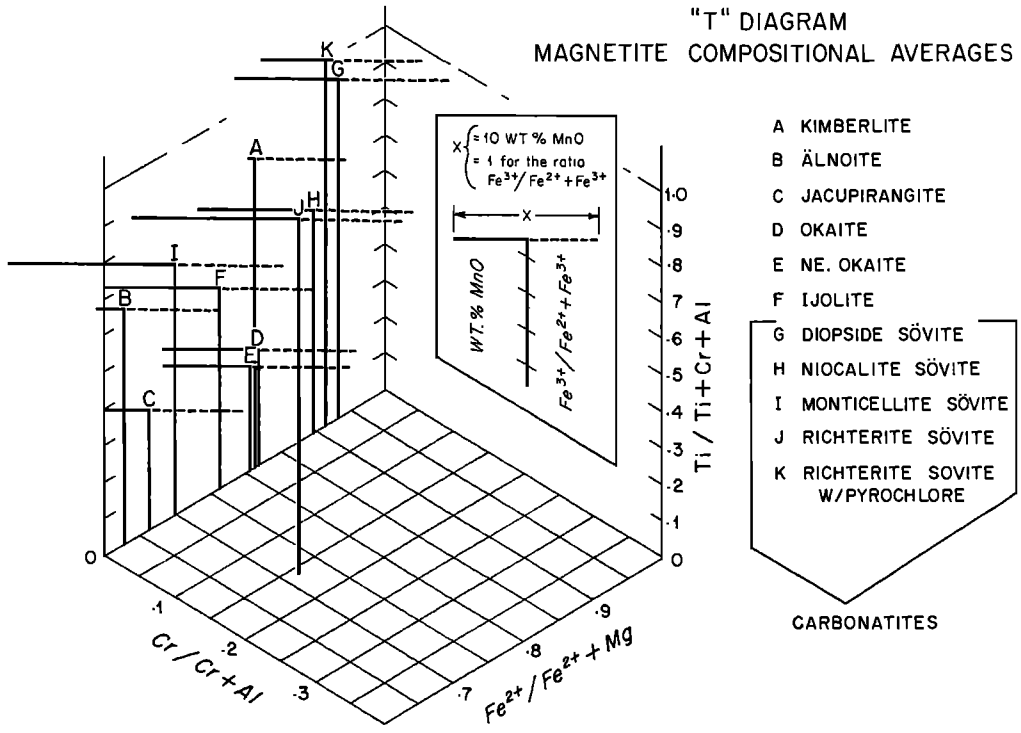

Fig. 4. The "T diagram" emphasizes site occupancy and oxidation ratios. Cr/Cr+Al *vs* Fe^{2+}/Fe^{2+}+Mg represents the base of the spinel prism. The vertical component of the "T" is the ratio Ti/Ti+Cr+Al; the horizontal components are wt% MnO and $Fe^{3+}/Fe^{2+}+Fe^{3+}$ to the left and right respectively, of the "T" apex.

ite end of the series and these magnetites are the most aluminous. MgO remains relatively uniform at 3.5 wt.% throughout the series, whereas Al_2O_3 reaches a maximum of 4.9 wt.% in nepheline-okaite and is at a minimum (2.5 wt.%) for the series in jacupirangite.

The magnetites of the nephelinite series (melteigite-urtite) are only abundant in the intermediate member, ijolite, in which the nepheline/pyroxene ratio ~ 1:1. In ijolite, MnO reaches a maximum for the alkaline silicate rocks at 8.01 wt.%. The contents of TiO_2, Al_2O_3, and MgO average 4.5, 2.2, and 2.8 wt.% respectively and these values are extremely close to those of magnetites in the diopside-bearing carbonatites (MnO = 7.29 wt.%, TiO_2 = 3.5-4.0 wt.%, Al_2O_3 <1 wt.%, MgO = 1.5 wt.%).

The magnetites in alnoites are low in MnO (0.5-2.0 wt.%), high in TiO_2 (3.5 wt.%) and MgO (7.5 wt.%) and have the lowest Fe^{2+}/Fe^{2+} + Mg encountered (0.630) as illustrated in Fig. 4. The magnetites in the Isle Bizard kimberlite have the lowest MnO content of any of the associated rocks (<0.25 wt.%), the lowest modal concentration, and the highest oxidation ratio (Fe^{3+}/Fe^{2+} + Fe^{3+}) = 0.636. TiO_2 is constant at ~5.5 wt.%, Al_2O_3 is <1 wt.% and MgO increases from 3.5 to 4.5 wt.% from crystal cores to mantles.

A comparison of spinel compositions determined in this study from the Oka carbonatite complex, with those of previous studies from Oka (Gold, 1966; Mitchell, 1978a), and with those from other carbonatite complexes (Fleischer, 1965; Prins, 1972; Bergstøl, 1972; Gittens et al., 1975; Mitchell, 1978b) may be summarized as follows: (1) the Oka carbonatite magnetites are low in Cr, Al, Ti and Mg and characteristically high in MnO; (2) the high MnO contents of the Oka magnetites are not typical of those from the East Africa carbonatites (0.4-1.0 wt.% MnO), and this results in part because of oxidation exsolution and the preferential partitioning of MnO into ilmenite along {111} spinel planes; (3) magneties from the Magnet Cove (1.8-2.1 wt.% MnO) and Kaiserstulh complexes are also typically low in MnO, but are high in MgO concentrations (2.6-9.5 wt.%), and this is coupled with the highly aluminous nature of these spinels (6.8-15.1 wt.%); (4) spinel ($MgAl_2O_4$) and Mg-rich magnetites are identified in the Jacupiranga carbonatite, and these are also low in MnO (0.5-0.6 wt.%); and (5) in closely associated carbonatite-kimberlite sequences (e.g. Premier, Oka and Arvida) relatively high MgO (~5 wt.%) and MnO (~12 wt.% max.) contents are typical of magnetites in the carbonatitic fraction of these complexes.

Pyrochlore Mineral Chemistry

The principle results of a detailed electron microprobe study of the pyrochlore mineral group in the Oka carbonatite complex are presented here and a more complete discussion will appear elsewhere. Our emphasis in this study, which is based on a 19 element matrix (F, Na, Mg, Al, Si, Sr, Y, Zr, Nb, Ca, Ti, La, Ce, Nd, Mn, Fe, Ta, Th, U), is related to the zonation trends that are present in pyrochlore, specifically with respect to the effects of coupled substitution, and is related also to the partitioning behavior of Ti in the context of the coexisting opaque mineral oxides, which are generally low in TiO_2.

The empirical formula for the pyrochlore mineral group may be expressed in two different forms:

AyB_2X_{7-z} where $0<y<2$ and $0<z<1.5$.

The A site = Ca, Na, U^{4+}, U^{6+}, Fe^{2+}, Th, Mn^{2+}, Sr, K, the light lanthanides La → Eu (ΣCe), and Y + the heavier lanthanides Ga → Lu (ΣY). The B site = Nb, Ta, Ti, Fe^{3+}, Sb^{5+}, Zr, Sn and W. X = O, OH, F and perhaps Cl, N.

Alternatively the formula may also be expressed as:

$A_{2-m}B_2O_6$ (O, OH, F)$_{1-n}.pH_2O$ (Hogarth, 1977). Three subgroups are recognized based on the B-atoms Nb, Ta, and Ti: the pyrochlore subgroup has Nb + Ta > 2Ti and Nb > Ta; the microlite subgroup in which Nb + Ta > 2Ti and Ta ≥ Nb; and the betafite subgroup in which 2Ti ≥ Nb + Ta. Within the subgroups individual species are defined with respect to the A-atoms (Na, Ca, K, Sn, Ba, REE, Pb, Bi, U) as outlined by Hogarth (1977).

Studies of the pyrochlore mineral group from the Oka complex have been undertaken by Hogarth (1961), Nickel (1962), Gold (1966), Perrault (1968), and by Petruk and Owens (1975). Complex optical and elemental zoning was recognized in these studies and our data support the broad color classification adopted by Gold (1966) which shows that at least 5 types of pyrochlore are present in the Oka complex. These are: Type 1 - deep red to reddish brown thorium-rich uranpyrochlore; Type 2 - chocolate brown ceriopyrochlore; Type 3 - red sodium-rich pyrochlore; Type 4 - black zirconium-rich pyrochlore; and Type 5 - buff pyrochlore with exceptionally high concentrations of Nb_2O_5 (65 wt% *versus* 40.0-57.0 wt%), fluorine (4.6 wt% F), and sodium (6.2 wt% Na_2O). In addition to these pyrochlores we have also observed a variety of green to greenish brown pyrochlores which are high in Na_2O (~3 wt%), F (~2 wt%), Nb_2O_5 (~60 wt%) and Ce_2O_3 (~5 wt%) but characteristically low in FeO (~1.5 wt%).

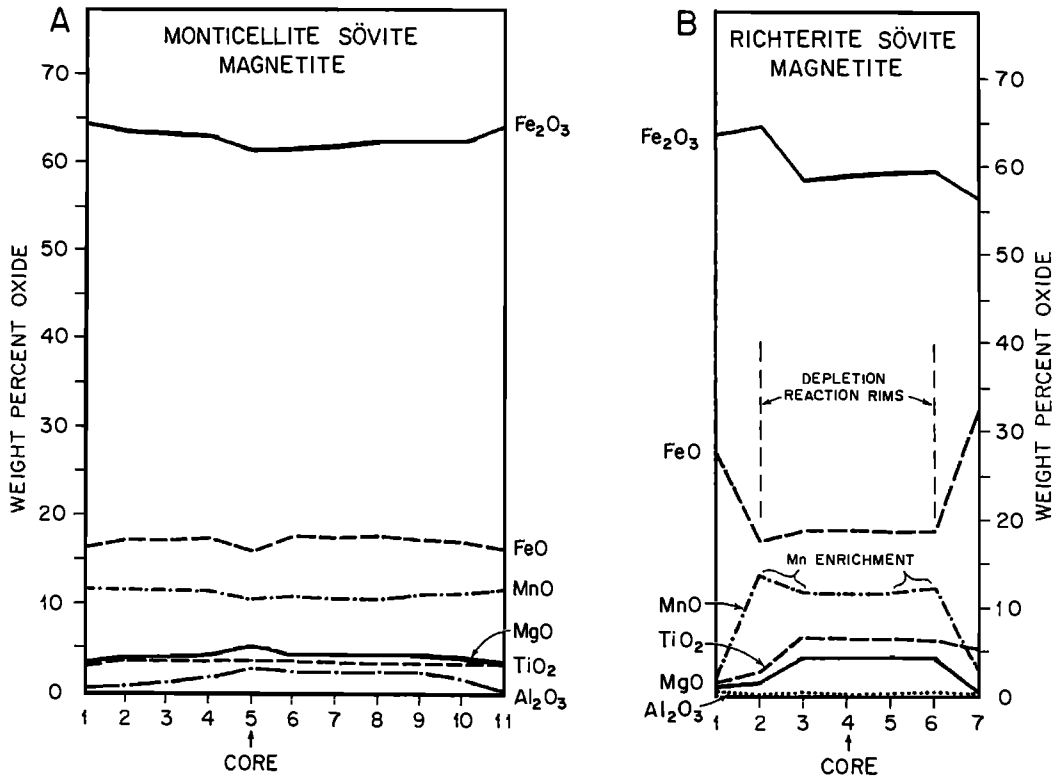

Fig. 5. Core-mantle compositional trends in monticellite sövite (A) and richterite sövite (B) magnetites, respectively. Mn-depletion reaction rims are present in (B), and these are associated with the *finger* textures illustrated in Fig. 1c-d.

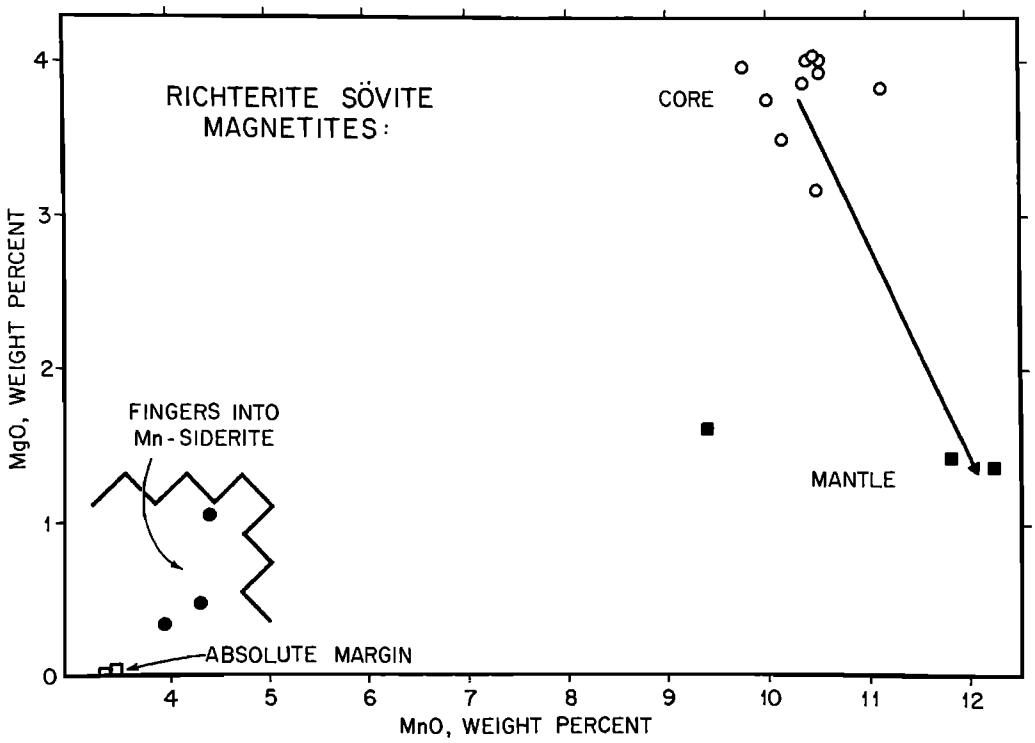

Fig. 6. A plot of MgO *versus* MnO for a magnetite in a richterite sövite which exhibits the *finger textured* reaction margin as illustrated in Fig. 1c-d.

In Fig. 7 we have contrasted the pyrochlore zonation in crystals from a diopside sövite with those from a richterite sövite for variations of TiO_2 *versus* Nb_2O_5, TiO_2 *versus* Ce_2O_3, and for Ce_2O_3 *versus* Nd_2O_3. These relationships are an expression of B site substitution (i.e. Ti and Nb), of A and B site substitution (i.e. Ti and Ce), and of cationic substitution exclusively in the B site (i.e. Ce and Nd). The A site trend and the A-B site trends, which involve titanium, show that TiO_2 increases towards the margins of pyrochlore crystals but the data also show: (1) that reversals in trends are possible; and (2) that hairpin loop variations are characteristic. High concentrations of Ce_2O_3 are clearly responsible, in part, for the variations in TiO_2 systematics in these richterite and diopside sovite pyrochlores, and the maximum of 10.6 wt.% Ce_2O_3 that we have observed at the margins of crystals is the highest that has yet been recorded from the Oka complex; values between 2 and 8 wt.% Ce_2O_3 appear to be more typical. Among the substitutional trends that are possible within the A site for the REE group, we note that Nd-Ce variations also exhibit the reversals and hairpin characteristics that are present in the Ti relationships. In particular, it is the outermost zones of these crystals that are the most complex and from these data we conclude: (1) that the magma was highly enriched in Ti and REE at the terminal stages of carbonatitic crystallization; (2) that the liquid was highly fluidal or that the magma chamber was intensely convective; and (3) that the relative partitioning coefficients of Ti among pyrochlore, co-crystallizing opaque mineral oxides, and liquid is that TiO_2 fractionation is highest in pyrochlore, followed by the oxides, and lastly by the residual liquid.

The betafite end member of the pyrochlore mineral group ($2Ti \geq Nb + Ta$), although not recognized in the Oka carbonatite complex, shows that Ti may be a significant component of this mineral series. The concentrations of TiO_2 that have been determined in this study and previous analyses of pyrochlore from the Oka complex vary between 2.6 and 10.4 wt.% TiO_2, and these contrast with the TiO_2 contents of coexisting magnetite solid solution members which range from 0.83 to 7.45 wt.% (Gold, 1966), but are most commonly in the 2-4 wt.% TiO_2 range for members of the carbonatite suite. An important facet of the behavior and the partitioning characteristics among crystal-liquid and crystal-crystal equilibria of Ti is related to the activity of Ca and the high affinity of Ca for Ti (Verhoogen, 1962a, 1962b). Our analyses of pyrochlore show that CaO is virtually constant at 18 wt%, a value that is consistently reported in the averages obtained in other investigations (Gold, 1966; Perrault, 1968; Petruk and Owens, 1975);

the only exceptions are those pyrochlores that are highly enriched in uranium (Petruk and Owens, 1975) in which the CaO content of the A site decreases to a minimum of 5 wt% CaO.

In summary, we have established: (1) that Nb is fractionated at an early stage in pyrochlore petrogenesis and is gradually replaced by Ti with increasing degrees of crystallization; (2) that the rare earth elements, Ce and Nd correlate with TiO_2 concentrations from pyrochlore crystal cores to margins; (3) that Ti, Ce and Nd vary in oscillatory patterns that are most complex at the margins of pyrochlore crystals; and (4) that in the absence of high uranium concentrations, the activity of Ca is relatively constant and that Ti is preferentially partitioned into pyrochlore, resulting in low Ti-magnetite and rare ilmenite.

Summary and Conclusions

A characteristic feature of the terminal stages of kimberlite crystallization is the high incidence of primary calcite, perovskite ($CaTiO_3$), and Mn-rich opaque mineral oxides (Haggerty, 1973; 1975; 1976; McMahon and Haggerty, 1976; Raber and Haggerty, 1978). These observations have resulted in the proposal that immiscible carbonatite liquids may fractionate from the more silicious kimberlite at the intrusive or fluidization stage of kimberlite formation. However, the overall relationship of carbonatites, kimberlites and their associated alkaline complexes is highly contentious and is, for example, regarded by Mitchell (1978) as a matter of "myth or fiction". The supportive documentation that Mitchell presents is impressive and we may conclude that although kimberlites and carbonatites may not in fact be related in the upper mantle petrogenesis of these rock types there is, nevertheless, a tantalizing episode of kimberlite formation which does result in carbonatitic fractionation. The extent of such fractionation may, of course, be limited to only a small scale as is the case of the Benfontein sill (Dawson and Hawthorne, 1973) and may not be applicable to large complexes.

Our approach to this study was motivated by the following questions: (1) How do carbonatite oxides differ from those of kimberlites?; (2) Do carbonatite oxides reflect the final stages of kimberlite oxide crystallization?; and (3) Because Ti and Ca are major constituents of intracrystalline kimberlite groundmass assem-

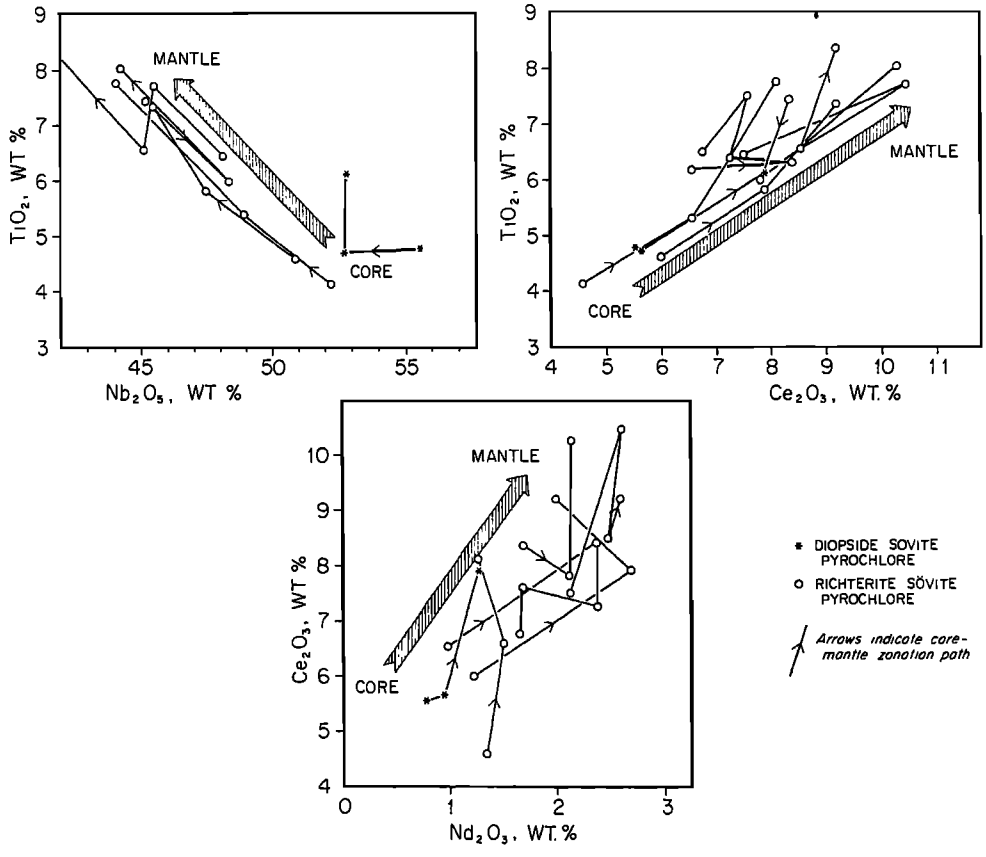

Fig. 7. Sövite-bearing pyrochlores illustrating core-mantle variations in the A site (TiO_2 *versus* Nb_2O_5), between the A and B sites (TiO_2 *versus* Ce_2O_3), and in the B site (Ce_2O_3 *versus* Nd_2O_3) exclusively.

blages and have the appearance of carbonatitic affinities, do these assemblages, in fact, bear any resemblance to the mineralogy and chemistry of carbonatites?

We conclude in general that the oxides from the Oka carbonatite complex are comparable, in terms of mineral chemistry, to those of the final stages of kimberlite formation and this is manifested specifically in the MnO contents of magnetite solid solution members along the join magnetite-jacobsite ($MnFe_2O_4$). A comparison between oxides in the Oka complex with those in other carbonatites is compounded by two independent effects: The first is related to the oxidation exsolution of magnetite solid solution members, which yield ilmenite-pyrophanite members along {111} spinel planes; induced separation of the rhombohedral phase results in an elemental partitioning of Mn and the spinel phase has, hence, been interpreted to contain low MnO contents (e.g. Prins, 1972), whereas in reality the primary magnetite must have contained substantial proportions of MnO. The second effect is related to the TiO_2 contents of carbonatitic magnetites; these are typically low in titanium in the Oka sövites and are also characteristically low in other carbonatites. An explanation of the Ti-deficiency in carbonatitic magnetites is perhaps most appropriately expressed in terms of the extraordinarily high Nb contents of carbonatites, the relationship of Nb and Ti, Ce and Ti, and of Ce and Nd in coexisting pyrochlore. From these data we suggest that because carbonatites are highly enriched in REE, are saturated in Ca, and have high Ti contents in their late stage liquids that titanium is preferentially fractionated into pyrochlore, and that this results in low Ti-magnetite and in low modal concentrations of ilmenite.

Magnetite compositional variations in the Oka carbonatite suite, and the associated alkaline complex show that these are typically characterized by high MnO contents, and that these range from a maximum of ~12 wt.% MnO in richterite sövites, to ~8 wt.% MnO in ijolites, ~6 wt.% in okaites, ~3 wt.% MnO in jacupirangite, ~1.5 wt.% MnO in alnoite, and ~0.25 wt.% MnO in the Isle Bizard kimberlite. Magnetite crystals are zoned with respect to MnO contents from crystal cores to margins, and in some instances have reacted with the carbonate matrix to produce Mn-siderite.

Although the regional relationships between kimberlites and carbonatites remain enigmatic, these rock types do appear to have some cogenetic association.

Acknowledgments

The sample collection used in this study was provided by David P. Gold of the Department of Geology, Pennsylvania State University. Laboratory support was provided by NSF under grant EAR76-23787 (principle investigator S.E.H.). The microprobe facility is supported by NSF (GA-74206) and by the University of Massachusetts. Detailed reviews of an earlier version of the manuscript were made by B. Mysen, D. Eggler and N. Boctor. Credit for skillful drafting is due to Marie Litterer. To all we express our sincere appreciation.

References

Bergstøl, S., The jacupirangite at Kodal, Vestfold, Norway, Min. Depos. (Berl.), 7, 233-246, 1972.

Dawson, J.B., and J.B. Hawthorne, Magmatic sedimentation and carbonatitic differentiation in kimberlite sills at Benfontein, South Africa, J. Geol. Soc. Lond., 129, 61-85, 1973.

Fleischer, M., Composition of magnetite as related to type of occurrence, U.S. Geol. Surv., 525-D, 82-84, 1965.

Gittins, J., R.H. Hewins, and A.F. Laurin, Kimberlitic-carbonatitic dikes of the Saguenay River Valley, Quebec, Canada, Phy. Chem. Earth, 9, 137-148, 1975.

Gold, D.P., The minerals of the Oka carbonatite and alkaline complex, Oka, Quebec, Min. Soc. India, IMA, 109-125, 1966.

Haggerty, S.E., Spinels of unique composition associated with ilmenite reactions in the Liqhobong kimberlite pipe, Lesotho, Lesotho National Development Corporation, Maseru, in Lesotho Kimberlites, edited by P.H. Nixon, pp. 149-158, 1973.

Haggerty, S.E., The chemistry and genesis of opaque minerals in kimberlites. Phy. Chem. Earth, 9, 295-307, 1975.

Hogarth, D.D., A study of pyrochlore and betafite, Can. Min., 6, 610-633, 1961.

Hogarth, D.D., Classifications and nomenclature of the pyrochlore group. Amer. Min., 62, 403-410, 1977.

McMahon, B.M., and S.E. Haggerty, Oka carbonatite complex: oxide mineral zoning in mantle petrogenesis, Geol. Soc. Amer. Abs. with Programs, 8, No. 6, 1006, 1976.

Mitchell, R.H., The kimberlite-carbonatite relationships--fact or fiction? (preprint), 1978a.

Mitchell, R.H., Manganoan magnesian ilmenite and titanoclinohumite from the jacupiranga carbonatite, Sao Paulo, Brazil (preprint), 1978b.

Nickel, E.H., Compositional variations in pyrochlore and niobian perovskite from a niobium deposit in the Oka district of Quebec. Dept. of Mines and Tech. Surveys, Canada, Tech. Bull., TB-31, 1-35, 1962.

Perrault, G., La composition chimique et la structure cristalline du pyrochlore d'Oka, P.Q., Can. Min., 9, 383-402, 1968.

Petruk, W., and D.R. Alton, Electron microprobe analyses for pyrochlores from Oka, Quebec, Can. Min., 13, 282-285, 1975.

Prins, P., Composition of magnetite from carbonatites, Lithos, 5, 227-240, 1972.

Raber, E., and S.E. Haggerty, Zircon-oxide reactions in diamond bearing kimberlites (this volume).

Shafigullah, M., W.M. Tupper, and T.J.S. Cole, K-Ar age of the carbonatite complex, Oka, Quebec, Can. Min., 10, 541-552, 1969.

Verhoogen, J., Oxidation of iron-titanium oxides in igneous rocks, J. Geol., 70, 168-181, 1962a.

Verhoogen, J., Distribution of titanium between silicates and oxides in igneous rocks, Amer. J. Sci., 260, 211-220, 1962b.

RELATIONSHIP OF THE MURFREESBORO KIMBERLITE AND OTHER IGNEOUS ROCKS OF ARKANSAS, U.S.A.

Kenneth F. Steele and George H. Wagner

Department of Geology, University of Arkansas, Fayetteville, Arkansas 72701

Abstract. Kimberlite, syenite lamprophyre and carbonatite are exposed in or along the border of the Ouachita Mountain Region in central Arkansas. These types of rocks are often found in intimate association with regard to space, time and tectonic environment. Although the kimberlite and some of the carbonatite exposures in Arkansas are not in close proximity to other types of igneous rocks, these igneous Arkansas rocks appear to be associated chemically, in time and in tectonic environment.

Introduction

Outcrops of igneous rocks in Arkansas are present in the Ouachita Mountain Region, or near its borders. The exposures are of a variety of unusual and rare rocks, including kimberlite, lamprophyre, carbonatite and syenite. However, the kimberlite is not found with these other igneous rocks as has been indicated (Dawson, 1967, p. 248). This paper will be concerned with the relationships of the kimberlite and other igneous rocks in terms of petrography, chemistry, space and time as revealed by the surface exposures.

Petrologic and Spatial Relationships

Murfreesboro Kimberlite

The Murfreesboro kimberlite located in Pike County in the Gulf Coastal Plains along the southern edge of the Ouachita Mountain Region is the site of the only diamond mine in North America (Fig. 1). There are four distinct outcrops of kimberlite, all within 4 km of Murfreesboro. The Prairie Creek intrusion covering 0.3 km^2 is the major one.

Three rock types are associated with the Murfreesboro intrusions: 1) massive porphyritic peridotite, 2) kimberlitic breccia, and 3) associated tuff (Fig. 2). The massive periodotite is composed primarily of olivine phenocrysts (many serpentinized) in a phlogopite groundmass. Pyroxene is also present, and perovskite and magnetite are present in minor amounts. Xenoliths of local sedimentary rock (mostly shale) are present as well as rare fragments of igneous rocks. The mineralogy of the breccia and tuff is similar to that of the massive peridotite (Lewis et al., 1976; Miser and Ross, 1923a). The absence of magnesian ilmenite, enstatite, and chrome diopside and the rarity of garnet are of special interest and have been noted by other workers. (Bolivar and Brookins, 1977). Most of the diamonds have been found in the weathered breccia at Prairie Creek (Thoenen et al., 1949).

Scott County Peridotite

A small 2 m wide peridotite sill resembling the kimberlite at Murfreesboro is exposed along Freedom Creek in Scott County (Fig. 1). This peridotite contains phenocrysts of phlogopite and serpentinized olivine in a groundmass of phlogopite, calcite and magnetite. The Scott County peridotite differs from the Murfreesboro samples in that no diamonds have been found and there is little brecciation at this site (Miser and Ross, 1923b).

Carbonatite

Arkansas carbonatite occur as massive carbonatites associated with the Magnet Cove and Potash Sulfur Springs complexes and as smaller brecciated types along the northern edge of the Ouachita Mountains in Perry and Conway Counties (Wagner and Steele, 1978, and Fig. 1). These smaller carbonatite intrusions differ from those associated with the igneous complexes in terms of: 1) size - they occur as dikes, sills and circular plugs only a few meters across, 2) xenoliths - they contain predominantly shale xenoliths from the country rock, although carbonatite xenoliths are present and at one locality rounded syenite xenoliths presumably from the basement are abundant. The larger carbonatites at Magnet Cove and Potash Sulfur Springs in comparison have appreciably fewer xenoliths or are devoid of them. 3) texture - they are composed of fine-grained, gray calcite crystals and many large biotite

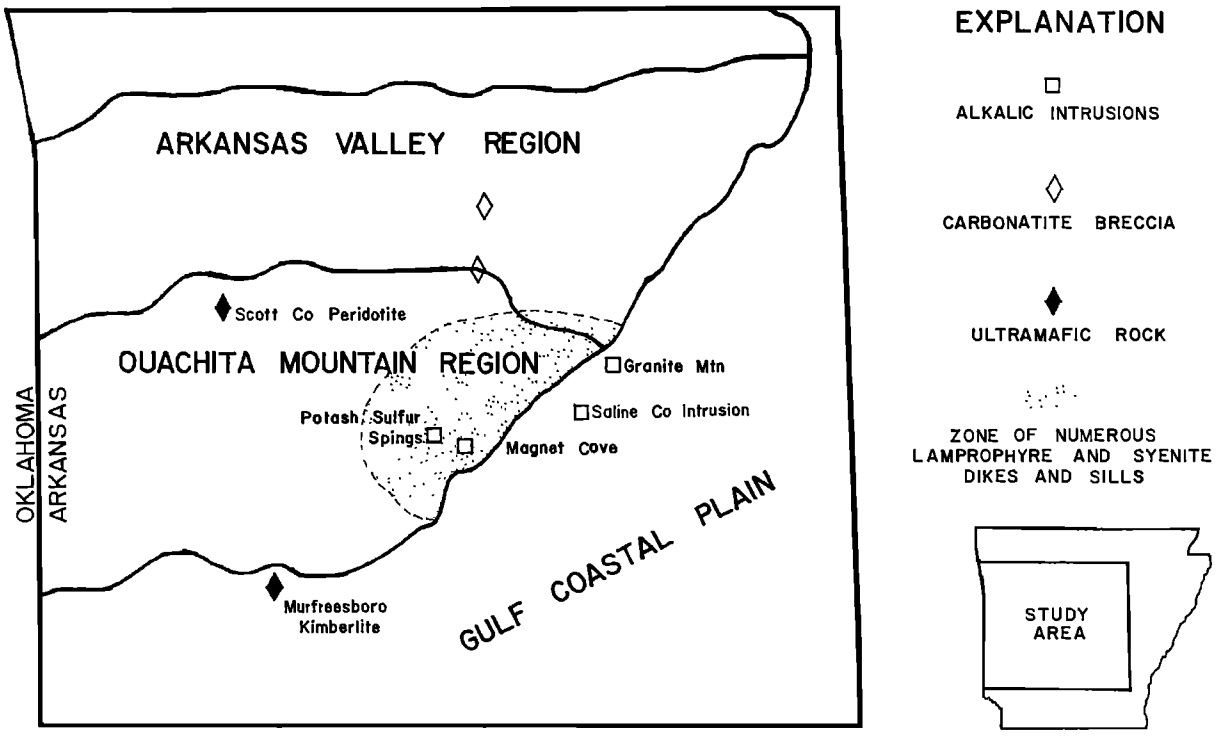

Fig. 1. Surface outcrops of major igneous activity in Arkansas, U.S.A. Small map shows location of Ouachita Mountain Region in Arkansas.

phenocrysts several centimeters across; whereas, the carbonatite associated with the syenite is composed of large, white calcite crystals and if biotite is present it may have a maximum diameter of about 0.5 centimeters. 4) associated igneous rocks - they are about 20 km from the nearest exposed igneous dikes.

Syenite and Lamprophyre

The most abundant rock types, lamprophyre and feldspathoidal syenite intrusions, are concentrated at the eastern edge of the Ouachita Mountains (Fig. 1). Althouth various types of lamprophyre are present as thin dikes and sills, monchiquite and ouachitite are the dominant varieties (Steele and Robison, 1976). Syenite occurs as tinguaite dikes and sills and also as larger intrusions. The largest intrusion is located at Granite Mountain in Pulaski County about 150 km northeast of the Murfreesboro kimberlite. Granite Mountain is predominantly pulaskite. Williams (1891) introduced the term pulaskite to include those rocks that are trachytic in texture and composed of orthoclase, biotite, hornblende, and lesser amounts of augite, nepheline and sodalite. Although several types of syenite dikes cut the pulaskite, the presence of miarolitic syenite warrants special note.

Twenty-four km southwest of Granite Mountain, similar syenite is exposed in Saline County. The nepheline syenite here is the parent material for the bauxite mined in the area. Orthoclase is the dominant constituent of the rock with nepheline, biotite, amphibole and pyroxene being other important constituents. Geophysical data (Stearn, 1930; Malamphy and Vallely, 1944; and Malamphy et al., 1948) indicate that the Granite Mountain and Saline County intrusions are a continuous body. The differences between the two intrusions can be attributed to cooling rate -- pulaskite having cooled more quickly than the nepheline syenite.

About 48 km west of these two larger syenite intrusions are the Magnet Cove, Potash Sulfur Springs and the "V" Intrusive complexes. Magnet Cove has been interpreted as a series of ring dikes: 1) an inner core of carbonatite and ijolite; 2) an intermediate ring of trachyte-phonolite, and 3) an outer ring of nepheline syenite and jacupirangite (Erickson and Blade, 1963). Potash Sulfur Springs has a crude ring structure with the outer part pulaskite, leucopulaskite and fenite, and the center is dominantly nepheline syenite. Isolated exposures of carbonatite and mafic rocks such as melteigite and ijolite are present throughout the complex. Pollack (1965) has interpreted the Potash Sulfur Springs complex as a ring dike similar to Magnet Cove; however, others have suggested that the leucopulaskite and pulaskite is the result of fenitization of the original nepheline syenite

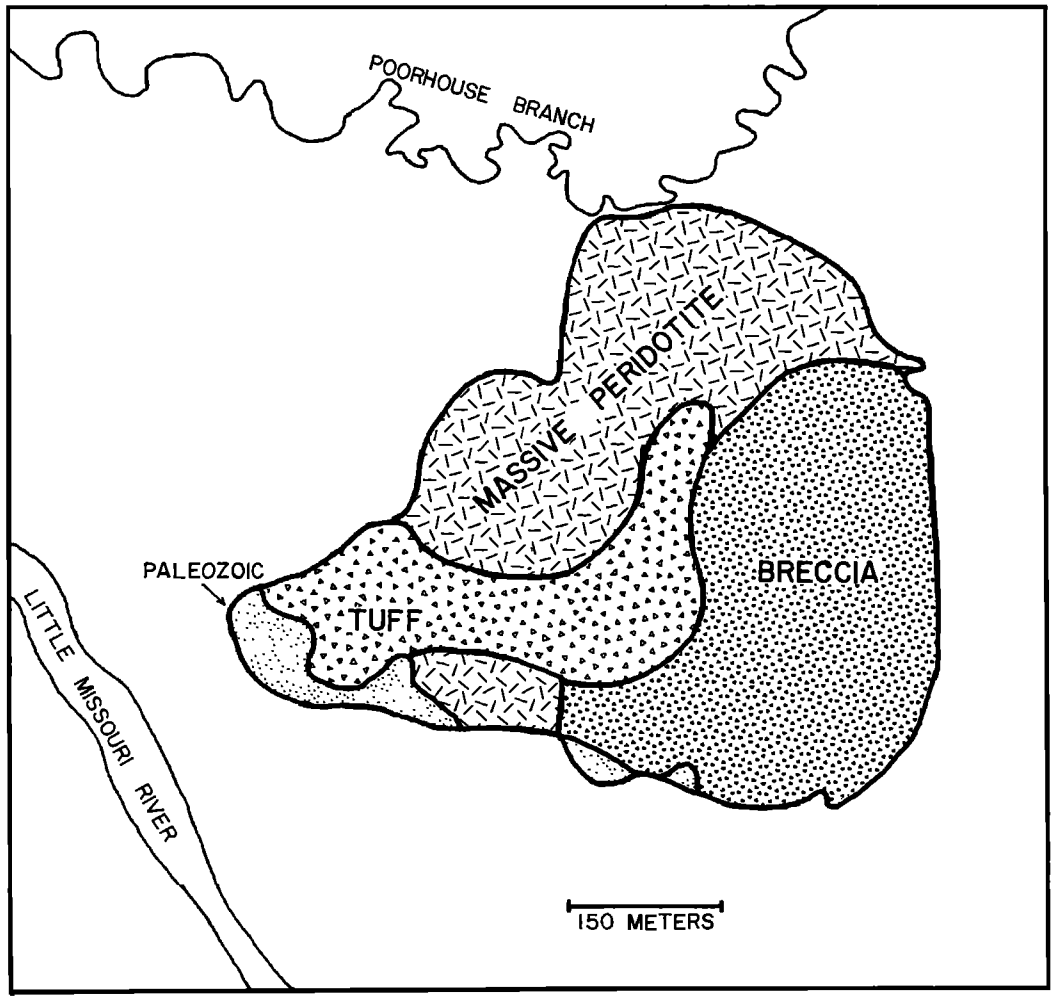

Fig. 2. Generalized geologic map of the Prairie Creek kimberlite intrusion near Murfreesboro, Arkansas.

(Howard and Steele, 1975). The "V" Intrusive is a complex system of criss-crossing dikes. The dikes are of various rock types which listed in order of decreasing age are malignite, melteigite, microijolite, sannaite, feldspathoidal syenite, pulaskite, alkali syenite, alkali syenite aplite and fluorite-pyrite-silica veins (Owens, 1967).

Discussion

From the above descriptions, two observations should be noted. Hypotheses concerning the origin of kimberlite often include rocks of the nepheline syenite-carbonatite suite (Dawson, 1967). The first observation is simply that these latter rocks are present in Arkansas. The second observation is that although there is often an intimate spatial association of rocks of the nepheline syenite-carbonatite suite and kimberlite (Mitchell, 1970; Dawson, 1967 and Heinrich, 1966), the Murfreesboro kimberlite is located 56 km from the nearest igneous outcrops, tinguaite and monchiquite dikes, in Garland County and the small carbonatite breccias are 20 km from other igneous rock types. However, it should be noted that there may be a much more intimate association at depth.

Chemical Relationships

The three varieties of kimberlite at Murfreesboro are similar chemically; however, the tuff contains less Fe, Mg, Ni and Ba than the other two and more Na and K. The massive peridotite has the highest Cr values and the lowest Li, V and Zn values. Differences in Ba content are difficult to ascertain because barite veins are present in the breccia. The Murfreesboro kimberlite exhibits the general chemical characteristics of other kimberlites when compared to other peridotites, namely higher K/Na and lower Mg/Fe ratios, and relatively high Ti, Al, Fe, Cr, K, Li, Sr and Ba. However, the Murfreesboro samples contain less Ca than most other kimberlites (Table 1; and Miser and Ross, 1923a).

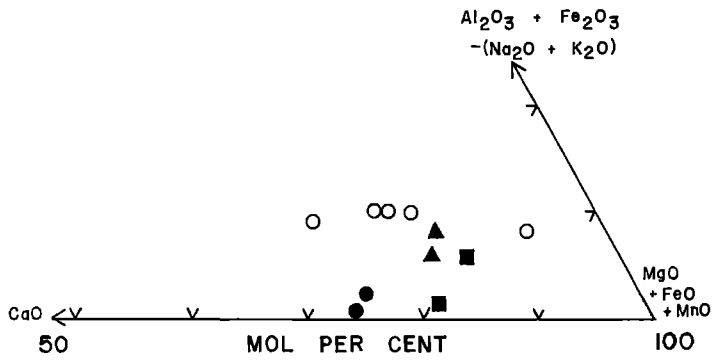

Fig. 3. Af-C-Fm diagram. Norris kimberlite (○; Meyer, 1975), and massive peridotite (■), breccia (▲), and tuff (●) from Murfreesboro, Arkansas.

The differences in the composition of these three varieties of kimberlite cannot be accounted for entirely by the xenoliths; thus, based on chemical data, the massive peridotite is slightly more mafic or primative than the breccia and the tuff is least mafic. Plots of Cr, Al_2O_3, K_2O+Na_2O versus mafic index yield smooth trends suggestive of some differentiation. Although Miser and Ross (1923a) originally considered the massive peridotite to have been intruded first followed by the breccia and then the tuff, recent work based on field and geophysical data (Bolivar and Brookins, 1977; Lewis and Meyer, 1976; and Bolivar et al., 1976) suggests the sequence of intrusion to be breccia, massive peridotite, and associated tuff.

Meyer (1975) suggests that the scatter of points for kimberlite from Norris Lake on an AFC diagram parallel to the CF side is a reflection of the extensive alteration of the samples. It is of interest to note that the Murfreesboro samples exhibit a similar trend (Fig. 3). It is also interesting that the gradual increase in Ca content corresponds with increase in felsic character.

The chemical composition of the Scott County peridotite is similar to other kimberlite. The greatest chemical difference between the Scott County and Murfreesboro rocks is that the Scott County peridotite contains about twice as much Ca. Slight differences in other element concentrations are also present, e.g., the Scott County peridotite also contains more Mn and V, but less Ti than the Murfreesboro samples (Table 1).

In comparing the carbonatites, generally the breccias have the highest elemental values, Magnet Cove next and Potash Sulfur Springs the least. These differences can be explained by varying amounts of minerals and calcite purity. The higher elemental values for the carbonatite breccias compared to the carbonatites from the igneous complexes may be in part due to the presence of xenoliths in these smaller carbonatites. The carbonatite breccias and the Potash Sulfur Springs carbonatite both have K>Na; whereas, the Magnet Cove carbonatite is lower in both K and Na and its Na content greatly exceeds K (Table 1).

Granite Mountain and Saline County syenite intrusions are very similar chemically (Table 1). The major difference is that all Granite Mountain rocks have Na>K. Samples from the Saline County intrusion may have either K or Na more abundant than the other; however, the average values for the Saline County intrusion indicate slightly more K than Na.

The feldspathoidal syenites from the complexes are somewhat chemically different from the two major intrusions discussed above (Table 1). Magnet Cove and the "V" intrusions contain much more Ca, Fe and Sr, and all three complexes contain more V than the major intrusions. Samples from the complexes may have K or Na more abundant than the other; however, the average values indicate the following K_2O/Na_2O ratios: Magnet Cove, 0.64; "V" Intrusive, 0.84; and Potash Sulfur Springs, 1.39 (Table 1).

The lamprophyre elemental values have a large range and it is not possible to distinguish the types based on chemistry. Because the ouachitite and monchiquite average values are similar, they have been combined as an average lamprophyre in Table 1. The lamprophyre have K_2O/Na_2O ratios (1.53), similar to the kimberlite. Although the various lamprophyre types exhibit considerable chemical overlap, the lamprophyre that has intruded the syenite complexes is characterized by both lower mafic indices and higher alkali content than the other lamprophyre samples and are most similar to the kimberlite.

Thus, many of the kimberlite, lamprophyre, syenite, and carbonatite samples exhibit similar chemical affinities, e.g. high K/Na ratios (Table 1). All of the rocks follow an alkali-olivine basalt trend on an AFM diagram (Fig. 4).

Time and Tectonic Relationship

Most workers consider the age of the majority of Arkansas igneous rocks to be Cretaceous; however, very few age determinations have been made for igneous rocks in Arkansas. Zartman et. al (1967) analyzed biotite from the Granite Mountain and Magnet Cove Intrusions using K/Ar and Rb/Sr methods and determined ages from 86±3 to 99±8 million years. Stone and Sterling (1964) report an average age for Granite Mountain based on two K/Ar analyses of biotite as 89 million years. A lamprophyre from Pope County, in the Arkansas Valley Region, has been dated as 83±6 million years based on K/Ar analysis of biotite (Stone, written communication, 1976). The Murfreesboro kimberlite is narrowly dated geologically because it intrudes Lower Cretaceous sediments and some kimberlite is found in the lower part of an Upper Cretaceous formation (Miser and Ross, 1923a).

Although there has been no investigation of the relationship of tectonic environment and igneous activity for Arkansas, major tectonic

TABLE 1. Average composition of Arkansas kimberlite, other igneous rocks of Arkansas and "average" kimberlite. Oxides are in weight percent and trace elements are in ppm by weight. Analyses were made by atomic absorption spectrometry.

	1	2	3	4	5+	6	7	8	9	10	11	12	13	14
TiO_2	2.26	2.24	2.22	1.20	2.03	1.20	0.24	0.09	0.92	0.63	0.63	1.65	0.88	3.43
Al_2O_3	2.94	3.92	4.60	2.46	4.9	3.67	0.58	1.72	17.90	16.55	18.79	13.83	18.61	13.39
Fe_2O_3*	9.16	9.52	6.11	10.02	11.67	9.09	4.70	1.01	3.21	2.44	3.76	10.07	5.49	12.04
MnO	0.15	0.15	0.16	0.24	0.10	0.50	0.21	0.22	0.22	0.24	0.21	0.30	0.26	0.21
MgO	20.89	19.49	10.38	18.61	23.9	4.89	2.35	0.73	0.69	0.36	0.83	2.47	0.92	7.21
CaO	5.84	5.32	5.49	11.60	10.6	39.08	46.13	45.86	1.80	1.39	1.23	8.74	6.22	12.27
Na_2O	0.48	0.35	1.72	0.19	0.31	2.99	0.22	0.69	6.89	6.77	5.64	5.10	7.77	1.79
K_2O	2.72	3.40	5.04	3.93	2.1	3.72	0.01	1.10	5.69	6.82	7.78	4.29	4.98	2.74
Ba	3045	3313	1433	2687	2060+	1491	481	1368	1079	513	1142	1558	1658	----
Sr	1272	1295	653	950	1100+	3931	5379	10,083	321	186	319	1088	1382	----
Rb	126	113	68	106	80+	----	2	12	----	223	209	125	181	----
Li	11	52	51	46	24+	17	5	8	28	31	20	30	19	----
V	38	115	83	205	120+	184	291	106	48	51	337	612	460	575
Co	58	92	39	70	70+	23	56	1	5	7	10	17	13	37
Zn	38	66	61	62	----	171	62	39	112	113	116	168	120	74
Ni	1100	1336	314	786	1100+	10	58	29	7	5	16	24	11	41
Cr	2531	1095	274	753	1505+	----	6	<1	10	12	16	22	13	54

1. Massive peridotite, Murfreesboro
2. Breccia, Murfreesboro
3. Tuff, Murfreesboro
4. Peridotite, Scott County
5. Micaceous kimberlite (Dawson, 1967)
6. Carbonatite breccia (Conway and Perry Counties)
7. Carbonatite, Magnet Cove
8. Carbonatite, Potash Sulfur Springs
9. Syenite, Granite Mountain (Van Buren, 1977)
10. Syenite, Saline County (Van Buren, 1977)
11. Syenite, Potash Sulfur Springs (Van Buren, 1977)
12. Syenite, "V" Intrusive (Van Buren, 1977)
13. Syenite, Magnet Cove (Van Buren, 1977)
14. Lamprophyre (Robison, 1976)

*Total iron as ferric iron
+Trace elements and oxides indicated from Dawson (1962)

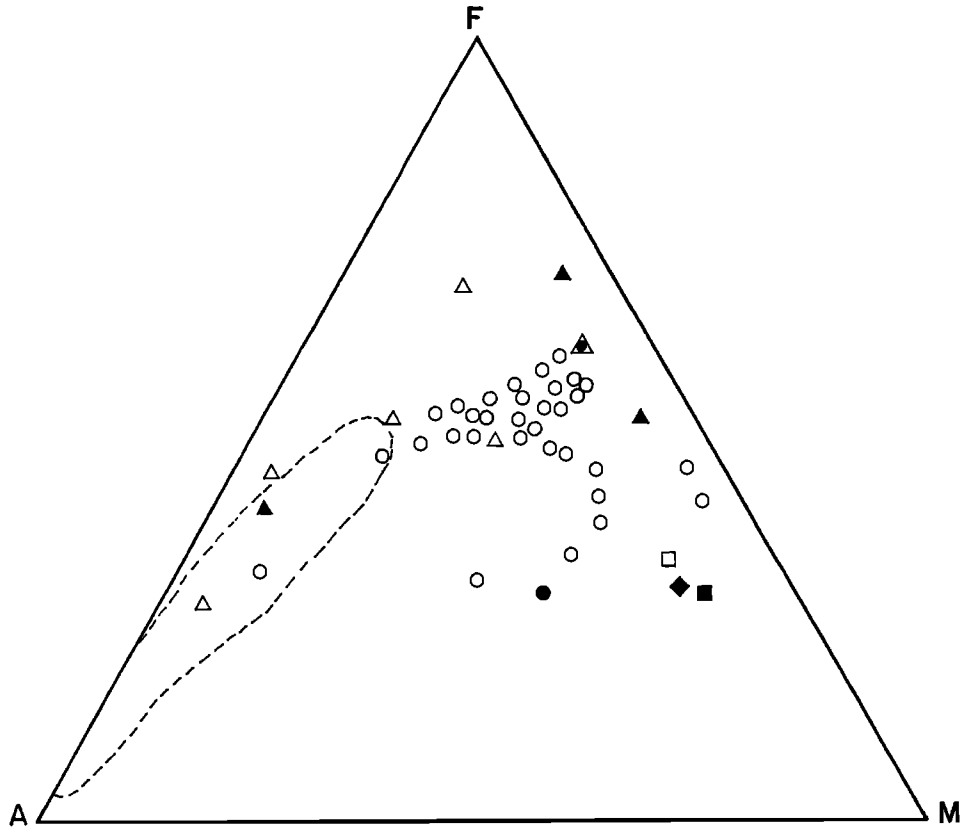

Fig. 4. AFM diagram. Syenite field is outlined by dashed line, lamprophyre (○), average carbonatite breccia (▲), Potash Sulfur Springs carbonatite (△), Magnet Cove carbonatite (▲), Murfreesboro peridotite (■), Murfreesboro breccia (◆), Murfreesboro tuff (●), and Scott County peridotite (□).

trends for the Ouachita Mountain Region and the Gulf Coastal Plains (King, 1969) suggests that the igneous rocks of Arkansas (including those encountered in wells in the Gulf Coastal Plains) are tectonically related. Dawson (1968) has pointed out that kimberlite and nepheline syenite-carbonatite suite rocks are associated in terms of time and tectonic environment, and although sufficient data is not available to adequately evaluate this statement for Arkansas, it is consistent with the available data.

Summary

The Murfreesboro kimberlite appears to be related in terms of age, tectonic environment and chemistry with the syenite, lamprophyre and carbonatite in Arkansas. The kimberlite is dated geologically as Cretaceous and radiometric dates for syenite and lamprophyre are about 89 million years. Many of the igneous rocks have K>Na, as does the kimberlite, and all of the rocks plot along a trend on an AFM plot. Most of the igneous rocks of Arkansas are exposed in the Ouachita Mountain Region, and although the Murfreesboro kimberlite is in the Gulf Coastal Plains, it is located close to the southern edge of the Ouachita Mountains which suggests a tectonic relationship for these igneous rocks. Finally, although an intimate spatial relationship between kimberlite and other igneous rocks may be lacking, there may be a more intimate spatial relationship at depth.

Acknowledgements. We greatly appreciate the assistance of the Arkansas Geological Commision during this project and financial support provided by the University of Arkansas.

References

Bolivar, S.L., D.G. Brookins, R.D. Lewis, H.O.A. Meyer, Geophysical studies of the Prairie Creek kimberlite, Murfreesboro, Arkansas, EOS Trans. AGU, 57, 762, 1976.

Bolivar, S.L., and D.G. Brookins, Geophysical and Rb-Sr study of the Elliott County, Kentucky and Prairie Creek, Arkansas kimberlites, Extended Abstracts, Second International Kimberlite Conference, Santa Fe, New Mexico, 1977.

Dawson, J.B., A review of the geology of kimberlite, in Ultramafic and Related Rocks, edited by P.J. Wyllie, pp. 241-251, Wiley, New York, 1967.

Dawson, J.B., Basutoland kimberlites, Geol. Soc. Am. Bull. 73, 545-560, 1962.

Erickson, R.L., and L.V. Blade, Geochemistry and petrology of the alkalic igneous ring dike complex at Magnet Cove, Arkansas: U.S. Geol. Surv. Prof. Paper 425, 95, 1963.

Heinrich, W.E., The Geology of Carbonatites, Rand McNally, Chicago, 555, 1966.

Howard, J.M., and Steele, K.F., Origin of the Potash Sulfur Springs intrusive complex, Arkansas: Programs Abstracts Geol. Soc. Amer., 7, 503, 1975.

King, P.B., Tectonic map of North America, U.S. Geol. Surv., 1969.

Lewis, R.D., H.O.A. Meyer, S.L. Bolivar, and D.G. Brookins, Mineralogy of the diamond bearing "kimberlite," Murfreesboro, Arkansas, EOS Trans. AGU, 57, 761, 1976.

Malamphy, M.C., G.K. Dale, T.M. Romslo, A.H. Reed, A. Ollar, and J.I. Tracy, Investigations of Arkansas bauxite, V.1: U.S. Bur. Mines, Rept. Inv. 4251, 63, 1948.

Malamphy, M.C., and J.L. Vallely, Geophysical Survey of the Arkansas bauxite region, Geophysics, 9, 324-366, 1944.

Meyer, H.O.A., Kimberlite from Norris Lake, eastern Tennessee: mineralogy and petrology, J. Geology, 83, 518-526, 1975.

Miser, H.D., and C.S. Ross, Diamond-bearing peridotite in Pike County, Arkansas, U.S. Geol. Surv. Bull. 735, 279-322, 1923a.

Miser, H.D., and C.S. Ross, Periodotite dikes in Scott County, Arkansas, U.S. Geol. Surv. Bull. 735, 271-278, 1923a.

Mitchell, R.H., Kimberlite and related rocks -- a critical reappraisal, J. Geol., 78, 686-704, 1970.

Owens, D.R., Bedrock geology of the "V" Intrusive, Garland County, Arkansas: Unpublished M.S. Thesis, University of Arkansas, 93, 1967.

Pollack, D.W., The Potash Sulfur Springs alkali complex, Garland County, Arkansas: (abstract), Mining Engr., 45-46, 1965.

Robison, E.C., Geochemistry of lamprophyric rocks of the eastern Ouachita Mountains, Arkansas, Unpublished M.S. Thesis, University of Arkansas, 147, 1976.

Stearn, N.H., A geomagnetic survey of the bauxite region in central Arkansas, Ark. Geol. Surv. Bull. 5, 16, 1930.

Steele, K.F., and E.C. Robison, Chemical relationships of lamprophyre, central Arkansas, EOS Trans. AGU, 56, 1018, 1976.

Stone, C.G., and P.T. Sterling, Relationship of igneous activity and mineral deposits in Arkansas, Ark. Geol. Comm. Publication, 55, 1964.

Thoenen, J.R., R.S. Hill, E.G. Howe, and S.M. Runke, Investigation of the Prairie Creek diamond area, Pike County, Arkansas, U.S. Bur. of Mines Rept. of Inv. 4549, 52, 1949.

Van Buren, W.M., Geochemistry of syenite in Arkansas, Unpublished M.S. Thesis, University of Arkansas, 100, 1977.

Wagner, G.H., and K.F. Steele, The chemical composition of carbonatite in Conway and Perry Counties of Arkansas, Proceedings of the Ark. Acad. of Sci., 31, 121-123, 1978.

Williams, J.F., The igneous rocks of Arkansas, Ark. Geol. Surv. Annual Rept., 2, 1-457, 1891.

Zartman, R.E., M.R. Brock, A.V. Heyl, and H.H. Thomas, K-Ar and Rb-Sr ages of some alkalic intrusive rocks from central and eastern United States, Am. J. Sci., 265, 848-870, 1967.

Author Index

The authors are indexed by the volume in which their papers appear. Volume I: Kimberlites, Diatremes, and Diamonds: their Geology, Petrology and Geochemistry is indicated by (I); Volume II: The Mantle Sample: Inclusions in Kimberlites and Other Volcanics is indicated by (II).